



*plants*

Special Issue Reprint

---

# 10th Anniversary of *Plants*

Recent Advances and Perspectives  
Volume III

---

Edited by  
Milan Stankovic, Paula Baptista and Petronia Carillo

[mdpi.com/journal/plants](https://mdpi.com/journal/plants)



**10th Anniversary of *Plants*—Recent  
Advances and  
Perspectives—Volume III**



# 10th Anniversary of *Plants*—Recent Advances and Perspectives—Volume III

Editors

**Milan Stankovic**

**Paula Baptista**

**Petronia Carillo**



Basel • Beijing • Wuhan • Barcelona • Belgrade • Novi Sad • Cluj • Manchester

*Editors*

Milan Stankovic  
University of Kragujevac  
Kragujevac  
Serbia

Paula Baptista  
Polytechnic Institute  
of Bragança  
Bragança  
Portugal

Petronia Carillo  
University of Campania  
“Luigi Vanvitelli”  
Caserta  
Italy

*Editorial Office*

MDPI  
St. Alban-Anlage 66  
4052 Basel, Switzerland

This is a reprint of articles from the Special Issue published online in the open access journal *Plants* (ISSN 2223-7747) (available at: [https://www.mdpi.com/journal/plants/special\\_issues/10th-anniversary\\_plants](https://www.mdpi.com/journal/plants/special_issues/10th-anniversary_plants)).

For citation purposes, cite each article independently as indicated on the article page online and as indicated below:

Lastname, A.A.; Lastname, B.B. Article Title. <i>Journal Name</i> <b>Year</b> , <i>Volume Number</i> , Page Range.
--

**Volume III**

**ISBN 978-3-0365-8422-5 (Hbk)**

**ISBN 978-3-0365-8423-2 (PDF)**

**[doi.org/10.3390/books978-3-0365-8423-2](https://doi.org/10.3390/books978-3-0365-8423-2)**

**Set**

**ISBN 978-3-0365-8372-3 (Hbk)**

**ISBN 978-3-0365-8373-0 (PDF)**

# Contents

<b>About the Editors</b> . . . . .	<b>ix</b>
<b>José Javier Martín-Gómez, Marco Porceddu, Gianluigi Bacchetta and Emilio Cervantes</b> Seed Morphology in Species from the <i>Silene mollissima</i> Aggregate (Caryophyllaceae) by Comparison with Geometric Models Reprinted from: <i>Plants</i> <b>2022</b> , <i>11</i> , 901, doi:10.3390/plants11070901 . . . . .	<b>1</b>
<b>Alessandra Marchica, Lorenzo Cotrozzi, Giacomo Lorenzini, Cristina Nali and Elisa Pellegrini</b> Antioxidants and Phytohormones Act in Coordination to Regulate Sage Response to Long Term Ozone Exposure Reprinted from: <i>Plants</i> <b>2022</b> , <i>11</i> , 904, doi:10.3390/plants11070904 . . . . .	<b>19</b>
<b>Hanna Bandurska</b> Drought Stress Responses: Coping Strategy and Resistance Reprinted from: <i>Plants</i> <b>2022</b> , <i>11</i> , 922, doi:10.3390/plants11070922 . . . . .	<b>31</b>
<b>Catello Di Martino, Valentina Torino, Pasqualino Minotti, Laura Pietrantonio, Carmine Del Grosso, Davide Palmieri, et al.</b> Mycorrhized Wheat Plants and Nitrogen Assimilation in Coexistence and Antagonism with Spontaneous Colonization of Pathogenic and Saprophytic Fungi in a Soil of Low Fertility Reprinted from: <i>Plants</i> <b>2022</b> , <i>11</i> , 924, doi:10.3390/plants11070924 . . . . .	<b>49</b>
<b>Min-Kyoung Kim, Geonha Park, Yura Ji, Yun-Gyo Lee, Minsik Choi, Seung-Hyeon Go, et al.</b> Design of Experiments-Based Optimization of Flavonoids Extraction from <i>Daphne genkwa</i> Flower Buds and Flavonoids Contents at Different Blooming Stages Reprinted from: <i>Plants</i> <b>2022</b> , <i>11</i> , 925, doi:10.3390/plants11070925 . . . . .	<b>69</b>
<b>Muhammad Jamil, Jian You Wang, Djibril Yonli, Tsuyoshi Ota, Lamis Berqdar, Hamidou Traore, et al.</b> <i>Striga hermonthica</i> Suicidal Germination Activity of Potent Strigolactone Analogs: Evaluation from Laboratory Bioassays to Field Trials Reprinted from: <i>Plants</i> <b>2022</b> , <i>11</i> , 1045, doi:10.3390/plants11081045 . . . . .	<b>85</b>
<b>Gustavo Arévalo-Rodrigues, Fernanda Hurbath, Erika Prado, Isabella Galvão, Inês Cordeiro and Diego Demarco</b> Adnate Leaf-Base and the Origin of Ribs in Succulent Stems of <i>Euphorbia</i> L. Reprinted from: <i>Plants</i> <b>2022</b> , <i>11</i> , 1076, doi:10.3390/plants11081076 . . . . .	<b>97</b>
<b>María de la Luz Riviello-Flores, Jorge Cadena-Iñiguez, Lucero del Mar Ruiz-Posadas, Ma. de Lourdes Arévalo-Galarza, Israel Castillo-Juárez, Marcos Soto Hernández, et al.</b> Use of Gamma Radiation for the Genetic Improvement of Underutilized Plant Varieties Reprinted from: <i>Plants</i> <b>2022</b> , <i>11</i> , 1161, doi:/10.3390/plants11091161 . . . . .	<b>109</b>
<b>Ramona Páltinean, Irina Ielciu, Daniela Hanganu, Mihaela Niculae, Eموke Pall, Luc Angenot, et al.</b> Biological Activities of Some Isoquinoline Alkaloids from <i>Fumaria schleicheri</i> Soy. Will. Reprinted from: <i>Plants</i> <b>2022</b> , <i>11</i> , 1202, doi:10.3390/plants11091202 . . . . .	<b>129</b>
<b>Robert Márquez Gutiérrez, Thales Henrique Cherubino Ribeiro, Raphael Ricon de Oliveira, Vagner Augusto Benedito and Antonio Chalfun-Junior</b> Genome-Wide Analyses of MADS-Box Genes in <i>Humulus lupulus</i> L. Reveal Potential Participation in Plant Development, Floral Architecture, and Lupulin Gland Metabolism Reprinted from: <i>Plants</i> <b>2022</b> , <i>11</i> , 1237, doi:10.3390/plants11091237 . . . . .	<b>143</b>

<b>Itziar Arnelas, Ernesto Pérez-Collazos, Josefa López-Martínez, Juan Antonio Devesa and Pilar Catalán</b> Molecular Systematics of <i>Valerianella</i> Mill. (Caprifoliaceae): Challenging the Taxonomic Value of Genetically Controlled Carpological Traits Reprinted from: <i>Plants</i> <b>2022</b> , <i>11</i> , 1276, doi:10.3390/plants11101276 . . . . .	159
<b>André Caeiro, Sandra Caeiro, Sandra Correia and Jorge Canhoto</b> Induction of Somatic Embryogenesis in Tamarillo ( <i>Solanum betaceum</i> Cav.) Involves Increases in the Endogenous Auxin Indole-3-Acetic Acid Reprinted from: <i>Plants</i> <b>2022</b> , <i>11</i> , 1347, doi:10.3390/plants11101347 . . . . .	181
<b>Diego José Fernández-López, José Ignacio Fernández-Fernández, Celia Martínez-Mora, Juan Antonio Bleda-Sánchez and Leonor Ruiz-García</b> Productiveness and Berry Quality of New Wine Grape Genotypes Grown under Drought Conditions in a Semi-Arid Wine-Producing Mediterranean Region Reprinted from: <i>Plants</i> <b>2022</b> , <i>11</i> , 1363, doi:10.3390/plants11101363 . . . . .	199
<b>Assunta Bertaccini</b> Plants and Phytoplasmata: When Bacteria Modify Plants Reprinted from: <i>Plants</i> <b>2022</b> , <i>11</i> , 1425, doi:10.3390/plants11111425 . . . . .	219
<b>Sara Vitalini, Marcello Iriti, Valentina Vaglia and Stefania Garzoli</b> Chemical Investigation and Dose-Response Phytotoxic Effect of Essential Oils from Two Gymnosperm Species ( <i>Juniperus communis</i> var. <i>saxatilis</i> Pall. and <i>Larix decidua</i> Mill.) Reprinted from: <i>Plants</i> <b>2022</b> , <i>11</i> , 1510, doi:10.3390/plants11111510 . . . . .	239
<b>Mohammad Ashrafal Alam, Marufur Rahman, Salahuddin Ahmed, Nasrin Jahan, Mohammad Al-Amin Khan, Mohammad Rafiqul Islam, et al.</b> Genetic Variation and Genotype by Environment Interaction for Agronomic Traits in Maize ( <i>Zea mays</i> L.) Hybrids Reprinted from: <i>Plants</i> <b>2022</b> , <i>11</i> , 1522, doi:10.3390/plants11111522 . . . . .	255
<b>Feyza Candan, Yuriy Markushin and Gulnihal Ozbay</b> Uptake and Presence Evaluation of Nanoparticles in <i>Cicer arietinum</i> L. by Infrared Spectroscopy and Machine Learning Techniques Reprinted from: <i>Plants</i> <b>2022</b> , <i>11</i> , 1569, doi:10.3390/plants11121569 . . . . .	271
<b>Chingchai Chaisiri, Xiangyu Liu, Yang Lin and Chaoxi Luo</b> <i>Diaporthe citri</i> : A Fungal Pathogen Causing Melanose Disease Reprinted from: <i>Plants</i> <b>2022</b> , <i>11</i> , 1600, doi:10.3390/plants11121600 . . . . .	285
<b>Nanami Sakata, Takumi Haraguchi, Shunsuke Masuo, Takako Ishiga and Yasuhiro Ishiga</b> <i>Pseudomonas cannabina</i> pv. <i>alisalensis</i> Virulence Factors Are Involved in Resistance to Plant-Derived Antimicrobials during Infection Reprinted from: <i>Plants</i> <b>2022</b> , <i>11</i> , 1742, doi:10.3390/plants11131742 . . . . .	305
<b>Caterina Catalano, Loredana Abbate, Sergio Fatta Del Bosco, Antonio Motisi, Francesco Carimi, Roberto De Michele, et al.</b> Different Cell Types Affect the Transition from Juvenile to Mature Phase in Citrus Plants Regenerated through Somatic Embryogenesis Reprinted from: <i>Plants</i> <b>2022</b> , <i>11</i> , 1811, doi:10.3390/plants11141811 . . . . .	319
<b>Manol Ognyanov, Petko Denev, Nadezhda Petkova, Zhana Petkova, Magdalena Stoyanova, Peter Zhelev, et al.</b> Nutrient Constituents, Bioactive Phytochemicals, and Antioxidant Properties of Service Tree ( <i>Sorbus domestica</i> L.) Fruits Reprinted from: <i>Plants</i> <b>2022</b> , <i>11</i> , 1832, doi:10.3390/plants11141832 . . . . .	333

<b>Widad AL-Juhani, Noha T. Al Thagafi and Rahmah N. Al-Qthanin</b> Gene Losses and Plastome Degradation in the Hemiparasitic Species <i>Plicosepalus acaciae</i> and <i>Plicosepalus curviflorus</i> : Comparative Analyses and Phylogenetic Relationships among Santalales Members Reprinted from: <i>Plants</i> <b>2022</b> , <i>11</i> , 1869, doi:10.3390/plants11141869 . . . . .	349
<b>Ghina Hajjar, Stéphane Quellec, Sylvain Challos, Lydia Bousset-Vaslin, Gisèle Joly, Christophe Langrume, et al.</b> Characterization of the Water Shortage Effects on Potato Tuber Tissues during Growth Using MRI Relaxometry and Biochemical Parameters Reprinted from: <i>Plants</i> <b>2022</b> , <i>11</i> , 1918, doi:10.3390/plants11151918 . . . . .	373
<b>Antonio Cano, Manuela Giraldo-Acosta, Sara García-Sánchez, Josefa Hernández-Ruiz and Marino B. Arnao</b> Effect of Melatonin in Broccoli Postharvest and Possible Melatonin Ingestion Level Reprinted from: <i>Plants</i> <b>2022</b> , <i>11</i> , 2000, doi:10.3390/plants11152000 . . . . .	395
<b>Sara Herrera, Jorge Lora, José I. Hormaza and Javier Rodrigo</b> Self-Incompatibility in Apricot: Identifying Pollination Requirements to Optimize Fruit Production Reprinted from: <i>Plants</i> <b>2022</b> , <i>11</i> , 2019, doi:10.3390/plants11152019 . . . . .	411
<b>Mei Han, Xianglei Xu, Yuan Xiong, Haikun Wei, Kejun Yao, Tingting Huang, et al.</b> Genome-Wide Survey and Expression Analyses of Hexokinase Family in Poplar ( <i>Populus trichocarpa</i> ) Reprinted from: <i>Plants</i> <b>2022</b> , <i>11</i> , 2025, doi:10.3390/plants11152025 . . . . .	429
<b>Ranjith Pathirana and Francesco Carimi</b> Management and Utilization of Plant Genetic Resources for a Sustainable Agriculture Reprinted from: <i>Plants</i> <b>2022</b> , <i>11</i> , 2038, doi:10.3390/plants11152038 . . . . .	445
<b>Manuel Pramsohler, Edith Lichtenberger and Gilbert Neuner</b> Seasonal Xylem Sap Acidification Is Governed by Tree Phenology, Temperature and Elevation of Growing Site Reprinted from: <i>Plants</i> <b>2022</b> , <i>11</i> , 2058, doi:10.3390/plants11152058 . . . . .	481
<b>Francesco Panara, Carlo Fasano, Loredana Lopez, Andrea Porceddu, Paolo Facella, Elio Fantini, et al.</b> Genome-Wide Identification and Spatial Expression Analysis of Histone Modification Gene Families in the Rubber Dandelion <i>Taraxacum kok-saghyz</i> Reprinted from: <i>Plants</i> <b>2022</b> , <i>11</i> , 2077, doi:10.3390/plants11162077 . . . . .	493
<b>Thomas Roach, Theresa Baur and Ilse Kranner</b> $\beta$ -Cyclocitral Does Not Contribute to Singlet Oxygen-Signalling in Algae, but May Down-Regulate Chlorophyll Synthesis Reprinted from: <i>Plants</i> <b>2022</b> , <i>11</i> , 2155, doi:10.3390/plants11162155 . . . . .	513
<b>Justyna Piotrowska, Yuki Jodoi, Nguyen Ha Trang, Anna Wawrzynska, Hideki Takahashi, Agnieszka Sirko, et al.</b> The C-Terminal Region of SLIM1 Transcription Factor Is Required for Sulfur Deficiency Response Reprinted from: <i>Plants</i> <b>2022</b> , <i>11</i> , 2595, doi:10.3390/plants11192595 . . . . .	525
<b>Aigerim Soltabayeva, Nurbanu Dauletova, Symbat Serik, Margulan Sandybek, John Okoth Omondi, Assylay Kurmanbayeva, et al.</b> Receptor-like Kinases (LRR-RLKs) in Response of Plants to Biotic and Abiotic Stresses Reprinted from: <i>Plants</i> <b>2022</b> , <i>11</i> , 2660, doi:10.3390/plants11192660 . . . . .	537

<b>Lyuben Zagorchev, Zhaokui Du, Yongbin Shi, Denitsa Teofanova and Junmin Li</b> <i>Cuscuta australis</i> Parasitism-Induced Changes in the Proteome and Photosynthetic Parameters of <i>Arabidopsis thaliana</i> Reprinted from: <i>Plants</i> <b>2022</b> , <i>11</i> , 2904, doi:10.3390/plants11212904 . . . . .	557
<b>Antonella Vitti, Israel Pagán, Brigida Bochicchio, Angelo De Stradis, Pasquale Piazzolla, Antonio Scopa, et al.</b> <i>Cucumber mosaic virus</i> Is Unable to Self-Assemble in Tobacco Plants When Transmitted by Seed Reprinted from: <i>Plants</i> <b>2022</b> , <i>11</i> , 3217, doi:10.3390/plants11233217 . . . . .	569
<b>Saverio Sciandrello, Salvatore Cambria, Gianpietro Giusso del Galdo, Pietro Minissale, Marta Puglisi, Gianmarco Tavilla, et al.</b> Ecological Features and Conservation of <i>Urtica rupestris</i> Guss. (Urticaceae): A Narrow Endemic Species of Sicily Reprinted from: <i>Plants</i> <b>2023</b> , <i>12</i> , 164, doi:10.3390/plants12010164 . . . . .	581

# About the Editors

## Milan Stankovic

Milan Stanković is an associate professor at the Department of Biology and Ecology, Faculty of Science, University of Kragujevac, Republic of Serbia and Head of Department of Biology and Ecology (2016-). His scientific and teaching career started at the Department of Biology and Ecology, Faculty of Science, University of Kragujevac (2008). He acquired his PhD degree in Plant Science (2012) at the same university and completed his postdoctoral research at the Université François-Rabelais de Tours, France. At the Faculty of Science, he was appointed as an assistant professor (2013), as well as an associate professor (2019), and he teaches several BSc, MSc, and PhD courses on plant science. His current research is focused on plant biology, ecology, and phytochemistry. Dr. Stanković is the (co-)author of over 300 references including articles in peer-reviewed journals, edited books, book chapters, conference papers, meeteng abstracts, etc. He is currently working as an associate editor of *Plants* (2012-).

## Paula Baptista

Paula Baptista is currently an associate professor at the Polytechnic Institute of Bragança (Portugal), the coordinator of the topic "Sustainable Agriculture and Innovative Agro-food Chains" of the Mountain Research Center (CIMO, <http://cimo.ipb.pt/web/>), and the general secretary of the International Organisation for Biological Control (IOBC-WPRS). More recently, she has become a member of the Plant Health (PLH) Panel of EFSA. She holds a bachelor's degree in agricultural engineering (1996, University of Trás-os-Montes), a master's degree in quality control (2000, University of Porto), and a PhD in science (2007, University of Minho). Her main interests are focused on agricultural microbiology and biotechnology, and in particular on the exploitation of beneficial microorganisms to improve plant health and yield. Her specific lines of research include the identification and characterization of microbial biological control agents, and the study of the molecular bases of plant(s)-pathogen(s)-biocontrol agent(s) interactions using '-omics' approaches. Her research has led to the publication of more than 150 ISI papers.

## Petronia Carillo

Petronia Carillo has been a full professor of agronomy at the University of Campania "Luigi Vanvitelli" in Caserta, Italy, since 2020, where she teaches agronomy, plant physiology, and post-harvest physiology. She was an associate professor of plant physiology (2010–2020) and permanent researcher of plant physiology (1999–2010) at the Second University of Naples, Italy. She studied at University Federico II of Naples, Italy, where she received her Ph.D. in plant physiology (1996) and MS (1992). She was a guest scientist at the Botanical Institute, Ruprecht-Karls-University of Heidelberg, Germany (4 months, 2000), and Max Planck Institute of Molecular Plant Physiology of Golm-Potsdam Germany (2–3 months a year from 2001 to 2010 and shorter visits from 2011 to 2020). She currently studies the metabolic and physiological responses of species of agronomic interest to nutrient deficiency, salt stress, and the type of cultivation (conventional, biological, hydroponic, eustress, microgravity, and the use of biostimulants).



## Article

# Seed Morphology in Species from the *Silene mollissima* Aggregate (Caryophyllaceae) by Comparison with Geometric Models

José Javier Martín-Gómez <sup>1</sup>, Marco Porceddu <sup>2,3,\*</sup>, Gianluigi Bacchetta <sup>2,3</sup> and Emilio Cervantes <sup>1</sup>

<sup>1</sup> Instituto de Recursos Naturales y Agrobiología del Consejo Superior de Investigaciones Científicas (IRNASA-CSIC), Cordel de Merinas 40, E-37008 Salamanca, Spain; jjavier.martin@irnasa.csic.es (J.J.M.-G.); emilio.cervantes@irnasa.csic.es (E.C.)

<sup>2</sup> Sardinian Germplasm Bank (BG-SAR), Hortus Botanicus Karalitanus (HBK), University of Cagliari (UNICA), Viale Sant'Ignazio da Laconi 9-11, 09123 Cagliari, Italy; bacchet@unica.it

<sup>3</sup> Centre for the Conservation of Biodiversity (CCB), Life and Environmental Sciences Department, University of Cagliari (UNICA), Viale Sant'Ignazio da Laconi 11-13, 09123 Cagliari, Italy

\* Correspondence: porceddu.marco@unica.it

**Abstract:** The description of seed shape by comparison with geometric models allows shape quantification, providing the means for an accurate comparison between different species or populations. Geometric models described for the lateral and dorsal views of the seeds of *Silene* species are applied to the quantification of the shape in the seeds belonging to twenty populations of the eleven taxa of *S. mollissima* aggregate. Cardioid models LM1, LM5 and LM6 adjust differentially to the lateral views of the seeds, while models DM1, DM5 and DM6 are applied to the dorsal views of the seeds. Quantification of the lateral view of seeds with LM5 results in two groups of species of different geographic origin. The seeds more resembling DM5 include *S. andryalifolia*, *S. badaroi*, *S. gazulensis*, *S. hifacensis* and *S. tomentosa*, i.e., the taxa with a continental distribution from southern Spain to northern Italy; in contrast, the group of seeds with lower similarity to DM5 includes those from species in northern Africa and the Mediterranean Tyrrhenian islands: *S. auriculifolia*, *S. hicesiae*, *S. ichnusae*, *S. mollissima*, *S. oenotriae* and *S. velutina*. The description of the seed shape based on geometric models contributes to investigating the relationships between related species and constitutes a promising technique for taxonomy.

**Keywords:** biogeography; cardioid; islands; geometric models; Mediterranean flora; morphology; *Silene*; super-ellipse

**Citation:** Martín-Gómez, J.J.; Porceddu, M.; Bacchetta, G.; Cervantes, E. Seed Morphology in Species from the *Silene mollissima* Aggregate (Caryophyllaceae) by Comparison with Geometric Models. *Plants* **2022**, *11*, 901. <https://doi.org/10.3390/plants11070901>

Academic Editors: Milan S. Stankovic, Paula Baptista and Petronia Carillo

Received: 9 March 2022

Accepted: 25 March 2022

Published: 28 March 2022

**Publisher's Note:** MDPI stays neutral with regard to jurisdictional claims in published maps and institutional affiliations.



**Copyright:** © 2022 by the authors. Licensee MDPI, Basel, Switzerland. This article is an open access article distributed under the terms and conditions of the Creative Commons Attribution (CC BY) license (<https://creativecommons.org/licenses/by/4.0/>).

## 1. Introduction

The genus *Silene* L., with more than 700 species, includes an important proportion of the diversity found in the family Caryophyllaceae Juss. The taxonomy of this genus was traditionally based on morphological criteria, and more recently has received the support of intensive DNA sequence analysis [1]. The genus was divided in three subgenera: *Lychnis*, *Silene* and *Behenantha*. The subg. *Silene* contains 11 sections, including Sect. *Siphonomorpha* Otth, a large group comprising about 150 species of perennial diploids [2], including both the *S. italica* and *S. mollissima* aggregates [3–5].

The *S. mollissima* aggregate contains 11 species found in different biogeographic provinces along the western Mediterranean Basin [6,7]. Among them, five species are endemic to the Tyrrhenian islands macro-hotspot (sensu Cañadas et al. 2014 [8]); these are: *Silene badaroi* Breistr. (= *S. tyrrhenia* Jeanmonod & Bocquet), *S. ichnusae* Brullo, De Marco and De Marco f., *S. hicesiae* Brullo & Signor., *S. oenotriae* Brullo and *S. velutina* Pourr. ex Loisel. *Silene hifacensis* Rouy ex Willk. and *S. mollissima* (L.) Pers. are Ibero-Levantine endemic, and the remaining four species of this aggregate are endemic to the Baetic-Riffan macro-hotspot: *S. andryalifolia* Pomel, *S. auriculifolia* Pomel, *S. gazulensis* A.Galán, J.E.Cortés,

Vicente Orell. & Mor. Alonso and *S. tomentosa* Otth. These species are currently identified by the morphological characters of their epigeal vegetative parts (leaves, hairs), as well as their inflorescence, flowers and capsules [4,9].

The 11 species of the *S. mollissima* aggregate that are the subject of this work constitute a paradigm for the study of plant diversity in the Mediterranean area, a region characterized by high rates of endemism due to isolation, either in islands, through mountain ranges or due to geographic micro-environments [10]. Thus, *S. tomentosa* is endemic to Gibraltar, a small area with very specific characteristics [11], while *S. gazulensis* is endemic to the Sierra de los Gazules in the surroundings of Gibraltar [12]. *S. andryaliifolia*, related to these species, has a broader distribution. The two Ibero-Levantine taxa, *S. hifacensis* and *S. mollissima*, are not sympatric. *S. hifacensis* only occurs on Ibiza and Alicante, while *S. mollissima* occurs on the Gymnesian islands of the Balearic Archipelago (Mallorca, Menorca and Cabrera) but not on the Pityusic islands (Ibiza or Formentera). Five of these species (*S. badaroi*, *S. ichnusae*, *S. hicesiae*, *S. oenotriae* and *S. velutina*) have a distribution centred in the Tyrrhenian area, with *S. badaroi* broadly distributed in the Provence and coast of north-western Italy; *S. velutina* is endemic to Sardinia and Corsica, and *S. ichnusae* is limited to north-western Sardinia while *S. hicesiae* and *S. oenotriae* occur in the southern Tyrrhenian sea. All these species are included in the section *Syphonomorpha* of subgen. *Silene* [1]. In this work, we have presented a morphological description of 20 populations from these species conserved in the Sardinian Germplasm Bank (BG-SAR; [13]) in order to find affinities between them as well as to investigate the variation in shape between species and populations.

Variations in the size and shape of the seeds represent an important source of information of high potential in taxonomy, particularly in *Silene* [14–19]. The application of image analysis techniques allows to obtain measurements related to the color, size and shape of seeds and to distinguish between different taxa or populations [20–25].

Based on previous studies on the seed morphology of the model plants *Arabidopsis thaliana* (L.) Heynh. [26,27], *Lotus japonicus* (Regel) K. Larsen and *Medicago truncatula* Gaertn. [28,29], seed shape descriptions based on the comparison with geometrical models have been applied to diverse plant genera and families [30–32], where the *J* index represents the percent of similarity between the geometric figure used as a model (cardioid) and the seed image. A striking similarity of the seed shape with the cardioid has been reported for the *Silene* species, in particular within *Silene* subg. *Behenantha*, with values of *J* index superior to 90 in a number of species (e.g., *S. noctiflora* L., *S. conica* L. and *S. latifolia* Poir.) [33]. In addition to the cardioid (Model 1, or LM1, where LM stands for lateral model), other models have already been described for the lateral views of *Silene* seeds [34,35]. LM2 is a flattened cardioid that demonstrated maximum similarity with the species *S. noctiflora* (*J* index 94.4) and *S. latifolia* (*J* index 93.0); LM3 was defined as an open cardioid curve having maximum similarity with *S. gallica* L. (*J* index 90.4) and LM4 was a flattened and elongated cardioid curve that indicated maximum similarity scores with *S. latifolia* (*J* index 92.5) and *S. declinis* (*J* index 91.5) [33]. LM5 and LM6 are modified forms from model 3 with variations in the hilum region. Values of *J* index superior to 90 were obtained in *S. diversifolia* Otth and *S. tridentata* Ramond ex DC. [34]. Models LM7 and LM8 present other morphological peculiarities and provide *J* index values superior to 90 with *S. portensis* L. (both models), *S. nicaensis* All., *S. littorea* Brot., *S. portensis* and *S. scabriflora* Brot. (model LM8) [34]. Models for the dorsal views of *Silene* seeds have also been described [35]. The *J* index values were more stable than the other typical morphological measures (i.e., area, length and width); hence, the association between the seed morphology and geometrical figures was stated as robust and could be used for classification purposes [33–35].

Concerning the seed morphology of the *S. mollissima* aggregate, morpho-colorimetric image analysis methods have been applied, revealing differences between the species [14,36]. By studying the seed morpho-colorimetric characteristics of *S. badaroi*, *S. ichnusae*, *S. hicesiae*, *S. oenotriae* and *S. velutina*, Murru et al. [36] reported that the current systematic treatment at the species level for these taxa is confirmed. However, the authors highlighted the need of

further investigations regarding the taxonomic position of *S. hicesiae* in the whole aggregate as well as regarding the differentiation of *S. ichnusae* from *S. velutina* [36]. Nevertheless, the results from automated image analysis reported so far do not discriminate between the differences in size and shape, and the differences resulting from the analysis may be due to a mixture of shape, size or even color characteristics, while we are interested by the identification of differences in seed shape. The seeds of a given species or population can have a conserved shape that corresponds to a geometric model. This is detected by values of *J* index superior to 90 and has been reported in populations of diverse species of *Silene* [33–35].

Previous studies on the seeds' characteristics in the taxa of a specific group membership proved that this type of analysis can be a useful tool for discriminating the species [23,24,29,35,36] or also in separating the taxa in different groups, such as, for example, the coastal species from the mountain ones [25]. These analyses are non-destructive, repeatable and, by incorporating the seed trait information with the leaves, hairs, flowers, fruit analysis or other morphological characteristics of a plant, may provide an important contribution for taxonomic studies.

Our objectives in this work are the following: (1) to describe the geometric models that define the seed shape in the species of *Silene mollissima* aggregate, and (2) to identify differences between the species in the shape of their seeds. We hypothesize that the new information provided by the geometric models analysis of seed shape may confer new knowledge useful to understand the relationships among species and to provide a new basis for the next taxonomic investigations regarding *Silene* taxa.

## 2. Results

### 2.1. General Morphology

#### 2.1.1. Lateral Views of Seeds

Table 1 presents a summary of the mean values and standard deviations for area (A), perimeter (P), length (L), width (W), aspect ratio (AR), circularity (C) and roundness (R) corresponding to the lateral views of the seeds in the 11 species of *S. mollissima* aggregate. Differences between the species were found in the size and shape for all the measurements. The mean area values were between 0.86 (*S. badaroi*) and 1.50 mm<sup>2</sup> (*S. andryalifolia*). Three groups of different sizes were defined. The largest seeds corresponded to *S. andryalifolia*, *S. auricolifolia* and *S. velutina*, the intermediate seeds to *S. hifacensis*, *S. ichnusae*, *S. mollissima*, *S. oenotriae* and *S. tomentosa* and the smallest seeds to *S. badaroi*, *S. gazulensis* and *S. hicesiae*.

The aspect ratio was between 1.15 in *S. auricolifolia* and 1.33 in *S. velutina*; three groups were defined corresponding to the rounded seeds with the smallest values of aspect ratio (*S. auricolifolia*), seeds with intermediate values (*S. andryalifolia*, *S. badaroi*, *S. gazulensis*, *S. hicesiae*, *S. hifacensis*, *S. ichnusae*, *S. mollissima* and *S. tomentosa*) and elongated seeds (*S. hicesiae*, *S. oenotriae* and *S. velutina*). The coefficient of variation had higher values in the measurements of size (A, P, L and W) than in the shape measurements (AR, C and R).

Different populations were analyzed in four species: *S. badaroi*, *S. hicesiae*, *S. hifacensis* and *S. velutina*. In the species with two populations analyzed (*S. hicesiae* and *S. velutina*), there was one population with larger seeds and the other with smaller seeds (not shown). There was no difference in aspect ratio, circularity or roundness in any of these two cases. There were also differences in seed size among the populations of *S. badaroi* (three populations) and *S. hifacensis* (six populations) (not shown). Differences in circularity were found between the populations of *S. badaroi* (not shown). In *S. hifacensis*, there were also differences in size, aspect ratio, circularity and roundness between the six populations studied (not shown).

#### 2.1.2. Dorsal View of Seeds

Table 2 presents a summary of the mean values and standard deviations for A, P, L, W, AR, C and R corresponding to the dorsal views of the seeds in the 11 species of

*S. mollissima* aggregate. Differences between the species were found in size and shape for all the measurements. The mean area values were between 0.71 (*S. hicesiae*) and 1.51 mm<sup>2</sup> (*S. auriculifolia*). Five groups of different sizes were defined. The largest seeds corresponded to *S. auriculifolia*, followed by the seeds of *S. andryalifolia*. The seeds of *S. oenotriae* and *S. velutina* were of intermediate size. *S. hifacensis*, *S. ichnusae*, *S. mollissima* and *S. tomentosa* were of small-intermediate size. The smallest seeds corresponded to *S. badaroi*, *S. gazulensis* and *S. hicesiae*.

**Table 1.** Results of Kruskal–Wallis and post hoc tests for the size and shape measurements in the lateral views of seeds in species of the *Silene mollissima* aggregate. Mean values and coefficient of variation (given in parentheses) are indicated for area (A), perimeter (P), length (L), width (W), aspect ratio (AR), circularity (C) and roundness (R). Values marked with the same superscript letter in each column correspond to populations that do not differ significantly at  $p < 0.05$ . N indicates the number of seeds analyzed.

Species	N	A (mm <sup>2</sup> )	P (mm)	L (mm)	W (mm)	AR	C	R
<i>S. andryalifolia</i>	30	1.50 <sup>e</sup> (9.28)	4.98 <sup>f</sup> (5.02)	1.55 <sup>e</sup> (5.29)	1.23 <sup>d</sup> (5.22)	1.27 <sup>bcd</sup> (5.06)	0.76 <sup>d</sup> (3.60)	0.79 <sup>bcd</sup> (4.67)
<i>S. auriculifolia</i>	15	1.44 <sup>de</sup> (18.80)	4.89 <sup>f</sup> (10.98)	1.45 <sup>d</sup> (9.31)	1.26 <sup>d</sup> (9.87)	1.15 <sup>a</sup> (5.17)	0.75 <sup>cd</sup> (6.27)	0.87 <sup>e</sup> (4.97)
<i>S. badaroi</i>	130	0.86 <sup>a</sup> (16.03)	3.77 <sup>a</sup> (8.50)	1.17 <sup>a</sup> (8.34)	0.93 <sup>a</sup> (8.40)	1.25 <sup>b</sup> (4.88)	0.76 <sup>d</sup> (4.00)	0.80 <sup>cd</sup> (4.82)
<i>S. gazulensis</i>	48	0.90 <sup>a</sup> (11.74)	4.01 <sup>c</sup> (6.57)	1.22 <sup>b</sup> (6.63)	0.94 <sup>a</sup> (7.01)	1.28 <sup>cde</sup> (7.40)	0.69 <sup>a</sup> (4.24)	0.77 <sup>abc</sup> (7.08)
<i>S. hicesiae</i>	130	0.87 <sup>a</sup> (14.91)	3.90 <sup>b</sup> (7.45)	1.21 <sup>b</sup> (8.25)	0.92 <sup>a</sup> (8.50)	1.32 <sup>e</sup> (8.30)	0.72 <sup>b</sup> (4.12)	0.76 <sup>a</sup> (8.11)
<i>S. hifacensis</i>	282	1.19 <sup>bc</sup> (18.18)	4.49 <sup>d</sup> (10.37)	1.38 <sup>c</sup> (9.46)	1.09 <sup>b</sup> (9.20)	1.26 <sup>bc</sup> (4.11)	0.74 <sup>c</sup> (5.99)	0.80 <sup>cd</sup> (4.05)
<i>S. ichnusae</i>	66	1.23 <sup>bc</sup> (17.21)	4.56 <sup>de</sup> (9.79)	1.41 <sup>cd</sup> (10.38)	1.11 <sup>b</sup> (8.74)	1.25 <sup>bc</sup> (7.97)	0.75 <sup>c</sup> (5.39)	0.79 <sup>cd</sup> (7.61)
<i>S. mollissima</i>	40	1.16 <sup>bc</sup> (13.57)	4.58 <sup>de</sup> (6.36)	1.36 <sup>c</sup> (6.78)	1.08 <sup>b</sup> (7.09)	1.26 <sup>bc</sup> (3.33)	0.69 <sup>a</sup> (3.71)	0.80 <sup>cd</sup> (3.35)
<i>S. oenotriae</i>	61	1.23 <sup>c</sup> (14.59)	4.80 <sup>f</sup> (7.23)	1.43 <sup>d</sup> (8.87)	1.09 <sup>b</sup> (9.72)	1.32 <sup>de</sup> (11.26)	0.68 <sup>a</sup> (5.50)	0.77 <sup>ab</sup> (10.73)
<i>S. tomentosa</i>	44	1.15 <sup>b</sup> (10.38)	4.62 <sup>e</sup> (6.28)	1.34 <sup>c</sup> (5.17)	1.09 <sup>b</sup> (6.38)	1.23 <sup>b</sup> (4.54)	0.68 <sup>a</sup> (4.87)	0.81 <sup>d</sup> (4.61)
<i>S. velutina</i>	135	1.38 <sup>d</sup> (15.01)	4.83 <sup>f</sup> (7.91)	1.53 <sup>d</sup> (8.43)	1.15 <sup>c</sup> (9.70)	1.33 <sup>e</sup> (9.82)	0.74 <sup>c</sup> (3.98)	0.76 <sup>a</sup> (9.80)

Similar to the lateral view, the aspect ratio was between 1.08 in *S. auriculifolia* and 1.78 in *S. velutina*. Four groups were defined by the seeds with large (*S. gazulensis*, *S. hicesiae*, *S. hifacensis*, *S. mollissima* and *S. velutina*), intermediate (*S. badaroi* and *S. ichnusae*), intermediate–small (*S. andryalifolia*, *S. oenotriae* and *S. tomentosa*) and smallest values of aspect ratio (*S. auriculifolia*). The coefficient of variation had higher values in the measurements of size (A, P, L and W) than in the shape measurements (AR, C and R).

In the species with two populations analyzed (*S. hicesiae* and *S. velutina*), there was no difference in size, aspect ratio, circularity or roundness between the populations (not shown). In contrast, there was a difference in the size and aspect ratio among the populations of *S. badaroi* (three populations) and *S. hifacensis* (six populations) (not shown).

## 2.2. Comparison of the Average Silhouette of Seeds with the Geometric Models

### 2.2.1. Lateral View of Seeds

The average silhouettes obtained for the lateral view of the seeds in all 20 populations belonging to 11 species are shown in Figure 1. They were compared with the models LM1 to LM8 described in Refs. [33,34].

**Table 2.** Results of Kruskal–Wallis and post hoc tests for the size and shape measurements of the seeds in species of the *Silene mollissima* aggregate. Mean values and coefficient of variation (given in parentheses) are indicated for area (A), perimeter (P), length (L), width (W), aspect ratio (AR), circularity (C) and roundness (R). Values marked with the same superscript letter in each column correspond to populations that do not differ significantly at  $p < 0.05$ . N indicates the number of seeds analyzed.

Species	N	A (mm <sup>2</sup> )	P (mm)	L (mm)	W (mm)	AR	C	R
<i>S. andryalifolia</i>	24	1.33 <sup>d</sup> (8.90)	4.88 <sup>d</sup> (5.91)	1.60 <sup>e</sup> (6.53)	1.06 <sup>e</sup> (4.49)	1.52 <sup>bc</sup> (6.92)	0.70 <sup>e</sup> (7.01)	0.66 <sup>cd</sup> (6.81)
<i>S. auriculifolia</i>	14	1.51 <sup>e</sup> (17.78)	4.96 <sup>d</sup> (9.68)	1.43 <sup>bc</sup> (8.04)	1.33 <sup>f</sup> (10.27)	1.08 <sup>a</sup> (4.46)	0.77 <sup>f</sup> (7.64)	0.93 <sup>e</sup> (4.46)
<i>S. badaroi</i>	74	0.75 <sup>a</sup> (16.11)	3.69 <sup>a</sup> (7.35)	1.22 <sup>a</sup> (7.14)	0.78 <sup>b</sup> (10.04)	1.56 <sup>c</sup> (7.00)	0.69 <sup>de</sup> (5.80)	0.64 <sup>c</sup> (6.76)
<i>S. gazulensis</i>	23	0.72 <sup>a</sup> (14.61)	3.78 <sup>ab</sup> (9.12)	1.24 <sup>a</sup> (7.95)	0.73 <sup>a</sup> (7.18)	1.71 <sup>def</sup> (5.29)	0.63 <sup>b</sup> (5.67)	0.59 <sup>ab</sup> (5.40)
<i>S. hicesiae</i>	43	0.71 <sup>a</sup> (17.35)	3.87 <sup>b</sup> (9.38)	1.24 <sup>a</sup> (8.66)	0.73 <sup>a</sup> (9.65)	1.68 <sup>de</sup> (6.35)	0.60 <sup>a</sup> (7.30)	0.59 <sup>b</sup> (6.12)
<i>S. hifacensis</i>	128	1.00 <sup>b</sup> (17.60)	4.35 <sup>c</sup> (9.68)	1.46 <sup>bc</sup> (9.56)	0.87 <sup>c</sup> (8.79)	1.68 <sup>d</sup> (5.76)	0.66 <sup>c</sup> (5.08)	0.60 <sup>b</sup> (5.69)
<i>S. ichmusae</i>	20	0.96 <sup>b</sup> (16.82)	4.26 <sup>c</sup> (7.67)	1.39 <sup>b</sup> (9.49)	0.87 <sup>c</sup> (8.75)	1.60 <sup>c</sup> (8.44)	0.66 <sup>c</sup> (8.77)	0.63 <sup>c</sup> (8.19)
<i>S. mollissima</i>	20	1.04 <sup>b</sup> (11.35)	4.45 <sup>c</sup> (5.82)	1.51 <sup>cd</sup> (5.20)	0.87 <sup>c</sup> (7.20)	1.74 <sup>ef</sup> (4.59)	0.66 <sup>c</sup> (4.11)	0.58 <sup>a</sup> (4.73)
<i>S. oenotriae</i>	20	1.19 <sup>c</sup> (11.87)	4.93 <sup>de</sup> (6.26)	1.53 <sup>d</sup> (4.97)	0.99 <sup>d</sup> (8.09)	1.55 <sup>bc</sup> (7.40)	0.61 <sup>a</sup> (7.18)	0.65 <sup>cd</sup> (6.83)
<i>S. tomentosa</i>	20	1.03 <sup>b</sup> (11.23)	4.37 <sup>c</sup> (4.25)	1.39 <sup>b</sup> (5.05)	0.94 <sup>d</sup> (6.92)	1.49 <sup>b</sup> (4.22)	0.68 <sup>cd</sup> (5.06)	0.67 <sup>d</sup> (4.26)
<i>S. velutina</i>	39	1.23 <sup>c</sup> (13.57)	5.12 <sup>e</sup> (7.37)	1.66 <sup>f</sup> (6.15)	0.94 <sup>d</sup> (9.94)	1.78 <sup>f</sup> (9.90)	0.59 <sup>a</sup> (9.43)	0.57 <sup>a</sup> (9.60)

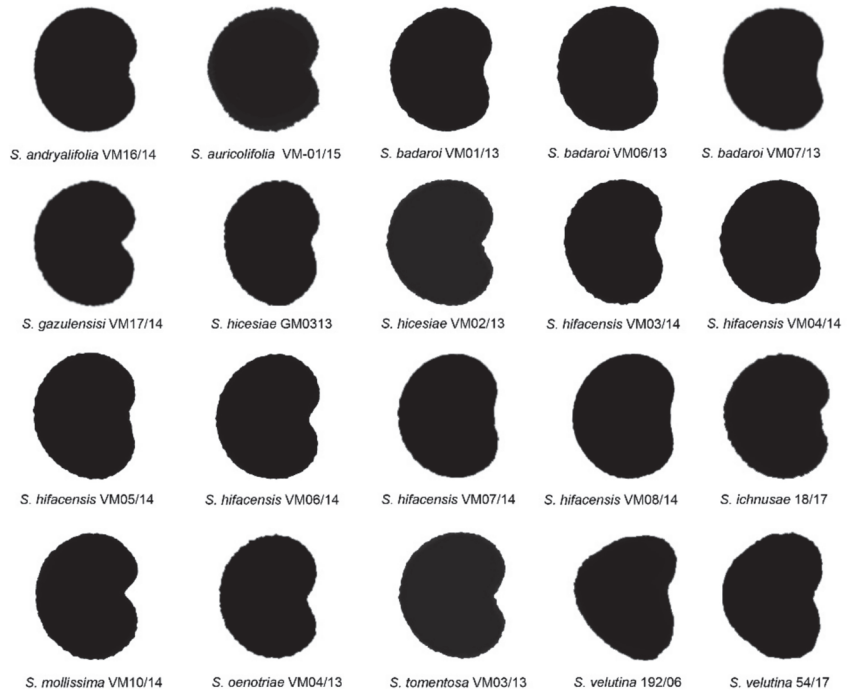


**Figure 1.** Average silhouettes obtained for the lateral views of 20 populations of 11 species in the *Silene mollissima* aggregate.

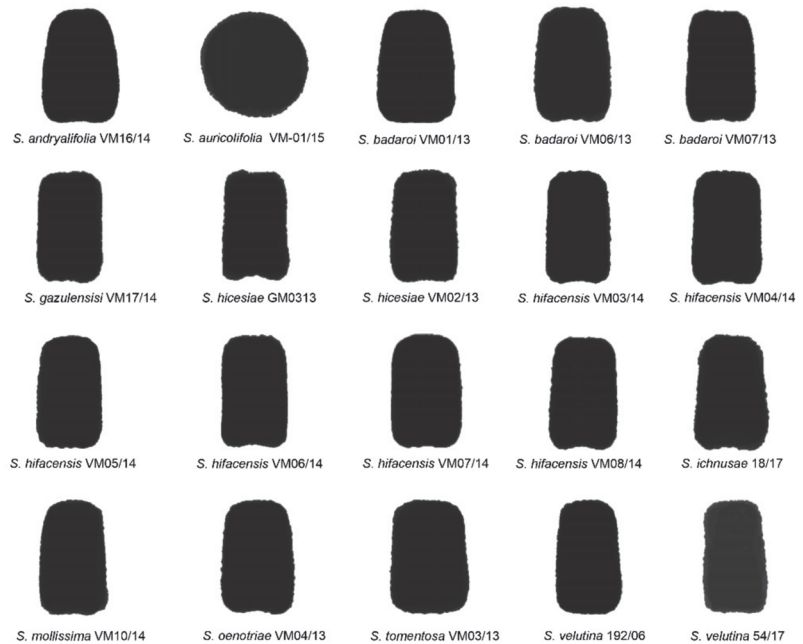
The average silhouette of each population was compared with the eight geometric models. The results of the comparison are given in Table 3. The values of  $J$  index (percent similarity to the models) superior to 90 were obtained in all the species tested. Maximum values were obtained with model LM1 for *S. andryalifolia*, *S. auriculifolia* and *S. ichmusae*, with model LM4 for *S. badaroi*, *S. hicesiae*, *S. hifacensis* and *S. oenotriae* and with model LM5 for *S. gazulensis*, *S. mollissima* and *S. tomentosa*. *S. velutina* showed the best score with model LM8. The  $J$  index was calculated with models LM1, LM4 and LM5 for all the species.

**Table 3.** Values of *J* index of the average silhouettes with lateral models LM1 to LM8. In bold, upper values obtained for each species.

Species	N	LM1	LM2	LM3	LM4	LM5	LM6	LM7	LM8
<i>S. andryalifolia</i>	24	<b>92.0</b>	91.8	88.3	91.9	91.9	84.2	88.5	89.0
<i>S. auriculifolia</i>	8	<b>92.9</b>	91.1	85.2	87.5	88.7	80.2	89.4	89.6
<i>S. badaroi</i>	70	91.0	91.0	90.4	<b>93.4</b>	91.7	86.3	89.3	90.3
<i>S. gazulensis</i>	32	90.6	88.4	90.4	90.8	<b>93.3</b>	87.7	91.4	90.0
<i>S. hicesiae</i>	48	88.1	87.3	89.2	<b>91.7</b>	90.1	88.7	87.5	86.8
<i>S. hifacensis</i>	128	91.9	91.0	90.4	<b>93.8</b>	92.0	86.3	89.1	90.5
<i>S. ichnusae</i>	20	<b>92.9</b>	91.7	88.3	90.5	91.9	82.9	89.4	91.8
<i>S. mollissima</i>	20	91.7	91.0	91.3	92.8	<b>93.4</b>	88.3	90.3	89.2
<i>S. oenotriae</i>	24	89.9	87.1	90.5	<b>92.0</b>	91.3	89.2	89.7	87.0
<i>S. tomentosa</i>	20	92.8	92.2	90.1	92.5	<b>93.2</b>	86.5	91.4	91.0
<i>S. velutina</i>	45	87.1	85.8	88.5	87.9	88.7	87.7	<b>89.1</b>	88.8

### 2.2.2. Dorsal View of Seeds

The average silhouettes obtained for the dorsal view of the seeds in all 20 populations belonging to 11 species are shown in Figure 2. They were compared with models DM1, DM5 and DM6 [35].

**Figure 2.** Average silhouettes obtained for the dorsal views of 20 populations of 11 species in the *Silene mollissima* aggregate.

The results of the comparison of the average silhouette of each species in the dorsal views of the seeds with the three geometric models tested are given in Table 4. Values superior to 90 were obtained for all the species except for *S. auriculifolia*, whose seeds are round in their lateral view. Maximum values were obtained with model DM5 for *S. andryalifolia*, *S. badaroi*, *S. oenotriae* and *S. tomentosa*. With model DM6, the highest values were obtained for *S. gazulensis*, *S. hicesiae*, *S. hifacensis*, *S. ichnusae*, *S. mollissima* and *S. velutina*. The *J* index values were tested with models DM1, DM5 and DM6 for the seeds of all the species.

**Table 4.** Values of *J* index of the average silhouettes with dorsal models DM1, DM5 and DM6. In bold, upper values obtained for each species.

Species	N	DM1	DM5	DM6
<i>S. andryalifolia</i>	24	90.5	<b>93.7</b>	90.1
<i>S. auricolifolia</i>	8	<b>79.2</b>	<b>79.2</b>	68.0
<i>S. badaroi</i>	70	91.9	<b>94.2</b>	90.9
<i>S. gazulensis</i>	32	92.0	91.7	<b>93.1</b>
<i>S. hicesiae</i>	48	89.2	91.0	<b>91.4</b>
<i>S. hifacensis</i>	128	91.4	92.5	<b>93.4</b>
<i>S. ichnusae</i>	20	92.0	92.8	<b>92.9</b>
<i>S. mollissima</i>	20	91.4	90.9	<b>93.2</b>
<i>S. oenotriae</i>	24	91.8	<b>92.9</b>	85.7
<i>S. tomentosa</i>	20	92.2	<b>93.9</b>	91.5
<i>S. velutina</i>	45	89.8	87.8	<b>91.8</b>

### 2.3. Shape Quantification with Models: The Mean *J* Index in the Seeds of Each Species

#### 2.3.1. Shape Quantification in the Lateral Views with Models LM1, LM4 and LM5

The percent similarity (*J* index) of the seeds with the models giving the highest values in the comparison with the average silhouettes (LM1, LM4 and LM5) was obtained for all the species (Table 5).

**Table 5.** Results of Kruskal–Wallis and post hoc tests for the *J* index values (percent of similarity of the lateral views of seeds with models LM1, LM4 and LM5) of the 11 species of the *Silene mollissima* aggregate. Mean values and coefficient of variation (given in parentheses) are indicated for *J* index values with the different models. Values marked with the same superscript letter in each column correspond to populations that do not differ significantly at  $p < 0.05$ . N indicates the number of seeds analyzed. In bold, upper values obtained for each species.

Species	N	LM1	LM4	LM5
<i>S. andryalifolia</i>	24	89.2 <sup>c</sup> (1.64)	88.8 <sup>cd</sup> (1.68)	<b>89.9<sup>b</sup></b> (1.72)
<i>S. auricolifolia</i>	8	<b>91.1<sup>d</sup></b> (1.80)	85.2 <sup>ab</sup> (4.00)	85.8 <sup>a</sup> (2.61)
<i>S. badaroi</i>	70	89.8 <sup>cd</sup> (1.60)	<b>90.0<sup>e</sup></b> (2.01)	89.7 <sup>b</sup> (1.42)
<i>S. gazulensis</i>	32	87.1 <sup>ab</sup> (2.80)	88.2 <sup>bcd</sup> (2.22)	<b>89.3<sup>b</sup></b> (2.07)
<i>S. hicesiae</i>	48	86.1 <sup>a</sup> (3.18)	<b>88.1<sup>bcd</sup></b> (2.76)	86.8 <sup>a</sup> (2.66)
<i>S. hifacensis</i>	128	90.2 <sup>cd</sup> (2.14)	<b>91.1<sup>f</sup></b> (1.51)	90.1 <sup>b</sup> (1.45)
<i>S. ichnusae</i>	20	<b>89.3<sup>cd</sup></b> (2.41)	88.2 <sup>bcd</sup> (2.70)	87.8 <sup>a</sup> (2.44)
<i>S. mollissima</i>	24	<b>87.7<sup>b</sup></b> (2.07)	86.8 <sup>abc</sup> (3.27)	86.2 <sup>a</sup> (2.59)
<i>S. oenotriae</i>	24	86.2 <sup>a</sup> (3.83)	<b>87.8<sup>bcd</sup></b> (2.25)	86.8 <sup>a</sup> (2.84)
<i>S. tomentosa</i>	20	<b>90.1<sup>cd</sup></b> (1.40)	89.5 <sup>de</sup> (2.10)	89.7 <sup>b</sup> (1.69)
<i>S. velutina</i>	45	84.8 <sup>a</sup> (4.93)	84.8 <sup>a</sup> (4.58)	<b>85.8<sup>a</sup></b> (3.61)

The analysis with each of the three models revealed a variable number of groups of low, intermediate and high *J* index values. Three species gave the lowest scores with model LM1 (*S. hicesiae*, *S. oenotriae* and *S. velutina*), and *S. auricolifolia* gave the highest values. Intermediate values of *J* index with LM1 were obtained in the remaining species. Three species gave the lowest scores with model LM4 (*S. auricolifolia*, *S. mollissima* and *S. velutina*), while the highest values were observed in *S. hifacensis* followed by *S. badaroi* and *S. tomentosa*; the remaining species had intermediate values. With model LM5, two groups were obtained of low (*S. auricolifolia*, *S. hicesiae*, *S. ichnusae*, *S. mollissima*, *S. oenotriae* and *S. velutina*) and high values of *J* index (*S. andryalifolia*, *S. badaroi*, *S. gazulensis*, *S. hifacensis* and *S. tomentosa*). Images of LM5 with *S. andryalifolia*, *S. badaroi*, *S. gazulensis*, *S. hifacensis* and *S. tomentosa* are shown in Figures A1–A5 of Appendix A, and images of LM5 with *S. auricolifolia*, *S. hicesiae*, *S. ichnusae*, *S. mollissima*, *S. oenotriae* and *S. velutina* are shown in Appendix A Figures A6–A11, respectively.

The coefficient of variation had lower values in the measurements of *J* index than in the other shape measurements (AR, C and R; see Table 1).

### 2.3.2. Shape Quantification in the Dorsal Views with Models DM1, DM5 and DM6

The percent similarity of the dorsal views of the seeds with models DM1, DM5 and DM6 (*J* index) was obtained for all the species (Table 6).

**Table 6.** Results of Kruskal–Wallis and post hoc tests for the *J* index values (percent of similarity of the dorsal views of seeds with models DM1, DM5 and DM6) of the 11 species of the *Silene mollissima* aggregate. Mean values and coefficient of variation (given in parentheses) are indicated for *J* index values with the different models. Values marked with the same superscript letter in each column correspond to populations that do not differ significantly at  $p < 0.05$ . N indicates the number of seeds analyzed. In bold, upper values obtained for each species.

Species	N	DM1	DM5	DM6
<i>S. andryalifolia</i>	24	87.3 <sup>cde</sup> (1.51)	<b>89.9<sup>ef</sup></b> (1.43)	87.8 <sup>bcde</sup> (3.43)
<i>S. auricolifolia</i>	14	73.3 <sup>a</sup> (3.75)	73.7 <sup>a</sup> (3.49)	68.0 <sup>a</sup> (3.56)
<i>S. badaroi</i>	69	88.0 <sup>de</sup> (2.27)	<b>90.1<sup>f</sup></b> (1.56)	88.4 <sup>bcde</sup> (2.78)
<i>S. gazulensis</i>	24	85.2 <sup>bcde</sup> (2.87)	85.4 <sup>bc</sup> (2.51)	<b>89.3<sup>cde</sup></b> (1.54)
<i>S. hicesiae</i>	40	83.9 <sup>bc</sup> (2.77)	85.2 <sup>bc</sup> (2.98)	<b>88.8<sup>bcde</sup></b> (1.64)
<i>S. hifacensis</i>	120	85.4 <sup>bcde</sup> (2.76)	86.3 <sup>bcd</sup> (2.67)	<b>90.4<sup>de</sup></b> (1.42)
<i>S. ichnusae</i>	20	84.8 <sup>bcd</sup> (3.28)	86.6 <sup>cde</sup> (2.94)	<b>87.4<sup>bc</sup></b> (3.31)
<i>S. mollissima</i>	20	84.4 <sup>bc</sup> (2.26)	84.6 <sup>bc</sup> (2.21)	<b>90.5<sup>e</sup></b> (1.31)
<i>S. oenotriae</i>	20	86.3 <sup>bcde</sup> (2.19)	<b>88.7<sup>def</sup></b> (1.77)	87.6 <sup>bcd</sup> (2.93)
<i>S. tomentosa</i>	20	<b>88.6<sup>e</sup></b> (1.81)	<b>90.0<sup>f</sup></b> (1.42)	86.1 <sup>b</sup> (2.31)
<i>S. velutina</i>	36	83.0 <sup>b</sup> (4.84)	83.2 <sup>b</sup> (5.04)	<b>87.8<sup>bcde</sup></b> (3.04)

The analysis with model DM1 revealed four groups: the highest scores were obtained in *S. tomentosa*, lowest in *S. auricolifolia* followed by *S. velutina* and intermediate in the remaining species. Nevertheless, better scores were obtained with DM5 and DM6. The values with model DM5 defined four groups: one formed by *S. andryalifolia*, *S. badaroi* and *S. tomentosa* with the highest scores, the lowest scores in *S. auricolifolia* followed by *S. velutina* and intermediate in the remaining species. The DM6 demonstrated the highest values of the *J* index in *S. mollissima* followed by *S. hifacensis*, with the lowest scores in *S. auricolifolia* followed by *S. tomentosa* while the remaining species had intermediate values. The coefficient of variation had lower values in the measurements of *J* index than in the other shape measurements (AR, C and R; see Table 2).

### 3. Discussion

The description of the seed shape by comparison with geometric models allows the quantification of shape, an important step for phenotype characterization in the analysis of differences between varieties and species as well as for the study of the effect of environmental factors. The information reported in this study allows to increase the knowledge on the seed traits of species of *Silene* [15,16,18,33,34], with particular reference to the members of *Silene mollissima* aggregate [36]. The overall seed shape in the lateral views of the *Silene* species resembles a cardioid and figures related to it, while, in the dorsal views, it is more elongated, resulting in shapes related to modified ellipses and hyper-ellipses. The models used in this work for the lateral views of the seeds (LM1 to LM8) were described by Martín-Gómez et al. and Juan et al. [33,34], while the models DM1, DM5 and DM6, used in the description of the dorsal views of the seeds, were recently described by Rodríguez-Lorenzo et al. [35]. This is the fourth publication reporting seed shape quantification in species of *Silene* by this method and the first time that a set of lateral and dorsal models has been applied simultaneously to a set of geographically and phylogenetically related species.

The first conclusion of this work confirms the previous observations detected by using this type of analysis (e.g., [33–35]) and especially refers to the stability of shape. In summary, (I) the coefficient of variation is smaller in shape than in size measurements, and (II) the coefficient of variation is smaller in a measurement that describes the overall similarity of a seed image with a geometric figure (*J* index) than in general shape measurements (aspect ratio, circularity or roundness). In this work, differences in the size between populations

were found in *S. badaroi*, *S. hicesiae*, *S. hifacensis* and *S. velutina*, while differences in the shape estimated as *J* index values with the different models were found only in the comparisons made with average silhouettes.

The differences in the size between the populations of the same species could not be correlated with known geographical factors. The populations having different seed size of species *S. badaroi*, *S. hicesiae*, *S. hifacensis* and *S. velutina* were located close to each other to attribute differences to climatic features, such as mean minimum temperatures or latitude. In the other cases reported, the differences in seed size in *S. dioica* were attributed to local, micro-environmental effects acting on a group of plants [37], similar to those described in *Arabidopsis helleri* (L.) O’Kane & Al-Shehbaz due to the presence of metals in the soil [38]. Differences in size between populations can also be attributed to the date of collection; for example, the seeds produced earlier in a plant are larger than seeds produced later [39].

A linear discriminant analysis (LDA) based on morpho-colorimetric measurements was applied to five Tyrrhenian species of the *S. mollissima* aggregate [36]. In this work, *S. badaroi* and *S. hicesiae* were separated from each other and from the other species analyzed (*S. ichnusae*, *S. oenotriae* and *S. velutina*). There are multiple factors influencing the result of LDA, while our analysis addresses more precisely the question of overall seed shape differences between species or populations independent of other considerations of size or color measurements.

The 11 species from the *S. mollissima* aggregate can be included in two groups for the lateral views and three for the dorsal views of seeds. Concerning the lateral views, the first group showing higher values of *J* index with model LM5 includes *S. andryalifolia*, *S. badaroi*, *S. gazulensis*, *S. hifacensis* and *S. tomentosa*; the second group, with lower values of *J* index with LM5, includes *S. auricolifolia*, *S. hicesiae*, *S. ichnusae*, *S. mollissima*, *S. oenotriae* and *S. velutina*. *S. gazulensis* is endemic in the Gibraltar area and its relatedness with *S. tomentosa* was already reported in the description of the former species [35].

In relation to the dorsal views, three groups resembling the results of the analysis of the aspect ratio were obtained. First, *S. auricolifolia*, with rounded seeds, forms an independent group. The second group contains all the species whose seeds have intermediate values of aspect ratio and whose dorsal views resemble model DM5 (*S. andryalifolia*, *S. badaroi*, *S. oenotriae* and *S. tomentosa*) and the third group, similar to species with higher values of aspect ratio, contains seeds resembling in their dorsal view the model DM6 (*S. gazulensis*, *S. hicesiae*, *S. hifacensis*, *S. ichnusae*, *S. mollissima* and *S. velutina*). According to their lateral and dorsal shape, and in relation to the other species studied by this method, the species of the *S. mollissima* aggregate resemble *S. conica* and *S. coutinhoi*, whose dorsal views adjust well to DM5 and DM6, respectively [35]. These two models have similar figures, with the only difference being that DM6 is narrower than DM5. The Iberian species *S. coutinhoi* is closely related to these species in the *Silene* sect. *Siphonomorpha* [40].

The analysis carried out in this work permitted to describe the seed shape of 20 populations of 11 taxa of *S. mollissima* aggregate as well as to detect two groups for the lateral views and three groups for the dorsal views of seeds of species of different geographic origin. The description of the seed shape by comparison with geometric models should be used as a complementary method in studies that take into consideration other morphological characteristics, such as the morpho-colorimetric quantitative and qualitative features of seeds, leaves, hairs, flowers, fruit or other characteristics of a plant, in order to ensure a more effective performance of classification among taxa. It is a low-cost and non-invasive approach, may contribute to the future studies on the other species of *Silene* and could be useful as the basis for a large-scale study.

## 4. Materials and Methods

### 4.1. Seeds of *Silene* Analyzed

Seeds of the 11 species of the *Silene mollissima* aggregate were obtained in the Sardinian Germplasm Bank (BG-SAR; [40]) and are described in Table 7. The localities of origin of the seed populations used in this work are shown in Figure 3. The accessions of each

species were stored at  $-25\text{ }^{\circ}\text{C}$  and preserved on the basis of established international protocols [41,42].

**Table 7.** Species and populations used in this work.

Species	Accession Code in BG-SAR	Locality (Date of Collection)	Seed Number (in Stock)	Mean Coordinates (WGS 84)	Mean Elevation (m a.s.l.)
<i>S. andryaliifolia</i>	VM16/14	Canellas de Alabaida, Malaga, Spain (20 May 2014)	30	36°50' N; 3°59' W	500
<i>S. auricolifolia</i>	VM01/15	Santa Cruz, Orano, Algeria (12 May 2015)	16	34°42' N; 00°40' W	316
<i>S. badaroi</i>	VM01/13	Capo Noli, Liguria, Italy (1 June 2013)	>200	44°11' N; 8°25' E	240
<i>S. badaroi</i>	VM06/13	Marciana, Isola d'Elba, Tuscan Archipelago, Italy (6 July 2012)	>200	42°48' N; 10°08' E	8
<i>S. badaroi</i>	VM07/13	Provence-Alpes-Côte d'Azur, Hyères, France (1 June 2013)	41	42°04' N; 6°06' E	10
<i>S. gazulensis</i>	VM17/14	Alcalá de los Gazules, Cadiz, Spain (15 June 2014)	48	36°27' N; 5°43' W	200
<i>S. hicesiae</i>	GM0313	Isole Eolie, Panarea, Sicily, Italy (2005)	66	38°38' N; 15°03' E	390
<i>S. hicesiae</i>	VM02/13	Isole Eolie, Panarea, Sicily, Italy (25 July 2013)	>200	38°38' N; 15°03' E	390
<i>S. hifacensis</i>	VM03/14	Passebret, Cap D'Or, Alicante, Spain (1 July 2013)	>200	38°40' N; 00°08' E	100
<i>S. hifacensis</i>	VM04/14	Morro de Toix, Calpe, Alicante, Spain (1 July 2013)	>200	38°37' N; 00°01' E	56
<i>S. hifacensis</i>	VM05/14	Cova Cendres, Cap D'Or, Alicante, Spain (1 July 2013)	>200	38°41' N; 00°09' E	80
<i>S. hifacensis</i>	VM06/14	Es Tossals, Cala Alabarca, Ibiza, Isole Baleari, Spain (16 June 2013)	92	39°03' N; 01°22' E	20
<i>S. hifacensis</i>	VM07/14	Illot de la Mona, Xabia, Alicante, Spain (1 July 2013)	49	38°48' N; 00°11' E	2
<i>S. hifacensis</i>	VM08/14	Morro de Toix, Calpe, Alicante, Spain (1 July 2014)	>200	38°37' N; 00°01' E	56
<i>S. ichnusae</i>	18/17	Capo Falcone, Stintino, Sardinia, Italy (1 July 2017)	67	40°58' N; 08°12' E	15
<i>S. mollissima</i>	VM10/14	Coma Freda, Maiorca, Isole Baleari, Spain (5 August 2014)	96	39°42' N; 02°52' E	650
<i>S. oenotriiae</i>	VM04/13	Massiccio del Pollino, Basilicata, Italy (2 June 2013)	62	39°49' N; 16°19' E	350
<i>S. tomentosa</i>	VM03/13	Gibraltar Botanical Garden, Gibraltar (unknown)	64	36°07' N; 05°20' W	250
<i>S. velutina</i>	192/06	Cala del Morto, Isola di La Maddalena, Sardinia, Italy (15 July 2006)	>200	41°14' N; 09°24' E	3
<i>S. velutina</i>	54/17	Abbatoggia, Isola di La Maddalena, Sardinia, Italy (12 August 2017)	73	41°14' N; 09°24' E	3

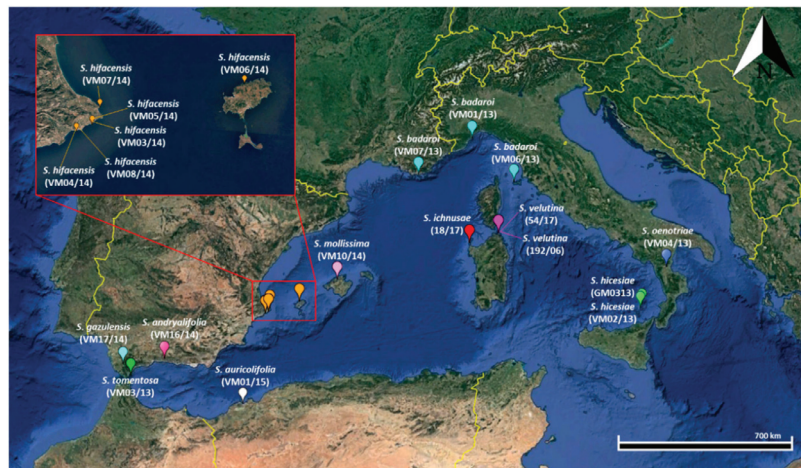


**Figure 3.** Map of the western Mediterranean biogeographic region showing the localities of origin of the seed populations used in this work.

#### 4.2. Seed Images

Photographs were taken with a Nikon Z6 camera with an objective AF-S Micro NIKKOR 60 mm f/2.8G ED. From an initial photograph made to the pool of seeds in each population and containing between 30 and 110 seeds, composed images containing 20–30 seeds regularly oriented per accession were prepared with Corel Photo Paint. In these images, the seeds were aligned to allow further analysis in ImageJ. The images are stored at: <https://zenodo.org/record/6205212#.YhOpUujMKM8> (accessed on 21 February 2022).

#### 4.3. General Morphological Description

Area (A), perimeter (P), length of the major axis (L), width (W), aspect ratio (AR is equal to L/W), circularity (C) and roundness (R) were obtained for the lateral views of seeds of each species from the initial photographs containing 16–110 seeds with ImageJ

program [43]. The seeds were oriented with the micropyle to the right. A ruler was the reference for the conversion of pixel units to length or surface units (mm or mm<sup>2</sup>). The circularity index and roundness were calculated as described [44]. Circularity is the ratio  $(4\pi \times A)/P^2$ , while roundness is  $(4 \times A)/\pi L^2$ ; in consequence, circularity decreases with irregularities of seed surface that increase the perimeter, but roundness is not affected.

#### 4.4. Obtention of an Average Silhouette

The average silhouette is a representative image of seed shape for each group of seeds. A total of 20 seeds were used for each studied species. The silhouette was obtained in Corel Photo Paint by the protocol described [45] (a detailed video is available at Zenodo: <https://zenodo.org/record/4478344#.YBPOguhKiM8>, accessed on 2 September 2021). The layers containing the seeds are superimposed and the opacity is given a value of 20 in all layers. All the layers are combined, and the brightness is adjusted to a minimum value. From this image, we are interested in the inner region representing the area where most of the seeds coincide, which is the darkest area. To select it, we use the magic wand tool and, with tolerance equal to 10, this selection is copied and pasted as a new layer.

#### 4.5. Geometric Models Used in the Comparisons

The models used in this work were: for the lateral views of seeds, the eight models already described for *Silene* seeds [33,34] that are stored in Zenodo <https://zenodo.org/record/5535612#.YbyrC2jMKM8> (accessed on 21 February 2022).

Models DM1, DM5 and DM6 for the dorsal views of seed models are available at: [https://zenodo.org/record/5997355#.Yg0zSN\\_MKM8](https://zenodo.org/record/5997355#.Yg0zSN_MKM8) (accessed on 21 February 2022).

#### 4.6. Comparison with Geometric Models: Calculation of the J Index

*J* index is defined by:

$$J \text{ index} = (\text{area } S)/(\text{area } T) \times 100$$

where *S* is the area shared between the seed image and the model and *T*, the total area occupied by both figures. *J* index ranges between 0 and 100, reaching maximum values when the geometric model and the seed image areas coincide. A high value of *J* index, i.e., high similarity with a given model, means a precise definition of seed shape for a particular species. A good adjustment to the model was considered when *J* index values were superior to 90 [33].

*J* index was calculated with the eight geometric models described for *Silene* on the average silhouettes of each species. Those models giving high values were applied to calculations of *J* index with the samples of 20–30 seeds.

Area calculation was carried out by superimposing the model on each seed image, searching a maximum adjustment between the shapes of the seeds and the geometric model (Figure 4). Three files were kept for each composition: (1) a document (PSD format) with the seeds and the geometric figure adapted to each of them, in which it is possible to make corrections; (2) a file (JPG format) with the geometric models in black, which is useful to obtain total area (*T*) with the software ImageJ and (3) another file in JPG format with the geometric models in white, useful to obtain the values of area shared between the geometric figure and the seed image (*S*) in ImageJ (Figure 4). Image composition with seeds and models was done in Corel PHOTO-PAINT X7, and area quantification in ImageJ. Figure 4 illustrates examples of the adjustment between seed images and the geometric models with indication of the areas measured for the calculation of the *J* index.

#### 4.7. Statistical Analysis

The raw data are available at: <https://zenodo.org/record/6378816#.YjrjbOfMKM8> (accessed on 23 March 2022). The mean, minimum and maximum values and the standard deviation were obtained for all the measurements indicated (A, P, L, W, AR, C and R) as well as for *J* index with the different models. Statistics were analyzed on IBM SPSS statistics

v28 (SPSS 2021) and R. software v. 4.1.2 [46]. As some of the populations did not follow a normal distribution, non-parametric tests were applied for the comparison of populations. Kruskal–Wallis test was completed followed by stepwise stepdown comparisons by the ad hoc procedure developed by Campbell and Skillings [47]. P values inferior to 0.05 were considered significant. The coefficient of variation was calculated as  $CV_{\text{trait}} = \text{standard deviation}_{\text{trait}} / \text{mean}_{\text{trait}} \times 100$  [48].



**Figure 4.** A sample of the composed images used for  $J$  index calculation. Seed images are combined with the geometric figure (model) in a different layer. In the upper part of this image, three seeds of *Silene mollissima* have the cardioid superimposed in black. They give the value of total area in ImageJ. The same seed images with model superimposed in white give the values of shared area between the seed and the model.

## 5. Conclusions

The seed morphology in the 11 species of the *S. mollissima* aggregate has been analyzed based on the comparison with geometric models both in the lateral and dorsal views. In the lateral view, the seeds resemble a cardioid (LM1) or models derived from it (LM4 and LM5). The comparison with LM5 revealed two groups of high and low similarity with this model. The group of high similarity to LM5 contains the species from Andalusie and Levant in southern Spain and the region of the Mediterranean coast in France and northern Italy with *S. andryalifolia*, *S. badaroi*, *S. gazulensis*, *S. hifacensis* and *S. tomentosa*. The group of lower similarity to LM5 includes the species of the islands along the Mediterranean Sea and north Africa: *S. auricolifolia*, *S. hicesiae*, *S. ichnusae*, *S. mollissima*, *S. oenotriae* and *S. velutina*. *S. auricolifolia* constitutes a separate group due to roundness in both the lateral and dorsal views.

In comparison with the other species analyzed by geometric models, and in particular in their dorsal views, the seeds of the *S. mollissima* aggregate, excluding *S. auricolifolia*, resemble species *S. conica* and *S. coutinhoi*.

Differences between the populations of the same species were found for seed size, circularity and roundness but not in shape quantification by similarity with a geometric model ( $J$  index), thus indicating the stability of the shape measured by comparison with a geometric model in comparison with the other measurements.

**Author Contributions:** Conceptualization, J.J.M.-G., M.P., G.B. and E.C.; methodology, J.J.M.-G., M.P., G.B. and E.C.; software, J.J.M.-G. and E.C.; formal analysis, J.J.M.-G., M.P., G.B. and E.C.; investigation, J.J.M.-G., M.P., G.B. and E.C.; resources, J.J.M.-G., M.P., G.B. and E.C.; data curation, J.J.M.-G.; writing—original draft preparation, E.C.; writing—review and editing, J.J.M.-G., M.P., G.B. and E.C.; visualization, J.J.M.-G. and E.C. All authors have read and agreed to the published version of the manuscript.

**Funding:** Project “CLU-2019-05-IRNASA/CSIC Unit of Excellence”, funded by the Junta de Castilla y León and co-financed by the European Union (ERDF “Europe drives our growth”).

**Data Availability Statement:** Not applicable.

**Conflicts of Interest:** The authors declare no conflict of interest.

### Appendix A

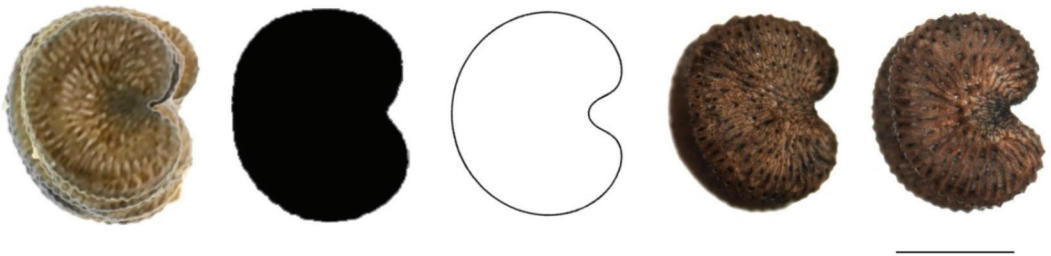


**Figure A1.** Superimposed images of the lateral view of *Silene andryaliifolia* seeds, the corresponding average silhouette, model LM5 and two seeds of this species. Bar represents 1 mm.

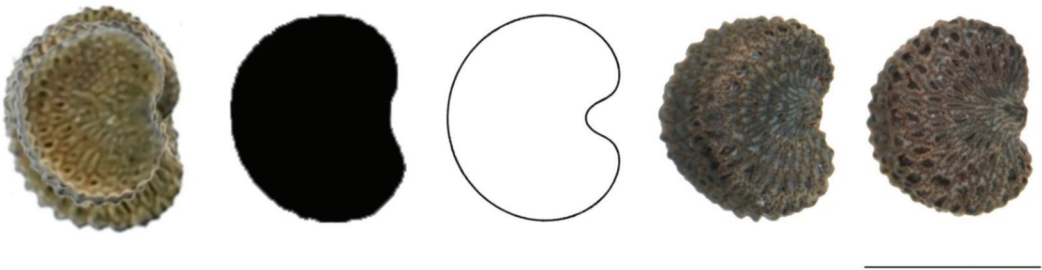


**Figure A2.** Superimposed images of the lateral view of *Silene badaroi* seeds, the corresponding average silhouette, model LM5 and two seeds of this species. Bar represents 1 mm.

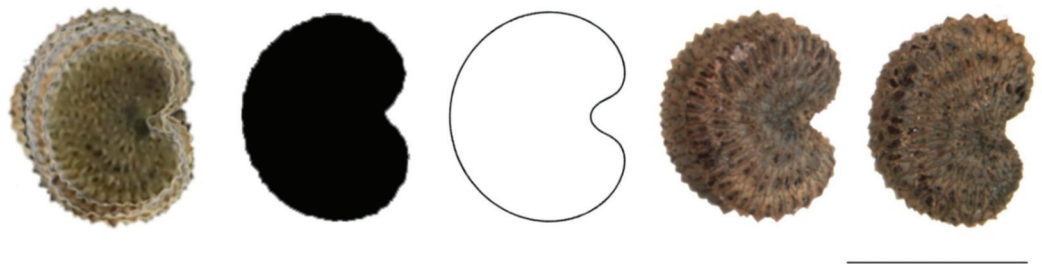


**Figure A3.** Superimposed images of the lateral view of *Silene gazulensis* seeds, the corresponding average silhouette, model LM5 and two seeds of this species. Bar represents 1 mm.

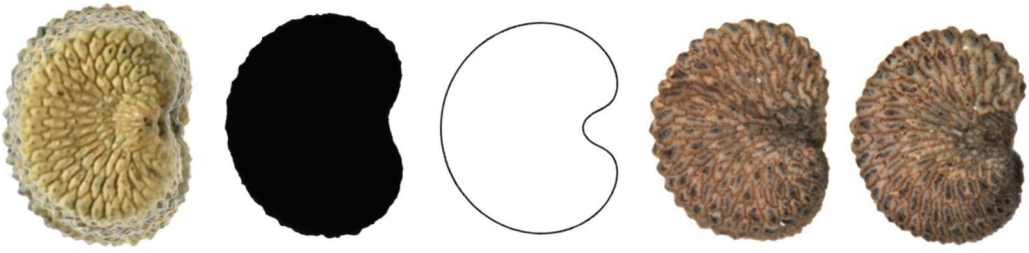


**Figure A4.** Superimposed images of the lateral view of *Silene hifacensis* seeds, the corresponding average silhouette, model LM5 and two seeds of this species. Bar represents 1 mm.

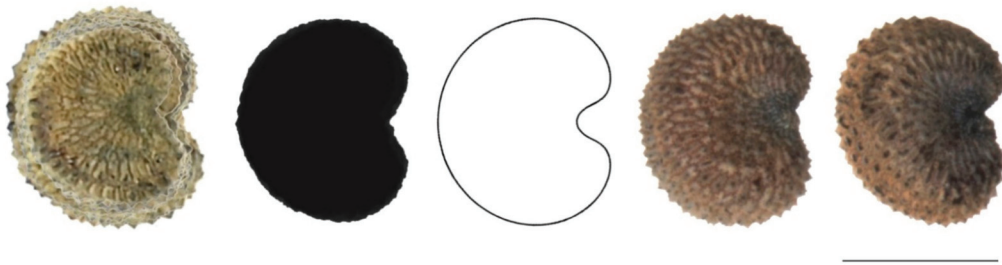


**Figure A5.** Superimposed images of the lateral view of *Silene tomentosa* seeds, the corresponding average silhouette, model LM5 and two seeds of this species. Bar represents 1 mm.

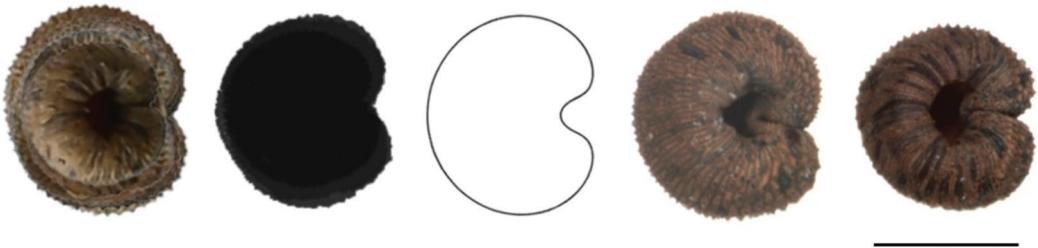


**Figure A6.** Superimposed images of the lateral view of *Silene auriculifolia* seeds, the corresponding average silhouette, model LM5 and two seeds of this species. Bar represents 1 mm.

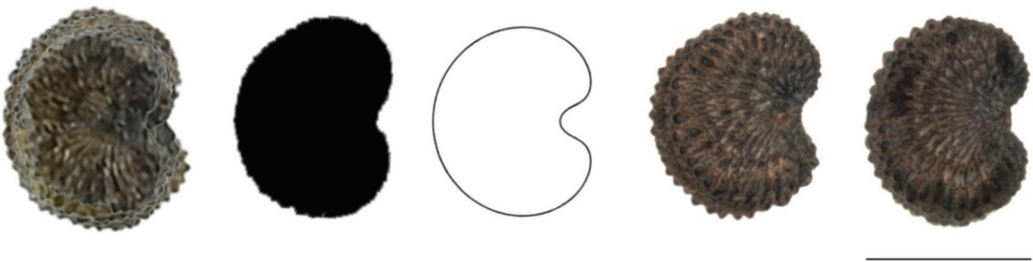


**Figure A7.** Superimposed images of the lateral view of *Silene hicesiae* seeds, the corresponding average silhouette, model LM5 and two seeds of this species. Bar represents 1 mm.

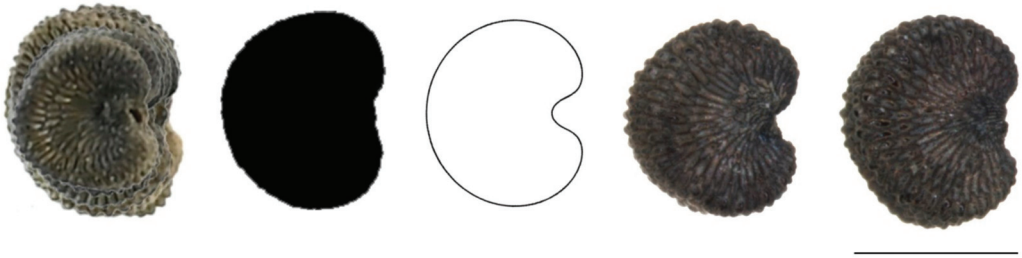


**Figure A8.** Superimposed images of the lateral view of *Silene ichnusae* seeds, the corresponding average silhouette, model LM5 and two seeds of this species. Bar represents 1 mm.

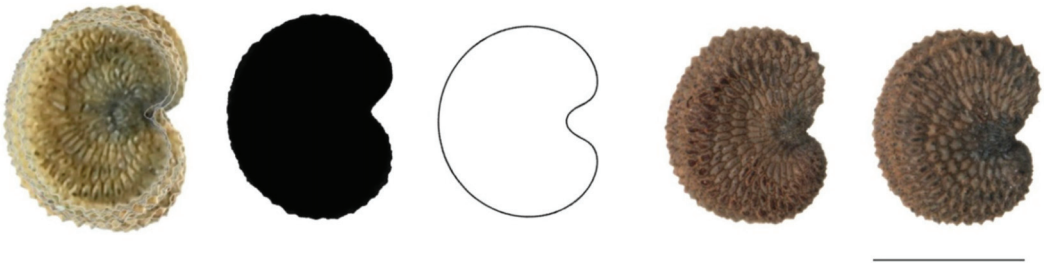


**Figure A9.** Superimposed images of the lateral view of *Silene mollissima* seeds, the corresponding average silhouette, model LM5 and two seeds of this species. Bar represents 1 mm.

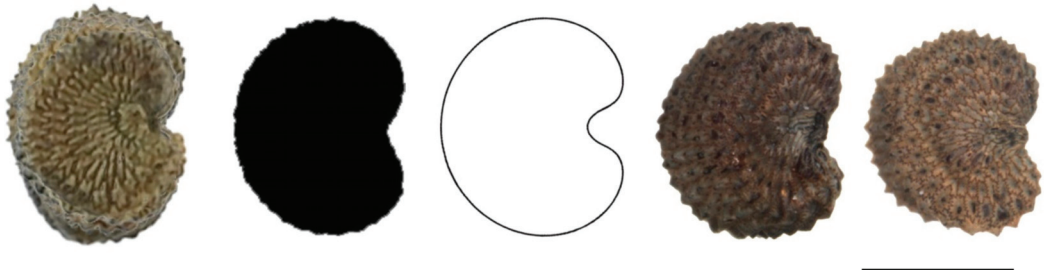


**Figure A10.** Superimposed images of the lateral view of *Silene oenotriae* seeds, the corresponding average silhouette, model LM5 and two seeds of this species. Bar represents 1 mm.

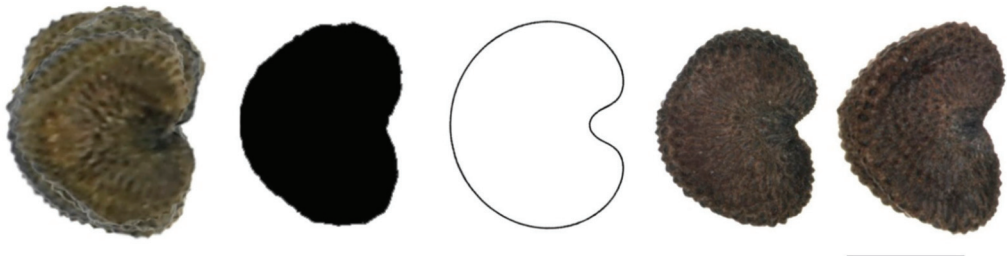


**Figure A11.** Superimposed images of the lateral view of *Silene velutina* seeds, the corresponding average silhouette, model LM5 and two seeds of this species. Bar represents 1 mm.

## References

- Jafari, F.; Zarre, S.; Gholipour, A.; Eggens, F.; Rabler, R.K.; Oxelman, B. A new taxonomic backbone for the infrageneric classification of the species-rich genus *Silene* (Caryophyllaceae). *Taxon* **2020**, *69*, 337–368. [CrossRef]
- Jafari, F.; Zarre, S.; Gholipour, A.; Eggens, F.; Rabler, R.K.; Oxelman, B. Notes on phylogeny and infrageneric classification of *Silene*, L. (Caryophyllaceae). Available online: <https://doi.org/10.13140/RG.2.2.25580.39040> (accessed on 30 June 2020).
- Jeanmonod, D. Révision de la section *Siphonomorpha* Otth du genre *Silene* L. en Méditerranée occidentale III: Aggrégat italica et espèces affines. *Candollea* **1984**, *39*, 549–639.
- Jeanmonod, D. Révision de la section *Siphonomorpha* Otth du genre *Silene* L. (Caryophyllaceae) en Méditerranée occidentale II: Le groupe de *S. mollissima*. *Candollea* **1984**, *39*, 195–259.
- Jeanmonod, D. Révision de la section *Siphonomorpha* Otth du genre *Silene* L. en Méditerranée occidentale. V: Synthèse. *Candollea* **1985**, *40*, 35–56.
- Murru, V.; Santo, A.; Piazza, C.; Hugot, L.; Bacchetta, G. Seed germination, salt stress tolerance, and the effect of nitrate on three Tyrrhenian coastal species of the *Silene mollissima* aggregate (Caryophyllaceae). *Botany* **2015**, *93*, 881–892. [CrossRef]
- Murru, V.; Santo, A.; Gallo, M.; Cardona, C.; Boi, M.; Bacchetta, G. Comparative germination ecology and seedling growth of two Ibero-Levantine endemic species belonging to the *Silene mollissima* aggregate (Caryophyllaceae). *Flora* **2017**, *227*, 10–17. [CrossRef]
- Cañadas, E.M.; Fenu, G.; Peñas, J.; Lorite, J.; Mattana, E.; Bacchetta, G. Hotspots within hotspots: Endemic plant richness, environmental drivers, and implications for conservation. *Biol. Conserv.* **2014**, *170*, 282–291. [CrossRef]
- Brullo, S. *Silene oenotriae* (Caryophyllaceae): A new species from S Italy. *Nord. J. Bot.* **1997**, *17*, 649–652. [CrossRef]
- Thompson, J.D. *Plant Evolution in the Mediterranean*; Oxford University Press: Oxford, UK, 2005; p. 302.
- Arroyo Marín, J. Plant diversity in the region of the strait of Gibraltar, a multilevel approach. *Lagascalia* **1997**, *19*, 393–404.
- Galán de Mera, A.; Morales Alonso, R.; Vicente Orellana, J.A.; Cortés, J.E. *Silene gazulensis* sp. nov. (Caryophyllaceae) un nuevo endemismo del entorno del estrecho de Gibraltar. *Acta Bot. Malac.* **1999**, *24*, 237–241. [CrossRef]
- Porceddu, M.; Santo, A.; Orrù, M.; Meloni, F.; Uccesu, M.; Picciau, R.; Sarigu, M.; Cuenca Lombrana, A.; Podda, L.; Sau, S.; et al. Seed conservation actions for the preservation of plant diversity: The case of the Sardinian Germplasm Bank (BG-SAR). *Plant Sociol.* **2017**, *54*, 111–117.
- Bacchetta, G.; Carta, A.; Paradis, G.; Piazza, C.; Peruzzi, L. Further insights into the taxonomy of the *Silene nocturna* species complex (Caryophyllaceae): A systematic survey of the taxa from Sardinia and Corsica. *Phytotaxa* **2014**, *175*, 037–044. [CrossRef]
- Camelia, I. Aspects regarding seeds morphology and germination peculiarities in some taxa from *Silene* L. genera. *J. Plant Dev.* **2011**, *18*, 5–10.
- Fawzi, N.; Fawzy, A.; Mohamed, A. Seed morphological studies of some species of *Silene* L. (Caryophyllaceae). *Int. J. Bot.* **2010**, *6*, 287–292. [CrossRef]
- Keshavarzi, M.; Mahdavinjad, M.; Sheidai, M.; Gholipour, A. Seed and pollen morphology of some *Silene* species (Caryophyllaceae) in Iran. *Phytol. Balc. Int. J. Balkan Flora Veg.* **2015**, *21*, 7–12.
- Yildiz, K. A morphological investigation of *Silene* L. (Caryophyllaceae) species distributed in West Anatolia and North Cyprus. *Pak. J. Bot.* **2006**, *38*, 67–83.
- Yildiz, K. Morphological and palynological investigation of *Silene gigantea* L. var. *gigantea* and *Silene behen* L. (Caryophyllaceae). *Turk. J. Bot* **2006**, *30*, 105–119.
- Mebatsion, H.K.; Paliwal, J.; Jayas, D.S. Evaluation of variations in the shape of grain types using principal components analysis of the elliptic Fourier descriptors. *Comput. Electron. Agric.* **2012**, *80*, 63–70. [CrossRef]
- Smykalova, I.; Grillo, O.; Bjelkova, M.; Pavelek, M.; Venora, G. Phenotypic evaluation of flax seeds by image analysis. *Ind. Crops Prod.* **2013**, *47*, 232–238.
- Lo Bianco, M.; Grillo, O.; Cañadas, E.; Venora, G.; Bacchetta, G. Inter- and intraspecific diversity in *Cistus* L. (Cistaceae) seeds, analysed with computer vision techniques. *Plant Biol.* **2017**, *19*, 183–190. [CrossRef]
- Lo Bianco, M.; Grillo, O.; Escobar Garcia, P.; Mascia, F.; Venora, G.; Bacchetta, G. Morpho-colorimetric characterization of *Malva* alliance taxa by seed image analysis. *Plant Biol.* **2017**, *19*, 90–98. [CrossRef] [PubMed]
- Sarigu, M.; Porceddu, M.; Schmitt, E.; Camarda, I.; Bacchetta, G. Taxonomic discrimination of the *Paeonia mascula* group in the Tyrrhenian Islands by seed image analysis. *Syst. Biodivers.* **2019**, *17*, 801–810. [CrossRef]
- Farris, E.; Orrù, M.; Uccesu, M.; Amadori, A.; Porceddu, M.; Bacchetta, G. Morpho-colorimetric characterization of the Sardinian endemic taxa of the genus *Anchusa* L. by seed image analysis. *Plants* **2020**, *9*, 1321. [CrossRef] [PubMed]
- Cervantes, E.; Martín, J.J.; Ardanuy, R.; de Diego, J.G.; Tocino, Á. Modeling the *Arabidopsis* seed shape by a cardioid: Efficacy of the adjustment with a scale change with factor equal to the Golden Ratio and analysis of seed shape in ethylene mutants. *J. Plant Physiol.* **2010**, *67*, 408–410. [CrossRef]
- Martín-Gómez, J.J.; Tocino, Á.; Ardanuy, R.; de Diego, J.G.; Cervantes, E. Dynamic analysis of *Arabidopsis* seed shape reveals differences in cellulose mutants. *Acta Physiol. Plant.* **2014**, *36*, 1585–1592. [CrossRef]
- Cervantes, E.; Martín, J.J.; Chan, P.K.; Gresshoff, P.M.; Tocino, Á. Seed shape in model legumes: Approximation by a cardioid reveals differences in ethylene insensitive mutants of *Lotus japonicus* and *Medicago truncatula*. *J. Plant Physiol.* **2012**, *169*, 1359–1365. [CrossRef]

29. Cervantes, E.; Saadaoui, E.; Tocino, Á.; Martín-Gómez, J.J. Seed shape quantification in the model legumes: Methods and applications. In *The Model Legume Medicago truncatula*; de Bruijn, F., Ed.; Wiley: Hoboken, NJ, USA, 2020; Chapter 3-1-6; pp. 92–98. [[CrossRef](#)]
30. Cervantes, E.; Martín-Gómez, J.J. Seed Shape Description and Quantification by Comparison with Geometric Models. *Horticulturae* **2019**, *5*, 60. [[CrossRef](#)]
31. Cervantes, E.; Martín-Gómez, J.J.; Saadaoui, E. Updated Methods for Seed Shape Analysis. *Scientifica* **2016**, *2016*, 5691825. [[CrossRef](#)]
32. Cervantes, E.; Martín Gómez, J.J.; Gutiérrez del Pozo, D.; Silva Dias, L. An Angiosperm species dataset reveals relationships between seed size and two-dimensional shape. *Horticulturae* **2019**, *5*, 71. [[CrossRef](#)]
33. Martín-Gómez, J.J.; Rewicz, A.; Rodríguez-Lorenzo, J.L.; Janoušek, B.; Cervantes, E. Seed morphology in *Silene* based on geometric models. *Plants* **2020**, *9*, 1787. [[CrossRef](#)]
34. Juan, A.; Martín-Gómez, J.J.; Rodríguez-Lorenzo, J.L.; Janoušek, B.; Cervantes, E. New techniques for seed shape description in *Silene* species. *Taxonomy* **2022**, *2*, 1. [[CrossRef](#)]
35. Rodríguez-Lorenzo, J.L.; Martín-Gómez, J.J.; Juan, A.; Tocino, Á.; Janoušek, B.; Cervantes, E. New geometric models for shape quantification of the dorsal view in seeds of *Silene* species. *Plants* **2022**. *submitted*.
36. Murru, V.; Grillo, O.; Santo, A.; Ucchesu, M.; Piazza, C.; Gaio, A.; Carta, A.; Bacchetta, G. Seed morpho-colorimetric analysis on some Tyrrhenian species of the *Silene mollissima* aggregate (Caryophyllaceae). *Flora* **2019**, *258*, 151445. [[CrossRef](#)]
37. Thomson, P.A. Variations in Seed Size Within Populations of *Silene dioica* (L.) Clairv. in Relation to Habitat. *Ann. Bot.* **1981**, *47*, 623–634. [[CrossRef](#)]
38. Murawska-Wlodarczyk, K.; Korzeniak, U.; Babst-Kostecka, A. Metalliferous habitats and seed microbes affect the seed morphology and reproductive strategy of *Arabidopsis helleri*. *Plant Soil* **2022**, *470*, 175–192. [[CrossRef](#)]
39. Cavers, P.B.; Steel, M.G. Patterns of Change in Seed Weight Over Time on Individual Plants. *Am. Nat.* **1984**, *124*, 324–335. [[CrossRef](#)]
40. Naciri, Y.; Du Pasquier, P.-E.; Lundberg, M.; Jeanmonod, D.; Oxelman, B. A phylogenetic circumscription of *Silene* sect. *Siphonomorpha* (Caryophyllaceae) in the Mediterranean Basin. *Taxon* **2017**, *66*, 91–108. [[CrossRef](#)]
41. Bacchetta, G.; Fenu, G.; Mattana, E.; Piotto, B.; Virevaire, M. *Manuale per la Raccolta, Studio, Conservazione e Gestione Ex Situ del Germoplasma*; APAT: Rome, Italy, 2006; Volume 37.
42. Bacchetta, G.; Bueno Sanchez, A.; Fenu, G.; Jiménez Alfaro, B.; Mattana, E.; Piotto, B.; Virevaire, M. *Conservación Ex Situ de Plantas Silvestres*; Obra Social La Caixa y Gobierno del Principado de Asturias; Principado de Asturias: Oviedo, Spain, 2008.
43. Rasband, W.S.; ImageJ U.S. National Institutes of Health: Bethesda, MA, USA. 2018. Available online: <http://imagej.nih.gov/ij/> (accessed on 21 February 2022).
44. Zdilla, M.J.; Hatfield, S.A.; McLean, K.A.; Cyrus, L.M.; Laslo, J.M.; Lambert, H.W. Circularity, solidity, axes of a best fit ellipse, aspect ratio, and roundness of the foramen ovale: A morphometric analysis with neurosurgical considerations. *J. Craniofacial Surg.* **2016**, *27*, 222–228. [[CrossRef](#)]
45. Cervantes, E.; Martín-Gómez, J.J.; Espinosa-Roldán, F.E.; Muñoz-Organero, G.; Tocino, Á.; Cabello-Sáenz de Santamaría, F. Seed Morphology in Key Spanish Grapevine Cultivars. *Agronomy* **2021**, *11*, 734. [[CrossRef](#)]
46. R Core Team. *R: A Language and Environment for Statistical Computing*; R Foundation for Statistical Computing: Vienna, Austria, 2020.
47. Campbell, G.; Skillings, J.H. Nonparametric Stepwise Multiple Comparison Procedures. *J. Am. Stat. Assoc.* **1985**, *80*, 998–1003. [[CrossRef](#)]
48. Sokal, R.R.; Braumann, C.A. Significance Tests for Coefficients of Variation and Variability Profiles. *Syst. Zool.* **1980**, *29*, 50. [[CrossRef](#)]



# Antioxidants and Phytohormones Act in Coordination to Regulate Sage Response to Long Term Ozone Exposure

Alessandra Marchica <sup>1</sup>, Lorenzo Cotrozzi <sup>1,2,3,\*</sup>, Giacomo Lorenzini <sup>1,2,3</sup>, Cristina Nali <sup>1,2,3</sup> and Elisa Pellegrini <sup>1,2,3</sup>

<sup>1</sup> Department of Agriculture, Food and Environment, University of Pisa, Via del Borghetto 80, 56124 Pisa, Italy; alessandra.marchica@agr.unipi.it (A.M.); giacomo.lorenzini@unipi.it (G.L.); cristina.nali@unipi.it (C.N.); elisa.pellegrini@unipi.it (E.P.)

<sup>2</sup> CIRSEC, Centre for Climate Change Impact, University of Pisa, Via del Borghetto 80, 56124 Pisa, Italy

<sup>3</sup> Nutrafood Research Center, University of Pisa, Via del Borghetto 50, 56124 Pisa, Italy

\* Correspondence: lorenzo.cotrozzi@unipi.it; Tel.: +39-050-2210563

**Abstract:** Antioxidants and phytohormones are hallmarks of abiotic stress responses in plants. Although it is known that they can offer cell protection or accelerate programmed cell death (PCD) depending on the level of stress, the involvement of these metabolites in stress acclimation is still not fully elucidated. Here, we showed the role of antioxidants and phytohormones in *Salvia officinalis* tolerance to long-term ozone (O<sub>3</sub>) exposure (120 ppb for 36 days, 5 h day<sup>-1</sup>). Salicylic acid (SA) content was increased under O<sub>3</sub> throughout the whole experiment (+150%, as average compared with control), being required to maintain the cellular redox state and potentiate defense responses. This accumulation was induced before the production of ethylene (ET), suggesting that ET was controlled by SA during O<sub>3</sub> exposure to modulate the magnitude of chlorosis formation and the cell redox balance (by regulating ascorbate and glutathione levels). The synthesis and/or regeneration of these antioxidants did not protect membranes from lipid peroxidation, as demonstrated by the accumulation of malondialdehyde (+23% as average). However, these processes of lipid oxidation did not include the synthesis of the membrane breakdown products, as confirmed by the unchanged values of jasmonic acid, thus indicating that this compound was not involved in the regulation of PCD strategies.

**Keywords:** abscisic acid; aromatic herb; ascorbate-glutathione cycle; jasmonic acid; lipoic acid; oxidative stress; salicylic acid; *Salvia officinalis*

**Citation:** Marchica, A.; Cotrozzi, L.; Lorenzini, G.; Nali, C.; Pellegrini, E. Antioxidants and Phytohormones Act in Coordination to Regulate Sage Response to Long Term Ozone Exposure. *Plants* **2022**, *11*, 904. <https://doi.org/10.3390/plants11070904>

Academic Editors: Milan S. Stankovic, Paula Baptista and Petronia Carillo

Received: 1 March 2022

Accepted: 25 March 2022

Published: 28 March 2022

**Publisher's Note:** MDPI stays neutral with regard to jurisdictional claims in published maps and institutional affiliations.



**Copyright:** © 2022 by the authors. Licensee MDPI, Basel, Switzerland. This article is an open access article distributed under the terms and conditions of the Creative Commons Attribution (CC BY) license (<https://creativecommons.org/licenses/by/4.0/>).

## 1. Introduction

Plants grow in a continuously changing environment, which has favored the evolution of a highly flexible metabolism and development essential for their sessile lifestyle [1]. Plant metabolism must be highly regulated in order to allow effective integration of a broad spectrum of biosynthetic pathways resulting in antioxidant accumulation and redox signaling activation [2]. Rather than involving simple signaling cassettes, emerging concepts indicate that the relationships between redox state and metabolism are subtle and complex. Plants can be considered as reducing–oxidizing systems in which catabolic processes produce energy, and anabolic processes assimilate it [3]. A key feature determining plant adaptive capability is the extent to which oxidative reactions can be closely controlled. If environmental changes are too extreme to allow short-term metabolic controls to maintain fluxes through primary metabolism, the stress-induced damage ensues [4]. In this situation, functional and genic alterations are induced in an attempt to restore redox homeostasis. If these responses are not occurring appropriately, then primary metabolism becomes impaired, oxidative stress becomes even more severe, and cell death and senescence responses are triggered [5]. Oxidative damage is a widespread phenomenon extensively observed in plants exposed to biotic and abiotic stress.

Tropospheric ozone ( $O_3$ ) is a major air pollutant that negatively affects many biological activities in living organisms, being a strong oxidant [6–9]. Although several efforts have been made to decrease the emission of  $O_3$  precursors, background  $O_3$  levels in the Northern Hemisphere are estimated to increase from the current 35–50 ppb to 42–84 ppb by the end of the century, with occasional peaks above 200 ppb [10,11]. Ozone enters the plant through open stomata, and in the apoplast, it breaks down into reactive oxygen species (ROS), whose excessive formation injures DNA, proteins, lipids, and carbohydrates, thus causing reduction of photosynthesis and growth, cell dehydration, accelerated leaf senescence, and the appearance of chlorotic/necrotic leaf injuries [6]. Ascorbate (Asc) and glutathione (Glu) are major ROS scavengers [4], but plant antioxidant power is not limited only to these metabolites, as the detoxification process is a complex network including also other enzymatic and non-enzymatic antioxidants [12]. The roles of some of these antioxidants (e.g., superoxide dismutase, catalase, polyphenols and carotenoids) in plant– $O_3$  interaction have been largely investigated (e.g., [4,13]), while those of other antioxidants (e.g., lipoic acid) remain understudied. Phytohormones are also crucial in the regulation of plant growth, development and response to biotic and abiotic stresses, including  $O_3$  [14,15]. However, it is largely known that cellular responses of plants to  $O_3$  are dose-dependent. Phytohormones (e.g., ethylene (ET), and jasmonic (JA), salicylic (SA) and abscisic (ABA) acids) have been investigated almost exclusively for their signaling roles in single pulse  $O_3$  studies (considering a pulse of  $O_3$  typically greater than 150 ppb, e.g., [16–18]), so another aspect that still needs to be elucidated regards the involvement of these molecules in stress acclimation or plant tolerance to long-term  $O_3$  exposure expected in the near future.

A plant species that has shown a good tolerance to  $O_3$  [19–22], as well as to other abiotic stresses (e.g., drought and salinity, [23,24]), is *Salvia officinalis* L. (sage, Lamiaceae family). Native to the Middle East and Mediterranean areas, and naturalized throughout the world, it is a major aromatic herb used in the food and pharmaceutical industries because of its important biological activities, including antioxidant and antimicrobial properties, mainly due to its foliar secondary metabolites [25,26]. Our research group has been studying the sage– $O_3$  interaction from different angles for about 10 years [19–22,27]. Among these investigations, Pellegrini et al. [27] carried out a monthly evaluation of the ecophysiological responses and some antioxidant regulators (i.e.,  $\beta$ -carotene and polyphenols) in sage exposed to 120 ppb of  $O_3$  for three consecutive months ( $5 \text{ h day}^{-1}$ ), and showed that although photosynthetic activity was reduced already after 1 month of exposure (i.e., the first time of analysis), sage was able to activate an adaptive survival mechanism to complete its life cycle. This capability was mainly attributed to an accumulation of polyphenols [27], and this interpretation seemed then confirmed by Marchica et al. [22], who reported an increased antioxidant capacity twinned with an enhancement of polyphenols occurring during the first weeks of exposure under the same  $O_3$  concentration (i.e., 120 ppb,  $5 \text{ h day}^{-1}$ ) but for only 36 consecutive days. Good  $O_3$  tolerance and increased antioxidant capacity were also reported by Marchica et al. [19] in sage exposed to a single pulse of  $O_3$  (200 ppb for 5 h), here highlighting also a key antioxidant role of Asc and Glu. Following the same experimental design, Marchica et al. [20] also reported a crucial signaling network including ROS and phytohormones (i.e., ET, JA, SA and ABA) activated by sage in response to a single pulse of  $O_3$  exposure. Overall, these researches have led to some very interesting results, but they have also opened up other equally interesting but still unanswered questions.

In the present study, sage was again exposed to 120 ppb of  $O_3$  for 36 consecutive days ( $5 \text{ h day}^{-1}$ ) in order to (i) evaluate the effects of long-term  $O_3$  on sage during the first weeks of exposure, and (ii) characterize the roles of antioxidants (both the most and less investigated) and phytohormones in sage tolerance to long-term  $O_3$  exposure.

## 2. Results

### 2.1. Leaf Symptoms and Chlorophyll Content

Ozone-treated plants showed a progressive leaf chlorosis from 14 days from the beginning of exposure (FBE) up to the experimental period (Figure 1a). No symptoms were observed on plants exposed to charcoal-filtered air (i.e., controls), throughout the whole experiment. The one-way repeated measures analysis of variance (ANOVA) of  $\text{Chl}_{\text{SPAD}}$  values showed that the effects of  $\text{O}_3$ , time, and their combination were significant (Figure 1b). Ozone also significantly decreased relative chlorophyll content by 23% at 14 days FBE, by 40% at 22 days FBE, and by approximately 60% at 29 and 36 days FBE (throughout the whole text, percentages of  $\text{O}_3$  effects are calculated in comparison with controls at the related times of analysis; Figure 1b).

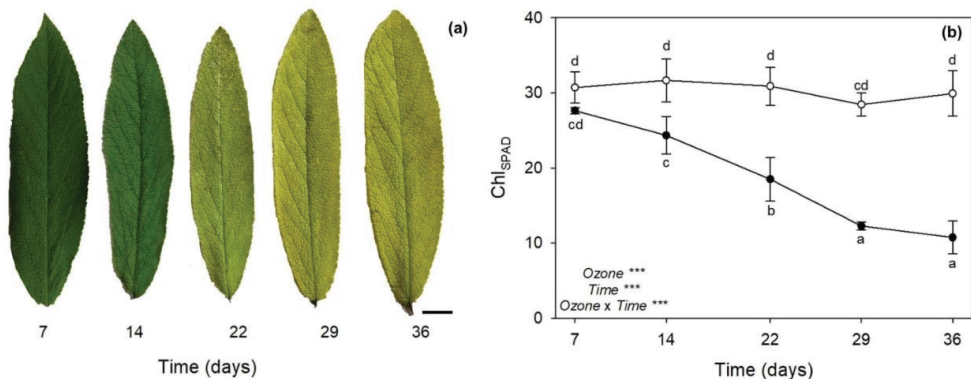


**Figure 1.** (a) Leaf symptoms of *Salvia officinalis* exposed to 120 ppb of ozone ( $5 \text{ h day}^{-1}$ ) for 7, 14, 22, 29 and 36 consecutive days. Bar: 1 cm. (b) Variation in relative chlorophyll content (determined in SPAD values,  $\text{Chl}_{\text{SPAD}}$ ) in leaves of sage exposed to charcoal-filtered air (open circle) or to 120 ppb of ozone ( $5 \text{ h day}^{-1}$ ) for 36 consecutive days (closed circle). Data are shown as mean  $\pm$  standard deviation.  $p$  levels for the effects of ozone, time, and their interaction from a one-way repeated measures ANOVA are shown (\*\*\*:  $p \leq 0.001$ ). According to Tukey's HSD post hoc test, different letters indicate significant differences among means ( $p \leq 0.05$ ).

### 2.2. Gas Exchange and Chlorophyll a Fluorescence

The one-way repeated measures ANOVA of ecophysiological parameters showed that the effects of  $\text{O}_3$ , time, and their combination were significant (Figure 2). Ozone significantly decreased  $\text{CO}_2$  assimilation rate ( $A$ ) from 14 days FBE ( $-51\%$ ), with great reductions observed at 29 and 36 days FBE (approximately  $-80\%$ , Figure 2a); whereas stomatal conductance ( $g_s$ ) was similarly reduced by  $\text{O}_3$  from 14 days FBE until the end of exposure (approximately  $-60\%$ , as average, Figure 2b). Conversely to  $A$ , intercellular  $\text{CO}_2$  concentration ( $C_i$ ) increased under  $\text{O}_3$  exposure from 14 days FBE ( $+11\%$ ), reaching higher values at 29 and 36 days FBE ( $+13\%$ , Figure 2c). Ozone decreased the maximum quantum efficiency of the photosystem II (PSII) photochemistry ( $F_v/F_m$ ) already at 7 days FBE ( $-9\%$ ), and this effect was almost consistent until the end of exposure (Figure 2d).

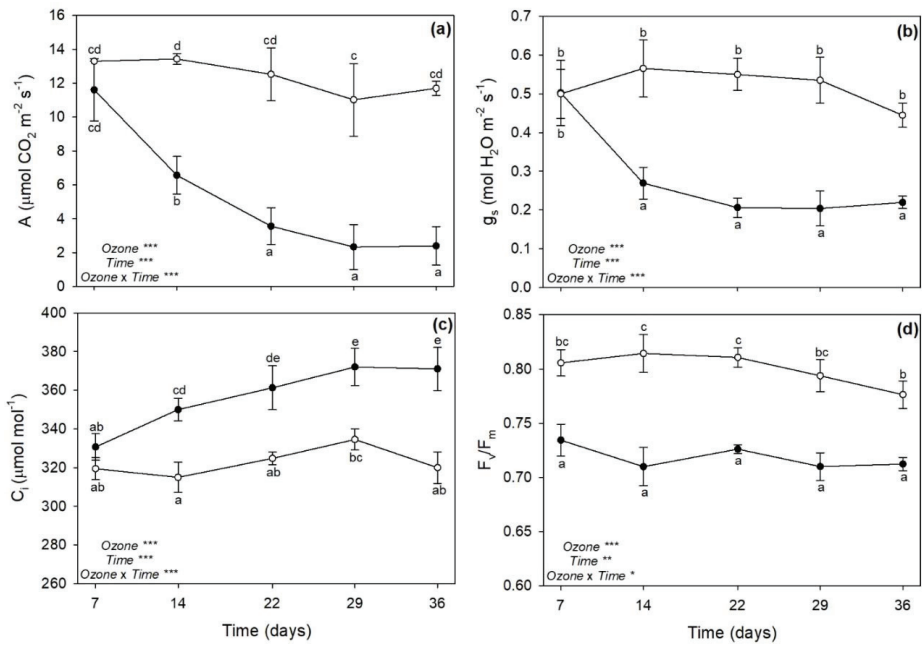


**Figure 2.** Variation in (a) CO<sub>2</sub> assimilation rate (A), (b) stomatal conductance (g<sub>s</sub>), (c) intercellular CO<sub>2</sub> concentration (C<sub>i</sub>), and (d) maximum quantum efficiency of the photosystem II photochemistry (F<sub>v</sub>/F<sub>m</sub>) in leaves of sage exposed to charcoal-filtered air (open circle) or to 120 ppb of ozone (5 h day<sup>-1</sup>) for 36 consecutive days (closed circle). Data are shown as mean  $\pm$  standard deviation. For each parameter, *p* levels for the effects of ozone, time, and their interaction from a one-way repeated measures ANOVA are shown (\*\*\*:  $p \leq 0.001$ , \*\*:  $p \leq 0.01$ , \*:  $p \leq 0.05$ ). According to Tukey's HSD post hoc test, different letters indicate significant differences among means ( $p \leq 0.05$ ).

### 2.3. Malondialdehyde and Lipoxygenase Activity

The two-way ANOVA of malondialdehyde (MDA) and lipoxygenase (LOX) activity showed that the effects of O<sub>3</sub>, time, and their combination were significant (Figure 3). Ozone significantly increased MDA content by 20% at 14 days FBE and by approximately 25% at later times of analysis (Figure 3a). A variable O<sub>3</sub> effect was instead reported on LOX activity: it was decreased at 7 and 14 days FBE (−65 and −76%, respectively), did not show differences at 22 days FBE, increased at 29 days FBE (+61%), and came back to control values at the end of exposure (Figure 3b).

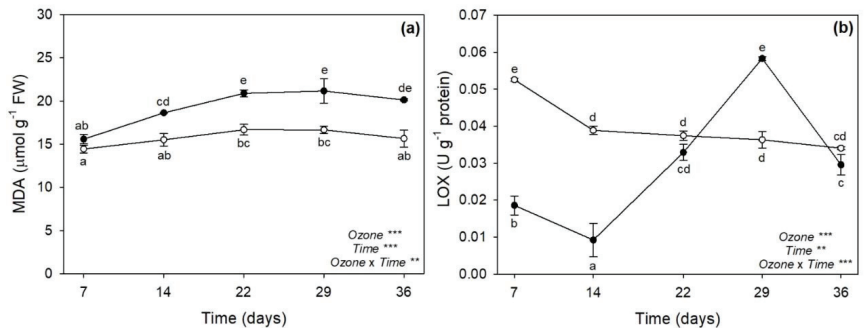


**Figure 3.** Variation in (a) malondialdehyde (MDA) content, and (b) lipoxygenase (LOX) activity in leaves of sage exposed to charcoal-filtered air (open circle) or to 120 ppb of ozone (5 h day<sup>-1</sup>) for

36 consecutive days (closed circle). Data are shown as mean  $\pm$  standard deviation. For each parameter, *p* levels for the effects of ozone, time, and their interaction from a two-way ANOVA are shown (\*\*\*:  $p \leq 0.001$ , \*\*:  $p \leq 0.01$ ). According to Tukey's HSD post hoc test, different letters indicate significant differences among means ( $p \leq 0.05$ ). FW: fresh weight.

#### 2.4. Low Molecular Weight Antioxidants

The two-way ANOVA of low molecular weight antioxidants showed that the effects of  $O_3$ , time, and their combination were significant (Figure 4). Ozone significantly increased the reduced form of Asc (AsA) at 14, 22 and 29 days FBE (+22, +21 and +27%, respectively; Figure 4a), as well as the oxidized form (DHA) at 22 and 29 days FBE (around +41%, Figure 4b). Differently,  $O_3$  increased reduced Glu (GSH) at 7 days FBE (+60%), as well as at 29 days FBE, and even more at 36 days FBE (+63%, Figure 4c). Additionally, oxidized Glu (GSSG) was increased by  $O_3$  at 22 and again at 36 days FBE (+53 and +56%, respectively; Figure 4d). Ozone also induced a marked accumulation of reduced and oxidized lipoic acid (DHLA and LA, respectively) at 14 days FBE (+109 and +352%, respectively). Conversely,  $O_3$  reduced LA content at 7 days FBE (−64%). No other significant effects were reported at other times of analysis for these parameters (Figure 4e,f).

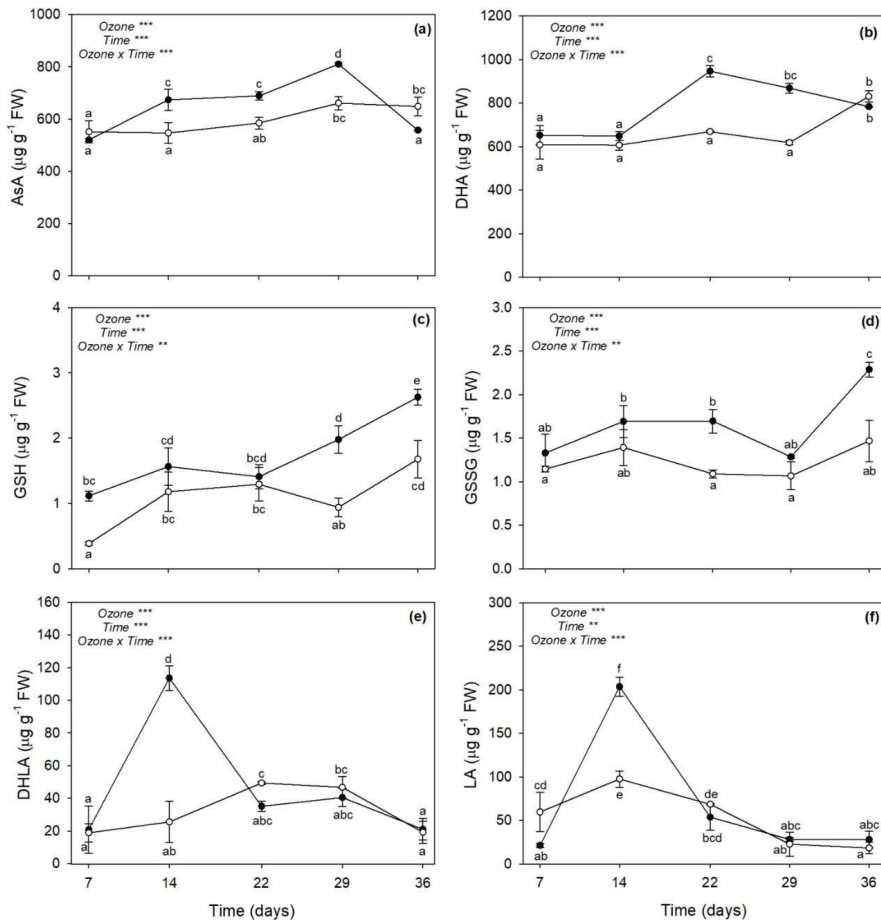


**Figure 4.** Variation in (a) reduced ascorbate (AsA), (b) oxidized ascorbate (DHA), (c) reduced glutathione (GSH), (d) oxidized glutathione (GSSG), (e) reduced lipoic acid (DHLA), and (f) oxidized

lipic acid (LA) contents in leaves of sage exposed to charcoal-filtered air (open circle) or to 120 ppb of ozone ( $5 \text{ h day}^{-1}$ ) for 36 consecutive days (closed circle). Data are shown as mean  $\pm$  standard deviation.  $p$  levels for the effects of ozone, time, and their interaction from a two-way ANOVA are shown (\*\*\*:  $p \leq 0.001$ , \*\*:  $p \leq 0.01$ ). According to Tukey's HSD post hoc test, different letters indicate significant differences among means ( $p \leq 0.05$ ). FW: fresh weight.

### 2.5. Phytohormones

The two-way ANOVA of phytohormones showed that the effects of  $\text{O}_3$ , time, and their combination were significant (except "ozone" and "ozone  $\times$  time" for JA; Figure 5). Ozone induced a marked accumulation of ET at 22 days FBE (+166%), which then lowered at 29 (+153%) and 36 (+66%) days FBE (Figure 5a). No  $\text{O}_3$  effects were reported on JA (Figure 5b). Ozone increased total SA (free plus conjugated forms of SA) already at 7 days FBE (+78%), and even more at all the other times of analysis (+150%, as average, Figure 5c). Moreover, ABA increased under  $\text{O}_3$  throughout the whole experiment, peaking at 14 days FBE and again at 36 days FBE (+145 and +49%, respectively; Figure 5d).

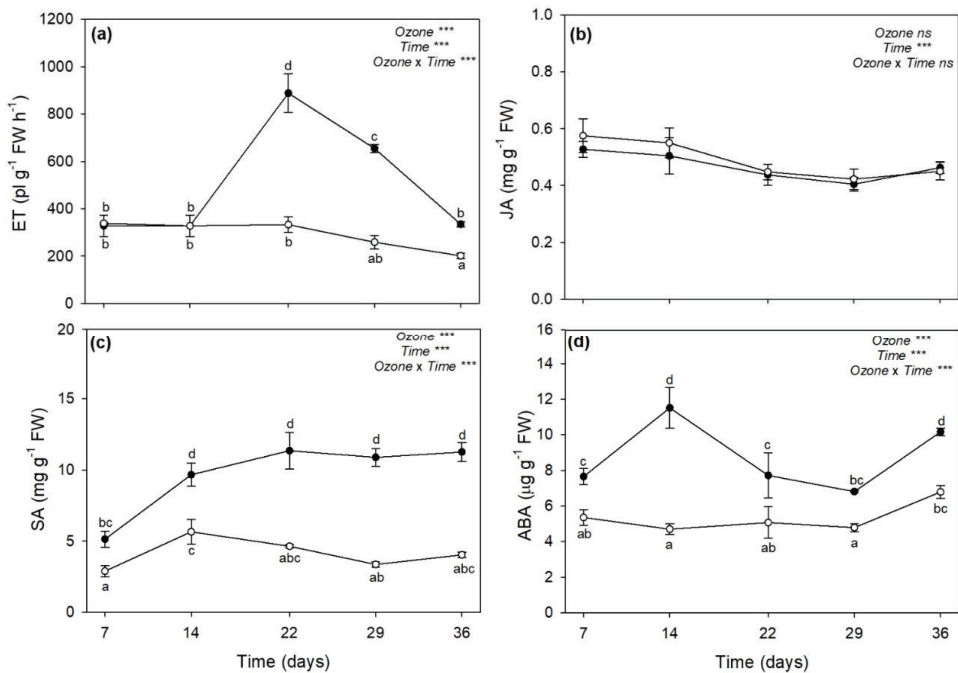


**Figure 5.** Variation in (a) ethylene (ET), (b) jasmonic acid (JA), (c) total salicylic acid (free plus conjugated forms of SA), and (d) abscisic acid (ABA) contents in leaves of sage exposed to charcoal-filtered air (open circle) or to 120 ppb of ozone ( $5 \text{ h day}^{-1}$ ) for 36 consecutive days. Data are shown as mean  $\pm$  standard deviation.  $p$  levels for the effects of ozone, time, and their interaction from a two-way ANOVA are shown (\*\*\*:  $p \leq 0.001$ , ns:  $p > 0.05$ ). According to Tukey's HSD post hoc test, different letters indicate significant differences among means ( $p \leq 0.05$ ). FW: fresh weight.

### 3. Discussion

As reported in a previous investigation performed by our research group [27], sage plants exposed to 120 ppb of  $\text{O}_3$  ( $5 \text{ h day}^{-1}$ ) for 90 consecutive days showed leaf yellowing, as well as some disorders in terms of leaf water status and photosynthetic performance, starting from 30 days FBE (i.e., the first time of analysis in that study). As expected, the present study showed that sage plants exposed to the same  $\text{O}_3$  concentration exhibited

similar O<sub>3</sub>-induced negative effects already in the first weeks of exposure. Indeed, the severity and incidence of visible injury that develops in plants are commonly utilized as indicators of O<sub>3</sub> damage [28]; here, a leaf chlorosis was clearly detectable at 14 days FBE, and it developed until the end of exposure. The reader should be aware that a single pulse of O<sub>3</sub> at a higher concentration (200 ppb for 5 h) did not induce any visible foliar injury in sage [19,20]. The appearance of visible leaf injury because of O<sub>3</sub> tends to occur by means of two processes. First, O<sub>3</sub> and O<sub>3</sub>-induced ROS directly harm plant cells by resulting in leaf chlorosis, necrosis and senescence [15]. Second, O<sub>3</sub>-derived ROS work as signal molecules that stimulate the hypersensitive response (HR; [29]). Because senescence and HR are genetically defined cell death programs and show several similarities, it has been speculated that common steps might exist for the induction and/or execution of these two processes [30]. In both cases, phytohormones and signaling molecules play a dual role, either offering protection or increasing/accelerating programmed cell death (PCD), depending on the intensity and duration of O<sub>3</sub> stress. A single pulse of O<sub>3</sub> (usually higher than 150 ppb) commonly induces an early synthesis of ET followed by the production of SA, JA, and ABA, where (i) ET and SA signaling triggers ROS production and PCD, establishing a feedback loop, (ii) JA attenuates this cycle by reducing the ROS production, and consequently ET biosynthesis and PCD, and (iii) ABA mainly acts as regulator of stomatal closure and O<sub>3</sub> influx [15,27]. This crosstalk was also reported in leaves of sage plants exposed to 200 ppb of O<sub>3</sub> for 5 h [20], but the present study showed a very different regulation of these compounds in sage under long-term O<sub>3</sub> treatment. In particular, the content of SA was significantly increased by O<sub>3</sub> throughout the whole period of the experiment, being probably required to maintain cellular redox state and potentiate defense responses [31]. It is known that SA may regulate Glu levels when plants are subjected to various stress factors, by acting as an antioxidant molecule through the Asc-Glu cycle [32]. In the present study, Glu was mainly accumulated at 7 (only the reduced GSH) and 36 days FBE (both GSH and GSSG), whereas both Asc forms were accumulated at 22 and 29 days FBE (likely the crucial stressful period), according to the outcomes reported above. The accumulation of SA was induced before the production of ET, supporting the hypothesis that the level of ET is controlled by SA during O<sub>3</sub> exposure in order to modulate the magnitude of lesion formation and HR-like cell death by contributing to the regulation of Asc and Glu levels. It should be noted that the synthesis and/or the regeneration of these low molecular weight antioxidant compounds to their reduced powerful antioxidant forms (due to LA after reduction to DHLA as observed at 7 and 14 days FBE) were not able to protect membranes from lipid peroxidation, as demonstrated by the accumulation of MDA (one of the major indicators of cell membrane damage; [33]) from 14 days FBE and even more at the last times of analysis. However, these processes of lipid oxidation did not include the synthesis of the membrane breakdown products formed by LOX, as confirmed by the highly variable response of this enzyme to O<sub>3</sub> exposure (which decreased at 7 and 14 days FBE, and increased only at 29 days FBE, when most severe symptoms and physiological impairments were first reported) and the unchanged values of JA (thus confirming that this compound was not involved in the regulation of PCD strategies; [34–36]). In addition, Marchica et al. [22] documented that the composition of volatile products of LOX pathway (such as C<sub>6</sub> aldehydes and alcohols and their derivatives) was slightly affected by O<sub>3</sub> exposure (under the same experimental conditions), suggesting that after a progression of oxidative pressure until 29 days FBE, sage then settled into a stable stress state until the end of exposure (in terms of free fatty acids released by phospholipases from membranes in response to O<sub>3</sub>), confirming a capability of this species to tolerate long-term O<sub>3</sub> exposure for several weeks.

Our results documented that the production of SA and ET is required to potentiate defense responses in O<sub>3</sub>-treated plants, although leaf injury through the induction of PCD is enhanced starting from 14 days FBE. Symptom observations were in accordance with Chl<sub>SPAD</sub> values, which confirmed a chlorophyll degradation that followed the same symptom development. A reduction of chlorophylls (i.e., chlorophyll *a* and *b*) as well as of

carotenoids (i.e.,  $\beta$ -carotene, antheraxanthin, lutein, and violaxanthin) was already reported at 30 days FBE in Pellegrini et al. [27]. Chlorosis is usually associated with alterations of the photosynthetic process [37]. An  $O_3$ -induced reduction of photosynthesis was indeed reported from 14 days FBE, and especially at the last two times of analysis (i.e., 29 and 36 days FBE), thus following the same trend reported for leaf symptoms and  $Chl_{SPAD}$ . This photosynthetic impairment was clearly due to stomatal limitations, as  $g_s$  showed reductions similar to those of A (although no higher  $g_s$  reductions were reported at 29 and 36 days FBE), and to mesophyll limitations, as  $C_i$  increased following an opposite trend to that of A (i.e., mesophyll cells did not consume  $CO_2$  for photosynthetic assimilation). The consistent increases in ABA observed throughout the whole experiment lead us to speculate that specific signaling pathways (i.e., xanthophyll and Asc-Glu cycles; [3,38]) are activated in order to modulate stomatal function, photosynthesis, and photoprotection under  $O_3$  exposure [36,39]. Pellegrini et al. [27] also observed a decrease in A and  $g_s$  values due to  $O_3$  at 30 days FBE, but no  $C_i$  increases were reported in that study ( $C_i$  decreased). The lack of mesophyll impairment in Pellegrini et al. [27] was likely due to the fact that plants were there exposed to  $O_3$  in a fumigation facility where temperature, relative humidity and photon flux density were controlled and set at optimal levels for plant growth, thus under better environmental conditions than those of the present study, where plants were exposed to  $O_3$  in fumigation chambers located inside a greenhouse with natural environmental conditions (except for  $O_3$  concentration). Indeed,  $F_v/F_m$  (i.e., the most widely used photo-oxidative stress marker, [40]) also was not affected by  $O_3$  in Pellegrini et al. [27], whereas a PSII photodamage was reported at all times of analysis in the present work, thus confirming both the environmental differences between the studies, and more importantly, the harsh  $O_3$  effects reported in the present study on mesophyll functioning. Finally, it should be noted that the  $F_v/F_m$  values were never below 0.70 in  $O_3$ -treated plants throughout the whole period of the experiment, suggesting the idea that  $F_v/F_m$  is sensitive not only to  $O_3$ , but also to environmental factors [41].

Overall, the outcomes of the present study suggest that sage was able to orchestrate the regulation of a number of antioxidants and phytohormones, and this capability allowed sage to tolerate long-term  $O_3$  stress. We speculated that a synergistic interaction among SA, ET and ABA may modulate the defense responses and, at the same time, the magnitude of chlorosis in response to  $O_3$  exposure. Similar results were previously reported by Guo et al. [35,36] and interpreted as a marker of  $O_3$ -induced leaf senescence [35,36]; this is an aspect that warrants more investigation in order to deeply understand the dual roles of these molecules, as well as the study of these stress-response pathways at a gene expression level. Furthermore, given that increasing  $O_3$  concentrations and other environmental stresses (e.g., elevated  $CO_2$  level, drought, and UV) usually occur together, more research would be interesting to further investigate the interactive impacts of multiple environmental stresses on the orchestrated regulations highlighted by the present study.

#### 4. Materials and Methods

##### 4.1. Plant Material and Experimental Design

Experimental activities were carried out at the field station of San Piero a Grado (Pisa, Italy) run by the Department of Agriculture, Food and Environment of the University of Pisa. At the beginning of spring 2019, 8-month-old seedlings of *S. officinalis* obtained from a local nursery were transplanted in 3.7 L plastic pots with a mix of steam-sterilized soil and peat (1:1, v/v), and kept under standard conditions until the beginning of the  $O_3$  exposure. In May 2019, sixty uniformly sized plants (ca. 30 cm tall) were placed in four fumigation chambers inside a greenhouse with natural lighting (the average photon flux density during measurements was around  $500 \mu\text{mol photons m}^{-2} \text{s}^{-1}$  at plant height), and kept under charcoal-filtered air (fifteen plants in each chamber). Ten days later, half of the plants at vegetative stage were exposed to a target concentration of 120 ppb of  $O_3$  (1 ppb =  $1.96 \mu\text{g m}^{-3}$ , at  $25^\circ\text{C}$  and  $101.325 \text{ kPa}$ ) for 36 consecutive days (5 h  $\text{day}^{-1}$ , in the form of a square wave from 10:00 a.m. to 03:00 p.m.), while the other plants at vegetative stage were maintained

under charcoal-filtered air (control, O<sub>3</sub> concentration < 5 ppb). Further details about the experimental conditions and methodology are reported in Marchica et al. [22].

Analyses were performed at 7, 14, 22, 29 and 36 days FBE (i.e., approximately weekly). At each time of analysis, at least five plants at vegetative stage per O<sub>3</sub> treatment ( $n \geq 5$ ) were randomly selected and measured in terms of gas exchange, chlorophyll *a* fluorescence and relative chlorophyll content (the same plants were repeatedly measured throughout the whole experiment; one leaf per plant). Then, using other plants at vegetative stage ( $n \geq 4$ ), five fully expanded leaves (equally distributed over plant height) per plant were excised for ET determination, and another 10 fully expanded leaves (again equally distributed over plant height) per plants were sampled, immediately frozen in liquid nitrogen, and stored at  $-80$  °C until biochemical analyses. All measurements were performed on leaves developed before the beginning of O<sub>3</sub> treatment.

#### 4.2. Gas Exchange and Chlorophyll *a* Fluorescence

The CO<sub>2</sub> assimilation rate (*A*), stomatal conductance (*g<sub>s</sub>*), and intercellular CO<sub>2</sub> concentration (*C<sub>i</sub>*) were determined using an LI-6400 portable photosynthesis system (Li-COR, Lincoln, NE, USA), operating at ambient CO<sub>2</sub> concentration and saturating light conditions (1500 μmol m<sup>-2</sup> s<sup>-1</sup> PAR). Chlorophyll *a* fluorescence measurements were collected using a PAM-2000 fluorometer (Walz, DE). The minimum and maximum fluorescence yields in the dark-adapted state (*F<sub>0</sub>* and *F<sub>m</sub>*, respectively) were determined immediately before and after the application of a saturating light pulse in 40 min dark-adapted leaves (the same used for gas-exchange measurements). The maximum quantum efficiency of PSII photochemistry was calculated as  $F_v/F_m = (F_m - F_0)/F_m$  [42]. A SPAD 502 m (Minolta, JP) was also used to determine leaf greenness and estimate relative chlorophyll content (Chl<sub>SPAD</sub>). Three measurements per leaf were made, and the mean of these measurements was recorded.

#### 4.3. Assessment of Oxidative Damage and Lipoxygenase Activity

Oxidative damage was assessed in terms of lipid peroxidation by measuring the accumulation of malondialdehyde (MDA) by-products [43]. Samples (40 mg fresh weight, FW) were extracted with 1 mL of 80% ethanol. The determination was performed with a fluorescence/absorbance microplate reader (Victor3 1420 Multilabel Counter, Perkin Elmer, Waltham, MA, USA) at 440, 532 and 600 nm.

The lipoxygenase (LOX) activity was assessed by analyzing the oxidation of Fe<sup>2+</sup> to Fe<sup>3+</sup> when linoleic acid was added [44]. Samples (150 mg FW) were homogenized with an LOX extraction solution (equal parts of 15 mM CaCl<sub>2</sub> solution, 13% (*v/v*) sucrose, and 60 mM Tris-HCl buffer at pH 6.8). The enzymatic activity was assessed using a UV-Vis 1900 spectrophotometer (Shimadzu, Kyoto, Japan) at 235 nm for 600 s at 50 °C.

#### 4.4. Determination of Low Molecular Weight Antioxidant Contents

The total (AsA plus DHA) and reduced ascorbate (AsA) contents were measured as described by Kampfenkel et al. [45], with minor modifications. Samples (60 mg FW) were homogenized with 500 μL of 80% methanol. The supernatant was divided in order to determine the total pool and the reduced form of Asc. The determination was performed using the same spectrophotometer reported before at 525 nm. The oxidized form of Asc was calculated as the difference between total ascorbate and AsA.

The total (GSH plus GSSG) and oxidized glutathione (GSSG) contents were determined according to Sgherri and Navari-Izzo [46]. Samples (50 mg FW) were homogenized with 500 μL of 5% TCA. The supernatant was divided in order to determine the total pool and the oxidized form of Glu. The determination was performed using the same spectrophotometer reported before at 412 nm, for 1 min at 25 °C. The amount of GSH was calculated as the difference between total glutathione and GSSG.

Lipoic and dihydrolipoic acids were extracted by acidic hydrolysis by adding samples (150 mg FW) with 1 mL of 6 N HCl [47]. The supernatants were mixed with 500 μL of chloroform, and the resultant organic fraction was collected and evaporated to dryness

under vacuum. Samples were recovered with 500  $\mu\text{L}$  of acetonitrile/0.1% acetic acid in water, 45:55 (*v/v*), which was the isocratic mobile phase eluted into an ultra-high-performance liquid chromatograph system (UHPLC; Dionex UltiMate 3000 system, Dionex UVD 170U UV-Vis detector; Thermo Scientific Waltham, MA, USA) equipped with an Acclaim Trinity P1 column (3  $\mu\text{m}$ , 3.0  $\times$  50 mm). The flow rate was 1 mL  $\text{min}^{-1}$ . Both LA and DHLA were detected at 210 nm.

#### 4.5. Determination of Phytohormone Contents

A few minutes after excision, ET production was measured by enclosing five leaves from each plant in air-tight containers. After 1 h of incubation at room temperature, gas samples were taken from the headspace of the containers. Separations were performed with a gas chromatograph (HP5890, Hewlett-Packard, Ramsey, MN, USA) equipped with a flame ionization detector and a stainless steel column (150 mm length  $\times$  0.4 cm internal diameter, packed with Hysep T). A detailed description of analytical conditions is available in Mensuali-Sodi et al. [48].

Jasmonic acid was determined by using a GC-MS according to Huang et al. [49], with minor modifications. Samples (100 mg FW) were extracted with 1 mL of methanol. The supernatants were evaporated at 37  $^{\circ}\text{C}$  under a vacuum for 10 min, and the residue was re-suspended with 750  $\mu\text{L}$  of ethyl acetate. The extract was injected into an Agilent 8890B gas chromatograph equipped with an Agilent DB-5MS (UI) capillary column (30 m  $\times$  0.25 mm; coating thickness 0.25  $\mu\text{m}$ ) and an Agilent 5977B single quadrupole mass detector (Agilent Technologies Inc., Santa Clara, CA, USA). A detailed description of analytical conditions is available in Huang et al. [49].

Free and conjugated SA were determined by UHPLC according to Zawoznik et al. [50] with some modifications. Samples (150 mg FW) were extracted with 1 mL of 90% (*v/v*) methanol. Separations were performed with the same UHPLC system reported above, equipped with an Acclaim 120 C18 column (5- $\mu\text{m}$  particle size, 4.6-mm internal diameter  $\times$  150-mm length) mounted in a Dionex TCC-100 column oven and a Dionex UltiMate 3000 RS fluorescence detector (Thermo Scientific) with excitation and emission at 305 and 407 nm, respectively. The flow rate was 1 mL  $\text{min}^{-1}$ .

Abscisic acid (ABA) content was determined after extracting leaf tissue in 1 mL of distilled water. The determination of ABA was performed at 415 nm with the same fluorescence/absorbance microplate reader reported before using the Phytodetek<sup>®</sup> Immunoassay Kit for ABA (Agdia, Elkhart, IN, USA).

#### 4.6. Statistical Analyses

The normal distribution of data was preliminarily tested by the Shapiro–Wilk test. The effects of O<sub>3</sub> (between factor), time (within factor), and their combination on Chl<sub>SPAD</sub>, gas-exchange parameters and F<sub>v</sub>/F<sub>m</sub> were analyzed using a one-way repeated measures analysis of variance (ANOVA). The effects of O<sub>3</sub>, time, and their combination on biochemical parameters were analyzed using a two-way ANOVA. Comparisons among parameter means were determined by the Tukey’s HSD post hoc test. Statistically significant effects were considered for  $p \leq 0.05$ . Analyses were performed in JMP 11 (SAS Institute Inc., Cary, NC, USA).

**Author Contributions:** Conceptualization, L.C., C.N. and E.P.; methodology, L.C., A.M. and E.P.; formal analysis, L.C. and A.M.; data curation, A.M.; writing—original draft preparation, L.C. and E.P.; writing—review and editing, L.C., E.P., G.L. and C.N.; supervision, G.L. and C.N. All authors have read and agreed to the published version of the manuscript.

**Funding:** This research received no external funding.

**Institutional Review Board Statement:** Not applicable.

**Informed Consent Statement:** Not applicable.

**Data Availability Statement:** The data presented in this study are available in the main text.

**Acknowledgments:** The authors gratefully acknowledge Anna Mensuali for ethylene determination and Andrea Parrini for supervising the growth chamber and the ozone exposure facilities.

**Conflicts of Interest:** The authors declare no conflict of interest.

## References

- Weng, J.-K.; Lynch, J.H.; Matos, J.O.; Dudareva, N. Adaptive mechanisms of plant specialized metabolism connecting chemistry to function. *Nat. Chem. Biol.* **2021**, *17*, 1037–1045. [[CrossRef](#)]
- Shao, H.-B.; Chu, L.-Y.; Shao, M.-A.; Jaleel, C.A.; Mi, H.-M. Higher plant antioxidants and redox signaling under environmental stresses. *Comptes Rendus Biol.* **2008**, *331*, 433–441. [[CrossRef](#)] [[PubMed](#)]
- Müller, M.; Munné-Bosch, S. Hormonal impact on photosynthesis and protection in plants. *Plant Physiol.* **2021**, *185*, 1500–1521. [[CrossRef](#)] [[PubMed](#)]
- Foyer, C.H.; Noctor, G. Ascorbate and glutathione: The heart of the redox hub. *Plant Physiol.* **2011**, *155*, 2–18. [[CrossRef](#)] [[PubMed](#)]
- Rejeb, I.B.; Pastor, V.; Mauch-Mani, B. Plant responses to simultaneous biotic and abiotic stress: Molecular mechanisms. *Plants* **2014**, *3*, 458–475. [[CrossRef](#)] [[PubMed](#)]
- Ainsworth, E.A. Understanding and improving global crop response to ozone pollution. *Plant J.* **2017**, *90*, 886–897. [[CrossRef](#)]
- Bhuyan, M.A.; Khan, H.U.R.; Zaman, K.; Hishan, S.S. Measuring the impact of global tropospheric ozone, carbon dioxide and sulfur dioxide concentrations on biodiversity loss. *Environ. Res.* **2018**, *160*, 398–411. [[CrossRef](#)]
- Nuvolone, D.; Petri, D.; Voller, F. The effects of ozone on human health. *Environ. Sci. Pollut. Res.* **2018**, *25*, 8074–8088. [[CrossRef](#)]
- Agathokleous, E.; Feng, Z.; Oksanen, E.; Sicard, P.; Wang, Q.; Saitanis, C.J.; Araminiene, V.; Blande, J.D.; Hayes, F.; Calatayud, V.; et al. Ozone affects plant, insect, and soil microbial communities: A threat to terrestrial ecosystems and biodiversity. *Sci. Adv.* **2020**, *6*, eabc1176. [[CrossRef](#)]
- Lefohn, A.S.; Malley, C.S.; Smith, L.; Wells, B.; Hazucha, M.; Simon, H.; Naik, V.; Mills, G.; Schultz, M.G.; Paoletti, E.; et al. Tropospheric ozone assessment report: Global ozone metrics for climate change, human health, and crop/ecosystem research. *Elementa* **2018**, *6*, 28. [[CrossRef](#)]
- IPCC, Intergovernmental Panel on Climate Change. Summary for Policymakers. In *Climate Change 2021: The Physical Science Basis*; Masson-Delmotte, V.P., Zhai, A., Pirani, S.L., Connors, C., Péan, S., Berger, N., Caud, Y., Chen, L., Goldfarb, M.I., Gomis, M., et al., Eds.; Contribution of Working Group I to the Sixth Assessment Report of the Intergovernmental Panel on Climate Change; Cambridge University Press: Cambridge, UK, 2021.
- Gill, S.S.; Tuteja, N. Reactive oxygen species and antioxidant machinery in abiotic stress tolerance in crop plants. *Plant Physiol. Biochem.* **2010**, *48*, 909–930. [[CrossRef](#)]
- Gandin, A.; Dizengremel, P.; Jolivet, Y. Integrative role of plant mitochondria facing oxidative stress: The case of ozone. *Plant Physiol. Biochem.* **2021**, *159*, 202–210. [[CrossRef](#)]
- Pellegrini, E.; Trivellini, A.; Cotrozzi, L.; Vernieri, P.; Nali, C. Involvement of phytohormones in plant responses to ozone. In *Plant Hormones Under Challenging Environmental Factors*; Golam, J.A., Jingquan, Y., Eds.; Springer: Dordrecht, The Netherlands, 2016; pp. 215–245.
- Hasan, M.M.; Rahman, M.A.; Skalicky, M.; Alabdallah, N.M.; Waseem, M.; Jahan, M.S.; Ahammed, G.J.; El-Mogy, M.M.; El-Yazied, A.A.; Ibrahim, M.F.M.; et al. Ozone induced stomatal regulations, MAPK and phytohormone signalling in plants. *Int. J. Mol. Sci.* **2021**, *22*, 6304. [[CrossRef](#)]
- Ogawa, D.; Nakajima, N.; Sano, T.; Tamaoki, M.; Aono, M.; Kubo, A.; Kanna, M.; Ioki, M.; Kamada, H.; Saji, H. Salicylic acid accumulation under O<sub>3</sub> exposure is regulated by ethylene in tobacco plants. *Plant Cell Physiol.* **2005**, *46*, 1062–1072. [[CrossRef](#)]
- Cotrozzi, L.; Pellegrini, E.; Guidi, L.; Landi, M.; Lorenzini, L.; Massai, R.; Remorini, D.; Tonelli, M.; Trivellini, A.; Vernieri, P.; et al. Losing the warning signal: Drought compromises the cross-talk of signaling molecules in *Quercus ilex* exposed to ozone. *Front. Plant Sci.* **2017**, *8*, 1020. [[CrossRef](#)]
- Landi, M.; Cotrozzi, L.; Pellegrini, E.; Remorini, D.; Tonelli, M.; Trivellini, A.; Nali, C.; Guidi, L.; Massai, R.; Vernieri, P.; et al. When “thirsty” means “less able to activate the signalling wave triggered by a pulse of ozone”: A case study in two Mediterranean deciduous oak species with different drought sensitivity. *Sci. Total Environ.* **2019**, *657*, 379–390. [[CrossRef](#)]
- Marchica, A.; Lorenzini, G.; Papini, R.; Bernardi, R.; Nali, C.; Pellegrini, E. Signalling molecules responsive to ozone-induced oxidative stress in *Salvia officinalis*. *Sci. Total Environ.* **2019**, *657*, 568–576. [[CrossRef](#)]
- Marchica, A.; Loré, S.; Cotrozzi, L.; Lorenzini, G.; Nali, C.; Pellegrini, E.; Remorini, D. Early detection of sage (*Salvia officinalis* L.) responses to ozone using reflectance spectroscopy. *Plants* **2019**, *8*, 346. [[CrossRef](#)]
- Marchica, A.; Cotrozzi, L.; Detti, R.; Lorenzini, G.; Pellegrini, E.; Petersen, M.; Nali, C. The biosynthesis of phenolic compounds is an integrated defence mechanism to prevent ozone injury in *Salvia officinalis*. *Antioxidants* **2020**, *9*, 1274. [[CrossRef](#)]
- Marchica, A.; Ascricchi, R.; Flamini, G.; Cotrozzi, L.; Tonelli, M.; Lorenzini, G.; Nali, C.; Pellegrini, E. Ozone as eustress for enhancing secondary metabolites and bioactive properties in *Salvia officinalis*. *Ind. Crops Prod.* **2021**, *170*, 113730. [[CrossRef](#)]
- Munné-Bosch, S.; Alegre, L. Drought-induced changes in the redox state of  $\alpha$ -tocopherol, ascorbate and the diterpene carnosic acid in chloroplast of Labiatae species differing in carnosic acid contents. *Plant Physiol.* **2003**, *131*, 1816–1825. [[CrossRef](#)] [[PubMed](#)]
- Tounekti, T.; Abreu, M.E.; Khemira, H.; Munné-Bosch, S. Canopy position determines the photoprotective demand and antioxidant protection of leaves in salt stressed *Salvia officinalis* L. plants. *Environ. Exp. Bot.* **2012**, *78*, 146–156. [[CrossRef](#)]

25. Martins, N.; Barros, L.; Santos-Buelga, C.; Henriques, M.; Silva, S.; Ferreira, I.C. Evaluation of bioactive properties and phenolic compounds in different extracts prepared from *Salvia officinalis* L. *Food Chem.* **2015**, *170*, 378–385. [[CrossRef](#)] [[PubMed](#)]
26. Trivellini, A.; Lucchesini, M.; Maggini, R.; Mosadegh, H.; Villamarin, T.S.S.; Vernieri, P.; Mensuali-Sodi, A.; Pardossi, A. Lamiaceae phenols as multifaceted compounds: Bioactivity, industrial prospects and role of “positive-stress”. *Ind. Crops Prod.* **2016**, *83*, 241–254. [[CrossRef](#)]
27. Pellegrini, E.; Francini, A.; Lorenzini, G.; Nali, C. Ecophysiological and antioxidant traits of *Salvia officinalis* under ozone stress. *Environ. Sci. Pollut. Res.* **2015**, *22*, 13083–13093. [[CrossRef](#)]
28. Cotrozzi, L.; Remorini, D.; Pellegrini, E.; Guidi, L.; Nali, C.; Lorenzini, G.; Massai, R.; Landi, M. Living in a Mediterranean city in 2050: Broadleaf or evergreen ‘citizens’? *Environ. Sci. Pollut. Res.* **2018**, *25*, 8161–8173. [[CrossRef](#)]
29. Rao, M.V.; Koch, J.R.; Davis, K.R. Ozone: A tool for probing programmed cell death in plants. *Plant Mol. Biol.* **2000**, *44*, 345–358. [[CrossRef](#)]
30. Rao, M.V.; Lee, H.-I.; Davis, K.R. Ozone-induced ethylene production is dependent on salicylic acid, and both salicylic acid and ethylene act in concert to regulate ozone-induced cell death. *Plant J.* **2002**, *32*, 447–456. [[CrossRef](#)]
31. Saleem, M.; Fariduddin, Q.; Castroverde, C.D.M. Salicylic acid: A key regulator of redox signalling and plant immunity. *Plant Physiol. Biochem.* **2021**, *168*, 381–387. [[CrossRef](#)]
32. Mateo, A.; Funck, D.; Mühlenthal, P.; Kular, B.; Mullineaux, P.M.; Karpinski, S. Controlled levels of salicylic acid are required for optimal photosynthesis and redox homeostasis. *J. Exp. Bot.* **2006**, *57*, 1795–1807. [[CrossRef](#)]
33. Morales, M.; Munné-Bosch, S. Malondialdehyde: Facts and artifacts. *Plant Physiol.* **2019**, *180*, 1246–1250. [[CrossRef](#)]
34. Tsukahara, K.; Sawada, H.; Kohno, Y.; Matsuura, T.; Mori, I.C.; Terao, T.; Oki, M.; Tamaoki, M. Ozone-induced rice grain yield loss is triggered via a change in panicle morphology that is controlled by *ABERRANT PANICLE ORGANIZATION 1* gene. *PLoS ONE* **2015**, *10*, e0123308. [[CrossRef](#)]
35. Guo, H.; Sun, Y.; Yan, H.; Li, C.; Ge, F. O<sub>3</sub>-induced leaf senescence in tomato plants is ethylene signaling-dependent and enhances the population abundance of *Bemisia tabaci*. *Front. Plant Sci.* **2018**, *9*, 764. [[CrossRef](#)]
36. Guo, H.; Sun, Y.; Yan, H.; Li, C.; Ge, F. O<sub>3</sub>-induced priming defense associated with the abscisic acid signaling pathway enhances plant resistance to *Bemisia tabaci*. *Front. Plant Sci.* **2020**, *11*, 93. [[CrossRef](#)]
37. Cotrozzi, L.; Campanella, A.; Pellegrini, E.; Lorenzini, G.; Nali, C.; Paoletti, E. Phenylpropanoids are key players in the antioxidant defense to ozone of European ash, *Fraxinus excelsior*. *Environ. Sci. Pollut. Res.* **2018**, *25*, 8137–8147. [[CrossRef](#)]
38. Wani, S.H.; Kumar, V.; Shriram, V.; Sah, S.K. Phytohormones and their metabolic engineering for abiotic stress tolerance in crop plants. *Crop J.* **2016**, *4*, 162–176. [[CrossRef](#)]
39. Proadhan, M.Y.; Munemasa, S.; Nahar, M.N.-E.-N.; Nakamura, Y.; Murata, Y. Guard cell salicylic acid signaling is integrated into abscisic acid signaling via the Ca<sup>2+</sup>/CPK-dependent pathway. *Plant Physiol.* **2018**, *178*, 441–450. [[CrossRef](#)]
40. Pintó-Marijuan, M.; Munné-Bosch, S. Photo-oxidative stress markers as a measure of abiotic stress-induced leaf senescence: Advantages and limitations. *J. Exp. Bot.* **2014**, *65*, 3845–3857. [[CrossRef](#)]
41. Bussotti, F.; Gerosa, G.; Digrado, A.; Pollastrini, M. Selection of chlorophyll fluorescence parameters as indicators of photosynthetic efficiency in large scale plant ecological studies. *Ecol. Indic.* **2020**, *108*, 105686. [[CrossRef](#)]
42. Genty, B.; Briantais, J.M.; Baker, N.R. The relationship between the quantum yield of photosynthetic electron transport and quenching of chlorophyll fluorescence. *Biochim. Biophys. Acta* **1989**, *990*, 87–92. [[CrossRef](#)]
43. Hodge, D.M.; DeLong, J.M.; Forney, C.F.; Prange, R.K. Improving the thiobarbituric acid reactive substances assay for estimating lipid peroxidation in plant tissues containing anthocyanin and other interfering compounds. *Planta* **1999**, *207*, 604–611. [[CrossRef](#)]
44. Silva, A.K.; de Almeida Ribeiro Oliveira, G.; Zaczek Bassinello, P.; Lanna, A.C.; Novotny, E.H.; Lião, L.M. Evaluation of lipoxygenase activity in common beans by UV and NMR spectroscopy: Proposal for a complementary technique for enzymatic studies. *Food Anal. Methods* **2020**, *13*, 35–43. [[CrossRef](#)]
45. Kampfenkel, K.; Van Montagu, M.; Inzé, D. Extraction and determination of ascorbate and dehydroascorbate from plant tissue. *Anal. Biochem.* **1995**, *225*, 165–167. [[CrossRef](#)]
46. Sgherri, C.L.M.; Navari-Izzo, F. Sunflower seedlings subjected to increasing water deficit stress: Oxidative stress and defence mechanisms. *Physiol. Plant* **1995**, *93*, 25–30. [[CrossRef](#)]
47. Sgherri, C.; Quartacci, M.F.; Izzo, R.; Navari-Izzo, F. Relation between lipoic acid and cell redox status in wheat grown in excess copper. *Plant Physiol. Biochem.* **2002**, *40*, 591–597. [[CrossRef](#)]
48. Mensuali Sodi, A.; Panizza, M.; Tognoni, F. Quantification of ethylene losses in different container-seal systems and comparison of biotic and abiotic contributions to ethylene accumulation in cultured tissues. *Physiol. Plant* **1992**, *84*, 472–476. [[CrossRef](#)]
49. Huang, Z.-H.; Wang, Z.-L.; Shi, B.-L.; Wei, D.; Chen, J.-X.; Wang, S.-L.; Gao, B.-J. Simultaneous determination of salicylic acid, jasmonic acid, methyl salicylate, and methyl jasmonate from *Ulmus pumila* leaves by GC-MS. *Int. J. Anal. Chem.* **2015**, *2015*, 698630. [[CrossRef](#)]
50. Zawoznik, M.S.; Groppa, M.D.; Tomaro, M.L.; Benavides, M.P. Endogenous salicylic acid potentiates cadmium-induced oxidative stress in *Arabidopsis thaliana*. *Plant Sci.* **2007**, *173*, 190–197. [[CrossRef](#)]

# Drought Stress Responses: Coping Strategy and Resistance

Hanna Bandurska

Department of Plant Physiology, Poznan University of Life Sciences, Wolyńska 35, 60-637 Poznań, Poland; hanna.bandurska@up.poznan.pl

**Abstract:** Plants' resistance to stress factors is a complex trait that is a result of changes at the molecular, metabolic, and physiological levels. The plant resistance strategy means the ability to survive, recover, and reproduce under adverse conditions. Harmful environmental factors affect the state of stress in plant tissues, which creates a signal triggering metabolic events responsible for resistance, including avoidance and/or tolerance mechanisms. Unfortunately, the term 'stress resistance' is often used in the literature interchangeably with 'stress tolerance'. This paper highlights the differences between the terms 'stress tolerance' and 'stress resistance', based on the results of experiments focused on plants' responses to drought. The ability to avoid or tolerate dehydration is crucial in the resistance to drought at cellular and tissue levels (*biological resistance*). However, it is not necessarily crucial in crop resistance to drought if we take into account agronomic criteria (*agricultural resistance*). For the plant user (farmer, grower), resistance to stress means not only the ability to cope with a stress factor, but also the achievement of a stable yield and good quality. Therefore, it is important to recognize both particular plant coping strategies (stress avoidance, stress tolerance) and their influence on the resistance, assessed using well-defined criteria.

**Keywords:** drought; state of stress; tolerance; avoidance; yield; stress survival

**Citation:** Bandurska, H. Drought Stress Responses: Coping Strategy and Resistance. *Plants* **2022**, *11*, 922. <https://doi.org/10.3390/plants11070922>

Academic Editors: Milan S. Stankovic, Paula Baptista and Petronia Carillo

Received: 17 March 2022

Accepted: 28 March 2022

Published: 29 March 2022

**Publisher's Note:** MDPI stays neutral with regard to jurisdictional claims in published maps and institutional affiliations.



**Copyright:** © 2022 by the author. Licensee MDPI, Basel, Switzerland. This article is an open access article distributed under the terms and conditions of the Creative Commons Attribution (CC BY) license (<https://creativecommons.org/licenses/by/4.0/>).

## 1. Introduction

Unfavorable environmental conditions frequently affect plants' performance, both in natural and agricultural settings. Cramer et al. [1] reported that only 3.5% of the global land area is free from any environmental constraints. Therefore, plants are often exposed to abiotic stress factors which affect their proper development and limit crop production [2–4]. Being immobile organisms, plants have been forced to develop specific adaptive traits and ability to adjust (acclimate) to adverse conditions (Figure 1). Adaptation includes developmental, morphological, and physiological traits which help the growth under adverse conditions. Acclimation (hardening) comprises structural, physiological, and biochemical changes responsible for the adjustment to new environmental conditions. It should be distinguished from adaptation, which usually refers to evolutionarily created and genetically determined traits. The ability to acclimate is determined by plant plasticity and includes activation of several complex cellular and molecular responses such as changes in hormone balance and gene expression [5].

The number of papers that focus on the mechanisms of plants response and resistance to stress factors has increased several folds since the beginning of this century [1,6]. It should be highlighted that the understanding of resistance to stress differs depending on the plant's strategy and plant user's expectations. Therefore, it is very important to correctly define resistance to stress using clear and appropriate criteria. Stress resistance should not be confused with stress tolerance, which often happens and leads to some misunderstanding which, in my opinion, makes it difficult to define the traits involved in crop resistance to environmental limits. Scientific research focused on identifying the mechanisms or traits responsible for the resistance of crops to stress factors should consider the differences between stress tolerance and stress resistance. The environmental constraint that most often causes the loss of yield throughout the world is drought [2,7]. This paper

discusses plant strategies responsible for coping with drought stress and the involvement of the components of these strategies in crop resistance to drought.

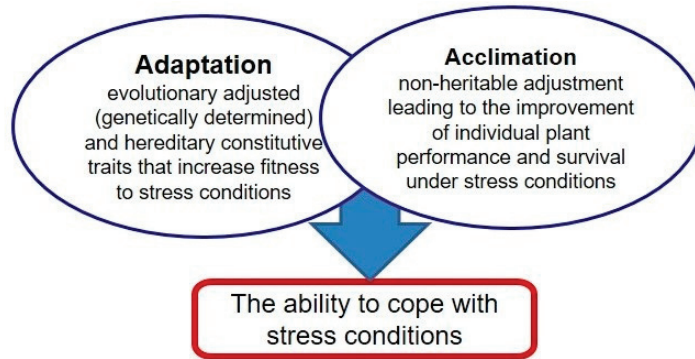


**Figure 1.** Stress adjustment developed in plants.

## 2. Concept of Stress and Terminology of Stress Resistance

A stress factor affects the state of stress (strain) in plant cells, which leads to structural or metabolic dysfunctions (growth inhibition, damage of structural and functional proteins, inhibition of enzyme activity) and death, or triggers changes that help the plant to adjust to adverse conditions. The plant response depends on the duration and severity of the stress factor, as well as on genetic traits that determine the ability to cope with stress. Depending on the level of stress and duration, plants can experience the state of eustress or distress (Figure 2). A low dose of stressor causes a slight strain (eustress), which triggers responses that help to cope with harmful conditions. Distress caused by a high dose of stressor rapidly triggers the state of stress in plants, leading to physiological destabilization and death or activation responses that protect against stress damage [8]. Plants' resistance to stress resulting from either adaptation or acclimation may be the effect of activation of diverse coping strategies including stressor escape, stress avoidance (avoidance of the state of stress in cells), and stress tolerance (tolerance of the state of stress in cells). The strategy of stressor escape (adaptive strategy) relies on the adjustment of the life cycle to the period when plants' needs are met. It can be observed in drought-sensitive plant species, growing in arid and semi-arid areas with regular water deficit, as well as in early spring plants living in a temperate climate. These plants start to develop at the end of winter (February/March) and complete their life cycle at the beginning of spring. Such a strategy is also observed in perennial plants of a temperate climate, which become dormant at the end of autumn to avoid low winter temperatures. The process of preparing plants to survive winter is autumn leaf senescence, controlled by environmental conditions (light, temperature) which affect the relocation of nitrogen, phosphorus, and other elements from leaves to other organs as well as increased levels of endogenous ABA, responsible for dormancy [9]. Maintaining seed dormancy under harsh conditions, regulated by the interplay between ABA and gibberellins, is also considered a stress escape strategy [10]. Stress avoidance is based on the traits and modifications that prevent the occurrence of the state of stress in plant cells, through retardation or weakening of the action of the stressor—as in, for example, stomatal closure responsible for the restriction of water loss through leaves, as well as osmotic adjustments in plant growing under water deficit conditions [2,11]. Stress tolerance, on the other hand, includes mechanisms responsible for coping with the ongoing state of stress in plant cells, such as the synthesis of compatible substances and proteins, which protects against the negative effect of osmotic and ionic stresses in drought- and salt-stressed plants [11,12]. In other words, it is the capacity to sustain plant functions, thanks to the modifications that counter negative effects of the occurrence of the state of stress, and to repair the damage after stress relief (Figure 2).

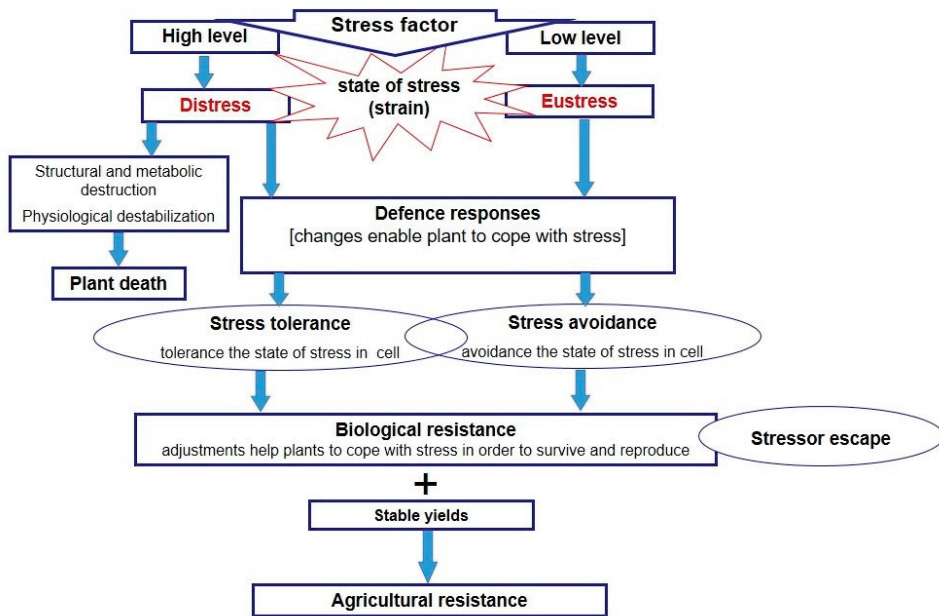


**Figure 2.** Plant responses to abiotic stress factors, coping strategy, and resistance.

Both stress avoidance and stress tolerance are responsible for resistance to stress, understood as the ability to cope with adverse environmental conditions, by keeping a balance between growth, reproduction, and activation of suitable coping strategies [13]. This kind of resistance can be called *biological resistance*, which is the strategy of an individual plant to tolerate and survive stress conditions. An example of *biological resistance* is also the stressor escape strategy which occurs in stress-sensitive plants. From the perspective of plant users, crop resistance to environmental stresses should be defined as the ability to cope with stress conditions thanks to defense responses (stress tolerance and/or avoidance) which enables maintenance of stable and good quality yields. Therefore, it can be called *agricultural resistance*.

### 3. Plant Responses to Drought

Drought is a meteorological term defined as a period of little or no rainfall, which reduces the amount of water in the soil, and is usually accompanied by high evaporative demand, leading to continuous loss of water by transpiration. It is considered the most frequent climate-related constraint in many regions of the world [3,14]. This stress factor generates the state of stress (strain) in plant cells, which is the reduction in water content (dehydration, water deficit), adversely affecting plant physiological activity, growth, reproduction, and crop productivity [15]. The level of dehydration depends on stress severity and duration, as well as on adaptive traits protecting against water loss (smaller leaves, leaves covered with cuticle or tomentose, as well as leaf folding) and supporting water uptake from deeper soil layers (extensive vertically orientated root system). Another example of an adaptive trait protecting from water loss is stomatal behavior (stomata open at night and closed during day) in crassulacean acid plants (CAM) having an alternative route of carbon assimilation which occurs during the night [5,16]. The above-mentioned adaptations do not usually occur in crop plants, which mostly belong to mesophytes, and are able to grow in an environment with a moderate supply of water. These plants may adjust to water scarcity through the activation of stress avoidance and/or tolerance mechanisms directed at preventing dehydration and/or dehydration damage, and surviving stress [11,13]. A suitable and commonly used marker to evaluate the level of dehydration

(state of stress) is relative water content (RWC). In leaves of well-irrigated plants RWC is  $\geq 90\%$ , but with mild drought stress it is in the range 60–70%, with moderate stress 40–60%, and in the case of severe stress it is lower than 40% [17].

Based on the ability to maintain stable leaf hydration under water deficit conditions the water management strategy of plants is classified as isohydric or anisohydric [18]. Isohydric species ('water savers') maintain nearly constant RWC through precise control of stomatal behavior. These plants respond to drought by a rapid decrease in stomatal conductance ( $g_s$ ) and restriction of excessive water loss without a reduction in leaf area but at the same time show a decrease in photosynthetic activity. In contrast, anisohydric plants ('water wasters') show a decrease in leaf water content and strong leaf area reduction but keep stomata open and maintain a high photosynthetic rate [19–21]. The extent of tissue dehydration is a signal triggering, directly or through ABA increase, the activation of appropriate metabolic and physiological changes responsible for plants' adjustment to drought [22]. Even a slight decrease in RWC triggers upstream signaling events, leading to ABA accumulation and stomatal closure [23]. It was suggested that ABA is primarily synthesized in roots, then it is moved to shoots via xylem vessels and acts as a signal of soil water shortage [24]. Recent research revealed that the source of ABA accumulation in roots under drought stress conditions is its transport from leaves [25,26]. In the model plant *Arabidopsis thaliana* it was observed that CLE-25 peptide is a root-derived molecule which moves via the vasculature to leaves and transmits a water deficit signal triggering ABA synthesis by the activation of biosynthetic enzymes [27]. The root–shoot signal mediating the effect of soil water deficit on stomata in tomato comprises a dialogue between ABA and strigolactones, ethylene precursor ACC, or sap pH [28]. Stomatal closure in response to soil water deficit in maize and poplar (isohydric species) is regulated by the interaction between the hydraulic signal as a primary message and ABA as a secondary message [18,28,29].

ABA is also involved in several downstream events responsible for the maintenance of tissue hydration (dehydration avoidance strategy), which include osmotic adjustment, comprising the accumulation of organic osmotic compounds (proline, glycine-betaine, soluble proteins, carbohydrates) in leaves and in roots [15,22]. It appears to be necessary for the activation of proline transport and deposition in the root growing region, allowing the maintenance of root growth and undisturbed water uptake under drought conditions [29]. Indeed, ABA plays a central role in plants' response to drought at different levels of organization; however, it does not act alone but through synergistic or antagonistic crosstalk with other hormones. Crosstalk between ABA, ethylene (ET), and auxin (AUX) regulates root growth and architecture [30]. Guard cells' aperture and water loss by stomata are controlled by the orchestration of ABA with jasmonic acid (JA), ET, salicylic acid (SA), as well as AUXs and cytokinins (CKs). Increased levels of JA, ET, and SA in drought-stressed plants promote the induction of stomatal closure which is maintained by the decline in CK and AUX levels [31–34]. Foliage-derived ABA promotes root growth under drought by lowering the level of ET, which is a root growth inhibitor [35]. Additionally, auxin-induced alteration of root architecture, which leads to the creation of more vertical and deeper roots, plays an important role in maintaining better water acquisition under drought conditions [27,36]. Brassinosteroid (BR)-induced root hydrotropism and accumulation of osmoprotectants (proline, trehalose, raffinose) in roots may also improve water uptake under drought [27,37]. The beneficial effect of ABA on water transport and tissue hydration under drought conditions may also be achieved by its influence on the improvement of root hydraulic conductivity through regulation of the activity of membrane water channels—aquaporins [38,39].

The strategy of dehydration avoidance (isohydric behavior) allows plants to sustain physiological functions under stress conditions and recover after stress termination. This strategy is effective in plants exposed to mild or moderate drought that does not last very long but under prolonged drought it affects carbon starvation [40]. Moreover, when stomata are closed plants absorb more light than can be used in carbon fixation, which triggers generation of reactive oxygen species (ROS), affecting secondary stress and damage

of PSII, leading to further weakness of photosynthesis [12,41]. What is more, during long-term drought the ability of plants to maintain stomatal closure may be weakened due to a decrease in ABA level and plant behavior changes to anisohydric [42]. The response to drought in anisohydric plants (barley, wheat, sunflower) is mainly regulated hydraulically. The maintenance of stomatal conductance in these plants is supported by the capacity for osmotic adjustment, controlled by the dehydration signal, which enables plants to extract water from soil to maintain tissue hydration [18,40]. In anisohydric wheat genotypes the level of ABA in leaves did not change under water deficit conditions, while in roots it increased but only after 21 days of stress [29]. Therefore, it is possible that, along with tissue dehydration, ABA may also play a role in the response of anisohydric species to prolonged drought. The stomatal conductance in anisohydric plants is also maintained by undisturbed water movement through cell membrane aquaporins responsible for roots' ability to conduct water [43]. It was reported that ABA increases the activity of aquaporins and improves root hydraulic conductivity [44]. The activity of aquaporins is also regulated by gibberellins (GAs), CKs, methyl jasmonate (MeJA), and AUXs at transcriptional and post-transcriptional levels ([45] and references therein). The anisohydric strategy is beneficial under mild to moderate drought conditions but may be a risk under severe and long-term stress, which may cause hydraulic failure and severe dehydration [20].

In plants exposed to severe and long-term drought, dehydration cannot be avoided, and activation of dehydration tolerance mechanisms becomes important. Dehydration has a deleterious effect on cell membranes and causes the disruption of many biochemical and physiological processes [2,46]. A frequently used indicator of dehydration tolerance is the cell membrane injury index or membrane stability index, which shows the ability to maintain membrane integrity at a given level of dehydration [47,48]. The dehydration tolerance mechanisms enable plants to maintain membrane integrity and cell homeostasis, and to regain physiological activity after stress cessation [12,41]. These mechanisms are controlled by ABA-dependent and -independent pathways and include synthesis of protective proteins (LEA proteins, dehydrins, chaperons) and compatible compounds (proline, glycine-betaine, proline-betaine, trehalose, raffinose mannitol, pinitol) involved in enzyme and membrane protection [2,22,41,49,50]. Dehydration-induced disturbance of the respiratory metabolic pathway exhibits generation of ROS, leading to a state of oxidative stress [2,46,51–53]. Moreover, in drought-stressed plants the enhanced build-up of ROS is caused by photosynthesis disruption and increased photorespiration due to the limitation of CO<sub>2</sub> uptake [53,54]. Overproduction of ROS (secondary stress), which includes superoxide radicals (O<sub>2</sub><sup>•−</sup>), hydrogen peroxide (H<sub>2</sub>O<sub>2</sub>), hydroxyl radical (OH<sup>•</sup>), and singlet oxygen (<sup>1</sup>O<sub>2</sub>), is harmful to organelles through lipid peroxidation and damage to nucleic acids and proteins [2,3,46]. In order to overcome oxidative damage, plants possess enzymatic and non-enzymatic ROS-scavenging systems. Enzymatic antioxidants include superoxide dismutase (SOD), catalase (CAT), and peroxidases (POX). The non-enzymatic components of the antioxidative system comprise ascorbic acid, α-tocopherol, flavonoid, glutathione, carotenoids, proline, and phenolic compounds which mitigate oxidative damage by direct reduction of ROS activity and by working together with antioxidant enzymes [53,55]. Additionally, alternative oxidase (AOX) is involved in avoidance of excess generation of ROS in mitochondrial electron transport chains [54]. ABA plays a pivotal role in the activation of antioxidant enzymes and synthesis of low molecular ROS scavengers [49,50]. Upregulation of the antioxidant system may also be controlled by JA, SA, and BRs [34,51–58].

Thanks to the efficient antioxidative system, plants can keep ROS at non-toxic levels, and these molecules are thought to act as signals for activation of stress defense responses [45,54]. It was also evidenced that NADPH oxidase localized in apoplastic fluid is involved in ROS production for integrating signaling networks involved in stress response processes. An increased level of this enzyme was detected in drought-stressed rice as well as in leaves of ABA- and Ca<sup>2+</sup>-treated maize seedlings [54,59]. Moreover, NADPH oxidase regulates H<sub>2</sub>O<sub>2</sub> production for the signaling cascade which affects ABA-dependent stomatal closure and antioxidant defense. The involvement of NADPH oxidase in brassinosteroid-

induced H<sub>2</sub>O<sub>2</sub> production and regulation of stomatal closure/opening and antioxidant defense was also reported [54,60].

Plant responses to drought are governed by a sophisticated regulatory system working at the molecular level. The decrease in turgor pressure leads to tension changes in plasma membranes, which are perceived by membrane proteins including receptor-like kinases (RLKs), histidine kinases (HKs), and integrin-like proteins (ILPs) working as osmotic stress sensors. ATHK1 is an *Arabidopsis thaliana* His kinase postulated to play a role in water stress perception triggering the mitogen-activated protein kinase (MAPK) signaling cascade both in ABA-dependent and ABA-independent regulatory systems [61]. A crucial role in the signal transduction route is played by transcription factors (TFs) that bind to TF binding sites (TFBS) in the promoter region and regulate gene expression. TF families involved in plants' response to drought include bZip (AREB/ABF), AP2/ERF (DREB/CBF), MYB/MYC, WRKY, and NAC [3,62]. In the ABA-dependent pathway the perception of ABA by receptor proteins is the primary event that triggers downstream signaling cascades to induce final physiological responses. The receptors for this hormone are small soluble cytosol/nucleus-localized pyrabactin resistance (PYR)/PYR-like (PYL)/regulatory components of ABA receptor (RCAR) proteins. The interaction of ABA with PYR/PYL/RCARs affects deactivation of protein phosphatase enzymes (PP2Cs), which are constitutive negative regulators of ABA-induced responses. The inhibition of PP2Cs leads to auto-phosphorylation of the protein kinases SnRK2s, which induces stomatal closure and stimulates nuclear targets that trigger expression of various water stress associated genes due to activation of TFs [62]. ABA-dependent gene expression systems involve activation of b-ZIP (AREBs/ABFs), MYC/MYB, as well as NAC transcription factors [63].

In ABA-independent responses to drought the dehydration signal from the cell surface to the nucleus is mediated by calcium, JA, and ROS [62]. Water deficit leads to membrane destabilization and Ca<sup>2+</sup> influx into the cytoplasm. The calcium signal is detected and transduced through calmodulin (CaM), calcium dependent protein kinases (CDPK), and calcineurin B-like proteins (CBLs) and interacts with the MAPK cascade, leading to activation of TFs (DREB, NAC) and expression of genes coding the synthesis of functional proteins (LEA proteins, chaperones, dehydrins, enzymes of osmolyte biosynthesis). JA, on the other hand, is engaged in activation of the MYC2 transcription factor, which triggers expression of stress-responsive genes [62]. Furthermore, JA along with ROS acts as a stress-signaling unit triggering the expression of genes involved in activation of enzymatic and non-enzymatic scavenging events [62,64]. The widespread plant response to drought is proline accumulation due to the stimulation of its synthesis from glutamate catalyzed by pyrroline-5-carboxylate synthetase (P5CS) and pyrroline-5-carboxylate reductase (P5CR) [65,66]. Synthesis of this amino acid under drought is driven by both ABA-dependent and ABA-independent signaling pathways engaged in triggering expression of *P5CS* and *P5CR* genes regulated by many TFs, which are also related to responses to drought controlled by other growth regulators [67].

Important components of the stress-factor-induced regulatory system are epigenetic modifications which are independent of DNA sequence changes. These changes include chromatin remodeling such as DNA methylation and histone modifications altering the structure and accessibility of chromatin, leading to changes in gene expression at the transcriptional and post-transcriptional levels [68]. Drought-stress-induced changes in DNA methylation have been observed in diverse plant species. These changes were related to the expression of genes encoding transcription factors and were involved in drought resistance mechanisms or were linked to drought sensitivity [69–71]. It was found that changes in DNA methylation (demethylation) in water deficit stressed rice were responsible for proline accumulation via the upregulation of proline metabolism-related gene expression [72]. In addition to DNA methylation, drought-induced histone modifications (methylation, acetylation) are involved in controlling gene expression in stressed plants [73]. It was observed that drought stress triggered histone H3 lisyne4 tri-

methylation (H3K4 me3) in the gene body region of nine cis-epoxycarotenoid dioxygenase 3 (NCED3), which is a key enzyme involved in ABA synthesis. Additionally, some studies reported the increase in H3K4me3 and H3 lisyne9 acetylation (H3K9Ac) in the promotor region of such genes as *RD29A*, *RD29B*, *RD22*, and *RELATED TO AP2.4 (RAP2.4)* encoding synthesis of LEA proteins. The abundance of histone modification and the number of genes expressed depend on stress duration and degree [70,73]. Most of the epigenetic modifications are removed when the stress is relived, but some of them persist, enabling plants to remember past stress and to prepare for future recurrent stress events which occur during plant life. This is so-called “plant stress memory”, which can also be transferred to further generations during sexual and vegetative reproduction [69,71,74]. Integral components of the stress response at the molecular level also involved in memory pathways are non-coding small RNAs (miRNAs, siRNAs), which can trigger DNA methylation and histone modifications. Plants exposed to drought can memorize stress events through DNA and histone modifications for specific gene expression thanks to up- and downregulation of small RNAs responsible for the increased resistance to future stress events through the control of TFs, ROS, and hormone levels [71,74].

#### 4. Drought Coping Strategies and Resistance

The ability to avoid or tolerate dehydration is crucial in dealing with drought at cellular and tissue levels (*biological resistance*), which allows plants to survive during water scarcity conditions and recovery. The tolerance and avoidance mechanisms were developed during evolution in order to adjust to environmental conditions but usually do not have beneficial effects in agricultural production. Plants can withstand drought without any visible signs of dehydration and/or dehydration damage, but their growth and yield may be lower than expected. This is an unwanted side effect of plant adjustment to stress, which has a negative impact on biomass accumulation and yield (*agricultural resistance*).

The activation of coping mechanisms is connected to increased energy and nutrient consumption, which results in the allocation of less energy and assimilates to growth processes, leading to yield reduction [15,75]. Furthermore, many traits associated with drought resistance have a dual effect (positive or negative) on plant productivity which depends on stress intensity and timing as well as on climatic conditions such as light intensity and evaporative demand [76]. The dehydration avoidance strategy, such as stomatal closure, reduces water loss from leaves. However, at the same time it causes the restriction of CO<sub>2</sub> uptake, ROS generation, damage of PSII, and the inhibition of photosynthesis, resulting in the reduction of crop production [12,41,77–79]. Moreover, changes in the hormonal balance, which is a part of the coping strategy consisting of an increase in the levels of ABA, JA, Et, and SA, and decrease in CKs, AUXs, and GAs, may also bring about photosynthesis inhibition, growth restriction, leaf senescence acceleration, and leaf fall, negatively affecting yield [32,34,80]. Therefore, there is a conflict between plant coping strategies (avoidance, tolerance) and resistance to drought essential for agricultural production. In the agricultural perspective, drought-resistant plants are those that maintain growth and stable yield during water-limited conditions. The priority in breeding research focusing on improving drought resistance is to obtain crop genotypes that can cope with drought stress without growth and yield reduction. Therefore, the research on plant stress physiology should concentrate on finding those features of coping strategies that ensure growth maintenance and stable yield (Table 1).

Many genes and processes involved in plants’ ability to cope and survive drought (*biological resistance*) in experiments conducted under laboratory conditions have been identified. However, the knowledge about their real function in the resistance to this stress, based on well-defined agronomic criteria (*agricultural resistance*), is rather poor [11,22,81,82]. It is hard to show the involvement of a particular trait or adjustment to drought in maintaining yield potential in a short-term experiment. The response to short-term drought conditions in soil pot experiments (limited rhizosphere) did not reflect the response to long-term water shortage in the field [83]. Drought resistance is the result of combined processes

that happen on different timescales and have a long-term impact on plant performance and yield. Short-term responses to drought include triggering physiological feedback processes responsible for stabilizing plant water and carbon status, which are often not correlated with the long-term effect. The favorable effects of these feedback strategies on yield depend on the drought scenario as well as on scalability and phenotypic distances between traits involved in particular coping strategies and those responsible for yield [28]. It is necessary to search for processes and adjustments that allow crops to continue to grow under water-limited conditions and rapid recovery after stress termination without yield reduction.

The source of traits valuable in developing new drought-resilient crop varieties may be wild genotypes and landraces originating from rainfed areas [3]. Another promising approach is the introduction of new crop species able to cope under water-limited conditions and maintain stable growth. An interesting species in this regard is quinoa (*Chenopodium quinoa* Willd.), which originated in the Andean region. It has begun to be called ‘the 21st century crop’, and recently it has been introduced into cultivation in many regions of the world. Quinoa has received special attention due to its high nutritional composition of seeds and strong natural ability to cope with drought [84,85]. There is wide diversity among quinoa genotypes in the traits of drought coping strategy (*biological resistance*) and resistance assessed based on the seed yields (*agricultural resistance*). The drought response mechanisms in quinoa to endure water deficits include accelerated root growth, high water-use efficiency (WUE), osmotic adjustment, turgor maintenance, increased synthesis of osmoprotectants such as amino acid proline, and soluble sugars (glucose, trehalose), ABA biosynthesis, antioxidant defense, heat-shock, and LEA protein synthesis [86]. Field studies have shown no significant yield reduction in the Danish quinoa cultivar Titicaca under water deficit conditions [84]. Soil pot experiments revealed that the capacity for growth in a drought-prone environment in ‘Titicaca’ was associated with the increase in WUE due to higher ABA concentration and nutrient content [87]. Recent studies revealed that drought resistance in quinoa var. Red Faro was due to elevated recovery capacities of PSII and PSI photochemical activities after re-watering [88]. There are numerous studies focused on molecular, biochemical, physiological, and morphological responses of varied quinoa genotypes to drought both under laboratory and field conditions. The sequencing of the quinoa genome creates the possibility of using new molecular tools to fully discover regulatory mechanisms involved in drought resistance of various quinoa genotypes [86].

A promising drought resistance strategy for crops is the ability to optimize water use, along with sustained high photosynthetic activity, which is an essential component of plant productivity [89]. It may be achieved by triggering varied metabolic and physiological responses of the dehydration avoidance strategy, which includes the modification of root conductivity and architecture, regulation of stomatal behavior allowing the maintenance of photosynthetic CO<sub>2</sub> fixation, as well as protection against non-stomatal photosynthesis limitation [90–92]. Plants with greater WUE assimilate more carbon per unit of transpired water. These plants are less susceptible to drought as they take less water from the soil and may access this water later in the season when a lack of water has become a limiting factor [79]. The improvement in WUE under water-limited conditions without trade-offs in carbon assimilation was revealed in transgenic tomato with overexpression of the gene encoding ABA biosynthesis enzyme (NCED3) as well as in *Arabidopsis* overexpressing ABA receptors [38,93]. The effect of increased ABA levels in roots and leaves of drought-stressed tomato lines was lower stomatal conductance and greater root conductivity [38]. However, ABA signaling-mediated changes in *Arabidopsis* transgenic lines affected reduced stomatal conductance, which was compensated by increased CO<sub>2</sub> gradients across stomata, allowing maintenance of a CO<sub>2</sub> influx [93]. These findings in *Arabidopsis* are being considered for translation to cereal crops to obtain drought-resistant genotypes through improving WUE [94,95]. A suitable criterion to measure WUE is carbon isotope discrimination ( $\Delta^{13}\text{C}$ ), which is used in breeding programs to select drought-resistant crop genotypes [76]. A significant positive relationship between  $\Delta^{13}\text{C}$  and yield was revealed in drought-stressed

quinoa cultivars under field conditions [86,96]. However, Tardieu [76] considers that  $\Delta^{13}\text{C}$  is a positive trait for yield under severe water deficit conditions but under mild to medium drought the positive traits that optimize yield are high stomatal conductance and growth maintenance.

Multiple biochemical and physiological changes that are components of drought coping strategies were revealed to have a favorable effect on yield (Table 1). Lower yield reduction under drought conditions was observed in a wheat cultivar that exhibited osmotic adjustment resulting from the accumulation of soluble sugars and proline as well as increased activity of enzymatic and non-enzymatic antioxidants. These changes allow for the maintenance of high photosynthetic  $\text{CO}_2$  fixation during drought and rapid recovery after re-watering, which are responsible for the final productivity [97]. Barley genotypes that yielded better under drought conditions exhibited increased expression of 34 genes which are involved in stress signaling, carbon metabolism, control of stomatal closure, proline synthesis, activation of the ROS scavenging system, and protective protein synthesis [82]. Elevated osmotic adjustment, increased expression of dehydrin genes, and a significant increase in alpha-tocopherol, which plays an important protective role for PSII, along with a higher photosynthetic rate, were observed in barley genotype, characterized by a smaller decrease in the performance index under drought stress conditions [98]. A large body of evidence has shown a beneficial role of proline in dealing with drought stress (*biological resistance*). Proline, involved in osmotic adjustment, is a free radical scavenger and acts as a compound that protects enzymes, proteins, and cell membranes against detrimental effects of dehydration and oxidative stress ([66,99] and references therein). It also serves as a carbon and nitrogen reserve after stress relief, and may act as a signaling molecule, able to activate defense responses [100]. Therefore, rapid proline accumulation at the beginning of drought stress may play an essential role in the dehydration avoidance strategy. Its increased level may also protect plants from the detrimental effect of dehydration (dehydration tolerance strategy), and it may be involved in the ability to recover after stress cessation. However, the involvement of this amino acid in the resistance to drought, understood as an adjustment without any negative effects on yield, is still not clear. The possible beneficial effect of greater leaf proline accumulation under drought on *agricultural resistance*, based on grain yield, was found in wheat [101]. Interesting results were obtained by Frimpong et al. [102], who observed that introgression barley lines, harboring a pyrroline-5-carboxylate synthase (*P5cs1*) allele, had markedly higher proline content in spikes and leaves, compared with other genotypes. These lines also showed milder drought symptoms, were able to maintain a high photosynthetic rate under drought, and achieved higher final seed production. Moreover, the barley near-isogenic line *NIL 143*, characterized by higher leaf and root proline content, showed less severe symptoms of drought, higher leaf water content, better stomatal conductance and net  $\text{CO}_2$  assimilation than other genotypes. This barley line also exhibited increased lateral root growth, probably due to high proline accumulation [103]. Considerable evidence obtained previously revealed that drought-stress-induced expression of proline biosynthetic genes is regulated by TFs related to almost all plant hormones [67].

One recently considered approach in attaining crop resistance to drought is focused on better understanding of the role of plant growth regulators (PGRs) in the coping strategy along with the mitigation of the negative effect of drought on productivity and yield. PGRs play an important role in triggering, directly or through specific signal cascades, a wide range of metabolic and physiological responses of plants to drought. Many of these responses, which are components of the drought stress coping strategy, are the result of positive or negative interactions between diverse PGRs [31,32,104]. Broadening knowledge about the impact of drought on the fluctuation of the level of PGRs and about the crosstalk between them in triggering appropriate responses seems to be essential in identifying components of drought coping strategies, which permit undisturbed growth and stable yield. The hormone that plays a key role in the plant response to drought is ABA, commonly called a “stress hormone”. An increased level of this PGR in drought-

stressed plants acts as a signal that regulates multiple responses at physiological and biochemical levels [10,50]. It was suggested that the interaction between plant hormones (ABA, AUXs, CKs, and ET) may play an important role in a diverse drought response of sensitive and resistant wheat lines [105]. The resistant wheat line was able to maintain growth and was characterized by lower yield reduction under drought. This line was temporarily anisohydric and closed the stomata only at a higher level of drought which correlated with the repression of ABA synthesis. At the same time, it had the ability to activate defense responses (ROS protection, LEA proteins, and cuticle synthesis) and to trigger expression of photosynthesis genes as well as genes involved in AUXs, CKs and Et metabolism, and signaling. However, the drought-sensitive wheat line was isohydric, had a higher ABA level, closed stomata at the start of stress and began photosynthesis inhibition. Certain recently obtained results of research focused on crosstalk between ABA, CKs, and BRs at physiological and molecular levels seem to be promising in finding drought coping strategies that prevent yield reduction [27,33]. ABA increase and the reduction in CK level under drought lead to a decrease in stomatal aperture and density, as well as accelerated leaf senescence, along with photosynthesis inhibition [32,106]. The manipulation of endogenous CK level and control of CK signaling pathway components in transgenic rice were effective in restoration of stomatal conductivity, reduction in leaf senescence, and amelioration of yield losses [32]. This transgenic rice also displayed increased expression of BR-related genes and repression of JA-related genes [107]. It was reported that BRs trigger the expression of various stress-related genes important in the maintenance of photosynthetic activity, stimulation of the antioxidant system, and accumulation of osmoprotectants [32,107,108]. Furthermore, overexpression of the BR receptor (BRL3) leads to activation of the synthesis of osmoprotectants (i.e., proline, trehalose, sucrose) in roots and overcoming growth arrest as well as modulating the root hydrotropic response during drought [27,37,104]. An interesting and promising mechanism leading to drought resistance appears to be the involvement of BRs in the expression of cell wall extension and release of enzymes, which lead to increased cell expansion [108]. The last several years of research have shown that crosstalk between BRs and other hormones is involved in the network of complex regulatory responses to drought, including stress perception and signaling leading to activation of various coping strategies [109]. Master regulators of abiotic stress responses whose expression is controlled by hormonal balance and crosstalk are TFs [110]. Gaining knowledge about the pattern of appropriate hormonal balance and crosstalk as well as identification of stress-responsive TFs and their role in activation of the components of the drought coping strategy without yield mortality is a powerful approach for achieving drought-resistant crop cultivars [3,62,111].

**Table 1.** Components of coping strategies and agricultural resistance in crops and model plants.

Plant Species/Genotypes	Stress Imposition Stress Level	Components of Coping Strategy	Agricultural Resistance	References
<i>Arabidopsis thaliana</i> transgenic line RCAR10-4	soil pot experiment water withholding 8 weeks severe stress RWC—not performed	increased expression of ABA receptor reduced stomatal conductance with maintenance of carbon assimilation overexpression of ABA biosynthesis of gene ( <i>NCED</i> )	improvement in WUE and growth	[93]
tomato transgenic line sp12	soil pot experiment water withholding at four- or five-leaf stage 5 days RWC—not performed	increased ABA level in root and leaves reduced stomatal conductance increased root hydraulic conductivity, water status improvement	improvement in WUE without trade-offs in carbon assimilation	[38]

Table 1. Cont.

Plant Species/Genotypes	Stress Imposition Stress Level	Components of Coping Strategy	Agricultural Resistance	References
wheat 'Luhan7'	soil pot experiment, irrigation withheld at tillering and jointing stage 10 days moderate stress RWC 85–89%	osmotic adjustment (proline, sugars) stomata closure activation of antioxidant system	high photosynthetic CO <sub>2</sub> fixation high drought index and harvest index	[97]
barley <i>H. vulgare</i> 'Martin' <i>H. spontaneum</i> HS41-1	soil pot experiment, water withholding at flowering stage 13 days severe stress RWC—not performed	high expression of signal transduction genes (TFs, CDPK, membrane binding proteins) and functional genes directly involved in coping strategy (stomatal behavior, synthesis of glycine-betaine, proline, antioxidants, dehydrins)	higher chlorophyll content and lower grain yield losses than in genotype without enhanced expression of coping strategy genes	[82]
barley 'Yousof' and 'Morocco'	soil pot experiment water withholding at two weeks seedling stress duration? mild stress RWC ~88%	high level of dehydrin and alpha-tocopherol involved in PSII protection in 'Yousof'	lower reduction in CO <sub>2</sub> assimilation rate and performance index in 'Yousof'	[98]
transgenic rice	soil pot experiment water withholding at pre-anthesis and post-anthesis 6–10 days mild stress RWC ~85%	increased CK synthesis, increased expression of BR related genes and repression of JA-related genes modification of source/sink relationships, a stronger sink capacity	higher grain yield with improved quality (nutrients and starch content)	[107]
wheat 'Zagros' and 'Marvdaht'	soil pot experiment soil moisture at about 50% of field capacity 31 days RWC—not performed	higher ABA and proline accumulation in 'Zagros' than 'Marvdaht'	higher harvest index and lower grain yield reduction in 'Zagros' than 'Marvdaht'	[101]
barley introgression lines with wild allele <i>p5cs1</i> - <i>S42IL-141</i> , <i>S42IL-141</i>	soil pot experiment reduction in irrigation at booting stage mild stress 15-day RWC ~83%	significantly higher spike and leaf proline level than other line	maintenance of high photosynthetic rate and inherent WUE, high final seed productivity	[102]
barley near-isogenic line with wild allele <i>P5cs1</i> - <i>NIL 143</i>	rhizoboxes filled with soil soil water content decreased from 40% at the beginning to 6% after 17 days (three-leaf seedling) severe stress RWC ~59%	higher root and shoot proline content than in other genotypes, less severe drought symptoms, better stomatal conductance, higher RWC, enhanced root growth	enhanced net assimilation rate	[103]
quinoa 'Titicaca'	field experiment soil pot experiment mild to severe RWC—not performed	ABA increase, high WUE	no yield reduction	[84,87]
quinoa 10 varieties	field experiment RWC—not performed	high carbon isotope discrimination	high yield	[96]

Table 1. Cont.

Plant Species/Genotypes	Stress Imposition Stress Level	Components of Coping Strategy	Agricultural Resistance	References
wheat drought-tolerant 'Halberd' drought-sensitive 'Cranbrook'	soil pot experiment growth chamber water withholding drought stress at the young microspore stage RWC—not performed	ABA increase, stomatal closure at the start of stress, inhibition of photosynthesis in 'Halberd' delayed stomatal closure and activation of defense response repression of ABA synthesis enrichment of genes involved in AUX, CK and ET metabolism/signaling in 'Cranbrook' increased CK level	lower yield reduction in 'Cranbrook'	[105]
transgenic <i>Oryza sativa</i> cotton	soil pot experiment in greenhouse and growth chamber irrigation reduction RWC—not performed	modifications of source/sink relationships delayed senescence increased expression of BR-related genes	improved grain yield and grain quality improved photosynthesis, biomass accumulation	[106,107]

## 5. Conclusions

Drought is the most frequent abiotic stress adversely affecting productivity of crop plants. As sessile organisms, plants have developed sophisticated regulatory mechanisms at molecular and physiological levels to cope with water scarcity conditions. These mechanisms are important for stress survival (*biological resistance*). However, activation of these mechanisms frequently does not prevent the negative effect of drought on growth and yields (*agricultural resistance*), which is important for plant users. Therefore, there is a need for continuous and extensive research expanding the knowledge required in breeding drought-resistant and high-yielding crop genotypes. The modern breeding technologies and biotechnological approaches aimed at developing crops resilient to drought with a high yield capacity should include genomic, molecular, and physiological research. It is crucial to determine the relationships between molecular, metabolic, and physiological changes involved in *biological resistance* to drought and *agricultural resistance* estimated using agronomic criteria (photosynthetic activity, growth traits, yield). At the molecular level, research based on marker-associated selection, genome-wide association studies, and genome selection with high throughput phenotyping are useful in identifying candidate genes and TFs effective for improving the resistance of crops to drought [3,28,104,112]. Currently used approaches to obtain drought resistance crops include the use of: (a) traditional breeding programs; (b) genetically modified plants; and (c) clustered regularly interspaced short palindromic repeats (CRISPR/Cas) editing strategy [4,113]. Presently, the new strategy with possible future application is the selection of epigenetic phenotypes with increased drought resistance [71].

A slightly different, non-genetic, approach for improving crop resistance to drought is the exogenous application of natural substances, including plant metabolites ([113] and references therein). The favorable effect of such metabolites on *biological resistance* has been demonstrated. It is reported in the literature that many of these metabolites are also involved in crop yield improvement under drought (*agricultural resistance*). It is a strategy that is easy and feasible to implement. However, the beneficial effects of application of this strategy depend on the concentration of the used compound, time of application, and crop species. The use of these metabolites by producers should be preceded by long-term experiments under field conditions in order to evaluate the dose, method, and time of application in different plant species as well as the cost of application in the field.

**Funding:** This publication was co-financed within the framework of the Polish Ministry of Science and Higher Education’s program: “Regional Initiative Excellence” in the years 2019–2022 (No.005/RID/2018/19).

**Conflicts of Interest:** The author declare no conflict of interest.

## References

1. Cramer, G.R.; Urano, K.; Delrot, S.; Pezzotti, M.; Shinozaki, K. Effects of abiotic stress on plants: A systems biology perspective. *BMC Plant Biol.* **2011**, *11*, 163. [[CrossRef](#)] [[PubMed](#)]
2. Farooq, M.; Wahid, A.; Kobayashi, N.; Fujita, D.; Basra, S.M.A. Plant drought stress: Effects, mechanisms and management. *Agron. Sustain. Dev.* **2009**, *29*, 185–212. [[CrossRef](#)]
3. Raza, A.; Razaq, A.; Mehmood, S.S.; Zou, X.; Zhang, X.; Lv, Y.; Xu, J. Impact of climate change on crops adaptation and strategies to tackle its outcome: A Review. *Plants* **2019**, *8*, 34. [[CrossRef](#)] [[PubMed](#)]
4. Imran, Q.M.; Falak, N.; Hussain, A.; Mun, B.-G.; Yun, B.-W. Abiotic stress in plants; stress perception to molecular response and role of biotechnological tools in stress resistance. *Agronomy* **2021**, *11*, 1579. [[CrossRef](#)]
5. Lambers, H.; Chapin III, F.S.; Pons, T.L. *Plant Physiological Ecology*, 2nd ed.; Springer Science + Business Media, LLC: New York, NY, USA, 2008; ISBN 978-0-387-78340-6.
6. Nuccio, M.; Paul, M.; Bate, N.J.; Cohn, J.; Cutler, S.R. Where are the drought tolerant crops? An assessment of more than two decades of plant biotechnology effort in crop improvement. *Plant Sci.* **2018**, *273*, 110–119. [[CrossRef](#)]
7. Yang, S.J.; Vanderbeld, B.; Wan, J.X.; Huang, Y.F. Narrowing down the targets: Towards successful genetic engineering of drought tolerant crops. *Mol. Plant* **2010**, *3*, 469–490. [[CrossRef](#)]
8. Hideg, E.; Jansen, M.A.K.; Strid, A. UV-B exposure, ROS, and stress: Inseparable companions or loosely linked associates? *Trends Plant Sci.* **2013**, *18*, 107–115. [[CrossRef](#)]
9. Keskitalo, J.; Bergquist, G.; Gardeström, P.; Jansson, S. A cellular timetable of autumn senescence. *Plant Physiol.* **2005**, *139*, 1635–1648. [[CrossRef](#)]
10. Basu, S.; Rabara, R. Abscisic acid—An enigma in the abiotic stress tolerance of crop plants. *Plant Gene* **2017**, *11*, 90–98. [[CrossRef](#)]
11. Dodd, I.C.; Ryan, A.C. Whole-plant physiological responses to water-deficit stress. In *eLS*; John Wiley & Sons, Ltd.: Chichester, UK, 2016. [[CrossRef](#)]
12. Dinakar, C.; Djilianov, D.; Bartels, D. Photosynthesis in desiccation tolerant plants: Energy metabolism and antioxidative stress defense. *Plant Sci.* **2012**, *182*, 29–41. [[CrossRef](#)]
13. Volaire, F. A unified framework of plant adaptive strategies to drought: Crossing scales and disciplines. *Glob. Change Biol.* **2018**, *24*, 2929–2938. [[CrossRef](#)] [[PubMed](#)]
14. Rojas, O. Agricultural extreme drought assessment at global level using FAO—Agricultural stress index system (ASIS). *Weather Clim. Extrem.* **2020**, *27*, 100184. [[CrossRef](#)]
15. Claeys, H.; Inzé, D. The agony of choice: How plants balance growth and survival under water-limiting conditions. *Plant Physiol.* **2013**, *162*, 1768–1779. [[CrossRef](#)] [[PubMed](#)]
16. Taiz, L.; Zeiger, E. *Plant Physiology*, 4th ed.; Sinauer Associates Inc.: Sunderland, MA, USA, 2010; ISBN 0-87893-856-7.
17. Laxa, M.; Liebthal, M.; Telman, W.; Chibani, K.; Dietz, K.-J. The role of the plant antioxidant system in drought tolerance. *Antioxidants* **2019**, *8*, 94. [[CrossRef](#)]
18. Tardieu, F.; Simonneau, T. Variability among species of stomatal control under fluctuating soil water status and evaporative demand: Modelling isohydric and anisohydric behaviours. *J. Exp. Bot.* **1998**, *49*, 419–432. [[CrossRef](#)]
19. Maseda, P.H.; Fernández, R.J. Stay wet or else: Three ways in which plants can adjust hydraulically to their environment. *J. Exp. Bot.* **2006**, *57*, 3963–3977. [[CrossRef](#)]
20. Sade, N.; Gebremedhin, A.; Moshelion, M. Risk-taking plants: Anisohydric behavior as a stress-resistance trait. *Plant Signal. Behav.* **2012**, *7*, 767–770. [[CrossRef](#)]
21. Skelton, R.P.; West, A.G.; Dawson, T.E. Predicting plant vulnerability to drought in biodiverse regions using functional traits. *Proc. Natl. Acad. Sci. USA* **2015**, *112*, 5744–5749. [[CrossRef](#)]
22. Takahashi, F.; Kuromori, T.; Sato, H.; Shinozaki, K. Regulatory gene networks in drought stress responses and resistance in plants. In *Survival Strategies in Extreme Cold and Desiccation. Advances in Experimental Medicine and Biology*; Iwaya-Inoue, M., Sakurai, M., Uemura, M., Eds.; Springer: Singapore, 2018; Volume 1081.
23. Verslues, P.E.; Zhu, J.-K. Before and beyond ABA: Upstream sensing and internal signals that determine ABA accumulation and response under abiotic stress. *Biochem. Soc. Trans.* **2005**, *33*, 375–379. [[CrossRef](#)]
24. Schachtman, D.P.; Goodger, J.Q.D. Chemical root to shoot signaling under drought. *Trends Plant Sci.* **2008**, *13*, 281–287. [[CrossRef](#)]
25. McAdam, S.A.N.; Brodribb, T.J.; Ross, J.J. Shoot derived abscisic acid promotes root growth. *Plant Cell Environ.* **2016**, *39*, 652–659. [[CrossRef](#)] [[PubMed](#)]
26. Castro, P.; Puértolas, J.; Dodd, I. Stem girdling uncouples soybean stomatal conductance from leaf water potential by enhancing leaf xylem ABA concentration. *Environ. Exp. Bot.* **2018**, *159*, 149–156. [[CrossRef](#)]
27. Gupta, A.; Rico-Medina, A.; Caño-Delgado, A.I. The physiology of plant responses to drought. *Science* **2020**, *368*, 266–269. [[CrossRef](#)] [[PubMed](#)]

28. Tardieu, F.; Simonneau, T.; Muller, B. The physiological basis of drought tolerance in crop plants: A scenario-dependent probabilistic approach. *Annu. Rev. Plant Biol.* **2018**, *69*, 733–759. [[CrossRef](#)]
29. Gallé, Á.; Csiszár, J.; Benyó, D.; Laskay, G.; Leviczky, T.; Erdei, L.; Tari, I. Isohydic and anisohydic strategies of wheat genotypes under osmotic stress: Biosynthesis and function of ABA in stress responses. *J. Plant Physiol.* **2013**, *170*, 1389–1399. [[CrossRef](#)]
30. Sharp, R.E.; Poroyko, V.; Hejlek, L.G.; Spollen, W.G.; Springer, G.K.; Bohnert, H.J.; Nguyen, H.T. Root growth maintenance during water deficits: Physiology to functional genomics. *J. Exp. Bot.* **2004**, *55*, 2343–2351. [[CrossRef](#)]
31. Verma, V.; Ravindran, P.; Kumar, P.P. Plant hormone-mediated regulation of stress responses. *BMC Plant Biol.* **2016**, *16*, 86. [[CrossRef](#)]
32. Peleg, Z.; Blumwald, E. Hormone balance and abiotic stress tolerance in crop plants. *Curr. Opin. Plant Biol.* **2011**, *14*, 290–295. [[CrossRef](#)]
33. Hai, N.N.; Chuong, N.N.; Tu, N.H.; Kisiala, A.; Hoang, X.L.T.; Thao, N.P. Role and regulation of cytokinins in plant response to drought stress. *Plants* **2020**, *9*, 422. [[CrossRef](#)]
34. Ciura, J.; Kruk, J. Phytohormones as targets for improving plant productivity and stress tolerance. *J. Plant Physiol.* **2018**, *229*, 32–40. [[CrossRef](#)]
35. Spollen, W.G.; LeNoble, M.E.; Samuels, T.D.; Bernstein, N.; Sharp, R.E. Abscisic acid accumulation maintains maize primary root elongations at low water potentials by restricting ethylene production. *Plant Physiol.* **2000**, *122*, 967–976. [[CrossRef](#)] [[PubMed](#)]
36. Ogura, T.; Goeschl, C.; Filiault, D.; Mírea, M.; Slovak, R.; Wolhrab, B.; Satbahai, S.B.; Busch, W. Root system depth in Arabidopsis is shaped by EXOCYST70A3 via the dynamic modulation of auxin transport. *Cell* **2019**, *178*, 400–412. [[CrossRef](#)] [[PubMed](#)]
37. Fábregas, N.; Lozano-Elena, F.; Blasco-Escámez, D.; Tohge, T.; Martínez-Andújar, C.; Albacete, A.; Osorio, S.; Bustamante, M.; Riechmann, J.L.; Nomura, T.; et al. Overexpression of the vascular brassinosteroid receptor BRL3 confers drought resistance without penalizing plant growth. *Nat. Commun.* **2018**, *9*, 4680. [[CrossRef](#)] [[PubMed](#)]
38. Thompson, A.J.; Andrews, J.; Mulholland, B.J.; McKee, J.M.T.; Hilton, H.W.; Horridge, J.S.; Farquhar, G.D.; Smeeton, R.C.; Smillie, I.R.A.; Black, C.R.; et al. Overproduction of abscisic acid in tomato increases transpiration efficiency and root hydraulic conductivity and influences leaf expansion. *Plant Physiol.* **2007**, *143*, 1905–1917. [[CrossRef](#)] [[PubMed](#)]
39. Aroca, R.; Porcel, R.; Ruiz-Lozano, J.M. Regulation of root water uptake under abiotic stress conditions. *J. Exp. Bot.* **2012**, *63*, 43–57. [[CrossRef](#)] [[PubMed](#)]
40. Blum, A. Towards a conceptual ABA ideotype in plant breeding for water limited environments. *Funct. Plant Biol.* **2015**, *42*, 502–513. [[CrossRef](#)] [[PubMed](#)]
41. Cruz de Carvalho, H.M. Drought stress and reactive oxygen species: Production, scavenging and signalling. *Plant Signal Behav.* **2008**, *3*, 156–165. [[CrossRef](#)]
42. Brodribb, T.J.; McAdam, S.A. Abscisic acid mediates a divergence in the drought response of two conifers. *Plant Physiol.* **2013**, *162*, 1370–1377. [[CrossRef](#)]
43. Vandeleur, R.K.; Mayo, G.; Shelden, M.C.; Gilliam, M.; Kaiser, B.N.; Tyerman, S.D. The role of plasma membrane intrinsic protein aquaporins in water transport through roots: Diurnal and drought stress responses reveal different strategies between isohydic and anisohydic cultivars of grapevine. *Plant Physiol.* **2009**, *149*, 445–460. [[CrossRef](#)]
44. Sharipova, G.; Ivanov, R.; Veselov, D.; Akhiyarova, G.; Shishova, M.; Nuzhnaya, T.; Kdoyarova, G. Involvement of reactive oxygen species in ABA-induced increase in hydraulic conductivity and aquaporin abundance. *Int. J. Mol. Sci.* **2021**, *22*, 9144. [[CrossRef](#)]
45. Ahmed, S.; Kouser, S.; Asgher, M.; Gandhi, S.G. Plant aquaporins: A frontward to make crop plants drought resistant. *Physiol. Plant.* **2021**, *172*, 1089–1105. [[CrossRef](#)] [[PubMed](#)]
46. Sharma, P.; Bhushan, A.; Rama, J.; Dubey, S.; Pessarakli, M. Reactive oxygen species, oxidative damage, and antioxidative defense mechanism in plants under stressful conditions. *J. Bot.* **2012**, *2012*, 217037. [[CrossRef](#)]
47. Bajji, M.; Kinet, J.-M.; Lutts, S. The use of electrolyte leakage method for assessing cell membrane stability as a water stress tolerance test in durum wheat. *Plant Growth Regul.* **2002**, *36*, 61–70. [[CrossRef](#)]
48. Blum, A.; Tuberosa, R. Dehydration survival of crop plants and its measurement. *J. Exp. Bot.* **2018**, *69*, 975–981. [[CrossRef](#)]
49. Rajashekar, G.; Jawahar, G.; Jalaja, N.; Kumar, S.A.; Kumari, P.H.; Punita, D.L.; Karumanchi, A.R.; Palakolanu, S.R.; Polavarapu, R.; Sreenivasulu, N.; et al. Chapter 27—Role and Regulation of Osmolytes and ABA Interaction in Salt and Drought Stress Tolerance. In *Plant Signaling Molecules*; Khan, M.I.R., Reddy, P.S., Ferrante, A., Khan, N.A., Eds.; Woodhead Publishing: Sawston, UK, 2019; pp. 417–436. [[CrossRef](#)]
50. Cardoso, A.A.; Gori, A.; Da-Silva, C.J.; Brunetti, C. Abscisic acid biosynthesis and signaling in plants: Key targets to improve water use efficiency and drought tolerance. *Appl. Sci.* **2020**, *10*, 6322. [[CrossRef](#)]
51. Bernardo, S.; Dinis, L.T.; Machado, N.; Moutinho-Pereira, J. Grapevine abiotic stress assessment and search for sustainable adaptation strategies in Mediterranean-like climates. A review. *Agron. Sustain. Dev.* **2018**, *38*, 66. [[CrossRef](#)]
52. Gómez, R.; Vicino, P.; Carrillo, N.; Lodeyro, A.F. Manipulation of oxidative stress responses as a strategy to generate stress-tolerant crops. From damage to signaling to tolerance. *Crit. Rev. Biotechnol.* **2019**, *39*, 693–708. [[CrossRef](#)]
53. Nadarajah, K.K. ROS Homeostasis in abiotic stress tolerance in plants. *Int. J. Mol. Sci.* **2020**, *21*, 5208. [[CrossRef](#)]
54. You, J.; Chan, Z. ROS regulation during abiotic stress responses in crop plants. *Front. Plant Sci.* **2015**, *6*, 1092. [[CrossRef](#)]
55. Meena, M.; Divyanshu, K.; Kumar, S.; Swapnil, P.; Zehra, A.; Shukla, V.; Yadav, M.; Upadhyay, R.S. Regulation of L-proline biosynthesis, signal transduction, transport, accumulation and its vital role in plants during variable environmental conditions. *Heliyon* **2019**, *5*, e02952. [[CrossRef](#)]

56. Anjum, S.A.; Wang, L.; Farooq, M.; Khan, I.; Xue, L. Methyl jasmonate-induced alteration in lipid peroxidation, antioxidative defence system and yield in soybean under drought. *J. Agron. Crop Sci.* **2011**, *197*, 296–301. [\[CrossRef\]](#)
57. Bandurska, H. Salicylic acid: An update on biosynthesis and action in plant response to water deficit and performance under drought. In *Salicylic Acid Plant Growth and Development*; Hayat, A., Ahmad, A., Alyemeni, M.N., Eds.; Springer: Dordrecht, The Netherlands; Heidelberg, Germany; New York, NY, USA; London, UK, 2013; pp. 1–14.
58. Chaudhry, S.; Sidhu, G.P.S. Climate change regulated abiotic stress mechanisms in plants: A comprehensive review. *Plant Cell Rep.* **2022**, *41*, 1–31. [\[CrossRef\]](#)
59. Duan, Z.-Q.; Bai, L.; Zhao, Z.-G.; Zhang, G.-P.; Cheng, F.-M.; Jiang, L.-X.; Chen, K.-M. Drought-stimulated activity of plasma membrane nicotinamide adenine dinucleotide phosphate oxidase and its catalytic properties in rice. *J. Integr. Plant Biol.* **2009**, *51*, 1104–1115. [\[CrossRef\]](#)
60. Wen, F.; Qin, T.; Wang, Y.; Dong, W.; Zhang, A.; Tan, M.; Jiang, M. OsHK3 is a crucial regulator of abscisic acid signaling involved in antioxidant defense in rice. *J. Integr. Plant Biol.* **2015**, *57*, 213–228. [\[CrossRef\]](#)
61. Takahashi, F.; Kuromori, T.; Urano, K.; Yamaguchi-Shinozaki, K.; Shinozaki, K. Drought stress responses and resistance in plants: From cellular responses to long-distance intercellular communication. *Front. Plant Sci.* **2020**, *11*, 556972. [\[CrossRef\]](#)
62. Mahmood, T.; Khalid, S.; Abdullah, M.; Ahmed, Z.; Shah, M.K.N.; Ghafoor, A.; Du, X. Insights into drought stress signaling in plants and the molecular genetic basis of cotton drought tolerance. *Cells* **2020**, *9*, 105. [\[CrossRef\]](#)
63. Abhilasha, A.; Choudhury, R.S. Molecular and physiological perspectives of abscisic acid mediated drought adjustment strategies. *Plants* **2021**, *10*, 2769. [\[CrossRef\]](#)
64. Ullah, A.; Sun, H.; Yang, X.; Zhang, X. Drought coping strategies in cotton: Increased crop per drop. *Plant Biotechnol. J.* **2017**, *15*, 271–284. [\[CrossRef\]](#)
65. Per, T.S.; Khan, N.A.; Reddy, P.S.; Masood, A.; Hasanuzzaman, M.; Khan, M.I.R.; Anjum, N.A. Approaches in modulating proline metabolism in plants for salt and drought stress tolerance: Phytohormones, mineral nutrients and transgenics. *Plant Physiol. Biochem.* **2017**, *115*, 126–140. [\[CrossRef\]](#)
66. Szabados, L.; Savouré, A. Proline: Multifunctional amino acid. *Trends Plant Sci.* **2010**, *15*, 89–97. [\[CrossRef\]](#)
67. Zarattini, M.; Forlani, G. Toward unveiling the mechanisms for transcriptional regulation of proline biosynthesis in the plant cell response to biotic and abiotic stress conditions. *Front. Plant Sci.* **2017**, *8*, 927. [\[CrossRef\]](#)
68. Kakoulidou, I.; Avramidou, E.V.; Baránek, M.; Brunel-Muguet, S.; Farrona, S.; Johannes, F.; Kaiserli, E.; Lieberman-Lazarovich, M.; Martinelli, F.; Mladenov, V.; et al. Epigenetics for crop improvement in times of global change. *Biology* **2021**, *10*, 766. [\[CrossRef\]](#)
69. Mozgova, I.; Mikulski, P.; Pecinka, A.; Farrona, S. Epigenetic mechanisms of abiotic stress response and memory in plants. In *Epigenetics in Plants of Agronomic Importance: Fundamentals and Applications*; Springer: Berlin/Heidelberg, Germany, 2019; pp. 1–64. [\[CrossRef\]](#)
70. Miryeganeh, M. Plants' Epigenetic mechanisms and abiotic stress. *Genes* **2021**, *12*, 1106. [\[CrossRef\]](#)
71. Sun, C.; Ali, K.; Yan, K.; Fiaz, S.; Dormatey, R.; Bi, Z.; Bai, J. Exploration of Epigenetics for improvement of drought and other stress resistance in crops: A Review. *Plants* **2021**, *10*, 1226. [\[CrossRef\]](#)
72. Zhang, C.Y.; Wang, N.N.; Zhang, Y.H.; Feng, Q.Z.; Yang, C.W.; Liu, B. DNA methylation involved in proline accumulation in response to osmotic stress in rice (*Oryza sativa*). *Genet. Mol. Res.* **2013**, *12*, 1269–1277. [\[CrossRef\]](#)
73. Chang, Y.N.; Zhu, C.; Jiang, J.; Zhang, H.; Zhu, J.K.; Duan, C.G. Epigenetic regulation in plant abiotic stress responses. *J. Integr. Plant Biol.* **2020**, *62*, 563–580. [\[CrossRef\]](#)
74. Thiebaut, F.; Hemerly, A.S.; Ferreira, P.C.G. A Role for epigenetic regulation in the adaptation and stress responses of non-model plants. *Front. Plant Sci.* **2019**, *10*, 246. [\[CrossRef\]](#)
75. Rodrigues, J.; Inzé, D.; Nelissen, H.; Saibo, N.J.M. Source–sink regulation in crops under water deficit. *Trends Plant Sci.* **2019**, *24*, 652–663. [\[CrossRef\]](#)
76. Tardieu, F. Any trait or trait-related allele can confer drought tolerance: Just design the right drought scenario. *J. Exp. Bot.* **2012**, *63*, 25–31. [\[CrossRef\]](#)
77. Flexas, J.; Bota, J.; Loreto, F.; Cornic, G.; Sharkey, T. Diffusive and metabolic limitations to photosynthesis under drought and salinity in C3 plants. *Plant Biol.* **2004**, *6*, 269–279. [\[CrossRef\]](#)
78. Flexas, J.; Ribas-Carbó, M.; Bot, J.; Galmés, J.; Henkle, M.; Martínez-Cañellas, S.; Medrano, H. Decreased Rubisco activity during water stress is not induced by decreased relative water content but related to conditions of low stomatal conductance and chloroplast CO<sub>2</sub> concentration. *New Phytol.* **2006**, *172*, 73–82. [\[CrossRef\]](#) [\[PubMed\]](#)
79. Gilliham, M.; Able, J.A.; Roy, S.J. Translating knowledge about abiotic stress tolerance to breeding programmes. *Plant J.* **2017**, *90*, 898–917. [\[CrossRef\]](#)
80. Munné-Bosch, S.; Leonor, A. Die and let live: Leaf senescence contributes to plant survival under drought stress. *Funct. Plant Biol.* **2004**, *31*, 203–216. [\[CrossRef\]](#) [\[PubMed\]](#)
81. Obidiegwu, J.E.; Bryan, G.J.; Jones, H.G.; Prashar, A. Coping with drought: Stress and adaptive responses in potato and perspectives for improvement. *Front. Plant Sci.* **2015**, *6*, 542. [\[CrossRef\]](#) [\[PubMed\]](#)
82. Guo, P.G.; Baum, M.; Grando, S.; Ceccarelli, S.; Bai, G.; Li, R.; von Korff, M.; Varshney, R.K.; Graner, A.; Volkoun, J. Differentially expressed genes between drought-tolerant and drought-sensitive barley genotypes in response to drought stress during the reproductive stage. *J. Exp. Bot.* **2009**, *60*, 3531–3544. [\[CrossRef\]](#)

83. Perlikowski, D.; Kosmala, A. Mechanisms of drought resistance in introgression forms of *Lolium multiflorum*/*Festuca arundinacea*. *Biol. Plant.* **2020**, *64*, 497–503. [[CrossRef](#)]
84. Pulvento, C.; Riccardi, M.; Lavini, A.; Iafelice, G.; Marconi, E.; d’Andria, R. Yield and quality characteristics of quinoa grown in open field under different saline and non-saline irrigation regimes. *J. Agron. Crop Sci.* **2012**, *198*, 254–263. [[CrossRef](#)]
85. Zurita-Silva, A.; Fuentes, F.; Zamora, P.; Jacobsen, S.-E.; Schwember, A.R. Breeding quinoa (*Chenopodium quinoa* Willd.): Potential and perspectives. *Mol. Breed.* **2014**, *34*, 13–30. [[CrossRef](#)]
86. Hinojosa, L.; González, J.A.; Barrios-Masias, F.H.; Fuentes, F.; Murphy, K.M. Quinoa abiotic stress responses: A review. *Plants* **2018**, *7*, 106. [[CrossRef](#)]
87. Yang, A.; Akhtar, S.S.; Amjad, M.; Iqbal, S.; Jacobsen, S.-E. Growth and physiological responses of quinoa to drought and temperature stress. *J. Agron. Crop Sci.* **2016**, *202*, 445–453. [[CrossRef](#)]
88. Manaa, A.; Goussi, R.; Derbali, W.; Cantamessa, S.; Essemine, J.; Barbato, R. Photosynthetic performance of quinoa (*Chenopodium quinoa* Willd.) after exposure to a gradual drought stress followed by a recovery period. *Biochim. Biophys. Acta (BBA) Bioenerg.* **2021**, *1862*, 148383. [[CrossRef](#)] [[PubMed](#)]
89. Simkin, A.J.; López-Calcano, P.E.; Raines, C.A. Feeding the world: Improving photosynthetic efficiency for sustainable crop production. *J. Exp. Bot.* **2019**, *70*, 1119–1140. [[CrossRef](#)] [[PubMed](#)]
90. Blum, A. Osmotic adjustment is a prime drought stress adaptive engine in support of plant production. *Plant Cell Environ.* **2017**, *40*, 4–10. [[CrossRef](#)]
91. Ruggiero, A.; Punzo, P.; Landi, S.; Costa, A.; Van Oosten, M.J.; Grillo, S. Improving plant water use efficiency through molecular genetics. *Horticulturae* **2017**, *3*, 31. [[CrossRef](#)]
92. Turner, N.C. Turgor maintenance by osmotic adjustment: 40 years of progress. *J. Exp. Bot.* **2018**, *69*, 3223–3233. [[CrossRef](#)]
93. Yang, Z.; Liu, J.; Tischer, S.V.; Christmann, A.; Windisch, W.; Schnyder, H.; Grill, E. Leveraging abscisic acid receptors for efficient water use in Arabidopsis. *Proc. Natl. Acad. Sci. USA* **2016**, *113*, 6791–6796. [[CrossRef](#)]
94. Dresselhaus, T.; Hückelhoven, R. Biotic and abiotic stress responses in crop plants. *Agronomy* **2018**, *8*, 267. [[CrossRef](#)]
95. Blankenagel, S.; Yang, Z.; Avramova, V.; Schön, C.-C.; Grill, E. Generating plants with improved water use efficiency. *Agronomy* **2018**, *8*, 194. [[CrossRef](#)]
96. González, J.A.; Bruno, M.; Valoy, M.; Prado, F.E. Genotypic variation of gas exchange parameters and leaf stable carbon and nitrogen isotopes in ten quinoa cultivars grown under drought. *J. Agron. Crop Sci.* **2011**, *197*, 81–93. [[CrossRef](#)]
97. Abid, M.; Ali, S.; Qi, L.K.; Zahoor, R.; Tian, Z.; Jiang, D.; Snider, J.L.; Dai, T. Physiological and biochemical changes during drought and recovery periods at tillering and jointing stages in wheat (*Triticum aestivum* L.). *Sci. Rep.* **2018**, *8*, 4615. [[CrossRef](#)]
98. Ghotbi-Ravandi, A.A.; Shahbazi, M.; Shariati, M.; Mulo, P. Effects of mild and severe drought stress on photosynthetic efficiency in tolerant and susceptible barley (*Hordeum vulgare* L.) genotypes. *J. Agron. Crop Sci.* **2014**, *200*, 403–415. [[CrossRef](#)]
99. Kavi Kishor, P.B.; Sreenivasulu, N. Is proline accumulation *per se* correlated with stress tolerance or is proline homeostasis a more critical issue? *Plant Cell Environ.* **2014**, *37*, 300–311. [[CrossRef](#)] [[PubMed](#)]
100. Hare, P.D.; Cress, W.A. Metabolic implications of stress-induced proline accumulation in plants. *Plant Growth Regul.* **1997**, *21*, 79–102. [[CrossRef](#)]
101. Saeedipour, S. Relationship of grain yield, ABA and proline accumulation in tolerant and sensitive wheat cultivars as affected by water stress. *Proc. Natl. Acad. Sci. India Sect. B Biol. Sci.* **2013**, *83*, 311–315. [[CrossRef](#)]
102. Frimpong, F.; Windt, C.W.; van Dusschoten, D.; Naz, A.A.; Frei, M.; Fiorani, F. A wild allele of pyrroline-5-carboxylate synthase1 leads to proline accumulation in spikes and leaves of barley contributing to improved performance under reduced water availability. *Front. Plant Sci.* **2021**, *12*, 633448. [[CrossRef](#)]
103. Frimpong, F.; Anokye, M.; Windt, C.W.; Naz, A.A.; Frei, M.; van Dusschoten, D.; Fiorani, F. Proline mediated drought tolerance in the barley (*Hordeum vulgare* L.) isogenic line is associated with lateral root growth at the early seedlings stage. *Plants* **2021**, *10*, 2177. [[CrossRef](#)]
104. Kundu, S.; Gantait, S. Abscisic acid signal crosstalk during abiotic stress response. *Plant Gene* **2017**, *11*, 61–69. [[CrossRef](#)]
105. Onyemaobi, O.; Sangma, H.; Garg, G.; Wallace, X.; Kleven, S.; Suwanchaikasem, P.; Roessner, U.; Dolferus, R. Reproductive stage drought tolerance in wheat: Importance of stomatal conductance and plant growth regulators. *Genes* **2021**, *12*, 1742. [[CrossRef](#)]
106. Kuppu, S.; Mishra, N.; Hu, R.; Sun, L.; Zhu, X.; Blumwald, E.; Payton, P.; Zhang, H. Water-deficit inducible expression of a cytokinin biosynthetic gene *IPT* improves drought tolerance in cotton. *PLoS ONE* **2013**, *8*, e64190. [[CrossRef](#)]
107. Peleg, Z.; Reguera, M.; Tumimbang, E.; Walia, H.; Blumwald, E. Cytokinin-mediated source/sink modifications improve drought tolerance and increase grain yield in rice under water-stress. *Plant Biotechnol. J.* **2011**, *9*, 747–758. [[CrossRef](#)]
108. Sharma, I.; Kaur, N.; Pati, P.K. Brassinosteroids: A promising option in deciphering remedial strategies for abiotic stress tolerance in rice. *Front. Plant Sci.* **2017**, *8*, 2151. [[CrossRef](#)] [[PubMed](#)]
109. Nolan, T.M.; Vukašinović, N.; Liu, D.; Russinova, E.; Yanhai, Y. Brassinosteroids: Multidimensional regulators of plant growth, development, and stress responses. *Plant Cell* **2020**, *32*, 295–318. [[CrossRef](#)] [[PubMed](#)]
110. Hrmova, M.; Hussain, S.S. Plant transcription factors involved in drought and associated stresses. *Int. J. Mol. Sci.* **2021**, *22*, 5662. [[CrossRef](#)] [[PubMed](#)]
111. Hoang, X.; Nhi, D.; Thu, N.; Thao, N.P.; Tran, L.P. Transcription factors and their roles in signal transduction in plants under abiotic stresses. *Curr. Genom.* **2017**, *18*, 483–497. [[CrossRef](#)] [[PubMed](#)]

112. Younis, A.; Ramzan, F.; Ramzan, Y.; Zulfiqar, F.; Ahsan, M.; Lim, K.B. Molecular markers improve abiotic stress tolerance in crops: A Review. *Plants* **2020**, *9*, 1374. [[CrossRef](#)]
113. Godoy, F.; Olivos-Hernández, K.; Stange, C.; Handford, M. Abiotic stress in crop species: Improving tolerance by applying plant metabolites. *Plants* **2021**, *10*, 186. [[CrossRef](#)]



## Article

# Mycorrhized Wheat Plants and Nitrogen Assimilation in Coexistence and Antagonism with Spontaneous Colonization of Pathogenic and Saprophytic Fungi in a Soil of Low Fertility

Catello Di Martino <sup>1,\*</sup>, Valentina Torino <sup>1</sup>, Pasqualino Minotti <sup>1</sup>, Laura Pietrantonio <sup>2</sup>, Carmine Del Grosso <sup>1</sup>, Davide Palmieri <sup>1</sup>, Giuseppe Palumbo <sup>1</sup>, Thomas W. Crawford, Jr. <sup>3</sup> and Simona Carfagna <sup>4</sup>

- <sup>1</sup> Department of Agriculture, Environmental and Food Sciences, University of Molise, Via De Sanctis, 86100 Campobasso, Italy; v.torino@studenti.unimol.it (V.T.); minottipasqualino@gmail.com (P.M.); c.delgrosso2@studenti.unimol.it (C.D.G.); davide.palmieri@unimol.it (D.P.); palumbo@unimol.it (G.P.)
- <sup>2</sup> MS Biotech SpA, c.da Piane di Larino, 35, 86035 Larino, Italy; laura.pietrantonio@msbiotech.net
- <sup>3</sup> Global Agronomy, LLC, Marana, AZ 85658, USA; globalagronomy@gmail.com
- <sup>4</sup> Dipartimento di Biologia, Università degli Studi di Napoli Federico II, 80126 Napoli, Italy; simona.carfagna@unina.it
- \* Correspondence: lello.dimartino@unimol.it; Tel.: +39-0874404692

**Abstract:** The aim of the work was to study the biological interference of the spontaneous colonization of pathogenic and saprophytic endophytes on the nitrogen assimilation of mycorrhized wheat plants cultivated in soils deficient in N and P. The nitrogen assimilation efficiency of mycorrhized plants was determined by measuring the activities of nitrate reductase assimilatory and glutamine synthetase enzymes and free amino acid patterns. Mycorrhizal plants at two different sites showed an assimilative activity of nitrate and ammonium approximately 30% greater than control plants. This activity was associated with significant increases in the amino acids Arg, Glu Gln and Orn in the roots where those amino acids are part of the inorganic nitrogen assimilation of mycorrhizal fungi. The nutrient supply of mycorrhizal fungi at the root guaranteed the increased growth of the plant that was about 40% greater in fresh weight and 25% greater in productive yield than the controls. To better understand the biological interaction between plant and fungus, microbiological screening was carried out to identify colonies of radicular endophytic fungi. Fourteen fungal strains belonging to nine different species were classified. Among pathogenic fungi, the genus *Fusarium* was present in all the examined roots with different frequencies, depending on the site and the fungal population present in the roots, providing useful clues regarding the principle of spatial conflict and fungal spread within the root system.

**Keywords:** amino acids; nitrate reductase; glutamine synthetase; plants mycorrhized; dark septate

**Citation:** Di Martino, C.; Torino, V.; Minotti, P.; Pietrantonio, L.; Del Grosso, C.; Palmieri, D.; Palumbo, G.; Crawford, T.W., Jr.; Carfagna, S. Mycorrhized Wheat Plants and Nitrogen Assimilation in Coexistence and Antagonism with Spontaneous Colonization of Pathogenic and Saprophytic Fungi in a Soil of Low Fertility. *Plants* **2022**, *11*, 924. <https://doi.org/10.3390/plants11070924>

Academic Editors: Milan S. Stankovic, Paula Baptista and Petronia Carillo

Received: 24 February 2022

Accepted: 27 March 2022

Published: 29 March 2022

**Publisher's Note:** MDPI stays neutral with regard to jurisdictional claims in published maps and institutional affiliations.



**Copyright:** © 2022 by the authors. Licensee MDPI, Basel, Switzerland. This article is an open access article distributed under the terms and conditions of the Creative Commons Attribution (CC BY) license (<https://creativecommons.org/licenses/by/4.0/>).

## 1. Introduction

About 80% of terrestrial plant roots are closely associated with mycorrhizal fungi [1], and many aspects of the physio-ecological roles played by these mycorrhizal fungi, such as plant nutrition, soil biology and soil chemistry, are well described [2]. The cytological interaction between fungus and root occurs at the interface between the plasma membranes of the arbuscular and cortical cells. Through these contact surfaces, nutritional exchanges take place between the plant that supply the fungus with carbonaceous skeletons and the fungus that transfers the mineral nutrients to the plant [3,4]. It has been reported that phosphate deficiency in soil stimulates mycorrhizal colonization [5]. The suppression of mycorrhizae arises from the high concentration of P and from other mineral nutrients present in the soil. In addition, a limitation of nitrogen in the soil also stimulates root colonization by mycorrhizal fungi [6]. Moreover, mycorrhizal fungi are implicated in absorbing inorganic nitrogen from the soil and moving it to the roots to be partly assimilated

by the root and partly by the leaves into organic nitrogen compounds. In both the roots and the leaves, the reduction of nitrate and the subsequent assimilation of ammonium require a significant energy quotient to generate organic N compounds through the consumption of the reduction equivalents of nicotinamide adenine dinucleotide (NAD(P)H) and adenosine triphosphate (ATP).

In mycorrhizae, nitrate is absorbed by the extra-radical hyphae and is then reduced to ammonium by nitrate reductase assimilatory (NRA) enzyme via the fugin metabolic pathway [7,8]. Ammonium absorbed from the soil or generated by nitrate reduction is the nitrogen substrate of two metabolic pathways: Glutamine synthetase (GS) and Glutamine-2-oxoglutarate aminotransferase (GOGAT) [9]. The glutamate (Glu) produced is quickly converted to arginine (Arg) that is then transferred into the intraradical mycelium. The disintegration of Arg releases  $\text{NH}_4^+$  from the arbuscules to the root cortex cells, which assimilate it through the GS/GOGAT pathway [10,11].

The roots of plants and mycorrhizae can also be colonized by the endophytic fungi, such as *Tricoderma* species, and dark septate fungi present in the rhizosphere. Interactions between plants and endophytic fungi in the roots do not always benefit the host. It is essential to clarify some fundamental concepts of phytopathology. When a plant and another organism come into contact, the interaction can be beneficial, harmless or harmful. Beneficial interactions, such as mutualism (each organism benefits from the association) and commensalism (all organisms in association are mutually beneficial), can be a source of great opportunity. Organisms involved in mutualism or commensalism can promote plant growth, induce abiotic stress resistance or make the plant more resistant to a disease. Harmful interactions include, on the other hand, competition, antagonism and parasitism [12]. These negative interactions can stress and damage cultivated plants and can negatively affect the treatments applied using biological agents. Therefore, considering the wide variety of species of endophytic fungi present in the soil, mycorrhizae can interact with phytopathogenic, saprophytic or symbiotic fungal colonies in the roots of the host plant [13,14].

Dark septate endophytes (DSE) are a group of endophytic fungi broadly classified as conidial or sterile septate fungal endophytes that form melanized structures, such as inter- and intracellular hyphae and microsclerotia in the plant roots, and DSE are believed to represent primary non-mycorrhizal root-inhabiting fungi [15]. Wild plant species may live in symbiosis with a unique and rich mycoflora, including DSE that may have been lost during the breeding of the cultivars used in agriculture [16,17]. However, some agronomic crops, such as grasses and cereal roots, are often colonized by DSE. Frequently DSE occur together with mycorrhizal fungi, such as arbuscular, ericoid, orchid and ectomycorrhiza [18]. Colonization by fungi through their hyphae enables host plants to acquire soluble mineral nutrients not otherwise available [18]. The relatively small diameter of DSE hyphae, with respect to the diameter of the root, allows roots to indirectly penetrate soil micropores and acquire resources from a volume of soil otherwise impenetrable to the plant's roots. It has been shown that *Piriformospora indica* colonizes the roots of many species of plants, favoring their growth [19,20].

In ways similar to mycorrhizal symbiosis, the symbiosis of *P. indica* with plant roots is characterized by a large intake of N [21,22]. In fact, Cruz et al. [23] observed that the absorption rate of  $\text{NH}_4^+$  labelled with  $^{15}\text{N}$  by the extraradical mycelium was greater in the tomato–*P. indica* interaction than in tomato–*Glomus intraradices* interaction. There is some evidence that different kinds of root-associated fungi interact. For example, ectomycorrhizae and DSE strains together are associated with increased plant biomass that is more than with either alone [24]. Cereal mycorrhizae, an ancient symbiotic, are often found with DSE associated with the roots of wheat (*Triticum aestivum*), wild barley (*Hordeum brevisubulatum* and *Hordeum bogdanii*), soybean (*Glycine max*) and maize (*Zea mays*) [25]. Even if there is little evidence of mutualistic interaction between plants and DSE [26,27], there are indications that the ecophysiological contribution DSE can provide to the plant include stress tolerance and resistance to pathogens. In other words, the presence of DSE in

plant roots could have a function very similar to a probiotic factor: the spores of DSE, once released, rapidly colonize the environment, occupying the ecological niche of other fungi and, by minimizing the carbon available in host rhizosphere environment, may prevent the development of other fungi. This indicates that when the soil is colonized by DSE, plants may be attacked less by fungal diseases of the root system. The relatively small diameter of DSE hyphae, especially when compared to the root diameter, allows the penetration of soil micropores and the acquisition of resources from a soil volume impenetrable to larger plant roots. As mentioned above, unlike mycorrhizal fungi, endophytes do not establish symbiosis with the host plant, but manage to live asymptotically within the plant tissue. To protect the host plant from biotic and abiotic stresses, endophytic fungi produce different bioactive compounds, and, in turn, the endophytic fungi benefit from nutrition provided by the host plant [28]. This exchange of benefits makes endophytes a potential resource for the production of beneficial metabolites, such as antimicrobial, antiviral and insecticidal compounds, which are antioxidants and compounds antagonistic to some kinds of cancer [28]. In view of the results of emerging research, many bioactive compounds attributed in the past to the secondary metabolism of plants may be, instead, of fungal origin [28]. Among the wide range of endophytic fungi present in the soil, the phytopathogens of cultivars of agronomic interest, such as wheat, have been a continuing source of great damage to humans and their health. Unfortunately, the roots of wheat can become colonized by *Fusarium* species, often resulting in severe crop disease, the accumulation of secondary metabolites toxic to man and reduced yields. The fungal species mainly associated with *Fusarium* head blight (FHB) in Europe are *F. graminearum*, *F. avenaceum* and *F. poae* [29–31]. Less frequently isolated species are *F. tricinctum*, *F. sporotrichioides*, *F. equiseti*, *F. langsethiae* and *F. culmorum* [32–34]. The purpose of the present work is to identify the effects of the biological interaction between endophytes and mycorrhizal durum wheat roots on nitrogen metabolism and the yield of durum wheat (*Triticum durum* Desf. or *Triticum turgidum* subsp. *durum* (Desf.) van Slageren) [35]) in fields with low rates of fertilization of phosphorus and nitrogen.

## 2. Results

### 2.1. Mycorrhization of Roots and Durum Wheat Development

The mycorrhizal colonization and durum wheat growth depicted in Figure 1 show the growth of mycorrhizal (M) and non-mycorrhizal control (NM) plants at two field sites. Spontaneous mycorrhization growth curves show a maximum value below 10% root length colonization (RLC) for NM particles under optimal soil fertilization for both sites A and B. Differently, M particles with low fertilization and mycorrhization growth curves show a maximum value of more than 50% (RLC) for both sites. These data show that the growth trend of the plants was influenced by the development of mycorrhizal colonies inside the root at both sites. Between 90 and approximately 130 days after sowing (DAS), i.e., during the phase of the beginning of stem elongation, the plants treated with mycorrhizae (M) grew approximately 30–40% less than the non-treated control plants (NM). At 130 DAS, i.e., during the beginning of the stem elongation stage, M and NM plants exhibited equivalent masses. Between 130 and 190 DAS, when root colonization was at the highest extent (reaching a maximum of 50 to 60% RLC), the shoots of M grew better than those of NM plants in both sites. In the range between 130 and 190 DAS, i.e., at the end of the raising stage and when the mycorrhization was maximal, the shoots of M plants had a greater mass than the shoots of NM plants, with a 25% and 35% increase for A and B sites, respectively.

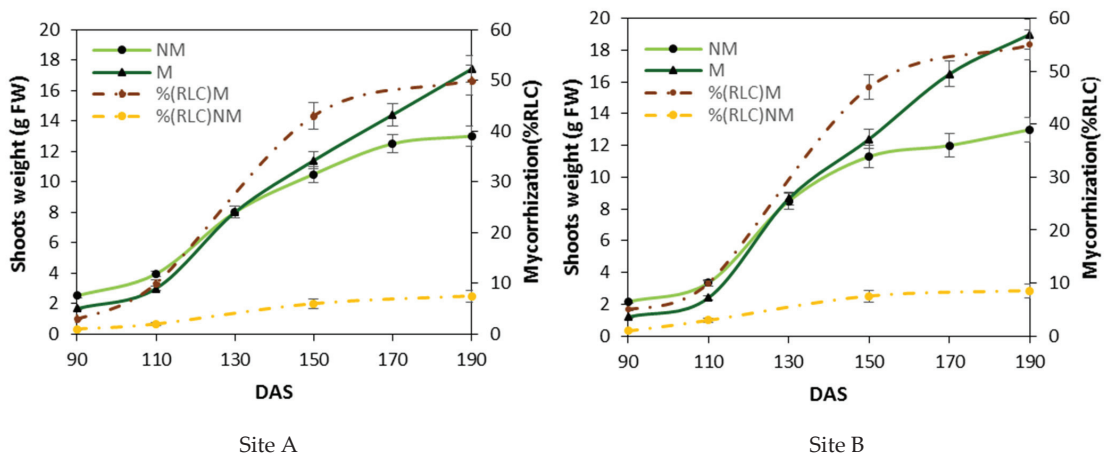


**Figure 1.** Differences in the aerial biomass weight between mycorrhized and non-mycorrhized plants. Shoot weights (a mean of ten shoots were in each parcel of control (NM) and mycorrhized plants (M)) and the corresponding root length colonization (% RLC) between 90 and 190 days after sowing (DAS) at two separate locations (Larino, Site A; Rotello, Site B). The mycorrhization index (dashed line) is expressed as a percentage of root length colonization % RLC by mycorrhizae. Bars indicate the standard deviation ( $\pm$ SD), and the means are the mean values of ten plants ( $n = 10$ ) randomly distributed in the experimental parcel.

## 2.2. Nitrogen Metabolism

In the present experiment, nitrogen in the soil was augmented with fertilizer containing 30%  $\text{NO}_3^-$ -N and 30% ureic N. Nitrogen fertilizer was scattered  $200 \text{ kg ha}^{-1}$  (NM) and  $100 \text{ kg ha}^{-1}$  (M) on the plants [36]. The activities of NRA and GS, crucial enzymes of N metabolism and assimilation, were studied in comparison to nitrogen sources and mycorrhiza–plant symbiosis (Figure 2). At 190 DAS in the control (NM) plants, the NRA activity was higher in leaves (Figure 2b) than in roots (Figure 2a). There was 27% and 30% more NRA activity at sites A and B, respectively. The values of NRA activity were greatest for plants treated with mycorrhizae (M) compared to NM plants in both roots and leaves at both sites. The largest increase in the NRA activity of M plants on NM plants was observed in the roots in both locations, with an average increase of 70% (Figure 2a). An analogous pattern was observed in leaves, but to a lesser extent in both locations with an average increase of 45% (Figure 2b).

It is particularly interesting to note that in NM plants, the specific activity of NRA was greater in the leaves than in the roots. On the contrary, in M plants, the percentage increase in NRA and its absolute values were higher in roots than in leaves. In NM plants, however, the enzyme with greater absolute activity in the leaves (Figure 2d) than in the roots was GS (Figure 2c). In the roots, however, the variations of GS-specific activity of M over NM plants, when comparing B (NM) and B (M) and A (NM) and A (M), were less than 40% and 35%, respectively.

In the leaves, the GS activity was markedly higher in the M than in the NM plants, where the percentage of activity increase in M compared NM plants in both locations was about 65%. This shows that in M plants, the specific activity of GS was greater in the leaves than in the roots, both in percentage increase and absolute value.

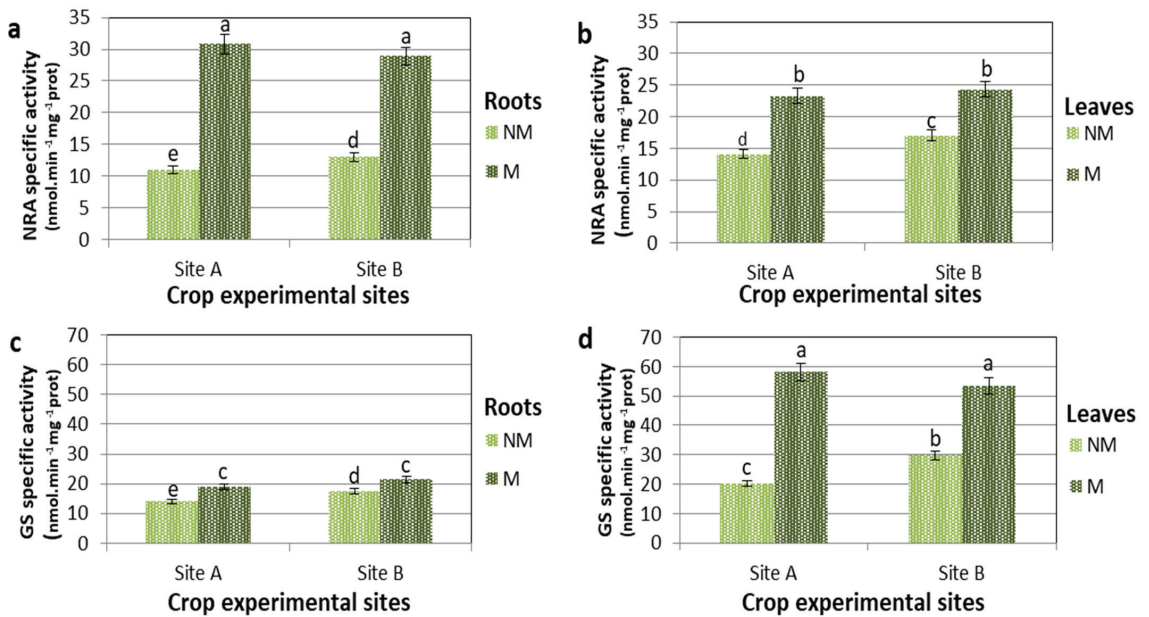


**Figure 2.** Nitrate reductase (NRA) and Glutamine synthetase (GS) specific activities of control (NM) and M plants of *Triticum durum* grown in two different soil sites (A and B) and collected at 190 DAS. Data are for NRA in roots (a) and in leaves (b), and GS in roots (c) and leaves (d). Specific activities are expressed in  $\text{nmol}\cdot\text{min}^{-1}\cdot\text{mg}^{-1}\cdot\text{prot}$ . The values are means  $\pm$  SD of ten biological replicates ( $n = 10$ ). Values marked by common letters are not statistically different at  $p \leq 5\%$  according to Tukey's test.

### 2.3. Free Amino Acids Content in NM and M Plants

Amino acid free content models showed significant differences in the roots (Figure 3a,c) and leaves (Figure 3b,d) when comparing the NM and M plants. At 190 DAS in the plants treated with mycorrhizae, the total free amino acid concentration increased to 70 and 100% in the roots and leaves of M, compared to the NM plants, for both A and B sites (Figure 3). The group of amino acids that showed a higher concentration in M than the NM roots includes glutamine (Gln), asparagine (Asn), alanine (Ala), arginine (Arg), ornithine (Orn) and citrulline (Cit). Although significant, smaller increases were observed for Glu and aspartate (Asp). The levels of leucine (Leu), valine (Val) and lysine (Lys) were over 100% higher in M than in NM roots. Glutamine, Arg, Asn and Cit, with high N/C ratios, are involved in N translocation and accumulation in roots. Large changes in concentration and distribution occurred also for the free amino acids in leaves (Figure 3b,d) of MS and NM plants at 190 DAS. The amino acids that contributed most to the total amount of N are Gln, Asn, Arg, Ala, Cit and Orn, which displayed the largest increase, reaching concentrations that were more than 200% greater, while Glu and Asp increased by about 75% in the leaves of M compared to NM plants in both sites (Figure 3b,d). In the leaves, however, only the Gln concentration was four times higher in the M compared to NM plants. Among the other amino acids, Leu, Val, Lys, Cit and Orn had concentrations higher than 200% also in the leaves of M plants relative to those of NM plants.

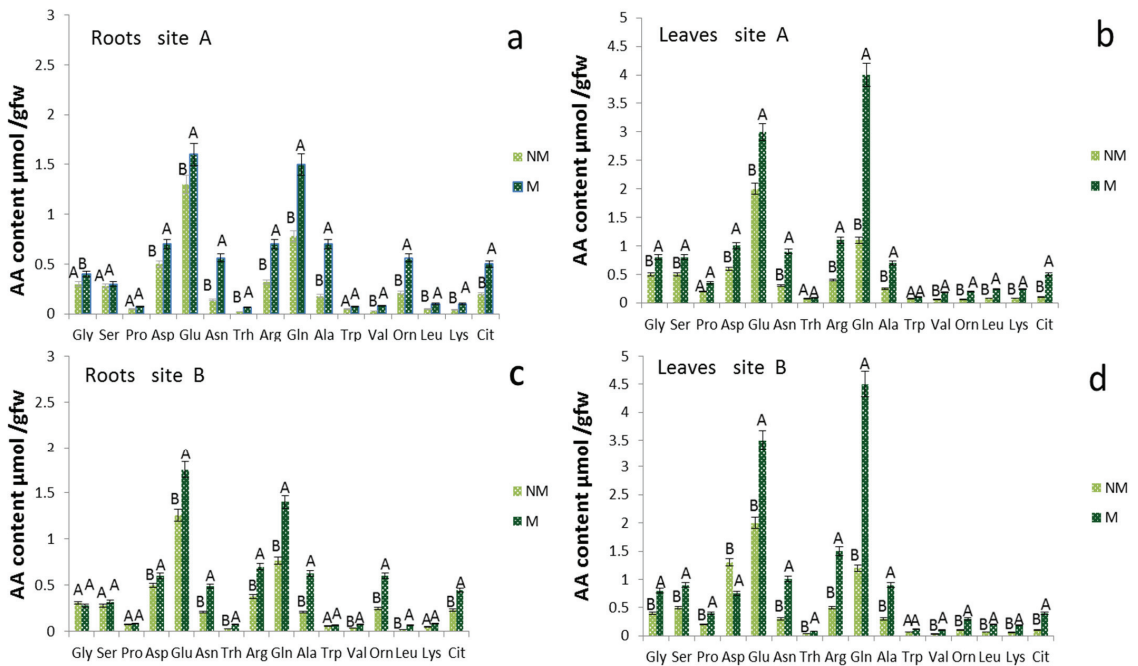


**Figure 3.** Amino acid concentrations of roots and leaves tissue of *Triticum durum* of control (NM) and mycorrhizal (M) treatments 190 d after sowing in two different soil sites (A and B; (a,c) refer to the roots, while (b,d) to the leaves). The values are means  $\pm$  SD of ten plants ( $n = 10$ ) in each experimental parcel. Bars indicate the standard deviation. Values marked by common letters are not statistically different at  $p \leq 5\%$  according to Tukey's test.

#### 2.4. Isolation and Identification of Endophytic Fungi from Plant Roots in the Field

Unlike plant growth in a greenhouse or growth chamber, which takes place in more controlled conditions, experimentation in the field includes various pedoclimatic factors and microbiological factors in the soil that can significantly affect the physiological processes and growth response of plants. For the purpose of the present research, an investigation was conducted on the nature of the endophytic colonies hosted by the roots of the plants collected in the two sites in the field at each of which the same two different fertilization treatments (Section 4.2) were utilized.

Nine endophytic fungal taxa were isolated from the roots of 20 plants randomly distributed in the two investigated sites (Table 1). *Alternaria* and *Fusarium* were the two most common genera that were detected in the roots of many plant species. *Fusarium* species were observed in all the sites studied, while *Alternaria* species were mostly isolated in plant roots from site B. Besides those two genera, the fungi of the *Cladorrhinum macrophomina* species were detected in the samples examined by root isolation and ITS pyrosequencing with different frequencies. The fungi of *Cladorrhinum australe*, *Macrophomina phaseolina*, *Fusarium equiseti* and *F. avenaceum* species were isolated much more from the plant roots of site A (NM), with a percentage of frequency on 20 plants examined being 5%, 75%, 70% and 90%, respectively. The fungi of *Alternaria alternata*, *A. infectoria*, *F. equiseti* and *F. avenaceum* species were isolated much more from the plant roots of the A (M) site, with a percentage of frequency of 20 plants examined being 50% 55%, 40% and 55%, respectively. On the other hand, in the plant roots of the B (NM) site, the most significant attendance rates were in favor of *F. avenaceum*, *M. phaseolina*, *F. equiseti* and *F. algeriense* (85%, 50%, 50% and 40%, respectively) and in the plant roots of site B (M), in favor of *A. alternata*, *A. infectoria*,

*F. avenaceum* and *M. phaseolina* (50%, 45%, 40% and 40%, respectively), as indicated in Table 1. and visibly evidentiary by the chromatism of the heat map Figure 4.

**Table 1.** Percentage frequency of endophytic fungi isolated from the roots of 20 *Triticum durum* plants harvested at sites A and B not treated with mycorrhizae NM and treated with mycorrhizae M. Different strains are indicated by superscript asterisks (“\*”, “\*\*\*”) and diamonds (“◊”, “◊◊”, “◊◊◊” and “◊◊◊◊”).

Microorganisms in Roots	Gene Bank Code	% Frequency Site A		% Frequency Site B	
		NM	M	NM	M
<i>Fusarium avenaceum</i>	OM417228	90%	55%	85%	40%
<i>Fusarium algeriense</i>	OM417243	20%	30%	40%	20%
<i>Alternaria alternata</i> *	OM422688	30%	50%	-	-
<i>Alternaria alternata</i> **	OM422689	-	-	35%	50%
<i>Alternaria infectoria</i>	OM422690	25%	55%	30%	45%
<i>Alternaria tellustris</i>	OM422702	20%	30%	20%	30%
<i>Cladorrhinum australe</i>	OM422711	65%	30%	30%	30%
<i>Macrophomina phaseolina</i>	OM422725	75%	30%	50%	40%
<i>Fusarium equiseti</i>	OM422743	70%	40%	50%	35%
<i>Fusarium chlamydosporum</i> ◊	OM422742	-	-	35%	20%
<i>Fusarium chlamydosporum</i> ◊◊	OM429358	15%	-	-	-
<i>Fusarium chlamydosporum</i> ◊◊◊	OM429359	15%	-	-	-
<i>Fusarium chlamydosporum</i> ◊◊◊◊	OM429357	35%	-	-	-

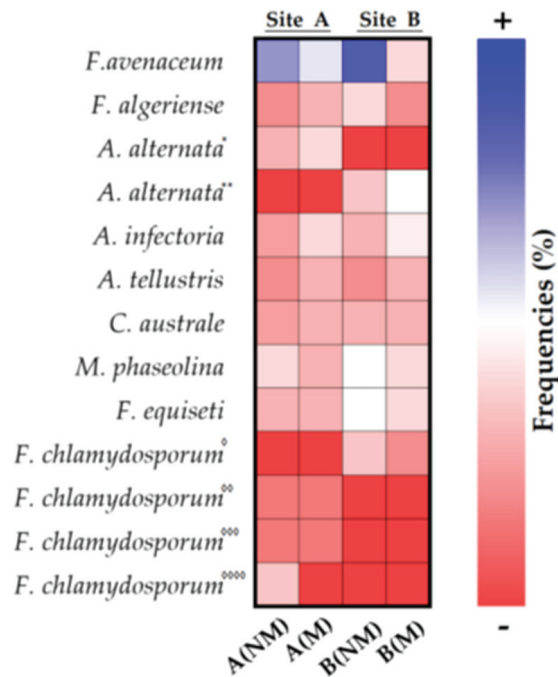


**Figure 4.** Heatmap of percentage frequency of endophytic fungi in the roots of *Triticum durum*. Different strains are indicated by superscript asterisks (“\*”, “\*\*\*”) and diamonds (“◊”, “◊◊”, “◊◊◊” and “◊◊◊◊”).

### 2.5. Cellulase Test on the Endophytic Fungi from Plant Roots

Cellulose, a linear polymer composed of  $\beta$ -D-glucopyranosyl units linked by  $\beta$ -1,4-D-glucosidic bonds, is a main component of plant cell walls. The cellulase test on isolated endophytes represents the response, using the cup plate method, of the ability of the fungi to lyse the cell wall of the host organism. Some of the strains isolated from the durum wheat roots in the two sites showed a positive test in the plate of the cellulase activity and, therefore, the ability of autonomous penetration into the root of the host plant (Table 2).

**Table 2.** Result of cellulase test on isolated endophytic strains in roots of *Triticum durum*.

Isolates	Results
<i>Fusarium avenaceum</i>	++
<i>Fusarium algeriense</i>	++
<i>Alternaria alternata</i> */**	+++
<i>Alternaria infectoria</i>	+++
<i>Alternaria tellustris</i>	++
<i>Cladorrhinum australe</i>	+
<i>Macrophomina phaseolina</i>	–
<i>Fusarium equiseti</i>	++
<i>Fusarium chlamydosporum</i> $\diamond/\diamond\diamond\diamond$	++

The + symbol corresponds to 0.5 cm radius of the cellulase activity halo. The minus (–) symbol corresponds to no-halo. \*/\*\* (one / two);  $\diamond/\diamond\diamond\diamond$  (one / four).

### 2.6. Root Microscopy

Although to different extents, all root samples examined showed endophyte colonization as observed via direct microscopy (Figure 5). In the seven images of Figure 5, it is possible to note also the presence of mycorrhizal colonization often associated with endophytic colonization in the same roots, highlighting vesicles and arbuscules.

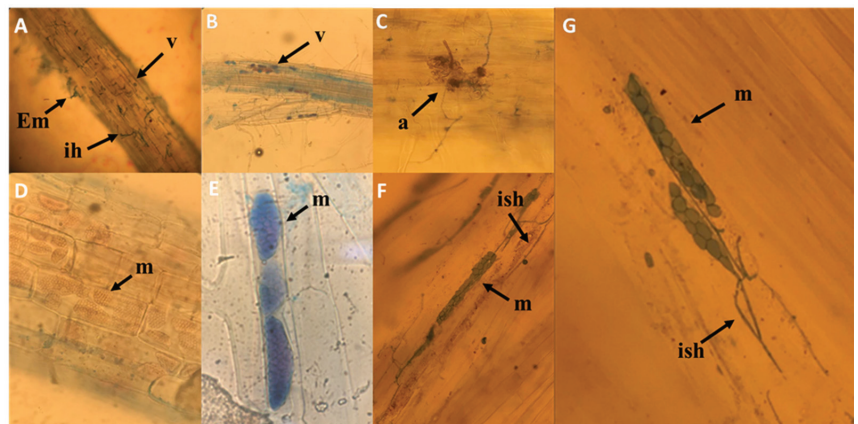


**Figure 5.** Light microscopy of root colonization by mycorrhizal fungi and DSE. Vesicles and arbuscules (A–C); intracellular growth of endophytic fungus with stained microscleptia at the young stage (arrowhead) in cortical cells without and with trypan blue (D–G). Em= external mycelium; ih = intracellular hyphae; v = vesicles; a = arbuscule; m = microscleptia; ish = intracellular septate hyphae.

The microscleptia are the result of single or contiguous hyphae that swell and develop numerous septa. The subsequent lateral sprouting produces groups of spherical cells that subsequently become pigmented. The typical morphology of conidia and the conidial chains of *Alternaria* spp. From site B (NM) are clearly observed without the aid of histochemical reagents, using an optical microscope (Figure 6).

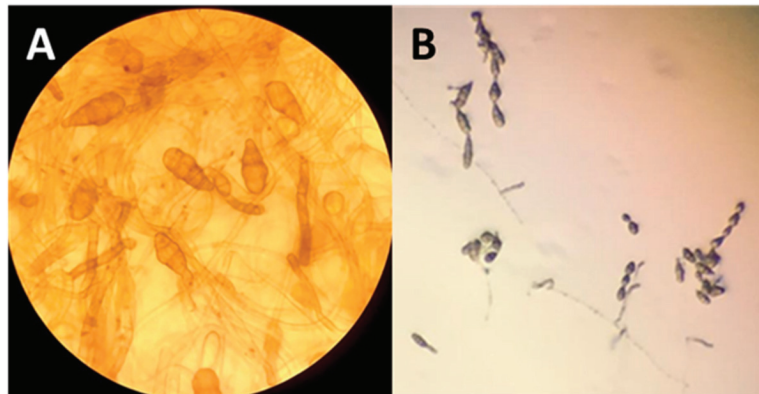


**Figure 6.** Morphology of *Alternaria* spp. isolated from roots. (A) Conidia and (B) conidial chains of *Alternaria* spp.

### 2.7. Evaluation of Fungal Competition via Dual Culture Assay of *Alternaria tellustris*

The DSE strain candidate *Alternaria tellustris* was isolated from healthy and mature roots of wheat plants and was evaluated for its fungal competition by using a dual culture assay. The results show that the DSE strain has an antagonistic activity against both the test pathogenic fungi *F. oxysporum* and *Rhizoctonia solani*. The degree of growth inhibition is 10.5% and 54.9% for *F. oxysporum* and 41.73% and 45.2 % for *R. solani* at 4 dpi and 8 dpi (days post-inoculation), respectively (Table 3, Figure 7).

**Table 3.** Percentage of growth inhibition by *A. tellustris* against *F. oxysporum* and *R. solani*. Data show the mean  $\pm$  SD of three replicas ( $n = 3$ ) at 4 and 8 days post-inoculation.

Days Post-Inoculation	% of Inhibition by <i>A. tellustris</i>	
	<i>Fusarium</i>	<i>Rhizoctonia</i>
4	10.5 $\pm$ 2.0	41.7 $\pm$ 1.1
8	54.9 $\pm$ 2.7	45.2 $\pm$ 0.8

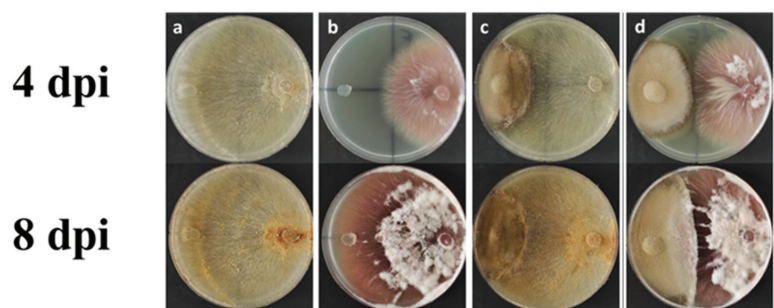


**Figure 7.** Representative pictures of the antagonistic activity assay via dual culture method at 4 and 8 days post-inoculation (dpi), respectively. (a,b) Control plates of *R. solani* and *F. oxysporum*, respectively; (c) dual culture assay of *A. tellustris* and *R. solani*; (d) dual culture assay of *A. tellustris* and *F. oxysporum*.

## 3. Discussion

### 3.1. Root Mycorrhization and Plant Growth

Durum wheat seeds treated with a mixture of fungal spores *Glomus mosseae*, *G. intraradices* and *G. coronatum* caused the mycorrhization of the roots of durum wheat seedlings

(M) in the open field where P availability was limited and N fertilization was reduced to 50% (i.e., 90 kg ha<sup>-1</sup>) compared to traditional treatments. The % RLC began to be significant only after 90 DAS at the beginning of stem elongation. Root samples obtained between 90 and 150 DAS showed hyperbolic growth in the percentage of mycorrhization, reaching a plateau of about 50% for both sites. In contrast, the percentage of spontaneous mycorrhization in roots that were nonmycorrhized (NM) does not exceed 10% at 100 DAS due to both the low microbiological load of the natural environment and the robust fertilization to which the non-mycorrhizal plants were treated. This reduction of mycorrhization is in accordance with the concept that the development of mycorrhizal colonization is affected by plant nutritional status and, more exactly, mycorrhization is reduced in response to the greater availability of macronutrients, in particular phosphorus and nitrogen, for the plant [37,38]. The mycorrhizal plants, compared to the non-mycorrhizal plants of the control, showed different growth responses: for both sites, the growth of mycorrhizal plants was initially slower, compared to control plants between 90 and about 130 DAS, suggesting that part of the energy resources of the plant is destined for the fungal colonization process, which slows down its growth. Subsequently, the plants treated with mycorrhizae showed an acceleration in the growth phase up to 150 DAS where the plants were strongly stimulated by the process of nitrogen assimilation, producing a significant increase in the amino acid pool that enhanced the overall, basic metabolism. These increases in metabolism were indirectly observed in the macroscopic evidence, with an increase in fresh weight of about 30%.

### 3.2. Nitrogen Assimilation

One of the most interesting, functional aspects of the symbiotic relationship between mycorrhizal fungi and the plant is the capacity of the fungus to assimilate inorganic nutrients from the soil and the subsequent transport of the mineral nutrients in the cortical parenchyma of the plant where metabolic photosynthates are exchanged. Arbuscular mycorrhizae can increase the absorption of N from the soil and its transfer to host plants [6,39]. Our results show that the activity of enzymes involved in nitrate assimilation, the reduction by NRA and the subsequent metabolism of ammonium by GS were highly correlated with root mycorrhization (Figure 2).

In site A at 130 DAS, when there was a high level of mycorrhization, M plants showed 55% and 40% higher NRA activity values compared to the NM plants for roots and leaves, respectively. In site B at 130 DAS during intense mycorrhization, M plants showed 80% and 55% higher NRA activity values compared to the NM plants for roots and leaves, respectively. Even with different values in mycorrhized plants there is a greater increase in NRA in the roots than in the leaves. Furthermore, at site B, this response was more pronounced: the increase was 45% and 37% more for site B than at site A for roots and leaves, respectively. In mycorrhizal maize roots, the improvement of the NRA activity has been assigned to the NADPH-dependent fungal NRA enzyme, which displayed activity four times greater with NADPH than with NADH [8]. This would suggest a hypothesis that the NRA activity, mainly due to the enzyme of the fungus, could be vastly higher. A confirmation of this comes from the fact that the fungus sends ammonium via the arbuscules to the cortical parenchyma where it is converted into glutamine [10]. However, nitrate reduction in the M plants was greater in both roots and leaves, indicating an interaction of mycorrhizal colonization with N nutrition.

Glutamine synthetase-specific activities (Figure 2) showed relatively small changes (<30%) in the roots for both sites, but GS activities increased significantly in the leaves of the plants treated with mycorrhizae (65% and 80%, compared to the NM plants for A and B sites, respectively). The high correlation between the percentage increase in NRA and GS activities of roots and leaves tends to generate a spatial separation between the assimilative reduction of nitrate (mostly in the roots) and ammonium metabolism (mostly in the leaves). Moreover, there is kinetic evidence that the chloroplast-localized GS isoform (GS2) of wheat (*Triticum aestivum* L. cv. Jubilejnaja-50) takes place at the carbon–nitrogen metabolic branch

point, and that its enzymatic activity is regulated also by the availability of C, whose main source in photosynthesis is the leaves [40].

### 3.3. Variation of Free Amino Acid Level and Distribution in Roots and Leaves of Mycorrhized Durum Wheat Plants

The amino acid patterns of mycorrhizal roots and leaves (Figure 3) include elevated levels of Gln and the low levels of Glu, further confirming that the assimilation of ammonium through the GS-GOGAT pathway occurred both in the plant and in the fungus [9,41].

The elevated concentrations of Arg and Orn strongly support the current model of conversion of nitrogenous forms in AM symbiosis, which includes the synthesis of Arg in the extra-radical mycelium and the transfer of Arg to the intraradical mycelium, where it is broken down by arginase and urease, and from whence it is subsequently transferred to the root cells as ammonium [10]. The elevated levels of Arg and the possibility that it can be transferred partly to the root cells demonstrate the increase in Cit derived from Orn through the Ornithine transcarbamylase and Carbamoyl phosphate synthetase by Gln.

Given the the high N/C ratio, we see that Cit predominates in transported N while, in some other instances, Arg is the major N-solute of xylem [42]. The decrease in Asp supports its role in the synthesis of argininosuccinate, an intermediate of Arg synthesis [43]. An inevitable increase in oxygen demand in the roots that developed from the seeds treated with mycorrhizae could trigger in the cells of the cortex a metabolic response, with low oxygen content, through the down-regulation of oxygen consumption pathways, such as respiration and enrichment in organic reserves [44,45]. The elevated levels of Ala in the roots treated with mycorrhizae suggest that glycolysis, more than overall respiration, was increased to support plants and fungi to form and maintain the high turnover rate of arbuscules [46,47]. In *Medicago truncatula*, a cytological change corresponding to an increased need for plastid and mitochondrial products during the establishment and functioning of symbiosis was observed. The mitochondria were thickened around the arbuscule, and this explains the change in the plastid ultrastructure caused by a reduction in carbohydrate reserves [45]. Finally, the Glu in the leaves reached, under various conditions, concentrations of 80–150% greater than in the roots, and together with the higher levels of Gln (Figure 3) and the activity of GS (Figure 2), it is probable that GOGAT enzymes were highly functional in the synthesis of nitrogen compounds from carbon and energy skeletons, supplied by photosynthesis.

### 3.4. Fungal Screening in Roots of Wheat Plants and Possible Antagonism between Mycorrhizal Fungi and Pathogenic Endophytes

An analysis to explore indigenous endophytic fungi in mycorrhized and non-mycorrhized durum wheat roots enables one to recognize indicators of healthiness and pathogenicity and reveals the potential ability of endophytes to colonize roots in competitive relationships with mycorrhizal fungi in soil intended for agricultural crops. At both sites, *F. avenaceum* and *F. equiseti* are the fungi with the highest rate of frequency in the NM roots with average values of 85% and 60%, respectively. They can be considered to be the most common species of *Fusarium* on cereals in temperate climates, and *Fusarium* fungi are generalist pathogens responsible for diseases in numerous crop species. *Fusarium* spp. produce mycotoxins, which are factors of pathogenicity and virulence in various plant–pathogen interactions. *Macrophomina phaseoline* was also found in the NM roots of both sites with significant frequencies and average values of approximately 60%. This necrotrophic fungus is an important pathogen of many crops, such as corn, sorghum, potato and soy.

The fungal screening performed on samples from the two sites indicated an interesting result that suggests the potential influence of mycorrhization on the fungal population. The presence of *F. avenaceum*, *F. equiseti* and *M. phaseoline* was strongly reduced by mycorrhization at both sites.

### 3.5. Spontaneous Colonization of Soil DSE, an Ecological Niche between Saprophytic Microorganisms and Pathogens of the Root System

Unlike the experiments conducted in growth chambers, in which the development of mycorrhizae, or mycorrhization, occurs in roots growing in relatively sterile soil, the experimental conditions in an open field may include the presence and possible conditioning of the endophytic fungi affecting the symbiotic action of mycorrhizae.

The molecular identification of isolated endophytic strains from durum wheat roots shows their presence in all the samples examined, including roots treated with mycorrhizae, suggesting the autonomous ability of mycorrhizae to colonize the root. This hypothesis of endophytic colonization was confirmed with the positive activity of mycorrhizae being demonstrated in the cellulase test, indicating that a group of hydrolytic enzymes was capable of hydrolyzing the organic polymer cellulose to smaller sugar components.

Among the isolated strains, fungi of the typically pathogenic genus *Fusarium* were found at both sites, but with different frequencies in the various root samples examined, depending on the site of origin of plants that already established mycorrhizal symbiosis. The other endophytic fungi present in the root system, such as *A. alternata*, also show different frequencies of distribution among the samples examined. These organisms, exerting an interaction with host plants, seem to play a wide range of ecological roles, constituting a continuum from mutualism to parasitism [48–50]. Particular interest has been shown in recent years regarding endophytic fungi considered to be dark septate endophytes (DSE), a group of endophytic fungi characterized by their morphology of melanized, septate hyphae. DSE are frequently observed in interaction with mycorrhizal fungi on shrubs, such as ericoid plants, and as ectomycorrhizae on orchid plants [51]. The effects of DSE on host plants range from pathogenic to mutualistic, depending on environmental factors and the genotypes of hosts and fungi [27]. The frequency of distribution of DSE in the cortical cells of the samples examined in the present report would confirm the tendency of DSE to colonize roots that are already mycorrhizal, with a percentage ranging from 20% to 40% more than in non-mycorrhizal roots. The greater presence of DSE coupled with mycorrhizal associations reduces the vital space for the development and colonization of pathogenic endophytes, including *Fusarium*, as confirmed by the low percentages of frequency in our mycorrhizal samples. On the other hand, some DSE, among which is *A. alternata*, have a wide range of metabolites that possess a great variety of biological activities, such as antimicrobial functions and antioxidant properties [52]. These DSE can effectively counteract, through biocontrol, the root contaminations of bacteria and fungi that are pathogenic to the plant. Some pathogenic fungi or bacteria that enter the xylem vessels that are the primary conduits for water and minerals of a vascular plant can proliferate within the vessels, causing the xylem flow to be blocked. This blockage can occur when fungi such as *F. oxysporum* gain entry to xylem vessels [53]. The ambiguous behavior of the genus *Alternaria* from leaf spot pathogen to root saprophyte can be attributed to the different conditions and availability of oxygen, which, at low levels in the roots, would reduce the virulence of the fungus by radically modifying the biotrophic response [54]. This hypothesis is visibly supported by the image in Figure 5D, where the colonization of cortical cells by *A. infectoria* (site B, M) does not generate cellular necrosis or damage. In fact, DSE produce microsclerotia and hyaline hyphae in the roots [55]. Moreover, it is possible to hypothesize, on the basis of the image (Figure 5D) that when microsclerotia colonized the epidermis and of the radical cortex, hyphae became connected inter- and intracellularly to the external mycelium. This type of cytological interaction between root and DSE facilitates the translocation of nutrients from soil to cortical cells through a network of fungal hyphae laying the foundation for an incipient symbiotic relationship between DSE and root system.

The capabilities of DSE to diminish the availability of nutrients and space to pathogenic fungi and also to promote plant defenses and plant growth [55] increases the interest in their role in the biological control of plant diseases. From our isolates among non-pathogenic DSE, plugs of mycelium of *A. tellustris* were used in an antimicrobial dual culture assay test to determine whether a DSE is able to counteract terrestrial plant pathogenic fungi,

such as *F. oxysporum* and *R. solani*. The analyses show that *A. tellustris* can diminish the nutrients and space available to both terrestrial pathogens. These results appear to indicate that DSE have an important role in diminishing the nutritional and spatial resources available to terrestrial plant pathogens, using different mechanisms of action, as mentioned by Santos et al. [56]. The present research suggests that endophytic fungi, such as *A. tellustris*, may have a role in the induction of a plant's defensive responses, such as systemic acquired resistance (SAR) and induced systemic resistance (ISR). The SAR response is caused by the activation of genes encoding several pathogenesis-related proteins (PRs) through the salicylic acid (SA) biosynthetic pathways. The induction of ISR is caused by upregulating several genes involved in the jasmonic acid (JA) and ethylene (ET) pathways. Lahlali et al. [57], for example, in one of the first reports on the molecular mechanisms of induced resistance mediated by a non-mycorrhizal endophytic fungus, report that the DSE *Heteroconium chaetospora* strain BC2HB1 is able to suppress the clubroot on canola through induced resistance via the concerted upregulation of genes involved in JA, ET and auxin biosynthesis. The PR-2 protein may also be involved in the plant's defenses [55].

#### 4. Materials and Methods

##### 4.1. Mycorrhizal Spore Inoculum for Seeds

Studies on the physiological effects of the mycorrhization of *durum wheat* (cv. Iride) were conducted in 2019 at two different sites within the same pedoclimatic area near Termoli Italy: Larino 700 m a. s. l. (A); Rotello 640 m a. s. l. (B). The mycorrhizal inoculum used contained a mixture of symbiotic fungi (*Glomus mosseae*, *G. intrardices* and *G. coronatum* 0.0001% w/w) provided by MS Biotech S.p.A. (Larino SS 87, km 204) and was sprayed with a backpack pump on about 450 kg of *durum wheat* seeds before sowing.

##### 4.2. Physical and Chemical Analysis of the Soil Samples

Physical and chemical analyses of the soil were performed in the laboratory in accordance with official Italian procedures [58]. Coarse sand (2.0–0.2 mm), fine sand (0.2–0.05 mm), silt (0.05–0.002 mm) and clay (<0.002 mm) fractions were separated via pipette and wet sieving following pre-treatment with H<sub>2</sub>O<sub>2</sub> and sodium hexametaphosphate. Textural classes were assigned according to Italian Soil Science Society standards [58]. Soil pH was measured potentiometrically in soil solution suspensions of 1:2.5 H<sub>2</sub>O. Total CaCO<sub>3</sub> (%) was determined using a De Astis calcimeter. Total organic carbon (TOC) was determined via wet digestion through a Walkley–Black procedure. Total nitrogen (N<sub>tot</sub>) was determined using the Kjeldahl method. Phosphorus was determined using Olsen's method. Cation exchange capacity (CEC) and exchangeable-base cations were extracted with 0.5 N BaCl<sub>2</sub>-TEA at pH 8.2 and determined by atomic absorptions spectrophotometry. The data were obtained by performing three replicas, and the mean ± SD was thus calculated (Table 4).

**Table 4.** Physico-chemical determinations of the soils of sites A and B.

Larino (A)		Rotello (B)	
coarse sand	18% ± 3%	coarse sand	11% ± 2%
fine sand	24% ± 4%	fine sand	36% ± 6%
silt	32% ± 6%	silt	13% ± 3%
clay	38% ± 7%	clay	40% ± 7%
pH	7.36 ± 0.2	pH	7.4 ± 0.1
CaCO <sub>3</sub> total	9% ± 1.5%	CaCO <sub>3</sub> total	9% ± 1.8%
CEC	18 cmol (+) kg <sup>-1</sup> ± 2	CEC	19 cmol (+) kg <sup>-1</sup> ± 2
total organic carbon	8.4 g kg <sup>-1</sup> ± 1.5	total organic carbon	8.5 g kg <sup>-1</sup> ± 1.5
total Nitrogen	1.1 g kg <sup>-1</sup> ± 0.2	total nitrogen	1.2 g kg <sup>-1</sup> ± 0.2
P <sub>2</sub> O <sub>5</sub>	19.2 mg kg <sup>-1</sup> ± 3	P <sub>2</sub> O <sub>5</sub>	19.7 mg kg <sup>-1</sup> ± 3
C/N	7.6 ± 1.5	C/N	7.1 ± 1.4

CEC: Cation exchange capacity. Data show the mean ± SD of three soil sample replicas (n = 3).

#### 4.3. Fertilization Plan

The cultivable area of each of the two sites was 0.25 ha, divided into two symmetrical parcels, one intended for the non-mycorrhized sowing (NM) of parcel 1, the other for the mycorrhized sowing (M) of parcel 2.

On the basis of the preliminary soil analyzes, 3 fertilizations were conducted: the first was background fertilization, the second was during the phenological phase of tillering and the third was during the phenological phase of the beginning of stem elongation. In the parcels cultivated with seeds and mycorrhizal spores, no basic fertilization was performed and no phosphorus fertilizer was added (Table 5).

- (1) Basic fertilization: 100 kg per hectare ( $\text{kg ha}^{-1}$ ) Fertilizer composition: 6% total nitrogen (1% organic N; 2%  $\text{NO}_3^-$ -N; 3% ureic N); 18% total phosphoric anhydride ( $\text{P}_2\text{O}_5$ ); 32% water-soluble  $\text{P}_2\text{O}_5$ ; 20% total CaO; 15% water-soluble sulfur anhydride ( $\text{SO}_3$ ); 7.5% organic carbon of biological origin.
- (2) Phenological phase of the beginning of tillering: nitrogen fertilizer 180  $\text{kg ha}^{-1}$  (NM) parcel 1 and 90  $\text{kg ha}^{-1}$  (M) parcel 2. Composition: 30% ureic N; 30%  $\text{NO}_3^-$ -N; 15% water-soluble  $\text{SO}_3$ . Fertilization was repeated after a week.
- (3) Phenological phase of the beginning of stem elongation: nitrogen fertilizer 200  $\text{kg ha}^{-1}$  (NM) parcel 100  $\text{kg ha}^{-1}$  (M) parcel 2. Composition: 30% ureic N; 30%  $\text{NO}_3^-$ -N; 20% water-soluble  $\text{SO}_3$ . Fertilization was repeated after a week.

**Table 5.** Fertilization plan.

Treatment	Date	Phenological Stage	A (NM)	A (M)	B (NM)	B (M)
Basic fertilization	2019/10/10	-	100 $\text{kg/ha}^{-1}$	-	100 $\text{kg/ha}^{-1}$	-
2nd fertilization	2020/02/04	Tillering	90 $\text{kg/ha}^{-1}$	45 $\text{kg/ha}^{-1}$	90 $\text{kg/ha}^{-1}$	45 $\text{kg/ha}^{-1}$
2nd fertilization	2020/02/18	Tillering	90 $\text{kg/ha}^{-1}$	45 $\text{kg/ha}^{-1}$	90 $\text{kg/ha}^{-1}$	45 $\text{kg/ha}^{-1}$
3rd fertilization	2020/03/14	Stem extension	100 $\text{kg/ha}^{-1}$	50 $\text{kg/ha}^{-1}$	100 $\text{kg/ha}^{-1}$	50 $\text{kg/ha}^{-1}$
3rd fertilization	2020/03/26	Stem extension	100 $\text{kg/ha}^{-1}$	50 $\text{kg/ha}^{-1}$	100 $\text{kg/ha}^{-1}$	50 $\text{kg/ha}^{-1}$

#### 4.4. Sampling, Plant Growth and Mycorrhizal Colonization Analyses

Samples were taken 90 (beginning of tillering stage), 110 (beginning of stem-elongation stage), 130, 150, 170 and 190 days after sowing (DAS) following the treatment of durum wheat seed with mycorrhizae. At each sampling, ten plants for each parcel of experimental land were collected at ten randomly distributed points, and were used for analyses.

The roots were cleaned in a container with water and then with sterile water, then dried with a paper towel and promptly used to determine the percentage of mycorrhization using the methods of Giovannetti and Mousse [59]. The shoots were used to calculate root fresh weight during the growth phase of the plants. Each subsample was counted three times by reorganizing the roots in the Petri dish, and the mean  $\pm$  SD was calculated.

#### 4.5. Primary Amino Acid Analyses

Proline was determined using high-performance liquid chromatography (HPLC) with a fluorescent 9-fluorenylmethoxycarbonyl derivative (P-FMOCCarbamate) using aliquots of root and leaf extracts that were formerly derivatized using o-Phthaldialdehyde Reagent Solution (OPA) solution to exclude the primary amino acids and was fluorometrically detected by excitation at 266 nm and emission at 305 nm [60].

Protein concentrations in root and leaf samples were determined using the methods of Lowry et al. [61]. The values are means  $\pm$  SD of ten plants ( $n = 10$ ). Values are statistically different at  $p \leq 5\%$  according to Tukey's test.

#### 4.6. Nitrate Reductase Assimilatory and Glutamine Synthetase Activity Assays

Portions of 300 mg FW and 1 g FW of leaf and root, respectively, after being immersed in liquid nitrogen, were finely ground in an agate mortar and subsequently extracted in 10 mL extraction buffer, and NRA and GS activities were determined using the methods of Gibon et al. [62]. The values are means  $\pm$  SD of ten biological replicates ( $n = 10$ ). Values are statistically different at  $p \leq 5\%$  according to Tukey's test.

#### 4.7. Root Microscopy

Direct observation of natural host root colonization by mycorrhizal and endophytic fungi was conducted using light microscopy as in Bordallo et al. [63]. Six to eight root pieces (c. 0.5 cm long) per plant sample were cut from each root system. Arbuscular mycorrhizal tissue was analyzed by evaluating the presence of aseptate hyphae, hyphal coils, arbuscules or arbusculate coils with or without vesicles. Root sections were then treated with Trypan blue, as previously indicated. The excess stain was removed with distilled water and the sample was blotted onto a filter paper. Root samples on microscope slides were observed and photographed with an Olympus BH-2 microscope.

#### 4.8. Isolation of Endophytic Fungi

Regarding dark septate endophytes, fungal colonization was characterized using regularly septate, melanized or hyaline hyphae with microsclerotia or moniliform cells that allowed us to discriminate the endophytic structures from the mycorrhizal structures.

Endophytic fungi were isolated from fresh plant roots that were disinfected by soaking in 75% ethanol (0.5 min), 3% sodium hypochlorite (5–8 min) and 75% ethanol (1 min), and which were then rinsed twice for 1 min in sterile water. The plant roots were cut into small pieces (0.5 cm) using a sterilized scalpel. Segments from each plant tissue sample were randomly chosen and placed in Petri dishes containing potato dextrose agar (PDA) supplemented with 50  $\mu\text{g mL}^{-1}$  streptomycin and 50  $\mu\text{g mL}^{-1}$  chloramphenicol. These plates were incubated at 28 °C until fungal growth appeared. The colonies were counted and grouped by their morphologic characteristics, and representative isolates of fungal diversity were collected, purified and preserved for future analysis. All the materials used were purchased from Merck KGaA, Darmstadt, Germany.

#### 4.9. Molecular Identification of Fungi

Due to the difficulty of identifying the morphological characteristics of endophytes isolated from the durum wheat roots, the identity of the groups of fungal isolates was confirmed by means of molecular methods.

Fourteen hypothetical endophytic fungi were analyzed. The isolated strains were aerobically cultured in 250 mL Erlenmeyer flasks containing PDA broth at 28 °C for 5 days without shaking. Each isolate (1 mL) was centrifuged at 14,000 rpm for 5 min at 4 °C, and the pellet obtained was subjected to DNA extraction using a DNA extraction kit (Macherey-Nagel, NucleoSpin Tissue Kit, Duren, Germany) according to the manufacturer's instructions. The quantity and purity of the DNA were assessed using the NanoDrop spectrophotometer 2000 (Thermo Scientific, Wilmington, DE, USA).

The amplification of internal transcribed spacer (ITS) region of rDNA was carried out using universal primers ITS1 (5'-TCCGTAGGTGAACCTGCGG-3') and ITS' (5'-TCCTCCG-CTTATTGATATC-3'). Polymerase chain reaction (PCR) determination was performed using a Mastercycler nexus gradient (Eppendorf, Hamburg, Germany). The reaction mixture consisted of 10  $\mu\text{L}$  TaqMan 2x PCR Master Mix (Norgen Biotek Corp., Thorold, ON, Canada), 2  $\mu\text{L}$  of each primer (2.5  $\mu\text{M}$ ), 2  $\mu\text{L}$  template DNA and the nuclease-free water were added to bring the final volume to 20  $\mu\text{L}$ .

PCR products were separated in 1.5% ( $w/v$ ) agarose gel via electrophoresis for 45 min at 80 V in 1X TAE buffer (Thermo Fisher Scientific, Waltham, MA, USA) and were subsequently visualized using a UV transilluminator (Bio-Rad molecular image Gel Doc XR, Hercules, CA, USA) after ethidium bromide (50  $\mu\text{g/mL}$ , Merck KGaA, Darmstadt,

Germany) staining. After purification (QIA-quick PCR Purification kit, QIAGEN GmbH, Hilden, Germany), the DNA products were sent to a commercial facility for sequencing (MacroGen Europe BV, Meibergdreef, Amsterdam, The Netherlands). The Basic Local Alignment Search Tool Nucleotide (BLASTN) tool encoded in NCBI suite [64] was applied to the GenBank [65] database to identify the sequences.

#### 4.10. Evaluation of Fungal Competition by Dual Culture Assay of *Alternaria tellustris*

*Alternaria tellustris* was used as a non-pathogenic DSE candidate to evaluate the potential antimicrobial activity of this strain against pathogenic fungi of terrestrial plants. The strain was screened for its antagonistic activity via the double culture method against two phytopathogenic fungi: (i) *Fusarium oxysporum* f.sp. *lycopersici* and (ii) *Rhizoctonia solani*. The plugs of mycelium (6 mm Ø) were taken under aseptic conditions every 4 to 5 days, selecting the pure cultures of *Alternaria tellustris* and each phytopathogenic fungus, and were then transferred to a Petri dish (90 mm Ø) containing 20 mL of potato dextrose agar (PDA) and kept 6 cm separate from each other. The plates were incubated at 28 °C for 8 days and the treatments were performed in triplicate. Pathogen and endophyte growth was observed daily, and radial growth was recorded by measuring the mean colony radius on day 4 and day 8 after inoculation (dpi). As a control, each fungus was plated by itself. The percentage of inhibition of the tested DSE and phytopathogenic fungi was calculated using the formula:

$$\% \text{ inhibition} = (R1 - R2/R1) \times 100$$

where R1 is the radial growth of the control plate, and R2 represents the radial growth of the dual culture plate. The data were obtained by performing three replicas and the mean and  $\pm$ SD was then calculated.

#### 4.11. Statistical Analysis

Data are presented as means  $\pm$  SD of the 10- or 20-plant samples randomly distributed in the experimental parcel. Each analysis of each sample was replicated two times. The statistical significance of differences was calculated at using Tukey's test ( $p \leq 5\%$ ). An analysis of variance was performed using the software IBM\_SPSS\_Statistics version 22.0 (SPSS Inc. Chicago, IL, USA, 2014).

## 5. Conclusions

Mycorrhized wheat plants showed a more efficient assimilation of inorganic nitrogen than did control plants at two sites in open fields. The increase in specific NRA and GS activities and the consequent enrichment of the amino acid pattern resulted in an increase in plant growth and yield under conditions of low fertilization and minimal environmental impact. The spontaneous colonization of the roots of durum wheat by endophytic fungi, such as DSE that were present in the soil, appears to be favored by the presence in the root of mycorrhizal fungi. The consociated interaction of DSE and mycorrhizal fungi appears to have been established, resulting in increased N absorption by the durum wheat. This relationship between DSE, mycorrhizal fungi and the roots resulted in (1) the improved the growth of the plant, (2) increased competitiveness between symbiotic fungi and pathogenic fungi, (3) reduced colonization spaces and (4) reduced pathogenic contamination, based upon measurements showing diminished presence of *Fusarium* species at two cultivation sites. Ultimately, it is possible to agree that the physiological role of these endophytic fungi could be relegated to the prevention of pathogenic infections and to the transport of nutrients from the soil to the roots in parallel with mycorrhizal associations.

**Author Contributions:** Conceptualization, C.D.M. and S.C.; methodology, C.D.M., S.C., G.P., C.D.G., L.P. and D.P. software, P.M.; validation, C.D.M., S.C. and T.W.C.J.; formal analysis, V.T., L.P. and C.D.G. investigation, C.D.G., V.T., D.P. and P.M.; data curation, C.D.M. and C.D.G.; writing—original draft preparation, C.D.M.; writing—review and editing, C.D.M., T.W.C.J. and S.C. All authors have read and agreed to the published version of the manuscript.

**Funding:** This research received no external funding.

**Institutional Review Board Statement:** Not applicable.

**Informed Consent Statement:** Not applicable.

**Data Availability Statement:** The data can be found and made available by the laboratory archive of Plant Physiology of the University of Molise.

**Conflicts of Interest:** The authors declare no conflict of interest.

## References

- Wang, B.; Qiu, Y.L. Phylogenetic distribution and evolution of mycorrhizas in land plants. *Mycorrhiza* **2006**, *16*, 299–363. [[CrossRef](#)]
- Di Martino, C.; Crawford, T.W., Jr. Roles and implications of arbuscular mycorrhizas in plant nutrition. In *Handbook of Plant and Crop Physiology*, 4th ed.; CRC Press: Boca Raton, FL, USA, 2021; Chapter 18; pp. 321–341. ISBN 978-036-755-454-5.
- Van der Heijden, M.G.A.; Sanders, I.R. *Mycorrhizal Ecology Ecological Studies*; Springer: Berlin/Heidelberg, Germany, 2003.
- Smith, S.E.; Read, D.J. *Mycorrhizal Symbiosis*, 3rd ed.; Academic Press: London, UK, 2008.
- Di Martino, C.; Palumbo, G.; Vitullo, D.; Di Santo, P.; Fuggi, A. Regulation of mycorrhiza development in durum wheat by P fertilization: Effect on plant nitrogen metabolism. *J. Plant Nutr. Soil Sci.* **2018**, *181*, 429–440. [[CrossRef](#)]
- Nouri, E.; Breuillin-Sessoms, F.; Feller, U.; Reinhardt, D. Phosphorus and nitrogen regulate arbuscular mycorrhizal symbiosis in *Petunia hybrida*. *PLoS ONE* **2014**, *9*, e90481. [[CrossRef](#)]
- Kaldorf, M.; Zimmer, W.; Bothe, H. Genetic evidence for the occurrence of assimilatory nitrate reductase in arbuscular-mycorrhizal and other fungi. *Mycorrhiza* **1994**, *5*, 23–28. [[CrossRef](#)]
- Kaldorf, M.; Schmelzer, E.; Bothe, H. Expression of maize and fungal nitrate reductase genes in arbuscular mycorrhiza. *Mol. Plant Microbe Int.* **1998**, *11*, 439–448. [[CrossRef](#)] [[PubMed](#)]
- Johansen, A.; Finlay, R.D.; Olsson, P.A. Nitrogen metabolism of external hyphae of the arbuscular mycorrhizal fungus *Glomus intraradices*. *New Phytol.* **1996**, *133*, 705–712. [[CrossRef](#)]
- Govindarajulu, M.; Pfeffer, P.E.; Jin, H.; Abubaker, J.; Doups, D.D.; Allen, J.W.; Bücking, H.; Lammers, P.J.; Shachar-Hill, Y. Nitrogen transfer in the arbuscular-mycorrhizal symbiosis. *Nature* **2005**, *435*, 819–823. [[CrossRef](#)] [[PubMed](#)]
- Tian, C.; Kasiborski, B.; Koul, R.; Lammers, P.J.; Bücking, H.; Shachar-Hill, Y. Regulation of the nitrogen transfer pathway in the arbuscular mycorrhizal symbiosis: Gene characterization and the coordination of expression with nitrogen flux. *Plant Physiol.* **2010**, *153*, 1175–1187. [[CrossRef](#)]
- Zeilinger, S.; Gupta, V.K.; Tanya, E.S.; Dahms, T.E.S.; Silva, R.N.; Singh, H.B.; Upadhyay, R.S.; Gomes, E.V.; Clement Kin-Ming Tsui, C.K.M.; Nayak, C. Friends or foes? Emerging insights from fungal interactions with plants. *FEMS Microbiol. Rev.* **2016**, *45*, 182–207. [[CrossRef](#)]
- Yang, H.; Dai, Y.; Wang, X.; Zhang, Q.; Zhu, L.; Bian, X. Meta-Analysis of Interactions between Arbuscular Mycorrhizal Fungi and Biotic Stressors of Plants. *Sci. World J.* **2014**, *2014*, 746506. [[CrossRef](#)]
- Liu, H.; Wu, M.; Liu, J.; Qu, Y.; Gao, Y.; Ren, A. Tripartite Interactions Between Endophytic Fungi, Arbuscular Mycorrhizal Fungi, and *Leymus chinensis*. *Microb. Ecol.* **2020**, *79*, 98–109. [[CrossRef](#)]
- Jumpponen, A.; Trappe, J.M. Dark septate endophytes: A review of facultative biotrophic root-colonizing fungi. *New Phytol.* **1998**, *140*, 295–310. [[CrossRef](#)]
- Mandyam, K.; Jumpponen, A. Seeking the elusive function of the root-colonising dark septate endophytic fungi. *Stud. Mycol.* **2005**, *53*, 173–189. [[CrossRef](#)]
- Lugtenberg, B.J.J.; Caradus, J.R.; Johnson, L.J. Fungal endophytes for sustainable crop production. *FEMS Microbiol. Ecol.* **2016**, *92*, fiw194. [[CrossRef](#)]
- Lukešová, T.; Kohout, P.; Větrovský, T.; Vohník, M. The Potential of Dark Septate Endophytes to Form Root Symbioses with Ectomycorrhizal and Ericoid Mycorrhizal Middle European Forest Plants. *PLoS ONE* **2005**, *10*, e0124752. [[CrossRef](#)]
- Varma, A.; Verma, S.; Sudha; Sahay, N.; Butehorn, B.; Franken, P. *Piriformospora indica*, a cultivable plant-growth-promoting root endophyte. *Appl. Environ. Microbiol.* **1999**, *65*, 2741–2744. [[CrossRef](#)]
- Kumari, R.; Kishan, H.; Bhoon, Y.K.; Varma, A. Colonization of cruciferous plants by *Piriformospora indica*. *Curr. Sci.* **2003**, *85*, 1672–1674.
- Bücking, H.; Kafle, A. Role of arbuscular mycorrhizal fungi in the nitrogen uptake of plants: Current knowledge and research gaps. *Agronomy* **2015**, *5*, 587–612. [[CrossRef](#)]
- Sherameti, I.; Shahollari, B.; Venus, U.; Aaltshmidt, L.; Varma, A.; Oelmüller, R. The endophytic fungus *Piriformospora indica* stimulates the expression of nitrate reductase and the starch-degrading enzyme glucan-water dikinase in tobacco and *Arabidopsis* roots through a homeodomain transcription factor that binds to a conserved motif in their promoters. *J. Biol. Chem.* **2005**, *280*, 26241–26247. [[CrossRef](#)]
- Cruz, C.; Fegghi, Z.; Martins-Loução, M.A.; Varma, A. Plant Nitrogen Use Efficiency May be Improved through Symbiosis with *Piriformospora indica*. In *Piriformospora indica: Sebaciniales and Their Biotechnological Applications*; Soil Biology, Varma, A., Kost, G., Oelmüller, R., Eds.; Springer: Berlin, Heidelberg, 2013; Volume 33, pp. 285–293. [[CrossRef](#)]

24. Reininger, V.; Sieber, T.N. Mitigation of antagonistic effects on plant growth due to root co-colonization by dark septate endophytes and ectomycorrhiza. *Environ. Microbiol. Rep.* **2013**, *5*, 892–898. [[CrossRef](#)]
25. Sawers, R.J.H.; Gutjahr, C.; Paszkowski, U. Cereal mycorrhiza: An ancient symbiosis in modern agriculture. *Trends Plant Sci.* **2008**, *13*, 96. [[CrossRef](#)] [[PubMed](#)]
26. Usuki, F.; Narisawa, K. A mutualistic symbiosis between a dark septate endophytic fungus, *Heteroconium chaetospira*, and a nonmycorrhizal plant, Chinese cabbage. *Mycologia* **2007**, *99*, 175–184. [[CrossRef](#)] [[PubMed](#)]
27. Jumpponen, A. Dark septate endophytes—Are they mycorrhizal? *Mycorrhiza* **2001**, *11*, 207–211. [[CrossRef](#)]
28. Chatterjee, S.; Ghosh, R.; Mandal, N.C. Production of bioactive compounds with bactericidal and antioxidant potential by endophytic fungus *Alternaria alternata* AE1 isolated from *Azadirachta indica* A. Juss. *PLoS ONE* **2019**, *14*, e0214744. [[CrossRef](#)]
29. Nicholson, P.; Chandler, E.; Draeger, R.C.; Gosman, N.E.; Simpson, D.R.; Thomsett, M.; Wilson, A.H. Molecular tools to study epidemiology and toxicology of Fusarium head blight of cereals. *Eur. J. Plant Pathol.* **2003**, *109*, 691–703. [[CrossRef](#)]
30. Somma, S.; Petruzzella, A.L.; Logrieco, A.F.; Meca, G.; Cacciola, O.S.; Moretti, A. Phylogenetic analyses of *Fusarium graminearum* strains from cereals in Italy, and characterisation of their molecular and chemical chemotypes. *Crop Pasture Sci.* **2014**, *65*, 52–60. [[CrossRef](#)]
31. Xu, X.-M.; Nicholson, P.; Thomsett, M.A.; Simpson, D.; Cooke, B.M.; Doohan, F.M.; Brennan, J.; Monaghan, S.; Moretti, A.; Mule, G.; et al. Relationship between the fungal complex causing Fusarium head blight of wheat and environmental conditions. *Phytopathology* **2008**, *98*, 69–78. [[CrossRef](#)]
32. Kosiak, B.; Torp, M.; Skjerve, E.; and Thrane, U. The prevalence and distribution of *Fusarium* species in Norwegian cereals: A survey. *Acta Agric. Scand. Sect. B Soil Plant Sci.* **2003**, *53*, 168–176. [[CrossRef](#)]
33. Logrieco, A.; Botalico, A.; Mulé, G.; Moretti, A.; Perrone, G. Epidemiology of toxigenic fungi and their associated mycotoxins for some Mediterranean crops. *Eur. J. Plant Pathol.* **2003**, *109*, 645–667. [[CrossRef](#)]
34. Xu, X.-M.; Parry, D.W.; Nicholson, P.; Thomsett, M.A.; Simpson, D.; Edwards, S.G.; Cooke, B.M.; Doohan, F.M.; Brennan, J.M.; Moretti, A.; et al. Predominance and association of pathogenic fungi causing Fusarium ear blight in wheat in four European countries. *Eur. J. Plant Pathol.* **2005**, *112*, 143–154. [[CrossRef](#)]
35. USDA, Agricultural Research Service. *National Plant Germplasm System*; Germplasm Resources Information Network (GRIN Taxonomy); National Germplasm Resources Laboratory: Beltsville, MD, USA, 2022.
36. Mojid, M.A.; Wyseure, G.C.L.; Biswas, S.K. Requirement of nitrogen, phosphorus and potassium fertilizers for wheat cultivation under irrigation by municipal wastewater. *J. Soil Sci. Plant Nutr.* **2012**, *12*, 655–665. [[CrossRef](#)]
37. Baum, C.; Makeschin, F. Effects of nitrogen and phosphorous fertilization on mycorrhizal formation of two poplar clones (*Populus trichocarpa* and *P. tremula* × *P. tremuloides*). *J. Plant Nutr. Soil Sci.* **2000**, *163*, 491–497. [[CrossRef](#)]
38. Grant, C.; Bittman, S.; Montreal, M.; Plenchette, C.; Morel, C. Soil and fertilizer phosphorus: Effects on plant P supply and mycorrhizal development. *Can. J. Plant Sci.* **2005**, *85*, 1. [[CrossRef](#)]
39. Tanaka, Y.; Yano, K. Nitrogen delivery to maize via mycorrhizal hyphae depends on the form of N supplied. *Plant Cell Environ.* **2005**, *28*, 1247–1254. [[CrossRef](#)]
40. Németh, E.; Nagy, Z.; Pécsváradi, A. Chloroplast glutamine synthetase, the key regulator of nitrogen metabolism in wheat, performs its role by fine regulation of enzyme activity via negative cooperativity of its subunits *Front. Plant Sci.* **2018**, *9*, 191. [[CrossRef](#)]
41. Breuninger, M.; Trujillo, C.G.; Serrano, E.; Fischer, R.; Requena, N. Different nitrogen source modulate activity but not expression of glutamine synthetase in arbuscular fungi. *Fungal Genet. Biol.* **2004**, *41*, 542–552. [[CrossRef](#)]
42. Millard, R.; Wendler, R.; Hepburn, A.; Smith, A. Variations in the amino acid composition of xylem sap of *Betula pendula* Roth. trees due to remobilization of stored N in the spring *P. Plant Cell Environ.* **1998**, *21*, 715–722. [[CrossRef](#)]
43. Cruz, C.; Eggsgaard, H.; Trujillo, C.; Ambus, P.; Requena, N.; Martins-Loução, M.A.; Jakobsen, I. Enzymatic evidence for the key role of arginine in nitrogen translocation by arbuscular mycorrhizal fungi. *Plant Physiol.* **2007**, *144*, 782–792. [[CrossRef](#)]
44. Summers, J.E.; Ratcliffe, R.G.; Jackson, M.B. Anoxia tolerance in the aquatic monocot *Potamogeton pectinatus*: Absence of oxygen stimulates elongation in association with an unusually large Pasteur effect. *J. Exp. Bot.* **2000**, *51*, 1413–1422.
45. Lohse, S.; Schliemann, W.; Ammer, C.; Kopka, J.; Strack, D.; Fester, T. Organization and metabolism of plastids and mitochondria in arbuscular mycorrhizal roots of *Medicago truncatula*. *Plant Physiol.* **2005**, *139*, 329–340. [[CrossRef](#)]
46. Hughes, J.K.; Hodge, A.; Fitter, A.H.; Atkin, O.K. Mycorrhizal respiration: Implications for global scaling relationships. *Trends Plant Sci.* **2008**, *13*, 583–588. [[CrossRef](#)] [[PubMed](#)]
47. Hughes, A.R.; Inouye, B.D.; Johnson, M.T.J.; Underwood, N.; Vellend, M. Ecological consequences of genetic diversity. *Ecol. Lett.* **2008**, *11*, 609–623. [[CrossRef](#)] [[PubMed](#)]
48. Saikkonen, K.; Faeth, S.H.; Helander, M.; Sullivan, T.J. Fungal endophytes: A continuum of interactions with host plants. *Annu. Rev. Ecol. Syst.* **1998**, *29*, 319–343. [[CrossRef](#)]
49. Schulz, B.; Rommert, A.K.; Dammann, U.; Aust, H.J.; Strack, D. The endophyte-host interaction: A balanced antagonism? *Mycol. Res.* **1999**, *103*, 1275–1283. [[CrossRef](#)]
50. Schulz, B.; Boyle, C. The endophytic continuum. *Mycol. Res.* **2005**, *109*, 661–686. [[CrossRef](#)]
51. Yeh, C.M.; Chung, K.M. between Orchids and Fungi. *Appl. Sci.* **2019**, *9*, 585. [[CrossRef](#)]
52. Hashad, N.; Ibrahim, R.; Mady, M.; Abdel-Aziz, M.S.; Moharram, F.A. Bioactive metabolites and host-specific toxins from endophytic fungi, *Alternaria alternata*. *Vietnam J. Chem.* **2021**, *59*, 732–759. [[CrossRef](#)]

53. de Sain, M.; Rep, M. The Role of pathogen-secreted proteins in fungal vascular wilt diseases. *Int. J. Mol. Sci.* **2015**, *16*, 23970–23993. [[CrossRef](#)]
54. Schleusner, Y.; Bandte, M.; Gossmann, M.; Heiermann, M.; Plöchl, M.; Büttner, C. Survival of *Alternaria alternata* during anaerobic digestion of biomass in stirred tank reactors *Commun. Agric. Appl. Biol. Sci.* **2012**, *77*, 79–84.
55. Harsonowati, W.; Surono, M.M.; Narisawa, K. The Effectiveness of a dark septate endophytic fungus, *Cladophialophora chaetospora* SK51, to mitigate Strawberry Fusarium Wilt Disease and with growth promotion activities. *Front Microbiol.* **2020**, *11*, 585. [[CrossRef](#)]
56. Santos, M.; Cesanelli, I.; Diáñez, F.; Sánchez-Montesinos, B.; Moreno-Gavira, A. Advances in the role of dark septate endophytes in the plant resistance to abiotic and biotic stresses. *J. Fungi* **2021**, *7*, 939. [[CrossRef](#)] [[PubMed](#)]
57. Lahlali, R.; Linda McGregor, L.; Song, T.; Gossen, B.D.; Narisawa, K.; Peng, G. *Heteroconium chaetospora* induces resistance to clubroot via upregulation of host genes Involved in jasmonic acid, ethylene, and auxin biosynthesis. *PLoS ONE* **2014**, *9*, e94144. [[CrossRef](#)] [[PubMed](#)]
58. MiPAF. Ministero delle Politiche Agricole e Forestali. In *Metodi di Analisi Chimica del Suolo*; Violante, P., Ed.; Franco Angeli Editore: Roma, Italy, 1999.
59. Giovannetti, M.; Mosse, B. An evaluation of techniques for measuring vesicular arbuscular mycorrhizal infection in roots. *New Phytol.* **1980**, *84*, 489–500. [[CrossRef](#)]
60. Di Martino, C.; Delfino, S.; Pizzuto, R.; Loreto, F.; Fuggi, A. Free amino acids and glycine betaine in leaf osmoregulation of spinach responding to increasing salt stress. *New Phytol.* **2003**, *158*, 455–463. [[CrossRef](#)]
61. Lowry, O.H.; Rosebrough, N.J.; Farr, A.L.; Randall, R.J. Protein measurement with the Folin phenol reagent. *J. Biol. Chem.* **1951**, *193*, 265–275. [[CrossRef](#)]
62. Gibon, Y.; Blaesing, O.E.; Hannemann, J.; Carillo, P.; Höhne, M.; Hendriks, J.H.M.; Palacios, N.; Cross, J.; Selbig, J.; Stitt, M. A robot-based platform to measure multiple enzyme activities in Arabidopsis using a set of cycling assays: Comparison of changes of enzyme activities and transcript levels during diurnal cycles and prolonged darkness. *Plant Cell* **2004**, *16*, 3304–3325. [[CrossRef](#)]
63. Bordallo, J.J.; Lopez-Llorca, L.V.; Jansson, H.B.; Salinas, J.; Persmark, L.; Asensio, L. Colonization of plant roots by egg-parasitic and nematode-trapping fungi. *New Phytol.* **2002**, *154*, 491–499. [[CrossRef](#)]
64. NCBI. Resource Coordinators Database Resources of the National Center for Biotechnology Information. *Nucleic Acids Res.* **2018**, *46*, D8–D13. [[CrossRef](#)]
65. Benson, D.A.; Cavanaugh, M.; Clark, K.; Karsch-Mizrachi, I.; Lipman, D.J.; Ostell, J.; Sayers, E.W. GenBank. *Nucleic Acids Res.* **2013**, *41*, D36–D42. [[CrossRef](#)]



## Article

# Design of Experiments-Based Optimization of Flavonoids Extraction from *Daphne genkwa* Flower Buds and Flavonoids Contents at Different Blooming Stages

Min-Kyoung Kim <sup>1</sup>, Geonha Park <sup>2</sup>, Yura Ji <sup>2</sup>, Yun-Gyo Lee <sup>3</sup>, Minsik Choi <sup>3</sup>, Seung-Hyeon Go <sup>3</sup>, Miwon Son <sup>4</sup> and Young-Pyo Jang <sup>2,3,5,\*</sup>

<sup>1</sup> Division of Pharmacognosy, College of Pharmacy, Kyung Hee University, Seoul 02447, Korea; mindung3@khu.ac.kr

<sup>2</sup> Department of Life and Nanopharmaceutical Sciences, Graduate School, Kyung Hee University, Seoul 02447, Korea; ginapark0326@khu.ac.kr (G.P.); j5620242@naver.com (Y.J.)

<sup>3</sup> Department of Biomedical and Pharmaceutical Sciences, Graduate School, Kyung Hee University, Seoul 02447, Korea; dbsry3733@khu.ac.kr (Y.-G.L.); alstlr7595@khu.ac.kr (M.C.); 2021310688@khu.ac.kr (S.-H.G.)

<sup>4</sup> Central Research Center, Mtherapharma Co., Seoul 07793, Korea; mwson2020@mtherapharma.com

<sup>5</sup> Department of Oriental Pharmaceutical Science, College of Pharmacy, Kyung Hee University, Seoul 02447, Korea

\* Correspondence: yjang@khu.ac.kr; Tel.: +82-2-961-9421

**Citation:** Kim, M.-K.; Park, G.; Ji, Y.; Lee, Y.-G.; Choi, M.; Go, S.-H.; Son, M.; Jang, Y.-P. Design of Experiments-Based Optimization of Flavonoids Extraction from *Daphne genkwa* Flower Buds and Flavonoids Contents at Different Blooming Stages. *Plants* **2022**, *11*, 925. <https://doi.org/10.3390/plants11070925>

Academic Editors: Milan S. Stankovic, Paula Baptista and Petronia Carillo

Received: 22 February 2022

Accepted: 25 March 2022

Published: 29 March 2022

**Publisher's Note:** MDPI stays neutral with regard to jurisdictional claims in published maps and institutional affiliations.



**Copyright:** © 2022 by the authors. Licensee MDPI, Basel, Switzerland. This article is an open access article distributed under the terms and conditions of the Creative Commons Attribution (CC BY) license (<https://creativecommons.org/licenses/by/4.0/>).

**Abstract:** The flower buds of *Daphne genkwa* have been reported as a potent resource associated with anti-angiogenic, anti-tumor, anti-rheumatoid arthritis activities, as well as immunoregulation. This paper aimed to establish an optimal extraction method for flavonoids, as active phytochemicals, and to conduct a comparative analysis by profiling the different blooming stages. Optimized shaking extraction conditions from the design of experiments (DoE), such as minutely mixture design, 2<sup>3</sup> full factorial design, and polynomial regression analysis, involved an agitation speed of 150 rpm and temperature of 65 °C for 12 h in 56% (v/v) acetone solvent. After, a comparative analysis was performed on three blooming stages, juvenile bud, mature purple bud, and complete flowering, by ultra-high-performance liquid chromatography-photodiode array-mass spectrometry (UHPLC-PDA-MS). Most flavonoids increased during bud growth and then decreased when the bud opened for blooming. In particular, apigenin 7-O-glucuronide, genkwanin 5-O-primeveroside, and genkwanin strikingly showcased this pattern. Furthermore, the raw spectrometric dataset was subjected to orthogonal projection to latent structures discriminant analysis (OPLS-DA) to find significant differences in the flavonoids from the juvenile bud, mature purple bud, and complete flowering. In conclusion, the present study facilitates an understanding of flavonoid change at different blooming stages and provides a momentous reference in the research of *D. genkwa*.

**Keywords:** *Daphne genkwa*; Thymelaeaceae; flavonoids; design of experiments; blooming stages

## 1. Introduction

Botanical medicine development, including interest in their health benefit and/or ability to protect our body from health disorders, is increasing worldwide [1]. The flower buds of *Daphne genkwa* Siebold & Zucc. (Thymelaeaceae) is a well-known traditional oriental medicine and are widely used in Korea and China. *D. genkwa* was found to contain important secondary metabolites including flavonoids, lignans, terpenoids, and coumarins that are actively studied for various biological activities [2,3]. In Eastern Asia, flower buds of *D. genkwa* (Genkwae Flos) are traditionally used as medicinal parts and have been studied for various pharmacological activities. Many studies have suggested daphnane-type diterpenes as active ingredients that are responsible for diverse biological activities such as antineoplastic, neuroprotective, anti-human immunodeficiency virus

(HIV), etc. [4–8]. Phytochemical analysis showed that the flower buds contain relatively smaller amounts of diterpenes than other plant parts such as roots and stems, and other parts were also studied for the biological activities [9]. Meanwhile, recent studies have shown that Genkwae Flos, which contain flavonoids as major components [10], exhibit anti-angiogenic, anti-inflammatory [11], anti-rheumatoid arthritis [12], and antitumor [13,14] activities. The analysis of flavonoids, which are major secondary metabolites of Genkwae Flos, is important to establish an efficient quality control strategy for Genkwae Flos as a medicinal raw material.

To the best of our knowledge, there is no research focusing on the comparative analysis for the classification of blooming stages of *D. genkwa* pertaining to the flavonoids profile. Indeed, flavonoids are very rich and primarily affected by the growth stage of the flower in diverse species such as *Chrysanthemum morifolium*, *Lycoris radiata*, *Agastache rugosa*, etc. [15–17]. Likewise, if Genkwae Flos shows a large difference in flavonoids content during the flowering period, this could be an important quality variable in the development of medicines using Genkwae Flos as a raw material. This study was conducted to provide scientific evidence for these questions.

According to the characteristic morphology and color, the medicinal part of *D. genkwa* flowers could be divided into three stages: juvenile bud (S1), mature purple bud (S2), and complete flowering (S3). As can be seen in Figure 1, the juvenile buds (S1) are green and densely covered with white downy hair. The mature purple buds (S2) are fully purple and the hair on the top has disappeared. Finally, at the complete flowering (S3), blooming purple flowers are gathered in an umbel [18].

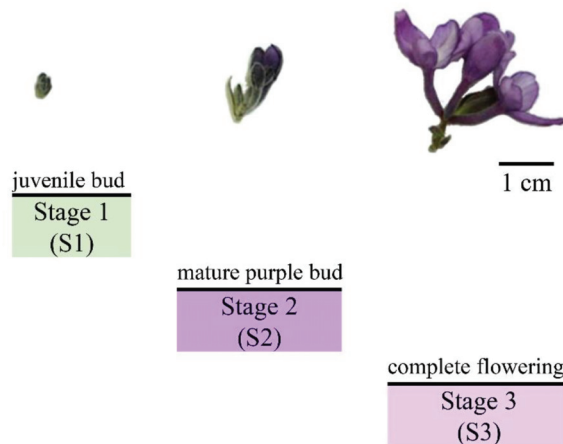


**Figure 1.** Morphological changes in the buds to flowers of *D. genkwa* at three blooming stages.

Our previous study [19] established a systematic and robust ultra-high-performance liquid chromatography-photodiode array (UHPLC-PDA) analysis that could identify and quantify eleven flavonoids of *D. genkwa*: (1) apigenin 5-*O*-glucoside, (2) apigenin 7-*O*-glucoside, (3) yuanhuanin, (4) apigenin 7-*O*-glucuronide, (5) genkwanin 5-*O*-primeveroside, (6) genkwanin 5-*O*-glucoside, (7) genkwanin 4'-*O*-rutinoside, (8) tiliroside, (9) apigenin, (10) 3'-hydroxygenkwanin, and (11) genkwanin. The representative chromatographic profile is shown in Figure 2 and eleven flavonoid peaks are indicated, with accompanying structural information. In this study, we tried to reveal the relationship between changes in the flavonoid profile and the three blooming stages using metabolomics technology.

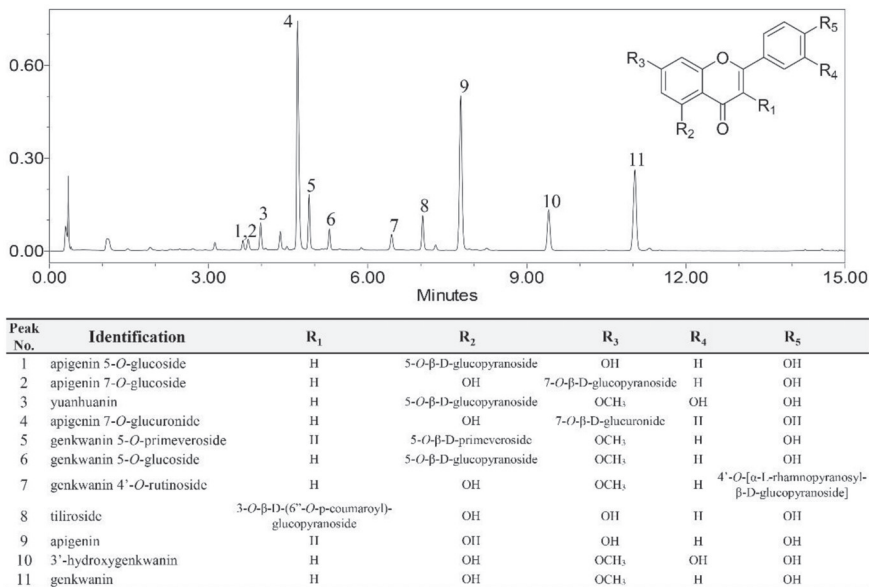


**Figure 2.** Representative UHPLC chromatogram of *D. genkwa* buds in 56% (*v/v*) acetone solvent. Flavonoids are indicated in the figure as 1–11: (1) apigenin 5-*O*-glucoside, (2) apigenin 7-*O*-glucoside, (3) yuanhuanin, (4) apigenin 7-*O*-glucuronide, (5) genkwanin 5-*O*-primeveroside, (6) genkwanin 5-*O*-glucoside, (7) genkwanin 4'-*O*-rutinoside, (8) tiliroside, (9) apigenin, (10) 3'-hydroxygenkwanin, and (11) genkwanin.

Prior to the metabolomics analysis, the optimized extraction solvents and conditions showing the maximum flavonoid extraction efficiency were needed to be optimized by design of experiments (DoEs) for reliable and consistent metabolomics studies. DoE is used to plan to-be-performed experiments for approaching the question to be solved and considers how to analyze the data using statistical methods in order to gather the maximum amount of information from a minimum number of experiments [20]. Experiments are conducted according to the experimental design and the responses are recorded for determining main effects and interaction effects between multi-variables. To extract flavonoids from plant matrix, solvent properties are very important to penetrate plant cell walls and dissolve intracellular metabolites. In this regard, a mixed composition of water and organic solvents was used for the extraction of phytochemicals with diverse degrees of polarity [21–23]. Therefore, the optimization of ternary mixtures was investigated with the mixture design method to test extraction efficacy in totality from non-polar aglycones (genkwanin and apigenin) to polar flavonoid glycosides.

After defining the optimal solvent mixture system, the best shaking extraction conditions were explored using 2<sup>3</sup> full factorial design (FFD) and polynomial regression analysis. Shaking extraction could minimize the degradation of the heat-sensitive natural products and consumes low energy, which is particularly advantageous for large-scale industrial processes [23,24]. The parameters that could affect the extract efficiency of the shaking procedure are agitation speed, extraction time, setting temperature, and solvent-to-material ratio [25]. Since these parameters influence each other and a complex interaction can be observed, DoE is widely used to evaluate multivariable effects based on statistical analysis [26]. Among the various approaches to design the experiments, FFD is utilized because it enables to discuss the joint effect of the studied factors (or design parameters) on a response with all possible combinations of levels for all factors [26]. In this study, the

significant parameters for shaking extraction were elucidated through FFD and the best condition was determined by polynomial regression analysis.

## 2. Results

### 2.1. Optimization of the Extraction Solvents

To penetrate the complex plant matrix, aqueous mixtures with alcoholic solvents, acetone, and ethyl acetate were considered suitable for diverse plant sources [27]. Also, flavonoids have polar (glycosidic form) to less polar (aglycone form, mainly flavones) constituents and predominant secondary metabolites in *D. genkwa* [19]. Therefore, water and two polar organic solvents, a dipole moment ( $\mu$ ) of  $>2$  (acetone 2.69 and methanol 2.87), were selected considering water-mixability.

Designing an approach to understand the best solvent for enriching target metabolites, flavonoids, we used the mixture design with the primary three solvents being selected: water ( $X_1$ ), acetone ( $X_2$ ), and methanol ( $X_3$ ). When performing the mixture design, the shaking extraction process was at 200 rpm,  $22 \pm 2$  °C, for 24 h, and in 30 mg/mL.

A total of 12 assays (Table 1) using the simplex-centroid design were executed and each response function was expressed as total flavonoids extraction efficacy, calculated by summing all identified flavonoid peak areas (Figure 2). The independent 12 assays were all performed in triplicate to evaluate the experimental error. The  $p$ -value (0.001) showed strong evidence that the model was very suitable. Also, the high  $R^2$  value (95.94%) and lack of fit (0.158) validated that all response functions fit the experimental data well with good predictability in the extraction of total flavonoids using various solvent mixtures (Table 2).

**Table 1.** Matrix of three variables in mixture design (simplex centroid) and experimental data for solvent mixture of maximum flavonoids extraction efficacy.

Runs	Variables			Total Flavonoids <sup>1</sup>
	Water $X_1$ % (v/v)	Acetone $X_2$ % (v/v)	Methanol $X_3$ % (v/v)	
1	100 (1)	0 (0)	0 (0)	146,058 $\pm$ 43,563
2	0 (0)	100 (1)	0 (0)	1,989,632 $\pm$ 31,687
3	0 (0)	0 (0)	100 (1)	5,451,037 $\pm$ 49,792
4	50 (1/2)	50 (1/2)	0 (0)	5,503,924 $\pm$ 33,794
5	50 (1/2)	0 (0)	50 (1/2)	2,702,388 $\pm$ 96,492
6	0 (0)	50 (1/2)	50 (1/2)	3,935,165 $\pm$ 81,567
7	66.7 (2/3)	16.7 (1/6)	16.7 (1/6)	3,330,635 $\pm$ 91,563
8	16.7 (1/6)	66.7 (2/3)	16.7 (1/6)	5,460,748 $\pm$ 78,409
9	16.7 (1/6)	16.7 (1/6)	66.7 (2/3)	5,005,935 $\pm$ 70,199
10	33.3 (1/3)	33.3 (1/3)	33.3 (1/3)	5,103,037 $\pm$ 93,384
11 (CP <sup>2</sup> )	33.3 (1/3)	33.3 (1/3)	33.3 (1/3)	5,559,679 $\pm$ 69,015
12	33.3 (1/3)	33.3 (1/3)	33.3 (1/3)	5,451,037 $\pm$ 77,357

<sup>1</sup> The sum of eleven flavonoids peak area, Mean  $\pm$  Standard Deviation; <sup>2</sup> Central Point.

**Table 2.** ANOVA for the mixture design and two-level for three variables ( $2^3$ ) FFD models.

Sources of Variations	Degree of Freedom	Sum of Squares	Mean Square	F-Value	p-Value
<b>Mixture design for solvent mixture of maximum flavonoids extraction efficacy</b>					
* Model	5	$3.269 \times 10^{13}$	$6.538 \times 10^{12}$	28.39	0.001
Total Error	6	$1.382 \times 10^{12}$	$2.303 \times 10^{11}$		
Lack of Fit	4	$1.268 \times 10^{12}$	$3.170 \times 10^{11}$	5.57	0.158
Pure Error	2	$1.138 \times 10^{11}$	$5.690 \times 10^{10}$		
Total Adjusted	11	$3.407 \times 10^{13}$			
<b><math>2^3</math> FFD for optimization of flavonoids shaking extraction conditions</b>					
* Model	8	$4.012 \times 10^{12}$	$5.015 \times 10^{11}$	54.13	0.001
Time ( $X_a$ )	1	$4.458 \times 10^9$	$4.458 \times 10^9$	0.48	0.495
* Temperature ( $X_b$ )	1	$3.757 \times 10^{12}$	$3.757 \times 10^{12}$	405.51	0.001
Shaking speed ( $X_c$ )	1	$5.442 \times 10^7$	$5.442 \times 10^7$	0.01	0.940
$X_a \cdot X_b$	1	$1.173 \times 10^7$	$1.173 \times 10^7$	0.00	0.972
* $X_a \cdot X_c$	1	$4.806 \times 10^{10}$	$4.806 \times 10^{10}$	5.15	0.032
$X_b \cdot X_c$	1	$3.102 \times 10^{10}$	$3.102 \times 10^{10}$	3.35	0.080
$X_a \cdot X_b \cdot X_c$	1	$1.158 \times 10^{10}$	$1.158 \times 10^{10}$	1.25	0.275
Pure Error	24	$2.223 \times 10^{11}$	$9.264 \times 10^9$		
Total Adjusted	32	$4.234 \times 10^{12}$			

\* Significant.

According to the analysis of regression coefficients at the 95% confidence level, the linear terms  $X_1$ ,  $X_2$ , and  $X_3$  and the interaction terms  $X_1X_2$  and  $X_1X_3$  were significant whereas the interaction term  $X_2X_3$  was not significant but contributed to the fitness of the model, therefore the following equation was mathematically calculated:

$$Y = -66788 \cdot X_1 + 2078100 \cdot X_2 + 5355400 \cdot X_3 + 19773000 \cdot X_1X_2 + 1275800 \cdot X_1X_3 + 3122300 \cdot X_2X_3 \quad (1)$$

where Y is expressed in summing eleven identified flavonoids peak areas, \* means significant parameters ( $p < 0.05$ ),  $X_1$  is water,  $X_2$  is acetone, and  $X_3$  is methanol.

The best solvent mixture was calculated by response surface methodology using upper multivariate Equation (1) by illustration with a 3D ternary graph (Figure 3A) and 2D contour plot (Figure 3B). In the 3D ternary graph (Figure 3A), the optimal zone where flavonoids are maximally extracted is shown at the top of the non-symmetrical open plane curve formed by interaction with acetone ( $X_2$ ) and water ( $X_1$ ). As can be seen from the optimization diagram (Figure 3C), both acetone ( $X_2$ ) and water ( $X_1$ ) have parabolic curve influence on the flavonoids extraction efficacy that can calculate the response of the maximum value. Methanol ( $X_3$ ) also has a parabolic curve effect but an opposite shape, and does not even contain an optimal mixture solvent point, which is indicated by a red line in each solvent of optimization diagram (Figure 3C).

Finally, a binary mixture consisting of water ( $X_1$ ) and acetone ( $X_2$ ) in a 44:56 ratio ( $X_1:X_2$ ) achieved the best extraction and yielded a Y value of 600,700 as shown in the optimization diagram (Figure 3C).

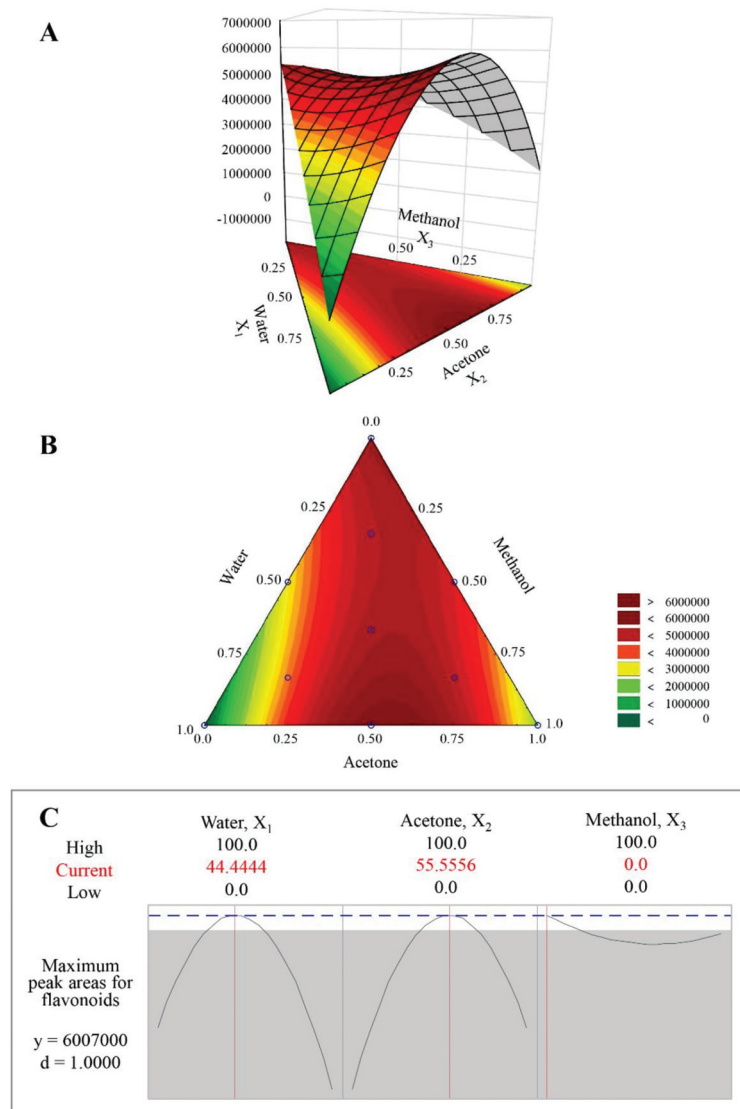


**Figure 3.** (A) 3D Response surface, (B) 2D Contour plot, and (C) optimization diagram obtained from mixture design for the solvent mixture of maximum flavonoids extraction efficacy.

### 2.2. Optimization of the Shaking Extraction Process

After the preliminary study for the solvent system, where the optimized solvent mixture was defined as 56% acetone in water, the detailed shaking procedure was optimized. The purpose of extraction is to efficiently separate the soluble metabolites of plants using selective solvents through appropriate procedures [27]. Among the various extraction methods, the shaking method is an economic and low-energy consumption extraction process that is often adopted in the natural products industry, and is very practical to yield high amounts of phytochemicals [28]. To optimize the shaking extraction conditions for maximum extraction of flavonoids, two stages of optimization were pursued: (a) a screening step, where three variables (extraction time, extraction temperature, shaking speed) were studied to identify those with significant effects on the dependent variable

(flavonoid extraction efficacy), and (b) the final optimization step, where the significant variable was further examined to determine the best condition. The two-level FFD is well-known for screening design to select meaningful factors and understand individual and/or synergetic effects in a multivariable system [29].

A  $2^3$  FFD was used to screen three variables such as extraction time ( $X_a$ ), extraction temperature ( $X_b$ ), and shaking speed ( $X_c$ ), which have an important influence on the extraction efficiency of the shaking method [28]. A total of eleven runs with three replicates in the central point (Table 3) was given by the expression  $2k + C$ , where  $k$  is the number of variables, and  $C$  is the number of central points [30], and all points were performed in triplicate for the evaluation of error. An ANOVA (Table 2) showed that shaking temperature ( $X_b$ ) and the interaction of shaking time and shaking speed ( $X_a \cdot X_c$ ) were significant with a great coefficient to the efficacy of flavonoids extraction evidenced by small  $p$ -values ( $<0.05$ ). In general, shaking speed and extraction time have a significant effect on the extraction efficiency of target metabolites, but in the case of plant samples with fragile tissues such as Genkwae Flos, these parameters do not seem to have a significant effect. Among the parameters, the extraction temperature ( $X_b$ ) showed a significant influence compared to the  $X_a \cdot X_c$  interaction which is shown from the much higher  $F$ -values. Also, the high  $R^2$  value (94.75%) and low  $p$ -value (0.001) showed good evidence of suitability and accuracy of this experimental model to predict the response. As can be seen in the Pareto chart (Figure 4A), main effect diagram (Figure 4B), and interaction effect diagram (Figure 4C), the  $X_b$  and  $X_a \cdot X_c$  had a striking positive influence on the flavonoids extraction efficacy and the temperature ( $X_b$ ) bar has the longest length in the Pareto chart (Figure 4A), which means this effect is the greatest. Those results were also summarized by the following equation:

$$Y = 7872868 + 5206 \cdot X_a + 24666 \cdot X_b + 1628 \cdot X_c - 91.2 \cdot X_a X_b - 39.4 \cdot X_a X_c - 35.4 \cdot X_b X_c + 0.595 \cdot X_a X_b X_c \quad (2)$$

where  $Y$  is expressed as the sum of the eleven identified flavonoids peak area, \* means significant parameters ( $p < 0.05$ ),  $X_a$  is shaking time,  $X_b$  is shaking temperature, and  $X_c$  is shaking speed.

**Table 3.** Matrix of  $2^3$  FFD and experimental data for optimization of flavonoids shaking extraction conditions.

Runs	Experimental Values			Coded Values			Total Flavonoids <sup>1</sup>
	Time $X_a$ h	Temp. $X_b$ °C	Speed $X_c$ rpm	Time $X_a$ h	Temp. $X_b$ °C	Speed $X_c$ rpm	
1	12	4	50	−1	−1	−1	8,081,710 ± 156,685
2	48	4	50	1	−1	−1	8,189,275 ± 95,743
3	12	45	50	−1	1	−1	8,990,219 ± 72,030
4	48	45	50	1	1	−1	9,007,132 ± 38,952
5	12	4	250	−1	−1	1	8,290,059 ± 155,656
6	48	4	250	1	−1	1	8,130,775 ± 65,101
7	12	45	250	−1	1	1	8,966,887 ± 100,054
8	48	45	250	1	1	1	8,892,662 ± 140,943
9	30	24	150	0	0	0	8,685,553 ± 57,434
10 (CP <sup>2</sup> )	30	24	150	0	0	0	8,719,852 ± 40,179
11	30	24	150	0	0	0	8,769,795 ± 45,904

<sup>1</sup> The sum of eleven flavonoids peak area, Mean ± Standard Deviation; <sup>2</sup> Central Point.

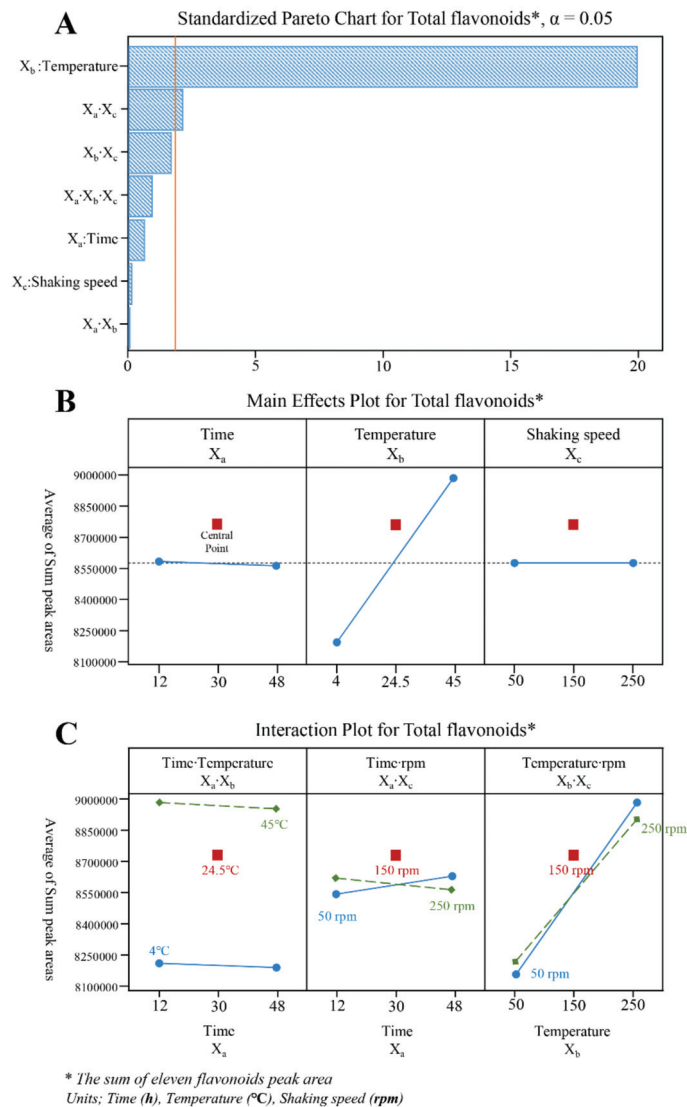


**Figure 4.** (A) Pareto Chart, (B) Main Effects Plot, and (C) Interaction Plot in  $2^3$  FFD for optimization of flavonoids shaking extraction conditions.

For the optimization step, the most influencing factor of temperature ( $X_b$ ) was further analyzed to define the best extraction condition. The designed  $X_b$  had four steps ranging from 20 to 80 °C considering the boiling point (70.2 °C) of the solvent mixture calculated from the mole % acetone in water [31]. Each of four experimental points was performed in triplicate and ANOVA analysis was performed to describe statistical suitability. To avoid overfitting, stepwise regression analysis (first-order, second-order, and third-order equations) was performed and compared the goodness of fit of the data based on two calculated evaluation measures, Akaike Corrected Information Criterion (AICc) and Bayesian Information Criterion (BIC) (Table 4). The smaller the AICc and BIC are, the better the model fits the data. As shown in Table 4, in the third-order equation model, AICc was the lowest at 851.65, and BIC was also the lowest at 857.57, which indicates the best fit for

the data. The high values of the regression coefficient ( $R^2 = 95.85\%$ ) and a high level of statistical significance ( $p$ -value  $< 0.001$ ) also validated the selection of the third-order model and high degree of data fitness (Table 4). The third-order regression equation is given as follows:

$$Y = 8672000 - 23670 \cdot X_b + 860 \cdot X_b^2 - 6.905 \cdot X_b^3 \quad (3)$$

where  $Y$  is defined as the sum of peak areas of the identified eleven flavonoids and  $X_b$  is temperature.

**Table 4.** Stepwise regression analysis along with coefficients of each equation and model parameters.

	First-Order		Second-Order		Third-Order	
	Coefficient	$p$ -Value	Coefficient	$p$ -Value	Coefficient	$p$ -Value
Constant	8,443,470	-	8,091,816	-	8,672,000	-
$X_b$	4881	0.0001	22,463	0.0001	-23,670	0.001
$X_b^2$	-	-	-175.8	0.0001	860	0.0001
$X_b^3$	-	-	-	-	-6.905	0.0001
S	86,755.6		48,564.3		29,786.3	
$R^2$	62.62%		88.63%		95.85%	
$R^2$ (adj)	61.52%		87.94/%		95.46%	
<sup>1</sup> AICc	925.56		885.25		851.65	
<sup>2</sup> BIC	929.56		890.29		857.57	

<sup>1</sup> AICc; Akaike Corrected Information Criterion; <sup>2</sup> BIC; Bayesian Information Criterion.

By mathematical approach, the maximum point of the three-order polynomial equation was found at 65.6 °C (Figure 5). Finally, the optimum shaking extraction conditions to maximize the flavonoids extraction from *D. genkwa* flower buds were determined as 44:56 ratio (water: acetone,  $v/v$ ) solvent mixture, 150 rpm shaking speed, 12 h shaking time, and 65 °C temperature. To validate this model, six replicates were extracted with the optimal conditions. The experimental value was  $8,955,360 \pm 36,450$  ( $N = 6$ ), which was close to the predicted value (8,871,048) with 0.94% percent error, sufficiently satisfying the predictability of the model.

### 2.3. Flavonoids Profile Change by Blooming Stages

In order to analyze the change in the content of individual flavonoid components according to the growth period of the buds (juvenile bud (S1), mature purple bud (S2), and complete flowering (S3)), the area values for the identified 11 flavonoid peaks were analyzed from the samples of the three different stages. A total of 108 chromatographic raw data (from triplicate of 36 samples) were converted into binary format and introduced to SIMCA-P for the multivariate analysis. Then Orthogonal Partial Least Squares Discriminant Analysis (OPLS-DA) was performed to investigate whether the discrimination of growth stages was possible in terms of the changes in flavonoid profiles. OPLS is an extension of PLS which can separate the systematic variation of data matrix into classes by finding important variables that maximize the variance between classes and also orthogonal latent variables to separate by classes [32]. In the present study, a score plot (Figure 6A) showed a clear clustering of three flowering stages with classification rate of 100%. The model was quite consistent and robust by the values of  $R^2X$  (0.982) and  $R^2Y$  (0.928) parameters. Also, the high value of  $Q^2Y$  (0.901) indicates great predictability. Besides, CV-ANOVA ( $p < 0.001$ ), Hotelling's  $T^2$  using 95% and 99% confidence limits, and permutation testing ( $N = 200$ ) were performed to exclude overfitting and validate the model (Figure 6B,C).

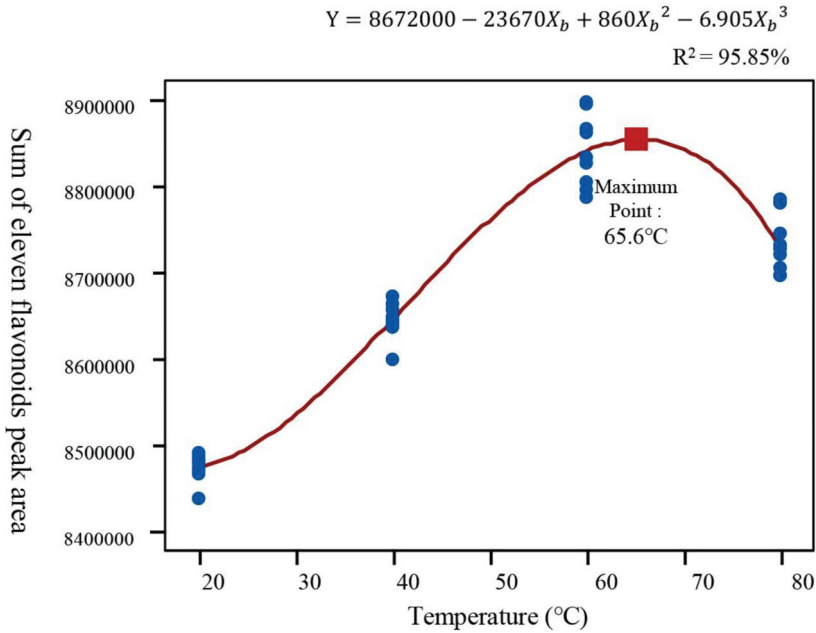


**Figure 5.** Polynomial regression curve by temperature (°C,  $X_b$ ) for the maximum flavonoids extraction efficacy.

In order to elucidate flavonoid component(s) responsible for the differentiation of each flowering stage, the Variable Importance in Projection (VIP) approach was applied. Three flavonoids possessing the highest VIP score > 1.000 (adjusted  $p < 0.5$ ) were selected as follows; apigenin 7-*O*-glucuronide (3.574), genkwanin 5-*O*-primeveroside (1.178), and genkwanin (1.208).

Afterwards, a heatmap of eleven flavonoids contents according to three stages was visualized (Figure 7A). The heatmap for three flavonoids of apigenin 7-*O*-glucuronide, genkwanin 5-*O*-primeveroside, and genkwanin were extracted separately because they showed a similar pattern of contents change according to the blooming stages. The relative content chart for these three flavonoids was represented to show the changing trend during growing stages (Figure 7B). These components increased when the bud matured (S1 to S2) and decreased when fully bloomed (S2 to S3).

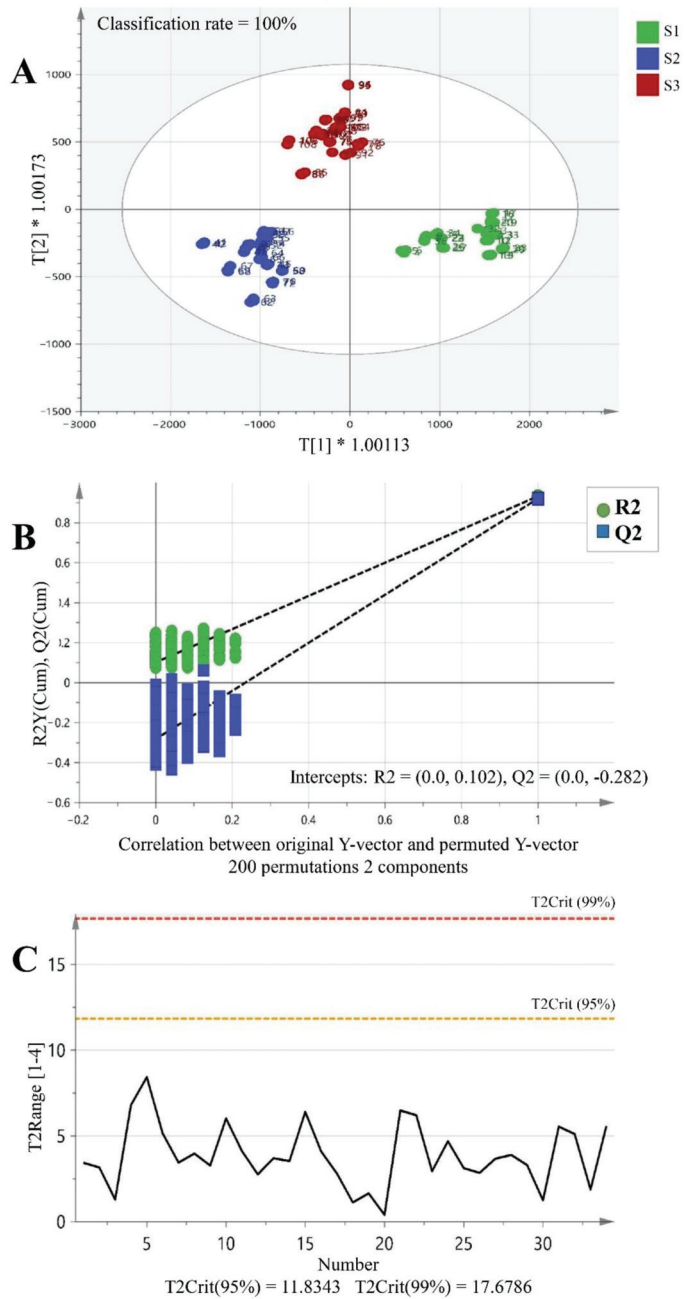


**Figure 6.** OPLS-DA score plot of samples from three stages (S1, S2, and S3) (A) and the validation of model using permutation test (B) and (C) Hotelling’s  $T^2$  test ( $R^2X = 0.982$ ,  $R^2Y = 0.928$ ,  $Q^2Y = 0.901$ ).  $T[1]*1.00113$  and  $T[2]*1.00173$  mean  $T[1] \times 1.00113$  and  $T[2] \times 1.00173$ , respectively.

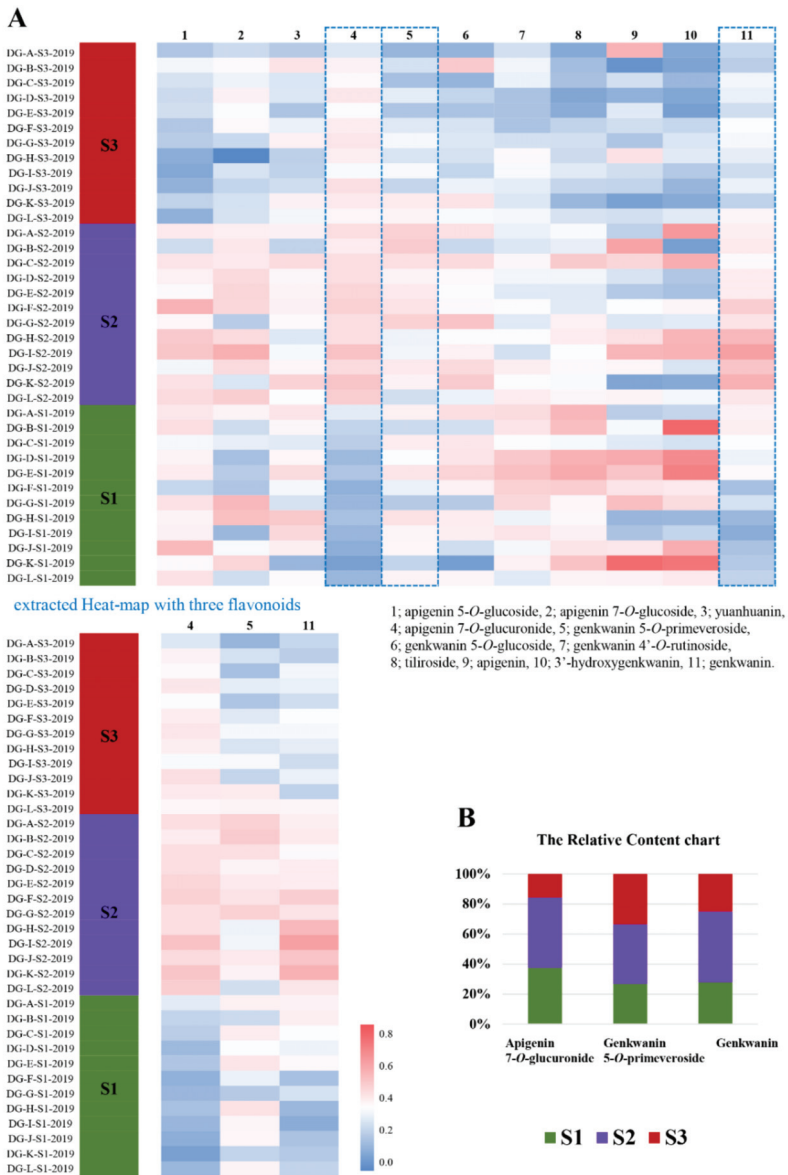


**Figure 7.** Significant changes in flavonoid biomarker candidates in S1, S2, and S3 blooming stages: (A) Heat-map visualization for 11 flavonoids and three significant flavonoids and (B) the relative content chart for three flavonoids.

### 3. Discussion

The quality control of botanical raw material is gradually progressing in the direction of identification and quantification of all possible phytochemicals using chemical fingerprinting and profiling approaches [33]. Optimization of the extraction process in the analysis of plant raw materials is the most basic step that must precede all analysis studies. Therefore, the best solvent mixture system and shaking extraction conditions

for the maximum extraction of flavonoids from *D. Genkwa* flower buds were optimized in this study by various DoEs. The metabolomics studies using the optimized extraction conditions could greatly improve the robustness of the experimental results. It is interesting that the shaking speed and extraction time, which are factors affecting the extraction efficiency of the shaking extraction method in general, have a lower effect than the extraction temperature in the case of Genkwae Flos. This is presumed to be due to the characteristics of the tissue of Genkwae Flos, which is softer and weaker than other plant parts, so that it is easily penetrated by solvents. Next, a series of metabolomics studies were performed to clarify whether flavonoid components, the main ingredient of Genkwae Flos, change by flowering stages, which will provide important data for the quality control of drug products developed with Genkwae Flos as a raw material. As a result, most flavonoids increased as the buds grew and then decreased when the buds were in full bloom (Table S2). In particular, this pattern is clearly observed in three unique flavonoids, apigenin 7-*O*-glucuronide, genkwanin 5-*O*-primeveroside, and genkwanin, which are also selected as the most influencing components for the discrimination of flowering stages by multivariate analysis. If further research is conducted on whether these components are deeply correlated with the biological activities of Genkwae Flos [10–14], it will be possible to know when it is most efficient to harvest the material using the information established through this study. As in this study, plant metabolomics studies systematically conducted through the design of experiments will be of great help in developing more accurate and reproducible quality control technologies for medicinal herbal products.

#### 4. Materials and Methods

##### 4.1. Chemicals and Reagents

Extra pure grade solvents (purity > 99.5%) of methanol, acetone, and water were supplied from Duksan Pure Chemicals (Seoul, Korea). For UHPLC-PDA analysis, HPLC-grade solvents (purity > 99.9%) of acetonitrile and water and HPLC-grade formic acid (purity > 99.0%) were purchased from Thermo Fisher Scientific (Seoul, Korea).

##### 4.2. Plant Material

The buds or flowers of *D. genkwa* at three different blooming stages, juvenile bud (S1), mature purple bud (S2), and complete flowering (S3), were collected from 12 Genkwa trees in Korea in April to June 2019. A dozen of biological replicates (A to L) were selected in this study, of which five (A to E) were collected from Medicinal Herb Garden of College of Pharmacy, Kyung Hee University, Seoul, and the other seven (F to L) from greenhouses in different places. The botanical origin of all trees (A to L) was authenticated by morphological examination including leaf arrangement, flower color, shape of leaf, number of stamens, inflorescent, etc., compared to the previous taxonomic literature [18,19]. The collected buds or flowers were immediately lyophilized and labeled as DG-A-S1-2019 to DG-L-S3-2019 (Table S1). The samples were stored in a deep freezer until analyses.

##### 4.3. Sample Preparation

Thirty milligrams of each lyophilized sample and 5 mm steel bead (QIAGEN) were placed in a 2 mL tube (Eppendorf) and ground to homogeneous fine powder by Tissue-Lyser (QIAGEN) in the frequency of 30 Hz for 3 min. For the comparative analysis in different blooming stages, those milled samples were added to 1 mL of the solvent established through mixture design and extracted according to the optimal shaking extraction conditions from the 2<sup>3</sup> full factorial design and polynomial regression analysis.

##### 4.4. UHPLC-PDA Analysis

Flavonoid identification was performed on a Waters ACQUITY™ H-class UPLC system with PDA detector and operated by Empower-3 software (Waters Corporation, Milford, MA, USA). A column Kinetex-C18 (2.1 × 50 mm, 1.7 μm, Phenomenex) was used for separation, with the column temperature set at 28 °C. For the mobile phase, the binary

gradient elution system consisted of acetonitrile (A) and 0.1% (v/v) formic acid in water (B). The elution method was as follows: linear gradient from 10 to 45% A (0–13 min), 45 to 100% A (13–13.5 min), 100 to 10% A (13.5–14 min), and isocratic 10% A (14–15 min). The flow rate and sample manager temperature were 0.35 mL/min and 25 °C, respectively. The detection wavelength was fixed at 335 nm. Those UHPLC conditions were optimized by analytical quality-by-design (AQbD) and validated in our previous report [25].

#### 4.5. Mixture Design

A mixture design was used to find the optimum solvent composition for the maximum flavonoids extraction. Twelve representative mixtures were set up by simplex centroid design (Table 1) using water, acetone, and methanol as follows: the triangle vertices at 1:0:0 ratio (v/v/v) as pure solvents; the edges at 1/2:1/2:0 ratio (v/v/v) as binary mixtures; three central points to estimate the pure error at 1/3:1/3:1/3 ratio (v/v/v) as equivalent ternary mixture; the axial points at 2/3:1/6:1/6 ratio (v/v/v) as non-equivalent ternary mixture. For the study of optimized solvents system, the extraction conditions were set as shaking speed of 200 rpm for 24 h at room temperature (22 ± 2 °C). All twelve points were performed in triplicate for the evaluation of experimental error. The content of total flavonoids was the dependent variable, which was obtained by summing eleven flavonoid peaks areas in each chromatographic result. The Minitab software ver. 18 and Statistica software ver. 13.3.0 (TIBCO Software Inc., Palo Alto, CA, USA) were employed for experimental design, statistical analysis, and model building. The following second-order polynomial Equation (4) represents this model:

$$Y = \beta_0 + \sum_{1 \leq i \leq 3} \beta_i x_i + \sum_{1 \leq i < j \leq 3} \beta_{ij} x_i x_j + \sum_{1 \leq i < j < k \leq 3} \beta_{ijk} x_i x_j x_k \quad (4)$$

where Y is the response,  $\beta_0$  is the corresponding coefficient for intercept,  $\beta_i$  is for each linear effect term, and  $\beta_{ij}$  and  $\beta_{ijk}$  are binary and ternary interaction effect terms. The independent variables are represented in the equation as  $x_i$ ,  $x_j$ , and  $x_k$ .

#### 4.6. Optimization of the Shaking Extraction Condition

To identify significant variables, an FFD of two levels (2<sup>3</sup>) was applied as shown in Table 3 for shaking time (h), temperature (°C), and speed of agitation (rpm). The dependent variable was the same as stated in the mixture design. Total experimental runs were eleven including triplicate of central point to estimate synergetic interactions in a multivariable system and to also estimate the significant factors deducing model coefficients. The results were fitted to a first-order Equation (5):

$$Y = \beta_0 + \sum_i \beta_i x_i + \sum_{i \neq j} \beta_{ij} x_i x_j \quad (5)$$

where Y is the response,  $x_i$  and  $x_j$  are independent variables, and  $\beta_0$ ,  $\beta_i$ , and  $\beta_{ij}$  are the corresponding coefficients for intercept, linear, and interaction terms, respectively.

After elucidation of the significant variable (temperature), further polynomial regression analysis was conducted to define the best extract conditions. The experimental points were four steps ranging from 20 °C to 80 °C. All the experimental designs were performed by Minitab software ver. 18, and an ANOVA was performed for statistical suitability.

#### 4.7. Multivariate Statistical Analysis

Multivariate statistical analysis was performed using SIMCA-P 14.0 (Umetrics, Malmo, Sweden). The acquired raw metabolomics dataset was elaborated for OPLS-DA study. The Hotelling's T<sup>2</sup> in 95% and 99% confidence limits were tested to investigate outliers. Cross-validation ANOVA ( $p < 0.001$ ) was carried out to define goodness-of-fit in R<sup>2</sup>X, R<sup>2</sup>Y, and Q<sup>2</sup>Y. Permutation testing ( $N = 200$ ) was applied to exclude model overfitting. The VIP was conducted to select marker phytochemicals having the highest classification potential. When constructing the heatmap, raw data was rescaled from 0 to 1 by variable transformation to remove any bias in actual concentration levels.

**Supplementary Materials:** The following supporting information can be downloaded at: <https://www.mdpi.com/article/10.3390/plants11070925/s1>, Table S1: List of *D. genkwa* buds or flowers from DG-A-S1-2019 to DG-L-S3-2019; Table S2: Peak area of each eleven flavonoids peak from DG-A-S1-2019 to DG-L-S3-2019.

**Author Contributions:** Conceptualization, M.-K.K., M.S. and Y.-P.J.; methodology, M.-K.K. and M.C.; software, G.P. and Y.-G.L.; formal analysis, Y.J. and S.-H.G.; data curation, M.-K.K.; writing—original draft preparation, M.-K.K. and G.P.; writing—review and editing, M.-K.K. and Y.-P.J.; funding acquisition, M.S. and Y.-P.J. All authors have read and agreed to the published version of the manuscript.

**Funding:** This research was supported by Basic Science Research Program through the National Research Foundation of Korea (NRF) funded by the Ministry of Education (grant number: 2018M3A9F3081538).

**Institutional Review Board Statement:** Not applicable.

**Informed Consent Statement:** Not applicable.

**Data Availability Statement:** The data is available from the authors upon request.

**Conflicts of Interest:** The authors declare no conflict of interest.

## References

- Upton, R.; David, B.; Gafner, S.; Glasl, S. Botanical ingredient identification and quality assessment: Strengths and limitations of analytical techniques. *Phytochem. Rev.* **2020**, *19*, 1157–1177. [\[CrossRef\]](#)
- Xu, W.C.; Shen, J.G.; Jiang, J.Q. Phytochemical and biological studies of the plants from the genus *Daphne*. *Chem. Biodivers.* **2011**, *8*, 1215–1233. [\[CrossRef\]](#) [\[PubMed\]](#)
- Hou, X.; Hou, X.; Li, L. Chemical constituents from the flower buds of *Daphne genkwa* (Thymelaeaceae). *Biochem. Syst. Ecol.* **2020**, *91*, 104055. [\[CrossRef\]](#)
- He, W.; Cik, M.; Appendino, G.; Puyvelde, L.V.; Leysen, J.E.; De Kimpe, N. Daphnane-type diterpene orthoesters and their biological activities. *Mini Rev. Med. Chem.* **2002**, *2*, 185–200. [\[CrossRef\]](#) [\[PubMed\]](#)
- Hong, J.-Y.; Nam, J.-W.; Seo, E.-K.; Lee, S.K. Daphnane diterpene esters with anti-proliferative activities against human lung cancer cells from *Daphne genkwa*. *Chem. Pharm. Bull.* **2010**, *58*, 234–237. [\[CrossRef\]](#) [\[PubMed\]](#)
- Li, F.; Sun, Q.; Hong, L.; Li, L.; Wu, Y.; Xia, M.; Ikejima, T.; Peng, Y.; Song, S. Daphnane-type diterpenes with inhibitory activities against human cancer cell lines from *Daphne genkwa*. *Bioorg. Med. Chem. Lett.* **2013**, *23*, 2500–2504. [\[CrossRef\]](#) [\[PubMed\]](#)
- Han, B.-S.; Kim, K.-S.; Kim, Y.J.; Jung, H.-Y.; Kang, Y.-M.; Lee, K.-S.; Sohn, M.-J.; Kim, C.-H.; Kim, K.-S.; Kim, W.-G. Daphnane diterpenes from *Daphne genkwa* activate Nurr1 and have a neuroprotective effect in an animal model of Parkinson's disease. *J. Nat. Prod.* **2016**, *79*, 1604–1609. [\[CrossRef\]](#)
- Han, B.; Kim, K.; Kim, Y.; Van Minh, N.; Jung, H.; Sohn, M.; Won, G.K. Nurr1-Activating Daphnane Diterpenes from *Daphne genkwa* and its Neuroprotective Effect in an Animal Model of Parkinson's Disease. *Planta Med. Int. Open* **2017**, *4* (Suppl. 1), S1–S202. [\[CrossRef\]](#)
- Han, B.-S.; Van Minh, N.; Choi, H.-Y.; Byun, J.-S.; Kim, W.-G. Daphnane and phorbol diterpenes, anti-neuroinflammatory compounds with Nurr1 activation from the roots and stems of *Daphne genkwa*. *Biol. Pharm. Bull.* **2017**, *40*, 2205–2211. [\[CrossRef\]](#)
- Moshiashvili, G.; Tabatadze, N.; Mshvildadze, V. The genus *Daphne*: A review of its traditional uses, phytochemistry and pharmacology. *Fitoterapia* **2020**, *143*, 104540. [\[CrossRef\]](#)
- Zhou, D.-C.; Zheng, G.; Jia, L.-Y.; He, X.; Zhang, C.-F.; Wang, C.-Z.; Yuan, C.-S. Comprehensive evaluation on anti-inflammatory and anti-angiogenic activities in vitro of fourteen flavonoids from *Daphne Genkwa* based on the combination of efficacy coefficient method and principal component analysis. *J. Ethnopharmacol.* **2021**, *268*, 113683. [\[CrossRef\]](#) [\[PubMed\]](#)
- Sun, Y.-W.; Bao, Y.; Yu, H.; Chen, Q.-J.; Lu, F.; Zhai, S.; Zhang, C.-F.; Li, F.; Wang, C.-Z.; Yuan, C.-S. Anti-rheumatoid arthritis effects of flavonoids from *Daphne genkwa*. *Int. Immunopharmacol.* **2020**, *83*, 106384. [\[CrossRef\]](#) [\[PubMed\]](#)
- Du, W.J.; Yang, X.L.; Song, Z.J.; Wang, J.Y.; Zhang, W.J.; He, X.; Zhang, R.Q.; Zhang, C.F.; Li, F.; Yu, C.H. Antitumor activity of total flavonoids from *Daphne genkwa* in colorectal cancer. *Phytother. Res.* **2016**, *30*, 323–330. [\[CrossRef\]](#)
- Zheng, W.; Gao, X.; Chen, C.; Tan, R. Total flavonoids of *Daphne genkwa* root significantly inhibit the growth and metastasis of Lewis lung carcinoma in C57BL6 mice. *Int. Immunopharmacol.* **2007**, *7*, 117–127. [\[CrossRef\]](#)
- Yue, J.; Zhu, C.; Zhou, Y.; Niu, X.; Miao, M.; Tang, X.; Chen, F.; Zhao, W.; Liu, Y. Transcriptome analysis of differentially expressed unigenes involved in flavonoid biosynthesis during flower development of *Chrysanthemum morifolium* 'Chuju'. *Sci. Rep.* **2018**, *8*, 13414. [\[CrossRef\]](#) [\[PubMed\]](#)
- Yeo, H.J.; Park, C.H.; Park, Y.E.; Hyeon, H.; Kim, J.K.; Lee, S.Y.; Park, S.U. Metabolic profiling and antioxidant activity during flower development in *Agastache rugosa*. *Physiol. Mol. Biol. Plants* **2021**, *27*, 445–455. [\[CrossRef\]](#) [\[PubMed\]](#)

17. Park, C.H.; Yeo, H.J.; Kim, Y.J.; Nguyen, B.V.; Park, Y.E.; Sathasivam, R.; Kim, J.K.; Park, S.U. Profiles of Secondary Metabolites (Phenolic Acids, Carotenoids, Anthocyanins, and Galantamine) and Primary Metabolites (Carbohydrates, Amino Acids, and Organic Acids) during Flower Development in *Lycoris radiata*. *Biomolecules* **2021**, *11*, 248. [[CrossRef](#)]
18. Lee, J.J.; Oh, S.H. A comparative morphological study of Thymelaeaceae in Korea. *Korean J. Plant Taxon.* **2017**, *47*, 207–221. [[CrossRef](#)]
19. Kim, M.K.; Park, S.C.; Park, G.; Choi, E.; Ji, Y.; Jang, Y.P. Analytical quality by design methodology for botanical raw material analysis: A case study of flavonoids in Genkwa Flos. *Sci. Rep.* **2021**, *11*, 11936. [[CrossRef](#)]
20. Chelladurai, S.J.S.; Murugan, K.; Ray, A.P.; Upadhyaya, M.; Narasimharaj, V.; Gnanasekaran, S. Optimization of process parameters using response surface methodology: A review. *Mater. Today Proc.* **2021**, *37*, 1301–1304. [[CrossRef](#)]
21. Shafiq, M.; Hussain, S.; Asif, S.; Pradhan, V.; Farooqui, M. Thermodynamic characteristics of solvents: A review. *Res. J. Chem. Sci.* **2013**, *3*, 98–104.
22. Ferreira, S.L.; Junior, M.M.S.; Felix, C.S.; da Silva, D.L.; Santos, A.S.; Neto, J.H.S.; de Souza, C.T.; Junior, R.A.C.; Souza, A.S. Multivariate optimization techniques in food analysis—A review. *Food Chem.* **2019**, *273*, 3–8. [[CrossRef](#)] [[PubMed](#)]
23. Ghafoor, K.; Al Juhaimi, F.; Özcan, M.M.; Uslu, N.; Babiker, E.E.; Mohamed Ahmed, I.A. Bioactive properties and phenolic compounds in bud, sprout, and fruit of Capparis spp. plants. *J. Food Process. Preserv.* **2020**, *44*, e14357. [[CrossRef](#)]
24. Azmir, J.; Zaidul, I.S.M.; Rahman, M.; Sharif, K.; Mohamed, A.; Sahena, F.; Jahurul, M.; Ghafoor, K.; Norulaini, N.; Omar, A. Techniques for extraction of bioactive compounds from plant materials: A review. *J. Food Eng.* **2013**, *117*, 426–436. [[CrossRef](#)]
25. Azwanida, N. A review on the extraction methods use in medicinal plants, principle, strength and limitation. *Med. Aromat. Plants* **2015**, *4*, 2167-0412.
26. Antony, J. *Design of Experiments for Engineers and Scientists*; Elsevier: Amsterdam, The Netherlands, 2014.
27. Altemimi, A.; Lakhssassi, N.; Baharlouei, A.; Watson, D.G.; Lightfoot, D.A. Phytochemicals: Extraction, Isolation, and Identification of Bioactive Compounds from Plant Extracts. *Plants* **2017**, *6*, 42. [[CrossRef](#)]
28. Sultana, B.; Anwar, F.; Ashraf, M. Effect of extraction solvent/technique on the antioxidant activity of selected medicinal plant extracts. *Molecules* **2009**, *14*, 2167–2180. [[CrossRef](#)]
29. Smucker, B.; Krzywinski, M.; Altman, N. Two-level factorial experiments. *Nat. Methods* **2019**, *16*, 211–212. [[CrossRef](#)]
30. Zhou, G.; Fu, L.; Li, X. Optimisation of ultrasound-assisted extraction conditions for maximal recovery of active monacolins and removal of toxic citrinin from red yeast rice by a full factorial design coupled with response surface methodology. *Food Chem.* **2015**, *170*, 186–192. [[CrossRef](#)]
31. Howard, K.S.; McAllister, R. Surface tension of acetone-water solutions up to their normal boiling points. *AIChE J.* **1957**, *3*, 325–329. [[CrossRef](#)]
32. Triba, M.N.; Le Moyec, L.; Amathieu, R.; Goossens, C.; Bouchemal, N.; Nahon, P.; Rutledge, D.N.; Savarin, P. PLS/OPLS models in metabolomics: The impact of permutation of dataset rows on the K-fold cross-validation quality parameters. *Mol. BioSyst.* **2015**, *11*, 13–19. [[CrossRef](#)] [[PubMed](#)]
33. Lee, S.L. A Totality-of-evidence approach to ensuring therapeutic consistency of naturally derived complex mixtures. In *The Science and Regulations of Naturally Derived Complex Drugs*; Springer: Berlin/Heidelberg, Germany, 2019; pp. 265–270.

## Article

# *Striga hermonthica* Suicidal Germination Activity of Potent Strigolactone Analogs: Evaluation from Laboratory Bioassays to Field Trials

Muhammad Jamil <sup>1</sup>, Jian You Wang <sup>1</sup>, Djibril Yonli <sup>2</sup>, Tsuyoshi Ota <sup>3</sup>, Lamis Berqdar <sup>1</sup>, Hamidou Traore <sup>2</sup>, Ouedraogo Margueritte <sup>2</sup>, Binne Zwanenburg <sup>4</sup>, Tadao Asami <sup>3</sup> and Salim Al-Babili <sup>1,5,\*</sup>

- <sup>1</sup> The BioActives Lab, Center for Desert Agriculture, King Abdullah University of Science and Technology (KAUST), Thuwal 23955-6900, Saudi Arabia; muhammad.jamil@kaust.edu.sa (M.J.); jianyong.wang@kaust.edu.sa (J.Y.W.); lamis.berqdar@kaust.edu.sa (L.B.)
  - <sup>2</sup> Institut de l'Environnement et de Recherches Agricoles (INERA), Ouagadougou 04 BP 8645, Burkina Faso; d.yonli313@gmail.com (D.Y.); hamitraore8@yahoo.com (H.T.); margoued616@gmail.com (O.M.)
  - <sup>3</sup> Applied Biological Chemistry, The University of Tokyo, 1-1-1 Yayoi, Bunkyo, Tokyo 113-8657, Japan; higenomoto.co@gmail.com (T.O.); asami@mail.ecc.u-tokyo.ac.jp (T.A.)
  - <sup>4</sup> Institute for Molecules and Materials, Radboud University, 6525 AJ Nijmegen, The Netherlands; b.zwanenburg@science.ru.nl
  - <sup>5</sup> Plant Science Program, Biological and Environmental Science and Engineering Division, King Abdullah University of Science and Technology (KAUST), Thuwal 23955-6900, Saudi Arabia
- \* Correspondence: salim.babili@kaust.edu.sa

**Citation:** Jamil, M.; Wang, J.Y.; Yonli, D.; Ota, T.; Berqdar, L.; Traore, H.; Margueritte, O.; Zwanenburg, B.; Asami, T.; Al-Babili, S. *Striga hermonthica* Suicidal Germination Activity of Potent Strigolactone Analogs: Evaluation from Laboratory Bioassays to Field Trials. *Plants* **2022**, *11*, 1045. <https://doi.org/10.3390/plants11081045>

Academic Editors: Milan S. Stankovic, Paula Baptista and Petronia Carillo

Received: 11 March 2022

Accepted: 11 April 2022

Published: 12 April 2022

**Publisher's Note:** MDPI stays neutral with regard to jurisdictional claims in published maps and institutional affiliations.



**Copyright:** © 2022 by the authors. Licensee MDPI, Basel, Switzerland. This article is an open access article distributed under the terms and conditions of the Creative Commons Attribution (CC BY) license (<https://creativecommons.org/licenses/by/4.0/>).

**Abstract:** The obligate hemiparasite *Striga hermonthica* is one of the major global biotic threats to agriculture in sub-Saharan Africa, causing severe yield losses of cereals. The germination of *Striga* seeds relies on host-released signaling molecules, mainly strigolactones (SLs). This dependency opens up the possibility of deploying SL analogs as “suicidal germination agents” to reduce the accumulated seed bank of *Striga* in infested soils. Although several synthetic SL analogs have been developed for this purpose, the utility of these compounds in realizing the suicidal germination strategy for combating *Striga* is still largely unknown. Here, we evaluated the efficacy of three potent SL analogs (MP3, MP16, and Nijmegen-1) under laboratory, greenhouse, and farmer’s field conditions. All investigated analogs showed around a 50% *Striga* germination rate, equivalent to a 50% reduction in infestation, which was comparable to the standard SL analog GR24. Importantly, MP16 had the maximum reduction of *Striga* emergence (97%) in the greenhouse experiment, while Nijmegen-1 appeared to be a promising candidate under field conditions, with a 43% and 60% reduction of *Striga* emergence in pearl millet and sorghum fields, respectively. These findings confirm that the selected SL analogs appear to make promising candidates as simple suicidal agents both under laboratory and real African field conditions, which may support us to improve suicidal germination technology to deplete the *Striga* seed bank in African agriculture.

**Keywords:** germination stimulant; witchweed; methyl phenlactonoates (MPs); Nijmegen-1; weed

## 1. Introduction

Cereal crops, particularly maize (*Zea mays*), sorghum (*Sorghum bicolor*), and pearl millet (*Pennisetum glaucum*), are important nutrient and livelihood sources for people in the region of sub-Saharan Africa [1]. However, the average yield of these cereals in Africa is very low, as compared to the world average. Increasing the per hectare yield of crops is one of the major challenges to alleviate hunger and poverty in sub-Saharan Africa [2]. Indeed, the agriculture practiced by the majority of smallholder farmers in Africa is facing a wide range of threats, such as low soil fertility, recurrent drought, and many biotic constraints, particularly parasitic weeds. One of the most troublesome and noxious weeds is *Striga*

*hermonthica* (*Striga*), which hinders crop production and causes more than 50% cereal yield losses in sub-Saharan Africa [3,4].

*Striga hermonthica* (also known as purple witchweed) is an obligate and hemiparasitic plant that parasitizes the root systems of cereals. It is now even becoming a persistent threat to crop production in sub-Saharan Africa, the Middle East, and parts of Asia [5–8]. It is estimated that *Striga* causes more than 50% cereal yield losses in sub-Saharan Africa and has already infested up to 40% (approximately 50 million hectares) of cropland in this region [9–11], thus building a large reservoir for further propagation and spreading of this weed. Although *Striga* has infested several regions of Africa, the most severely infested countries are Burkina Faso, Gambia, Mali, Niger, Nigeria, Senegal, Togo (West Africa), Ethiopia, Eritrea, Kenya, Mozambique, Malawi, Somalia, Tanzania (East Africa), and Sudan. Beyond those, *Striga* infestation is gradually spreading to other African countries, such as Cameroon, Rwanda, Congo, Burundi, Zambia, and Zimbabwe. The ever-increasing *Striga* problem incurs an annual loss of US \$7–10 billion per annum to the livelihoods of African farmers, and its elevated levels in vast areas will further worsen situations of food insecurity, hunger, and poverty for millions of subsistence farmers [12–15]. Hence, developing suitable *Striga* control strategies to minimize the damage is of urgent need for African agriculture.

Despite the debilitating yield losses caused by *Striga*, effective control measures are still far beyond success. Production of more than 200,000 tiny (0.3 nm × 0.15 nm), light (4–7 µg), and long-lived (>15 years) viable seeds by a single *Striga* plant, characterized by a complex life cycle and underground parasitism, makes *Striga* control burdensome [16,17]. Even though local farmers are aware of the *Striga* problem, many factors, such as poverty, limited resources, and harsh weather have impeded the control of this parasite in infested areas. In such cases, the key principles for effective control of *Striga* should be prevention of new seed production, significant reduction in the soil seed bank, and avoiding spreading of seeds from infested to non-infested soils [18–21].

The tiny *Striga* seeds have developed a host detection strategy by perceiving host-released signaling molecules, mainly the phytohormone strigolactones (SLs), which trigger their germination [22–24]. Strigolactones (SLs) are a group of evolutionarily conserved carotenoid-derived plant hormones that regulate many aspects of plant biology [25–27]. The well-known reason why plants release SLs is to successfully communicate with the surrounding arbuscular mycorrhiza (AM) for symbiotic interactions [23,28]. In the parasitic plant *Striga*, the receptors responsible for SL-induced seed germination are *Striga hermonthica* hyposensitive to light (ShHTLs), a group of  $\alpha/\beta$  s that are assumed to be evolutionarily derived from a karrikin-insensitive2 (KAI2) receptor and to arise through gene duplication with functional replacement by SLs [29]. Among the several SL receptors, ShHTL7 is the most sensitive to SLs, suggesting a major role in modulating the seed germination of *Striga* [30,31]. Recently, ShHTL7 has been further characterized as a non-canonical receptor by noting how covalently linked intermediate molecule (CLIM), the SL hydrolysis intermediate, interacts with the F-box proteins ShMAX2 and SMAX1 to mediate SL signaling transduction [32], in a similar way as to rice D14. After successful germination and attachment to the host roots, *Striga* seedlings start siphoning off nutrients and water [33,34]. This dependency of *Striga* germination on host-released SLs and host attachment can be utilized as an effective management strategy [15,35]. The induction of *Striga* seeds' germination through synthetic SL analogs in the absence of the host leads to the death of germinating seedlings at the latest a few days after germination [36,37]. This mechanism builds the basis for a promising control strategy, known as “suicidal germination”, which can reduce the *Striga* seed bank in the infested soils [38–40]. However, the assessment of utility and the employment of suicidal germination relies on the development of cheap and potent SL analogs. Although this technology has been suggested and advocated in several studies to combat not only *Striga* [37–43] but also other root parasites of the *Orobanchaceae* family, in the past 40 years, its application in real African fields remains contested. Despite the availability of several SL analogs and mimics, the selection of simple SL analogs to be used

as potential *Striga* suicidal agents, especially under field conditions, is still a challenge. In the present study, we selected two potent methyl phenlactonoates (MP3 and MP16) [24,37] and a well-known, easy-to-synthesize SL analog, Nijmegen-1 [43], for a comparative study on inducing *Striga* seed germination, first under laboratory conditions.

## 2. Results

### 2.1. *Striga* Seed Germination Bioassays in Response to Various Strigolactone Analogs

The structures of the selected SL analogs are shown in Figure 1. All selected SL analogs at the 1  $\mu\text{M}$  concentration showed a 49–52% *Striga* germination rate, which is statistically equal to the standard SL analog GR24 (64%) (Figure 2). However, *Striga* seeds were more sensitive to a lower concentration of GR24 (0.1  $\mu\text{M}$ ) with a maximum germination rate (66%), compared to the two other analogs at the same concentration (34–37%). Interestingly, higher concentrations, (1–10  $\mu\text{M}$ ) did not show any significant differences between SL analogs. Next, we applied these SL analogs to *Striga* seeds collected from Kenya, Burkina, and Niger to account for differences between *Striga* populations from different origins (Supplementary Figure S1). At a concentration of 1  $\mu\text{M}$ , GR24 and MP3 showed a higher germination rate (20–22%) than MP16 and Nijmegen-1 (14%) in the *Striga* seeds collected from Burkina Faso. In contrast, the four SL analogs exhibited statistically equal *Striga* germinating activity (11–16%) on the seeds collected from Kenya and Niger. These results unraveled differences in the sensitivity of *Striga* populations toward SL analogs but also indicated that the selected analogs could be candidates for testing and realizing the introduction of suicidal germination technology in various parts of Africa.

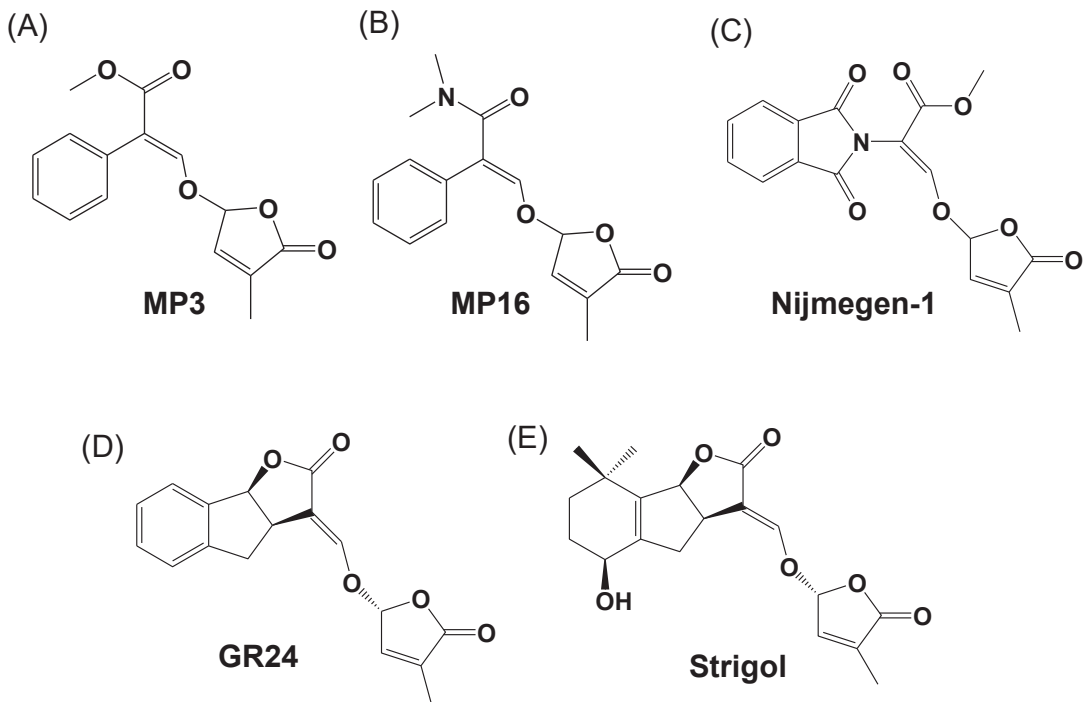


**Figure 1.** Chemical structures of strigolactone analogs (A) MP3, (B) MP16, (C) Nijmegen-1, (D) GR24, and (E) strigol, a natural strigolactone.

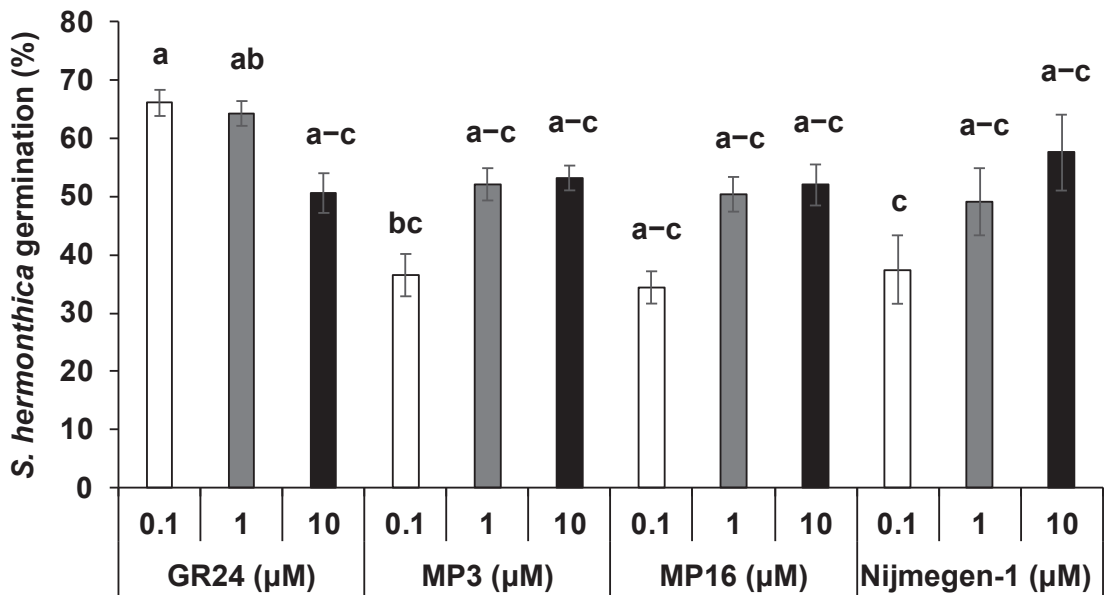


**Figure 2.** *Striga* seed germination rate in response to MP3, MP16, Nijmegen-1, and GR24. Various concentrations ( $10^{-5}$ – $10^{-7}$  M) of selected SL analogs were applied to 10-day preconditioned *Striga* seeds. GR24 was used as a positive control and water as a negative control. For each SL analog, treatments with various letters differed significantly according to one-way analysis of variance (ANOVA) and Tukey's post-hoc test ( $p < 0.05$ ). Error bars represent the standard error of the mean.

### 2.2. *Striga* Emergence on Strigolactone Analogs' Treatment under Greenhouse Conditions

Surprisingly, all three SL analogs showed a significant reduction in *Striga* emergence in comparison to the control treatment (Figure 3A–C). The reducing effect of MP16 on *Striga* emergence was strongest (97%), followed by Nijmegen-1 (89%) and MP3 (73%). As expected, the application of SLs led to improved growth of the host plant due to lower infection of viable *Striga* plants. In particular, MP16-treated pots had the same plant heights as non-infested plants. Application of MP3 and Nijmegen-1 also improved plant growth as compared to the control treatment, but to a lesser extent than MP16, which indicated that the latter is the most potent suicidal agent among the selected analogs under greenhouse conditions (Figure 3C).

### 2.3. Effect of Strigolactone Analogs on *Striga* Infection under Field Conditions

In the pearl millet field, application of Nijmegen-1 led a smaller number of *Striga* plants to emerge ( $32 \pm 6.1$ ), followed by MP16 ( $33 \pm 9.8$ ) and MP3 ( $37 \pm 6.7$ ), as compared to the control plot ( $56 \pm 16.4$ ). In other words, treatment with Nijmegen-1, MP16, and MP3 led to a 43%, 41%, and 33% reduction of *Striga* emergence, respectively (Figure 4C). In the sorghum field, formulated Nijmegen-1 also exhibited the highest reduction of *Striga* emergence (60%), followed by formulated MP3 (52%) and MP16 (11%) (Figure 5C). With respect to the host plants, we observed a 38% increase in pearl millet grain yield and 64% for the stalk yield on MP16 application, whereas MP3 showed a moderate effect on grain yield (9%) and biomass yield (30%). Surprisingly, the application of Nijmegen-1 showed a reduction of pearl millet grain yield (13% less than blank), accompanied by a 31% increase in biomass yield (Figure 4D). In contrast, the application of this SL analog to sorghum led to the maximum observed increase in grain yield (13% higher than blank), while MP3 and MP16 did not show a pronounced effect (−4% and 3%, respectively). All the treatments

showed a 1–37% increase in sorghum biomass yield over the blank treatment (Figure 5D). These results indicate the applicability of the selected SL analogs under real field conditions and their potential to solve the severe food security threats caused by *Striga*.

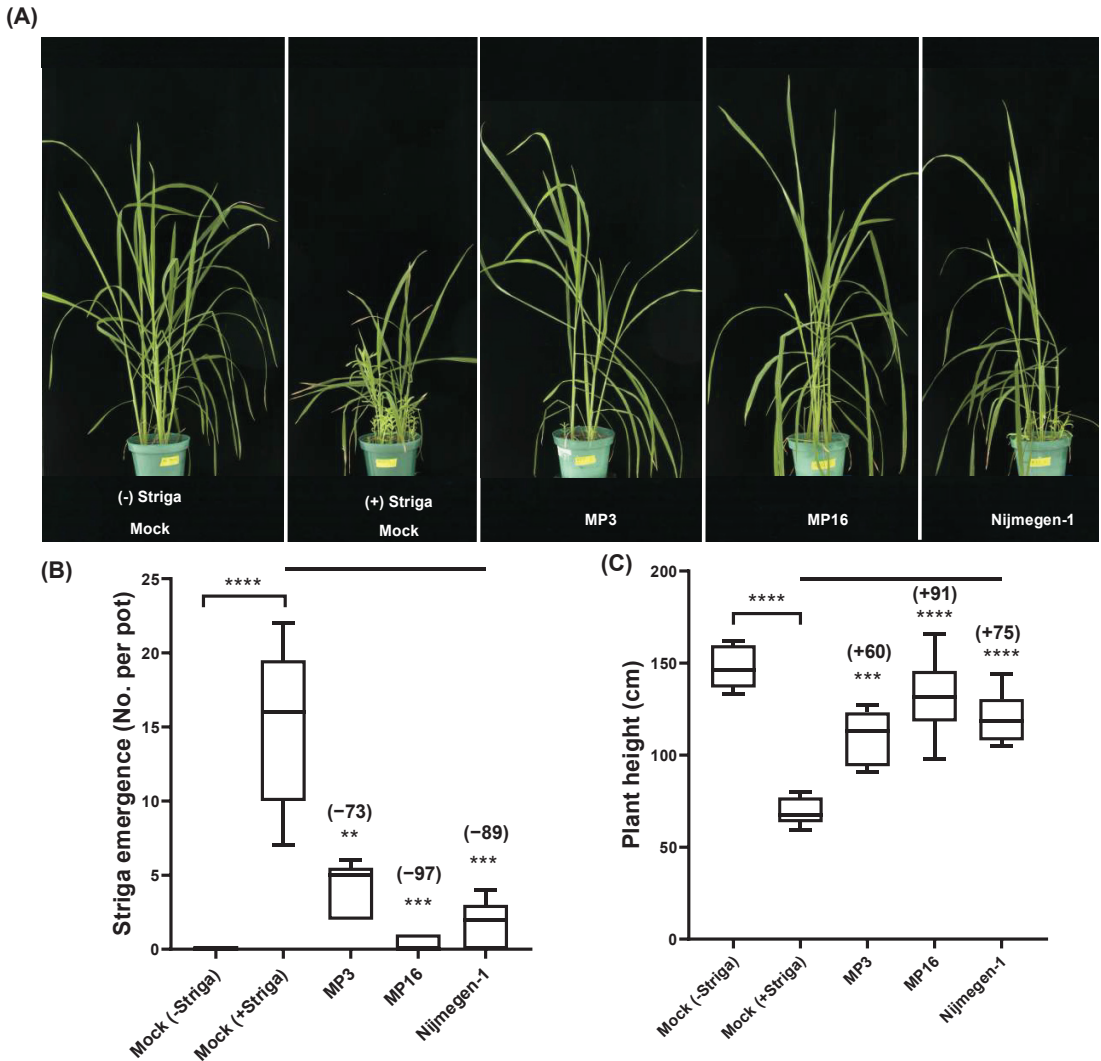


**Figure 3.** *Striga* emergence in response to the application of various SL analogs in pots under greenhouse conditions. (A) Representative pots of greenhouse study, showing *Striga* emergence under different treatments. (B) Number of *Striga* plants that emerged in mock, MP3, MP16, or Nijmegen-1 treatment. The selected SL analogs were applied twice at a 1  $\mu$ M concentration to 10-day preconditioned *Striga*-infested pots. (C) Rice plant height in response to different treatments. Data are means  $\pm$  SE ( $n = 6$ ). Error bars represent the standard error of the mean. Values in parenthesis show the percentage increase (+) or decrease (–) over mock treatment. For each SL analog, treatments with various asterisks differ significantly according to one-way analysis of variance (ANOVA), \*\*  $p < 0.005$ , \*\*\*  $p < 0.005$ , \*\*\*\*  $p < 0.0005$ ).

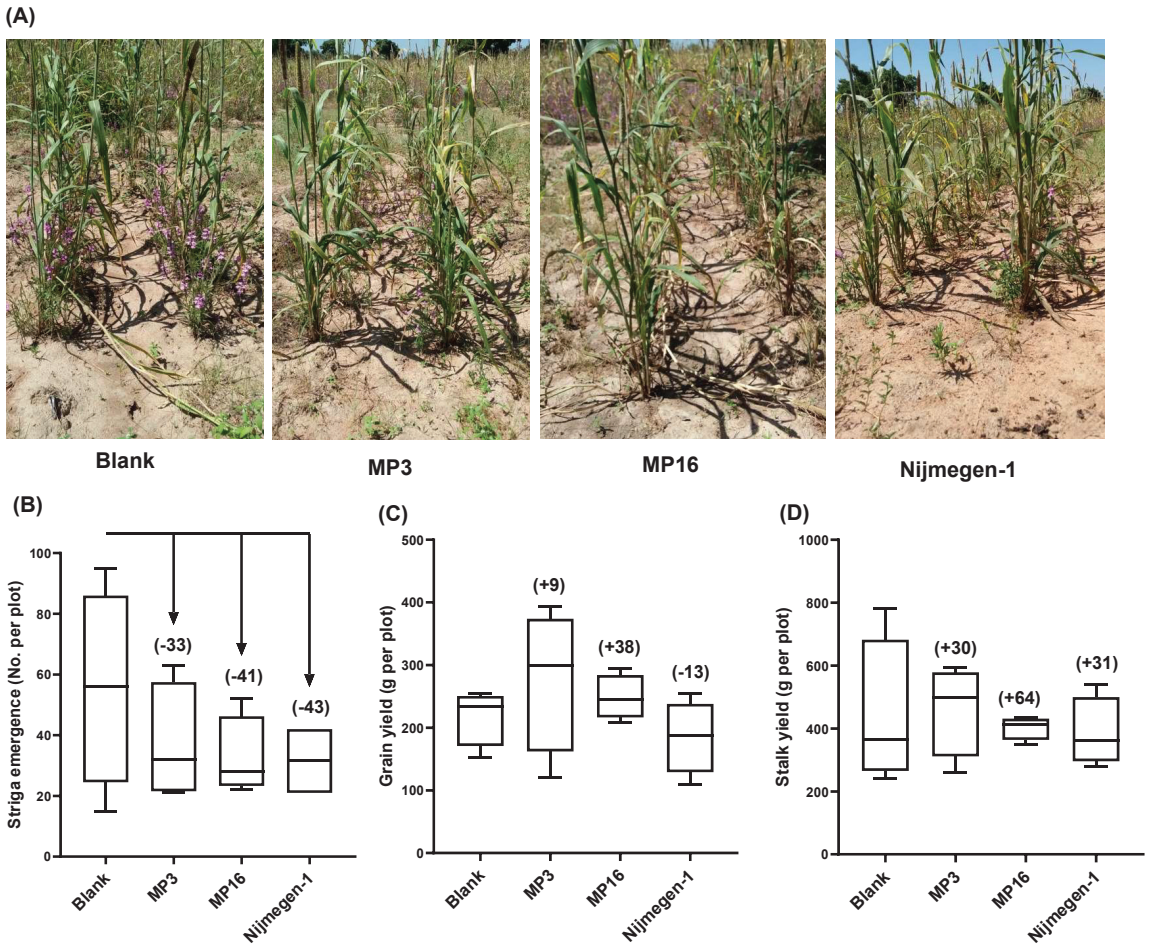


**Figure 4.** *Striga* emergence in response to different SL analogs for a naturally infested pearl millet field in Burkina Faso. **(A)** Representative pearl millet plots of farmer’s field, showing *Striga* emergence under different treatments. **(B)** Number of *Striga* plants that emerged in pearl millet field under mock, MP3, MP16, or Nijmegen-1 treatment. **(C)** Pearl millet grain yield per plot. **(D)** Pearl millet stalk yield per plot. Data are means  $\pm$  SE ( $n = 4$ ). Values in parenthesis show the percentage increase (+) or decrease (–) over mock treatment.

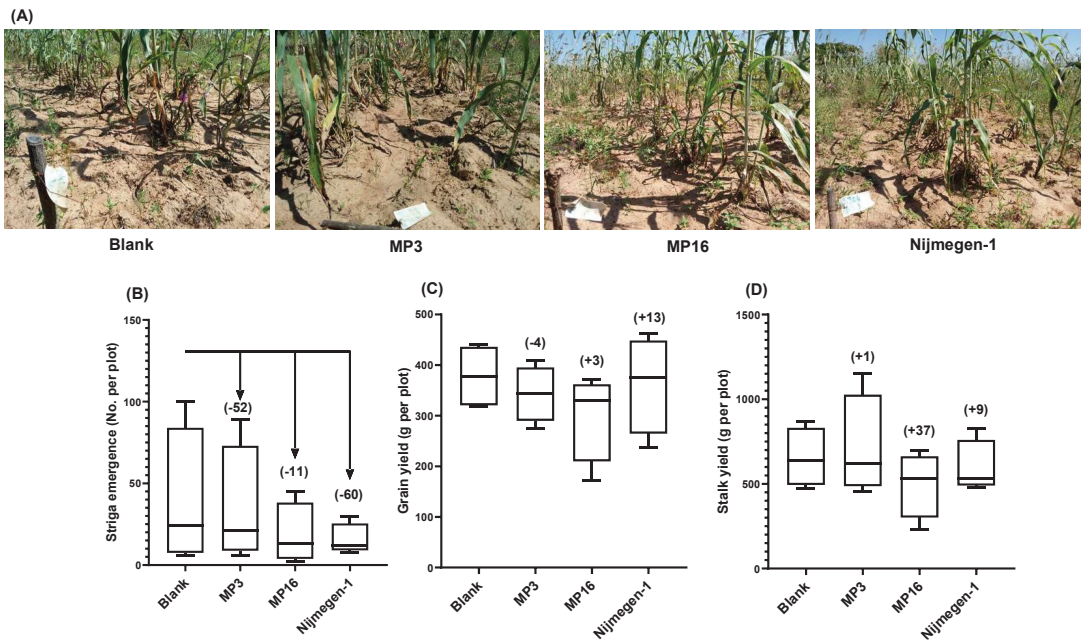


**Figure 5.** *Striga* emergence in response to different SL analogs for a naturally infested sorghum field in Burkina Faso. (A) Representative sorghum plots of farmer field, showing *Striga* emergence under different treatments. (B) Number of *Striga* plants that emerged in sorghum field under mock, MP3, MP16, or Nijmegen-1 treatment. (C) Sorghum grain yield per plot. (D) Sorghum stalk yield per plot. Data are means  $\pm$  SE ( $n = 4$ ). Values in parenthesis are showing the percentage increase (+) or decrease (–) over mock treatment.

### 3. Discussion

The performance of three selected synthetic SL analogs (Figure 1) for *Striga* control was first assessed and confirmed using *in vitro* bioassays. The results showed that MP3, MP16, and Nijmegen-1 are all potent SL analogs inducing *Striga* seed germination (Figure 2). Previously, the moderate activity of Nijmegen-1 was reported for *Striga* germination [43–45], but our bioassays showed its comparable *Striga* germination activity at a high dose (1–10  $\mu$ M). Similarly, we recently reported that MP3 and MP16 exhibit high bioactivity in stimulating *Striga* seed germination [24,37], which is in agreement with the outcome of this work. In addition, these SL analogs were also tested on different *Striga* batches collected from Burkina Faso, Niger, and Kenya. Although all SL analogs (at 1  $\mu$ M) induce *Striga* seed germination ranging from 12–20%, this activity level is not as high as we observed in a *Striga* batch collected from Sudan. This result demonstrates that the sensitivity toward a certain SL analog depends on the ecotype of the *Striga* population. In addition, it shows the need to have an array of SL analogs to realize the suicidal germination strategy in different parts of Africa. Nevertheless, the results obtained with different *Striga* populations indicate that the selected SL analogs can be used in different regions of Africa, although with different efficiency levels.

The bioactivity of Nijmegen-1 was previously tested under pot conditions at a lower concentration (0.5  $\mu$ M) and reported to be relatively weak [39]. In the present pot study, we modified the testing protocol by increasing the concentration of SL analogs to 1  $\mu$ M and the number of applications to two. The results obtained indicated that increasing the dose and frequency of SL analogs might be an effective way to improve their efficacy as suicidal agents against *Striga*. The maximum 97% reduction in *Striga* emergence on the application of MP16 showed its potential to be used as a suicidal agent (Figure 3).

Although we reported a high *Striga* germination-inducing activity of MP1, which carries a 4-nitro substituent on the benzene ring of MP3 [24,39], its synthesis is complex and expensive due to the involvement of additional synthesis steps and introduction of a 4-nitro group. So, alternately, we redesigned and synthesized another SL analog MP16, which is comparatively simple and easy to synthesize at a low cost. The *Striga* germination-inducing activity of the proposed MP16 was comparable to MP1. Similarly, the selected SL analogs might also potentially regulate the plant root architecture and above-ground shoot development when applied to a field [46]. However, there is still a lack of experimental evidence to support our understanding of the mechanisms involved. The actual molecular basis for the SL analogs on crop plants and crosstalk with other phytohormones still needs to be further investigated.

In field trials, we observed that all selected analogs caused a reduction in *Striga* emergence for both pearl millet and sorghum fields; however, these differences were statistically non-significant (Figures 4 and 5). This might be attributed to the great variation in *Striga* infestation level between each plot. Moreover, the *Striga* seed density in the soil, soil texture, structure, pH, farmer's cultural practices, and the amount of rainfall to the field are all possible factors affecting the observed variations between two fields and their replications. Weak activity of MP3 and Nijmegen-1 in clay soil and high in sandy loam-mixture soil has already been reported [39]. In addition, the inconsistency in the performance of MP3 and Nijmegen-1 for farmer's fields has been indicated in a previous study [39], showing reductions of 55% and 65% in *Striga* emergence in a pearl millet field (sandy soil) but no significant impact (12–20%) in a sorghum field (clay soil). In the present study, we increased the number of applications from two to four and observed 33–43% and 60–52% reductions in *Striga* emergence by MP3 and Nijmegen-1 in a pearl millet and sorghum field, respectively. Due to seed dormancy or pre-conditioning requirements, *Striga* seeds are not synchronous in their germination response to SL analogs; hence, we suggested at least four-time repeated applications of SL analogs for maximum eradication of the seed bank in the infested soil. Then, the compound should reach *Striga* seeds to induce their germination. The success of the suicidal germination depends on many factors that are not restricted to the frequency and concentration of the suicidal agents but also include the type of the soil, climate conditions, and amount and frequency of rainfall [39,47]. In addition, it is very important to develop a handy, cost-effective, and stable formulation of suicidal agents that must be easily accessible to African farmers [48].

In summary, our results demonstrate the potential of the three selected simple SL analogs in combating *Striga*. The selected SL analogs will allow the development of further analogs as well as testing and optimizing of formulations and application protocols that aim at depleting the *Striga* seed bank and increasing food security. Moreover, combining the suicidal germination strategy with resistant crop varieties and/or suitable crop rotation or intercropping will likely alleviate the *Striga* problem significantly in the infested regions of Africa.

## 4. Materials and Methods

### 4.1. Plant Materials and Chemicals

The SL analogs *rac*-GR24, MP3, and Nijmegen-1 were synthesized and provided by Prof. Binne Zwanenburg, Radboud University, The Netherlands. The SL analog MP16 was synthesized and provided by Prof. Tadao Asami, University of Tokyo, Japan. The procedure for the synthesis of SL analogs has already been described previously [24,37,43,49]. *Striga hermonthica* seeds were collected from an infested sorghum field during 2020 in Sudan (Prof. A. G. Babiker), from a maize field during 2018 in Kenya (Prof. Steven Runo, Kenyatta University), from a pearl millet field during 2020 in Burkina Faso (Dr. Djibril Yonli, INERA), and a pearl millet field during 2019 in Niger (Dr. Mohammed Riyazaddin, ICRISAT). Seeds of rice IAC-165 were obtained from Africa Rice, Tanzania (Dr. Jonne Rodenburg). The emulsifier Atlas G-1086, a polyoxyethylene sorbitol hexaoleate, was obtained from CRODA, The Netherlands.

#### 4.2. *Striga* Seed Germination Bioassays

The germination activity of the selected SL analogs on *Striga hermonthica* seeds was determined by using a previously described procedure [50,51]. For pre-conditioning, *Striga* seeds were surface sterilized with 50% commercial bleach for seven minutes, followed by six washing steps with MiliQ water in a laminar fume hood. Then, about 50–100 surface-sterilized *Striga* seeds were uniformly spread on a glass-fiber filter-paper disc (9 mm), and 12 discs with *Striga* seeds were put in a Petri dish on sterilized filter paper moistened with 3 mL MiliQ water. The sealed Petri dishes were incubated in the dark at 30 °C for 10 days. On the 11th day, the discs were dried under a laminar flow cabinet, and the SL analogs (50 µL) were applied to each disc with various concentration ranges ( $10^{-5}$  M to  $10^{-7}$  M). Being very active, the synthetic SL analog GR24 was used as a standard positive control instead of natural SL, which is very scarce in plants, unstable, and difficult to extract. After application, the *Striga* seeds were induced to germinate in the dark for 24 h at 30 °C. The discs were scanned under a binocular microscope and germinated, and non-germinated seeds were counted by SeedQuant [52], with a germination rate (in %) then calculated.

#### 4.3. *Striga* Emergence under Greenhouse Conditions

To further evaluate their bioactivity, we tested the three SL analogs in *Striga*-infested pots under greenhouse conditions, using a highly susceptible rice cv. IAC 165 as a host crop. The SL analogs were applied twice at 1 µM concentration to artificially infested preconditioned *Striga* pots. After 10 days of application, three one-week-old rice seedlings were planted in each pot, and *Striga* emergence was counted at 10 weeks after sowing (WAS). A mixture of soil (Stender, Basissubstrat) with sand (3:1 ratio) was prepared [53] and about 0.5 L of this mixture without *Striga* seeds was added to the bottom of a 3-L perforated plastic pot. Then, about 20 mg (~8000) *Striga* seeds were thoroughly mixed in a 1.5-L soil mixture and added on the top of clean soil in the same pot. The *Striga* seeds were preconditioned in a greenhouse under hot (30 °C) and moist conditions for 10 days. On the 11th day, each pot was supplied with 500 ml (1 µM) SL analogs, and *Striga* seeds were allowed to germinate for suicidal death without a host for another 10 days. Then, three one-week-old rice seedlings (IAC-165, a *Striga*-sensitive variety) were planted in the middle of each pot. The rice plants were allowed to grow under normal growth conditions (30 °C, 65% RH, normal sunlight). After 10 weeks, *Striga* emergence was observed in each pot and compared with the mock treatment.

#### 4.4. *Striga* Emergence under Field Conditions

Next, the suicidal germinating bioactivity of three selected SL analogs was further investigated under naturally infested rainfed farmer's field conditions in Burkina Faso (Figures 4 and 5). Formulated SL analogs were applied at a 1 µM final concentration four times on the onset of rainfall. The three selected candidate SL analogs were further evaluated under field conditions in eastern Burkina Faso. Two highly *Striga*-infested pearl millet and sorghum fields, located near the Kouaré research station (11°58'49" N, 0°18'30" E) of INERA (Institut de l'Environnement et de Recherches Agricoles), were selected. Trials were established in each farmer's field, following a randomized complete block design with four independent replications using 4 m × 4 m (or 16 m<sup>2</sup>) plots. Each plot consisted of five (5) ridges/rows, and the distance between ridge/row was 0.80 m; all plots were spaced with four (4) ridges/rows to avoid any SL contamination through run-off. The emulsifier Atlas G-1086 was used to formulate MP3, MP16, and Nijmegen-1. Each SL analog was applied (25 mL/m<sup>2</sup> at 400 µM) in formulated form four times in each field after the onset of rainfall (≥10 mm) to make a final concentration of 1 µM. A blank treatment (Atlas-G only) was included as the control. The experimental crops pearl millet (local cultivar Idipiéni) and sorghum (local cultivar Itchoari) were sown at least one week after the last application. The rainfall was 391.5 mm recorded in 25 days and 617 mm in 27 days during the pearl millet and sorghum growth period, respectively. Plots were weeded twice (15 and 30 days after sowing (DAS)) with hand hoeing before *Striga* emergence. Then,

weeds other than *Striga* plants were hand-pulled until crop harvest. The emerged *Striga* plants were counted at 80 DAS, corresponding to the period of maximum emergence of *Striga* plants in the plots.

#### 4.5. Statistical Analysis

Collected data were analyzed using statistical software package R (version 3.2.2) and GraphPad Prism (version 9.1.1). One-way analysis of variance (ANOVA) with the least significant difference (LSD) multiple range test and unpaired *t*-test were used to analyze the effect of different SL analogs on *Striga* infestation.

**Supplementary Materials:** The following supporting information can be downloaded at: <https://www.mdpi.com/article/10.3390/plants11081045/s1>, Figure S1: *Striga* seed germination in response to MP3, MP16, and Nijmegen-1 treatments.

**Author Contributions:** S.A.-B. and M.J. conceived and designed the experiments. M.J., J.Y.W. and L.B. performed laboratory and greenhouse studies. D.Y., H.T. and O.M. conducted field trials. B.Z., T.O. and T.A. helped with the synthesis of SL analogs. J.Y.W., M.J. and S.A.-B. wrote the manuscript. All authors have read and agreed to the published version of the manuscript.

**Funding:** This study was supported by the Bill and Melinda Gates Foundation (grant number OPP1136424 to S.A.), King Abdullah University of Science and Technology, and a JSPS Grant-in-Aid for Scientific Research (grant number 18H05266 to T.A.).

**Institutional Review Board Statement:** Not applicable.

**Informed Consent Statement:** Not applicable.

**Data Availability Statement:** Not applicable.

**Acknowledgments:** We are grateful to Abdel Gabar Babiker, The National Research Center, Sudan; Steven Runo, Kenyatta University, Kenya; Mohammed Riyazaddin, ICRISAT, Niger for providing *S. hermonthica* seeds. We are thankful to Jonne Rodenburg, Africa Rice, Tanzania for providing seeds of rice cv. IAC-165. We thank Boubacar A. Kountché for his valuable time spent discussing this work.

**Conflicts of Interest:** The authors declare no conflict of interest.

## References

- Ejeta, G. Breeding for *Striga* Resistance in Sorghum: Exploitation of an Intricate Host-Parasite Biology. *Crop Sci.* **2007**, *47*, 216–227. [[CrossRef](#)]
- Khan, Z.R.; Midega, C.A.O.; Pittchar, J.O.; Murage, A.W.; Birkett, M.A.; Bruce, T.J.A.; Pickett, J.A. Achieving Food Security for one Million Sub-Saharan African Poor Through Push-Pull Innovation by 2020. *Philos. Trans. R. Soc. B-Biol. Sci.* **2014**, *369*, 1–11. [[CrossRef](#)] [[PubMed](#)]
- Scott, D.; Scholes, J.D.; Randrianjafizanaka, M.T.; Randriamampianina, J.A.; Autfray, P.; Freckleton, R.P. Identifying Existing Management Practices in the Control of *Striga asiatica* within Rice–Maize Systems in Mid-West Madagascar. *Ecol. Evol.* **2021**, *11*, 13579–13592. [[CrossRef](#)] [[PubMed](#)]
- Rodenburg, J.; Riches, C.R.; Kayeke, J.M. Addressing Current and Future Problems of Parasitic Weeds in Rice. *Crop Prot.* **2010**, *29*, 210–221. [[CrossRef](#)]
- Gressel, J.; Hanafi, A.; Head, G.; Marasas, W.; Obilana, A.B.; Ochanda, J.; Souissi, T.; Tzotzos, G. Major Heretofore Intractable Biotic Constraints to African Food Security that may be Amenable to Novel Biotechnological Solutions. *Crop Prot.* **2004**, *23*, 661–689. [[CrossRef](#)]
- Ejeta, G. The *Striga* Scourge in Africa: A Growing Pandemic. In *Integrating New Technologies for Striga Control: Towards Ending the Witch-Hunt*, 2nd ed.; Ejeta, G., Gressel, J., Eds.; World Scientific: Singapore, 2007; pp. 3–16.
- Scholes, J.D.; Press, M.C. *Striga* Infestation of Cereal Crops—an Unsolved Problem in Resource Limited Agriculture. *Curr. Opin. Plant Biol.* **2008**, *11*, 180–186. [[CrossRef](#)]
- Parker, C. Parasitic Weeds: A World Challenge. *Weed Sci.* **2012**, *60*, 269–276. [[CrossRef](#)]
- Rich, P.J.; Grenier, U.; Ejeta, G. *Striga* Resistance in the Wild Relatives of Sorghum. *Crop Sci.* **2004**, *44*, 2221–2229. [[CrossRef](#)]
- Pennisi, E. Armed and Dangerous. *Science* **2010**, *327*, 804–805.
- Rodenburg, J.; Demont, M.; Zwart, S.J.; Bastiaans, L. Parasitic Weed Incidence and Related Economic Losses in Rice in Africa. *Agri. Econ. Environ.* **2016**, *235*, 306–317. [[CrossRef](#)]
- Rodenburg, J.; Bastiaans, L.; Weltzien, E.; Hess, D.E. How can Field Selection for *Striga* Resistance and Tolerance in Sorghum be Improved? *Field Crop. Res.* **2005**, *93*, 34–50. [[CrossRef](#)]

13. Westwood, J.H.; Depamphilis, C.W.; Das, M.; Fernández-Aparicio, M.; Honaas, L.A.; Timko, M.P.; Wafula, E.K.; Wickett, N.J.; Yoder, J.I. The Parasitic Plant Genome Project: New Tools for Understanding the Biology of Orobanche and Striga. *Weed Sci.* **2012**, *60*, 295–306. [[CrossRef](#)]
14. Pennisi, E. How Crop-Killing Witchweed Senses its Victims. *Science* **2015**, *350*, 146–147. [[CrossRef](#)] [[PubMed](#)]
15. Jamil, M.; Kountche, B.A.; Al-Babili, S. Current Progress in Striga Management. *Plant Physiol.* **2021**, *185*, 1339–1352. [[CrossRef](#)] [[PubMed](#)]
16. Bebawi, F.F.; Eplee, R.E.; Harris, C.E.; Norris, R.S. Longevity of Witchweed (*Striga asiatica*) Seed. *Weed Sci.* **1984**, *32*, 494–497. [[CrossRef](#)]
17. Gbèhounou, G.; Pieterse, A.H.; Verkleij, J.A. Longevity of Striga Seeds Reconsidered: Results of a Field Study on Purple Witchweed (*Striga hermonthica*) in Benin. *Weed Sci.* **2003**, *51*, 940–946. [[CrossRef](#)]
18. Berner, D.; Kling, J.; Singh, B. Striga Research and Control. A Perspective from Africa. *Plant Dis.* **1995**, *79*, 652–660. [[CrossRef](#)]
19. Joel, D.M. The Long-term Approach to Parasitic Weeds Control: Manipulation of Specific Developmental Mechanisms of the Parasite. *Crop Prot.* **2000**, *19*, 753–775. [[CrossRef](#)]
20. Kim, S.; Adetimirin, V.; The, C.; Dossou, R. Yield Losses in Maize due to Striga hermonthica in West and Central Africa. *Int. J. Pest Manag.* **2002**, *48*, 211–217. [[CrossRef](#)]
21. Gbèhounou, G.; Adango, E. Trap Crops of Striga hermonthica: In vitro Identification and Effectiveness in situ. *Crop Prot.* **2003**, *22*, 395–404. [[CrossRef](#)]
22. Yoneyama, K.; Awad, A.A.; Xie, X.; Yoneyama, K.; Takeuchi, Y. Strigolactones as Germination Stimulants for Root Parasitic Plants. *Plant Cell Physiol.* **2010**, *51*, 1095–1103. [[CrossRef](#)] [[PubMed](#)]
23. Al-Babili, S.; Bouwmeester, H.J. Strigolactones, a Novel Carotenoid-Derived Plant Hormone. *Ann. Rev. Plant Biol.* **2015**, *66*, 161–186. [[CrossRef](#)] [[PubMed](#)]
24. Jamil, M.; Kountche, B.A.; Haider, I.; Guo, X.J.; Ntui, V.O.; Jia, K.P.; Ali, S.; Hameed, U.S.; Nakamura, H.; Lyu, Y.; et al. Methyl Phenlactonoates are Efficient Strigolactone Analogs with Simple Structure. *J. Exp. Bot.* **2018**, *69*, 2319–2331. [[CrossRef](#)] [[PubMed](#)]
25. Xie, X.N.; Yoneyama, K.; Yoneyama, K. The Strigolactone Story. *Ann. Rev. Phytopath.* **2010**, *48*, 93–117. [[CrossRef](#)]
26. Felemban, A.; Braguy, J.; Zurbriggen, M.D.; Al-Babili, S. Apocarotenoids Involved in Plant Development and Stress Response. *Front. Plant Sci.* **2019**, *10*, 1–16. [[CrossRef](#)]
27. Wang, J.Y.; Lin, P.-Y.; Al-Babili, S. On the Biosynthesis and Evolution of Apocarotenoid Plant Growth Regulators. *Sem. Cell Dev. Biol.* **2021**, *109*, 3–11. [[CrossRef](#)]
28. Fiorilli, V.; Wang, J.Y.; Bonfante, P.; Lanfranco, L.; Al-Babili, S. Apocarotenoids: Old and New Mediators of the Arbuscular Mycorrhizal Symbiosis. *Front. Plant Sci.* **2019**, *10*, 1186. [[CrossRef](#)]
29. Conn, C.E.; Nelson, D.C. Evidence that KARRIKIN-INSENSITIVE2 (KAI2) Receptors may Perceive an Unknown Signal that is not Karrikin or Strigolactone. *Front. Plant Sci.* **2016**, *6*, 1219–1225. [[CrossRef](#)]
30. Tsuchiya, Y.; Yoshimura, M.; Sato, Y.; Kuwata, K.; Toh, S.; Holbrook-Smith, D.; Zhang, H.; Mccourt, P.; Itami, K. Probing strigolactone receptors in Striga hermonthica with fluorescence. *Science* **2015**, *349*, 864–868. [[CrossRef](#)]
31. Zarban, R.A.; Hameed, U.F.S.; Jamil, M.; Ota, T.; Wang, J.Y.; Arold, S.; Asami, T.; Al-Babili, S. Rational Design of Striga hermonthica-Specific Seed Germination Inhibitors. *Plant Physiol.* **2022**, *188*, 1369–1384. [[CrossRef](#)]
32. Yao, R.; Wang, F.; Ming, Z.; Du, X.; Chen, L.; Wang, Y.; Zhang, W.; Deng, H.; Xie, D. SHHTL7 is a Non-canonical Receptor for Strigolactones in Root Parasitic Weeds. *Cell Res.* **2017**, *27*, 838–841. [[CrossRef](#)] [[PubMed](#)]
33. Shen, H.; Ye, W.; Hong, L.; Huang, H.; Wang, Z.; Deng, X.; Yang, Q.; Xu, Z. Progress in Parasitic Plant Biology: Host Selection and Nutrient Transfer. *Plant Biol.* **2006**, *8*, 175–185. [[CrossRef](#)] [[PubMed](#)]
34. Westwood, J.H. The Physiology of the Established Parasite–Host Association. In *Parasitic Orobancheaceae*; Springer: Berlin/Heidelberg, Germany, 2013; pp. 87–114.
35. Rubiales, D.; Fernández-Aparicio, M.; Vurro, M.; Eizenberg, H. Advances in Parasitic Weed Research. *Front. Plant Sci.* **2018**, *9*, 236–245. [[CrossRef](#)] [[PubMed](#)]
36. Zwanenburg, B.; Pospíšil, T. Structure and Activity of Strigolactones: New Plant Hormones with a Rich Future. *Mol. Plant* **2013**, *6*, 38–62. [[CrossRef](#)] [[PubMed](#)]
37. Jamil, M.; Kountche, B.A.; Wang, J.Y.; Haider, I.; Jia, K.-P.; Takahashi, I.; Ota, T.; Asami, T.; Al-Babili, S. A New Series of Carlactonoic Acid Based Strigolactone Analogs for Fundamental and Applied Research. *Front. Plant Sci.* **2020**, *11*, 1–13. [[CrossRef](#)]
38. Zwanenburg, B.; Pospíšil, T.; Zeljkovic, S.C. Strigolactones: New Plant Hormones in Action. *Planta* **2016**, *243*, 1311–1326. [[CrossRef](#)]
39. Kountche, B.A.; Jamil, M.; Yonli, D.; Nikiema, M.P.; Blanco-Ania, D.; Asami, T.; Zwanenburg, B.; Al-Babili, S. Suicidal Germination as a Control Strategy for Striga hermonthica (Benth.) in Smallholder Farms of Sub-Saharan Africa. *Plants People Planet* **2019**, *1*, 107–118. [[CrossRef](#)]
40. Eplee, R.E. Ethylene: A Witchweed Seed Germination Stimulant. *Weed Sci.* **1975**, *23*, 433–436. [[CrossRef](#)]
41. Samejima, H.; Babiker, A.G.; Takikawa, H.; Sasaki, M.; Sugimoto, Y. Practicality of the Suicidal Germination Approach for Controlling Striga hermonthica. *Pest Manag. Sci.* **2016**, *72*, 2035–2042. [[CrossRef](#)]
42. Zwanenburg, B.; Blanco-Ania, D. Strigolactones: New Plant Hormones in the Spotlight. *J. Exp. Bot.* **2018**, *69*, 2205–2218. [[CrossRef](#)]

43. Nefkens, G.H.; Thuring, J.W.J.; Beenackers, M.F.; Zwanenburg, B. Synthesis of a Phthaloylglycine-Derived Strigol Analogue and its Germination Stimulatory Activity Toward Seeds of the Parasitic Weeds *Striga hermonthica* and *Orobancha crenata*. *J. Agric. Food Chem.* **1997**, *45*, 2273–2277. [[CrossRef](#)]
44. Mwakaboko, A.S.; Zwanenburg, B. Single Step Synthesis of Strigolactone Analogues from Cyclic Keto Enols, Germination Stimulants for Seeds of Parasitic Weeds. *Bioorg. Med. Chem.* **2011**, *19*, 5006–5011. [[CrossRef](#)] [[PubMed](#)]
45. Jamil, M.; Kountche, B.A.; Haider, I.; Wang, J.Y.; Aldossary, F.; Zarban, R.A.; Jia, K.P.; Yonli, D.; Hameed, U.F.S.; Takahashi, I.; et al. Methylation at the C-3' in D-Ring of Strigolactone Analogs Reduces Biological Activity in Root Parasitic Plants and Rice. *Front. Plant Sci.* **2019**, *10*, 1–14. [[CrossRef](#)] [[PubMed](#)]
46. Aliche, E.B.; Screpanti, C.; De Mesmaeker, A.; Munnik, T.; Bouwmeester, H.J. Science and Application of Strigolactones. *New Phytol.* **2020**, *227*, 1001–1011. [[CrossRef](#)]
47. Wigchert, S.; Kuiper, E.; Boelhouwer, G.; Nefkens, G.; Verkleij, J.; Zwanenburg, B. Dose—Response of Seeds of the Parasitic Weeds *Striga* and *Orobancha* Toward the Synthetic Germination Stimulants GR24 and Nijmegen 1. *J. Agric. Food Chem.* **1999**, *47*, 1705–1710. [[CrossRef](#)]
48. Jamil, M.; Wang, J.Y.; Yonli, D.; Patil, R.H.; Riyazaddin, M.; Gangashetty, P.; Berqdar, L.; Chen, G.-T.E.; Traore, H.; Margueritte, O.; et al. A New Formulation for Strigolactone Suicidal Germination Agents, Towards Successful *Striga* Management. *Plants* **2022**, *11*, 808. [[CrossRef](#)]
49. Mangnus, E.M.; Dommerholt, F.J.; De Jong, R.L.; Zwanenburg, B. Improved Synthesis of Strigol Analog GR24 and Evaluation of the Biological Activity of its Diastereomers. *J. Agric. Food Chem.* **1992**, *40*, 1230–1235. [[CrossRef](#)]
50. Jamil, M.; Charnikhova, T.; Houshyani, B.; van Ast, A.; Bouwmeester, H.J. Genetic Variation in Strigolactone Production and Tillering in Rice and its Effect on *Striga hermonthica* Infection. *Planta* **2012**, *235*, 473–484. [[CrossRef](#)]
51. Jamil, M.; Kanampiu, F.K.; Karaya, H.; Charnikhova, T.; Bouwmeester, H.J. *Striga hermonthica* Parasitism in Maize in Response to N and P Fertilisers. *Field Crop. Res.* **2012**, *134*, 1–10. [[CrossRef](#)]
52. Braguy, J.; Ramazanova, M.; Giancola, S.; Jamil, M.; Kountche, B.A.; Zarban, R.A.Y.; Felemban, A.; Wang, J.Y.; Lin, P.-Y.; Haider, I.; et al. SeedQuant: A Deep Learning-Based Tool for Assessing Stimulant and Inhibitor Activity on Root Parasitic Seeds. *Plant Physiol.* **2021**, *186*, 1632–1644. [[CrossRef](#)]
53. Wang, J.Y.; Jamil, M.; Lin, P.-Y.; Ota, T.; Fiorilli, V.; Novero, M.; Zarban, R.A.; Kountche, B.A.; Takahashi, I.; Martínez, C. Efficient Mimics for Elucidating Zaxinone Biology and Promoting Agricultura Applications. *Mol. Plant* **2020**, *13*, 1654–1661. [[CrossRef](#)] [[PubMed](#)]

## Article

# Adnate Leaf-Base and the Origin of Ribs in Succulent Stems of *Euphorbia* L.

Gustavo Arévalo-Rodrigues<sup>1</sup>, Fernanda Hurbath<sup>2</sup>, Erika Prado<sup>3</sup>, Isabella Galvão<sup>3</sup>, Inês Cordeiro<sup>1</sup> and Diego Demarco<sup>3,\*</sup>

<sup>1</sup> Núcleo de Conservação da Biodiversidade, Instituto de Pesquisas Ambientais-PEFI, Sao Paulo 04301-902, SP, Brazil; arevalogustavo92@gmail.com (G.A.-R.); inescordeiro@sp.gov.br (I.C.)

<sup>2</sup> Unidade Passos, Universidade do Estado de Minas Gerais, Passos 37900-106, MG, Brazil; fhurbath@gmail.com

<sup>3</sup> Departamento de Botânica, Instituto de Biociências, Universidade de São Paulo, Sao Paulo 05508-090, SP, Brazil; erikapradomaximo@usp.br (E.P.); isabellagalvao97@gmail.com (I.G.)

\* Correspondence: diegodemarco@usp.br

**Abstract:** Stem succulence evolved independently in many plant lineages as an adaptation to arid environments. One of the most interesting cases is the convergence between Cactaceae and *Euphorbia*, which have anatomical adaptations mostly to increase photosynthetic capability and water storage. Our goal was to describe the shoot development in two succulent species of *Euphorbia* using light microscopy coupled with high-resolution X-ray-computed tomography. Collateral cortical bundles were observed associated with the stem ribs in both species. The analysis of vasculature demonstrated that these bundles are, in fact, leaf traces that run axially along a portion of the internode. That structural pattern is due to an ontogenetic alteration. During shoot development, the leaf-bases remain adnate to the stem near the SAM, forming an axial component. When the internode elongates, the leaf bundles stretch as cortical bundles. The meristematic activity associated with the bundles forms the stem ribs, as leaf veins near the node, and induce rib formation along the entire internode even in the portion where the leaf traces join the stele. In addition, heterochronic shifts are also involved in the evolution of the shoot system in these *Euphorbia*, being related to early deciduous reduced leaves and the transference of the main photosynthetic function to the stem. This study demonstrates for the first time the influence of leaf developmental shifts and stem rib formation in *Euphorbia* and sheds new light on the evolution of stem succulence.

**Keywords:** plant development; vasculature; leaf traces; structure; microtomography; Euphorbiaceae

**Citation:** Arévalo-Rodrigues, G.; Hurbath, F.; Prado, E.; Galvão, I.; Cordeiro, I.; Demarco, D. Adnate Leaf-Base and the Origin of Ribs in Succulent Stems of *Euphorbia* L. *Plants* **2022**, *11*, 1076. <https://doi.org/10.3390/plants11081076>

Academic Editors: Milan S. Stankovic, Paula Baptista and Petronia Carillo

Received: 5 March 2022

Accepted: 11 April 2022

Published: 15 April 2022

**Publisher's Note:** MDPI stays neutral with regard to jurisdictional claims in published maps and institutional affiliations.



**Copyright:** © 2022 by the authors. Licensee MDPI, Basel, Switzerland. This article is an open access article distributed under the terms and conditions of the Creative Commons Attribution (CC BY) license (<https://creativecommons.org/licenses/by/4.0/>).

## 1. Introduction

Among the numerous adaptive strategies found in arid environments, stem succulence plays a pivotal role in plant survival. This evolutionary innovation probably occurred in more than 30 families [1–5], as an important convergence which favored the occupation of environments lacking water by distinct angiosperm lineages [6]. This strategy involves organ thickening by means of the expansion of parenchyma (chlorophyll and water or starch storage tissues) in the cortex or pith [6–9]. A most remarkable convergence case is observed comparing cactiform species of *Euphorbia* (Euphorbiaceae) and cacti (Cactaceae) [10–14], but it is not restricted to these two families. Stem succulence based on parenchyma expansion has also been reported for several unrelated genera, such as *Caralluma*, *Duvalia*, *Echidnopsis*, *Hoodia*, *Huernia*, *Larryleachia*, *Pachypodium*, *Plumeria*, *Pseudolithos*, and *Stapelia* in Apocynaceae, *Othonna* and *Senecio* in Asteraceae, *Tylecodon* in Crassulaceae, *Pelargonium* and *Sarcocaulon* in Geraniaceae, *Dorstenia* in Moraceae, and *Cissus* in Vitaceae [1,2,4,5,9,15–17].

Despite the fact that many valuable data on the origin and structure of the succulence are available for leaves of some families [18–20] and stems of Cactaceae [9,21–24], little is known about the succulent stems of *Euphorbia* (Euphorbiaceae). Even though some xeromorphic characters related to succulence are apparently of the same morphological

nature, their development and evolutionary shifts are practically unexplored, particularly in groups with non-succulent ancestors [14], such as *Euphorbia* [25]. The need for further studies to determine the origin of succulence in different lineages is reinforced by a study of Mauseth [9], who reported the lack of many features typically considered xeromorphic in succulent stems of 28 species from seven families other than Cactaceae.

*Euphorbia* L. is the largest genus of Euphorbiaceae and one of the largest within angiosperms [26], with about 2000 species occurring worldwide, especially in arid and semi-arid environments in the Tropics [27]. The genus has many life forms, such as herbs, geophytes, trees and shrubs, which encompass the major diversity of succulent species of the genus and are morphologically characterized as xerophytic cactiform species and pencil-stem species [25]. The cactiform species usually have organs modified into thorns and succulent and/or ribbed stems which are photosynthetic, at least in the young parts. The pencil-stem species have similar features, but the stems are thinner and permanently photosynthetic along the entire shoot system [25]. Remarkably, species of *Euphorbia* with those morphologies usually have highly reduced leaves but some other species retained large foliage leaves, decreasing the dependence on the stem photosynthesis, a trait much rarer in Cactaceae [25,28,29].

The subgenus *Euphorbia* is recognized by the most intricate evolution of xeromorphic growth form with five independent origins in the genus [25] and a wide diversity of species found in Africa and Madagascar. Fifteen species occur in the Neotropics [30], whose main monophyletic section is *Euphorbia* sect. *Brasilienses* V.W. Steinm. & Dorsey with five succulent pencil-stem species: *E. attastoma* var. *attastoma* Rizzini, *E. attastoma* var. *xanthochlora* Rizzini, *E. holochlorina* Rizzini, *E. phosphorea* Mart., *E. sipolisii* N.E.Br. and *E. tetragularis* Hurbath & Cordeiro. These five species are shrubs, usually ramified, with succulent photosynthetic stems with 4–8 ribs, bearing reduced, early deciduous leaves. They are endemic to Brazil, occurring in environments with sandy soils such as “caatinga” (shrubland vegetation common to the arid climate of northeast Brazil) and rocky uplands [31].

Succulent stems usually have abundant water-storage tissue and chlorenchyma [6–8,32–35] and may have vascular modifications since the succulence is recurrently associated with anatomical changes in the vascular tissues [19,20,36–40]. Although the xeromorphic features of the cactiform *Euphorbia* are widely known, anatomical investigations of their stems and early deciduous leaves are lacking.

Among the few anatomical studies performed in the genus, the presence of cortical vascular bundles stands out as one of the striking unexpected features found in some species [9,30,32,41,42], also reported for some Cactaceae [9,43–47]. The main function assigned to these bundles is to improve the transport of photo-assimilates from the chlorenchyma to secondary vascular system and to provide mechanical support to the shoot [30,46,48]. Additionally, Solereder [32] and Metcalfe & Chalk [33] reported a high development of the cortex in succulent stems, mainly due to the activity of marginal meristem. However, its action mechanism remains unclear.

Our study aimed to investigate the development and vascular architecture of pencil stems and reduced leaves in *Euphorbia* in order to provide a model to understand the origin of some xeromorphic features in succulent stems of the genus.

## 2. Results

*Euphorbia attastoma* and *E. tetragularis* are candelabriform shrubs with succulent branches of pencil-stem type. The leaves are reduced and restricted to the apex with early abscission (Figure 1A). Both species have ribbed stems, showing six ribs and spiral phyllotaxis in *E. attastoma* (Figure 1B) and four ribs and alternate, distichous leaves in *E. tetragularis* (Figure 1C). The ribs are found only in the internodes, arranged in alternate groups of three projections, which coincide with the base of the leaves, which are simple and sessile.

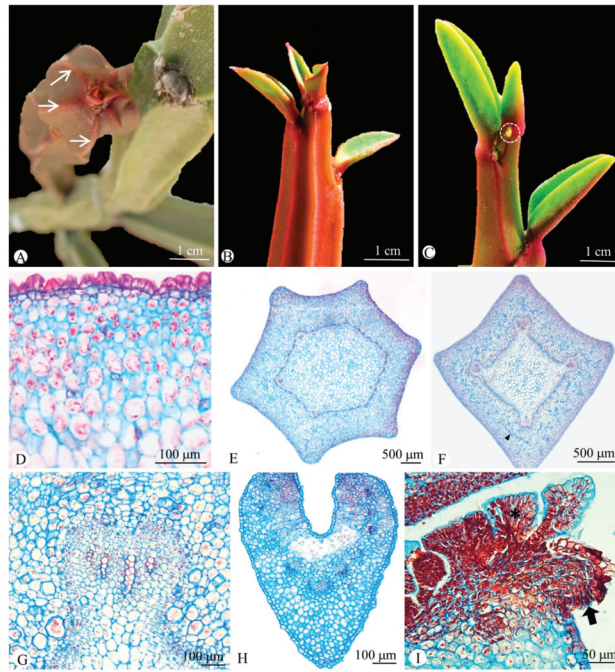


**Figure 1.** Stem morphology and anatomy of *Euphorbia attastoma* (A,B,D,E) and *E. tetragonalis* (C,F–I). Cross sections (D,E,F–I). (A) Stem ribs in frontal view (arrows) with leaves restricted to the shoot apex. (B,C) Note the spiral leaves in (B) and alternate, distichous leaves with stipules in the leaf base (dashed circle) in (C). (D) Detail of a rib showing many layers of chlorenchyma and a papillate epidermis. (E,F) Stem with a prominent vascular bundle in the eustele in each radius of the ribs, numbering six in *E. attastoma* (E) and four in *E. tetragonalis* (F). Note the numerous branched laticifers (arrowhead in (F)). (G) Detail of a vascular bundle of the eustele. (H) Median portion of the leaf with chlorenchyma and vascular bundles. (I) Detail of the leaf axil with colleters (asterisk) and one of the glomeriform stipules (arrow).

### 2.1. Anatomy

The stem of both species has a uniseriate papillate epidermis with stomata and a cortex particularly thicker in the ribbed region due to the presence of dozens of layers of parenchyma (Figure 1D). The cortex is divided in two regions: an outer cortex formed by chlorenchyma with elongate cells near the epidermis and an inner cortex containing several layers of parenchyma with starch grains. The vascular system is arranged in an eustele of irregular shape (polygonal), whose angles vary according to the number of ribs (Figure 1E,F). Each angle has a large bundle, which is considerably larger than the other bundles (Figure 1G). In addition to the stele, vascular bundles are observed in the cortex, opposite to the ribs, whose number varies according to the number of ribs (Figure 2A–F). Branched laticifers occur throughout parenchyma and vascular bundles (Figure 1F).

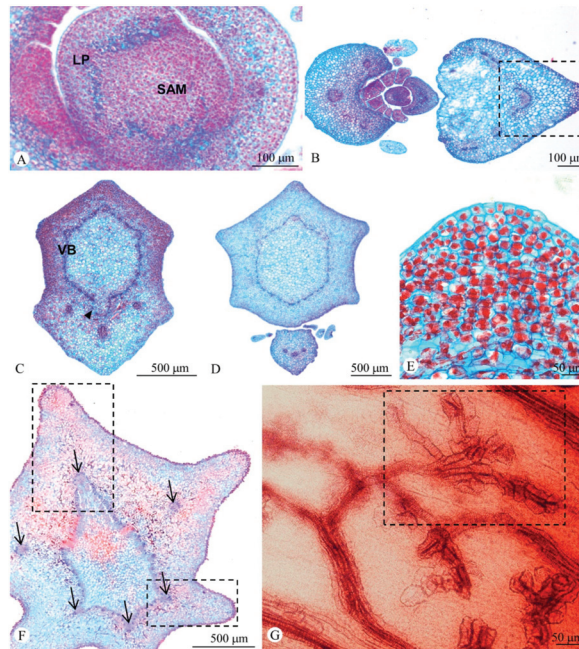


**Figure 2.** Ontogeny and vasculature of the shoot in *Euphorbia attastoma* (A,C,D,F) and *E. tetragularis* (B,E,G). (A) Origin of the leaf primordium (LP) in the flank of the shoot apical meristem (SAM). (B) Leaves from distinct nodes in different developmental stages. Note the parenchymatic expansion of the midrib of the leaf (dashed square). (C) Nodal region showing three leaf traces associated with their respective ribs and the leaf gap (arrowhead). (D) Reduced leaf with three bundles and the ribbed stem. (E) Detail of the anticlinal and periclinal division of the ground meristem cells during rib development. (F) Divergence of leaf traces from the eustele, evidencing their relationship with the stem ribs (arrows). Note the profuse multiplication of parenchyma in front of each trace, forming the ribs (dashed squares). (G) Leaf terminal venation with areoles composed of tracheids (dashed square). VB = vascular bundle.

The leaves are relatively small, varying from  $6.7\text{--}11 \times 2.2\text{--}3$  mm and have a uniseriate epidermis with stomata and chlorenchyma (Figure 1H). They have three vascular bundles in the base, which subsequently branch in five to nine in the median portion (Figure 1H). Laterally to the base of the leaf blade, a pair of glanduliform stipules with papillate epidermis are formed together with a profusion of sessile colleters, which extend from one stipule to the other along the leaf axil (Figure 2B). These colleters are formed by a secretory palisade epidermis and a non-secretory parenchyma core (Figure 1I).

## 2.2. Shoot Ontogeny and Vasculature

The leaf primordium originates from the peripheral zone in the flank of shoot apical meristem (SAM). The initiation occurs in regular plastochrons, which vary according to the phyllotaxis (Figure 2A). During the expansion of the leaf primordium, its base remains united to the stem primordium, becoming part of the axis. The subsequent intercalary growth of the stem primordium elongates this adnate region, and the leaf-base is stretched along a portion of the internode, where the leaf traces are observed as stem collateral cortical bundles.

In this second stage of the shoot morphogenesis, the ground meristem in front of the collateral cortical bundles (leaf bundles) generates numerous layers of parenchyma (Figure 2E), which correspond to leaf veins. Ontogenetically, these veins are the ribs of the stem, formed by the cortical bundle and a large amount of parenchyma, which doubles

the thickness of the cortex. In regions without ribs, the cortex of both species is 1.5–2 mm thick, but in the rib radius the cortex is about 4–4.5 mm. This relationship of the leaf base as an axial component can also be perceived through the analysis of vasculature (Figures 2 and 3), but it is not restricted to the portion of leaf-base adnation. In fact, since the leaf-base becomes an axial component in the shoot apex, its incorporated vasculature induces the proliferation of the ground meristem basipetally, both in the region with cortical bundles and in the region without bundles, which, actually, corresponds to the most length of the internode.

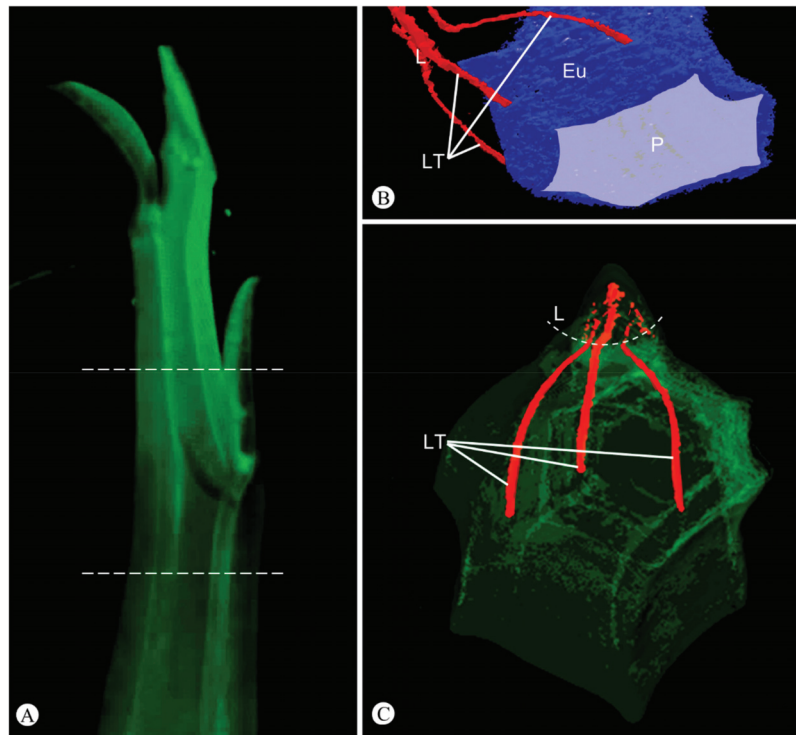


**Figure 3.** Microtomography with 3D-reconstruction of the shoot of *Euphorbia attastoma*. (A) General view of the shoot. (B,C) Reconstructions of the area enclosed by the dashed lines in (A). (B) Detail of the leaf traces (LT in red) connected to the eustele (Eu in blue) surrounding the medullary parenchyma (P in gray). Note that the three leaf traces do not branch until reach the free portion of the leaf (L). (C) Nodal region showing the leaf traces (LT in red).

Leaf morphogenesis is rapid. The free portion of the leaf, found around 1.5–2 cm above the node, is comprised exclusively of the leaf blade. Early in leaf development, meristems differentiate into mature tissues, stopping the leaf expansion. As a consequence, the leaves remain small and are also early deciduous, being restricted to the apex portion of the shoot. Thus, the photosynthesis of the plant is supplied almost entirely by the stem with adnate leaf-bases.

Shoot vasculature varies according to evolutionary developmental shifts. In the nodal region, three leaf traces diverge from the stele and occupy a peripheral position in the cortex in the region of the stem rib, running parallel to the surface along the internode, profoundly altering the stem morphology. These traces remain unbranched until the base of the free portion of the leaf (Figure 3, Supplementary Material Video S1). In the leaf blade, the three bundles ramify, forming secondary and tertiary veins, which terminate with tracheids in the areoles (Figure 2G).

### 3. Discussion

The present study revealed the origin and nature of the ribs of the succulent stems in two Neotropical species of *Euphorbia* for the first time. Using developmental analysis and 3D-reconstruction techniques, we were able to demonstrate that the leaf-base is congenitally adnate to the stem, as an axial component, and the development of the three main veins of this base induces rib formation along the entire internode of the succulent pencil stems.

Succulent stems are common in *Euphorbia*, exhibiting ribs with reduced, early deciduous leaves. Rudimentary leaves occur in other New World lineages with ribbed stems of the subgenus *Euphorbia*, such as in *E. pteroneura* A. Berger (sect. *Euphorbiastrum* (Klotzsch & Garcke) Boiss.), a Mexican species (sensu Dorsey et al. [27]). Ribbed stems also occur in herbs, particularly in *E.* sect. *Stachydium* Boiss., the sister group of *E.* sect. *Brasilienses*, e.g., *E. heterodoxa* Müll. Arg., an endemic species from rocky outcrops in Northeastern of Brazil. Other succulent lineages within the genus also have rudimentary leaves with succulent ribbed and/or tuberculate stems. Those species belong to the Old World and are currently classified in the subgenus *Euphorbia* and *E.* subg. *Athymalus* Neck. ex Rchb. [27,49]. Given the diversity of species bearing ribbed stems in unrelated lineages, the main common trait is the presence of rudimentary leaves. This fact is certainly involved in the stem organogenesis in *Euphorbia* since the stem ribs are concomitantly produced with the leaf primordium, exhibiting an easily recognizable relationship between both organs.

Restriction of leaf blade development and transference of function to stem, which becomes the main photosynthetic organ of the plant, is usually related to succulent stems in arid environments [9,48,50–53]. The enlargement of the cortex of these stems appears to be related to the expansion of the photosynthetic tissue, in addition to the increment in water and starch storage [9,48,51,54–58].

The cortex may be extremely broad in Cactaceae due to cortical bundles which produce intrafascicular secondary phloem and xylem in many species [9,48,50]. On the other hand, we did not observe any expansion of the stem tissues in *Euphorbia* due to vascular proliferation of the cortical bundles. Actually, the non-separation of the leaf-base from the SAM flank during the leaf primordium development seems to be the reason for the succulence of the pencil stem in the genus. The maintenance of the leaf-base forming an axial component has already been reported for plants of other families [59].

Fusion of the leaf adaxial side to the stem is not an uncommon process for bud protection in xerophytes since it reduces the water loss to the environment. This process usually involves expansion of the leaf-base. In succulent species of Aizoaceae and Amaranthaceae, a large expansion of the leaf-base around the SAM and a reduction in the leaf blade have previously been reported [18,20,60]. This foliar characteristic appears to have evolved multiple times in these two families, coinciding with the aridification of southern Africa in the Late Miocene [60–62]. However, there is no fusion of the leaf-base to the stem, as observed in *Euphorbia*. Conversely, leaf fusion may be total in other lineages. In Podostemaceae, the leaf-base is completely united to the promeristem, originating shoots apparently devoid of SAM in the subfamily Podostemoideae [63].

In general, main xeromorphic features of the succulent stems are the increase in parenchyma tissue of the cortex or pith, reduction of leaf size and number, and establishment of mechanisms for water protection and its storage [9]. Regardless of the origin of expanded cortical tissues of the succulent stems, the enlargement is associated with the presence of cortical bundles. The emergence of cortical bundles was a key innovation in the evolution of Cactoideae (Cactaceae), which allow some species to develop cortices up to 30 cm thick keeping all their tissues hydrated [48,64]. If the cortex is unvascularized, the slow transport of water by diffusion appears to limit the increase in cortex thickness [55,64].

Extrastelar vascular bundles, such as the collateral cortical bundles (leaf traces) observed in the Neotropical *Euphorbia* sect. *Brasilienses*, have also been reported for *E. weberbaueri* Mansf. (*E.* sect. *Euphorbiastrum*) (Klotzsch & Garcke) Boiss. [30], another Neotropical species with ribs very similar to those described herein, and also for African species as *Euphorbia fortuita* A.C. White, R.A. Dyer & B. Sloane, *Euphorbia horrida* Boiss.,

*Euphorbia obesa* Hook. f. and *Euphorbia officinarum* L. [9]. Those additional bundles have been reported for 55 eudicot families, extending along the internodes, as cortical bundles or medullary bundles [33]. In the case of cortical bundles, Howard [65] observed that their relationship with the leaves varies depending on the group analyzed and can be found in the stem (1) unrelated to the leaf vasculature, (2) partially related to leaf vasculature or (3) completely related to leaf vasculature. This third condition is the one discovered here in *Euphorbia attastoma* and *E. tetragonalis*. This variation indicates that the mere occurrence of cortical bundles in the stem does not necessarily imply adnation of the leaf to the stem. The main example is the cacti, whose extensive set of cortical bundles, observed in addition to the leaf/bud traces, are truly cauline, derived from procambial cells originated in the cortical area near the shoot apical meristem [44,48,64].

Despite the fact that the origin of ribbed stems has not been investigated in other species of *Euphorbia*, further anatomical studies may reveal similarities in relation to our results, indicating the likely evolution of this character in other clades of the genus. Mauseth [9] found that the leaf traces are related to the stem ribs in nine species of *Euphorbia*. If this relationship exists between this type of stem succulence and leaf traces in other species, we can assume that the number of ribs and their disposition depends on the phyllotaxis and plastochron. This hypothesis is supported by the difference observed between *E. attastoma* (six ribs) and *E. tetragonalis* (four ribs). This is related to the three leaf traces that diverge from the eustele in different times during development, indicating a case of heterochrony in closely phylogenetically related species. The ribs are surely associated with the stem thickness, allowing the candelabriform morphology observed in *E. sect. Brasilienses* and seems to be important to accommodate seasonal expansion and contraction of stem [66].

The evolutionarily shift of plants from one form into another involves modifications of the developmental patterns [48]. In this study, we verified that during the initial development of leaf primordia, the leaf-base remains adnate to the developing stem in *Euphorbia*. This congenital fusion of tissues displaces the orientation of the leaf traces, which are oblique/horizontal and run directly to the leaf-base at the nodes in the vast majority of angiosperms [65], to run roughly parallel to the surface of the stem along a short portion of the internode (Figure 4).

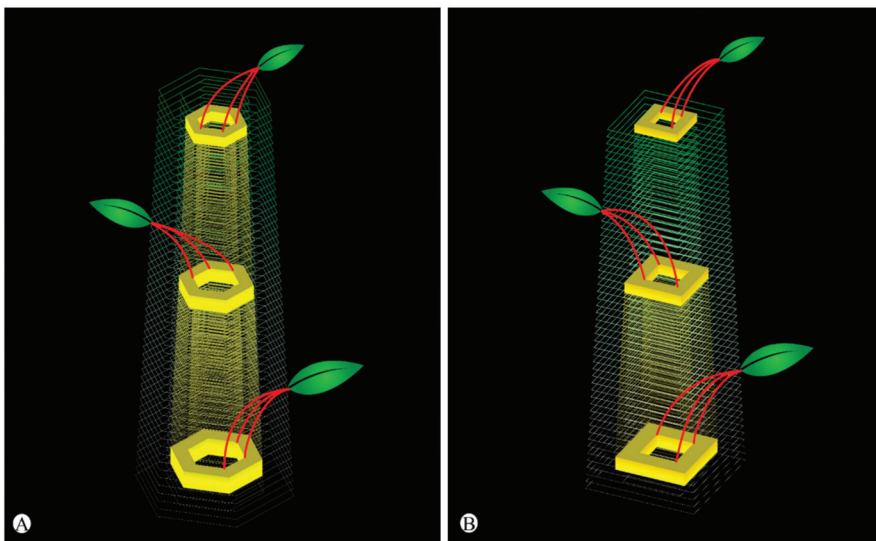


**Figure 4.** Diagrams showing the leaf traces diverging from stele in *Euphorbia attastoma* (A) and *E. tetragonalis* (B). Note that the leaf traces (red) diverge in groups of three in both species.

Fusion of the leaf-base to the stem is not an uncommon event in angiosperms [67], but the developmental process observed in *Euphorbia* appears to be an evolutionary novelty and is described for the first time in this study. Despite the fact that the general leaf development is well known and widely analyzed in textbooks and articles, the origin of the stem is often neglected. After the formation of the leaf primordia in the shoot apex and the establishment of the nodal regions, there is an elongation of the internode by multiplication and elongation of the cells of the primary meristems [65]. This second stage of the stem morphogenesis has been altered in the *Euphorbia* pencil stem. When the internode elongates, the leaf-base united to the stem also elongates (Figure 5), stretching the leaf traces along the internode. Consequently, the leaf is “displaced” to another region above its point of origin (Figure 4).

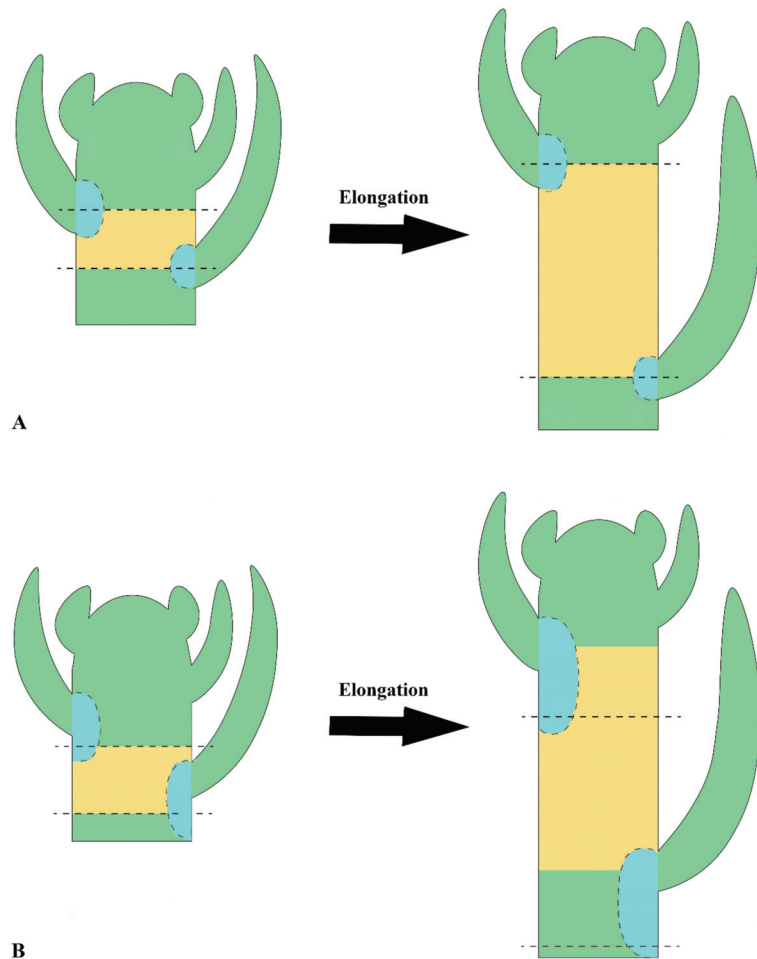


**Figure 5.** Schematic drawings of two stages of shoot development. **(A)** Regular shoot development. Note that the leaf-base participation in the axis is restricted to its point of origin at the node, even after the internode elongation. **(B)** Shoot of *Euphorbia attastoma* and *E. tetragonalis*. Note that adnate leaf-base forms an axial component, displacing the leaf to a region above the node. The fused portion elongates along with the internode. The origins of axial tissues were colored in one plastochron. Dashed line: node; blue: leaf-base component; yellow: cauline component; green: indiscriminant components.

The increment of foliar tissues into the stem considerably expanded the cortex, increasing its photosynthetic capacity (Figure 5). Additionally, there is an early maturation of the leaf meristems, interrupting the leaf blade development and producing very reduced leaves. This type of developmental shift of the tissue differentiation timing is known as heterochrony and has been shown to be one of the main processes in plant evolution [68]. In addition, some heterochronic changes may lead to transfer of function (heterotopy) due to spatial relationships that change over time [69]. This can be observed in the cactiform species of *Euphorbia*, whose stem becomes the main photosynthetic organ of the plant due to the early leaf abscission.

Despite our observation that cortical bundles (leaf traces) elongate for a short region of the stem above the node, these vascular bundles undoubtedly stimulate parenchyma proliferation, forming the ribs continuously along the entire internode. To date, it is not possible to infer which endogenous signal is responsible for this change in stem tissues. However, previous studies show that the hormonal stimulus responsible for the differentiation of procambium, and consequently the vascular bundles in shoots, is the auxin. Polar auxin gradients induce procambium differentiation along the path of its flow and may regulate vascular adaptation to the plant's environment [70,71]. Thus, if auxin is related to the differentiation of cortical bundles, we can hypothesize that auxin is also related to rib differentiation regardless of the presence of cortical bundles from one node to the other, deviating from the expected transport pathway due to the adnation of the leaf base to the stem. Further immunocytochemical studies are needed to definitively verify this hypothesis and clarify the physiological regulation of succulence evolution in *Euphorbia*.

#### 4. Materials and Methods

For this study two species of *E. sect. Brasilienses* were selected: *E. attastoma* (Hurbath 853, 854) and *E. tetragonalis* (Hurbath 844). The samples were collected from three individuals of each species cultivated in glasshouse at Instituto de Biociências at the Universidade de São Paulo. Vouchers of the species were deposited at SP Herbarium.

Shoots were fixed in FAA for 24 h (formalin, acetic acid, 50% ethanol 1:1:18 v:v) [72] and then stored in 70% ethanol. Entire leaves were first cleared using 100% ethanol, then treated with 10% sodium hydroxide for 2 h, followed by 5% sodium hypochlorite. The leaves were stained with 1% safranin and mounted in Kaiser's glycerin gelatin [73]. For anatomical analyses, shoot apices were isolated, dehydrated in a butyl series [72], embedded in Paraplast® (Leica Microsystems, Wetzlar, Germany) and transversely or longitudinally sectioned using a Leica RM2145 rotary microtome. Sections 12 µm thick were stained with astra blue and safranin [74], and the slides were mounted in Permount® (Fisher Scientific, Pittsburgh, PA, USA). The photomicrographs were taken using a Leica DMLB light microscope coupled with a digital camera.

For high-resolution X-ray-computed tomography (HRXCT), we used the fixed shoots of *E. attastoma*, which were treated with phosphotungstic acid in 70% ethanol for one week. Subsequently, the samples were dehydrated in an ascending ethyl series containing 1% phosphotungstic acid (1:1; v:v) and wrapped with parafilm in a tube filled with 100% ethanol. Finally, the samples were scanned using a SkyScan 1176 microtomograph (Bruker, Billerica, MA, USA). The exposure time was approximately 4 h per sample and for the 3D reconstruction we used the software CTVox and CTVol, 3D Doctor (Able Software Corp., Lexington, KY, USA) and 3D Slicer. Image sequences and the video (Supplementary Material) were segmented automatically and manually.

The vasculature diagrams were made based on the microscopic observations and the high-resolution X-ray-computed tomography, using the software Cinema 4D (Friedrichsdorf, Hesse, Germany) and Adobe Photoshop (San Jose, CA, USA).

#### 5. Conclusions

We demonstrate for the first time that the succulence of the pencil stem in *Euphorbia* is due to the incorporation of the leaf-base as an axial component during shoot development.

This joining of tissues doubles the thickness of the cortex of stem and its amount of photosynthetic tissue. The elongation of the internode joined to the leaf-base transforms the leaf traces into cortical bundles that are associated with proliferation of the parenchyma, forming the stem ribs. A likely hormonal signal from the leaf is transported basipetally along the entire internode, inducing rib formation regardless of the presence of cortical bundles. Heterochronic shifts are also involved in the evolution of the very small leaves of *Euphorbia*, their early abscission and the transference of the main photosynthetic function to the stem. A major sampling is needed to evaluate the specific role of these features in the adaptive success of the *Euphorbia* and its diversification in arid environments.

**Supplementary Materials:** The following supporting information can be downloaded at: <https://www.mdpi.com/article/10.3390/plants11081076/s1>, Video S1: Microtomographic reconstruction of the shoot of *Euphorbia attastoma*.

**Author Contributions:** Conceptualization: D.D.; data curation: G.A.-R., E.P., I.G. and D.D.; funding acquisition: G.A.-R. and I.C.; investigation: G.A.-R., F.H., E.P., I.G., I.C. and D.D.; methodology: G.A.-R., E.P., I.G. and D.D.; resources: G.A.-R., I.C. and D.D.; supervision: I.C. and D.D.; validation: G.A.-R., E.P., I.G., I.C. and D.D.; visualization: G.A.-R., E.P., I.G. and D.D.; writing—original draft: G.A.-R., I.C. and D.D.; writing—review and editing: G.A.-R., F.H., E.P., I.G., I.C. and D.D. All authors have read and agreed to the published version of the manuscript.

**Funding:** This research was funded by Conselho Nacional de Desenvolvimento Científico e Tecnológico (CNPq proc. #169737/2018-7 and #311275/2019-2) and Fundação de Apoio à Pesquisa do Estado de São Paulo (FAPESP proc. 11812-1/2015).

**Institutional Review Board Statement:** Not applicable.

**Informed Consent Statement:** Not applicable.

**Data Availability Statement:** All figures and tables of this manuscript have been unpublished and were made specifically for this article.

**Acknowledgments:** This study is part of the PhD dissertation of the first author in the Programa de Pós-Graduação em Biodiversidade Vegetal e Meio Ambiente of the Instituto de Pesquisas Ambientais-PEFI, São Paulo, Brazil. The authors thank CNPq for financial support and Instituto de Biociências at Universidade de São Paulo and Instituto de Botânica, where this study took place.

**Conflicts of Interest:** The authors declare no conflict of interest.

## References

- Jacobsen, H. *A Handbook of Succulent Plants*; Blandford Press: London, UK, 1960.
- Albers, F.; Meve, U. *Illustrated Handbook of Succulent Plants: Asclepiadaceae*; Springer: Berlin, Germany, 2002.
- Eggle, U. *Illustrated Handbook of Succulent Plants: Monocotyledons*; Springer: Berlin, Germany, 2001.
- Eggle, U. *Illustrated Handbook of Succulent Plants: Dicotyledons*; Springer: Berlin, Germany, 2002.
- Eggle, U. *Illustrated Handbook of Succulent Plants: Crassulaceae*; Springer: Berlin, Germany, 2003.
- von Willert, D.B.; Eller, M.; Weger, M.J.A.; Brinckmann, E.; Ihlenfeldt, H.D. *Life Strategies of Succulents in Deserts with Special Reference to the Namib Desert*; Cambridge University Press: Cambridge, UK, 1992.
- Gibson, A.C. The Anatomy of Succulence. In *Crassulacean Acid Metabolism: Proceedings of the Fifth Annual Symposium in Botany, Los Angeles, CA, USA, 14–16 January 1982*; Ting, I.P., Gibbs, M., Eds.; American Society of Plant Physiologists: Rockville, MD, USA, 1982; pp. 1–15.
- Gibson, A.C.; Nobel, P.S. *The Cactus Primer*; Harvard University Press: Cambridge, MA, USA, 1986.
- Mauseth, J.D. The structure of photosynthetic succulent stems in plants other than cacti. *Int. J. Plant Sci.* **2004**, *165*, 1–9. [[CrossRef](#)]
- Raven, P.H.; Evert, R.F.; Eichhorn, S.E. *Biology of Plants*, 4th ed.; Worth Publishers: New York, NY, USA, 1986.
- Futuyma, D.J. *Evolutionary Biology*, 3rd ed.; Sinauer Associates: Sunderland, MA, USA, 1997.
- Niklas, K. *The Evolutionary Biology of Plants*; The University of Chicago Press: Chicago, IL, USA, 1997.
- Stearn, S.C.; Hoekstra, R.F. *Evolution: An Introduction*, 2nd ed.; Oxford University Press: Oxford, UK, 2005.
- Hearn, D.J. Developmental patterns in anatomy are shared among separate evolutionary origins of stem succulent and storage root-bearing growth habits in *Adenia* (Passifloraceae). *Am. J. Bot.* **2009**, *96*, 1941–1956. [[CrossRef](#)] [[PubMed](#)]
- Ihlenfeldt, H.D. Lebensformen und Überlebensstrategien bei Sukkulenten. *Ber. Deut. Bot. Ges.* **1985**, *98*, 409–423.
- Sajeva, M.; Costanzo, M. *Succulents: The Illustrated Dictionary*; Timber Press: Portland, OR, USA, 1994.
- Sajeva, M.; Costanzo, M. *Succulents II: The New Illustrated Dictionary*; Le Lettere: Florence, Italy, 2000.

18. Melo-de-Pinna, G.F.A.; Ogura, A.S.; Arruda, E.C.P.; Klak, C. Repeated evolution of endoscopic peripheral vascular bundles in succulent leaves of Aizoaceae (Caryophyllales). *Taxon* **2014**, *63*, 1037–1052. [[CrossRef](#)]
19. Melo-de-Pinna, G.F.A.; Hernandes-Lopes, J.; Ogura, A.S.; Santos, L.K.; Silva, D.C.; Haevermans, T. Growth patterns and different arrangements of vascular tissues in succulent leaves. *Int. J. Plant. Sci.* **2016**, *177*, 643–660. [[CrossRef](#)]
20. Ogura, A.S.; Hernandes-Lopes, J.; Melo-de-Pinna, G.F.A. A new anatomical interpretation for abaxialization in unifacial leaf blade of stone plants (Aizoaceae, Caryophyllales). *Braz. J. Bot.* **2018**, *41*, 751–764. [[CrossRef](#)]
21. Mauseth, J.D.; Kiesling, R. Comparative anatomy of *Neoraimondia roseiflora* and *Neocardenasia herzogiana* (Cactaceae). *Haseltonia* **1997**, *5*, 37–50.
22. Mauseth, J.D. Theoretical aspects of surface-to-volume ratios and water-storage capacities of succulent shoots. *Am. J. Bot.* **2000**, *88*, 1107–1115. [[CrossRef](#)]
23. Anderson, E.F. *The Cactus Family*; Timber Press: Portland, OR, USA, 2001.
24. Terrazas, S.T.; Mauseth, J.D. Shoot Anatomy and Morphology. In *Cacti: Biology and Uses*; Nobel, P.S., Ed.; University of California Press: Berkeley, CA, USA, 2002; pp. 23–40.
25. Horn, J.W.; van Ee, B.W.; Morawetz, J.J.; Riina, R.; Steinmann, V.W.; Berry, P.E.; Wurdack, K.J. Phylogenetics and the evolution of major structural characters in the giant genus *Euphorbia* L. (Euphorbiaceae). *Mol. Phylogenet. Evol.* **2012**, *63*, 305–326. [[CrossRef](#)]
26. Frodin, D.G. History and concepts of big plant genera. *Taxon* **2004**, *53*, 753–776.
27. Dorsey, B.L.; Haevermans, T.; Aubriot, X.; Morawetz, J.J.; Riina, R.G.; Steinmann, V.W.; Berry, P.E. Phylogenetics, morphological evolution, and classification of *Euphorbia* subgenus *Euphorbia*. *Taxon* **2013**, *62*, 291–315. [[CrossRef](#)]
28. Edwards, E.J.; Nyffeler, R.; Donoghue, M.J. Basal cactus phylogeny: Implications of the *Pereskia* (Cactaceae) paraphyly for the transition to the cactus life form. *Am. J. Bot.* **2005**, *92*, 1177–1188. [[CrossRef](#)]
29. Hernández-Hernández, T.; Hernández, H.M.; Arturo De-Nova, J.; Puente, R.; Eguiarte, L.E.; Magallón, S. Phylogenetic relationships and evolution of growth form in Cactaceae (Caryophyllales, Eudicotyledoneae). *Am. J. Bot.* **2011**, *98*, 44–61. [[CrossRef](#)] [[PubMed](#)]
30. Steinmann, V.W. The Evolution of Succulence in the New World Species of *Euphorbia* (Euphorbiaceae). Ph.D. Thesis, Claremont Graduate University, Claremont, CA, USA, 2001.
31. Hurbath, F. Sistemática, Estrutura Genética de Populações e Filogeografia de *Euphorbia* sect. *Brasilenses* V.W. Steinm. & Dorsey (Euphorbiaceae). Ph.D. Thesis, Instituto de Botânica, São Paulo, SP, Brazil, 2018.
32. Solereder, H. *Systematic Anatomy of the Dicotyledons*, 2nd ed.; Clarendon Press: Oxford, UK, 1908.
33. Metcalfe, C.R.; Chalk, L. *Anatomy of the Dicotyledons*; Clarendon Press: Oxford, UK, 1950.
34. Bobich, E.G.; North, G.B. Structural implications of succulence: Architecture, anatomy, and mechanics of photosynthetic stem succulents, pachycauls, and leaf succulents. In *Perspectives in Biophysical Plant Ecophysiology: A Tribute to Park S. Nobel*; De la Barrera, E., Smith, W.K., Eds.; Universidad Nacional Autónoma de México: Mexico City, Mexico, 2009; pp. 3–37.
35. Rowley, G.D. *Caudiciform and Pachycaul Succulents: Pachycauls, Bottle-, Barrel- and Elephant Trees and Their Kin*; Strawberry Press: Mill Valley, CA, USA, 1987.
36. Eames, A.J.; MacDaniels, L.H. *An Introduction to Plant Anatomy*; McGraw-Hill: New York, NY, USA, 1947.
37. Esau, K. *Anatomy of Seed Plants*, 2nd ed.; Wiley: New York, NY, USA, 1977.
38. Kaplan, D.R. Fundamental concepts of leaf morphology and morphogenesis: A contribution to the interpretation of molecular genetic mutants. *Int. J. Plant. Sci.* **2001**, *162*, 465–474. [[CrossRef](#)]
39. Ogburn, R.M.; Edwards, E.J. Repeated origin of three-dimensional leaf venation releases constraints on the evolution of succulence in plants. *Curr. Biol.* **2013**, *23*, 1–5. [[CrossRef](#)] [[PubMed](#)]
40. Hernandes-Lopes, J.; Oliveira-Neto, M.A.; Melo-de-Pinna, G.F.A. Different ways to build succulent leaves in Portulacineae (Caryophyllales). *Int. J. Plant Sci.* **2016**, *177*, 198–208. [[CrossRef](#)]
41. Kniep, H. Über die Bedeutung des Milchsafts der Pflanzen. *Flora Allg. Bot. Ztg.* **1905**, *94*, 129–205.
42. Trumpke, H. *Beiträge zur Anatomie der Sukkulen Euphorbien*; Schlesische Volkszeitung: Breslau, Poland, 1914.
43. Sajeva, M.; Mauseth, J.D. Leaf-like structure in the photosynthetic, succulent stems of cacti. *Ann. Bot.* **1991**, *68*, 405–411. [[CrossRef](#)]
44. Mauseth, J.D. *Blossfeldia* lacks cortical bundles and persistent epidermis; is it basal within Cactoideae? *Bradleya* **2006**, *24*, 73–82. [[CrossRef](#)]
45. Terrazas, T.; Escamilla-Molina, R.; Vázquez-Sánchez, M. Variation in the tracheary elements in species of *Coryphantha* (Cactaceae-Cactoideae) with contrasting morphology: The bottleneck model. *Braz. J. Bot.* **2016**, *39*, 669–678. [[CrossRef](#)]
46. Schwager, H.; Neinhuis, C.; Mauseth, J.D. Secondary growth of the leaf and bud traces in *Hylocereus undatus* (Cactaceae) during the formation of branches or flowers. *Int. J. Plant. Sci.* **2015**, *176*, 762–769. [[CrossRef](#)]
47. Mauseth, J. Many cacti have clusters of terminal tracheids on their cortical bundles. *Haseltonia* **2018**, *24*, 64–74. [[CrossRef](#)]
48. Mauseth, J.D.; Sajeva, M. Cortical bundles in the persistent, photosynthetic stems of Cacti. *Ann. Bot.* **1992**, *70*, 317–324. [[CrossRef](#)]
49. Peirson, J.; Bruyns, P.; Riina, R.; Morawetz, J.; Berry, P. A molecular phylogeny and classification of the largely succulent and mainly African *Euphorbia* subg. *Athymalus* (Euphorbiaceae). *Taxon* **2013**, *62*, 1178–1199. [[CrossRef](#)]
50. Boke, N.H. Developmental morphology and anatomy in Cactaceae. *BioScience* **1980**, *30*, 605–610. [[CrossRef](#)]
51. Nobel, P.S. Water relations and photosynthesis of a barrel cactus, *Ferocactus acanthodes*, in the Colorado desert. *Oecologia* **1977**, *27*, 117–133. [[CrossRef](#)] [[PubMed](#)]

52. Nobel, P.S. Interception of photosynthetically active radiation by cacti of different morphology. *Oecologia* **1980**, *45*, 160–166. [[CrossRef](#)]
53. Darling, M.S. 1989. Epidermis and hypodermis of the saguaro cactus (*Cereus giganteus*): Anatomy and spectral properties. *Am. J. Bot.* **1989**, *76*, 1698–1706. [[CrossRef](#)]
54. Boke, N.H. Histogenesis of the vegetative shoot in *Echinocereus*. *Am. J. Bot.* **1951**, *38*, 23–38. [[CrossRef](#)]
55. Barcikowski, W.; Nobel, P.S. Water relations of cacti during desiccation: Distribution of water in tissues. *Bot. Gaz.* **1984**, *145*, 110–115. [[CrossRef](#)]
56. Mauseth, J.D.; Ross, R.G. Systematic anatomy of the primitive cereoid cactus *Leptocereus quadricostatus*. *Bradleya* **1988**, *6*, 49–64. [[CrossRef](#)]
57. Mauseth, J.D. Comparative structure-function studies within a strongly dimorphic plant, *Melocactus intortus* (Cactaceae). *Bradleya* **1989**, *1*, 1–12. [[CrossRef](#)]
58. Mauseth, J.D. Morphogenesis in a highly reduced plant; the endophyte of *Tristerix aphyllus* (Loranthaceae). *Bot. Gaz.* **1990**, *151*, 348–353. [[CrossRef](#)]
59. Mitra, G.C.; Majumdar, G.P. The leaf-base and the internode: Their true morphology. *Palaeobotanist* **1952**, *1*, 351–367.
60. Kadereit, G.; Mucina, I.; Freitag, H. Phylogeny of Salicornioideae (Chenopodiaceae): Diversification, biogeography, and evolutionary trends in leaf and flower morphology. *Taxon* **2006**, *55*, 617–642. [[CrossRef](#)]
61. Klak, C.; Reeves, G.; Hedderson, T.A.J. Unmatched tempo of evolution in southern African semi-desert ice plants. *Nature* **2004**, *427*, 63–65. [[CrossRef](#)]
62. Valente, L.M.; Britton, A.W.; Powell, M.P.; Papadopoulos, A.S.T.; Burgoyne, P.M.; Savolainen, V. Correlates of hyperdiversity in southern African ice plants. *Bot. J. Linn. Soc.* **2014**, *174*, 110–129. [[CrossRef](#)]
63. Jäger-Zürn, I. Shoot apex and spathella: Two problematical structures of Podostemaceae–Podostemoideae. *Plant Syst. Evol.* **2005**, *253*, 209–218. [[CrossRef](#)]
64. Mauseth, J.D. Structure–function relationships in highly modified shoots of Cactaceae. *Ann. Bot.* **2006**, *98*, 901–926. [[CrossRef](#)]
65. Howard, R. The stem-node-leaf continuum of the dicotyledoneae. *J. Arnold Arbor.* **1974**, *55*, 125–181. [[CrossRef](#)]
66. Gibson, A.C.; Horak, K.E. Systematic anatomy and phylogeny of Mexican columnar cacti. *Ann. Mo. Bot. Gard.* **1978**, *65*, 999–1057. [[CrossRef](#)]
67. Majumdar, G.P. Stipules, stipels, ligules and leaf-sheath. *Proc. Indian Acad. Sci.* **1956**, *43*, 9–22. [[CrossRef](#)]
68. Kellogg, E.A. Are Macroevolution and Microevolution Qualitatively Different? Evidence from Poaceae and Other Families. In *Developmental Genetics and Plant Evolution*; Cronk, Q.C.B., Bateman, R.M., Hawkins, J.A., Eds.; Taylor & Francis: London, UK, 2002; pp. 70–84.
69. Baum, D.A.; Donoghue, M.J. Transference of Function, Heterotopy and the Evolution of Plant Development. In *Developmental Genetics and Plant Evolution*; Cronk, Q.C.B., Bateman, R.M., Hawkins, J.A., Eds.; Taylor & Francis: London, UK, 2002; pp. 52–69.
70. Aloni, R. The Induction of Vascular Tissues by Auxin. In *Plant Hormones*; Davies, P.J., Ed.; Springer: Dordrecht, The Netherlands, 2010; pp. 485–506.
71. Aloni, R. Ecophysiological implications of vascular differentiation and plant evolution. *Trees* **2015**, *29*, 1–16.
72. Johansen, D.A. *Plant Microtechnique*; McGraw-Hill: New York, NY, USA, 1940.
73. Kraus, J.E.; Arduin, M. *Manual Básico de Métodos em Morfologia Vegetal*; Editora da Universidade Federal Rural do Rio de Janeiro: Seropédica, Brazil, 1997.
74. Gerlach, D. *Botanische Mikrotechnik: Eine Einführung*, 3rd ed.; Georg Thieme: Stuttgart, Germany, 1984.

Review

# Use of Gamma Radiation for the Genetic Improvement of Underutilized Plant Varieties

María de la Luz Riviello-Flores<sup>1</sup>, Jorge Cadena-Iñiguez<sup>2,\*</sup>, Lucero del Mar Ruiz-Posadas<sup>1</sup>,  
Ma. de Lourdes Arévalo-Galarza<sup>1</sup>, Israel Castillo-Juárez<sup>1</sup>, Marcos Soto Hernández<sup>1</sup>  
and Carlos Roman Castillo-Martínez<sup>3</sup>

<sup>1</sup> Colegio de Postgraduados, Campus Montecillo, Km. 36.5, Carretera México-Texcoco, Montecillo, Texcoco 56230, Mexico; marluriviello@gmail.com (M.d.l.L.R.-F.); lucpo@colpos.mx (L.d.M.R.-P.); larevalo@colpos.mx (M.d.L.A.-G.); israel.castillo@colpos.mx (I.C.-J.); msoto@colpos.mx (M.S.H.)

<sup>2</sup> Colegio de Postgraduados, Campus San Luis Potosí, Salinas de Hidalgo, San Luis Potosí 78622, Mexico

<sup>3</sup> CENID-COMEF, Instituto Nacional de Investigación Forestales, Agrícolas y Pecuarias (INIFAP), Progreso Núm. 5, Barrio de Santa Catarina, Alcaldía Coyoacán 04010, Mexico; castillo.carlos@inifap.gob.mx

\* Correspondence: jocadena@colpos.mx; Tel.: +52-5951149532

**Abstract:** Agricultural biodiversity includes many species that have biological variants (natives, ecotypes, races, morphotypes). Their use is restricted to local areas because they do not fulfill the commercial requirements; however, it is well documented that these species are a source of metabolites, proteins, enzymes, and genes. Rescuing and harnessing them through traditional genetic breeding is time-consuming and expensive. Inducing mutagenesis may be a short-time option for its genetic improvement. A review of outstanding research was carried out, in order to become familiar with gene breeding using gamma radiation and its relevance to obtain outstanding agronomic characteristics for underutilized species. An approach was made to the global panorama of the application of gamma radiation in different conventional crop species and in vitro cultivated species, in order to obtain secondary metabolites, as well as molecular tools used for mutation screening. The varied effects of gamma radiation are essentially the result of the individual responses and phenotypic plasticity of each organism. However, even implicit chance can be reduced with specific genetic breeding, environmental adaptation, or conservation objectives.

**Keywords:** in vitro crop; phytochemicals; gamma radiation; ionizing radiation; mutants

**Citation:** Riviello-Flores, M.d.l.L.; Cadena-Iñiguez, J.; Ruiz-Posadas, L.d.M.; Arévalo-Galarza, M.d.L.; Castillo-Juárez, I.; Soto Hernández, M.; Castillo-Martínez, C.R. Use of Gamma Radiation for the Genetic Improvement of Underutilized Plant Varieties. *Plants* **2022**, *11*, 1161. <https://doi.org/10.3390/plants11091161>

Academic Editors: Milan S. Stankovic, Paula Baptista and Petronia Carillo

Received: 8 April 2022  
Accepted: 23 April 2022  
Published: 26 April 2022

**Publisher's Note:** MDPI stays neutral with regard to jurisdictional claims in published maps and institutional affiliations.



**Copyright:** © 2022 by the authors. Licensee MDPI, Basel, Switzerland. This article is an open access article distributed under the terms and conditions of the Creative Commons Attribution (CC BY) license (<https://creativecommons.org/licenses/by/4.0/>).

## 1. Introduction

Beneficial mutations are changes to the genotypic structure that increase the variability of the species and favor their adaptation to various selection pressures [1]. These can be induced by physical mutagenic agents such as ionizing radiation (X-rays and gamma rays), non-ionizing radiation (ultraviolet), and corpuscular radiation (protons, neutrons, alpha, and beta particles) [1,2]. Ionizing radiation (IR) induces the change from neutral molecules or atoms to their ionized forms; this change requires ionization energy, which is the minimum amount of energy that separates the electron from a free atom in its lower energy state [1,2], through two effects: Compton and photoelectric [3].

IR can directly induce physical, biological, and chemical changes in the cells altering the chemical nature of the molecules [1,2,4]. It can induce specific changes in the genome [5] and indirectly induce an alteration of free radicals generated mainly by the ionization of water molecules [1,2,4] (Figure 1).

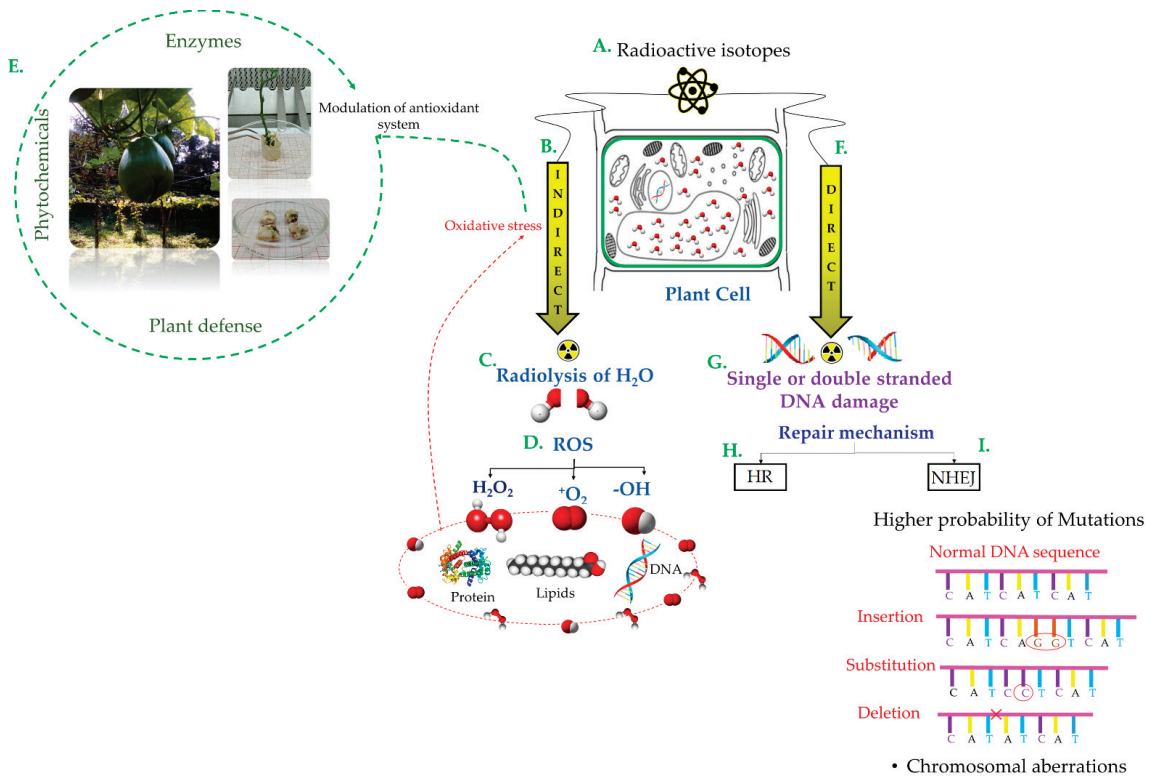


**Figure 1.** Scheme of Mutation Inductions by gamma radiation for the genetic improvement of plants. (A) Gamma radiation (GR) is one of the most widely used mutagenic agents in plants, because it is reported to induce high genetic variability. This type of radiation can be generated by radioisotopes such as carbon-14 (<sup>14</sup>C), cobalt-60 (<sup>60</sup>Co), cesium-137 (<sup>137</sup>Cs), and plutonium-239 (<sup>239</sup>Pu) [1]. Gamma rays (B) interact indirectly through (C) Radiolysis of water produces (D) reactive oxygen species (ROS) (hydrogen peroxide (H<sub>2</sub>O<sub>2</sub>), superoxide anion (O<sub>2</sub><sup>•</sup>), hydroxyl radical (OH), and singlet oxygen (O=O)) that generate lipid peroxidation and alter the structure of DNA and proteins [2–4]. (E) By increasing the ROS concentration, oxidative stress triggers the defense of the plant, which is modulated by enzymes such as peroxidase, ascorbate peroxidase, superoxide dismutase, and glutathione reductase [2,6]. Primary gamma radiation lesions delay or inhibit cell division and affect mitotic activity, growth rate or habit, dilation of thylakoid membranes, photosynthesis, modulation of the antioxidant system, and accumulation of phenolic compounds [7]. (F) Direct gamma radiation can generate base modifications and (G) single or double DNA strand breaks [8]. A twofold mechanism is involved in the natural repair of these errors: (H) Homologous Recombination (HR), an error-free repair mechanism; and (I) Non-Homologous End-Joining (NHEJ), a mechanism with a greater probability of generating mutations in the repair site, including deletions, insertions, and substitutions, among others [9].

Ionizing energy has been used for approximately 60 years to develop new varieties with economic value, improved resistance to pests and disease, higher agricultural yield, better quality, and high nutritional value, among other advantages. Population growth, food shortages, the economic situation of some regions of the world, the excessive use of non-renewable energy resources (fossil fuels), and climate change have led to the search for new uses and the genetic improvement of underutilized vegetables [10]. So-called underutilized plant species varieties (neglected, orphan or minor) are an option to substitute

crops with broad commercial demand [9]. Although they are considered popular crops for local consumption or self-consumption (not commercially competitive), they represent a potential option for diet diversification, owing to their wide possibility of improvement, processing, and adaptation to the environment [9]. This review focuses on the research about plant breeding mediated by GR in recent years and its relevance to obtain good agronomic characteristics for agriculture. In addition, future perspectives for its application in underutilized genetic varieties—as an alternative for the use of little valued genetic resources—is highlighted.

The information search was carried out in Google Academic, Scopus, and SciELO. The following search words were used: “ionizing radiation in plants”, “the effect of gamma irradiation on secondary metabolites”, “induced mutation by gamma irradiation”, “effect of ionizing radiation on DNA-plant”, “plant mutation breeding”, “in vitro mutagenesis”, and “secondary metabolites”. The mutant varieties database of the International Atomic Energy Agency (IAEA) was also consulted, using the search criteria “physical agent” and “gamma radiation”.

## 2. Radiosensitivity

Efficient induction of mutagenesis by gamma radiation (GR) requires determination of the optimal radiation dose; that is, the dose that reduces 50% of the population (median lethal dose, LD<sub>50</sub>). It also requires variables such as: survival, mass, or number of germinated specimens, among others; or, the radiation dose that reduces growth in 50% of the population (median growth reduction, GR<sub>50</sub>). Both doses depend on the plant tissue (seed, meristem, callus, etc.), stage of development and moisture content, among other parameters [11,12]. High radiation doses can induce radioinhibition by affecting growth promoters and eventually tissue destruction [13]. It can also cause loss of regenerative capacity and malformation of plant tissues as well as tissue destruction [14]. Radiosensitivity assays allow determining the appropriate radiation dose to induce the highest mutation rate with the most negligible effects on the gene complex [1,15]. Radiation stimulation can be obtained with low radiation doses that favor the induction of metabolites and biochemical changes involved in plant regeneration [13,16], thus generating chimeric plants [13]. Some studies have reported that radiation stimulation by GR is demonstrated in plant varieties. Kaolack and Crimson irradiated sweet varieties of *Citrullus lanatus* (watermelon) inducing an LD<sub>50</sub> of 225.40 and 221.56 Gy, respectively [17]. While in *Coffea arabica* L. var. *typica* with an LD<sub>50</sub> of 100 Gy, morphological changes were induced in the leaf (color, number, length, and width), plant height, and distance from the cotyledon to the first node [18]. An LD<sub>50</sub> of 2486 Gy was recommended for the *Eragrostis superba* (Wilman lovegrass) plant [12], while 628, 712, 698, and 411 Gy were recommended for the seeds of *Eragrostis curvula* (weeping grass), *Pennisetum ciliare* (Buffel), *Bouteloua curtipendula* (Banderita), and *Bouteloua gracilis* (Navajita), respectively [19]. In corns and seedlings of *Agave tequilana* var. *blue*, a LD<sub>50</sub> between 20 and 25 Gy induced the number of shoots and increased the size of the seedlings, while 16 Gy increased the callus area [20]. For *Solanum tuberosum* var. Désirée (potato), an LD<sub>50</sub> of 10 Gy increased the regeneration of vegetable callus by 71% [21]. Meanwhile, GR-induced DNA breaks the form of harmful genomic and chromosomal abnormalities [22]. The erroneous nature of DNA repair can lead to aberrations that can be latently transmitted to the progeny [23]. Some examples are reported in the axillary buds of *Physalis peruviana* (Golden Berry/Uchuva): at 100 Gy cytological changes were induced and the number of lagging chromosomes increased, while at 200 Gy, the formation of anaphase, telophase, and isolated chromosome bridges increased [24]. The alterations during anaphase revealed that GR influences the function of the mitotic spindle; the bridges are caused by the formation of dicentric chromosomes that originate from the chromosome exchange after DNA breakage [25]. Another example can be found in *Chrysanthemum morifolium* “Donglinruixue” (chrysanthemum): a 35-Gy radiation increased the number of cells with chromosomal aberrations (adhesion, univalent, unipolar, lagging chromosomes) and the formation of micronuclei [26]. In *Saccharum* spp. hybrid var. “SP 70-1284” (sugar-

cane) doses higher than 30 Gy compromise callus growth and regeneration [27]. In general, ionizing radiation-induced DNA repair uses mechanisms similar to those that regulate the integrity of foreign sequences in plant genomes [5,23]. It can occur by a double-strand break (DSB) repair route: the first recovers information through homologous recombination (HR), and the second uses a non-homologous end-joining (NHEJ) system that often results in the deletion of a DNA fragment and therefore a mutation [9]. The adaptive and developmental process of plants provides them with greater resistance to the production of DSB by ionizing radiation than other eukaryotic organisms, triggering much more effective and rapid DNA repair and defense reactions.

### 3. Gamma Radiation and In Vitro Culture

In vitro mutagenesis in a plant organ, tissue, and cell cultures provides the opportunity for the rapid and massive spread of mutant plants [1]. The induction of mutations through GR has been reported in buds and seeds collected in the field, as well as in tissue cultures, protoplasts, and callus [28]. With this technique, large populations of plants can be managed under controlled conditions, in reduced spaces, and at any time of the year [9]. On the one hand, in vitro biotechnological techniques guarantee quality and safety, which combined with mutagenesis techniques, allow the selection of outstanding agronomic characteristics in plants of economic and productive importance [29]. On the other hand, although the aim is to obtain improved characteristics with GR, negative responses on growth have also been reported, as is the case of *Gerbera jamesonii* calluses in which an 11% reduction of fresh weight was recorded after subjecting them to 20 Gy from GR [30]. Therefore, using wide ranges of GR to cover the radioinduction and radioinhibition intervals must be taken into consideration. Also, the basic physiological and taxonomic aspects and the oxygen and water content of the plant material to be irradiated must be determined. In this regard, the effect of low GR doses on the growth and accumulation of 20-hydroxyecdysone in *Sesuvium portulacastrum* tissue culture has been reported. When the dose of 20 Gy doubled the concentration of the metabolite (0.139 mg/dry weight), the GR was proved to induce metabolic changes and obtain mutants with a higher in vitro production of secondary metabolites [31]. Another research reported the effect of 15–45 Gy doses combined with monochromatic lights on the growth of in vitro shoots of the *Dendrobium sonia* orchid. GR decreased shoot length, fresh weight, and leaf area, but its combination with yellow light increased shoot survival and length, fresh weight, and chlorophyll content [32]. Similarly, using different GR doses (10, 30, and 50 Gy) on in vitro cultured explants of *Eriobotrya japonica* L. (Loquat) made it possible to accelerate the reproduction programs in which the combination of apical explants grown in MS medium with 10 Gy of GR favored a greater growth of callus diameter and height, the number of leaf shoots, and seedling height [33]. Likewise, good results have been reported in species of difficult reproduction. For example, the vegetative cycle of *Musa paradisiaca*—which reproduces vegetatively—requires a long generational time; this makes genetic variation difficult. The effect of radiation on the diversity of the Pisang Ambon crop was determined, when 10 and 20 Gy were found to increase the length and width of the leaves, as well as the height and diameter of the stem. These results are important, because they support the massive propagation of banana plants of better quality and with greater resistance to biotic and abiotic stress [34]. Additionally, positive effects of GR have been reported on different plant structures of various varieties of *Citrus* spp. However, since all the material was susceptible to GR-induced mutagenesis, the seeds showed the highest resistance (LD<sub>50</sub> at 127 Gy in “Alemow”, and 156 Gy in sour orange), followed by the buds (LD<sub>50</sub> around 50 Gy for all cultivars) and the nodal segments (LD<sub>50</sub> of 25 Gy for both lemon cultivars) [35]. Therefore, the GR applied to in vitro cultures allows the development of multiple responses in plant materials, either to promote variability in a short time in species where it is difficult to obtain it traditionally or to enhance the metabolic expression.

#### 4. Gamma Radiation as a Tool for Plant Breeding

The induction of mutations by physical agents allows to obtain genetic variations in crops of agronomic importance that are not found in nature [35]. The alteration caused by the formation of free radicals promotes structural and metabolic changes in the plant [10]. For example, studies about the effect of GR on chloroplasts show that they were mainly sensitive to high radiation and that mutations occurred after 50 Gy [36]. In addition, high doses of GR affect protein synthesis, hormonal balance, enzymatic activity, and gas and water exchange [36]. Currently, there is great interest in generating new variations to develop more nutritious, resilient, and productive crops [37,38].

Although the generation of new varieties by GR is random, they can be identified and selected in a short time, accelerating the establishment and release process; compared to the process used to obtain Genetically Modified Organisms (GMOs) this is a more efficient method [1]. According to the mutant varieties database of the International Atomic Energy Agency (IAEA), from 1960 to 2020, 1703 plants of agronomic importance with GR-induced mutations were recorded. Specimens such as the Rosa mutant (Pink Hat)—generated by radiating terminal buds—were approved in 1960; their advantages include a two-tone flower color and resistance to mold [39]. Recently, *Oryza sativa* L., *Solanum lycopersicum* L., and *Bougainvillea* spp. mutants were registered [39]. In the case of *O. sativa* (rice), the organoleptic characteristics, yield, and early maturation, as well as their resistance to *Nilaparvata lugens* infection increased in the mutants generated with GR [39]. When the seeds of *S. lycopersicum* (tomato) were subject to radiation, mutants with higher yields and fruit quality (shape, size, and color of the leaves) were obtained; they also have a greater tolerance to heat stress. As a consequence of its success, one of its varieties has been transferred to the industrial sector, where it is used to produce different food products [39]. Also, it was reported that doses of 10 and 20 Gy of GR increases the stomatal parameters (density, length, and width of the stomata) of three varieties of sugarcane (NIA-0819, NIA-98, and BL4), which has an impact on gas exchange and photosynthetic activity [40]. In *Triticum aestivum* L., radiation on the seeds of two genotypes (Roshan and T-65-58-8) decreased the number of shoots, the length of the root, and the dry weight of the seedlings, without affecting germination. However, when the seedlings were irradiated with 100 Gy, proline and chlorophyll A content increased by 85%. Therefore, the expressed phenotype depends on the radiation dose, which may enhance resistance to radiation, drought or saline stress [36].

With GR, mutants resistant to heavy metals, salt stress, and pests can also be obtained. *Hordeum vulgare* L. (mountain barley) seedlings irradiated with 50 Gy and subjected to lead and cadmium stress presented less hydrogen peroxide and malondialdehyde. In addition, a high concentration of proline and antioxidant enzymatic activity suggested the expression of heavy metal transporters [41]. The effect of GR on the induction of resistance to saline stress was reported in *S. tuberosum* L. (potato) and *O. sativa* L. (rice) cultures, in which several mutants resistant to high concentrations of salt were generated [42,43]. On the one hand, three lines of *Cicer arietinum* L. (chickpea) were also induced with GR (LD<sub>50</sub> of 150 Gy) and became resistant to *Ascochyta rabiei* (chickpea blight) [44]. On the other hand, GR has also been used in difficult-to-handle cultivars with long harvest times: for example, Mentik Susu, a variety of rice that is very difficult to harvest, as a consequence of its great height. Using GR (200 Gy), smaller, more productive mutants with a better seed yield were obtained; harvest time was also shorter [45]. Finally, mutants with higher commercial quality characteristics can be obtained with GR—for example, *Pamindo agrihorti* (grapefruit), derived from *Citrus maxima*. The stability of the characters and greater vigor were also demonstrated.

## 5. Effect of Gamma Radiation on the Concentration of Secondary Metabolites

Secondary metabolites are organic compounds with low molecular weight; they are biosynthesized from or share substrates of origin with the primary metabolism. They include phenolic compounds, terpenoids, and compounds that have nitrogen in their structure [46]. They are of utmost importance because they help the plant to interact with biotic and abiotic factors in the hostile environment in which they develop, creating defense and protection mechanisms [46]. In some cases, the secondary metabolites are highly specific to the species, providing them with important qualities for their application as therapeutic or medicinal agents [46]. One area of interest is the profitable production of secondary metabolites through biotechnological mechanisms and mutagenesis. Under this approach, the GR technologies that have been applied increase the concentration of phytochemicals of interest in both sexually or vegetative propagated (in vitro) plants of commercial or medicinal value. GR interacts with the biosynthetic mechanism of the plant forming free radicals (ROS) caused by the radiolysis of water. This triggers the oxidative stress response, producing various defense enzymes and antioxidants [47], which is proportional to the concentrations of secondary metabolites. It is important to highlight that a low GR dose generates accelerated cell proliferation, germination rate, cell growth, enzymatic activity, resistance to stress, and increased crop yield and contraction of secondary metabolites [31,47].

When the calluses of *Rosmarinus Officinalis* L. (Rosemary) are irradiated, the activity of phenylalanine ammonium lyase (PAL) increases and, at the same time, the concentration of total phenols also increases. This enzyme is key in the pathway of the phenylpropanoids responsible for the synthesis of phenolic acids [48].

Moghaddam et al. [49] demonstrated that, after eight weeks, the seedlings of the accession CA23 of *Centella asiatica* irradiated with 20 and 30 Gy doses contained the highest concentrations of total flavonoids ( $16.827 \pm 0.02$ ; and  $16.837 \pm 0.008$  mg g<sup>-1</sup> dry weight, respectively): 54.7% and 46.8% more than control.

Flavonoid biosynthesis is stimulated by enhancing the phenylalanine content, the phenylalanine ammonia-lyase (PAL) activity, and the chalcone synthase enzyme (CHS) activity. Specifically, regarding the response to gamma radiation, PAL activity affects flavonoid synthesis in the phenylpropanoid pathway, where this enzyme acts as a catalyst for the conversion of phenylalanine to cinnamic acid. However, the enzyme chalcone synthase (CHS), key in the biosynthesis of flavonoids or isoflavonoids, also catalyzes the formation of chalcones from malonyl-coA and coumaroyl-coA. Chalcones are a major intermediate in the flavonoid pathway that gives rise to several classes of flavonoids. There is a correlation between the upregulation of CHS genes and increased flavonoid content in response to gamma radiation [49].

In other researches, seeds of *Onobrychis viciifolia* Scop were irradiated. The leaf extract of *Syn. Onobrychis sativa* L. (Sainfoin) irradiated with 90 Gy had a greater phenolic content than non-irradiated extract. Likewise, the alkaloid Berberine increased from 0.000152% to 0.000203% [50].

Sheikhi et al. [51] studied the effect of gamma radiation on calluses of *Ferula gummosa* Boiss. and found that the phenolic content increased by 36.5% and 38.9%, when they were irradiated with 20 and 25 Gy doses.

It should be mentioned that the effect of gamma radiation on the concentration of terpenoids, alkaloids and other metabolites of medicinal importance has also been studied. Muhallilin et al. [52] researched the diversity of morphological characteristics and chemical content of the seedlings of *Celosia cristata* L., an ornamental plant valued for its application in traditional medicine. They selected a clone (labeled C1U3 2.3.1) irradiated with 25 Gy dose, which showed a remarkable triterpenic compounds content that was not present in the controls.

Magdy et al. [53] identified that the M2 offspring of a rhizome of *Zingiber officinale* Rosc (parental ginger) irradiated with 20 Gy had 73.76% more 6-gingerol content than the control:  $38.4 \pm 0.01 \text{ mg g}^{-1}$  of methanol extract compared to  $22.1 \pm 0.03 \text{ mg g}^{-1}$  of methanol extract in the non-irradiated control samples.

Kapare et al. [31] studied the impact of low doses of gamma radiation (range: 5–40 Gy) on the growth and accumulation of 20-hydroxyecdysone in *Sesuvium portulacastrum* shoots. They verified that ex vitro plants obtained from shoots exposed to 20 Gy had 66% more ecdysteroid 20-hydroxyecdysone content ( $0.321 \text{ mg dry weight of the plant}^{-1}$ ) than the control.

Azeez et al. [54] studied the effect of gamma radiation on the yield of pharmacologically-profitable secondary metabolites in callus cultures obtained from the leaf, stem, and root of *Hypericum triquetrifolium* Turra, irradiated with doses of 10, 20, 40, and 50 Gy. They specified that the best irradiation doses that stimulated epicatechin concretion were 10 and 20 Gy in leaf and stem callus ( $126.39$  and  $148.80 \text{ mg } 100 \text{ g}^{-1}$ ) regarding the control ( $98.81$  and  $101.72$  respectively). Likewise, they registered that the foliar callus irradiated with doses of 10 Gy had higher naphthodianthrones hypericin and pseudohypericin content than the control samples (hypericin 10 Gy:  $0.294 \text{ mg } 100 \text{ g}^{-1}$ ; control:  $0.251 \text{ mg } 100 \text{ g}^{-1}$ ; pseudohypericin 10 Gy:  $4.01 \text{ mg } 100 \text{ g}^{-1}$ ; control:  $3.57 \text{ mg } 100 \text{ g}^{-1}$ ).

The concentration of alkaloids such as trigonelline and nicotinic acid (two secondary metabolites of medicinal importance) was significantly affected by the gamma radiation incidence on *Trigonella foenum-graecum* L. (fenugreek) seeds. In this research, the highest result was obtained with the 100 Gy dose, with 7% and 9% increases of these secondary metabolites compared to the control [55].

Mariadoss et al. [56] applied gamma radiation to obtain high-performance cell cultures of *Rubia cordifolia*. Callus irradiated with 8 Gy accumulated a maximum alizarin and purpurin levels that were 6 and 11 times higher than non-irradiated callus cultures. From the mutants, a suspension cell bioreactor protocol was established, obtaining 63.58% more anthraquinones.

Overall, the application of GR technology to increase secondary metabolites such as those mentioned and others—capsaicinoids [57], steviosides [58], saponins, ginsenosides [59], camptothecin [60]—offers an impressive study window about various plant species with medicinal applications; at the same time, it provides an opportunity to move towards a more sustainable agriculture. Therefore, further research about the potential for the application of technologies—such as ionizing radiation and biotechnological protocols—are necessary. When they work together, the success in the objectives set increases.

## 6. Molecular Analysis for the Identification and Screening of Mutants

The genetic breeding process through physical agents such as GR is strengthened when a molecular identification of specific agronomic traits is carried out; this allows the screening of DNA polymorphisms between mutants or point mutations. This screening identifies whether the mutations are the results of single base substitutions, deletions, insertions, inversions, duplications, reciprocal translocations, among others. Meanwhile specific researches obtained useful plant material for the application of functional genetics. Whole genome resequencing, molecular markers (such as ISSR, RAPD-PCR), or more complex methodologies (such as QTls, TILLING or transcriptomics supported with bioinformatic analysis) can be used to achieve these objectives.

Magdy et al. [53] recorded some examples of these molecular methodologies, which they used to obtain variability in curl-mas of *Z. officinale* Roscoe (ginger), confirming it through RAPD-PCR analyzes; they used five primers and obtained 58 bands; 15 monomorphic and 43 polymorphic (74.14% polymorphism). The polymorphism levels varied with each primer, confirming the genetic variation in the plants irradiated with gamma rays compared to the control.

ISSR (Inter Simple Sequence Re-peats) markers were used to identify DNA polymorphism among gamma-radiation mutants of *Sophora davidii* (Franch.) Kom. ex Pavol (medicinal plant and food scrub of ecological value). This analysis allowed the generation of 183-point fragments with 51.37% polymorphism. The genetic similarity based on the ISSR data ranged from 0.6885 to 1.000 (Jaccard coefficients of dissimilarity), with an average genetic similarity of 0.7884, which indicated the level of genetic variation between mutants. Therefore, gamma ray treatment proved to be an effective way to induce mutations in *S. davidii* and that mutants were successfully detected by ISSR analysis [61].

Li et al. [62] characterized GR and ion beam-induced mutations in *Oryza sativa* L. mutant lines of the M5 generation by whole genome resequencing and bioinformatic analysis. Fifty-seven single-base substitutions (SBS), 17.7 deletions, and 5.9 insertions were detected in each irradiated mutant. An analysis of structural variation (SV) was performed and an average 0.6 SV (spanning large deletions or insertions, inversions, duplications, and reciprocal translocations) were detected in each mutant.

2-Acetyl-1-pyrroline (2AP) is a volatile compound responsible of the aroma in rice and it is biosynthesized when the BADH2 gene loses its function as a suppressor gene. Aromatic rice cultivars naturally incur the BADH2 gene mutation at 8 bp. Some homozygous mutant rice lines were obtained by gamma radiation with a 100 Gy dose and various aroma-related primers of rice were used to identify the point mutation. PCR was performed and 254-bp and 355-bp DNA fragments were sequenced to identify the genetic mutation. The nucleotide sequence data of these DNA fragments showed that point mutations (deletions and substitutions of purine for pyrimidine or vice versa) occurred in the BADH2 gene in exon 7; these are called second mutations and were caused by gamma rays [63].

Tan et al. [64] characterized mutations in coding regions of a *Hordeum vulgare* (barley) dwarf mutant induced by gamma radiation, using a transcriptome sequencing strategy. They found 1193 genetic mutations in gene transcription regions: 97% of these were concentrated in the 5H and 7H chromosome regions. They also found that the mutations were not uniformly distributed throughout the genome, but that they were located in several concentrated regions. This is a clear example that provides a deeper understanding of the mechanisms of gamma radiation mutation and its application in the analysis of genetic function.

Regarding the monitoring of induced mutations in cultivars of agronomic and economic importance, outstanding molecular methodologies have been developed, including QTL (identification of quantitative trait loci). In other cases, the outstanding application of gamma radiation to induce mutations enables important research lines for the application of functional genomics, such as the creation of TILLING populations.

TILLING is a reverse genetics methodology in functional genomics research that helps the functional identification of mutations in specific genes [65]. It has been used together with gamma radiation to obtain cultivars with outstanding agronomic characteristics. To achieve this procedure, approximately 15,000 m<sup>3</sup> of cultivars were developed by applying gamma radiation to rice seeds (*O. sativa* subsp. Japonica cv. Donganbyeon). The salient characteristics in the TILLING population were analyzed, using AFLP molecular markers and evaluating genetic diversity. Subsequently, 28 polymorphic loci of the TILLING lines were cloned. Overall, this study proposed the TILLING rice population as a valuable genetic source that can be used in functional genomic studies about the species [66].

Continuing with the use of more sophisticated methodologies for the screening of gamma radiation-induced mutations, Hwang et al. [67] researched the QTL to determine the flowering time of a rice mutant obtained by gamma radiation, whose importance is associated with crop yield and quality. To achieve their objective, they developed a linkage map of 36 InDel markers and six SNP markers with F2 plants derived from the “WT 9 EMT1” cross. They detected a main QTL region in chromosome 6 and a candidate gene to control the early heading date in EMT1 by genetic linkage analysis, sequence variation and expression study. The results obtained suggested that the genes related to the temperature-sensitive flowering pathways could promote the regulation of flowering, such as the EMT1

gene, which provides the clearest explanation for the flowering mechanisms of rice under LD conditions and for the development of new early flowering rice cultivars.

Recently, technologies such as transcriptomics have been used to provide a specific response to the effect of gamma radiation on the genome. Kang et al. [68], researched the gene expression changes of *Vigna unguiculata* (L.) Walp. (cowpeas) plants subjecting them to different doses of ionizing radiation: gamma radiation and proton beam. They identified differentially expressed genes (DEG) in the entire genome of the irradiated plant through the classification of the genes; subsequently, they were able to make a general description of the metabolic pathways that were involved in the stimulation of change in the plant. The response to irradiations doses was diverse: three genes were identified and expressed differently with each irradiation dose (32, 75, and 69) than control. In contrast with control, 168, 434, and 387 DEG were identified for each proton beam irradiation dose. The number of genes related to defense, photosynthesis, reactive oxygen species (ROS), plant hormones, and transcription factors (TF) that were up- or down-regulated was higher in proton beam treatment than in gamma ray treatment.

Kim et al. [69] observed a 208-lines gene expression pattern in a group of mutant diversity (MDP) of M12-generation *Glycine max* L. (soybean), obtained by gamma radiation; they selected and studied the metabolic properties observing the isoflavones and fatty acids content of the seeds. Six lines with altered isoflavone content and six lines with altered oleic acid content were selected and compared with wild types in order to measure gene expression. The isoflavone biosynthetic genes were different in each stage and expression patterns and, in the mutants that presented a higher concentration of isoflavones, the MaT7 gene showed a higher expression level. Fatty acid biosynthetic genes were classified into two groups that reflect the development stages of the seeds. Consequently, the bases were established for a future functional analysis of the regulatory genes that are involved in the biosynthetic pathway of isoflavones and fatty acids in soybeans.

## 7. Prospects for the Application of Gamma Radiation in Underutilized Genetic Varieties

Plant genetic resources for food and agriculture (PGRFA) are also considered as part of agricultural biodiversity. These are defined as plant material (including reproductive and vegetative propagation) with actual or potential value for food and agriculture [70]. Currently, thirty main crops are used commercially to supply the global food demand, but only wheat, rice, corn, and potatoes (13.3%) are classified as food security [71,72]. Meanwhile, approximately 23% of the 30,000 edible plant species are collected and used as food. However, although they can diversify the diet with new nutritional sources, there have been few studies and evaluations in this regard. Since they lack commercial interest, some species have been cataloged as underutilized (forgotten, obsolete, or minor) and their nutritional and cultural properties, as well as their role as a source of genetic diversity, have not been valued. It is important to note that many of these plants are used in local agriculture and they have been the basis of community food for centuries. However, although commercially important crops have replaced many of them, they have now been incorporated into genetic improvement studies [73].

Padulosi et al. [74] mention that underutilized species depend on the geographical area, as well as the social and economic impact. In certain places, the species is well known and widely used, while in others, it is classified as underutilized. An example is *Cicer arietinum* (chickpea), which is in Italy considered an underutilized species, but which in Syria is a staple food and the basis of their diet.

Other species are the vegetables *Eruca sativa*, *Diplotaxis tenuifolia*, and *D. muralis* (arugula), which have significant economic value in Europe; meanwhile, in Egypt, they provide nutrients to the poorest population and are therefore unexpensive and locally used [74].

Cateano et al. [73] mention some crops with different marginality categories in countries such as Ecuador, Brazil, Bolivia, Spain, Peru, Colombia, and the Andean Region. Furthermore, they identify many orphan, obsolete, promising, and underutilized crops in Colombia.

Bravo, Arteaga and Herrera [7] recorded 91 species used for food and medicinal use in northern Venezuela. Forty-six of these species are known as alternative or underutilized plants, they are used for self-consumption, their commercialization is very limited, many of them exist in the wild, and they have the potential to strengthen the local diet. This group includes *Annona cherimola* (custard apple), *Annona squamosa* (Anón), *Spondias mombin* (Jobo), *Spondias purpurea* (stone plum), *Chrysophyllum cainito* (caimillo), *Coleus forskohlii* (oregano), *Curcuma longa* (turmeric), *Portulaca oleracea* (purslane), *Eryngium foetidum* (wild coriander).

In Mexico, some research centers have undertaken to conserve and make use of the PGRFA, rescuing several crops that are a priority for food sovereignty whose basis is the underutilized biological variants (Table 1). The scheme integrates the rescue, conservation, characterization, and development of capacities following the Second World Plan of Action for Plant Genetic Resources for Food and Agriculture of the FAO [75,76]. Forty-four networks were established per crop and a Thematic Network of Conservation Centers, carrying out actions in four strategic areas and eighteen lines of action.

**Table 1.** Priority crops and Network of Conservation Centers in Mexico [75].

Basic and Industrial	Fruit Trees	Vegetables	Impulse	Ornamental
<i>Agave</i> spp.	<i>Persea</i> spp.	<i>Capsicum</i> spp.	<i>Bixa orellana</i> L.	Bromeliaceae
<i>Gossypium barbadense</i> L.	<i>Theobroma</i> spp.	<i>Solanum lycopersicum</i> L.	<i>Suaeda acuminata</i> (C. A. Mey.) Moq.	Cactaceae
<i>Phaseolus vulgaris</i> L.	<i>Juglans</i> spp.	<i>Cucurbita</i> spp.	<i>Portulaca oleracea</i> L.	<i>Tagetes</i> spp.
<i>Helianthus annuus</i> L.	<i>Carica</i> spp.	<i>Ipomoea</i> spp.	<i>Yucca</i> spp.	<i>Dahlia</i> spp.
<i>Jatropha curcas</i> L.	<i>Vitis</i> spp.	<i>Sechium</i> spp.		<i>Echeveria</i> spp.
<i>Zea mays</i> L.	<i>Annona</i> spp.	<i>Solanum cardiophyllum</i> Lindl.		<i>Hymenocallis</i> spp.
<i>Vanilla</i> spp.	<i>Spondias</i> spp.	<i>Physalis</i> spp.		Euphorbiaceae
<i>Amaranthus</i> spp.	<i>Psidium guajava</i> L.			Orchidaceae
<i>Simmondsia chinensis</i> (Link) C. K. Schneid	<i>Byrsonima crassifolia</i> (L.)Kunth			<i>Beaucarnea recurvata</i> Lem.
	<i>Opuntia</i> spp.			<i>Tigridia</i> spp.
	<i>Philodendron</i> spp.			
	<i>Pouteria</i> spp.			
	<i>Crataegus</i> spp.			

Genetic resources are a reservoir for conducting bioprospective studies (Table 1) and identifying new sources of nutrients and compounds that provide health benefits. They also offer a potential solution to the growing demand of the food industry and favor its protection as a material that generates value for local communities.

Although they have been undervalued, the group of plants known as quelites is currently classified within the Priority Biocultural Regions of Mexico and it is linked to the Great Geoeconomic Regions of the country [75]. Approximately 127 native herbaceous species that grow in the *milpas* fall within the denomination of quelite, out of which 12 species are the most representative, including: *Portulaca oleracea* (purslane), *Amaranthus* spp. (amaranth), *Dhysphania ambrosioides* (epazote), *Porophyllum ruderale* subsp. *macrocephalum* (papalo), *Chenopodium berlandieri* (quelite), *Solanum americanum* (blackberry), *S. nigrescens* (divine nightshade), *Anoda cristata* (alache), *Jaltomata procumbens* (jaltomate), *Lepidium virginicum* (virgina pepperweed), and *Phytolacca icosandra* (amolquelite) [76].

On the one hand, quelites are semi-domesticated plants of local and traditional consumption. Its production has been remained under the protection of small producers; additionally, several quelites have agronomic qualities such as resistance to drought and low maintenance [76]. They also have great commercial potential, including *ruderalis* subsp. *macrocephalum*, *P. oleracea*, *Amaranthus* spp., *Suaeda edulis* (romerito), and *Chenopodium berlandieri* subsp. *nuttalliae* (huauzontle); they are produced on a large scale, with national and export demand [76]. Therefore, quelites are a clear example that underutilized crops can contribute to food sovereignty [76].

On the other hand, *Annona purpurea* Moc. & Sessé ex Dunal is a semi-domesticated fruit tree for local consumed in certain regions of Mexico that, as a consequence of the lack of enough information, was classified as an underutilized species. Nevertheless, around 44 alkaloids, 27 essential oils, four flavonoids, and two steroids—which represent potentially bioactive compounds—have been currently identified [77] in this fruit.

Underutilized crops are also candidates for genetic improvement using biotechnological and molecular tools. In this regard, the application of nuclear energy was analyzed to improve native Mexican pseudo cereals—classified as underutilized, but which have high nutritional value—including *Chenopodium berlandieri* ssp. *nuttalliae* (red chia), *Amaranthus hypochondriacus* Aztec race (white chia), and Mixteca race (black chia), as well as *Chenopodium berlandieri* ssp. *nuttalliae* (huauzontle). Genetic improvement was achieved through GR induction of the seeds and a subsequent establishment of the mutant line in the field, where it is expected to achieve improvements, such as reduced dehiscence, larger seed size, large and compact spike, among others [78].

Conservation models must be directly correlated to use; otherwise, there is a risk of losing agrobiodiversity as a consequence of the lack of consumers [79]. Few reports yet include the underutilized species category; however, due to the characteristics of the crops, several researches can be identified in which GR has been used to improve species that fall into this category.

This review gives examples of genetic improvement using GR (Table 2) in crops with high impact on food and plant species which are considered unusual, forgotten, in danger of extinction, of local use, and with a crucial bio prospective potential.

**Table 2.** Gamma radiation treatment and LD<sub>50</sub> determination to obtain putative mutant lines of different plant species.

Common Name	Scientific Name	Irradiated Tissue Material	Treatment	LD <sub>50</sub>	Observations	Reference
Watermelon	<i>Citrullus lanatus</i> (Thunb.) Matsum. & Nakai var. <i>Kaolack</i> and var. <i>Crimson sweet</i>	Seeds	100, 200, 300, 400, and 600 Gy	<i>Kaolack</i> 225.40 Gy and <i>Crimson sweet</i> 221.56 Gy	Radiosensitivity of the two most frequently cultivated varieties in Cameroon and determination of LD <sub>50</sub> .	[16]
Coffee plant	<i>Coffea arabica</i> L. var. <i>typica</i>	Seeds	0, 50, 100, and 150 Gy	100 Gy	Determination of LD <sub>50</sub> and morphological changes in plant	[17]
Wilman lovegrass	<i>Eragrostis superba</i> Peyr.	Seeds	100, 200, 300, 450, 600, 900, 1400, 2000, and 4000 Gray	2486 Gy	Determination of LD <sub>50</sub> .	[18]
Grasses: llorón, buffel, banderita, and navajita	Lloron ( <i>Eragrostis curvula</i> ), buffel ( <i>Pennisetum ciliare</i> ), banderita ( <i>Bouteloua curtipendula</i> ), and navajita ( <i>Bouteloua gracilis</i> )	Seeds	100, 200, 300, 450, 600, and 900 Gray	Pasto lloron 628 Gy, buffel 712 Gy, banderita 698 Gy, and navajita 411 Gy	Determination and comparison of LD <sub>50</sub> in pastures.	[19]
Agave	<i>Agave tequilana</i> Weber var. <i>Azul</i>	Callus cultures and seedlings	10, 20, 30, 40, and 50 Gy	seedlings 20–25 Gy; Callus 16 Gy	Determination of LD <sub>50</sub> and comparison between plant material.	[20]
Potato	<i>Solanum tuberosum</i> L. var. <i>Désirée</i>	Callus cultures	5, 10, 15, 20, and 30 Gy	10 Gy	Determination of mean lethal dose.	[21]

Table 2. Cont.

Common Name	Scientific Name	Irradiated Tissue Material	Treatment	LD <sub>50</sub>	Observations	Reference
Golden berry/Uchuva	<i>Physalis peruviana</i> L.	Axillary buds	50, 100, 200, and 300 Gy		Higher percentage of cells with chromosomal alterations.	[24]
Chrysanthemum	<i>Chrysanthemum morifolium</i> (Ramat.) "Donglinruixue"	Seeds	0, 15, 20, 25, 30, and 35 Gy *	35 Gy	The seeds will form genomic and chromosomal abnormalities during anaphase.	[26]
Sugar cane	<i>Saccharum</i> spp. Hibrido var. "SP 70-1284"	Callus cultures	10, 20, 30, 40, 50, 60, 70, and 80 Gy	30 Gy	Determination of LD <sub>50</sub> .	[27]
Gerbera	<i>Gerbera jamesonii</i> H. Bolus	In vitro explant growth, callus cultures and seedlings	10, 20, 30, 40, 50, and 60 Gy	20 gy	Callus fresh weight decrease response.	[30]
Beach purslane	<i>Sesuvium portulacastrum</i> L.	Shoots	5 to 40 Gy	20 Gy	Increased concentration of ecysteroid 20-hydroxyecdysone.	[31]
Orchid	<i>Dendrobium sonia</i>	Shoots	15–45 Gy	30 GY	GR decreased shoot length, fresh weight, and leaf area, but its combination with yellow light increased shoot survival and length, fresh weight, and chlorophyll content	[32]
Loquat	<i>Eriobotrya japonica</i> L.	Callus cultures and seedlings	(0, 10, 30, and 50 Gy)	10 Gy	Response in growth traits: callus diameter, callus height, number of shoots, number of leaves, and height of seedlings.	[33]
Banana	<i>Musa paradisiaca</i> L.	In vitro sprout seedlings	10 Gy, 20 Gy, and 30 Gy	10 and 20 Gy	Seedling morphological properties. Bases of mass propagation.	[34]
Citrus	<i>Citrus</i> spp. (several varieties: 'Alemow' and sour orange as citrus rootstock, lemon cv. 'Fino 49' and 'Verna 51', tangerine cv. 'Nova', and lime cv. 'Bearss')	Seeds, buds, and nodal segments	Seeds 0, 50, 100, 150, 200, and 250 Gy Buds 0, 25, 50, 75, and 100 Gy Nodal segments 0, 10, 20, 30, 40, and 50 Gy	Seeds (LD <sub>50</sub> of 127 Gy in <i>Alemow</i> , and 156 Gy in <i>sour orange</i> ). Buds (LD <sub>50</sub> around 50 Gy for all cultivars) and nodal segments (LD <sub>50</sub> around 25 Gy for both lemon cultivars).	Difficult-breeding species.	[35]
Wheat	<i>Triticum aestivum</i> L.	Seeds	100, 200, 300 and 400 Gy	100 Gy	85% increase in proline concentration and higher chlorophyll a concentration in seedlings.	[36]
Chickpea	<i>Cicer arietinum</i> L.	Seeds	50 a 750 Gy (frequency of 50 Gy) with a dose rate of 10.606 Gy min <sup>-1</sup>	150 Gy	Lines resistant to <i>Ascochyta blight</i> .	[44]
Rice	<i>Oryza sativa</i> L. var. Mentik Susu	M3 Seeds		200 gGy	Mutants with short plant height, high productivity, higher seed yield, and short harvest age.	[45]
Asiatic spark	<i>Centella asiatica</i> (L.) Urb.	Axillary buds	0, 10, 20, 30, 40, 50, 60, 70, 80, 90, 100, and 120 Gy	20 and 30 Gy	Higher concentrations of total flavonoids.	[49]
Esparceta, Sainfoin	<i>Onobrychis vicifolia</i> Scop. Syn. <i>Onobrychis sativa</i> L.	Seeds	30, 60, 90, and 120 Gy	90 Gy	Remarkable increase in the phenolic content of the leaf extract and increase of alkaloid Berberine.	[50]
Barijeh	<i>Ferula gummosa</i> Boiss.	Callus cultures	0 to 25 Gy	Of 20 and 25 Gy	Increased phenolic content.	[51]
Jengger Ayam	<i>Celosia cristata</i> L.	Seedlings	0, 25, 50, and 75 Gy	25 Gy	The CIU3 2.3.1 mutant presents triterpenic compounds that were not found in the controls.	[52]
Curled-leaved St. John's-wort	<i>Hypericum triquetrifolium</i> Turra	Callus cultures	10, 20, 40, and 50 Gy	10 Gy	Higher content of phytochemicals than in the control samples.	[54]
Fenugreek	<i>Trigonella foenum-graecum</i> L.	Seeds	0, 100, 200, 300, and 400 Gy	100 Gy	7% and 9% increases in trigonelline and nicotinic acid.	[55]

Table 2. Cont.

Common Name	Scientific Name	Irradiated Tissue Material	Treatment	LD <sub>50</sub>	Observations	Reference
Common madder or Indianmadder	<i>Rubia cordifolia</i> L.	Callus cultures	2, 4, 6, 8, 10, 12, 14, and 16 Gy	8 Gy	Radiation dose for kinetic study of cell growth and anthraquinone content. They accumulated a maximum level of alizarin and glitter that were 6 and 11 times higher than the non-irradiated callus cultures.	[56]
Barley	<i>Hordeum vulgare</i> L.	Seedlings	50–300 Gy	50 Gy	High concentration of proline and antioxidant enzyme activity. Heavy metal stress resistance.	[61]

\* Gy-Gray unit of measure ( $J\ Kg^{-1}$ ): absorption of one joule of radiation energy per kilogram of matter.

Within this context, a general genetic improvement route with GR and cobalt 60 is proposed, based on the effect they have on different crops (Figure 2). A summary of the methodology with GR in combination with genetic improvement biotechnological techniques is shown. The proposal includes five stages. The first includes aspects that give value to the underutilized species, such as traditional knowledge, morphological characteristics, nutritional contribution, and socioeconomic impact (Figure 2: Knowledge of the species). The use of GR during the second stage (Figure 2: Objectives) depends on the purpose of the research, including: genetic improvement, increased secondary metabolites, phenotypic improvements, tolerance to water stress, salinity, resistance to pests, and increased postharvest life. Once the objectives and scope have been established, we propose using biotechnological techniques, such as in vitro culture and cobalt 60 radiation. In the third stage, the plants should be placed in a greenhouse (Figure 2), to control its environment and protect it from any pollutant, pathogen, or pest. After the mother plant is obtained, the buds or shoots are established in vitro for their multiplication and induction of morphogenesis. Since undifferentiated cells can be worked with, allowing the generation of mutants from the first irradiated generation, indirect morphogenesis guarantees that radiation will have a more significant impact. The fourth stage consists of generating a radiosensitivity curve, to obtain the median lethal dose (LD<sub>50</sub>) or the median growth reduction (GR<sub>50</sub>), and to guarantee the generation of point mutations. Finally, the fifth stage includes plants obtained through regeneration and the evaluation of the morphometric, phytochemical, and physiological differences with the aim of identifying beneficial characteristics.

In this way, the phenomenon of mutagenesis and how a different variety is obtained can be explained. It is essential to highlight that this route is proposed for underutilized plant resources that do not compete in agricultural markets. However, experience indicates some intangible values are essential for society and that conservation actions should be favored [80].

Finally, following the callus irradiation line can reduce the time required to obtain an improved variety. Figure 3 describes the traditional improvement of the variety of *Secchium edule* var. countryside to obtain better quality fruits and longer shelf life. Using the Stratified Mass Selection method, it was possible to obtain these characteristics for the export market in five years [81]. Meanwhile, genetic improvement (biotechnological techniques) and GR were used to obtain the same results in two years (personal communication, unpublished data).

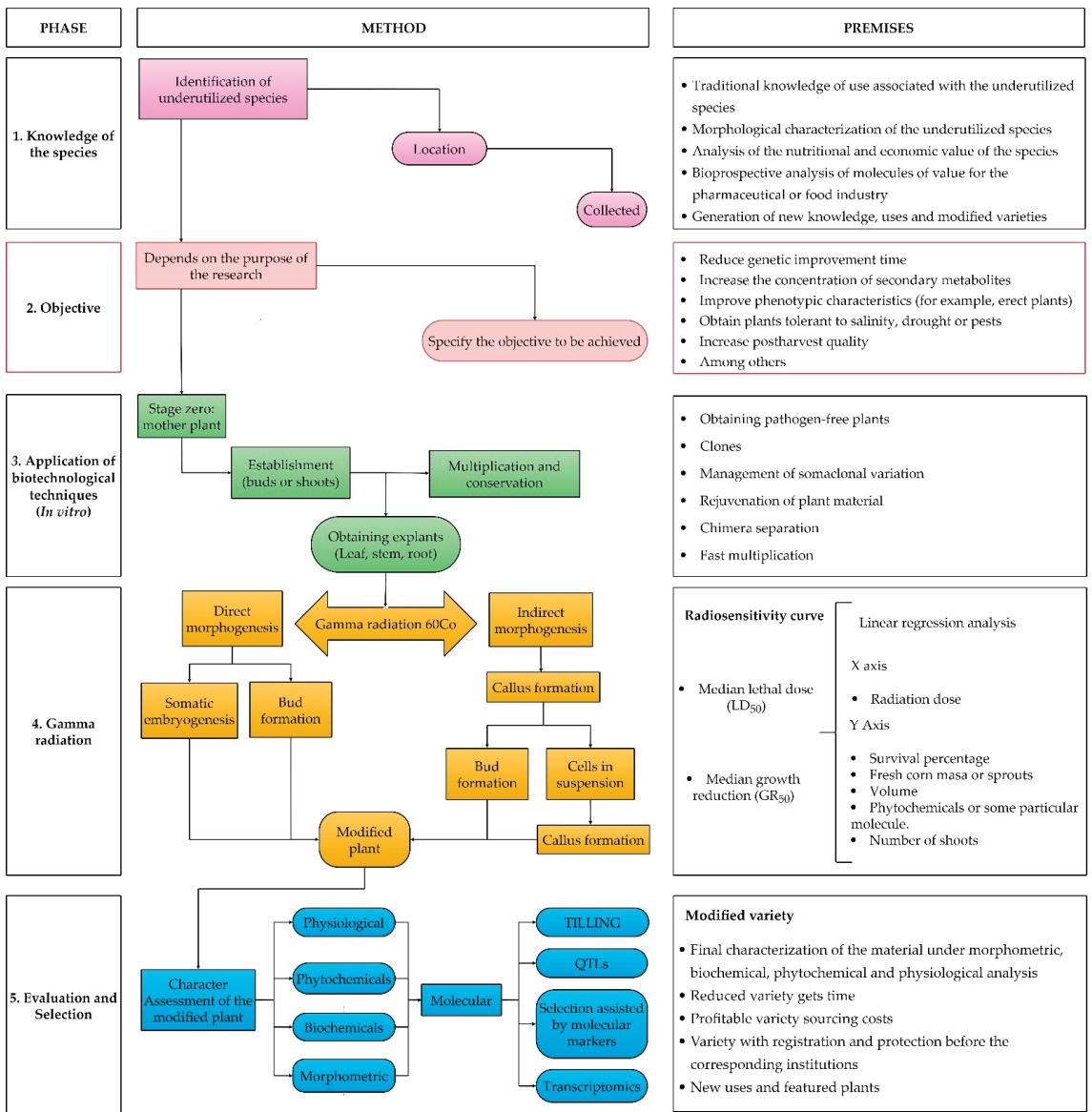


**Figure 2.** Proposal for the induction of *in vitro* mutagenesis with cobalt-60 for the genetic improvement of underutilized varieties. 1.—knowledge of the species, 2.—objectives, 3.—application of biotechnological techniques, 4.—Gamma radiation, and 5.—evaluation and selection.

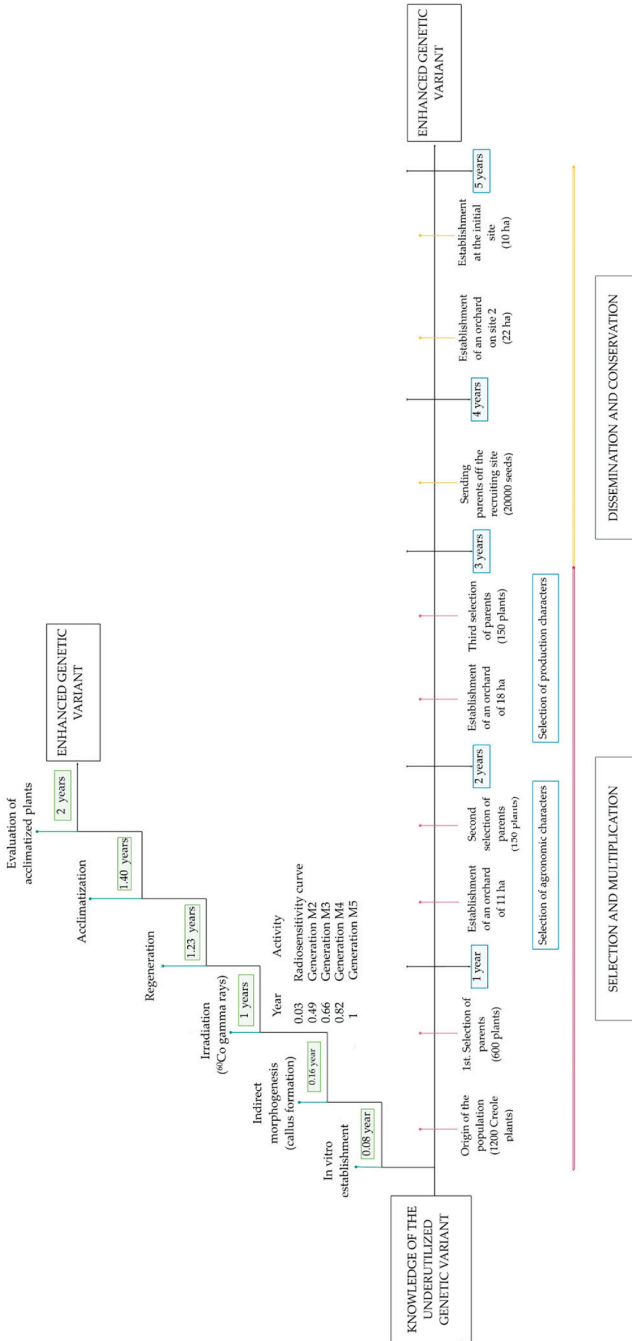


**Figure 3.** Comparative representation of the time reduction between traditional participatory breeding [81] and GR combined with in vitro techniques for the fruit of *S. adule*.

## 8. Conclusions

As a tool for plant breeding, GR has opened several options for food and agriculture. Some reports indicate that the effects that GR generates in specialized organelles and plant cells are aimed at practical applications, promoting new values in cultivars, which also involve a source of nutrients, active pharmaceutical principles, innovative standards for agriculture, or adaptive changes to the environment. A significant number of species which have undergone GR-induced mutations are included among the underutilized varieties—in which genetically improved cultivars have been discovered. The diversity of GR effects results essentially from individual responses and the phenotypic plasticity of each organism. It is important to point out that, although this irradiation technology is based on chance, good results can be obtained if it is directed towards a target and is linked to biotechnological techniques.

**Author Contributions:** Conceptualization, J.C.-I. and M.d.I.L.R.-F.; methodology, J.C.-I. and M.d.L.A.-G.; validation, L.d.M.R.-P., M.S.H. and I.C.-J.; investigation, M.d.I.L.R.-F., J.C.-I. and C.R.C.-M.; resources, L.d.M.R.-P.; writing—original draft preparation, J.C.-I., I.C.-J. and M.d.L.A.-G.; writing—review and editing, J.C.-I. and L.d.M.R.-P. All authors have read and agreed to the published version of the manuscript.

**Funding:** This research received no external funding.

**Institutional Review Board Statement:** Not applicable.

**Informed Consent Statement:** Not applicable.

**Data Availability Statement:** Not applicable.

**Conflicts of Interest:** The authors declare no conflict of interest.

## References

- Spencer, L.M.M.; Forster, B.P.; Jankuloski, L. *Manual on Mutation Breeding*, 3rd ed.; Food and Agriculture Organization of the United Nations (FAO): Rome, Italy, 2018.
- Ludovici, G.M.; Oliveira de Souza, S.; Chierici, A.; Cascone, M.G.; d’Errico, F.; Malizia, A. Adaptation to Ionizing Radiation of Higher Plants: From Environmental Radioactivity to Chernobyl Disaster. *J. Environ. Radioact.* **2020**, *222*, 106375. [[CrossRef](#)] [[PubMed](#)]
- Obodovskiy, I. Chapter 2-Nuclei and Nuclear Radiations. *Radiation* **2019**, 41–62. [[CrossRef](#)]
- Jan, S.; Parween, T.; Siddiqi, T.O.; Mahmooduzzafar. Effect of Gamma Radiation on Morphological, Biochemical, and Physiological Aspects of Plants and Plant Products. *Environ. Rev.* **2012**, *20*, 17–39. [[CrossRef](#)]
- Caplin, N.; Willey, N. Ionizing Radiation, Higher Plants, and Radioprotection: From Acute High Doses to Chronic Low Doses. *Front. Plant Sci.* **2018**, *9*, 847. [[CrossRef](#)] [[PubMed](#)]
- De la Cruz, T.E.; Hasbach, G.P.; Andrade, J.M.G.; Sánchez, C.M.; Jiménez, J.G.; Bárcenas, T.F.; Arriaga, O.V. The genus *Chenopodium*: A potential food source. In *Biotechnology of Neglected and Underutilized Crops*; Springer: Dordrecht, The Netherlands, 2013; pp. 3–31.
- Bravo, M.; Arteaga, M.I.; Herrera, F.F. Bioinventario de especies subutilizadas comestibles y medicinales en el norte de Venezuela. *Boletín Latinoam. Caribe Plantas Med. Aromát.* **2017**, *16*, 347–360.
- Khan, S.A.; Rahman, L.; Verma, R.; Shanker, K. Physical and Chemical Mutagenesis in *Stevia Rebaudiana*: Variant Generation with Higher UGT Expression and Glycosidic Profile but with Low Photosynthetic Capabilities. *Acta Physiol. Plant* **2016**, *38*, 1–12. [[CrossRef](#)]
- Hernández, M.S.; Pedraza, S.M.E.; Antonio, L.P.; Gómez, S.J.M.; Morales, G.J.L. Mutagenesis in the Improvement of Ornamental Plants. *Rev. Chapingo Ser. Hortic.* **2019**, *25*, 151–167. [[CrossRef](#)]
- Wi, S.G.; Chung, B.Y.; Kim, J.H.; Baek, M.H.; Yang, D.H.; Lee, J.W.; Kim, J.S. Ultrastructural changes of cell organelles in *Arabidopsis* stems after gamma irradiation. *J. Plant Biol.* **2005**, *48*, 195–200. [[CrossRef](#)]
- Datta, S.K.; Silva, J.A. Role of Induced Mutagenesis for Development of New Flower Colour and Type in Ornamentals. In *Floriculture, Ornamental and Plant Biotechnology: Advances and Topical*, 1st ed.; Global Science Books: Carrollton, GA, USA, 2006; pp. 640–645. Available online: <http://www.globalsciencebooks.info/Journals/GSBjournals.html> (accessed on 10 January 2022).
- Álvarez, H.A.; Morales, N.R.C.; Avendaño, A.H.C.; Corrales, L.R.; Villarrea, G.F.; Santellano, E.E.; Gomez, S.Y. Mean Lethal Dose (LD50) and Growth Reduction (GR (50)) Due to Gamma Radiation in Wilman Lovegrass (*Eragrostis superba*). *Rev. Mex. Cienc. Pecu.* **2019**, *10*, 227–238.

13. Surakshitha, N.C.; Soorianathasundaram, K. Determination of Mutagenic Sensitivity of Hardwood Cuttings of Grapes 'Red Globe' and 'Muscat' (*Vitis vinifera* L.) to gamma rays. *Sci. Hortic.* **2017**, *226*, 152–156. [CrossRef]
14. Chakravarty, B.; Sen, S. Enhancement of Regeneration Potential and Variability by  $\gamma$ -Irradiation in Cultured Cells of *Scilla Indica*. *Biol. Plant.* **2001**, *44*, 189–193. [CrossRef]
15. FAO. *Laboratory Training Manual on the Use of Isotopes and Radiation in Entomology*; FAO: Rome, Italy, 1977; Volume 61, p. 271.
16. Al-Safadi, B.; Ayyoubi, Z.; Jawdat, D. The Effect of Gamma Irradiation on Potato Microtuber Production in vitro. *Plant Cell Tissue Organ Cult.* **2000**, *61*, 183–187. [CrossRef]
17. Ernest, F.P.; Noëlle, M.A.H.; Godswill, N.N.; Thiruvengadam, M.; Simon, O.A.; Bille, N.H.; Shariati, M.A. Radiosensitivity of Two Varieties of Watermelon (*Citrullus lanatus*) to Different Doses of Gamma Irradiation. *Braz. J. Bot.* **2020**, *43*, 897–905. [CrossRef]
18. Quintana, V.; Alvarado, L.; Alvarado, L.; Saravia, D.; Saravia, D.; Borjas, R.; Borjas, R.; Gómez, L.; Castro, C.V.; Julca, O.A.; et al. Gamma Radiosensitivity of Coffee (*Coffea arabica* L. Var. Typica). *Peruv. J. Agron.* **2019**, *3*, 74. [CrossRef]
19. Álvarez, H.A.; Corrales, L.R.; Morales, N.C.R.; Avendaño, A.C.H.; Villarreal, G.F. Dosis Óptima de Irradiación Gamma Con Co 60 Para Inducción de Mutagénesis En Pastos. *Nova Sci.* **2017**, *9*, 65–82. [CrossRef]
20. Ángeles, E.A.; Valencia, B.A.J.; Virgen, C.G.; Ramírez, S.C.; Paredes, G.L.; Hurtado-De la Peña, S. Determinación de la dosis letal (dl50) con CO60 en vitroplántulas de Agave Tequilana Var. Azul. *Rev. Fitotec. Mex.* **2013**, *36*, 381.
21. Veitia, N.; García, L.R.; Bermúdez, C.I.; Orellana, P.; Padrón, Y.; Torres, D. Efecto de Las Radiaciones Gamma Sobre Callos de Papa Var. 'Desirée'. *Biotechnol. Veg.* **2007**, *7*, 57–61.
22. Mba, C.; Afza, R.; Shu, Q.Y. Mutagenic radiations: X-rays, ionizing particles and ultraviolet. In *Plant Mutation Breeding and Biotechnology*; Shu, Q.Y., Forster, B.F., Nakagawa, H., Eds.; CAB International and FAO: Rome, Italy, 2012; pp. 83–106.
23. Esnault, M.A.; Legue, F.; Chenal, C. Ionizing Radiation: Advances in Plant Response. *Environ. Exp. Bot.* **2010**, *68*, 231–237. [CrossRef]
24. Caro, M.D.P.; Estupiñán, R.S.Y.; Rache, C.L.Y.; Pacheco, M.J.C. Effect of Gamma Rays on Vegetative Buds of *Physalis peruviana* L. *Acta Agronómica* **2012**, *61*, 305–314.
25. Zaka, R.; Chenal, C.; Misset, M.T. Study of External Low Irradiation Dose Effects on Induction of Chromosome Aberrations in Pisum Sativum Root Tip Meristem. *Mutat. Res. Genet. Toxicol. Environ. Mutagen.* **2002**, *517*, 87–99. [CrossRef]
26. Wang, L.; Wu, J.; Lan, F.; Gao, P. Morphological, Cytological and Molecular Variations Induced by Gamma Rays in Chrysanthemum Morifolium 'Donglinruixue'. *Folia Hortic.* **2020**, *32*, 87–96. [CrossRef]
27. Balero, A.V.; Pérez, P.A.O.; Rodríguez, N.V.; Rodríguez, D.T. Crecimiento, Regeneración y Radiosensibilidad de Callos de Caña de Azúcar (*Saccharum* spp. Híbrido Var. "SP 70-1284") Tratados Con Radiación Gamma Fuente 60Co. *Biotechnol. Veg.* **2004**, *4*, 165–169.
28. Suprasanna, P.; Vitthal, S.B.; Yadav, P.V. In vitro Mutagenesis and Selection in Plant Tissue Cultures and Their Prospects for Crop Improvement. *Bioresources. Biodivers. Bioavailab.* **2012**, *6*, 6–14.
29. Al-Safadi, B.; Elias, R. Improvement of Caper (*Capparis spinosa* L.) Propagation Using in vitro Culture and Gamma Irradiation. *Sci. Hortic.* **2011**, *127*, 290–297. [CrossRef]
30. Hasbullah, N.A.; Taha, R.M.; Saleh, A.; Mahmud, N. Irradiation Effect on in vitro Organogenesis, Callus Growth and Plantlet Development of Gerbera Jamesonii. *Hortic. Bras.* **2012**, *30*, 252–257. [CrossRef]
31. Kapare, V.; Satdive, R.; Fulzele, D.P.; Malpathak, N. Impact of Gamma Irradiation Induced Variation in Cell Growth and Phytoecdysteroid Production in Sesuvium portulacastrum. *J. Plant Growth Regul.* **2017**, *36*, 919–930. [CrossRef]
32. Billore, V.; Mirajkar, S.J.; Suprasanna, P.; Jain, M. Gamma Irradiation Induced Effects on in vitro Shoot Cultures and Influence of Monochromatic Light Regimes on Irradiated Shoot Cultures of Dendrobium Sonia Orchid. *Biotechnol. Rep.* **2019**, *22*, e00343. [CrossRef] [PubMed]
33. Surya, M.I.; Ismaini, L.; Lailaty, I.Q. 'In vitro' regeneration and Induction of Loquat (*Eriobotrya japonica* L.). *Aust. J. Crop Sci.* **2019**, *13*, 701. [CrossRef]
34. Due, M.S.; Susilowati, A.; Yunus, A. The Effect of Gamma Rays Irradiation on Diversity of Musa Paradisiaca Var. Sapientum as Revealed by ISSR Molecular Marker. *Biodiversitas* **2019**, *20*, 1416–1422. [CrossRef]
35. Pérez, J.M.; Tallón, C.I.; Pérez, T.O. Inducing Mutations in *Citrus* spp.: Sensitivity of Different Sources of Plant Material to Gamma Radiation. *Appl. Radiat. Isot.* **2020**, *157*, 109030. [CrossRef]
36. Borzouei, A.; Kafi, M.; Khazaei, H.; Naseriyan, B.; Majdabadi, A. Effects of Gamma Radiation on Germination and Physiological Aspects of Wheat (*Triticum aestivum* L.) seedlings. *Pak. J. Bot.* **2010**, *42*, 2281–2290.
37. Amri-Tiliouine, W.; Laouar, M.; Abdelguerfi, A.; Jankowicz-Cieslak, J.; Jankuloski, L.; Till, B.J. Genetic variability induced by gamma rays and preliminary results of low-cost TILLING on M2 generation of chickpea (*Cicer arietinum* L.). *Front. Plant Sci.* **2018**, *9*, 1568. [CrossRef] [PubMed]
38. Shuryak, I.; Tkavc, R.; Matrosova, V.Y.; Volpe, R.P.; Grichenko, O.; Klimenkova, P.; Conze, I.H.; Balygina, I.A.; Gaidamakova, E.K.; Daly, M.J. Chronic gamma radiation resistance in fungi correlates with resistance to chromium and elevated temperatures, but not with resistance to acute irradiation. *Sci. Rep.* **2019**, *9*, 11361. [CrossRef]
39. FAO/IAEA. MVD-Search. (s. f.). Available online: <https://mvd.iaea.org/#/Search> (accessed on 21 January 2021).
40. Yasmeen, S.; Khan, M.T.; Khan, I.A. Revisiting the Physical Mutagenesis for Sugarcane Improvement: A Stomatal Prospective. *Sci. Rep.* **2020**, *10*, 16003. [CrossRef] [PubMed]
41. Wang, P.; Zhang, Y.; Zhao, L.; Mo, B.; Luo, T. Effect of Gamma Rays on Sophora Davidii and Detection of DNA Polymorphism through ISSR Marker. *Biomed Res. Int.* **2017**, *2017*, 8576404.

42. Yaycili, O.; Alikamanoglu, S. Induction of Salt-Tolerant Potato (*Solanum tuberosum* L.) Mutants with Gamma Irradiation and Characterization of Genetic Variations via RAPD-PCR Analysis. *Turk. J. Biol.* **2012**, *36*, 405–412.
43. Abdelnour-Esquivel, A.; Perez, J.; Rojas, M.; Vargas, W.; Gatica-Arias, A. Use of Gamma Radiation to Induce Mutations in Rice (*Oryza sativa* L.) and the Selection of Lines with Tolerance to Salinity and Drought. *Vitr. Cell. Dev. Biol.-Plant* **2020**, *56*, 88–97. [[CrossRef](#)]
44. Mabrouk, Y.; Charaabi, K.; Mahiout, D.; Rickauer, M.; Belhadji, O. Evaluation of Chickpea (*Cicer arietinum* L.) Irradiation-Induced Mutants for Resistance to Ascochyta Blight in Controlled Environment. *Braz. J. Bot.* **2018**, *41*, 311–318. [[CrossRef](#)]
45. Rachmawati, D.; Hanifah, W.N.; Parjanto; Yunus, A. Selection of Short Stem Mentik Susu Rice M3 from Gamma Ray Irradiation. *IOP Conf. Ser. Earth Environ. Sci.* **2019**, *250*, 012020. [[CrossRef](#)]
46. Vardhan, P.V.; Shukla, L.I. Gamma Irradiation of Medicinally Important Plants and the Enhancement of Secondary Metabolite Production. *Int. J. Radiat. Biol.* **2017**, *93*, 967–979. [[CrossRef](#)]
47. Choi, H.I.; Han, S.M.; Jo, Y.D.; Hong, M.J.; Kim, S.H.; Kim, J.B. Effects of Acute and Chronic Gamma Irradiation on the Cell Biology and Physiology of Rice Plants. *Plants* **2021**, *10*, 439. [[CrossRef](#)]
48. El-Beltagi, H.S.; Ahmed, O.K.; El-Desouky, W. Effect of Low Doses  $\gamma$ -Irradiation on Oxidative Stress and Secondary Metabolites Production of Rosemary (*Rosmarinus officinalis* L.) Callus Culture. *Radiat. Phys. Chem.* **2011**, *80*, 968–976. [[CrossRef](#)]
49. Moghaddam, S.S.; Jaafar, H.; Ibrahim, R.; Rahmat, A.; Aziz, M.A.; Philip, E. Effects of Acute Gamma Irradiation on Physiological Traits and Flavonoid Accumulation of Centella asiatica. *Molecules* **2011**, *16*, 4994–5007. [[CrossRef](#)]
50. Mohajer, S.; Taha, R.M.; Lay, M.M.; Esmaeili, A.K.; Khalili, M. Stimulatory Effects of Gamma Irradiation on Phytochemical Properties, Mitotic Behaviour, and Nutritional Composition of Sainfoin (*Onobrychis viciifolia* Scop.). *Sci. World J.* **2014**, *2014*, 854093. [[CrossRef](#)]
51. Ashouri Sheikhi, A.; Hassanpour, H.; Jonoubi, P.; Ghorbani Nohooji, M.; Nadimifar, M.S. The Effect of Gamma Irradiation on In vitro Total Phenolic Content and Antioxidant Activity of Ferula gummosa Bioss. *J. Med. Plants* **2016**, *3*, 122–131.
52. Muhallilin, I.; Aisyah, S.I.; Sukma, D. The Diversity of Morphological Characteristics and Chemical Content of Celosia Cristata Plantlets Due to Gamma Ray Irradiation. *Biodiversitas* **2019**, *20*, 862–866. [[CrossRef](#)]
53. Magdy, A.M.; Fahmy, E.M.; Al-Ansary, A.E.R.M.F.; Awad, G. Improvement of 6-Gingerol Production in Ginger Rhizomes (*Zingiber officinale* Roscoe) Plants by Mutation Breeding Using Gamma Irradiation. *Appl. Radiat. Isot.* **2020**, *162*, 109193. [[CrossRef](#)]
54. Azeez, H.; Ibrahim, K.; Pop, R.; Pamfil, D.; Hârta, M.; Bobiş, O. Changes Induced by Gamma Ray Irradiation on Biomass Production and Secondary Metabolites Accumulation in Hypericum Triquetrifolium Turra Callus Cultures. *Ind. Crops Prod.* **2017**, *108*, 183–189. [[CrossRef](#)]
55. Parchin, R.A.; Ghomi, A.A.N.; Badi, H.N.; Eskandari, A.; Navabpour, S.; Mehrafarin, A. Growth Characteristics and Phytochemical Responses of Iranian Fenugreek (*Trigonella foenum-graecum* L.) Exposed to Gamma Irradiation. *Ind. Crops Prod.* **2019**, *139*, 111593. [[CrossRef](#)]
56. Mariados; Satdive, R.; Fulzele, D.P.; Ramamoorthy, S.; Doss, G.P.; Zayed, H.; Younes, S.; Rajasekaran. Enhanced Production of Anthraquinones by Gamma-Irradiated Cell Cultures of Rubia Cordifolia in a Bioreactor. *Ind. Crops Prod.* **2020**, *145*, 111987. [[CrossRef](#)]
57. Topuz, A.; Ozdemir, F. Influences of Gamma Irradiation and Storage on the Capsaicinoids of Sun-Dried and Dehydrated Paprika. *Food Chem.* **2004**, *86*, 509–515. [[CrossRef](#)]
58. Khalil, S.A.; Ahmad, N.; Zamir, R. Gamma Radiation Induced Variation in Growth Characteristics and Production of Bioactive Compounds during Callogenesis in *Stevia rebaudiana* (Bert.). *New Negat. Plant Sci.* **2015**, *1–2*, 1–5. [[CrossRef](#)]
59. Kim, D.S.; Song, M.; Kim, S.H.; Jang, D.S.; Kim, J.B.; Ha, B.K.; Kim, S.H.; Lee, K.J.; Kang, S.Y.; Jeong, I.Y. The Improvement of Ginsenoside Accumulation in Panax ginseng as a Result of  $\gamma$ -Irradiation. *J. Ginseng Res.* **2013**, *37*, 332–340. [[CrossRef](#)]
60. Fulzele, D.P.; Satdive, R.; Kamble, S.; Singh, S.; Singh, S. Improvement of Anticancer Drug Camptothecin Production by Gamma Irradiation on Callus Cultures of Nothapodytes Foetida. *Int. J. Pharm. Res. Allied Sci.* **2015**, *4*, 19–27.
61. Wang, X.; Ma, R.; Cui, D.; Cao, Q.; Shan, Z.; Jiao, Z. Physio-Biochemical and Molecular Mechanism Underlying the Enhanced Heavy Metal Tolerance in Highland Barley Seedlings Pre-Treated with Low-Dose Gamma Irradiation. *Sci. Rep.* **2017**, *7*, 14233. [[CrossRef](#)]
62. Li, F.; Shimizu, A.; Nishio, T.; Tsutsumi, N.; Kato, H. Comparison and Characterization of Mutations Induced by Gamma-Ray and Carbon-Ion Irradiation in Rice (*Oryza sativa* L.) Using Whole-Genome Resequencing. *G3 Genes Genomes Genet.* **2019**, *9*, 3743–3751. [[CrossRef](#)]
63. Ishak, I. Identification of the Second Mutation of BADH2 Gene Derived from Rice Mutant Lines Induced by Gamma Rays. *At. Indones.* **2016**, *42*, 39. [[CrossRef](#)]
64. Tan, C.; Zhang, X.Q.; Wang, Y.; Wu, D.; Bellgard, M.I.; Xu, Y.; Shu, X.; Zhou, G.; Li, C. Characterization of Genome-Wide Variations Induced by Gamma-Ray Radiation in Barley Using RNA-Seq. *BMC Genom.* **2019**, *20*, 783. [[CrossRef](#)]
65. González, T.M.; Prat, M. Desarrollo de Una Plataforma de Tilling En Melón (*Cucumis melo* L.). Doctoral Thesis, Universitat Autònoma de Barcelona, Bellaterra, Spain, 2014.
66. Cho, H.Y.; Park, S.J.; Kim, D.S.; Jang, C.S. A TILLING Rice Population Induced by Gamma-Ray Irradiation and Its Genetic Diversity. *Korean J. Breed. Sci.* **2010**, *42*, 365–373.

67. Hwang, S.G.; Kim, J.H.; Jang, C.S. A Major QTL and a Candidate Gene for Heading Date in an Early Maturing Rice Mutant Induced by Gamma Ray Irradiation. *Genes Genom.* **2016**, *38*, 747–756. [[CrossRef](#)]
68. Kang, R.; Seo, E.; Park, A.; Kim, W.J.; Kang, B.H.; Lee, J.H.; Kim, S.H.; Kang, S.Y.; Ha, B.K. A Comparison of the Transcriptomes of Cowpeas in Response to Two Different Ionizing Radiations. *Plants* **2021**, *10*, 567. [[CrossRef](#)]
69. Kim, D.G.; Lyu, J.I.; Lim, Y.J.; Kim, J.M.; Hung, N.N.; Eom, S.H.; Kim, S.H.; Kim, J.B.; Bae, C.H.; Kwon, S.J. Differential Gene Expression Associated with Altered Isoflavone and Fatty Acid Contents in Soybean Mutant Diversity Pool. *Plants* **2021**, *10*, 1037. [[CrossRef](#)]
70. Domínguez García, I.A. *El Marco Jurídico Para el Aprovechamiento, Conservación y Promoción de los Recursos Fitogenéticos Para la Alimentación y la Agricultura*; Chapingo: Texcoco, Mexico, 2014.
71. FAO. *Primer Informe Sobre El Estado de Los Recursos Fitogenéticos en el Mundo*; FAO: Roma, Italy, 1996.
72. Arora, R.K. *Diversity in Underutilized Plant Species: An Asia-Pacific Perspective*; Bioversity International: New Delhi, India, 2014.
73. Caetano, C.M.; Peña Cuellar, R.D.; Maigual Juajibioy, J.L.; Vásquez Ávila, L.N.; Caetano Nunes, D.G.; Caetano Nunes de Pazdiora, B.R. Mejoramiento Participativo: Herramienta Para La Conservación de Cultivos Subutilizados y Olvidados. *Acta Agron.* **2015**, *64* (Suppl. S3), 307–327. [[CrossRef](#)]
74. Padulosi, S.; Hodgkin, T.; Williams, J.; Haq, N.; Engles, J.M.M.; Rao, V.R.; Jackson, M.T. 30 underutilized crops: Trends, challenges and opportunities in the 21st century. *Manag. Plant Genet. Divers.* **2002**, *323*. Available online: <https://eprints.soton.ac.uk/53786/> (accessed on 10 January 2022).
75. González, S.R.; Cadena, I.J.; Morales, F.F.J.; Ruiz, V.V.M.; Pimentel, L.J.; Peña, L.A. Model for the conservation and sustainable use of plant genetic resources in México. *Wulfenia J.* **2015**, *22*, 333–353.
76. Linares, E.; Bye, R. Las especies subutilizadas de la milpa. *Rev. Digit. Univ.* **2015**, *16*, 22.
77. Luna, C.L.M.; González, E.A.R. La chincuya (*Annona purpurea* Moc. & Sessé ex Dunal): Una planta mesoamericana. In *Anonáceas*; Universidad Autónoma Chapingo: Texcoco, Mexico, 2015; p. 229.
78. De la Cruz Torres, E. Aplicación de la Energía Nuclear en el Mejoramiento de Pseudocereales Nativos de México. 2010. Available online: <https://xdoc.mx/documents/aplicacion-de-la-energia-nuclear-en-el-mejoramiento-de-5e9229009c7b4> (accessed on 10 January 2022).
79. FAO. *Segundo Plan de Acción Mundial Para los Recursos Fitogenéticos Para la Alimentación y la Agricultura*; FAO: Roma, Italy, 2011; 108p.
80. Iñiguez, L.M.I.; Cadena, I.J.; Soto, H.R.M.; Morales, F.F.J.; Cortes, C.M.; Watanabe, K.N.; Cadena, Z.J.D. Bioprospecting of *Sechium* spp. varieties for the selection of characters with pharmacological activity. *Sci. Rep.* **2021**, *11*, 6185. [[CrossRef](#)]
81. Avendaño, A.C.H.; Cadena, I.J.; Arévalo, G.M.L.C.; Cisneros, S.V.M.; Morales, F.F.J.; Ruiz, P.L.M. Mejoramiento genético participativo en chayote. *Agroproductividad* **2014**, *7*, 6.



## Article

# Biological Activities of Some Isoquinoline Alkaloids from *Fumaria schleicheri* Soy. Will.

Ramona Păltinean <sup>1,†</sup>, Irina Ielciu <sup>1,\*</sup>, Daniela Hanganu <sup>2</sup>, Mihaela Niculae <sup>3</sup>, Eموke Pall <sup>3</sup>, Luc Angenot <sup>4</sup>, Monique Tits <sup>4</sup>, Andrei Mocan <sup>1</sup>, Mihai Babotă <sup>1,†</sup>, Oleg Frumuzachi <sup>1</sup>, Mircea Tămaş <sup>1</sup>, Gianina Crişan <sup>1</sup> and Michel Frederich <sup>4</sup>

<sup>1</sup> Department of Pharmaceutical Botany, “Iuliu Hațieganu” University of Medicine and Pharmacy, 400337 Cluj-Napoca, Romania; rpaltinean@umfcluj.ro (R.P.); mocan.andrei@umfcluj.ro (A.M.); mihai.babota@umfcluj.ro (M.B.); oleg.frumuzachi@gmail.com (O.F.); mtbotanica@yahoo.com (M.T.); gcrisan@umfcluj.ro (G.C.)

<sup>2</sup> Department of Pharmacognosy, “Iuliu Hațieganu” University of Medicine and Pharmacy, 400010 Cluj-Napoca, Romania; dhanganu@umfcluj.ro

<sup>3</sup> Department of Clinical Sciences, University of Agricultural Sciences and Veterinary Medicine, 400372 Cluj-Napoca, Romania; mihaela.niculae@usamvcluj.ro (M.N.); emoke.pall@usamvcluj.ro (E.P.)

<sup>4</sup> Center of Interdisciplinary Research on Medicines, Laboratory of Pharmacognosy, University of Liège, 4000 Liège, Belgium; l.angenot@uliege.be (L.A.); m.tits@uliege.be (M.T.); m.frederich@uliege.be (M.F.)

\* Correspondence: irina.ielciu@umfcluj.ro

† These authors contributed equally to this work.

**Citation:** Păltinean, R.; Ielciu, I.; Hanganu, D.; Niculae, M.; Pall, E.; Angenot, L.; Tits, M.; Mocan, A.; Babotă, M.; Frumuzachi, O.; et al. Biological Activities of Some Isoquinoline Alkaloids from *Fumaria schleicheri* Soy. Will. *Plants* **2022**, *11*, 1202. <https://doi.org/10.3390/plants11091202>

Academic Editors: Milan S. Stankovic, Paula Baptista and Petronia Carillo

Received: 11 April 2022

Accepted: 27 April 2022

Published: 29 April 2022

**Publisher’s Note:** MDPI stays neutral with regard to jurisdictional claims in published maps and institutional affiliations.



**Copyright:** © 2022 by the authors. Licensee MDPI, Basel, Switzerland. This article is an open access article distributed under the terms and conditions of the Creative Commons Attribution (CC BY) license (<https://creativecommons.org/licenses/by/4.0/>).

**Abstract:** *Fumaria schleicheri* Soy. Will. is a species belonging to the Papaveraceae family, being widespread in East-Central and Southern Europe. As with numerous other species of the genus, it is used in traditional medicine for the treatment of hepatobiliary and digestive disorders. The aim of the present study consisted of the evaluation of its alkaloid content and the assessment of its in vitro antioxidant, anti-cholinesterase and cytotoxic potential. Total alkaloid content in the composition of the species was quantified by a spectrophotometrical method and they were individually identified and quantified by HPLC-DAD. The antioxidant capacity was investigated by the DPPH and FRAP methods, while the anti-cholinesterase activity was assessed by an adapted Ellman’s method. The in vitro cytotoxic activity was evaluated on BJ human fibroblasts and DLD-1 human colon adenocarcinoma cell lines. Results showed the presence of bicuculline, protopine, chelidonine, stylopine and sanguinarine, among which bicuculline, protopine, stylopine and sanguinarine were quantified, while the antioxidant and anti-cholinesterase assays showed valuable potentials. No cytotoxic effect was observed on BJ cell lines and selective cytotoxicity was expressed towards tumoral cells. In this context, *F. schleicheri* appears as an important medicinal species with significant potential of substitution with the officinal species.

**Keywords:** *Fumaria schleicheri* Soy. Will.; isoquinoline alkaloids; HPLC-DAD; in vitro anti-cholinesterase; cytotoxic; antioxidant

## 1. Introduction

In Europe, almost 60 taxons of the genus *Fumaria* (Papaveraceae) can be found in the spontaneous flora of different countries [1], especially in the Mediterranean basin and in the Eastern and Western parts of the continent [1,2]. Due to the nomenclatural and taxonomic confusion of the categories at the same level, this genus has been successively introduced in the Papaveraceae family and in the Fumariaceae family, being actually included in the Papaveraceae family, Fumarieae tribe [2,3]. Species of the *Fumaria* genus present similar morphological characters; thus, their identification is difficult and laborious [3,4].

The *Fumaria schleicheri* Soy. Will. species is widespread in East-Central and Southern Europe [1] and can be identified by small sepals, deep pink corolla and bracts about as long

as the erect fruiting pedicels [4]. It is one of seven species included in the *Fumaria* genus that can be found in the Romanian flora and is widespread in the Western and Central regions of Romania [3,5,6].

*Fumaria* species have been used since ancient times in folk medicine, especially to treat hepatobiliary and digestive disorders, but also for the treatment of skin and respiratory disorders, rheumatism, hypertension, different types of infections or constipation [7–9]. Studies performed on different species of the genus have proven the analgesic, antioxidant, hepatoprotective, antiproliferative, antiplasmodial, antibacterial, antifungal and anti-inflammatory activities of *Fumaria* species [3,8–11]. These biological activities are attributed to the composition in isoquinoline alkaloids, among which protopine derivatives (e.g., protopine, allocryptopine), protoberberine derivatives (e.g., stylopine), benzophenanthridine derivatives (e.g., sanguinarine, chelidonine, chelerythrine) and phthalide-isoquinoline derivatives (e.g., bicuculline, hydrastine) (Figure 1) are the predominant classes of compounds [8,9,11–14].

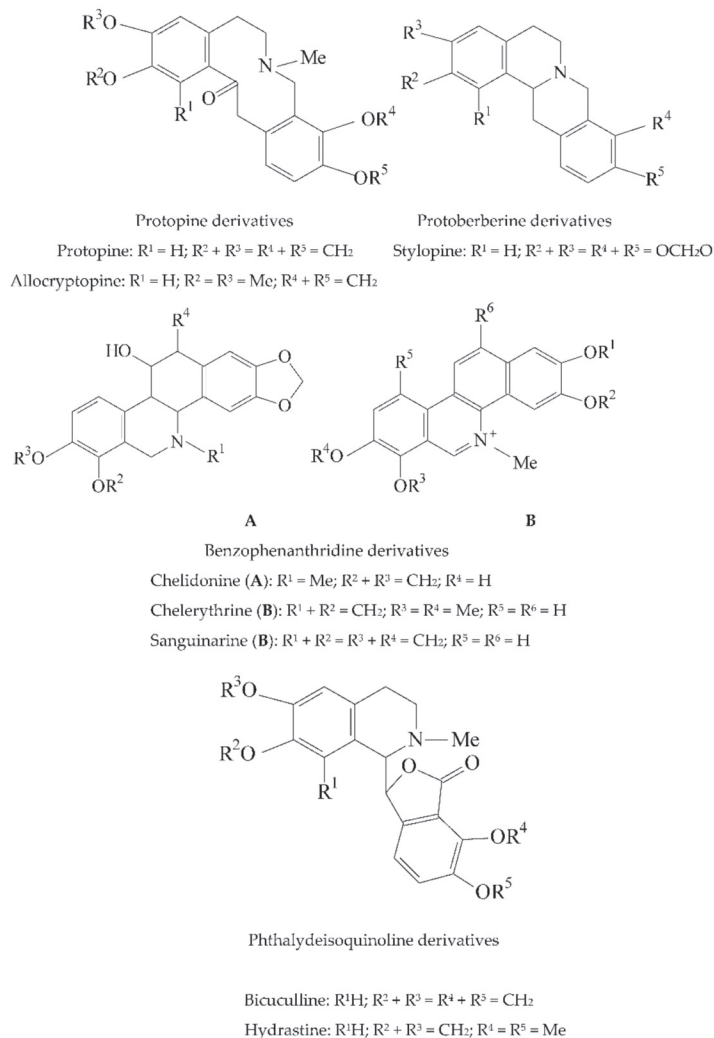


**Figure 1.** Structures of alkaloids that can be found in the composition of *F. schleicheri* species [11,13,14].

Among the species of the *Fumaria* genus, *F. schleicheri* Soy.-Will. is a species that is lesser studied. The few existing studies cite its anticonvulsant [15–18] and neuroprotective activities [19], which are assigned also to the composition in alkaloids, such as protopine [17,20], parfumidine, fumaricine, cryptopine, allocryptopine [11,20], stylophine [21] or fumschleicherine [11,20,22]. Other compounds that can be found in the composition of the species in significant amounts are polyphenols, which offer the species antioxidant and diuretic properties [3]. To the best of our knowledge, these studies are the only ones that describe this species from the point of view of its chemical composition and biological activities.

Cytotoxic activity is reported for species belonging to the *Fumaria* genus, especially for the officinal one [11,23] and it is studied towards various cancerous cell lines (e.g., melanoma, breast cancer, leukemia) [11,23–25]. The compounds that are responsible for this activity are the isoquinoline alkaloids [11,14], while the underlying mechanism is related to the antioxidant potential of these compounds [11,23].

The acetylcholinesterase inhibitory activity represents the basis of the studies that aim to develop a treatment for Alzheimer's disease. *Fumaria* species represent one of the numerous genera of plants that have been studied for this biological activity. *F. vaillantii* Loisel [11,26,27], *F. kralikii* Jord [28], *F. indica* Lam [29] and *F. officinalis* L. [14] proved to be the most efficient ones.

The antioxidant activity is one of the biological activities that is highly studied for the species belonging to the *Fumaria* genus [3,9], being assigned both to their polyphenolic composition [10,30], but also to their alkaloid composition [13,31,32]. It is one of the activities that not only forms the basis of cytotoxic activity [11,23,33], but also the basis of numerous other biological activities, such as hepatoprotective activity [34], antibacterial [13] or antidiabetic one [35].

The link between all these concepts represents the purpose of the present study. Therefore, taking all these into consideration, the study of the *F. schleicheri* species and its biological activities appears to be an important subject. In this context, the aim of the present study consisted of the identification and quantification of the isoquinoline alkaloids present in *F. schleicheri* and the evaluation of their biological activities, such as the anti-cholinesterase, antioxidant and cytotoxic ones. In order to evaluate the chemical composition of the species, specimens harvested from different environments were tested. In this way, both the chemical composition of the species and the effect of pedo-climatic conditions on the total alkaloid content could be evaluated. This represents a first argument that sustains the originality of this study, which also consists of the fact that it is one of the few studies existing in scientific literature that aims to bring arguments regarding the cytotoxic, anti-cholinesterase and antioxidant activity of the species and to further confirm these biological activities, which are cited for the alkaloids of the *Fumaria* genus. Moreover, the present study is one of the few studies performed on the species that proves it can be a valuable medicinal product, having important potential for the substitution with the officinal species.

## 2. Results

Three *F. schleicheri* samples (FS1–FS3) obtained from different Romanian environments were subjected to the phytochemical analysis and antioxidant and acetylcholinesterase inhibitory properties evaluation. The sample with the highest alkaloid content was selected and further investigated for its in vitro cytotoxic potential against both normal and tumoral cells.

### 2.1. Quantification of the Total Alkaloids Content

The quantification of the total alkaloid content revealed a significant concentration of total alkaloids for all the tested samples ( $p < 0.05$ ) (Table 1).

**Table 1.** The total alkaloid content of the tested *F. schleicheri* samples.

Sample	Total Alkaloid Content (g Chelidonine/100 g Vegetal Product %)
FS1	0.52 ± 0.23 <sup>b</sup>
FS2	0.60 ± 0.03 <sup>b</sup>
FS3	0.86 ± 0.11 <sup>a</sup>

Note: Values represent the mean ± standard deviations of three independent measurements. Superscript letters indicate statistically significant differences between the total alkaloid content of the tested samples ( $p < 0.05$ ).

It can be clearly observed that the results obtained for the determination of the total alkaloid content highlighted important amounts of alkaloids, with a significantly higher value for the FS3 sample ( $0.86 \pm 0.11$ ) ( $p < 0.05$ ). All samples were collected in the same maturation stages of the species (in May–June, at the complete flowering and fruiting setting stage of the species). It could be observed that the obtained results for all the tested samples depended on the pedo-climatic conditions of the harvested samples, varying accordingly. Results of this quantification of alkaloids represent an element of novelty of the present study, which reports the quantification of this total alkaloid content for the first time. In order to identify the individual alkaloids that are present in the chemical composition of the species, total alkaloids determination was completed by the HPLC-DAD quantification of individual alkaloids from each sample.

## 2.2. Identification and Quantification of Alkaloids from *F. schleicheri* Extracts by HPLC-DAD

In the composition of the tested extracts, the presence of alkaloids such as bicuculline, protopine, stylophine, chelidonine and sanguinarine could be observed (Figures S1–S3). Identification of these compounds could be performed by comparison of the obtained results for the tested extract with the ones obtained in the same conditions for commercially available references.

Identification of individual compounds was achieved by HPLC-DAD and highlighted the presence of bicuculline, protopine, chelidonine, stylophine and sanguinarine. The obtained parameters for each compound (UV spectra) and the retention times ( $R_t$ ) were compared to the ones obtained for commercially available references and allowed us to confirm the presence of these compounds in the composition of the tested samples (Table 2).

**Table 2.** Alkaloids identified in the tested *F. schleicheri* extracts.

Compound	Retention Time $R_t$ (min)	UV $\lambda_{max}$ (nm)
Protopine	24.79 ± 0.14	210, 290
Bicuculline	22.40 ± 0.04	200, 230
Chelidonine	26.29 ± 0.08	200, 290
Stylophine	27.25 ± 0.10	200, 290
Sanguinarine	29.13 ± 0.03	280, 330

Note: Values represent the mean ± standard deviations of three independent measurements.

Results of the quantification of individual alkaloids showed important amounts especially in the case of protopine, stylophine, bicuculline, chelidonine and sanguinarine (Table 3). In particular, FS1 sample contained the highest amount of stylophine, bicuculline and sanguinarine. Furthermore, for all tested extracts, these amounts were proved to be in direct correlation with the amount of total alkaloids obtained in the spectrophotometrical assays.

**Table 3.** Quantification of alkaloids in the tested *F. schleicheri* samples.

Compound (mg/100 g Dry Weight)	FS1	FS2	FS3
Protopine	191.08 ± 0.56	217.49 ± 0.02	126.45 ± 0.11
Stylopine	24.59 ± 0.20 <sup>a</sup>	<LoQ	3.55 ± 0.02 <sup>b</sup>
Bicuculline	67.16 ± 0.55 <sup>a</sup>	3.77 ± 0.03 <sup>c</sup>	26.84 ± 0.20 <sup>b</sup>
Sanguinarine	5.61 ± 0.04 <sup>a</sup>	2.11 ± 0.03 <sup>b</sup>	1.67 ± 0.016 <sup>c</sup>
Chelidonium	<LoQ	<LoQ	<LoQ

Note: Values represent the mean ± standard deviations of three independent measurements. <LoQ—identified, but not quantified (below quantification limit). The superscript letters indicate statistically significant differences between the quantified alkaloids values ( $p < 0.05$ ).

### 2.3. Antioxidant Activity of the *F. schleicheri* Extract

The results obtained using the DPPH and the FRAP assays are presented in Table 4. Important antioxidant properties were observed for all the tested samples, with the most relevant potential exhibited by the FS1 sample for the FRAP ( $p < 0.05$ ) and DPPH (values statistically not significant) assays.

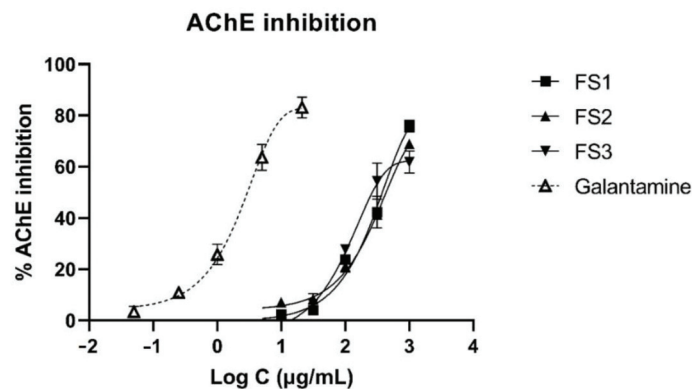
**Table 4.** Results for the antioxidant activity assays for the tested *F. schleicheri* samples.

Sample	DPPH (mg Trolox Equivalents/g Dry Extract)	FRAP (mg Trolox Equivalents/g Dry Extract)
FS1	38.93 ± 0.59	68.03 ± 0.46 <sup>a</sup>
FS2	32.50 ± 1.35	39.30 ± 0.13 <sup>c</sup>
FS3	29.07 ± 1.36	50.65 ± 0.65 <sup>b</sup>

Note: Values represent the mean ± standard deviations of three independent measurements. The superscript letters indicate statistically significant differences between antioxidant activity of the tested samples ( $p < 0.05$ ).

### 2.4. Anti-Cholinesterase Activity of the *F. schleicheri* Extract

Inhibitory potential of alkaloid fractions or individual alkaloids isolated from different *Fumaria* species on acetyl- and butyrylcholinesterase was indicated by several studies [14,26,36]. In this regard, dry extracts of *F. schleicheri* were tested in vitro for their ability to inhibit acetylcholinesterase using Ellman colorimetric assay adapted to a microplate reader method. Inhibition was expressed as IC<sub>50</sub> (µg/mL) using galantamine as positive control (IC<sub>50</sub> = 2.00 ± 0.47 µg/mL). All tested samples exerted a medium inhibitory activity, while FS3 proved to be the most active against acetylcholinesterase ( $p < 0.05$ ) (Table 5, Figure 2).

**Figure 2.** Achetylcholinesterase (AChE) inhibition by *F. schleicheri* extracts and galantamine as reference inhibitor.

**Table 5.** Results of the anti-cholinesterase activity assays for the tested *F. schleicheri* samples.

Sample	AChE Inhibition IC <sub>50</sub> (µg/mL)	Galantamine IC <sub>50</sub> (µg/mL)
FS1	456.72 ± 50.63 <sup>b</sup>	
FS2	381.83 ± 102.90	2.00 ± 0.47
FS3	349.24 ± 51.42 <sup>a</sup>	

Note: Values represent the mean ± standard deviations of three independent measurements. The superscript letters indicate statistically significant differences between the anti-cholinesterase activity of the tested samples ( $p < 0.05$ ).

### 2.5. In Vitro Cytotoxic Activity of the *F. schleicheri* Extract

For the evaluation of the in vitro cytotoxic activity, the FS3 sample was selected, as it was proved to have the highest alkaloids content. In order to evaluate its inhibitory activity, DLD-1 and BJ cells were incubated with five different concentrations of the extract. In DLD-1 cells the extracts caused inhibitory activity in a dose-dependent manner (Figure 3). A significant increase in the cytotoxic activity ( $p < 0.0001$ ) compared to the untreated control was revealed at a concentration of 30 µg/mL extract followed by concentrations of 20 and 25 µg/mL, respectively. The cytotoxic potential was also indicated by calculating the required concentration that inhibited 50% of the DLD-1 cell line (IC<sub>50</sub> in µg/mL). The concentration of extract required to reduce DLD-1 cell viability by 50% was 21.91 ± 0.38 µg/mL at 24 h. At a concentration of 15 µg/mL, the percentage of cell viability was 77.69 ± 1.26% and 97.53 ± 1.81% at the concentration of 10 µg/mL. At the same concentrations, the average viability of BJ cells was 99.68 ± 0.57% (Figure 4) with no statistically significant ( $p > 0.05$ ) differences between the viability values determined by these concentrations and the negative control. Thus, the tested extract of *F. schleicheri* was considered non-cytotoxic on BJ cells. Selective cytotoxicity was expressed only towards tumoral cells.

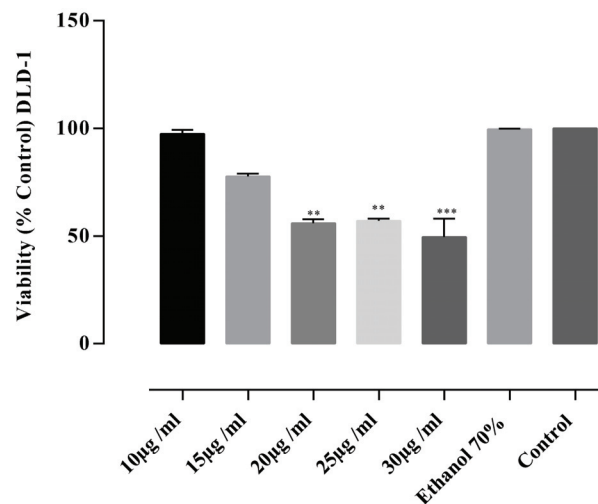


**Figure 3.** Cytotoxic activity assay results of *F. schleicheri* (FS3) extract on DLD cell line. The extract was tested at five different concentrations 10–30 µg/mL. Negative control—untreated cells. Internal control—cells treated with 70% ethanolic solution. Values represent the mean ± SD of three independent evaluations; \*\*  $p < 0.001$ ; \*\*\*  $p < 0.0001$ .

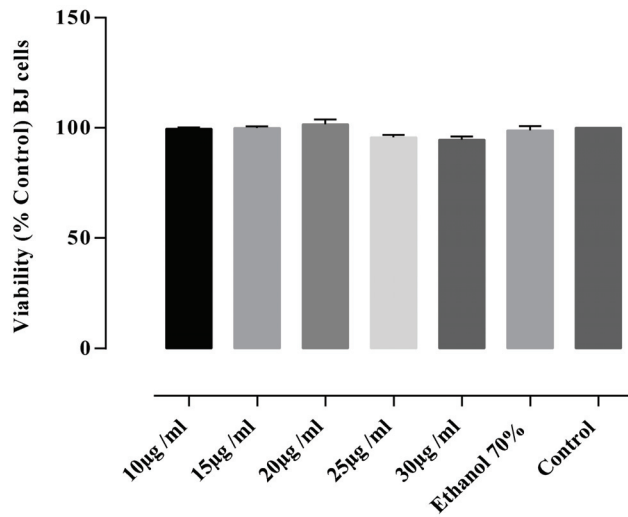


**Figure 4.** Cytotoxic activity assay results of *F. schleicheri* extract (FS3) on BJ cell line. Negative control—untreated cells. Internal control—cells treated with 70% ethanol solution. Values represent the mean  $\pm$  SD of three independent evaluations.

### 3. Discussion

*F. schleicheri* is a Papaveraceae species that has received lesser attention in scientific studies along time. However, it is one of the most widespread species in the *Fumaria* genus [3]. In this context, its study appears important, especially as the ethnopharmacological potential of *Fumaria* species is largely known [9], and the existing studies prove the possibility to use its vegetal medicinal products as substitutes for the officinal species [16–19].

The total alkaloid content was assessed spectrophotometrically hereby for the first time for the *F. schleicheri* species. Other similar studies cite the total quinolizidine contents, which were of 0.43% for *F. capreolata* and 0.52% for *F. bastardii* [37], which proved to be similar with the amount of isoquinoline alkaloids quantified here. Suau et al. assessed the total alkaloids from the aerial parts for *F. sepium* at 0.88% and at 0.83% for *F. agraria* [38]. However, these studies do not use spectrophotometrical methods, which represents therefore an element of novelty of the present study. The only existing study which cites similar results is, to the best of our knowledge, also performed by our team on the officinal species and showed similar amounts of total alkaloids [39]. The sample that showed superior results compared to the for *F. schleicheri* is the FS3 sample, which was also chosen for the cytotoxicity assays.

The chemical composition of the 70% aqueous ethanolic extract was further investigated using a HPLC-DAD method and compounds were identified by comparison of the obtained parameters with the results obtained for commercially available references that were tested in the same conditions. Among the compounds that were identified, only protopine [11,17,20] and stylophine [21] were previously identified in the composition of the species. For the other compounds, to the best of our knowledge, it is the first scientific evidence of their presence in the composition of the species growing in Romania. The presence of bicuculline, chelidonine and sanguinarine is therefore an element of novelty that this study presents (Table 2). They are valuable compounds, important for the biological activities of this species, that were previously reported in the composition of other *Fumaria* species [7,9,12,39], but not in the composition of *F. schleicheri*. Results obtained in the phytochemical analysis of the *F. schleicheri* extract not only represent elements of originality and are reported for the first time hereby but are also related to the biological activities of the species.

The antioxidant capacity of *F. schleicheri* is reported hereby for the first time, being assigned to its alkaloids content. Other existing studies on the same species assigned this

activity to the composition in polyphenolic compounds [3,10]. DPPH and FRAP assays were used to establish the total antioxidant capacity and showed important results for this species. For the officinal species, this activity was assigned to the alkaloid's composition [13]. The attribution of the antioxidant activity to alkaloids represents therefore another element of novelty of the present study and becomes even more important as this activity seems to represent the basis of numerous other pharmacological activities [13].

The results obtained for the acetylcholinesterase (AChE) inhibitory activity can be explained based on the different distribution of each individual alkaloid in the analyzed samples. In a previous study focused on the evaluation of anti-cholinesterase potential of several *Fumaria* species from Turkey, Sener et al. [36] noticed that this activity varied in a dependent manner by the content in three main alkaloids, the most important being protopine. The most recent studies showed also that the anticholinesterase potential of isoquinolinic alkaloid-rich fractions can be influenced both by the type and amount of each individual compound through a synergistic effect. For example, Tuzimski et al. [40] highlighted a strong in vitro synergistic effect for the pairs protopine-sanguinarine and protopine-chelerythrine which exerted inhibition rates over 97% in comparison with galantamine. Moreover, anti-cholinesterase potential of an alkaloid extract obtained from *F. schleicheri* was evaluated for the first time in the present work, this representing one of the main original elements of the present study.

A significative negative correlation was noticed between the values obtained for the total alkaloid content and the anti-cholinesterase activity (Pearson correlation coefficient  $-0.97$ ,  $p < 0.05$ ), indicating that this therapeutic activity depends on the alkaloid concentrations. Given the interpretation of the AChE Inhibition based on the  $IC_{50}$  ( $\mu\text{g}/\text{mL}$ ) values, the results suggest a most intense activity with an increasing alkaloid content.

Treatment of BJ cells with 10–30  $\mu\text{g}/\text{mL}$  concentration of the extract, did not express a cytotoxic effect (Figure 4). On the other side, the same concentrations of the tested extract, proved selective cytotoxicity towards the human colon adenocarcinoma DLD-1 cell line. This pharmacological activity was previously reported for the officinal species [23,24], being assigned to the isoquinoline alkaloids [14,23]. The in vitro cytotoxic potential of the *F. schleicheri* species adds novelty and originality to the present study, as it is pointed out hereby for the first time, alongside with the other biological activities.

All these biological activities were previously cited and evaluated for the *F. officinalis* species [9]. Taking into consideration that a significant cytotoxic, anti-cholinesterase and antioxidant properties are revealed in the present study for the *F. schleicheri* species and also the fact that the studied species has an important ethnopharmacological background, it appears that *F. schleicheri* may be taken into consideration for further studies that may highlight the possibility of replacing the vegetal medicinal product with vegetal medicinal products obtained from *F. schleicheri*.

## 4. Materials and Methods

### 4.1. Chemicals and Reagents

Stylopine and chelidonine were purchased from ChromaDex Inc. (Los Angeles, CA, USA), sanguinarine chloride hydrate and chelidonine from Sigma-Aldrich (Darmstadt, Germany), protopine from Extrasynthese (Genay, France) and bicuculline from Cayman Chemical Company (Ann Arbor, Michigan, USA). All references were of analytical standard. Trifluoroacetic acid for HPLC, HPLC grade acetonitrile and methanol were purchased from Sigma-Aldrich (Darmstadt, Germany). The ultra-pure water used for HPLC analysis was obtained from a Millipore system (Milli-Q RG) (Millipore, France). Acetylcholine for the antispastic assays was obtained from Sigma-Aldrich (Darmstadt, Germany). Ferric chloride, 6-hydroxy-2,5,7,8-tetramethylchromane-2-carboxylic acid (Trolox) (97%); diammonium 2,2'-azino-bis(3-ethylbenzothiazoline-6-sulfonate) (ABTS) (>98%), 2,2-diphenyl-1-(2,4,6-trinitrophenyl) hydrazine (DPPH), 2,4,6-tris (2-pyridyl)-striazine (TPTZ) for antioxidant assays, acetylthiocholine iodide (ATCI), acetylcholinesterase from *Electrophorus electricus* (elec-

tric eel) (AChE), 5,5'-dithiobis(2-nitrobenzoic acid) (DTNB) and galantamine hydrobromide for the AChE inhibition assay were purchased from Sigma-Aldrich (Darmstadt, Germany).

#### 4.2. Plant Material

Aerial parts of *Fumaria schleicheri* Soy. Will. were collected from its natural habitat at the flowering and fruit setting stages. The specimens were obtained from different Romanian environments (Table 6, Figures S4–S6) and identified by the Department of Botany, Faculty of Pharmacy, University of Medicine and Pharmacy “Iuliu Hațieganu” Cluj-Napoca, Romania and deposited at the herbarium of the department (Voucher no. 28.3.3.6-9) [12,39].

**Table 6.** The collected *F. schleicheri* samples and their harvesting place.

Sample	Harvesting Place
FS1	Deva. Hunedoara County
FS2	Târgu Mureș, Mureș county
FS3	Nădășel, Cluj county

The fresh aerial parts of plants material were mechanically cleaned and left to dry at 23 °C for 14 days. The dried herbal material was crushed with a Retsch grinder at 350 μm and preserved in the dark at 20 °C [41].

#### 4.3. Extraction Technique

An amount of 1 g air-dried aerial parts of *Fumaria schleicheri* Soy. Will was mixed with 15 mL of diluted ammonia and extracted with ethyl acetate (3 × 30 mL). The solvent was evaporated to dryness in a rotary evaporator at 40 °C under reduced pressure. The residue was taken up with 100 mL sulfuric acid 0.05 M. After homogenization, the aqueous acid solution was adjusted to pH 9–10 with concentrated ammonia and extracted with ethyl acetate (3 × 30 mL). The extracts were dried over anhydrous sodium sulphate and the solvent was evaporated to dryness in a rotary evaporator at 40 °C under reduced pressure. The residue was dissolved in methanol and transferred into a 10 mL volumetric flask. The solution was diluted to volume with the same solvent and then filtered through 0.45 μm membrane before use. Then, 10 μL of the solution was injected for HPLC-DAD [42–46].

#### 4.4. Preparation of Standard Solutions and Sample Preparation for HPLC-DAD

Reference standards were diluted in methanol to achieve a concentration of 1 mg/mL. All solutions were stored in a refrigerator at 4 °C prior to analysis. Then, 10 μL of each solution was injected for HPLC-DAD [12,39,42].

#### 4.5. Quantification of Total Alkaloid Content

The quantification of total alkaloid content was performed using a method described in the *Chelidonium herba* monograph in the European Pharmacopoeia, 10th edition. The colorimetric quantification assay was carried out using chromotropic acid, which reacts with the formaldehyde released by the methylenedioxy groups of the isoquinoline alkaloids in an acidic medium to form the stable, colored, dibenzoxanthylum cation, which can be revealed by spectrophotometry at 570 nm. The total alkaloids content was calculated using the following formula:  $A \times 2.23/m$ , considering A the absorbance at 570 nm and m the mass of vegetal powder. Results were expressed as g chelidonine/100 g vegetal product (%). All experiments were performed in triplicate (n = 3) [39,47].

#### 4.6. HPLC-DAD Conditions

Chromatographic analysis was performed on an Agilent 1100 HPLC system equipped with a binary pump, an autosampler, a column compartment and a UV-VIS diode array detector. Samples were separated on an Inertsil Phenyl RP column (5 μm, 4.6 × 250 mm, Phenomenex, Torrance, CA, USA). The column temperature was set to 25 °C. The mobile

phase was composed of a gradient of acetonitrile (A) and 0.1 M triethylamine and 0.01 M sodium heptanesulphonate, adjusted with  $H_3PO_4$  to pH 2.5 (B). The gradient program was set as it follows: 0–1 min 85% B; 1–20 min 70% solution B; 20–30 min 50% solution B, 30–35 min 40% solution B, 35–40 min 85% solution B. The flow rate was kept constantly at 1 mL/min and the injected volume was 10  $\mu$ L. The UV detection of alkaloids and their references were performed at 210, 240 and 290 nm for protopine, stylophine, bicuculline and chelidoneine and at 280 and 330 for sanguinarine [12,39].

#### 4.7. Antioxidant Activity Assays

Preliminary evaluation of in vitro antioxidant potential of the *F. schleicheri* extract was made using two complementary assays (DPPH and FRAP). In the DPPH assay, 30 L of sample was mixed with 270  $\mu$ L of DPPH solution (0.004% in absolute methanol). The reaction mix was incubated at room temperature in a dark place for 30 min; after incubation, the absorbance of each sample was read at 517 nm. In the FRAP assay, a reaction mixture containing 25  $\mu$ L of sample and 175  $\mu$ L of FRAP reagent—acetate buffer (0.3 M, pH 3.6); 2,4,6-tris(2-pyridyl)-s-triazine (TPTZ) (10 mM) in 40 mM HCl; and ferric chloride (20 mM) in a ratio of 10:1:1 (*v/v/v*)—was incubated for 30 min at room temperature, followed by the reading of the absorbance at 593 nm. For both assays, the results were expressed as mg Trolox equivalents/g dry extract (mg TE/g d.e) [43,45,46].

#### 4.8. Anti-Cholinesterase Activity Assays

The extracts were supposed to serial dilutions (10, 31.5, 100, 315, 1000  $\mu$ g/mL in 50 mM Tris-HCl, pH = 8 containing 5% DMSO) and tested for acetylcholinesterase (AChE) inhibitory activity using an Ellman's method adapted for 96-wells microplate reader. First, 25  $\mu$ L of the sample, 50  $\mu$ L of Tris-HCl buffer (pH = 8, 50 mM), 125  $\mu$ L of DTNB (0.9 mM in the same buffer) and 25  $\mu$ L of AchE (0.078 U/mL in same buffer) were mixed in each well and incubated for 15 min at room temperature in a dark place. After incubation, 25  $\mu$ L of ATCI (4.5 mM in Tris-HCl buffer) were added to each well and incubated again for 10 min. The absorbance of the samples was measured at 405 nm and  $IC_{50}$  values ( $\mu$ g/mL) were expressed using galantamine as positive control [46,48].

#### 4.9. Cytotoxic Activity Assessment

The cytotoxicity assay of *F. schleicheri* ethanolic extract (FS3) was performed using human fibroblasts BJ (ATCC<sup>®</sup> CRL-2522<sup>™</sup>) and human colon adenocarcinoma cell line DLD-1 (ATCC<sup>®</sup> CCL-221<sup>™</sup>). The cells were cultured according to standard conditions. The potential cytotoxicity of the tested extract was assessed with (4,5-dimethylthiazol-2-yl)-2,5-diphenyltetrazolium bromide (MTT) assay. To obtain cell suspensions, the cells were treated with 0.25% trypsin-EDTA, and after centrifugation (1500 rpm for 5 min),  $1 \times 10^4$  cells/well were seeded on 96 wells plates in 200  $\mu$ L complete culture medium. After 24 h, the *F. schleicheri* extract in five different concentrations (10–30  $\mu$ g/mL) was added. Negative control samples were represented by untreated cells. The internal control was represented by cells treated with 70% ethanol. Each experimental condition was performed in triplicate. Cell proliferation analysis was performed after 24 h. After 24 h, the medium was removed and 100  $\mu$ L of 1 mg/mL MTT solution (Sigma-Aldrich, St. Louis, MO, USA) was added. After 3 h of incubation at 37 °C in dark, the MTT solution was removed from each well and 150  $\mu$ L of DMSO (dimethyl sulfoxide) solution (Fluka, Buchs, Switzerland) was added. Spectrophotometric readings at 450 nm were performed with a BioTek Synergy 2 microplate reader (Winooski, VT, USA). Cytotoxicity was expressed as viability percentage (%) based on the absorbance ratio between cell cultures treated with extract and the negative controls (untreated cells) multiplied by 100. Additionally, the concentration required to inhibit 50% of the cell line ( $IC_{50}$  in  $\mu$ g/mL) was calculated from the dose–response curve obtained using non-linear regression [49–51].

#### 4.10. Statistical Analysis

Statistical analysis was performed using ANOVA GraphPad Prism software, version 6.0 (San Diego, CA, USA). The results were presented as mean  $\pm$  standard deviation (SD). One-way analysis of variance (ANOVA) was conducted, followed by Tukey's post hoc test, to determine statistical significance. The Pearson correlation analysis was performed to determine the correlation between the total alkaloids content in tested extracts and the anticholinesterase activity. A *p* value lower than 0.05 was considered statistically significant.

#### 5. Conclusions

Phytochemical analysis of *Fumaria schleicheri* Soy. Will. highlighted the presence of several isoquinolinic alkaloids, namely bicuculline, chelidionine and sanguinarine, which were not previously reported in the composition of the species. Furthermore, the extracts belonging to the aerial parts of this species displayed valuable in vitro antioxidant, anticholinesterase and cytotoxic activities. In this way, the species proved to have important potential to be considered in the future as a promising substitute for the officinal species belonging to the *Fumaria* genus. Further studies are necessary in order to establish the mechanisms of action for the biological activities, but the antioxidant activity may represent an important basis for these activities.

**Supplementary Materials:** The following supporting information can be downloaded at: <https://www.mdpi.com/article/10.3390/plants11091202/s1>, Figure S1. HPLC-DAD chromatogram of the FS1 sample, Figure S2. HPLC-DAD chromatogram of the FS2 sample, Figure S3. HPLC-DAD chromatogram of the FS3 sample, Figure S4. FS1 sample during the harvesting stage, Figure S5. FS2 sample during the conditioning phase, Figure S6. FS3 sample during the drying phase.

**Author Contributions:** Conceptualization, R.P., I.I., D.H., L.A., M.T. (Monique Tits), M.T. (Mircea Tămaș), G.C. and M.F.; methodology, R.P., I.I., M.N., E.P., A.M., M.B. and O.F.; software, R.P., I.I., D.H., M.N., E.P., M.B. and O.F.; formal analysis, R.P., I.I., M.N., E.P., A.M., M.B. and O.F.; investigation, R.P., I.I., M.N., E.P., A.M., M.B. and O.F.; resources, R.P., I.I., L.A., M.T. (Monique Tits), M.T. (Mircea Tămaș), G.C. and M.F.; writing—original draft preparation, R.P., I.I. and M.B.; writing—review and editing, R.P., I.I., D.H., M.N., E.P., L.A., M.T. (Monique Tits), A.M., M.B., O.F., M.T. (Mircea Tămaș), G.C. and M.F.; supervision, R.P., I.I., D.H., L.A., M.T. (Monique Tits), M.T. (Mircea Tămaș), G.C. and M.F.; project administration, R.P.; funding acquisition, R.P. All authors have read and agreed to the published version of the manuscript.

**Funding:** This work was supported by a grant of Romanian Ministry of Education and Research, CNCS-UEFISCDI, project number PN-III-P1-1.1-PD-2019-0603, within PNCDI III and a grant of USAMVCN, project number 24905-2021-1108.

**Institutional Review Board Statement:** Not applicable.

**Informed Consent Statement:** Not applicable.

**Data Availability Statement:** Data sharing not applicable.

**Acknowledgments:** We are grateful to Jean-Noël Wauters for providing help with the identification of compounds and HPLC-DAD analysis.

**Conflicts of Interest:** The authors declare no conflict of interest.

#### References

1. Tutin, T.G.; Burges, N.A.; Chater, A.O.; Edmonson, J.R.; Heywood, V.H.; Moore, D.M.; Valentine, D.H.; Walters, S.M.; Webb, D.A. *Flora Europaea, Vol. 1 (Psilotaceae to Platanaceae)*, 2nd ed.; Cambridge University Press: Cambridge, UK, 2010.
2. Pérez-Gutiérrez, M.A.; Romero-García, A.T.; Salinas, M.J.; Blanca, G.; Carmen Fernández, M.; Suárez-Santiago, V.N. Phylogeny of the Tribe Fumarieae (Papaveraceae s.l.) Based on Chloroplast and Nuclear DNA Sequences: Evolutionary and Biogeographic Implications. *Am. J. Bot.* **2012**, *99*, 517–528. [[CrossRef](#)] [[PubMed](#)]
3. Păltinean, R.; Mocan, A.; Vlase, L.; Gheldiu, A.M.; Crișan, G.; Ielciu, I.; Voștinaru, O.; Crișan, O. Evaluation of Polyphenolic Content, Antioxidant and Diuretic Activities of Six *Fumaria* Species. *Molecules* **2017**, *22*, 639. [[CrossRef](#)] [[PubMed](#)]
4. Păltinean, R.; Wauters, J.N.; Tits, M.; Frédérich, M.; Angenot, L.; Tămaș, M.; Crișan, G. Comparative Morphological Studies on Some Species of the Genus *Fumaria*. *Farmacia* **2013**, *61*, 371–377.

5. Săvulescu, T. *Flora Republicii Populare Române*; Editura Academiei R.P.R.: București, Romania, 1955; Volume III.
6. Ciocârlan, V. *Flora Ilustrată a României, Pteridophyta et Spermatophyta*; Editura Ceres: București, Romania, 2000; pp. 579–582.
7. Goetz, P.; Ghedira, K.; Le Jeune, R. *Fumaria officinalis* L. (Fumariaceae). *Phytotherapie* **2009**, *7*, 221–225. [[CrossRef](#)]
8. Dutta, R.; Sharma, M.K.; Jha, M. A Review on Ethnobotanical, Phytochemistry, Bioactivities and Medicinal Mysteries of *Fumaria officinalis* (Common Fumitory). *EAS J. Pharm. Pharmacol.* **2019**, *1*, 99–105. [[CrossRef](#)]
9. Al-Snafi, A.E. Constituents and Pharmacology of *Fumaria officinalis*—A Review. *IOSR J. Pharm.* **2020**, *10*, 17–25.
10. Ivanov, I.G.; Vrancheva, R.Z.; Marchev, A.S.; Petkova, N.T.; Aneva, I.Y.; Panteley, D.P.; Georgiev, V.G.; Pavlov, A.I. Antioxidant Activities and Phenolic Compounds in Bulgarian *Fumaria* Species. *Int. J. Curr. Microbiol. Appl. Sci.* **2014**, *3*, 296–306.
11. Zhang, R.; Guo, Q.; Kennelly, E.J.; Long, C.; Chai, X. Diverse Alkaloids and Biological Activities of *Fumaria* (Papaveraceae): An Ethnomedicinal Group. *Fitoterapia* **2020**, *146*, 104697. [[CrossRef](#)]
12. Păltinean, R.; Toiu, A.; Wauters, J.N.; Frédéricich, M.; Tits, M.; Angenot, L.; Tămaș, M.; Crișan, G. Identification and Determination of Alkaloids in *Fumaria* Species from Romania. *Dig. J. Nanomater. Biostruct.* **2013**, *8*, 817–824.
13. Khamtache-Abderrahim, S.; Lequart-Pillon, M.; Gontier, E.; Gaillard, I.; Pilard, S.; Mathiron, D.; Djoudad-Kadji, H.; Maiza-Benabdesselam, F. Isoquinoline Alkaloid Fractions of *Fumaria officinalis*: Characterization and Evaluation of Their Antioxidant and Antibacterial Activities. *Ind. Crop. Prod.* **2016**, *94*, 1001–1008. [[CrossRef](#)]
14. Chlebek, J.; Novák, Z.; Kassemová, D.; Šafratová, M.; Kostelník, J.; Malý, L.; Ločárek, M.; Opletal, L.; Hošťálková, A.; Hrabínová, M.; et al. Isoquinoline Alkaloids from *Fumaria officinalis* L. and Their Biological Activities Related to Alzheimer's Disease. *Chem. Biodivers.* **2016**, *13*, 91–99. [[CrossRef](#)] [[PubMed](#)]
15. Tsyvunin, V.; Shtrygol, S.Y. Antiepileptic Potential of *Fumaria schleicheri* and *Ocimum basilicum* Dry Extracts. *News Pharm.* **2015**, *1*, 64–68. [[CrossRef](#)]
16. Tsyvunin, V.; Shtrygol, S.; Gorbach, T.; Shtrygol', D. Anticonvulsant Activity of *Fumaria schleicheri* Dry Extract and Sodium Valproate: Role of Neurotrophin and Cytokine Pathways. *Thai J. Pharm. Sci.* **2020**, *44*, 46–51.
17. Prokopenko, Y.; Tsyvunin, V.; Shtrygol, S.; Georgiyants, V. In Vivo Anticonvulsant Activity of Extracts and Protopine from the *Fumaria schleicheri* Herb. *Sci. Pharm.* **2016**, *84*, 547–554. [[CrossRef](#)]
18. Tsyvunin, V.; Shtrygol, S.Y.; Gorbach, T.V. Experimental Investigation of Antiepileptic Potential and Mechanisms of Anticonvulsant Action of Dry Extract of *Fumaria schleicheri*. *News Pharm.* **2015**, 341–342.
19. Tsyvunin, V.; Shtrygol, S.Y.; Prokopenko, Y.S. Neuroprotective Properties of Dry Extracts of *Fumaria schleicheri* and *Ocimum basilicum*. *Rev. Clin. Pharmacol. Drug Ther.* **2013**, *11*, 66–71. [[CrossRef](#)]
20. Kiryakov, H.G.; Mardirosyan, Z.H.; Panov, P.P. Alkaloids from *Fumaria schleicheri* Soy Will. *Comptes Rendus L'acad. Bulg. Sci.* **1980**, *33*, 1377–1379.
21. Radu, A.; Tămaș, M.; Olah, B. Cercetări Asupra Alcaloizilor Din Unele Specii de *Fumaria*. *Farmaciază* **1979**, *26*, 1–5.
22. Kiryakov, H.G.; Mardirosian, Z.H.; Hughes, D.W.; Maclean, D.B. Fumschleicherine, an Alkaloid of *Fumaria schleicheri*. *Phytochemistry* **1980**, *19*, 2507–2509. [[CrossRef](#)]
23. Adham, A.N.; Naqishbandi, A.M.; Efferth, T. Cytotoxicity and Apoptosis Induction by *Fumaria officinalis* Extracts in Leukemia and Multiple Myeloma Cell Lines. *J. Ethnopharmacol.* **2021**, *266*, 113458. [[CrossRef](#)]
24. Petruczynik, A.; Plech, T.; Tuzimski, T.; Misiurek, J.; Kapron, B.; Misiurek, D.; Szultka-Mlynska, M.; Buszewski, B.; Waksmundzka-Hajnos, M. Determination of Selected Isoquinoline Alkaloids from *Mahonia aquifolia*; *Meconopsis cambrica*; *Corydalis lutea*; *Dicentra spectabilis*; *Fumaria officinalis*; *Macleaya cordata* Extracts by HPLC-DAD and Comparison of Their Cytotoxic Activity. *Toxins* **2019**, *11*, 575. [[CrossRef](#)]
25. Chlebek, J.; Doskočil, I.; Hulcová, D.; Breiterová, K.; Šafratová, M.; Havelek, R.; Habartová, K.; Hošťálková, A.; Volštatová, T.; Cahliková, L. Cytotoxicity of Naturally Occurring Isoquinoline Alkaloids of Different Structural Types. *Nat. Prod. Commun.* **2016**, *11*, 753–756. [[CrossRef](#)] [[PubMed](#)]
26. Orhan, I.; Sener, B. Acetylcholinesterase Inhibitors from Natural Resources. *J. Pharm. Sci.* **2003**, *28*, 51–58.
27. Dhivya, P.S.; Sobiya, M.; Selvamani, P.; Latha, S. An Approach to Alzheimer's Disease Treatment with Cholinesterase Inhibitory Activity from Various Plant Species. *Int. J. PharmTech Res.* **2014**, *6*, 1450–1468.
28. Vrancheva, R.Z.; Ivanov, I.G.; Aneva, I.Y.; Dincheva, I.N.; Badjakov, I.K.; Pavlov, A.I. Alkaloid Profiles and Acetylcholinesterase Inhibitory Activities of *Fumaria* Species from Bulgaria. *Zeitschrift Naturforsch.—Sect. C J. Biosci.* **2016**, *71*, 9–14. [[CrossRef](#)] [[PubMed](#)]
29. Singh, G.K.; Rai, G.; Chatterjee, S.S.; Kumar, V. Effects of Ethanolic Extract of *Fumaria indica* L. on Rat Cognitive Dysfunctions. *AYU Int. Q. J. Res. Ayurveda* **2013**, *34*, 421–429. [[CrossRef](#)]
30. Vrancheva, R.Z.; Ivanov, I.G.; Aneva, I.Y.; Dincheva, I.N.; Badjakov, I.K.; Pavlov, A.I. GC-MS Based Metabolite Profiling of Five Bulgarian *Fumaria* Species. *J. Biosci. Biotechnol.* **2014**, *3*, 195–201.
31. Roy, A. A Review on the Alkaloids an Important Therapeutic Compound from Plants. *Int. J. Plant Biotechnol.* **2017**, *3*, 9.
32. Dey, P.; Kundu, A.; Kumar, A.; Gupta, M.; Lee, B.M.; Bhakta, T.; Dash, S.; Kim, H.S. *Analysis of Alkaloids (Indole Alkaloids, Isoquinoline Alkaloids, Tropane Alkaloids)*; Elsevier Inc.: Amsterdam, The Netherlands, 2020. [[CrossRef](#)]
33. Hanganu, D.; Niculae, M.; Ielciu, I.; Olah, N.-K.; Munteanu, M.; Burtescu, R.; Ștefan, R.; Olar, L.; Pall, E.; Andrei, S.; et al. Chemical Profile, Cytotoxic Activity and Oxidative Stress Reduction of Different *Syringa vulgaris* L. Extracts. *Molecules* **2021**, *26*, 3104. [[CrossRef](#)]

34. Ielciu, I.; Sevastre, B.; Olah, N.-K.; Turdean, A.; Chișe, E.; Marica, R.; Oniga, I.; Uifălean, A.; Sevastre-Berghian, A.C.; Niculae, M.; et al. Evaluation of Hepatoprotective Activity and Oxidative Stress Reduction of *Rosmarinus officinalis* L. Shoots Tincture in Rats with Experimentally Induced Hepatotoxicity. *Molecules* **2021**, *26*, 1737. [[CrossRef](#)]
35. Sevastre-Berghian, A.C.; Ielciu, I.; Mitre, A.O.; Filip, G.A.; Oniga, I.; Vlase, L.; Benedec, D.; Gheldiu, A.-M.; Toma, V.A.; Mihart, B.; et al. Targeting Oxidative Stress Reduction and Inhibition of HDAC1, MECP2, and NF- $\kappa$ B Pathways in Rats With Experimentally Induced Hyperglycemia by Administration of *Thymus marshallianus* Willd. Extracts. *Front. Pharmacol.* **2020**, *11*, 581470. [[CrossRef](#)] [[PubMed](#)]
36. Sener, B.; Orhan, I. Exploring Turkish Biodiversity: A Rich Source of Chemical Diversity for Drug Leads Discovery. *Pure Appl. Chem.* **2011**, *83*, 1699–1707. [[CrossRef](#)]
37. Maiza-Benabdeslam, F.; Chibane, M.; Madani, K.; Max, H.; Adach, S. Determination of Isoquinoline Alkaloids Contents in Two Algerian Species of *Fumaria* (*Fumaria capreolata* and *Fumaria bastardi*). *Afr. J. Biotechnol.* **2007**, *6*, 2487–2492. [[CrossRef](#)]
38. Suau, R.; Cabezudo, B.; Rico, R.; López-Romero, J.M.; Nájera, F. Alkaloids from *Fumaria sepium* and *Fumaria agraria*. *Biochem. Syst. Ecol.* **2002**, *30*, 263–265. [[CrossRef](#)]
39. Păltinean, R.; Toiu, A.; Wauters, J.N.; Frédérich, M.; Tits, M.; Angenot, L.; Tămaș, M.; Crișan, G. Phytochemical Analysis of *Fumaria officinalis* L. (Fumariaceae). *Farmacia* **2016**, *64*, 409–413.
40. Tuzimski, T.; Petruczynik, A. Application of HPLC-DAD for In Vitro Investigation of Acetylcholinesterase Inhibition Activity of Selected Isoquinoline Alkaloids from *Sanguinaria canadensis* Extracts. *Molecules* **2021**, *26*, 230. [[CrossRef](#)]
41. Ielciu, I.; Hanganu, D.; Păltinean, R.; Vlase, L.; Frédérich, M.; Gheldiu, A.-M.; Benedec, D.; Crișan, G. Antioxidant Capacity and Polyphenolic Content of the Echinocystis Lobata (Michx.) Torr. et A.Gray Flowers. *Pak. J. Pharm. Sci.* **2018**, *31* (Suppl. 2), 677–683.
42. Ielciu, I.; Mouithys-Mickalad, A.; Franck, T.; Angenot, L.; Ledoux, A.; Păltinean, R.; Ciekiewicz, E.; Etienne, D.; Tits, M.; Crișan, G.; et al. Flavonoid Composition, Cellular Antioxidant Activity and (Myelo)Peroxidase Inhibition of a *Bryonia alba* L. (Cucurbitaceae) Leaves Extract. *J. Pharm. Pharmacol.* **2019**, *71*, 230–239. [[CrossRef](#)]
43. Ielciu, I.; Frederich, M.; Hanganu, D.; Angenot, L.; Olah, N.-K.; Ledoux, A.; Crisan, G.; Păltinean, R. Flavonoid Analysis and Antioxidant Activities of the *Bryonia alba* L. Aerial Parts. *Antioxidants* **2019**, *8*, 108. [[CrossRef](#)]
44. Ledoux, A.; St-Gelais, A.; Ciekiewicz, E.; Jansen, O.; Bordignon, A.; Illien, B.; Di Giovanni, N.; Marvilliers, A.; Hoareau, F.; Pendeville, H.; et al. Antimalarial Activities of Alkyl Cyclohexenone Derivatives Isolated from the Leaves of *Poupartia borbonica*. *J. Nat. Prod.* **2017**, *80*, 1750–1757. [[CrossRef](#)]
45. Babotă, M.; Voștinaru, O.; Păltinean, R.; Mihali, C.; Dias, M.I.; Barros, L.; Ferreira, I.C.F.R.; Mocan, A.; Crișan, O.; Nicula, C.; et al. Chemical Composition, Diuretic, and Antityrosinase Activity of Traditionally Used Romanian *Cerasorum stipites*. *Front. Pharmacol.* **2021**, *12*, 1–11. [[CrossRef](#)] [[PubMed](#)]
46. Mocan, A.; Babotă, M.; Pop, A.; Fizeșan, I.; Diuzheva, A.; Locatelli, M.; Carradori, S.; Campestre, C.; Menghini, L.; Sisea, C.R.; et al. Chemical Constituents and Biologic Activities of Sage Species: A Comparison between *Salvia officinalis* L., *S. glutinosa* L. and *S. transsylvanica* (Schur Ex Griseb. & Schenk) Schur. *Antioxidants* **2020**, *9*, 480. [[CrossRef](#)]
47. European Directorate for the Quality of Medicines & Health Care. *European Pharmacopoeia*, 9th ed.; European Directorate for the Quality of Medicines & Health Care: Strasbourg, France, 2017.
48. Coetzee, D.D.; López, V.; Smith, C. High-Mesembrine Scelletium Extract (Trimesemine<sup>TM</sup>) Is a Monoamine Releasing Agent, Rather than Only a Selective Serotonin Reuptake Inhibitor. *J. Ethnopharmacol.* **2016**, *177*, 111–116. [[CrossRef](#)] [[PubMed](#)]
49. Sevastre, B.; Sárpataki, O.; Stan, R.L.; Taulescu, M.; Sevastre-Berghian, A.C.; Olah, N.K.; Furtuna, F.; Hanganu, D.; Hangan, A.C.; Cenariu, M.; et al. Anticancer Activity of *Euonymus europaeus* Fruits Extract on Human Melanoma Cells. *Farmacia* **2017**, *65*, 56–62.
50. Rugină, D.; Hanganu, D.; Diaconeasa, Z.; Tăbăran, F.; Coman, C.; Leopold, L.; Bunea, A.; Pinte, A. Antiproliferative and Apoptotic Potential of Cyanidin-Based Anthocyanins on Melanoma Cells. *Int. J. Mol. Sci.* **2017**, *18*, 949. [[CrossRef](#)]
51. Stan, R.L.; Hangan, A.C.; Dican, L.; Sevastre, B.; Hanganu, D.; Cătoi, C.; Sárpataki, O.; Ionescu, C.M. Comparative Study Concerning Mistletoe Viscotoxins Antitumor Activity. *Acta Biol. Hung.* **2013**, *64*, 279–288. [[CrossRef](#)]



## Article

# Genome-Wide Analyses of MADS-Box Genes in *Humulus lupulus* L. Reveal Potential Participation in Plant Development, Floral Architecture, and Lupulin Gland Metabolism

Robert Márquez Gutiérrez<sup>1</sup>, Thales Henrique Cherubino Ribeiro<sup>1</sup>, Raphael Ricon de Oliveira<sup>1</sup>,  
Vagner Augusto Benedito<sup>2,\*</sup> and Antonio Chalfun-Junior<sup>1,\*</sup>

<sup>1</sup> Laboratory of Plant Molecular Physiology, Plant Physiology Sector, Department of Biology, Federal University of Lavras (UFLA), Lavras 37200-900, MG, Brazil; robertmarquez993@gmail.com (R.M.G.); thalescherubino@gmail.com (T.H.C.R.); rapharicon@gmail.com (R.R.d.O.)

<sup>2</sup> Laboratory of Plant Functional Genetics, Plant and Soil Sciences Division, 3425 Agricultural Sciences Building, West Virginia University, Morgantown, WV 26506-6108, USA

\* Correspondence: vagner.benedito@mail.wvu.edu (V.A.B.); chalfunjunior@ufla.br (A.C.-J.)

**Abstract:** MADS-box transcription factors (TFs) are involved in multiple plant development processes and are most known during the reproductive transition and floral organ development. Very few genes have been characterized in the genome of *Humulus lupulus* L. (Cannabaceae), an important crop for the pharmaceutical and beverage industries. The MADS-box family has not been studied in this species yet. We identified 65 MADS-box genes in the hop genome, of which 29 encode type-II TFs (27 of subgroup MIKCC and 2 MIKC\*) and 36 type-I proteins (26  $\alpha$ , 9  $\beta$ , and 1  $\gamma$ ). Type-II MADS-box genes evolved more complex architectures than type-I genes. Interestingly, we did not find FLOWERING LOCUS C (FLC) homologs, a transcription factor that acts as a floral repressor and is negatively regulated by cold. This result provides a molecular explanation for a previous work showing that vernalization is not a requirement for hop flowering, which has implications for its cultivation in the tropics. Analysis of gene ontology and expression profiling revealed genes potentially involved in the development of male and female floral structures based on the differential expression of ABC homeotic genes in each whorl of the flower. We identified a gene exclusively expressed in lupulin glands, suggesting a role in specialized metabolism in these structures. *In toto*, this work contributes to understanding the evolutionary history of MADS-box genes in hop, and provides perspectives on functional genetic studies, biotechnology, and crop breeding.

**Keywords:** ABC model; hop; transcription factors; type-II MADS box; type-I MADS-box

**Citation:** Márquez Gutiérrez, R.; Cherubino Ribeiro, T.H.; de Oliveira, R.R.; Benedito, V.A.; Chalfun-Junior, A. Genome-Wide Analyses of MADS-Box Genes in *Humulus lupulus* L. Reveal Potential Participation in Plant Development, Floral Architecture, and Lupulin Gland Metabolism. *Plants* **2022**, *11*, 1237. <https://doi.org/10.3390/plants11091237>

Academic Editor: Alex Troitsky

Received: 22 March 2022

Accepted: 26 April 2022

Published: 3 May 2022

**Publisher's Note:** MDPI stays neutral with regard to jurisdictional claims in published maps and institutional affiliations.



**Copyright:** © 2022 by the authors. Licensee MDPI, Basel, Switzerland. This article is an open access article distributed under the terms and conditions of the Creative Commons Attribution (CC BY) license (<https://creativecommons.org/licenses/by/4.0/>).

## 1. Introduction

MADS-box proteins are transcription factors (TFs) that interact with the promoters of their target genes through the binding to CARG-box *cis*-elements [1]. Phylogenetic data have classified MADS-box proteins into two groups: types I (e.g., SRF from human) and II (e.g., Mcm1 from yeast) [2]. A highly conserved sequence of about 60 amino acids called the MADS domain characterizes this family of TFs. In plants, MADS-box TFs have largely diversified and can be sub-classified into several clades. Type-I proteins are split into three groups: M $\alpha$ , M $\beta$ , and M $\gamma$ , whereas type-II proteins are classified into two groups: MIKC\* and MIKCC [3]. MIKC represents the protein structure of type-II MADS-box TFs, which has the conserved MADS-box for DNA-binding closed to the N-terminus followed by an intervening domain (I), a keratin-like domain (K) for protein-protein interaction, and the variable C-terminal domain. MIKCC MADS-box proteins are sub-classified into 13 subfamilies, including the TM8 subfamily that is absent in *Arabidopsis* [4].

MADS-box TFs orchestrate multiple developmental programs in plants, most notably vegetative and reproductive development programs. More recently, a novel MADS-box

TF in apple was implicated in regulating dormancy cycles in response to environmental cues [5]. MADS-box TFs are also involved in maintaining the spike morphology of barley under high-temperature stress [6], promoting bud break in ecodormant poplar [7], and controlling nitrogen fixation symbiosis in common beans [8]. Flowering transition is another process governed by MADS-box genes. In *Arabidopsis*, SUPPRESSOR OF OVER-EXPRESSION OF CONSTANS 1 (SOC1) integrates multiple flowering signals derived from photoperiod, temperature, hormone, and age-related signals [9–11]. SOC1 interacts with AGAMOUS-like 24 (AGL24) and FRUITFULL (FUL) to promote flowering [12,13]. In addition, the transition from the vegetative to the reproductive phase in *Arabidopsis* is controlled by the MADS-box protein, SHORT VEGETATIVE PHASE (SVP), which is a repressor of flowering under short days [14] alike to what FLOWERING LOCUS C (FLC) does prior to vernalization [15,16]. FLC is a TF that acts as a floral repressor and is negatively regulated by cold periods or vernalization, being essential to synchronize flowering and winter [17,18]. FLC homologs were described in the three major eudicot lineages [19,20], including sugar-beet, apple, and coffee [19,21,22]. However, despite the role of FLC being described in the Brassicaceae [23] and more recently cereal crops and grasses [24,25], the extent to which the molecular mechanisms underlying vernalization have been conserved during the diversification of the angiosperms remains elusive.

Some of the most studied MADS-box transcription factors are involved in the development of floral organs in angiosperms [26]. Such genes are called homeotic, since their misexpression in a given whorl leads to the formation of a different floral organ [27–29]. This led to the formulation of the ABC model [30], which encompasses the combinatorial transcription of MADS-box TFs that elicit the developmental program of specific organs in each whorl of the flower. In this model, a class-A gene expressed alone in the first whorl leads to the formation of sepals, the co-expression of class A and B genes in the second whorl leads to the development of petals, the co-expression of class B and C genes in the third whorl elicits the formation of anthers, and finally, the expression of a C-class gene alone in the fourth whorl leads to the formation of carpels.

Further research extended the ABC model to an ABCDE model, where D-class genes expressed in the carpel lead to the formation of ovules, and E-class genes expressed in all whorls form tetramers with ABC TFs that coordinate the development of each whorl [1,31]. In *Arabidopsis*, the ABCDE model encompasses the A-class APETALA1 (AP1) [32]; the B-class APETALA3 (AP3) and PISTILLATA (PI) [33,34]; the C-class AGAMOUS (AG) [35]; the D-class AGAMOUS-like 1, 5, and 11 (AGL1, AGL5, and AGL11) [36]; and the E-class SEPAL-LATA 1,2,3,4 (SEP1, SEP2, SEP3, and SEP4) [37]. The ABCDE model has been conserved throughout angiosperm evolution. The genes encompassing each homeotic class have been determined in different species, from monocots, such as rice [38,39], wheat [40], and Easter lily [28]; to dicots, such as soybean [41,42], coffee [22], and the New Zealand endemic species, *Clianthus maximus* [43], among many others. Moreover, studies have also revealed the significance of type-I MADS-box transcription factors in plant reproduction [44].

Hop (*Humulus lupulus* L.) is a perennial crop that belongs to the Cannabaceae family. It blooms in short days once it develops a particular number of nodes. It has been phenotypically demonstrated that vernalization and dormancy do not influence flower yield and quality [45,46]. Moreover, hop is an economically important species because its cones (female inflorescences) are widely utilized in the pharmaceutical and beer industries [47–49]. However, the mechanisms involved in the reproductive phase transition and flower development remain poorly explored at the molecular genetics level. We carried out a genome-wide approach, identified 65 MADS-box genes in the hop genome, and further studied their phylogenetic relationships, genetic structure, and gene expression profiles using publicly available RNA-Seq data. This study revealed TFs that potentially coordinate critical aspects of plant development, phase transition, and glandular metabolism. Therefore, this work advances our understanding of the evolutionary history of the MADS-box TFs in hop and opens new avenues for functional genetic research and crop breeding toward expanding its production zones in the world, especially in the tropics.

## 2. Results

### 2.1. MADS-Box Genes Encoded in the Hop Genome and Gene Ontology Annotation

Using AUGUSTUS on RNA-Seq libraries, our bioinformatics pipeline identified 47 genes coding for proteins with canonical MADS-box domains. Moreover, the hop genome sequence has 69 genes annotated as coding for MADS-box proteins. The overlap of our results with the official hop genome annotation shows a set of 65 non-redundant genes (unigenes: HIMADS01 to HIMADS65), seven of which exclusively from our prediction, 23 exclusively in the hop genome annotation, and 35 represented in both sets. All seven novel genes identified in our *de novo* prediction pipeline were MIKC<sup>C</sup>-type proteins (HIMADS28–33 and HIMADS65). The encoded protein length ranged from 135 to 547 amino acid residues (aa), with an average of 249 aa; the molecular mass varied from 16 to 60 kDa, and the isoelectric point was between 4.55 and 10.25 (Table S1).

Gene Ontology (GO) analysis was performed on the 65 hop MADS-box proteins with the Blast2GO software (Table S3). All hop MADS-box proteins were classified into the three main categories (cellular component, molecular function, and biological process) and their subcategories (Figure S6). In this analysis, 48 proteins returned for cellular component and further split into six subgroups, being the ‘cell part, cell, and organelle’ subcategory the most over-represented subgroup (74%), which is a share even greater than that of *Arabidopsis* (56%), according to our analyses. In addition, 1.5% of the hop MADS-box proteins were annotated into the membrane subcategory, in contrast with 2.8% in *Arabidopsis*. On the other hand, all 65 hop MADS-box proteins were annotated in the subcategory binding of the category molecular function, a result identical to *Arabidopsis*. The second most represented molecular function subcategory in the hop MADS-box protein set was transcription regulator activity, with 75% of the proteins, in contrast with 87% for *Arabidopsis*. The subcategory catalytic activity did not contain any hop MADS-box proteins. Finally, the category biological process contained 51 hop MADS-box proteins (79%). The subcategories biological regulation, cellular processes, regulation of biological processes, and metabolic process were the most overrepresented (97.5%) in hop, followed by positive regulation of biological process subcategory (92.5%). All other subcategories were represented by less than 20% of the hop MADS-box protein set.

### 2.2. Phylogenetic Analyses Revealed Clades and Potential Functions of Hop MADS-Box Genes

Protein domain analyses identified 29 type-II and 36 type-I MADS-box proteins encoded in the hop genome. Each set was submitted to separate phylogenetic analyses to further classify them into subfamilies (Figures 1, 2 and S1). Our results revealed five members in the SEP clade, two in the A clade (AP1-FUL), two in the B clade (AP3-PI), three in the C/D clade (AG), four in the AGL6, two in the AGL12, two in the AGL15, three in the TM8, one in the BS (TT16), two in the SVP, and one in the SOC1 clade (Figure 1, Table S1). Two type-II proteins were classified as MIKC\* (Figure S1). Remarkably, the FLC and AGL17 subfamilies are not represented in the hop genome. The only member of the SOC1 subfamily (HIMADS65) was found when a tBLASTn was performed using the *Arabidopsis* SOC1 protein sequence as a query, and AUGUSTUS was run on the genome region identified in the output. HIMADS65 lies within the region annotated as an intron of 000453F.g47 (Figure S2). The same approach was used for other genes, resulting in no new sequences.

For the type-I MADS-box proteins, the  $\alpha$ -subfamily encompasses the most represented group, with 26 members, followed by the  $\beta$ -subfamily (nine members). In contrast, the  $\gamma$ -subfamily is represented by a single member (Figure 2).

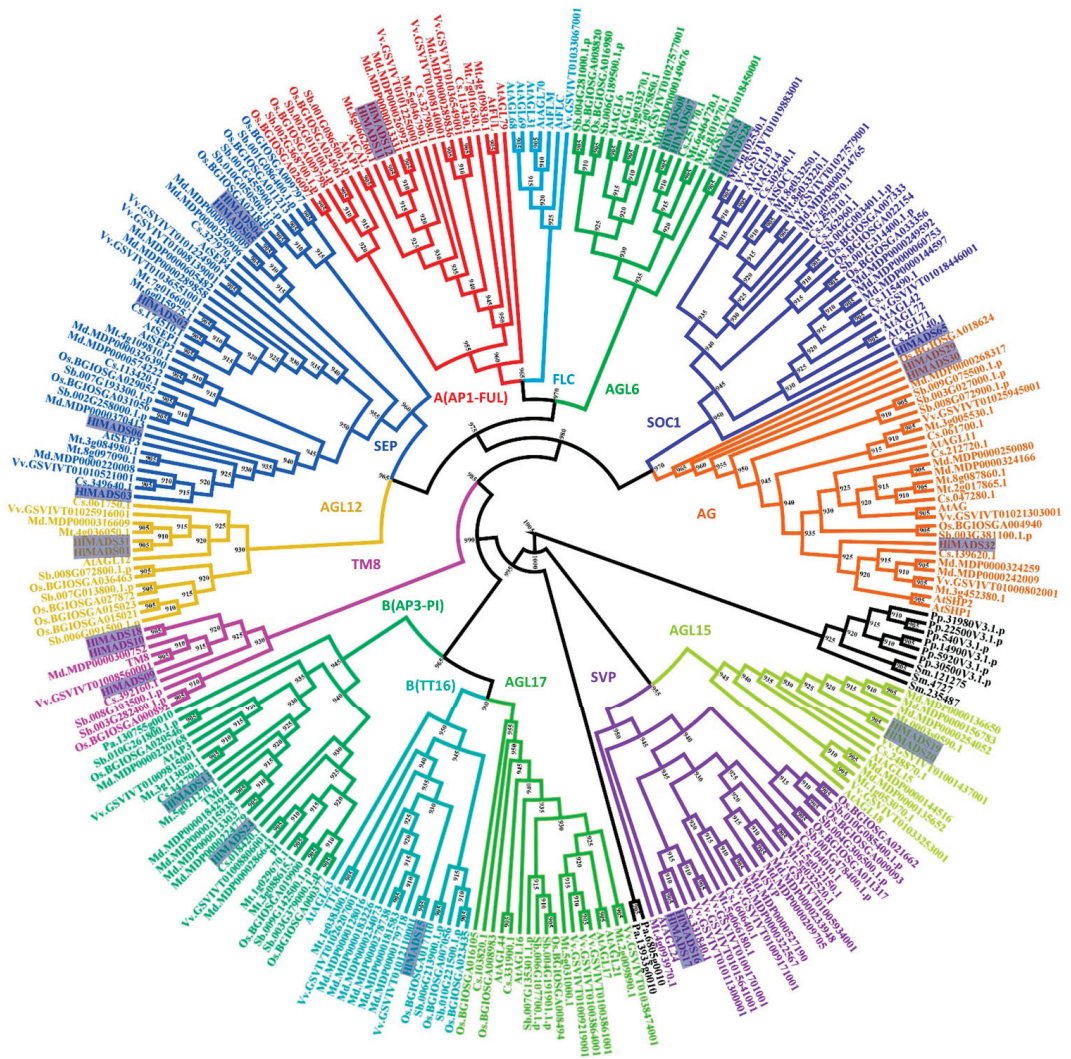


**Figure 1.** Phylogenetic tree of MIKCC-type MADS-box proteins of *Humulus lupulus* (Hl) (27 sequences, highlighted), *Arabidopsis thaliana* (At)(39), *Solanum lycopersicum* (TM6 and TM8), *Physcomitrella patens* (Pp) (6), *Selaginella moellendorffii* (Sm) (3), *Picea abies* (Pa) (3), *Sorghum bicolor* (Sb) (32), *Oryza sativa* subsp. *indica* (Os) (32), *Cucumis sativus* (Cs) (26), *Malus domestica* (Md) (42), *Medicago truncatula* (Mt) (35), and *Vitis vinifera* (Vv) (33). Sequences from *Selaginella moellendorffii*, *Physcomitrella patens*, and *Picea abies* were used as outgroups (in black font).

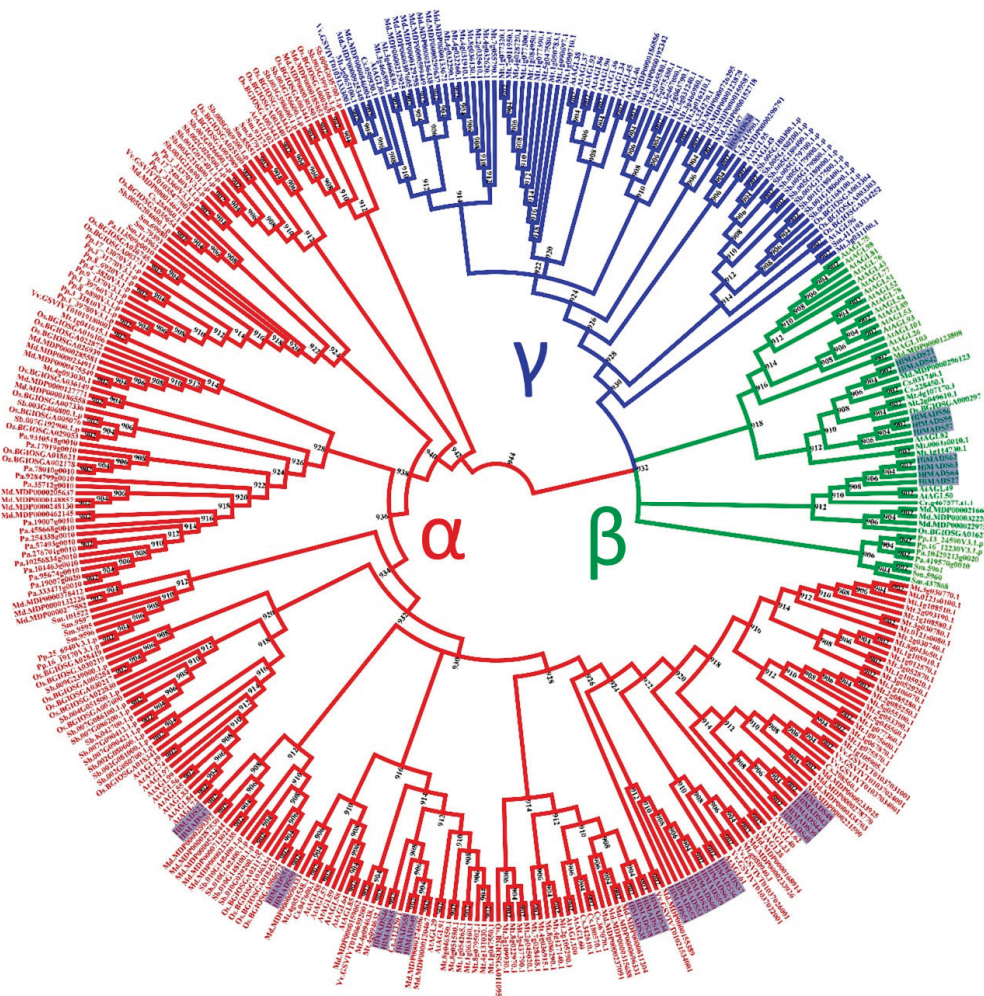


**Figure 2.** Phylogenetic tree of I-type MADS-box proteins of *Humulus lupulus* (Hl) (36 sequences, highlighted), *Arabidopsis thaliana* (At) (58), *Chlamydomonas reinhardtii* (Cr) (1), *Physcomitrella patens* (Pp) (16), *Selaginella moellendorffii* (Sm) (14), *Piceaabies* (Pa) (18), *Sorghum bicolor* (Sb) (38), *Oryza sativa* subsp. *indica* (Os) (36), *Cucumis sativus* (Cs) (12), *Malus domestica* (Md) (56), *Medicago truncatula* (Mt) (79), and *Vitis vinifera* (Vv) (10).

### 2.3. Structural and Motif Analyses of Hop MADS-Box Genes

To confirm our phylogenetic relationships and gain further insights into gene functions, we explored the exon-intron architecture of MADS-box genes. The number of exons among the 29 type-II MADS-box genes varied from 2 (*HIMADS33* and *HLMADS65*) to 13 (*HIMADS22*, the sole member of the MIKC\* group). In hop, *HIMADS05* is the longest type-II MADS-box gene (12.5 kb), with nine exons and eight introns. In the type-I group, the exon number varied from one to five. Overall, *HIMADS61* was the longest gene (16 kb), whereas the shortest ones were *HIMADS46* (584 bp) and *HIMADS47* (613 bp), both with only one exon each (Figure 3), all falling in the type-I clade.

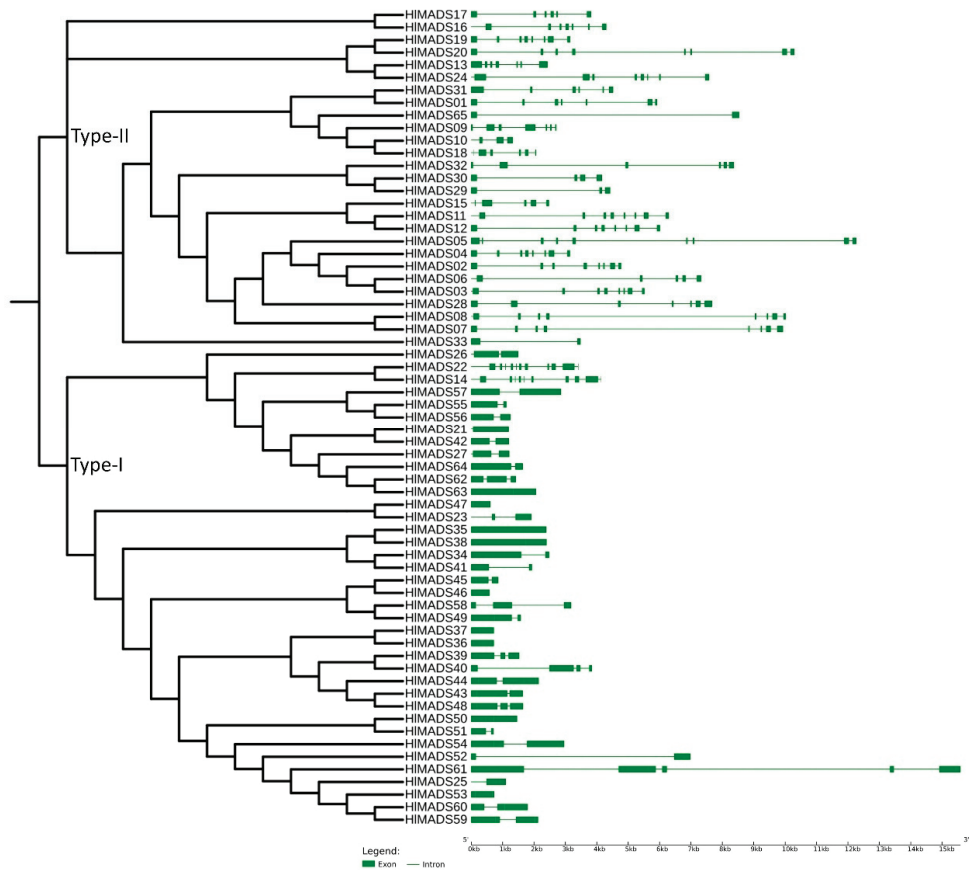


**Figure 3.** Phylogenetic tree and structure of 65 hop MADS-box genes. Exons are represented by green solid boxes, and introns by green lines.

The MEME tool was used to visualize conserved protein domains. While all type-II proteins displayed the MADS-box domain in the tool output, only 21 proteins had the K-box domain, even though this motif is a characteristic feature of this group (Figure 4). However, the NCBI's Conserved Domain Search tool resulted in 23 proteins with the K-box domain, consequently adding HIMADS28 and HIMADS29 to the list. Even though the MADS domain did not appear for HIMADS55, HIMADS56, and HIMADS57, in the MEME analyses, the domain presence was confirmed by NCBI and PFAM conserved domain inference tools. All I-type proteins displayed the MADS domain in MEME but at diverse locations of the peptide sequence (Figures S3 and S4).

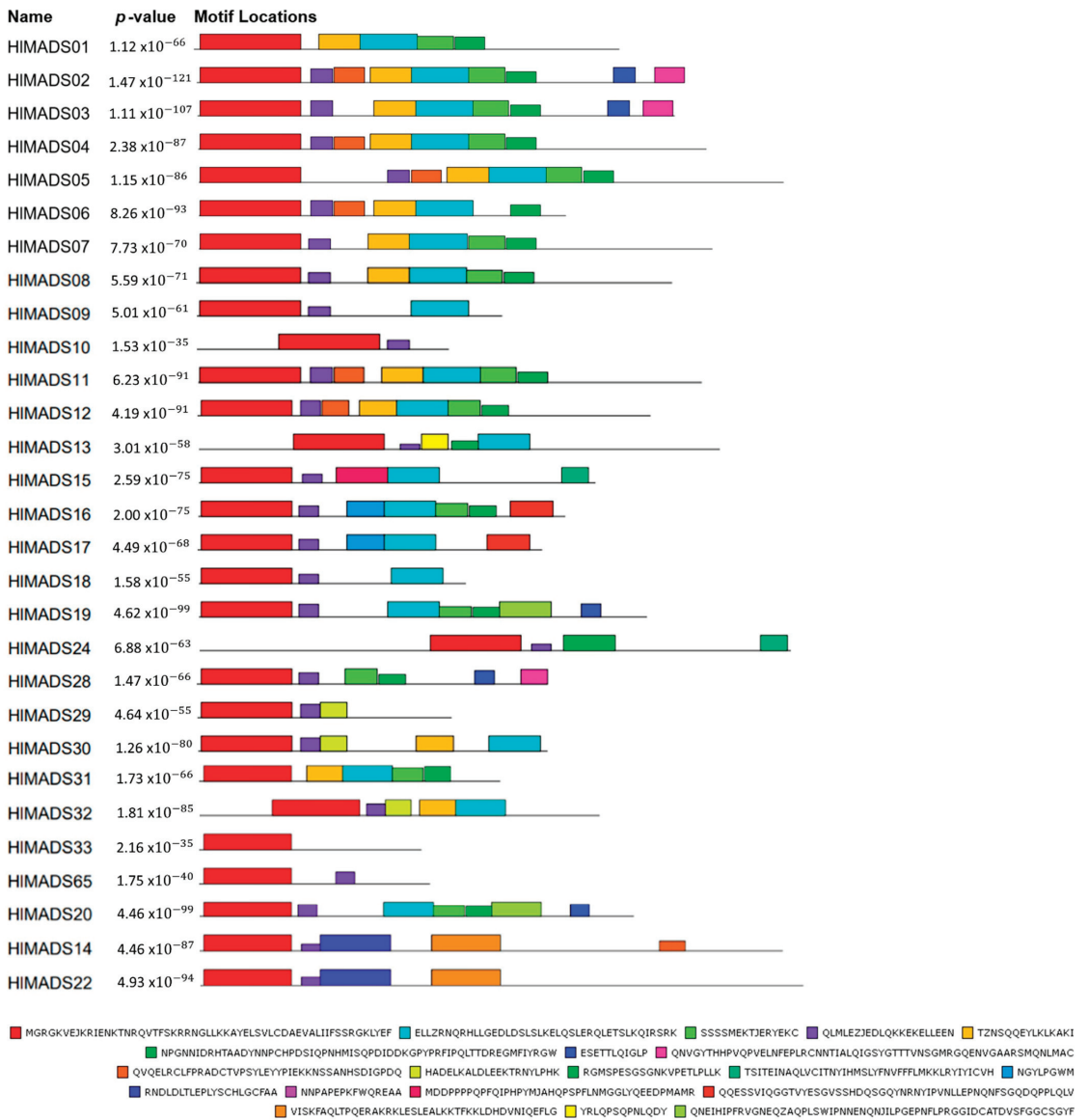


**Figure 4.** Motif distribution of hop type-I MADS-box proteins. Protein sequences are represented by black lines, and the conserved motifs are represented by colored boxes with the MADS-box domain in red.

**2.4. Transcriptional Profile of Hop MADS-Box Genes in Different Tissues**

The expression profiling of MADS-box genes in different hop tissues was determined through the analysis of publicly available RNA-Seq data deposited in the NCBI-SRA database. Thirty genes were expressed in different samples (Figure 5), whereas 35 were not expressed. Of the expressed genes, 18 are of the MIKCC type, and 12 are type I. Some genes belonging to the same subfamily showed distinct expression patterns. For example, in the SEP subfamily, *HIMADS03* and *HIMADS04* were expressed in all samples analyzed, whereas *HIMADS06* was expressed only in the stem, meristem, glands, mature leaves,

and cones without glands. Interestingly, young leaves and bracts showed an identical expression pattern for the MADS-box genes. Moreover, *HIMADS17*, *HIMADS30*, and *HIMADS31* (respective members of the SVP, C/D(AG), and AGL12 clades) were expressed in young leaves compared with the mature organ, indicating a possible function during leaf development and expansion.

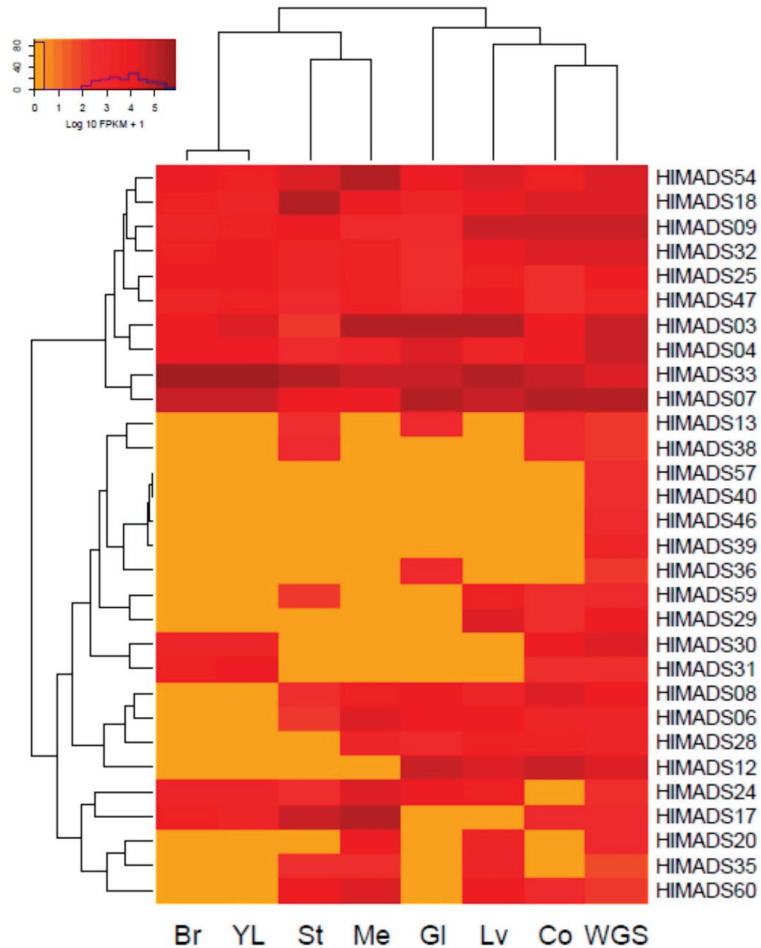


**Figure 5.** Expression profiling of hop MADS-box genes in RNA-Seq libraries: bracts (Br), young leaves (YL), stem (St), vegetative meristem (Me), glands (Gl), mature leaves (Lv), cones without glands (Co), and a mélange of plant tissues collected throughout the whole growing season (WGS).

We identified two gene groups regarding the expression profile (Figure 5). The first encompassed constitutive genes: two SEP (*HIMADS03* and *HIMADS04*), two TM8 (*HIMADS09* and *HIMADS18*), two AGL6-like (*HIMADS07* and *HIMADS33*), one of the C/D (AG) subfamily (*HIMADS32*), and three type-I  $\alpha$  (*HIMADS25*, *HIMADS47*, and *HIMADS54*). The second group included 20 genes (9 type-I and 11 MIKC<sup>c</sup>) that showed variable expression among the samples. The B (AP3-PI) subfamily member, *HIMADS13*, was expressed in the stem, glands, and cones, whereas four type-I genes (*HIMADS57*, *HIMADS40*, *HIMADS46*, and *HIMADS39*) were expressed only in the whole plant sample. Interestingly, a type-I  $\alpha$  gene, *HIMADS36*, was expressed only in the glands. On the other hand, two C/D(AG) subfamily genes (*HIMADS29* and *HIMADS30*) are in this group, with *HIMADS29*

being expressed in mature leaves and cones, while *HIMADS30* expressed in the bracts and young leaves, similar to *HIMADS31*. Meanwhile, *HIMADS06* (SEP) and *HIMADS08* (AGL6) did not express in bracts or young leaves; *HIMADS28* (AGL6) expressed in the meristem, glands, mature leaf, and cones; *HIMADS12* [A(API-FUL)] expressed in glands, leaf, and cones; *HIMADS24* [B(AP3-PI)] expressed in all samples but cones without glands. In turn, *HIMADS17* (SVP) was expressed in all samples but glands and mature leaves, whereas *HIMADS20* was expressed only in the meristem and mature leaves. Lastly, *HIMADS35* and *HIMADS60* (type-I  $\alpha$ -subfamily) expressed in the stem, meristem, and mature leaves, while *HIMADS60* expressed in cones, and *HIMADS35* did not.

### 3. Discussion

Many MADS-box proteins function as master regulatory transcription factors controlling critical aspects of plant development and agricultural traits. The genomic characterization of this gene family has been carried out for several plant species, such as *Arabidopsis* (107 genes: [50]), rice (75 genes: [51]), grapevine (74 genes: [52]), *Pyrus* (75 genes: [53]), to name a few. This work identified and provided the transcriptional profiling of 65 MADS-box genes in the hop (*H. lupulus* L.) genome. First, we carried out a *de novo* gene annotation of the hop genome and combined it with the official one available on the HopBase platform [54]. This pipeline identified seven novel MADS-box genes (*HIMADS28-33* and *HIMADS65*) in the hop genome with reads from RNAseq libraries aligned on these genes (Figures S2 and S7). Additionally, it was possible to find some genes (i.e., *HIMADS01* and *HLMADS02*) which were only identified when AUGUSTUS was run with the UTR parameters turned off. This finding shows that *de novo* gene prediction outputs, as well as the official functional genome annotation, must be interpreted with caution.

In our phylogenetic analyses, 27 MADS-box proteins were classified into 11 clades based on their relationships with the *Arabidopsis* MIKCC-type and TM8 subfamilies. We discovered that the AGL17 subfamily is not represented in the hop genome, similarly to pears [53]. Neither the FLC subfamily is represented in the hop genome, suggesting that the species lacks the vernalization route completely. Accordingly, it has been demonstrated that hop does not require vernalization to trigger flowering [45], but instead, the process must involve other induction routes, such as photoperiod and age [46].

According to the photoperiod route in *Arabidopsis*, SOC1 integrates photoperiod signals to promote flowering under long-day conditions [55]. It was possible that in hop, a functional homolog was similarly involved in flowering induction. However, no SOC1 ortholog was identified in our gene prediction pipelines. Notwithstanding, the HopBase genome annotation includes a gene (*000453F.g47*) that contains only the K-box domain characteristic of the SOC subfamily. That may be the reason our BlastP analysis using the MADS-box consensus sequence as the query did not identify this gene in the hop proteome. However, the MADS domain for this gene was recognized by AUGUSTUS in the first annotated intron of *000453F.g47*, where RNA-Seq reads aligned (Figure S2). This gene displays two exons and encodes a protein with the MADS domain but without the K-box, suggesting that it was incorrectly annotated or may undergo intron retention, which is the most predominant mechanism of alternative splicing in plants [56]. Moreover, two SVP subfamily genes were identified in the hop genome, with *HIMADS17* expressed in young leaves only, indicating potential participation in leaf development and expansion. Finally, two AGL15 subfamily genes (*HIMADS19* and *HIMADS20*) were identified, with the latter expressed in mature leaves and the meristem. In hop, these genes could act as repressors of flowering transition since members of this subfamily act as flowering repressors in *Arabidopsis* [57] and promote the expression of miR156, a *bona fide* marker of plant juvenility [58].

Our phylogenetic study also identified two API-FUL subfamily genes (*HIMADS11* and *HIMADS12*) in the hop genome. In *Arabidopsis*, API determines floral meristem identity and, later, also in petal and sepal development [32,59]. The expression of *HIMADS12* in hop cones suggests a possible participation in determining floral organ identity (Figure 5).

Even though female flowers of hop (cones or strobiles) entirely lack the perianth (sepals and petals), male flowers have sepals [60], thus showing that the A function of the ABC model of flower development is present in hop. Another hypothesis for the lack of perianth structures in female hop flowers could be a lack of the E-class (SEP subfamily) function. However, this subfamily is the most represented within the MIKCC clade in this species, with five genes expressed in different tissues (Figure 5). The repression mechanism of the A- and B-functions in the first two whorls during cone development remain to be ascertained. Figure 1 shows the B-class *HIMADS13* was closest to AP3 while *HIMADS24* was closest to PI. These genes showed distinct gene structures, with *HIMADS24* being longer than *HIMADS13*, containing an extra exon (Figure 3), and lacking the K-box (Figure 4). When comparing GO terms between *HIMADS13* and *HIMADS24* (Table S3), both displayed the same terms, results which are comparable for the *Arabidopsis* AP3 and PI. Therefore, it is plausible that the B-function in hop is conserved during flower development.

Dioecious reproduction is a common feature found in the Cannabaceae, including *Cannabis* and *Humulus*. The organ positions in male (staminate) and female (pistillate) hop flowers deviate from the prevalent four-whorl scheme (sepals-petals-stamens-carpels) observed in many angiosperm groups [60]. After the shoot meristem undergoes flowering transition, the formation of floral organs is initiated. Male and female inflorescence meristems are distinguishable at the anatomical level very early on [60], when the program of floral organ developmental fate has already been decided. According to the classic ABC model, also known as the ABCDE model, the expression of class A and C genes are mutually exclusive in the floral meristem [30]. Three C/D-class genes were identified in the hop genome (Figure 1). The presence of sepals in the first of the two whorls of the male flower suggests a partial presence of the A-class function. In contrast, the development of stamens in the second whorl reveals the expression of B and C class genes and repression of the class A gene function. On the other hand, in female flowers (cones), the formation of a rudimentary perianth (without the development of sepals or petals) indicates an absence of ABC gene expression. In contrast, the development of two carpels in its second whorl indicates the exclusive expression of the C function. Finally, *HIMADS29* probably carries out the D-class function because it is expressed in the cones (Figure 5) and its gene annotation is associated with ovule development (GO:0048481). A more refined definition of gene expression within the developing flower and functional analyses to define the role of ABCDE genes are warranted to better understand the genetics of floral organ development in this species.

The 36 type-I MADS-box genes identified in the hop genome were classified into three subfamilies,  $\alpha$  (26 genes),  $\beta$  (9), and  $\gamma$  (1). These genes were more structurally diverse but contained fewer exons than the type-II genes (Figure 3). Previous research reported similar results in other species [50,53,61]. The amino acid sequence in this group was also more diverse than in the type-II group, and the MADS-box was not detected in some analyses for three members of the  $\beta$ -subfamily (*HIMADS55*, *HIMADS56*, and *HIMADS57*), although they were present when manually inspected (Figure S4). The MADS motif is somewhat divergent in these three proteins and required a higher sensitivity from the sequence analysis tool. According to the gene expression profile, 12 type-I *MADS-box* were expressed in the RNA-Seq libraries analyzed, with *HIMADS57* the only member of the  $\beta$ -subfamily to be expressed. Interestingly, *HIMADS36* was exclusively expressed in all three gland samples analyzed (Figure S5), which allowed us to hypothesize that it may coordinate the biosynthesis of resin and specialized metabolites [62] or participate in gland development. Therefore, it is important to further verify the exact timing expression domain and function of *HIMADS36*. Moreover, *HIMADS36* is associated with a GO term (0045944) involved in multiple processes related to transcriptional induction of genes related to the metabolism of organic compounds. Overall, our findings provide perspectives on functional analyses and breeding of hop.

## 4. Materials and Methods

### 4.1. Gene Prediction

*H. lupulus* L. gene prediction was performed using AUGUSTUS version 3.3.3 [63]. RNA-seq libraries retrieved from the NCBI's SRA database guided the proper identification of exon-intron gene boundaries (Table S2; accessed on 7 January 2020). After quality evaluation with FastQC, the libraries were processed with Trimmomatic v.0.39 [64] to remove adapter sequences and fragments with poor overall Phred quality. High-quality libraries were then aligned to the *H. lupulus* L. masked genome sequence from the HopBase platform [54] (accessed on 7 January 2020) using HISAT2 v.2.1 [65]. During the training phase to establish AUGUSTUS metaparameters for the species, RNA-seq libraries from glands, leaf, cones without glands, and meristem (SRR575195, SRR10589377, SRR575201, SRR10320794, respectively) were assembled using Trinity v.2.11.0 [66]. Candidate coding regions were identified with TransDecoder v.5.5.0 [47]. Subsequently, protein sequences were generated and utilized to train AUGUSTUS according to Alternate protocol 1 [67]. The training was also enriched with EST and UTR coordinates utilizing coding sequences from Transdecoder and the PASA pipeline [68]. Sorted BAM files were used to generate exon (with Bam2wig) and intron hints. Finally, the trained metaparameters were fed into AUGUSTUS for gene prediction.

### 4.2. Identification of MADS-Box Genes in the Hop Genome

We used the Basic Local Alignment Search Tool BLAST v.2.11.0 [69] to scan the hop proteome searching for MADS-box proteins. A conserved domain sequence from Serum Response Factor (SRF) retrieved from the Pfam database (<http://pfam.xfam.org/>, accessed on 14 May 2021) was used as a query in BlastP against proteins obtained previously in the gene prediction step. In parallel, BlastP was carried out against the hop proteome retrieved from the HopBase platform. We only considered MADS-box proteins with sequences presenting a conserved domain with all three Pfam, SMART, and NCBI-BlastP analyses. Redundant proteins reported on the same locus were combined after manually curating genomic loci with IGV. Putative MADS-box protein sequences with less than 100 amino acid residues were re-submitted to AUGUSTUS, with UTR parameters turned off, until new sequences were no longer retrieved. Each non-redundant, putative MADS-box protein sequence identified in these analyses was named HIMADS01 to 65. Their physicochemical properties (length of amino acid sequence, molecular weight, and isoelectric point) were determined with the ExPASy Proteomics tool (<https://web.expasy.org/protparam/>, accessed on 14 May 2021).

### 4.3. Phylogenetic Analysis

MADS-box protein sequences retrieved from species spanning the plant kingdom (*Chlamydomonas reinhardtii*, *Physcomitrella patens*, *Selaginella moellendorffii*, *Piceaabies*, *Sorghum bicolor*, *Oryza sativa*, *Cucumis sativus*, *Malus domestica*, *Medicago truncatula*, and *Vitis vinifera*) were retrieved from the PlantTFDB database v.5.0 [70] along with those from *Arabidopsis thaliana* and *Solanum lycopersicum* retrieved from the NCBI database, along with those from *H. lupulus* identified above, were used in our phylogenetic analysis. For sequence types I, MIKC<sup>c</sup>, and MIKC<sup>\*</sup>, multiple sequence alignment jobs were performed separately with MAFFT v.7.475 [71]. The alignment quality was evaluated with GUIDANCE 2 v.2.02 [72]. Both steps used default parameters. Phylogenetic trees were inferred with PHYLIP v.3.696 [73] with 1000 bootstrap replicates, using the Jones-Taylor-Thornton matrix and neighbor-joining method [74]. Finally, the tree was visualized with FigTree, and the hop MADS-box proteins were classified into subgroups according to the *Arabidopsis* MADS-box subfamilies [50] plus the subfamily TM8 first reported in tomato [4]. When a subfamily was absent in a first search, tBLASTn was performed using the protein sequence from *Arabidopsis* of that subfamily as the query.

#### 4.4. MADS-Box Gene Structure and Conserved Protein Motif Analyses in Hop

The exon-intron structures of MADS-box genes were identified with the Gene Structure Display Server GSDS2.0 [75] using the GFF files generated from our gene prediction as well as the annotation available at the HopBase. The MEME suite online analysis tool [76] was used to identify putative motifs of hop MADS-box proteins with the following parameters: maximum of 20 motifs to be identified and motif width between 6 and 60. In this case, we used sequences from *Chlamydomonas reinhardtii*, *Physcomitrella patens*, *Selaginella moellendorffii*, *Picea abies*, *Sorghum bicolor*, *Oryza sativa*, *Cucumis sativus*, *Malus domestica*, *Medicago truncatula*, and *Vitis vinifera*, as background normalization. Finally, the conserved motifs obtained were verified with PFAM, SMART, and NCBI conserved domain inference tools.

#### 4.5. Gene Ontology (GO) Annotation of the Hop MADS-Box Genes

The MADS-box genes of hop were annotated into each of the three categories of Gene Ontology (GO: biological process, molecular function, and cellular component) using the Blast2GO software [77], and the results were visualized with WEGO [78].

#### 4.6. Expression Analysis of MADS-Box Genes in Hop Tissues

Gene transcription profiling of hop MADS-box genes was generated with NCBI-SRA RNA-seq libraries of meristems (SRR10320793), stems (SRR10320795), leaves (SRR575205), young leaves (ERR2040411), cones without glands (SRR575201), bracts (SRR10541757), glands (SRR575193), and a sample of the whole plant during the growing season (SRR4242068). The data were aligned to the hop masked genome sequence with STAR v.2.7.7 [79] using default parameters. The number of aligned reads was quantified with the htseq-count function in HTseq v.0.11.5 [80] assuming no strand specificity. The quantified reads were normalized as FPKM (Fragments Per Kilobase of transcript per Million mapped reads) with the edgeR package. Finally, a heatmap of MADS-box gene expression was generated in R v.3.6.3 using the gplots package. To corroborate these results, we used Samtoolsto filter all reads uniquely mapped to the genome. Subsequently, each locus was visualized with IGV, and the alignments for selected genes are reported in Figure S7.

## 5. Conclusions

In this work, we identified 65 MADS-box genes in the hop genome, with 36 being of type I and 29 genes of type II. Phylogenetic analyses showed that 27 type-II MADS-box genes belonged to 12 subfamilies, while two genes were of type MIKC\*. Meanwhile, type-I MADS-box genes were classified in  $\alpha$ -subfamily (26 members),  $\beta$ -subfamily (nine members), and  $\gamma$ -subfamily (a single member). The gene structure of type-I genes was less complex than that of type II genes, with fewer exons, even though the longest MADS-box gene was of type I. Some MIKC<sup>C</sup>-type MADS-box proteins did not display the K-box domain. Members of the FLC subfamily were not found in the hop genome. The only SOC1 subfamily member in the hop genome may undergo alternative splicing with intron retention. Genes of the ABCDE model of flower development were expressed in cones. One gene, a member of the  $\alpha$ -subfamily, was found exclusively expressed in lupulin glands, with potential implications for specialized metabolism. Thus, this work contributes to understanding the evolutionary history of MADS-box in hop and provides perspectives on functional analysis and crop breeding.

**Supplementary Materials:** The following supporting information can be downloaded at: <https://www.mdpi.com/article/10.3390/plants11091237/s1>, Table S1: MADS-box genes identified in the hop genome. Table S2: RNA-seq libraries used to guide AUGUSTUS gene prediction and transcriptional profiling. Table S3: Gene Ontology terms of the hop MADS-box gene family. Figure S1: Phylogenetic tree of MIKC\*-type MADS-box proteins of *H. lupulus* (2, in red font), *Arabidopsis* (6, in black font). Figure S2: RNA-Seq reads aligned on the gene *000453F.g47*. Figure S3: Motif distribution of type-I MADS-box proteins in hop. Protein sequences are represented by black lines, and the conserved motifs are represented by colored boxes. Figure S4: Motif distribution of hop  $\beta$ -subfamily MADS-box proteins. Protein sequences are represented by black lines, and the conserved motifs are represented by colored boxes. (A) Logo of MADS-box domain. (B): Motif distribution of the hop  $\beta$ -subfamily MADS-box proteins. (C) Amino acid residues within MADS-box domains. Figure S5: Expression profile of the hop MADS-box genes in three RNA-Seq libraries from cones, leaves, and glands. Figure S6: Gene Ontology classification of MADS-box genes in hop and *Arabidopsis*. Figure S7: RNAseq reads that are uniquely mapped on six novel MADS-box genes (HIMADS28-33).

**Author Contributions:** R.R.d.O. and A.C.-J. conceptualized the project. R.M.G. conducted the analyses of the data. T.H.C.R. supported the bioinformatics analyses. T.H.C.R., R.R.d.O. and A.C.-J. supervised the project. R.M.G., R.R.d.O., V.A.B. and A.C.-J. discussed data analyses and results. R.M.G. wrote the first version of the manuscript. R.R.d.O., V.A.B. and A.C.-J. revised and contributed to the writing of the manuscript's final version. All authors have read and agreed to the published version of the manuscript.

**Funding:** Student scholarship was funded by CNPq (grant 149043/2019-8). The Laboratory of Plant Molecular Physiology (LFMP) is partially supported by the Instituto Brasileiro de Ciência e Tecnologia do Café (INCT/Café), Coordenação de Aperfeiçoamento de Pessoal de Nível Superior (CAPES), and Conselho Nacional de Desenvolvimento Científico e Tecnológico (CNPq).

**Institutional Review Board Statement:** Not applicable.

**Informed Consent Statement:** Not applicable.

**Data Availability Statement:** Main data supporting the findings of this study are available in the manuscript and online supplementary materials. The raw data used for the analyses and figures are available upon request to A.C.-J.

**Acknowledgments:** The authors thank the Federal University of Lavras (UFLA/Brazil) and the members of the Laboratory of Plant Molecular Physiology (LFMP, UFLA/Brazil) for structural support of the experiments and data analyses; Léo Rufato (Universidade do Estado de Santa Catarina, UDESC) is thanked for the corrections and suggestions provided in a preliminary version of the manuscript; the Instituto Brasileiro de Ciência e Tecnologia do Café (INCT/Café), Coordenação de Aperfeiçoamento de Pessoal de Nível Superior (CAPES) and Conselho Nacional de Desenvolvimento Científico e Tecnológico (CNPq) are acknowledged for financial support.

**Conflicts of Interest:** The authors declare no conflict of interest and that the funders had no role in the design of the study, data collection, analyses, interpretation, writing of the manuscript, or in the decision to publish the work.

## References

1. Riechmann, J.L.; Krizek, B.A.; Meyerowitz, E.M. Dimerization Specificity of Arabidopsis MADS Domain Homeotic Proteins APETALA1, APETALA3, PISTILLATA, and AGAMOUS. *Proc. Natl. Acad. Sci. USA* **1996**, *93*, 4793–4798. [[CrossRef](#)] [[PubMed](#)]
2. Becker, A.; Theissen, G. The Major Clades of MADS-Box Genes and Their Role in the Development and Evolution of Flowering Plants. *Mol. Phylogenet. Evol.* **2003**, *29*, 464–489. [[CrossRef](#)]
3. Smaczniak, C.; Immink, R.G.H.; Angenent, G.C.; Kaufmann, K. Developmental and Evolutionary Diversity of Plant MADS-Domain Factors: Insights from Recent Studies. *Development* **2012**, *139*, 3081–3098. [[CrossRef](#)] [[PubMed](#)]
4. Daminato, M.; Masiero, S.; Resentini, F.; Lovisetto, A.; Casadoro, G. Characterization of TM8, a MADS-Box Gene Expressed in Tomato Flowers. *BMC Plant Biol.* **2014**, *14*, 319. [[CrossRef](#)]
5. da Silveira Falavigna, V.; Severing, E.; Lai, X.; Estevan, J.; Farrera, I.; Hugouvieux, V.; Revers, L.F.; Zubieta, C.; Coupland, G.; Costes, E.; et al. Unraveling the Role of MADS Transcription Factor Complexes in Apple Tree Dormancy. *New Phytol.* **2021**, *232*, 2071–2088. [[CrossRef](#)]
6. Li, G.; Kuijter, H.N.J.; Yang, X.; Liu, H.; Shen, C.; Shi, J.; Betts, N.; Tucker, M.R.; Liang, W.; Waugh, R.; et al. MADS1 Maintains Barley Spike Morphology at High Ambient Temperatures. *Nat. Plants* **2021**, *7*, 1093–1107. [[CrossRef](#)]

7. Gómez-Soto, D.; Ramos-Sánchez, J.M.; Alique, D.; Conde, D.; Triozzi, P.M.; Perales, M.; Allona, I. Overexpression of a SOC1-Related Gene Promotes Bud Break in Ecodormant Poplars. *Front. Plant Sci.* **2021**, *12*, 670497. [[CrossRef](#)]
8. Ayra, L.; Reyero-Saavedra, M.d.R.; Isidra-Arellano, M.C.; Lozano, L.; Ramírez, M.; Leija, A.; Fuentes, S.-I.; Girard, L.; Valdés-López, O.; Hernández, G. Control of the Rhizobia Nitrogen-Fixing Symbiosis by Common Bean MADS-Domain/AGL Transcription Factors. *Front. Plant Sci.* **2021**, *12*, 1061. [[CrossRef](#)]
9. Hyun, Y.; Richter, R.; Vincent, C.; Martínez-Gallegos, R.; Porri, A.; Coupland, G. Multi-Layered Regulation of SPL15 and Cooperation with SOC1 Integrate Endogenous Flowering Pathways at the Arabidopsis Shoot Meristem. *Dev. Cell* **2016**, *37*, 254–266. [[CrossRef](#)]
10. Immink, R.G.H.; Posé, D.; Ferrario, S.; Ott, F.; Kaufmann, K.; Valentim, F.L.; de Folter, S.; van der Wal, F.; van Dijk, A.D.J.; Schmid, M.; et al. Characterization of SOC1's Central Role in Flowering by the Identification of Its Upstream and Downstream Regulators. *Plant Physiol.* **2012**, *160*, 433–449. [[CrossRef](#)]
11. Lee, J.; Lee, I. Regulation and Function of SOC1, a Flowering Pathway Integrator. *J. Exp. Bot.* **2010**, *61*, 2247–2254. [[CrossRef](#)] [[PubMed](#)]
12. Liu, C.; Chen, H.; Er, H.L.; Soo, H.M.; Kumar, P.P.; Han, J.-H.; Liou, Y.C.; Yu, H. Direct Interaction of AGL24 and SOC1 Integrates Flowering Signals in Arabidopsis. *Dev. Camb. Engl.* **2008**, *135*, 1481–1491. [[CrossRef](#)] [[PubMed](#)]
13. Torti, S.; Fornara, F. AGL24 Acts in Concert with SOC1 and FUL during Arabidopsis Floral Transition. *Plant Signal. Behav.* **2012**, *7*, 1251–1254. [[CrossRef](#)] [[PubMed](#)]
14. Hartmann, U.; Höhmann, S.; Nettesheim, K.; Wisman, E.; Saedler, H.; Huijser, P. Molecular Cloning of SVP: A Negative Regulator of the Floral Transition in Arabidopsis. *Plant J.* **2000**, *21*, 351–360. [[CrossRef](#)]
15. Michaels, S.D.; Amasino, R.M. Flowering Locus C Encodes a Novel MADS Domain Protein That Acts as a Repressor of Flowering. *Plant Cell* **1999**, *11*, 949–956. [[CrossRef](#)]
16. Mateos, J.L.; Madrigal, P.; Tsuda, K.; Rawat, V.; Richter, R.; Romera-Branchat, M.; Fornara, F.; Schneeberger, K.; Krajewski, P.; Coupland, G. Combinatorial Activities of Short Vegetative Phase and Flowering Locus C Define Distinct Modes of Flowering Regulation in Arabidopsis. *Genome Biol.* **2015**, *16*, 31. [[CrossRef](#)]
17. Madrid, E.; Chandler, J.W.; Coupland, G. Gene Regulatory Networks Controlled by FLOWERING LOCUS C That Confer Variation in Seasonal Flowering and Life History. *J. Exp. Bot.* **2021**, *72*, 4–14. [[CrossRef](#)]
18. Kim, D.-H.; Doyle, M.R.; Sung, S.; Amasino, R.M. Vernalization: Winter and the Timing of Flowering in Plants. *Annu. Rev. Cell Dev. Biol.* **2009**, *25*, 277–299. [[CrossRef](#)]
19. Reeves, P.A.; He, Y.; Schmitz, R.J.; Amasino, R.M.; Panella, L.W.; Richards, C.M. Evolutionary Conservation of the FLOWERING LOCUS C-Mediated Vernalization Response: Evidence from the Sugar Beet (*Beta Vulgaris*). *Genetics* **2007**, *176*, 295–307. [[CrossRef](#)]
20. Ruelens, P.; de Maagd, R.A.; Proost, S.; Theißen, G.; Geuten, K.; Kaufmann, K. Flowering Locus C in Monocots and the Tandem Origin of Angiosperm-Specific MADS-Box Genes. *Nat. Commun.* **2013**, *4*, 2280. [[CrossRef](#)]
21. Kagaya, H.; Ito, N.; Shibuya, T.; Komori, S.; Kato, K.; Kanayama, Y. Characterization of FLOWERING LOCUS C Homologs in Apple as a Model for Fruit Trees. *Int. J. Mol. Sci.* **2020**, *21*, 4562. [[CrossRef](#)] [[PubMed](#)]
22. de Oliveira, R.R.; Cesarino, I.; Mazzafera, P.; Dornelas, M.C. Flower Development in *Coffea arabica* L.: New Insights into MADS-Box Genes. *Plant Reprod.* **2014**, *27*, 79–94. [[CrossRef](#)] [[PubMed](#)]
23. Calderwood, A.; Lloyd, A.; Hepworth, J.; Tudor, E.H.; Jones, D.M.; Woodhouse, S.; Bilham, L.; Chinoy, C.; Williams, K.; Corke, F.; et al. Total FLC Transcript Dynamics from Divergent Parologue Expression Explains Flowering Diversity in Brassica Napus. *New Phytol.* **2021**, *229*, 3534–3548. [[CrossRef](#)] [[PubMed](#)]
24. Kennedy, A.; Geuten, K. The Role of Flowering Locus C Relatives in Cereals. *Front. Plant Sci.* **2020**, *11*, 617340. [[CrossRef](#)]
25. Sharma, N.; Ruelens, P.; D'hauw, M.; Maggen, T.; Dochy, N.; Torfs, S.; Kaufmann, K.; Rohde, A.; Geuten, K. A Flowering Locus C Homolog Is a Vernalization-Regulated Repressor in Brachypodium and Is Cold Regulated in Wheat. *Plant Physiol.* **2017**, *173*, 1301–1315. [[CrossRef](#)]
26. Ma, H.; dePamphilis, C. The ABCs of Floral Evolution. *Cell* **2000**, *101*, 5–8. [[CrossRef](#)]
27. Bowman, J.L.; Smyth, D.R.; Meyerowitz, E.M. Genes Directing Flower Development in Arabidopsis. *Plant Cell* **1989**, *1*, 37–52. [[CrossRef](#)]
28. Benedito, V.A.; Visser, P.B.; van Tuyl, J.M.; Angenent, G.C.; de Vries, S.C.; Krens, F.A. Ectopic Expression of LLAG1, an Agamous Homologue from Lily (*Lilium longiflorum* Thunb.) Causes Floral Homeotic Modifications in Arabidopsis. *J. Exp. Bot.* **2004**, *55*, 1391–1399. [[CrossRef](#)]
29. Thomson, B.; Wellmer, F. Chapter Eight—Molecular Regulation of Flower Development. In *Current Topics in Developmental Biology*; Grossniklaus, U., Ed.; Plant Development and Evolution; Academic Press: Cambridge, MA, USA, 2019; Volume 131, pp. 185–210.
30. Coen, E.S.; Meyerowitz, E.M. The War of the Whorls: Genetic Interactions Controlling Flower Development. *Nature* **1991**, *353*, 31–37. [[CrossRef](#)]
31. Theißen, G.; Saedler, H. Floral Quartets. *Nature* **2001**, *409*, 469–471. [[CrossRef](#)]
32. Irish, V.F.; Sussex, I.M. Function of the Apetala-1 Gene during Arabidopsis Floral Development. *Plant Cell* **1990**, *2*, 741–753. [[PubMed](#)]
33. Goto, K.; Meyerowitz, E.M. Function and Regulation of the Arabidopsis Floral Homeotic Gene Pistillata. *Genes Dev.* **1994**, *8*, 1548–1560. [[CrossRef](#)] [[PubMed](#)]

34. Jack, T.; Brockman, L.L.; Meyerowitz, E.M. The Homeotic Gene APETALA3 of Arabidopsis Thaliana Encodes a MADS Box and Is Expressed in Petals and Stamens. *Cell* **1992**, *68*, 683–697. [[CrossRef](#)]
35. Yanofsky, M.F.; Ma, H.; Bowman, J.L.; Drews, G.N.; Feldmann, K.A.; Meyerowitz, E.M. The Protein Encoded by the Arabidopsis Homeotic Gene Agamous Resembles Transcription Factors. *Nature* **1990**, *346*, 35–39. [[CrossRef](#)]
36. Savidge, B.; Rounsley, S.D.; Yanofsky, M.F. Temporal Relationship between the Transcription of Two Arabidopsis MADS Box Genes and the Floral Organ Identity Genes. *Plant Cell* **1995**, *7*, 721–733. [[CrossRef](#)] [[PubMed](#)]
37. Pelaz, S.; Ditta, G.S.; Baumann, E.; Wisman, E.; Yanofsky, M.F. B and C Floral Organ Identity Functions Require SEPALLATA MADS-Box Genes. *Nature* **2000**, *405*, 200–203. [[CrossRef](#)] [[PubMed](#)]
38. Kyozuka, J.; Kobayashi, T.; Morita, M.; Shimamoto, K. Spatially and Temporally Regulated Expression of Rice MADS Box Genes with Similarity to Arabidopsis Class A, B and C Genes. *Plant Cell Physiol.* **2000**, *41*, 710–718. [[CrossRef](#)]
39. Wu, F.; Shi, X.; Lin, X.; Liu, Y.; Chong, K.; Theißen, G.; Meng, Z. The ABCs of Flower Development: Mutational Analysis of AP1/FUL-like Genes in Rice Provides Evidence for a Homeotic (A)-Function in Grasses. *Plant J.* **2017**, *89*, 310–324. [[CrossRef](#)]
40. Kuijter, H.N.J.; Shirley, N.J.; Khor, S.F.; Shi, J.; Schwerdt, J.; Zhang, D.; Li, G.; Burton, R.A. Transcript Profiling of MIKCC MADS-Box Genes Reveals Conserved and Novel Roles in Barley Inflorescence Development. *Front. Plant Sci.* **2021**, *12*, 1834. [[CrossRef](#)]
41. Chi, Y.; Huang, F.; Liu, H.; Yang, S.; Yu, D. An APETALA1-like Gene of Soybean Regulates Flowering Time and Specifies Floral Organs. *J. Plant Physiol.* **2011**, *168*, 2251–2259. [[CrossRef](#)]
42. Huang, F.; Xu, G.; Chi, Y.; Liu, H.; Xue, Q.; Zhao, T.; Gai, J.; Yu, D. A Soybean MADS-Box Protein Modulates Floral Organ Numbers, Petal Identity and Sterility. *BMC Plant Biol.* **2014**, *14*, 89. [[CrossRef](#)] [[PubMed](#)]
43. Song, J.; Clemens, J.; Jameson, P.E. Expression of Floral Identity Genes in Cilianthus Maximus during Mass Inflorescence Abortion and Floral Development. *Ann. Bot.* **2011**, *107*, 1501–1509. [[CrossRef](#)] [[PubMed](#)]
44. Masiero, S.; Colombo, L.; Grini, P.E.; Schnittger, A.; Kater, M.M. The Emerging Importance of Type I MADS Box Transcription Factors for Plant Reproduction. *Plant Cell* **2011**, *23*, 865–872. [[CrossRef](#)] [[PubMed](#)]
45. Bauerle, W.L. Disentangling Photoperiod from Hop Vernalization and Dormancy for Global Production and Speed Breeding. *Sci. Rep.* **2019**, *9*, 16003. [[CrossRef](#)]
46. Thomas, G.G.; Schwabe, W.W. Factors Controlling Flowering in the Hop (*Humulus lupulus* L.). *Ann. Bot.* **1969**, *33*, 781–793. [[CrossRef](#)]
47. Benkherouf, A.Y.; Logrén, N.; Somborac, T.; Kortesiemi, M.; Soini, S.L.; Yang, B.; Salo-Ahen, O.M.H.; Laaksonen, O.; Uusi-Oukari, M. Hops Compounds Modulatory Effects and 6-Prenylningenin Dual Mode of Action on GABAA Receptors. *Eur. J. Pharmacol.* **2020**, *873*, 172962. [[CrossRef](#)]
48. Jiang, C.-H.; Sun, T.-L.; Xiang, D.-X.; Wei, S.-S.; Li, W.-Q. Anticancer Activity and Mechanism of Xanthohumol: A Prenylated Flavonoid From Hops (*Humulus lupulus* L.). *Front. Pharmacol.* **2018**, *9*, 530. [[CrossRef](#)]
49. Yamashita, M.; Fukizawa, S.; Nonaka, Y. Hop-Derived Prenylflavonoid Isoxanthohumol Suppresses Insulin Resistance by Changing the Intestinal Microbiota and Suppressing Chronic Inflammation in High Fat Diet-Fed Mice. *Eur. Rev. Med. Pharmacol. Sci.* **2020**, *24*, 1537–1547. [[CrossRef](#)]
50. Parenicová, L.; de Folter, S.; Kieffer, M.; Horner, D.S.; Favalli, C.; Busscher, J.; Cook, H.E.; Ingram, R.M.; Kater, M.M.; Davies, B.; et al. Molecular and Phylogenetic Analyses of the Complete MADS-Box Transcription Factor Family in Arabidopsis: New Openings to the MADS World. *Plant Cell* **2003**, *15*, 1538–1551. [[CrossRef](#)]
51. Arora, R.; Agarwal, P.; Ray, S.; Singh, A.K.; Singh, V.P.; Tyagi, A.K.; Kapoor, S. MADS-Box Gene Family in Rice: Genome-Wide Identification, Organization and Expression Profiling during Reproductive Development and Stress. *BMC Genom.* **2007**, *8*, 242. [[CrossRef](#)]
52. Grimplet, J.; Martínez-Zapater, J.M.; Carmona, M.J. Structural and Functional Annotation of the MADS-Box Transcription Factor Family in Grapevine. *BMC Genom.* **2016**, *17*, 80. [[CrossRef](#)] [[PubMed](#)]
53. Meng, D.; Cao, Y.; Chen, T.; Abdullah, M.; Jin, Q.; Fan, H.; Lin, Y.; Cai, Y. Evolution and Functional Divergence of MADS-Box Genes in Pyrus. *Sci. Rep.* **2019**, *9*, 1266. [[CrossRef](#)] [[PubMed](#)]
54. Hill, S.T.; Sudarsanam, R.; Henning, J.; Hendrix, D. HopBase: A Unified Resource for Humulus Genomics. *Database* **2017**, *2017*, bax009. [[CrossRef](#)]
55. Jung, J.-H.; Ju, Y.; Seo, P.J.; Lee, J.-H.; Park, C.-M. The SOC1-SPL Module Integrates Photoperiod and Gibberellic Acid Signals to Control Flowering Time in Arabidopsis. *Plant J.* **2012**, *69*, 577–588. [[CrossRef](#)] [[PubMed](#)]
56. Ullah, F.; Hamilton, M.; Reddy, A.S.N.; Ben-Hur, A. Exploring the Relationship between Intron Retention and Chromatin Accessibility in Plants. *BMC Genom.* **2018**, *19*, 21. [[CrossRef](#)]
57. Adamczyk, B.J.; Lehti-Shiu, M.D.; Fernandez, D.E. The MADS Domain Factors AGL15 and AGL18 Act Redundantly as Repressors of the Floral Transition in Arabidopsis. *Plant J. Cell Mol. Biol.* **2007**, *50*, 1007–1019. [[CrossRef](#)]
58. Serivichyaswat, P.; Ryu, H.-S.; Kim, W.; Kim, S.; Chung, K.S.; Kim, J.J.; Ahn, J.H. Expression of the Floral Repressor MiRNA156 Is Positively Regulated by the AGAMOUS-like Proteins AGL15 and AGL18. *Mol. Cells* **2015**, *38*, 259–266. [[CrossRef](#)]
59. Gustafson-Brown, C.; Savidge, B.; Yanofsky, M.F. Regulation of the Arabidopsis Floral Homeotic Gene APETALA1. *Cell* **1994**, *76*, 131–143. [[CrossRef](#)]
60. Shephard, H.L.; Parker, J.S.; Darby, P.; Ainsworth, C.C. Sexual Development and Sex Chromosomes in Hop. *New Phytol.* **2000**, *148*, 397–411. [[CrossRef](#)]

61. Zhang, L.; Zhao, J.; Feng, C.; Liu, M.; Wang, J.; Hu, Y. Genome-Wide Identification, Characterization of the MADS-Box Gene Family in Chinese Jujube and Their Involvement in Flower Development. *Sci. Rep.* **2017**, *7*, 1025. [[CrossRef](#)]
62. Okada, Y.; Ito, K. Cloning and Analysis of Valerophenone Synthase Gene Expressed Specifically in Lupulin Gland of Hop (*Humulus lupulus* L.). *Biosci. Biotechnol. Biochem.* **2001**, *65*, 150–155. [[CrossRef](#)] [[PubMed](#)]
63. Stanke, M.; Diekhans, M.; Baertsch, R.; Haussler, D. Using Native and Syntenically Mapped CDNA Alignments to Improve de Novo Gene Finding. *Bioinformatics* **2008**, *24*, 637–644. [[CrossRef](#)] [[PubMed](#)]
64. Bolger, A.M.; Lohse, M.; Usadel, B. Trimmomatic: A Flexible Trimmer for Illumina Sequence Data. *Bioinformatics* **2014**, *30*, 2114–2120. [[CrossRef](#)] [[PubMed](#)]
65. Pertea, M.; Kim, D.; Pertea, G.M.; Leek, J.T.; Salzberg, S.L. Transcript-Level Expression Analysis of RNA-Seq Experiments with HISAT, StringTie and Ballgown. *Nat. Protoc.* **2016**, *11*, 1650–1667. [[CrossRef](#)]
66. Haas, B.J.; Papanicolaou, A.; Yassour, M.; Grabherr, M.; Blood, P.D.; Bowden, J.; Couger, M.B.; Eccles, D.; Li, B.; Lieber, M.; et al. De Novo Transcript Sequence Reconstruction from RNA-Seq Using the Trinity Platform for Reference Generation and Analysis. *Nat. Protoc.* **2013**, *8*, 1494–1512. [[CrossRef](#)] [[PubMed](#)]
67. Hoff, K.J.; Stanke, M. Predicting Genes in Single Genomes with AUGUSTUS. *Curr. Protoc. Bioinform.* **2019**, *65*, e57. [[CrossRef](#)] [[PubMed](#)]
68. Haas, B.J.; Delcher, A.L.; Mount, S.M.; Wortman, J.R.; Smith, R.K.; Hannick, L.I.; Maiti, R.; Ronning, C.M.; Rusch, D.B.; Town, C.D.; et al. Improving the Arabidopsis Genome Annotation Using Maximal Transcript Alignment Assemblies. *Nucleic Acids Res.* **2003**, *31*, 5654–5666. [[CrossRef](#)]
69. Altschul, S.F.; Madden, T.L.; Schäffer, A.A.; Zhang, J.; Zhang, Z.; Miller, W.; Lipman, D.J. Gapped BLAST and PSI-BLAST: A New Generation of Protein Database Search Programs. *Nucleic Acids Res.* **1997**, *25*, 3389–3402. [[CrossRef](#)]
70. Jin, J.; Zhang, H.; Kong, L.; Gao, G.; Luo, J. PlantTFDB 3.0: A Portal for the Functional and Evolutionary Study of Plant Transcription Factors. *Nucleic Acids Res.* **2014**, *42*, D1182–D1187. [[CrossRef](#)]
71. Katoh, K.; Misawa, K.; Kuma, K.; Miyata, T. MAFFT: A Novel Method for Rapid Multiple Sequence Alignment Based on Fast Fourier Transform. *Nucleic Acids Res.* **2002**, *30*, 3059–3066. [[CrossRef](#)]
72. Sela, I.; Ashkenazy, H.; Katoh, K.; Pupko, T. GUIDANCE2: Accurate Detection of Unreliable Alignment Regions Accounting for the Uncertainty of Multiple Parameters. *Nucleic Acids Res.* **2015**, *43*, W7–W14. [[CrossRef](#)] [[PubMed](#)]
73. Felsenstein, J. PHYLIP—Phylogeny Inference Package (Version 3.2). *Cladistics* **1989**, *5*, 164–166. [[CrossRef](#)]
74. Saitou, N.; Nei, M. The Neighbor-Joining Method: A New Method for Reconstructing Phylogenetic Trees. *Mol. Biol. Evol.* **1987**, *4*, 406–425. [[CrossRef](#)] [[PubMed](#)]
75. Hu, B.; Jin, J.; Guo, A.-Y.; Zhang, H.; Luo, J.; Gao, G. GSDB 2.0: An Upgraded Gene Feature Visualization Server. *Bioinformatics* **2015**, *31*, 1296–1297. [[CrossRef](#)] [[PubMed](#)]
76. Bailey, T.L.; Johnson, J.; Grant, C.E.; Noble, W.S. The MEME Suite. *Nucleic Acids Res.* **2015**, *43*, W39–W49. [[CrossRef](#)] [[PubMed](#)]
77. Conesa, A.; Götz, S.; García-Gómez, J.M.; Terol, J.; Talón, M.; Robles, M. Blast2GO: A Universal Tool for Annotation, Visualization and Analysis in Functional Genomics Research. *Bioinformatics* **2005**, *21*, 3674–3676. [[CrossRef](#)]
78. Ye, J.; Zhang, Y.; Cui, H.; Liu, J.; Wu, Y.; Cheng, Y.; Xu, H.; Huang, X.; Li, S.; Zhou, A.; et al. WEGO 2.0: A Web Tool for Analyzing and Plotting GO Annotations, 2018 Update. *Nucleic Acids Res.* **2018**, *46*, W71–W75. [[CrossRef](#)]
79. Dobin, A.; Davis, C.A.; Schlesinger, F.; Drenkow, J.; Zaleski, C.; Jha, S.; Batut, P.; Chaisson, M.; Gingeras, T.R. STAR: Ultrafast Universal RNA-Seq Aligner. *Bioinformatics* **2013**, *29*, 15–21. [[CrossRef](#)]
80. Anders, S.; Pyl, P.T.; Huber, W. HTSeq—A Python Framework to Work with High-Throughput Sequencing Data. *bioRxiv* **2014**. [[CrossRef](#)]

## Article

# Molecular Systematics of *Valerianella* Mill. (Caprifoliaceae): Challenging the Taxonomic Value of Genetically Controlled Carpological Traits

Itziar Arnelas<sup>1,2,\*</sup>, Ernesto Pérez-Collazos<sup>3,4,†</sup>, Josefa López-Martínez<sup>5,\*</sup>, Juan Antonio Devesa<sup>1,\*</sup> and Pilar Catalán<sup>3,4,\*</sup>

- <sup>1</sup> Departamento de Botánica, Ecología y Fisiología Vegetal, Universidad de Córdoba, E-14071 Córdoba, Spain  
<sup>2</sup> Departamento de Ciencias Biológicas y Agropecuarias, Universidad Técnica Particular de Loja, CP 11-01-608 Loja, Ecuador  
<sup>3</sup> Departamento de Ciencias Agrarias y del Medio Natural, Escuela Politécnica Superior de Huesca, Universidad de Zaragoza, E-22071 Huesca, Spain; ernestop@unizar.es  
<sup>4</sup> Grupo de Bioquímica, Biofísica y Biología Computacional (BIFI, UNIZAR), Unidad Asociada al CSIC, E-50059 Zaragoza, Spain  
<sup>5</sup> Departamento de Biología Vegetal, Ecología y Ciencias de la Tierra, Universidad de Extremadura, E-06006 Badajoz, Spain  
\* Correspondence: iarnelas@utpl.edu.ec (I.A.); josefalopez@unex.es (J.L.-M.); bv1dealj@uco.es (J.A.D.); pcatalan@unizar.es (P.C.)  
† These authors contributed equally to this work.

**Citation:** Arnelas, I.; Pérez-Collazos, E.; López-Martínez, J.; Devesa, J.A.; Catalán, P. Molecular Systematics of *Valerianella* Mill. (Caprifoliaceae): Challenging the Taxonomic Value of Genetically Controlled Carpological Traits. *Plants* **2022**, *11*, 1276. <https://doi.org/10.3390/plants11101276>

Academic Editors: Cássio Van den Berg and Igor Bartish

Received: 27 March 2022

Accepted: 4 May 2022

Published: 10 May 2022

**Publisher's Note:** MDPI stays neutral with regard to jurisdictional claims in published maps and institutional affiliations.



**Copyright:** © 2022 by the authors. Licensee MDPI, Basel, Switzerland. This article is an open access article distributed under the terms and conditions of the Creative Commons Attribution (CC BY) license (<https://creativecommons.org/licenses/by/4.0/>).

**Abstract:** *Valerianella* (cornsalad) is a taxonomically complex genus formed by 50–65 annual Holarctic species classified into at least four main sections. Carpological traits (sizes and shapes of achenes and calyx teeth) have been used to characterize its sections and species. However, the potential systematic value of these traits at different taxonomic ranks (from sections to species (and infraspecific taxa)) has not been tested phylogenetically yet. Here, we have assessed the evolutionary systematic value of *Valerianella* diagnostic carpological traits at different hierarchical ranks and have demonstrated their ability to separate taxa at the sectional level but not at species level for species of several species pairs. A total of 426 individuals (17 species, 4 sections) of *Valerianella* were analyzed using AFLP and plastid data. Genetic clusters, phylogenetic trees, and haplotype networks support the taxonomic classification of *Valerianella* at the four studied sectional levels (*V. sects. Valerianella, Cornigerae, Coronatae, Platycoelae*) but show admixture for ten taxa from five species pairs (*V. locusta*—*V. carinata*, *V. coronata*—*V. pumila*, *V. multidentata*—*V. discoidea*, *V. dentata*—*V. ramosa*, *V. eriocarpa*—*V. microcarpa*), which are not reciprocally monophyletic. Dating analyses indicate that the *Valerianella* sections are relatively old (mid-Miocene), while most species diverged in the Pliocene–Pleistocene. A new section *Valerianella* sect. *Stipitae* is described to accommodate the highly divergent and taxonomically distinct *V. fusiformis* type species. Taxonomic treatments that recognize the sectional ranks and that subsume the separate species of each species pair into single species represent a natural classification for *Valerianella*.

**Keywords:** AFLP; carpological traits; genetic structure; phylogeny; molecular systematics; plastid phylogeny; taxonomy; *Valerianaceae*

## 1. Introduction

Molecular systematics has revolutionized the taxonomic circumscriptions of many plant groups. Genetically supported phylogenies have provided evolutionary frameworks for a natural classification of the angiosperms and for a critical revision of some morphological traits used to identify species and other taxonomic ranks [1]. The cornsalad genus *Valerianella* Mill. comprises 50 [2,3] to 65 species [4] distributed mainly in the temperate regions of the northern hemisphere and classified into at least four main sections [2]. Many

of them (c. 39) are present in the Mediterranean region, a probable center of origin of the genus [5]. Up to 11 species have been recorded from the Western Mediterranean region [6], including some of the taxonomically most complex groups of closely related species pair aggregates with a specific genetic control system in their diagnostic fruit characters [7,8]. In Flora Europaea, the classification of the separate *Valerianella* species from each of these species pairs was based solely on a few carpological features, such as inflated vs. uninflated sterile locules of the achene and the presence vs. absence (or sizes) of the calyx teeth [9], while the other reproductive and vegetative traits of the species were the same. The discovery of the genetic regulatory mechanism of the fruit morphotype led some taxonomists to postulate that these phenotypes resulted from the co-segregation of alleles that did not represent a speciation process and, therefore, the two taxa of each species pair should be treated as the same species [6,10].

*Valerianella* taxa are annual, self-pollinating plants displaying small flowers with slightly colored corollas, little or no scent, low pollen production, and most likely no nectar [8,11]. Species recognition has traditionally been based on fruit characteristics, as flowers are similar across taxa. In contrast, fruits are highly polymorphic, and both homocarpny and heterocarpny (the production of two or more types of fruit by the same individual) have been detected between and within several taxa [6–8,10–14]. Furthermore, fruit polymorphism can occur within populations, where each individual plant produces only one type of fruit but two or more fruit morphotypes are present within populations [7]. The fruits have three locules, one fertile and two sterile, with unequal development in the different species, which can sometimes culminate in a more or less developed, persistent calyx [6,15–17]. Fruit traits have been used as the main diagnostic features for the delineation of sectional boundaries in the genus and for the description of infrageneric taxa [2,6,10,15,16,18–25].

Although fruit morphology is a diagnostic character of indisputable value in the taxonomy of *Valerianella*, its use alone in the circumscription of new taxa has given rise to several uncertainties [9] and the description of spurious taxa (e.g., *V. cupulifera* Legrand). Martin and Mathez [8], in a pioneer genetic study of Mediterranean species of *Valerianella*, detected the existence of a genetically controlled fruit polymorphism system that caused the coexistence in the same population of individuals with two different types of fruits. A similar fruit morphotype genetic regulatory system was found in other self-pollinating genera of the Valerianoideae (e.g., *Fedia*, [26]) and was also attributed to some American *Valerianella* [7] and *Plectritis* [27] taxa.

Inheritance patterns of fruit morphotype deduced for the *V. coronata*–*V. pumila* complex was also suspected to be found in other species pair groups of Mediterranean *Valerianella* species, namely in *V. locusta*–*V. carinata* and *V. dentata*–*V. rimosa* [6,8,10]. Based on these hypotheses and the observed occurrence of the different species pairs in sympatric areas, Devesa et al. [10] and Devesa and López [6] proposed new specific re-circumscriptions of these groups. Therefore, *V. coronata* and *V. pumila*, previously treated as separate species, were classified as two forms of *V. coronata* within *V. sect. Coronatae*, *V. locusta* and *V. carinata* as two forms of *V. locusta* subsp. *locusta* within *V. sect. Valerianella*, and *V. dentata* and *V. rimosa* as two forms of *V. dentata* within *V. sect. Platycocelae*.

The phylogenetic studies conducted on the Valerianoideae have demonstrated that the diploid *Valerianella* and its derived allotetraploid *Fedia* taxa form a monophyletic group within a large paraphyletic lineage of *Valeriana* [5,28–32]. Evolutionary analyses within *Valerianella* have shown the close relationships between the genotypes of some of the species pairs mentioned [33,34], indirectly supporting their respective common ancestors and the convenience of classifying them at the infraspecific level within each group, leading to the new taxonomic treatment proposed for *V. locusta*, *V. coronata*, and *V. dentata* by [6,10]. However, exhaustive population-level evolutionary studies within and between these *Valerianella* species pair complexes and other related taxa have yet to be conducted, questioning how widespread the genetic regulatory mechanism of the *Valerianella* fruit morphotype might be across different taxonomic ranks and time scales and whether it might have affected speciation processes within these complexes. Conserved

plastid DNA sequences have provided useful information to reconstruct the evolutionary history of the Valerianoideae and their lineages [5,28,29,31,32,35–37]. Highly variable nuclear AFLP markers have proven their value in characterizing the genetic structure and relationships of many plant groups [38,39] and, in particular, among representatives of the Valerianoideae [33,34,40].

In order to reconstruct the genetic and evolutionary relationships between the populations of five *Valerianella* species pairs within a large suprageneric phylogenetic framework and to investigate the phylogenetic value of the diagnostic carpological traits of the *Valerianella* sections and species (Table 1) and the number of times that the mechanism of genetic regulation of fruit morphotype has evolved along *Valerianella* lineages, we have performed a large evolutionary and population genetic study of *Valerianella* species based on plastid *trnT-L* and *trnL-F* DNA sequences and nuclear AFLP data. Our study aimed to: (i) reconstruct the evolutionary relationships of *Valerianella* species and sections, using plastid data from a representative sample of Western Mediterranean and American taxa; (ii) estimate the times of divergence and origins of its main lineages; (iii) analyze genetic relationships and the role of genetic isolation in shaping the morphological differentiation of populations; (iv) elucidate the systematic value of carpological traits in sectional and specific taxonomic ranks; and (v) evaluate the evolution of the inheritance system of the fruit–calyx morphotype both at the population level and at the species level of the *Valerianella* species pairs studied. Our approach is based on the assumption that if the diagnostic carpological traits that taxonomically separate species from each species pair are exclusively controlled by co-segregating genotypes of two linked loci, sympatric populations of the two morphs would be genetically and evolutionarily closer to each other than populations of the same morph that are geographically separated. Conversely, if the diagnostic carpological features that characterize each species derive from the expression of other genes, similar morphotypes from distant populations would share a common ancestor, thus representing a single speciation event.

**Table 1.** A summary of the carpological diagnostic features characterizing the four main sections of *Valerianella* (*V.* sects. *Cornigerae*, *Coronatae*, *Platycoelae*, and *Valerianella*) and the newly described *V.* sect. *Stipitae* analyzed in this study.

<i>Valerianella</i> Sections and Species	Fruit Diversity	Calix Shape	Achene Type and Shape	Achene Compression	Spongy Tissue in Fertile and Sterile Cavities of Achene
<i>Coronatae</i> <i>V. coronata</i> <i>V. discoidea</i> <i>V. multidentata</i> <i>V. pumila</i>	Homocarpous plant	Persistent in the fruit, forming a toothed crown with hooked teeth, a trilobulated disk, or a narrow-toothed ring	Monomorphic or dimorphic, not fusiform, not stipitate	Not (strongly) laterally compressed	Not developed
<i>Cornigerae</i> <i>V. echinata</i>	Heterocarpous plant	Persistent in the fruit, formed by 3 teeth, all of them horn-shaped	Only dimorphic, not fusiform, not stipitate	Not (strongly) laterally compressed	Well developed
<i>Platycoelae</i> <i>V. eriocarpa</i> <i>V. dentata</i> <i>V. microcarpa</i> <i>V. rimosa</i>	Homocarpous plant	Persistent in the fruit, forming a toothed crown with unhooked teeth, an entire tongue, toothed or denticulate, or a truncated cylinder with a tooth	Monomorphic or dimorphic, not fusiform, not stipitate	Not (strongly) laterally compressed	Not developed
<i>Stipitae</i> <i>V. fusiformis</i>	Homocarpous plant	Not persistent in the fruit	Only monomorphic, fusiform, stipitate	Not (strongly) laterally compressed	Not developed
<i>Valerianella</i> <i>V. carinata</i> <i>V. locusta</i> <i>V. lusitanica</i>	Homocarpous plant	Not persistent in the fruit, or formed by 3 small teeth, one of them horn-shaped	Monomorphic or dimorphic, not fusiform, not stipitate	(Strongly) laterally compressed	Not developed/ well developed

## 2. Results

### 2.1. Phylogeny of *Valerianella* Based on Plastid Data

To test our evolutionary hypotheses, we reconstructed a largely sectional and population-level sampled phylogeny of *Valerianella sensu lato* (diploid *Valerianella* clade plus its derived allotetraploid *Fedia* lineage) using 51 individuals from the Western Mediterranean and American regions corresponding to 16 *Valerianella* species, which covered the four main sections of the genus, and two species of *Fedia* (Figure 1, Table S1). Maximum likelihood (ML) phylogenetic analysis and Bayesian phylogenetic dating (BEAST) analysis of the plastid *trnL-F* and *trnT-L* data (Table S1) were performed using also sequences of the close core Valerianoideae *Centranthus*, *Valeriana*, and *Plectritis* and of less related Dipsacales *Nardostachys*, *Patrinia*, and *Triplostegia* species as outgroups (Table S1; see Section 4).

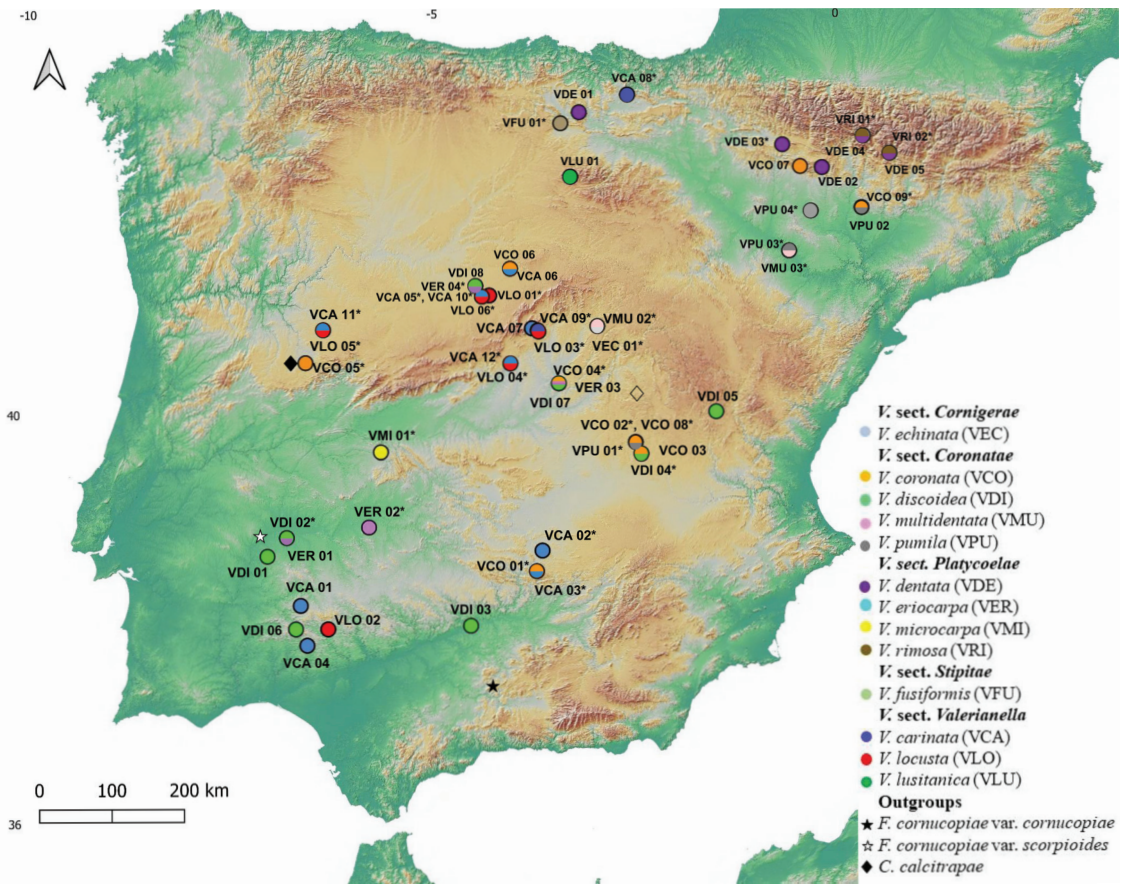


**Figure 1.** Geographical distributions of the studied populations of the *Valerianella* species, *Fedia cornucopiae* var. *cornucopiae* (white star) and var. *scorpioides* (black star) and *Centranthus calcitrapae* (diamonds) in the Iberian Peninsula. Color codes of *Valerianella* species are indicated in the chart.

Optimal ML (Figures 2 and S1) and Maximum Clade Credibility (MCC) BEAST (Figure 3) phylogenetic trees based on *trnL-F* data only, and the best ML tree (Figure S2A,B) based on *trnT-L* + *trnL-F* combined data, retrieved highly supported and consistent topologies for the major *Valerianella* lineages. Both ML and BEAST *trnL-F* trees showed the early split of *V. fusiformis*, traditionally classified within *V. sect. Platycolae*, from the rest (0.99 posterior probability support (PPS); 100% bootstrap support (BS)), followed by the strongly to well-supported divergences of the *Valerianella* + *Fedia* clade (0.99 PPS; 100% BS), which

in turn showed the split of the sister FCV (*Fedia* and *V.* sects. *Cornigerae* + *Valerianella*) (0.97 PPS; 94% BS) and PC (*V.* sects. *Platycoelae* + *Coronatae*) (0.99 PPS; 72% BS) subclades (Figures 2, S1 and S2). The better-rooted ML and BEAST *trnL-F* topology recovered the early split of *V. fusiformis*, traditionally classified within *V.* sect. *Platycoelae*, from the rest (0.99 PPS) (Figures 2, 3 and S1), while the ML *trnT-L* + *trnL-F* tree placed it as a sister to the PC clade but with less support (72% BS; Figure S2B). Within the FCV clade, the BEAST and ML analyses recovered a sister relationship for the *Fedia* and *V.* sect. *Cornigerae* + *Valerianella* lineages (0.97 PPS, 94% BS), followed by the split of the *V.* sect. *Cornigerae* (*V. echinata*) and *V.* sect. *Valerianella* lineages (0.99 PPS, 98% BS) (Figures 2, S1 and S2). The strongly supported *V.* sect. *Valerianella* clade (0.99 PPS, 100% BS) showed mixed resolution of samples from the species pair *V. carinata* and *V. locusta* (and its close taxon *V. lusitanica*, also treated as a subspecies of *V. locusta*; [6,10]). The two topologies supported the divergence of the sister lineages V1 and V2 (0.99, 0.78 PPS; 89%, 98% BS), the first containing samples of *V. carinata* and *V. lusitanica* from the W Iberian Peninsula and the second showing the well to poorly supported splits of *V. carinata* and *V. locusta* samples from the NW, Central, and NE Iberian Peninsula (Figures 2, S1 and S2). Within the PC clade, the two analyses revealed a strongly supported sister relationship for the *V.* sect. *Platycoelae* (0.93 PPS; 100% BS) and *V.* sect. *Coronatae* (0.98 PPS; 100% BS) clades. *Valerianella* sect. *Platycoelae* in turn was divided into Old World (0.98 PPS; 100% BS) and New World (American *V. florifera* / (*V. amarella*, *V. radiata*) species) (0.99 PPS; 100% BS) well-supported clades. The Old World clade consisted of two sister lineages of strongly supported species pairs, the *V. microcarpa*–*V. eriocarpa* (0.99 PPS; 98% BS) and *V. dentata*–*V. ramosa* (0.99 PPS; 100% BS) clades. Although less largely sampled, both clades showed an admixture of species samples from each pair in each group (Figures 2, S1 and S2). *Valerianella* sect. *Coronatae* included two other species pair sister lineages, the *V. coronata*–*V. pumila* (0.99 PPS; 100% BS) clade with strong support and the *V. discoidea*–*V. multidentata* (0.66 PPS; 97% BS) clade with relatively good support. These lineages also showed the admixture of samples from each of the two species of each pair (Figures 2, S1 and S2). The topology of the combined *trnT-L* + *trnL-F* ML tree (Figure S2A,B) was similar to that of the ML and BEAST *trnL-F* trees, except for the position of *V. fusiformis*. In the *trnT-L* + *trnL-F* ML tree, this lineage was resolved as sister to the *V.* sects. *Coronatae* + *Platycoelae* clade but with low to moderate support (55% and 72% BS without and with indels, respectively; Figure S2A,B). The exchange position of *V. fusiformis* in the *trnL-F* and *trnT-L* + *trnL-F* trees was caused by homoplasies in the *trnL-F* and *trnT-L* characters (Figures 2, 3 and S2); however, in both analyses, *V. fusiformis* fell apart from its co-sectional *V.* sect. *Platycoelae* taxa and these divergences received high support.

The inspection of the plastid DNA data set (*trnT-L* + *trnL-F*) revealed 36 informative indels for different lineages of the *Valerianella sensu lato* clade and *C. calcitrapae* when they were mapped onto the ML *trnL-F* tree (FCV clade 7, *V.* sect. *Valerianella* 1, PC clade 3, PC clade except *V. multidentata* and *V. discoidea* subclades 1, *V.* sect. *Coronatae* 3, *V.* sect. *Platycoelae* 1, *V. dentata*–*V. ramosa* 1, *V. discoidea*–*V. multidentata* 1, all species except *V.* sect. *Coronatae* 1, *F. cornucopiae* 1, all species except *F. cornucopiae* 7, *F. cornucopiae* + PC clade (except VCO05) + *V. fusiformis* 1, *C. calcitrapae* 2, all species except *C. calcitrapae* 2, *C. calcitrapae* + *F. cornucopiae* + *V. fusiformis* + PC clade 1, *C. calcitrapae* + *F. cornucopiae* + *V.* sect. *Cornigerae* + PC clade 1) (Figure S2B, Table S2).

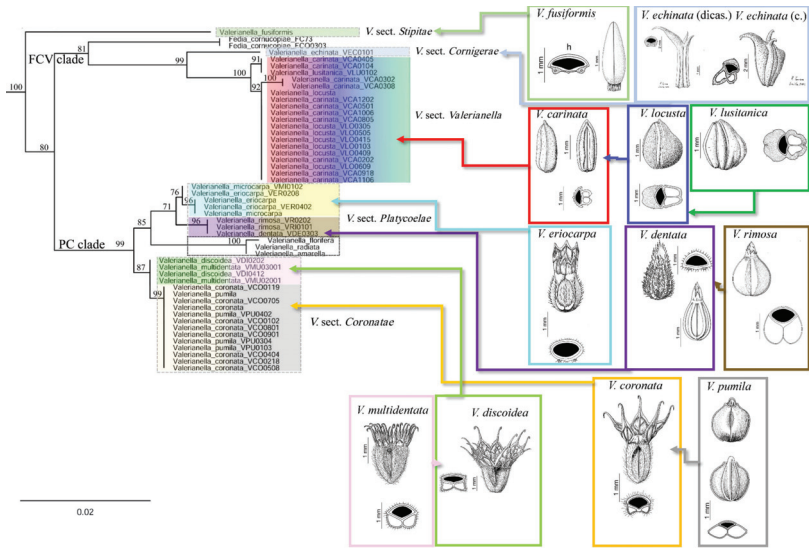


**Figure 2.** Maximum likelihood plastid *trnL*-F tree constructed with IQTREE showing the relationships between the *Valerianella* and *Fedia* species studied. Dipsacaceae sequences were used to root the tree (see Figure S1). FCV (*Fedia* + *V. sect. Valerianella* clade), PC (*V. sect. Platycoclae* + *Coronatae* clade). Numbers on branches indicate UltraFast Bootstrap support (BS) values. The icons show the different types of carpological traits (fruit and vestigial calyx) of the *Valerianella* species studied (reprinted and adapted with permission from Editorial Board from [6], Copyright 2007, Real Jardín Botánico de Madrid-CSIC).

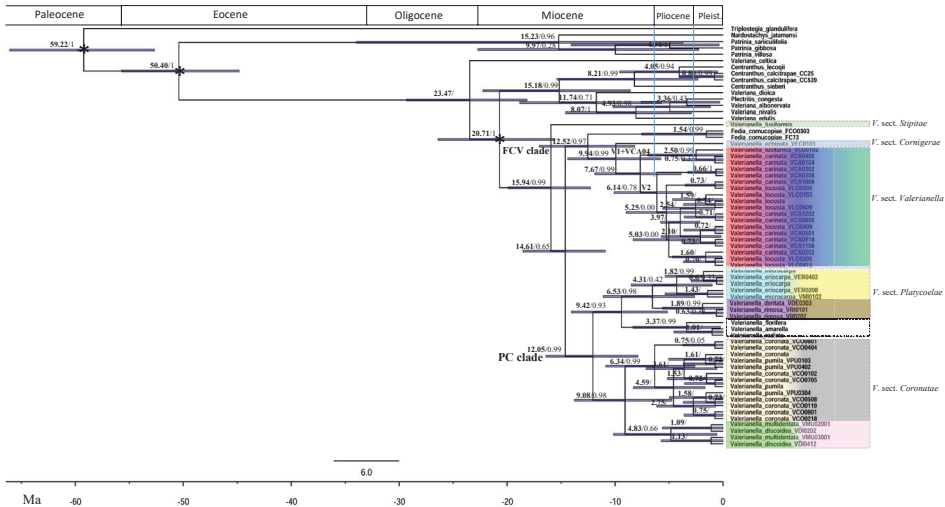


**Figure 3.** BEAST maximum clade credibility (MCC) tree based on *trnL*-F plastid data showing the estimated mean nodal ages of the *Valerianella* and *Fedia cornucopiae* lineages studied. Asterisk represents the imposed calibrations (see text). Numbers above the branches indicate the estimated ages (in bold) and the Bayesian posterior probability support (PPS) values (plain text). Bars represent 95% highest posterior density (HDP) intervals. Main clades: FCV (*Fedia* + *sect. Valerianella*), PC (*sect. Platycoclae* + *sect. Coronatae*).

## 2.2. Divergence Time Estimation of *Valerianella* Lineages

To infer the ages of the different *Valerianella* lineages and the times of origin of the sectional diagnostic carpological traits and fruit morphotypes of species pairs, divergence times for all the MCC BEAST clades were estimated using the Bayesian search and imposing secondary calibrations for the ancestors of Dipsacoideae + Valerianoideae, Valerianoideae, core Valerianoideae (*Plectritis*, *Centranthus*, *Valeriana*, *Valerianella*, and *Fedia*), and *Valerianella* + *Fedia* following [36].

According to the BEAST chronogram, the diversification of the Valerianoideae could have started in the early Miocene at  $20.7 \pm 11.1$  Ma (Figures 3 and S2), and the split of *V. fusiformis*, a species phenotypically distinct from all its congeners (Figure 3, Table 1), from the *Valerianella* + *Fedia* clade could have occurred in the mid-Miocene at  $15.9 \pm 10.7$  Ma. Within the FCV clade, the split of *Fedia* from *Valerianella* sects. *Cornigerae* + *Valerianella* was dated to the mid-Miocene at  $12.5 \pm 8.8$  Ma. These two sections of *Valerianella*, *Cornigerae*, and *Valerianella*, characterized by their unique carpological traits (Table 1), were estimated to have diverged from their common ancestor at  $9.9 \pm 8.6$  Ma, while the diversification of the admixed lineages of *V. sect. Valerianella* (*V. carinata* and *V. locusta*–*V. lusitanica*) was estimated to have occurred in the late Miocene,  $7.6 \pm 7.9$  Ma. The most recent sectional splits date from the late Miocene (e.g., V2,  $6.1 \pm 8$  Ma) to the late Pliocene (e.g., V1,  $2.5 \pm 6.9$  Ma) (Figures 3 and S2).

The origins of the PC clade and the *V. sect. Platycoelae* and *V. sect. Coronatae* subclades, also characterized by their unique carpological features (Table 1), were dated to the mid-late Miocene at  $12.0 \pm 7.6$ ,  $9.4 \pm 8.8$  Ma and  $9.0 \pm 9.0$  Ma, respectively. Diversifications of the phenotypically admixed *V. coronata*–*V. pumila* lineages were estimated to have occurred in the late Miocene ( $6.5 \pm 8.4$  Ma), and those of the also admixed *V. multidentata*–*V. discoidea* and *V. microcarpa*–*V. eriocarpa* lineages in the early Pliocene at  $4.8 \pm 9.6$  Ma and  $4.3 \pm 7.5$  Ma, respectively. North American *Valerianella* species were inferred to have diverged in the mid-Pliocene,  $3.3 \pm 8.0$  Ma (node l), and the admixed *V. dentata*–*V. rimosa* lineages in the Pleistocene ( $1.8 \pm 5.3$  Ma, node n) (Figures 2 and S2).

## 2.3. Plastid Haplotype Network of *Valerianella*

To investigate the extent of maternal haplotype exchange between species of each of the studied *Valerianella* species pairs, we built a plastid haplotype network using concatenated plastid *trnT-L* + *trnL-F* sequences from the more exhaustively studied Western Mediterranean samples (Figure 1; Table S1). The statistical parsimony haplotypic network of *Valerianella* was fully resolved (Figure 4); it showed no internal loops, suggesting the absence of introgressions between these diploid species. The analysis detected a total of 18 haplotypes and the network topology was highly consistent with that of the ML and BEAST plastid trees (Figures 2, 3 and S2). The highly divergent haplotype XVIII, characteristic of *V. fusiformis*, separated by 69 steps from the rest. The network showed the divergences of four main groups within the remaining haplotypes, corresponding to each of the four *Valerianella* sections (Figure 4). Haplotypes of *V. sect. Coronatae* occupied the central part of the network. The most common haplotype, X, was shared by 11 *V. coronata* and *V. pumila* samples, while its derived XI and XII haplotypes were unique to one *V. pumila* and one *V. coronata* sample each. Haplotype XVII, separated from the previous group by eight steps, was shared by four samples of *V. multidentata* and *V. discoidea* (Figure 4). A subnetwork of four *V. sect. Platycoelae* peripheral haplotypes separated from the central haplotypes by 18 steps. Haplotype XVI was shared by three *V. rimosa* and *V. dentata* samples, whereas the remaining three haplotypes were unique to *V. eriocarpa* (XIII, XIV) and *V. microcarpa* (XV) samples (Figure 4). Another peripheral subnetwork of nine *V. sects. Cornigerae* and *Valerianella* haplotypes was separated from the central group by 35 steps. *V. echinata* (*V. sect. Cornigerae*) presented a single haplotype (IX) isolated by 31 steps from those of *V. sect. Valerianella*. Within the latter group, the most frequent haplotype, I, was shared by samples of *V. carinata* and *V. locusta* from the Central Iberian Peninsula, while haplotype

IV (*V. carinata*) was distributed in its NW range and haplotypes VII (*V. carinata*) and VIII (shared by two samples of *V. carinata* and *V. lusitanica*) in its W range (Figure 4).

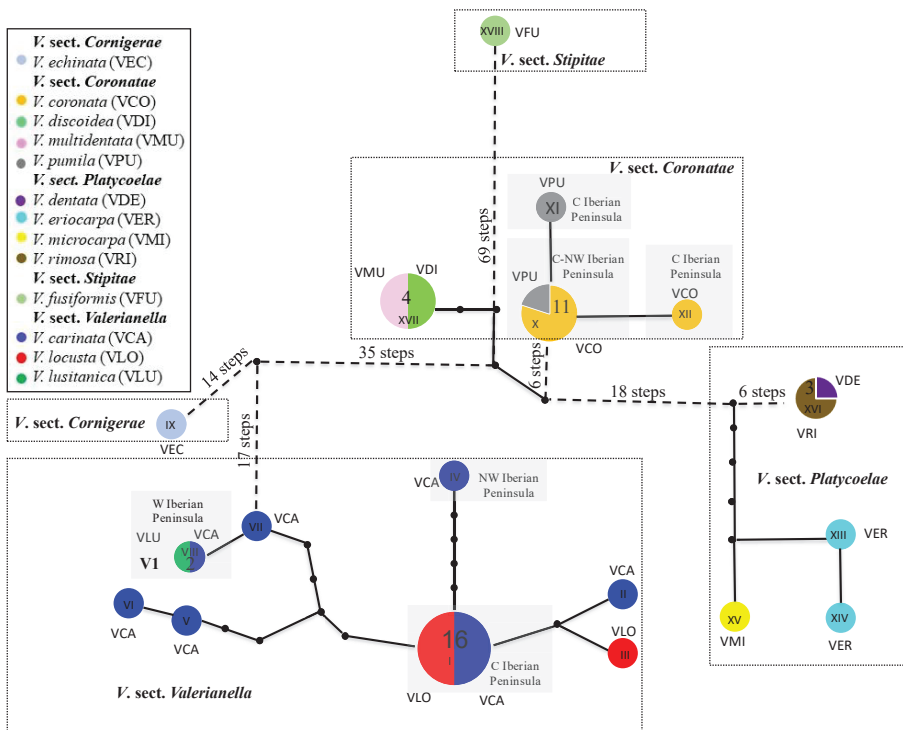


**Figure 4.** *Valerianella* *trnL-F* + *trnT-L* plastid haplotype parsimony network. Mutation steps are represented by dots (numbers of mutation steps are indicated within parentheses). Color codes of *Valerianella* species are indicated in the chart.

#### 2.4. Genetic Diversity and Structure of *Valerianella* Populations

To analyze the genetic structure and diversity of the sections and species pairs of *Valerianella* studied, nuclear AFLP analysis was performed on the most extensively sampled Western Mediterranean populations (Table S1). Two out of the ten AFLP primer-pair combinations (E-ACA/M-CTG and E-ACG/M-CAT) assayed generated 230 reliable bands, of which 221 were polymorphic (96.09%). At the sectional level, the amount of genetic diversity measured by the percentage of polymorphic loci (*PLP*), within species (*hsp*) and among species (*Hsp*) Bayesian diversity, and Nei's genetic diversity (*h*) was relatively equivalent for *V. sect. Valerianella* (*PLP* = 40.7; *Br* = 1.221; *Hsp* = 0.150; *h* = 0.789), *V. sect. Coronatae* (*PLP* = 38.8; *Br* = 1.221; *Hsp* = 0.128; *h* = 0.844), and *V. sect. Platycycoelae* (*PLP* = 24.5; *Br* = 1.176; *Hsp* = 0.165; *h* = 0.603), while the values for *V. sect. Cornigerae* could not be compared with those of the other sections since it only contained a single population (Table 2). Within sections, the genetic diversity parameters of taxa of each species pair were also equivalent when they had similar sample sizes (e.g., *V. carinata* (*PLP* = 55.8; *Br* = 1.267) vs. *V. locusta* (*PLP* = 53.6; *Br* = 1.261); *V. coronata* (*PLP* = 33.9; *Br* = 1.188) vs. *V. pumila* (*PLP* = 38.8; *Br* = 1.186)). In other species, the values varied, although it depended mainly on the size of the sampling (Table 2). Unique AFLP fragments were present in almost all the taxa studied, from one in *V. eriocarpha* to seven in *V. carinata*, although only *V. echinata* presented diagnostic fragments (*fd* = 8), fixed in all individuals of its single population (Table 2). Similar rank values were found in the genetic diversity parameters at a population level for populations of close sizes (Table S3). Almost all populations of

each species pair presented relatively high to very high Nei's  $h$  genetic diversity values (0.650–1.000), except for three populations that were less variable and did not present unique fragments (*V. rimosa* VEC01, 0.415; *V. lusitanica* VLU01, 0.323; *V. echinata* VEC01, 0.048) (Table S3). Analysis of the genetic structure of the Iberian populations of *Valerianella* revealed a higher probability for two genetic groups ( $K = 2$ ), one that includes all *V. sect. Valerianella* populations and the other populations of the remaining sections (Figure 5A). The next best probability was for  $K = 11$  genetic groups showing (i) a single group for *V. sect. Valerianella* (VCA, VLO, VLU); (ii) six groups within *V. sect. Coronatae*, five corresponding to the species pair *V. coronata* (three groups)—*V. pumila* (two, one of them showing admixture between VCO and VPU in some individuals), and one to *V. discoidea* (VDI); (iii) three groups for the *V. sect. Platycoelae* species pair *V. dentata* (one, VDE, plus another group shared with VRI)—*V. rimosa*, and one for *V. eriocarpa* (VER); (iv) one group for *V. sect. Cornigerae* *V. echinata* (VEC) (Figure 5B). Separate Bayesian genetic structure analysis detected genetic substructuring within each section and a few species pairs (Figure S3A–C). Interestingly, the analysis detected three genetic groups within *V. carinata*–*V. locusta* that were geographically structured; a first group joined populations of *V. carinata* from SW-C Spain with *V. lusitanica* (*V. locusta* subsp. *lusitanica*), a second group populations of *V. carinata* from Central and NE Spain, and a third group populations of *V. locusta* from across Spain. Geographical genetic substructuring was also detected within the *V. coronata*–*V. pumila* species pair, with some populations of *V. pumila* from Central Spain grouping together with populations of *V. coronata* from all over Spain, while populations of *V. pumila* from NE Spain were merged into a separate group (Figure S3B,C). In contrast, the genetic structure detected within the *V. dentata*–*V. rimosa* species pair was not connected to geography; a population of *V. dentata* from NE Spain formed a group with two populations of *V. rimosa* from the same site and nearby, while other populations of *V. dentata* from NE Spain formed a second group with a population from N Spain (Figure S3D). Analysis of Molecular Variance (AMOVA) revealed that 70.13% of the variability resided among populations and among taxa and 29.87% within populations.

**Table 2.** Genetic diversity values of the 10 Iberian species of *Valerianella* studied. Number of populations studied ( $N$ ), number of rare fragments ( $fr$ ), number of unique fragments ( $fu$ ), number of diagnostic fragments ( $fd$ ), percentage of polymorphic loci at the 99% criterion ( $P_{99}$ ), percentage of polymorphic loci at the 1% criterion after rarefaction ( $PLP$ ), band richness after rarefaction ( $Br$ ), Bayesian diversity within species ( $h_{Sp}$ ) and between species ( $H_{Sp}$ ), Nei's genetic diversity ( $h$ ).

Taxon	$N$	$fr$	$fu$	$fd$	$P_{99}$	$PLP(6)$	$Br(6)$	$h_{Sp}$	$h$
<b>Sect. <i>Valerianella</i></b>									
<i>V. locusta</i>	6	20	3	0	50.8	53.6	1.261	0.113	0.720
<i>V. carinata</i>	11	25	7	0	47.8	55.8	1.267	0.120	0.752
<i>V. lusitanica</i>	1	0	2	0	16.1	12.9	1.137	0.082	0.323
Sect. <i>Valerianella</i>	18	45	12	0	32.8	40.7	1.221	$H_{Sp} = 0.150$	0.789
<b>Sect. <i>Coronatae</i></b>									
<i>V. coronata</i>	9	12	2	0	37.8	38.8	1.188	0.083	0.707
<i>V. pumila</i>	4	0	2	0	33.0	33.9	1.186	0.087	0.695
<i>V. discoidea</i>	8	0	6	0	42.6	43.8	1.262	0.116	0.805
Sect. <i>Coronatae</i>	21	12	10	0	37.8	38.8	1.212	$H_{Sp} = 0.128$	0.844
<b>Sect. <i>Platycoelae</i></b>									
<i>V. dentata</i>	5	0	3	0	46.5	47.8	1.298	0.132	0.797
<i>V. rimosa</i>	1	0	0	0	14.3	11.6	1.112	0.067	0.415
<i>V. eriocarpa</i>	4	0	1	0	14.8	14.3	1.119	0.067	0.551
Sect. <i>Platycoelae</i>	10	0	4	0	25.2	24.5	1.176	$H_{Sp} = 0.139$	0.835
<b>Sect. <i>Cornigerae</i></b>									
<i>V. echinata</i>	1	0	0	8	6.2	-	1.009	0.058	0.048
Sect. <i>Cornigerae</i>	1	0	0	8	6.2	-	1.009	$H_{Sp} = 0.348$	0.048
Total	50	57	26	8	30.5	-	-	$H_{Sp} = 0.207$	0.892

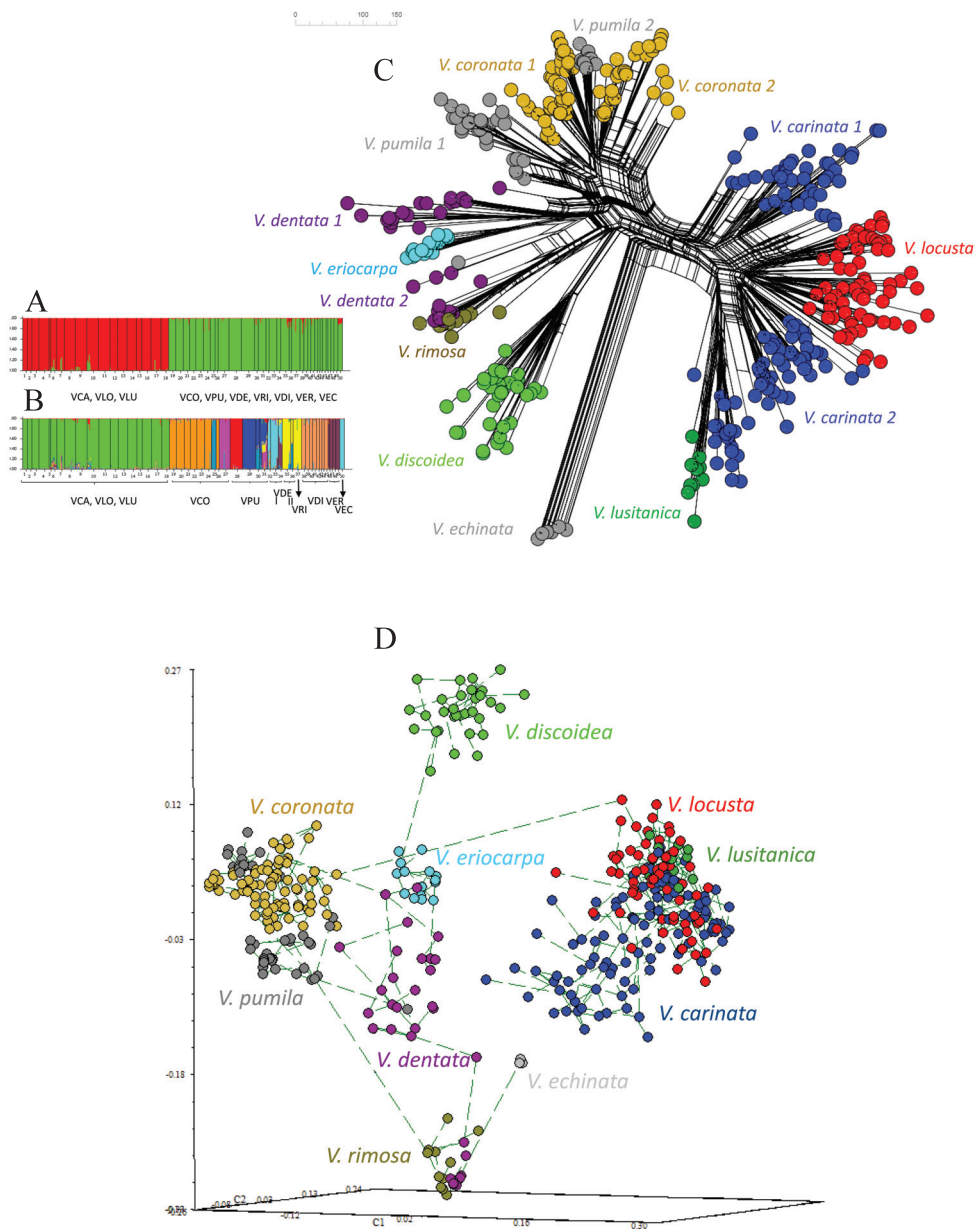


**Figure 5.** Genetic structure and relationships among 414 individuals of the *Valerianella* species studied based on total genomic AFLP data. STRUCTURE Bayesian inference analysis for the best  $K = 2$  (A) and  $K = 10$  (B) hypothetical populations. Neighbor joining network topology (C). Three-dimensional PCoA plot with superimposed MST showing the genetic relationships among the 414 individuals of *Valerianella* (D). *V.* Sect. *Valerianella* (*V. carinata* (VCA), *V. locusta* (VLO), *V. lusitanica* (VLU)); *V.* sect. *Coronatae* (*V. coronata* (VCO), *V. pumila* (VPU), *V. discoidea* (VDI)); *V.* sect. *Platycoelae* (*V. dentata* (VDE), *V. rimosa* (VRI), *V. eriocarpa* (VER)); *V.* sect. *Cornigerae* (*V. echinata* (VEC)). Color codes of *Valerianella* species correspond to those indicated in Figure 1.

### 2.5. Genetic Relationships of Valerianella Populations

To assess our evolutionary hypotheses using nuclear data, we framed the genetic relationships between Iberian populations of *Valerianella* through neighbor joining network (NJ network) analysis and principal coordinate analysis with Minimum Spanning Tree superimposed on it (PCoA-MST).

The NJ network topology obtained from the analysis of all individuals (Figure 5C) showed high congruence with the plastid tree topology for all four *Valerianella* sections and for their respective species pairs (Figures 2 and 3). The AFLP network showed the isolation of *V. sect. Valerianella* samples from the rest and from the population of *V. echinata* (*V. sect. Cornigerae*) (Figure 5C). Within *V. sect. Coronatae*, *V. discoidea* samples did not cluster close to those of *V. coronata–V. pumila*, while, within *V. sect. Platycoclae*, all sectional samples were closely related to each other, although the *V. dentata–V. rimosa* group also included *V. eriocarpa* (Figures 5C and S3). Independent NJ network analysis of *V. sect. Valerianella* retrieved geographical genetic patterns similar to those observed in the STRUCTURE groups (Figure S3E–G), although it additionally showed the clustering of SW Iberian *V. carinata* populations with *V. lusitanica* and the separation of Central Iberian *V. carinata* populations into two genetic groups, each related to SW–central and to central *V. locusta* populations, respectively (Figure S3E). The independent NJ network relationships inferred for the species pairs *V. coronata–V. pumila* and *V. dentata–V. rimosa* (Figure S3F,G) agreed with the geographical structuring retrieved from the respective genetic structure analyses (Figure S3B–D). The 3D PCoA plot recovered similar genetic relationships for the Iberian *Valerianella* samples as those uncovered by the NJ network topology (Figure 5C), although the MST connected *V. echinata* with the *V. dentata–V. rimosa* group from NE Spain instead of with the *V. sect. Valerianella* group (Figure 5D).

### 2.6. Genetic Divergence and Differentiation of the Sectional Carpological Traits of Valerianella

To test the potential effect of long-term genetic divergence between populations on the morphological variation of *Valerianella* carpological traits, we conducted a distance-based redundant analysis (dbRDA) with randomization. Genetic differentiation between populations, estimated using pairwise  $F_{ST}$  values from AFLP data, was tested against the morphological PCo scores of the populations obtained from a principal coordinate analysis (PCoA) performed with the carpological traits scored as binary characters (Table 1). dbRDA analyses could be only performed at the sectional level, for which up to six diagnostic characters could be analyzed, but not at species pair level due to a lack of sufficient diagnostic traits. The dbRDA results revealed that the genetic divergence of populations explained the morphological differentiation of their sectional carpological traits (57.28% of the variation,  $p = 0.001$ ; Table 3).

**Table 3.** Results of the distance-based redundancy analysis (dbRDA) of the four *Valerianella* sections obtained from the marginal test that tested the correlation between the genetic distances of the populations ( $F_{ST}$ ) (explanatory variable) and the morphological differentiation of the sections based on their diagnostic carpological traits (response variable, see Table 1). Significance of predictors test:  $p < 0.001$  \*\*\*.

dbRDA			
Marginal Test			
Variable	F	p	% Var
$F_{ST}$ (PC1)	65.34	0.001 ***	57.28
$F_{ST}$ (PC2)	1.95	0.258	1.71
$F_{ST}$ (PC3)	0.76	0.521	0.67

### 3. Discussion

#### 3.1. Molecular Systematics Supports the Sectional Classification of *Valerianella* s.l. and the Value of Its Diagnostic Carpological Traits

Our plastid and nuclear phylogenetic analyses have generated congruent topologies and provided a robust evolutionary scenario for the divergence of the *Valerianella* + *Fedia* lineages. The plastid tree and the nuclear network reveal the clear split of the *V.* sects. *Valerianella* + *Cornigerae* and *V.* sects. *Coronatae* + *Platycoelae* clades and also support the isolation of each of the four *Valerianella* sections (Figures 2, 3 and 5). Our more largely sampled plastid topology also recovers the sister relationship of *Fedia* with *V.* sects. *Valerianella* + *Cornigerae* and the nesting of North American *Valerianella* species within its *V.* sect. *Platycoelae* clade (Figures 2 and 3). Our results generally agree with previous evolutionary studies of Valerianaceae [35] and partially disagree with those of *Valerianella* [33,34] and *Valerianella* plus *Fedia* [5]. However, all the studies of valerians and cornsalads coincide in the nesting of the polyploid *Fedia* clade within the large diploid *Valerianella* clade [5,28,30–32,35,36,41], forming a natural group described as subtribe Fediinae Graebn. *sensu* Weberling [42]. The morphological similarities between the two genera refer to their annual habit and type of inflorescence [43] and the genetic polymorphism of the fruit [11,26], while they differ in the presence of three stamens in *Valerianella* and two in *Fedia* [6,44]. Our widely sampled phylogeny of cornsalads allows us to hypothesize that the polyploid ancestor of *Fedia* was probably derived from a diploid ancestor of *V.* sects. *Valerianella* + *Cornigerae* (Figures 2 and 3).

The strong monophyly and isolation revealed for each of the four main sections of *Valerianella* in the ML and Bayesian plastid trees (Figures 2 and 3) and the statistical parsimony haplotypic network (Figure 4) are corroborated with the same topology obtained from a larger sampled population analysis in the nuclear neighbor-net AFLP tree (Figure 5C). The only exception is the more divergent position of *V. discoidea* with respect to its co-sectional *V. coronata*–*V. pumila* group in the AFLP network than in the plastid tree (Figures 2, 3 and 5), although the *V. discoidea*–*V. multidentata* haplotype XVII was also differentiated from haplotypes X, XI, and XII of *V. coronata*–*V. pumila* by 10 steps in the plastid haplotype network (Figure 4). However, these two species pairs of *V.* sect. *Coronatae* resolve as sister lineages with high support in the plastid topologies (Figures 2 and 3).

The four sectional lineages are morphologically differentiated by their unique carpological traits (Figure 2, Table 1), although they also share some fruit features that relate them to each other [6]. Thus, *V.* sect. *Cornigerae*, represented in our study by the circum-Mediterranean species *V. echinata*, has heterocarpic plants and is characterized by its persistent calyx in the fruit, consisting of three well-developed horn-like teeth; in contrast, Mediterranean and Eurasian species of *V.* sect. *Valerianella* are characterized by their laterally compressed achenes and their non-persistent calyx in the fruit or their persistent calyx formed by three small teeth, one of them horn-shaped. Both sections share achenes with well-developed spongy tissue in the fertile and sterile cavities of the fruit, although, in *V.* sect. *Valerianella*, these are not always present (Figure 2, Table 1). The Mediterranean species of *V.* sect. *Coronatae* and the Old and New World species of *V.* sect. *Platycoelae* share a persistent crown-toothed fruit calyx; however, while the crown-toothed fruit has hooked teeth or is replaced by a trilobed disc, or a narrow (toothed) ring in the former group, it consists of unhooked teeth or is replaced by a toothed or denticulate tongue or by a truncated cylinder with a tooth in the second group (Figure 2, Table 1) [6]. Population-level dbRDA tests detected a significant correlation of genetic distances with morphological traits (Table 3); therefore, long-term genetic isolation significantly explains the carpological differentiation of the main sections of *Valerianella*. Dating analysis conducted on the plastid phylogeny estimates that the early *Valerianella* + *Fedia* splits (15.9 Ma, node b; 14.6 Ma, Figure 3) coincided with a global warming event [45]. At that time, a period of increasing seasonality could have occurred in Central Europe and the Mediterranean area, where two major seasonal phases of hot and dry and cold and wet climate date from around 16.3–15.7 and 14.7–14.5 Ma, respectively [45]. Our dating analysis also indicates

that the four main *Valerianella* sectional lineages diverged in the late Miocene (9.9–7.6 Ma; Figure 3). These ages are coincident with a warmer and wetter period characteristic of the Upper Tortonian [46]. These changing climate conditions could have caused the origin of diverse environments, promoting the successful diversification of several herbaceous lineages such as the *Valerianella* sectional ancestors and those of other Mediterranean angiosperms [47]. Evolutionary (Figures 2 and 3) and statistical (Table 3) analyses support the phylogenetic value of the diagnostic carpological traits separating the four monophyletic sections of *Valerianella*.

### 3.2. A New Taxonomic Section of *Valerianella* to Accommodate *V. fusiformis*

One of the *Valerianella* species studied, *V. fusiformis*, did not fit into its putative *V.* sect. *Platycoelae* group [6,10] or in any other major sectional group of *Valerianella* in our plastid topologies (Figures 2, 3 and S1) and haplotypic network (Figure 4). This species, endemic to Northern and Eastern Spain, which grows in therophytic pastures on stony substrates, preferably limestones, was classified within *V.* sect. *Platycoelae* based on its monomorphic fruits with developed sterile cavity and sterile cavities reduced to arched ribs [6]. However, our plastid phylogenies placed it either as an early split within the *Valerianella* + *Fedia* clade based on *trnL-F* data (Figures 2 and 3) or as a separate, early diverging lineage within the *V.* sect. *Coronatae* + *Platycoelae* clade based on combined *trnT-L* + *trnL-F* data (Figure S1). The haplotypic network based on the later data set also showed the isolation of the *V. fusiformis* haplotype XVIII, which was separated by 69 steps from its closest *V.* sect. *Coronatae* haplotypes (Figure 4). Despite the different topological resolutions for *V. fusiformis*, which are caused by homoplasies between the plastid *trnT-L* and *trnL-F* characters, both trees support the placement of *V. fusiformis* outside of the *V.* sect. *Platycoelae* clade, a lineage that includes correctly classified species from the Old and the New Worlds (Figures 2, 3 and S1). Careful inspection of the carpological traits of *V. fusiformis* allows us to separate this species from the other *Valerianella* species based on the unique features of its fruit (Figure 2, Table 1). Due to the taxonomic singularity of the *V. fusiformis* carpological traits and its large phylogenetic divergence from the remaining *Valerianella* sections (Figures 2, 3 and S1), we propose its classification into a newly described *Valerianella* section *Stipitae* (see below).

### 3.3. *Valerianella* Species Pairs Are Constituted by a Single Species with a Genetic Regulatory Mechanism for Different Carpological Traits

In contrast to the strongly supported phylogenetic divergences of *Valerianella* sectional lineages (Figures 1, 2 and S1) and their clear taxonomic differentiation based on several statistically significantly different carpological traits (Figure 2, Table 3), our evolutionary and population-level analyses do not separate the species of each of the studied species pairs of *V.* sects. *Valerianella*, *Coronatae*, and *Platycoelae* as reciprocally monophyletic lineages or genetically diversified groups (Figures 2–5 and S1), despite their distinctive fruiting characteristics (Figure 2; [6,10]). Both the plastid phylogenetic trees plus the haplotypic network and the nuclear AFLP clusters show the mixture of individuals of both species in each of the studied *V. carinata*–*V. locusta* (+ *V. lusitanica*), *V. coronata*–*V. pumila*, and *V. dentata*–*V. ramosa* species pairs (Figures 2–4, 5A–D and S1–S3). Plastid reconstructions also recovered a mix of individuals from both species within the *V. discoidea*–*V. multidentata* and *V. eriocarpa*–*V. microcarpa* species pairs (Figures 2–4 and S1). Furthermore, in the three more extensively studied species pairs (*V. carinata*–*V. locusta* (+*V. lusitanica*), *V. coronata*–*V. pumila*, *V. dentata*–*V. ramosa*), our evolutionary and genetic analyses have detected a geographic structure between the populations of each pair, instead of a taxonomic structure (Figures 2–5, S1, S2A,B and S3A–G). It represents a typical scenario for a single species where isolation-by-distance is the main factor responsible for the divergence of populations, as in many other Mediterranean or North American annual plants (e.g., *Brachypodium distachyon*, [48]; *Arabidopsis thaliana*, [49]; *Mimulus guttatus*, [50]). Within the *V. carinata*–*V. locusta* (+*V. lusitanica*) species pair, three to five genetic groups have been identified in the

STRUCTURE plot and the neighbor network tree, respectively (Figures 5A–C and S3A,E), corresponding to SW Iberian populations of VCA + VLU, Central–S Iberian populations of VCA + VLO, Central Iberian populations of VCA + VLO, and Central Iberian populations of VLO, with individuals from two of the last groups showing admixed genetic profiles between those of the three main STRUCTURE groups. This nuclear genetic profiling pattern fits the plastid haplotypic pattern where individuals of each of the five *V. carinata*–*V. locusta* (+*V. lusitanica*) geographic groups have private haplotypes separated from each other by several steps (Figure 4), except for the Central Iberian VCA and VCO groups that share the most common haplotype I (Figure 4). Within the *V. coronata*–*V. pumila* species pair, two genetic groups have been differentiated in the STRUCTURE and neighbor network analyses (Figures 5A–D and S3C–E), corresponding to Central and NE Iberian populations of VCO+VPU and NE Iberian populations of VPU, which are also partially reflected in their common and private plastid haplotypes (Figure 4). Within the *V. dentata*–*V. rimosa* species pair, two other genetic groups have been differentiated; one of them is formed by two sympatric populations of VDE+VRI from easternmost NE Spain and the other by VDE populations from N and NE Spain (Figures 5B,C and S3D–G), although all the individuals share the same plastid haplotype (Figure 4). The genetic admixture of individuals from different species is only restricted to each of the five *Valerianella* species pairs studied (Figures 2–5, S1 and S2) and not between other *Valerianella* species. It is demonstrated by the fact that sympatric populations of *Valerianella* species, even from the same section but from different species pairs (e.g., *V. pumila* and *V. multidentata*, NE Spain; *V. coronata* and *V. discoidea*, C Spain; Figure 1), do not show mixing between their individuals (Figures 2–5, S1 and S2).

Although our conservative plastid-based age estimates indicate that these *Valerianella* species pairs could have originated as early as the Late Miocene (e.g., *V. carinata*–*V. locusta* (+*V. lusitanica*), 7.6 Ma; *V. coronata*–*V. pumila*, 6.3 Ma), in the Pliocene (e.g., *V. discoidea*–*V. multidentata* 4.8 Ma; *V. eriocarpa*–*V. microcarpa*, 4.3 Ma), or more recently in the Pleistocene (e.g., *V. dentata*–*V. rimosa* 1.8 Ma) (Figure 3), their respective genetic admixtures are not a consequence of the lack of evolutionary time for speciation, since it is accepted that the radiations of most Mediterranean plants occurred during these late Neogene–Pleistocene time periods [51,52]. Their genetic admixture cannot be attributed to recent hybridizations because these *Valerianella* species show a predominant selfing breeding system [8] and homoploid hybrid plant species are known to have speciated until recently [48]. Furthermore, we hypothesize that the high selfing rates shared by the annual *Valerianella* species might have been acquired from their common Late Miocene ancestor (Figure 3). The aridification of the circum-Mediterranean region at the end of the Miocene probably favored the development of annual and biennial self-fertilizing species [53] since, in limited environments with low abundance of pollinators or changes between seasons to provide reproductive assurance, selfing is reproductively more efficient than outbreeding [54]. Similar evolutionary patterns have been suggested for other lineages of annual self-pollinating plants that constitute the majority of the Mediterranean flora [51,53,55]. However, the relatively high to moderate values of genetic diversity detected in some populations of the studied *Valerianella* species pairs are surprising ( $P_{99}$ , *PLP*, *hsp*, *h*; Table 2, Table S3). These values are higher than those detected in populations of other highly self-fertilizing annual plants (e.g., *B. distachyon*, [48]). This could be a consequence of the large population sizes and rapid mutation rate of some of the annual *Valerianella* species and occasional interbreeding between individuals, as indicated for the *V. coronata*–*V. pumila* group, where outcrossing can occur randomly in nature [8]. In contrast, genetic structure is high among populations (70.13%), as previously described for *Valerianella* [34] and expected for self-pollinated plants [56–58], where selfing increases the genetic structure between populations due to the absence of gene flow [59]. The probable existence of a mixed mating system (selfing, crossbreeding) in the *Valerianella* species pairs [8] would explain the balance between the moderate values of genetic diversity and the high genetic structuring of their populations, since complete selfing is extremely rare in nature [60].

The morphological differentiation of the separately recognized species within each of the *Valerianella* species pairs studied is based on only one (presence vs. absence of inflated sterile cavities of the achene) or up to two carpological traits (presence vs. absence of remaining calyx or presence of two calyx shapes in the fruit), while they are similar in the rest of the vegetative and reproductive features [6,10]. Alternative fruit morphotypes of *Valerianella* and *Fedia* species pairs have been shown to be caused by a genetic regulatory mechanism governed by two linked loci [8,26]. Self-pollinating experiments of the two parental *V. coronata* and *V. pumila* individuals and of their cross-bred F1 progeny showed that the fruit shapes of *V. coronata* and *V. pumila* were determined by two codominant alleles at a single locus, and that the two morphs resulted from the expression of different segregating genotypes [8]. Since eventual crosses between both morphotypes can occur spontaneously, they produced an intermediate heterozygous morphotype that other authors misinterpreted as different species (e.g., *V. cupulifera* Legrand, [8]). However, these heterozygous morphotypes are rare and rapidly disappearing from nature as a consequence of the predominant selfing reproductive system of the parental morphotypes. Similarly, self-pollination experiments in di-morphic and tri-morphic populations of *Fedia pallescens* demonstrated that two diallelic loci are linked on the same chromosome in a functional supergene, and that one allele from each locus shows a dominant effect at the heterozygous stage, causing the co-segregation of the two morphs in the populations [26]. Both experiments suggest that the fruit morphotype regulatory system occurs within a single species and that it develops into distinct intraspecific carpological morphs when two segregating genotypes coexist in the same heteromorphic population or when each genotype is present in separate monomorphic populations. Our evolutionary and population genetics analyses of *Valerianella* have demonstrated that this genetic regulatory system of fruit morphotype occurs in all five species pairs studied from three sections of *Valerianella*, *V. sect. Valerianella* (*V. carinata*–*V. locusta* (+ *V. lusitanica*)), *V. sect. Coronatae* (*V. coronata*–*V. pumila*, *V. discoidea*–*V. multidentata*), and *V. sect. Platycoelae* (*V. dentata*–*V. rimosa*, *V. eriocarpa*–*V. microcarpa*) (Figures 1–3 and 5), suggesting that the two linked loci responsible for these carpological traits were likely present in the ancestor of the *Valerianella* + *Fedia* clade. Interestingly, in the studied representative of *V. sect. Cornigerae*, *V. echinata*, the two fruit-bearing forms exist in the same heterocarpic plant; the flowers of the axillary branches have achenes without inflated sterile cavities and a long vestigial calyx, while the flowers of the terminal branches have achenes with inflated sterile cavities and a short remaining calyx (Figure 2; [6]), which suggests that the regulatory mechanism is expressed differently in different parts of the inflorescence. More comprehensive gene expression analyses would be needed to investigate the allelic composition of the two linked loci in the *Valerianella* species pairs studied to confirm their role in determining fruit morphotypes and their inheritance. Taxonomically, the five *Valerianella* species pairs studied must be considered single species. Devesa and López [6,10] treated three of them as a single species and their different fruit morphs as forms of the same species (i.e., *V. locusta* subsp. *locusta* f. *locusta* and f. *carinata*, and *V. lusitanica* as subspecies of *V. locusta*, *V. locusta* subsp. *lusitanica*, although it should probably be considered as a third form, f. *lusitanica*, due to its evolutionary closeness to some populations of *F. carinata* (Figures 2–5 and S2); *V. coronata* f. *coronata* and f. *pumila*; *V. dentata* f. *dentata* and f. *rimosa*). Our study supports an intraspecific taxonomic treatment for the fruit morphotypes of these species pairs of *Valerianella* and also for those of *V. discoidea*–*V. multidentata* and *V. eriocarpa*–*V. microcarpa*, either as forms or as any other infraspecific rank, for a natural classification of cornsalads. Future reproductive and genomic studies of these *Valerianella* species will contribute to a better understanding of the breeding system and the evolution of this economically and ecologically important genus.

### 3.4. Description of *Valerianella* sect. *Stipitae*, sect. *nova*

*Valerianella* sect. *Stipitae* López & Devesa, sect. *nov.*

*Description:* Homocarpic plants presenting monomorphic, stipitated, and fusiform achenes showing a highly developed convex fertile cavity not filled with spongy tissue and

two sterile cavities reduced to arched ribs filled almost completely with spongy tissue, and absence of calyx in the fruit.

*Typus*: *Valerianella fusiformis* Pau in Bol. Soc. Esp. Hist. Nat., 21: 144 (1921) [*Ind. loc.*: “Nieva de Cameros (Logroño), 5 julio 1905”; *lectotypus*: Caroli Pau Herbarium Hispanicum/Nieva de Cameros (Logroño)/5 Julii 1905 (MA 119385), designated here by J. López & J.A. Devesa].

The section is integrated only by *Valerianella fusiformis* Pau. It differs from the rest of the sections by the fusiform and stipitate achenes of the plants (Figure 2; [6]).

#### 4. Materials and Methods

##### 4.1. Population Sampling and DNA Isolation

A total of 414 individual samples were collected from 54 populations of 16 different species of *Valerianella* (13; Figure 1), *Fedia* (2), and the outgroup *Centranthus* (1) throughout the Iberian Peninsula. The number of samples collected per population ranged from 5 (VPU03, VDI03) to 30 (VDE02) depending on the size of the population and the availability of individuals. Sampling was more exhaustive on populations of the three *V. coronata*–*V. pumila*, *V. carinata*–*V. locusta*, and *V. dentata*–*V. ramosa* species pairs, including both sympatric and allopatric populations of one and the other fruit morphotype in each case (Table S1). Total genomic DNA was extracted using the DNAeasy kit (Quiagen). The extracted genomic DNA was quantified in 1% agarose gels by comparing the intensity of the band with a control DNA sample of 100 ng /  $\mu$ L (Invitrogen).

##### 4.2. Plastid DNA Sequence Analysis

The *trnT-L* and *trnL-F* plastid regions were amplified and sequenced in a total of 37 (*trnL-F-trnT-L*) and 43 (*trnL-F*) individuals from 13 representative *Valerianella* species plus 2 from *Fedia cornucopiae* (Table S1) and 2 from *Centranthus calcitrapae* used to root the ML phylogenetic tree. PCR amplification and sequencing were carried out with the external forward/reverse primer–pair combinations “a”/“b” and “c”/“f” for, respectively, the *trnT-L* and *trnL-F* regions [61], following the protocols indicated in [62]. Corrected consensus sequences were aligned with the Clustal X algorithm using Se-AL v.2.0 [63] and manually adjusted. The indels were encoded as binary characters; only those gaps that were unambiguous and potentially informative [64] were added to the corresponding data matrices and used in the statistical parsimony network analysis and maximum likelihood *trnT-L* + *trnL-F* analysis.

Forty samples were selected for phylogenetic, dating, and haplotype network analysis (Table S2). Phylogenetic maximum likelihood analysis of the combined *trnT-L* and *trnL-F* data sets was conducted in IQTREE [65]. We imposed the best-fit nucleotide substitution model (K3Pu+F+I) that was automatically selected by the ModelFinder option of the program [66] according to the Bayesian Information Criterion (BIC). Each search was performed through the automated computation of 20 maximum likelihood (ML) starting trees from 98 alternative randomized maximum parsimony (MP) trees, searching for the best-scoring ML trees and estimating branch support for the best tree from 1000 bootstrap replicates (BS) using the UltraFast Bootstrap option implemented in the software [67,68].

We used the most widely sampled *trnL-F* data set to compute a large Valerianoideae ML tree and to estimate the divergence times of the studied *Valerianella* and allied lineages using BEAST v1.8.0 [69]. For this, we downloaded from GenBank additional sequences of 8 American *Valerianella* species [36] and 5 species of *Valeriana*, 1 of *Plectritis*, 3 of *Centranthus*, 1 of *Nardostachys*, 3 of *Patrinia*, and 1 of *Triplostegia* that were used to root the tree (Table S1; [36,70]). Due to the lack of *Valerianella* fossils, we used secondary calibrations according to the family-wide phylogeny of [36]. The estimated ages for the most recent common ancestors of Caprifoliaceae subfam. Dipsacoideae and subfam. Valerianoideae were set at  $62.48 \pm 3.6$  Ma and  $51.58 \pm 2.9$  Ma, respectively, and those of the core Valerianoideae (*Plectritis*, *Centranthus*, *Valeriana*, *Valerianella*, and *Fedia*) and *Valerianella* + *Fedia* were set at  $20.34 \pm 3.7$  Ma and  $10.71 \pm 2.8$  Ma, respectively (Figure 3). The BEAUti interface was used

to create the BEAST input file using the following parameters: (i) General Time Reversible model with a gamma distribution with four categories of rates and proportion of invariant sites (GTR+I+G), (ii), a relaxed molecular clock model with uncorrelated rates drawn from a log-normal distribution, (iii), a Yule model of evolutionary process with random start to infer the tree topologies, and (iv) an angiosperm molecular evolutionary mutation rate (UCDL) of  $1e-4$  to  $1e-1$  typical of most angiosperms. We used BEAST to infer the topology, branch lengths, and tree node dates. BEAST MCMC chain length analysis was run for 200 million generations, saving data every 1500 generations. We used Tracer v1.6. [71] to evaluate parameter convergence statistics for Effective Sample Size (ESS) values  $>200$ . The maximum clade credibility tree with mean ages and 95% highest posterior probability density (HPD) of nodes was summarized with TreeAnnotator and visualized with FigTree v.1.3.1 [72].

Statistical parsimony haplotype networks of *Valerianella* species were constructed using the combined *trnT-L + trnL-F* plastid data set with TCS v1.2.1 [73], considering gaps as a 5th state, and establishing a maximum connection of 72 steps.

#### 4.3. AFLP Analysis

In total, 414 individuals from 10 species of *Valerianella* were used in the AFLP-based analysis (Table S1). The AFLP procedure followed the protocol of [74]. Briefly, 200 nanograms of the genomic DNA was digested by two restriction enzymes (EcoRI/MseI) and ligated to double-stranded EcoRI and MseI adaptors in successive steps. These fragments were pre-amplified using EcoRI and MseI primers with one selective nucleotide, and then amplified using more specific primers with three selective nucleotides. Products were separated on 6% denatured polyacrylamide gels. Electrophoresis was conducted for two hours at 80 watts. Bands were visualized by silver staining following Bassam et al. (1991). Ten combinations of ECO/MSE primer-pairs were tested in a preliminary assay to select the most informative and reliable primer combinations. Repeatability analysis was performed for each primer-pair combination on a reduced subset of the samples (10) to test consistency in the multilocus profiles obtained.

AFLP bands were scored as present (1) or absent (0). Genetic diversity estimators such as number of rare fragments ( $f_r$ ), unique (exclusive) fragments ( $f_u$ ), and diagnostic ( $f_d$ ) fragments were calculated at species pair, species, and population levels. The fragments were treated as “rare” and “diagnostic” when the frequencies were less than 0.02 or greater than 0.99, respectively [75]. The percentage of polymorphic AFLP fragments was calculated using the TFGPA v.1.3 software [76] at the 1% level ( $P_{99}$ ). The intrapopulation genetic diversity of each taxon was measured from all loci in each data set as band richness after rarefaction ( $B_r$ ), and the percentage of polymorphic loci at 1% level for a standardized sample size ( $PLP$ ) calculated using *Aflpdiv* 1.1 [77]. Bayesian genetic diversity was calculated as the average panmictic heterozygosity within each population ( $hs$ ) and each species ( $hsp$ ), and its average value was estimated between the studied species ( $Hsp$ ) using HICKORY v.1.0.4 [78]. Nei’s (1973) genetic diversity index was calculated for each species and at the population level.

Genetic relationship between individuals was revealed through (i) neighbor joining network analysis conducted on SplitsTree5 [79], and (ii) three-dimensional principal coordinate analysis (PCoA) with a Minimum Spanning Tree (MST, [80,81]) superimposed on the PCoA plots using NTSYSpc v. 2.11a [82]. Neighbor joining network analyses were also performed separately for each *Valerianella* species pair. Neighbor joining clustering based on  $F_{ST}$  statistics obtained from the analysis of molecular variance (AMOVA, [83]) was conducted in MEGA v.5 [84] at the population level.

A Bayesian genetic structure analysis was performed to infer the structure of *Valerianella* samples and their sections, species pairs, and populations using STRUCTURE v.2.2 [85]. We imposed the admixture ancestry model with correlated allele frequencies. We ran the analysis for a range of K values starting from 1 to 50, using a burn-in period and a run length of the Monte Carlo Markov Chain of 75,000 and 150,000 iterations, re-

spectively. Chain convergence was estimated through visual inspection of the posterior values excluding the burn-in. Ten iterations were conducted using the ad hoc parameter  $\Delta K$  of [86] to estimate the rate of change of likelihood values between successive K values, using STRUCTURE HARVESTER [87]. Genetic substructuring within *Valerianella* sections was further assessed through independent analyses of the split data matrices using the same procedures indicated above (for K groups ranging from 1 to the number of analyzed populations plus two).

A distance-based redundancy analysis (dbRDA; [88]) was conducted to examine whether genetic distances could explain the observed morphological differentiation in diagnostic carpological traits of *Valerianella* sections. The dbRDA analysis is a multivariate method that allows testing of the influence of genetic factors on the values of a linearly dependent dissimilarity matrix (in this case, the morphological distance). To perform the dbRDA analysis, we encoded as binary traits the most important morphological qualitative diagnostic characters for the 13 *Valerianella* species studied that belong to each of the four main sections plus the newly described *V. sect. Stipitae* (Table 1). To calculate the phenotypic distance between populations, we used the PCoA function of the ape package [89], which computes the PCo scores of the main axes obtained from the PCoA. The first three PCo component scores of PCoA were used for dbRDA analysis. We calculated pairwise population  $F_{ST}$  distances as genetic data and converted them to a square data set using the prcomp function of the stats package. dbRDA analysis (marginal test) was performed with the R package VEGAN [90] using the capscale function. The statistical significance of the predictors, assigned using multivariate F statistics with 9999 permutations and variance components, was obtained with the anova.cca and RsquareAdj functions. All statistical analyses were performed in R version 3.4.3 [91].

**Supplementary Materials:** The following supporting information can be downloaded at: <https://www.mdpi.com/article/10.3390/plants11101276/s1>, Figure S1: Maximum likelihood plastid *trnL-F* tree constructed with IQTREE showing the relationships between the *Valerianella* and *Fedia* species studied. Dipsacaceae sequences were used to root the tree. FCV (*Fedia* + *V. sect. Valerianella* clade), PC (*V. sects. Platycoclae* + *Coronatae* clade). Numbers on branches indicate UltraFast Bootstrap support (BS) values, Figure S2: Maximum likelihood plastid *trnT-L+trnL-F* tree constructed with IQTREE showing the relationships between the *Valerianella* and *Fedia* species studied. *Centranthus calcitrapae* was used to root the tree. FCV (*Fedia* + *V. sect. Valerianella* clade), PC (*V. sects. Platycoclae* + *Coronatae* clade). Numbers on branches indicate UltraFast Bootstrap support (BS) values. Vertical bars on branches indicate informative *trnT-L+trnL-F* gap positions for the respective lineages (see Table S2), Figure S3: Bayesian genetic structure (STRUCTURE) and relationships (neighbor joining network topology) among individuals of the *Valerianella* species studied based on nuclear AFLP data for three *Valerianella* sections. (A) *V. sect. Valerianella*: *V. carinata* (VCA), *V. locusta* (VLO), *V. lusitanica* (VLU). (B) *V. sect. Coronatae*: *V. coronata* (VCO), *V. pumila* (VPU), *V. discoidea* (VDI). (C) *V. sect. Platycoclae*: *V. dentata* (VDE), *V. ramosa* (VRI), *V. eriocarpa* (VER). Color codes of *Valerianella* species correspond to those indicated in Figure 1, Table S1: List of the *Valerianella*, *Fedia*, and *Centranthus* taxa sampled in the Iberian Peninsula and the outgroups used in the plastid and nuclear AFLP studies. For each entry, the population codes used in AFLP analysis and the localities of origin are indicated. GenBank accession codes in bold correspond to new data generated in this study. Taxonomic classification of *Valerianella* follows [6,91]. Herbaria acronyms: COFC (Córdoba University, Spain), K (Kew Royal Botanic Garden), UNEX (University of Extremadura, Spain), YU (University of Alabama, US), Table S2: Summary of the nucleotide site variation found across the plastid *trnT-L + trnL-F* aligned data matrices of the *Valerianella*, *Fedia*, and *Centranthus* taxa studied, Table S3: Genetic diversity indices calculated from AFLP data of 50 populations of the *Valerianella* species under study. Taxon, population code, number of studied individuals (*N*), number of unique fragments (*fu*), number of diagnostic fragments (*fd*), percentage of polymorphic loci at the 99% criterion (*P99*), Bayesian diversity within population (*hs*), Nei's genetic diversity (*h*).

**Author Contributions:** P.C., J.L.-M. and J.A.D. designed the study. J.L.-M. and J.A.D. collected the samples. J.L.-M. and E.P.-C. developed the experimental work. I.A., E.P.-C., J.L.-M., J.A.D. and P.C. analyzed the data and interpreted the results. I.A., E.P.-C. and P.C. wrote the manuscript. All authors have read and agreed to the published version of the manuscript.

**Funding:** This work has been supported by a Spanish Government grant project CGL005-25122-E to J. A. Devesa, a co-funded Spanish Aragón Government and European Social Fund grant to the University of Zaragoza BIOFLORA research group, and a BBVA Foundation post-doctorate fellowship to E. Pérez-Collazos.

**Institutional Review Board Statement:** Not applicable.

**Informed Consent Statement:** Not applicable.

**Data Availability Statement:** <https://github.com/Bioflora/Valerianella/>.

**Acknowledgments:** We thank the COFC, K, UNEX, and YU herbaria for loaning *Valerianella* specimens for our study, Francisco Bueno Carrillo for his help with data processing, and three anonymous reviewers and the handling editor for valuable comments on an early version of the manuscript.

**Conflicts of Interest:** The authors declare no conflict of interest.

## References

- Otero, A.; Fernández-Mazuecos, M.; Vargas, P. Evolution in the Model Genus *Antirrhinum* Based on Phylogenomics of Topotypic Material. *Front. Plant Sci.* **2021**, *12*, 35. [[CrossRef](#)] [[PubMed](#)]
- Krok, T. *Anteckningar till en Monografi Öfver Växtfamiljen Valerianaceae: Valerianella, Hall*; PA Norstedt & Söner: Stockholm, Sweden, 1864; pp. 1–105.
- Judd, W.S.; Campbell, C.S.; Kellogg, E.A.; Stevens, P.F.; Donoghue, M.J. *Plant Systematics. A Phylogenetic Approach*; Sinauer Associates: Sunderland, MA, USA, 2008.
- Stevens, P.F. Angiosperm Phylogeny Website. 2017. Available online: <http://www.mobot.org/MOBOT/research/APweb/> (accessed on 3 May 2022).
- Bell, C.D. Phylogenetic placement and biogeography of the North American species of *Valerianella* (Valerianaceae: Dipsacales) based on chloroplast and nuclear DNA. *Mol. Phylogenet. Evol.* **2007**, *44*, 929–941. [[CrossRef](#)] [[PubMed](#)]
- Devesa, J.A.; López, J. *Valerianella*. In *Flora Iberica*; Devesa, J., Gonzalo, R., Herrero, A., Eds.; CSIC: Madrid, Spain, 2007; Volume XV, pp. 233–258.
- Eggers-Ware, M.D. Genetic fruit polymorphism in North American *Valerianella* (Valerianaceae) and its taxonomic implications. *Syst. Bot.* **1983**, *8*, 33–44. [[CrossRef](#)]
- Martin, A.; Mathez, J. Polymorphisme et taxinomie chez les Valerianaceae: Quelques indications sur les valerianelles proches 862 de *Valerianella coronata*. *Nat. Monspel. Ser. Bot.* **1990**, *55*, 61–75.
- Ernet, D.; Richardson, I.B.K. *Valerianella* Mill. In *Flora Europaea*; Tutin, T.G., Ed.; Cambridge University Press: Cambridge, UK, 1976; Volume 4, pp. 48–52.
- Devesa, J.A.; López, J.; Gonzalo, R. Notas taxonómicas sobre el género *Valerianella* Mill. (Valerianaceae) para la Flora Ibérica. *Acta Bot. Malacit.* **2005**, *30*, 41–48. [[CrossRef](#)]
- Ernet, D. Blütenbau und Fortpflanzungsbiologie von *Valerianella* und *Fedia* (Valerianaceae). *Plant Syst. Evol.* **1977**, *128*, 1–22. [[CrossRef](#)]
- Jacobs, B.; Bell, C.; Smets, E. Fruits and seeds of the valeriana clade (Dipsacales): Diversity and evolution. *Int. J. Plant Sci.* **2010**, *171*, 421–434. [[CrossRef](#)]
- Al-Edhari, A.H.; ALRegawi, M.; Sardar, A.S.; Guda, M.A.; Almayahi, B.A. Morphological study for *Valerianella kotschy* Boiss. and *V. muricata* (Stev.) Baxt. (Valerianaceae) in Kurdistan, Iraq. *Plant Arch.* **2018**, *18*, 2417–2424.
- Al-Dabbagh, S.T.S.; Saeed, J.F. Morphological and anatomical variations of fruits in some taxa of Valerianaceae Batsch family. *Iraqi J. Agric. Sci.* **2020**, *51*, 101–115. [[CrossRef](#)]
- Candolle, A.P. *Prodromus Systematis Naturalis Regni Vegetabilis*; Treutel & Würtz: Paris, France, 1830.
- Boissier, E. *Flora Orientalis*; H. Georg: Geneve, Switzerland, 1875.
- Coode, M.J.E.; Matthews, V.A. *Valerianella* Miller. In *Flora of Turkey and East Aegean Islands*; Davis, P.H., Ed.; Edinburgh 790 University Press: Edinburgh, Scotland, 1972; Volume 4, pp. 559–581.
- Soyer-Willemet, H.F. *Valerianella*. In *Flore de France*; Grenier, J.C.M., Godron, D.A., Eds.; chez J.B. Baillièrre, libraire de l'Académie nationale de Médecine: Paris, France, 1850; pp. 37–58.
- Fanlo, R. Valerianelas ibéricas. Nota primera. *An. Inst. Bot. Cavanilles* **1975**, *32*, 151–157.
- Fanlo, R. El género *Valerianella* en la Península Ibérica. II. *Acta Bot. Malacit.* **1975**, *1*, 47–52.
- Fanlo, R. *Valerianella* (Valerianaceae) en la Península Ibérica. *Lazaroa* **1981**, *3*, 131–135.
- Fanlo, R. El género *Valerianella* Miller en la Península Ibérica. III. *An. Jard. Bot. Madr.* **1981**, *38*, 61–66.

23. Charpin, A.; Molero, J. *Valerianella orientalis* (Schlecht.) Boiss. et Bal. in Boiss., novedad para la flora española. *Collect. Bot.* **1984**, *15*, 153–157.
24. Martín-Blanco, C.J. Sinopsis del género *Valerianella* Miller (Valerianaceae) en la Península Ibérica. *Bot. Complut.* **1993**, *18*, 151–180.
25. DoĖru-Koca, A.; Zare, G.; Çeçen, Ö. *Valerianella turcica* (Caprifoliaceae), a new species from Turkey. *Phytotaxa* **2016**, *272*, 157–164. [[CrossRef](#)]
26. Xena De Enrech, N.; Mathez, J. Genetic control of fruit polymorphism in the Genus *Fedia* (Valerianaceae) in the light of dimorphic and trimorphic populations of *F. pallescens*. *Plant Syst. Evol.* **1998**, *210*, 199–210. [[CrossRef](#)]
27. Dempster, L.T. Dimorphism in the fruits of *Plectritis* and its taxonomic implications. *Brittonia* **1958**, *10*, 14–28. [[CrossRef](#)]
28. Raymúndez, M.B.; Mathez, J.; Xena De Enrech, N.; Dubuisson, J.-Y. Évolution/Evolution Coding of insertion-deletion events of the chloroplastic intergene atp-rbcL for the phylogeny of the *Valerianeae* tribe (Valerianaceae). *Comptes Rendus Biol.* **2002**, *325*, 131–139. [[CrossRef](#)]
29. Bell, C.D. Preliminary phylogeny of Valerianaceae (Dipsacales) inferred from nuclear and chloroplast DNA sequence data. *Mol. Phylogenet. Evol.* **2004**, *31*, 340–350. [[CrossRef](#)]
30. Bell, C.D.; Donoghue, M.J. Phylogeny and biogeography of Valerianaceae (Dipsacales) with special reference to the South American valerians. *Org. Divers. Evol.* **2005**, *5*, 147–159. [[CrossRef](#)]
31. Hidalgo, O.; Garnatje, T.; Susanna, A.; Mathez, J. Phylogeny of valerianaceae based on matK and ITS markers, with reference to matK individual polymorphism. *Ann. Bot.* **2004**, *93*, 283–293. [[CrossRef](#)] [[PubMed](#)]
32. Bell, C.D.; Calderon, G.; Gonzalez, L.; Scholz, A.; Liede-Schumann, S. Resolving relationships within valerianaceae (dipsacales): New insights and hypotheses from low-copy nuclear regions. *Syst. Bot.* **2015**, *40*, 327–335. [[CrossRef](#)]
33. Muminovic, J.; Melchinger, A.E.; Lübberstedt, T. Genetic diversity within lamb’s lettuce (*Valerianella locusta* L.) and across related species determined by AFLP markers. *Eucarpia Leafy Veg.* **2003**, 91–97.
34. Muminovic, J.; Melchinger, A.E.; Lübberstedt, T. Genetic diversity in cornsalad (*Valerianella locusta*) and related species as determined by AFLP markers. *Plant Breed* **2004**, *123*, 460–466. [[CrossRef](#)]
35. Hidalgo, O.; Mathez, J.; Garcia, S.; Garnatje, T.; Pellicer, J.; Vallès, J. Genome Size Study in the Valerianaceae: First Results and New Hypotheses. *J. Bot.* **2010**, *2010*, 797246. [[CrossRef](#)]
36. Bell, C.D.; Donoghue, M.J. Dating the dipsacales: Comparing models, genes, and evolutionary implications 1. *Am. J. Bot.* **2005**, *92*, 284–296. [[CrossRef](#)]
37. Winkworth, R.C.; Bell, C.D.; Donoghue, M.J. Mitochondrial sequence data and Dipsacales phylogeny: Mixed models, partitioned Bayesian analyses, and model selection. *Mol. Phylogenet. Evol.* **2008**, *46*, 830–843. [[CrossRef](#)]
38. Perez-Collazos, E.; Sanchez-Gomez, P.; Jimenez, J.F.; Catalan, P. The phylogeographical history of the Iberian steppe plant *Ferula loscosii* (Apiaceae): A test of the abundant-centre hypothesis. *Mol. Ecol.* **2009**, *18*, 848–861. [[CrossRef](#)]
39. Arnelas, I.; Pérez-Collazos, E.; Devesa, J.A.; Manzaneda, A.J.; Catalan, P. Taxonomic Differentiation of Iberian Knapweeds (*Centaurea* sects. *Jacea* and *Lepteranthus*, Asteraceae) and Genetic Isolation of Intraspecific Floral Morphotypes. *Ann. Missouri Bot. Gard.* **2020**, *105*, 481–501. [[CrossRef](#)]
40. Grassi, F.; Imazio, S.; Gomarasca, S.; Citterio, S.; Aina, R.; Sgorbati, S.; Sala, F.; Patrignani, G.; Labra, M. Population structure genetic variation within *Valeriana wallrothii* Kreyer in relation to different ecological locations. *Plant Sci.* **2004**, *166*, 1437–1441. [[CrossRef](#)]
41. Bell, C.D.; Edwards, E.J.; Kim, S.-T.; Donoghue, M.J. Dipsacales phylogeny based on chloroplast DNA sequences. *Harvard Pap. Bot.* **2001**, *6*, 481–499.
42. Weberling, F. Familie Valerianaceae. In *Illustrierte Flora von Mitteleuropa*; Hegi, G., Ed.; Cari Hanser: Munich, Germany, 1970; pp. 97–176.
43. Donoghue, M.J.; Bell, C.D.; Winkworth, R.C. The evolution of reproductive characters in Dipsacales. *Int. J. Plant Sci.* **2003**, *164*, S453–S464. [[CrossRef](#)]
44. Böhme, M. The Miocene Climatic Optimum: Evidence from ectothermic vertebrates of Central Europe. *Palaeogeogr. Palaeoclim. Palaeoecol.* **2003**, *195*, 389–401. [[CrossRef](#)]
45. Pound, M.J.; Haywood, A.M.; Salzmann, U.; Riding, J.B.; Lunt, D.J.; Hunter, S.J. A Tortonian (late Miocene, 11.61–7.25 Ma) global vegetation reconstruction. *Palaeogeogr. Palaeoclim. Palaeoecol.* **2011**, *300*, 29–45. [[CrossRef](#)]
46. Vargas, P.; Fernández-Mazuecos, M.; Heleno, R. Phylogenetic evidence for a Miocene origin of Mediterranean lineages: Species diversity, reproductive traits and geographical isolation. *Plant Biol.* **2018**, *20*, 157–165. [[CrossRef](#)]
47. Shiposha, V.; Catalán, P.; Olonova, M.; Marques, I. Genetic structure and diversity of the selfing model grass *Brachypodium stacei* (Poaceae) in Western Mediterranean: Out of the Iberian Peninsula and into the islands. *PeerJ* **2016**, *2016*, e2407. [[CrossRef](#)]
48. Castilla, A.R.; Méndez-Vigo, B.; Marcer, A.; Martínez-Minaya, J.; Conesa, D.; Picó, F.X.; Alonso-Blanco, C. Ecological, genetic and evolutionary drivers of regional genetic differentiation in *Arabidopsis thaliana*. *BMC Evol. Biol.* **2020**, *20*, 71. [[CrossRef](#)]
49. Twyford, A.D.; Wong, E.L.Y.; Friedman, J. Multi-level patterns of genetic structure and isolation by distance in the widespread plant *Mimulus guttatus*. *Heredity (Edinb)* **2020**, *125*, 227–239. [[CrossRef](#)]
50. Thompson, J.D. *Plant Evolution in the Mediterranean*; Oxford Scholarship Online: Oxford, UK, 2007. [[CrossRef](#)]
51. Feliner, G.N. Southern European glacial refugia: A tale of tales. *Taxon* **2011**, *60*, 365–372. [[CrossRef](#)]
52. Hellwig, F.H. *Centaureinae* (Asteraceae) in the Mediterranean—History of ecogeographical radiation. *Plant Syst. Evol.* **2004**, *246*, 137–162. [[CrossRef](#)]

53. Solbrig, O.T. On the relative advantages of cross-and self-fertilization. *Ann. Missouri Bot. Gard.* **1976**, *63*, 262–276. [CrossRef]
54. Alarcón, M.L.; Roquet, C.; Aldasoro, J.J. Evolution of pollen/ovule ratios and breeding system in *Erodium* (Geraniaceae). *Syst. Bot.* **2011**, *36*, 661–676. [CrossRef]
55. Abbott, R.J.; Gomes, M.F. Population genetic structure and outcrossing rate of *Arabidopsis thaliana* (L.) Heynh. *Heredity (Edinb)* **1989**, *62*, 411–418. [CrossRef]
56. Tremetsberger, K.; Stuessy, T.F.; Guo, Y.-P.; Baeza, C.M.; Weiss, H.; Samuel, R.M. Amplified Fragment Length Polymorphism (AFLP) variation within and among populations of *Hypochaeris acaulis* (Asteraceae) of Andean southern South America. *Taxon* **2003**, *52*, 237–245. [CrossRef]
57. Hughes, P.W.; Simons, A.M. Microsatellite evidence for obligate autogamy, but abundant genetic variation in the herbaceous monocarp *Lobelia inflata* (Campanulaceae). *J. Evol. Biol.* **2015**, *28*, 2068–2077. [CrossRef]
58. Burgarella, C.; Glémin, S. Population Genetics and Genome Evolution of Selfing Species. In *eLS*; Wiley: Hoboken, NJ, USA, 2017; pp. 1–8.
59. Wright, S.I.; Kalisz, S.; Slotte, T. Evolutionary consequences of self-fertilization in plants. *Proc. Biol. Sci.* **2013**, *280*, 20130133. [CrossRef]
60. Taberlet, P.L.; Gielly, L.; Pautou, G.; Baubet, J. Universal primers for amplification of the tree non-coding regions of chloroplast DNA. *Plant Mol. Biol.* **1991**, *17*, 1105–1109. [CrossRef]
61. Arnelas, I.; Pérez-Collazos, E.; Devesa, J.A.; López, E.; Catalan, P. Phylogeny of highly hybridogenous Iberian *Centaurea* L. (Asteraceae) taxa and its taxonomic implications. *Plant Biosyst.* **2018**, *152*, 1182–1190. [CrossRef]
62. Rambaut, A. Se-AL: Sequence Alignment Editor 1999. Available online: <http://tree.bio.ed.ac.uk/software/seal/> (accessed on 1 May 2021).
63. Catalán, P.; Torrecilla, P.; López Rodríguez, J.Á.; Olmstead, R.G. Phylogeny of the festucoid grasses of subtribe Loliinae and allies (Poeae, Pooideae) inferred from ITS and trnL-F sequences. *Mol. Phylogenet. Evol.* **2004**, *31*, 517–541. [CrossRef]
64. Nguyen, L.-T.; Schmidt, H.A.; von Haeseler, A.; Minh, B.Q. IQ-TREE: A fast and effective stochastic algorithm for estimating maximum-likelihood phylogenies. *Mol. Biol. Evol.* **2015**, *32*, 268–274. [CrossRef] [PubMed]
65. Kalyaanamoorthy, S.; Minh, B.Q.; Wong, T.K.F.; von Haeseler, A.; Jermini, L.S. ModelFinder: Fast model selection for accurate phylogenetic estimates. *Nat. Methods* **2017**, *14*, 587–589. [CrossRef] [PubMed]
66. Minh, B.Q.; Nguyen, M.A.T.; Von Haeseler, A. Ultrafast approximation for phylogenetic bootstrap. *Mol. Biol. Evol.* **2013**, *30*, 1188–1195. [CrossRef] [PubMed]
67. Chernomor, O.; von Haeseler, A.; Minh, B.Q. Terrace Aware Data Structure for Phylogenomic Inference from Supermatrices. *Syst. Biol.* **2016**, *65*, 997–1008. [CrossRef] [PubMed]
68. Drummond, A.J.; Suchard, M.A.; Xie, D.; Rambaut, A. Bayesian phylogenetics with BEAUti and the BEAST 1.7. *Mol. Biol. Evol.* **2012**, *29*, 1969–1973. [CrossRef]
69. Niu, Y.T.; Ye, J.F.; Zhang, J.L.; Wan, J.Z.; Yang, T.; Wei, X.X.; Lu, L.M.; Li, J.H.; Chen, Z.D. Long-distance dispersal or postglacial contraction? Insights into disjunction between Himalaya–Hengduan Mountains and Taiwan in a cold-adapted herbaceous genus, *Triplostegia*. *Ecol. Evol.* **2018**, *8*, 1131–1146. [CrossRef]
70. Rambaut, A.; Suchard, M.A.; Xie, D.; Drummond, A.J. Tracer 2014. Available online: <http://beast.bio.ed.ac.uk/Tracer> (accessed on 3 May 2022).
71. Rambaut, A. FigTree 2009. Available online: <http://tree.bio.ed.ac.uk/software/figtree/> (accessed on 3 May 2022).
72. Clement, M.; Posada, D.; Crandall, K.A. TCS: A computer program to estimate gene genealogies. *Mol. Ecol.* **2000**, *9*, 1657–1659. [CrossRef]
73. Vos, P.; Hogers, R.; Bleeker, M.; Reijmans, M.; Van De Lee, T.; Hornes, M.; Friters, A.; Pot, J.; Paleman, J.; Kuiper, M.; et al. AFLP: A new technique for DNA fingerprinting. *Nucleic Acids Res.* **1995**, *23*, 4407–4414. [CrossRef]
74. Martínez-Ortega, M.M.; Delgado, L.; Albach, D.C.; Elena-Rosselló, J.A.; Rico, E. Species boundaries and phylogeographic patterns in cryptic taxa inferred from AFLP markers: *Veronica* subgen. *Pentasepalae* (Scrophulariaceae) in the Western Mediterranean. *Syst. Bot.* **2004**, *29*, 965–986. [CrossRef]
75. Miller, M.P. Tools for Population Genetic Analyses (TFPGA) 1997. Available online: <https://www.ccg.unam.mx/~{vinuesa/flem09/docs/TFPGADOC.PDF> (accessed on 3 May 2022).
76. Coart, E.; Van Glabeke, S.; Petit, R.J.; van Bockstaele, E.; Roldan-Ruiz, I. Range wide versus local patterns of genetic diversity 788 in holsbeam (*Carpinus betulus* L.). *Conserv. Genet.* **2005**, *6*, 259–273. [CrossRef]
77. Holsinger, K.E.; Lewis, P.O. *HICKORY*; University of Connecticut: Storrs, CT, USA, 2003.
78. Huson, D.H.; Bryant, D. Application of phylogenetic networks in evolutionary studies. *Mol. Biol. Evol.* **2006**, *23*, 254–267. [CrossRef] [PubMed]
79. Gower, J.C.; Ross, G.J.S. Minimum Spanning Tree and single-linkage cluster analysis. *Appl. Stat.* **1969**, *18*, 54–64. [CrossRef]
80. Dunn, G.; Everitt, B. *A Introduction to Mathematical Taxonomy*; Courier Corporation: North Chelmsford, MA, USA, 2004; p. 152.
81. Rohlf, F.J. *NtSYSpc, Numerical Taxonomy and Multivariate Analysis System*; Applied Biostatistics Inc.: New York, NY, USA, 2002.
82. Excoffier, L.; Smouse, P.E.; Quattro, J.M. Analysis of Molecular Variance Inferred from Metric Distances Among DNA Haplotypes: Application to Human Mitochondrial DNA Restriction Data. *Genetics* **1992**, *131*, 79–91. [CrossRef] [PubMed]
83. Tamura, K.; Stecher, G.; Kumar, S. MEGA11: Molecular Evolutionary Genetics Analysis Version 11. *Mol. Biol. Evol.* **2021**, *38*, 3022–3027. [CrossRef]

84. Falush, D.; Stephens, M.; Pritchard, J.K. Inference of population structure using multilocus genotype data: Dominant markers and null alleles. *Mol. Ecol. Notes* **2007**, *7*, 574. [[CrossRef](#)]
85. Evanno, G.; Regnaut, S.; Goudet, J. Detecting the number of clusters of individuals using the software STRUCTURE: A simulation study. *Mol. Ecol.* **2005**, *14*, 2611–2620. [[CrossRef](#)]
86. Earl, D.A.; vonHoldt, B.M. Structure Harvester: A website and program for visualizing STRUCTURE output and implementing the Evanno method. *Conserv. Genet. Res.* **2012**, *4*, 359–361. [[CrossRef](#)]
87. Legendre, P.; Fortin, M.J. Comparison of the Mantel test and alternative approaches for detecting complex multivariate relationships in the spatial analysis of genetic data. *Mol. Ecol. Resour.* **2010**, *10*, 831–844. [[CrossRef](#)]
88. Paradis, E.; Schliep, K. ape 5.0: An environment for modern phylogenetics and evolutionary analyses in R. *Bioinformatics* **2019**, *35*, 526–528. [[CrossRef](#)]
89. Oksanen, J.; Blanchet, F.G.; Friendly, M.; Kindt, R.; Legendre, P.; McGlenn, D.; Minchin, P.R.; O'Hara, R.B.; Simpson, G.L.; Solymos, P.; et al. VEGAN: Community Ecology Package. R Package Version 2019. Available online: <https://cran.r-project.org/web/packages/vegan/index.html> (accessed on 3 May 2022).
90. R Core Team. *R: A Language and Environment for Statistical Computing*; R Core Team: Vienna, Austria, 2022.
91. Euro+Med. Euro+Med PlantBase—The Information Resource for Euro-Mediterranean Plant Diversity. Available online: <http://ww2.bgbm.org/EuroPlusMed/> (accessed on 3 May 2022).

## Article

# Induction of Somatic Embryogenesis in Tamarillo (*Solanum betaceum* Cav.) Involves Increases in the Endogenous Auxin Indole-3-Acetic Acid

André Caeiro, Sandra Caeiro, Sandra Correia and Jorge Canhoto \*

Center for Functional Ecology, Department of Life Sciences, University of Coimbra, 3000-456 Coimbra, Portugal; andreaeiro91@gmail.com (A.C.); caeirosandra@hotmail.com (S.C.); sandraimc@ci.uc.pt (S.C.)

\* Correspondence: jorgecan@uc.pt

**Abstract:** Somatic embryogenesis (SE) is a complex biological process regulated by several factors, such as the action of plant growth regulators, namely auxins, of which the most physiologically relevant is indole-3-acetic acid (IAA). In tamarillo, an optimized system for induction of SE creates, after an induction process, embryogenic (EC) and non-embryogenic *callus* (NEC). In this work the endogenous levels of auxin along the induction phase and in the *calli* samples were investigated using chemical quantifications by colorimetric reactions and HPLC as well as immunohistochemistry approaches. Differential gene expression (*IAA 11*, *IAA 14*, *IAA 17*, *TIR 1*, and *AFB3*) analysis during the induction phase was also carried out. The results showed that the endogenous IAA content is considerably higher in embryogenic than in non-embryogenic *calli*, with a tendency to increase as the dedifferentiation of the original explant (leaf segments) evolves. Furthermore, the degradation rates of IAA seem to be related to these levels, as non-embryogenic tissue presents a higher degradation rate. The immunohistochemical results support the quantifications made, with higher observable labeling on embryogenic tissue that tends to increase along the induction phase. Differential gene expression also suggests a distinct molecular response between EC and NEC.

**Keywords:** auxins; embryogenic *calli*; gene expression; HPLC; IAA; immunohistochemistry

**Citation:** Caeiro, A.; Caeiro, S.; Correia, S.; Canhoto, J. Induction of Somatic Embryogenesis in Tamarillo (*Solanum betaceum* Cav.) Involves Increases in the Endogenous Auxin Indole-3-Acetic Acid. *Plants* **2022**, *11*, 1347. <https://doi.org/10.3390/plants11101347>

Academic Editors: Milan S. Stankovic, Paula Baptista and Petronia Carillo

Received: 17 April 2022

Accepted: 17 May 2022

Published: 19 May 2022

**Publisher's Note:** MDPI stays neutral with regard to jurisdictional claims in published maps and institutional affiliations.



**Copyright:** © 2022 by the authors. Licensee MDPI, Basel, Switzerland. This article is an open access article distributed under the terms and conditions of the Creative Commons Attribution (CC BY) license (<https://creativecommons.org/licenses/by/4.0/>).

## 1. Introduction

Tamarillo, *Solanum betaceum* (Cav.) Sendt. (syn. *Cyphomandra betacea*) is a small (2–4 m high) solanaceous tree indigenous to South America, specifically to the Andean regions of Argentina, Bolivia Chile, Ecuador, and Peru, and currently cultivated around the globe, namely in California and New Zealand [1]. In its natural environment, tamarillo is found between 700 and 2000 m, preferring lower altitudes in colder climates [2]. It is grown for its edible fruits, which can be consumed fresh, incorporated in recipes [3], or used to prepare jams or other types of processed foods or drinks [4]. Moreover, the fruit presents low caloric and high vitamin content, as well as several natural antioxidants with potential therapeutic activities, making it a possible source of interesting secondary metabolites [5,6].

Conventional means such as seeds, cuttings, or grafting into wild *Solanum mauritianum* trees can be used for propagation of tamarillo [4]. However, these techniques present problems such as the genetic variability of seeds, the low interspecific hybridization rate in grafting, and phytosanitary problems [7,8]. In this context, biotechnological tools have been an alternative for plant breeding with several in vitro methodologies described for tamarillo cloning such as micropropagation through axillary shoot proliferation [9], organogenesis [10,11], and somatic embryogenesis (reviewed in [12]).

Somatic embryogenesis (SE) can be defined as a process by which a somatic cell or tissue creates a structure that resembles an embryo (somatic embryo) without fecundation [13]. This structure has embryonic characteristics, such as bipolar organization, lack of vascular contact with the parental tissue and, through a series of developmental stages

similar to a zygotic embryo, germinates into a plant [14,15]. The first successful attempt of SE in tamarillo was reported in mature zygotic embryos and hypocotyls [16]. In this protocol, embryogenesis was induced using the auxin 1-naphthaleneacetic acid (NAA) with formation of a small *callus* mass followed by differentiation into somatic embryos in a “one-step” system. On the other hand, if the auxin used was either 2,4-Dichlorophenoxyacetic acid (2,4-D) or picloram, the zygotic embryos and young leaf explants produced an embryogenic *callus* that could be successfully maintained by successive subcultures in the same auxin-containing medium [12,17]. Interestingly, on this type of system a second type of *callus* without embryogenic competence (non-embryogenic) is also obtained. Additionally, in both induction systems, the embryogenic yield was greatly increased by the addition of high levels of sucrose (26 mM) to the culture medium [18].

Auxins, particularly 2,4-D, are the main plant growth regulators (PGRs) used in somatic embryogenesis experiments, with most protocols starting with an induction phase in an auxin supplemented medium followed by an embryo maturation phase on auxin-free or auxin-reduced medium [19]. This typical induction scheme, varying the types of synthetic auxins depending on the original explant, has been followed in tamarillo [6,12].

The level of endogenous plant growth regulators (PGRs), namely auxins, is considered one of the most important embryogenic controlling factors [20,21]. Auxin gradients are related with the establishment of bilateral symmetry necessary for proper embryo development in both zygotic and somatic embryos [15]. External stimulation by auxin-like molecules is believed to cause an increase in the endogenous levels of this PGR; thus initiating the cell reprogramming stages necessary for embryogenesis [13,22]. Specifically, with the increase in endogenous levels of indole-3-acetic acid (IAA), particularly in the early stages of SE, induction has been extensively reported in several model species, such as carrot (*Daucus carota* L.) and *Arabidopsis thaliana* [23]. The auxin mechanism of action has been related with gene expression modulation, and several proteins have been closely linked to this regulation pathway, namely in embryogenesis [20]. The auxin-responsive protein family (*Aux/IAAs*), auxin response factors (ARFs), and the transport inhibitor response 1 protein (*TIR1*) have been identified as the main response factors active during embryogenesis induction [23].

The aim of this work was to analyze the endogenous levels of auxins, namely indole-3-acetic acid (IAA), the main natural auxin, during somatic embryogenesis and in embryogenic and non-embryogenic *callus* of tamarillo, by chemical quantification of this PGR. Furthermore, quantitative studies were applied along the induction protocol to establish the evolution of auxin concentration. In addition, the distribution of IAA in the tissue was investigated through immunofluorescence microscopy. Finally, the expression of the main genes related to auxin response in embryogenesis was investigated along the induction path in order to relate the genetic effects of this regulator with its endogenous concentrations.

## 2. Results

### 2.1. Somatic Embryogenesis Induction and Callus Proliferation

In order to obtain enough tissue during the induction phase, leaf segments were culture in the presence 20  $\mu$ M of picloram, presenting an embryogenic yield of 44%. The IAA levels were investigated on the final stages of induction starting at 8 weeks until 12 weeks (Figure 1A). Additionally, established embryogenic and non-embryogenic *calli* was also used with embryogenic tissue forming a characteristic white compact structure and non-embryogenic forming a mucilaginous, friable *callus*. For the study of embryogenic competence, previously established embryogenic *callus* (EC) and non-embryogenic *callus* (NEC) of both leaf segments (EC1 and NEC1) and zygotic embryos were used (EC2, NEC 2, and EC3) (Figure 1B).

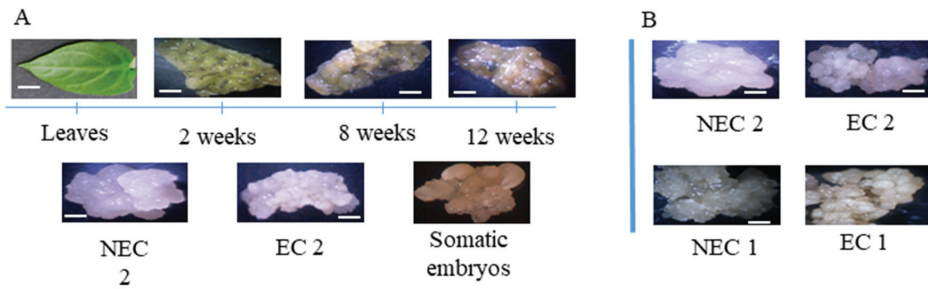


**Figure 1.** Plant material. (A) Time course of leaf explant SE induction; leaves from *in vitro* established plantlets were used. EC 2 and NEC 2 are the embryogenic and non-embryogenic calli resulting from the induction process. (B) EC 2 and NEC 2 were previously established from zygotic embryos and used in the IAA quantifications. The bars in each figure represent 1 mm with exception of the leaves in which the length is 1 cm.

To confirm the embryogenic competence, embryogenic and non-embryogenic tissue were transferred to development medium, with the embryogenic tissue forming somatic embryos after 4 weeks, whereas the non-embryogenic tissue became necrotic. In this phase, the influence of auxin polar transport was also assayed as described, with the embryogenic callus exposed to different concentrations of 2,3,5-Triiodobenzoic acid (TIBA) (Table 1). In the maturation assay, proliferation of proembryogenic mass was observed in all treatments, while concentrations of TIBA higher than 5  $\mu\text{M}$  show a statistic significant decrease in the formation of normal somatic embryos, while the number of abnormally formed embryos shows no specific trend in relation to TIBA concentration.

**Table 1.** Results of the auxin polar transport inhibitors assay. Values are presented as mean  $\pm$  SD ( $n = 4$ ); values in the same column with different letters are statistically different by Tukey test ( $p < 0.05$ ) in the case of the mass increment, while for abnormal embryo formation the letters refer to Dunn's multiple comparison test.

TIBA ( $\mu\text{M}$ )	Mass Increment (g)	Embryo Formation (Number/g of Tissues)	
		Normal	Abnormal
0	1.057 $\pm$ 0.140 <sup>a,b</sup>	22.16 $\pm$ 9.58 <sup>a</sup>	9.08 $\pm$ 8.02 <sup>b</sup>
0.5	1.140 $\pm$ 0.201 <sup>a</sup>	17.42 $\pm$ 1.99 <sup>a</sup>	3.86 $\pm$ 1.18 <sup>b,c</sup>
1	1.132 $\pm$ 0.102 <sup>a</sup>	14.4 $\pm$ 3.45 <sup>a</sup>	1.71 $\pm$ 0.20 <sup>c</sup>
5	1.045 $\pm$ 0.217 <sup>b</sup>	7.77 $\pm$ 2.90 <sup>b</sup>	10.13 $\pm$ 2.62 <sup>a,b</sup>
10	0.695 $\pm$ 0.190 <sup>b</sup>	2.08 $\pm$ 1.50 <sup>b</sup>	1.51 $\pm$ 0.744 <sup>c</sup>

## 2.2. IAA Location on the Induction of SE

The later stages of embryogenic induction were taken from the 8th week onward. All the samples presented some autofluorescence observed in the controls without the antibody labeling (Figure 2A); however, it is possible to observe distinct labeled spots on the proembryogenic tissue, increasing in frequency along the induction phase. The embryogenic tissue follows this pattern with diffuse spots with marked presence of IAA. The presence of IAA appears in the cell peripheral zone. With respect to the non-embryogenic tissue, the labeling is less frequent and even absent in some parts of the tissue.

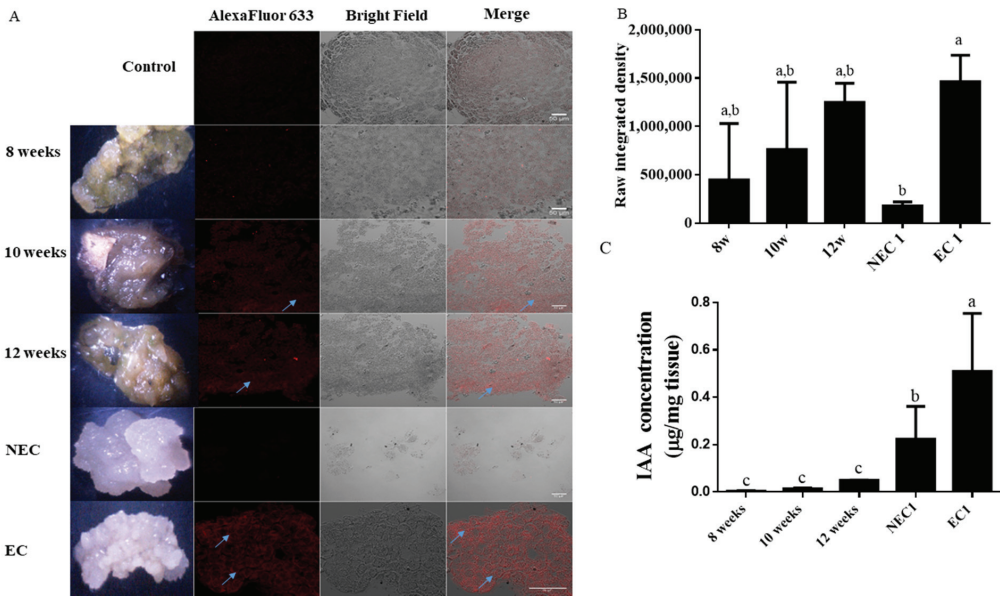


**Figure 2.** IAA assays in time courses from leaf segment induction. NEC and EC are non-embryogenic and embryogenic calli, respectively, similar to EC 1 and NEC 1 represented in Figure 1. (A) Immunohistochemistry observations. Fluorescence, transmission, and composed image of the different tissues, unlabeled tissue samples from EC were used as control (C—control; 8 w—8 weeks induction; 10 w—10 weeks induction; 12 w—12 weeks induction; NEC—non-embryogenic callus; EC—embryogenic callus). (B) Raw integrated intensity for each sample. (C) IAA quantification by HPLC. Results are presented as mean  $\pm$  SD. Different letters are significantly different according to Tukey test ( $p < 0.05$ ).

In terms of quantification (Figure 2B), the integrated density of the samples showed an increasing tendency along the induction phase, although not statistically significant. The embryogenic tissue, however, presents a higher level of labeling in comparison to the non-embryogenic tissue.

IAA quantification by High Performance Liquid Chromatography (HPLC) (Figure 2C) shows tendency of IAA increase in the induction phase starting with a small, statistically insignificant difference between the 8th and 10th weeks of induction ( $0.004 \pm 0.001$  and  $0.013 \pm 0.004$   $\mu\text{g IAA/mg.f.w}$  for EC3, respectively), and a marked increase by the 12th week ( $0.496 \pm 0.001$   $\mu\text{g IAA/mg.f.w}$ ). These values are still comparatively lower to those presented by embryogenic callus sub cultivated in the same media.

### 2.3. IAA Levels Increment in EC

The previously induced callus lines were assayed for IAA by Ehrlich method and HPLC quantification. When assayed by the Ehrlich reaction and statistically analyzed based on type of synthetic auxin present (Figure 3A), the difference between the endogenous auxin levels in NEC 1 and EC 1 is statistically significant, with EC 1 showing the highest values of IAA ( $10.49 \pm 2.51$   $\mu\text{g IAA/mg f.w.}$ ). In the case of picloram-induced calli, the difference between embryogenic (EC2 and EC3) and non-embryogenic callus (NEC2) is statistically relevant ( $p < 0.05$ ), with EC2 showing higher IAA values than EC3, although not statistically different at the confidence interval used. Further statistic comparison between embryogenic calli (Figure 3B) indicated a significant statistical difference between the embryogenic tissues induced with different synthetic auxins, with 2,4-D apparently leading to a marked increase in the endogenous level of IAA. A similar statistical test on

the non-embryogenic tissue (Figure 3C) showed no differences between non-embryogenic tissues, regardless of biological origin.

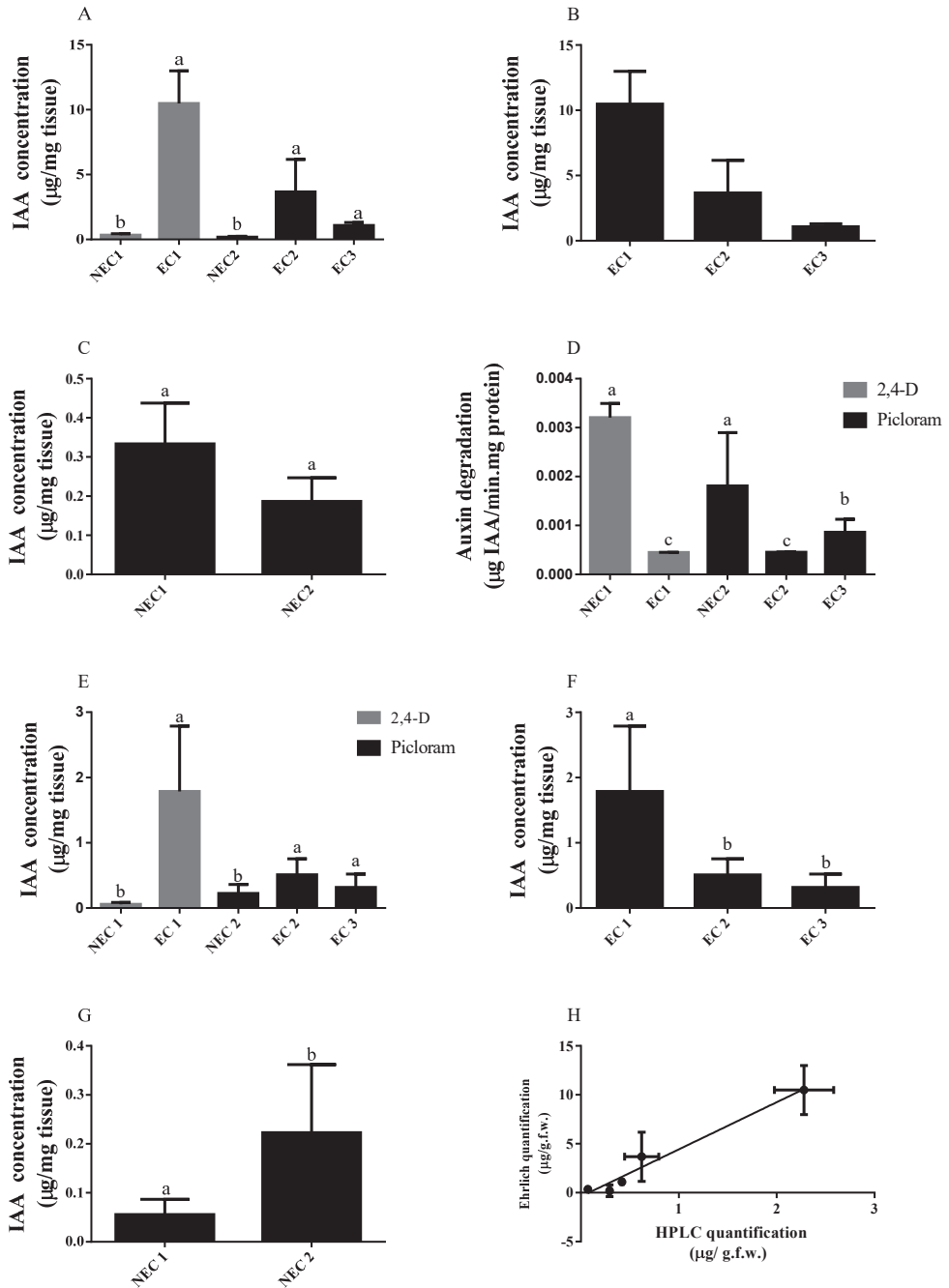


**Figure 3.** IAA quantification on induced embryogenic (EC) and non-embryogenic (NEC) calli, where EC 1 and NEC 1 are induced from zygotic embryos in 2,4-D supplemented medium and NEC 2, EC 2,

and EC 3 are from leaf segments in a picloram-supplemented medium. (A) IAA quantification by Ehrlich reaction. (B) Statistical analysis of IAA in embryogenic *calli* assayed by Ehrlich reaction. (C) Statistical analysis of IAA in non-embryogenic *calli* assayed by Ehrlich reaction. (D) IAA degradation measured by discontinuous assay. (E) IAA quantification by HPLC. (F) Statistical analysis of IAA in embryogenic *calli* assayed by HPLC. (G) Statistical analysis of IAA in non-embryogenic *calli* assayed by HPLC. (H) Comparison of IAA measurement Ehrlich reaction and HPLC comparison between HPLC and Ehrlich reaction. Results of HPLC quantification (x axis) were plotted against the results of Ehrlich quantification (y axis) for each *callus* tissue tested. The linear fit equation is  $y = 4.818x - 0.3963$  ( $R^2 = 0.969$ ). Results are presented as mean  $\pm$  SD. Different letters are significantly different according to Tukey test or by the unpaired *t*-test in the case of non-embryogenic *calli* analysis ( $p < 0.05$ ;  $n = 3$ ).

IAA degradation analysis (Figure 3D) was carried out in the *calli* samples, through the quantification of the amount of auxin degraded over a known and fixed period of time (60 min). The results are presented in terms of total intracellular protein to have a specific rate of degradation that can be readily compared between samples (Table 2). This quantification shows no clear distinction in the protein content of embryogenic tissue in relation to the auxin used in the induction phase ( $0.693 \pm 0.075$  mg/mL for 2,4-D and  $0.625 \pm 0.071$  mg/mL for picloram). Similarly, the non-embryogenic tissue is also not significantly different between 2,4-D and picloram treatments ( $0.112 \pm 0.029$  and  $0.290 \pm 0.067$  mg/mL, respectively). However, the comparison of embryogenic and non-embryogenic *callus* shows a significant difference. Interestingly, EC3 shows an intermediary value between embryogenic and non-embryogenic *callus*.

**Table 2.** Total protein content in the different *calli*. Results are presented as mean  $\pm$  SD ( $n = 3$ ). Different letters are significantly different according to Tukey test ( $p < 0.05$ ).

Tissue	Protein Concentration (mg/mL) $\pm$ SD
NEC1	$0.112 \pm 0.029^c$
NEC2	$0.290 \pm 0.067^c$
EC1	$0.693 \pm 0.075^a$
EC2	$0.625 \pm 0.071^a$
EC3	$0.388 \pm 0.290^{a,b}$

In the case of 2,4-D-induced tissue (Figure 3D), there were significantly higher rates of degradation in the non-embryogenic tissue (NEC 1 =  $1.80 \times 10^{-3} \pm 1.088 \times 10^{-3}$   $\mu$ g IAA/mg protein.min), a tendency also observed in the case of picloram-induced tissue where the non-embryogenic presented the highest value of IAA degradation (NEC 2 =  $3.21 \times 10^{-3} \pm 3.06 \times 10^{-4}$   $\mu$ g IAA/mg protein.min). In this case, EC2 and EC3 showed a statistically similar degradation of IAA.

IAA content in this case was also analyzed by HPLC (Figure 3E). The IAA was identified via UV-visible spectrum and retention time (Figure 4A–C) and quantified taking into account a calibration curve (Figure 4D). In general, the data obtained by this analysis shows the same trends found when the tissue was subjected to IAA quantification by Ehrlich: EC *callus* lines present significantly higher levels of IAA ( $2.280 \pm 0.303$  and  $0.621 \pm 0.175$   $\mu$ g IAA / mg.f.w for EC1 and EC2, respectively) when compared to the respective NEC line. Furthermore, a separate comparison between the embryogenic *calli* (Figure 3F) revealed statistically higher value in 2,4-D-induced *calli* while in non-embryogenic tissues (Figure 3G) the amounts of auxin were not significantly different. Finally, the results obtained for both analytic methods were compared (Figure 3F) showing a good linear fit ( $R^2 = 0.9694$ ) and a systematic higher value of concentration given by Ehrlich quantification.

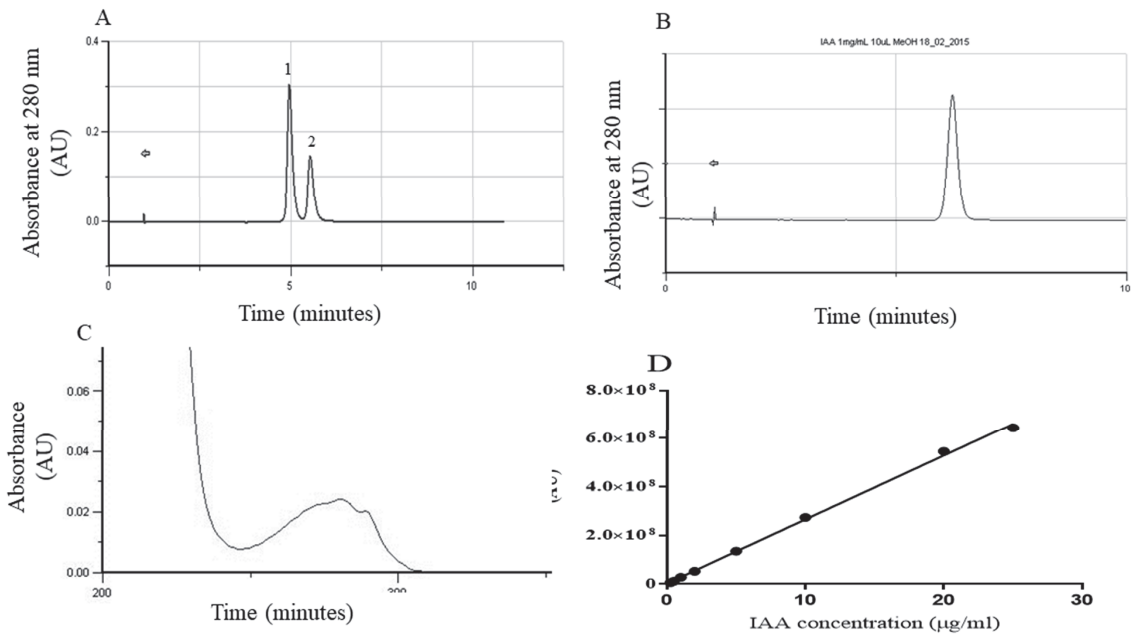


**Figure 4.** HPLC quantification parameters. (A) Retention time of IPA (peak 1,  $R_t = 5.34$  min) and IAA (peak 2,  $R_t = 6.00$  min) in a sample. (B) IAA standard ( $R_t = 5.98$  min). (C) UV-spectrum of IAA. (D) Calibration curve used in the quantification of IAA with the linear equation  $\text{Area} = 2.633 \times 10^7 [\text{IAA}] + 2.094 \times 10^6$  ( $R^2 = 0.9984$ ).

#### 2.4. Auxin-Related Gene Expression Relates with IAA Levels during SE Induction

In terms of gene expression, 3 Aux/IAA genes and 2 auxin intracellular receptors were analyzed. In terms of the first group, there is a general trend of decrease in gene expression along the induction course, with statistically significant differences between the initial explant (leaf segment) and non-embryogenic *calli*. (Figure 5A–C). Furthermore, in *IAA 11* and *IAA 17*, although statistically insignificant, there appears to be a trend in higher expression in EC when compared to NEC. Both auxin response genes assayed, *TIR 1* and *AFB3* (Figure 5D,E), show a higher expression in the initial induction explants (leaf segments) and a statistically insignificant variation along the induction period and between EC and NEC.

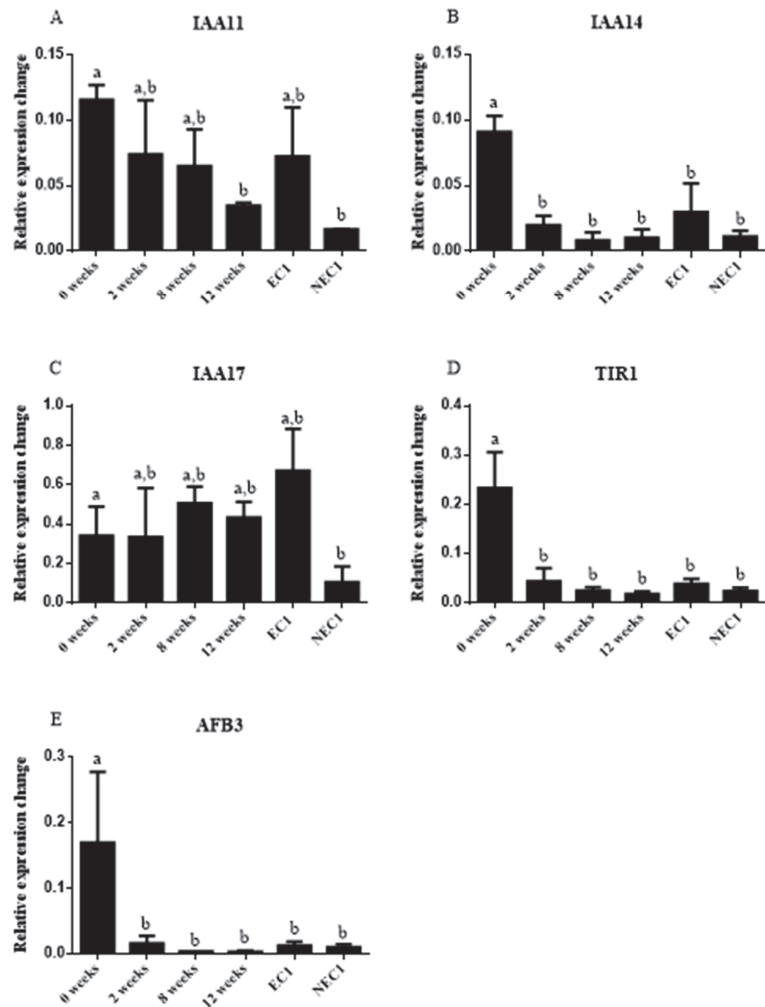


**Figure 5.** Relative gene expression. Relative expression was calculated in relation to reference genes previously validated for tamarillo. Results are presented as mean  $\pm$  SD. Different letters are significantly different according to Tukey test ( $p < 0.05$ ).

### 3. Discussion

#### 3.1. IAA Distribution Is Important for Somatic Embryo Conversion

Indirect *in vitro* SE induction protocols can be divided in two stages, one in which somatic cells enter in a dedifferentiated cell state and acquire embryogenic potential and another in which these cells evolve into somatic embryos [24]. These two stages are usually applied *in vitro* by changing the external stimuli, usually stress or PGR [25]. Tamarillo is one of these cases, where the SE process is induced in an auxin-rich medium, and the proembryogenic masses formed during this stage transform into somatic embryos upon transference to an auxin-free medium [12].

Early studies have shown, in both zygotic and somatic embryos, that the endogenous auxin content is important to the developmental program of embryos as well as their germination [26,27]. Therefore, the auxin polar transport inhibitor assays made in this work aimed to test whether somatic embryo development of tamarillo was also affected by the

mechanism of polar auxin transport, when the proembryogenic masses are transferred to a medium without auxins. In this stage of embryo development, the endogenous auxin is greatly responsible for the organized division and specification of cells, or embryo patterning [28].

Previous studies have shown that TIBA can inhibit somatic embryogenesis even in the presence of strong auxins such as 2,4-D [29]. Several other studies have also demonstrated that TIBA affects the maturation of somatic embryos, particularly in the earlier stages of globular and heart-shaped embryos [26].

The TIBA mechanism of action is based on blocking auxin transport by binding to PIN regulator efflux carriers [30] without directly antagonizing the response cascade triggered by the auxin, with the auxin polar transport being fundamental for the effective response of the tissue. In fact, several studies seem to support the idea that the polarity of cells is achieved by cell-to-cell communication, greatly influenced by auxins [28,31].

The results here presented support this hypothesis, that the cell-to-cell communication mediated by auxins is fundamental for the development of somatic embryos, as the high concentrations of TIBA affected the number of somatic embryos formed.

### 3.2. IAA Quantification through SE Induction

Endogenous levels of PGRs are extremely important in the regulation of plant development [32]. Consequently, their quantification has been extensively carried out in several contexts to understand the biochemical and molecular mechanisms underlying different aspects of morphogenesis [33]. In particular, experiments carried out with different species, such as *Coffea canephora* [34] and *Cunninghamia lanceolata* [35], have shown that the levels of IAA or other auxins strongly affect somatic embryo formation and development.

The Ehrlich reagent has been used to measure several indole-containing molecules, from tryptamines to ergoloid compounds [36], and has been optimized for colorimetric quantifications of IAA [37] and, in specific conditions, IAA and indole-3-butyric acid (IBA) [38], also allowing a discontinuous method for determination of IAA degradation as colorimetric reactions can be applied to protein solutions, in specified conditions, to measure auxin degradation and, therefore, indirectly determine the catalytic activity of the enzymes involved in its oxidation, namely IAA oxidase and peroxidases. This type of discontinuous assay to determine the activity of these enzymes has been previously reported [39].

Auxins are enzymatically degraded by either oxidation of the side chains by peroxidases or the oxidation of the indole ring by indole-3-acetaldehyde oxidase (EC 1.2.3.7) or IAA oxidase [40]. This degradation is physiologically important because it leads to the permanent inactivation of IAA [41].

The results showed the endogenous level of IAA inversely related to the degradation rate, i.e., tissues with lower IAA levels presented the highest levels of IAA degradation (NEC1 and NEC2), while the tissues with high values of endogenous auxin presented the lowest degradation rate. Data have also indicated that the degradation of IAA in the non-embryogenic *callus* is at least partially responsible for the low concentration of endogenous auxin in this tissue, caused by a higher biotransformation rate. In this context, the homeostasis of auxin in embryogenic and non-embryogenic *calli* of tamarillo seems to be related to the degradation pathway of the complex auxin metabolism. This type of attenuation of the auxin signaling system has been described in *A. thaliana*, where the oxidation of auxin by enzymatic systems was unable to generate the activation of certain auxin-responsive genes [42].

The quantifications made by HPLC differed, in absolute values, from those made by the Ehrlich reaction. However, the overall relationship between the two types of *callus* was similar, with the embryogenic *callus* displaying a higher endogenous IAA concentration than the non-embryogenic one.

Overall, the endogenous IAA level was dependent on the induction phase and the embryogenic competence of the tissue. These differences have been observed in other

SE plant models such as carrot (*Daucus carota* L.) [43] and alfalfa (*Medicago sativa*) [44], systems where 2,4-D is also the auxin used to trigger somatic embryogenesis. 2,4-D appears to be necessary not only for initiation of the somatic embryogenesis process but for the maintenance of embryogenic competence *in vitro*. The mechanism of action is not completely understood, but clearly involves the expression modulation of several genes related to the metabolism of auxins, mainly IAA biosynthesis, degradation, and transport [24]. The role of 2,4-D as an auxin (directly or indirectly) is still in dispute, with some authors hypothesizing that the dedifferentiation process that the cells experience is a response to the stress caused by the herbicide action of this compound [45].

After the recognition of the differences between embryogenic and non-embryogenic *calli*, the auxin kinetics was investigated along with the induction phase of SE in leaf segments. These have shown a greater embryogenic yield than zygotic embryos, the other explant commonly used on induction protocols [2]. Another important factor to consider is that the leaves were gathered from *in vitro* cloned plants sharing the same genotype, and because of this the genetic variability factors were less determinant, although genetic variations in plants regenerated from embryogenic embryos have been reported [18]. However, by the 12th week the IAA concentration was still about five times lower than that of the embryogenic *calli*. These results are in accordance with other studies of auxin variation during the SE process, namely those of Yang and co-workers [24] who found, in the somatic embryogenesis process of cotton, a profile of endogenous IAA concentration that decreased in the first stages of cell dedifferentiation and increased in the end of the induction phase, with the final embryogenic tissue presenting values 11-fold higher than the initial explants. In the present work, the endogenous level of IAA in the early cell dedifferentiation periods was not possible to determine; however, the results indicated that the induction phase is characterized by a lower level of IAA, while the maintenance of embryogenic competence is largely dependent on high concentrations of IAA. In fact, tissues with minor embryogenic competence (such as the *callus* tissue EC 3) presented a significantly lower concentration of IAA.

Several studies have shown that the endogenous auxins are responsible for the activation of a complex pathway, which leads to the activation of several genes, either related with the metabolism of auxin or metabolic pathways, such as basic metabolic pathways, and the biosynthesis of secondary metabolites [46]. Additionally, Yang and co-workers (2012) [24] also found distinct transcription profiles in embryogenic and non-embryogenic tissues, related with the auxin signal pathway. Comparative proteomic studies in tamarillo have also shown differently expressed proteins in embryogenic and non-embryogenic *callus*, despite the type of auxin used for induction [47].

Given the results presented here, and the analogy to other species, it can be assumed that the endogenous auxin level is influencing the proteome of the different cell lines.

### 3.3. Immunolocalization of IAA during SE Induction

The distribution of auxin in the tissue is an important factor for somatic embryogenesis with several signaling events related with this hormone linked to early somatic embryogenesis [48]. Furthermore, the induction process for tamarillo SE applied in this work gives rise to both embryogenic and non-embryogenic tissue, a result that could be, at least partially, related to the distribution of IAA in the proembryogenic tissue along the induction phase. Our results point to an increase in this level along the induction phase consistent with the chemical quantifications, and a distribution seems to be ubiquitous in the proembryogenic masses and the embryogenic tissue. The only significant distinction can be seen when the embryogenic and non-embryogenic tissue is compared. Similar differences have been reported in other woody plants [49]. Overall, these results seem to indicate that distribution of IAA in the tissues is directly related to the embryogenic competence, with a similar result described for other model species such as *Arabidopsis thaliana* [50].

### 3.4. Auxin-Related Gene Differential Expression Is Influenced by IAA Endogenous Levels

The differential genetic expression triggered by auxin or auxin-like stimulation is considered central to almost all plant development processes, namely SE [23]. In this work, as the endogenous IAA levels were shown to be different along the induction process and between EC and NEC lines, gene expression assays were carried out to elucidate some of the molecular aspects of cell response to the embryogenic trigger. Several similar studies have been carried out and show that certain genes are over- or under-expressed in SE protocols and can be related to embryogenic competence [23,51]. The molecular mechanism of auxin regulation mediated by these genes is partially known: in the absence of auxin, the *Aux/IAA* gene family interacts with Auxin Responsive Factor (ARF), inhibiting its activity and decreasing auxin response, whereas in auxin presence they are targeted for ubiquitin-mediated degradation [52,53]. These genes, namely *IAA 17*, have been shown to be over-expressed in initial SE stages of *A. thaliana* [53]. In this work the *Aux/IAA* genes (*IAA 11* and *IAA 17*) were found over-expressed in several stages of SE when compared to non-embryogenic *calli*. As these genes are repressors of auxin-induced gene expression [54], it is possible that their higher relative expression is linked with a proper cell response to the highly auxin enriched culture medium resulting in embryogenic competence [55]. Furthermore, the low expression values of NEC *calli* might directly explain the low embryogenic competence that this tissue presents. Previous studies have hinted to this type of response by studying the genetic expression profile of highly responsive cultivars of *Gossypium hirsutum* in comparison to recalcitrant ones [56]. However, these expression levels can also be related to the low concentration and high degradation rates of IAA that have been found in NEC *calli*. In fact, the presence of synthetic auxins has increased the endogenous concentration of IAA in EC *calli*. Therefore, it is possible that a distinct molecular mechanism is responsible for the low concentration of auxins in NEC and this factor is influencing the low expression of *Aux/IAA*. This hypothesis should be further investigated in future works.

Lastly, the ubiquitin ligase complex responsible for degradation of *Aux/IAA* contains the *TIR1*- and *AFB*-encoded genes and these proteins are considered auxin receptors [57]. These genes were found under-expressed in all tissues when compared to the initial explant used in the induction protocol (leaf segments). Again, this fact might hint to a “low auxin sensitive” environment that is effectively suppressed in EC by a higher level of endogenous IAA that does not exist in NEC; therefore critically influencing the embryogenic competence of both *calli*. This hypothesis, along with the precise molecular mechanism of auxin increase in EC, should be further investigated.

## 4. Materials and Methods

### 4.1. Somatic Embryogenesis Induction from Leaf Segments of In Vitro Propagated Shoots

Tamarillo plants (red variety) were used for SE induction, were micropropagated from previously established shoot cultures from in vitro germinated seeds in MS [58] propagation medium supplemented with 8.6 mM sucrose, 0.88  $\mu\text{M}$  of 6-benzylaminopurine (BAP), and 6 g/L of agar (Sigma-Aldrich, St. Louis, MI, USA) and pH was adjusted to 5.6–5.8 before autoclaving. The plants were segmented (1–1.5 cm) and subcultured monthly in the same medium and kept in a growth chamber at 25 °C, in a 16 h photoperiod, at 25–35  $\mu\text{mol m}^{-2} \text{s}^{-1}$  (white cool fluorescent lamps). The apical leaves from the clones (2–4 for each plantlet) were aseptically removed, after one month in propagation medium, and used for SE inductions as previously described [12,17]. Briefly, the leaves were segmented (area of approximately 0.25 cm<sup>2</sup>), randomly punctured on the abaxial side and placed on test tubes (15 cm  $\times$  2.2 cm) containing approximately 12.5 mL of MS medium supplemented with 26 mM sucrose and a synthetic auxin, 20  $\mu\text{M}$  of picloram. The pH was adjusted to 5.6–5.8 before autoclaving and 2.5 g/L of phytigel<sup>TM</sup> (Sigma-Aldrich, St. Louis, MI, USA) was added as the gelling agent. All the culture media used were autoclaved at 121 °C for 20 min.

#### 4.2. Embryogenic and Non-Embryogenic Calli Subcultures and Maintenance

The induction of proembryogenic *calli* as previously described and its subculture were carried out in the same culture medium in dark conditions in a growth chamber at a temperature of  $24 \pm 1$  °C for 12 weeks. During the later stages of the induction stage (8–12 weeks), samples of dedifferentiating explants from leaf segments were periodically (every 2 weeks) removed from the induction medium and frozen in liquid nitrogen for further analysis. Additionally, for genetic analysis, samples of early-stage dedifferentiation (2 weeks) were also removed from the culture medium and immediately frozen. Unless otherwise stated, all samples were made in triplicate.

At the end of the induction period (12 weeks), masses of EC were transferred to Petri dishes (90 mm in diameter and 15.9 mm in height) containing 30 mL of a hormone-free embryo development MS medium, supplemented with 11.6 mM sucrose and 2.5 g/L of phytigel™ (Sigma), to evaluate embryogenic competence by the development of somatic embryos. Based on their embryogenic ability two lines of EC were selected: EC2 (high embryogenic ability) and EC3 (low embryogenic ability). Furthermore, to study the influence of auxin gradients in somatic embryo conversion, TIBA was added to the embryo development medium in a concentration between 0.5 and 10 µM. The TIBA solution was sterilized by filtration with a 0.2 µm filter and added to the medium at a temperature of about 60 °C to avoid thermal degradation. An initial mass of about 200 mg of *callus* tissue was used and after 4 weeks of growth in dark conditions at a temperature of  $24 \pm 1$  °C the final mass was registered and number of somatic embryos (morphologically normal and abnormal) counted. The results are presented as a percentage of mass increment ((final mass – initial mass)/initial mass × 100) and number of somatic embryos per gram of tissue. The conversion assays were carried out in quadruplicate.

Additionally, to access the endogenous auxin levels of embryogenic and non-embryogenic masses from other tissues (particularly in terms of the synthetic auxin used), previously induced EC and NEC *calli* form zygotic embryos were used. These were maintained in test tubes ( $15 \times 2.2$  cm<sup>2</sup>) containing approximately 12.5 mL of MS medium supplemented with MS medium with 26 mM sucrose and 9 µM of 2,4-D with and 2.5 g/L of phytigel™ (Sigma). These were termed EC 1 and NEC 1, respectively.

#### 4.3. Quantification of IAA

##### 4.3.1. Ehrlich Reaction

In a first approach, the IAA content in the established *calli* lines (from zygotic embryos, EC 1 and NEC 1, and leaf explants, EC 2, EC 3, and NEC 3) was assayed using the colorimetric method described by Anthony and Street [37]. This methodology was applied to broadly evaluate the IAA endogenous concentration in the proembryogenic masses and evaluate the IAA degradation rates of these *calli* to access if the embryogenic competence and culture medium influenced the endogenous levels of auxins in the same patterns. Ehrlich reagent was prepared by dissolving 2 g of *p*-dimethylaminobenzaldehyde (PDAB, Sigma-Aldrich, St. Louis, MI, USA) in 100 mL HCl 2.5 M. The plant material, on average 600 mg of fresh mass, was ground in a sterilized mortar with K-phosphate buffer 0.01 M (pH 6.0) (1 mL/500 mg.f.w) and centrifuged (4800 g; 20 min). After centrifugation, the supernatant was used for the quantification. The reaction was initiated with successive addition of 2 mL of TCA (100%) (Sigma) and Ehrlich reagent to 1 mL of sample. After an incubation period of 30 min, the absorbance at 530 was measured against a blank solution of K-phosphate in a Jenway 7305 spectrometer. A calibration curve was prepared using buffered solutions of IAA with concentrations between 2 and 50 µg/mL. The results are presented as µg of IAA per mg of fresh tissue (µg/mg.f.w).

To measure the degradation of IAA by the tissue, *callus* samples were treated as before and incubated in IAA solution (0.02 mM IAA; 0.02 mM MnCl<sub>2</sub>, K-phosphate buffer) for 90 min before the Ehrlich reaction was carried out. The results are presented as µg of IAA degraded per mg of protein per minute (µg IAA/mg protein.min).

The total protein was assayed using Bio-Rad Protein Assay based on Bradford's reaction (Bradford, 1976) in a 96-well microplate. A calibration curve was constructed using concentrations of BSA between 5 and 40  $\mu\text{g}/\text{mL}$ . All measurements were made simultaneously and in triplicate at 595 nm in a SPECTRAMax PLUS 384 spectrophotometer (Molecular Devices, Sunnyvale, CA, USA).

#### 4.3.2. HPLC

The colorimetric quantifications showed differences in both endogenous levels of auxin and degradation rates; however, this quantification method is described as less sensitive than other methods, namely chromatographic methods such as HPLC, and proved less precise in differentiating leaf segments. Therefore, to have a more sensitive approach that also allowed the analysis of time courses, HPLC analysis was employed. The quantification of IAA by HPLC was based on the method described by Kim and co-workers [59] with modifications. Briefly, the plant material (8, 10, and 12 weeks of induction as well as EC1EC2, EC2, NEC 1, and NEC 2) was extracted in 100% methanol (2.5 mL per gram of fresh weight tissue), IPA was added as an internal standard (10  $\mu\text{g}/\text{g.f.w.}$ ), and the resulting extract was cleared by centrifugation (16,000 $\times g$ , 10 min) at 4 °C. Before the next steps, the polarity of the extract was increased by adding one volume of pure water. The sample was then extracted by two steps of serial partition against 100% ethyl acetate. In the first, the pH of the aqueous phase was adjusted to higher than 9 (1 M KOH) and after separation of phases by centrifugation (16,000 $\times g$ , 10 min), the aqueous phase was transferred to a new tube and the pH was reduced to less than 3 and again partitioned against ethyl acetate. After separation of phases by centrifugation (16,000 $\times g$ , 10 min), the organic phase was collected, completely dried in vacuum, and dissolved in a minimal volume of 100% methanol, micro-filtered, and injected in the HPLC apparatus.

The samples were then analyzed in an HPLC system composed of a Gilson 234 injector, Gilson 305 pumps, and Waters Spherisorb<sup>®</sup> 5  $\mu\text{m}$  ODS2 (C18) 4.6  $\times$  250 mm column and a Gilson 170 diode array detector (Gilson, Madison, WI, USA). The compounds were resolved with an isocratic elution similar to that used by Nakurte and co-workers [60], consisting of 56% methanol and 44% water and orthophosphoric acid (pH = 2.3) with a flow rate of 1 mL/min. The system used the control and analysis software Gilson Unipoint v 5.11. The detector wavelength was set at 282 nm. Calibration curves of standard concentrations of both IAA and IPA between 0.5 and 25  $\mu\text{g}$  were prepared in triplicate. Additionally, the resolving power of the isocratic elution was tested with mixtures of both the components in different concentrations.

#### 4.4. Immunohistochemistry IAA Localization

The total quantification of IAA during late induction phase was complemented with IAA immunolocalization studies. For the localization of IAA in specific cells/tissues during SE induction, samples were collected from several time-points during induction from leaf explants (8, 10, and 12 weeks) and from embryogenic and non-embryogenic *callus* tissue previously induced (EC2 and NEC2) also from leaf explants and in the presence of picloram. The samples were subjected to a fixation protocol with an overnight fixation step in cold ethanol:acetic acid 3:1 (*v:v*) followed by successive incubations in solutions with increasing amounts of sucrose in PBS buffer (0.01 M, pH 7.4): 10% sucrose for 3 h, 15% sucrose for 3 h, and finally 34% sucrose and 0.01% safranin overnight. Before each incubation the samples were vacuum infiltrated for 15 min. After the fixation process, the samples were frozen in optimal temperature cutting compound (OCT, Sakura<sup>®</sup> Finetek, Torrance, CA, USA), cut in a cryostat microtome into 14  $\mu\text{m}$  thick sections that were mounted into poly-L-Lysine-coated slides. The sections were then digested in a 2% driselase<sup>®</sup> (Fluka) solution for 30 min at 37 °C and washed with PBS. After the digestion, the samples were blocked with a 10% (*w:v*) bovine serum albumin (BSA, Thermofisher, Waltham, MA, USA) in PBS buffered solution for 1 h. The samples were then stained with 0.01% indole-3-acetic acid polyclonal antibody in 0.3% (*w:v*) BSA/PBS buffer for 24 h, washed three times with PBS,

and labeled with the secondary antibody 0.002% (*v:v*) Alexa fluor<sup>®</sup> 633 goat anti-rabbit (ThermoFisher, Waltham, MA, USA). Sections were then mounted in DakoCytomation fluorescent mounting medium (Abcam, Cambridge, UK) and examined under a confocal microscope (Zeiss LSM510 META; Carl Zeiss, Jena, Germany).

#### 4.5. Expression of Auxin-Related Genes

Total RNA was extracted from multiple samples during the SE induction and from maintained *calli*, using the kit NucleoSpin<sup>®</sup> RNA Plant (MACHEREY-NAGEL GmbH & Co. KG, Duren, Germany) following the manufacturer's instructions. The final concentration of RNA of each sample was measured using a spectrophotometer (NanoDrop<sup>™</sup>, Thermo Scientific, MA, USA). RNA quality was confirmed with the A260/A280 and A260/A230 ratios and in an agarose gel electrophoresis. cDNA was produced from 1 µg of total RNA from each sample using NZY First-Strand cDNA Synthesis Kit (NZYTech, Lda.—Genes and Enzymes, Lisbon, Portugal) according to the manufacturer's instructions.

Quantitative PCR gene expression analysis of three genes coding Aux/IAA proteins (*IAA11*, *IAA14*, and *IAA17*) and two auxin receptors (TRANSPORT INHIBITOR RESPONSE 1, *TIR1* and AUXIN SIGNALING F-BOX 3, *AFB3*) was made using NZYSpeedy qPCR Green Master Mix (2x) (NZYTech, Lda.—Genes and Enzymes, Lisbon, Portugal), following the instructions provided with the samples diluted 50 times. Samples with the mix were pooled in a 96-well qPCR plate and measured in C1000 Touch<sup>™</sup> Thermal Cycler (Bio-Rad Laboratories, Lda., Amadora, Portugal). For reliable quantitative PCRs, two reference genes were also chosen in order to normalize the data of *Ef1α* and IRON SUPEROXIDE DISMUTASE, *FeSOD* [61]. All the primers (Table 3), with the exception of *TIR1* gene primers (designed for *Solanum lycopersicum* GQ370812.1), were designed for *Solanum betaceum* transcript sequences obtained from embryogenic cell RNAseq libraries (data not published), using the NCBI primer design tool.

**Table 3.** Primers used for the gene expression assay.

Gene	Forward Primer	Reverse Primer	Amplicon Length (bp)
<i>Ef1α</i>	ACAAGCGTGTTCATCGAGAGG	TGTGTCCAGGGGCATCAATC	183
<i>FeSOD</i>	TCACCATCGACGTTTGGG AG	GACTGCTTCCCATGACACCA	114
<i>IAA11</i>	AGGAAGGGTGCTAGTTAGC	TGACACCCCTCGAGTAAGGA	631
<i>IAA14</i>	AGTTTTCCGACGAAGAGGGT	GTGGCCACCACTGAGATCAT	332
<i>IAA17</i>	TTGATGAAGAGCTCGGAGGC	CCCCGTGGCCTTATTTACGA	335
<i>TIR1</i>	AGATGGCTGTCCAAAGCTCC	GAGCCTGTCTCCAAACGGA	389
<i>AFB3</i>	CTGTACGGAAATGGGGTGCT	GCAGAGTACGGGGAACCAAA	284

The expression values (Cq) obtained were first normalized using the mean Cq values for the reference genes used. The method used to analyze the qPCR data was the relative quantification method, or  $2^{-\Delta\Delta CT}$  method, where the  $\Delta\Delta CT$  value = (CQ Target—CQ Reference) [62].

#### 4.6. Statistical and Data Analysis

The homogeneity of variances was tested with the Brown–Forsythe test ( $p < 0.05$ ). In the case of homogeneity of variances, the data was analyzed with a one-way analysis of variance (ANOVA) and, where necessary, the means were compared by Tukey test ( $p < 0.05$ ). In the case non-homogenous variances, a Kruskal–Wallis one-way analysis of variance was used and the means compared by Dunn's multiple comparison test ( $p < 0.05$ ).

To compare outputs between the two IAA quantification methods, a linear interpolation was used with a 95% confidence interval using the program GraphPad<sup>®</sup> Prism version 6.1 for windows.

Immunofluorescent results were analyzed using Fiji software [63], taking the control without antibody labeling for threshold determination and computation of the integrated density of fluorescents.

## 5. Conclusions

Somatic embryogenesis is complex biological process mediated and regulated by several molecular mechanisms. One the most important aspects is the level of endogenous auxin present in the explants. The present work aimed to further study the influence of auxins, namely IAA, in the induction of SE and the conversion of the proembryogenic masses into somatic embryos in indirect somatic embryogenesis of tamarillo, a system that has been extensively optimized and studied. As such, several quantification assays were carried out along the induction phase and on both embryogenic and non-embryogenic *calli*, as well as some differential gene expression studies.

The results in this work show the kinetics of the endogenous IAA content as increasing along the induction phase and a higher concentration of EC over NEC, as well as a decreased IAA degradation rate in EC. Some changes in gene expression level have also been found in some of the main auxin response genes. Furthermore, an assay with TIBA, an auxin polar transport inhibitor, has shown indirectly that IAA is important of the conversion of EC into somatic embryos.

Altogether, the results hint that IAA endogenous concentration is important in induction of proembryogenic masses as it tends to increase along the dedifferentiation process. Additionally, it appears to be relevant for the acquisition and maintenance of embryogenic competence as EC systematically presented a higher concentration of NEC. The genetic expression results presented a general difference between the initial explants of SE and the final proembryogenic masses. Interestingly, the expression values are not quantitatively different between both types of *calli* assayed, a fact that might suggest a different molecular mechanism, either at the biosynthetic or degradation steps in the complex metabolic pathway of auxin homeostasis. Therefore, future studies should aim to further characterize the biosynthesis of IAA in the *calli* as well as a deeper molecular characterization.

**Author Contributions:** Conceptualization: S.C. (Sandra Correia) and J.C.; methodology: A.C. and S.C. (Sandra Caeiro); writing—original draft preparation: A.C. All authors have read and agreed to the published version of the manuscript.

**Funding:** Foundation for Science and Technology (Portugal) supported André Caeiro fellowship (SFRH/BD/137819/2018). This work was carried out at the R&D Unit Center for Functional Ecology—Science for People and the Planet (CFE), with reference UIDB/04004/2020, financed by FCT/MCTES through national funds (PIDDAC). The work was also financed by P2020 | COMPETE grant number PTDC/BAA-AGR/32265/2017, BP4BP—Tamarillo breeding: better plants for better products; and the Centre for Functional Ecology of the University of Coimbra.

**Data Availability Statement:** Not applicable.

**Conflicts of Interest:** The authors declare no conflict of interest.

## References

1. Kahia, J.; Sallah, P.K.; Diby, L.; Kouame, C.; Kirika, M.; Niyitegeka, S.; Asimwe, T. A novel regeneration system for tamarillo (*Cyphomandra betacea*) via organogenesis from hypocotyl, leaf, and root explants. *HortScience* **2015**, *50*, 1375–1378. [[CrossRef](#)]
2. Correia, S.; Lopes, M.L.; Canhoto, J.M. Somatic embryogenesis induction system for cloning an adult *Cyphomandra betacea* (Cav.) Sendt. (tamarillo). *Trees* **2011**, *25*, 1009–1020. [[CrossRef](#)]
3. Diep, T.T.; Rush, E.C.; Yoo, M.J.Y. Tamarillo (*Solanum betaceum* Cav.): A Review of Physicochemical and Bioactive Properties and Potential Applications. *Food Rev. Int.* **2020**, 1–25. [[CrossRef](#)]
4. Prohens, J.; Nuez, F. The tamarillo (*Cyphomandra betacea*): A review of a promising small fruit crop. *Small Fruits Rev.* **2001**, *1*, 43–68. [[CrossRef](#)]
5. Kou, M.-C.; Yen, J.-H.; Hong, J.-T.; Wang, C.-L.; Lin, C.-W.; Wu, M.-J. *Cyphomandra betacea* Sendt. phenolics protect LDL from oxidation and PC12 cells from oxidative stress. *LWT-Food Sci. Technol.* **2009**, *42*, 458–463. [[CrossRef](#)]
6. Correia, S.; Canhoto, J. Biotechnology of tamarillo (*Cyphomandra betacea*): From in vitro cloning to genetic transformation. *Sci. Hortic. (Amst.)* **2012**, *148*, 61–168. [[CrossRef](#)]
7. Mossop, D.W. Isolation, purification, and properties of tamarillo mosaic virus, a member of the potato virus Y group. *N. Z. J. Agric. Res.* **1977**, *20*, 535–541. [[CrossRef](#)]
8. Correia, S.; Canhoto, J. Somatic embryogenesis of tamarillo (*Solanum betaceum* Cav.). In *Vegetative Propagation of Forest Trees*; Jain, S., Gupta, P., Eds.; Springer: Cham, Switzerland, 2016.

9. Cohen, D.; Elliott, D. Micropropagation methods for blueberries and tamarillos [*Cyphomandra betacea*, tree-tomato]. In *Combined Proceedings International Plant Propagators' Society*; International Plant Propagators' Society: Monroe, CT, USA, 1979.
10. Guimarães, M.L.; Tomé, M.C.; Cruz, G.S. *Cyphomandra betacea* (Cav.) Sendtn. (Tamarillo) BT-Trees IV; Bajaj, Y.P.S., Ed.; Springer: Berlin/Heidelberg, Germany, 1996; pp. 120–137.
11. Obando, M.; Goreux, A.; Jordan, M. In vitro regeneration of *Cyphomandra betacea* (Tamarillo) and Andean fruit species. *Cienc. Investig. Agrar.* **1992**, *19*, 125–130. [[CrossRef](#)]
12. Correia, S.; Canhoto, J. Somatic Embryogenesis of Tamarillo (*Solanum betaceum* Cav.). In *Step Wise Protocols for Somatic Embryogenesis on Important Woody Plants*; Jain, S.M., Gupta, P., Eds.; Springer International Publishing: New York, NY, USA, 2018; Volume 2, pp. 171–179.
13. Méndez-Hernández, H.A.; Ledezma-Rodríguez, M.; Avilez-Montalvo, R.N.; Juárez-Gómez, Y.L.; Skeete, A.; Avilez-Montalvo, J.; De-la-Pena, C.; Loyola-Vargas, V.M. Signaling Overview of Plant Somatic Embryogenesis. *Front. Plant Sci.* **2019**, *10*, 77. [[CrossRef](#)]
14. Stasolla, C.; Yeung, E.C. Recent advances in conifer somatic embryogenesis: Improving somatic embryo quality. *Plant Cell. Tissue Organ Cult.* **2003**, *74*, 15–35. [[CrossRef](#)]
15. Jiménez, V.M. Regulation of in vitro somatic embryogenesis with emphasis on the role of endogenous hormones. *Rev. Bras. Fisiol. Veg.* **2001**, *13*, 196–223. [[CrossRef](#)]
16. Guimarães, M.L.S.; Cruz, G.S.; Montezuma-De-Carvalho, J.M. Somatic embryogenesis and plant regeneration in *Cyphomandra betacea* (Cav.) Sendt. *Plant Cell. Tissue Organ Cult.* **1988**, *15*, 161–167. [[CrossRef](#)]
17. Lopes, M.L.; Ferreira, M.R.; Carloto, J.M.; Cruz, G.S.; Canhoto, J.M. Somatic Embryogenesis Induction in Tamarillo (*Cyphomandra betacea*). In *Somatic Embryogenesis in Woody Plants*; Springer: Dordrecht, The Netherlands, 2000; pp. 433–455.
18. Canhoto, J.M.; Lopes, M.L.; Cruz, G.S. Protocol for Somatic Embryogenesis: Tamarillo (*Cyphomandra betacea* (Cav.) Sendtn.). In *Protocol for Somatic Embryogenesis in Woody Plants*; Jain, P., Gupta, S.M., Eds.; Springer: Dordrecht, The Netherlands, 2005.
19. Raghavan, V. Role of 2,4-dichlorophenoxyacetic acid (2,4-D) in somatic embryogenesis on cultured zygotic embryos of Arabidopsis: Cell expansion, cell cycling, and morphogenesis during continuous exposure of embryos to 2,4-D. *Am. J. Bot.* **2004**, *91*, 1743–1756. [[CrossRef](#)] [[PubMed](#)]
20. Winnicki, K. The Winner Takes It All: Auxin-The Main Player during Plant Embryogenesis. *Cells* **2020**, *9*, 606. [[CrossRef](#)]
21. Gaj, M.D. Direct somatic embryogenesis as a rapid and efficient system for in vitro regeneration of *Arabidopsis thaliana*. *Plant Cell. Tissue Organ Cult.* **2001**, *64*, 39–46. [[CrossRef](#)]
22. Hazubska-Przybył, T.; Ratajczak, E.; Obarska, A.; Pers-Kamczyc, E. Different roles of auxins in somatic embryogenesis efficiency in two picea species. *Int. J. Mol. Sci.* **2020**, *21*, 3394. [[CrossRef](#)]
23. Wójcik, A.M.; Wójcikowska, B.; Gaj, M.D. Current perspectives on the auxin-mediated genetic network that controls the induction of somatic embryogenesis in plants. *Int. J. Mol. Sci.* **2020**, *21*, 1333. [[CrossRef](#)]
24. Yang, X.; Zhang, X.; Yuan, D.; Jin, F.; Zhang, Y.; Xu, J. Transcript profiling reveals complex auxin signalling pathway and transcription regulation involved in dedifferentiation and redifferentiation during somatic embryogenesis in cotton. *BMC Plant Biol.* **2012**, *12*, 110. [[CrossRef](#)]
25. Fehér, A. Somatic embryogenesis—Stress-induced remodeling of plant cell fate. *Biochim. Biophys. Acta—Gene Regul. Mech.* **2015**, *1849*, 385–402. [[CrossRef](#)]
26. Liu, C.M.; Xu, Z.H.; Chua, N.H. Auxin polar transport is essential for the establishment of bilateral symmetry during early plant embryogenesis. *Plant Cell* **1993**, *5*, 621–630. [[CrossRef](#)]
27. Vondrakova, Z.; Dobrev, P.I.; Pesek, B.; Fischerova, L.; Vagner, M.; Motyka, V. Profiles of endogenous phytohormones over the course of norway spruce somatic embryogenesis. *Front. Plant Sci.* **2018**, *9*, 1283. [[CrossRef](#)] [[PubMed](#)]
28. Möller, B.; Weijers, D. Auxin control of embryo patterning. *Cold Spring Harb. Perspect. Biol.* **2009**, *1*, a001545. [[CrossRef](#)] [[PubMed](#)]
29. Verma, S.K.; Das, A.K.; Gantait, S.; Gurel, S.; Gurel, E. Influence of auxin and its polar transport inhibitor on the development of somatic embryos in *Digitalis trojana*. *3 Biotech* **2018**, *8*, 99. [[CrossRef](#)] [[PubMed](#)]
30. Teale, W.; Palme, K. Naphthylphthalamic acid and the mechanism of polar auxin transport. *J. Exp. Bot.* **2018**, *69*, 303–312. [[CrossRef](#)]
31. Jenik, P.D.; Gillmor, C.S.; Lukowitz, W. Embryonic patterning in *Arabidopsis thaliana*. *Annu. Rev. Cell Dev. Biol.* **2007**, *23*, 207–236. [[CrossRef](#)]
32. Jiang, K.; Asami, T. Chemical regulators of plant hormones and their applications in basic research and agriculture. *Biosci. Biotechnol. Biochem.* **2018**, *82*, 1265–1300. [[CrossRef](#)]
33. Stuepp, C.A.; Wendling, I.; Trueman, S.J.; Koehler, H.S.; Zuffellato-Ribas, K.C. The use of auxin quantification for understanding clonal tree propagation. *Forests* **2017**, *8*, 27. [[CrossRef](#)]
34. Ayil-Gutiérrez, B.; Galaz-Ávalos, R.M.; Peña-Cabrera, E.; Loyola-Vargas, V.M. Dynamics of the concentration of IAA and some of its conjugates during the induction of somatic embryogenesis in *Coffea canephora*. *Plant Signal. Behav.* **2013**, *8*, e26998. [[CrossRef](#)]
35. Zhou, X.; Zheng, R.; Liu, G.; Xu, Y.; Zhou, Y.; Laux, T.; Zhen, Y.; Harding, S.A.; Shi, J.; Chen, J. Desiccation treatment and endogenous IAA levels are key factors influencing high frequency somatic embryogenesis in *Cunninghamia lanceolata* (Lamb.) hook. *Front. Plant Sci.* **2017**, *8*, 2054. [[CrossRef](#)]
36. Ehmann, A. The van URK-Salkowski reagent—a sensitive and specific chromogenic reagent for silica gel thin-layer chromatographic detection and identification of indole derivatives. *J. Chromatogr. A* **1977**, *132*, 267–276. [[CrossRef](#)]
37. Anthony, A.; Street, H. A colorimetric method for the estimation of certain indoles. *New Phytol.* **1969**, *69*, 47–50. [[CrossRef](#)]

38. Guo, J.M.; Xin, Y.Y.; Yin, X.B. Selective differentiation of indoleacetic acid and indolebutyric acid using colorimetric recognition after ehrlich reaction. *J. Agric. Food Chem.* **2010**, *58*, 6556–6561. [[CrossRef](#)] [[PubMed](#)]
39. Pujari, D.S.; Chanda, S.V. Effect of salinity stress on growth, peroxidase and IAA oxidase activities in *Vigna* seedlings. *Acta Physiol. Plant.* **2002**, *24*, 435–439. [[CrossRef](#)]
40. Simon, S.; Petrášek, J. Why plants need more than one type of auxin. *Plant Sci.* **2011**, *180*, 454–460. [[CrossRef](#)]
41. Paciorek, T.; Friml, J. Auxin signaling. *J. Cell Sci.* **2006**, *119*, 1199–1202. [[CrossRef](#)]
42. Peer, W.A.; Cheng, Y.; Murphy, A.S. Evidence of oxidative attenuation of auxin signalling. *J. Exp. Bot.* **2013**, *64*, 2629–2639. [[CrossRef](#)]
43. Michalczyk, L.; Cooke, T.J.; Cohen, J.D. Auxin levels at different stages of carrot somatic embryogenesis. *Phytochemistry* **1992**, *31*, 1097–1103. [[CrossRef](#)]
44. Pasternak, T.P.; Prinsen, E.; Ayaydin, F.; Miskolczi, P.; Potters, G.; Asard, H.; Van Onckelen, H.A.; Dudits, D.; Fehér, A. The Role of auxin, pH, and stress in the activation of embryogenic cell division in leaf protoplast-derived cells of alfalfa. *Plant Physiol.* **2002**, *129*, 1807–1819. [[CrossRef](#)]
45. Grossmann, K. Auxin Herbicide Action. *Plant Signal. Behav.* **2007**, *2*, 421–423. [[CrossRef](#)]
46. Yang, X.; Zhang, X. Regulation of Somatic Embryogenesis in Higher Plants. *CRC Crit. Rev. Plant Sci.* **2010**, *29*, 36–57. [[CrossRef](#)]
47. Correia, S.; Vinhas, R.; Manadas, B.; Lourenço, A.S.; Veríssimo, P.; Canhoto, J.M. Comparative Proteomic Analysis of Auxin-Induced Embryogenic and Nonembryogenic Tissues of the Solanaceous Tree *Cyphomandra betacea* (Tamarillo). *J. Proteome Res.* **2012**, *11*, 1666–1675. [[CrossRef](#)] [[PubMed](#)]
48. Su, Y.H.; Liu, Y.B.; Bai, B.; Zhang, X.S. Establishment of embryonic shoot-root axis is involved in auxin and cytokinin response during Arabidopsis somatic embryogenesis. *Front. Plant Sci.* **2015**, *5*, 792. [[CrossRef](#)] [[PubMed](#)]
49. Rodríguez-Sanz, H.; Manzanera, J.A.; Solís, M.T.; Gómez-Garay, A.; Pintos, B.; Risueño, M.C.; Testillano, P.S. Early markers are present in both embryogenesis pathways from microspores and immature zygotic embryos in cork oak, *Quercus suber* L. *BMC Plant Biol.* **2014**, *14*, 224. [[CrossRef](#)] [[PubMed](#)]
50. Bai, B.; Su, Y.H.; Yuan, J.; Zhang, X.S. Induction of Somatic Embryos in Arabidopsis Requires Local YUCCA Expression Mediated by the Down-Regulation of Ethylene Biosynthesis. *Mol. Plant* **2013**, *6*, 1247–1260. [[CrossRef](#)] [[PubMed](#)]
51. Santos, I.R.; Maximiano, M.R.; Almeida, R.F.; da Cunha, R.N.V.; Lopes, R.; Scherwinski-Pereira, J.E.; Mehta, A. Genotype-dependent changes of gene expression during somatic embryogenesis in oil palm hybrids (*Elaeis oleifera* x *E. guineensis*). *PLoS ONE* **2019**, *13*, e0209445. [[CrossRef](#)]
52. Luo, J.; Zhou, J.J.; Zhang, J.Z. Aux/IAA gene family in plants: Molecular structure, regulation, and function. *Int. J. Mol. Sci.* **2018**, *19*, 259. [[CrossRef](#)]
53. Elhiti, M.; Stasolla, C. Transduction of Signals during Somatic Embryogenesis. *Plants* **2022**, *11*, 178. [[CrossRef](#)]
54. Kulaeva, O.N.; Prokoptseva, O.S. Recent Advances in the Study of Mechanisms of Action of Phytohormones. *Biochemical* **2004**, *69*, 233–247. [[CrossRef](#)]
55. Gulzar, B.; Mujib, A.; Malik, M.Q.; Sayeed, R.; Mamgain, J.; Ejaz, B. Genes, proteins and other networks regulating somatic embryogenesis in plants. *J. Genet. Eng. Biotechnol.* **2020**, *18*, 31. [[CrossRef](#)]
56. Sun, R.; Wang, S.; Ma, D.; Li, Y.; Liu, C. Genome-Wide Analysis of Cotton Auxin Early Somatic Embryogenesis. *Genes* **2019**, *10*, 730. [[CrossRef](#)]
57. Dharmasiri, N.; Dharmasiri, S.; Estelle, M. The F-box protein TIR1 is an auxin receptor. *Nature* **2005**, *435*, 441–445. [[CrossRef](#)] [[PubMed](#)]
58. Murashige, T.; Skoog, F. A Revised Medium for Rapid Growth and Bio Assays with Tobacco Tissue Cultures. *Physiol. Plant.* **1962**, *15*, 474–497. [[CrossRef](#)]
59. Kim, Y.; Oh, Y.J.; Park, W.J. HPLC-based quantification of indole-3-acetic acid in the primary root tip of maize. *J. Nanobiotechnol.* **2006**, *3*, 40–45.
60. Nakurte, I.; Keisa, A.; Rostoks, N. Development and validation of a reversed-phase liquid chromatography method for the simultaneous determination of indole-3-acetic acid, indole-3-pyruvic acid, and abscisic acid in Barley (*Hordeum vulgare* L.). *J. Anal. Methods Chem.* **2012**, *2012*, 103575. [[CrossRef](#)]
61. Cordeiro, D.; Rito, M.; Borges, F.; Canhoto, J.; Correia, S. Selection and validation of reference genes for qPCR analysis of miRNAs and their targets during somatic embryogenesis in tamarillo (*Solanum betaceum* Cav.). *Plant Cell Tissue Organ Cult.* **2020**, *143*, 109–120. [[CrossRef](#)]
62. Livak, K.J.; Schmittgen, T.D. Analysis of Relative Gene Expression Data Using Real-Time Quantitative PCR and the  $2^{-\Delta\Delta CT}$  Method. *Methods* **2001**, *25*, 402–408. [[CrossRef](#)]
63. Schindelin, J.; Arganda-Carreras, I.; Frise, E.; Kaynig, V.; Longair, M.; Pietzsch, T.; Preibisch, S.; Rueden, C.; Saalfeld, S.; Schmid, B. Fiji: An open-source platform for biological-image analysis. *Nat. Methods* **2012**, *9*, 676–682. [[CrossRef](#)]



## Article

# Productiveness and Berry Quality of New Wine Grape Genotypes Grown under Drought Conditions in a Semi-Arid Wine-Producing Mediterranean Region

Diego José Fernández-López <sup>1</sup>, José Ignacio Fernández-Fernández <sup>2</sup>, Celia Martínez-Mora <sup>1</sup>, Juan Antonio Bleda-Sánchez <sup>2</sup> and Leonor Ruiz-García <sup>1,\*</sup>

<sup>1</sup> Equipo de Mejora Genética Molecular, Departamento de Biotecnología, Genómica y Mejora Vegetal, Instituto Murciano de Investigación y Desarrollo Agrario y Medioambiental, 30150 Murcia, Spain; diegoj.fernandez@carm.es (D.J.F.-L.); celia.martinez@carm.es (C.M.-M.)

<sup>2</sup> Equipo de Enología y Viticultura, Departamento de Desarrollo Rural, Enología y Agricultura Sostenible, Instituto Murciano de Investigación y Desarrollo Agrario y Medioambiental, 30150 Murcia, Spain; josei.fernandez@carm.es (J.I.F.-F.); juanantonio.bleda@carm.es (J.A.B.-S.)

\* Correspondence: leonor.ruiz@carm.es

**Abstract:** One alternative for adapting viticulture to high temperatures and the scarcity of water is the development of new varieties adapted to such conditions. This work describes six new genotypes, derived from “Monastrell” × “Cabernet Sauvignon” (MC16, MC19, MC72, MC80) and “Monastrell” × “Syrah” (MS104, MS49) crosses, grown under deficit irrigation and rainfed conditions in a semi-arid wine-producing area (Murcia, southeastern Spain). The effect of genotype, year, and irrigation treatment on the phenological, productiveness, morphological, and grape quality data was evaluated. The study material was obtained and selected as part of a breeding program run by the *Instituto Murciano de Investigación y Desarrollo Agrario y Medioambiental* (IMIDA). The results obtained show that under rainfed conditions, the values for productive variables decreased, while those referring to the phenolic content increased. Notable variation in the parameters evaluated was also seen for the different genotypes studied. The behavior of the genotypes MC80 and MS104 under rainfed conditions was noteworthy. In addition to maintaining very adequate yields, phenolic contents, must pH, and total acidity values, MC80 fell into the best ‘phenolic quality group’ and MS104 returned a low °Baumé value, ideal for the production of low-alcohol-content wines. These genotypes could favor the development of sustainable quality viticulture in dry and hot areas.

**Keywords:** deficit irrigation; drought; grape quality; phenology; productivity

**Citation:** Fernández-López, D.J.; Fernández-Fernández, J.I.; Martínez-Mora, C.; Bleda-Sánchez, J.A.; Ruiz-García, L. Productiveness and Berry Quality of New Wine Grape Genotypes Grown under Drought Conditions in a Semi-Arid Wine-Producing Mediterranean Region. *Plants* **2022**, *11*, 1363. <https://doi.org/10.3390/plants11101363>

Academic Editors: Petronia Carillo, Paula Baptista and Milan S. Stankovic

Received: 11 April 2022

Accepted: 17 May 2022

Published: 20 May 2022

**Publisher’s Note:** MDPI stays neutral with regard to jurisdictional claims in published maps and institutional affiliations.



**Copyright:** © 2022 by the authors. Licensee MDPI, Basel, Switzerland. This article is an open access article distributed under the terms and conditions of the Creative Commons Attribution (CC BY) license (<https://creativecommons.org/licenses/by/4.0/>).

## 1. Introduction

One of the most severe abiotic stresses expected with climate change in the Mediterranean Basin is drought, which will doubtlessly be aggravated by increased temperatures and solar radiation [1]. The IPCC has reported that areas with Mediterranean climates are likely to face increased drought and reduced renewable surface water and groundwater resources [2]. Despite its ability to adapt to different environmental conditions, the grapevine is one of the most sensitive fruit crops with respect to water scarcity and severe drought; hence, it represents a major concern among viticulturists, winemakers, and enologists regarding the effects of climate change on the production and conservation of wine. This is especially true in the Mediterranean Basin where water resources are particularly vulnerable, and where most grapevine-growing areas are located [3–5]. The climatic scenario for the region, which involves increased drought and raised temperatures, will have consequences for vine development, such as the earlier appearance of the different phenological stages; indeed, this is already taking place [6,7]. Changes may also occur at the physiological level, and the qualitative characteristics of the grapes and eventual

wine will likely be affected [8–15]. Smaller yields can be expected in line with reductions in berry and bunch weight, together with restricted growth, smaller leaf surface areas (with early senescence and premature leaf fall), increased respiration and evapotranspiration, and reduced photosynthetic activity [3,13–17].

Preventive and adaptive measures need to be taken by the wine sector if the adverse effects of climate change are to be mitigated [18–21]. A short-term preventive measure could be the use of deficit irrigation techniques, which may improve the quality of grapes and wine [22–29] while maintaining good yields—as long as the water-stress threshold is not exceeded (which would lead to a reduction in wine quality) [30]. However, Fraga et al. (2018) [31] observed that, in hot and dry regions in Portugal, yields were significantly reduced even when efficient irrigation was available, a consequence of water and heat stress; daytime temperatures above 35 °C negatively affect flowering and fruit set [32] and therefore yield. High temperatures have been correlated to the elevated synthesis of anthocyanins, although at temperatures above 35 °C, anthocyanins stop accumulating and may even be degraded [33–35]. Thus, in hot and dry regions, viticulture cannot be sustained simply by the use of deficit irrigation techniques; it will be necessary to adopt other measures to maintain the sustainability of the system. The selection of suitable plant material (variety/clone and rootstock) from the existing vine biodiversity is one of the most powerful long-term strategies for adapting wine production to water scarcity [1,3,13,36–40]. Another alternative is the development and selection, through directed crosses, of new vines that are better adapted to the specific conditions of the viticulture zone [37,41,42] while still showing good agronomic properties, grape quality, and enological characteristics [43,44]. Changes in vineyard management will, of course be needed too, combining efficient irrigation (if possible) with the use of more drought-tolerant plant material [19,31,45].

Different varieties adapted to current drought conditions have been identified, such as “Monastrell”, “Cabernet Sauvignon”, and “Syrah”, among others [9,22,30,46]. However, the quality of these varieties might fall with the higher temperatures and greater water scarcity expected in the coming years. In fact, climate change forecasts in semi-arid areas, where the availability of water is already limited, indicate that the climate will become warmer and drier, threatening the sustainability of vineyards in the near future [43,47]. Hence, the importance of taking adaptation measures in these areas, especially those related to obtaining and selecting new material that is better adapted to water scarcity and rising temperatures. Since the combination of temperatures > 35 °C and water scarcity can reduce yields and the concentration of polyphenols and anthocyanins in the berries, the selection of new varieties with higher-than-normal concentrations of polyphenols and anthocyanins is of great interest. Excessive sugar accumulation may also occur under hot conditions, with a consequent increase in the alcohol content of the eventual wine. Thus, varieties are also needed that ripen with a lower sugar concentration under such conditions. This would be of great interest since it might lead to products suitable for consumers who demand quality wines with lower alcohol contents.

The Instituto Murciano de Investigación y Desarrollo Agrario y Medioambiental (IMIDA), in Murcia, Spain, has been running a program to develop grapevine varieties with better phenolic quality for semi-arid wine-producing areas since the 1990s. The program is based on new genotypes obtained from crosses between ‘Monastrell’ and other varieties such as Cabernet Sauvignon, Syrah, Tempranillo, Verdejo and Barbera [48–50]. ‘Monastrell’ is cultivated in different parts of Spain (particularly the southeast); it is the main variety grown in the Jumilla, Bullas and Yecla Denominations of Origin (occupying 81% of the cultivated area)—all of which have a semi-arid Mediterranean climate, with hot summers, mild winters, and scant rainfall that averages between 300 and 350 mm/year. It is also cultivated in France (where it is known as ‘Mourvedre’), California (where it is known as ‘Mataró’), and Chile, and in recent years, it has been increasingly planted in Australia [51].

Using study material produced within the above IMIDA breeding program, the present work examines the effect of genotype, year, and irrigation treatment (collecting phenological, productiveness, morphological, and grape quality data) for six new genotypes

obtained via “Monastrell” × “Cabernet Sauvignon” and “Monastrell” × “Syrah” crosses, when grown under controlled deficit irrigation and rainfed conditions. The final objective of this work is the identification and selection of new genotypes best adapted to the conditions of drought and high temperatures in semi-arid zones, as a measure of adaptation to the adverse effects of climate change.

## 2. Results

### 2.1. Phenological Stages

Table 1 shows that for most of the phenological stages studied, significant variation ( $p < 0.001$ ) existed among the genotypes and the year of study within the same irrigation treatment. No significant differences were found between irrigation treatments for the phenological stages.

**Table 1.** Mean data (2018–2021) for the phenological stage dates of the six new genotypes grown under regulated deficit irrigation (RDI) and rainfed conditions.

Genotype	Budbreak		Flowering		Veraison		Harvest		Leaf Fall Start		Total Leaf Fall	
	RDI	Rainfed	RDI	Rainfed	RDI	Rainfed	RDI	Rainfed	RDI	Rainfed	RDI	Rainfed
MC16	Apr 16 ab,α	Apr 16 ab,α	May 28 ab,α	May 29 a,α	Aug 09 c,α	Aug 10 c,α	Sep 14 b,α	Sep 11 c,α	Oct 13 b,α	Oct 13 b,α	Nov 27 c,α	Nov 29 cd,α
MC19	Apr 21 c,α	Apr 24 c,α	Jun 03 c,α	Jun 04 b,α	Aug 04 b,α	Aug 06 b,α	Aug 29 a,α	Sep 05 b,α	Oct 30 d,α	Oct 27 cd,α	Dec 03 d,α	Dec 02 cd,α
MC72	Apr 12 a,α	Apr 12 a,α	May 27 a,α	May 28 a,α	Aug 01 a,α	Aug 02 a,α	Aug 26 a,α	Aug 25 a,α	Nov 08 e,α	Nov 06 e,α	Dec 06 d,α	Dec 05 d,α
MC80	Apr 19 bc,α	Apr 19 bc,α	Jun 01 bc,α	Jun 01 ab,α	Aug 12 d,β	Aug 10 c,α	Sep 13 b,α	Sep 13 c,α	Nov 03 de,α	Nov 02 de,α	Nov 27 c,α	Nov 27 c,α
MS49	Apr 16 b,α	Apr 16 ab,α	May 29 ab,α	May 28 a,α	Jul 31 a,α	Aug 02 a,α	Aug 30 a,α	Aug 29 a,α	Sep 19 a,β	Sep 15 a,α	Nov 09 a,α	Nov 08 a,α
MS104	Apr 16 b,α	Apr 17 ab,α	May 30 abc,α	Jun 01 ab,α	Aug 09 c,α	Aug 11 c,α	Sep 09 b,α	Sep 06 b,α	Oct 21 c,α	Oct 20 bc,α	Nov 22 b,α	Nov 20 b,α
Irrigation Year	Apr 17 α	Apr 18 α	May 30 α	May 31 α	Aug 06 α	Aug 07 α	Sep 04 α	Sep 04 α	Oct 21 α	Oct 20 α	Nov 26 α	Nov 26 α
2018	Apr 11 a,α	Apr 11 a,α	May 27 a,α	May 26 b,α	Aug 04 a,α	Aug 06 ab,α	Sep 10 b,α	Sep 14 c,α	-	-	-	-
2019	Apr 25 c,α	Apr 27 c,α	Jun 08 b,α	Jun 10 c,β	Aug 07 a,α	Aug 09 b,β	Sep 04 ab,α	Sep 04 b,α	Oct 31 b,α	Oct 31 b,α	Nov 30 b,α	Nov 29 b,α
2020	Apr 13 a,α	Apr 13 a,α	May 26 a,α	May 25 a,α	Aug 06 a,α	Aug 05 a,α	Aug 30 a,α	Aug 30 a,α	Oct 14 a,α	Oct 12 a,α	Nov 26 b,α	Nov 27 b,α
2021	Apr 16 b,α	Apr 16 b,α	May 27 a,α	May 28 b,α	Aug 06 a,α	Aug 05 a,α	Sep 06 b,α	Sep 03 b,α	Oct 18 a,α	Oct 17 a,α	Nov 21 a,α	Nov 19 a,α

For each genotype and year, different letters in the same column (a–e) indicate significant differences among genotypes and years, respectively, at the 5% level, according to Duncan’s multiple range test. For each phenological stage date, different letters in the same row (α, β) indicate significant differences between the irrigation treatments (Duncan test,  $p < 0.05$ ).

The mean duration of the period from budbreak to total leaf fall was very similar under both the RDI and rainfed conditions (223 and 222 days, respectively). MS104 had the shortest mean duration of this phenological period under both (RDI 207 days, and rainfed 205 days), while MC72 had the longest (238 days and 237 days, respectively).

The ripening period, i.e., from the date of veraison to the date of harvest, averaged 29 days under RDI, and 28 days under the rainfed conditions. MC72 had the shortest maturation period under both conditions (mean 25 and 23 days, respectively), while MC16 had the longest under the RDI conditions (mean 36 days), and MC80 the longest under the rainfed conditions (mean 34 days). Taking into account the mean harvest date, MC16, MC80, and MS49 were the latest maturing genotypes, while MC19, MC72, and MS104 were the earliest (Table 1). Finally, the overall mean period of leaf fall, calculated from the starting date to total leaf fall, was 36 and 37 days under the RDI and rainfed conditions, respectively. Again, there were differences among the genotypes: MS104 had the longest period of leaf fall (mean 52 and 54 days under the RDI and rainfed conditions, respectively), whereas MC80 had the shortest (mean 24 and 25 days, respectively). MS104 entered its rest period the earliest (9–8 December), and MC72 the latest (5–6 December).

### 2.2. Yield Parameters

The yield values varied significantly among the genotypes (G), irrigation treatments (T), and year of study (Y) (Table 2), with the interaction  $G \times Y$  strongest ( $p < 0.001$ ) with respect to most yield variables. The interaction  $G \times T \times Y$  was significant ( $p < 0.001$ ) only for the parameters related to the weight of the berry. The total yield ( $\text{kg vine}^{-1}$ ) was significantly lower under the rainfed conditions than under RDI, with a mean reduction for the study period (2018–2021) of 39.4%, mainly due to the reduced mean weight of the bunches (33.5%), berries (20.5%) and number of bunches (14.3%). MS104 was the most productive genotype under both the RDI (mean  $2.52 \text{ kg vine}^{-1}$ ) and rainfed (mean

1.51 kg vine<sup>-1</sup>) conditions, mainly due to a higher mean bunch weight under both (mean RDI 131.04 g, mean rainfed 87.46 g). MC19 and MC72 were the least productive under both RDI (mean 1.76 kg vine<sup>-1</sup>) and rainfed (mean value of 1.03 kg vine<sup>-1</sup>) conditions, probably because MC19 had one of the lowest number of bunches and MC72 one of the lowest mean bunch weights (Table 2).

**Table 2.** Yield components of the six genotypes grown under regulated deficit irrigation (RDI) and rainfed conditions over the four-year study period (2018–2021), and the mean values for that period.

Genotype	2018		2019		2020		2021		2018–2021		ANOVA							
	RDI	Rainfed	RDI	Rainfed	RDI	Rainfed	RDI	Rainfed	RDI	Rainfed	G	T	Y	G × T	G × Y	T × Y	G × T × Y	
Yield (kg vine <sup>-1</sup> )	MC16	2.55 b,α	2.10 b,α	1.97 bc,β	0.86 ab,α	1.12 a,α	0.68 ab,α	2.29 ab,α	1.53 ab,α	1.94 a,β	1.38 ab,α	***	***	***	*	**	ns	ns
	MC19	1.83 a,β	1.56 a,α	1.10 a,α	0.50 a,α	1.29 a,β	0.63 a,β	2.43 abc,β	1.32 ab,α	1.76 a,β	1.03 a,α							
	MC72	1.75 a,β	1.25 a,α	1.50 abc,β	0.54 a,α	1.82 b,β	0.83 ab,α	1.84 ab,β	1.24 ab,α	1.76 a,β	1.03 a,α							
	MC80	2.89 bc,β	2.07 b,α	1.30 ab,α	0.77 ab,α	1.04 a,α	0.79 ab,α	1.78 a,α	1.51 ab,α	1.77 a,β	1.39 ab,α							
	MS104	2.90 bc,β	2.00 b,α	2.18 c,α	1.33 b,α	1.39 ab,α	0.92 b,α	3.47 c,β	1.70 b,α	2.52 b,β	1.51 b,α							
	MS49	3.17 c,β	2.27 b,α	2.03 bc,β	0.62 ab,α	1.34 ab,β	0.42 a,α	2.95 bc,β	0.90 a,α	2.47 b,β	1.14 ab,α							
	Average	2.54 β	1.88 α	1.67 β	0.74 α	1.33 β	0.71 α	2.40 β	1.39 α	2.03 β	1.23 α							
	N° bunches vine <sup>-1</sup>	MC16	20 a,α	20 a,α	bc,α	23 c,α	19 a,α	21 c,α	19 a,α	19 b,α	20 a,α	***	***	***	ns	***	**	*
MC19		22 a,α	27 b,α	13 a,α	10 a,α	19 a,β	12 a,α	18 a,α	13 a,β	19 a,β								
MC72		25 ab,α	22 ab,α	21 bc,α	15 b,α	23 b,β	18 bc,α	21 a,β	18 b,α	23 b,β	18 abc,α							
MC80		22 a,α	21 a,α	21 bc,α	17 bc,α	17 a,α	15 ab,α	19 a,α	17 ab,α	19 a,α	17 ab,α							
MS104		22 a,α	20 a,α	17 ab,α	19 bc,α	18 a,α	14 ab,α	18 a,α	17 b,α	19 a,α	17 ab,α							
MS49		28 b,α	33 c,β	23 c,α	17 b,α	20 ab,β	16 abc,α	22 a,α	16 ab,β	23 b,α	22 c,α							
Average		23 α	24 α	20 β	16 α	19 β	16 α	20 β	16 α	21 β	18 α							
Bunch weight (g)		MC16	130.90 c,α	108.97 b,α	88.59 a,β	37.15 a,α	58.03 a,β	30.10 ab,α	115.20 abc,α	79.60 abc,α	97.60 ab,β	69.21 bc,α	***	***	***	*	***	ns
	MC19	89.05 ab,β	62.70 a,α	80.21 a,β	43.56 a,α	67.26 ab,β	45.66 bc,α	130.05 b,β	88.12 bc,α	93.53 ab,β	61.79 abc,α							
	MC72	70.25 a,α	61.84 a,α	69.46 a,β	34.78 a,α	78.40 b,β	46.66 bc,α	86.38 a,β	67.83 ab,α	77.52 a,β	55.54 ab,α							
	MC80	139.49 c,β	99.12 b,α	60.92 a,α	38.41 a,α	62.40 ab,α	44.88 bc,α	92.83 a,α	89.26 bc,α	90.99 ab,α	74.25 cd,α							
	MS104	148.07 c,α	112.31 b,α	124.78 b,β	68.28 a,α	73.39 ab,α	60.49 c,α	176.14 c,β	98.11 c,α	131.04 c,β	87.46 d,α							
	MS49	118.03 bc,β	70.57 a,α	87.14 a,β	36.37 a,α	64.52 ab,β	24.91 a,α	133.74 b,β	56.37 a,α	104.10 b,β	48.93 a,α							
	Average	116.10 β	85.36 α	84.56 β	42.82 α	66.82 β	42.17 α	119.41 β	79.38 α	98.53 β	65.51 α							
	Berry weight (g)	MC16	0.97 b,β	0.75 a,α	0.71 a,β	0.52 a,α	0.85 a,β	0.64 a,β	1.39 b,β	0.93 a,α	0.96 a,β	0.78 a,α	***	***	***	***	***	**
MC19		1.17 c,β	0.79 a,α	0.98 b,β	0.64 ab,α	1.00 ab,α	0.89 bc,α	1.42 b,β	1.03 ab,α	0.99 ab,β	0.86 b,α							
MC72		0.94 b,β	0.78 a,α	0.97 b,β	0.77 b,α	1.13 b,β	0.83 abc,α	1.17 a,α	1.13 b,α	1.06 ab,β	0.86 b,α							
MC80		1.17 c,α	0.88 a,α	1.08 b,β	0.66 ab,α	1.04 ab,α	0.96 c,α	1.34 b,α	1.27 c,α	1.09 b,α	1.03 c,α							
MS104		0.72 a,α	0.70 a,α	1.03 b,α	0.78 b,α	1.19 b,α	1.02 c,α	1.61 c,β	1.34 c,α	1.22 c,β	1.03 c,α							
MS49		1.20 c,β	0.82 a,α	1.19 b,β	0.59 ab,α	1.19 b,β	0.66 ab,α	1.75 d,β	1.01 a,α	1.39 d,β	0.81 ab,α							
Average		1.05 β	0.88 α	1.00 β	0.77 α	1.00 β	0.82 α	1.44 β	1.12 α	1.12 β	0.89 α							
% skin		MC16	18.63 d,β	15.11 c,α	9.98 b,α	11.71 b,α	12.27 c,α	13.49 c,α	11.04 d,α	12.57 c,β	13.48 e,α	14.21 d,α	***	*	***	***	***	ns
	MC19	8.66 a,α	12.45 b,β	9.39 c,α	8.77 a,α	08.37 a,α	7.98 a,α	7.72 a,α	8.66 a,β	9.99 a,α	9.03 a,α							
	MC72	13.41 c,β	11.00 b,α	9.60 c,α	9.17 a,α	11.67 b,α	10.13 b,α	10.33 c,α	10.22 b,α	10.72 c,α	11.23 b,α							
	MC80	13.46 c,α	15.46 d,α	12.31 b,α	12.19 b,α	11.96 bc,α	12.04 e,α	12.67 c,α	12.41 c,α	12.40 d,α	13.11 c,β							
	MS104	11.20 b,α	10.99 b,α	7.87 b,α	7.51 a,α	7.10 a,α	6.85 a,α	8.77 a,α	8.70 a,α	9.65 a,α	9.10 a,α							
	MS49	7.31 a,α	8.17 a,α	5.83 a,α	8.26 a,β	7.50 a,α	7.93 a,α	7.89 a,α	9.80 b,β	8.29 a,α	10.87 b,β							
	Average	11.69 α	11.27 α	9.78 α	11.25 β	11.25 α	11.68 α	9.74 α	10.39 β	10.75 α	11.26 β							

Table 2. Cont.

Genotype	2018		2019		2020		2021		2018–2021		ANOVA						
	RDI	Rainfed	RDI	Rainfed	RDI	Rainfed	RDI	Rainfed	RDI	Rainfed	G	T	Y	G × T	G × Y	T × Y	G × T × Y
MC16	7.51 bcd,α	8.13 ab,α	8.86 b,α	13.87 c,β	8.97 b,α	10.23 c,α	6.89 d,α	9.55 e,β	8.68 d,α	10.88 e,β	***	***	***	***	***	ns	***
MC19	4.47 a,α	8.38 abc,β	5.73 a,α	7.40 a,α	6.41 a,α	5.61 a,α	3.90 a,α	5.18 a,β	5.27 a,α	6.20 a,β							
MC72	7.92 cd,α	10.10 c,α	6.66 a,α	8.43 ab,α	8.95 b,α	10.67 c,α	7.09 d,α	7.27 c,α	7.76 c,α	10.30 de,β							
MC80	5.70 ab,α	6.59 a,α	8.54 b,α	8.96 ab,α	8.43 b,α	10.29 c,α	7.94 e,α	8.52 d,β	9.32 e,α	9.36 c,α							
MS104	8.39 d,α	9.51 bc,α	7.11 a,α	9.90 ab,β	6.29 a,α	7.84 b,β	5.01 b,α	6.40 b,β	6.57 b,α	7.92 b,β							
MS49	6.47 bc,α	9.36 bc,β	6.65 a,α	10.08 b,β	7.49 ab,α	9.82 bc,β	5.53 c,α	8.06 d,β	6.63 b,α	9.87 cd,β							
Average	6.74 α	8.68 β	7.26 α	9.77 β	7.76 α	9.08 β	6.06 α	7.49 β	7.38 α	9.11 β							

For each productive variable, year and irrigation treatment, different letters in the same column (a–e) indicate significant differences among genotypes (Duncan’s multiple range test,  $p < 0.05$ ). For each productive variable, genotype and year, different letters in the same row (α, β) indicate significant differences between the irrigation treatments (Duncan’s multiple range test,  $p < 0.05$ ). %skin, percentage contribution of the skin to berry weight; %seeds, percentage contribution of the seeds to berry weight. Analysis of variance (three-way ANOVA) by genotype (G), irrigation treatment (T), year (Y) and their interactions: ns: non-significant; \*  $p < 0.05$ ; \*\*  $p < 0.01$ ; \*\*\*  $p < 0.001$ .

MC80 returned the least affected total yield under the rainfed conditions compared to RDI, with a mean reduction of 21%, mainly due to less reduced bunch (18%) and berry weights (6%). MS49 was the genotype most affected by the rainfed conditions, with an average reduction of 54% compared to under RDI, mainly due to a greater reduction in the bunch (53%) and berry weights (41%). A progressive reduction in the mean total yield (i.e., of all genotypes) was also observed from 2018 to 2020, under both the RDI (48%) and rainfed conditions (62%), coinciding with a reduction in bunch weight (42% under RDI and 51% under rainfed conditions) and in the number of bunches (16% and 34%, respectively). Compared to 2020, in 2021, there was a recovery in the total yield (80% under RDI and 96% under rainfed conditions) and in the mean bunch weight (79% under RDI and 88% under rainfed conditions) (Table 2).

The berry weight variables were those most significantly influenced by the interactions  $G \times T$ ,  $G \times Y$  and  $G \times T \times Y$  ( $p < 0.001$ ). The mean berry weight was significantly reduced under the rainfed conditions compared to RDI, with a mean reduction of 20%; MS49 showed the mean berry weight most affected, with a reduction of 41% compared to 6% for MC80 (Table 2). The mean percentage contribution of the skin (%skin) and of the seeds (%seeds) to berry weight increased under the rainfed conditions by 5% and 23%, respectively, compared to RDI. MC80 was the genotype with the most increased %skin under the rainfed compared to the RDI conditions (57%). %skin values are a sign of quality; MC16 and MC80 returned the highest %skin contributions to berry weight, both under the RDI (13.48% and 12.40%, respectively) and rainfed (14.21% and 13.11%, respectively) conditions; MC16 also returned the lowest mean berry weight (0.96 g under RDI and 0.78 g under rainfed conditions). All genotypes maintained a mean berry weight under 1.80 g (a quality criterion used in the initial selection process) under both irrigation treatments.

### 2.3. Characterization of the Bunches and Berries

Table 3 shows that the values for most of the variables used in the characterization of the bunches and berries varied significantly ( $p < 0.001$ ) between the genotypes (G), irrigation treatments (T), and years of study (Y), and in terms of the influence of the interaction  $G \times T$  and  $G \times Y$ . The interaction of  $G \times T \times Y$  was strong ( $p < 0.001$ ) only for the berry width. MC16, MC19, and MC72 showed the least compact clusters under both irrigation treatments, coinciding with a greater cluster length and shorter berry length and width (Table 3).

**Table 3.** Morphological characterization of the bunches and berries of the new genotypes grown under regulated deficit irrigation (RDI) and rainfed conditions over the four-year study period (2018–2021), and the mean values for that period.

Genotype	2018		2019		2020		2021		2018–2021		ANOVA							
	RDI	Rainfed	RDI	Rainfed	RDI	Rainfed	RDI	Rainfed	RDI	Rainfed	G	T	Y	G × T	G × Y	T × Y	G × T × Y	
Bunch length (mm)	MC16	173 bc,α	176 c,α	136 ab,α	127 a,α	147 ab,α	156 b,α	162 ab,α	161 c,α	155 bc,α	155 d,α	***	***	***	**	***	ns	*
	MC19	191 c,β	164 bc,α	129 ab,α	125 a,α	167 bc,α	152 b,α	163 ab,β	128 a,α	162 cd,β	142 c,α							
	MC72	174 bc,α	156 abc,α	154 b,β	121 a,α	174 c,α	148 b,α	170 b,β	145 abc,α	168 d,β	143 c,α							
	MC80	156 ab,α	137 a,α	121 a,α	117 a,α	152 abc,β	127 ab,α	150 a,α	153 bc,α	145 ab,β	134 bc,α							
	MS104	132 a,α	130 a,α	128 a,α	111 a,α	144 ab,β	113 a,α	157 ab,α	143 ab,α	140 a,β	124 ab,α							
	MS49	151 ab,α	141 ab,α	139 ab,β	99 a,α	156 a,β	113 a,α	164 ab,β	131 a,α	148 ab,β	121 a,α							
	Average	163 α	151 α	135 β	117 α	153 β	135 α	161 β	143 α	153 β	136 α							
	MC16	94 abc,α	112 d,β	95 ab,α	79 ab,α	88 ab,α	81 bc,α	87 a,α	86 b,α	91 b,α	90 c,α	***	***	***	***	***	ns	*
	MC19	115 cd,α	97 bcd,α	92 ab,α	78 ab,α	87 ab,α	87 71 b,α	97 ab,β	70 a,α	98 bc,β	79 b,α							
	MC72	129 d,β	106 cd,α	114 b,β	81 ab,α	119 c,α	103 c,α	128 c,β	102 c,α	123 d,β	123 98 d,α							
MC80	100 bc,α	87 ab,α	80 a,α	79 ab,α	89 ab,α	89 77 b,α	108 b,α	99 c,α	95 bc,β	85 bc,α								
MS104	85 ab,α	89 abc,α	116 b,α	93 b,α	95 b,α	93 bc,α	109 b,β	95 bc,α	101 c,β	93 cd,α								
MS49	75 a,α	71 a,α	71 a,α	59 a,α	70 a,β	47 a,α	87 a,β	70 a,α	76 a,β	62 a,α								
Average	100 α	94 α	95 β	78 α	91 β	79 α	103 β	87 α	97 β	84 α								
Bunch compactness (OIV)	MC16	5	5	3	3	3	3	5	5	3–5	3–5							
	MC19	5	3	5	3	5	3	7	5	5	3							
	MC72	3	3	1	1	1	1	1	1	1	1							
	MC80	7	7	5	5	7	7	7	7	7	7							
	MS49	7	7	7	7	7	7	7	7	7	7							
Average	7	7	7	7	7	7	7	7	7	7								
Berry length (mm)	MC16	11.50 bc,α	11.29 c,α	10.49 a,β	9.08 a,α	10.45 a,α	10.44 a,α	11.56 a,β	10.86 a,α	11.00 a,β	10.42 a,α	***	***	***	**	***	ns	**
	MC19	12.16 cd,β	10.59 ab,α	10.83 ab,α	9.77 ab,α	11.05 a,α	10.74 a,α	12.85 b,β	11.17 a,α	11.72 bc,β	10.57 ab,α							
	MC72	10.91 ab,α	10.67 abc,α	11.15 ab,α	10.07 bc,β	12.23 a,α	10.97 ab,α	12.24 ab,α	12.04 b,α	11.63 b,β	10.94 abc,α							
	MC80	12.44 d,β	11.07 bc,α	11.95 c,β	9.74 ab,α	11.86 b,α	11.29 a,α	12.26 ab,α	12.07 b,α	12.13 bc,β	11.04 bc,α							
	MS104	10.59 a,α	10.28 a,α	11.48 bc,α	10.69 b,α	11.95 b,β	11.00 a,α	14.84 c,β	13.13 c,α	12.21 c,β	11.27 c,α							
	MS49	13.95 e,β	12.10 d,α	12.96 d,β	10.35 b,α	12.96 c,β	10.73 a,α	14.20 c,β	12.77 c,α	13.52 d,β	11.49 c,α							
	Average	11.93 β	11.00 α	11.48 β	9.95 α	11.75 β	10.86 α	12.99 β	12.01 α	12.04 β	10.95 α							
	MC16	11.44 b,α	10.89 b,α	10.296 a,β	9.33 a,α	10.70 a,β	9.11 a,α	11.51 a,β	10.62 a,α	10.98 a,β	9.99 a,α	***	***	***	**	***	ns	***
	MC19	12.08 bc,β	10.55 ab,α	10.81 a,α	10.05 ab,α	11.09 ab,α	10.85 b,α	12.55 ab,β	11.38 b,α	11.63 bc,β	10.71 bc,α							
	MC72	10.50 a,α	10.45 ab,α	10.87 ab,α	9.99 ab,α	12.05 c,β	10.61 b,α	11.69 bc,α	11.74 bc,α	11.28 bc,α	10.70 bc,α							
MC80	12.20 c,β	10.74 bc,α	11.64 ab,α	10.11 bc,α	11.61 bc,α	11.49 b,α	12.33 c,α	12.10 cd,α	11.94 cd,β	11.11 c,α								
MS104	9.95 a,α	10.06 a,α	10.93 ab,α	10.56 b,α	12.06 b,α	11.19 c,β	13.63 d,α	12.60 bc,α	11.64 bc,α	11.10 c,α								
MS49	12.02 bc,β	10.84 b,α	11.89 c,β	11.89 ab,α	9.73 c,β	12.44 a,α	9.58 d,β	12.48 bc,α	11.46 d,β	10.40 ab,α								
Average	11.36 β	10.59 α	11.07 β	9.96 α	11.66 β	10.47 α	12.37 β	11.65 α	11.61 β	10.67 α								

For each morphological variable, year and irrigation treatment, different letters in the same column (a–e) indicate significant differences among genotypes (Duncan’s multiple range test,  $p < 0.05$ ). For each morphological variable, genotype and year, different letters in the same row (α, β) indicate significant differences between the irrigation treatments (Duncan’s multiple range test,  $p < 0.05$ ). OIV 204 descriptor (bunch compactness): 1, very loose; 3, loose; 5, medium; 7, compact; 9, very compact. Analysis of variance (three-way ANOVA) by genotype (G), irrigation treatment (T), year (Y) and their interactions: ns: non-significant; \*  $p < 0.05$ ; \*\*  $p < 0.01$ ; \*\*\*  $p < 0.001$ .

The mean length and width of both the bunches and the berries were significantly reduced under rainfed conditions compared to RDI, coinciding with a reduction in the bunch and berry mean weight (Table 2). The mean reduction was 11% for the bunch length, 13% for the bunch width, 9% for the berry length, and 8% for the berry width. Under rainfed conditions, MC19 and MS49 showed a reduction in bunch compactness, coinciding with one of the greatest reductions in bunch length (12% and 18%, respectively) and width (19% and 18%, respectively), and with one of the largest reductions in berry length (10% and 15%, respectively) and width (8% and 15%, respectively).

No variation was seen among the genotypes or irrigation treatments in terms of berry skin and pulp color pulp, or berry flavor. All had a blue-black skin color (OIV 225 rank 9), showed an absence of anthocyanin pigmentation in the pulp (OIV 231 rank 1), and had a flavor catalogued as not moscatel, foxé, or herbaceous (OIV 236 rank 5).

### 2.4. Grape Quality

The mean values for all the variables used to characterize grape quality (Table 4) varied significantly ( $p < 0.001$ ) among the genotypes (G), but only some varied significantly between the irrigation treatments (T) and year of study (Y). Only the interaction  $G \times Y$  and  $G \times T \times Y$  had any significant influence on all these variables ( $p < 0.001$ ). Both the TPC skin–seed and the anthocyanin contents were significantly higher under the rainfed than the RDI conditions, with a mean increase (period 2018–2021) of 16% and 10%, respectively. Under rainfed conditions, the greatest percentage increase in TPC skin–seed was for MS49 (47%), while MC72 showed the lowest (7%). Except for MC72, which remained in ‘quality group’ 2 (based on mean TPC skin–seed values), a trend was observed for the quality group to improve under these conditions, especially for MS49 (Table 4). The greatest percentage increase in the anthocyanin content was again seen for MS49 (35%), while MC80 had the lowest percentage increase (3%). MC16 and MC80 fell into the best “quality groups” (for both TPC skin–seed and anthocyanin content) under both the RDI and rainfed conditions.

**Table 4.** Values of different quality variables for the grapes of the new genotypes grown under regulated deficit irrigation (RDI) and rainfed conditions over the four-year study period (2018–2021), and the mean values for that period.

	Genotype	2018		2019		2020		2021		2018–2021		ANOVA						
		RDI	Rainfed	RDI	Rainfed	RDI	Rainfed	RDI	Rainfed	RDI	Rainfed	G	T	Y	G × T	G × Y	T × Y	G × T × Y
TPC skin–seed (mg kg <sup>-1</sup> berry)	MC16	2849 c,α	3217 b,β	3289 b,α	3764 de,β	3560 d,α	3352 c,β	2915 d,α	3627 c,β	3222 d,α	3504 c,β	***	***	ns	***	***	ns	***
	MC19	2038 a,α	3093 b,β	2432 a,α	5204 c,β	2479 b,α	2485 a,α	2053 a,α	2429 a,β	2271 ab,α	2603 b,β							
	MC72	2098 a,α	3316 b,β	2598 a,β	2101 a,α	2148 a,α	2443 a,α	2340 a,α	2346 b,α	2262 a,α	2415 a,β							
	MS104	3483 d,α	2462 c,β	2445 b,α	2609 d,β	2356 c,α	2749 d,β	2276 e,α	2674 d,α	2391 e,α	2688 d,β							
	MS49	2408 b,α	3138 b,β	2371 a,α	4010 e,β	2203 a,α	3222 c,β	2654 c,α	3846 d,β	2421 c,α	3563 c,β							
	Average	2686 α	3178 β	2725 α	3207 β	2661 α	3042 β	2665 α	3125 β	2662 α	3090 β							
	TPC Quality group <sup>Y</sup>	MC16	2–3	3–4	4	4	4	4	3	4	3–4	4						
	MC19	1–2	3	2	3–4	2	2	1–2	2	2	2–3	2						
	MC72	1–2	4	2–3	2	2	2	2	2	2	2	2						
	MC80	3–4	4	3–4	4	3–4	4	4	4	4	4	4						
MS104	4	2	2	2–3	2	2–3	2	2–3	2	2–3	2							
MS49	2	3	2	4	2	3–4	2–3	4	4	2	4							
Average	2–3	3	2–3	3–4	2–3	3	2–3	3	2–3	3								
Anthocyanins (mg kg <sup>-1</sup> berry)	MC16	2844 d,α	3322 c,β	2637 c,α	3393 d,β	3525 e,α	3473 d,α	2725 c,α	3217 d,β	3059 f,α	3349 e,β	***	***	***	***	***	ns	***
	MC19	2103 b,α	3344 c,β	2724 c,α	2913 d,α	2806 d,α	2815 b,α	2146 b,α	2323 b,β	2483 c,α	2645 c,β							
	MC72	1213 a,α	2254 b,β	1437 a,α	1470 a,β	2108 a,α	2000 a,α	2143 b,α	2056 a,α	2015 a,α	1983 a,α							
	MC80	2807 d,α	3224 c,β	3144 d,α	3268 d,β	2841 d,α	3081 c,β	2947 d,β	2792 c,α	2916 e,α	2999 d,α							
	MS104	2362 bc,β	1935 a,α	2190 b,α	2220 b,α	2463 b,α	2669 b,β	1963 a,α	2127 a,β	2218 b,α	2355 b,β							
	MS49	2385 c,α	3173 c,β	2734 c,α	4115 e,β	2636 c,α	3577 d,β	2618 c,α	3415 e,β	2625 d,α	3544 f,β							
	Average	2286 α	2875 β	2478 α	2897 β	2730 α	2936 β	2424 α	2655 β	2543 α	2796 β							
	Anthoc Quality group <sup>Y</sup>	MC16	4	4	4	4	4	4	4	4	4	4						
	MC19	2–3	4	4	4	4	4	2–3	3	3	3	4						
	MC72	2	3	2	2	2	2–3	2–3	2–3	2–3	2–3	2–3						
MC80	4	4	4	4	4	4	4	4	4	4	4							
MS104	3	2–3	2–3	2–3	3	4	2–3	2–3	2–3	2–3	3							
MS49	3	4	4	4	4	4	4	4	4	4	4							
Average	3	4	3	4	4	4	3	4	3	4								
°Baumé	MC16	13.8 d,α	13.8 d,α	12.8 b,α	14.2 c,β	14.8 c,α	14.6 d,α	14.2 d,α	13.8 cd,α	14.2 d,α	14.2 c,α	***	ns	**	**	***	ns	***
	MC19	11.6 b,β	11.2 b,α	13.8 e,β	13.6 d,α	14.2 de,α	13.9 c,α	13.2 bc,α	12.4 b,β	13.5 c,α	13.0 bc,α							
	MC72	14.1 e,β	13.3 e,α	14.2 f,β	13.3 b,α	13.1 cd,β	13.1 b,α	14.1 d,α	14.2 d,α	13.9 cd,α	13.5 cd,α							
	MC80	11.5 b,α	12.7 d,β	13.2 d,α	13.4 c,β	12.4 b,α	12.9 b,β	13.5 cd,α	12.0 b,β	12.8 b,α	12.6 b,α							
	MS104	9.4 a,α	10.5 a,β	10.8 a,β	9.0 a,α	11.3 a,α	11.1 a,α	10.3 a,α	10.2 a,α	10.7 a,α	10.5 a,α							
	MS49	12.6 c,β	11.9 c,α	13.1 c,α	15.2 f,β	13.2 c,α	14.4 cd,α	12.5 b,α	13.4 c,β	12.9 b,α	13.8 de,β							
	Average	12.2 α	12.2 α	13.0 α	13.13 α	13.2 α	13.3 α	13.0 α	12.7 α	13.0 α	12.9 α							

Table 4. Cont.

Genotype	2018		2019		2020		2021		2018–2021		ANOVA							
	RDI	Rainfed	RDI	Rainfed	RDI	Rainfed	RDI	Rainfed	RDI	Rainfed	G	T	Y	G × T	G × Y	T × Y	G × T × Y	
pH	MC16	4.17	4.08	3.84	3.86	3.97	4.02	4.14	4.27	4.04	4.11	***	ns	***	ns	***	ns	***
		d,β	c,α	b,α	c,α	c,α	cd,α	bc,α	bc,α	c,β	d,α							
	MC19	3.95	3.99	3.93	4.02	3.96	3.90	3.94	3.91	3.95	3.93							
		b,α	b,β	c,α	d,β	c,α	b,α	a,α	ab,α	bc,α	b,α							
	MC72	4.18	4.14	4.02	4.01	3.85	4.03	4.20	4.23	4.02	4.11							
		d,α	d,α	d,α	d,α	b,α	d,β	c,α	c,α	cd,α	c,α							
TA (g L <sup>-1</sup> tartaric)	MC16	3.98	4.10	3.69	3.58	3.64	3.70	4.06	3.96	3.85	3.83							
		c,α	c,β	a,β	a,α	a,α	a,α	b,α	b,α	a,α	a,α							
	MC19	3.82	3.91	3.93	3.69	3.88	3.91	3.90	3.85	3.88	3.86							
		a,α	a,β	c,β	b,α	b,α	bc,α	a,α	a,α	ab,α	ab,α							
	MS104	4.00	4.01	4.03	4.11	4.05	4.08	3.97	3.96	4.01	4.03							
		c,α	b,α	d,α	e,β	d,α	d,α	a,α	b,α	cd,α	c,α							
Average	4.01 α	4.04 α	3.91 α	3.88 α	3.89 α	3.94 α	4.04 α	4.03 α	3.96 α	3.98 α								
Tar (g L <sup>-1</sup> )	MC16	4.10	4.89	6.11	6.93	4.86	4.93	3.86	4.37	4.51	4.90	***	ns	***	**	***	ns	***
		d,α	c,β	d,α	e,β	e,α	d,α	bc,α	c,β	c,α	c,α							
	MC19	3.50	3.02	3.92	4.21	3.23	3.46	4.01	3.51	3.64	3.51							
		b,β	ab,α	a,α	b,β	a,α	a,β	c,β	a,α	a,α	a,α							
	MC72	3.92	3.56	3.91	3.57	3.76	3.68	3.59	3.51	3.72	3.59							
		c,β	ab,α	a,α	a,α	b,α	ab,α	b,α	a,α	a,α	a,β							
Mal (g L <sup>-1</sup> )	MC16	3.36	3.11	4.98	5.41	4.57	4.65	3.10	3.75	3.90	4.21							
		a,α	a,α	c,α	d,β	d,α	c,α	a,α	a,β	ab,α	b,α							
	MC19	4.26	4.22	4.35	4.90	4.26	3.77	4.84	4.08	4.50	4.05							
		a,α	a,α	a,α	b,α	b,α	b,α	e,β	b,α	c,β	b,α							
	MS104	3.45	4.98	4.48	5.26	3.84	3.84	4.49	4.57	4.13	4.39							
		e,α	bc,α	b,α	c,β	c,β	b,α	e,β	b,α	c,β	b,α							
Tar/Mal	MC16	5.99	6.85	4.61	3.70	4.20	4.01	5.68	5.48	5.01	4.85	***	ns	***	ns	***	ns	***
		d,α	e,β	a,α	a,α	a,α	a,α	c,β	ab,α	ab,α	a,α							
	MC19	5.88	4.98	5.50	5.61	5.23	5.24	5.92	5.66	5.57	5.46							
		c,β	bc,α	c,α	c,α	c,α	d,α	cd,β	b,α	c,α	b,α							
	MC72	5.62	5.96	6.49	5.44	5.26	4.55	6.12	6.51	5.71	5.47							
		c,α	d,α	d,β	c,α	c,β	bc,α	d,α	c,α	c,α	b,α							
MI	MC16	3.98	3.30	4.58	4.59	4.33	5.00	4.81	5.16	4.51	4.85							
		a,β	a,α	a,α	b,α	a,α	d,β	a,α	a,α	a,α	a,α							
	MC19	2.61	1.88	1.93	1.65	1.99	2.26	2.21	1.90	2.12	2.04							
		b,β	c,α	c,β	c,α	b,α	b,β	b,β	c,α	b,α	b,α							
	MS104	1.78	1.65	1.70	1.34	1.51	1.40	1.40	1.44	1.51	1.43							
		b,α	b,α	b,β	a,α	a,α	a,α	a,α	b,α	a,α	a,α							
MI	MC16	2.82	2.09	2.05	3.04	2.98	3.17	3.24	2.95	3.24	2.95	***	ns	**	ns	***	ns	***
		bc,β	a,α	a,α	b,α	a,α	cd,β	b,α	b,β	b,β	b,α							
	MC19	3.31	3.72	3.52	3.23	4.40	4.02	3.31	3.57	3.77	3.73							
		b,α	b,β	e,β	e,α	d,β	c,α	c,α	c,α	c,α	c,α							
	MC72	3.59	3.75	3.65	3.73	3.62	3.56	3.94	4.05	3.74	3.77							
		d,α	b,α	f,α	f,α	c,α	b,α	d,α	d,α	c,α	c,α							
MI	MC16	3.43	4.10	2.65	2.47	2.72	2.78	4.40	3.25	3.46	3.07							
		c,α	b,β	c,β	c,α	a,α	a,α	e,β	bc,α	bc,α	b,α							
	MC19	2.22	2.49	2.50	1.84	2.65	2.95	2.17	2.52	2.40	2.62							
		a,α	a,β	b,β	a,α	a,α	a,β	a,β	a,β	a,α	a,β							
	MS104	3.66	2.43	2.92	2.89	3.45	3.77	2.81	2.95	3.16	3.22							
		a,α	a,α	d,α	d,α	c,α	b,α	b,α	b,α	b,α	b,α							
Average	3.26 α	3.22 α	2.89 α	2.70 α	3.31 α	3.34 α	3.38 α	3.25 α	3.30 α	3.24 α								

TPC, total phenolic content in skin and seed; TA, total acidity; Tar, tartaric acid; Mal, malic acid; Tar/Mal, ratio of tartaric acid to malic acid; MI, maturity index expressed as the ratio of the °Baumé value to total acidity. ¥: classification according to the values shown in Supplementary Table S3. For each quality variable, year and irrigation treatment, different letters in the same column (a–f) indicate significant differences among genotypes (Duncan’s multiple range test,  $p < 0.05$ ). For each quality variable, genotype and year, different letters in the same row (α, β) indicate significant differences between the irrigation treatments (Duncan’s multiple range test,  $p < 0.05$ ). Analysis of variance (three-way ANOVA) by genotype (G), irrigation treatment (T), year (Y) and their interactions: ns: non-significant; \*  $p < 0.05$ ; \*\*  $p < 0.01$ ; \*\*\*  $p < 0.001$ .

The mean values of parameters such as °Baumé, pH, total acidity and tartaric acid content (period 2018–2021) varied significantly ( $p < 0.001$ ) among the genotypes (G) and year of study (Y), and in terms of the influence of the interaction  $G \times Y$  and  $G \times T \times Y$ . However, it did not vary significantly with respect to irrigation treatment (Table 4). MS104

reached physiological maturity with the lowest °Baumé value under both the RDI (10.7) and rainfed conditions (10.5) (Table 4) (period 2018–2021). In contrast, MC16 was harvested with the highest °Baumé value (14.2 under both RDI and rainfed conditions).

The mean pH values of MC19, MC80, and MS104 were below the overall mean value under both the RDI and rainfed conditions (Table 4). Moreover, MC80 and MS104 maintained a pH below pH 3.9 in both treatments; this is an initial quality requirement for the pre-selection of genotypes and is of great interest for the production of quality wines in the area).

MC16 had the highest total acidity value (g/L, tartaric acid) under the RDI (4.51) and rainfed (4.90) conditions. In contrast, MC19 had the lowest (3.64 and 3.51, respectively). Although the mean total acidity was slightly higher under the rainfed conditions than under RDI, MC72 and MS104 had significantly lower mean values under the former (3% and 10% lower, respectively). In contrast to the total acidity, the mean tartaric acid content (g/L) tended to be lower under rainfed conditions, except in MC80, which saw an increase of 8% compared to under the RDI condition, although this was not statistically significant (Table 4). MC72 had the highest tartaric acid content (g/L) under the RDI (5.71) and rainfed (5.47) conditions; MC80 had the lowest under RDI (4.51), and MS49 had the lowest under the rainfed conditions (4.72).

The mean malic acid content (period 2018–2021) varied significantly ( $p < 0.001$ ) among the genotypes (G), and in terms of the influence of the interaction  $G \times Y$  and  $G \times T \times Y$ . It also differed ( $p < 0.01$ ) among irrigation treatments (T) and in terms of the influence of the interaction  $G \times T$ , but it did not vary significantly between study years (Table 4). MC16 had the highest malic acid content (g/L) under RDI (2.83) and rainfed (2.78) conditions. In contrast, MC80 had the lowest content under RDI (1.51), and MC19 (1.25) under the rainfed conditions. The mean malic acid content was significantly lower under the rainfed than the RDI conditions, particularly for MC19 (22%) and MS104 (27%). The mean tartaric/malic ratio was lowest in MC16—probably explaining it having the highest total acidity value—and was highest in MC19—probably explaining it having the lowest total acidity value.

The maturity index (MI) at the time of harvest, expressed as the relationship °Baumé/total acidity, was estimated for each genotype and irrigation treatment (Table 4). The mean MI (period 2018–2021) varied significantly ( $p < 0.001$ ) among the genotypes (G), and in terms of the influence of the interaction  $G \times Y$  and  $G \times T \times Y$ . Differences ( $p < 0.01$ ) were also seen with respect to the year of study (Y), but not between the irrigation treatments (Table 4). MS104 had the lowest mean MI under the RDI (2.40) and rainfed conditions (2.62), while MC19 had the highest under RDI (3.77), and MC72 the highest under the rainfed conditions (3.77). The MC19 and MC72 genotypes had values above the overall mean under both treatments, unlike MC16, MS104 and MS49. In general, these findings indicate that higher MI values are more related to a reduction in total acidity than to an increase in the °Baumé value.

### 2.5. Vine Water Status

The cumulative water stress, calculated as  $S_{\Psi}$  (Figure 1), was significantly higher under the rainfed conditions (mean 86 MPa day) than under RDI (mean 69 MPa day), with a mean increase of 26% compared to the latter. MC16 showed the greatest increase (34%) compared to under RDI, and MS104 the lowest (16%). Differences among the genotypes were significant only under the rainfed conditions, ranging from the lowest value of 82 MPa day returned by MS104, to 99 MPa day returned by MC16. A negative correlation was detected between  $S_{\Psi}$  and the yield and quality characteristics ( $p < 0.05$ ), both under the RDI and rainfed conditions, i.e., between the  $S_{\Psi}$  and the total yield ( $r = -0.26$  and  $r = -0.37$ ), weight of the bunches ( $r = -0.18$  and  $r = -0.35$ ), and number of bunches ( $r = -0.29$  and  $r = -0.25$ ) (probability level  $p < 0.001$ ). In contrast, the  $S_{\Psi}$  correlated positively with the anthocyanin content under both the RDI and rainfed conditions ( $r = 0.22$  and  $r = 0.24$ ), and TPC ( $r = 0.36$  and  $r = 0.31$ , for a probability level of  $p < 0.001$ ).

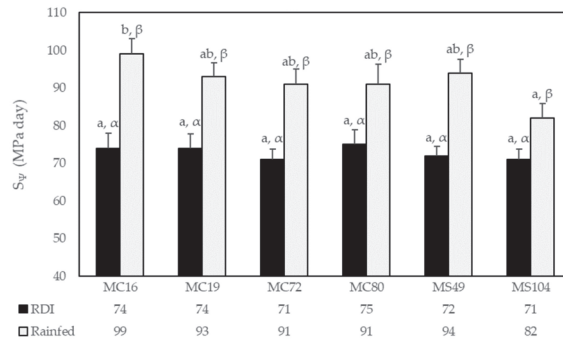


**Figure 1.** Mean annual water-stress integral ( $S_{\Psi}$ ) values for each genotype and irrigation treatment. Vertical bars represent the standard error. RDI, regulated deficit irrigation. For each irrigation treatment, different letters (a–b) indicate significant differences among genotypes (Duncan’s multiple range test,  $p < 0.05$ ). For each genotype, different letters ( $\alpha$ ,  $\beta$ ) indicate significant differences between irrigation treatments (Duncan’s multiple range test,  $p < 0.05$ ).

### 3. Discussion

The results presented in this work are of great importance given the risk that the current semi-arid wine-growing areas could undergo in the near future, mainly due to the extreme scarcity of water and high temperatures expected [43], which could cause the exclusion of these areas for wine production [47]. Most of the varieties grown in these areas are adapted to the current conditions of drought and high temperatures, but they may not resist a climate that is drier and warmer as expected. Hence, the importance of obtaining and selecting new plant material that can adapt to these new adverse climatic conditions, maintaining adequate production and good quality in these growing areas. The phenotypic variability found among the six new genotypes studied has allowed us to identify those that could better adapt to the new climate scenario in semi-arid zones.

Some of the phenological and grape quality variables (such as °Baumé, pH and acidity) measured in this work were not significantly affected by the tested irrigation treatments. In contrast, all the productive and morphological variables measured, and those related to phenolic content, were significantly affected (under rainfed conditions the values for productive variables decreased, while those referring to phenolic content increased). Notable variation around the mean change in value was also seen for the different genotypes studied.

In grapevines, the phenology of the plant determines the production window and influences the ability to adapt to climate change [52,53]. One way to adapt vineyards to drought conditions and high temperatures, such as those found in the study area, is the cultivation of late-ripening varieties; this would avoid plants suffering high temperatures during the ripening period. Alternatively, varieties with longer ripening periods or that ripen slowly could be used. Of the six genotypes studied, MC16 and MC80 were the slowest and latest to ripen. Therefore, they could be good candidates for cultivation under hot and dry conditions.

The present results confirm the negative effect of water stress on total yield reported by other authors [26,39,54], and agree with the associated high skin/pulp ratios reported [55,56]. They also confirm that different genotypes show different sensitivities to water scarcity [57,58]. Thus, under rainfed conditions, MS104 was the most productive genotype (34% higher than the least productive) and returned the highest bunch and berry weights. On the other hand, compared to that recorded under RDI conditions, in the present work, MC80 showed the least reduced yield, bunch, and berry weights under rainfed conditions.

There is a relationship between the high phenolic content of the berry and wine quality attributes such as aroma, color, body, etc., particularly in red wines [59,60]. In this

regard, under rainfed conditions, MC80 showed the highest TCP skin–seed content and MS49 the highest anthocyanin content, exceeding those of MC72 (which had the lowest contents) by 61% and 79%, respectively. Although phenolic quality is associated with a reduction in production and a smaller berry size [27,61], the present results also show a strong genotypic component since the differences in phenolic variables did not always coincide with differences in the yield variables. For example, the lowest production and the smallest berry size of MC72 and MC19 (Table 2) did not correlate with the highest TCP skin–seed content (Table 4), as might be expected, while the highest production of MS104 did correlate with one of the lowest TCP skin–seed contents. Based on these results, new experiments will be designed to evaluate and confirm the highest quality of wine obtained from the varieties with the highest phenolic content.

In general, when vines have adequate availability of water, their sugar content, must pH, and total acidity will be higher than under conditions of water stress [62]; higher values for these variables were therefore expected under RDI than under the rainfed conditions. However, water availability seemed to have no significant effect on these variables, in agreement with that reported by other authors for total acidity [63], pH [64–66], and sugars [66–69]. Nevertheless, differences were seen at the genotype level with respect to these variables, allowing, for example, for the selection of genotypes such as MS104 with a lower berry sugar content at harvest for use in making wines with a lower alcohol content. This is important given the increase in the accumulation of sugars that normally occurs with rising temperatures, as well as rising consumer demands for low-alcohol wines.

The malic acid content was significantly lower under the rainfed than under the RDI conditions, as reported by other authors [70–73]. It is known that if water stress intensifies, malic acid is metabolized more [74], while tartaric acid values remain more stable [75]. This might explain why the Tar/Mal ratio was significantly higher under the rainfed conditions, further confirming that the lower acidity recorded in some genotypes is mainly due to their lower malic acid content. Acidity is essential in wine, both from the point of view of its conservation and its organoleptic properties, so a reduction in total acidity, and in particular malic acid, can lead to unbalanced and flat wines [68,76,77]. For this reason, in hot climates, it is necessary to make acidity corrections during fermentation to guarantee the conservation and good evolution of the wine over time. In this regard, under rainfed conditions, MC16 and MC80 showed the highest total acidity, exceeding that of MC19 (which had the lowest total acidity) by 40% and 20%, respectively.

The year of measurement had a significant effect on most of the studied variables, with some exceptions such as TPC skin–seed, malic acid, and the Tar/Mal ratio. The earliest ripening occurred in 2020—the year with the highest maximum temperature during the ripening period (veraison–harvest). This effect was particularly noticeable in the earlier maturing genotypes MC19, MC72, and MS104.

Daytime temperatures > 35 °C during the period from flowering to the beginning of veraison can lead to reduced yields since both flowering and fruit setting are affected [32], and in the present work, such temperatures were recorded for 7 days during this period in 2018, for 10 days in 2019, for 11 days in 2020, and for 9 days in 2021. This may have influenced the reduction in yield and the mean bunch weight recorded in 2019 and 2020.

After the harvest, the plant accumulates reserves for the following year and produces the reproductive meristems responsible for the following year’s production [78]. The present results show that in 2020, during this phase, there was more rainfall than in previous years of study, which might explain the increase in the total yield, bunch weight, and berry weight recorded in 2021.

High temperatures have been correlated with a greater synthesis of anthocyanins and sugars, and with a reduction in acidity [33,34], and the present results show that in 2020—the year with the warmest ripening period—there was an increase in the synthesis of anthocyanins and in the °Baumé value, while the content of tartaric acid was reduced. Nevertheless, despite the effect of the year, the particular behavior of the genotypes was generally maintained over the different years. For example, in most years, MC80 was

among the genotypes with the latest harvest dates and one of the genotypes in which the contribution of the skin to the weight of the berry was greatest. It also had among the highest TPC skin–seed and anthocyanin values in most years. MS104 was one of the most productive genotypes, reached physiological maturity with the lowest °Baumé value, and, along with MC80, had one of the lowest must pH values.

#### 4. Conclusions

Starting from the premise that genotypes that behave better under rainfed conditions should be those that can best adapt to the effects of climate change in semi-arid areas, and taking into account that temperatures above 35 °C can reduce the yield, total acidity, and phenolic quality and increase the must pH and sugar content (and, therefore, the wine alcohol content), MC80 and MS104 would appear to be candidates for cultivation as climate change takes hold. MC80 suffered below-average water stress, fell into the best “phenolic quality group” for TPC and anthocyanins, and maintained very adequate yield, pH, and total acidity values. MS104 suffered the least water stress and returned the highest yields while maintaining very adequate anthocyanin, pH, and total acidity values. MS104 also had the lowest °Baumé value, rendering it of interest for the production of low-alcohol wines. This genotype might satisfy the requirements of winemakers who seek to produce such wines in hot climates.

The effect of controlled deficit irrigation and drought on other variables, such as leaf area, gas exchange, and wine quality, is now being examined. Having more complete information will aid in our understanding of grapevine responses to drought and high temperatures, and in the selection of the genotypes best adapted to them.

#### 5. Materials and Methods

##### 5.1. Location and Climate

The plant material used in the present work was cultivated in El Chaparral (Cehegín, Murcia, SE Spain) at the IMIDA’s “Hacienda Nueva” experimental farm (38°06′40.7″ N; 1°40′50.3″ W; altitude 433 m). This site is located in one of the warmest wine-producing areas of the region of Murcia, with hot summers (daily maximum temperatures can exceed 40 °C) and low rainfall (perhaps <350 mm per year). Supplementary Table S1 shows the values for the different meteorological variables—reference evapotranspiration (ET<sub>o</sub>, mm), precipitation (mm), vapor pressure deficit (VPD, KPa), daily maximum (T<sub>MAX</sub>, °C), average (T<sub>MED</sub>, °C), minimum (T<sub>MIN</sub>, °C) air temperature, cumulative radiation (RAD<sub>CUM</sub>, MJ/m<sup>2</sup>), maximum radiation (RAD<sub>MAX</sub>, W/m<sup>2</sup>), and mean radiation (RAD<sub>MEAN</sub>, W/m<sup>2</sup>)—recorded during the crops’ different phenological periods for the four years of the present study (2018–2021). These variables were monitored daily at a meteorological station (Campbell mod. CR 10 X) belonging to the Murcia Agricultural Information Service (SIAM, <http://siam.imida.es/> (accessed on 25 January 2022)), located on the experimental farm. Over 2018–2021 period, a mean annual ET<sub>o</sub> of 1125 mm was recorded, along with a mean annual rainfall of 384 mm and a mean annual atmospheric VPD of 1.16 KPa.

##### 5.2. Plant Material

The plant material used in this study included six new genotypes selected from crosses between “Monastrell” (M) and “Cabernet Sauvignon” (C), and between “Monastrell” (M) and “Syrah” (S): MC16, MC19, MC72, MC80, MS49, and MS104. All genotypes were unequivocally identified (Supplementary Table S2) via PCR and the analysis of eight simple sequence repeat (SSR) markers, as described by Bayo-Canha et al. (2012) [79]. In 2016, scions were grafted onto 110-Ritcher rootstocks planted in 2015; this is the rootstock most commonly used in the area since it shows good adaptation to drought and promotes good grape quality [1,80]. The assessed genotypes were 2 years old at the start of the study, and 5 years old at the end.

The six new genotypes were initially classified into “quality groups”, according to the content of total phenolic compounds in the skins and seeds (TPC skin–seed), and

anthocyanins in the skin (Supplementary Table S3; [48,49]). All were selected for their phenolic quality—which was very superior to that of the parentals (Table 5)—based on data obtained over 2012–2017 from the analysis of 20 plants per genotype (on 110-Richter rootstocks), cultivated under sustained deficit irrigation at 40–60% of crop evapotranspiration (ETc) throughout the growing season. The TCP skin–seed and anthocyanin contents were  $>3100 \text{ mg kg}^{-1}$  berry and  $>2200 \text{ mg kg}^{-1}$  berry, respectively, for all six genotypes (Table 5). This exceeds the values for the reference variety of the area ‘Monastrell’ ( $1528 \text{ mg kg}^{-1}$  berry and  $939 \text{ mg kg}^{-1}$  berry, respectively), as well as for ‘Cabernet Sauvignon’ ( $2220 \text{ mg kg}^{-1}$  berry and  $1450 \text{ mg kg}^{-1}$  berry, respectively) and ‘Syrah’ ( $1984 \text{ mg kg}^{-1}$  berry and  $1583 \text{ mg kg}^{-1}$  berry, respectively), all of which are well adapted to the warm climate of the area. MC16, MC80, MS49 and MS104 gave yields similar to or slightly higher than those obtained with ‘Monastrell’ ( $2.00 \text{ kg vine}^{-1}$ ), while MC19 and MC72 returned the lowest yields (below that of Syrah at  $1.59 \text{ kg vine}^{-1}$ , the least productive parental under rainfed conditions).

**Table 5.** Mean data (2012–2017) for production and phenolic quality of the six new genotypes and their parentals when grown under sustained deficit irrigation (40–60% ETc).

Genotype	Yield (kg Vine <sup>-1</sup> )	Berry Weight (g)	TPC Skin-Seed (mg kg <sup>-1</sup> berry)	TPC Quality Group †	Anthocyanins (mg kg <sup>-1</sup> berry)	Anthocyanins Quality Group †
Monastrell	2.83 abc	1.52 d	1528 a	1	939 a	1
Cabernet Sauvignon	3.01 abc	1.06 abc	2220 a	2	1450 a	2
Syrah	3.29 bc	1.49 d	1984 a	1	1583 a	2
MC16	3.33 bc	0.96 ab	3848 b	4	2948 c	4
MC19	3.46 c	1.10 abc	3152 b	3	2713 bc	4
MC72	1.97 ab	0.91 a	3549 b	4	2223 b	3
MC80	1.69 a	1.21 bcd	3970 b	4	2709 bc	4
MS104	3.53 c	1.38 cd	3497 b	4	2913 c	4
MS49	2.11 abc	1.27 bcd	3468 b	4	3191 c	4
<b>Average</b>	<b>2.80</b>	<b>1.21</b>	<b>3024</b>	<b>3</b>	<b>2296</b>	<b>3</b>

TPC, total phenol content in skin and seed. Different letters in the same column indicate significant differences among genotypes (Duncan’s multiple range test,  $p < 0.05$ ). †: classification according to the values shown in Supplementary Table S3.

### 5.3. Experimental Design and Irrigation Treatments

A randomized block design was followed with two irrigation treatments and three replicates per genotype, irrigation treatment, and parameter evaluated. Each replicate involved six vines per genotype and treatment, of which the outside plants in each row were discounted to avoid potential edge effects. Thus, for each genotype, 24 plants were studied, 12 for each irrigation treatment and parameter evaluated (4 plants per replicate). The training system used was a bilateral cordon trellis with a vertical three-wire system. The rows had a N-NW to S-SE orientation. The distance between rows was 2.5 m, and that between vines was 1 m. The vines were pruned to six two-bud spurs (12 nodes).

The two irrigation treatments were: (1) regulated deficit irrigation (RDI), which contributed 25–30% of the ETc; and (2) rainfed, in which the only water received was from rainfall. This particular RDI treatment was selected since it maintains adequate yields and allows for very good enological quality in the area [39]. Supplementary irrigation (equivalent to the mean historical rainfall of the area for the last 10 years) was allowed for both treatments when necessary to avoid irreversible damage due to very severe water stress ( $\Psi_S < -1.6 \text{ MPa}$ ): this was needed twice in 12 and 30 August 2018, twice in 6 and 20 August 2019, and once in 22 August 2020; in 2021, it was not required. This covered the entire plot to maintain the total water difference between the treatments. The ETc was calculated as described in Romero et al. (2018) [39].

The irrigation system consisted of two irrigation lines for each row of vines. One of these irrigation lines contained one self-compensating dripper per plant (flow rate of 4 l/h) for applying fertilizer treatments and supplementary irrigation. The other line had 8 l/h self-compensating drippers for use in the RDI treatment, but no drippers for the rainfed rows. In 2015, 2016, and 2017, irrigation (252 mm/plant per year) was applied for the correct establishment of the plot. In 2018, 2019, 2020, and 2021, the experimental irrigation treatments were applied between April and October (sprouting to post-harvest), with an average 143 mm/plant provided per year under the RDI conditions. The cultivation techniques—fertilizer use, phytosanitary treatments, and soil maintenance—were the same throughout the experimental plot. Weed removal was carried out using herbicides in the dripper line and, in the lanes between the rows, using agricultural machinery.

#### 5.4. Vines Water Status

The water potential of the stem ( $\Psi_S$ ) was determined fortnightly at noon (12:00–13:30 solar hour) from mid-May–June to the end of September–October, using a Model 600 pressure chamber (Soil Moisture Equipment, Santa Barbara, CA, USA). For each genotype and irrigation treatment, four mature, healthy, fully exposed, and expanded leaves located on the main shoots of the upper-middle part of the canopy were selected. These leaves were covered with totally airtight aluminum foil bags for at least 2 h before taking measurements.

The cumulative effect of the water deficit was determined as the water-stress integral ( $S\Psi$ ) calculated, as defined by Myers (1988) [81], as the sum of the mean difference between two consecutive measurements of water potential ( $\bar{\Psi}_{i,i+1}$ ) and the maximum (least negative) value recorded during the study period ( $c$ ), multiplied by the number of days in the interval between one measurement and the next ( $n$ ) (1).

$$S\Psi = \sum_{i=0}^{i=t} (\bar{\Psi}_{i,i+1} - c)n \quad (1)$$

#### 5.5. Phenotypic Evaluation

##### 5.5.1. Phenological Characteristics

During 2018, 2019, 2020 and 2021, the dates for the different phenological stages—budbreak, flowering, veraison, and harvest—for each genotype and irrigation treatment were recorded [82]. In 2019, 2020 and 2021, the dates for the beginning of leaf fall and its completion were also recorded. The date of budbreak was considered as that on which 50% of the buds on a plant were in Baggioolini phenological stage C (green tip); the date of flowering as that on which 50% of the flowers were in phenological stage I (visible stamens); the veraison date as that on which 50% of the berries had started to change color and/or showed a loss of chlorophyll and softening had started (phenological stage M); the date of harvest (phenological stage N) as that on which appropriate physiological maturity had been reached; the date of the start of leaf fall as that on which 5% of the leaves fell (phenological state O1); and the date of total leaf fall as that on which leaf fall was complete (phenological state O2). Physiological maturity was deemed to begin when the grape reached its maximum size and its highest concentration of sugars. At this point, the berry begins to decrease in size due to water loss and some dehydrated berries appear in the cluster, the organoleptic maturity of the skin is good, and the seeds are mature (brown color).

##### 5.5.2. Productive and Morphological Characteristics

For each genotype, irrigation treatment, and replicate (4 plants per replicate), the productiveness and morphological characteristics of representative bunches were assessed at the time of harvest. The yield was recorded as the total number of bunches per plant, total yield (kg/plant), and mean bunch weight (total yield/number of bunches); the mean berry weight was calculated from the weight of 100 randomly selected berries. The morphological characterization of the bunches was performed based on the bunch length (mm), bunch

width (mm), and bunch compactness as per OIV 204 descriptors (1, very loose; 3, loose; 5, medium; 7, compact; 9, very compact) [83]. Morphological characterization of the berries was performed using 30 representative berries per replicate and treatment (randomly selected from the different areas of the representative bunches) and based on the berry length (mm) and width (mm) as measured with a Mitutoyo CD-15D digital caliper.

### 5.6. Grape Quality

The grape quality (for each genotype, irrigation treatment, and replicate) was assessed at the IMIDA experimental winery. For each replicate and irrigation treatment, 350 berries were randomly selected from the different areas of the bunches. From this representative sample, 30 berries were taken for the extraction and analysis in triplicate of the TPC skin–seed (mg/kg berry), and of the total anthocyanins (mg/kg berry), as described by Rustioni et al. (2014) [84]. The rest of the berry sample (320 berries) was crushed, without breaking the seed, and centrifuged. The °Baumé value (OIV-MA-AS2-02), total acidity (OIV-MA-AS313-01), must pH (OIV-MA-AS313-15), tartaric acid content (following the modified Rebelein method [85]), and malic acid content (OIV-MA-AS313-11) were analyzed in the must obtained by centrifugation, adhering to the protocols described by Fernández-Fernández et al. (2020) [49]. The grape maturity index (MI) was calculated as the ratio between the °Baumé value and the total acidity. All analyses were performed using randomly selected berries from each replicate per genotype and irrigation treatment.

### 5.7. Statistical Analysis

The collected data were subjected to analysis of variance (three-way ANOVA), using the genotype, irrigation treatment, and year as factors. Means were compared using Duncan's multiple range test ( $p < 0.05$ ). The correlation between  $S_V$  and the productiveness and quality traits was calculated using the Spearman test ( $p < 0.05$ ). All analyses were performed using StatGraphics Centurion XVI v.16.1.18 software (StatGraphics Technologies, Inc., The Plains, VA, USA).

**Supplementary Materials:** The following supporting information can be downloaded at: <https://www.mdpi.com/article/10.3390/plants11101363/s1>. Table S1: Meteorological variables recorded in the years 2018, 2019, 2020 and 2021; Table S2: Genetic profile of grapevine material for eight identificatory SSRs. Alleles expressed in base pairs (bp); Table S3: Grape phenolic quality groups based on mean data of six years (2012–2017).

**Author Contributions:** Conceptualization, L.R.-G.; methodology and formal analysis, D.J.F.-L. and J.I.F.-F.; field experiments, calculation and application of irrigation treatment, physiological data collection, D.J.F.-L.; phenological, productiveness and morphological data collection, D.J.F.-L.; statistical analysis of the data, D.J.F.-L.; molecular marker analysis, C.M.-M.; grape quality analysis, J.I.F.-F. and J.A.B.-S.; writing—original draft preparation, D.J.F.-L. and L.R.-G.; writing—review, D.J.F.-L., J.I.F.-F., C.M.-M., J.A.B.-S. and L.R.-G.; editing, D.J.F.-L. and L.R.-G.; funding acquisition, L.R.-G. All authors have read and agreed to the published version of the manuscript.

**Funding:** This work was financed by the *Instituto Nacional de Investigación y Tecnología Agraria y Alimentaria* (INIA) via project RTA2014-00016-C03-02, Ministerio de Ciencia e Innovación via project PID2020-119263RR-100, and by the European Regional Development Fund (80%), with the collaboration of the Region of Murcia (20%), via project FEDER1420-29.

**Institutional Review Board Statement:** Not applicable.

**Informed Consent Statement:** Not applicable.

**Data Availability Statement:** All data generated is provided in this manuscript.

**Acknowledgments:** The authors thank Ana Fuentes-Denia, José Cayetano Gómez-Martínez and Juan Corredor for technical assistance; Carlos V. Padilla, Eliseo Salmerón and Isidro Hita for crop health control; Adrián Yepes-Hita, Sergio Lucas-Miñano and José Antonio Martínez-Jiménez for plant management in the field; and Pascual Romero for the initial design of the plantation and irrigation treatments. The English manuscript was prepared by Adrian Burton.

**Conflicts of Interest:** The authors declare that they have no competing financial interests or personal relationships that might influence the work reported in this paper.

## References

- van Leeuwen, C.; Destrac-Irvine, A. Modified grape composition under climate change conditions requires adaptations in the vineyard. *OENO One* **2017**, *51*, 147. [[CrossRef](#)]
- IPCC. *Climate Change and Land: An IPCC Special Report on Climate Change, Desertification, Land Degradation, Sustainable Land Management, Food Security, and Greenhouse Gas Fluxes in Terrestrial Ecosystems*; Shukla, P.R., Skea, J., Calvo Buendia, E., Masson-Delmotte, V., Pörtner, H.-O., Roberts, D.C., Zhai, P., Slade, R., Connors, S., van Diemen, R., et al., Eds.; 2019; p. 205, in press.
- Fraga, H.; Malheiro, A.C.; Moutinho-Pereira, J.; Santos, J.A. An overview of climate change impacts on European viticulture. *Food Energy Secur.* **2012**, *1*, 94–110. [[CrossRef](#)]
- van Leeuwen, C.; Schultz, H.R.; de Cortazar-Atauri, I.G.; Duchêne, E.; Ollat, N.; Pieri, P.; Bois, B.; Goutouly, J.-P.; Quéno, H.; Touzard, J.-M.; et al. Why climate change will not dramatically decrease viticultural suitability in main wine-producing areas by 2050. *Proc. Natl. Acad. Sci. USA* **2013**, *110*, E3051–E3052. [[CrossRef](#)] [[PubMed](#)]
- Medrano, H.; Tomás, M.; Martorell, S.; Escalona, J.-M.; Pou, A.; Fuentes, S.; Flexas, J.; Bota, J. Improving water use efficiency of vineyards in semi-arid regions. A review. *Agron. Sustain. Dev.* **2015**, *35*, 499–517. [[CrossRef](#)]
- Edwards, E.J.; Unwin, D.; Kilmister, R.; Treeby, M. Multi-seasonal effects of warming and elevated CO<sub>2</sub> on the physiology, growth and production of mature, field grown, Shiraz grapevines. *OENO One* **2017**, *51*, 127–132. [[CrossRef](#)]
- Venios, X.; Korkas, E.; Nisioutou, A.; Banilas, G. Grapevine Responses to Heat Stress and Global Warming. *Plants* **2020**, *9*, 1754. [[CrossRef](#)]
- Jones, G.V.; Davis, R.E. Climate influences on grapevine phenology, grape composition, and wine production and quality for Bordeaux, France. *Am. J. Enol. Vitic.* **2000**, *51*, 249–261.
- Jones, G.V.; White, M.A.; Cooper, O.R.; Storchmann, K. Climate Change and Global Wine Quality. *Clim. Chang.* **2005**, *73*, 319–343. [[CrossRef](#)]
- Duchêne, E.; Huard, F.; Dumas, V.; Schneider, C.; Merdinoglu, D. The challenge of adapting grapevine varieties to climate change. *Clim. Res.* **2010**, *41*, 193–204. [[CrossRef](#)]
- Schultz, H.R.; Jones, G.V. Climate Induced Historic and Future Changes in Viticulture. *J. Wine Res.* **2010**, *21*, 137–145. [[CrossRef](#)]
- Mosedale, J.R.; Abernethy, K.E.; Smart, R.E.; Wilson, R.; Maclean, I. Climate change impacts and adaptive strategies: Lessons from the grapevine. *Glob. Chang. Biol.* **2016**, *22*, 3814–3828. [[CrossRef](#)] [[PubMed](#)]
- Gambetta, G.A.; Herrera, J.C.; Dayer, S.; Feng, Q.; Hochberg, U.; Castellarin, S.D. The physiology of drought stress in grapevine: Towards an integrative definition of drought tolerance. *J. Exp. Bot.* **2020**, *71*, 4658–4676. [[CrossRef](#)] [[PubMed](#)]
- Rienth, M.; Vigneron, N.; Darriet, P.; Sweetman, C.; Burbidge, C.; Bonghi, C.; Walker, R.P.; Famiani, F.; Castellarin, S.D. Grape Berry Secondary Metabolites and Their Modulation by Abiotic Factors in a Climate Change Scenario—A Review. *Front. Plant Sci.* **2021**, *12*, 643258. [[CrossRef](#)] [[PubMed](#)]
- van Leeuwen, C.; Darriet, P. The Impact of Climate Change on Viticulture and Wine Quality. *J. Wine Econ.* **2016**, *11*, 150–167. [[CrossRef](#)]
- de Orduña, R.M. Climate change associated effects on grape and wine quality and production. *Food Res. Int.* **2010**, *43*, 1844–1855. [[CrossRef](#)]
- Mirás-Avalos, J.M.; Intrigliolo, D.S. Grape Composition under Abiotic Constraints: Water Stress and Salinity. *Front. Plant Sci.* **2017**, *8*, 851. [[CrossRef](#)]
- Viguie, V.; Lecocq, F.; Touzard, J.-M. Viticulture and adaptation to climate change. *J. Int. Sci. Vigne du Vin.* **2014**, *7*, 55–60.
- Santos, J.A.; Fraga, H.; Malheiro, A.C.; Moutinho-Pereira, J.; Dinis, L.-T.; Correia, C.; Moriondo, M.; Leolini, L.; DiBari, C.; Costafreda-Aumedes, S.; et al. A Review of the Potential Climate Change Impacts and Adaptation Options for European Viticulture. *Appl. Sci.* **2020**, *10*, 3092. [[CrossRef](#)]
- Naulleau, A.; Gary, C.; Prévot, L.; Hossard, L. Evaluating Strategies for Adaptation to Climate Change in Grapevine Production—A Systematic Review. *Front. Plant Sci.* **2021**, *11*, 2154. [[CrossRef](#)]
- Romero, P.; Navarro, J.M.; Ordaz, P.B. Towards a sustainable viticulture: The combination of deficit irrigation strategies and agroecological practices in Mediterranean vineyards. A review and update. *Agric. Water Manag.* **2022**, *259*, 107216. [[CrossRef](#)]
- Romero, P.; Fernández-Fernández, J.I.; Gil-Muñoz, R.; Botía, P. Vigour-yield-quality relationships in long-term deficit irrigated winegrapes grown under semiarid conditions. *Theor. Exp. Plant Physiol.* **2016**, *28*, 23–51. [[CrossRef](#)]
- Romero, P.; García, J.G.; Fernández-Fernández, J.I.; Gil Muñoz, R.; Saavedra, F.D.A.; Martínez-Cutillas, A. Improving berry and wine quality attributes and vineyard economic efficiency by long-term deficit irrigation practices under semiarid conditions. *Sci. Hortic.* **2016**, *203*, 69–85. [[CrossRef](#)]
- Scholasch, T.; Rienth, M. Review of water deficit mediated changes in vine and berry physiology; Consequences for the optimization of irrigation strategies. *OENO One* **2019**, *3*, 423–444. [[CrossRef](#)]
- Romero Azorín, P.; García García, J. The Productive, Economic, and Social Efficiency of Vineyards Using Combined Drought-Tolerant Rootstocks and Efficient Low Water Volume Deficit Irrigation Techniques under Mediterranean Semiarid Conditions. *Sustainability* **2020**, *12*, 1930. [[CrossRef](#)]

26. Pérez-Álvarez, E.; Molina, D.I.; Vivaldi, G.; García-Esparza, M.; Lizama, V.; Álvarez, I. Effects of the irrigation regimes on grapevine cv. Bobal in a Mediterranean climate: I. Water relations, vine performance and grape composition. *Agric. Water Manag.* **2021**, *248*, 106772. [[CrossRef](#)]
27. Pérez-Álvarez, E.P.; Intrigliolo, D.S.; Almajano, M.P.; Rubio-Bretón, P.; Garde-Cerdán, T. Effects of Water Deficit Irrigation on Phenolic Composition and Antioxidant Activity of Monastrell Grapes under Semiarid Conditions. *Antioxidants* **2021**, *10*, 1301. [[CrossRef](#)]
28. Torres, N.; Yu, R.; Martínez-Luscher, J.; Girardello, R.C.; Kostaki, E.; Oberholster, A.; Kurtural, S.K. Shifts in the phenolic composition and aromatic profiles of Cabernet Sauvignon (*Vitis vinifera* L.) wines are driven by different irrigation amounts in a hot climate. *Food Chem.* **2022**, *371*, 131163. [[CrossRef](#)]
29. Lizama, V.; Pérez-Álvarez, E.; Intrigliolo, D.; Chirivella, C.; Álvarez, I.; García-Esparza, M. Effects of the irrigation regimes on grapevine cv. Bobal in a Mediterranean climate: II. Wine, skins, seeds, and grape aromatic composition. *Agric. Water Manag.* **2021**, *256*, 107078. [[CrossRef](#)]
30. Romero, P.; Fernández-Fernández, J.; Martínez-Cutillas, A. Physiological thresholds for efficient regulated deficit irrigation management in winegrapes under semiarid conditions. *Am. J. Enol. Vitic.* **2010**, *61*, 300–312.
31. Fraga, H.; de Cortázar Atauri, I.G.; dos Santos, J.C.A. Viticultural irrigation demands under climate change scenarios in Portugal. *Agric. Water Manag.* **2018**, *196*, 66–74. [[CrossRef](#)]
32. Pagay, V.; Collins, C. Effects of timing and intensity of elevated temperatures on reproductive development of field-grown Shiraz grapevines. *OENO One* **2017**, *51*, 409–421. [[CrossRef](#)]
33. Spayd, S.E.; Tarara, J.M.; Mee, D.L.; Ferguson, J.C. Separation of sunlight and temperature effects on the composition of *Vitis vinifera* cv. Merlot berries. *Am. J. Enol. Vitic.* **2002**, *53*, 171–182.
34. Mori, K.; Goto-Yamamoto, N.; Kitayama, M.; Hashizume, K. Loss of anthocyanins in red-wine grape under high temperature. *J. Exp. Bot.* **2007**, *58*, 1935–1945. [[CrossRef](#)] [[PubMed](#)]
35. de Rosas, I.; Deis, L.; Baldo, Y.; Cavagnaro, J.B.; Cavagnaro, P.F. High Temperature Alters Anthocyanin Concentration and Composition in Grape Berries of Malbec, Merlot, and Pinot Noir in a Cultivar-Dependent Manner. *Plants* **2022**, *11*, 926. [[CrossRef](#)] [[PubMed](#)]
36. Pavloušek, P. Evaluation of drought tolerance of new grapevine rootstock hybrids. *J. Environ. Biol.* **2011**, *32*, 543–549.
37. Reynolds, A.G. *Grapevine Breeding Programs for the Wine Industry: Traditional and Molecular Techniques*, 1st ed.; Reynolds, A., Ed.; Woodhead Publishing: Oxford, UK, 2015; ISBN 978-1-78242-075-0. [[CrossRef](#)]
38. Berdeja, M.; Nicolas, P.; Kappel, C.; Dai, Z.W.; Hilbert, G.; Peccoux, A.; Lafontaine, M.; Ollat, N.; Gomes, E.; Delrot, S. Water limitation and rootstock genotype interact to alter grape berry metabolism through transcriptome reprogramming. *Hortic. Res.* **2015**, *2*, 15012. [[CrossRef](#)]
39. Romero, P.; Botía, P.; Navarro, J.M. Selecting rootstocks to improve vine performance and vineyard sustainability in deficit irrigated Monastrell grapevines under semiarid conditions. *Agric. Water Manag.* **2018**, *209*, 73–93. [[CrossRef](#)]
40. Zombardo, A.; Mica, E.; Puccioni, S.; Perria, R.; Valentini, P.; Mattii, G.B.; Cattivelli, L.; Storchi, P. Berry Quality of Grapevine under Water Stress as Affected by Rootstock–Scion Interactions through Gene Expression Regulation. *Agronomy* **2020**, *10*, 680. [[CrossRef](#)]
41. Santos, J.A.; Costa, R.; Fraga, H. New insights into thermal growing conditions of Portuguese grapevine varieties under changing climates. *Theor. Appl. Climatol.* **2018**, *135*, 1215–1226. [[CrossRef](#)]
42. Nicolle, P.; Williams, K.A.; Angers, P.; Pedneault, K. Changes in the flavan-3-ol and polysaccharide content during the fermentation of *Vitis vinifera* Cabernet-Sauvignon and cold-hardy *Vitis* varieties Frontenac and Frontenac blanc. *OENO One* **2021**, *55*, 337–347. [[CrossRef](#)]
43. Guiot, J.; Cramer, W. Climate change: The 2015 Paris Agreement thresholds and Mediterranean basin ecosystems. *Science* **2016**, *354*, 465–468. [[CrossRef](#)] [[PubMed](#)]
44. Santillán, D.; Garrote, L.; Iglesias, A.; Sotes, V. Climate change risks and adaptation: New indicators for Mediterranean viticulture. *Mitig. Adapt. Strat. Glob. Chang.* **2020**, *25*, 881–899. [[CrossRef](#)]
45. Tortosa, I.; Escalona, J.M.; Toro, G.; Douthe, C.; Medrano, H. Clonal Behavior in Response to Soil Water Availability in Tempranillo Grapevine cv: From Plant Growth to Water Use Efficiency. *Agronomy* **2020**, *10*, 862. [[CrossRef](#)]
46. Fraga, H.; Santos, J.A.; Malheiro, A.C.; Oliveira, A.A.; Moutinho-Pereira, J.; Jones, G.V. Climatic suitability of Portuguese grapevine varieties and climate change adaptation. *Int. J. Climatol.* **2015**, *36*, 1–12. [[CrossRef](#)]
47. Morales-Castilla, I.; de Cortázar-Atauri, I.G.; Cook, B.I.; Lacombe, T.; Parker, A.; van Leeuwen, C.; Nicholas, K.A.; Wolkovich, E.M. Diversity buffers winegrowing regions from climate change losses. *Proc. Natl. Acad. Sci. USA* **2020**, *117*, 2864–2869. [[CrossRef](#)] [[PubMed](#)]
48. Fernández-Fernández, J.I.; Gil-Muñoz, R.; Bleda-Sánchez, J.A.; Martínez-Mora, C.; Corredor-Cano, J.; Cebrián-Pérez, A.; Martínez-Balsas, D.; Gómez-Martínez, J.C.; Martínez-Jiménez, J.A.; García-Pérez, G.; et al. Selección final de cruces de Monastrell por su composición fenólica. Años 1997 a 2017. In Proceedings of the 34 Reunión del Grupo de Trabajo de Experimentación en Viticultura y Enología, Pastriz, Spain, 10–11 April 2018; pp. 131–138.
49. Fernández-Fernández, J.I.; Gil-Muñoz, R.; Bleda-Sánchez, J.A.; Corredor-Cano, J.; Moreno-Olivares, J.D.; Cebrián-Pérez, A.; Martínez-Balsas, D.; Gómez-Martínez, J.C.; Palencia-Sigüenza, M.S.; Carcelén-Cutillas, J.C.; et al. Nuevas variedades procedentes de Monastrell adaptadas a clima cálido. Cosechas 2016–2019. *Rev. Enólogos* **2020**, *126*, 78–88.

50. Ruiz-García, L.; Gil-Muñoz, R.; Martínez-Mora, C.; Bleda, J.A.; Fuentes-Denia, A.; Martínez-Jiménez, J.A.; Martínez-Cutillas, A.; Fernández-Fernández, J.I. Nuevas variedades de vid obtenidas en la Región de Murcia. *Actas Hortic.* **2018**, *80*, 226–229.
51. Focus OIV. *Distribution of the World's Grapevine Varieties*; International Organisation of Vine and Wine: Paris, France, 2017; p. 54. Available online: <https://www.oiv.int> (accessed on 25 April 2022).
52. Jackson, R.S. *Wine Science Principles and Applications*, 3rd ed.; Elsevier: Amsterdam, The Netherlands; Academic Press: San Diego, CA, USA, 2008.
53. Wolkovich, E.M.; Burge, D.O.; Walker, M.A.; Nicholas, K. Phenological diversity provides opportunities for climate change adaptation in winegrapes. *J. Ecol.* **2017**, *105*, 905–912. [[CrossRef](#)]
54. Girona, J.; Mata, M.; del Campo, J.; Arbonés, A.; Bartra, E.; Marsal, J. The use of midday leaf water potential for scheduling deficit irrigation in vineyards. *Irrig. Sci.* **2006**, *24*, 115–127. [[CrossRef](#)]
55. Roby, G.; Matthews, M.A. Relative proportions of seed, skin and flesh, in ripe berries from Cabernet Sauvignon grapevines grown in a vineyard either well irrigated or under water deficit. *Aust. J. Grape Wine Res.* **2004**, *10*, 74–82. [[CrossRef](#)]
56. Chacón-Vozmediano, J.L.; Martínez-Gascuña, J.; García-Navarro, F.J.; Jiménez-Ballesta, R. Effects of Water Stress on Vegetative Growth and 'Merlot' Grapevine Yield in a Semi-Arid Mediterranean Climate. *Horticulturae* **2020**, *6*, 95. [[CrossRef](#)]
57. Carbonell-Bejerano, P.; Carvalho, L.C.; Dias, J.E.E.; Martínez-Zapater, J.M.; Amâncio, S. Exploiting *Vitis* genetic diversity to manage with stress. In *Grapevine in a Changing Environment: A Molecular and Ecophysiological Perspective*, 1st ed.; Gerós, H., Chaves, M., Medrano, H., Delrot, S., Eds.; John Wiley & Sons, Ltd.: Hoboken, NJ, USA, 2016; pp. 347–380. [[CrossRef](#)]
58. Molitor, D.; Keller, M. Yield of Müller-Thurgau and Riesling grapevines is altered by meteorological conditions in the current and previous growing seasons. *OENO One* **2016**, *50*, 245–258. [[CrossRef](#)]
59. Kennedy, J.A.; Saucier, C.; Glories, Y. Grape and wine phenolics: History and perspective. *Am. J. Enol. Vitic.* **2006**, *57*, 239–248.
60. Ivanova, V.; Vojnoski, B.; Stefova, M. Effect of winemaking treatment and wine aging on phenolic content in Vranec wines. *J. Food Sci. Technol.* **2011**, *49*, 161–172. [[CrossRef](#)]
61. Howell, G.S. Sustainable grape productivity and the growth-yield relationship: A review. *Am. J. Enol. Vitic.* **2001**, *52*, 165–174.
62. Dai, A. Drought under global warming: A review. *Wiley Interdiscip. Rev. Clim. Change* **2011**, *2*, 45–65. [[CrossRef](#)]
63. Alatzas, A.; Theocharis, S.; Miliordos, D.-E.; Leontaridou, K.; Kanellis, A.K.; Kotseridis, Y.; Hatzopoulos, P.; Koundouras, S. The Effect of Water Deficit on Two Greek *Vitis vinifera* L. Cultivars: Physiology, Grape Composition and Gene Expression during Berry Development. *Plants* **2021**, *10*, 1947. [[CrossRef](#)]
64. De La Hera, M.L.; Martínez-Cutillas, A.; Lopez-Roca, J.M.; Gómez-Plaza, E. Effect of moderate irrigation on grape composition during ripening. *Span. J. Agric. Res.* **2005**, *3*, 352–356. [[CrossRef](#)]
65. Etchebarne, F.; Ojeda, H.; Hunter, J. Leaf:Fruit Ratio and Vine Water Status Effects on Grenache Noir (*Vitis vinifera* L.) Berry Composition: Water, Sugar, Organic Acids and Cations. *South Afr. J. Enol. Vitic.* **2010**, *31*, 110–115. [[CrossRef](#)]
66. Cabral, I.L.; Teixeira, A.; Lanoue, A.; Unlubayir, M.; Munsch, T.; Valente, J.; Alves, F.; da Costa, P.L.; Rogerson, F.S.; Carvalho, S.M.P.; et al. Impact of Deficit Irrigation on Grapevine cv. 'Touriga Nacional' during Three Seasons in Douro Region: An Agronomical and Metabolomics Approach. *Plants* **2022**, *11*, 732. [[CrossRef](#)]
67. Santesteban, L.G.; Miranda, C.; Royo, J.B. Regulated deficit irrigation effects on growth, yield, grape quality and individual anthocyanin composition in *Vitis vinifera* L. cv. 'Tempranillo'. *Agric. Water Manag.* **2011**, *98*, 1171–1179. [[CrossRef](#)]
68. Junquera, P.; Lissarrague, J.R.; Jiménez, L.; Linares, R.; Baeza, P. Long-term effects of different irrigation strategies on yield components, vine vigour, and grape composition in cv. Cabernet-Sauvignon (*Vitis vinifera* L.). *Irrig. Sci.* **2012**, *30*, 351–361. [[CrossRef](#)]
69. Casasa, L.F.; Keller, M.; Harbertson, J.F. Regulated Deficit Irrigation Alters Anthocyanins, Tannins and Sensory Properties of Cabernet Sauvignon Grapes and Wines. *Molecules* **2015**, *20*, 7820–7844. [[CrossRef](#)]
70. Girona, J.; Marsal, J.; Mata, M.; DEL Campo, J.; Basile, B. Phenological sensitivity of berry growth and composition of Tempranillo grapevines (*Vitis vinifera* L.) to water stress. *Aust. J. Grape Wine Res.* **2010**, *15*, 268–277. [[CrossRef](#)]
71. Intrigliolo, D.S.; Castel, J.R. Response of grapevine cv. 'Tempranillo' to timing and amount of irrigation: Water relations, vine growth, yield and berry and wine composition. *Irrig. Sci.* **2009**, *28*, 113–125. [[CrossRef](#)]
72. Bellvert, J.; Marsal, J.; Mata, M.; Girona, J. Yield, Must Composition, and Wine Quality Responses to Preveraison Water Deficits in Sparkling Base Wines of Chardonnay. *Am. J. Enol. Vitic.* **2016**, *67*, 1–12. [[CrossRef](#)]
73. Cooley, N.; Clingeleffer, P.; Walker, R. Effect of water deficits and season on berry development and composition of Cabernet Sauvignon (*Vitis vinifera* L.) grown in a hot climate. *Aust. J. Grape Wine Res.* **2017**, *23*, 260–272. [[CrossRef](#)]
74. Bucchetti, B.; Matthews, M.A.; Falginella, L.; Peterlunger, E.; Castellarin, S.D. Effect of water deficit on Merlot grape tannins and anthocyanins across four seasons. *Sci. Hortic.* **2011**, *128*, 297–305. [[CrossRef](#)]
75. Iland, P.G.; Coombe, B.G. Malate, tartrate, potassium, and sodium in flesh and skin of Shiraz grapes during ripening: Concentration and compartmentation. *Am. J. Enol. Vitic.* **1988**, *39*, 71–76.
76. Jones, G. Climate Change and the Global Wine Industry. In Proceedings of the 13th Annual Australian Wine Industry Technical Conference, Adelaide, Australia, 28 July–2 August 2007.
77. Keller, M. Managing grapevines to optimise fruit development in a challenging environment: A climate change primer for viticulturists. *Aust. J. Grape Wine Res.* **2010**, *16*, 56–69. [[CrossRef](#)]
78. Hidalgo, L. *Tratado de Viticultura General*, 3rd ed.; Mundi-Prensa Libros: Madrid, Spain, 2002.

79. Bayo-Canha, A.; Fernández-Fernández, J.I.; Martínez-Cutillas, A.; Ruiz-García, L. Phenotypic segregation and relationships of agronomic traits in Monastrell × Syrah wine grape progeny. *Euphytica* **2012**, *186*, 393–407. [[CrossRef](#)]
80. Ollat, N.; Peccoux, A.; Papura, D.; Esmenjaud, D.; Marguerit, E.; Tandonnet, J.-P.; Bordenave, L.; Cookson, S.; Barrieu, F.; Rossdeutsch, L.; et al. Rootstocks as a component of adaptation to environment. In *Grapevine in a Changing Environment: A Molecular and Ecophysiological Perspective*, 1st ed.; Geros, H., Chaves, M., Medrano, H., Delrot, S., Eds.; John Wiley & Sons, Ltd.: Hoboken, NJ, USA, 2016; pp. 68–108. [[CrossRef](#)]
81. Myers, B.J. Water stress integral—A link between short-term stress and long-term growth. *Tree Physiol.* **1988**, *4*, 315–323. [[CrossRef](#)] [[PubMed](#)]
82. Baggiolini, M. Les stades repères dans le développement annuel de la vigne et leur utilisation pratique. *Rev. Romande Agric. Vitic. Arboric.* **1952**, *8*, 4–6.
83. International Organization of Vine and Wine (O.I.V). *Compendium of International Methods of Wine and Must Analysis*, 2020th ed.; International Organization of Vine and Wine: Paris, France, 2020; Volume I, ISBN 978-2-85038-017-4.
84. Rustioni, L.; Maghradze, D.; Popescu, C.F.; Cola, G.; Abashidze, E.; Aroutiounian, R.; Brazão, J.; Coletti, S.; Cornea, V.; De-jeu, L.; et al. First results of the European grapevine collections collaborative network: Validation of a standard enocarpological phenotyping method. *Vitis-J. Grapevine Res.* **2014**, *53*, 219–226. [[CrossRef](#)]
85. García-Barceló, J. *Técnicas Analíticas Para Vinos*, 1st ed.; GAB: Barcelona, Spain, 1990; ISBN 84-404-7827-5.



Review

# Plants and Phytoplasmas: When Bacteria Modify Plants

Assunta Bertaccini

Department of Agricultural and Food Sciences, Alma Mater Studiorum—University of Bologna, 40127 Bologna, Italy; [assunta.bertaccini@unibo.it](mailto:assunta.bertaccini@unibo.it)

**Abstract:** Plant pathogen presence is very dangerous for agricultural ecosystems and causes huge economic losses. Phytoplasmas are insect-transmitted wall-less bacteria living in plants, only in the phloem tissues and in the emolymph of their insect vectors. They are able to manipulate several metabolic pathways of their hosts, very often without impairing their life. The molecular diversity described (49 ‘*Candidatus* Phytoplasma’ species and about 300 ribosomal subgroups) is only in some cases related to their associated symptomatology. As for the other plant pathogens, it is necessary to verify their identity and recognize the symptoms associated with their presence to appropriately manage the diseases. However, the never-ending mechanism of patho-adaptation and the copresence of other pathogens makes this management difficult. Reducing the huge impact of phytoplasma-associated diseases in all the main crops and wild species is, however, relevant, in order to reduce their effects that are jeopardizing plant biodiversity.

**Keywords:** plant diseases; bacterium; symptoms; pathogenicity; molecular classification

## 1. Introduction

Plant pathogen presence is usually known as a very dangerous component of agricultural ecosystems and is associated with huge economic losses. The world history was also often shaped by dangerous plant epidemics or pandemics such as the wheat rust that was among the main causes of the Roman empire failure, the potato late blight by *Phytophthora infestans* producing the Irish migration to America due to the famine, and the coffee rust obliging to stop the coffee cultivation in several areas, mainly in islands. Recently plant pathogenic bacteria have played an important role in reducing kiwi cultivation, due to the canker by *Pseudomonas syringae* pv. *actinidiae* [1], and citrus, through the greening (‘*Candidatus* Liberibacter’ species) [2] diseases. Moreover, there are bacteria hosted by plants and insects that are both associated with severe epidemic or with useful changes in plant behavior. While their presence in apple trees causes severe losses in production and kills millions of coconut palm trees in the Caribbean, the presence of a poinsettia branching bacterium is allowing its commercial production as pot plant (Figure 1).

**Citation:** Bertaccini, A. Plants and Phytoplasmas: When Bacteria Modify Plants. *Plants* **2022**, *11*, 1425. <https://doi.org/10.3390/plants11111425>

Academic Editors: Milan S. Stankovic, Paula Baptista and Petronia Carillo

Received: 3 May 2022  
Accepted: 24 May 2022  
Published: 27 May 2022

**Publisher’s Note:** MDPI stays neutral with regard to jurisdictional claims in published maps and institutional affiliations.



**Copyright:** © 2022 by the author. Licensee MDPI, Basel, Switzerland. This article is an open access article distributed under the terms and conditions of the Creative Commons Attribution (CC BY) license (<https://creativecommons.org/licenses/by/4.0/>).

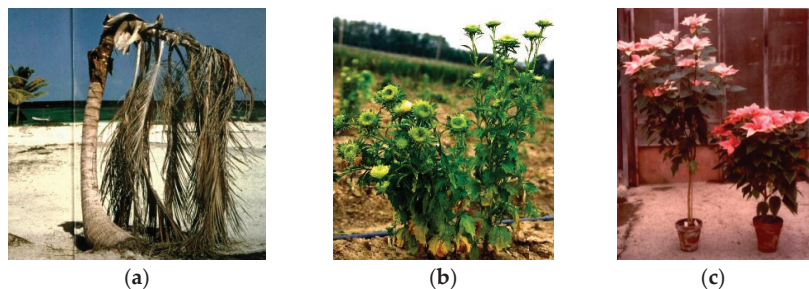


**Figure 1.** Coconut (a), aster (b), and poinsettia (c) infected by phytoplasmas.

Phytoplasmas are insect-transmitted wall-less bacteria provisionally classified to be the '*Candidatus Phytoplasma*' species [3,4]. They live only in the plant phloem tissues and in the emolymph of their insect vectors, especially concentrated in the salivary glands. Their relationship with both plants and insects is very intimate and they are able to manipulate several metabolic pathways, very often without impairing the host's life [5].

## 2. Phytoplasma Discovery

The phytoplasma presence in plants historically dates back about 1000 years, when special tree peonies exhibiting green flowers were given to the Chinese court during the Song dynasty (900 BC) as the most precious and beautiful flower of the empire. However, scientific records of phytoplasma-associated plant diseases started when, in 1967, mulberry dwarf, rice yellow dwarf, and sweet potato witches' broom, long considered to be caused by viruses, using electron microscopy, were found to be colonized by small pleomorphic bodies (80–800 nm in diameter) resembling mycoplasmas (bacterial pathogens of humans and animals) and were named mycoplasma-like organisms (MLOs) [6]. Their discovery stimulated worldwide investigation and numerous plant diseases were associated with the consistent presence of MLOs. These bacteria were long considered unculturable, but about 10 years ago, colonies containing molecularly different phytoplasmas began to be obtained in artificial media from different infected plant species (Figure 2) [7–11].

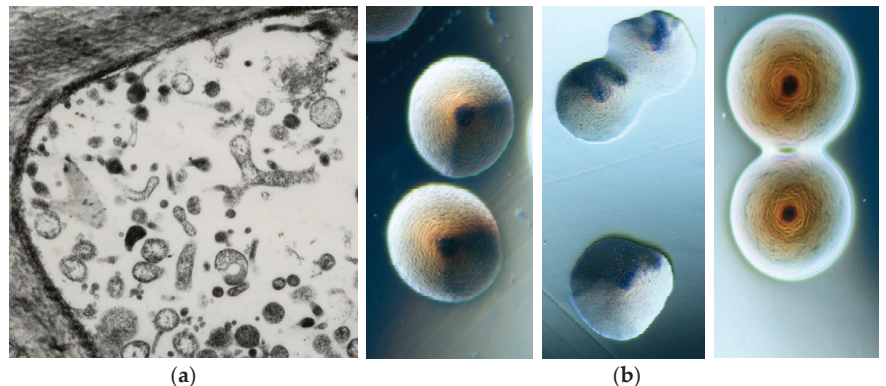


**Figure 2.** Transmission electron microscopy picture of a thin section in the phloematic tissue of a phytoplasma infected gladiolus plant showing the presence of strong pleomorphism ( $\times 8000$ ) (a). Tree morphotypes of colonies containing phytoplasmas under binocular microscope ( $\times 40$ ) (b).

## 3. Phytoplasma Classification

The '*Candidatus Phytoplasma*' genus provisional classification is highly relevant due to its application in epidemiological and ecological studies, mainly aimed at keeping the severe phytoplasma plant diseases under control worldwide. The updated proposed guidelines accommodate those '*Ca. Phytoplasma*' species strains sharing  $> 98.65\%$  sequence identity of their full or nearly full 16S rRNA gene sequences, obtained with at least 2-fold coverage of the sequence, compared with those of the reference strain of such species [4]. The officially published '*Candidatus Phytoplasma*' species are 49; however, they do not cover all the relevant biodiversity, especially in reference to differential geographic distribution and/or host species. Therefore, the differentiation in ribosomal groups and subgroups [12] is still valuable and should be used to be able to work on their epidemiology and prevention in the different areas of the world. The main distribution of strains is tightly related to the geographic areas and to the dissemination performed by propagation materials, such as cuttings and seeds, that are also infected, even if only in low percentages (1–3%).

#### 4. Relationship between Phytoplasma Symptomatology and Classification

Together with the study on the diseases associated with the presence of these bacteria, the first step was to give them a name according to the diverse disease in which the association was detected with specific phytoplasmas. Today, 30 years after this exercise started it appears clear that the molecular diversity described in phytoplasmas (49 ‘*Candidatus* Phytoplasma’ species and about 200 ribosomal subgroups) using the 16S ribosomal gene as basic standard is only in some cases related to a differential symptomatology. Identical symptoms are associated with different phytoplasmas and vice versa. Moreover, phytoplasmas associated with decline symptoms in some species could be associated with phyllody/virescence in others, such as ‘*Ca. P. solani*’ infecting potatoes, tomatoes, and grapevine. Therefore, contrary to the other plant pathogens it is necessary to verify the pathogen identity by molecular tools on a case-by-case basis; however, at the same time, it is of utmost importance to also recognize the symptoms associated with the presence of the phytoplasmas in order to appropriately manage the disease. This review of the main symptoms and several associated phytoplasmas worldwide is aimed at helping the recognition of the presence of these bacteria in plants, further clarifying their relationship with the host plants. This feature is, however, not stable over time also in the same plant species, considering the never-ending mechanism of patho-adaption that is part of life also in microorganisms; pathogens are special microorganisms that are simply looking for new ecological niches to ensure their survival and do not aim to destroy or kill the hosts.

##### 4.1. Shoot Proliferation and Witches’ Broom

Diseases with symptoms of witches’ broom can be caused by basidiomycetes but could also be associated with the presence of phytoplasmas. In both cases they are economically important in a number of crop plant species, including the cocoa tree, jujube, citrus, and apple and timber trees, such as poplar, *Melia azedarach*, and paulownia (Figure 3). Among woody species, this malformation is almost always associated with the presence of specific phytoplasmas, such as in apple (‘*Ca. P. mali*’), lime (‘*Ca. P. aurantifolia*’), lilac (‘*Ca. P. fraxini*’), paulownia (‘*Ca. P. asteris*’), almond (‘*Ca. P. phoenicium*’), *Juniperus* (16SrIX-E), walnut (16SrIII-G), *Balanites triflora* (‘*Ca. P. balanites*’), spartium (‘*Ca. P. spartii*’), black alder (16SrX-E), hibiscus (‘*Ca. P. brasiliense*’), *Guazuma* spp. (16SrXV-B), chestnut (‘*Ca. P. castaneae*’), *Cassia italica* (‘*Ca. P. omanense*’), and salt cedar (‘*Ca. P. tamaricis*’). In herbaceous host plants, the presence of witches’ broom was reported in diverse species, some of them as hosts of new phytoplasma strains (Table 1), such as strawberry, peanut, cactus, tabebuja, tomatillo, chayote, black raspberry, erigeron, alfalfa, and pigeon pea.

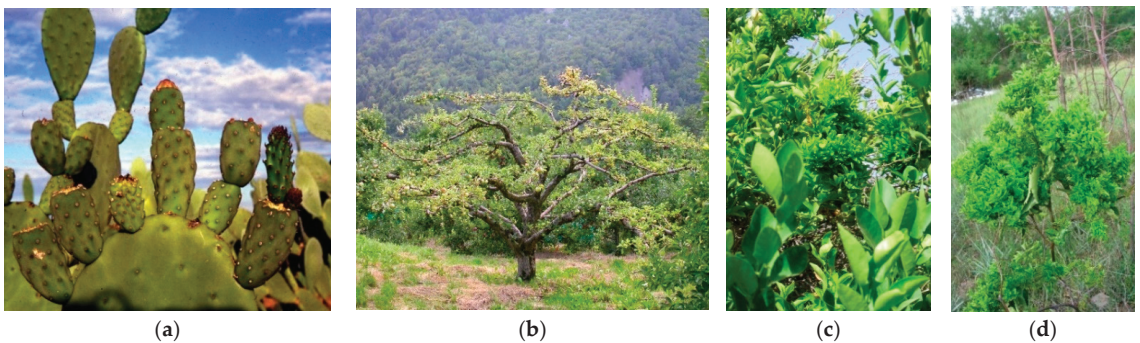


**Figure 3.** Cactus pear (*Opuntia ficus-indica*) proliferation (a), apple proliferation (b), citrus witches’ broom (c), and jujube witches’ broom (d) are associated with the presence of phytoplasmas in diverse areas of the world.

**Table 1.** Molecular diversity and geographic distribution of selected phytoplasmas belonging to different ribosomal groups/‘*Candidatus* Phytoplasma’ species (marked by different color) associated with witches’ broom symptoms.

Disease (Acronym)	Continent	16Sr Subgroups	‘ <i>Candidatus</i> Phytoplasma’ Species	GenBank Accession Number	References
Aster yellows w. b. (AY-WB)	America	16SrI-A	‘ <i>Ca. P. asteris</i> ’	NC_007716	[13]
Paulownia w. b. (PaWB)	Asia	16SrI-D		AY265206	[14]
Strawberry witches’ broom (STRAWB1), (STRAWB2)	America	16SrI-I / -K		U96614, U96616	[15]
Peach rosette-like (PRU0382)	America	16SrI-W		HQ450211	[16]
Peanut witches’ broom (PnWB)	America	16SrII-A		L33765	[17]
Lime witches’ broom (WBDL)	Asia	16SrII-B	‘ <i>Ca. P. aurantifolia</i> ’	U15442	[18]
Cactus witches’ broom (CWB)	Asia	16SrII-G to -L		EU099568, EU099552, EU099569, EU099572, EU099551, EU099546, EF647744	[19]
Tabebuia witches’ broom	America	16SrII-O			[20]
Tomatillo witches’ broom	America	16SrII-T		U125185	[21]
Walnut witches’ broom (WWB)	America	16SrIII-G		AF190226, AF190227	[22]
Poinsettia branch-inducing (PoiBI)	Europe, America	16SrIII-H		AF190223	[22]
Chayote w. b. (ChWBIII)	America	16SrIII-J		AF147706	[23]
Black raspberry w. b. (BRWB7)	America	16SrIII-Q		AF302841	[24]
Conyza witches’ broom	America	16SrIII-X		KC412026	[25]
Jujube witches’ broom (JWB-G1)	Asia	16SrV-B	‘ <i>Ca. P. ziziphi</i> ’	AB052876	[26]
<i>Balanites triflora</i> w. b. (BlfWB)	Asia	16SrV-F	<i>Ca. P. balanitae</i> ’	AB689678	[27]
Korean jujube witches’ broom	Asia	16SrV-G		AB052879	[26]
<i>Bischofia polycarpa</i> witches’ broom	Asia	16SrV-H		KJ452547	[28]
Blackberry witches’ broom	Europe	16SrV-I		KR233473	[29]
Clover proliferation (CP)	America	16SrVI-A	‘ <i>Ca. P. trifolii</i> ’	AY390261	[30]
Erigeron witches’ broom (ErWB)	America	16SrVII-B		AY034608	[31]
Argentinian alfalfa w.b. (ArAWB)	America	16SrVII-C		AY147038	[32]
Erigeron w. b. (EboWB-Br0)	America	16SrVII-D		KJ831066	[33]
Loofah witches’ broom (LufWB)	Asia	16Sr VIII-A	‘ <i>Ca. P. luffae</i> ’	AF086621	[34]
Pigeon pea w. b. (PPWB)	America	16SrIX-A		AF248957	[35]
Almond witches’ broom (AlWB)	Asia	16SrIX-B/-D	‘ <i>Ca. P. phoenicium</i> ’	AF515636, AF515637	[36]
Juniperus witches’ broom	America	16SrIX-E		GQ925918	[37]
Almond and stone fruit witches’ broom (N27-2), (A1-1)	Asia	16SrIX-F/-G	‘ <i>Ca. P. phoenicium</i> ’	HQ407532, HQ407514	[38]
Apple proliferation (AP)	Europe, Asia	16SrX-A	‘ <i>Ca. P. mali</i> ’	AJ542541	[39]
Spartium witches’ broom (SpaWB)	Europe	16SrX-D	‘ <i>Ca. P. spartii</i> ’	X92869	[40]

Table 1. Cont.

Disease (Acronym)	Continent	16Sr Subgroups	'Candidatus Phytoplasma' Species	GenBank Accession Number	References
Black alder w. b. (BAWB, BWB)	Europe	16SrX-E		X76431	[41]
Hibiscus witches' broom (HibWB)	America, Asia	16SrXV-A	'Ca. P. brasiliense'	AF147708	[42]
Guazuma w. b. (GWB)	America	16SrXV-B		HQ258882	[43]
Chestnut witches' broom	Asia	16SrXIX-A	'Ca. P. castaneae'	AB054986	[44]
Rhamnus witches' broom	Europe	16SrXX-A	'Ca. P. rhamni'	AJ583009	[40]
Weeping tea witches' broom	Oceania	16SrXXV-A *		AF521672	[ ]
Cassia w. b. (CaWB)	Asia	16SrXXIX-A	'Ca. P. omanense'	EF666051	[45]
Bindweed witches' broom (RBiWB)	Asia	16SrXXIX-B		KY047493	[47]
Salt cedar witches' broom	Asia	16SrXXX-A	'Ca. P. tamaricis'	FJ432664	[48]

w. b., witches' broom; \*, described as sequence deposited in GenBank only.

The excessive shoot proliferation results in poor or no fruit production and severely reduces the cultivation of some of these crops. Citrus in the Arabian Peninsula, jujube in China, and apple proliferation in Europe are some of the most severe cases that greatly reduce the possibility to produce and commercialize popular fruits. This modification is due to the loss of apical dominance of the shoots linked to disorders in the hormone balance.

#### 4.2. Stunting and Little Leaf

Stunting in plants could be due to virus or phytoplasma presence; however, it must also be verified that glyphosate or similar pesticides were not applied in the area in which these malformations are present in plants in the past years, since this can produce indistinguishable symptoms (Figure 4). The presence of phytoplasmas is reported in several plant species enclosing small fruits, vegetables, corn, and soybean; in some cases, these bacteria were associated with the presence of little leaf or stunting also in trees, such as cherry, eucalyptus, and *Sophora japonica* [49] (Table 2). In strawberries the case *Fragaria multicipita* was discovered to be not a true species, but just a cloned phytoplasma-infected genotype [15]. The hormone imbalance, according with the diverse infected species, is usually present and the transportation of starch and other metabolites for the appropriate development is very often impaired.

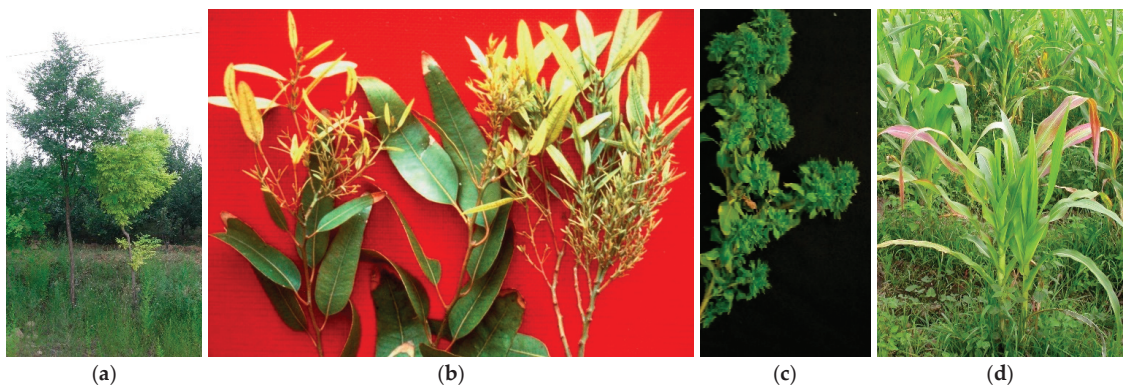


Figure 4. *Sophora japonica* stunting and yellows (a); *Eucalyptus* little leaf (b), periwinkle little leaf (c), and corn stunting (d).

**Table 2.** Molecular diversity and geographic distribution of selected phytoplasmas belonging to different ribosomal groups/‘*Candidatus* Phytoplasma’ species (marked by different color) associated with little leaf and stunting symptoms.

Disease (Acronym)	Continent	16Sr Subgroups	‘ <i>Candidatus</i> Phytoplasma’ Species	GenBank Accession Number	References
Blue dwarf wheat (BDW)	Asia	16SrI-C	‘ <i>Ca. P. tritici</i> ’	DQ078304	[50]
Blueberry stunt (BBS3)	America	16SrI-E		AY265213	[14]
Cherry little leaf (ChLL)	Europe	16SrI-Q		AY034089	[51]
Pepper little leaf (PeLL)	America	16SrI-S		DQ092321	[52]
Tomato little leaf (ToLL)	America	16SrI-T		DQ375238	[52]
<i>Vasconcellea cundinamarcensis</i> little leaf	China	16SrII-U		KP057205	[53]
Spiraea stunt (SP1)	America	16SrIII-E		AF190228	[23]
<i>Heterothalamus</i> little leaf (HetLL)	America	16SrIII-W		KC412029	[26]
Broccoli stunt (BSP-21)	America	16SrIII-Z		JX626327	[22]
Rubus stunt (RuS)	Europe	16SrV-E	‘ <i>Ca. P. rubi</i> ’	AY197648	[54]
<i>Fragaria multicipita</i> , multiplier disease	America	16SrVI-B		AF190224	[15]
Periwinkle little leaf (PLL-Bd)	Asia	16SrVI-D		AF228053	[55]
Portulaca little leaf (PLL-Ind)	Asia	16SrVI-H		EF651786	[56]
Soybean stunt (SoyST1c1)	America	16SrXXXI-A	‘ <i>Ca. P. costaricanum</i> ’	HQ225630	[57]

#### 4.3. Phyllody and Virescence

The transformation of different plant organs into leaves is a very relevant symptom among those associated with phytoplasma presence and is known as phyllody; this type of malformation could also be due to the application of pesticides based on hormone-like molecules. The virescence is the change of the color of flowers to green, which is due to phytoplasma presence, but in some cases the diagnostics can be tricked by the existence of flowers that are green and the presence of genetic factors modifying the anthocyanin distribution in the plant, as can be seen in a Chinese variety of rose and in some special clones of periwinkle (Figure 5). The most relevant phytoplasma-associated diseases are reported in flowering species for commercialization; however, virescence is also present in horticultural and seed crops, such as tomatoes, cabbages, strawberries, and clover, among several other species (Table 3).

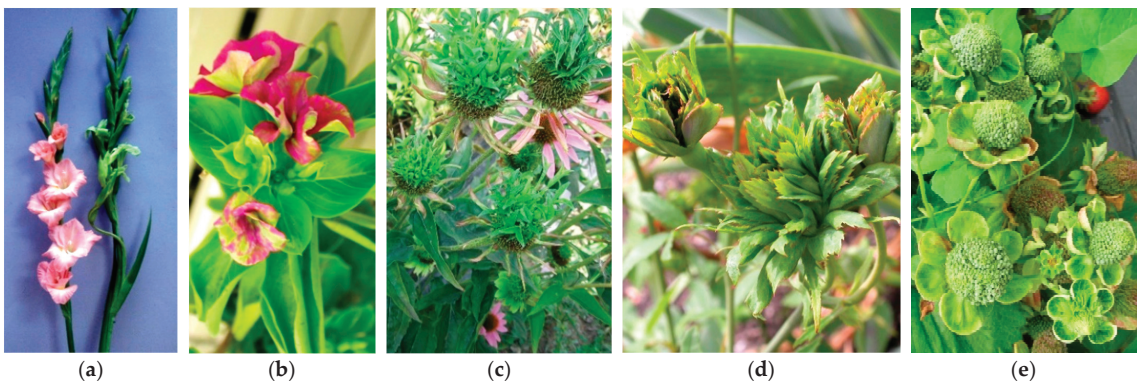


**Figure 5.** Virescence in gladiolus (a) and in periwinkle (b); phyllody in echinacea (c), rose (d), and strawberry (e). The rose flowers are showing virescence and phyllody due to genetics, rather than the phytoplasma presence in all the others.

**Table 3.** Molecular diversity and geographic distribution of selected phytoplasmas belonging to different ribosomal groups/‘*Candidatus* Phytoplasma’ species (marked by different color) and associated with phyllody and virescence symptoms.

Disease (Acronym)	Continent	16Sr Subgroups	‘ <i>Candidatus</i> Phytoplasma’ Species	GenBank Accession Number	References
Clover phyllody (CPh)	America	16SrI-C		AF222065	[15]
Faba bean phyllody (FBP)	Asia, Africa	16SrII-C		X83432	[58]
<i>Pichris echioides</i> phyllody (PEY)	Europe	16SrII-E		Y16393	[58]
Cotton phyllody (CoP)	Africa	16SrII-F		EF186827	[59]
Strawberry leafy fruit (SLF)	America	16SrIII-K		AF274876	[15]
Dandelion virescence (DanVir)	Europe	16SrIII-O/-P		AF370120, AF370119	[60]
<i>Heterothalamus</i> little leaf (HetLL)	America	16SrIII-W		KC412029	[26]
<i>Centarurea solstitialis</i> virescence (CSVI)	Europe	16SrVI-E		AY270156	[61]
<i>Catharanthus</i> phyllody (CPS)	Africa	16SrVI-F		EF186819	[59]
Naxos periwinkle virescence (NAXOS)	Europe, Asia, America	16SrIX-C		HQ589191	[62]
Sarsoon phyllody	Asia	16SrIX-H		KU892213	[63]
Japanese hydrangea phyllody	Asia	16SrXII-D	‘ <i>Ca. P. japonicum</i> ’	AB010425	[64]
Mexican periwinkle virescence (MPV)	America	16SrXIII-A	‘ <i>Ca. P. hispanicum</i> ’	AF248960	[65]
Strawberry green petal (STRAWB2)	America	16SrXIII-B		U96616	[15]
Malaysian periwinkle virescence (MaPV)	Asia	16SrXXXII-A	‘ <i>Ca. P. malaysianum</i> ’	EU371934	[66]

#### 4.4. Yellowing and Decline

One of the main symptoms associated with the presence of phytoplasmas is the yellowing, in several cases these bacteria are also known as agents of yellows diseases. Generally, the yellowing of the aerial portions of the plant is complemented by a general decline that led to a huge, and in several cases complete, loss of production (Figures 6 and 7). However, these symptoms can also be due to lack of nutrients, poor fertilization, and the presence of other pathogens infecting the root apparatus. The presence of phytoplasmas in plants exhibiting decline and yellowing must be considered together with these other factors in complex syndromes. The phytoplasmas associated with these symptoms are detected in some of the most economically relevant woody species, such as grapevine, fruit trees, and palms (especially coconut and other species for nut production) (Table 4). The metabolic basis for these symptoms is still very poorly understood, but the excessive consumption of sugar and the lack of its mobilization to the sink organs are involved.

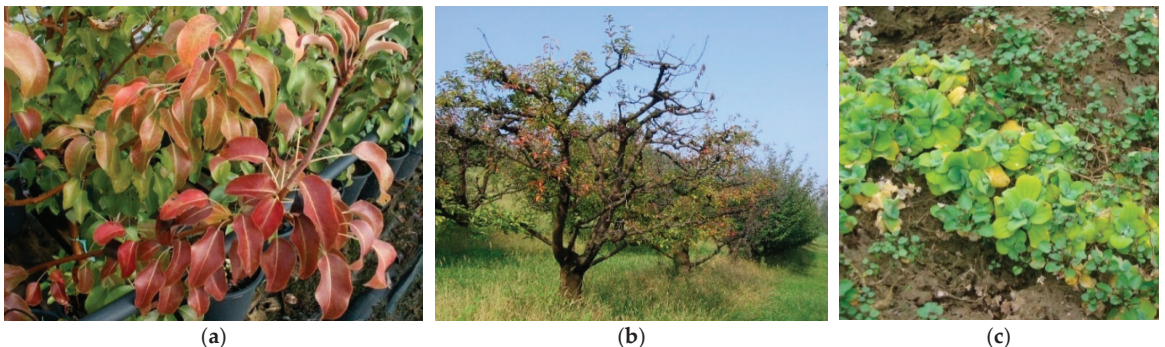


**Figure 6.** Reddening in pear decline (a), yellowing in plum (b) and watercress (c).

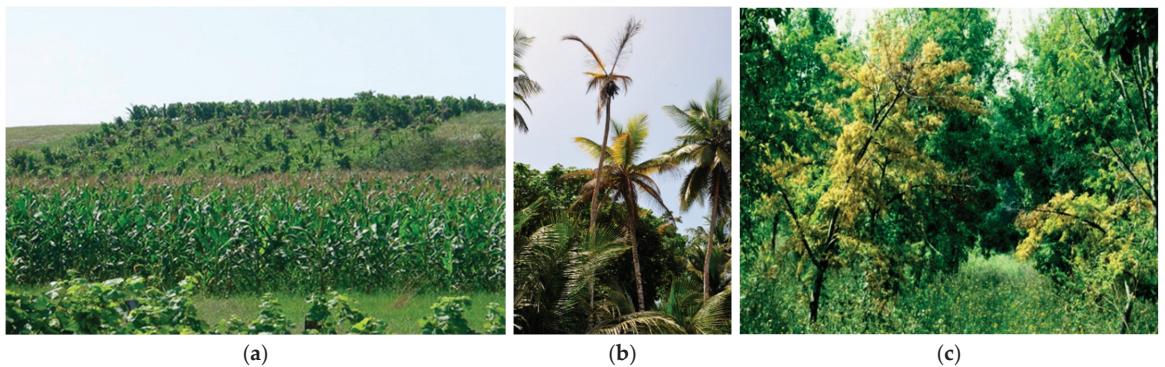


**Figure 7.** Grapevine yellows (a), coconut lethal yellowing (b), and elm yellows (c) associated with the presence of diverse phytoplasmas.

**Table 4.** Molecular diversity and geographic distribution of selected phytoplasmas belonging to different ribosomal groups/‘*Candidatus* Phytoplasma’ species (marked by different color) associated with yellows and decline symptoms.

Disease (Acronym)	Continent	16Sr Subgroups	‘ <i>Candidatus</i> Phytoplasma’ Species	GenBank Accession Number	References
Aster yellows (MAY)	America	16SrI-B	‘ <i>Ca. P. asteris</i> ’	M30790	[14]
Aster yellows apricot Spain (A-AY)	Europe, America	16SrI-F		AY265211	[14]
Aster yellows (AV2192)	Europe	16SrI-L		AY180957	[67]
Aster yellows (AVUT)	Europe	16SrI-M		AY265209	[17]
Aster yellows (IoWB)	America	16SrI-N		AY265205	[17]
Aster yellows from <i>Populus</i> (PopAY)	Europe	16SrI-P		AF503568	[68]
Papaya mosaic (PpM)	Oceania	16SrII-D	‘ <i>Ca. P. australasia</i> ’	Y10096	[69]
<i>Echinopsis</i> yellow patch	America	16SrII-R		DQ535900	[21]
Peach X-disease (PX11CT1)	America	16SrIII-A	‘ <i>Ca. P. pruni</i> ’	JQ044393	[22]
Clover yellow edge (CYE)	America, Europe	16SrIII-B		AF173558	[22]
Goldenrod yellows (GR1)	America	16SrIII-D		GU004372	[22]
Milkweed yellows (MW1)	America	16SrIII-F		AF510724	[22]
Virginia grapevine yellows (VGYIII)	America	16SrIII-I		AF060875	[70]
Western peach X-disease (WX)	America	16SrIII-S		L04682	[71]
Coconut lethal yellowing (LYJ-C8)	America	16SrIV-A	‘ <i>Ca. P. palmae</i> ’	AF498307	[4]
Yucatan coconut lethal decline (LDY)	America	16SrIV-B		U18753	[72]
Tanzanian coconut lethal decline (LDT)	Africa	16SrIV-C	‘ <i>Ca. P. cocostanzaniae</i> ’	X80117	[72]
Texas phoenix decline (TPD)	America	16SrIV-D		AF434969	[73]
Coconut lethal yellowing (LYDR-B5)	America	16SrIV-E		DQ631639	[74]
<i>Washingtonia robusta</i> decline	America	16SrIV-F		EU241512	[73]
Elm yellows (EY)	Europe, America	16SrV-A	‘ <i>Ca. P. ulmi</i> ’	AY197655	[75]
‘Flavescence dorée’ (FD-C)	Europe	16SrV-C		X76560	[76]
‘Flavescence dorée’ (FD-D)	Europe	16SrV-D		AJ548787	[76]
Illinois elm yellows (EY-IL1)	America	16SrVI-C		AF409069	[77]

Table 4. Cont.

Disease (Acronym)	Continent	16Sr Subgroups	'Candidatus Phytoplasma' Species	GenBank Accession Number	References
Ash yellows (AshY)	America, Europe, Asia	16SrVII-A	'Ca. P. fraxini'	AF092209	[78]
European stone fruit yellows (ESFY)	Europe, Asia	16SrX-B	'Ca. P. prunorum'	AJ542544	[39]
Pear decline (PD)	Europe, America	16SrX-C	'Ca. P. pyri'	AJ542543	[39]
Rice yellow dwarf (RYD)	Asia	16SrXI-A	'Ca. P. oryzae'	AB052873	[79]
"Stolbur" (STOL11)	Europe, America, Asia, Africa	16SrXII-A	'Ca. P. solani'	AF248959	[80]
Australian grapevine yellows (AUSGY)	Oceania	16SrXII-B	'Ca. P. australiense'	L76865	[81]
Strawberry lethal yellows (StrawLY)	Oceania	16SrXII-C		AJ243045	[82]
Yellows diseased strawberry (StrawY)	Europe	16SrXII-E	'Ca. P. fragariae'	DQ086423	[83]
"Bois noir" (BN-Op30), (BN-Fc3)	Europe	16SrXII-F /-G		EU836652, EU836647	[84]
Bindweed yellows (BY-S57/11)	Europe	16SrXII-H	'Ca. P. convolvuli'	JN833705	[85]
Chinaberry yellows (CBY1)	America	16SrXIII-C		AF495882	[86]
Chinaberry yellowing (ChTY)	America	16SrXIII-G	'Ca. P. meliae'	KU850940	[86]
Sugarcane yellow leaf syndrome	America	16SrXVI-A	'Ca. P. graminis'	AY725228	[87]
Pinus phytoplasma (PinP)	Europe, America, Africa	16SrXXI-A	'Ca. P. pini'	AJ310849	[88]
Lethal yellowing Mozambique (LYDM 178)	Africa	16SrXXII-A	'Ca. P. palmicola'	KF751387	[89]
Cape Saint Paul Wilt Ghana (LDG)	Africa	16SrXXII-B		Y13912	[90]
Buckland valley grapevine yellows	Oceania	16SrXXIII-A *		AY083605	[45]
Malayan yellow dwarf (MYD)	Asia	16SrXXXII-B		EU498727	[66]
Malayan oil palm (MOP)	Asia	16SrXXXII-C		EU498728	[66]
Allocasuarina phytoplasma	Oceania	16SrXXXIII-A	'Ca. P. allocasuarinae'	AY135523	[40]
Bogia coconut syndrome (BCS)	Oceania	Not determ.	'Ca. P. noviguineense'	LC228755	[91]
Palm decline (RID7692)	Oceania	Not determ.	'Ca. P. dypsidsis'	MT233886	[92]
Not described	Oceania	Not determ.	'Ca. P. stylosanthis'	MT431550	[93]
Palm decline	Oceania	16SrXXXVI	'Ca. P. wodyetiae'	KY069029	[94]

\*, described as sequence deposited in GenBank only.

#### 4.5. White Leaf

The white leaf symptomatology (Figure 8) is limited to a small range of species, monocotyledonous, and is reported to be associated with phytoplasma presence only in Asia and Europe (Table 5). The main economically relevant disease is the sugarcane white leaf that is severely infecting this crop in all Asian countries. The presence of diverse phytoplasmas is associated in sugarcane also with other symptoms, such as yellow leaf and grassy shoots. These diseases are insect- and cutting-transmitted and in some cases also transovarially [95]. The lack of chlorophyll in the leaves is the main modification, which is often accompanied by a strong shortening of the cycle span and early drying; inappropriate photosynthesis is the mechanism involved in this modification of plants.

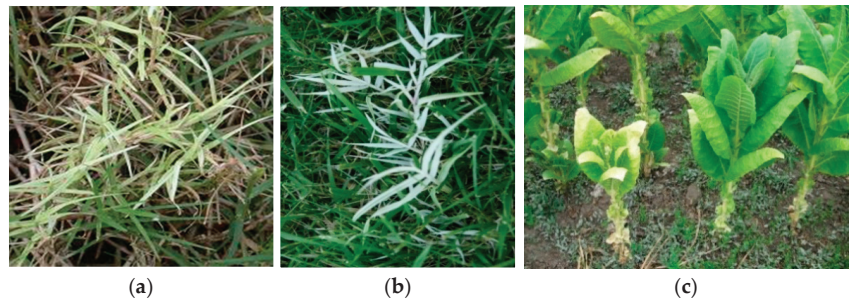


**Figure 8.** Bermudagrass white leaf in *Cynodon dactylon* (a,b) and yellow and stunting in tobacco (c).

**Table 5.** Molecular diversity and geographic distribution of selected phytoplasmas belonging to different ribosomal groups/‘*Candidatus* Phytoplasma’ species (marked by different color) associated with white leaf symptoms.

Disease (Acronym)	Continent	16Sr Subgroups	‘ <i>Candidatus</i> Phytoplasma’ Species	GenBank Accession Number	References
Cirsium white leaf (CirWL)	Europe	16SrIII-R		AF373105	[72]
Cirsium white leaf (CWL)	Europe	16SrIII-U		AF373105, AF373106	[81]
Sugarcane white leaf (SCWL)	Asia	16SrXI-B	‘ <i>Ca. P. sacchari</i> ’	X76432	[96]
Sugarcane white leaf (SCWL)	Asia	16SrXI-D		KR020685	[97]
Bermudagrass white leaf (BGWL)	Europe	16SrXIV-A	‘ <i>Ca. P. cynodontis</i> ’	AJ550984	[98]
Bermudagrass white leaf Iran	Asia	16SrXIV-B		EF444485	[99]
Bermudagrass white leaf (RS304/13)	Europe	16SrXIV-C		KP019339	[100]

#### 4.6. Purple Top and Other Malformations

The presence of phytoplasmas in the sieve tube also interferes with the composition of the phloem sap and is associated with hormone imbalance; therefore, several diverse malformations in roots, flowers, tubers, and leaves can be observed in infected plants (Figure 9). Phytoplasmas that induce these malformations infect mainly herbaceous crops (Table 6).



**Figure 9.** Cassava frog skin (a), tomato (b) and potato “stolbur” (c), potato purple top (d), and carrot reddening (e).

**Table 6.** Molecular diversity and geographic distribution of selected phytoplasmas belonging to different ribosomal groups/‘*Candidatus* Phytoplasma’ species (marked by different color) associated with purple top and other malformations.

Disease (Acronym)	Continent	16Sr Subgroups	‘ <i>Candidatus</i> Phytoplasma’ Species	GenBank Accession Number	References
Soybean purple stem (SPS)	America	16SrI-O		AF268405	[101]
Mexican potato purple top (JAL8), (SON18)	America	16SrI-U/-V		FJ914650, FJ914642	[53]
Papaya bunchy top (BTS)	America	16SrI-X		JF781308	[102]
Tomato “brote grande”	America	16SrI-Y	‘ <i>Ca. P. lycopersici</i> ’	EF199549	[103]
Papaya bunchy top (BTS)	America	16SrI-Z		JF781311	[104]
Potato purple top	Asia	16SrII-M		FJ914643	[105]
Papaya BTSp	America	16SrII-N		JF781309	[102]
Cuban papaya	America	16SrII-P		DQ286948	[22]
Papaya bunchy top (TSpHav02-IIA)	America	16SrII-Q		JF78131	[22]
<i>Echinopsis</i> yellow patch	America	16SrII-R		DQ535900	[22]
<i>Amaranthus hypochondriacus</i> 52A	America	16SrII-S		FJ357164	[22]
Pecan bunch (PB)	America	16SrIII-C		GU004371	[23]
Cassava frog skin (CFSD)	America	16SrIII-L		EU346761	[106]
Potato purple top (MT117)	America	16SrIII-M		FJ226074	[23]
Potato purple top (AKpot6)	America	16SrIII-N		GU004365	[23]
Sweet and sour cherry (ChD)	Europe	16SrIII-T		FJ231728	[107]
Passion fruit phytoplasma (PassWB-Br4)	America	16SrIII-V		GU292082	[108]
Cranberry false-blossom	America	16SrIII-Y		KF62652	[109]
Passionfruit (WB-Br4)	America	16SrVI-I	‘ <i>Ca. P. sudamericanum</i> ’	GU292081	[110]
Leafhopper-borne (BVK)	Europe	16SrXI-C		X76429	[13]
Cirsium phytoplasma	Europe	16SrXI-E	‘ <i>Ca. P. cirsii</i> ’	KR869146	[111]
Sugarcane grassy shoot (SCGS)	Asia	16SrXI-F		HF586636	[112]
Potato (169/Hezuo 88)	Asia	16SrXII-I		EU338445	[112]
Mexican potato purple top (SINPV)	America	16SrXIII-D		FJ914647	[53]
Papaya apical curl necrosis (PACN)	America	16SrXIII-E		EU719111	[113]
Strawberry red leaf	America	16SrXIII-F		KJ921641	[114]
Papaya bunchy top	America	16SrXVII-A	‘ <i>Ca. P. caricae</i> ’	AY725234	[88]
American potato purple top wilt	America	16SrXVIII-A	‘ <i>Ca. P. americanum</i> ’	DQ174122	[115]
Sorghum bunchy shoot	Oceania	16SrXXIV-A *		AF509322	[45]
Sugarcane phytoplasma D3T1	Africa	16SrXXVI-A *		AJ539179	[45]
Sugarcane phytoplasma D3T2	Africa	16SrXXVII-A *		AY539180	[45]
Derbid phytoplasma	Africa	16SrXXVIII-A *		AY744945	[45]

\*, described as sequence deposited in GenBank only.

## 5. Phytoplasma Genomics

Unlike common bacteria and many other organisms, including animals and plants, mycoplasmas use the UGA stop codon as a tryptophan-encoding codon; moreover, a gene encoding peptide chain release factor 2 that recognizes UGA as a termination codon is present in the phytoplasma genome [116]. The first complete genome sequence of 860,631 bp of the mutant OY-M that was reported in 2004 with a GC content of 28% [117]. Gene annotation analysis revealed that although the genome encoded basic cellular functions including DNA replication, transcription, translation, and protein translocation, the genes required for amino acid and fatty acid biosynthesis, the tricarboxylic acid cycle, and electron transport/oxidative phosphorylation were not present. Although metabolic genes were few in number, the OY-M genome contained many transporter genes. The phytoplasma genome is also rich in repeat regions with duplicated genes and transposon-like elements called potential mobile units; these features are similar to genes and organized in

a conservative manner and are thought to play roles in the regulation of gene expression and serve as drivers for phytoplasma interaction with insects and plants [13,118–120].

## 6. Mechanisms to Infect Plants and Insects

The longtime search for pathogenicity factors still did not elucidate this important aspect and very little clarification is available about a basic question, which is: are phytoplasmas always pathogenic? The finding of several cases of phytoplasma presence in asymptomatic plants do not allow to answer to this question yet. Phytoplasmas are spread between plants by phloem-feeding insects, such as leafhoppers, planthoppers, and psyllids [121]. Due to their wide range of plant hosts, phytoplasmas are often detected in various crops and wild plants [122]. Because phytoplasmas are transmitted transovarially in several cases [123], the presence or absence of insect hosts is a critical determinant of their survival in the natural environment. When phytoplasmas invade insects, their extracellular membrane proteins play important roles for host interactions. Notably, antigenic membrane protein (AMP), a representative of phytoplasma membrane proteins that is predominantly detected on the phytoplasma cell surface, was found to form a complex with host microfilaments determining whether an insect can transmit a phytoplasma [124–127]. Furthermore, microarray and gene expression patterns analyses revealed that phytoplasmas dramatically alter the expression of approximately one-third of their genes using transcription factors to establish host switching between plants and insects [128].

## 7. Genetic Factors Determining Symptom Development

Some of the molecular mechanisms by which phytoplasmas induce their most typical symptoms were elucidated. Comparing the genome sequences of OY-W and OY-M revealed the duplication of glycolytic gene clusters in the OY-W genome. It has been suggested that this difference is responsible for the high consumption of carbon sources, resulting in high growth rates and severe symptoms, such as yellowing, dwarfism, and decline, at least in the case of the OY-W phytoplasma strain [129]. Furthermore, the mechanisms of purple top symptoms have been revealed. Phytoplasma infection activates the anthocyanin biosynthetic pathway. The increased accumulation of anthocyanin not only changes the color of the leaves to purple, but also acts as an antioxidant that protects plant cells from damage caused by reactive oxygen species, which results in leaf cell death [130].

A comprehensive search for pathogenicity-related genes, in which phytoplasma genes encoding secreted proteins were expressed. In 2009, the first phytoplasma effector protein, TENGU, a secreted peptide of 38 amino acids, was identified as an inducer of witches' broom [131]. It is conserved among various phytoplasma strains. Following secretion from the phytoplasma cell, TENGU is cleaved in planta to a peptide of 12 amino acids, which is then transported to the shoot apical meristem, wherein it inhibits the signaling pathway of the plant hormone auxin and induces witches' broom symptoms [132]. TENGU also induces the sterility of male and female flowers by inhibiting the signaling pathway of jasmonic acid (JA) [133]. The reduction in endogenous JA levels is thought to contribute to attracting insect vectors. Similarly, another secreted protein, SAP11, downregulates JA synthesis and increases the fecundity of insect vectors.

In phytoplasma-infected plants, phyllody often affects sepals, and abnormal expression patterns of MTFs genes were found in all floral organs except stamens in phytoplasma-infected petunias [134,135]. Recently, SAP54 and PHYLL1 were found to be homologous proteins that induce phyllody in the floral organs of *Arabidopsis thaliana*. The proteins interact with and then degrade A- and E- class MTFs via the ubiquitin–proteasome pathway and are genetically and functionally conserved among phytoplasma strains and species. Therefore, the phyllody-inducing gene/protein (phyllogen) family was demonstrated to induce flower phyllody and related malformations (virescence and proliferation). Phyllogens induce flower phyllody in various angiosperms and MTF degradation in non-flowering plants. These molecules induce virescence, phyllody, and proliferation symptoms, indicating that these flower symptoms are not independent symptoms induced by distinct

effectors but a series of gradually changing phenotypes. Flower virescence can be considered just a mild form of phyllody, and the loss of flower meristem determinacy can be considered a severe form of phyllody [136–139].

Why do phytoplasmas induce symptoms accompanied by unique morphological changes, such as witches' broom and phyllody? Both symptoms increase the prevalence of short branches and small young leaves, which are preferred by sap-feeding insects. Furthermore, phyllody flowers remain green even when healthy flowers wither. These features are likely to enhance the attraction of insect vectors and thus the spread of phytoplasmas. Such manipulations of the morphology of host plants appear to be a common strategy for the survival of phytoplasmas.

## 8. Management

Because phytoplasmas are difficult to culture, electron microscopy observation using ultrathin sections of sieve elements and plant recovery after tetracycline treatment were the only diagnostic methods available when phytoplasmas were discovered. Subsequently, several DNA-based technologies to detect phytoplasmas have been developed and applied routinely [140] to detect and correctly identify the phytoplasmas present in diseased crops and devise appropriate management strategies [141]. Although treatment using tetracycline-class antibiotics suppresses phytoplasma multiplication in infected plants cultured *in vitro*, high concentrations of antibiotics damage the plant tissues [142–145]. Recently, a comprehensive screening of 40 antibiotics showed that phytoplasmas were eliminated from infected plants not only by the application of tetracycline but also by using rifampicin. Diverse alternative and more sustainable methods were tested and are under trial for practical application; however, the production of phytoplasma-free nursery stocks is still the basis of a friendly and sustainable management, since curing plants is time- and money-consuming, considering that these pathogens are insect- and seed-transmitted. Methods to eliminate phytoplasmas from crops using diverse molecules and resistance inducers showed increased plant performances but not pathogen elimination, and in many cases the scaling up of these systems has not yet been exploited.

## 9. Concluding Remarks

In the last quarter century, although there have been many barriers to the study of phytoplasmas, such as the difficulty of culturing them and the necessity of producing plant or insect hosts to maintain them for scientific purposes, several phytoplasma molecular and biological properties have been elucidated. Further research work, including the development of effective and ecofriendly strategies to control phytoplasma-associated diseases, will greatly contribute to both the understanding of phytoplasma biology and their physiopathological role in agricultural productions.

**Funding:** This research received no external funding.

**Institutional Review Board Statement:** Not applicable.

**Informed Consent Statement:** Not applicable.

**Acknowledgments:** The author thanks their colleagues, Nicoletta Contaldo, Bojan Duduk, Alberto Calari, Carmen Castillo Carrillo, Luciano Rovesti, Gian Luigi Rana, and Giovanni Granata, for kindly providing some of the pictures.

**Conflicts of Interest:** The author declares no conflict of interest.

## References

- McCann, H.C.; Li, L.; Liu, Y.; Li, D.; Pan, H.; Zhong, C.; Rikkerink, E.; Templeton, M.D.; Straub, C.; Colombi, E.; et al. Origin and evolution of the kiwifruit canker pandemic. *Gen. Biol. Evol.* **2017**, *9*, 932–944. [[CrossRef](#)] [[PubMed](#)]
- Bové, J.-M. Huanglongbing: A destructive, newly-emerging, century-old disease of citrus. *J. Plant Pathol.* **2006**, *88*, 7–37.
- IRPCM. 'Candidatus Phytoplasma', a taxon for the wall-less, non-helical prokaryotes that colonise plant phloem and insects. *Int. J. Syst. Evol. Microbiol.* **2004**, *54*, 1243–1255. [[CrossRef](#)] [[PubMed](#)]

4. Bertaccini, A.; Arocha-Rosete, Y.; Contaldo, N.; Duduk, B.; Fiore, N.; Montano, H.G.; Kube, M.; Kuo, C.-H.; Martini, M.; Oshima, K.; et al. Revision of the ‘*Candidatus Phytoplasma*’ species description guidelines. *Int. J. Syst. Evol. Microbiol.* **2022**, *74*, 005353. [[CrossRef](#)]
5. Namba, S. Molecular and biological properties of phytoplasmas. *Proc. Jpn. Acad. Ser. B Phys. Biol. Sci.* **2019**, *95*, 401–418. [[CrossRef](#)]
6. Doi, Y.; Teranaka, M.; Yora, K.; Asuyama, H. Mycoplasma or PLT grouplike microorganisms found in the phloem elements of plants infected with mulberry dwarf, potato witches’ broom, aster yellows or pawlownia witches’ broom. *Ann. Phytopath. Soc. Jpn.* **1967**, *33*, 259–266. [[CrossRef](#)]
7. Contaldo, N.; Bertaccini, A.; Paltrinieri, S.; Windsor, H.M.; Windsor, G.D. Axenic culture of plant pathogenic phytoplasmas. *Phytopath. Medit.* **2012**, *51*, 607–617. [[CrossRef](#)]
8. Contaldo, N.; Satta, E.; Zambon, Y.; Paltrinieri, S.; Bertaccini, A. Development and evaluation of different complex media for phytoplasma isolation and growth. *J. Microbiol. Meth.* **2016**, *127*, 105–110. [[CrossRef](#)]
9. Contaldo, N.; D’Amico, G.; Paltrinieri, S.; Diallo, H.A.; Bertaccini, A.; Arocha Rosete, Y. Molecular and biological characterization of phytoplasmas from coconut palms affected by the lethal yellowing disease in Africa. *Microbiol. Res.* **2019**, *223–225*, 51–57. [[CrossRef](#)]
10. Luis Pantoja, M.; Paredes-Tomás, C.; Uneau, Y.; Myrie, W.; Morillon, R.; Satta, E.; Contaldo, N.; Pacini, F.; Bertaccini, A. Identification of ‘*Candidatus Phytoplasma*’ species in “huanglongbing” infected citrus orchards in the Caribbean. *Eur. J. Plant Pathol.* **2021**, *160*, 185–198. [[CrossRef](#)]
11. Betancourt, C.; Pardo, J.; Muñoz, J.; Alvarez, E. Isolation of phytoplasmas associated to frogskin disease in cassava. *Rev. UDCA Actual. Divulg. Cient.* **2019**, *22*, e1177. [[CrossRef](#)]
12. Lee, I.-M.; Gundersen-Rindal, D.E.; Davis, R.E.; Bartoszyk, I.M. Revised classification scheme of phytoplasmas based on RFLP analyses of 16S rRNA and ribosomal protein gene sequences. *Int. J. Syst. Evol. Microbiol.* **1998**, *48*, 1153–1169. [[CrossRef](#)]
13. Bai, X.; Zhang, J.; Ewing, A.; Miller, S.A.; Radek, A.J.; Shevchenko, D.V.; Tsukerman, K.; Walunas, T.; Lapidus, A.; Campbell, J.W.; et al. Living with genome instability: The adaptation of phytoplasmas to diverse environments of their insect and plant hosts. *J. Bacteriol.* **2006**, *188*, 3682–3696. [[CrossRef](#)]
14. Lee, I.-M.; Gundersen-Rindal, D.E.; Davis, R.E.; Bottner, K.D.; Marccone, C.; Seemüller, E. ‘*Candidatus Phytoplasma asteris*’, a novel taxon associated with aster yellows and related diseases. *Int. J. Syst. Evol. Microbiol.* **2004**, *54*, 1037–1048. [[CrossRef](#)] [[PubMed](#)]
15. Jomantiene, R.; Davis, R.E.; Maas, J.; Dally, E.L. Classification of new phytoplasmas associated with diseases of strawberry in Florida, based on analysis of 16S rRNA and ribosomal protein gene operon sequences. *Int. J. Syst. Evol. Microbiol.* **1998**, *48*, 269–277. [[CrossRef](#)]
16. Arocha-Rosete, Y.; Zunnoon-Khan, S.; Krukovets, I.; Crosby, W.; Scott, J.; Bertaccini, A.; Michelutti, R. Identification and molecular characterization of the phytoplasma associated with peach rosette-like disease at the Canadian clonal Genebank based on the 16S rRNA gene analysis. *Can. J. Plant Pathol.* **2011**, *33*, 127–134. [[CrossRef](#)]
17. Gundersen, D.E.; Lee, I.-M.; Rehner, S.A.; Davis, R.E.; Kingsbury, D.T. Phylogeny of mycoplasmalike organisms (phytoplasmas): A basis for their classification. *J. Bacteriol.* **1994**, *176*, 5244–5254. [[CrossRef](#)] [[PubMed](#)]
18. Zreik, L.; Carle, P.; Bové, J.-M.; Garnier, M. Characterization of the mycoplasmalike organism associated with witches’ broom disease of lime and proposition of a ‘*Candidatus*’ taxon for the organism, ‘*Candidatus Phytoplasma aurantifolia*’. *Int. J. Syst. Bacteriol.* **1995**, *45*, 449–453. [[CrossRef](#)]
19. Cai, H.; Wei, W.; Davis, R.E.; Chen, H.; Zhao, Y. Genetic diversity among phytoplasmas infecting *Opuntia* species: Virtual RFLP analysis identifies new subgroups in the peanut witches’ broom phytoplasma group. *Int. J. Syst. Evol. Microbiol.* **2008**, *58*, 1448–1457. [[CrossRef](#)]
20. Mafia, R.G.; Barreto, R.W.; Vanetti, C.A.; Hodgetts, J.; Dickinson, M.; Alfenas, A.C. A phytoplasma is associated with witches’ broom disease of *Tabebuia pentaphylla* in Brazil. *New Dis. Rep.* **2007**, *15*, 49. [[CrossRef](#)]
21. Perez-López, E.; Luna-Rodríguez, M.; Olivier, C.Y.; Dumonceaux, T.J. The underestimated diversity of phytoplasmas in Latin America. *Int. J. Syst. Evol. Microbiol.* **2016**, *66*, 492–513. [[CrossRef](#)] [[PubMed](#)]
22. Davis, R.E.; Zhao, Y.; Dally, E.L.; Lee, I.-M.; Jomantiene, R.; Douglas, S. ‘*Candidatus Phytoplasma pruni*’, a novel taxon associated with X-disease of stone fruits, *Prunus* spp.: Multilocus characterization based on 16S rRNA, secY, and ribosomal protein genes. *Int. J. Syst. Evol. Microbiol.* **2013**, *63*, 766–776. [[CrossRef](#)] [[PubMed](#)]
23. Montano, H.G.; Davis, R.E.; Dally, E.L.; Pimentel, J.P.; Brioso, P.S.T. Identification and phylogenetic analysis of a new phytoplasma from diseased chayote in Brazil. *Plant Dis.* **2000**, *84*, 429–436. [[CrossRef](#)] [[PubMed](#)]
24. Davis, R.E.; Dally, E.L.; Converse, R.H. Molecular identification of a phytoplasma associated with witches’-broom disease of black raspberry in Oregon and its classification in group 16SrIII, new subgroup Q. *Plant Dis.* **2001**, *85*, 1121. [[CrossRef](#)] [[PubMed](#)]
25. Galdeano, E.; Guzmán, F.A.; Fernández, F.; Conci, R.G. Genetic diversity of 16SrIII group phytoplasmas in Argentina. Pre-dominance of subgroups 16SrIII-J and B and two new subgroups 16SrIII-W and X. *Eur. J. Plant Pathol.* **2013**, *137*, 753–764. [[CrossRef](#)]
26. Jung, H.-Y.; Sawayanagi, T.; Kakizawa, S.; Nishigawa, H.; Wei, W.; Oshima, K.; Miyata, S.; Ugaki, M.; Hibi, T.; Namba, S. ‘*Candidatus Phytoplasma ziziphi*’, a novel phytoplasma taxon associated with jujube witches’ broom disease. *Int. J. Syst. Evol. Microbiol.* **2003**, *53*, 1037–1041. [[CrossRef](#)]

27. Win, N.K.K.; Lee, S.-Y.; Bertaccini, A.; Namba, S.; Jung, H.-Y. ‘*Candidatus* Phytoplasma balanitae’ associated with witches’ broom disease of *Balanites triflora*. *Int. J. Syst. Evol. Microbiol.* **2013**, *63*, 636–640. [[CrossRef](#)]
28. Lai, F.; Song, C.S.; Ren, Z.G.; Lin, C.L.; Xu, Q.C.; Li, Y.; Piao, C.G.; Yu, S.S.; Guo, M.W.; Tian, G.Z. Molecular characterization of a new member of the 16SrV group of phytoplasma associated with *Bischofia polycarpa* (Lévl.) Airy Shaw witches’ broom disease in China by a multiple gene-based analysis. *Austral. Plant Pathol.* **2014**, *43*, 557–569. [[CrossRef](#)]
29. Fránová, J.; de Sousa, E.; Mimoso, C.; Cardoso, F.; Contaldo, N.; Paltrinieri, S.; Bertaccini, A. Multigene characterization of a new ‘*Candidatus* Phytoplasma rubi’-related strain associated with blackberry witches’ broom in Portugal. *Int. J. Syst. Evol. Microbiol.* **2016**, *66*, 1438–1446. [[CrossRef](#)]
30. Hiruki, C.; Wang, K. Clover proliferation phytoplasma: ‘*Candidatus* Phytoplasma trifolii’’. *Int. J. Syst. Evol. Microbiol.* **2004**, *54*, 1349–1353. [[CrossRef](#)]
31. Barros, T.S.L.; Davis, R.E.; Resende, R.O.; Dally, E.L. Erigeron witches’ broom phytoplasma in Brazil represents new subgroup VII-B in 16S rRNA gene group VII, the ash yellows phytoplasma group. *Plant Dis.* **2002**, *86*, 1142–1148. [[CrossRef](#)] [[PubMed](#)]
32. Conci, L.; Meneguzzi, N.; Galdeano, E.; Torres, L.; Nome, C.; Nome, S. Detection and molecular characterisation of an alfalfa phytoplasma in Argentina that represents a new subgroup in the 16S rDNA ash yellows group (‘*Candidatus* Phytoplasma fraxini’). *Eur. J. Plant Pathol.* **2005**, *113*, 255–265. [[CrossRef](#)]
33. Flores, D.; Amaral Mello, A.O.; Pereira, T.B.C.; Rezende, J.A.M.; Bedendo, I.P. A novel subgroup 16SrVII-D phytoplasma identified in association with erigeron witches’ broom. *Int. J. Syst. Evol. Microbiol.* **2015**, *65*, 2761–2765. [[CrossRef](#)] [[PubMed](#)]
34. Davis, R.E.; Zhao, Y.; Wei, W.; Dally, E.L.; Lee, I.-M. ‘*Candidatus* Phytoplasma luffae’, a novel taxon associated with witches’ broom disease of loofah, *Luffa aegyptica* Mill. *Int. J. Syst. Evol. Microbiol.* **2017**, *67*, 3127–3133. [[CrossRef](#)] [[PubMed](#)]
35. Gundersen, D.E.; Lee, I.-M.; Schaff, D.A.; Harrison, N.A.; Chang, C.J.; Davis, R.E.; Kinsbury, D.T. Genomic diversity among phytoplasma strains in 16S rRNA group I (aster yellows and related phytoplasmas) and III (X-disease and related phytoplasmas). *Int. J. Syst. Bacteriol.* **1996**, *46*, 64–75. [[CrossRef](#)]
36. Verdin, E.; Salar, P.; Danet, J.-L.; Choueiri, E.; Jreijiri, F.; El Zammar, S.; Gélie, B.; Bové, J.-M.; Garnier, M. ‘*Candidatus* Phytoplasma phoenicium’ sp. nov., a novel phytoplasma associated with an emerging lethal disease of almond trees in Lebanon and Iran. *Int. J. Syst. Evol. Microbiol.* **2003**, *53*, 833–838. [[CrossRef](#)]
37. Davis, R.E.; Dally, E.; Zhao, Y.; Lee, I.-M.; Jomantiene, R.; Detweiler, A.J.; Putnam, M.L. First report of a new subgroup 16SrIX-E (‘*Candidatus* Phytoplasma phoenicium’-related) phytoplasma associated with juniper witches’ broom disease in Oregon, USA. *Plant Pathol.* **2010**, *59*, 1161. [[CrossRef](#)]
38. Molino Lova, M.; Quaglino, F.; Abou-Jawdah, Y.; Choueiri, E.; Sobh, H.; Casati, P.; Tedeschi, R.; Alma, A.; Bianco, P.A. Identification of new 16SrIX subgroups, -F and -G, among ‘*Candidatus* Phytoplasma phoenicium’ strains infecting almond, peach and nectarine in Lebanon. *Phytopath. Medit.* **2011**, *50*, 273–282. [[CrossRef](#)]
39. Seemüller, E.; Schneider, B. ‘*Candidatus* Phytoplasma mali’, ‘*Candidatus* Phytoplasma pyri’ and ‘*Candidatus* Phytoplasma prunorum’, the causal agents of apple proliferation, pear decline and European stone fruit yellows, respectively. *Int. J. Syst. Evol. Microbiol.* **2004**, *54*, 1217–1226. [[CrossRef](#)]
40. Marcone, C.; Gibb, K.S.; Streten, C.; Schneider, B. ‘*Candidatus* Phytoplasma spartii’, ‘*Candidatus* Phytoplasma rhamnii’ and ‘*Candidatus* Phytoplasma allocasuarinae’, respectively associated with *Spartium* witches’ broom, buckthorn witches’ broom and *Allocasuarina* yellows diseases. *Int. J. Syst. Evol. Microbiol.* **2004**, *54*, 1025–1029. [[CrossRef](#)]
41. Seemüller, E.; Schneider, B.; Maurer, R.; Ahrens, U.; Daire, X.; Kison, H.; Lorenz, K.; Firrao, G.; Avinent, L.; Sears, B.B.; et al. Phylogenetic classification of phytopathogenic mollicutes by sequence analysis of 16S ribosomal DNA. *Int. J. Syst. Bacteriol.* **1994**, *44*, 440–446. [[CrossRef](#)] [[PubMed](#)]
42. Montano, H.G.; Davis, R.E.; Dally, E.L.; Hogenhout, S.; Pimentel, J.P.; Brioso, P.S. ‘*Candidatus* Phytoplasma brasiliense’, a new phytoplasma taxon associated with hibiscus witches’ broom disease. *Int. J. Syst. Evol. Microbiol.* **2001**, *51*, 1109–1118. [[CrossRef](#)] [[PubMed](#)]
43. Villalobos, W.; Martini, M.; Garita, L.; Muñoz, M.; Osler, R.; Moreira, L. *Guazuma ulmifolia* (Sterculiaceae), a new natural host of 16SrXV phytoplasma in Costa Rica. *Trop. Plant Pathol.* **2011**, *36*, 2. [[CrossRef](#)]
44. Jung, H.-Y.; Sawayanagi, T.; Kakizawa, S.; Nishigawa, H.; Miyata, S.; Oshima, K.; Ugaki, M.; Lee, J.T.; Hibi, T.; Namba, S. ‘*Candidatus* Phytoplasma castaneae’, a novel phytoplasma taxon associated with chestnut witches’ broom disease. *Int. J. Syst. Evol. Microbiol.* **2002**, *52*, 1543–1549. [[CrossRef](#)] [[PubMed](#)]
45. Wei, W.; Davis, R.E.; Lee, I.-M.; Zhao, Y. Computer-simulated RFLP analysis of 16S rRNA genes: Identification of ten new phytoplasma groups. *Int. J. Syst. Evol. Microbiol.* **2007**, *57*, 1855–1867. [[CrossRef](#)]
46. Al-Saady, N.A.; Khan, A.J.; Calari, A.; Al-Subhi, A.M.; Bertaccini, A. ‘*Candidatus* Phytoplasma omanense’, associated with witches’ broom of *Cassia italica* (Mill.) Spreng in Oman. *Int. J. Syst. Evol. Microbiol.* **2008**, *58*, 461–466. [[CrossRef](#)]
47. Esmailzadeh Hosseini, S.A.; Salehi, M.; Mirchenari, S.M.; Contaldo, N.; Paltrinieri, S.; Bertaccini, A. Occurrence of a ‘*Candidatus* Phytoplasma omanense’-related strain in bindweed showing a witches’ broom disease in Iran. *Phytopath. Moll.* **2016**, *6*, 87–92. [[CrossRef](#)]
48. Zhao, Y.; Sun, Q.; Wei, W.; Davis, R.E.; Wu, W.; Liu, Q. ‘*Candidatus* Phytoplasma tamaricis’, a novel taxon discovered in witches’-broom-diseased salt cedar (*Tamarix chinensis* Lour.). *Int. J. Syst. Evol. Microbiol.* **2009**, *59*, 2496–2504. [[CrossRef](#)]

49. Duduk, B.; Tian, J.B.; Contaldo, N.; Fan, X.P.; Paltrinieri, S.; Chen, Q.F.; Zhao, Q.F.; Bertaccini, A. Occurrence of phytoplasmas related to “stolbur” and to ‘*Candidatus Phytoplasma japonicum*’ in woody host plants in China. *J. Phytopath.* **2010**, *158*, 100–104. [\[CrossRef\]](#)
50. Zhao, Y.; Wei, W.; Davis, R.E.; Lee, I.-M.; Bottner-Parker, K.D. The agent associated with blue dwarf disease in wheat represents a new phytoplasma taxon, ‘*Candidatus Phytoplasma tritici*’. *Int. J. Syst. Evol. Microbiol.* **2021**, *71*, 004604. [\[CrossRef\]](#)
51. Valiunas, D.; Jomantiene, R.; Davis, R.E. A ‘*Candidatus Phytoplasma asteris*’-related phytoplasma associated with cherry little leaf disease represents a new subgroup, 16SrI-Q. *Phytopathology* **2005**, *95*, S106.
52. Santos-Cervantes, M.E.; Chávez-Medina, J.A.; Acosta-Pardini, J.; Flores-Zamora, G.L.; Méndez-Lozano, J.; Leyva-López, N.E. Genetic diversity and geographical distribution of phytoplasmas associated with potato purple top disease in Mexico. *Plant Dis.* **2010**, *94*, 388–395. [\[CrossRef\]](#) [\[PubMed\]](#)
53. Yang, Y.; Jiang, L.; Che, H.; Cao, X.; Luo, D. Identification of a novel subgroup 16SrII-U phytoplasma associated with papaya little leaf disease. *Int. J. Syst. Evol. Microbiol.* **2016**, *66*, 3485–3491. [\[CrossRef\]](#) [\[PubMed\]](#)
54. Malembic-Maher, S.; Salar, P.; Filippin, L.; Carle, P.; Angelini, E.; Foissac, X. Genetic diversity of European phytoplasmas of the 16SrV taxonomic group and proposal of ‘*Candidatus Phytoplasma rubi*’. *Int. J. Syst. Evol. Microbiol.* **2011**, *61*, 2129–2134. [\[CrossRef\]](#) [\[PubMed\]](#)
55. Siddique, A.B.M.; Agrawal, G.K.; Alam, N.; Krishina Reddy, M. Electron microscopy and molecular characterization of phytoplasmas associated with little leaf disease of brinjal (*Solanum melongena*) and periwinkle (*Catharanthus roseus*) in Bangladesh. *J. Phytopath.* **2001**, *149*, 237–244. [\[CrossRef\]](#)
56. Samad, A.; Ajayakumar, P.V.; Shasany, A.K.; Gupta, M.K.; Alam, M.; Rastogi, S. Occurrence of a clover proliferation (16SrVI) group phytoplasma associated with little leaf disease of *Portulaca grandiflora* in India. *Plant Dis.* **2008**, *92*, 832. [\[CrossRef\]](#)
57. Lee, I.-M.; Bottner-Parker, K.D.; Zhao, Y.; Villalobos, W.; Moreira, L. ‘*Candidatus Phytoplasma costaricanum*’ a novel phytoplasma associated with an emerging disease in soybean (*Glycine max*). *Int. J. Syst. Evol. Microbiol.* **2011**, *61*, 2822–2826. [\[CrossRef\]](#)
58. Seemüller, E.; Marcone, C.; Lauer, U.; Ragozzino, A.; Göschl, M. Current status of molecular classification of the phytoplasmas. *J. Plant Pathol.* **1998**, *80*, 3–26.
59. Martini, M.; Lee, I.-M.; Bottner, K.D.; Zhao, Y.; Botti, S.; Bertaccini, A.; Harrison, N.A.; Carraro, L.; Marcone, C.; Khan, J.; et al. Ribosomal protein gene-based phylogeny for finer differentiation and classification of phytoplasmas. *Int. J. Syst. Evol. Microbiol.* **2007**, *57*, 2037–2051. [\[CrossRef\]](#)
60. Jomantiene, R.; Maas, J.L.; Takeda, F.; Davis, R.E. Molecular identification and classification of strawberry phylloid fruit phytoplasma in group 16SrI, new subgroup. *Plant Dis.* **2002**, *86*, 920. [\[CrossRef\]](#)
61. Faggioli, F.; Pasquini, G.; Lumia, V.; Campobasso, G.; Widmer, T.L.; Quimby, P.C. Molecular identification of a new member of the clover proliferation phytoplasma group (16SrVI) associated with yellow starthistle virescence in Italy. *Eur. J. Plant Pathol.* **2004**, *110*, 353–360. [\[CrossRef\]](#)
62. Duduk, B.; Mejia, J.F.; Calari, A.; Bertaccini, A. Identification of 16SrIX group phytoplasmas infecting Colombian periwinkles and molecular characterization on several genes. In Proceedings of the 17th IOM Congress, Tienjin, China, 6–11 July 2008; p. 83.
63. Ahmad, J.N.; Ahmad, S.J.N.; Irfan, M.; Paltrinieri, S.; Contaldo, N.; Bertaccini, A. Molecular detection, identification, characterization and transmission study of sarsoon phyllody in Punjab–Pakistan associated with phytoplasmas affiliated to the new subgroup 16SrIX-H. *Eur. J. Plant Pathol.* **2017**, *149*, 117–125. [\[CrossRef\]](#)
64. Sawayanagi, T.; Horikoshi, N.; Kanehira, T.; Shinohara, M.; Bertaccini, A.; Cousin, M.-T.; Hiruki, C.; Namba, S. ‘*Candidatus Phytoplasma japonicum*’, a new phytoplasma taxon associated with Japanese hydrangea phyllody. *Int. J. Syst. Evol. Microbiol.* **1999**, *49*, 1275–1285. [\[CrossRef\]](#) [\[PubMed\]](#)
65. Davis, R.E.; Harrison, N.A.; Zhao, Y.; Wei, W.; Dally, E.L. ‘*Candidatus Phytoplasma hispanicum*’, a novel taxon associated with Mexican periwinkle virescence disease of *Catharanthus roseus*. *Int. J. Syst. Evol. Microbiol.* **2016**, *66*, 3463–3467. [\[CrossRef\]](#)
66. Nejat, N.; Vadamalai, G.; Davis, R.E.; Harrison, N.A.; Sijam, K.; Dickinson, M.; Abdullah, S.N.A.; Zhao, Y. ‘*Candidatus Phytoplasma malaysianum*’, a novel taxon associated with virescence and phyllody of Madagascar periwinkle (*Catharanthus roseus*). *Int. J. Syst. Evol. Microbiol.* **2013**, *63*, 540–548. [\[CrossRef\]](#)
67. Lee, I.-M.; Martini, M.; Bottner, K.D.; Dane, R.A.; Black, M.C.; Troxclair, N. Ecological implications from a molecular analysis of phytoplasmas involved in an aster yellows epidemic in various crops in Texas. *Phytopathology* **2003**, *93*, 1368–1377. [\[CrossRef\]](#)
68. Šeruga, M.; Škorić, D.; Botti, S.; Paltrinieri, S.; Juretić, N.; Bertaccini, A. Molecular characterization of a phytoplasma from the aster yellows (16SrI) group naturally infecting *Populus nigra* L. ‘Italica’ trees in Croatia. *For. Pathol.* **2003**, *33*, 113–125. [\[CrossRef\]](#)
69. White, D.T.; Blackall, L.L.; Scott, P.T.; Walsh, K.B. Phylogenetic positions of phytoplasmas associated with dieback, yellow crinkle and mosaic diseases of papaya, and their proposed inclusion in ‘*Candidatus Phytoplasma australiense*’ and a new taxon, ‘*Candidatus Phytoplasma australasia*’. *Int. J. Syst. Bacteriol.* **1998**, *48*, 941–951. [\[CrossRef\]](#)
70. Davis, R.E.; Jomantiene, R.; Dally, E.L.; Wolf, T.K. Phytoplasmas associated with grapevine yellows in Virginia belong to group 16SrI, subgroup A (tomato big bud phytoplasma subgroup), and group 16SrIII, new subgroup I. *Vitis* **1998**, *37*, 131–137. [\[CrossRef\]](#)
71. Zhao, Y.; Wei, W.; Lee, I.-M.; Shao, J.; Suo, X.; Davis, R.E. Construction of an interactive online phytoplasma classification tool, iPhyClassifier, and its application in analysis of the peach X-disease phytoplasma group (16SrIII). *Int. J. Syst. Evol. Microbiol.* **2009**, *59*, 2582–2593. [\[CrossRef\]](#)
72. Harrison, N.A.; Richardson, P.A.; Kramer, J.B.; Tsai, J.H. Detection of the mycoplasma-like organism associated with lethal yellowing disease of palms in Florida by polymerase chain reaction. *Plant Pathol.* **1994**, *43*, 998–1008. [\[CrossRef\]](#)

73. Harrison, N.A.; Helmick, E.E.; Elliott, M.L. Lethal yellowing-type diseases of palms associated with phytoplasmas newly identified in Florida, USA. *Ann. Appl. Biol.* **2008**, *153*, 85–94. [[CrossRef](#)]
74. Martinez, R.T.; Narvaez, M.; Fabre, S.; Harrison, N.A.; Oropeza, C.; Dollet, M.; Hichez, E. Coconut lethal yellowing on the southern coast of the Dominican Republic is associated with a new 16SrIV group phytoplasma. *New Dis. Rep.* **2007**, *15*, 39. [[CrossRef](#)]
75. Lee, I.-M.; Martini, M.; Marcone, C.; Zhu, S.F. Classification of phytoplasma strains in the elm yellows group (16SrV) and proposal of ‘*Candidatus Phytoplasma ulmi*’ for the phytoplasma associated with elm yellows. *Int. J. Syst. Evol. Microbiol.* **2004**, *54*, 337–347. [[CrossRef](#)] [[PubMed](#)]
76. Martini, M.; Murari, E.; Mori, N.; Bertaccini, A. Identification and epidemic distribution of two “flavescence dorée”-related phytoplasmas in Veneto (Italy). *Plant Dis.* **1999**, *83*, 925–930. [[CrossRef](#)]
77. Jacobs, K.A.; Lee, I.-M.; Griffiths, H.M.; Miller, F.D., Jr.; Bottner, K.D. A new member of the clover proliferation phytoplasma group (16SrVI) associated with elm yellows in Illinois. *Plant Dis.* **2003**, *87*, 241–246. [[CrossRef](#)]
78. Griffiths, H.M.; Sinclair, W.A.; Smart, C.D.; Davis, R.E. The phytoplasma associated with ash yellows and lilac witches’ broom: ‘*Candidatus Phytoplasma fraxini*’. *Int. J. Syst. Bacteriol.* **1999**, *49*, 1605–1614. [[CrossRef](#)]
79. Jung, H.-Y.; Sawayanagi, T.; Wongkaew, P.; Kakizawa, S.; Nishigawa, H.; Wei, W.; Oshima, K.; Miyata, S.; Ugaki, M.; Hibi, T.; et al. ‘*Candidatus Phytoplasma oryzae*’, a novel phytoplasma taxon associated with rice yellow dwarf disease. *Int. J. Syst. Evol. Microbiol.* **2003**, *53*, 1925–1929. [[CrossRef](#)]
80. Quaglino, F.; Zhao, Y.; Casati, P.; Bulgari, D.; Bianco, P.A.; Wei, W.; Davis, R.E. ‘*Candidatus Phytoplasma solani*’, a novel taxon associated with “stolbur” and “bois noir”-related diseases of plants. *Int. J. Syst. Evol. Microbiol.* **2013**, *63*, 2879–2894. [[CrossRef](#)]
81. Davis, R.E.; Dally, E.L.; Gundersen, D.E.; Lee, I.-M.; Habili, N. ‘*Candidatus Phytoplasma australiense*’ a new phytoplasma taxon associated with Australian grapevine yellows. *Int. J. Syst. Bacteriol.* **1997**, *47*, 262–269. [[CrossRef](#)]
82. Padovan, A.; Gibb, K.; Persley, D. Association of ‘*Candidatus Phytoplasma australiense*’ 38 with green petal and lethal yellows diseases in strawberry. *Plant Pathol.* **2000**, *49*, 362–369. [[CrossRef](#)]
83. Valiunas, D.; Staniulis, J.; Davis, R.E. ‘*Candidatus Phytoplasma fragariae*’, a novel phytoplasma taxon discovered in yellows diseased strawberry, *Fragaria × ananassa*. *Int. J. Syst. Evol. Microbiol.* **2006**, *56*, 277–281. [[CrossRef](#)] [[PubMed](#)]
84. Quaglino, F.; Zhao, Y.; Bianco, P.A.; Wei, W.; Casati, P.; Durante, G.; Davis, R.E. New 16Sr subgroups and distinct single nucleotide polymorphism lineages among grapevine “bois noir” phytoplasma populations. *Ann. Appl. Biol.* **2009**, *154*, 279–289. [[CrossRef](#)]
85. Martini, M.; Marcone, C.; Mitrovic, J.; Maixner, M.; Delic, D.; Myrta, A.; Ermacora, P.; Bertaccini, A.; Duduk, B. ‘*Candidatus Phytoplasma convolvuli*’, a new phytoplasma taxon associated with bindweed yellows in four European countries. *Int. J. Syst. Evol. Microbiol.* **2012**, *62*, 2910–2915. [[CrossRef](#)]
86. Fernández, F.D.; Galdeano, E.; Kornowski, M.V.; Arneodo, J.D.; Conci, L.R. Description of ‘*Candidatus Phytoplasma meliae*’, a phytoplasma associated with Chinaberry (*Melia azedarach* L.) yellowing in South America. *Int. J. Syst. Evol. Microbiol.* **2016**, *66*, 5244–5251. [[CrossRef](#)] [[PubMed](#)]
87. Arocha, Y.; López, M.; Piñol, B.; Fernández, M.; Picornell, B.; Almeida, R.; Palenzuela, I.; Wilson, M.R.; Jones, P. ‘*Candidatus Phytoplasma graminis*’ and ‘*Candidatus Phytoplasma caricae*’, two novel phytoplasmas associated with diseases of sugarcane, weeds and papaya in Cuba. *Int. J. Syst. Evol. Microbiol.* **2005**, *55*, 2451–2463. [[CrossRef](#)]
88. Schneider, B.; Torres, E.; Martín, M.P.; Schröder, M.; Behnke, H.D.; Seemüller, E. ‘*Candidatus Phytoplasma pini*’, a novel taxon from *Pinus silvestris* and *Pinus halepensis*. *Int. J. Syst. Evol. Microbiol.* **2005**, *55*, 303–307. [[CrossRef](#)]
89. Harrison, N.A.; Davis, R.E.; Oropeza, C.; Helmick, E.E.; Narvaez, M.; Eden-Green, S.; Dollet, M.; Dickinson, M. ‘*Candidatus Phytoplasma palmicola*’, associated with a lethal yellowing-type disease of coconut (*Cocos nucifera* L.) in Mozambique. *Int. J. Syst. Evol. Microbiol.* **2014**, *64*, 1890–1899. [[CrossRef](#)]
90. Tymon, A.M.; Jones, P.; Harrison, N.A. Phylogenetic relationships of coconut phytoplasmas and the development of specific oligonucleotide PCR primers. *Ann. Appl. Biol.* **1998**, *132*, 437–452. [[CrossRef](#)]
91. Miyazaki, A.; Shigaki, T.; Koinuma, H.; Iwabuchi, N.; Rauka, G.B.; Kembu, A.; Saul, J.; Watanabe, K.; Nijo, T.; Maejima, K.; et al. ‘*Candidatus Phytoplasma noviguineense*’, a novel taxon associated with Bogia coconut syndrome and banana wilt disease on the island of New Guinea. *Int. J. Syst. Evol. Microbiol.* **2018**, *68*, 170–175. [[CrossRef](#)]
92. Jones, L.M.; Pease, B.; Perkins, S.L.; Constable, F.E.; Kinoti, W.M.; Warmington, D.; Allgood, B.; Powell, S.; Taylor, P.; Pearce, C.; et al. ‘*Candidatus Phytoplasma dypsidsis*’, a novel taxon associated with a lethal wilt disease of palms in Australia. *Int. J. Syst. Evol. Microbiol.* **2021**, *71*, 004818. [[CrossRef](#)] [[PubMed](#)]
93. Jardim, B.R.; Kinoti, W.M.; Tran-Nguyen, L.T.T.; Gambley, C.; Rodoni, B.; Constable, F.E. ‘*Candidatus Phytoplasma stylosanthis*’, a novel taxon with a diverse host range in Australia, characterised using multilocus sequence analysis of 16S rRNA, secA, tuf, and rp genes. *Int. J. Syst. Evol. Microbiol.* **2021**, *71*, 004589. [[CrossRef](#)]
94. Naderali, N.; Nejat, N.; Vadamalai, G.; Davis, R.E.; Wei, W.; Harrison, N.A.; Kong, L.L.; Kadir, J.; Tan, H.-Y.; Zhao, Y. ‘*Candidatus Phytoplasma wodyetiae*’, a new taxon associated with yellow decline disease of foxtail palm (*Wodyetia bifurcata*) in Malaysia. *Int. J. Syst. Evol. Microbiol.* **2017**, *67*, 3765–3772. [[CrossRef](#)] [[PubMed](#)]
95. Tedeschi, R.; Bertaccini, A. Transovarial transmission in insect vectors. In *Phytoplasmas: Plant Pathogenic Bacteria-II Transmission and Management of Phytoplasma Associated Diseases*; Bertaccini, A., Weintraub, P.G., Rao, G.P., Mori, N., Eds.; Springer: Singapore, 2019; pp. 115–130.

96. Kirdat, K.; Tiwarekar, B.; Thorat, V.; Sathe, S.; Shouche, Y.; Yadav, A. ‘*Candidatus* Phytoplasma sacchari’, a novel taxon-associated with sugarcane grassy shoot (SCGS) disease. *Int. J. Syst. Evol. Microbiol.* **2020**, *71*, 004591. [[CrossRef](#)]
97. Zhang, R.Y.; Li, W.F.; Huang, Y.K.; Wang, X.Y.; Shan, H.L.; Luo, Z.-M.; Yin, J. Group 16SrXI phytoplasma strains, including subgroup 16SrXI-B and a new subgroup, 16SrXI-D, are associated with sugar cane white leaf. *Int. J. Syst. Evol. Microbiol.* **2016**, *66*, 487–491. [[CrossRef](#)]
98. Marcone, C.; Schneider, B.; Seemüller, E. ‘*Candidatus* Phytoplasma cynodontis’, the phytoplasma associated with Bermuda grass white leaf disease. *Int. J. Syst. Evol. Microbiol.* **2004**, *54*, 1077–1082. [[CrossRef](#)]
99. Salehi, M.; Izadpanah, K.; Siampour, M.; Taghizadeh, M. Molecular characterization and transmission of bermuda grass white leaf phytoplasma in Iran. *J. Plant Pathol.* **2009**, *91*, 655–661.
100. Mitrovic, J.; Smiljković, M.; Seemüller, E.; Reinhardt, R.; Hüttel, B.; Büttner, C.; Bertaccini, A.; Kube, M.; Duduk, B. Differentiation of ‘*Candidatus* Phytoplasma cynodontis’ based on 16S rRNA and groEL genes and identification of a new subgroup, 16SrXIV-C. *Plant Dis.* **2015**, *99*, 1578–1583. [[CrossRef](#)]
101. Lee, M.E.; Grau, C.R.; Lukaesko, L.A.; Lee, I.-M. Identification of aster yellows phytoplasmas in soybean in Wisconsin based on RFLP analysis of PCR-amplified products (16S rDNAs). *Can. J. Plant Pathol.* **2002**, *24*, 125–130. [[CrossRef](#)]
102. Acosta, K.I.; Zamora, L.; Piñol, B.E.; Fernández, A.; Chávez, A.; Flores, G.; Méndez, J.; Santos, M.; Leyva, N.; Arocha, Y. Identification and molecular characterization of phytoplasmas and rickettsia pathogens associated with bunchy top symptom (BTS) and papaya bunchy top (PBT) of papaya in Cuba. *Crop Prot.* **2013**, *45*, 49–56. [[CrossRef](#)]
103. Arocha, Y.; Antesana, O.; Montellano, E.; Franco, P.; Plata, G.; Jones, P. ‘*Candidatus* Phytoplasma lycopersici’, a phytoplasma associated with “hoja de perejil” disease in Bolivia. *Int. J. Syst. Evol. Microbiol.* **2007**, *57*, 1704–1710. [[CrossRef](#)] [[PubMed](#)]
104. Acosta-Pérez, K.I.; Piñol-Pérez, B.E.; Zamora-Gutierrez, L.; Quiñones-Pantoja, M.L.; Miranda-Cabrera, I.; Leyva-López, N.E.; Arocha-Rosete, Y. A phytoplasma representative of a new subgroup 16SrI-Z associated with bunchy top symptoms (BTS) on papaya in Cuba. *Rev. Protec. Veg.* **2017**, *32*, 52–59.
105. Yadav, A.; Bhale, U.; Thorat, V.; Shouche, Y. First report of a new subgroup 16SrII-M ‘*Candidatus* Phytoplasma aurantifolia’ associated with witches’ broom disease of *Tephrosia purpurea* in India. *Plant Dis.* **2014**, *98*, 990. [[CrossRef](#)]
106. Alvarez, E.; Mejía, J.F.; Llano, G.A.; Loke, J.B.; Calari, A.; Duduk, B.; Bertaccini, A. Detection and molecular characterization of a phytoplasma associated with frogskin disease in cassava. *Plant Dis.* **2009**, *93*, 1139–1145. [[CrossRef](#)] [[PubMed](#)]
107. Valiunas, D.; Jomantiene, R.; Ivanauskas, A.; Abraitis, R.; Staniene, G.; Zhao, Y.; Davis, R.E. First report of a new phytoplasma subgroup, 16SrIII-T, associated with decline disease affecting sweet and sour cherry trees in Lithuania. *Plant Dis.* **2009**, *93*, 550. [[CrossRef](#)]
108. Davis, R.E.; Zhao, Y.; Dally, E.L.; Jomantiene, R.; Lee, I.-M.; Wei, W.; Kitajima, E.W. ‘*Candidatus* Phytoplasma sudamericanum’, a novel taxon, and strain PassWB-Br4, a new subgroup 16SrIII-V phytoplasma, from diseased passion fruit (*Passiflora edulis* f. *flavicarpa* Deg.). *Int. J. Syst. Evol. Microbiol.* **2012**, *62*, 984–989. [[CrossRef](#)] [[PubMed](#)]
109. Lee, I.-M.; Polashock, J.; Bottner-Parker, K.D.; Bagadia, P.G.; Rodriguez-Saona, C.; Zhao, Y.; Davis, R.E. New subgroup 16SrIII-Y phytoplasmas associated with false-blossom diseased cranberry (*Vaccinium macrocarpon*) plants and with known and potential insect vectors in New Jersey. *Eur. J. Plant Pathol.* **2014**, *139*, 393–400. [[CrossRef](#)]
110. Šafárová, D.; Zemánek, T.; Válková, P.; Navrátil, M. ‘*Candidatus* Phytoplasma cirsii’, a novel taxon from creeping thistle [*Cirsium arvense* (L.) Scop]. *Int. J. Syst. Evol. Microbiol.* **2016**, *66*, 1745–1753. [[CrossRef](#)]
111. Yadav, A.; Thorat, V.; Deokule, S.; Shouche, Y.; Prasad, D.T. New subgroup 16SrXI-F phytoplasma strain associated with sugarcane grassy shoot (SCGS) disease in India. *Int. J. Syst. Evol. Microbiol.* **2017**, *67*, 374–378. [[CrossRef](#)]
112. Cheng, M.; Dong, J.; Lee, I.-M.; Bottner-Parker, K.D.; Zhao, Y.; Davis, R.E.; Laski, P.J.; Zhang, Z.; McBeath, J.H. Group 16SrXII phytoplasma strains, including subgroup 16SrXII-E (‘*Candidatus* Phytoplasma fragariae’) and a new subgroup, 16SrXII-I, are associated with diseased potatoes (*Solanum tuberosum*) in the Yunnan and Inner Mongolia regions of China. *Eur. J. Plant Pathol.* **2014**, *142*, 305–318. [[CrossRef](#)]
113. Melo, L.; Silva, E.; Flóres, D.; Ventura, J.; Costa, H.; Bedendo, I. A phytoplasma representative of a new subgroup, 16SrXIII-E, associated with papaya apical curl necrosis. *Eur. J. Plant Pathol.* **2013**, *137*, 445–450. [[CrossRef](#)]
114. Fernández, F.D.; Meneguzzi, N.G.; Guzmán, F.A.; Kirschbaum, D.S.; Nome, C.F.; Conci, L.R. Detection and identification of a novel 16SrXIII subgroup phytoplasma associated with strawberry red leaf disease in Argentina. *Int. J. Syst. Evol. Microbiol.* **2015**, *65*, 2741–2747. [[CrossRef](#)] [[PubMed](#)]
115. Lee, I.-M.; Bottner, K.D.; Secor, G.; Rivera-Varas, V. ‘*Candidatus* Phytoplasma americanum’, a phytoplasma associated with a potato purple top wilt disease complex. *Int. J. Syst. Evol. Microbiol.* **2006**, *56*, 1593–1597. [[CrossRef](#)]
116. Kakizawa, S.; Oshima, K.; Kuboyama, T.; Nishigawa, H.; Jung, H.-Y.; Sawayanagi, T.; Tsuchizaki, T.; Miyata, S.; Ugaki, M.; Namba, S. Cloning and expression analysis of phytoplasma protein translocation genes. *Mol. Plant Microbe Interact.* **2001**, *14*, 1043–1050. [[CrossRef](#)]
117. Oshima, K.; Kakizawa, S.; Nishigawa, H.; Jung, H.-Y.; Wei, W.; Suzuki, S.; Arashida, R.; Nakata, D.; Miyata, S.; Ugaki, M.; et al. Reductive evolution suggested from the complete genome sequence of a plant-pathogenic phytoplasma. *Nat. Genet.* **2004**, *36*, 27–29. [[CrossRef](#)] [[PubMed](#)]
118. Arashida, R.; Kakizawa, S.; Hoshii, A.; Ishii, Y.; Jung, H.-Y.; Kagiwada, S.; Yamaji, Y.; Oshima, K.; Namba, S. Heterogeneous dynamics of the structures of multiple gene clusters in two pathogenetically different lines originating from the same phytoplasma. *DNA Cell Biol.* **2008**, *27*, 209–217. [[CrossRef](#)]

119. Jomantiene, R.; Davis, R.E. Clusters of diverse genes existing as multiple, sequence-variable mosaics in a phytoplasma genome. *FEMS Microbiol. Lett.* **2006**, *255*, 59–65. [[CrossRef](#)]
120. Toruño, T.Y.; Musić, M.S.; Simi, S.; Nicolaisen, M.; Hogenhout, S.A. Phytoplasma PMU1 exists as linear chromosomal and circular extrachromosomal elements and has enhanced expression in insect vectors compared with plant hosts. *Mol. Microbiol.* **2010**, *77*, 1406–1415. [[CrossRef](#)]
121. Weintraub, P.G.; Beanland, L. Insect vectors of phytoplasmas. *Annu. Rev. Entomol.* **2006**, *51*, 91–111. [[CrossRef](#)]
122. Wei, W.; Kakizawa, S.; Suzuki, S.; Jung, H.-Y.; Nishigawa, H.; Miyata, S.; Oshima, K.; Ugaki, M.; Hibi, T.; Namba, S. In planta dynamic analysis of onion yellows phytoplasma using localized inoculation by insect transmission. *Phytopathology* **2004**, *94*, 244–250. [[CrossRef](#)]
123. Bertaccini, A.; Oshima, K.; Kakizawa, S.; Duduk, B.; Namba, S. Dissecting the multifaceted mechanisms that drive leafhopper host–phytoplasma specificity. In *Vector-Mediated Transmission of Plant Pathogens*; Brown, J.K., Ed.; APS Press: St. Paul, MN, USA, 2016; Volume 2, pp. 21–28. [[CrossRef](#)]
124. Kakizawa, S.; Oshima, K.; Ishii, Y.; Hoshi, A.; Maejima, K.; Jung, H.-Y.; Yamaji, Y.; Namba, S. Cloning of immunodominant membrane protein genes of phytoplasmas and their in planta expression. *FEMS Microbiol. Lett.* **2009**, *293*, 92–101. [[CrossRef](#)] [[PubMed](#)]
125. Suzuki, S.; Oshima, K.; Kakizawa, S.; Arashida, R.; Jung, H.-Y.; Yamaji, Y.; Nishigawa, H.; Ugaki, M.; Namba, S. Interaction between the membrane protein of a pathogen and insect microfilament complex determines insect-vector specificity. *Proc. Natl. Acad. Sci. USA* **2006**, *103*, 4252–4257. [[CrossRef](#)] [[PubMed](#)]
126. Galetto, L.; Bosco, D.; Balestrini, R.; Genre, A.; Fletcher, J.; Marzachi, C. The major antigenic membrane protein of ‘*Candidatus* Phytoplasma asteris’ selectively interacts with ATP synthase and actin of leafhopper vectors. *PLoS ONE* **2011**, *6*, e22571. [[CrossRef](#)] [[PubMed](#)]
127. Boonrod, K.; Munteanu, B.; Jarausch, B.; Jarausch, W.; Krczal, G. An immunodominant membrane protein (Imp) of ‘*Candidatus* Phytoplasma mali’ binds to plant actin. *Mol. Plant Microbe Interact.* **2012**, *25*, 889–895. [[CrossRef](#)] [[PubMed](#)]
128. Oshima, K.; Ishii, Y.; Kakizawa, S.; Sugawara, K.; Neriya, Y.; Himeno, M.; Minato, N.; Miura, C.; Shiraishi, T.; Yamaji, Y.; et al. Dramatic transcriptional changes in an intracellular parasite enable host switching between plant and insect. *PLoS ONE* **2011**, *6*, e23242. [[CrossRef](#)]
129. Oshima, K.; Kakizawa, S.; Arashida, R.; Ishii, Y.; Hoshi, A.; Hayashi, Y.; Kagiwada, S.; Namba, S. Presence of two glycolytic gene clusters in a severe pathogenic line of ‘*Candidatus* Phytoplasma asteris’. *Mol. Plant Pathol.* **2007**, *8*, 481–489. [[CrossRef](#)]
130. Himeno, M.; Kitazawa, Y.; Yoshida, T.; Maejima, K.; Yamaji, Y.; Oshima, K.; Namba, S. Purple top symptoms are associated with reduction of leaf cell death in phytoplasma-infected plants. *Sci. Rep.* **2014**, *4*, 4111. [[CrossRef](#)]
131. Hoshi, A.; Oshima, K.; Kakizawa, S.; Ishii, Y.; Ozeki, J.; Hashimoto, M.; Komatsu, K.; Kagiwada, S.; Yamaji, Y.; Namba, S. A unique virulence factor for proliferation and dwarfism inplants identified from a phytopathogenic bacterium. *Proc. Natl. Acad. Sci. USA* **2009**, *106*, 6416–6421. [[CrossRef](#)]
132. Sugawara, K.; Honma, Y.; Komatsu, K.; Himeno, M.; Oshima, K.; Namba, S. The alteration of plant morphology by small peptides released from the proteolytic processing of the bacterial peptide TENGU. *Plant Physiol.* **2013**, *162*, 2005–2014. [[CrossRef](#)]
133. Minato, N.; Himeno, M.; Hoshi, A.; Maejima, K.; Komatsu, K.; Takebayashi, Y.; Kasahara, H.; Yusa, A.; Yamaji, Y.; Oshima, K.; et al. The phytoplasmal virulence factor TENGU causes plant sterility by downregulating of the jasmonic acid and auxin pathways. *Sci. Rep.* **2014**, *4*, 7399. [[CrossRef](#)]
134. Arashida, R.; Kakizawa, S.; Ishii, Y.; Hoshi, A.; Jung, H.-Y.; Kagiwada, S.; Yamaji, Y.; Oshima, K.; Namba, S. Cloning and characterization of the antigenic membrane protein (Amp) gene and in situ detection of Amp from malformed flowers infected with Japanese hydrangea phyllody phytoplasma. *Phytopathology* **2008**, *98*, 769–775. [[CrossRef](#)] [[PubMed](#)]
135. Himeno, M.; Neriya, Y.; Minato, N.; Miura, C.; Sugawara, K.; Ishii, Y.; Yamaji, Y.; Kakizawa, S.; Oshima, K.; Namba, S. Unique morphological changes in plant pathogenic phytoplasma-infected petunia flowers are related to transcriptional regulation of floral homeotic genes in an organ-specific manner. *Plant J.* **2011**, *67*, 971–979. [[CrossRef](#)] [[PubMed](#)]
136. MacLean, A.M.; Sugio, A.; Makarova, O.V.; Findlay, K.C.; Grieve, V.M.; Toth, R.; Nicolaisen, M.; Hogenhout, S.A. Phytoplasma effector SAP54 induces indeterminate leaf-like flower development in *Arabidopsis* plants. *Plant Physiol.* **2011**, *157*, 831–841. [[CrossRef](#)]
137. Maejima, K.; Iwai, R.; Himeno, M.; Komatsu, K.; Kitazawa, Y.; Fujita, N.; Ishikawa, K.; Fukuoka, M.; Minato, N.; Yamaji, Y.; et al. Recognition of floral homeotic MADS domain transcription factors by a phytoplasmal effector, phyllogen, induces phyllody. *Plant J.* **2014**, *78*, 541–554. [[CrossRef](#)] [[PubMed](#)]
138. MacLean, A.M.; Orlovskis, Z.; Kowitzanich, K.; Zdzarska, A.M.; Angenent, G.C.; Immink, R.G.; Hogenhout, S.A. Phytoplasma effector SAP54 hijacks plant reproduction by degrading MADS-box proteins and promotes insect colonization in a RAD23-dependent manner. *PLoS Biol.* **2014**, *12*, e1001835. [[CrossRef](#)] [[PubMed](#)]
139. Kitazawa, Y.; Iwabuchi, N.; Himeno, M.; Sasano, M.; Koinuma, H.; Nijo, T.; Tomomitsu, T.; Yoshida, T.; Okano, Y.; Yoshikawa, N.; et al. Phytoplasma-conserved phyllogen proteins induce phyllody across the Plantae by degrading floral MADS domain proteins. *J. Exp. Bot.* **2017**, *68*, 2799–2811. [[CrossRef](#)] [[PubMed](#)]
140. Bertaccini, A.; Paltrinieri, S.; Contaldo, N. Standard detection protocol: PCR and RFLP analyses based on 16S rRNA gene. In *Phytoplasmas*; Humana Press: New York, NY, USA, 2019; pp. 83–95. [[CrossRef](#)]

141. Bianco, P.A.; Romanazzi, G.; Mori, N.; Myrie, W.; Bertaccini, A. Integrated management of phytoplasma diseases. In *Phytoplasmas: Plant Pathogenic Bacteria-II Transmission and Management of Phytoplasma Associated Diseases*; Bertaccini, A., Weintraub, P.G., Rao, G.P., Mori, N., Eds.; Springer: Singapore, 2019; Volume 2, pp. 237–258.
142. Tanno, K.; Maejima, K.; Miyazaki, A.; Koinuma, H.; Iwabuchi, N.; Kitazawa, Y.; Nijo, T.; Hashimoto, M.; Yamaji, Y.; Namba, S. Comprehensive screening of antimicrobials to control phytoplasma diseases using an in vitro plant-phytoplasma co-culture system. *Microbiology* **2018**, *164*, 1048–1058. [[CrossRef](#)]
143. Davies, D.L.; Clark, M.F. Maintenance of mycoplasma-like organisms occurring in *Pyrus* species by micropropagation and their elimination by tetracycline therapy. *Plant Pathol.* **1994**, *43*, 819–823.
144. Aldaghi, M.; Massart, S.; Druart, P.; Bertaccini, A.; Jijakli, M.H.; Lepoivre, P. Preliminary in vitro evaluation of antimicrobial activity of some chemicals and essential oils on apple proliferation disease. *Commun. Appl. Biol. Sci. Ghent Univ.* **2008**, *73*, 335–341.
145. Bertaccini, A. Containment of phytoplasma-associated plant diseases by antibiotics and other antimicrobial molecules. *Antibiotics* **2021**, *10*, 1398. [[CrossRef](#)]

Article

# Chemical Investigation and Dose-Response Phytotoxic Effect of Essential Oils from Two Gymnosperm Species (*Juniperus communis* var. *saxatilis* Pall. and *Larix decidua* Mill.)

Sara Vitalini <sup>1,2,†</sup>, Marcello Iriti <sup>2,3,†</sup>, Valentina Vaglia <sup>4</sup> and Stefania Garzoli <sup>5,\*</sup>

- <sup>1</sup> Department of Food, Environmental and Nutritional Sciences, Milan State University, Via Mangiagalli 25, 20133 Milan, Italy; sara.vitalini@unimi.it
- <sup>2</sup> National Interuniversity Consortium of Materials Science and Technology, Via G. Giusti 9, 50121 Firenze, Italy; marcello.iriti@unimi.it
- <sup>3</sup> Department of Biomedical, Surgical and Dental Sciences, Milan State University, Via G. Celoria 2, 20133 Milan, Italy
- <sup>4</sup> Department of Environmental Science and Policy, Milan State University, Via G. Celoria 2, 20133 Milan, Italy; valentina.vaglia@unimi.it
- <sup>5</sup> Department of Drug Chemistry and Technology, Sapienza University, P.le Aldo Moro 5, 00185 Rome, Italy
- \* Correspondence: stefania.garzoli@uniroma1.it
- † Those authors contributed equally to this work.

**Abstract:** The chemical composition of the liquid and vapor phases of leaf essential oils (EOs) obtained from two species of Gymnosperms (*Juniperus communis* var. *saxatilis* Willd. and *Larix decidua* Mill.) was investigated using the SPME-GC-MS technique. The results highlighted a composition characterized by 51 identified volatile compounds (34 in *J. communis* and 39 in *L. decidua*). In both blooms, monoterpenes prevailed over the sesquiterpenes, albeit with qualitative and quantitative differences. Sabinene (37.5% and 34.5%, respectively) represented the two most abundant components in the liquid and vapor phases of *J. communis*, and  $\alpha$ -pinene (51.0% and 63.3%) was the main constituent in *L. decidua*. The phytotoxic activity of the two EOs was assessed in pre-emergence conditions using three concentrations in contact (2, 5, 10  $\mu$ L/mL) and non-contact (2, 20, 50  $\mu$ L) tests against *Lolium multiflorum* Lam. (Poaceae) and *Sinapis alba* L. (Brassicaceae). Treatments were effective in a dose-dependent manner by significantly reducing the germination (up to 100% and 45–60%, respectively, with filter paper and soil as a substrate) and the seedling development (1.3 to 8 times) of both target species. Moreover, an exploratory survey on the residual presence of volatile compounds in the soil at the end of the tests was carried out.

**Citation:** Vitalini, S.; Iriti, M.; Vaglia, V.; Garzoli, S. Chemical Investigation and Dose-Response Phytotoxic Effect of Essential Oils from Two Gymnosperm Species (*Juniperus communis* var. *saxatilis* Pall. and *Larix decidua* Mill.). *Plants* **2022**, *11*, 1510. <https://doi.org/10.3390/plants11111510>

Academic Editor: Fabrizio Araniti

Received: 16 May 2022

Accepted: 1 June 2022

Published: 4 June 2022

**Publisher's Note:** MDPI stays neutral with regard to jurisdictional claims in published maps and institutional affiliations.



**Copyright:** © 2022 by the authors. Licensee MDPI, Basel, Switzerland. This article is an open access article distributed under the terms and conditions of the Creative Commons Attribution (CC BY) license (<https://creativecommons.org/licenses/by/4.0/>).

**Keywords:** common juniper; common larch; Cupressaceae; Pinaceae; SPME-GC-MS; volatile compounds; herbicidal activity; weed control

## 1. Introduction

Since man became a farmer 10,000 years ago, he has always had to fight against weeds, which have been a constant component of the agro-ecosystem. They have adapted to crop systems and co-evolved with them, significantly interfering with the human activities. From an ecological point of view, weeds are plants capable of colonizing potentially productive environments, managing to persist in conditions of repeated disturbance [1]. In the field, they cause significant damage for farmers. The most relevant effects include a decrease in crop production and a deterioration in its quality, in addition to an obstacle to mechanical operations. Another equally important aspect concerns the enrichment of the stock of seeds in the soil following the dissemination caused by their uncontrolled development [2]. Weeds can be controlled by various means (physical, ecological, mechanical, and chemical). Synthetic herbicides have been widely used since their discovery in the first decades of the previous century [3]. However, the growing problems related to weed management, such

as resistance to herbicides, their low biodegradability, and high percolation and persistence in the soil, are increasing concerns relating to human health and environmental issues [4].

As a result of these problems, in recent years, various natural products have been studied for their allelopathic activity, including essential oils (EOs) and some of their constituents. EOs are multicomponent mixtures of plant volatiles able to exert a phytotoxic effect by providing an eco-chemical approach [5]. Their contact action causes rapid drying of the green plant parts by destroying the leaf cuticle and cell membranes [6]. In detail, allelochemicals can affect physiological functions, such as seed germination, respiration, photosynthesis, ion uptake, enzyme activity, transpiration, and hormone levels. They can also alter gene expression, the signal transduction chain, and permeability of the cell wall and membrane, and enhance the production of reactive oxygen species, or modify both the division and differentiation of cells [7]. The inhibition of germination and plant growth by EOs has been mainly attributed to terpenes, in particular, monoterpenes [8]. In general, essential oils offer an interesting class of compounds for management of parasites and weeds due to their low persistence in soil, relatively low toxicity towards mammals, and less stringent regulatory approval mechanisms [9].

In this work, we focused on the phytotoxic potential of EOs from two species of gymnosperms, namely *Juniperus communis* var. *saxatilis* Pall. (Cupressaceae) and *Larix decidua* Mill. (Pinaceae). The allelopathic activity of gymnosperms has long been known [10]. Several families—Araucariaceae, Cupressaceae, Pinaceae, Podocarpaceae, and Taxaceae—shows a strong negative allelopathic effect on the germination and growth of other plants [11]. In most of the cases, the allelochemicals identified as responsible for these interactions are the phenolic compounds leached from the litter consisting mainly of tree needles [10,11]. Until now, few reports have documented the phytotoxicity including autotoxicity of EOs obtained from leaves of species belonging to *Juniperus* [12–14] and *Larix* [15–17] genera. Our aim was to evaluate and compare the inhibitory effects of the two EOs used in different ways—via air and direct contact—on the germination and seedling growth of both monocot and dicot weed species, after determining the chemical composition of both liquid and vapor phases by means of the solid-phase micro-extraction gas chromatography-mass spectrometry (SPME-GC-MS) technique. The changes in the volatile profile occurring in the soil samples after the treatments with the EOs were also investigated.

## 2. Results

### 2.1. Essential Oil Chemical Composition

To describe the chemical profile of the liquid and vapor phases, the EOs were analyzed using the SPME-GC-MS technique. In total, 51 compounds were identified, of which 34 were in *J. communis* and 39 in *L. decidua* (Table 1). In both oils, the monoterpenes prevailed over the sesquiterpenes. Among the former, sabinene (37.5%, 34.5%) was the most abundant component in the liquid and vapor phases of *J. communis*, respectively, and  $\alpha$ -pinene (51.0%, 63.3%) was the main constituent of *L. decidua*. Furthermore, the vapor phase of *J. communis* was enriched with limonene (14.0%), *p*-cymene (7.5%), and  $\beta$ -myrcene (12.6%), and that of *L. decidua* was enriched with  $\beta$ -ocimene (10.2%),  $\beta$ -pinene (7.9%),  $\beta$ -myrcene (6.2%) and limonene (4.5%) as principal compounds.

**Table 1.** Chemical composition (percentages mean values  $\pm$  standard deviation) of EO liquid and vapor phases.

N°	Component <sup>1</sup>	LRI <sup>2</sup>	LRI <sup>3</sup>	<i>Juniperus communis</i> EO <sup>4</sup>	<i>Juniperus communis</i> EO <sup>5</sup>	<i>Larix decidua</i> EO <sup>6</sup>	<i>Larix decidua</i> EO <sup>7</sup>
1	$\alpha$ -thujene	821	823	4.2 $\pm$ 0.02	4.9 $\pm$ 0.06	0.3 $\pm$ 0.02	0.5 $\pm$ 0.03
2	$\alpha$ -pinene	942	943	19.0 $\pm$ 0.04	10.3 $\pm$ 0.03	51.0 $\pm$ 0.05	63.3 $\pm$ 0.03
3	camphene	945	946	0.2 $\pm$ 0.02	-	1.4 $\pm$ 0.02	1.2 $\pm$ 0.01
4	dehydroabinene	960	956	-	-	-	0.4 $\pm$ 0.02
5	sabinene	976	972	37.5 $\pm$ 0.03	34.5 $\pm$ 0.02	0.8 $\pm$ 0.02	1.0 $\pm$ 0.03

Table 1. Cont.

N°	Component <sup>1</sup>	LRI <sup>2</sup>	LRI <sup>3</sup>	<i>Juniperus communis</i> EO <sup>4</sup>	<i>Juniperus communis</i> EO <sup>5</sup>	<i>Larix decidua</i> EO <sup>6</sup>	<i>Larix decidua</i> EO <sup>7</sup>
6	$\beta$ -pinene	985	978	3.0 ± 0.04	12.6 ± 0.03	2.3 ± 0.02	7.9 ± 0.02
7	$\beta$ -myrcene	990	987	1.1 ± 0.03	-	9.7 ± 0.03	6.2 ± 0.02
8	$\alpha$ -phellandrene	1007	1005	0.7 ± 0.03	1.4 ± 0.03	0.3 ± 0.03	0.2 ± 0.07
9	3-carene	1010	1008	-	0.9 ± 0.03	-	-
10	$\alpha$ -terpinene	1012	1010	2.4 ± 0.06	5.8 ± 0.03	-	-
11	<i>p</i> -cymene	1020	1016	1.2 ± 0.02	7.5 ± 0.05	1.1 ± 0.03	1.1 ± 0.01
12	limonene	1026	1023	5.8 ± 0.03	14.0 ± 0.07	3.9 ± 0.06	4.5 ± 0.02
13	$\beta$ -ocimene	1029	1024	-	-	10.2 ± 0.04	10.2 ± 0.02
14	1,8-cineole	1030	1025	-	-	3.2 ± 0.06	1.9 ± 0.05
15	$\gamma$ -terpinene	1053	1054	5.0 ± 0.04	1.0 ± 0.02	0.5 ± 0.03	0.3 ± 0.02
16	terpinolene	1082	1080	2.6 ± 0.03	4.3 ± 0.06	1.0 ± 0.04	0.5 ± 0.03
17	<i>p</i> -cymenene	1093	1091	-	-	0.3 ± 0.02	0.1 ± 0.01
18	$\alpha$ -campholenal	1127	1125	-	-	0.3 ± 0.03	-
19	trans-pinocarveol	1137	1134	-	-	1.1 ± 0.02	0.3 ± 0.03
20	pinocarvone	1149	1145	-	-	0.2 ± 0.02	-
21	borneol	1160	1155	-	-	0.2 ± 0.03	-
22	terpinen-4-ol	1165	1160	4.2 ± 0.02	2.7 ± 0.02	0.8 ± 0.02	0.1 ± 0.02
23	$\alpha$ -terpineol	1182	1183	0.2 ± 0.01	-	0.4 ± 0.02	-
24	carveol	1202	1201	-	-	-	0.1 ± 0.02
25	cuminal	1215	1211	-	-	0.1 ± 0.01	-
26	phellandral	1255	1249	-	-	0.1 ± 0.04	-
27	bornyl acetate	1294	1290	0.3 ± 0.02	-	2.6 ± 0.07	0.1 ± 0.01
28	4-terpinenyl acetate	1307	1304	0.1 ± 0.01	-	0.8 ± 0.02	-
29	$\alpha$ -terpinyl acetate	1336	1333	0.4 ± 0.03	-	-	-
30	$\alpha$ -cubebene	1352	1348	0.2 ± 0.03	-	-	-
31	copaene	1390	1385	0.3 ± 0.02	-	0.1 ± 0.02	-
32	$\beta$ -elemene	1408	1406	1.8 ± 0.05	-	0.1 ± 0.02	-
33	longifolene	1410	1408	-	-	0.2 ± 0.02	tr
34	$\beta$ -caryophyllene	1427	1424	1.3 ± 0.03	-	2.2 ± 0.07	tr
35	cis-thujopsene	1438	1435	2.1 ± 0.03	-	-	-
36	humulene	1471	1465	0.8 ± 0.04	-	0.7 ± 0.03	-
37	$\gamma$ -muurolene	1490	1486	0.5 ± 0.02	-	0.3 ± 0.02	-
38	germacrene D	15,001	1500	0.1 ± 0.02	-	0.5 ± 0.05	-
39	$\alpha$ -muurolene	1507	*	1.0 ± 0.02	-	0.5 ± 0.02	-
40	guaia-1(10), 11-diene	1509	1505	0.3 ± 0.02	-	-	-
41	$\delta$ -cadinene	1533	1530	2.4 ± 0.03	-	-	-
42	$\alpha$ -cadinene	1539	*	-	-	0.1 ± 0.02	-
43	$\alpha$ -calacorene	1541	1539	-	-	0.1 ± 0.02	-
44	spathulenol	1576	1571	0.1 ± 0.02	-	-	-
45	caryophyllene oxide	1616	1613	0.1 ± 0.02	-	0.2 ± 0.02	-
46	epicubenol	1620	1618	0.1 ± 0.02	-	-	-
47	humulene epoxide II	1622	*	-	-	0.1 ± 0.02	-
48	$\delta$ -cadinol	1627	*	-	-	0.2 ± 0.01	-
49	$\tau$ -cadinol	1630	1625	-	-	0.1 ± 0.02	-
50	$\tau$ -muurolol	1641	1639	0.6 ± 0.02	-	-	-
51	$\alpha$ -cadinol	1678	1676	0.4 ± 0.03	-	-	-
	SUM			100.0	99.9	97.9	99.9
	Terpenoids			87.6	99.9	89.6	99.7
	Sesquiterpenoids			11.8	-	5.1	-
	Others			0.6	-	3.2	0.2

<sup>1</sup> The components are reported according to their elution order on apolar column; <sup>2</sup> Linear Retention indices measured on apolar column; <sup>3</sup> Linear Retention indices from literature; \* LRI not available; <sup>4</sup> Percentage values of *J. communis* liquid phase components; <sup>5</sup> Percentage values of *J. communis* vapor phase components; <sup>6</sup> Percentage values of *L. decidua* liquid phase components; <sup>7</sup> Percentage values of *L. decidua* vapor phase components; - Not detected; tr: traces (mean value < 0.1%).

Qualitative differences between the two EOs were noted. In particular,  $\beta$ -ocimene (10.2%), 1,8-cineole (3.2%), and trans-pinovcarveol (1.1%) were detected only in *L. decidua*; cis-thujopsene (2.1%),  $\delta$ -cadinene (2.4%),  $\tau$ -muurolol (0.6%), and  $\alpha$ -cadinol (0.4%) were characteristic only in *J. communis*; and a number of other minor compounds (ranging from 0.1% to 0.3%) were detected in one of the EOs.

## 2.2. Soil Chemical Composition

The chemical composition of the EO residual vapor phase emitted from the soils at the end of both non-contact and contact tests was investigated using the SPME-GC/MS technique. The compounds detected in the samples with 20 or 50  $\mu$ L of *J. communis* EO submitted to the non-contact test are listed in Table 2. In total, 55.9% of the starting compounds remained. cis-Thujopsene was the most abundant compound in all soils with percentage values equal to 30.2% and 40.5% in the samples where *L. multiflorum* seeds were sown at 20 and 50  $\mu$ L, respectively, and 26.7% and 32.2% in the corresponding samples with *S. alba* seeds. This compound was followed by  $\alpha$ -pinene (19.0% and 20.4%) in the presence of *L. multiflorum* and by  $\beta$ -elemene (12.9% and 13.7%) in the presence of *S. alba*. No residual volatile component was found in the soils treated with 2  $\mu$ L of EOs.

**Table 2.** Chemical composition (percentage mean values  $\pm$  standard deviation) of soil samples with *L. multiflorum* and *S. alba* seeds in non-direct contact with *J. communis* EO.

N <sup>o</sup>	Component <sup>1</sup>	LRI <sup>2</sup>	LRI <sup>3</sup>	Soil <sup>4</sup>	Soil <sup>5</sup>	Soil <sup>6</sup>	Soil <sup>7</sup>
1	$\alpha$ -thujene	821	823	4.2 $\pm$ 0.02	0.1 $\pm$ 0.02	4.0 $\pm$ 0.03	3.7 $\pm$ 0.03
2	$\alpha$ -pinene	942	943	19.0 $\pm$ 0.05	0.4 $\pm$ 0.02	20.4 $\pm$ 0.02	1.2 $\pm$ 0.02
3	Sabinene	976	972	2.5 $\pm$ 0.02	-	3.2 $\pm$ 0.02	3.2 $\pm$ 0.02
4	$\alpha$ -terpinene	1012	1010	5.1 $\pm$ 0.02	0.3 $\pm$ 0.02	4.5 $\pm$ 0.02	6.0 $\pm$ 0.06
5	<i>p</i> -cymene	1020	1016	9.0 $\pm$ 0.02	0.6 $\pm$ 0.03	4.8 $\pm$ 0.04	6.5 $\pm$ 0.03
6	Limonene	1026	1023	4.9 $\pm$ 0.02	0.3 $\pm$ 0.02	2.9 $\pm$ 0.02	4.6 $\pm$ 0.02
7	$\gamma$ -terpinene	1053	1054	6.3 $\pm$ 0.02	0.3 $\pm$ 0.04	6.5 $\pm$ 0.02	7.8 $\pm$ 0.02
8	Terpinolene	1082	1080	2.2 $\pm$ 0.02	1.0 $\pm$ 0.06	-	-
9	$\alpha$ -cubebene	1352	1348	-	2.3 $\pm$ 0.02	0.5 $\pm$ 0.03	2.1 $\pm$ 0.01
10	Copaene	1390	1385	0.3 $\pm$ 0.02	2.8 $\pm$ 0.02	0.9 $\pm$ 0.02	3.2 $\pm$ 0.02
11	$\beta$ -elemene	1408	1406	9.7 $\pm$ 0.02	12.9 $\pm$ 0.02	7.1 $\pm$ 0.02	13.7 $\pm$ 0.02
12	$\beta$ -caryophyllene	1427	1424	1.6 $\pm$ 0.02	4.2 $\pm$ 0.03	2.1 $\pm$ 0.02	4.4 $\pm$ 0.01
13	cis-thujopsene	1438	1435	30.2 $\pm$ 0.02	26.7 $\pm$ 0.04	40.5 $\pm$ 0.03	32.2 $\pm$ 0.02
14	Humulene	1471	1465	1.5 $\pm$ 0.02	2.1 $\pm$ 0.02	1.0 $\pm$ 0.05	3.0 $\pm$ 0.02
15	$\gamma$ -muurolene	1490	1486	-	4.9 $\pm$ 0.04	-	-
17	$\alpha$ -muurolene	1507	*	-	1.9 $\pm$ 0.04	-	-
16	$\delta$ -cadinene	1533	1530	0.6 $\pm$ 0.04	10.6 $\pm$ 0.02	0.3 $\pm$ 0.02	2.6 $\pm$ 0.01
18	$\tau$ -muurolol	1641	1639	-	0.9 $\pm$ 0.02	-	-
19	$\alpha$ -cadinol	1678	1676	2.9 $\pm$ 0.02	27.7 $\pm$ 0.04	1.2 $\pm$ 0.02	5.6 $\pm$ 0.02
	SUM			100.0	100.0	99.9	99.8
	Terpenoids			53.2	3.0	46.3	33.0
	Sesquiterpenoids			46.5	94.2	52.7	63.6
	Others			0.3	2.8	0.9	3.2

<sup>1</sup> The components are reported according to their elution order on apolar column; <sup>2</sup> Linear Retention indices measured on apolar column; <sup>3</sup> Linear Retention indices from literature; \* LRI not available; <sup>4</sup> Percentage mean values of the volatiles from soil with 20  $\mu$ L of *J. communis* EO and *L. multiflorum* seeds; <sup>5</sup> Percentage values of the volatiles from soil with 20  $\mu$ L of *J. communis* EO and *S. alba* seeds; <sup>6</sup> Percentage mean values of the volatiles from soil with 50  $\mu$ L of *J. communis* EO and *L. multiflorum* seeds; <sup>7</sup> Percentage mean values of the volatiles from soil with 50  $\mu$ L of *J. communis* EO and *S. alba* seeds; - Not detected.

The compounds released from the soils with 20 or 50  $\mu$ L of *L. decidua* EO without direct contact with seeds are listed in Table 3. Among the five detected components,  $\alpha$ -pinene was the most abundant in all the samples, with values ranging from 37.8% (soil with *S. alba* at 20  $\mu$ L EO) to 87.7% (soil with *L. multiflorum* at 20  $\mu$ L EO). Moreover, in this case, no residual volatile component was found to be emitted from the soils treated with 2  $\mu$ L of EOs.

Only three compounds were detected for the soil samples containing *L. multiflorum* and *S. alba* seeds in direct contact with 5 and 10  $\mu$ L of *J. communis* and *L. decidua* EOs

(Tables 4 and 5).  $\alpha$ -Thujene was the main volatile for the soils treated with *J. communis* EO, regardless of the type of seed species. In particular, it was the only one for the sample with *S. alba* seeds subjected to the action of 5  $\mu$ L of *L. decidua* EO (Table 4). In contrast,  $\alpha$ -pinene ( $\geq 81.8\%$ ) characterized the chemical composition of the volatile emission of the soils in direct contact with *L. decidua* EO (Table 5).

**Table 3.** Chemical composition (percentages mean values  $\pm$  standard deviation) of soil samples with *L. multiflorum* and *S. alba* seeds in non-contact with *L. decidua* EO.

N <sup>o</sup>	Component <sup>1</sup>	LRI <sup>2</sup>	LRI <sup>3</sup>	Soil <sup>4</sup>	Soil <sup>5</sup>	Soil <sup>6</sup>	Soil <sup>7</sup>
1	$\alpha$ -pinene	942	943	87.7 $\pm$ 0.05	37.8 $\pm$ 0.03	72.5 $\pm$ 0.03	66.7 $\pm$ 0.05
2	$\beta$ -pinene	985	978	4.6 $\pm$ 0.02	3.3 $\pm$ 0.02	2.8 $\pm$ 0.03	7.1 $\pm$ 0.02
3	$\beta$ -myrcene	990	987	7.7 $\pm$ 0.02	10.2 $\pm$ 0.03	12.6 $\pm$ 0.03	19.1 $\pm$ 0.02
4	$\beta$ -ocimene	1029	1024	-	13.8 $\pm$ 0.03	7.7 $\pm$ 0.02	4.6 $\pm$ 0.02
5	$\beta$ -caryophyllene	1427	1424	-	34.9 $\pm$ 0.04	4.4 $\pm$ 0.02	2.5 $\pm$ 0.03
SUM				100.0	100.0	100.0	100.0

<sup>1</sup> The components are reported according to their elution order on apolar column; <sup>2</sup> Linear Retention indices measured on apolar column; <sup>3</sup> Linear Retention indices from literature; <sup>4</sup> Percentage mean values of the volatiles from soil with 20  $\mu$ L of *L. decidua* EO and *L. multiflorum* seeds; <sup>5</sup> Percentage mean values of the volatiles from soil with 20  $\mu$ L of *L. decidua* EO and *S. alba* seeds; <sup>6</sup> Percentage mean values of the volatiles from soil with 50  $\mu$ L of *L. decidua* EO and *L. multiflorum* seeds; <sup>7</sup> Percentage mean values of the volatiles from the soil with 50  $\mu$ L of *L. decidua* EO and *S. alba* seeds; - Not detected.

**Table 4.** Chemical composition (percentages mean values  $\pm$  standard deviation) of soil samples with *L. multiflorum* and *S. alba* seeds in contact with *J. communis* EO.

N <sup>o</sup>	Component <sup>1</sup>	LRI <sup>2</sup>	LRI <sup>3</sup>	Soil <sup>4</sup>	Soil <sup>5</sup>	Soil <sup>6</sup>	Soil <sup>7</sup>
1	$\alpha$ -thujene	821	823	-	100.0 $\pm$ 0.02	42.2 $\pm$ 0.03	87.9 $\pm$ 0.03
2	$\beta$ -elemene	1408	1406	-	-	17.4 $\pm$ 0.02	12.1 $\pm$ 0.02
3	cis-thujopsene	1438	1435	-	-	40.4 $\pm$ 0.03	-
SUM					100.0	100.0	100.0

<sup>1</sup> The components are reported according to their elution order on apolar column; <sup>2</sup> Linear Retention indices measured on apolar column; <sup>3</sup> Linear Retention indices from literature; <sup>4</sup> Percentage mean values of the volatiles from soil with 5  $\mu$ L of *J. communis* EO and *L. multiflorum* seeds; <sup>5</sup> Percentage mean values of the volatiles from soil with 5  $\mu$ L of *J. communis* EO and *S. alba* seeds; <sup>6</sup> Percentage mean values of the volatiles from soil with 10  $\mu$ L of *J. communis* EO and *L. multiflorum* seeds; <sup>7</sup> Percentage mean values of the volatile from soil with 10  $\mu$ L of *J. communis* EO and *S. alba* seeds; - Not detected.

**Table 5.** Chemical composition (percentages mean values  $\pm$  standard deviation) of soil samples with *L. multiflorum* and *S. alba* seeds in direct contact with *L. decidua* EO.

N <sup>o</sup>	Component <sup>1</sup>	LRI <sup>2</sup>	LRI <sup>3</sup>	Soil <sup>4</sup>	Soil <sup>5</sup>	Soil <sup>6</sup>	Soil <sup>7</sup>
1	$\alpha$ -pinene	942	943	96.4 $\pm$ 0.05	93.7 $\pm$ 0.03	88.9 $\pm$ 0.03	81.8 $\pm$ 0.05
2	$\beta$ -pinene	985	978	3.6 $\pm$ 0.02	4.7 $\pm$ 0.02	11.1 $\pm$ 0.03	18.2 $\pm$ 0.02
3	$\beta$ -myrcene	990	987	-	1.6 $\pm$ 0.03	-	-
SUM				100.0	100.0	100.0	100.0

<sup>1</sup> The components are reported according to their elution order on apolar column; <sup>2</sup> Linear Retention indices measured on apolar column; <sup>3</sup> Linear Retention indices from literature; <sup>4</sup> Percentage mean values of the volatiles from soil with 5  $\mu$ L of *L. decidua* EO and *L. multiflorum* seeds; <sup>5</sup> Percentage mean values of the volatiles from soil with 5  $\mu$ L of *L. decidua* EO and *S. alba* seeds; <sup>6</sup> Percentage mean values of the volatiles from soil with 10  $\mu$ L of *L. decidua* EO and *L. multiflorum* seeds; <sup>7</sup> Percentage mean values of the volatiles from soil with 10  $\mu$ L of *L. decidua* EO and *S. alba* seeds; - Not detected.

### 2.3. Effectiveness of EOs in Non-Contact Germination Test (Filter Paper Substrate)

The results for *J. communis* and *L. decidua* EOs showed a significant impact ( $p$ -values = 0.000) on all the considered indices, in both target species (Table 6). In particular, the treatments performed with the highest dose (50  $\mu$ L) of *J. communis* EO totally inhibited the *L. multiflorum* germination ( $G = 0\%$ ) and reduced that of *S. alba* by 67.3%, also

affecting the other considered parameters (CVG =  $-75\%$ ; MGT =  $+11.6\%$ ; SVI =  $-92.3\%$ ; root length =  $-90.3\%$ ; shoot length =  $-71.2\%$ ). The same dose of *Larix decidua* EO was even more effective, preventing the germination of both *L. multiflorum* and *S. alba*. Moreover, the obtained data evidenced that *L. multiflorum* was the most susceptible species. The values of its indices, except for MGT in some cases, were also significantly decreased by the lowest doses (2 and 20  $\mu\text{L}$ ) of both EOs.

**Table 6.** Germination and growth values of two target species (*Lolium multiflorum* and *Sinapis alba*) under the phytotoxic effects of different doses of *Juniperus communis* var. *saxatilis* and *Larix decidua* EOs using filter paper as a substrate.

Target Species	EO ( $\mu\text{L}$ )	G (%)	CVG	MGT	SVI	Root (mm)	Shoot (mm)
<i>Juniperus communis</i> var. <i>saxatilis</i>							
<i>Lolium multiflorum</i>	0	93.3 $\pm$ 5.3 a	89.8 $\pm$ 9.0 a	5.1 $\pm$ 0.1 a	11,064 $\pm$ 306 a	72.3 $\pm$ 6.5 a	46.6 $\pm$ 2.0 a
	2	80.3 $\pm$ 9.4 b	67.7 $\pm$ 6.6 b	5.1 $\pm$ 0.1 a	5129 $\pm$ 720 b	41.5 $\pm$ 4.5 b	22.3 $\pm$ 3.2 b
	20	35.0 $\pm$ 8.5 c	21.5 $\pm$ 7.0 c	5.4 $\pm$ 0.2 b	772 $\pm$ 314 c	15.7 $\pm$ 3.6 c	5.8 $\pm$ 0.7 c
	50	0.0 $\pm$ 0.0 d	n.d.	n.d.	n.d.	n.d.	n.d.
	F	154.856	157.288	1721.960	580.626	214.413	476.953
	p-value	0.000 *	0.000 *	0.000 *	0.000 *	0.000 *	0.000 *
<i>Sinapis alba</i>	0	83.3 $\pm$ 8.7 a	102.6 $\pm$ 13.9 a	4.3 $\pm$ 0.1 a	4522 $\pm$ 301 a	30.9 $\pm$ 2.5 a	23.6 $\pm$ 1.6 a
	2	78.5 $\pm$ 8.3 a	89.9 $\pm$ 13.1 a	4.3 $\pm$ 0.1 a	3711 $\pm$ 354 b	29.3 $\pm$ 3.2 a	18.1 $\pm$ 1.6 b
	20	70.0 $\pm$ 8.5 a	85.7 $\pm$ 15.8 a	4.4 $\pm$ 0.1 a	2195 $\pm$ 120 c	18.6 $\pm$ 3.3 b	13.0 $\pm$ 0.9 c
	50	35.0 $\pm$ 6.3 b	26.8 $\pm$ 3.0 b	4.8 $\pm$ 0.2 b	349 $\pm$ 99 d	3.0 $\pm$ 0.6 c	6.8 $\pm$ 0.9 d
	F	29.702	28.903	9.183	225.386	96.659	121.614
	p-value	0.000	0.000	0.002	0.000	0.000	0.000
<b>Interaction species <math>\times</math> treatment</b>							
	F	20.398	10.168	749.786	209.782	68.815	150.270
	p-value	0.000 *	0.000 *	0.000 *	0.000 *	0.000 *	0.000 *
<i>Larix decidua</i>							
<i>Lolium multiflorum</i>	0	90.0 $\pm$ 3.5 a	92.0 $\pm$ 3.2 a	5.0 $\pm$ 0.2 a	10,450 $\pm$ 116 a	68.6 $\pm$ 1.4 a	47.5 $\pm$ 3.4 a
	2	63.0 $\pm$ 8.2 b	46.8 $\pm$ 6.9 b	5.2 $\pm$ 0.1 ab	2662 $\pm$ 590 b	20.0 $\pm$ 1.6 b	21.9 $\pm$ 3.1 b
	20	54.0 $\pm$ 15.4 b	28.3 $\pm$ 9.9 c	5.5 $\pm$ 0.3 b	907 $\pm$ 366 c	3.6 $\pm$ 1.3 c	13.0 $\pm$ 1.5 c
	50	0.0 $\pm$ 0.0 c	n.d.	n.d.	n.d.	n.d.	n.d.
	F	71.962	151.869	814.006	731.639	2514.839	275.249
	p-value	0.000 *	0.000 *	0.000 *	0.000 *	0.000 *	0.000 *
<i>Sinapis alba</i>	0	83.3 $\pm$ 11.6 a	106.0 $\pm$ 17.6 a	4.3 $\pm$ 0.1 a	3440 $\pm$ 891 a	20.0 $\pm$ 4.3 a	20.9 $\pm$ 3.5 a
	2	81.8 $\pm$ 6.7 a	101.0 $\pm$ 13.9 a	4.4 $\pm$ 0.0 b	2734 $\pm$ 537 a	18.2 $\pm$ 5.4 a	15.5 $\pm$ 2.2 b
	20	71.8 $\pm$ 11.5 a	72.3 $\pm$ 16.1 b	4.8 $\pm$ 0.0 c	2444 $\pm$ 525 a	17.5 $\pm$ 0.9 a	16.4 $\pm$ 2.3 b
	50	0.0 $\pm$ 0.0 b	n.d.	n.d.	n.d.	n.d.	n.d.
	F	81.159	50.067	6953.429	26.377	28.495	59.168
	p-value	0.000 *	0.000 *	0.000 *	0.000 *	0.000 *	0.000 *
<b>Interaction species <math>\times</math> treatment</b>							
	F	4.164	11.159	15.836	127.252	215.139	63.298
	p-value	0.017 *	0.000 *	0.000 *	0.000 *	0.000 *	0.000 *

Values are mean  $\pm$  standard deviation; asterisk and different letters indicate statistically significant differences at  $p$ -value  $\leq 0.05$  among treatments in each species.  $F$ -value and  $p$ -value of the ANOVA test. Abbreviations: G%, Germination Percentage; CVG, Coefficient of Velocity of Germination; MGT, Mean Germination Time, SVI, Seedling Vigor Index.

#### 2.4. Effectiveness of EOs in Non-Contact Germination Test (Soil Substrate)

The data reported in Table 7 also confirmed the efficacy of the *J. communis* and *L. decidua* EOs in the tests carried out using the soil as a substrate. All the indices, except G for *L. multiflorum* under the effect of *J. communis* EO, underwent significant variations

( $p$ -values < 0.05), if only due to the action of the highest tested dose. In detail, CVG of *L. multiflorum* and shoot length decreased by 49.5% and 33%, respectively, while MGT increased by 12.8% with 50  $\mu$ L of *J. communis* EO. These values reached  $-60.8\%$ ,  $-59.4\%$ , and  $+6.1\%$  in the presence of the 50  $\mu$ L of *L. decidua* EO. Regarding *S. alba*, the same treatments, respectively, reduced G by 26.6% and 43.2%, CVG by 32.4 and 60.2%, and shoot length by 25.5% and 42.6%, and increased MGT to  $+6.8\%$  and  $+10.9\%$ . In some cases, lower doses of both EOs were able to significantly affect the germination (e.g.,  $-15\%$  for *S. alba* at 2  $\mu$ L of *J. communis* and  $-35.5\%$  for *L. multiflorum* at 20  $\mu$ L of *L. decidua*) and development (e.g.,  $-9.9$  for *L. multiflorum* at 2  $\mu$ L of *J. communis* and  $-23.6\%$  for *S. alba* at 20  $\mu$ L of *L. decidua*) of the two target species.

**Table 7.** Germination and growth values of two target species (*Lolium multiflorum* and *Sinapis alba*) under the phytotoxic effects of different doses of *Juniperus communis* var. *saxatilis* and *Larix decidua* EOs using soil as a substrate.

Target Species	EO ( $\mu$ L)	G (%)	CVG	MGT	Shoot (mm)
<i>Juniperus communis</i> var. <i>saxatilis</i>					
<i>Lolium multiflorum</i>	0	86.8 $\pm$ 5.3	92.0 $\pm$ 5.8 a	4.7 $\pm$ 0.1 a	73.1 $\pm$ 2.2 a
	2	78.3 $\pm$ 6.7	82.0 $\pm$ 11.6 a	4.8 $\pm$ 0.1 a	66.6 $\pm$ 2.8 b
	20	76.5 $\pm$ 4.0	71.5 $\pm$ 5.3 a	5.0 $\pm$ 0.2 b	65.6 $\pm$ 3.6 b
	50	63.3 $\pm$ 20.1	46.5 $\pm$ 19.2 b	5.3 $\pm$ 0.0 c	49.0 $\pm$ 4.9 c
	F	3.073	10.652	19.886	34.017
	$p$ -value	0.069	0.001 *	0.000 *	0.000 *
<i>Sinapis alba</i>	0	88.5 $\pm$ 3.0 a	101.5 $\pm$ 6.5 a	4.4 $\pm$ 0.1 a	29.8 $\pm$ 1.1 a
	2	75.3 $\pm$ 9.9 b	75.2 $\pm$ 11.2 b	4.4 $\pm$ 0.1 ab	29.4 $\pm$ 1.3 a
	20	65.0 $\pm$ 6.3 b	72.5 $\pm$ 1.9 b	4.6 $\pm$ 0.1 ab	24.5 $\pm$ 1.6 b
	50	65.0 $\pm$ 6.3 b	68.6 $\pm$ 5.5 b	4.7 $\pm$ 0.1 b	22.2 $\pm$ 1.4 b
	F	10.649	18.279	5.742	30.647
	$p$ -value	0.001 *	0.000 *	0.011 *	0.000 *
<b>Interaction species <math>\times</math> treatment</b>					
	F	0.921	3.165	4.787	15.100
	$p$ -value	0.446	0.043 *	0.009 *	0.000 *
<i>Larix decidua</i>					
<i>Lolium multiflorum</i>	0	88.0 $\pm$ 10.0 a	93.3 $\pm$ 12.4 a	4.9 $\pm$ 0.1 a	72.1 $\pm$ 2.8 a
	2	86.5 $\pm$ 7.5 a	82.3 $\pm$ 16.1 a	5.0 $\pm$ 0.1 a	69.3 $\pm$ 2.8 a
	20	56.8 $\pm$ 8.7 b	55.2 $\pm$ 8.1 b	4.9 $\pm$ 0.0 a	44.4 $\pm$ 3.6 b
	50	48.3 $\pm$ 5.5 b	36.6 $\pm$ 6.0 b	5.2 $\pm$ 0.2 b	29.3 $\pm$ 3.2 c
	F	25.388	20.468	5.965	176.381
	$p$ -value	0.000 *	0.000 *	0.010 *	0.000 *
<i>Sinapis alba</i>	0	76.5 $\pm$ 7.0 a	80.5 $\pm$ 11.3 a	4.6 $\pm$ 0.1 a	30.5 $\pm$ 1.1 a
	2	76.8 $\pm$ 8.7 a	77.8 $\pm$ 10.5 a	4.6 $\pm$ 0.0 a	31.3 $\pm$ 0.7 a
	20	68.5 $\pm$ 3.0 a	68.5 $\pm$ 6.2 a	4.7 $\pm$ 0.1 a	23.3 $\pm$ 2.0 b
	50	43.5 $\pm$ 7.0 b	32.0 $\pm$ 4.9 b	5.1 $\pm$ 0.1 b	17.5 $\pm$ 2.0 c
	F	21.634	27.273	30.000	69.892
	$p$ -value	0.000 *	0.000 *	0.000 *	0.000 *
<b>Interaction species <math>\times</math> treatment</b>					
	F	4.055	2.357	0.583	66.368
	$p$ -value	0.018 *	0.097	0.632	0.000 *

Values are mean  $\pm$  standard deviation; asterisk and different letters indicate statistically significant differences at  $p$ -value  $\leq$  0.05 among treatments in each species.  $F$ -value and  $p$ -value of the ANOVA test. Abbreviations: G%, Germination percentage; CVG, Coefficient of Velocity of Germination; MGT, Mean Germination Time.

The “interaction species  $\times$  treatment” (EO doses) was not significant ( $p$ -value > 0.05) for G% after the *J. communis* treatment and for CVG and MGT indices after *L. decidua* use.

### 2.5. Effectiveness of EO in Contact Germination Test (Filter Paper Substrate)

The *J. communis* and *L. decidua* EOs tested in direct contact with seeds using filter paper as a substrate showed phytotoxic activity against both *L. multiflorum* and *S. alba*, influencing most of their germination and growth parameters (Table 8). In this case, the “interaction species × treatment” (EO doses) was not significant only for CVG ( $p$ -value > 0.05) after the *J. communis* treatments.

**Table 8.** Germination and growth values of two target species (*Lolium multiflorum* and *Sinapis alba*) under the phytotoxic effects of different doses of *Juniperus communis* var. *saxatilis* and *Larix decidua* EOs using filter paper as a substrate.

Target Species	EO (μL/mL)	G (%)	CVG	MGT	SVI	Root (mm)	Shoot (mm)
<i>Juniperus communis</i> var. <i>saxatilis</i>							
<i>Lolium multiflorum</i>	0	90.0 ± 3.5 a	84.8 ± 4.6 a	5.0 ± 0.1 a	7037 ± 568 a	42.9 ± 3.3 a	35.2 ± 0.5 a
	2	53.5 ± 13.0 b	37.1 ± 14.7 b	5.4 ± 0.1 b	2632 ± 678 b	34.9 ± 2.9 b	14.4 ± 3.8 b
	5	31.8 ± 13.9 c	17.8 ± 8.9 c	5.4 ± 0.2 b	1020 ± 660 c	20.4 ± 6.7 c	9.3 ± 2.0 c
	10	0.0 ± 0.0 d	n.d.	n.d.	n.d.	n.d.	n.d.
	<i>F</i> <i>p</i> -value	61.330 0.000 *	68.439 0.000 *	2630.647 0.000 *	126.727 0.000 *	88.602 0.000 *	187.572 0.000 *
<i>Sinapis alba</i>	0	81.8 ± 6.7 a	103.8 ± 9.4 a	4.3 ± 0.1 a	2780 ± 361 a	16.8 ± 1.9 a	17.2 ± 1.7 a
	2	49.8 ± 8.3 b	41.9 ± 9.9 b	4.5 ± 0.2 ab	1686 ± 326 b	20.6 ± 1.9 b	13.2 ± 0.7 b
	5	39.8 ± 13.5 b	35.2 ± 3.7 b	4.9 ± 0.3 b	705 ± 165 c	7.7 ± 1.2 c	10.4 ± 2.1 b
	10	38.3 ± 3.5 b	31.6 ± 16.9 b	5.0 ± 0.2 b	683 ± 155 c	7.3 ± 2.3 c	10.5 ± 1.1 b
	<i>F</i> <i>p</i> -value	21.253 0.000 *	37.024 0.000 *	7.728 0.004 *	55.029 0.000 *	51.470 0.000 *	17.225 0.000 *
<b>Interaction species × treatment</b>							
<i>F</i> <i>p</i> -value	10.297 0.000 *	2.403 0.092	460.778 0.000 *	48.706 0.000 *	39.572 0.000 *	79.502 0.000 *	
<i>Larix decidua</i>							
<i>Lolium multiflorum</i>	0	91.5 ± 3.0 a	84.0 ± 8.3 a	5.2 ± 0.1 a	8338 ± 714 a	49.4 ± 3.6 a	41.7 ± 3.9 a
	2	51.5 ± 12.8 b	31.2 ± 8.9 b	5.5 ± 0.1 b	2227 ± 824 b	16.6 ± 5.7 b	36.2 ± 8.2 b
	5	0.0 ± 0.0 c	n.d.	n.d.	n.d.	n.d.	n.d.
	10	0.0 ± 0.0 c	n.d.	n.d.	n.d.	n.d.	n.d.
	<i>F</i> <i>p</i> -value	183.326 0.000 *	169.513 0.000 *	15,155.667 0.000 *	208.653 0.000 *	191.104 0.000 *	214.739 0.000 *
<i>Sinapis alba</i>	0	71.8 ± 6.2 a	76.3 ± 6.6 a	4.5 ± 0.2 a	2892 ± 288 a	16.9 ± 1.3 a	23.4 ± 1.8 a
	2	66.5 ± 12.2 a	62.4 ± 21.3 a	4.9 ± 0.2 b	2029 ± 461 b	14.0 ± 2.5 a	16.3 ± 1.3 ab
	5	64.8 ± 9.9 a	56.3 ± 11.1 a	5.0 ± 0.1 b	1610 ± 315 b	9.7 ± 2.4 b	15.3 ± 2.1 b
	10	18.3 ± 6.7 b	12.8 ± 5.5 b	5.0 ± 0.2 b	252 ± 108 c	9.2 ± 1.9 b	18.3 ± 6.7 ab
	<i>F</i> <i>p</i> -value	29.871 0.000 *	18.409 0.000 *	7.446 0.004 *	47.666 0.000 *	12.202 0.001 *	3.851 0.038 *
<b>Interaction species × treatment</b>							
<i>F</i> <i>p</i> -value	38.219 0.000*	14.891 0.000 *	1426.056 0.000 *	96.108 0.000 *	99.856 0.000 *	60.698 0.000 *	

Values are mean ± standard deviation; asterisk and different letters indicate statistically significant differences at  $p$ -value ≤ 0.05 among treatments in each species. *F*-value and *p*-value of the ANOVA test. Abbreviations: G%, Germination Percentage; CVG, Coefficient of Velocity of Germination; MGT, Mean Germination Time, SVI, Seedling Vigor Index.

Both EOs completely inhibited the germination of *L. multiflorum* (G = 0%) at the 50 μL dose. *L. decidua* also had the same effect at 20 μL, preventing the calculation of the related indices. At 2 μL, it inhibited G of *L. multiflorum* by 43.7%, CVG by 63%, SVI by 66.4%, and brought MGT to +5.8%. Its impact on *S. alba* was comparable (higher for some indices, lower for others) to that of *J. communis* when used at 50 μL (G, −74.5% vs. −53.2%; CVG,

–83.2% vs. –69.6%; MGT, +11.1% vs. +16.3%, SVI, 91.3% vs. –75.4%, root length, –45.6% vs. –56.6%, shoot length, –21.8% vs. –39%), and was generally less effective at the two lower doses.

## 2.6. Effectiveness of EO Vapor Phase in Contact Germination Test (Soil Substrate)

The data shown in Table 9 corroborated the above results regarding the effectiveness of the *J. communis* and *L. decidua* EOs against the two target species, despite the presence of the soil and the resulting interference. In general, they were able to similarly reduce the germination of *L. multiflorum* (by up to –53.9% and 50.2%, respectively). *J. communis* EO more influenced its CVG (–21.3% to –76.9%) and MGT (+8.3% to +16.7%) values than *L. decidua* EO. However, the latter limited the shoot elongation of *L. multiflorum* to 2.4 times compared to 1.3 times for *J. communis* EO. A similar trend was observed with respect to *S. alba* (G, –10.7% to –62.5% vs. –12.6% to –38.9%; CVG, –30.6% to –77.5% vs. –32.8% to –58.2%; MGT, +6.7% to 11.1% vs. +11.1% to +13.3%; shoot length, –0.7% to –35.3% vs. –17% to –40%).

**Table 9.** Germination and growth values of two target species (*Lolium multiflorum* and *Sinapis alba*) under the phytotoxic effects of different doses of *Juniperus communis* var. *saxatilis* and *Larix decidua* EOs using soil as a substrate.

Target Species	EO (μL/mL)	G (%)	CVG	MGT	Shoot (mm)
<i>Juniperus communis</i> var. <i>saxatilis</i>					
<i>Lolium multiflorum</i>	0	98.3 ± 3.5 a	112.8 ± 11.5 a	4.8 ± 0.1 a	71.7 ± 3.2 a
	2	83.5 ± 4.0 b	88.8 ± 9.4 b	4.8 ± 0.1 a	69.6 ± 3.6 a
	5	56.5 ± 13.8 c	47.5 ± 18.3 c	5.2 ± 0.0 a	66.9 ± 1.3 a
	10	45.3 ± 3.5 c	26.0 ± 9.2 c	5.6 ± 0.4 b	43.0 ± 8.7 b
	F	41.002	38.913	14.510	28.223
	p-value	0.000 *	0.000 *	0.000 *	0.000 *
<i>Sinapis alba</i>	0	93.3 ± 5.5 a	115.2 ± 13.7 a	4.5 ± 0.1 a	28.3 ± 0.5 a
	2	83.5 ± 4.0 ab	80.0 ± 4.7 b	4.8 ± 0.1 b	28.1 ± 3.6 a
	5	70.0 ± 14.1 b	63.2 ± 13.6 b	5.0 ± 0.0 c	22.4 ± 1.9 b
	10	35.0 ± 12.3 c	25.7 ± 11.0 c	5.0 ± 0.1 c	18.3 ± 1.4 c
	F	26.273	43.250	25.826	19.860
	p-value	0.000 *	0.000 *	0.000 *	0.000 *
<b>Interaction species × treatment</b>					
	F	2.655	1.436	4.688	11.654
	p-value	0.071	0.257	0.010 *	0.000 *
<i>Larix decidua</i>					
<i>Lolium multiflorum</i>	0	90.0 ± 8.5 a	102.3 ± 19.0 a	4.7 ± 0.0 a	72.1 ± 3.4 a
	2	71.8 ± 9.9 b	68.0 ± 3.3 b	4.9 ± 0.0 ab	59.6 ± 2.8 b
	20	71.5 ± 3.0 b	57.1 ± 16.0 bc	5.2 ± 0.5 ab	57.0 ± 2.8 b
	50	44.8 ± 9.9 c	35.0 ± 14.6 c	5.4 ± 0.1 c	29.5 ± 11.2 c
	F	19.881	15.100	4.696	33.525
	p-value	0.000 *	0.000 *	0.022 *	0.000 *
<i>Sinapis alba</i>	0	81.8 ± 3.5 a	96.0 ± 9.5 a	4.5 ± 0.1 a	31.2 ± 2.1 a
	2	71.5 ± 8.3 ab	64.5 ± 11.1 ab	5.1 ± 0.1 b	25.9 ± 2.2 b
	20	58.3 ± 17.3 ab	48.5 ± 25.2 b	5.1 ± 0.3 b	20.4 ± 0.7 c
	50	50.0 ± 16.7 c	40.1 ± 19.1 b	5.0 ± 0.1 b	18.7 ± 2.1 c
	F	4.799	8.060	8.892	36.371
	p-value	0.020 *	0.003 *	0.002 *	0.000 *

Table 9. Cont.

Target Species	EO (μL/mL)	G (%)	CVG	MGT	Shoot (mm)
<b>Interaction species × treatment</b>					
	F	1.155	1.140	1.387	17.195
	p-value	0.347	0.353	0.271	0.000 *

Values are mean ± standard deviation; asterisk and different letters indicate statistically significant differences at  $p$ -value  $\leq 0.05$  among treatments in each species.  $F$ -value and  $p$ -value of the ANOVA test. Abbreviations: G%, Germination percentage; CVG, Coefficient of Velocity of Germination; MGT, Mean Germination Time.

Lastly, the “interaction species × treatment” (EO doses) was not significant for G and CVG after the *J. communis* EO treatment ( $p$ -value  $> 0.05$ ), whereas it was significant only for the shoot length parameter in the presence of *L. decidua* EO ( $p$ -value = 0.00).

### 3. Discussion

The chemical composition of the liquid and vapor phases of two EOs obtained from leaves of *J. communis* var. *saxatilis* and *L. decidua* was determined by SPME-GC/MS analyses. Gymnosperms and, in particular, conifers produce EOs characterized by compounds belonging to the family of terpenes such as monoterpenes, sesquiterpenes, and their derivatives [18]. In agreement with previous works [19–22], our results showed monoterpenes prevail over sesquiterpenes. In particular, the two major components of *J. communis* and *L. decidua* EOs were  $\alpha$ -pinene or sabinene, which were also found in other *Juniperus* [23,24] and *Larix* species [17,25,26]. Nevertheless, qualitative and/or quantitative differences in the chemical composition can be found, especially for minor compounds [27–31]. This is due to the different genotype or species [32,33], environmental conditions and soil composition [34,35], geographical area of origin [36] and harvesting period, in addition to different extraction methods and plant parts [37,38].

It is known that monoterpenes possess phytotoxic effects capable of leading to anatomical and physiological changes in plant seedlings, probably due to the inhibition of DNA synthesis or the rupture of mitochondrial membranes [39,40]. In particular, it was reported that  $\alpha$ -pinene strongly inhibited mitochondrial ATP production [41] and root growth, also causing oxidative damage [42]. Furthermore, several monoterpenes, including  $\alpha$ -pinene, have been shown to have inhibiting abilities on germination and radicle elongation of *Raphanus sativus* L. and *Lepidium sativum* L. [43]. Regarding sabinene, some studies documented the phytotoxicity of different EOs having this compound among the main constituents [44–46]. For example, a sabinene chemotype identified for EO from *Ravensara aromatica* Sonn. showed strong toxicity against *Oryza sativa* L. and *Lepidium sativum* L. [44]. Nonetheless, the higher percentage of  $\alpha$ -pinene in our *L. decidua* EO may justify its greater effectiveness compared to the *J. communis* EO, in which sabinene was the most abundant. However, it is highly probable that the herbicidal activity of both EOs found in this work cannot be exclusively attributed to  $\alpha$ -pinene and/or sabinene, but to the combined effect (synergistic or additive) of several molecules, including the minor ones. Indeed, as has been recently confirmed, mixtures of compounds are much more active and trigger different and more drastic responses [47].

EOs from conifer leaves have been reported to have high therapeutic potential [48] and, therefore, they are widely used in the treatment of infections and inflammatory phenomena [49]. Several studies demonstrated their biological properties [20,50–57], including allelopathic effects [10,11]. Nevertheless, EOs obtained from *Juniperus* and *Larix* species have been rather neglected from this point of view. Recently, Semerdjieva and co-authors [58] investigated the allelopathic activity of *J. sabina* L. and *J. excelsa* Bieb. EOs, reporting different inhibitory actions depending on the target species, the type of used EO, and the relative concentrations. Previously, Mehdizadeh et al. [14] documented the phytotoxic potential of EO obtained from the leaves of *J. polycarpos* var. *turcomanica* (B.Fedtsch.) R.P. Adams against three species of weeds, namely, *Portulaca oleracea* L., *Amaranthus retroflexus* L., and *Datura*

*stramonium* L., attributing it to its major group of constituents, namely, monoterpenes hydrocarbons. Herbicidal effects were also reported for *J. oxycedrus* L. subsp. *macrocarpa* and *J. phoniceae* EOs, which were able to strongly reduce the germination and seedling growth of all tested weeds, in a dose-dependent manner [13,59]. In the case of *J. phoniceae*, its EO also increased the proline level and caused severe electrolyte leakage from the roots of all target weeds, indicating membrane disruption and loss of integrity [59]. Finally, the *J. communis* EO exhibited no phytotoxic effect against *Ailanthus altissima* (Mill.) Swingle, resulting in 0% seedling mortality [23]. Few data are also available on the phytotoxicity of EOs from the genus *Larix*. The most recent work [17] studied the herbicidal effects of *L. kaempferi* (Lamb.) Carrière, demonstrating its capacity to inhibit the growth of *Brassica napus* L. by 50% in a seed bioassay and its inability to stop the development of new shoots after a foliar application of 10% EO in a greenhouse experiment. Previously, the negative effect of volatile substances of *L. gmelinii* (Rupr.) Kuzen. EO on the growth of *Fraxinus mandshurica* Rupr. was mainly attributed to  $\alpha$ -pinene [15], while the EO from leaves and branches of *L. principis-rupprechtii* affected its own regeneration with significant inhibitory effects on the germination rate, radicle and hypocotyl length, and fresh mass [16].

In general, our data, in addition to highlighting a greater efficacy of the *L. decidua* EO, showed the different susceptibility of the two target species. *L. multiflorum* (monocotyledon) was more sensitive to treatments than *S. alba* (dicotyledon). Furthermore, the effects of both EOs were reduced by the interaction with the soil, with significant results still being obtained. In this type of substrate, we wanted to check for the possible presence of residual volatile terpenes. As expected, after 7 days, most of them were not detected, with differences between the two tests. Their absence, which may be due to the ability of soil particles to adsorb the volatile terpenes and subsequently release them to penetrate the seeds and exert their possible toxicity, deserves to be further investigated [60].

## 4. Materials and Methods

### 4.1. Plant Material

Bio EOs from leaves of *J. nana* and *L. decidua* were directly supplied from Bergila GmbH Srl (Falzes/Issengo-Bolzano, Italy) and stored at 4 °C until use.

Target seeds of *L. multiflorum* (grass) and *S. alba* L. (broadleaf) were provided by the organic farm “Terre di Lomellina” (Pavia, Italy) and purchased from the company “Padana Sementi” (Padua, Italy), respectively. Before use, they were sterilized with 1% sodium hypochlorite solution for 10 min, then repeatedly rinsed with distilled water.

### 4.2. Solid-Phase Microextraction (SPME)

To describe the chemical profile of the headspace from two EOs and of soil samples, a SPME device from Supelco (Bellefonte, PA, USA) was used for the sampling. The soil (~1 g) and the EOs (~2 mL) were individually placed into a 15 mL glass vial with PTFE-coated silicone septum. The chosen fiber was coated with 50/30 $\mu$ m DVB/CAR/PDMS (divinylbenzene/carboxen/polydimethylsiloxane). Before sampling, the fiber was conditioned at 270 °C for 20 min. First, the samples were equilibrated for 30 min at 50 °C prior to analysis. Subsequently, the fiber was exposed to the equilibrated headspace for 10 and 30 min to capture the volatile components from EOs and soil samples, respectively. Later, the fiber was inserted in a GC injector maintained at 250 °C for the desorption of collected components.

### 4.3. Gas Chromatography/Mass Spectrometry (GC/MS)

All analyses were performed using a Clarus 500 model Perkin Elmer (Waltham, MA, USA) gas chromatograph coupled with a mass spectrometer and equipped with an FID (flame detector ionization). In the GC oven was housed a Varian Factor Four VF-1 capillary column and helium was used as carrier gas at a flow rate of 1 mL/min. The adopted chromatographic conditions followed a previous study [61]. The mass spectra were obtained in the electron impact mode (EI), at 70 eV in scan mode in the range 35–400  $m/z$ . The

identification of volatile compounds was performed by matching their mass spectra with those stored in the Wiley 2.2 and Nist 02 mass spectra libraries database and by comparison of their linear retention indices (LRIs), relative to C<sub>8</sub>–C<sub>25</sub> *n*-alkanes analyzed under the same conditions, with those available in the literature. Relative amounts of compounds, expressed as a percentage, were calculated in relation to the total area of the chromatogram by normalizing the peak area without the use of an internal standard and any factor correction. All analyses were carried out in triplicate.

#### 4.4. Phytotoxic Studies

##### 4.4.1. Non-Contact Germination Test with EOs

Seeds (15) of the target species *L. multiflorum* and *S. alba* were sown in 9 cm diameter Petri dishes lined with filter paper (Whatman No. 1) wetted with 4 mL of sterilized water. The EOs of *J. communis* or *L. decidua* were pipetted (2, 20, or 50 µL) into a small handmade aluminum container placed in the center of each Petri dish to avoid direct contact with seeds. To evaluate the phytotoxic activity of the EOs using a different substrate, the seeds (15) were also sown in 9 cm diameter Petri dishes filled with 25 g of non-fertilized soil (Vigorplant® SER CA 98 V7, Fombio (Lo), Italy) wetted with 15 mL of sterilized water. Sterile 6 mm diameter disks (1 or 3) impregnated with different amounts (2, 20, or 50 µL) of *J. nana* or *L. decidua* EO were placed at the same depth as the seeds and covered with soil. In their respective controls, the EOs were absent and replaced by distilled water (2, 20 or 50 µL). Tests were carried out under a biological hood with vertical laminar flow. Subsequently, the suitably sealed (double layer of Parafilm) and initialed Petri dishes were incubated for 16 h light at 23 °C and 8 h darkness at 18 °C in a climatic chamber for 7 days. The experimental design included 3 quantities of each EO (treated samples) or distilled water (control samples) × 2 target species × 3 replicates × 2 runs.

##### 4.4.2. Contact Germination Test with EOs

Seeds (15) of the target species *L. multiflorum* and *S. alba* were sown in 9 cm diameter Petri dishes lined with filter paper (Whatman No. 1) wetted with 4 mL of an oily solution prepared with different concentrations (2, 5, and 10 µL/mL) of *J. communis* or *L. decidua* EO and using 0.1% Tween® 20 (Sigma-Aldrich, Milan, Italy) as surfactant. To evaluate the same phytotoxic activity of the EOs using a different substrate, the seeds (15) were also sown in 9 cm diameter Petri dishes filled with 25 g of non-fertilized soil (Vigorplant® SER CA 98 V7 Fombio (Lo), Italy) wetted with 15 mL of the same oily solutions prepared with different concentrations (2, 5, and 10 µL/mL) of *J. communis* or *L. decidua* EO and using 0.1% Tween® 20 (Sigma-Aldrich, Milan, Italy) as surfactant. In their respective controls, the EOs were absent and replaced by 0.1% Tween® 20 solution (4 or 15 mL). The test was carried out under a biological hood with vertical laminar flow. Subsequently, the suitably sealed (double layer of Parafilm) and initialed Petri dishes were incubated for 16 h light at 23 °C and 8 h darkness at 18 °C in a climatic chamber for 7 days. The experimental design included 3 quantities of each EO (treated samples) or distilled water (control samples) × 2 target species × 3 replicates × 2 runs.

#### 4.5. Data Analysis

Phytotoxic effects of the *J. communis* and *L. decidua* EOs on germination and seedling development of the target species were described using the following indices:

1. Germination percentage (G) = (Germinated seed number)/(Seed total number) × 100;
2. Coefficient of Velocity of Germination (CVG) =  $N_1 + N_2 + \dots + N_i / 100 \times N_1 T_1 + \dots + N_i T_i$ , where N is the number of seeds germinated every day; T is the number of days from seeding corresponding to N [62];
3. Mean Germination Time (MGT) =  $(\sum D \times \text{Germinated seed number}) / (\sum \text{Germinated seed number})$ , where D is the number of days from the beginning of germination, plus the number of seeds germinated on day D [63];
4. Seedling Vigor Index (SVI) = (Mean Root length + Mean Shoot length) × Germination %. [64].

The number of germinated seeds was detected every day for a week, and the measurements on the radicle and shoot of the seedlings were carried out at the end of the test, seven days after sowing.

#### 4.6. Statistical Analysis

The data were evaluated with the support of IBM SPSS software, through the analysis of variance carried out separately for each EO (i.e., from the two species *J. communis* and *L. decidua*) and substrate (i.e., filter paper and soil). The germination and growth indices (i.e., G%, CVG, MGT, SVI, root length, shoot length) measured for the two target species (i.e., *L. multiflorum* and *S. alba*) under different treatments were taken into account as dependent variables.

The one-way ANOVA and the Turkey's-b post hoc test were performed in order to establish the significant effect (at  $\alpha \leq 0.05$ ) of the treatments with EOs (i.e., the different levels of concentration or quantity in EOs, respectively) on the target species and describe the homogenous subsets.

Moreover, the two-way ANOVA was performed, considering as factors the treatments with EOs and the species, in order to highlight the significant interaction ( $\alpha \leq 0.05$ ) between "species  $\times$  treatments" and then highlighting the species-specific effects of the treatments and the different behavior or susceptibility of *L. multiflorum* (grass) and *S. alba* (broadleaf).

## 5. Conclusions

Essential oils extracted from certain species of plants can represent a valid alternative to the use of synthetic chemicals as natural herbicidal agents capable of guaranteeing a phytotoxic effect but, at the same time, respectful of the environment and human health.

In our study, *J. communis* and *L. decidua* EOs were investigated in order to evaluate and compare their allelopathic effects, and on the basis of their chemical compositions. The findings showed that both EOs were active in a dose-dependent manner, but with greater efficacy shown in *L. decidua* EO against *Lolium multiflorum* and *Sinapis alba* L.

In conclusion, due to the obtained data, we can confirm that the EOs from gymnosperms, and their main components, may represent an important source for the development of new low-impact natural products against weeds.

**Author Contributions:** Conceptualization, S.G. and S.V.; investigation, S.G. and S.V.; data curation, M.I., S.G., S.V. and V.V.; writing—original draft preparation, S.G., S.V. and V.V.; writing—review and editing, M.I., S.G. and S.V.; funding acquisition, M.I. and S.G. All the authors critically edited the manuscript before submission. All authors have read and agreed to the published version of the manuscript.

**Funding:** This research received no external funding.

**Institutional Review Board Statement:** Not applicable.

**Informed Consent Statement:** Not applicable.

**Data Availability Statement:** All generated data are included in this article.

**Acknowledgments:** The authors are thankful to Bergila, GmbH Srl (Falzes/Issengo-Bolzano) Italy, for providing *J. communis* var. *saxatilis* and *L. decidua* essential oils.

**Conflicts of Interest:** The authors declare no conflict of interest.

## References

1. Liebman, M.; Mohler, C.L.; Staver, C.P. (Eds.) *Ecological Management of Agricultural Weeds*; Cambridge University Press: Cambridge, UK, 2001.
2. Chauhan, B.S. Grand challenges in weed management. *Front. Agron.* **2020**, *1*, 3. [[CrossRef](#)]
3. Dayan, F.E. Current status and future prospects in herbicide discovery. *Plants* **2019**, *8*, 341. [[CrossRef](#)] [[PubMed](#)]
4. Tataridas, A.; Kanatas, P.; Chatzigeorgiou, A.; Zannopoulos, S.; Travlos, I. Sustainable crop and weed management in the era of the EU Green Deal: A survival guide. *Agronomy* **2022**, *12*, 589. [[CrossRef](#)]

5. Ibáñez, M.D.; Blázquez, M.A. Phytotoxic effects of commercial essential oils on selected vegetable crops: Cucumber and tomato. *Sustain. Chem. Pharm.* **2020**, *15*, 100209. [[CrossRef](#)]
6. Ahuja, N.; Batish, D.R.; Singh, H.P.; Kohli, R.K. Herbicidal activity of eugenol towards some grassy and broad-leaved weeds. *J. Pest Sci.* **2015**, *88*, 209–218. [[CrossRef](#)]
7. Scognamiglio, M.; D'Abrosca, B.; Esposito, A.; Pacifico, S.; Monaco, P.; Fiorentino, A. Plant growth inhibitors: Allelopathic role or phytotoxic effects? Focus on Mediterranean biomes. *Phytochem. Rev.* **2013**, *12*, 803–830. [[CrossRef](#)]
8. Ishii-Iwamoto, E.L.; Pergo Coelho, E.M.; Reis, B.; Moscheta, I.S.; Moacir Bonato, C. Effects of monoterpenes on physiological processes during seed germination and seedling growth. *Curr. Bioact. Compd.* **2012**, *8*, 50–64. [[CrossRef](#)]
9. Raveau, R.; Fontaine, J.; Lounès-Hadj Sahraoui, A. Essential oils as potential alternative biocontrol products against plant pathogens and weeds: A review. *Foods* **2020**, *9*, 365. [[CrossRef](#)]
10. Singh, H.P.; Kohli, R.K.; Batish, D.R.; Kaushal, P.S. Allelopathy of gymnospermous trees. *J. For. Res.* **1999**, *4*, 245–254. [[CrossRef](#)]
11. Teixeira da Silva, J.A.; Karimi, J.; Mohsenzadeh, S.; Dobránszki, J. Allelopathic potential of select gymnospermous trees. *J. For. Sci.* **2015**, *31*, 109–118.
12. Young, G.P.; Bush, J.K. Assessment of the allelopathic potential of *Juniperus ashei* on germination and growth of *Bouteloua curtipendula*. *J. Chem. Ecol.* **2009**, *35*, 74–80. [[CrossRef](#)] [[PubMed](#)]
13. Ismail, A.; Lamia, H.; Hanana, M.; Jamoussi, B. Chemical composition of *Juniperus oxycedrus* L. subsp. *macrocarpa* essential oil and study of their herbicidal effects on germination and seedling growth of weeds. *Asian J. Appl. Sci.* **2011**, *4*, 771–779. [[CrossRef](#)]
14. Mehdizadeh, L.; Taheri, P.; Ghasemi Pirbalouti, A.; Moghaddam, M. Phytotoxicity and antifungal properties of the essential oil from the *Juniperus polycarpus* var. *turcomanica* (B. Fedtsch.) R.P. Adams leaves. *Physiol. Mol. Biol. Plants* **2020**, *26*, 759–771. [[CrossRef](#)] [[PubMed](#)]
15. Wu, J.M.; Li, B.N.; Liu, G.P.; Wang, X.S.; Wu, B.G. Effect of volatile substances of larch on the growth of ash in a mixed forest plantation. *J. Northeast For. Univ.* **2000**, *28*, 25–28.
16. Fen, H.A.N.; Hui, W.; Yin-Xia, B.; Yong-Bing, L.I. Chemical components and their allelopathic effects of the volatiles from *Larix principis-rupprechtii* leaves and branches. *Chin. J. Appl. Ecol.* **2008**, *19*, 2327–2332.
17. Yun, M.S.; Cho, H.M.; Yeon, B.-R.; Choi, J.S.; Kim, S. Herbicidal activities of essential oils from pine, nut pine, larch and khangnan fir in Korea. *Weed Turf. Sci.* **2013**, *2*, 30–37. [[CrossRef](#)]
18. Bhardwaj, K.; Islam, M.T.; Jayasena, V.; Sharma, B.; Sharma, S.; Sharma, P.; Kuča, K.; Bhardwaj, P. Review on essential oils, chemical composition, extraction, and utilization of some conifers in Northwestern Himalayas. *Phyther. Res.* **2020**, *34*, 2889–2910. [[CrossRef](#)]
19. Bali, A.S.; Batish, D.R.; Singh, H.P. Allelopathic effect of aromatic plants: Role of volatile essential oils. *J. Global. Biosci.* **2016**, *5*, 4386–4395.
20. Visan, D.-C.; Oprea, E.; Radulescu, V.; Voiculescu, I.; Biris, I.-A.; Cotar, A.I.; Saviuc, C.; Chifiriuc, M.C.; Marinas, I.C. Original contributions to the chemical composition, microbicidal, virulence-arresting and antibiotic-enhancing activity of essential oils from four coniferous species. *Pharmaceuticals* **2021**, *14*, 1159. [[CrossRef](#)]
21. Sahin, H.T.; Yalcin, O.U. Chemical Composition and Utilization of Conifer Needles-A Review. *J. Appl. Life Sci. Int.* **2017**, *14*, 1–11. [[CrossRef](#)]
22. Garcia, G.; Garcia, A.; Gibernau, M.; Bighelli, A.; Tomi, F. Chemical compositions of essential oils of five introduced conifers in Corsica. *Nat. Prod. Res.* **2017**, *31*, 1697–1703. [[CrossRef](#)] [[PubMed](#)]
23. Karalija, E.; Dahija, S.; Parić, A.; Zeljković, S.Č. Phytotoxic potential of selected essential oils against *Ailanthus altissima* (Mill.) Swingle, an invasive tree. *Sustain. Chem. Pharm.* **2020**, *15*, 100219. [[CrossRef](#)]
24. Zheljzkov, V.D.; Cantrell, C.L.; Semerdjieva, I.; Radoukova, T.; Stoyanova, A.; Maneva, V.; Kačaniová, M.; Astatkie, T.; Borisova, D.; Dincheva, I.; et al. Essential oil composition and bioactivity of two juniper species from Bulgaria and Slovakia. *Molecules* **2021**, *26*, 3659. [[CrossRef](#)] [[PubMed](#)]
25. Holm, Y.; Laakso, I.; Hiltunen, R. Variation and inheritance of monoterpenes in *Larix* species. *Flavour Fragr. J.* **1997**, *12*, 335–339. [[CrossRef](#)]
26. Doi, M.; Toeda, K.; Myoda, T.; Hashidoko, Y.; Fujimori, T. Seasonal fluctuations of aroma components of essential oils from *Larix leptolepis*. *J. Oleo Sci.* **2019**, *68*, 671–677. [[CrossRef](#)]
27. Loizzo, M.R.; Saab, A.M.; Tundis, R.; Menichini, F.; Bonesi, M.; Statti, G.A.; Menichini, F. Chemical composition and antimicrobial activity of essential oils from *Pinus brutia* (calabrian pine) growing in Lebanon. *Chem. Nat. Compd.* **2008**, *44*, 6. [[CrossRef](#)]
28. Thai, T.H.; Hien, N.T.; Cuong, N.; Casanova, J.; Tomi, F.; Paoli, M. Chemical composition of essential oils isolated from leaves, twigs, roots and cones of Vietnamese *Keteleeria evelyniana* Mast. *J. Essent. Oil Res.* **2022**, *34*, 148–154. [[CrossRef](#)]
29. Lee, J.H.; Lee, B.K.; Kim, J.H.; Lee, S.H.; Hong, S.K. Comparison of chemical compositions and antimicrobial activities of essential oils from three conifer trees; *Pinus densiflora*, *Cryptomeria japonica*, and *Chamaecyparis obtusa*. *J. Microbiol. Biotechnol.* **2009**, *19*, 391–396. [[CrossRef](#)]
30. Höferl, M.; Stoilova, I.; Schmidt, E.; Wanner, J.; Jirovetz, L.; Trifonova, D.; Krastev, L.; Krastanov, A. Chemical composition and antioxidant properties of juniper berry (*Juniperus communis* L.) essential oil. Action of the essential oil on the antioxidant protection of *Saccharomyces cerevisiae* model organism. *Antioxidants* **2014**, *3*, 81–98. [[CrossRef](#)]

31. Cabral, C.; Francisco, V.; Cavaleiro, C.; Gonçalves, M.J.; Cruz, M.T.; Sales, F.; Batista, M.T.; Salguero, L. Essential oil of *Juniperus communis* subsp. *alpina* (Suter) Čelak needles: Chemical composition, antifungal activity and cytotoxicity. *Phytother. Res.* **2012**, *26*, 1352–1357. [[CrossRef](#)]
32. Zheljazzkov, D.; Astatkie, T.; Jeliaskova, E.A.; Heidel, B.; Ciampa, L. Essential oil content, composition and bioactivity of *Juniper* species in Wyoming, United States. *Nat. Prod. Commun.* **2017**, *12*, 201–204. [[CrossRef](#)] [[PubMed](#)]
33. Holubová, V.; Hrdlicka, P.; Kubán, V. Age and space distributions of monoterpenes in fresh needles of *Picea abies* (L) Karst. determined by gas chromatography-mass spectrometry. *Phytochem. Anal.* **2001**, *12*, 243–249. [[CrossRef](#)] [[PubMed](#)]
34. Kupcinskiene, E.; Stikliene, A.; Judzentiene, A. The essential oil qualitative and quantitative composition in the needles of *Pinus sylvestris* L. growing along industrial transects. *Environ. Pollut.* **2008**, *155*, 481–491. [[CrossRef](#)] [[PubMed](#)]
35. Arlinda, A.; Kadiasi, N.; Alban, I. Effect of soil composition elements on essential oils content of *Juniperus communis* L. berries in north populations in Albania. *Int. J. Curr. Res.* **2021**, *13*, 19794–19797.
36. Hajdari, A.; Mustafa, B.; Nebija, D.; Miftari, E.; Quave, C.L.; Novak, J. Chemical Composition of *Juniperus communis* L. Cone Essential Oil and Its Variability among Wild Populations in Kosovo. *Chem. Biodivers.* **2015**, *12*, 1706–1717. [[CrossRef](#)]
37. Angioni, A.; Barra, A.; Russo, M.T.; Coroneo, V.; Dessi, S.; Cabras, P. Chemical composition of the essential oils of *Juniperus* from ripe and unripe berries and leaves and their antimicrobial activity. *J. Agric. Food Chem.* **2003**, *7*, 3073–3078. [[CrossRef](#)]
38. Koukos, P.K.; Papadopoulou, K.I. Essential oil of *Juniperus communis* L. grown in Northern Greece: Variation of fruit oil yield and composition. *J. Essent. Oil Res.* **1997**, *9*, 35–39. [[CrossRef](#)]
39. Nishida, N.; Tamotsu, S.; Nagata, N.; Saito, C.; Sakai, A. Allelopathic effects of volatile monoterpenoids produced by *Salvia leucophylla*: Inhibition of cell proliferation and DNA synthesis in the root apical meristem of *Brassica campestris* seedlings. *J. Chem. Ecol.* **2005**, *31*, 1187–1203. [[CrossRef](#)]
40. Dehsheikh, A.B.; Sourestani, M.M.; Dehsheikh, P.B.; Mottaghipisheh, J.; Vitalini, S.; Iriti, M. Monoterpenes: Essential oil components with valuable features. *Mini Rev. Med. Chem.* **2020**, *20*, 958–974. [[CrossRef](#)]
41. Abraham, D.; Francischini, A.C.; Pergo, E.M.; Kelmer-Bracht, A.M.; Ishii-Iwamoto, E.L. Effects of  $\alpha$ -pinene on the mitochondrial respiration of maize seedlings. *Plant Physiol. Biochem.* **2003**, *41*, 985–991. [[CrossRef](#)]
42. Singh, H.P.; Batish, D.R.; Kaur, S.; Arora, K.; Kohli, R.K.  $\alpha$ -Pinene inhibits growth and induces oxidative stress in roots. *Ann. Bot.* **2006**, *98*, 1261–1269. [[CrossRef](#)] [[PubMed](#)]
43. De Martino, L.; Mancini, E.; De Almeida, L.F.R.; De Feo, V. The antigerminative activity of twenty seven monoterpenes. *Molecules* **2010**, *15*, 6630–6637. [[CrossRef](#)] [[PubMed](#)]
44. Andrianjafinandrasana, S.N.; Andrianoelisoa, H.S.; Jeanson, M.L.; Ramonta, I.R.; Danthu, P. Allelopathic effects of volatile compounds of essential oil from *Ravensara aromatica* Sonnerat chemotypes. *Allelopathy J.* **2013**, *31*, 333–344.
45. Wright, C.; Chhetri, B.K.; Setzer, W.N. Chemical composition and phytotoxicity of the essential oil of *Encelia farinosa* growing in the sonoran desert. *Am. J. Essent. Oils Nat. Prod.* **2013**, *1*, 18–22.
46. Verma, R.S.; Joshi, N.; Padalia, R.C.; Singh, V.R.; Goswami, P.; Verma, S.K.; Iqbal, H.; Chanda, D.; Verma, K.; Darokar, M.P.; et al. Chemical composition and antibacterial, antifungal, allelopathic and acetylcholinesterase inhibitory activities of cassumunarginger. *J. Sci. Food Agric.* **2018**, *98*, 321–327. [[CrossRef](#)]
47. Scognamiglio, M.; Schneider, B. Identification of potential allelochemicals from donor plants and their synergistic effects on the metabolome of *Aegilops geniculata*. *Front. Plant Sci.* **2020**, *11*, 1046. [[CrossRef](#)]
48. Tahir, A.; Jilani, M.I.; Khera, R.A.; Nadeem, F. *Juniperus communis*: Biological activities and therapeutic potentials of a medicinal plant—A comprehensive study. *Int. J. Chem. Biochem. Sci.* **2016**, *9*, 85–91.
49. Süntar, I.; Tumen, I.; Ustün, O.; Keleş, H.; Küpeli Akkol, E. Appraisal on the wound healing and anti-inflammatory activities of the essential oils obtained from the cones and needles of *Pinus* species by in vivo and in vitro experimental models. *J. Ethnopharmacol.* **2012**, *139*, 533–540. [[CrossRef](#)] [[PubMed](#)]
50. Garzoli, S.; Masci, V.L.; Caradonna, V.; Tiezzi, A.; Giacomello, P.; Ovidi, E. Liquid and vapor Phase of four conifer-derived essential oils: Comparison of chemical compositions and antimicrobial and antioxidant properties. *Pharmaceuticals* **2021**, *14*, 134. [[CrossRef](#)]
51. Hong, E.J.; Na, K.J.; Choi, I.G.; Choi, K.C.; Jeung, E.B. Antibacterial and antifungal effects of essential oils from coniferous trees. *Biol. Pharm. Bull.* **2004**, *27*, 863–866. [[CrossRef](#)]
52. Pérez-Rosés, R.; Risco, E.; Vila, R.; Peñalver, P.; Cañigueral, S. Biological and nonbiological antioxidant activity of some essential oils. *J. Agric. Food Chem.* **2016**, *64*, 4716–4724. [[CrossRef](#)] [[PubMed](#)]
53. Emami, S.A.; Javadi, B.; Hassanzadeh, M.K. Antioxidant activity of the essential oils of different parts of *Juniperus communis* subsp. *hemisphaerica*. and *Juniperus oblonga*. *Pharm. Biol.* **2007**, *4*, 769–776. [[CrossRef](#)]
54. Emami, S.A.; Sadeghi-aliabadi, H.; Saeidi, M.; Jafarian, A. Cytotoxic evaluations of Iranian conifers on cancer cells. *Pharm. Biol.* **2005**, *43*, 299–304. [[CrossRef](#)] [[PubMed](#)]
55. Thi Hoai, N.; Viet Duc, H.; Thi Thao, D.; Orav, A.; Raa, A. Selectivity of *Pinus sylvestris* extract and essential oil to estrogen-insensitive breast cancer cells *Pinus sylvestris* against cancer cells. *Pharmacogn. Mag.* **2015**, *11*, S290.
56. Maurya, A.K.; Devi, R.; Kumar, A.; Kundal, R.; Thakur, S.; Sharma, A.; Kumar, R.; Padwad, Y.S.; Chand, G.; Singh, B.; et al. Chemical composition, cytotoxic and antibacterial activities of essential oils of cultivated clones of *Juniperus communis* and wild *Juniperus* species. *Chem. Biodivers.* **2018**, *15*, e1800183. [[CrossRef](#)]

57. Wedge, D.; Tabanca, N.; Sampson, B.; Werle, C.; Demirci, B.; Can Baser, K.H.; Nan, P.; Duan, J.; Liu, Z. Antifungal and insecticidal activity of two *Juniperus* essential oils. *Nat. Prod. Commun.* **2009**, *4*, 123–127.
58. Semerdjieva, I.; Atanasova, D.; Maneva, V.; Zhelezkov, V.; Radoukova, T.; Astatkie, T.; Dincheva, I. Allelopathic effects of *Juniper* essential oils on seed germination and seedling growth of some weed seeds. *Ind. Crops Prod.* **2022**, *180*, 114768. [[CrossRef](#)]
59. Ismail, A.; Lamia, H.; Mohsen, H.; Bassem, J. Herbicidal potential of essential oils from three mediterranean trees on different weeds. *Curr. Bioact. Compd.* **2012**, *8*, 3–12. [[CrossRef](#)]
60. Muller, C.H.; del Moral, R. Soil toxicity induced by terpenes from *Salvia leucophylla*. *Bull. Torrey Bot. Club.* **1966**, *93*, 130–137. [[CrossRef](#)]
61. Vitalini, S.; Iriti, M.; Garzoli, S. GC-MS and SPME-GC/MS Analysis and bioactive potential evaluation of essential oils from two *Viola* species belonging to the *V. calcarata* complex. *Separations* **2022**, *9*, 39. [[CrossRef](#)]
62. Al-Mudaris, M. Notes on various parameters recording the speed of seed germination. *Der. Trop.* **1998**, *99*, 147–154.
63. Ellis, R.A.; Roberts, E.H. The quantification of ageing and survival in orthodox seeds. *Seed Sci. Technol.* **1981**, *9*, 373–409.
64. Abdul-Baki, A.A.; Anderson, J.D. Vigour determination in soybean seed by multiple criteria. *Crop Sci.* **1973**, *1*, 630–633. [[CrossRef](#)]

## Article

# Genetic Variation and Genotype by Environment Interaction for Agronomic Traits in Maize (*Zea mays* L.) Hybrids

Mohammad Ashraf Alam<sup>1</sup>, Marufur Rahman<sup>2</sup>, Salahuddin Ahmed<sup>3</sup>, Nasrin Jahan<sup>4</sup>,  
Mohammad Al-Amin Khan<sup>5</sup>, Mohammad Rafiqul Islam<sup>6</sup>, Amnah Mohammed Alsuhaibani<sup>7</sup>, Ahmed Gaber<sup>8</sup>  
and Akbar Hossain<sup>9,\*</sup>

- <sup>1</sup> Spices Research Centre, Bangladesh Agricultural Research Institute, Bogura 5810, Bangladesh; a.alam\_83@yahoo.com
  - <sup>2</sup> Regional Station, Bangladesh Institute of Research and Training on Applied Nutrition, Rangapur 5470, Bangladesh; marufur@birtan.gov.bd
  - <sup>3</sup> Maize Breeding Division, Bangladesh Wheat and Maize Research Institute, Dinajpur 5200, Bangladesh; su\_ahmed66@yahoo.com
  - <sup>4</sup> Plant Genetic Resources Research Centre, Bangladesh Agricultural Research Institute, Gazipur 1701, Bangladesh; nasrin.jahan83@gmail.com
  - <sup>5</sup> Regional Spices Research Centre, Bangladesh Agricultural Research Institute, Gazipur 1701, Bangladesh; mithunkhan93@gmail.com
  - <sup>6</sup> Regional Agricultural Research Station, Bangladesh Agricultural Research Institute, Pabna 6620, Bangladesh; rafiq\_bari2@yahoo.com
  - <sup>7</sup> Department of Physical Sport Science, College of Education, Princess Nourah bint Abdulrahman University, P.O. Box 84428, Riyadh 11671, Saudi Arabia; amalsuhaibani@pnu.edu.sa
  - <sup>8</sup> Department of Biology, College of Science, Taif University, P.O. Box 11099, Taif 21944, Saudi Arabia; a.gaber@tu.edu.sa
  - <sup>9</sup> Department of Agronomy, Bangladesh Wheat and Maize Research Institute, Dinajpur 5200, Bangladesh
- \* Correspondence: akbar.hossain@bwmri.gov.bd

**Citation:** Alam, M.A.; Rahman, M.; Ahmed, S.; Jahan, N.; Khan, M.A.-A.; Islam, M.R.; Alsuhaibani, A.M.; Gaber, A.; Hossain, A. Genetic Variation and Genotype by Environment Interaction for Agronomic Traits in Maize (*Zea mays* L.) Hybrids. *Plants* **2022**, *11*, 1522. <https://doi.org/10.3390/plants11111522>

Academic Editors: Milan S. Stankovic, Petronia Carillo, Paula Baptista and Othmane Merah

Received: 28 February 2022

Accepted: 2 June 2022

Published: 6 June 2022

**Publisher's Note:** MDPI stays neutral with regard to jurisdictional claims in published maps and institutional affiliations.



**Copyright:** © 2022 by the authors. Licensee MDPI, Basel, Switzerland. This article is an open access article distributed under the terms and conditions of the Creative Commons Attribution (CC BY) license (<https://creativecommons.org/licenses/by/4.0/>).

**Abstract:** In order to develop high-yielding genotypes of adapted maize, multilocation trials of maize were performed including forty-five maize hybrids exploiting genetic variability, trait associations, and diversity. The experiments were laid out in an RCB design and data were recorded on eight yield and yield-contributing traits, viz., days to anthesis (AD), days to silking (SD), anthesis–silking interval (ASI), plant height (PH), ear height (EH), kernels per ear (KPE), thousand-kernel weight (TKW), and grain yield (GY). An analysis of variance (ANOVA) showed significant variation present among the different traits under study. The phenotypic coefficient of variance (PCV) showed a higher value than the genotypic coefficient of variance (GCV), indicating the environmental influence on the expression of the traits. High heritability coupled with high genetic advance was found for these traits, indicative of additive gene action. The trait associations showed that genotypic correlation was higher than phenotypic correlation. Based on genetic diversity, the total genotypes were divided into four clusters, and the maximum number of 16 genotypes was found in cluster IV. Among the eight yield and yield-contributing traits, PH, ASI, EH, and TKW were the important traits for variability creation and were mostly responsible for yield. Genotypes G5, G8, G27, G29, and G42 were in the top ranks based on grain yield over locations, while a few others showed region-centric performances; all these genotypes can be recommended upon validation for commercial release. The present findings show the existence of proper genetic variability and divergence among traits, and the identified traits can be used in a maize improvement program.

**Keywords:** genetic diversity; trait association; GCV; genetic variability; genetic advance; heritability; PCV

## 1. Introduction

Maize (*Zea mays* L.) is a popular staple cereal after rice and wheat [1,2]. It is also used as a raw material for human food, as well as animal feed products. The nutrition quality of

maize (i.e., starch, protein, oil, fiber, sugar, and ash) is very rich [3]. In addition, corn oil and corn flakes are popular across the globe [3]. China, Brazil, Argentina, and Ukraine are the best maize-producing countries, and the USA is ranked first in maize production [4].

In Bangladesh, maize stands in the second position for production after rice and is ranked third as a staple cereal [5]. The last decade's maize production increased three times in Bangladesh, and surprisingly, the growth rate per year is 11.40% [5]. Although the maize production area has expanded and the adaptation rate is high, we are still behind in achieving sustainable food security with the existing available commercial cultivar. Hence, it is urgent to create high-yielding new varieties of maize to break the yield ceiling. It is most important to enhance the qualities of yield-contributing traits to develop the best variety. Yield is a polygenic and complex trait and is related to other yield-contributing traits that are easily inherited [2,3]. The genetic diversity, variability, and heritability inside the current germplasm are key thrusts that improve the efficiency of the breeding program [1,6,7].

Hence, trait selection for any crops solely based on the heritability of the particular traits sometimes may lead to an incorrect choice, where considering genetic advances along with it might be more effective. Heritability explains the degree of extent for heritable traits from parents to segregants; in addition, genetic advance is a powerful tool in searching for the original advance predicted under selection [8]. Correlation and path analysis provide relationships among the traits and also show the importance of a trait in contributing to the yield. Traits having high values of the genotypic coefficients of variations indicate that the traits are highly heritable and have good potential for perfect selection [9–11].

Along with trait selection, breeders have also intensely emphasized the development of stable genotypes for different climatic conditions and locational variations. Those varieties are suitable for a wide range of planting. The ideal variety should have a high mean yield with low fluctuations in diverse environments and locations [12,13], although region-centric varieties can meet the demand of a specific region. The responses of genotype and location interactions on yield and yield-attributed traits have been well-recognized for a while. Improvement is possible either by reducing the genotype  $\times$  location interaction through breeding for a region-centric adaptation or by identifying a germplasm having wide adaptation from selection across varying environments. Apart from adaptivity, a genotype  $\times$  location interaction study can also provide information about similarities of locations for a variety of responses that may help in making decisions for adaption targets and test sites [14].

Considering the above aspects, a few attempts have already been made to enhance the trait qualities of maize in Bangladesh. The present investigation is undertaken to screen variability, genetic advance, trait associations, and diversity among the genotypes and traits of maize for the development of high-yielding cultivars suitable for different locations.

## 2. Materials and Methods

### 2.1. Plant Genetic Materials

Forty-five test crosses of maize hybrids were used in the present study. A list and the pedigrees of the test crosses of hybrids are given in Table S1. The female parents were developed locally at the Ishwardi location, comprising a screened sample of the population pool, and they were further bulked for one more season. The male counterparts were collected from the plant-breeding division of the Bangladesh Agricultural Research Institute (BARI), followed by three more seasons of regeneration. A large number of the test crosses were made at the Ishwardi location, but only a few hybrids were included in the study (only those successful hybrids representing a female parental line with all three male inbred lines).

### 2.2. Experimental Site and Design

The present investigation was carried out at three regional stations (Barishal, Ishwardi, and Jashore) of the Bangladesh Agricultural Research Institute (BARI) during 2015–2016. Among these locations, the Barishal region is under the agro-ecological zone of the Ganges

Tidal Floodplain. The soil type is noncalcareous grey floodplain with 15–20 inches of total annual rainfall and a tropical monsoon climate with 25.6 °C as the average temperature. The Ishwardi location is under the active Brahmaputra-Jamuna Floodplain zone. The soil type is sandy and silty alluvium. The yearly maximum temperature is 36.8 °C, and the minimum temperature is 9.6 °C with an annual rainfall of 1872 mm. The regional station at Jashore is under the AEZ High Ganges River Floodplain. The soil in the AEZ falls under dark grey calcareous floodplain soil. The annual average temperature ranges from 15.4 to 34.6 °C with rainfall of 60.5 inches. Details of the weather that prevailed during the cropping season at the studied locations are given in Table S2. In all three locations, all the materials were arranged in a randomized complete block design (RCBD) and repeated three times.

### 2.3. Experimental Details

The unit plot size was 7.5 m<sup>2</sup>. The distance from row to row was 75 cm, and the plant-to-plant distance was 25 cm. Standard intercultural operations were performed during plant production. Well-decomposed farmyard manure (FYM) at 6 t ha<sup>-1</sup> was applied one week before sowing, and a mixture of N:P:K at 120:60:40 kg ha<sup>-1</sup> was mixed into the soil immediately before sowing. During the growth stages of the crop, two hand weedings were conducted, one at 18 days after sowing (DAS), while the second one was performed at 36 DAS. Earthing-up was conducted two times during the whole cropping cycle. A total of three irrigations (i.e., one at the vegetative stage, the second during anthesis (to avoid pollen desiccation), and the third during the grain-filling stage) were applied during the whole cropping cycle. For plant protection, one spray was applied against leaf feeders during the late vegetative stage.

### 2.4. Evaluation of Agronomic Traits

Data on different traits were collected according to the standard methods stated in the IBPGR [15]. Data on the days to anthesis (AD), days to silking (SD), anthesis–silking interval (ASI), plant height (PH), ear height (EH), kernels per ear (KPE), thousand-kernel weight (TKW), and grain yield (GY) were recorded for all three locations. Data on yield and yield-related traits were collected during the flowering-to-harvesting stage. In each replication, 3 plants were selected to collect these yield and yield-related traits.

### 2.5. Statistical Analysis

An analysis of variance (ANOVA) for all the recorded data and mean separation tests at the 5% and 1% levels of probability were performed using SAS software (version 9.2). The details of the analysis were as follows.

#### 2.5.1. Analysis of Variance

The analysis of variance for individual traits was carried out using R software version 4.1.2 [16]. The linear model of observations in an alpha lattice design was as follows:

$$Y_{ij} = \mu + t_i + r_j + e_{ij}$$

where  $Y_{ij}$  is the observed trait's value for  $i$ th treatment at the  $j$ th replicate;  $t_i$  is the fixed effect of the  $i$ th treatment;  $r_j$  is the effect of the  $j$ th replicate; and  $e_{ij}$  is the experimental error.

ANOVA for yield was performed for genotype  $\times$  location using the R platform [16] and the 'Plant breeding' package software [17].

The model was written as below:

$$Y_{ij} = \mu + g_i + l_j + g_i \times l_j + \epsilon_{ij}$$

where  $Y_{ij}$  is the observed mean yield for  $i$ th genotype at the  $j$ th location;  $g_i$  is the genotype effect;  $l_j$  is the effect of the location;  $g_i \times l_j$  is the interaction effect of  $i$ th genotype at the  $j$ th location; and  $\epsilon_{ij}$  is the residual error.

Pi is the phenotypic index, which was estimated as:

Pi = the mean of a particular genotype over all the locations – the grand mean of all genotypes over all locations, and

Li is the locational index, which was estimated as:

Li = the mean of all the genotypes in a particular location – the grand mean of all genotypes over all locations.

### 2.5.2. Variability Estimates

Variability estimates including genotypic and phenotypic variances, heritability, genotypic and phenotypic coefficients of variations, and genetic advance were estimated according to [18–21].

#### Phenotypic and Genotypic Variance

These parameters were calculated according to the formula given by [21] for genotypic variance:

$$\delta^2g = \frac{MSG - MSE}{r} \times 100$$

where MSG is the mean sum of square for the genotypes; MSE is the mean sum of square for the error; and  $r$  is the number of replications.

The phenotypic variance was calculated as follows:

$$\delta^2p = \delta^2g + \delta^2e$$

where  $\delta^2g$  is the genotypic variance, and  $\delta^2e$  is the environmental variance equal to the mean square error.

The genotypic and phenotypic coefficients of variation were calculated with the following formula [22]:

$$GCV = \frac{\delta_g \times 100}{\bar{x}}$$

$$PCV = \frac{\delta_p \times 100}{\bar{x}}$$

where GCV is the genotypic coefficient of variation; PCV is the phenotypic coefficient of variation;  $\delta_g$  is the genotypic standard deviation;  $\delta_p$  is the phenotypic standard deviation; and  $\bar{x}$  is the population.

#### Estimation of Heritability

Heritability, in a broad sense for all the traits, was computed as suggested by [21]:

$$h^2 \% = \frac{\sigma_g^2}{\sigma_p^2} \times 100$$

where  $h^2$  is heritability in a broad sense;  $\sigma_g^2$  is the genotypic variance; and  $\sigma_p^2$  is the phenotypic variance.

The heritability was classified as low (0–30%), moderate (30–60%), or high (>60%), as suggested by [23].

#### Estimation of Genetic Advance

The genetic advance was calculated as follows:

$$GA = K \cdot h^2 \cdot \sigma_p$$

or as genetic advance:

$$GA = K \cdot \frac{\sigma_g^2}{\sigma_p^2} \cdot \sigma_{ph}$$

where  $K$  is the selection intensity, or the value that is 2.06 at a 5% selection intensity;  $\sigma_{ph}$  is the phenotypic standard deviation;  $h^2$  is heritability in a broad sense;  $\sigma_g^2$  is the genotypic variance; and  $\sigma_p^2$  is the phenotypic variance.

#### Association Analysis

To observe associations among the studied traits, a correlation analysis was performed with R software [16] using the ‘Agricolae’ package [24].

#### Regression Analysis

A multiple regression analysis was performed to determine the extent of the relationship between GY with the other studied traits. Stepwise regression was also performed to find the most-contributing traits to GY in different locations. The analysis and visualization were performed using the ‘ggplot2’ [25] package in R software [16].

#### Grouping or Clustering

Grouping for all the genotypes was conducted using a cluster analysis, as suggested by D2 analysis [26,27]. The grouping method divided the genotypes into more or less homogeneous groups. The grouping of traits was also helpful to find the closeness of the traits. The analysis and visualization were performed with R software [16].

### 3. Results and Discussion

The study was conducted to discover the variations of yield and yield-contributing traits in forty-five maize genotypes. Data for eight traits were collected from three locations (Barishal, Ishwardi, and Jashore) and statistical analyses were conducted for probable explanations. The ANOVA of eight yield and yield-related traits of maize is shown in Table 1. The data in Table 1 showed significant ( $p \leq 0.05$ ) variations among the genotypes for AD, SD, ASI, PH, EH, KPE, TKW, and GY at the three locations.

**Table 1.** Estimation of genetic parameters in eight traits of 45 genotypes of maize grown in multiple locations.

Traits	X	LSD	CV%	$\sigma_g^2$	$\sigma_p^2$	$\sigma_e^2$	GCV	PCV	ECV	$h^2$	GA
Barishal location											
AD	88.03	4.40	2.37	4.10 **	8.44	4.34	2.30	3.30	24.69	0.65	11.37
SD	89.12	4.78	2.60	3.47 *	8.85	5.38	2.09	3.34	26.22	0.56	10.26
ASI	1.20	1.34	52.07	0.00 <sup>ns</sup>	0.39	0.39	0.00	52.07	160.05	0.00	0.00
PH	218.06	36.99	8.08	111.73 <sup>ns</sup>	422.02	310.29	4.85	9.42	4.17	0.42	363.96
EH	119.18	33.00	13.56	129.77 *	390.86	261.09	9.56	16.59	4.13	0.50	401.39
KPE	510.99	123.35	11.18	1288.16 <sup>ns</sup>	4551.01	3262.85	7.02	13.20	1.26	0.44	4136.42
TKW	352.83	74.45	10.33	578.54 *	1907.60	1329.07	6.82	12.38	1.91	0.47	1828.90
GY	10.75	2.61	11.87	0.90 *	2.53	1.63	8.83	14.79	50.46	0.53	2.74
Ishwardi location											
AD	97.40	1.64	0.82	11.25 **	11.89	0.64	3.44	3.54	6.75	0.97	23.82
SD	98.51	1.69	0.83	9.47 **	10.13	0.67	3.12	3.23	8.05	0.97	20.16
ASI	1.12	0.99	39.18	0.67 **	0.86	0.19	73.22	83.04	50.77	0.87	1.56
PH	220.95	16.42	3.34	103.48 **	157.90	54.42	4.60	5.69	4.67	0.79	257.54
EH	115.04	15.02	5.90	78.14 **	124.15	46.01	7.68	9.69	5.46	0.77	197.59
KPE	465.02	50.52	5.12	2258.45 **	2826.25	567.79	10.22	11.43	0.84	0.89	5171.93
TKW	326.60	23.13	3.47	1170.97 **	1299.27	128.30	10.48	11.04	0.87	0.95	2537.49
GY	11.65	1.64	6.79	1.84 **	2.47	0.63	11.65	13.48	32.04	0.85	4.35

Table 1. Cont.

Traits	X	LSD	CV%	$\sigma^2_g$	$\sigma^2_p$	$\sigma^2_e$	GCV	PCV	ECV	h <sup>2</sup>	GA
Jashore location											
AD	92.33	1.38	0.72	4.13 **	4.57	0.44	2.20	2.32	14.58	0.95	8.94
SD	93.55	1.90	0.92	4.41 **	5.16	0.75	2.24	2.43	16.78	0.92	9.79
ASI	1.22	1.48	53.54	0.18 <sup>ns</sup>	0.61	0.43	34.37	63.62	108.06	0.45	0.56
PH	224.18	28.95	5.85	222.41 **	394.22	171.81	6.65	8.86	3.32	0.72	585.82
EH	115.23	12.45	4.57	215.42 **	243.16	27.74	12.74	13.53	2.17	0.94	470.62
KPE	497.40	81.36	8.01	1776.91 **	3363.96	1587.05	8.47	11.66	1.18	0.69	4790.46
TKW	351.33	55.03	7.62	1758.71 **	2476.29	717.57	11.94	14.16	1.08	0.83	4236.82
GY	10.51	2.05	9.16	0.60 *	1.53	0.93	7.38	11.76	62.97	0.57	1.78

\* 5% level of probability, \*\* 1% level of probability; <sup>ns</sup> non-significant; AD: days to anthesis, SD: days to silking, ASI: anthesis–silking interval, PH: plant height, EH: ear height, KPE: kernels per plant, TKW: thousand-kernel weight, GY: grain yield, X: mean value, LSD: least significant difference, CV%: coefficient of variation,  $\sigma^2_g$ : genotypic variance,  $\sigma^2_p$ : phenotypic variance,  $\sigma^2_e$ : environmental variance, GCV: genotypic coefficient of variation, PCV: phenotypic coefficient of variation, ECV: environmental coefficient of variation, h<sup>2</sup>: heritability, GA: genetic advance.

### 3.1. Genetic Variability among Genotypes

The variations among the tested genotypes for the target traits allowed for the selection of desirable genotypes for future crop improvement. In the current study, the differences among the genotypes in response to eight traits under three locations were explained, and the results are shown in Table 1. It was noted that the minimum number of days for AD and SD were required at the Barishal (88.03 and 89.12 days, respectively) location, followed by Jashore (92.33 and 93.55 days, respectively). The ASI and PH showed almost similar values at the three locations. In the cases of EH (119.18), KPE (510.99), and TKW (352.83), the maximum values were found at the Barishal location, and the lowest values for KPE (465.02) and TKW (326.60) were observed at the Ishwardi location. Considering the grain yield, the maximum value was recorded at Ishwardi (11.65), and the minimum was found at Jashore (10.51). The expression of every trait depends on the interaction between genes and environmental factors. Sometimes, more environmental influences hinder the expression of traits. The variances due to genotype and phenotype indicate the contribution of the heritable part within a trait-based phenotypic expression. In the present study, the phenotypic variance appeared to be higher than the genotypic variance for all the traits under the three different locations for all the genotypes (Table 1). This information suggested that the environmental impact on the phenotypic expression of genes is controlled by these traits. Previous results of some researchers [28–30] also agree with the findings of the present study.

The present investigation at three locations showed a wide range of variations for different traits. This variation indicated that there is a way to identify promising genotypes based on the traits. The PCV and GCV for all the genotypes in multiple locations were divided into three categories (above 20% was high, 10–20% was medium, and below 10% was low). At the Ishwardi and Jashore locations, high levels of PCV and GCV were found for the ASI. On the other hand, only PCV was high. Moderate levels of PCV and lower levels of GCV were recorded for the EH, KPE, TKW, and GY traits only for the Barishal location. At the Ishwardi location, the PCV of KPE, TKW, and GY were observed at a medium level; however, the EH was at low level for this location. However, the PCV and GCV were moderate for EH and TKW at the Barishal location. In this location, PCV were also moderate for KPE and GY, but the GCV was recorded as low. Both GCV and PCV were at lower levels for AD, SD, and PH in all three locations (Table 1). A medium level of the coefficient of variation implies an equal influence of additive and nonadditive gene action. Medium levels of genotypic coefficients of variance were found for some traits, as reported by several earlier findings [4,31,32].

In the present investigation, the PCV was comparatively higher than the GCV for all the traits, but the ranges of difference between the PCV and GCV were low for AD, SD, and PH at the three locations, indicating the low impact of the environment on the expression of the traits, a symptom of the heritable nature of the traits. Several researchers have also observed a similar but higher PCV than GCV in their studies [33,34]. In our study, closer GCV and PCV were found for EH, KPE, TKW, and GY at the Ishwardi and Jashore locations, indicating low environmental influence on the expression of the traits. Therefore, a huge scope for the perfect selection of traits existed based upon the phenotypic expression of these traits. Similar findings were also observed by [35]. The GCV and PCV values were also close in the cases of AD, SD, and PH at all three locations, but the low levels of GCV and PCV (<10%) were not suitable for selection. A wider PCV and GCV value was observed for ASI at the three locations. At the Barishal location, wider GCV and PCV values were also observed for EH, KPE, TKW, and GY, indicating the dominant role of the environment on the expression of the traits, which was not suitable for effective selection. A high level of environmental influence was also found by Patil et al. [35] in the case of some traits.

### 3.2. Heritability and Genetic Advance

Heritability is a tool that is used to estimate the degree of variation in a group population. The heritability in a group of the population can be classified into three groups (i.e., >80% is high, 40–80% is medium, and low is <40%). In the present investigation, at the Ishwardi location, high heritability was observed for all the traits. For the AD, SD, EH, and TKW traits, heritability was shown to be high at the Jashore location. However, a moderate level of heritability was found for all the traits except the ASI at the Barishal location. At the Jashore location, medium levels of heritability were observed for ASI, PH, KPE, and GY (Table 1). Several earlier findings have revealed that a high level of heritability for any trait indicates a low level of environmental impact on genotypes. The information from the current study related to heritability is helpful for selecting the best traits for the improvement of crops [9,36,37]. The current study also reported a high level of heritability for different traits of maize. However, only heritability-based trait selection may not be successful sometimes, as the broad sense of heritability counts on total genetic variance, which involves additive, dominant, and epistatic variances. Therefore, estimation of the heritability of a group of genotypes coupled with high genetic advance is more reliable and efficient for the selection of desirable traits for a group of the population [38]. According to the categorization of genetic advance as a percentage of mean (GAM) <10 is low, 10–20% is medium, and >20% is high. High heritability coupled with high genetic advances were found in almost all the traits, except ASI and GY at the Ishwardi location. At the Jashore location, high heritability with high genetic advance was also observed for EH and TKW (Table 1). These findings are in accordance with a previous study [39]. High heritability with moderate genetic advance was also observed for AD and SD at the Ishwardi location, which indicates influence from dominance or epistasis. Similar findings have been observed by [4,28]. Moderate heritability with high genetic advance were observed for PH, EH, KPE, and TKW at the Barishal location; on the other hand, at the Jashore location, it was observed for EH and KPE. Moderate heritability coupled with moderate genetic advance was found for AD and SD at the Barishal location. Low estimates of genetic gain were revealed for grain yield (GY) at all the locations, except for the AD and SD value, which showed low genetic gain at the Jashore location. The traits showed high heritability coupled with high genetic advance, which gave information to select superior genotypes. These traits governed by additive gene action would be favorable for a breeding program.

### 3.3. Association of Traits among Genotypes

Polygenic traits are sensitive to environmental influence. Therefore, the selection of promising genotypes based on only yield may not be effective. For yield improvement or plant architecture improvement, selection has to be performed through associated

traits. In our study, correlation coefficient analyses for seven traits were performed at both the phenotypic and genotypic levels (Tables 2–4). At three locations, a higher genotypic correlation coefficient was found than the phenotypic correlation coefficient in the present investigation, while a strong inborn association was decreased at the phenotypic level due to environmental effects. The same type of results was also observed [40]. At the Barishal and Jashore locations, the results indicated that some yield-contributing traits, such as PH, EH, and TKW, had a significant positive correlation at the phenotypic, as well as genotypic, level with maize grain yield (Tables 2–4). A significant and positive correlation was also observed for PH and EH with grain yield at the Ishwardi location (Table 3). At the Barishal location, the highest value of positive and significant correlation was found between AD and SD (0.99 and 0.92), closely followed by EH and PH (0.99 and 0.70) and GY and PH (0.99 and 0.51). TKW and KPE (−0.77 and −0.31) showed the highest value of significant negative correlation. A significant correlation was found between AD and SD (0.97 and 0.96), closely followed by EH and PH (0.78 and 0.75); on the other hand, ASI and AD (−0.48 and −0.44) exhibited the highest value of negative and significant correlation at the Ishwardi location (Table 3). At the Jashore location, a significant correlation was found between AD and SD (0.99 and 0.95), closely followed by EH and PH (0.84 and 0.81); on the other hand, TKW and KPE (−0.81 and −0.54) exhibited the highest value of negative and significant correlation (Table 4). The recent findings agree with several research observations on different traits of maize [8,35,41]. Hence, selection based on these traits will result in improving the grain yield of maize.

**Table 2.** Associations of different traits from trial evaluated at Barishal location.

Traits		AD	SD	ASI	PH	EH	KPE	TKW
SD	$r_g$	0.99 **						
	$r_p$	0.92 **						
ASI	$r_g$	-	-					
	$r_p$	0.06	0.02					
PH	$r_g$	0.80 **	0.74 **	-				
	$r_p$	0.43 **	0.39 *	0.07				
EH	$r_g$	0.36 *	0.27	-	0.99 **			
	$r_p$	0.32 *	0.30 *	0.17	0.70 **			
KPE	$r_g$	0.17	0.22	-	0.62 **	0.35 *		
	$r_p$	0.23	0.27	0.21	0.29	0.18		
TKW	$r_g$	−0.33 *	−0.19	-	0.23	24	−0.77 **	
	$r_p$	−0.19	−0.11	−0.04	0.13	0.15	−0.31 *	
GY	$r_g$	0.43 **	0.40 *	-	0.99 **	0.73 **	0.61 **	0.48 **
	$r_p$	0.24	0.23	0.26	0.51 **	0.42 **	0.28	0.41 *

\* 5% level of probability, \*\* 1% level of probability, AD: days to anthesis, SD: days to silking, ASI: anthesis–silking interval, PH: plant height, EH: ear height, KPE: kernels per plant, TKW: thousand kernel-weight, GY: grain yield,  $r_g$ : genotypic correlation coefficient,  $r_p$ : phenotypic correlation coefficient.

The association of traits as measured by the correlation coefficient may not always show a perfect picture of the relationships among traits. In this way, the regression coefficient helps to examine the relationships of traits and to identify the relative importance of each in contributing to the yield. The regression analysis showed that ASI, PH, KPE, and TKW were effective traits for yield at the Barishal location, and the regression value was 0.42; KPE and TKW were effective traits at the Ishwardi location, and a value of 0.47 contributed towards yield. AD, ASI, EH, KPE, and TKW were effective for the yield of maize at the Jashore location, and the regression value was found to be 0.57 for these traits (Table 5).

**Table 3.** Associations of different traits from trial evaluated at Ishwardi location.

Traits		AD	SD	ASI	PH	EH	KPE	TKW
SD	$r_g$	0.97 **						
	$r_p$	0.96 **						
ASI	$r_g$	−0.48 **	−0.29					
	$r_p$	−0.44 **	−0.18					
PH	$r_g$	0.2	0.21	−0.06				
	$r_p$	0.15	0.18	0.04				
EH	$r_g$	0.43 **	0.53 **	0.2	0.78 **			
	$r_p$	0.25	0.35 *	0.24	0.75 **			
KPE	$r_g$	0.32 *	0.37 *	0.13	0.23	0.46 **		
	$r_p$	0.28	0.32 *	0.04	0.26	0.34 *		
TKW	$r_g$	−0.16	−0.16	0.04	0.04	0.2	−0.19	
	$r_p$	−0.15	−0.16	0.03	0.08	0.14	−0.17	
GY	$r_g$	0.09	0.13	0.02	0.36 *	0.52 **	0.50 **	0.27
	$r_p$	0.08	0.11	0.05	0.33 *	0.37 *	0.62	0.28

\* 5% level of probability, \*\* 1% level of probability, AD: days to anthesis, SD: days to silking, ASI: anthesis–silking interval, PH: plant height, EH: ear height, KPE: kernels per plant, TKW: thousand-kernel weight, GY: grain yield,  $r_g$ : genotypic correlation coefficient,  $r_p$ : phenotypic correlation coefficient.

**Table 4.** Associations of different traits from the trial were evaluated at the Jashore location.

Traits		AD	SD	ASI	PH	EH	KPE	TKW
SD	$r_g$	0.99 **						
	$r_p$	0.95 **						
ASI	$r_g$	0.04	0.24					
	$r_p$	−0.03	0.27					
PH	$r_g$	0.54 **	0.57 **	0.30 *				
	$r_p$	0.42 **	0.41 *	0.00				
EH	$r_g$	0.61 **	0.59 **	0.15	0.84 **			
	$r_p$	0.53 **	0.54 **	0.07	0.81 **			
KPE	$r_g$	0.69 **	0.71 **	0.27	0.63 **	0.58 **		
	$r_p$	0.56 **	0.55 **	0.05	0.42 **	0.43 **		
TKW	$r_g$	−0.32 *	−0.29	0.15	0.26	0.10	−0.81 **	
	$r_p$	−0.27	−0.25	0.04	0.12	−0.01	−0.54 **	
GY	$r_g$	0.10	0.03	−0.38 *	0.85 **	0.78 **	−0.05	0.54 **
	$r_p$	0.08	0.00	−0.26	0.49 **	0.42 **	0.20	0.44 **

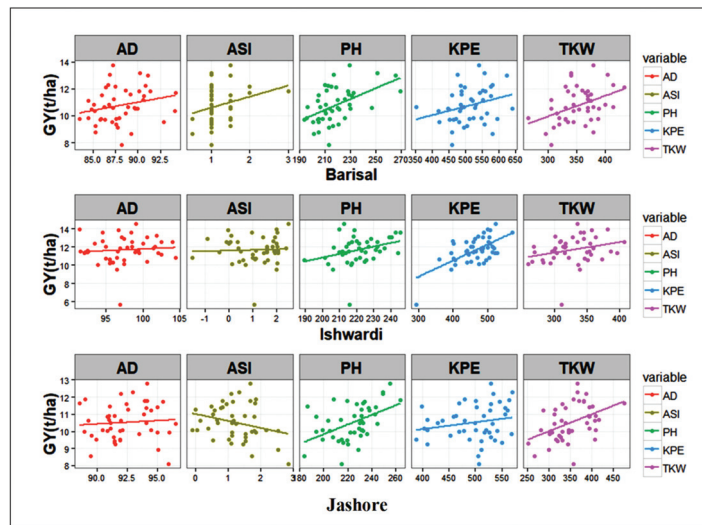
\* 5% level of probability, \*\* 1% level of probability, AD: days to anthesis, SD: days to silking, ASI: anthesis–silking interval, PH: plant height, EH: ear height, KPE: kernels per plant, TKW: thousand-kernel weight, GY: grain yield,  $r_g$ : genotypic correlation coefficient,  $r_p$ : phenotypic correlation coefficient.

Figure 1 displays the contributions of different traits to the grain yield variation. In order to obtain the highest grain yields for different genotypes, the improvement of these traits could obtain a high yield of maize [42]; these traits were used in a stepwise regression in which the grain yield was a dependent variable against other traits as the independent variables [43]. Among the independent variables, TKW, KPE, and PH were the most important traits contributing to the final grain yield of maize.

**Table 5.** Initial model and final models for different locations were obtained from stepwise regression.

Traits		AD	SD	ASI	PH	EH	KPE	TKW	Multiple Regression	Stepwise Regression
Barishal	b	0.122	0.121	0.820	0.040	0.030	0.006	0.015	0.42	0.45
	r <sup>2</sup>	0.056	0.053	0.070	0.256	0.170	0.070	0.167		
	p-value	0.116	0.120	0.082	0.000	0.004	0.060	0.005		
Ishwardi	b	0.036	0.050	0.070	0.040	0.046	0.017	0.012	0.47	0.51
	r <sup>2</sup>	0.006	0.011	0.001	0.106	0.133	0.380	0.070		
	p-value	0.587	0.486	0.774	0.029	0.010	<0.000	0.060		
Jashore	b	0.038	0.000	−0.400	0.028	0.027	0.004	0.009	0.57	0.59
	r <sup>2</sup>	0.006	0.000	0.060	0.236	0.176	0.038	0.193		
	p-value	0.608	0.990	0.080	0.001	0.004	0.190	0.002		

AD: days to anthesis, SD: days to silking, ASI: anthesis–silking interval, PH: plant height, EH: ear height, KPE: kernels per plant, TKW: thousand-kernel weight, b: slope, r<sup>2</sup>: coefficient of determination.

**Figure 1.** Graph displaying contributions of different traits to the grain yield variation.

The initial model and final models for different locations obtained from the stepwise regression were as follows:

Initial model:  $GY \sim AD + SD + ASI + PH + EH + KPE + TKW$ .

Final model for Barishal:  $GY \sim ASI + PH + KPE + TKW$ .

Final model for Ishwardi:  $GY \sim KPE + TKW$ .

Final model for Jashore:  $GY \sim AD + ASI + EH + KPE + TKW$ .

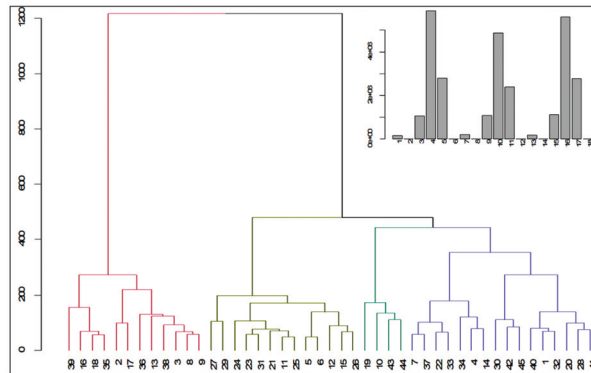
### 3.4. Genetic Diversity

Cluster analysis is a perfect biometrical tool for grouping data according to similarity. Data can be categorized into homogenous and distinct groups with cluster analysis. In the current study, all the genotypes were classified into four different clusters, with cluster IV having the maximum genotypes (16, 35.55%), followed by cluster II and cluster I (13 and 12, respectively) genotypes (Table 6).

**Table 6.** Cluster analysis of forty-five maize genotypes.

Cluster	Number of Genotypes	Percentage (%)	Accession Number
I	12	26.66	G39, G16, G18, G35, G2, G47, G36, G13, G33, G3, G8, G9
II	13	28.88	G27, G29, G24, G23, G31, G21, G11, G25, G5, G6, G12, G15, G26
III	4	8.88	G19, G10, G13, G44
IV	16	35.55	G7, G37, G22, G33, G34, G4, G14, G30, G42, G45, G40, G1, G32, G20, G28, G41

Cluster III contained the lowest number of genotypes (8.88%) and occupied the lowest rank. Remarkably, cluster I had the (G39, G16, G18, G35, G2, G47, G36, G13, G33, G3, G8, and G9) genotypes, whereas cluster II had the (G27, G29, G24, G23, G31, G21, G11, G25, G5, G6, G12, G15, and G26) genotypes. Furthermore, cluster III had (G19, G10, G13, and G44), and cluster IV showed sixteen genotypes: (G7, G37, G22, G33, G34, G4, G14, G30, G42, G45, G40, G1, G32, G20, G28, and G41) (Table 6 and Figure 2). Similar observations have also been found [34,44]. Some parents of the genotypes collected from the same or nearby locations did not fall in the same cluster, informing that geographical closeness did not always give better genetic uniformity. Therefore, there might be underlying factors playing a role behind the genetic differences among genotypes originating from the same areas that may have various genetic make-ups. The dendrogram represents the index of genetic diversity among the clusters and genotypes (Figure 2). Inter- and intracluster distances informed us that there was existing diversity among genotypes. In the case of maize, ref. [45] also found similar findings. By using a covariance matrix in the case of maize nonhierarchical clustering, ref. [46] observed clusters, and ref. [45] also found clusters from maize advance lines.

**Figure 2.** Dendrogram showing the grouping of genotypes based on AD, ASI, PH, KPE, TKW, and GY traits of all locations.

The biplot depicts the positions of different studied traits except for GY and their clustering patterns based on the traits' weights (Figure 3). The biplot reveals that the studied traits could broadly be classified into two groups. The traits of SD, AD, and ASI were in one set, whereas TKW, KPE, PH, and EH were in the other one. It was found that the traits in such groups looked to be the same type. The PCA explained the partitioning of total variation into principal components (PCs). In the analysis, across the locations, PC1 accounted for 95.83% of the total variation, and PC2 contributed only 3.33%. At the Barishal location, the biplot reveals similar results, as across one plot, the traits were majorly grouped into two, and in the other, they were sub-grouped into four: traits KPE, PH, and EH were together in a subgroup with AD and SD in one subgroup, ASI in another subgroup, and lastly, TKW was the furthest in the fourth subgroup. At this location, PC1 accounted for 94.83% and PC2 for 4.56% of the total variability (Figure S1). At the Ishwardi

location, PC1 contributed 80.98%, while PC2 accounted for 16.3% of the total diversity (Figure S2). The biplot depicts that the traits of PH and EH, as well as KPE and TKW, were included largely in one group together, whereas AD, SD, and ASI were in another group, following a similar pattern as before. At the Jashore location, the biplot shows the traits of PH, EH, KPE, and TKW together into a major group, whereas AD, SD, and ASI were in another one. The PC1 accounted for 72.71% of the variability, and PC2 accounted for 23.9% of the total diversity (Supplementary Figure S3). PCA analysis accounted for the traits and variables and reduced them into PCs, where in the present study, the most variability (~99%) was conferred by the first two PCs. Similar findings have been observed in cases of maize by [11,47].

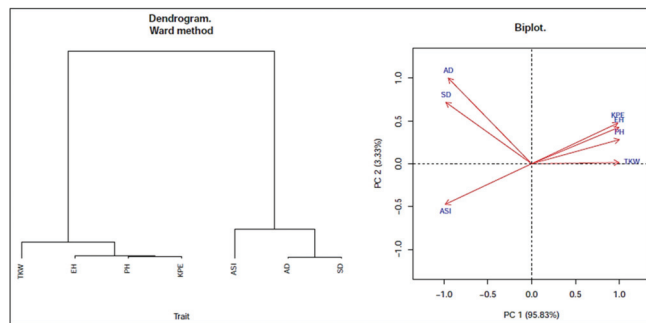


**Figure 3.** Dendrogram showing clustering of different traits (left); position of different traits depicted on biplot from principal component analysis of combined data.

### 3.5. Genotype $\times$ Location Interaction Analysis

A genotype  $\times$  location interaction analysis was performed based on grain yield observations at different locations. Ample variation ( $p \leq 0.01$ ) was observed for the studied genotypes in the combined analysis of variance (Table 7), which indicated the differential responses of genotypes at different locations.

**Table 7.** Genotype–location interaction ANOVA for grain yield studied at three locations.

Source of Variation	Degrees of Freedom	Sum Squares	Mean Squares	% Total SS
Location	2	53.901	26.951	11.286
Genotype	44	219.712	4.993 **	46.004
Genotype $\times$ Location	88	203.979	2.318 **	42.709
Residuals	132	139.081	1.0536	-

\*\* 1% level of probability.

The highest portion (46.004%) of the total sum of squares was explained by the genotypic effect, which indicated the presence of ample genetic variability among the studied genotypes and the possibility of selection for stable, high-yielding genotypes. The location was the least source of variation and contributed only a small portion (11.286%) to the total sum of squares. Moreover, location was not significant, indicating that across the genotypes, the means at locations were not varied statistically. However, a significant difference was spotted for genotype  $\times$  location interaction, suggesting that the grain yield of genotypes varied across the locations and reflecting the existence of locational effects in the genotype  $\times$  location interaction. A high percentage (42.709%) of the total sum of squares for the genotype  $\times$  location interaction displayed the significance of this source of variation and also implicated a truncated effectiveness of indirect selection for potential genotypes disregarding the genotype  $\times$  location interaction. Genotype–location interactions had a role in the stability of the tested genotypes. Therefore, the stability of the genotypes was

measured because the difference in locations accounted for most of the population [48–50]. Parag et al. [51] also found significant variation due to a genotype  $\times$  location interaction for the yield of maize. Hence, a significant genotype  $\times$  location interaction may influence crop development, which a plant breeder can use in a maize variety development program if genotypes are to be adopted to explicit climates.

### 3.6. Top Yielder at Locations

The yield of maize under the investigation varied with locations. The mean grain yield of the genotypes over the locations ranged from 8.46 t/ha to 12.70 t/ha with a total mean of 11.02 t/ha (Table 8). Quite a few genotypes showed wider adaptation, but some also showed region-centric better performances. Overall, genotypes G5, G8, G27, G29, and G42 were the top five based on yield performance for wider adaption, in which genotype G42 ranked first. At the Barishal location, the highest value for yield was 13.79 t/ha, and the lowest value was 7.80 t/ha. The best-performing five genotypes at this location were G8, G29, G30, G42, and G45. G42 was the top performer here, whereas G8 and G45 showed somewhat region-specific yielders compared to the other two locations. The maximum value for yield was found to be 14.51 t/ha, and the minimum value was 5.68 t/ha at Ishwardi. The best five performers were the G5, G7, G13, G27, and G37 genotypes, of which G37 was the top yielder. At this particular location, most of the top-yielding genotypes were region-centric in nature, except G5 and G27. On the other hand, the maximum value for yield was 12.89 t/ha, and the minimum value was 8.27 t/ha at the Jashore location. The five best-yielding genotypes were G28, G29, G30, G41, and G42, and G29 was the highest yielder. The region-specific adaption was observed for genotype G28. The experimental locations were ranked based on yield potential as Ishwardi > Barishal > Jashore. The present findings showed differential yield potentials at the three locations. The locations of Barishal, Jashore, and Ishwardi were also distinct and suggested the existence of genotype–location interactions. Similar observations have been found [52,53]. A vast majority of the genotypes showed unstable performances among the locations. In a study with maize genotypes, Badu-Apraku et al. [54] found some high-yielding, unstable genotypes in West Africa. In the present study, a few other genotypes exhibited near-perfect performances, i.e., better yielding ability across the locations. A perfect genotype must have a high mean value of yield and a high level of stability in vast environments [53,55].

**Table 8.** Mean grain yield performances of the studied genotypes at different locations.

Gen	Bar	Ish	Jas	Mean	Pi	Gen	Bar	Ish	Jas	Mean	Pi
G1	11.12	11.35	11.43	11.30	0.28	G24	10.54	10.17	10.61	10.44	−0.58
G2	10.82	12.53	11.00	11.45	0.43	G25	10.20	11.88	9.57	10.55	−0.48
G3	9.78	12.05	10.10	10.64	−0.38	G26	11.86	13.19	9.94	11.66	0.64
G4	10.38	11.54	8.53	10.15	−0.87	G27	12.18	13.62 *	10.44	12.08 *	1.06
G5	11.68	13.58 *	11.53	12.26 *	1.24	G28	10.58	11.92	12.07 *	11.52	0.50
G6	11.46	11.51	9.61	10.86	−0.16	G29	13.00 *	11.84	12.89 *	12.57 *	1.55
G7	11.51	13.91 *	9.90	11.77	0.75	G30	13.19 *	10.37	12.15 *	11.90	0.88
G8	13.04 *	12.51	11.39	12.31 *	1.29	G31	8.63	13.09	9.14	10.28	−0.74
G9	12.13	12.91	10.88	11.97	0.95	G32	11.57	11.31	10.73	11.20	0.18
G10	9.81	10.56	8.27	9.55	−1.48	G33	10.59	13.05	11.24	11.62	0.60
G11	9.79	11.53	10.32	10.55	−0.48	G34	9.22	11.32	10.18	10.24	−0.78
G12	9.35	10.10	9.92	9.79	−1.23	G35	9.73	12.65	11.04	11.14	0.12
G13	10.83	13.86 *	10.12	11.60	0.58	G36	10.48	11.99	11.40	11.29	0.27
G14	9.80	11.38	10.88	10.68	−0.34	G37	9.70	14.51 *	10.65	11.62	0.60
G15	11.21	11.62	11.39	11.41	0.39	G38	8.78	12.52	10.97	10.75	−0.27
G16	9.51	10.02	9.60	9.71	−1.31	G39	10.62	11.14	10.75	10.83	−0.19
G17	10.62	10.63	11.22	10.82	−0.20	G40	9.53	11.39	11.19	10.70	−0.32

Table 8. Cont.

Gen	Bar	Ish	Jas	Mean	Pi	Gen	Bar	Ish	Jas	Mean	Pi
G18	10.33	10.68	9.76	10.26	−0.76	G41	11.80	11.99	12.11 *	11.97	0.95
G19	9.75	5.68	9.97	8.46	−2.56	G42	13.79 *	12.35	11.97 *	12.70 *	1.68
G20	10.56	10.83	10.92	10.77	−0.25	G43	7.80	9.48	9.67	8.98	−2.04
G21	11.83	10.57	11.05	11.15	0.13	G44	9.12	10.83	10.13	10.03	−0.99
G22	12.24	12.38	10.26	11.63	0.61	G45	12.31 *	10.32	11.79	11.47	0.45
G23	11.17	11.71	11.10	11.32	0.30						
Mean	10.75	11.65	10.66	11.02		Mean	10.75	11.65	10.66	11.02	
Li	−0.27	0.63	−0.36			Li	−0.27	0.63	−0.36		

Gen: genotype; Bar: Barishal; Ish: Ishwardi; Jas: Jashore; Pi: phenotypic index; Li: locational index; \* indicates the five best-performing genotypes in terms of grain yield; Significant at 5% level of probability.

#### 4. Conclusions

Improvement of maize yield-contributing traits was possible using phenotypic selection for PH, ASI, EH, and TKW, of which all locations showed high values for the genotypic and phenotypic coefficients of variation coupled with  $h^2b$  (heritability) and GA (genetic advance). These traits also revealed positive or negative direct effects on maize yield. Therefore, priority should be given to these traits for crop improvement. The diversity analysis provided a way to choose the best recombinants for different traits and further create variations in these traits in future segregants. Hence, traits controlled by additive gene action may be amenable to a breeding program. These traits can be used for the improvement of maize through selection. Quite a few genotypes were found to be better either for wider adaption or specific to a particular location, which needs to be further validated before recommending for cultivation.

**Supplementary Materials:** The following supporting information can be downloaded at: <https://www.mdpi.com/article/10.3390/plants11111522/s1>. Table S1: Details of the studied genotypes; Table S2: Weather conditions prevailing for vegetative and reproductive phases during cropping period at different locations; Figure S1: Dendrogram showing clustering of different traits (left); the position of different traits depicted on biplot from principal component analysis for data on Barishal environment; Figure S2: Dendrogram showing clustering of different traits (left); the position of different traits depicted on biplot from principal component analysis for data on Ishwardi environment; Figure S3: Dendrogram showing clustering of different traits (left); position of different traits depicted on biplot from principal component analysis for data on Jashore environment.

**Author Contributions:** Conceptualization, M.A.A. and S.A.; methodology, M.A.A.; software, M.A.A.; validation, S.A.; formal analysis, M.A.A.; investigation, N.J., M.A.-A.K. and M.A.A.; data curation, M.A.A. and M.R.I.; writing—original draft preparation, M.A.A. and M.R.; writing—review and editing, M.A.A., M.R., S.A., A.G., A.M.A. and A.H.; funding acquisition, A.M.A. and A.H. All authors have read and agreed to the published version of the manuscript.

**Funding:** This research was funded by the Bangladesh Agricultural Research Institute (BARI), Gazipur, Bangladesh, and was partially funded by the Princess Nourah bint Abdulrahman University's Researchers Support Project number (PNURSP2022R65) of Princess Nourah bint Abdulrahman University, Riyadh, Saudi Arabia.

**Institutional Review Board Statement:** Not applicable.

**Informed Consent Statement:** Not applicable.

**Data Availability Statement:** Not applicable.

**Acknowledgments:** We would like to thank the Bangladesh Agricultural Research Institute (BARI). In addition, the authors gratefully thank the Princess Nourah bint Abdulrahman University's Researchers Support Project number (PNURSP2022R65) of Princess Nourah bint Abdulrahman University, Riyadh, Saudi Arabia, for supporting this study.

**Conflicts of Interest:** The authors declare no conflict of interest.

## References

- Ogunniyan, D.J.; Olakojo, S.A. Genetic variation, heritability, genetic advance and agronomic character association of yellow elite inbred lines of maize (*Zea mays* L.). *Niger. J. Genet.* **2014**, *28*, 24–28. [CrossRef]
- Nzuve, F.; Githiri, S.; Mukunya, D.M.; Gethi, J. Genetic variability and correlation studies of grain yield and related agronomic traits in maize. *J. Agric. Sci.* **2014**, *6*, 166–176. [CrossRef]
- Kumar, G.P.; Reddy, V.N.; Kumar, S.S.; Rao, P.V. Genetic variability, heritability and genetic advance studies in newly developed maize genotypes (*Zea mays* L.). *Int. J. Pure Appl. Biosci.* **2014**, *2*, 272–275.
- Ali Abdikadir, H.; Abdikadir, M.; Hasan, M.; Kalam Azad, M.A.; Hasanuzzaman, M. Genetic variability and diversity studies in maize (*Zea mays* L.) Inbred lines. *IOSR J. Agric. Vet. Sci.* **2018**, *11*, 69–76. [CrossRef]
- Islam, S.; Ferdousi, A.; Sweetey, A.Y.; Das, A.; Ferdoush, A.; Haque, M.A. Morphological characterization and genetic diversity analyses of plant traits contributed to grain yield in maize (*Zea mays* L.). *J. Biosci. Agric. Res.* **2020**, *25*, 2047–2059. [CrossRef]
- Maruthi, R.T.; Rani, K.J. Genetic variability, heritability and genetic advance estimates in maize (*Zea mays* L.) Inbred lines. *J. Appl. Natl. Sci.* **2015**, *7*, 149–154. [CrossRef]
- Sesay, S.; Ojo, D.K.; Ariyo, O.J.; Meseke, S. Genetic variability, heritability and genetic advance studies in top-cross and three-way cross maize (*Zea mays* L.) hybrids. *Maydica* **2016**, *61*, 1–7.
- Kinfe, H.; Tsehaye, Y. Studies of heritability, genetic parameters, correlation and path coefficient in elite maize hybrids. *Acad. Res. J. Agric. Sci. Res.* **2015**, *3*, 296–303. [CrossRef]
- Olakojo, S.A.; Olaoye, G. Correlation and heritability estimates of maize agronomic traits for yield improvement and striga asiatica (L.) kuntze tolerance. *Plant Sci.* **2011**, *5*, 365–369.
- Roy, P.; Haque, M.; Ferdousi, A.; Bari, M. Field performance based in-depth genetic analysis of selected maize (*Zea mays* L.) genotypes. *Fundam. Appl. Agric.* **2018**, *3*, 1. [CrossRef]
- Syafii, M.; Cartika, I.; Ruswandi, D. Multivariate analysis of genetic diversity among some maize genotypes under maize-albizia cropping system in Indonesia. *Asian J. Crop. Sci.* **2015**, *7*, 244–255. [CrossRef]
- Ashraf, M.; Qureshi, A.G.; Khan, N.A. Genotype-environment interaction in wheat. *Online J. Biol. Sci.* **2001**, *50*, 356–367. [CrossRef]
- Tarakanovas, P.; Ruzgas, V. Additive main effect and multiplicative interaction analysis of grain yield of wheat varieties in Lithuania. *Agron. Res.* **2006**, *491*, 91–98.
- Annicchiarico, P. Additive main effects and multiplicative interaction (AMMI) analysis of genotype-location interaction in variety trials repeated over years. *Theor. Appl. Genet.* **1997**, *4*, 1072–1077. [CrossRef]
- International Board for Plant Genetic Resources (IBPGR); International Maize and Wheat Improvement Center (CIMMYT). *Descriptors for Maize/Descriptores Para Maiz/Descripteurs Pour Le Maïs*; International Board for Plant Genetic Resources: Wageningen, The Netherlands, 1991; p. 100.
- R Core Team. *R: A Language and Environment for Statistical Computing*; R Foundation for Statistical Computing: Vienna, Austria, 2017; Available online: <https://www.R-project.org/> (accessed on 1 December 2017).
- Rosyara, U.R. Plant Breeding: Analysis and Visualization of Data from Plant Breeding and Genetics Experiments. R Package Version 1.1.1/r37. 2014. Available online: <https://R-Forge.R-project.org/projects/plantbreeding/> (accessed on 1 December 2014).
- Johnson, H.W.; Robinson, H.F.; Comstock, R.E. Estimates of genetic and environmental variability in soybeans. *Agron. J.* **1955**, *47*, 314–318. [CrossRef]
- Hanson, C.H.; Robinson, H.F.; Comstock, R.E. Biometrical studies of yield in segregating populations of korean lespedeza. *Agron. J.* **1956**, *48*, 268–272. [CrossRef]
- Burton, G.W.; DeVane, E.H. Estimating heritability in tall fescue (*Festuca arundinacea*) from replicated clonal material. *Agron. J.* **1953**, *45*, 478–481. [CrossRef]
- Lush, J.L. Heritability of quantitative characters in farm animals. In *Heritability of Quantitative Characters in Farm Animals*; CABI: Wallingford, UK, 1949; pp. 356–375.
- Burton, G.W. Quantitative inheritance in grasses. In Proceedings of the 6th International Grassland Congress, State College, PA, USA, 17–23 August 1952; pp. 277–283.
- Robinson, H.F.; Comstock, R.E.; Harvey, P.H. Estimates of heritability and degree of dominance in corn. *Agron. J.* **1949**, *41*, 353–359. [CrossRef]
- De Mendiburu, F. *Agricolae: Statistical Procedures for Agricultural Research*. 2017. Available online: <https://CRAN.R-project.org/package=agricolae> (accessed on 12 January 2017).
- Wickham, H. *ggplot2: Elegant Graphics for Data Analysis*; Springer: New York, NY, USA, 2009.
- Mahalanobis, P.C. On the generalized distance in statistics. *Proc. Natl. Inst. Sci. India* **1936**, *2*, 49–55.
- Rao, C.R. *Advance Statistical Method in Biometrical Research*; John Willey and Sons: New York, NY, USA, 1952.
- Maurya, A.K.; Kumar, R.; Kumar, V.; Verma, R.K.; Shweta, S.; Yadav, B.K.; Kumar, S. Studies on heritability and genetic advance estimates in maize genotypes. *Plant Arch.* **2014**, *14*, 1155–1157.
- Zaman, M.A.; Alam, M.A. Genetic diversity in exotic maize. *Bangladesh J. Agric. Res.* **2013**, *38*, 335–341. [CrossRef]
- Vishnuvardhan, K.M.; Kumar, K.P.; Murthy, K.D.; Sreevalli, M. Genetic variability, heritability and association analysis of morphological and yield components in maize hybrids. *Ann. Plant Soil Res.* **2021**, *23*, 424–431. [CrossRef]

31. Gazal, A.; Nehvi, F.A.; Lone, A.A.; Dar, Z.A. Assessment of genetic variability of a set of maize inbred lines for drought tolerance under temperate conditions. *Int. J. Curr. Microb. Appl. Sci.* **2017**, *6*, 2380–2389. [[CrossRef](#)]
32. Gazal, A.; Nehvi, F.; Lone, A.A. Morphological and molecular characterization of maize inbred lines showing variability for drought tolerance. *Genet. Mol. Res.* **2018**, *17*, 2. [[CrossRef](#)]
33. Nagalakshmi, R.M.; Ravikesavan, R.; Paranidharan, V.; Manivannan, N.; Firoz, H.; Vignesh, M.; Senthil, N. Genetic variability, heritability and genetic advance studies in backcross populations of maize (*Zea mays* L.). *Electron. J. Plant Breed.* **2018**, *9*, 1137–1145. [[CrossRef](#)]
34. Ganesan, K.N.; Nallathambi, G.; Senthil, N.; Tamilarasi, P.M. Genetic divergence (*Zea mays* L.) Analysis in indigenous maize. *Electron. J. Plant Breed.* **2010**, *1*, 1241–1243.
35. Patil, S.M.; Kumar, K.; Jakhar, D.S.; Rai, A.; Borle, U.M.; Singh, P. Studies on variability, heritability, genetic advance and correlation in maize (*Zea mays* L.). *Int. J. Agric. Environ. Biotech.* **2016**, *9*, 1103. [[CrossRef](#)]
36. Aminu, D.; Izge, A.U. Heritability and correlation estimates in maize (*Zea mays* L.) Under drought conditions in northern guinea and sudan savannas of Nigeria. *World J. Agric. Sci.* **2012**, *8*, 598–602. [[CrossRef](#)]
37. Azam, M.G.; Sarker, U.; Maniruzzaman, M.; Banik, B.R. Genetic variability of yield and its contributing characters on CIMMYT maize inbreds under drought stress. *Bangladesh J. Agric. Res.* **2015**, *39*, 419–426. [[CrossRef](#)]
38. Prakash, R.; Ravikesavan, R.; Vinodhana, N.K.; Senthil, A. Genetic variability, character association and path analysis for yield and yield component traits in maize (*Zea mays* L.). *Electron. J. Plant Breed* **2019**, *10*, 518–524. [[CrossRef](#)]
39. Akeel, A.; Kameel Azzam, H.; Al-Ahmad, S.A. Breeding and potentials of high—Biomass rice varieties for bioenergy production in japan. *Agric. Biol. J. N. Am.* **2008**, *4*, 11–13.
40. Mustafa, H.S.B.; Ahsan, M.; Aslam, M.; Ali, Q.; Hasan, E.; Bibi, T.; Mehmood, T. Genetic variability and traits association in maize (*Zea mays* L.). *Agric. Res.* **2013**, *51*, 231–238.
41. Gokenapally, S.; Jabeen, F. *Heritability, Character Association and Path Analysis for Grain Yield and Yield Contributing Characters in Maiz*; Department of Genetics and Plant Breeding College of Agriculture, Central Agricultural University: Bihar, India, 2013.
42. Mousavi, S.M.N.; Nagy, J. Evaluation of plant characteristics related to grain yield of FAO410 and FAO340 hybrids using regression models. *Cereal Res. Commun.* **2020**, *49*, 161–169. [[CrossRef](#)]
43. Mirzamasoumzadeh, B.; Ahadzadeh, B.; Mollasadeghi, V. Effect of drought stress on yield of maize hybrids. *Adv. Environ. Biol.* **2014**, *8*, 120–122. [[CrossRef](#)]
44. Chen, F.-B.; Yang, K.; Rong, T.; Pan, G. Analysis of genetic diversity of maize hybrids in the regional tests in sichuan and southwest China. *Frontiers Agric. China* **2008**, *2*, 162. [[CrossRef](#)]
45. Biswas, A.; Sarker, U.; Banik, B.R.; Rohman, M.M.; Mian, M.A.K. Genetic divergence study in salinity stress tolerant maize (*Zea mays* L.). *Bangladesh J. Agric. Res.* **2015**, *39*, 621–630. [[CrossRef](#)]
46. Rohman, M.M.; Banik, B.R.; Biswas, A.; Rahman, M.S. Genetic diversity of maize (*Zea mays* L.) inbreds under salinity stress. *Bangladesh J. Agric. Res.* **2016**, *40*, 529–536. [[CrossRef](#)]
47. Kamara, A.Y.; Kling, J.G.; Menkir, A.; Ibikunle, O. Agronomic performance of maize (*Zea mays* L.) Breeding lines derived from a low nitrogen maize population. *J. Agric. Sci.* **2003**, *141*, 221–230. [[CrossRef](#)]
48. Kandus, M.; Almora, D.; Ronceros, R.B.; Salenro, J.C. Statistical models for evaluating the genotype environment interaction in maize (*Zea mays* L.). *Phyton* **2010**, *79*, 39–46.
49. Abakemal, D.; Shimelis, H.; Derera, J. Genotype-by-environment interaction and yield stability of quality protein maize hybrids developed from tropical highland adapted inbred lines. *Euphytica* **2016**, *209*, 757–769. [[CrossRef](#)]
50. Amare, K.B.; Adisu, G. Adaptability and stability analysis of groundnut genotypes using AMMI model and GGE-biplot. *J. Crop. Sci. Biotechnol.* **2017**, *20*, 343–349.
51. Parag-Agarwal, S.S.; Verma, S.N.; Mishra Agrarwal, P. Phenotypic stability for different quantitative traits in maize hybrids. *Ind. J. Agric. Res.* **2000**, *34*, 107–111.
52. Malla, S.; Ibrahim, A.M.H.; Little, R.; Kalsbeck, S.; Glover, K.D.; Ren, C. Comparison of shifted multiplicative model, rank correlation, and biplot analysis for clustering winter wheat production environments. *Euphytica* **2010**, *174*, 357–370. [[CrossRef](#)]
53. Makumbi, D.; Diallo, A.; Kanampiu, K.; Mugo, S.; Karaya, H. Agronomic performance and genotype x environment interaction of herbicide-resistant maize varieties in Eastern Africa. *Crop. Sci.* **2015**, *55*, 540–555. [[CrossRef](#)]
54. Badu-Apraku, B.; Oyekunle, M.; Obeng-Antwi, K.; Osuman, A.; Ado, S.; Coulibaly, N.; Yallou, C.; Abdulai, M.; Boakyewaa, G.; Didjeira, A. Performance of extra-early maize cultivars based on GGE biplot and AMMI analysis. *J. Agric. Sci Camb.* **2012**, *150*, 473–483. [[CrossRef](#)]
55. Yan, W.; Tinker, N.A. Biplot analysis of multi-environment trial data: Principles and applications. *Can. J. Plant Sci.* **2006**, *86*, 623–645. [[CrossRef](#)]

## Article

# Uptake and Presence Evaluation of Nanoparticles in *Cicer arietinum* L. by Infrared Spectroscopy and Machine Learning Techniques

Feyza Candan <sup>1</sup>, Yuriy Markushin <sup>2</sup> and Gulnihal Ozbay <sup>3,\*</sup>

<sup>1</sup> Department of Biology, Faculty of Science and Letters, Manisa Celal Bayar University, 45140 Manisa, Turkey; feyza.candan@cbu.edu.tr

<sup>2</sup> Division of Physics, Engineering, Mathematics, and Computer Science, College of Agriculture, Science and Technology, Delaware State University, Dover, DE 19901, USA; ymarkushin@desu.edu

<sup>3</sup> Department of Agriculture and Natural Resources, College of Agriculture, Science and Technology, Delaware State University, Dover, DE 19901, USA

\* Correspondence: gozbay@desu.edu

**Abstract:** The aim of this work was to study the applicability of infrared spectroscopy combined with machine learning techniques to evaluate the uptake and distribution of gold nanoparticles (AuNPs) and single-walled carbon nanotubes (CNTs) in *Cicer arietinum* L. (chickpea). Obtained spectral data revealed that the uptake of AuNPs and CNTs by the *C. arietinum* seedlings' root resulted in the accumulation of AuNPs and CNTs at stem and leaf parts, which consequently led to the heterogeneous distribution of nanoparticles. principal component analysis and support vector machine classification were applied to assess its usefulness for evaluating the results obtained using the attenuated total reflectance-Fourier transform infrared spectroscopy method of *C. arietinum* plant grown at different conditions. Specific wavenumbers that could classify the different nanoparticle constituents of *C. arietinum* plant extracts according to their ATR-FTIR spectra were identified within three specific regions: 450–503 cm<sup>-1</sup>, 750–870 cm<sup>-1</sup>, and 1022–1218 cm<sup>-1</sup>, based on larger PCA loadings of *C. arietinum* ATR-FTIR spectra with distinct spectral differences between samples of interest. The current work paves a path to the future fabrication strategies for AuNPs and single-walled CNTs via plant-based routes and highlights the diversity of the applications of these materials in bio-nanotechnology. These results indicate the importance of family-plant selection, choice of methods, and pathways for the efficient biomolecule delivery, drug cargo, and optimal conditions in the wide spectrum of bioapplications.

**Keywords:** *Cicer arietinum* L.; gold nanoparticles; carbon nanotubes; ATR-FTIR spectroscopy; machine learning techniques; principal component analysis; support vector machine classification

**Citation:** Candan, F.; Markushin, Y.; Ozbay, G. Uptake and Presence Evaluation of Nanoparticles in *Cicer arietinum* L. by Infrared Spectroscopy and Machine Learning Techniques. *Plants* **2022**, *11*, 1569. <https://doi.org/10.3390/plants11121569>

Academic Editors: Milan S. Stankovic, Paula Baptista and Petronia Carillo

Received: 6 April 2022

Accepted: 7 June 2022

Published: 14 June 2022

**Publisher's Note:** MDPI stays neutral with regard to jurisdictional claims in published maps and institutional affiliations.



**Copyright:** © 2022 by the authors. Licensee MDPI, Basel, Switzerland. This article is an open access article distributed under the terms and conditions of the Creative Commons Attribution (CC BY) license (<https://creativecommons.org/licenses/by/4.0/>).

## 1. Introduction

Effects of nanoparticles (NPs) on biological systems and for the environment are known according to recent studies [1–5]. Plants are one of the most important organisms of our ecosystem and they also face toxicity caused by contamination of NPs in the soil. Thus, it is necessary to understand the interactions of NPs with plants, essential base components of all ecosystems [6–8]. On the other hand, as NPs are being increasingly used in many sectors of the industry, there is growing interest in the biological and environmental safety of their production by using plant extracts as a model system [9]. Considerably, studying all of these NPs-related topics will face challenges without having an efficient, robust, and cost-effective system to differentiate the NPs composition, and to identify the uptake and presence of SNPs inside the plants.

In the 21st century, many investigations have been related to the economic plants uptake, distribution, translocation, and accumulation of NPs, for example: silver NPs

(SNPs) in *Brassica juncea* and *Medicago sativa* [10], ceria NPs in cucumber [11], Au NPs in rice, radish, pumpkin, and perennial ryegrass [12], SNPs in wheat [13], Au NPs and SNPs in rice [14–16], AuNPs and CNTs in pea green [17,18], and SNPs in tomato [19].

*Cicer arietinum* L. is an annual plant from the Fabaceae family and it is one of the first plants cultivated in the world. Molecular analysis demonstrates that the *C. arietinum* is from the southeastern Anatolia region of Turkey, and the first information about the *C. arietinum* wild species in the world is documented from the Hacilar village in Turkey [20]. In this region, *C. arietinum* has been grown for about 7000–7500 years [21–23].

Because of its economic value (16.2 billion USD global trade in 2020) and its easy adaptive conditions for laboratory, *C. arietinum* was selected as a plant model to observe the absorption potential into the seeds and transportation-translocation of AuNPs and single-walled CNTs as regards the root, stem, and leaf of the *C. arietinum* seedlings. The spectral differences between the control group and Au NPs- or CNTs-exposed *C. arietinum* seeds obtained with ATR-FTIR were studied by employing machine learning techniques. Data obtained from the Au NPs- and CNTs-exposed seedlings and from the control samples were compared and evaluated according to Au NPs and CNTs concentration distribution-accumulation on the plant organs and their comparative significant importance, thus its general value in other perspectives.

Attenuated total reflectance-Fourier transform infrared spectroscopy (ATR-FTIR) has become an attractive analytical method because it can be used with a little or essentially no sample preparation, and analysis is relatively rapid [24]. These advantages and the small sample volume result in time and cost savings, which consequently lead to an increase in the number of analyzed samples. That is important for the future in-field applications.

Support vector machine (SVM) is a pattern recognition and classification method that is used widely in data mining applications for the purpose of supervised classification of data representing different classes of interest [25]. SVM is based on statistical learning to determine a hyperplane for optimal separation of classes. SVM uses an iterative training algorithm to achieve separation of different classes.

Principal component analysis (PCA) is typically used to provide a visual representation of the relationships between samples and variables and to combine samples into classes [26]. In this work, PCA was applied especially for the translation of spectroscopic data into lower dimensional space, and PCA score plots were used to objectively classify extract samples of *C. arietinum* plant, whereas SVM analysis allowed for the classification of the plant root, stem, and leaf extract samples based on the similarities of their spectroscopic properties (due to NPs components). The hypothesis of the study was to differentiate the NPs composition of the plant samples using *C. arietinum* as a model based on its spectroscopical data.

## 2. Materials and Methods

### 2.1. Seedling Growth and Extract Preparation

In our study, the water soluble single-walled CNTs functionalized with polyethylene glycol (PEG) obtained from Carbon Solutions at the concentration of 1.25 mg/mL in sterile distilled water was used for the seed-NPs exposure. We also used 10 nm of diameter Au NPs (optical density (OD) 1, stabilized suspension in 0.1 mM phosphate-buffered saline (PBS), reactant free). The Au NPs was obtained from Millipore Sigma and subsequently, a 4x-dilution with sterile distilled water was used for the seed-NPs exposure.

The following are CNT properties obtained from [27]: type of material P7-CNTs; individual tube lengths range from 0.5 to 3  $\mu\text{m}$  and have an average diameter of 1.4 nm. CNTs tend to occur as bundles with bundle lengths of 1–5  $\mu\text{m}$  and average bundle diameters of 2–10 nm and bundle length: 500–600 nm; bundle diameter: 4–5 nm [27]. The same commercial CNTs that we used in our work were characterized in [28]. In this work P7-CNTs were obtained from commercial P3-CNTs by derivatizing with PEG to give water solubility. According to [28], the characterization of P7-CNTs revealed that the zeta potential of CNTs in a pH range of the soil used in our work (from pH 6 to pH 8) is about  $-50$  mV.

The following are 10 nm diameter gold nanoparticles properties obtained from [28]: polydispersity index (PDI)  $\leq 0.2$ , core size: 8–12 nm, hydrodynamic diameter (Z): 11–25 nm; concentration of particles/mL:  $5.38 \times 10^{12}$ – $6.58 \times 10^{12}$ , absorption max: 510–525 nm, OD 1, zeta potential of  $-25.8$  mV at pH 7.4 in stabilized suspension in 0.1 mM PBS (reactant free) that we used in our work [29].

In the next step, 18 *C. arietinum* seeds (*cv.* dried raw garbanzo beans) were sterilized with sodium hypochlorite (7.5%) for 20 min. Subsequently, seeds were rinsed with autoclaved-distilled water 3 times and seeds were taken to sterile tubes for further analysis [30]. Later, 6 seeds were treated for duration of 2 days with 15 mL Au NPs (1.25 mg mL<sup>-1</sup>, 10 nm of diameter): water (group I). In parallel, 6 other *C. arietinum* seeds were treated with 15 mL CNTs (OD: 0.25): water for the duration of 2 days (group II); and 6 other *C. arietinum* seeds were used as control (group III) and seeds were treated with 15 mL pure water for duration of 2 days.

After 2 days, all three groups of seeds were planted into 0.5 L pots (10.5 cm  $\times$  9 cm) for 3 weeks in growth chamber ( $22 \pm 24$  °C, humidity = 60%, 10-h light period, intensity: 250  $\mu$ mol/m<sup>2</sup>/s). The residual water (group III) and two NPs solutions (group I and II) which remained in each tube after 2 days seeds NPs treated cultures were poured directly onto the seeds during planting process. All the groups were checked every 24 h and each pot was irrigated with 8 mL distilled water.

After 3 weeks, the control, Au NPs, and CNTs groups were photographed, and different parts of the *C. arietinum* plants (root, stem, and leaf) were sampled, and homogenized and washed by deionized water. Afterward, the samples were collected for centrifugal filtration, and for agitation, the plant samples were vortexed (10 s) and centrifuged for 30 min at the speed of 13,000 rpm (24 °C).

## 2.2. Data Collection and Analysis

For analysis of the ATR-FTIR spectral data, we used the multivariate data analysis and machine learning techniques using PCA and SVM. For this purpose, we utilized the Unscrambler software (CAMO Analytics). The SVM method was applied with the following parameters: SVM type: Classification (nu-SVC), Kernel type: Radial basis function, Gamma: 0.0005353319, Nu value: 0.5, Weights: All1.00, Cross validation segments: 10. We used 26 *C. arietinum* plant samples for multivariate data analysis, with 1868 variables representing ATR-FTIR spectral wavenumbers for the 400–4000 cm<sup>-1</sup> spectral range and 572 wavenumbers for the specific range from 400 to 1500 cm<sup>-1</sup>. The cross-validation procedure involved taking the training set and splitting it into 10 segments in a random way and then to be trained with the SVM algorithm on 9 parts to test on the 10th part.

In this study, the SVM classification method was used based on our previous comparisons among other classification methods such as K-nearest neighbor, classification and regression trees, neural networks, SVM, adaptive local hyperplane, and linear discriminant classifiers for spectroscopic data sets. Our previous studies strongly show that SVM is one of the most robust and accurate algorithms for spectroscopic data sets [24,31]. To minimize a very strong IR absorption of water in several regions related to its O–H stretching and different bending vibrations [32], we used dried samples for ATR-FTIR analysis. Nevertheless, some residual water might still be present in dried samples. It is well known that the general regions of the infrared spectrum in which various kinds of vibrational bands have been observed are associated to water molecule (i.e.,  $\sim 1595$ , and  $\sim 3657$  cm<sup>-1</sup>) [32]. Therefore, the spectra were collected over the range 400–1500 cm<sup>-1</sup> to minimize the potential influence of several regions related to O–H stretching and different bending vibrations of water molecule.

Finally, 5  $\mu$ L aliquots from each tested group were placed on the diamond crystal plate of the spectrometer and dried (room temperature for 30 min). The dried samples were subsequently analyzed by the ATR-FTIR (Nicolet 6700 ATR-FTIR Spectrometer from Thermo Electron Corporation, Waltham, MA, USA). Drops of the plant extract samples were deposited over an aperture on the top of the device, and the aperture was connected to

the surface of a diamond prism where the total reflection occurs. The ATR-FTIR spectra are collected with a resolution of  $4\text{ cm}^{-1}$ . A total of 100 scans were averaged for each spectrum. The background for the ATR-FTIR spectra is a spectrum of empty ATR crystal in the air.

### 3. Results

#### 3.1. Morphological Results

The physical interactions related to the Au NPs and CNTs in the water occur via passing the seed coat and semipermeable cell walls with the pure water. Since the seeds had no endosperm at the maturity stages in *C. arietinum*, two developed cotyledons interfaced with the NPs. Accordingly, the embryo of the seeds which were treated for 2 days with Au NPs and CNTs solutions through their development process had cotyledons, which gave the nutrients to the plumula (which gave nutrients to the stem), radicle (which gave nutrients to the root), and hypocotyl (which gave nutrients to the part between root and stem). These embryos interfaced the two tested NPs via the swollen cotyledons processes, and later, the NPs interfered with other parts of the plant through transport and development processes.

Bioimages revealed that our tested groups had different morphologies (Figure 1a,b), and the stem was growing more vertically and branched in our control plants (4.8–5.5 cm).

We also found that, among the tested groups, the highest stems (height: 14.8–26.2 cm) were recorded for the CNTs, and the most leaves and lateral branching were observed on stems with Au NPs (height: 15.2–17.8 cm) (Figure 1). In all three analyzed groups, the leaves had alternate arrangement, with an imparipinnate compound leaf shape, and serrate edges. We did not observe any morphological changes on the leaflets (foliole) in Au NPs and CNTs groups compared to the control. However, in all the AuNPs and CNTs samples, the imparipinnate leaves' number, size, and leaflets were increased in length and width, and leaflet colors were observed in dark green (Figure 1). The study of the root system in our analyzed groups revealed that even though the *C. arietinum* in our control group had a taproot rooting system consisting of primary root (0.9–4.6 cm) (Figure 1a (#1)) the Au NPs and CNTs groups had longer and more lateral roots. The lengths of the root were recorded as 5.3–7.2 cm and 1.8–3.9 cm, respectively, for Au NPs and CNTs.



**Figure 1.** Photos of typical *C. arietinum* seedling of the control group (#1 in frame (a)) and the sample treated with: Au NPs (#2 in frame (a)) and with CNTs (#3 and #4 in frame (b)) (Pictures taken by F. Candan).

The efficiency of the carbon nanoparticles (CNPs) was also studied on the morphology and physiology of *Vigna radiate* from the Fabaceae family. The results revealed the CNPs (100 to 150  $\mu\text{M}$ ) had a positive influence on the growth of the *V. radiate* and the plant biomass (fresh weight) increased 1.12-fold, total concentration and protein content also increased 1.9- and 1.14-fold, respectively [33].

### 3.2. Spectroscopic Results

It is documented that the NPs can be transported to the above-ground portion of the plants and to the shoots and leaves through the plant vascular systems [34]. The Au NPs and CNTs possible transportation and translocation from the roots to stem and ultimately to the leaves by vascular system was evaluated by analyzing the spectral data in our study (Figures 2 and 3). These data are presented in tables (Tables 1–3) and graphs (Figures 2 and 4–6). For this purpose, the ATR-FTIR results from the root, stem, and leaves in all of our tested groups were collected, and consequently the PCA-SVM technique was used to classify samples based on the spectral differences due to the presence of AuNPs or CNTs.

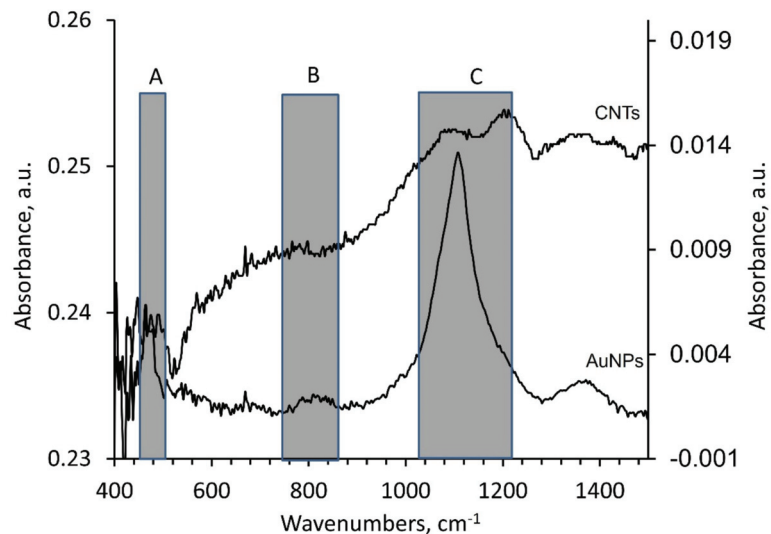


**Figure 2.** ATR-FTIR spectra of gold nanoparticles (AuNPs, right Y-axis) and carbon nanotube samples (CNTs, left Y-axis). Marked spectral ranges: (A) 450–503  $\text{cm}^{-1}$ , (B) 750–870  $\text{cm}^{-1}$ , (C) 1022–1218  $\text{cm}^{-1}$ .

Previously, we reported an efficient statistical framework for automatic classification of the ATR-FTIR spectra of various proteins which potentially can be used as biomarkers of ovarian cancer: monoclonal antibodies and antigens of ovarian cancer marker CA125, Osteopontin, Leptin, and insulin-like growth factor II [24]. We also applied this efficient established method in our lab for the classification of different plant extract samples (Figure 3). Through this framework, we follow several steps as follows: (1) dimensionality reduction (the number of wavenumbers in ATR-FTIR spectra is reduced using PCA method), (2) the obtained principal components values are used as an input for the classification of ATR-FTIR spectra.

PCA is a commonly used dimensionality reduction method [26]. By this method, the PCA analysis reduces the dimensionality of a dataset consisting of multiple interrelated variables and retaining of the variation present in the dataset. PCA creates the new variables by transforming the original variables in a dataset to a new set of variables, called the principal components (PC). The first PC typically accounts for the maximal variation of data.

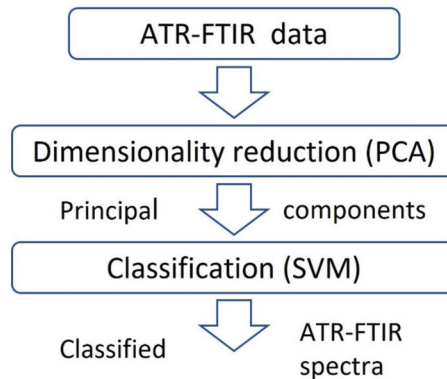


**Figure 3.** Statistical framework for automatic ATR-FTIR spectra classification (adapted from [24]).

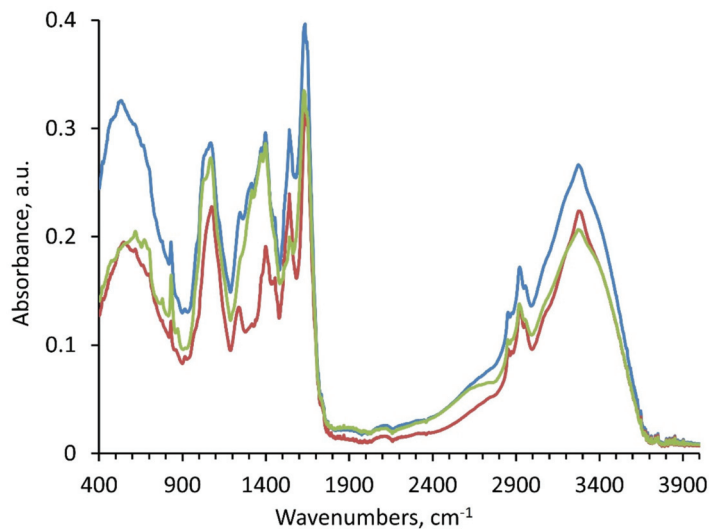


**Figure 4.** ATR-FTIR spectra of *C. arietinum* plant samples grown under the influence of Au NPs and CNTs. Note: Control—red line, Au NPs-treated plant—blue line, and CNTs-treated plants—green line. The ATR-FTIR clearly identified three tested groups.

We propose the identification of specific ATR-FTIR wavenumbers that could classify samples based on inclusion of AuNPs or CNTs from the aqueous extracts of *C. arietinum* grown under the influence of AuNPs or CNTs, based on the collection of ATR-FTIR spectra within three specific spectral ranges as follow, (A) 450–503  $\text{cm}^{-1}$ , (B) 750–870  $\text{cm}^{-1}$ , and (C) 1022–1218  $\text{cm}^{-1}$  (Figure 2). These spectral ranges were selected based on distinct spectral differences between the ATR-FTIR spectra of Au NPs and CNTs samples, which are important for the classification of the plant samples treated by NPs (Figure 2).

Figure 5 demonstrates the PCA loading plot in order to identify the variables (wavenumbers) with the largest effect on the studied NPs. In this regard, larger PCA loadings indicate that the variable strongly influences the component, and the PCA loadings close to 0 indicate the variable has a weak influence on the component. Table 1 shows the comparison of spectral ranges for PCA loading with stronger effect on the PC for the following classes of samples: (1) root samples of *C. arietinum* plant grown at three conditions (column 1 in Table 1) and (2) the specific ATR-FTIR spectral peaks/valleys of AuNPs- (column 2 in Table 1) and CNTs-standards (column 3 in Table 1).

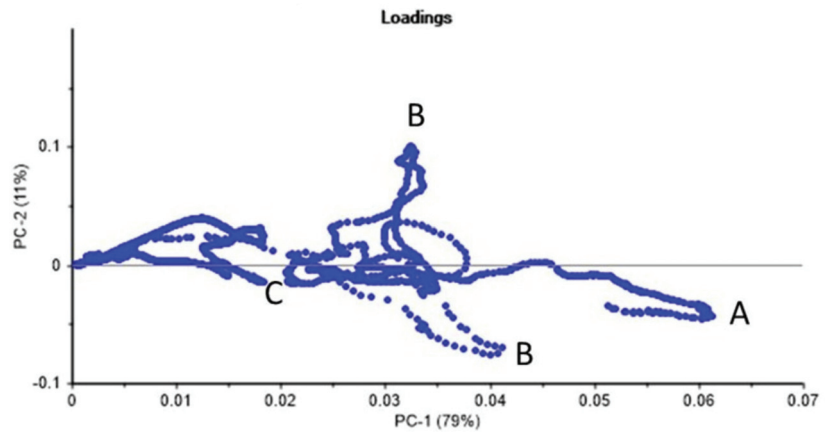


**Figure 5.** PCA loading ATR-FTIR spectral ranges (A, B, C) for *C. arietinum* root samples grown at three conditions (Class). See text and Table 1 for more details.

The variable PCA loadings for PC-1 and PC-2 presented in Figure 5 show peaks A, B, and C related to the following spectral ranges in Table 1 and in Figure 2: (1) range A at 450–503  $\text{cm}^{-1}$ ; (2) range B at 750–870  $\text{cm}^{-1}$ ; and (3) range C at 1022–1218  $\text{cm}^{-1}$ . We used these identified spectral ranges A, B, and C for the dimensionality reduction by PCA analysis and for the classification of the NPs-treated plant samples using the SVM method.

**Table 1.** Comparison of spectral ranges for PCA loading with stronger effect on the PC of the *C. arietinum* root samples grown under influence of NPs with the ATR-FTIR spectral peaks/valleys of AuNPs and CNTs standard samples. (A): Range A at 450–503  $\text{cm}^{-1}$ ; (B): range B at 750–870  $\text{cm}^{-1}$ ; and (C): range C at 1022–1218  $\text{cm}^{-1}$ .

Spectral Ranges for PCA Loading with Stronger Effect on the PC for <i>C. arietinum</i> Root Samples Grown under Influence of NPs, ( $\text{cm}^{-1}$ )	ATR-FTIR Peaks, AuNPs-Standard, ( $\text{cm}^{-1}$ )	ATR-FTIR Peaks/Valleys CNTs-Standard, ( $\text{cm}^{-1}$ )
450–503 (A)	450–503	490–560
750–870 (B)	750–870	790–850
1022–1218 (C)	1022–1218	1130–1260

Since the main purpose of the PCA is the dimensionality reduction of the spectral dataset, the purpose of using the SVM classification is to compute a separation hyperplane for optimal separation of the spectral data assigned to different classes, to maximize the minimal distance between points and the separation hyperplane [24,25]. Such constructed hyperplane provides the best generalization of unknown examples. SVM utilizes the structural risk minimization principle with the goal to achieve zero training error while minimizing the complexity of the model [24,25].

PC analysis has also been applied for the feature extraction of ATR-FTIR spectral data to visually demonstrate class separability (Figure 5). Note that dimensionality reduction is essential in classification [31]. The number of attributes can be large (e.g., 1868 variables representing ATR-FTIR spectral wavenumbers for the 400–4000  $\text{cm}^{-1}$  spectral range and 572 wavenumbers for the specific range from 400 to 1500  $\text{cm}^{-1}$ ). It is also known that not all the attributes available to a learning algorithm are useful [35].

In our study, we used the first two or three PCs for classification of experimental data, mostly because of our daily experience in inhabiting a space of three dimensions. Therefore, when researchers visually analyze the three-dimensional data (Figure 3), they implicitly

perform relevant discrimination leading to really good classification results with the visual inspection.

Figure 6 represents the PCA score graph of the first three PC for the ATR-FTIR spectral data of *C. arietinum*. Our results clearly demonstrated that even the first three PCs are sufficient to achieve separation of 2 NPs-based and 1 control group classes (blue squares for Au NPs, red circles for CNTs, and green triangles for control group) for ATR-FTIR spectral data of *C. arietinum* root (A), stem (B), and leaf (C) samples.

The first principal component in Figure 6A explains 79% of the variability, the second PC explains 11%, and the third only 6% of variability. Together, the first three PCs explain 96% of the variability. PC-1 in Figure 6B explains 92% of the variability, PC-2 explains 5%, and PC-3—only 2%. Together, the first three PCs explain 99% of the variability. At the same time, PC-1 in Figure 6C explains 86% of the variability, PC-2 explains 8%, and PC-3—only 3%. Together, the first three PCs explain 97% of the variability. As the explained variability values are close to 100% (e.g., 96%, 99%, and 97%), and in order to minimize the possible overfitting, the cross-validation for the SVM classification was performed.

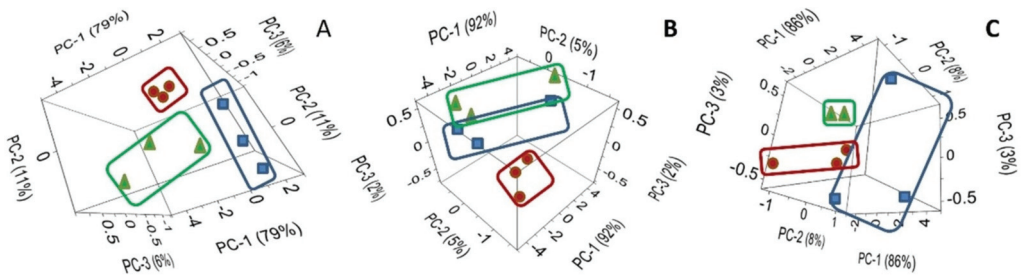


**Figure 6.** The PCA score graph of the first three PC for ATR-FTIR spectral data of *C. arietinum* root (A), stem (B), and leaf (C) samples grown in the presence of: (1) Au NPs (blue), (2) CNTs (red), and (3) control group (green).

Table 2 includes SVM classification for ATR-FTIR spectral data of *C. arietinum* samples (all plant parts combined for the analysis) grown at three conditions (Class): (1) Au NPs (CP Au NPs), (2) CNTs (CP CNTs), and (3) control ground (CP control). Correct SVM prediction is marked by the bold green fonts (green is correct prediction and red is wrong prediction). The SVM prediction matrix presented in Table 2 indicates the classification determined for each plant sample. From a total of 26 samples analyzed, 22 samples had correct SVM prediction of the class and 4 had incorrect SVM prediction of the class with total SVM prediction accuracy of about 85%. Therefore, the application of SVM is able to provide about 85% prediction accuracy on the *C. arietinum* samples grown at three conditions with all the plant parts combined for the analysis.

Table 3 presents the training and cross-validation accuracy of the SVM classification for ATR-FTIR spectral data of various plant parts of the *C. arietinum* samples grown at three conditions: (1) Au NPs, (2) CNTs, and (3) control ground. In this regard, Table 3 shows: 1st table row-data related to all plant parts analyzed; 2nd table row-data related to the plant root samples; and 3rd table row-data related to the plant stem samples.

The comparison of the cross-validation accuracy values for the root samples (~78%), the stem (~44%), and for the leaves (~33%) shows that the accuracy of the proposed model for the unknown samples was in good agreement with the possible translocation and accumulation pathway of nano-inclusions inside the plant structure (from root-to stem-to leaves). Larger cross-validation accuracy value for root samples is likely associated with larger concentration of Au NPs and CNTs in the root-extracts of *C. arietinum* plant grown at different conditions, as compared with the stem- or leaf-extracts.

**Table 2.** SVM classification for ATR-FTIR spectral data of *C. arietinum* samples (all plant parts combined for the analysis) grown at 3 conditions (Class): (1) Au NPs (Au NPs), (2) carbon nanotubes (CNTs) and (3) control ground (control). Correct SVM prediction is marked by the bold green font (green is correct prediction and red is wrong prediction).

Samples	Class	SVM Prediction
CP leaf1	Au NPs	Au NPs
CP root1	Au NPs	Au NPs
CP stem1	Au NPs	Au NPs
CP leaf1	CNTs	CNTs
CP root1	CNTs	CNTs
CP stem1	CNTs	CNTs
CP root1	control	control
CP stem1	control	Au NPs
CP leaf2	Au NPs	Au NPs
CP root2	Au NPs	Au NPs
CP stem2	Au NPs	control
CP leaf2	CNTs	control
CP root2	CNTs	CNTs
CP stem2	CNTs	CNTs
CP leaf2	control	control
CP root2	control	control
CP stem2	control	control
CP leaf3	Au NPs	Au NPs
CP root3	Au NPs	Au NPs
CP stem3	Au NPs	Au NPs
CP leaf3	CNTs	Au NPs
CP root3	CNTs	CNTs
CP stem3	CNTs	CNTs
CP leaf3	control	control
CP root3	control	control
CP stem3	control	control

Note: In the current study for the ATR-FTIR measurements, we used 9 plants grown in 3 different conditions (3 plants per each condition). From each plant, we collected 3 types of samples: leaf, steam, and root. The total is 27 samples. One control leaf sample was lost.

**Table 3.** Training and cross-validation accuracy of the SVM classification for ATR-FTIR spectral data.

Plant Parts	Training Accuracy	Cross-Validation Accuracy
All parts	84.62	61.54
Root	100	77.78
Stem	88.84	44.44
Leaf	100	33.33

Note: Data are presented as the mean value of various plant parts of the *C. arietinum* samples grown in 3 conditions: (1) Au NPs, (2) CNTs, and (3) control group. The results demonstrate the possibility of automatic classification of plants based on nanoparticle-inclusion in plant samples using PCA and linear SVM with accuracy of nearly 85%.

#### 4. Discussion

In our study, the obtained spectral data were in agreement with heterogeneous distribution of AuNPs and CNTs in *C. arietinum* seedlings' root, stem, and leaf (Figure 6, Table 3). Moreover, as it is clearly demonstrated in Figure 6, in the analysis of the PCA scores of the first three PCs for the ATR-FTIR spectral data of *C. arietinum*, even the first three PCs are sufficient to achieve the visual separation (clustering) of 2 NPs-based and 1 control group classes for ATR-FTIR spectral data of *C. arietinum* root, stem, and leaf samples (Figures 5 and 6).

By comparing the spectra of the Au NPs and CNTs samples (Figure 2), we identified three specific spectral ranges, 450–503  $\text{cm}^{-1}$ , 750–870  $\text{cm}^{-1}$ , and 1022–1218  $\text{cm}^{-1}$ , to be used for the dimensionality reduction by PCA and for the classification by SVM of the aqueous extracts of *C. arietinum* used as a model plant grown under influence of Au NPs and CNTs. Those spectral ranges were chosen based on larger PCA loadings of *C. arietinum* ATR-FTIR spectral ranges (Figure 5, Table 1), which also overlap with spectral ranges with distinct visual differences between spectra of Au NPs and CNTs samples (Figure 2). We hypothesize that the *C. arietinum* root samples demonstrate stronger PCA class separability than either the leaf or the stem samples, due to the most probable route of nanoparticulate transportation in plants. We also observed that the Au NPs and CNTs appeared in the spectral study differently (Figure 6B,C and Table 3). These differences might be related to possible variance of the chemical bonds created between NPs and the plant components or to photocatalytic effects or due to possible promotion of higher photosynthetic activity in the *C. arietinum* by CNTs [36].

Previously, it was shown in the AuNPs-exposed barley plants that the AuNPs were accumulated in the plants root up to a certain extent and it permanently inhibited the root growth [16]. Based on our findings, the Au NPs- and CNTs-exposure of *C. arietinum* seeds at our used concentration leads to an increase in the length of roots, stems, and leaves in *C. arietinum* Plant (Figure 1). The spectral results are in agreement with the hypothesis of more significant translocal distribution of AuNPs and CNTs in the root system of the plant than the leaf or the stem parts (Figure 6, Table 3). The difference of our results from the previous reported work [16] could be explained by the difference of the Au NPs size used in our study (10 nm of diameter), by the specific type of the plant family (Poaceae-Fabaceae), or based on the specific interactions of the monocotyl-dicotyl plants with our tested NPs.

Previously, in the work [37], different sizes of Au NPs (6–100 nm of diameter) were synthesized from *Lantana camara* (Verbenaceae family) leaf extracts by various methods and ATR-FTIR studies were done as well. Therefore, this plant was recommended for various medicinal and biomedical applications [37]. The ATR-FTIR results in our study also showed permissible results for our tested NPs (Figures 2, 5 and 6). At the same time, the Fabaceae (Leguminosae) family taxa is more common, it is easier to grow, and it has greater economic value when compared with the Verbenaceae family. Therefore, this type of plant can be recommended for nanotechnological applications.

It is known that cucumber seedlings treated with 7 nm of diameter ceria particles showed significantly higher ceria contents in both roots and shoots than those exposed to 25 nm of diameter ceria particles at all test concentrations. Only very limited amounts of ceria nanoparticles could be transferred from the roots to shoots because the entry of nanoparticles into the roots was difficult [11]. As is seen, diameters of NPs and nano-materials transport differentiation change from plant to plant. Because of that, our study provides valuable information about *C. arietinum*-Au NPs (10 nm of diameter) harmony and *C. arietinum*-CNTs harmony, which are both remarkable for other fields of study, especially for biomedical-based ones (Figures 5 and 6, Tables 1–3).

Effects of Au NPs (from 10 to 14 nm of diameter) on leaves and chloroplasts have been also studied with the conclusion that photosynthetic capacity is greater in the presence of Au NPs [38]. On the other hand, it was also demonstrated that CNTs are capable of developing the chloroplast carbon capture and photosynthesis by improving the chloroplast activities [39]. According to our study, even with a naked eye, leaves of seedlings treated with Au NPs and CNTs being dark green is the result of an increase in chloroplast caused

by physiologic activities in the plant (Figure 1) [5,40]. In addition to that, the detailed stereo microscopic analyses of the leaves also showed the same result. However, detailed comparative physiological studies are needed on this subject.

Cano et al. [41] studied CNTs and the effects on corn (*Zea mays* L.) relative to uptake, accumulation, and stress features. As a result, they reported that CNTs were taken up into corn roots, stems, and leaves, and that CNTs accumulated mostly in roots, with minimal accumulation in stems and leaves. All these results are in very good agreement with our study (Figure 6, Table 3), despite the different methods employed in both studies.

On the other hand, root nodules appeared as a result of root trichomes and soil bacterium synergy in Fabaceae family and then the nitrogen fixation could be provided to soil [42,43]. The increase of the lateral roots and correlatedly with the *Rhizobium* bacteria means that the particle concentration was shown to enhance all yields on the soil and under the soil development in a more effective way than lower concentrations of the CNTs or of the multiwalled CNTs. According to our study, increasing in lateral roots can be clearly seen in Figure 1. This information highlights the possible structural adaptation and correlations between *C. arietinum* and the microbial biota increasing by adding CNTs. On the other hand, our study shows the possibility of the CNTs application directly to seeds water solution, not to soil, which is cheaper and easier to implement in practice.

The limits of uptake of the metallic silver by two common metallophytes, *Brassica juncea* and *Medicago sativa*, and assessing of the form and distribution of the SNPs by the plants was also studied in [10]. According to this study, *M. sativa* belonging to Fabaceae family translocated more SNPs than *B. juncea* which belongs to Brassicaceae family [10]. *Medicago sativa* and *C. arietinum* plants showed a preference trend to SNPs and Au NPs and they both belong to the Fabaceae family. Thus, we recommend the *C. arietinum* as a potential metallophyte model in future studies (Tables 1–3, Figures 1, 2, 5 and 6).

The role of the Au NPs and CNTs in *C. arietinum* plant signal transduction between cells of the roots, stems, and leaves and developmental differences, especially in their physiology metabolism, can be studied further in light of the current investigation. However, this work showed that *C. arietinum* seeds are potentially capable of absorbing Au NPs and CNTs, with possible transfer and translocation pathways as it can be seen from the plant morphology and spectral graphs (Figures 1, 2, 5 and 6).

## 5. Conclusions

The present study relates to the applicability evaluation of infrared spectroscopy combined with machine learning techniques for monitoring the uptake and distribution of Au NPs and CNTs in *C. arietinum* samples. The results indicate that the principal component analysis of the infrared spectroscopic data leads to good classification results with the visual inspection. The obtained results further demonstrate the possibility of automatic classification of plant parts based on NPs-inclusion in plant samples using PCA and linear SVM with an accuracy of nearly 85%. It was also shown that application of the ATR-FTIR for NPs-inclusion in plant samples can potentially lead to the development of future analytical techniques and applications.

Additionally, the obtained results might be helpful in evaluating plants, especially economically valuable plants as an important component of the ecological systems and need to be considered when developing possible transportation and accumulation pathways of nanomaterials from the environment to the human body.

The results of the current study showed that rapid-growing plants such as Fabaceae family members such as *C. arietinum* might be useful in environmental remediation, phyto-remediation, and phyto-mining, since our study showed the transfer and translocation of NPs from the root system to the upper part (stem and leaves) of *C. arietinum*. Because of that, we recommend more studies on NPs combined with *C. arietinum* in other fields such as biomedical studies.

Moreover, the plant morphogenesis and differentiation are formations that are complementary to each other but essentially do not control each other, as their formations are

controlled by different genes or gene complexes. Therefore, it is thought that because of NPs accumulation observed in seedlings treated with Au NPs and CNTs, there might be remarkable change in the genes which control plant growth and differentiation. Consequently, we plan to carry out a complementary study to evaluate the *C. arietinum* samples of plants treated with Au NPs and CNTs by comparing them with the control group in terms of genetics.

**Author Contributions:** F.C. planned, initiated, conducted initial methods and analysis, analyzed the data, and was involved in manuscript preparation. Y.M. conducted spectroscopic analyses, provided resources and facilities, analyzed the data, and was involved in manuscript preparation. G.O. provided assistance with the logistics involved in preparing and analyzing the samples, provided resources and funding support, participated in spectroscopic analyses, and was involved in manuscript preparation. All authors have read and agreed to the published version of the manuscript.

**Funding:** This research received partial support by USDA NIFA Grant Awards# 2016-06642 and 2016-06476.

**Data Availability Statement:** Data generated in this article are available upon request from the authors. Authors' e-mail addresses are provided as: F. Candan at feyzacandan2002@yahoo.com; Y. Markushin at ymarkushin@desu.edu; and G. Ozbay at gozbay@desu.edu.

**Acknowledgments:** The authors would like to thank Qi Lu at the Department of Physics and Engineering in Delaware State University for providing resources and facilities for F. Candan to initiate this work and Aliya Lackings for her assistance with sampling and analyzing spectroscopic images. Special thanks to Ali Parsaeimehr for his thorough review and editing of our manuscript. The funding for the research was provided by USDA NIFA Grant Award# 2016-06642 and the undergraduate internship support by USDA NIFA Grant Award# 2016-06476.

**Conflicts of Interest:** The authors declare no conflict of interest.

## References

1. Monica, R.C.; Cremonini, R. Nanoparticles and higher plants. *Caryologia* **2009**, *62*, 161–165. [[CrossRef](#)]
2. Iravani, S. Green synthesis of metal nanoparticles using plants. *Green Chem.* **2011**, *13*, 2638–2650. [[CrossRef](#)]
3. Rico, C.M.; Majumdar, S.; Duarte-Gardea, M.; Peralta-Videa, J.R.; Gardea-Torresdey, J.L. Interaction of nanoparticles with edible plants and their possible implications in the food chain. *J. Agric. Food Chem.* **2011**, *59*, 3485–3498. [[CrossRef](#)]
4. Zaytseva, O.; Neumann, G. Carbon nanomaterials: Production, impact on plant development, agricultural and environmental applications. *Chem. Biol. Technol. Agric.* **2016**, *3*, 17. [[CrossRef](#)]
5. Candan, F. Plant Communities and Their Environment. In *Plant Phenology and an Assessment of the Effects Regarding Heavy Metals, Nanoparticles, and Nanotubes on Plant Development: Runner Bean, Artichoke, and Chickpea Seedlings*, 1st ed.; Oliveira, M.T., Candan, F., Fernandes-Silva, A., Eds.; IntechOpen Press: London, UK, 2020; pp. 3–25.
6. Stampoulis, D.; Sinha, S.K.; Whita, J.C. Assay dependent phytotoxicity of nanoparticles to plants. *Environ. Sci. Technol.* **2009**, *43*, 9473–9479. [[CrossRef](#)]
7. Schwab, F.; Zhai, G.; Kern, M.; Turner, A.; Schnoor, J.L.; Barriers, W. Pathways and processes for uptake, translocation and accumulation of nanomaterials in plants—Critical review. *Nanotoxicology* **2016**, *10*, 257–278. [[CrossRef](#)]
8. Bashri, G.; Parihar, P.; Singh, R.; Patel, A.; Prasad, S.M. Plant and nanoparticle interface at the molecular level: An integrated overview. *Nanomater. Plants Algae Microorg.* **2018**, *1*, 325–344.
9. Makarov, V.V.; Love, A.J.; Sinitsyna, O.V.; Makarova, S.S.; Yaminsky, I.V.; Taliansky, E.M.; Kalinina, O.N. Green nanotechnologies: Synthesis of metal nanoparticles using plants. *Acta Nat.* **2014**, *6*, 35–44. [[CrossRef](#)]
10. Harris, A.T.; Bali, R. On the formation and extent of uptake of silver nanoparticles by live plants. *J. Nanopart. Res.* **2008**, *10*, 691–695. [[CrossRef](#)]
11. Zhang, Z.; He, X.; Zhang, H.; Ma, Y.; Zhang, P.; Ding, Y.; Zhao, Y. Uptake and distribution of ceria nanoparticles in cucumber plants. *Metallomics* **2011**, *8*, 816–822. [[CrossRef](#)]
12. Zhu, Z.J.; Wang, H.; Yan, B.; Zheng, H.; Jiang, Y.; Miranda, O.R.; Rotello, V.M.; Xing, B.; Vachet, R.W. Effect of surface charge on the uptake and distribution of gold nanoparticles in four plant species. *Environ. Sci. Technol.* **2012**, *46*, 12391–12398. [[CrossRef](#)]
13. Dimkpa, C.O.; Mclean, J.E.; Martineau, N.; Britt, D.W.; Haverkamp, R.; Anderson, A.J. Silver nanoparticles disrupt wheat (*Triticum aestivum* L.) growth in a sand matrix. *Environ. Sci. Technol.* **2013**, *47*, 1082–1090. [[CrossRef](#)]
14. Koelmel, J.; Leland, T.; Wang, H.; Amarasiriwardena, D.; Xing, B. Investigation of gold nanoparticles uptake and their tissue level distribution in rice plants by laser ablation-inductively coupled-mass spectrometry. *Environ. Pollut.* **2013**, *174*, 222–228. [[CrossRef](#)]
15. Nair, P.M.G.; Chung, I.M. Physiological and molecular level effects of silver nanoparticles exposure in rice (*Oryza sativa* L.) seedlings. *Chemosphere* **2014**, *112*, 105–113. [[CrossRef](#)]

16. Feichtmeier, N.S.; Walther, P.; Leopold, K. Uptake, effects, and regeneration of barley plants exposed to gold nanoparticles. *Environ. Sci. Pollut. Res.* **2015**, *22*, 8549–8558. [[CrossRef](#)]
17. Candan, F.; Lu, Q. Anatomical Study on Translocation of Carbon Nanomaterials Distribution in Leaf and Stem of the Pea Green (*Pisum sativum*) Plant. In Proceedings of the 3rd International Symposium on EuroAsian Biodiversity, SEAB, Minsk, Belarus, 7–8 July 2017.
18. Candan, F.; Markushin, Y. Spectroscopic Study of the Gold Nanoparticles (AuNPs) Distribution in Leaf, Stem, and Root of the Pea Green (*Pisum sativum*) Plant. In Proceedings of the 3rd International Symposium on EuroAsian Biodiversity, SEAB, Minsk, Belarus, 7–8 July 2017.
19. Çekiç, F.Ö.; Ekinci, S.; İnal, M.S.; Ünal, D. Silver nanoparticles induced genotoxicity and oxidative stress in tomato plants. *Turk. J. Biol.* **2017**, *41*, 700–707. [[CrossRef](#)]
20. Helbaek, H. *Excavations at Hacilar*; Mellart, J., Ed.; University Press: Edinburgh, UK, 1970; pp. 189–244.
21. Van der Maesen, L.J.G. *Cicer L. A Monograph of the Genus with Spezial Reference to Chickpea (Cicer arietinum L.), Its Ecology and Cultivation*; Communications Agricultural University: Wageningen, The Netherlands, 1972; pp. 72–100.
22. Van der Maesen, L.J.G. *Cicer L. Origin, History and Taxonomy of Chickpea*. In *The Chickpea*; Saxena, M.C., Singh, K.B., Eds.; CABI International Publ.: Wallingford, UK, 1987; pp. 11–34.
23. Auckland, L.J.G.; Maesen, V.D. Chickpea. In *Hybridization of Crop Plants*; Walter, R.F., Hedley, H.H., Eds.; American Society of Agronomy and Crop Science Society of America: Madison, WI, USA, 1980; pp. 249–259.
24. Marcano, A.; Pokrajac, D.; Lazarevic, A.; Smith, M.; Markushin, Y.; Melikechi, N. *Statistical Analysis for Automatic Identification of Ovarian Cancer Protein-Biomarkers Based on Fast Fourier Transform Infrared Spectroscopy: Fourier Transforms-New Analytical Approaches and FTIR Strategies*; IntechOpen Press: London, UK, 2011; Chapter 8; pp. 147–166.
25. Vapnik, V. *The Nature of Statistical Learning Theory*; Springer: New York, NY, USA, 2000.
26. Jolliffe, I.T. *Principal Component Analysis*; Springer: New York, NY, USA, 2002.
27. Carbonsolution. Available online: <https://carbonsolution.com> (accessed on 5 April 2022).
28. Zhao, B.; Hu, H.; Yu, A.; Perea, D.; Robert, C.; Haddon, R.C. Synthesis and characterization of water soluble single-walled carbon nanotube graft copolymers. *J. Am. Chem. Soc.* **2005**, *127*, 8197–8203. [[CrossRef](#)]
29. Cytodiagnosics. Available online: [www.cytodiagnosics.com/collections/reactant-free-gold-nanoparticles/products/10nm-reactant-free-gold-nanoparticles?variant=31523912810570](http://www.cytodiagnosics.com/collections/reactant-free-gold-nanoparticles/products/10nm-reactant-free-gold-nanoparticles?variant=31523912810570) (accessed on 5 April 2022).
30. Demiray, H.; EşizDereboylu, A. Effects of excess and deficient boron and niacin on the ultrastructure of root cells in *Daucus carota* cv *nantes*. *Turk. J. Bot.* **2013**, *37*, 160–166.
31. Pokrajac, D.; Lazarevic, A.; Kecman, V.; Marcano, A.; Markushin, Y.; Vance, T.; Reljin, N.; McDaniel, S.; Melikechi, N. Automatic classification of laser-induced breakdown spectroscopy (LIBS) data of protein biomarker solutions. *Appl. Spectrosc.* **2014**, *68*, 1067–1075. [[CrossRef](#)]
32. Coker, D.F.; Reimers, J.R.; Watts, R.O. The Infrared Absorption Spectrum of Water. *Aust. J. Phys.* **1982**, *35*, 623–638. [[CrossRef](#)]
33. Shekhawat, G.S.; Mahawar, L.; Rajput, P.; Rajput, V.D.; Minkina, T.; Singh, R.K. Role of engineered carbon nanoparticles (CNPs) in promoting growth and metabolism of *Vigna radiata* (L.) Wilczek: Insights into the biochemical and physiological responses. *Plants* **2021**, *7*, 1317. [[CrossRef](#)]
34. Talebi, S.M. Nanoparticle-Induced Morphological Responses of Roots and Shoots of Plants. In *Nanomaterials in Plants, Algae, and Microorganisms*; Tripathi, D.K., Ahmad, P., Sharma, S., Chauhan, D.K., Dubey, N.K., Eds.; Academic Press: Cambridge, UK, 2017; Volume 1, pp. 119–141.
35. Duda, R.O.; Hart, P.E.; Stork, D.G. *Pattern Classification*; Wiley: New York, NJ, USA, 2001.
36. Giraldo, J.P.; Landry, M.P.; Faltermeier, S.M.; McNicholas, T.P.; Iverson, N.M.; Boghossian, A.A.; Reuel, N.F.; Hilmer, A.J.; Sen, F.; Brew, J.A.; et al. Plant nanobionics approach to augment photosynthesis and biochemical sensing. *Nat. Mater.* **2014**, *13*, 400–408. [[CrossRef](#)]
37. Dash, S.S.; Bag, B.G.; Hota, P. *Lantana camara* Linn leaf extract mediated green synthesis of gold nanoparticles and study of its catalytic activity. *Appl. Nanosci.* **2015**, *5*, 343–350. [[CrossRef](#)]
38. Torres, R.; Diz, V.E.; Lagorio, M.G. Effects of gold nanoparticles on the photophysical and photosynthetic parameters of leaves and chloroplasts. *Photochem. Photobiol. Sci.* **2018**, *17*, 505–516. [[CrossRef](#)]
39. Khatri, K.; Rathore, M.S. Plant Nanobionics and Its Applications for Developing Plants with Improved Photosynthetic Capacity. In *Photosynthesis: From Its Evolution to Future Improvements in Photosynthetic Efficiency Using Nanomaterials*; Cañedo, J.C.G., López Lizárraga, J.C.G., Eds.; IntechOpen Press: Rijeka, Croatia, 2018; pp. 95–112.
40. Candan, F.; Lu, Q. Comparative Effects of Gold (Au) and Carbon (C<sub>70</sub>) Nanomaterials Translocation on Chick pea (*Cicer arietinum* L.) Plant Morphology. In Proceedings of VIII International Symposium on Ecology and Environmental Problems, ISEEP, Çanakkale, Turkey, 4–7 October 2017.
41. Cano, A.M.; Kohl, K.; Deleon, S.; Payton, P.; Irin, F.; Saed, M.; Shah, S.A.; Green, M.J.; Cañas-Carrell, J.E. Determination of uptake, accumulation, and stress effects in corn (*Zea mays* L.) grown in single-wall carbon nanotube contaminated soil. *Chemosphere* **2016**, *152*, 117–122. [[CrossRef](#)]
42. Duke, J.A. *Handbook of Legumes of World Economic Importance*; Plenum Press: New York, NY, USA, 1981; pp. 52–57.
43. Singh, K.B. Chickpea (*Cicer arietinum* L.). *Field Crops Res.* **1997**, *53*, 161–170. [[CrossRef](#)]



Review

# Diaporthe citri: A Fungal Pathogen Causing Melanose Disease

Chingchai Chaisiri <sup>1,2,3</sup>, Xiangyu Liu <sup>1,2,3</sup>, Yang Lin <sup>2,3</sup> and Chaoxi Luo <sup>1,2,3,\*</sup>

<sup>1</sup> Key Lab of Horticultural Plant Biology, Ministry of Education, Wuhan 430070, China; chaisiri.ch@webmail.hzau.edu.cn (C.C.); xiangyuli@webmail.hzau.edu.cn (X.L.)

<sup>2</sup> Hubei Key Lab of Plant Pathology, Huazhong Agricultural University, Wuhan 430070, China; yanglin@mail.hzau.edu.cn

<sup>3</sup> College of Plant Science and Technology, Huazhong Agricultural University, Wuhan 430070, China

\* Correspondence: cxluo@mail.hzau.edu.cn

**Abstract:** Citrus melanose is a fungal disease caused by *Diaporthe citri* F.A. Wolf. It is found in various citrus-growing locations across the world. The host range of *D. citri* is limited to plants of the *Citrus* genus. The most economically important hosts are *Citrus reticulata* (mandarin), *C. sinensis* (sweet orange), *C. grandis* or *C. maxima* (pumelo), and *C. paradisi* (grapefruit). In the life cycle of *D. citri* throughout the citrus growing season, pycnidia can be seen in abundance on dead branches, especially after rain, with conidia appearing as slimy masses discharged from the dead twigs. Raindrops can transmit conidia to leaves, twigs, and fruits, resulting in disease dispersion throughout small distances. Persistent rains and warm climatic conditions generally favor disease onset and development. The melanose disease causes a decline in fruit quality, which lowers the value of fruits during marketing and exportation. High rainfall areas should avoid planting susceptible varieties. In this article, information about the disease symptoms, history, geographic distribution, epidemiology, impact, and integrated management practices, as well as the pathogen morphology and identification, was reviewed and discussed.

**Keywords:** citrus; melanose; *Diaporthe citri*; epidemiology; symptomatology

**Citation:** Chaisiri, C.; Liu, X.; Lin, Y.; Luo, C. *Diaporthe citri*: A Fungal Pathogen Causing Melanose Disease. *Plants* **2022**, *11*, 1600. <https://doi.org/10.3390/plants11121600>

Academic Editors: Milan S. Stankovic, Paula Baptista and Petronia Carillo

Received: 19 April 2022

Accepted: 12 June 2022

Published: 17 June 2022

**Publisher's Note:** MDPI stays neutral with regard to jurisdictional claims in published maps and institutional affiliations.



**Copyright:** © 2022 by the authors. Licensee MDPI, Basel, Switzerland. This article is an open access article distributed under the terms and conditions of the Creative Commons Attribution (CC BY) license (<https://creativecommons.org/licenses/by/4.0/>).

## 1. Introduction

### 1.1. Major Fungal Diseases on Citrus

Several citrus diseases are currently documented in China and around the world. The generally occurring fungal diseases include melanose, gummosis, and stem-end rot caused by *Diaporthe* spp.; branch cankers caused by *Botryosphaeriaceae* [1,2]; scab caused by *Elsinoë* spp. [3–9]; black rot caused by *Alternaria* spp. [10–14]; greasy leaf spot caused by *Cercosporoid* genus [15,16]; anthracnose caused by *Colletotrichum* spp. [17–25]; and blue and green mold caused by *Penicillium* spp. [26–28]. Among these fungal diseases, melanose, gummosis, and stem-end rot caused by *Diaporthe* spp. have a significant impact on citrus production [29,30]. At the same time, some *Diaporthe* spp. have also been reported as endophytes and/or saprobes on citrus [29–37].

Melanose disease was not a major problem in citrus crops prior to the 1990s. However, the accumulation of a large number of dead branches or trees results in an increase in fungal inocula in old citrus orchards worldwide. Currently, melanose has become the major fungal disease of citrus in China, dramatically reducing the commercial value of citrus fruits (Figure 1). *Diaporthe* spp., have been isolated from citrus hosts in many citrus-growing regions of China, e.g., Jiangxi, Zhejiang, Guangxi, Guangdong, Shaanxi, Fujian, Hunan, Chongqing, Yunnan, etc.

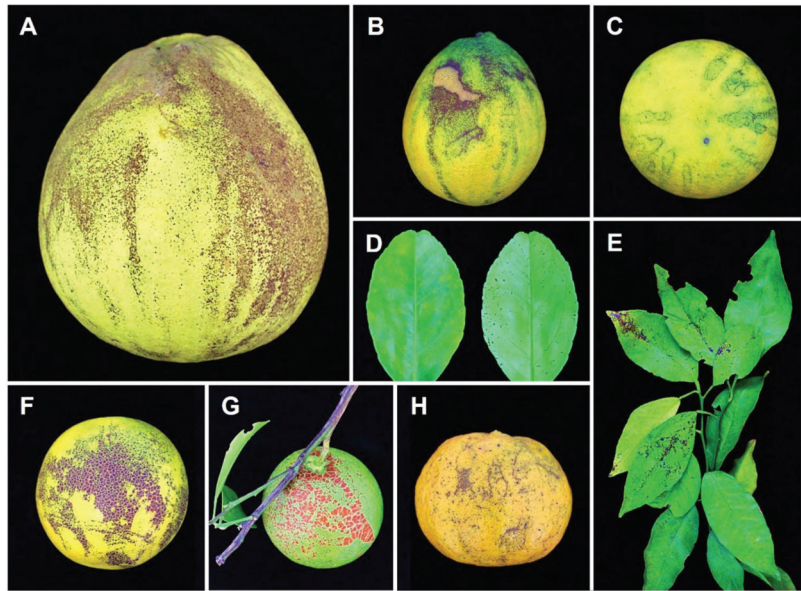


**Figure 1.** The typical symptoms of melanose disease in the field with different citrus tissue causal agents by *Diaporthe* species: (A) pumelo fruit (*C. maxima*) from Chongqing; (B,C) orange fruits (*C. sinensis*) from Chongqing; (D) young orange leaf (*C. sinensis* var. *Brasiliensis*) from Guizhou; (E) mandarin leaf (*Citrus* sp.) from Zhejiang; (F) orange fruits (*C. sinensis*) from Chongqing; (G) citrus fruit (*C. changshan-huyou*) from Zhejiang; and (H) mandarin fruit (*C. reticulata*) from Zhejiang.

### 1.2. *Diaporthe* Species Associated with Citrus

Previous studies about *Diaporthe* spp. have largely concentrated on species identification, especially the species associated with specific hosts. The molecular taxonomy of the genus *Diaporthe* related to citrus and allied taxa has made great advances in recent years. The phylogenies based on multiple loci provide a more robust and comprehensible taxonomy and nomenclature for *D. citri* and will serve as a starting point for field study by plant pathologists, breeders, and mycologists. Such information may be used to improve disease management and the deployment of citrus cultivars with species-specific and/or broad-spectrum resistance.

All citrus species, including grapefruit, clementine, lemon, lime, mandarin, orange, satsuma, and tangerine, are susceptible to melanose. *Phomopsis citri* was first recorded as a citrus parasitic fungus causing stem-end rot symptoms in Florida, USA [38]. Its teleomorph (sexual stage) is *D. citri* [39]. In addition to *D. citri*, many other *Diaporthe* species were also detected in citrus hosts. They could be pathogens, endophytes, or saprobes on citrus [29,31,40–45]. The summary of the global distribution of *Diaporthe* species associated with citrus hosts and their allied genera confirmed with DNA sequences is shown in Table 1.

**Table 1.** Summary of the global distribution of *Diaporthe* species associated with *Citrus* hosts and their allied genera confirmed with DNA sequences.

<i>Diaporthe</i> Species	<i>Citrus</i> Host and Allied Genera	Locality Distribution	Symptom/Tissue	Reference(s)
<i>D. apiculatum</i>	<i>Citrus grandis</i> cv. Tomentosa	China	non-symptom / twig	[34]
<i>D. aquatica</i>	<i>C. grandis</i> cv. Tomentosa	China	non-symptom / fruit	[34]
<i>D. arecae</i>	<i>C. grandis</i>	China	non-symptom / twig, leaf	[31]
	<i>C. limon</i>	China	non-symptom / branch	[31]
	<i>C. reticulata</i>	China	non-symptom / branch, twig	[31]
	<i>C. sinensis</i>	China	non-symptom / branch, twig	[31]
	<i>C. sinensis</i>	China	Decaying / fruit	[35]
<i>D. biconispora</i>	<i>C. unshiu</i>	Suriname	non-symptom / twig	[31]
	<i>C. grandis</i>	China	non-symptom / branch	[31]
	<i>C. sinensis</i>	China	non-symptom / branch	[31]
<i>D. biguttulata</i>	<i>Fortunella margarita</i>	China	non-symptom / branch	[31]
	<i>C. limon</i>	China	Melanose, stem-end rot, dead wood / fruit, leaf	[30,31,37,46]
<i>D. citri</i>	<i>C. reticulata</i>	China		
	<i>C. reticulata</i>	New Zealand	N.A. / stem	[37]
	<i>C. reticulata</i>	Portugal (Azores)	Blight / shoot	[47]
	<i>C. reticulata</i> cv. Nanfengmiju	China	Melanose / fruit, leaf, twig	[32]
	<i>C. sinensis</i>	Brazil	N.A. / fruit	[37]
	<i>C. sinensis</i>	China	Melanose / twig, leaf	[32,46,48]
	<i>C. sinensis</i>	USA, Florida	Stem-end rot / fruit	[30]
	<i>C. unshiu</i>	China	non-symptom / twig	[31]
	<i>C. unshiu</i> var. Juwadeun	Korea	N.A. / fruit	[37]
	<i>Citrus</i> sp.	USA, Florida	N.A. / leaf	[37]
<i>D. citriasiana</i>	<i>C. grandis</i> cv. Shatianyou	China	Anonymous spot / leaf	[31]
	<i>C. reticulata</i> cv. Nanfengmiju	China	Melanose-like / leaf	[32]
	<i>C. sinensis</i>	China	Melanose-like / leaf	[32]
	<i>C. unshiu</i>	China	Dead wood, non-symptom / branch, leaf	[30,31]
	<i>C. grandis</i>	China	non-symptom / branch	[31]
<i>D. citrichimensis</i>	<i>C. unshiu</i>	China	Dead wood, scab / branch, leaf	[30,31]
<i>D. cytosporella</i>	<i>Fortunella margarita</i>	China	non-symptom / branch	[31]
	<i>C. limon</i>	Spain	N.A. / fruit	[37]
	<i>C. limonia</i>	Italy	N.A.	[37]
	<i>C. sinensis</i>	USA, California	N.A. / twig	[37]
<i>D. discoidispora</i>	<i>C. reticulata</i> cv. Nanfengmiju	China	Melanose-like / fruit, leaf	[32]
	<i>C. sinensis</i>	China	non-symptom / twig	[30,31]
	<i>C. unshiu</i>	China	non-symptom / twig	[31]
<i>D. endocitricola</i>	<i>C. grandis</i> cv. Tomentosa	China	non-symptom / fruit	[34]

Table 1. Cont.

Diaporthe Species	Citrus Host and Allied Genera	Locality Distribution	Symptom/Tissue	Reference(s)
<i>D. endophytica</i>	<i>C. unshiu</i>	China	Scab/leaf	[31]
<i>D. eres</i>	<i>C. reticulata</i> cv. Nanfengmiju	China	Melanose-like/twig, fruit, leaf	[32]
	<i>C. unshiu</i>	China	Non-symptom/twig	[31]
	<i>Fortunella margarita</i>	China	Non-symptom/branch	[31]
	<i>Citrus</i> sp.	China	Non-symptom/branch, fruit	[31]
<i>D. foeniculina</i>	<i>C. aurantifolia</i>	Greece	Blight, canker/shoot, branch	[49]
	<i>C. aurantifolia-limon</i>	Greece	Blight, canker/shoot, branch	[49]
	<i>C. bergamia</i>	Greece	Canker/branch	[29]
	<i>C. japonica</i>	Malta	Dieback/twig	[29]
	<i>C. latifolia</i>	USA, California	N.A./trunk	[37]
	<i>C. limon</i>	Greece	Blight, canker/shoot, branch	[29,49]
	<i>C. limon</i>	Italy	Canker/trunk	[29]
	<i>C. limon</i>	Malta	Canker/trunk	[29]
	<i>C. limon</i>	New Zealand	N.A.	[37]
	<i>C. limon</i>	Portugal	Dieback/twig	[29]
	<i>C. limon</i>	Spain	Dieback/twig	[29]
	<i>C. limon</i>	Turkey	Rot/fruit	[50]
	<i>C. limon</i>	USA, California	N.A./branch	[29,37]
	<i>C. limon</i>	Lebanon	Blight/shoot	[42]
	<i>C. maxima</i>	Greece	Canker/branch	[29]
	<i>C. maxima</i>	Italy	Canker/branch	[29]
	<i>C. medica</i>	Greece	Blight, canker/shoot, branch	[49]
	<i>C. mitis</i>	Italy	Canker, dieback/branch, twig	[29]
	<i>C. paradisi</i>	Italy	Canker/branch	[29]
	<i>C. paradisi</i>	Malta	Canker/trunk	[29]
	<i>C. paradisi</i>	Portugal	Canker/branch	[29]
	<i>C. reticulata</i>	Greece	Canker/trunk	[29]
	<i>C. reticulata</i>	Italy	Dieback/twig	[29]
	<i>C. reticulata</i>	Italy	Dieback/twig	[29]
	<i>C. sinensis</i>	Spain	Dieback/twig	[29]
	<i>C. sinensis</i>	Iran	Non-symptom/leaf	[51]
	<i>C. sinensis</i>	Italy	Canker/branch, trunk	[29]
	<i>C. sinensis</i>	Malta	Canker/branch	[29]
	<i>C. sinensis</i>	Portugal	Canker, dieback/branch, twig	[29]
	<i>Microcitrus australasica</i>	Italy	Dieback/twig	[29]
	<i>Poncirus trifoliata</i> × <i>C. paradisi</i>	Greece	Blight, canker/shoot, branch	[49]
<i>D. foeniculina</i> ( <i>D. baccae</i> )	<i>C. limon</i>	Italy	Blight, canker/shoot, branch	[29]

Table 1. Cont.

Diaporthe Species	Citrus Host and Allied Genera	Locality Distribution	Symptom/Tissue	Reference(s)
	<i>C. paradisi</i>	Italy	Canker/branch	[29]
	<i>C. reticulata</i>	Italy	Canker/trunk	[29]
	<i>C. sinensis</i>	Italy	Canker, dieback/trunk, twig	[29]
<i>D. guangdongensis</i>	<i>C. grandis</i> cv. Tomentosa	China	non-symptom/fruit	[34]
<i>D. hongkongensis</i>	<i>C. grandis</i>	China	Non-symptom/twig	[31]
	<i>C. reticulata</i>	China	Scab/leaf	[31]
	<i>C. reticulata</i> cv. Nanfengmiju	China	Non-symptom/twig	[31]
	<i>C. sinensis</i>	China	Non-symptom/twig	[31]
	<i>C. unshiu</i>	China	Non-symptom/twig	[31]
<i>D. infertilis</i>	<i>C. sinensis</i>	Suriname	Decaying/fruit	[29,35]
<i>D. limonicola</i>	<i>C. grandis</i> cv. Tomentosa	China	non-symptom/fruit	[34]
	<i>C. limon</i>	Malta	Canker/branch, trunk	[29]
<i>D. masirevicii</i>	<i>C. grandis</i> cv. Tomentosa	China	non-symptom/fruit, twig	[34]
<i>D. melitensis</i>	<i>C. limon</i>	Malta	Canker/branch	[29]
<i>D. multiguttulata</i>	<i>C. grandis</i>	China	Non-symptom/branch	[31]
	<i>C. maxima</i>	China	Symptomatic/branches	[48]
<i>D. novem</i>	<i>C. aurantiifolia</i>	China	Dieback/twig	[29]
	<i>C. japonica</i>	Italy	Dieback/twig	[29]
	<i>C. limon</i>	Italy	Dieback/twig	[29]
<i>D. ovalispora</i>	<i>C. grandis</i> cv. Tomentosa	China	non-symptom/twig	[31]
<i>D. passifloricola</i>	<i>C. reticulata</i> cv. Nanfengmiju	China	non-symptom/fruit, twig	[34]
	<i>C. grandis</i> cv. Tomentosa	China	Stem-end rot/fruit	[52]
<i>D. persae</i>	<i>C. limon</i>	China	non-symptom/leaf	[34]
<i>D. pluscolorum</i>	<i>C. grandis</i> cv. Tomentosa	Cameroon	non-symptom/leaf	[41]
<i>D. sennae</i>	<i>C. sinensis</i>	China	non-symptom/fruit	[34]
<i>D. siamensis</i>	<i>C. limon</i>	China	Stem-end rot/fruit	[53]
<i>D. sojae</i>	<i>C. limon</i>	China	Non-symptom/twig	[31]
	<i>C. limon</i>	Cameroon	non-symptom/leaf	[41]
	<i>C. reticulata</i>	China	Non-symptom/twig	[31]
<i>D. subclavata</i>	<i>C. reticulata</i> cv. Nanfengmiju	China	Melanose-like, scab/twig, fruit, leaf	[31,32]
	<i>C. unshiu</i>	China	Non-symptom/twig	[31]
	<i>C. grandis</i> cv. Shatianyou	China	Unidentified symptom/fruit	[31]
	<i>C. unshiu</i>	China	Scab/leaf	[31]
<i>D. taicicola</i>	<i>C. sinensis</i>	China	Stem-end rot/fruit	[53]
<i>D. unshiuensis</i>	<i>C. reticulata</i> cv. Nanfengmiju	China	Melanose-like/fruit, twig	[32]
	<i>C. sinensis</i>	China	Melanose-like/twig, leaf	[32]
	<i>C. unshiu</i>	China	Unidentified symptom/fruit	[31]

Table 1. Cont.

<i>Diaporthe</i> Species	<i>Citrus</i> Host and Allied Genera	Locality Distribution	Symptom/Tissue	Reference(s)
<i>Diaporthe</i> sp.	<i>Fortunella margarita</i>	China	Non-symptom/branch	[31]
	<i>C. aurantium</i>	Taiwan	non-symptom/N.A.	[54]
	<i>C. limon</i>	India	Dieback/shoot, branch	[55]
	<i>C. limon</i>	Cameroon	non-symptom/leaf	[41]
	<i>C. reticulata</i>	Iran	non-symptom/N.A.	[56]
	<i>Fortunella margarita</i>	China	Non-symptom/branch	[31]

N.A.: not available.

### 1.3. Identification and Molecular Diagnostics

Citrus melanose is caused by *D. citri*, which belongs to Kingdom Fungi; Ascomycota; Sordariomycetes; Diaporthales; Diaporthaceae; *Diaporthe* [57–64]. The genus of *Diaporthe* was established by Nitschke [65]. *Phomopsis* is the anamorphic (asexual stage) name of *Diaporthe* [38,63,66–70]. The genus *Diaporthe* shows high species diversity; more than 1200 species named “*Diaporthe*” and about 1050 species named “*Phomopsis*” have been recorded in MycoBank lists (<http://www.mycobank.org>; accessed on 9 June 2021).

#### 1.3.1. Morphological Characteristics

For taxonomy of *Diaporthe* species, morphological characterization based on conidia morphology, fruiting body structure, and culture characteristics has been the basis of this study [71–74]. On PDA culture medium, mycelium is typically fan-shaped and white in color [75]. Teleomorphic ascomata, which are usually immersed in the substrate erumpent through pseudostromata mostly surrounding the ascomata, have more or less elongated perithecial necks. The pseudostromata are distinct and often delimited by dark lines [76]. The perithecia are circular, flattened at the base, with long black beaks [39,77]. The perithecia generally remain within the plant’s bark but protrude out of the stem surface, which makes them easily visible under a dissecting microscope. Asci are unitunicate and clavate to cylindrical, loosening from the ascogenous cells at an early stage and lying free in the ascocarp. Ascospores are biseriolate to uniseriate, and there are two oil droplets or guttulae within each cell, which are fusoid, ellipsoid to cylindrical, septate, straightly constricted at the septum, inequilateral or curved, hyaline, and sometimes with appendages [76,78]. Because ascospores are forcibly ejected from the asci, they become windborne and are responsible for the long-distance spread of the pathogen [39]. Upon finding a suitable substrate, spores may germinate, producing hyphae that quickly become septate mycelium [77].

The anamorphic state of this fungus is the most important stage for the disease cycle. The pycnidia (asexual fruiting bodies) of *D. citri* are scattered on the substratum and are dark in color, ovoid, thick-walled, and erumpent. Conidiophores are hyaline and branched, and occasionally, they are short and 1–2 septate. Conidiogenous cells were phialidic, hyaline, and slightly tapering toward the apex [30,37]. Generally, they are multiseptate and filiform with enteroblastic and monophialadic conidiogenesis [79,80]. It may produce three types of hyaline, non-septate conidia, namely, alpha, beta conidia [81], as well as an intermediate between these two conidial types, namely, gamma conidia [82–84]. The alpha conidia are functional, aseptate, single-celled, hyaline, fusiform, and usually biguttulate but sometimes lack guttula (lipid drop) or have more guttulae. The beta conidia tend to be produced in older pycnidia and are also aseptate, hyaline, long, slender, rod-shaped structures. They may be filiform and straight, but more often they are hooked at one end, lack guttula, and do not germinate [85]. The gamma conidia are hyaline, multiguttulate, fusiform to subcylindrical, with an acute or rounded apex, while the base is sometimes truncate [73,82–84,86,87]. The asexual morphology and cultural characteristics of *D. citri* are shown in Figure 2.

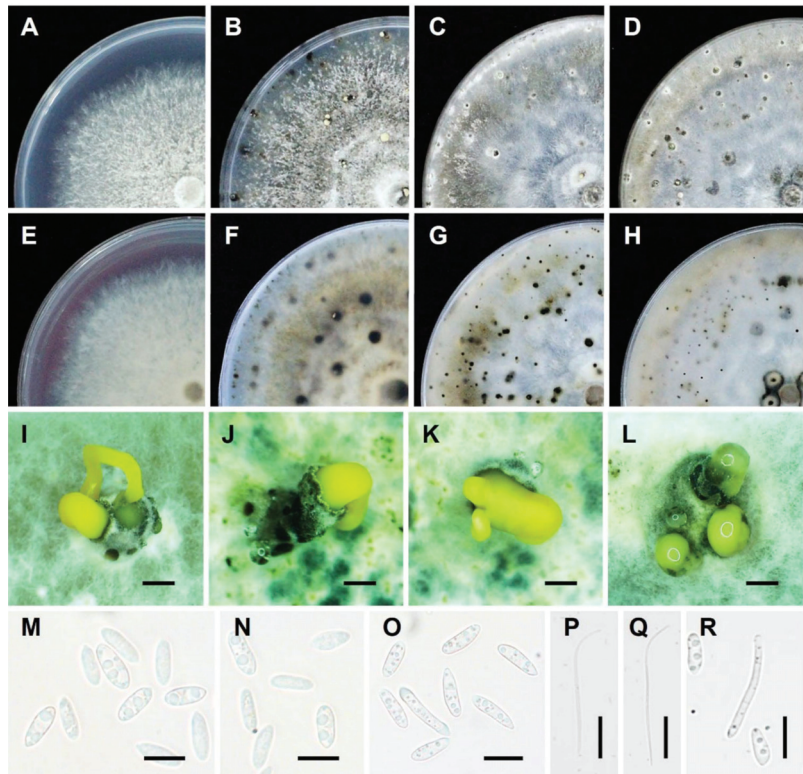


**Figure 2.** Asexual morphology and cultural characteristics of *D. citri*: (A,E) culture on PDA medium after 7 days; (B,F) culture on potato dextrose agar (PDA) medium after 30 days; (C,G) culture on corn meal agar (CMA) medium after 30 days; (D,H) culture on oatmeal agar (OMA) medium after 30 days; (I–L) conidiomata sporulating on PDA medium after 30 days; (M–O) Alpha conidia; (P,Q) Beta conidia; and (R) Alpha and Gamma conidia. Note: (A–D) surface and (E–H) reversed sides of colony culture. Scale bar: (I–L) = 200 µm; (M–R) = 10 µm.

### 1.3.2. Molecular Identification

Currently, four nuclear genome sequences of *D. citri* have been deposited in GenBank with the accession numbers JACTAD000000000, JADAZQ000000000, JADAZP000000000, and JADAZO000000000 for strains NFHF-8-4, ZJUD2, ZJUD14, and Q7, respectively [88,89]. The genome assembly sizes of ZJUD2 (59.5 Mp) and ZJUD14 (52.0 Mp) were relatively shorter, while NFHF-8-4 and Q7 contained longer assembly size (more than 63 Mp) [88,89].

Taylor et al. [90] proposed genealogical concordance phylogenetic species recognition (GCPSR), which compares individual gene sequences to find inconsistencies, and it has been shown to be very useful in defining species boundaries in morphologically conserved fungi [91]. Although each cluster in combined trees is usually considered a separate lineage, the common approach of concatenating sequenced data to delimit species without using the GCPSR principle overestimates the real diversity of species placement [91–96]. Since the widespread use of DNA sequences [35], genus *Diaporthe* species identification has progressed beyond host association and morphological characterization [73,81]. The *Diaporthe* genus is commonly represented by using traditional molecular barcoding for fungal species identification based on nuclear ribosomal internal transcribed spacer regions (ITS) [70,97–99]. As a result, some *Diaporthe* species have been reported to be perplexing, with contradictory findings when only the ITS sequence is used to produce a phylogenetic tree [35,67,99–102].

According to previous studies, multi-locus phylogenetic analysis has been proved more efficient to identify isolates at the species level [29,35,102–105]. Several loci, including large subunit of the ribosomal DNA (LSU), intergenic spacers of the ribosomal DNA (IGS), ITS, translation elongation factor 1- $\alpha$  gene (*TEF1- $\alpha$* ),  $\beta$ -tubulin gene (*TUB2*), histone 3 gene (*HIS3*), calmodulin gene (*CAL*), actin gene (*ACT*), DNA-lyase gene (*APN2*), 60S ribosomal protein L37 gene (*FG1093*), and mating type genes (*MAT-1-1-1* and *MAT-1-2-1*), are demonstrated as efficient tools to determine *Diaporthe* species. Even molecular sequences are already being used to identify species and rebuild phylogenies, complete genome sequences for *Diaporthe* species are still in the future. Currently, the most frequently used molecular loci in this genus are the ITS, *TEF1- $\alpha$* , *TUB2*, *HIS3*, and *CAL* [35,58,98,104]. Among them, *TEF1- $\alpha$*  is the most efficient tool in resolving the phylogenetic signal of the *D. eres* species complex [101,106]. Similarly, the highly variable *TEF1- $\alpha$*  was also shown to be the most efficient locus in distinguishing *Diaporthe* species [99,101,104,106,107]. Although the ITS region showed the relatively limited delimitation of *Diaporthe* species in phylogenetic analyses, it is still informative and should not be excluded from concatenation analysis of multi-locus DNA sequences [58,94,98,104]. A summary of universal and species-specific primers used for species determination within the *Diaporthe* genus is shown in Table 2.

**Table 2.** Summary of published universal primers and species-specific primers used for species determination within *Diaporthe* spp.

Gene/Locus <sup>1</sup>	Primer Name	Primer Sequences (5' to 3')	Reference
<i>ACT</i>	ACT-512F	ATGTGCAAGGCCGGTTTCGC	[108]
	ACT-783R	TACGAGTCCTTCTGGCCCAT	[108]
	ACT878R	ATCTTCTCC ATGTCGTCCCAG	[37]
<i>APN2</i>	apn2fw2	GCMATGTTYGAMATYCTGGAG	[101]
	apn2rw2	CTTGGTCTCCCAGCAGGTGAAC	[101]
<i>CAL</i>	CAL-228F	GAGTTCAAGGAGGCCTTCTCCC	[108]
	CAL-737R	CATCTTCTGGCCATCATGG	[108]
	CL1	GARTWCAAGGAGGCCTTCTC	[109]
	CL2A	TTTTTGCATCATGAGTTGGAC	[109]
	CAL563F	GACAAATCA CCACCAARGAGC	[37]
<i>FG1093</i>	FG1093 E1F1	GCGCCACAMCAAGWCSACRC	[110]
	FG1093 E3R1	TTCTBCGCTTGGCCTTCTCRS	[110]
<i>GAPDH</i>	Gpd1-LM	ATTGGCCGCATCGTCTTCCGCAA	[111]
	Gpd2-LM	CCCACCTCGTTGTCGTACCA	[111]
<i>HIS3</i>	CYLH3F	AGGTCCACTGGTGGCAAG	[112]
	H3-1b	GCGGGCGAGCTGGATGTCCTT	[113]
<i>IGS</i>	IGS-12a	AGTCTGTGGATTAGTGGCCG	[114]
	NS1R	GAGACAAGCATATGACTAC	[114]
<i>ITS</i>	ITS1	TCCGTAGGTGAACCTGCGG	[115]
	ITS-1F	CTTGGTCATTTAGAGGAAGTAA	[116]
	ITS4	TCCTCCGCTTATTGATATGC	[115]
	DcitriF	GTTTAACTACTGCGCTCGGGGTCCTG	[117]
	DcitriR	CTTACTGTTGCCTCGGCGCAGG	[117]
<i>LSU</i>	LSU1Fd	GRATCAGGTAGGRATACCCG	[118]
	LR5	TCCTGAGGGAAAACCTTCG	[119]
<i>MAT1-1-1</i>	MAT1-1-1FW	GCAAMIGTKTIKACTACA	[99]
	MAT1-1-1RV	GTCTMTGACCARGACCATG	[99]
	MAT1 141F	GGTCAAGAAGAAGAAGTCC	[120]
<i>MAT1-2-1</i>	MAT1-2-1FW	GCCCKCCYAAAYCCATTTCATC	[99]
	MAT1-2-1RV	TTGACYTCAGAAGACTTGGCGTG	[99]
<i>MS204</i>	MAT2 188F	CCAGCTCCATCACAAAC	[120]
	MS204 E1F1	AAGGGCACCTGGAGGGCCAC	[110]
<i>SSU</i>	MS204 E5R1	GATGGTGACGGYTTGATGTA	[110]
	NMS1	CAGCAGTGAGGAATATTGGTCAATG	[121]

Table 2. Cont.

Gene/Locus <sup>1</sup>	Primer Name	Primer Sequences (5' to 3')	Reference
<i>TEF-α</i>	NMS2	GCGGATCATCGAATTAATAACAT	[121]
	EF1-728F	CATCGAGAAGTTCGAGAAGG	[108]
	EF1-986R	TACTTGAAGGAACCCCTTACC	[108]
<i>TUB2</i>	EF-2	GGARGTACCAGTSATCATGTT	[122]
	Bt2a	GGTAACCAAATCGGTGCTGCTTTC	[113]
	Bt2b	ACCCCTCAGTGTAGTGACCCCTGGC	[113]
	TUBDcitri-F1	CCATTGACCATCTGCAACAT	[32]
	TUBD-R1	CCTTGGCCAGTTGTTTCC	[32]
	Dc-F	CCCTCGAGGCATCATTAC	[46]
	Dc-R	ATGTTGCAGATGGTCAAATGG	[46]
	Tub2FD	GTBCACCTYCARACCGGYCARTG	[123]
	T22	TCTGGATGTTGTTGGGAATCC	[124]
T1	AACATGCGTGAGATTGTAAGT	[124]	

<sup>1</sup> *ACT*: actin gene, *APN2*: DNA-lyase gene, *CAL*: calmodulin gene, *FG1093*: 60s ribosomal protein L37 gene, *GAPDH*: glyceraldehyde-3-phosphate dehydrogenase, *HIS3*: histone 3 gene, IGS: intergenic spacers of the ribosomal DNA, ITS: nuclear ribosomal internal transcribed spacer, LSU: large subunit of the ribosomal DNA, *MAT-1-1-1/MAT-1-2-1*: mating type genes, *MS204*: guanine nucleotide-binding protein subunit beta-like protein gene, SSU: small subunit 18S ribosomal RNA, *TEF1-α*: translation elongation factor 1-α gene, and *TUB2*: β-tubulin gene.

### 1.3.3. Molecular Diagnosis

A conventional species-specific PCR method has been developed to distinguish *D. citri* from other *Diaporthe* species [32,46,117]. The PCR-based technique showed outstanding specificity and sensitivity, indicating that it may be used to effectively detect *D. citri* in practice. Effective PCR with citrus tissues infected by *D. citri*, as well as modern PCR, isothermal amplification, or any technique that is fast, low-cost, and accurate for alternative detection of certain diseases, should be developed, because such methods may also be applied for phytosanitary detection in plant quarantine.

### 1.3.4. Genetic Populations

Although *D. citri* and other *Diaporthe* infections are well-known, information about their diversity, population genetics, reproductive methods, and pathogenicity is limited [125,126]. Our understanding of the infection process, host range, and fungicide resistance of *D. citri* would improve if we understood its population genetics in nature. Such information is also useful for making long-term management strategies for this disease [127–129]. In China, the population genetics of *D. citri* was analyzed by using polymorphic simple sequence repeat (SSR) markers and the mating type idiomorphs. The majority of the analyzed samples came from southern China, including Fujian, Zhejiang, Jiangxi, Hunan, and Guizhou provinces. It was shown that alleles at the 14 SSR loci were not substantially different from linkage equilibrium, and most subpopulations exhibited equal frequencies of the two mating types. The findings suggest that teleomorphic reproduction is important in *D. citri* populations in southern China, and the ascospores seem to be a major contributor to citrus disease [46]. The presence of significant genetic differences among different geographical populations, however, does not eliminate the possibility of migration. Closely related strains were detected from many geographically diverse regions. They also found signs of genetic mixing between two extremely distinct genetic populations. These findings imply that *D. citri* populations are evolving, which might be accelerated by either increasing human impacts through frequent citrus seedling exchange or by global climate change [46].

## 2. Epidemiology, Life Cycle, and Symptomatology

Citrus melanose is caused by *D. citri*, which attacks foliage, fruits, and twigs when they are immature. Since mature tissues are more immune to pathogen attack, the first 8 to 9 weeks of the citrus growing season are the most vulnerable to pathogen attack. Melanose

signs can differ depending on the severity of the infection. At the end of the susceptibility cycle, the flyspeck melanose symptoms appear [130,131].

The fungal inocula can be scattered over a wide range since ascospores are released forcefully and can be spread over a long distance. *D. citri* is primarily a saprophyte that feeds on and receives its nutrition from dead wood [44,132]. Perithecia and pycnidia are only found on dead and dying twigs and fruits showing stem-end rot. The conidia provided by pycnidia are the primary source of inoculum [133]. Ascospores are ejected forcibly and play a significant role in long-distance dispersal [132]. As a result of the widespread dissemination of a vast number of ascospores, the number of cases of infection is rising [134]. When ascospores or conidia of *Diaporthe* land on the surface of a plant, the disease will be triggered. Pathogens thrive in dry environments with temperatures ranging from 17 to 35 °C [44].

The germination of spores requires approximately 10 to 24 h of moisture, depending on the temperature [44,134], and the germination and formation of a germ tube takes 36 to 48 h [133]. After that, the citrus melanose pathogen directly penetrates the cuticle layer tissue and infects the plant.

*D. citri* could overwinter on debris, e.g., mummy fruits, dead stems, branches, and dry leaves. Perithecia could form on debris next year. Ascospores are produced in proportion to the amount of dead wood present in a canopy. These spores contribute slightly to the disease severity of an orchard, but they are carried by the wind and spread across long distances. Conidia, developed in mature pycnidia, can continuously infect citrus during the growing season. Conidia can be dispersed to nearby citrus trees with raindrops, which most probably cause the majority of fruit infections (Figure 3). Nevertheless, conidia can also be transmitted through the air over long distances when rainfall is scarce.

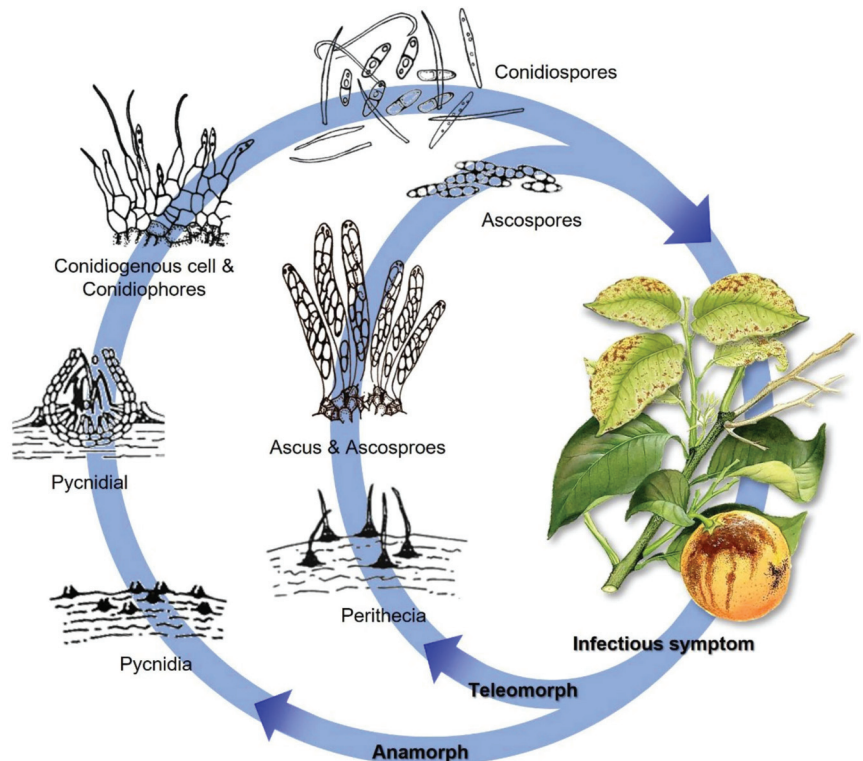


**Figure 3.** Representative *Diaporthe* disease cycle: melanose disease cycle on citrus caused by *D. citri*. Revised and redrawn from Burnett [135], Timmer et al. [75], and Udayanga et al. [63].

Symptoms appear as discrete small, sunken, brown spots about one week after infection, which later become raised and filled with reddish-brown gum. The leaf pustules are initially surrounded by a yellow halo. Diseased areas regreen later and create corky pustules. On fruits, pustules can grow relatively large and can crack, creating a pattern of mudcake. The severity of the disease is determined mainly by the amount of inoculum-bearing dead wood in the canopy of the tree and the duration of the wetting period following rainfall or sprinkler irrigation. Wet, rainy conditions, especially when rain showers occur late in the day, and fruits staying continuously wet on warm nights are conducive to infection.

### 3. Geographic Distribution and Host Associations

The USDA's Agricultural Research Service's Systematic Mycology and Microbiology Laboratory (SMML database: <https://nt.ars-grin.gov/fungalatabases/>, accessed on 10 December 2021) and the Centre for Agriculture and Bioscience International (CABI database: <https://www.cabi.org/isc/>, accessed on 15 January 2022) obtained some information about *D. citri*, including the geographic distribution and host associations. According to the SMML and CABI databases, *D. citri* has been discovered on citrus hosts and related species all over the world. The *D. citri* is the most predominant species in the *Diaporthe* genus, which occurs widely in citrus-growing countries, e.g., China, Philippines, Japan, Korea, Thailand, Myanmar, Cambodia, Fiji, Mauritius, United States, Mexico, Haiti, Cuba, Dominican Republic, Panama, Puerto Rico, Venezuela, Trinidad and Tobago, Brazil, Cyprus, Portugal (Azores Islands), New Zealand, Niue, Samoa, Tonga, Cook Islands, Cote d'Ivoire, and Zimbabwe, which has also been summarized previously [32]. A global geographic distribution map of *D. citri* associated with the citrus hosts is available on the CABI database (accessed and last modified on 16 November 2021) and is shown in Figure 4. The green disease-free areas may mean that no data is in the CABI database, but this does not necessarily mean that the disease is absent.

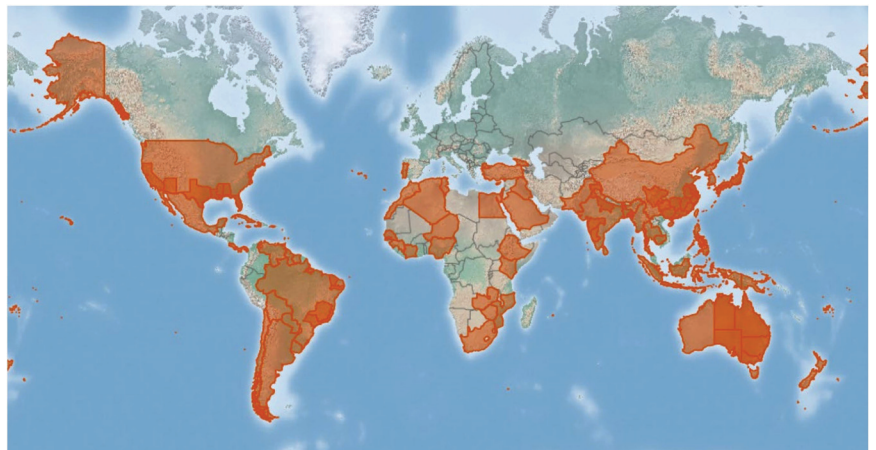


**Figure 4.** A global geographic distribution map of *D. citri* associated with the citrus-host plant is available on the CABI database.

### 4. Main Management Approaches of Melanose Disease

The yield is almost unaffected by melanose disease, and the juice processing is unaffected as well. However, the quality of the fruit for marketing and exportation suffers the consequences. In order to avoid poor quality and fruit deterioration caused by citrus melanose, integrated management practices should be implemented. Integrated pest management (IPM) is now largely recognized as the most effective way to protect plants. Its ultimate objective will be to maintain pest populations below economically injurious levels

without or just with minimal pesticides. Although IPM must rely on pesticides currently, minimizing chemical inputs while maintaining crop quality at an economically viable level is a basic requirement for plant protection. To achieve this goal, it is critical to understand the disease epidemiology at various points in time while performing pest control [132,136].

Currently, no resistance cultivars are available for melanose control in practice. The removal of dead wood to reduce the pressure of melanose fungus is both time-consuming and labor-intensive. Nevertheless, pruning dead branches should be performed on a regular basis. Proper pruning enhances air circulation within the canopy of the plant, keeping it dry and reducing opportunities for pathogens to survive and cause infections. It will also improve the effectiveness of fungicide infiltration into the foliage [43,137]. Furthermore, avoid planting sensitive citrus cultivars or species in high-rainfall zones, such as sweet orange, grapefruit, and pumelo [137,138]. Other management practices, such as citrus plantations in low-rainfall and sunny zones, should be implemented. Interplanting citrus with non-susceptible hosts is also a feasible measure [137,139].

#### 4.1. Chemical Control

Application of fungicides is still the most commonly used method to control melanose disease on citrus. Many fungicides have been tested for melanose control. Copper is a protective compound, which forms a layer on the surface of plant tissue, e.g., fruit, protecting it from infection. The gap in the protective copper layer, however, grows larger as the fruit grows and expands. If conditions are favorable for the pathogen infection, the copper layer needs to be renewed through another spray. The melanose fungus stored in dead wood is slightly affected by copper spraying. The use of copper fungicides before flowering will not reduce infection. A copper fungicide must be applied on the fruit surface to provide efficient melanose control. In the case of serious infection in late summer, additional protectant spray should be applied [140]. Applications of pyraclostrobin to the spring flush growth of citrus trees are much more efficient for controlling melanose, scab, and *Alternaria* brown spot than those of famoxadone or copper hydroxide [44,141–144]. Bushong and Timmer [145] demonstrated that azoxystrobin was a highly effective preventative spray for melanose, whereas benomyl and fenbuconazole were not. As post-infection treatments for melanose, none of the fungicides are successful. In Japan, dithianon and mancozeb were used to spray alternately from June to August to control this disease [146]. In Pakistan, five chemicals were tested at recommended doses, including penflufen, copper hydroxide, tebuconazole plus trifloxystrobin, and difenoconazole, for controlling melanose disease. When used as a protectant, copper hydroxide was found to be the most effective for the management of citrus melanose [147]. Whereas Anwar et al. [148] evaluated six different fungicides for citrus melanose control, the use of mancozeb led to a significant inhibition of fungal growth. Similarly, several chemicals, including mancozeb and fenbuconazole, were found to be effective in controlling citrus melanose in China and other countries [40,43,148–150].

#### 4.2. Biological Control

Although chemical control plays an important role in managing plant diseases, overuse of chemical pesticides has raised severe issues about food contamination, environmental pollution, and phytotoxicity. Biocontrol is a viable option as it is friendly to the environment. Biological control of plant diseases with antagonistic bacteria is a viable alternative to chemical control. Many antagonistic bacteria are known to play important roles in the sustainability of natural ecosystems, and some of them can be employed as inoculants to stimulate plant growth and resistance.

For melanose control, more and more biocontrol candidates have been developed, e.g., *Burkholderia gladioli*: TRH423-3, MRL408-3, *Pseudomonas pudia*: THJ609-3, and *P. fluorescens*: TRH415-2, and selected for their antifungal effectiveness against *D. citri* using dual-culture testing. Disease suppression was observed after pretreatment with the rhizobacterial strains, with varying degrees of protection rates for each rhizobacterial strain. Following the pathogen inoculation, subsequent treatment with the rhizobacterial strains

also enhanced protection rates. The rhizobacterial strains might be especially useful in organic citrus production where chemicals are strictly forbidden [151]. Similarly, pretreatment with *P. putida* strain THJ609-3 resulted in a decreased disease incidence. When the infection behaviors of *D. citri* and necrosis deposits on plant tissues were examined using a fluorescent microscope, it was shown that the process of disease development was reduced after being treated with the bacterial strain, especially the conidia germination rates, which were significantly lower after being pretreated with the strain THJ609-3. Furthermore, morphological abnormalities of the germ tubes were also observed. These results pointed to the bacterial-direct antifungal action on the leaf surfaces as a potential cause of disease reduction [152]. *Thiobacillus* species were used to generate bio-sulfur, which was investigated as an alternative to managing citrus melanose. It was found that melanose disease severity was lower on bio-sulfur pretreated citrus leaves than on untreated leaves, suggesting that bio-sulfur might be applied as an environmentally friendly alternative to control citrus melanose [153]. *Bacillus velezensis* CE 100, an effective biocontrol agent, has been used to control *D. citri*. In dual culture plates, *D. citri* mycelial growth was significantly suppressed by strain CE 100, suggesting that some volatile substances inhibited the growth of *D. citri*. It was also observed that the bacterial culture filtrate (BCF) of strain CE 100 inhibited *D. citri* growth. Microscopic examination indicated that BCF had a substantial impact on the pathogen hyphal shape, most probably the result of numerous cell-wall disintegrating enzymes and metabolites generated by strain CE 100. Interestingly, *D. citri* conidial germination was decreased by approximately 80% when 50% BCF of strain CE 100 was used [154].

## 5. Conclusions

In this paper, the history of citrus melanose, pathogen morphology, molecular identification, population studies, epidemiology of disease symptoms and life cycle, global distribution, and integrated disease management are documented. At present, there are no cases of plants bred or engineered specifically for resistance to diseases caused by *D. citri*. Does the teleomorph *D. citri* have higher opportunities for surviving on different hosts? Does genetic recombination play an important role in survival or in variability in this species? Are teleomorph ascospores spread differently from anamorphic conidia? Do ascospores and conidia infect citrus tissues in the same way? Which defense reactions occur in infected plants? At what level is the pathogen *D. citri* recognized by the plant? Are signal cascades of defensive reactions known? These are some of the questions about pathogen epidemiology that still need to be answered as they directly impact disease management. However, more understanding of the molecular mechanisms that confer virulence on *D. citri* is helpful in the development of alternative disease management strategies, especially when it is urgent to develop environmentally friendly approaches or tools to maintain the plant health in the future.

**Author Contributions:** Conceptualization, C.C.; writing—original draft preparation, C.C. and X.L.; writing—review and editing, C.C., X.L., Y.L. and C.L.; supervision, C.L.; project administration and funding acquisition, Y.L. and C.L. All authors have read and agreed to the published version of the manuscript.

**Funding:** This study was funded by the Fundamental Research Funds for the Central Universities (No. 2662020ZKPY018) and the National Key Research and Development Program of China (No. 2017YFD020200103).

**Institutional Review Board Statement:** Not applicable.

**Informed Consent Statement:** Not applicable.

**Data Availability Statement:** Not applicable.

**Acknowledgments:** The authors would like to thank Margaret Senior (<https://www.dpi.nsw.gov.au/about-us/services/collections/scientific-illustrations/senior/citrus/melanose-citrus> (accessed on 1 June 2021); Department of Primary Industries, Government of New South Wales) for providing

an illustration of melanose infected by *D. citri* to re-draw the general life cycle of citrus melanose disease. The authors also sincerely thank the reviewers for their contributions during the revision process.

**Conflicts of Interest:** The authors declare no conflict of interest. The funders had no role in the design of the study; in the collection, analyses, or interpretation of data; in the writing of the manuscript or in the decision to publish the results.

## References

1. BeZerra, J.D.P.; Crous, P.W.; Aiello, D.; Gullino, M.L.; Polizzi, G.; Guarnaccia, V. Genetic diversity and pathogenicity of *Botryosphaeriaceae* species associated with symptomatic citrus plants in Europe. *Plants* **2021**, *10*, 492. [[CrossRef](#)] [[PubMed](#)]
2. Xiao, X.E.; Wang, W.; Crous, P.W.; Wang, H.K.; Jiao, C.; Huang, F.; Pu, Z.X.; Zhu, Z.R.; Li, H.Y. Species of *Botryosphaeriaceae* associated with citrus branch diseases in China. *Persoonia* **2021**, *47*, 106–135. [[CrossRef](#)]
3. Chung, K.R. *Elsinoë fawcettii* and *Elsinoë australis*: The fungal pathogens causing citrus scab. *Mol. Plant Pathol.* **2011**, *12*, 123–135. [[CrossRef](#)]
4. Fan, X.L.; Barreto, R.W.; Groenewald, J.Z.; Bezerra, J.D.; Pereira, O.L.; Cheewangkoon, R.; Mostert, L.; Tian, C.M.; Crous, P.W. Phylogeny and taxonomy of the scab and spot anthracnose fungus *Elsinoë* (*Myriangiiales*, *Dothideomycetes*). *Stud. Mycol.* **2017**, *87*, 1–41. [[CrossRef](#)] [[PubMed](#)]
5. Gopal, K.; Govindarajulu, B.; Ramana, K.T.V.; Kumar, C.S.K.; Gopi, V.; Sankar, T.G.; Lakshmi, L.M.; Lakshmi, T.N.; Sarada, G. Citrus scab (*Elsinoë fawcettii*): A review. *J. Agric. Allied Sci.* **2014**, *3*, 49–58.
6. Hyun, J.W.; Yi, S.H.; MacKenzie, S.J.; Timmer, L.W.; Kim, K.S.; Kang, S.K.; Kwon, H.M.; Lim, H.C. Pathotypes and genetic relationship of worldwide collections of *Elsinoë* spp. causing scab disease of citrus. *Phytopathology* **2009**, *99*, 721–728. [[CrossRef](#)]
7. Miles, A.K.; Tan, Y.P.; Shivas, R.G.; Drenth, A. Novel pathotypes of *Elsinoë australis* associated with *Citrus australasica* and *Simmondsia chinensis* in Australia. *Trop. Plant Pathol.* **2015**, *40*, 26–34. [[CrossRef](#)]
8. Timmer, L.W.; Priest, M.; Broadbent, P.; Tan, M.K. Morphological and pathological characterization of species of *Elsinoë* causing scab diseases of citrus. *Phytopathology* **1996**, *86*, 1032–1038. [[CrossRef](#)]
9. Whiteside, J.O. Biological characteristics of *Elsinoë fawcettii* pertaining to the epidemiology of sour orange scab. *Phytopathology* **1975**, *65*, 1170–1177. [[CrossRef](#)]
10. Peever, T.L.; Carpenter-Boggs, L.; Timmer, L.W.; Carris, L.M.; Bhatia, A. Citrus black rot is caused by phylogenetically distinct lineages of *Alternaria alternata*. *Phytopathology* **2005**, *95*, 512–518. [[CrossRef](#)]
11. Timmer, L.W.; Peever, T.L.; Solel, Z.; Akimitsu, K. *Alternaria* diseases of citrus—Novel pathosystems. *Phytopathol. Mediterr.* **2003**, *42*, 99–112.
12. Timmer, L.W.; Solel, Z.; Orozco-Santos, M. *Alternaria* Brown Spot of Mandarins. In *Compendium of Citrus Diseases*; Timmer, L.W., Garnsey, S.M., Graham, J.H., Eds.; The American Phytopathological Society Press: Saint Paul, MI, USA, 2000.
13. Woudenberg, J.H.C.; Groenewald, J.Z.; Binder, M.; Crous, P.W. *Alternaria* redefined. *Stud. Mycol.* **2013**, *75*, 171–212. [[CrossRef](#)] [[PubMed](#)]
14. Woudenberg, J.H.C.; Seidl, M.F.; Groenewald, J.Z.; de Vries, M.; Stielow, J.B.; Thomma, B.P.H.J.; Crous, P.W. *Alternaria* section *alternaria*: Species, *formae speciales* or pathotypes? *Stud. Mycol.* **2015**, *82*, 1–21. [[CrossRef](#)] [[PubMed](#)]
15. Pretorius, M.C.; Crous, P.W.; Groenewald, J.Z.; Braun, U. Phylogeny of some cercosporoid fungi from *Citrus*. *Sydowia* **2003**, *55*, 286–305.
16. Huang, F.; Groenewald, J.Z.; Zhu, L.; Crous, P.W.; Li, H.Y. Cercosporoid diseases of *Citrus*. *Mycologia* **2015**, *107*, 1151–1171. [[CrossRef](#)]
17. Bragança, C.A.D.; Damm, U.; Baroncelli, R.; Júnior, N.S.M.; Crous, P.W. Species of the *Colletotrichum acutatum* complex associated with anthracnose diseases of fruit in Brazil. *Fungal Biol.* **2016**, *120*, 547–561. [[CrossRef](#)]
18. Damm, U.; Cannon, P.F.; Woudenberg, J.H.C.; Johnston, P.R.; Weir, B.S.; Tan, Y.P.; Shivas, R.G.; Crous, P.W. The *Colletotrichum boninense* species complex. *Stud. Mycol.* **2012**, *73*, 75–78. [[CrossRef](#)]
19. Damm, U.; Woudenberg, J.H.C.; Cannon, P.F.; Crous, P.W. *Colletotrichum* species with curved conidia from herbaceous hosts. *Fungal Divers.* **2009**, *39*, 45–87.
20. Guarnaccia, V.; Groenewald, J.Z.; Polizzi, G.; Crous, P.W. High species diversity in *Colletotrichum* associated with citrus diseases in Europe. *Persoonia* **2017**, *39*, 32–50. [[CrossRef](#)]
21. Honger, J.O.; Offei, S.K.; Oduro, K.A.; Odamten, G.T.; Nyaku, S.T. Identification and molecular characterisation of *Colletotrichum* species from avocado, citrus and pawpaw in Ghana. *S. Afr. J. Plant Soil* **2016**, *33*, 177–185. [[CrossRef](#)]
22. Huang, F.; Chen, G.Q.; Hou, X.; Fu, Y.S.; Cai, L.; Hyde, K.D.; Li, H.Y. *Colletotrichum* species associated with cultivated citrus in China. *Fungal Divers.* **2013**, *61*, 61–74. [[CrossRef](#)]
23. Peng, L.J.; Yang, Y.L.; Hyde, K.D.; Bahkali, A.H.; Liu, Z.Y. *Colletotrichum* species on citrus leaves in Guizhou and Yunnan provinces, China. *Cryptogam. Mycol.* **2012**, *33*, 267–283.
24. Wang, W.; de Silva, D.D.; Moslemi, A.; Edwards, J.; Ades, P.K.; Crous, P.W.; Taylor, P.W.J. *Colletotrichum* species causing anthracnose of citrus in Australia. *J. Fungi* **2021**, *7*, 47. [[CrossRef](#)] [[PubMed](#)]

25. Weir, B.S.; Johnston, P.R.; Damm, U. The *Colletotrichum gloeosporioides* species complex. *Stud. Mycol.* **2012**, *73*, 115–180. [[CrossRef](#)] [[PubMed](#)]
26. Holmes, G.J.; Eckert, J.W.; Pitt, J.I. Revised description of *Penicillium ulaiense* and its role as a pathogen of citrus fruits. *Phytopathology* **1994**, *84*, 719–727. [[CrossRef](#)]
27. Tashiro, N.; Manabe, K.; Ide, Y. First report of whisker mold, a postharvest disease on citrus caused by *Penicillium ulaiense* (in Japan). *J. Gen. Plant Pathol.* **2012**, *78*, 140–144. [[CrossRef](#)]
28. Louw, J.P.; Korsten, L. Pathogenicity and host susceptibility of *Penicillium* spp. on citrus. *Plant Dis.* **2015**, *99*, 21–30. [[CrossRef](#)]
29. Guarnaccia, V.; Crous, P.W. Emerging citrus diseases in Europe caused by species of *Diaporthe*. *IMA Fungus* **2017**, *8*, 317–334. [[CrossRef](#)]
30. Huang, F.; Hou, X.; Dewdney, M.M.; Fu, Y.S.; Chen, G.Q.; Hyde, K.D.; Li, H.Y. *Diaporthe* species occurring on citrus in China. *Fungal Divers.* **2013**, *61*, 237–250. [[CrossRef](#)]
31. Huang, F.; Udayanga, D.; Wang, X.H.; Hou, X.; Mei, X.F.; Fu, Y.S.; Hyde, K.D.; Li, H.Y. Endophytic *Diaporthe* associated with citrus: A phylogenetic reassessment with seven new species from China. *Fungal Biol.* **2015**, *119*, 331–347. [[CrossRef](#)]
32. Chaisiri, C.; Liu, X.Y.; Lin, Y.; Li, J.B.; Xiong, B.; Luo, C.X. Phylogenetic analysis and development of molecular tool for detection of *Diaporthe citri* causing melanose disease of citrus. *Plants* **2020**, *9*, 329. [[CrossRef](#)] [[PubMed](#)]
33. Dangomen, A.; Visarathanonh, N.; Manoch, L.; Piasai, O. Morphological studies of endophytic and plant pathogenic *Phomopsis liquidambaris* and *Diaporthe phaseolorum* (*P. phaseoli* anamorph) from healthy plants and diseased fruits. *Thai J. Agric. Sci.* **2013**, *46*, 157–164.
34. Dong, Z.Y.; Manawasinghe, I.S.; Huang, Y.H.; Shu, Y.X.; Phillips, A.J.; Dissanayake, A.J.; Hyde, K.D.; Xiang, M.M.; Luo, M. Endophytic *Diaporthe* associated with *Citrus grandis* cv. Tomentosa in China. *Front. Microbiol.* **2021**, *11*, 609387. [[CrossRef](#)] [[PubMed](#)]
35. Gomes, R.R.; Glienke, C.; Videira, S.I.R.; Lombard, L.; Groenewald, J.Z.; Crous, P.W. *Diaporthe*: A genus of endophytic, saprobic and plant pathogenic fungi. *Persoonia* **2013**, *31*, 1–41. [[CrossRef](#)] [[PubMed](#)]
36. Tan, Y.P.; Edwards, J.; Grice, K.R.E.; Shivas, R.G. Molecular phylogenetic analysis reveals six new species of *Diaporthe* from Australia. *Fungal Divers.* **2013**, *61*, 251–260. [[CrossRef](#)]
37. Udayanga, D.; Castlebury, L.A.; Rossman, A.Y.; Hyde, K.D. Species limits in *Diaporthe*: Molecular re-assessment of *D. citri*, *D. cytosporella*, *D. foeniculina* and *D. rudis*. *Persoonia* **2014**, *32*, 83–101. [[CrossRef](#)]
38. Fawcett, H.S. The cause of stem-end rot of citrus fruits (*Phomopsis citri* n. sp.). *Phytopathology* **1912**, *2*, 109–113.
39. Wolf, F.A. The perfect stage of the fungus which causes melanose of citrus. *J. Agric. Res.* **1926**, *33*, 621–625.
40. Chen, G.Q.; Jiang, L.Y.; Xu, F.S.; Li, H.Y. In vitro and in vivo screening of fungicides for controlling citrus melanose caused by *Diaporthe citri*. *J. Zhejiang Univ. (Agric. Life Sci.)* **2010**, *36*, 440–444. (In Chinese)
41. Douanla-Meli, C.; Langer, E.; Mouafo, F.T. Fungal endophyte diversity and community patterns in healthy and yellowing leaves of *Citrus limon*. *Fungal Ecol.* **2013**, *6*, 212–222. [[CrossRef](#)]
42. Habib, W.; Gerdes, E.; Antelmi, I.; Baroudy, F.; Choueiri, E.; Nigro, F. *Diaporthe foeniculina* associated with severe shoot blight of lemon in Lebanon. *Phytopathol. Mediterr.* **2015**, *54*, 149–150.
43. Jiang, L.Y.; Xu, F.S.; Huang, Z.D.; Huang, F.; Chen, G.Q.; Li, H.Y. Occurrence and control of citrus melanose caused by *Diaporthe citri*. *Acta Agric. Zhejiangensis* **2012**, *24*, 647–653. (In Chinese)
44. Mondal, S.N.; Vicent, A.; Reis, R.F.; Timmer, L.W. Saprophytic colonization of citrus twigs by *Diaporthe citri* and factors affecting pycnidial production and conidial survival. *Plant Dis.* **2007**, *91*, 387–392. [[CrossRef](#)] [[PubMed](#)]
45. Murali, T.S.; Suryanarayanan, T.S.; Geeta, R. Endophytic *Phomopsis* species: Host range and implications for diversity estimates. *Can. J. Microbiol.* **2006**, *52*, 673–680. [[CrossRef](#)]
46. Xiong, T.; Zeng, Y.T.; Wang, W.; Li, P.D.; Gai, Y.P.; Jiao, C.; Zhu, Z.R.; Xu, J.P.; Li, H.Y. Abundant genetic diversity and extensive differentiation among geographic populations of the citrus pathogen *Diaporthe citri* in Southern China. *J. Fungi* **2021**, *7*, 749. [[CrossRef](#)] [[PubMed](#)]
47. Guarnaccia, V.; Crous, P.W. Species of *Diaporthe* on *Camellia* and *Citrus* in the Azores Islands. *Phytopathol. Mediterr.* **2018**, *57*, 307–319.
48. Yang, Q.; Jiang, N.; Tian, C.M. New species and records of *Diaporthe* from Jiangxi province, China. *MycKeys* **2021**, *77*, 41–64. [[CrossRef](#)]
49. Vakalounakis, D.J.; Ntougias, S.; Kavroulakis, N.; Protopapadakis, E. *Neofusicoccum parvum* and *Diaporthe foeniculina* associated with twig and shoot blight and branch canker of citrus in Greece. *J. Phytopathol.* **2019**, *167*, 527–537. [[CrossRef](#)]
50. Tekiner, N.; Tozlu, E.; Guarnaccia, V. First report of *Diaporthe foeniculina* causing fruit rot of lemon in Turkey. *J. Gen. Plant Pathol.* **2020**, *102*, 277. [[CrossRef](#)]
51. Juybari, H.Z.; Tajick Ghanbary, M.A.; Karimi, H.; Arzanlou, K.; Seasonal, M. Seasonal, tissue and age influences on frequency and biodiversity of endophytic fungi of *Citrus sinensis* in Iran. *For. Pathol.* **2019**, *6*, e12559. [[CrossRef](#)]
52. Chaisiri, C.; Liu, X.Y.; Yin, W.X.; Luo, C.X.; Lin, Y. Morphology characterization, molecular phylogeny, and pathogenicity of *Diaporthe passifloricola* on *Citrus reticulata* cv. Nanfengmiju in Jiangxi province, China. *Plants* **2021**, *10*, 218. [[CrossRef](#)] [[PubMed](#)]
53. Cui, M.J.; Wei, X.; Xia, P.L.; Yi, J.P.; Yu, Z.H.; Deng, J.X.; Li, Q.L. *Diaporthe taicola* and *D. siamensis*, two new records on *Citrus sinensis* in China. *Mycobiology* **2021**, *49*, 267–274. [[CrossRef](#)] [[PubMed](#)]

54. Ho, M.Y.; Chung, W.C.; Huang, H.C.; Chung, W.H.; Chung, W.H. Identification of endophytic fungi of medicinal herbs of Lauraceae and Rutaceae with antimicrobial property. *Taiwania* **2012**, *57*, 229–241.
55. Mahadevakumar, S.; Yadav, V.; Tejaswini, G.S.; Sandeep, S.N.; Janardhana, G.R. First report of *Phomopsis citri* associated with dieback of *Citrus lemon* in India. *Plant Dis.* **2014**, *98*, 1281. [[CrossRef](#)] [[PubMed](#)]
56. Sadeghi, F.; Samsampour, D.; Seyahooei, M.A.; Bagheri, A.; Soltani, J. Diversity and spatiotemporal distribution of fungal endophytes associated with *Citrus reticulata* cv. Siyahoo. *Curr. Microbiol.* **2019**, *76*, 279–289. [[CrossRef](#)]
57. Hongsanan, S.; Maharachchikumbura, S.S.N.; Hyde, K.D.; Samarakoon, M.C.; Jeewon, R.; Zhao, Q.; Al-Sadi, A.M.; Bahkali, A.H. An updated phylogeny of Sordariomycetes based on phylogenetic and molecular clock evidence. *Fungal Divers.* **2017**, *84*, 25–41. [[CrossRef](#)]
58. Hyde, K.D.; Nilsson, R.H.; Alias, S.A.; Ariyawansa, H.A.; Blair, J.E.; Cai, L.; de Cock, A.W.A.M.; Dissanayake, A.J.; Glockling, S.L.; Goonasekara, I.D.; et al. One stop shop: Backbones trees for important phytopathogenic genera: I (2014). *Fungal Divers.* **2014**, *67*, 21–125. [[CrossRef](#)]
59. Jayasiri, S.C.; Hyde, K.D.; Ariyawansa, H.A.; Bhat, J.; Buyck, B.; Cai, L.; Dai, Y.C.; Abd-Elsalam, K.A.; Ertz, D.; Hidayat, I.; et al. The faces of fungi database: Fungal names linked with morphology, phylogeny and human impacts. *Fungal Divers.* **2015**, *74*, 3–18. [[CrossRef](#)]
60. Maharachchikumbura, S.S.N.; Hyde, K.D.; Jones, E.B.G.; McKenzie, E.H.C.; Bhat, J.D.; Dayarathne, M.C.; Huang, S.K.; Norphanphoun, C.; Senanayake, I.C.; Perera, R.H.; et al. Families of Sordariomycetes. *Fungal Divers.* **2016**, *79*, 1–317. [[CrossRef](#)]
61. Maharachchikumbura, S.S.N.; Hyde, K.D.; Jones, E.B.G.; McKenzie, E.H.C.; Huang, S.K.; Abdel-Wahab, M.A.; Daranagama, D.A.; Dayarathne, M.; D'souza, M.J.; Goonasekara, I.D.; et al. Towards a natural classification and backbone tree for Sordariomycetes. *Fungal Divers.* **2015**, *72*, 199–301. [[CrossRef](#)]
62. Senanayake, I.C.; Crous, P.W.; Groenewald, J.Z.; Maharachchikumbura, S.S.N.; Jeewon, R.; Phillips, A.J.L.; Bhat, J.D.; Perera, R.H.; Li, Q.R.; Li, W.J.; et al. Families of *Diaporthales* based on morphological and phylogenetic evidence. *Stud. Mycol.* **2017**, *86*, 217–296. [[CrossRef](#)] [[PubMed](#)]
63. Udayanga, D.; Liu, X.Z.; McKenzie, E.H.C.; Chukeatirote, E.; Bahkali, A.H.A.; Hyde, K.D. The genus *Phomopsis*: Biology, applications, species concepts and names of common phytopathogens. *Fungal Divers.* **2011**, *50*, 189–225. [[CrossRef](#)]
64. Wijayawardene, N.N.; Hyde, K.D.; Rajeshkumar, K.C.; Hawksworth, D.L.; Madrid, H.; Kirk, P.M.; Braun, U.; Singh, R.V.; Crous, P.W.; Kukwa, M.; et al. Notes for genera: Ascomycota. *Fungal Divers.* **2017**, *86*, 1–594.
65. Nitschke, T.R.J. *Pyrenomyces germanici*. In *Die Kernpilze Deutschlands Bearbeitet von dr. Th. Nitschke*; Eduard Trewendt: Breslau, Germany, 1870; Volume 2, pp. 161–320.
66. Diogo, E.L.F.; Santos, J.M.; Phillips, A.J.L. Phylogeny, morphology and pathogenicity of *Diaporthe* and *Phomopsis* species on almond in Portugal. *Fungal Divers.* **2010**, *44*, 107–115. [[CrossRef](#)]
67. Farr, D.F.; Castlebury, L.A.; Rossman, A.Y.; Putnam, M.L. A new species of *Phomopsis* causing twig dieback of *Vaccinium vitis-idaea* (lingonberry). *Mycol. Res.* **2002**, *106*, 745–752. [[CrossRef](#)]
68. Gao, Y.H.; Liu, F.; Duan, W.J.; Crous, P.W.; Cai, L. *Diaporthe* is paraphyletic. *IMA Fungus* **2017**, *8*, 153–187. [[CrossRef](#)] [[PubMed](#)]
69. Ko, Y.; Sun, S.K. *Phomopsis* fruit rot of subtropical peach in Taiwan. *Plant Pathol. Bull.* **2003**, *12*, 212–214.
70. Santos, J.M.; Phillips, A.J.L. Resolving the complex of *Diaporthe* (*Phomopsis*) species occurring on *Foeniculum vulgare* in Portugal. *Fungal Divers.* **2009**, *34*, 111–125.
71. Brayford, D. Variation in *Phomopsis* isolates from *Ulmus* species in the British Isles and Italy. *Mycol. Res.* **1990**, *94*, 691–697. [[CrossRef](#)]
72. Chi, P.K.; Jiang, Z.D.; Xiang, M.M. *Flora Fungorum Sinicorum*; Science Press: Beijing, China, 2007; Volume 34. (In Chinese)
73. Mostert, L.; Crous, P.W.; Kang, J.C.; Phillips, A.J.L. Species of *Phomopsis* and a *Libertella* sp. occurring on grapevines with specific reference to South Africa: Morphological, cultural, molecular and pathological characterization. *Mycologia* **2001**, *93*, 146–167. [[CrossRef](#)]
74. Uecker, F.A. A world list of *Phomopsis* names with notes on nomenclature, morphology and biology. *Mycol. Mem.* **1988**, *13*, 1–231.
75. Timmer, L.W.; Mondal, S.N.; Peres, N.A.R.; Bhatia, A. Fungal Diseases of Fruit and Foliage of Citrus Trees. In *Diseases of Fruits and Vegetables*; Naqvi, S.A.M.H., Ed.; Springer: Dordrecht, The Netherlands, 2004; Volume 1, pp. 247–290.
76. Wehmeyer, L.E. *The Genus Diaporthe Nitschke and Its Segregates*; Science Series; University of Michigan Studies: Ann Arbor, MI, USA, 1933; Volume 9, pp. 1–349.
77. Whiteside, J.O.; Garnsey, S.M.; Timmer, L.W. Melanose. In *Compendium of Citrus Diseases*; Whiteside, J.O., Ed.; APS Press: St. Paul, MN, USA, 1988; pp. 20–21.
78. Muntanola-Cvetković, M.; Mihaljević, M.; Petrov, M. On the identity of the causative agent of a serious *Phomopsis-Diaporthe* disease in sunflower plants. *Nova Hedwig.* **1981**, *34*, 417–435.
79. Punithalingam, E. *Phomopsis anacardii*. *CMI Descr. Pathog. Fungi Bact.* **1985**, *826*, 1–2.
80. Cristescu, C. A new species of *Phomopsis* Sacc. (*Mitosporic fungi*) in Romania. *Rom. J. Biol.-Plant Biol.* **2003**, *48*, 45–49.
81. Rehner, S.A.; Uecker, F.A. Nuclear ribosomal internal transcribed spacer phylogeny and host diversity in the coelomycete *phomopsis*. *Can. J. Bot.* **1994**, *72*, 1666–1674. [[CrossRef](#)]
82. Cristescu, C. The morphology and anatomy of structure somatic and reproductive of species of *Phomopsis* (Sacc.) Bubák. *Bul. Grădini Bot. Iași Tomul* **2007**, *14*, 19–27.

83. Roskopf, E.N.; Charudattan, R.; Shabana, Y.M.; Benny, G.L. *Phomopsis amaranthicola*, a new species from *Amaranthus* sp. *Mycologia* **2000**, *92*, 114–122. [[CrossRef](#)]
84. Roskopf, E.N.; Charudattan, R.; Valero, J.T.; Stall, W.M. Field evaluation of *Phomopsis amaranthicola*, a biological control agent of *Amaranthus* spp. *Plant Dis.* **2000**, *84*, 1225–1230. [[CrossRef](#)]
85. Sutton, B.C. *The Coelomycetes. Fungi Imperfecti with Pycnidia, Acervuli and Stromata*; Commonwealth Mycological Institute: Kew, Surrey, UK, 1980.
86. Punithalingam, E. Studies on Sphaeropsidales in culture, II. *Mycol. Pap.* **1974**, *136*, 1–63.
87. Rodeva, R.; Stoyanova, Z.; Pandeva, R. A new fruit disease of pepper in Bulgaria caused by *Phomopsis capsici*. *Acta Hortic.* **2009**, *830*, 551–556. [[CrossRef](#)]
88. Liu, X.Y.; Chaisiri, C.; Lin, Y.; Yin, W.X.; Luo, C.X. Whole-genome sequence of *Diaporthe citri* isolate NFHF-8-4 the causal agent of citrus melanose. *Mol. Plant Microbe. Interact.* **2021**, *34*, 845–847. [[CrossRef](#)] [[PubMed](#)]
89. Gai, Y.P.; Xiong, T.; Xiao, X.; Li, P.D.; Zeng, Y.T.; Li, L.; Riely, B.K.; Li, H.Y. The genome sequence of the citrus melanose pathogen *Diaporthe citri* and two citrus-related *Diaporthe* species. *Phytopathology* **2021**, *111*, 779–783. [[CrossRef](#)] [[PubMed](#)]
90. Taylor, J.W.; Jacobson, D.J.; Kroken, S.; Kasuga, T.; Geiser, D.M.; Hibbett, D.S.; Fisher, M.C. Phylogenetic species recognition and species concepts in fungi. *Fungal Ecol.* **2000**, *31*, 21–32. [[CrossRef](#)] [[PubMed](#)]
91. Liu, F.; Wang, M.; Damm, U.; Crous, P.W.; Cai, L. Species boundaries in plant pathogenic fungi: A *Colletotrichum* case study. *BMC Evol. Biol.* **2016**, *16*, 81. [[CrossRef](#)] [[PubMed](#)]
92. Achari, S.R.; Kaur, J.; Dinh, Q.; Mann, R.; Sawbridge, T.; Summerell, B.A.; Edwards, J. Phylogenetic relationship between australian *Fusarium oxysporum* isolates and resolving the species complex using the multispecies coalescent model. *BMC Genom.* **2020**, *21*, 248. [[CrossRef](#)]
93. Hilário, S.; Gonçalves, M.F.M.; Alves, A. Using genealogical concordance and coalescent-based species delimitation to assess species boundaries in the *Diaporthe eres* complex. *J. Fungi* **2021**, *7*, 507. [[CrossRef](#)]
94. Hilário, S.; Santos, L.; Alves, A. *Diaporthe amygdali*, a species complex or a complex species? *Fungal Biol.* **2021**, *125*, 505–518. [[CrossRef](#)]
95. Kubatko, L.S.; Degnan, J.H. Inconsistency of phylogenetic estimates from concatenated data under coalescence. *Syst. Biol.* **2007**, *56*, 17–24. [[CrossRef](#)]
96. Stewart, J.E.; Timmer, L.W.; Lawrence, C.B.; Pryor, B.M.; Peever, T.L. Discord between morphological and phylogenetic species boundaries: Incomplete lineage sorting and recombination results in fuzzy species boundaries in an asexual fungal pathogen. *BMC Evol. Biol.* **2014**, *14*, 38. [[CrossRef](#)]
97. Castlebury, L. The *Diaporthe vaccinii* complex of fruit pathogens. *Inoculum* **2005**, *56*, 12.
98. Marin-Felix, Y.; Hernández-Restrepo, M.; Wingfield, M.J.; Akulov, A.; Carnegie, A.J.; Cheewangkoon, R.; Gramaje, D.; Groenewald, J.Z.; Guaraccia, V.; Halleen, F.; et al. Genera of phytopathogenic fungi: GOPHY 2. *Stud. Mycol.* **2019**, *92*, 47–133. [[CrossRef](#)] [[PubMed](#)]
99. Santos, J.M.; Correia, V.G.; Phillips, A.J.L.; Spatafora, J.W. Primers for mating-type diagnosis in *Diaporthe* and *Phomopsis*: Their use in teleomorph induction in vitro and biological species definition. *Fungal Biol.* **2010**, *114*, 255–270. [[CrossRef](#)] [[PubMed](#)]
100. Farr, D.F.; Castlebury, L.A.; Rossman, A.Y. Morphological and molecular characterization of *Phomopsis vaccinii* and additional isolates of *phomopsis* from blueberry and cranberry in the Eastern United States. *Mycologia* **2002**, *94*, 494–504. [[CrossRef](#)] [[PubMed](#)]
101. Udayanga, D.; Castlebury, L.A.; Rossman, A.Y.; Chukeatirote, E.; Hyde, K.D. Insights into the genus *Diaporthe*: Phylogenetic species delimitation in the *D. eres* species complex. *Fungal Divers.* **2014**, *67*, 203–229. [[CrossRef](#)]
102. Udayanga, D.; Castlebury, L.A.; Rossman, A.Y.; Chukeatirote, E.; Hyde, K.D. The *Diaporthe sojae* species complex: Phylogenetic re-assessment of pathogens associated with soybean, cucurbits and other field crops. *Fungal Biol.* **2015**, *119*, 383–407. [[CrossRef](#)]
103. Dissanayake, A.J.; Liu, M.; Zhang, W.; Chen, Z.; Udayanga, D.; Chukeatirote, E.; Li, X.H.; Yan, J.Y.; Hyde, K.D. Morphological and molecular characterisation of *Diaporthe* species associated with grapevine trunk disease in China. *Fungal Biol.* **2015**, *119*, 283–294. [[CrossRef](#)]
104. Santos, L.; Alves, A.; Alves, R. Evaluating multi-locus phylogenies for species boundaries determination in the genus *Diaporthe*. *PeerJ* **2017**, *5*, e3120. [[CrossRef](#)]
105. Van Niekerk, J.M.; Groenewald, J.Z.; Farr, D.F.; Fourie, P.H.; Halleen, F.; Crous, P.W. Reassessment of *Phomopsis* species on grapevine. *Australas. Plant Pathol.* **2005**, *34*, 27–39. [[CrossRef](#)]
106. Chaisiri, C.; Liu, X.Y.; Lin, Y.; Fu, Y.P.; Zhu, F.X.; Luo, C.X. Phylogenetic and haplotype network analyses of *Diaporthe eres* species in China based on sequences of multiple loci. *Biology* **2021**, *10*, 179. [[CrossRef](#)]
107. Castlebury, L.A.; Farr, D.F.; Rossman, A.Y. Phylogenetic distinction of *Phomopsis* isolates from cucurbits. *Inoculum* **2001**, *52*, 25.
108. Carbone, I.; Kohn, L.M. A method for designing primer sets for speciation studies in filamentous ascomycetes. *Mycologia* **1999**, *91*, 553–556. [[CrossRef](#)]
109. O'Donnell, K.; Kistler, H.C.; Tacke, B.K.; Casper, H.C. Gene genealogies reveal global phylogeographic structure and reproductive isolation among lineages of *Fusarium graminearum*, the fungus causing wheat scab. *Proc. Natl. Acad. Sci. USA* **2000**, *97*, 7905–7910. [[CrossRef](#)] [[PubMed](#)]
110. Walker, D.M.; Castlebury, L.A.; Rossman, A.Y.; White, J.F. New molecular markers for fungal phylogenetics: Two genes for species-level systematic in the Sordariomycetes (Ascomycota). *Mol. Phylogenet. Evol.* **2012**, *64*, 500–512. [[CrossRef](#)] [[PubMed](#)]

111. Myllys, L.; Stenroos, S.; Thell, A. New genes for phylogenetic studies of lichenized fungi: Glyceraldehyde-3-phosphate dehydrogenase and betatubulin genes. *Lichenologist* **2002**, *34*, 237–246. [[CrossRef](#)]
112. Crous, P.W.; Groenewald, J.Z.; Risède, J.M.; Simoneau, P.; Hywel-Jones, N.L. *Calonectria* species and their *Cylindrocladium* anamorphs: Species with clavate vesicles. *Stud. Mycol.* **2004**, *50*, 415–430. [[CrossRef](#)]
113. Glass, N.L.; Donaldson, G.C. Development of primer sets designed for use with the PCR to amplify conserved genes from filamentous Ascomycetes. *Appl. Environ. Microb.* **1995**, *61*, 1323–1330. [[CrossRef](#)]
114. Pecchia, S.; Mercatelli, E.; Vannacci, G. Intraspecific diversity within *Diaporthe helianthi*: Evidence from rDNA intergenic spacer (IGS) sequence analysis. *Mycopathologia* **2004**, *157*, 317–326. [[CrossRef](#)]
115. White, T.J.; Bruns, T.; Lee, S.; Taylor, J. Amplification and Direct Sequencing of Fungal Ribosomal RNA Genes for Phylogenetics. In *PCR Protocols: A Guide to Methods and Applications*; Innis, M.A., Gelfand, D.H., Sninsky, J.J., White, T.J., Eds.; Academic Press: San Diego, CA, USA, 1990; pp. 315–322.
116. Gardes, M.; Bruns, T.D. ITS primers with enhanced specificity for basidiomycetes—Application to the identification of mycorrhizae and rusts. *Mol. Ecol.* **1993**, *2*, 113–118. [[CrossRef](#)]
117. Choi, C.W.; Jung, K.E.; Kim, M.J.; Yoon, S.H.; Park, S.M.; Jin, S.B.; Hyun, J.W. Development of molecular marker to detect citrus melanose caused by *Diaporthe citri* from citrus melanose-like symptoms. *Plant Pathol. J.* **2021**, *37*, 681–686. [[CrossRef](#)]
118. Crous, P.W.; Schoch, C.L.; Hyde, K.D.; Wood, A.R.; Gueidan, C.; de Hoog, G.S.; Groenewald, J.Z. Phylogenetic lineages in the *Capnodiales*. *Stud. Mycol.* **2009**, *64*, 17–47. [[CrossRef](#)]
119. Vilgalys, R.; Hester, M. Rapid genetic identification and mapping of enzymatically amplified ribosomal DNA from several *Cryptococcus* species. *J. Bacteriol.* **1990**, *172*, 4238–4246. [[CrossRef](#)] [[PubMed](#)]
120. Hilário, S.; Amaral, I.A.; Gonçalves, M.F.M.; Lopes, A.; Santos, L.; Alves, A. *Diaporthe* species associated with twig blight and dieback of *Vaccinium corymbosum* in Portugal, with description of four new species. *Mycologia* **2020**, *112*, 293–308. [[CrossRef](#)]
121. Li, K.N.; Rouse, D.I.; German, T.L. PCR primers that allow intergenetic differentiation of ascomycetes and their application to *Verticillium* spp. *Appl. Environ. Microb.* **1994**, *60*, 4324–4331. [[CrossRef](#)] [[PubMed](#)]
122. O'Donnell, K.; Cigelnik, E.; Nirenberg, H.I. Molecular systematics and phylogeography of the *Gibberella fujikuroi* species complex. *Mycologia* **1998**, *90*, 465–493. [[CrossRef](#)]
123. Aveskamp, M.M.; Verkley, G.J.M.; Gruyter, J.; Perelló, A.; Woudenberg, J.H.C.; Groenewald, J.Z.; Crous, P.W. DNA phylogeny reveals polyphyly of *Phoma* section *Peyronellaea* and multiple taxonomic novelties. *Mycologia* **2009**, *101*, 363–382. [[CrossRef](#)]
124. O'Donnell, K.; Cigelnik, E. Two divergent intragenomic rDNA ITS2 types within a monophyletic lineage of the fungus *Fusarium* are nonorthologous. *Mol. Phylogenet. Evol.* **1997**, *7*, 103–116. [[CrossRef](#)] [[PubMed](#)]
125. Ruocco, M.; Baroncelli, R.; Cacciola, S.O.; Pane, C.; Monti, M.M.; Firrao, G.; Vergara, M.; Lio, G.M.S.; Vannacci, G.; Scala, F. Polyketide synthases of *Diaporthe helianthi* and involvement of DHPK51 in virulence on sunflower. *BMC Genom.* **2018**, *19*, 27. [[CrossRef](#)]
126. SAYS-LESAGE, V.; ROECKEL-DREVET, P.; VIGUIÉ, A.; TOURVIEILLE, J.; NICOLAS, P.; LABROUHE, D.T. Molecular variability within *Diaporthe/Phomopsis helianthi* from France. *Phytopathology* **2002**, *92*, 308–313. [[CrossRef](#)]
127. Croll, D.; McDonald, B.A. The genetic basis of local adaptation for pathogenic fungi in agricultural ecosystems. *Mol. Ecol.* **2017**, *26*, 2027–2040. [[CrossRef](#)]
128. Stukenbrock, E.H.; McDonald, B.A. The origins of plant pathogens in agro-ecosystems. *Annu. Rev. Phytopathol.* **2008**, *46*, 75–100. [[CrossRef](#)]
129. Xu, J. *Evolutionary Genetics of Fungi*; Horizon Scientific Press: Norfolk, UK, 2005.
130. Timmer, L.W.; Garnsey, S.M.; Graham, J.H. *Scab Diseases, revised edition: 31–32 ed.*; American Phytopathological Society Press: St. Paul, MN, USA, 2000; p. 92.
131. Kuhara, S. *The Application of the Epidemiologic Simulation Model “Melan” to Control Citrus Melanose Caused by Diaporthe Citri (Faw.) Wolf*; ASPAC Food and Fertilizer Technology Center: Taipei, China, 1999; p. 481.
132. Kucharek, T.; Whiteside, J.; Brown, E. Melanose and Phomopsis Stem-End Rot of Citrus. In *Plant Pathology Fact Sheet, Florida Cooperative Extension Service*; Institute of Food and Agricultural Sciences, University of Florida: Gainesville, FL, USA, 2000; pp. 26–30.
133. Bach, W.J.; Wolf, F.A. The isolation of the fungus that causes citrus melanose and the pathological anatomy of the host. *J. Agric. Res.* **1928**, *37*, 243–252.
134. Agostini, J.P.; Bushong, P.M.; Bhatia, A.; Timmer, L.W. Influence of environmental factors on severity of citrus scab and melanose. *Plant Dis.* **2003**, *87*, 1102–1106. [[CrossRef](#)] [[PubMed](#)]
135. Burnett, H.C. *Melanose Diaporthe Citri (Faw.) Wolf*; Florida Department of Agriculture and Consumer Services, Division of Plant Industry: Gainesville, FL, USA, 1962; p. 1.
136. Hardy, S.; Donovan, N. *Managing Melanose in Citrus*; Profitable & sustainable primary industries, New South Wales Department of Primary Industries: Orange, NSW, Australia, 2007; Volume 751, pp. 1–3.
137. Nelson, S. Citrus Melanose. In *Plant Disease*; Cooperative Extension Service, College of tropical Agriculture and Human Resources, University of Hawaii: Honolulu, HI, USA, 2008; pp. 1–5.
138. Barkley, P.B.; Schubert, T.; Schutte, G.C.; Godfrey, K.; Hattingh, V.; Telford, G.; Beattie, G.A.C.; Hoffman, K.M. *Invasive Pathogens in Plant Biosecurity. Case Study: Citrus Biosecurity*; Springer: Dordrecht, The Netherlands, 2014; pp. 547–592.

139. Rehman, F.U.; Kalsoom, M.; Sultan, A.; Adnan, M.; Junaid, S.; Akram, H.; Tariq, M.A.; Shafique, T.; Zafar, M.I. Citrus melanose and quality degradation of fruit by this disease: A review. *J. Biogeneric Sci. Res.* **2020**, *3*, 1–4. [[CrossRef](#)]
140. Dewdney, M.M.; Timmer, L.W. Florida Citrus Pest Management Guide. Available online: <http://edis.ifas.ufl.edu> (accessed on 19 August 2021).
141. Driscoll, P.J. Copper toxicity on florida citrus—Why did it happen? *Proc. Fla. State Hort. Soc.* **2004**, *117*, 124–127.
142. Narciso, J.; Widmer, W.; Ference, C.; Ritenour, M.; Diaz, R. Use of carnauba based carrier for copper sprays reduces infection by *Xanthomonas citri* subsp. *citri* and *Diaporthe citri* in Florida commercial grapefruit groves. *Agric. Sci.* **2012**, *3*, 962–970.
143. Stover, E.D.; Ciliento, S.; Albrigo, G. Copper fungicide spray timings for melanose control in grapefruit: Comparison of computer modelling of copper residues vs. calendar sprays. *Hortscience* **2004**, *39*, 886A–886. [[CrossRef](#)]
144. Timmer, L.W.; Zitko, S.E. Evaluation of copper fungicides and rates of metallic copper for control of melanose on grapefruit in florida. *Plant Dis.* **1996**, *80*, 166–169. [[CrossRef](#)]
145. Bushong, P.M.; Timmer, L.W. Evaluation of postinfection control of citrus scab and melanose with benomyl, fenbuconazole, and azoxystrobin. *Plant Dis.* **2007**, *84*, 1246–1249. [[CrossRef](#)]
146. Inuma, T. Decreasing the frequency of control of citrus melanose by using the fungicides dithianon for satsuma mandarin cultivation (in Japanese). *Ann. Rept. Kansai Pl. Prot.* **2014**, *56*, 85–87. [[CrossRef](#)]
147. Idrees, M.; Naz, S.; Ehetisham-Ul-Haq, M.; Mehboob, S.; Kamran, M.; Ali, S.; Iqbal, M. Protectant and curative efficacy of different fungicides against citrus melanose caused by *Phomopsis citri* under in vivo conditions. *Int. J. Biosci.* **2019**, *15*, 194–199.
148. Anwar, U.; Mubeen, M.; Iftikhar, Y.; Zeshan, M.A.; Shakeel, Q.; Sajid, A.; Umer, M.; Abbas, A. Efficacy of different fungicides against citrus melanose disease in Sargodha, Pakistan. *Pak. L. Phytopathol.* **2021**, *33*, 67–74. [[CrossRef](#)]
149. Liu, X.; Wang, M.S.; Mei, X.F.; Jiang, L.Y.; Han, G.X.; Li, H.Y. Sensitivity evaluation of *Diaporthe citri* populations to mancozeb and screening of alternative fungicides for citrus melanose control. *J. Plant Protec.* **2018**, *45*, 373–381. (In Chinese)
150. Qin, S.Y.; Zhou, X.Y.; Jiang, Y.L. Screening of fungicides for controlling citrus melanose in lab. *Guangdong Agric. Sci.* **2012**, *39*, 77–79. (In Chinese)
151. Ko, Y.J.; Kang, S.Y.; Jeun, Y.C. Suppression of citrus melanose on the leaves treated with rhizobacterial strains after inoculation with *Diaporthe citri*. *Res. Plant Dis.* **2012**, *18*, 331–337. (In Korean) [[CrossRef](#)]
152. Ko, Y.J.; Kim, J.S.; Kim, K.D.; Jeun, Y.C. Microscopical observation of inhibition-behaviors against *Diaporthe citri* by pre-treated with *Pseudomonas putida* strain THJ609-3 on the leaves of citrus plants. *J. Microbiol.* **2014**, *52*, 879–883. [[CrossRef](#)] [[PubMed](#)]
153. Shin, Y.H.; Ko, E.J.; Kim, S.J.; Hyun, H.N.; Jeun, Y.C. Suppression of melanose caused by *Diaporthe citri* on citrus leaves pretreated with bio-sulfur. *Plant Pathol. J.* **2019**, *35*, 417–424. [[CrossRef](#)] [[PubMed](#)]
154. Lee, D.R.; Maung, C.E.H.; Choi, T.G.; Kim, K.Y. Large scale cultivation of *Bacillus velezensis* CE 100 and effect of its culture on control of citrus melanose caused by *Diaporthe citri*. *Korean J. Soil Sci. Fert.* **2021**, *54*, 297–310. [[CrossRef](#)]

## Article

# *Pseudomonas cannabina* pv. *alisalensis* Virulence Factors Are Involved in Resistance to Plant-Derived Antimicrobials during Infection

Nanami Sakata <sup>1</sup>, Takumi Haraguchi <sup>1</sup>, Shunsuke Masuo <sup>1,2</sup>, Takako Ishiga <sup>1</sup> and Yasuhiro Ishiga <sup>1,\*</sup>

- <sup>1</sup> Faculty of Life and Environmental Sciences, University of Tsukuba, 1-1-1 Tennodai, Tsukuba 305-8572, Ibaraki, Japan; sakata.nanami.td@alumni.tsukuba.ac.jp (N.S.); takku\_yakult@icloud.com (T.H.); masuo.shunsuke.fp@u.tsukuba.ac.jp (S.M.); takakoishiga@gmail.com (T.I.)
- <sup>2</sup> Microbiology Research Center for Sustainability (MiCS), University of Tsukuba, 1-1-1 Tennodai, Tsukuba 305-8572, Ibaraki, Japan
- \* Correspondence: ishiga.yasuhiro.km@u.tsukuba.ac.jp; Tel./Fax: +81-029-853-4792

**Abstract:** Bacteria are exposed to and tolerate diverse and potentially toxic compounds in the natural environment. While efflux transporters are generally thought to involve bacterial antibiotic resistance in vitro, their contributions to plant bacterial virulence have so far been poorly understood. *Pseudomonas cannabina* pv. *alisalensis* (*Pcal*) is a causal agent of bacterial blight of Brassicaceae. We here demonstrated that NU19, which is mutated in the resistance-nodulation-cell division (RND) transporter encoded gene, showed reduced virulence on cabbage compared to WT, indicating that the RND transporter contributes to *Pcal* virulence on cabbage. We also demonstrated that brassinin biosynthesis was induced after *Pcal* infection. Additionally, the RND transporter was involved in resistance to plant-derived antimicrobials and antibiotics, including the cabbage phytoalexin brassinin. These results suggest that the RND transporter extrudes plant-derived antimicrobials and contributes to *Pcal* virulence. We also found that the RND transporter contributes to *Pcal* virulence on Brassicaceae and tomato, but not on oat. These results suggest that the RND transporter contributes to *Pcal* virulence differentially depending on the host-plant species. Lastly, our expression-profile analysis indicated that the type-three secretion system (TTSS), which is essential for pathogenesis, is also involved in suppressing brassinin biosynthesis. Taken together, our results suggest that several *Pcal* virulence factors are involved in resistance to plant-derived antimicrobials and bacterial survival during infection.

**Citation:** Sakata, N.; Haraguchi, T.; Masuo, S.; Ishiga, T.; Ishiga, Y.

*Pseudomonas cannabina* pv. *alisalensis* Virulence Factors Are Involved in Resistance to Plant-Derived Antimicrobials during Infection. *Plants* **2022**, *11*, 1742. <https://doi.org/10.3390/plants11131742>

Academic Editors: Milan S. Stankovic, Paula Baptista and Petronia Carillo

Received: 26 May 2022  
Accepted: 28 June 2022  
Published: 30 June 2022

**Publisher's Note:** MDPI stays neutral with regard to jurisdictional claims in published maps and institutional affiliations.



**Copyright:** © 2022 by the authors. Licensee MDPI, Basel, Switzerland. This article is an open access article distributed under the terms and conditions of the Creative Commons Attribution (CC BY) license (<https://creativecommons.org/licenses/by/4.0/>).

**Keywords:** *Pseudomonas cannabina* pv. *alisalensis*; resistance-nodulation-cell division transporter; type-three secretion system; phytoalexin; brassinin; glucosinolate; cabbage

## 1. Introduction

Plants produce diverse specialized secondary metabolites to protect against pathogens and pests [1]. Specialized metabolites differ between plant clades [2]. The simplest functional definitions recognize “phytoalexins” as metabolites that are synthesized de novo in response to a pathogen, and “phytoanticipins” as constitutively biosynthesized infection inhibitors [3]. Phytoanticipins and phytoalexins are structurally diverse and different in plant species. So far, at least 44 phytoalexins have been isolated from Brassicaceae, most of which are derived from the amino acid tryptophan [4]. These defense metabolites have inhibitory activity in vitro against various bacteria and fungi, and they confer disease resistance in plant–pathogen interactions [4–7].

The Brassicaceae family includes many economically important crops. More than 40 phytoalexins have been identified from cultivated and wild Brassicaceae. *Brassica* species produce indole sulfur phytoalexins, which are hallmarks of the Brassicaceae with different subsets produced by different edible crucifers [8,9]. The role of phytoalexins in pathogen

resistance has been well-studied in the model plant *Arabidopsis thaliana*. Camalexin is a major phytoalexin of *A. thaliana*, and its production can be induced in *A. thaliana* leaves by a range of biotrophic and necrotrophic plant pathogens [4,10]. Camalexin antimicrobial activity was shown in vitro against bacteria, oomycetes, and fungi [11–17]. A mutation in the *PHYTOALEXIN DEFICIENT 3 (PAD3)* gene abolishes camalexin biosynthesis, resulting in enhanced susceptibility to necrotrophic pathogens, including *Botrytis cinerea* [16,18] and *Alternaria brassicicola* [19,20]. Several studies highlighted the importance of camalexin in response to hemibiotrophic pathogens [21,22], although camalexin accumulation was not always correlated with pathogen resistance. For instance, camalexin production was induced in response to various *Pseudomonas syringae* strains, but a *pad3* mutant showed the same susceptibility to those strains [23–25].

Klein and Sattely (2017) identified the biosynthetic genes required to generate the cruciferous phytoalexin brassinin. Brassinin is a glucosinolate downstream product and is a starting point for the various other phytoalexins [26]. Brassinin is not present in *A. thaliana* but is produced by many cultivated Brassica species. The inability of *A. thaliana* to synthesize or tailor brassinin is associated with the absence of enzymes, including brassinin-associated  $\beta$ -glucosidase (BABG) and dithiocarbamate 5-methyltransferase (DTCMT) [8]. Brassinin antifungal activity in vitro has been reported [13]. Brassinin primarily targets mitochondrial functions in *A. brassicicola*, then induces secondary effects such as reactive oxygen species (ROS) production and changes in lipid homeostasis [27]. Camalexin contributes to plant resistance against various fungal and oomycete pathogens [11,18,21,28,29]. However, few studies have investigated the importance of brassinin in plant resistance, and especially focused on the importance of phytoalexin in resistance against bacterial pathogens.

*Pseudomonas cannabina* pv. *alisalensis* (*Pcal*) is a causal agent of bacterial blight of Brassicaceae [30]. *Pcal* has a wide plant-host range: the Brassicaceae family (including cabbage, broccoli, Japanese radish, Chinese cabbage), tomato, and portions of Poaceae families such as oat (*Avena strigosa*) and timothy (*Phleum pratense*) [30]. Currently, copper fungicides and antibiotics have mainly been used for bacterial disease control. However, bacterial strains (including a *Pcal* strain) have developed a resistance against these chemicals [31]. To develop new strategies for *Pcal* disease control, we need to identify *Pcal* infection mechanisms. We previously identified potential *Pcal* virulence factors [32]. Multiple virulence factors are needed for successful infection such as the type-three secretion system (TTSS), membrane transporters, transcriptional factors, and amino-acid metabolism [32]. Among these mutants, a NU19 mutant (where Tn5 is inserted in the resistance-nodulation-cell division (RND) transporter encoded gene (PMA4326\_12408)), showed reduced virulence on cabbage [32]. However, the function of the RND transporter in *Pcal* virulence remains largely unclear.

For successful infection, plant pathogens need to eliminate the effects of host-derived antimicrobial compounds through extruding antimicrobials outside the cell, suppressing biosynthesis, and converting them to ineffective ones [7,33]. To extrude antimicrobials, bacteria have five structural groups of multidrug resistance (MDR) efflux-pump transporters: RND, small multidrug resistance, multiantimicrobial extrusion, the major facilitator superfamily, and ATP-binding cassette superfamilies. The RND efflux system functions to extrude various substrates, including antibiotics and host-derived molecules [34]. Fan et al. (2011) demonstrated that the *sax* (*survival in Arabidopsis extracts*) genes in *P. syringae* pv. *tomato* (*Pto*) DC3000 are required to overwhelm isothiocyanate-based defenses and facilitate a disease outcome. The *sax* genes form a subgroup of the RND efflux system [7]. In *P. syringae*, there are different operons for the RND efflux-pump transporter, *mexAB-oprM* and *mexEF-oprN*. *mexAB-oprM* deletion mutants in *Pto* DC3000, *P. syringae* pv. *phaseolicola* (*Pph*) 1448A, *P. syringae* pv. *syringae* (*Psy*) B728a, and *P. amygdali* pv. *tabaci* (formerly *P. syringae* pv. *tabaci*; *Pta*) 6605 exhibited increased antimicrobial susceptibility [35–37]. Helmann et al. (2022) demonstrated that *Psy* B728a *MexB* contributes to virulence differentially depending on the host-plant species. Therefore, although it is tempting to speculate that the *Pcal* RND transporter also contributes to virulence differentially depending on the

host-plant species, few RND transporter studies focused on host-derived phytoalexin and its virulence contributions on different host plants.

We here investigated the importance of the RND transporter in *Pcal* virulence by inoculating the NU19 strain [32] on Brassicaceae crops. We demonstrated that brassinin accumulated in several brassica crops, and is induced by *Pcal* infection. We also showed that the RND transporter is involved in diverse antimicrobial sensitivity, including brassinin. Moreover, our results also indicated that the TTSS might be involved in suppressing brassinin biosynthesis. Together, our results suggest that several *Pcal* virulence factors are involved in resistance to plant-derived antimicrobials and bacterial survival during infection.

## 2. Results

### 2.1. RND Transporter Contributes to *Pcal* Virulence

To investigate the RND transporter contributions to *Pcal* virulence, we conducted an inoculation assay with the RND transporter mutant NU19, which was isolated as a reduced virulence strain in a previous screening [32]. We firstly confirmed no significant differences in bacterial growth in KB medium between WT and NU19 after 12 h and 24 h incubation (Supplementary Figure S1). When we dip-inoculated plants with WT, cabbage showed chlorosis and necrosis (Figure 1A). However, cabbage inoculated with NU19 showed reduced symptoms (Figure 1A). Bacterial populations were also significantly reduced in plants inoculated with NU19 (Figure 1B). These results indicate that the RND transporter contributes to *Pcal* virulence on cabbage.

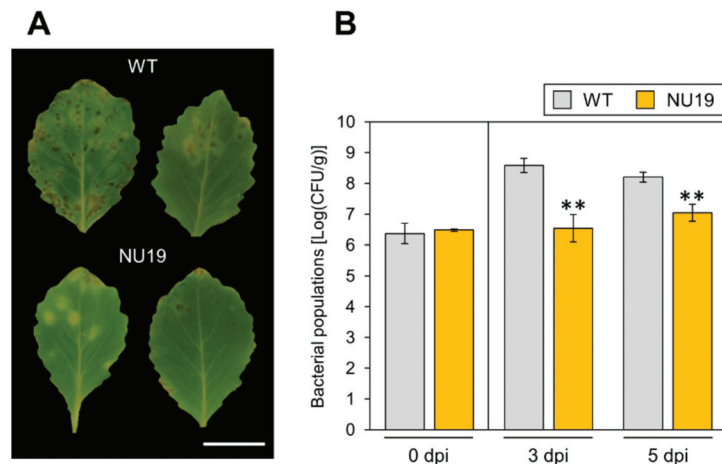


**Figure 1.** Disease symptoms (A) and bacterial populations (B) on cabbage leaves dip-inoculated with *Pseudomonas cannabina* pv. *alisalensis* KB211 WT and NU19. Cabbage plants were dip-inoculated with  $5 \times 10^7$  CFU/mL of inoculum containing 0.025% Silwet L-77. The bacterial populations in the plant were evaluated at 0, 3, and 5 dpi. The leaves were photographed at 5 dpi. Scale bar shows 2 cm. Vertical bars indicate the standard error for at least three independent experiments. Asterisks indicate a significant difference from the *Pcal* WT in a *t*-test (\*\*  $p < 0.01$ ).

### 2.2. Brassinin Biosynthesis Is Induced after *Pcal* Infection

The RND transporter functions to extrude a wide range of substrates, including antibiotics and host-derived molecules [34]. We then hypothesized that NU19 exhibited reduced virulence by impairment in cabbage-derived antimicrobial efflux. Therefore, we firstly examined whether cabbage secondary metabolites, glucosinolate biosynthesis, are induced after *Pcal* infection. We investigated expression profiles of brassinin biosynthesis-related genes (*CYP83B1*, *BABG.a*, *BABG.b*, and *DTCMT*), indole glucosinolate biosynthesis-related genes (*CYP81F2* and *CYP81F4*), and aliphatic glucosinolates biosynthesis-related

genes (*CYP83A1*, *FMOGS-OX2*, and *FMOG-OX5*) (Figure 2A). Brassinin biosynthesis-related genes, except *BABG.a*, showed greater expression after *Pcal* infection (Figure 2B–E). However, aliphatic glucosinolate biosynthesis-related genes, including *CYP83A1*, *FMOGS-OX2*, and *FMOGS-OX5*, showed less expression after infection (Supplementary Figure S2A–C). Moreover, the indole glucosinolate pathway, *CYP81F2* and *CYP81F4*, also showed greater expression after infection, same as the brassinin biosynthesis pathways (Supplementary Figure S2D,E).

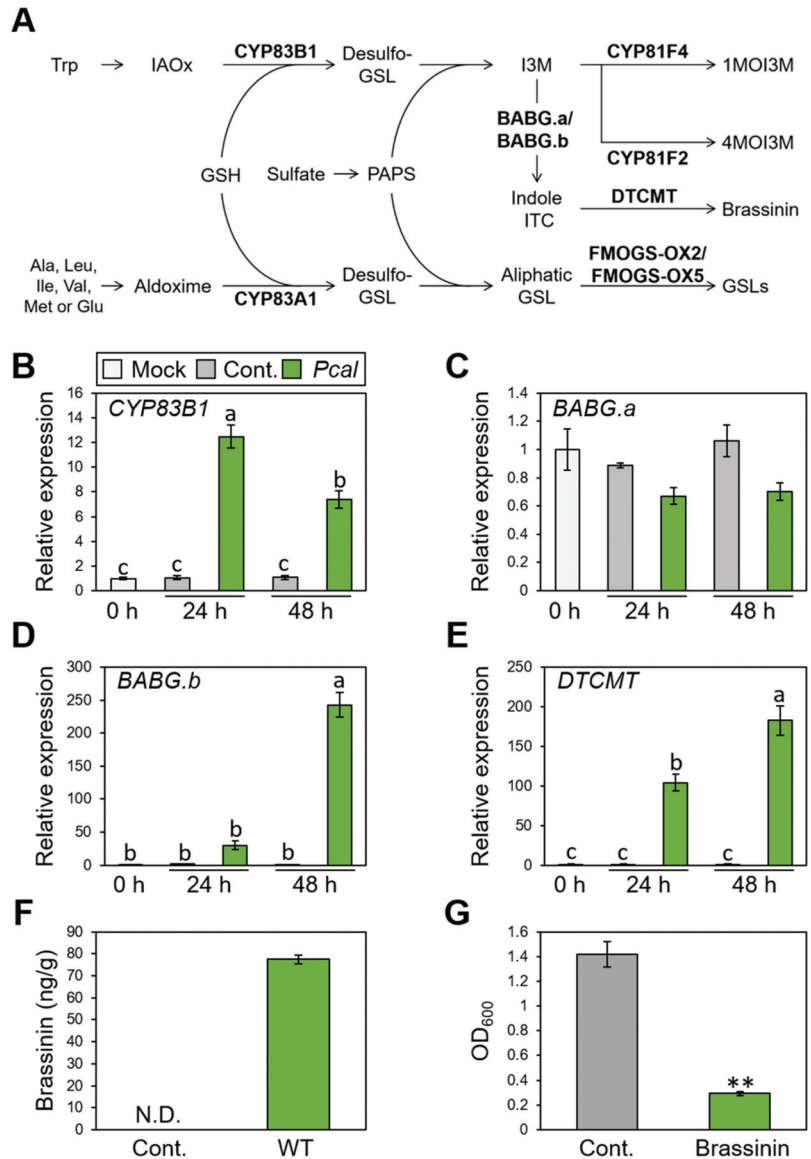


**Figure 2.** Expression profiles of brassinin-related genes and brassinin production during *Pseudomonas cannabina* pv. *alisalensis* KB211 WT infection, and antimicrobial activity of brassinin. (A) The aliphatic and indolic glucosinolate biosynthesis pathways in cabbage. Schematic biosynthetic pathways with the specific biosynthetic enzyme locations used in this study are shown in bold. GSH, glutathione;

GSL, glucosinolate; IAOx, indole-3-acetaldoxime; ITC, isothiocyanate; I3M, indole glucosinolates; PAPS, 3'-phosphoadenosine-5'-phosphosulfate; 1MOI3M, 1-Methoxyindole-3-yl methyl glucosinolate; 4MOI3M, 4-Methoxyindole-3-yl methyl glucosinolate. Brassinin biosynthesis gene expression profiles after syringe-inoculation with water (mock), or *Pseudomonas cannabina* pv. *alisalensis* KB211 WT. Expression profiles of *CYP83B1* (B), *BABG.a* (C), *BABG.b* (D), and *DTCMT* (E) were determined 24 and 48 h after inoculation with  $5 \times 10^5$  CFU/mL of WT or mock water-inoculated control, using real-time quantitative reverse-transcription PCR with gene-specific primer sets. Expression in cabbage was normalized using *BoUBQ1*. Vertical bars indicate the standard error for three biological replicates. Different letters indicate a significant difference among treatments based on a Tukey's honestly significant different test ( $p < 0.05$ ). (F) Total brassinin production in cabbage after syringe inoculation with *Pcal* WT or with water as a control. Cabbage leaves were collected at 48 hpi and were extracted with 80% methanol. Then, total brassinin were quantified by RP-LC-ESI-MS/MS. Vertical bars indicate the standard error for at least three independent experiments. N.D. indicates not detected. (G) Bacterial growth in LB medium after 24 h incubation with or without brassinin. The bacterial suspension was standardized to an OD<sub>600</sub> of 0.01 in LB and coincubated with or without 200  $\mu$ M brassinin. After 24 h, bacterial growth was measured at OD<sub>600</sub>. Asterisks indicate a significant difference from the water-treatment control in a *t*-test (\*\*  $p < 0.01$ ).

We next examined brassinin quantification using LC-MS/MS. The brassinin amount reached around 80 ng/g after *Pcal* infection at 48 h post inoculation (hpi) (Figure 2F). Moreover, brassinin has antimicrobial activity against *Pcal* (Figure 2G). Taken together, these results indicate that brassinin functions as a phytoalexin against *Pcal* infection.

### 2.3. RND Transporter Contributes to Resistance to Diverse Toxicants

To investigate whether the RND transporter is involved in resistance to various toxicants, we firstly examined the brassinin sensitivity of WT and NU19. The NU19 growth rate was reduced compared to WT (Figure 3A), suggesting that the RND transporter contributes to brassinin resistance. We next examined the sensitivity to other plant-derived metabolites. NU19 was significantly susceptible to sulforaphane, genistein, indole, and phloretin in these experimental conditions (Figure 3B–G). Furthermore, NU19 was more sensitive to spectinomycin and streptomycin than WT (Table 1). Taken together, these results indicate that the RND transporter contributes to resistance to several plant-derived antimicrobials and antibiotics.

**Table 1.** Antimicrobial susceptibility of *Pcal* KB211 WT and NU19.

Strain	MIC ( $\mu$ g/mL) in KB Medium						
	Sp	Sm	Nal	Cef	Tet	Amp	Car
WT	8	4	4	16	1	32	>1000
NU19	4	2	4	16	1	32	>1000

Sp, Spectinomycin; Sm, Streptomycin; Nal, Nalidixic acid; Cef, Cefotaxime; Tet, Tetracycline; Amp, Ampicillin; Car, Carbenicillin.

### 2.4. RND Transporter Contributes to *Pcal* Virulence on Multiple Host Plants

We next investigated whether the RND transporter contributes to *Pcal* virulence on multiple host plants. Disease symptoms and bacterial populations of NU19 were reduced in Brassica plants, including broccoli, Japanese radish, and Chinese cabbage (Figure 4A–C; Supplementary Figure S3A–C). These results indicate the RND transporter contributes to *Pcal* virulence on Brassica crops. Moreover, disease symptoms and bacterial populations of NU19 were reduced compared to WT in tomato (Figure 4D; Supplementary Figure S3D). Interestingly, however, disease symptoms and bacterial populations of NU19 and WT were almost the same in oat (Figure 4E; Supplementary Figure S4E). These results suggest that the RND transporter contributes less or does not contribute to disease on oat. Taken

together, although the RND transporter contribution to *Pcal* virulence differed in infection on oat, the RND transporter contributes to disease on multiple host plants.

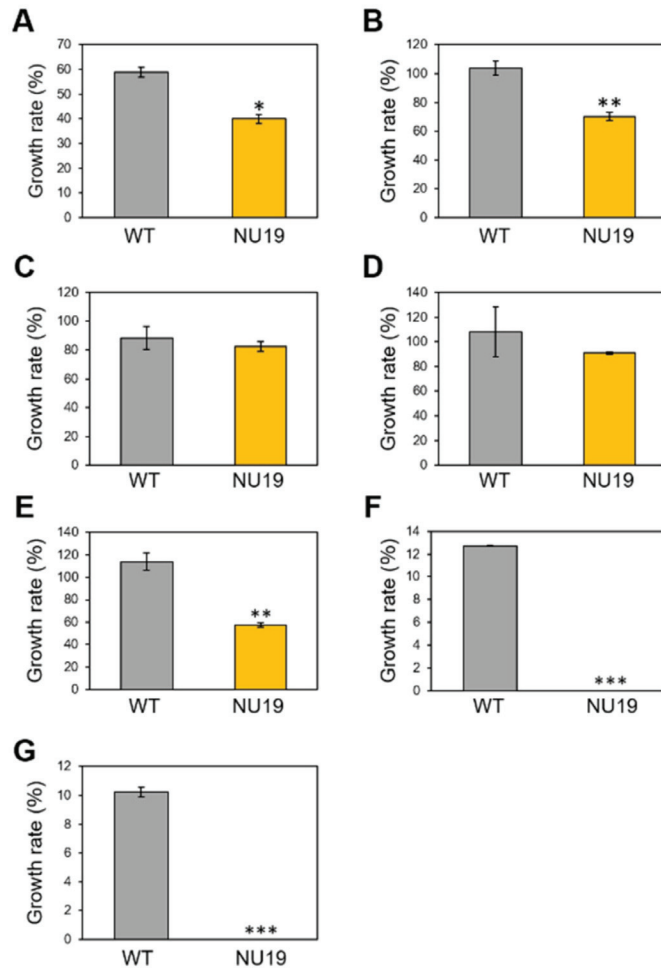


**Figure 3.** Growth rate of *Pseudomonas cannabina* pv. *alisalensis* KB211 WT and NU19 in KB medium with or without plant-derived antimicrobials. The bacterial suspensions were standardized to an OD<sub>600</sub> of 0.01 with KB, and after 6 h incubation, 200 μM brassinin (A), sulforaphane (B), camalexin (C), daidzein (D), genistein (E), indole (F), and phloretin (G) were added to each sample. Bacterial growth was measured at OD<sub>600</sub> after 24 h incubation. Asterisks indicate a significant difference from the *Pcal* WT in a *t*-test (\*  $p < 0.05$ , \*\*  $p < 0.01$ , \*\*\*  $p < 0.001$ ).

### 2.5. TTSS Suppresses Brassinin Biosynthesis

We demonstrated that brassinin biosynthesis is induced by *Pcal* infection. Therefore, it is tempting to speculate that efflux or detoxification of host-derived antimicrobials, including brassinin, is a critical step for successful *Pcal* infection. Thus, we assumed that the RND transporter is not the only virulence factor that suppresses brassinin accumulation. Therefore, to investigate whether the TTSS and coronatine (COR), which are important *Pcal* virulence factors [32,38], are involved in brassinin suppression, we examined the expression profiles of brassinin biosynthesis related-genes during infection with WT, NB35 (a TTSS mutant), and  $\Delta cmaA$ . Since NB35 and  $\Delta cmaA$  showed significantly reduced populations

compared to WT [32,38,39], we first determined the time point at which these three strains have the same bacterial populations. Bacterial populations in cabbage inoculated with these strains were not significantly different at 6 hpi (Supplementary Figure S4). Therefore, we examined the expression profiles in plants inoculated with these *Pcal* strains at 6 hpi. All genes involved in brassinin biosynthesis, except *BABG.a*, showed significantly or tended to show greater expression during NB35 infection compared to WT and  $\Delta cmaA$  (Figure 5A–D). These results indicate that the TTSS might be involved in brassinin biosynthesis suppression.

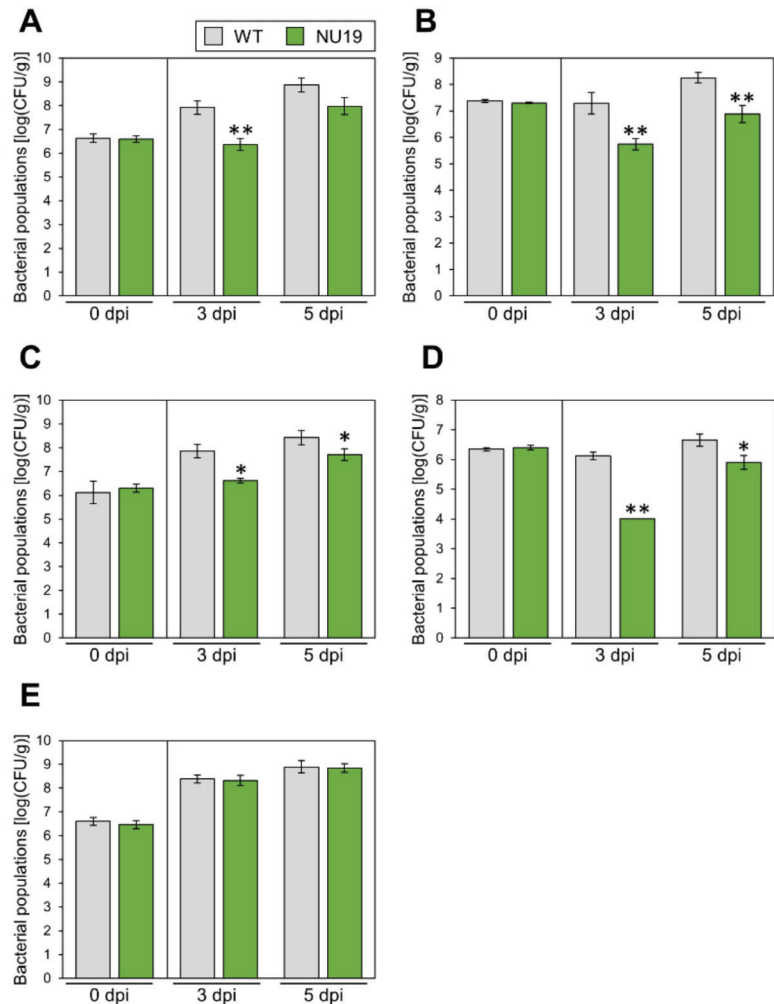


**Figure 4.** Bacterial populations of *Pseudomonas cannabina* pv. *alisalensis* KB211 WT and NU19 in broccoli (A), Japanese radish (B), Chinese cabbage (C), tomato (D), and oat (E). All plants were dip-inoculated with  $5 \times 10^7$  CFU/mL of inoculum containing 0.025% Silwet L-77. The bacterial populations in the plant were evaluated at 0, 3, and 5 dpi. Vertical bars indicate the standard error for at least three independent experiments. Asterisks indicate a significant difference from the *Pcal* WT in a *t*-test (\*  $p < 0.05$ , \*\*  $p < 0.01$ ).

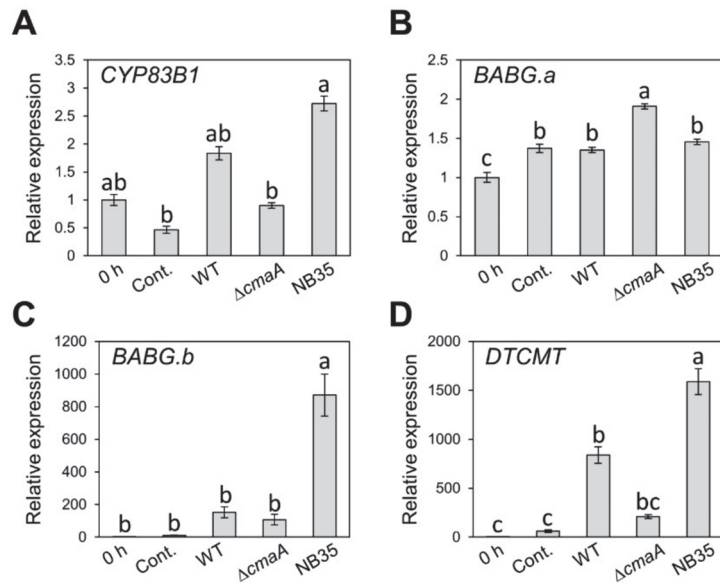


**Figure 5.** Gene expression profiles of brassinin biosynthesis-related genes after syringe inoculation with water (mock), or *Pseudomonas cannabina* pv. *alisalensis* KB211 WT,  $\Delta cmaA$ , and NB35 (TTSS mutant). Expression profiles of *CYP83B1* (A), *BAG.a* (B), *BAG.b* (C), and *DTCMT* (D) were determined 6 h after inoculation with  $5 \times 10^7$  CFU/mL of WT,  $\Delta cmaA$ , NB35 or mock water-inoculated control, using real-time quantitative reverse transcription PCR with gene-specific primer sets. Expression in cabbage was normalized using *BoUBQ1*. Vertical bars indicate the standard error for three biological replicates. Different letters indicate a significant difference among treatments based on a Tukey's honestly significant different test ( $p < 0.05$ ).

### 3. Discussion

Bacteria are exposed to, and tolerate, diverse and potentially toxic compounds in the natural environment [40]. While efflux transporters are generally thought to involve bacterial antibiotic resistance in vitro, their contributions to plant bacterial virulence have so far been poorly understood. We here demonstrated that NU19, which is mutated in the RND transporter encoded gene, showed reduced virulence on cabbage compared to WT (Figure 1), indicating that the RND transporter contributes to *Pcal* virulence on cabbage. We also demonstrated that brassinin biosynthesis was induced after *Pcal* infection (Figure 2). Additionally, the RND transporter was involved in resistance to several plant-derived antimicrobials and antibiotics, including brassinin (Figure 3). These results suggest that the RND transporter contributes to *Pcal* virulence through extruding host-derived antimicrobials. The RND transporter also contributes to *Pcal* virulence on Brassicaceae plants and tomato, but not on oat (Figure 4), suggesting that RND transporter contributes to *Pcal* virulence differentially depending on the host plant species. Lastly, our expression-profile analysis indicates that the TTSS is also involved in brassinin biosynthesis suppression (Figure 5). Taken together, our results suggest that several *Pcal* virulence factors are involved in resistance to plant-derived antimicrobials and bacterial survival during infection.

Brassinin biosynthesis was induced in response to *Pcal* infection (Figure 2). Moreover, indole glucosinolates biosynthesis-related gene expression, including brassinin, were induced after *Pcal* infection (Figure 2; Supplementary Figure S2D,E). Conversely, aliphatic glucosinolate biosynthesis-related gene expression was downregulated in response to *Pcal* infection (Supplementary Figure S2A–C). Indeed, in *A. thaliana*, when the aliphatic glucosinolate pathway is blocked because of a *cyp83a1* mutation, the pathways for indole

glucosinolate and camalexin were enhanced [41]. One possible explanation for how the glucosinolate synthetase *CYP83A1* gene mutation affects camalexin accumulation is that it may cause crosstalk between the aliphatic glucosinolates and indole glucosinolates biosynthetic pathways [41]. Consistent with this, our data also indicated that indole glucosinolate pathways, including brassinin, were induced after *Pcal* infection, while aliphatic glucosinolate pathways were downregulated (Figure 2; Supplementary Figure S2). Accumulation of indole indolic metabolites has been observed in response to *P. syringae* [23,24,42,43], and these indole metabolites, such as camalexin, 4-methoxyglucobrassicin, and 4-hydroxyindole-3-carbonyl nitrile, are important in *A. thaliana* basal defense [19,43–46]. Importantly, the increased biosynthesis of various glucosinolate classes depends on the type of challenging pathogens [26]. Together, the rapid and precise regulation of glucosinolate biosynthesis work in response to pathogen infection, and the downstream products of indole glucosinolates might function as the cabbage defense metabolites against bacterial pathogens.

The RND transporter contributes to *Pcal* virulence on Brassicaceae crops (Figures 1 and 4A–C). We also demonstrated that the RND transporter contributes to susceptibility to the cabbage phytoalexin brassinin (Figure 3A), suggesting that RND transporters contribute to *Pcal* virulence by providing resistance to host-derived antimicrobials. The *mexAB-oprM* deletion mutants of *Pto* DC3000, *Pph* 1448A, *Psy* B728a, and *Pta* 6605 exhibited increased susceptibility to antimicrobials, and reduced disease-symptom development and bacterial populations [35–37]. In *Pta*, the RND transporter contributed not only directly to extrude antimicrobials, but also indirectly to regulate motility and N-acyl-homoserine lactone (AHL) production [36]. Thus, further investigation will lead to understanding the importance of the RND transporter in bacterial virulence.

Brassinin biosynthesis-related genes showed greater expression during the TTSS mutant infection compared to WT and the COR mutant (Figure 5), suggesting that the TTSS is involved in suppressing brassinin biosynthesis. Bais et al. (2005) also demonstrated that the TTSS and perhaps other virulence factors under HrpL control (but not COR) are required for blocking the synthesis or exudation of antimicrobial compounds in *Pto* DC3000 [47]. Moreover, *P. syringae* HopZ1 targeted a host enzyme to suppress isoflavone biosynthesis in soybean, which are important secondary metabolites during plant–microbe interactions in soybean [48]. These results suggest that the TTSS suppressed host-derived antimicrobial biosynthesis in addition to those emitted by the RND transporter. Conversely, a phytoanticipin, sulforaphane, inhibits *P. syringae* TTSS genes [49]. Chemoproteomics analyses showed that sulforaphane covalently modified the cysteine at position 209 of HrpS, a key transcriptional factor controlling TTSS gene expression [49]. This study indicated that sulforaphane inhibited virulence gene expression instead of targeting general bacterial activity. Taken together, although further analysis will be needed, there is a possibility that plant-derived antimicrobials and bacterial virulence factors target each other.

Moreover, although the RND transporter contributes to *Pcal* virulence on multiple host plants (Figure 4A–D), the NU19 multiplication defect was not observed on oat, indicating that the RND transporter has less or no contribution to disease on oat (Figure 4E). *Psy* B728a MexB contributes to virulence in common bean, but was not required for growth in lima bean, fava bean, pepper, *Nicotiana benthamiana*, sunflower, and tomato [50]. Additionally, *Sclerotinia sclerotiorum* induced both camalexin and aliphatic glucosinolate biosynthesis genes, while *B. cinerea* did not induce aliphatic glucosinolate and induced camalexin biosynthesis genes [14]. Therefore, the plant–microbe interaction must be considered. Moreover, despite the high degree of primary homology between two RND transporters, AcrAB-TolG and MexAB-OprM, these pumps do not efflux all substrates with equal efficiency [51]. These results indicated that RND transporters have substrate specificity. Related plant families generally make use of related chemical structures for defense [2]. Indeed, oat major specialized metabolites are amphiphilic saponins [52], while brassicaceae major specialized metabolites are glucosinolates and indole alkanoids [53]. Given these very different polarities, it is unlikely that the same RND transporter would be suitable to efflux them out of the cells. However, the reason for the difference in RND transporter contribution

depending on the host plant remains unclear. Further studies on oat secondary metabolites and RND transporter roles in *Pcal* virulence on different host plants are necessary.

We here demonstrated that the RND transporter contributes to *Pcal* virulence on Brassicaceae plants. The RND transporter plays an important role in resistance to plant-derived antimicrobials and antibiotics. Moreover, we revealed that the TTSS might be involved in suppressing brassinin biosynthesis. Our study shed light on the importance of efflux or suppressing host-derived antimicrobials for successful bacterial infection. Further study on plant–bacterial interactions over host-derived metabolites will be needed to understand *Pcal* host diversity and virulence mechanisms.

#### 4. Materials and Methods

##### 4.1. Bacterial Strains, Plasmids, and Growth Conditions

The bacterial strains and plasmids used in this study are described in Supplementary Table S1. *Pseudomonas cannabina* pv. *alisalensis* strain KB211 (*Pcal* KB211) was used as the pathogenic strain to inoculate cabbage, broccoli, Japanese radish, Chinese cabbage, tomato, and oat. *Pcal* wild type (WT) and  $\Delta cmaA$  were grown on King's B (KB; [54]) medium at 28 °C NU19 and NB35 were grown on KB medium containing kanamycin (10 µg/mL) (Km) (Supplementary Table S1). Before *Pcal* inoculation, bacteria were suspended in sterile distilled H<sub>2</sub>O, and the bacterial cell densities at 600 nm (OD<sub>600</sub>) were measured using a Biowave CO8000 Cell Density Meter (Funakoshi, Tokyo, Japan).

##### 4.2. Bacterial In Vitro Growth Measurements

WT and NU19 were grown at 28 °C on Luria–Bertani (LB; [55]) medium. The bacterial suspensions were standardized to an OD<sub>600</sub> of 0.01 with LB, and bacterial growth was measured at OD<sub>600</sub> for 6, 9, 12, and 24 h.

##### 4.3. Plant Materials

Plants used for *Pcal* virulence assays include cabbage (*Brassica oleracea* var. *capitata*) cv. Kinkei 201, broccoli (*Brassica oleracea* var. *italica*) cv. Midoribue, Japanese radish (*Raphanus sativus* var. *longipinnatus*) cv. Natsutsukasa, Chinese cabbage (*Brassica rapa* var. *pekinensis*) cv. Akimeki, tomato (*Solanum lycopersicum*) cv. Moneymaker, and oat (*Avena strigosa*) cv. Hayoat. All plants were grown from seed at 23–25 °C with a light intensity of 200 µEm<sup>-2</sup>s<sup>-1</sup> and a 16 h light/8 h dark photoperiod. Seedlings were used for dip-inoculation assays around two weeks after germination.

##### 4.4. Bacterial Inoculation

To assay for disease on cabbage, broccoli, Japanese radish, Chinese cabbage, tomato, and oat plants, dip inoculations were conducted by soaking seedlings in bacterial suspensions ( $5 \times 10^7$  CFU/mL) containing 0.025% Silwet L-77 (OSI Specialities, Danbury, CT, USA). The seedlings were then incubated in growth chambers at 85–95% RH for the first 24 h, then at 80–85% RH for the rest of the experimental period. Disease symptoms were photographed at 5 days postinoculation (dpi) for all plants. To assess bacterial growth in all plants, the internal bacterial populations were measured after dip inoculation. Inoculated seedlings were collected, and two inoculated leaves were measured. The leaves were surface-sterilized with 10% H<sub>2</sub>O<sub>2</sub> for 3 min. After washing with sterile distilled water three times, the leaves were homogenized in sterile distilled water, and diluted samples were plated onto solid KB agar medium. Two or three days after dilution sample plating, the bacterial colony-forming units (CFUs) were counted and normalized as CFU per gram, using the total leaf weight. The bacterial populations at 0 dpi were estimated using leaves harvested at 1 hpi without surface sterilization. The bacterial populations were evaluated in at least three independent experiments.

Cabbage was syringe-inoculated with *Pcal* WT,  $\Delta cmaA$ , and NB35 ( $5 \times 10^7$  CFU/mL) with a 1 mL blunt syringe. The plants were then incubated at 70–80% RH for the rest of the experimental period. To assess bacterial growth in cabbage, the internal bacterial

population was measured at 6 hpi. Leaf disks were harvested using a 3.5 mm-diameter cork-borer from syringe-infiltrated zones. The bacterial populations were evaluated in at least three independent experiments.

#### 4.5. Monitoring Gene Expression in Planta

To analyze plant gene expression profiles during infection, we syringe-inoculated cabbage plants with *Pcal* WT ( $5 \times 10^5$  CFU/mL), and sampled at 24 and 48 hpi. To compare gene expression profiles during infection, cabbage plants were syringe-inoculated with *Pcal* WT,  $\Delta$ *cmnA*, and NB35 ( $5 \times 10^7$  CFU/mL), and sampled at 6 hpi, where the bacterial populations of even the virulence pathogen WT had not yet significantly increased. The total RNAs, including plant and bacterial RNAs, were extracted from infected leaves and purified. Total RNA extraction and real-time quantitative RT-PCR (RT-qPCR) were performed as described previously [56]. Two micrograms of total RNA were treated with gDNA Remover (Toyobo, Osaka, Japan) to eliminate genomic DNA, and the DNase-treated RNA was reverse-transcribed using the ReverTra Ace qPCR RT Master Mix (Toyobo). The cDNA (1:10) was then used for RT-qPCR using the primers shown in Table S2 with THUNDERBIRD SYBR qPCR Mix (Toyobo) on a Thermal Cycler Dice Real-Time System (Takara Bio, Kusatsu, Japan). Cabbage *UBIQUITIN EXTENSION PROTEIN 1* (*BoUBQ1*) was used as an internal control to normalize gene expression. The reagent blank (no-template) controls were used to detect contamination. The expression profiles were evaluated in at least six independent samples.

#### 4.6. Brassinin Quantification by RP-LC-ESI-MS/MS

*Pcal* WT bacterial suspension ( $5 \times 10^5$  CFU/mL), or water (mock) were infiltrated into three-week-old cabbage. Twenty leaf discs (3.5 mm diameter) from four cabbage leaves were collected 48 hpi, the weight was measured, and samples were frozen in liquid nitrogen and stored at  $-80$  °C. Samples were extracted with 300  $\mu$ L of 80% methanol.

Brassinin was measured by using the multiple reaction monitoring (MRM) mode on the LC-ESI-MS/MS (LCMS-8045; Shimadzu, Kyoto, Japan) under the following conditions: capillary voltage, 4.5 kV; desolvation line, 300 °C; heat block, 500 °C; nebulizer nitrogen gas 3 L/min; drying gas, 10 L/min. Ion-source polarity was set in the negative-ion mode. The separation was performed with the LC system equipped with a 150  $\times$  2.1 mm ACQUITY UPLC CSH C18 Column (Waters Corp., Milford, MA, USA) with a particle and pore size of 1.7  $\mu$ m and 130 Å, respectively. The initial mobile phase was solvent A: solvent B = 95:5 (solvent A, 0.025% formic acid; solvent B, acetonitrile (LC/MS Grade, Merck KGaA, Darmstadt, Germany) and maintained for 4 min. The solvent B concentration was increased to 50% for 11 min and then maintained at that ratio for another 5 min. The column was re-equilibrated for 3 min. The 0.4 mL min<sup>-1</sup> flow rate and the 40 °C column temperature were maintained throughout the analysis. The MRM-transition *m/z* 235→58 was used as a precursor and as productions, respectively. The dwell time, Q1 pre-bias, collision energy, and Q3 pre-bias were set at 100 ms, 26 V, 7 eV, 21 V, respectively. The brassinin ion peak was detected at the retention of 15.3 min, and the fragment ion peak area of *m/z* = 58 was used for the quantification.

#### 4.7. Antimicrobial-Activity Assay

To analyze brassinin antimicrobial activity against bacteria, the *Pcal* suspension was standardized to an OD<sub>600</sub> of 0.01 in LB and coinoculated with or without 200  $\mu$ M brassinin (Merck KGaA). After 24 h, bacterial growth was measured at OD<sub>600</sub>.

#### 4.8. Inhibition Assay

To analyze WT and NU19 susceptibility to plant-derived antimicrobials, WT and NU19 were grown at 28 °C on KB medium. The bacterial suspensions were standardized to an OD<sub>600</sub> of 0.01 with KB, and after 6 h incubation, 200  $\mu$ M antimicrobials, including brassinin (Merck KGaA), sulforaphane (Funakoshi), camalexin (Merck KGaA), daidzein (INDOFINE

Chemical Company, Hillsborough, NJ, USA), genistein (Tokyo Chemical Industry, Tokyo, Japan), indole (Tokyo Chemical Industry), and phloretin (Funakoshi), was added to each sample. Bacterial growth was measured at OD<sub>600</sub> after 24 h incubation.

#### 4.9. Drug-Susceptibility Tests

The minimum inhibitory concentrations (MICs) of antibiotics for WT and NU19 were determined via cell growth in 2-fold dilutions of test compounds, including spectinomycin, streptomycin, nalidixic acid, cefotaxime, tetracycline, ampicillin, and carbenicillin (Merck KGaA), in 96-well plates containing KB medium to reach a total volume of 100 µL per well. The bacterial suspensions were standardized to an OD<sub>600</sub> of 0.01 with KB, and bacterial growth was examined by visual inspection after 24 h of static incubation.

#### 4.10. Statistical Analysis

All data are expressed as the mean with SE. All statistical analyses were performed using EZR (Saitama Medical Centre, Jichi Medical University, Saitama, Japan; [57]), a graphical user interface for R (version 3.6.3; R Foundation for statistical Computing, Vienna, Austria). Tukey's honestly significant difference (HSD) test was used to analyze gene expression profiles. Differences of  $p < 0.05$  were considered statistically significant.

**Supplementary Materials:** The following supporting information can be downloaded at: <https://www.mdpi.com/article/10.3390/plants11131742/s1>, Table S1: Bacterial strains and plasmids used in this study; Table S2: Primer sets used in this study; Figure S1: *Pseudomonas cannabina* pv. *alisalensis* KB211 WT and NU19 growth in KB medium; Figure S2: Expression profiles of *CYP83A1* (A), *FMOG-OX2* (B), *FMOG-OX5* (C), *CYP81F2* (D), *CYP81F4* (E) were determined 24 and 48 h after inoculation with  $5 \times 10^5$  CFU/mL of WT or mock water-inoculated control, using real-time quantitative reverse transcription PCR with gene-specific primer sets; Figure S3: Disease symptoms on broccoli (A), Japanese radish (B), Chinese cabbage (C), tomato (D), and oat (E) dip-inoculated with *Pseudomonas cannabina* pv. *alisalensis* KB211 WT and NU19; Figure S4: Bacterial populations in cabbage syringe-inoculated with *Pseudomonas cannabina* pv. *alisalensis* KB211 WT,  $\Delta$ *cmaA*, and NB35 (TTSS mutant); Spreadsheets: The data presented in this study.

**Author Contributions:** N.S. and Y.I. designed the experiments; N.S., T.H., S.M., T.I. and Y.I. performed the experiments; N.S. and Y.I. wrote the manuscript. All authors have read and agreed to the published version of the manuscript.

**Funding:** This work was supported: in part, by the Japan Society for the Promotion of Science (JSPS), Grant Number: 19K06045 (Y.I.), and by the JSPS, Grant Number: 21J10765 (N.S.).

**Institutional Review Board Statement:** Not applicable.

**Informed Consent Statement:** Not applicable.

**Data Availability Statement:** The data presented in this study are openly available in Supplementary Materials here.

**Acknowledgments:** We thank Christina Baker for editing the manuscript. *Pcal* KB211 was kindly given from the Nagano vegetable and ornamental crops experiment station, Nagano, Japan.

**Conflicts of Interest:** The authors declare no conflict of interest.

## References

1. Piasecka, A.; Jedrzejczak-Rey, N.; Bednarek, P. Secondary metabolites in plant innate immunity: Conserved function of divergent chemicals. *New Phytol.* **2015**, *206*, 948–964. [CrossRef] [PubMed]
2. Dixon, R.A. Natural products and plant disease resistance. *Nature* **2001**, *411*, 843–847. [CrossRef]
3. VanEtten, H.D.; Mansfield, J.W.; Bailey, J.A.; Farmer, E.E. Two classes of plant antibiotics: Phytoalexins versus phytoanticipins. *Plant Cell* **1994**, *6*, 1191–1192. [CrossRef] [PubMed]
4. Ahuja, I.; Kissen, R.; Bones, A.M. Phytoalexins in defense against pathogens. *Trends Plant Sci.* **2012**, *17*, 73–90. [CrossRef] [PubMed]
5. González-Lamothe, R.; Mitchell, G.; Gattuso, M.; Diarra, M.S.; Malouin, F.; Bouarab, K. Plant antimicrobial agents and their effects on plant and human pathogens. *Int. J. Mol. Sci.* **2009**, *10*, 3400–3419. [CrossRef]

6. Pedras, M.S.C.; Abdoli, A. Pathogen inactivation of cruciferous phytoalexins: Detoxification reactions, enzymes and inhibitors. *RSC Adv.* **2017**, *7*, 23633–23646. [[CrossRef](#)]
7. Fan, J.; Doerner, P.; Lamb, C. *Pseudomonas sax* genes overcome non-host resistance in *Arabidopsis*. *Science* **2011**, *1185*, 1185–1188. [[CrossRef](#)]
8. Klein, A.P.; Sattely, E.S. Biosynthesis of cabbage phytoalexins from indole glucosinolate. *Proc. Natl. Acad. Sci. USA* **2017**, *114*, 1910–1915. [[CrossRef](#)]
9. Pedras, M.S.C.; Yaya, E.E.; Glawischnig, E. The phytoalexins from cultivated and wild crucifers: Chemistry and biology. *Nat. Prod. Rep.* **2011**, *28*, 1381–1405. [[CrossRef](#)]
10. Glawischnig, E. Camalexin. *Phytochemistry* **2007**, *68*, 401–406. [[CrossRef](#)]
11. Schlaeppi, K.; Abou-Mansour, E.; Buchala, A.; Mauch, F. Disease resistance of *Arabidopsis* to *Phytophthora brassicae* is established by the sequential action of indole glucosinolates and camalexin. *Plant J.* **2010**, *62*, 840–851. [[CrossRef](#)] [[PubMed](#)]
12. Rogers, E.E.; Glazebrook, J.; Ausubel, F.M. Mode of action of the *Arabidopsis thaliana* phytoalexin camalexin and its role in *Arabidopsis*-pathogen interactions. *Mol. Plant. Microbe. Interact.* **1996**, *9*, 748–757. [[CrossRef](#)] [[PubMed](#)]
13. Sellam, A.; Iacomini-Vasilescu, B.; Hudhomme, P.; Simoneau, P. In vitro antifungal activity of brassinin, camalexin and two isothiocyanates against the crucifer pathogens *Alternaria brassicicola* and *Alternaria brassicae*. *Plant Pathol.* **2007**, *56*, 296–301. [[CrossRef](#)]
14. Stotz, H.U.; Sawada, Y.; Shimada, Y.; Hirai, M.Y.; Sasaki, E.; Krischke, M.; Brown, P.D.; Saito, K.; Kamiya, Y. Role of camalexin, indole glucosinolates, and side chain modification of glucosinolate-derived isothiocyanates in defense of *Arabidopsis* against *Sclerotinia sclerotiorum*. *Plant J.* **2011**, *67*, 81–93. [[CrossRef](#)]
15. Sanchez-Vallet, A.; Ramos, B.; Bednarek, P.; López, G.; Piślewska-Bednarek, M.; Schulze-Lefert, P.; Molina, A. Tryptophan-derived secondary metabolites in *Arabidopsis thaliana* confer non-host resistance to necrotrophic *Plectosphaerella cucumerina* fungi. *Plant J.* **2010**, *63*, 115–127. [[CrossRef](#)]
16. Kliebenstein, D.J.; Rowe, H.C.; Denby, K.J. Secondary metabolites influence *Arabidopsis/Botrytis* interactions: Variation in host production and pathogen sensitivity. *Plant J.* **2005**, *44*, 25–36. [[CrossRef](#)]
17. Pedras, M.S.; Khan, A.Q. Biotransformation of the phytoalexin camalexin by the phytopathogen *Rhizoctonia solani*. *Phytochemistry* **2000**, *53*, 59–69. [[CrossRef](#)]
18. Ferrari, S.; Plotnikova, J.M.; De Lorenzo, G.; Ausubel, F.M. *Arabidopsis* local resistance to *Botrytis cinerea* involves salicylic acid and camalexin and requires *EDS4* and *PAD2*, but not *SID2*, *EDS5* or *PAD4*. *Plant J.* **2003**, *35*, 193–205. [[CrossRef](#)]
19. Thomma, B.P.; Nelissen, I.; Eggermont, K.; Broekaert, W.F. Deficiency in phytoalexin production causes enhanced susceptibility of *Arabidopsis thaliana* to the fungus *Alternaria brassicicola*. *Plant J.* **1999**, *19*, 163–171. [[CrossRef](#)]
20. Nafisi, M.; Goregaoker, S.; Botanga, C.J.; Glawischnig, E.; Olsen, C.E.; Halkier, B.A.; Glazebrook, J. *Arabidopsis* cytochrome P450 monooxygenase 71A13 catalyzes the conversion of indole-3-acetaldoxime in camalexin synthesis. *Plant Cell* **2007**, *19*, 2039–2052. [[CrossRef](#)]
21. Bohman, S.; Staal, J.; Thomma, B.P.H.J.; Wang, M.; Dixelius, C. Characterisation of an *Arabidopsis-Leptosphaeria maculans* pathosystem: Resistance partially requires camalexin biosynthesis and is independent of salicylic acid, ethylene and jasmonic acid signalling. *Plant J.* **2004**, *37*, 9–20. [[CrossRef](#)] [[PubMed](#)]
22. Lemarié, S.; Robert-Seilaniantz, A.; Lariagon, C.; Lemoine, J.; Marnet, N.; Levrel, A.; Jubault, M.; Manzaneres-Dauleux, M.J.; Grivot, A. Camalexin contributes to the partial resistance of *Arabidopsis thaliana* to the biotrophic soilborne protist *Plasmodiophora brassicae*. *Front. Plant Sci.* **2015**, *6*, 539. [[CrossRef](#)] [[PubMed](#)]
23. Glazebrook, J.; Ausubel, F.M. Isolation of phytoalexin-deficient mutants of *Arabidopsis thaliana* and characterization of their interactions with bacterial pathogens. *Proc. Natl. Acad. Sci. USA* **1994**, *91*, 8955–8959. [[CrossRef](#)] [[PubMed](#)]
24. Zhou, N.; Tootle, T.L.; Glazebrook, J. *Arabidopsis* *PAD3*, a gene required for camalexin biosynthesis, encodes a putative cytochrome P450 monooxygenase. *Plant Cell* **1999**, *11*, 2419–2428. [[CrossRef](#)] [[PubMed](#)]
25. Nguyen, N.H.; Trotel-Aziz, P.; Villaume, S.; Rabenoelina, F.; Clément, C.; Baillieux, F.; Aziz, A. Priming of camalexin accumulation in induced systemic resistance by beneficial bacteria against *Botrytis cinerea* and *Pseudomonas syringae* pv. *tomato* DC3000. *J. Exp. Bot.* **2022**, *73*, 3743–3757. [[CrossRef](#)]
26. Plaszkó, T.; Szűcs, Z.; Vasas, G.; Gonda, S. Interactions of fungi with non-isothiocyanate products of the plant glucosinolate pathway: A review on product formation, antifungal activity, mode of action and biotransformation. *Phytochemistry* **2022**, *200*, 113245. [[CrossRef](#)]
27. N’Guyen, G.Q.; Raulo, R.; Porquier, A.; Iacomini, B.; Pelletier, S.; Renou, J.-P.; Bataillé-Simoneau, N.; Champion, C.; Hamon, B.; Kwasiborski, A.; et al. Responses of the necrotrophic fungus *Alternaria brassicicola* to the indolic phytoalexin brassinin. *Front. Plant Sci.* **2021**, *11*, 2216. [[CrossRef](#)]
28. Chassot, C.; Buchala, A.; Schoonbeek, H.-J.; Métraux, J.-P.; Lamotte, O. Wounding of *Arabidopsis* leaves causes a powerful but transient protection against *Botrytis* infection. *Plant J.* **2008**, *55*, 555–567. [[CrossRef](#)]
29. Van Baarlen, P.; Woltering, E.J.; Staats, M.; VAN Kan, J.A.L. Histochemical and genetic analysis of host and non-host interactions of *Arabidopsis* with three *Botrytis* species: An important role for cell death control. *Mol. Plant Pathol.* **2007**, *8*, 41–54. [[CrossRef](#)]
30. Takikawa, Y.; Takahashi, F. Bacterial leaf spot and blight of crucifer plants (Brassicaceae) caused by *Pseudomonas syringae* pv. *maculicola* and *P. cannabina* pv. *alisalensis*. *J. Gen. Plant Pathol.* **2014**, *80*, 466–474. [[CrossRef](#)]

31. Takahashi, F.; Ochiai, M.; Ikeda, K.; Takikawa, Y. Streptomycin and copper resistance in *Pseudomonas cannabina* pv. *alisalensis*. *Jpn. J. Phytopathol.* **2013**, *35*. (abstract in Japanese).
32. Sakata, N.; Ishiga, T.; Saito, H.; Nguyen, V.T.; Ishiga, Y. Transposon mutagenesis reveals *Pseudomonas cannabina* pv. *alisalensis* optimizes its virulence factors for pathogenicity on different hosts. *PeerJ* **2019**, *7*, e7698. [[CrossRef](#)] [[PubMed](#)]
33. Piddock, L.J.V. Multidrug-resistance efflux pumps - not just for resistance. *Nat. Rev. Microbiol.* **2006**, *4*, 629–636. [[CrossRef](#)] [[PubMed](#)]
34. Blair, J.M.A.; Piddock, L.J.V. Structure, function and inhibition of RND efflux pumps in gram-negative bacteria: An update. *Curr. Opin. Microbiol.* **2009**, *12*, 512–519. [[CrossRef](#)] [[PubMed](#)]
35. Stoitsova, S.O.; Braun, Y.; Ullrich, M.S.; Weingart, H. Characterization of the RND-type multidrug efflux pump MexAB-OprM of the plant pathogen *Pseudomonas syringae*. *Appl. Environ. Microbiol.* **2008**, *74*, 3387–3393. [[CrossRef](#)]
36. Ichinose, Y.; Nishimura, T.; Harada, M.; Kashiwagi, R.; Yamamoto, M.; Noutoshi, Y.; Toyoda, K.; Taguchi, F.; Takemoto, D.; Matsui, H. Role of two sets of RND-type multidrug efflux pump transporter genes, *MexAB-OprM* and *MexEF-OprN*, in virulence of *Pseudomonas syringae* pv. *tabaci* 6605. *Plant Pathol. J.* **2020**, *36*, 148–156. [[CrossRef](#)]
37. Helmann, T.C.; Ongsarte, C.L.; Lam, J.; Deutschbauer, A.M.; Lindow, S.E. Genome-wide transposon screen of a *Pseudomonas syringae* *mexB* mutant reveals the substrates of efflux transporters. *MBio* **2019**, *10*, e02614-19. [[CrossRef](#)]
38. Sakata, N.; Ishiga, T.; Masuo, S.; Hashimoto, Y.; Ishiga, Y. Coronatine contributes to *Pseudomonas cannabina* pv. *alisalensis* virulence by overcoming both stomatal and apoplastic defenses in dicot and monocot plants. *Mol. Plant. Microbe. Interact.* **2021**, *34*, 746–757. [[CrossRef](#)]
39. Sakata, N.; Ishiga, T.; Ishiga, Y. *Pseudomonas cannabina* pv. *alisalensis* TrpA is required for virulence in multiple host plants. *Front. Microbiol.* **2021**, *12*, 659734. [[CrossRef](#)]
40. Mareri, L.; Parrotta, L.; Cai, G. Environmental stress and plants. *Int. J. Mol. Sci.* **2022**, *23*, 5416. [[CrossRef](#)]
41. Liu, S.; Bartnikas, L.M.; Volko, S.M.; Ausubel, F.M.; Tang, D. Mutation of the glucosinolate biosynthesis enzyme cytochrome P450 83A1 monooxygenase increases camalexin accumulation and powdery mildew resistance. *Front. Plant Sci.* **2016**, *7*, 227. [[CrossRef](#)] [[PubMed](#)]
42. Forcat, S.; Bennett, M.; Grant, M.; Mansfield, J.W. Rapid linkage of indole carboxylic acid to the plant cell wall identified as a component of basal defence in *Arabidopsis* against *hrp* mutant bacteria. *Phytochemistry* **2010**, *71*, 870–876. [[CrossRef](#)] [[PubMed](#)]
43. Rajniak, J.; Barco, B.; Clay, N.K.; Sattely, E.S. A new cyanogenic metabolite in *Arabidopsis* required for inducible pathogen defence. *Nature* **2015**, *525*, 376–379. [[CrossRef](#)] [[PubMed](#)]
44. Bednarek, P.; Pislewski-Bednarek, M.; Svatos, A.; Schneider, B.; Doubsky, J.; Mansurova, M.; Humphry, M.; Consonni, C.; Panstruga, R.; Sanchez-Vallet, A.; et al. A glucosinolate metabolism pathway in living plant cells mediates broad-spectrum antifungal defense. *Science* **2009**, *323*, 101–106. [[CrossRef](#)]
45. Clay, N.K.; Adio, A.M.; Denoux, C.; Jander, G.; Ausubel, F.M. Glucosinolate metabolites required for an *Arabidopsis* innate immune response. *Science* **2009**, *323*, 95–101. [[CrossRef](#)]
46. Millet, Y.A.; Danna, C.H.; Clay, N.K.; Songnuan, W.; Simon, M.D.; Werck-Reichhart, D.; Ausubel, F.M. Innate immune responses activated in *Arabidopsis* roots by microbe-associated molecular patterns. *Plant Cell* **2010**, *22*, 973–990. [[CrossRef](#)]
47. Bais, H.P.; Prithiviraj, B.; Jha, A.K.; Ausubel, F.M.; Vivanco, J.M. Mediation of pathogen resistance by exudation of antimicrobials from roots. *Nature* **2005**, *434*, 217–221. [[CrossRef](#)]
48. Zhou, H.; Lin, J.; Johnson, A.; Morgan, R.L.; Zhong, W.; Ma, W. *Pseudomonas syringae* type III effector HopZ1 targets a host enzyme to suppress isoflavone biosynthesis and promote infection in soybean. *Cell Host Microbe* **2011**, *9*, 177–186. [[CrossRef](#)]
49. Wang, W.; Yang, J.; Zhang, J.; Liu, Y.X.; Tian, C.; Qu, B.; Gao, C.; Xin, P.; Cheng, S.; Zhang, W.; et al. An *Arabidopsis* secondary metabolite directly targets expression of the bacterial type III secretion system to inhibit bacterial virulence. *Cell Host Microbe* **2020**, *27*, 601–613.e7. [[CrossRef](#)]
50. Helmann, T.; King, D.; Lindow, S. Differential virulence contributions of the efflux transporter MexAB-OprM in *Pseudomonas syringae* infecting variety of host plants. *Mol. Plant. Microbe. Interact.* **2022**, in press. [[CrossRef](#)]
51. Tikhonova, E.B.; Wang, Q.; Zgurskaya, H.I. Chimeric Analysis of the Multicomponent Multidrug Efflux Transporters from Gram-Negative Bacteria. *J. Bacteriol.* **2002**, *184*, 6499–6507. [[CrossRef](#)] [[PubMed](#)]
52. Raguindin, P.F.; Adam Itodo, O.; Stoyanov, J.; Dejanovic, G.M.; Gamba, M.; Asllanaj, E.; Minder, B.; Bussler, W.; Metzger, B.; Muka, T.; et al. A systematic review of phytochemicals in oat and buckwheat. *Food Chem.* **2021**, *338*, 127982. [[CrossRef](#)] [[PubMed](#)]
53. Nafisi, M.; Sonderby, I.E.; Hansen, B.G.; Geu-Flores, F.; Nour-Eldin, H.H.; Nørholm, M.H.H.; Jensen, N.B.; Li, J.; Halkier, B.A. Cytochromes P450 in the biosynthesis of glucosinolates and indole alkaloids. *Phytochem. Rev.* **2006**, *5*, 331–346. [[CrossRef](#)]
54. King, E.O.; Ward, M.K.; Raney, D.E. Two simple media for the demonstration of pyocyanin and fluorescin. *J. Lab. Clin. Med.* **1954**, *44*, 301–307. [[CrossRef](#)] [[PubMed](#)]
55. Sambrook, J.; Fritsch, E.F.; Maniatis, T. *Molecular cloning: A laboratory manual*, 2nd ed.; Cold Spring Harbor Laboratory: Huntington, NY, USA, 1989.
56. Ishiga, Y.; Ichinose, Y. *Pseudomonas syringae* pv. *tomato* OxyR is required for virulence in tomato and *Arabidopsis*. *Mol. Plant. Microbe. Interact.* **2016**, *29*, 119–131. [[CrossRef](#)]
57. Kanda, Y. Investigation of the freely available easy-to-use software “EZR” for medical statistics. *Bone Marrow Transplant.* **2013**, *48*, 452–458. [[CrossRef](#)]

## Article

# Different Cell Types Affect the Transition from Juvenile to Mature Phase in Citrus Plants Regenerated through Somatic Embryogenesis

Caterina Catalano <sup>1,†</sup>, Loredana Abbate <sup>1,†</sup>, Sergio Fatta Del Bosco <sup>1</sup>, Antonio Motisi <sup>1</sup>, Francesco Carimi <sup>1,\*</sup>, Roberto De Michele <sup>1</sup>, Francesco Mercati <sup>1</sup>, Anna Maria D'Onghia <sup>2</sup> and Angela Carra <sup>1</sup>

- <sup>1</sup> CNR—Istituto di Bioscienze e BioRisorse, Corso Calatafimi 414, 90129 Palermo, Italy; caterina.catalano@ibbr.cnr.it (C.C.); loredana.abbate@ibbr.cnr.it (L.A.); sergio.fatta@ibbr.cnr.it (S.F.D.B.); antonio.motisi@ibbr.cnr.it (A.M.); roberto.demichale@ibbr.cnr.it (R.D.M.); francesco.mercati@ibbr.cnr.it (F.M.); angela.carra@ibbr.cnr.it (A.C.)
- <sup>2</sup> CIHEAM—Centre International de Hautes Etudes Agronomiques Méditerranéennes of Bari, Via Ceglie 9, 70010 Valenzano, Italy; donghia@iamb.it
- \* Correspondence: francesco.carimi@ibbr.cnr.it
- † These authors contributed equally to this work.

**Abstract:** Robust protocols for the regeneration of somatic embryos *in vitro* are essential for the efficient use of the most modern biotechnologies. Unfortunately, in perennial trees such as *Citrus*, plants regenerated from juvenile tissues usually exhibit strong, undesirable juvenile characters such as thorny habit and delayed flowering and fruit production. In this work, we tested whether the cell types (nucellar and stigma/style) used to regenerate *Citrus* plants through somatic embryogenesis affected the transition from the juvenile to mature phase. The results show that regenerants from nucellar cells presented persistent juvenile characters, whereas plants originating from stigma/style explants transitioned to the mature phase more rapidly. Our observations support the hypothesis that the totipotent cells originated from different cell types are not equivalent, possibly by maintaining memory of their previously differentiated state.

**Keywords:** flowering; juvenile traits; genetic stability; flow cytometry; plant tissue culture; somaclonal variation; thorniness

**Citation:** Catalano, C.; Abbate, L.; Fatta Del Bosco, S.; Motisi, A.; Carimi, F.; De Michele, R.; Mercati, F.; D'Onghia, A.M.; Carra, A. Different Cell Types Affect the Transition from Juvenile to Mature Phase in Citrus Plants Regenerated through Somatic Embryogenesis. *Plants* **2022**, *11*, 1811. <https://doi.org/10.3390/plants11141811>

Academic Editors: Milan S. Stankovic, Paula Baptista and Petronia Carillo

Received: 10 May 2022

Accepted: 4 July 2022

Published: 8 July 2022

**Publisher's Note:** MDPI stays neutral with regard to jurisdictional claims in published maps and institutional affiliations.



**Copyright:** © 2022 by the authors. Licensee MDPI, Basel, Switzerland. This article is an open access article distributed under the terms and conditions of the Creative Commons Attribution (CC BY) license (<https://creativecommons.org/licenses/by/4.0/>).

## 1. Introduction

The relevance of the *Citrus* industry and the continuous introduction of new improved genotypes encourage the use of biotechnologies based on somatic embryogenesis as an effective tool to rapidly regenerate genotypes of interest. One of the main problems that may limit the use of somatic embryogenesis is the occurrence of somaclonal variation. Plantlets derived from *in vitro* culture might develop altered characteristics and provide a wide range of culture-induced genetic variants [1] called somaclonal variations [2]. Several factors influence the onset of somaclonal variation, with the type and origin of explant being the most influencing elements [3]. Moreover, plantlets regenerated *in vitro* through somatic embryogenesis may display ploidy change that induces several anatomical and morphological changes in regenerants [4]. However, the detection of genetic instability in regenerants can be easily addressed through flow cytometric analysis and DNA-based techniques, such as RFLP, RAPD, ISSR, AFLP and microsatellites [5].

Improvement by conventional breeding for *Citrus* is problematic due to several factors such as sterility, nucellar embryony and long juvenile periods [6,7]. The long juvenile period is probably the major constraint for breeders. In *Citrus*, the mature and juvenile forms show distinct morphological characters such as leaf shape, branch habit, growth habit and degree of thorniness. The transition time from juvenile to mature forms varies from species to species [8] and it is also affected by environmental clues [9–11]. Early

fruit production is a strongly desired character in *Citrus* and, as a consequence, attempts for shortening juvenile period is one of the greatest challenges. There are both historical work and ongoing efforts to use horticultural methods such as hybridization and clonal selection for shortening the juvenile period [12–17]. More recently, protocols for genetic transformation aimed to reduce juvenile period have been proposed [18–22].

*Citrus* genetic and sanitary improvement by conventional methods alone has many limitations that can be overcome using in vitro biotechnologies as somatic embryogenesis, which is reported as a key regeneration pathway in many experimental approaches to cultivar improvement [6]. The final success depends on several factors including the age of the explant. In *Citrus*, the best in vitro results, in terms of rapid proliferation rate, are normally obtained using stock material in the juvenile phase as explant source. Sim et al. [23] and Cervera et al. [24] have reported that explants collected from juvenile *Citrus* plants provide the best regeneration frequency in plant tissue culture as compared to explants collected from adult plants. The limited use of adult explants is due to the low morphogenetic potential of explants, and poor rooting of the shoots obtained [25,26]. For this reason, the regeneration of *Citrus* is usually achieved through the culture of nucellar tissues collected from immature, aborted and unfertilized ovules [27]. Unfortunately, plants regenerated from juvenile tissues usually exhibit strong and undesirable juvenile characters for several years. Other subsequent studies indicated the embryogenic potential of somatic tissues which are neither nucellar nor ovular in origin: anthers [28], juice vesicles [29] and stigmas/styles [30]. Among these three different types of explants, stigmas/styles showed the highest embryogenic potential in different *Citrus* species.

In this study, the effects of different cell types (nucellar and stigma/style) on the transition from the juvenile to the mature phase were evaluated on plants regenerated through somatic embryogenesis in four *Citrus* species. Flowering and morphological traits were assessed on plants, grafted onto sour orange, maintained in greenhouse and field conditions. Since DNA and ploidy variation may induce several morphological changes that could influence regenerant growth, the genetic fidelity of the regenerated plants was verified by flow cytometric analysis and DNA analysis (ISSR and RAPD).

## 2. Materials and Methods

### 2.1. Plant Regeneration

Somatic embryos were generated from stigma/style explants dissected from flowers before opening (Figure 1A,B) and undeveloped ovules were dissected from mature fruits (Figure 1C). Plant material of six cultivars belonging to four *Citrus* species ('Femminello comune' and 'Lunario' lemon (*Citrus limon* (L.) Burman F.), 'Tardivo di Ciacculli' mandarin (*Citrus deliciosa* Tenore), 'AA CNR 31' sour orange (*Citrus aurantium* L.), 'Brasilian NL92' and 'Valencia late' sweet orange (*Citrus sinensis* (L.) Osbeck)) was collected from plants growing in the Collesano field station (38° N, 14° E), Sicily. Flowers were surface sterilized by immersion for 5 min in 70% ethanol, 15 min in 2% sodium hypochlorite, followed by three 3 min rinses in sterile distilled water. Stigmas and styles were excised with a scalpel and vertically plated as single explants into medium-sized Petri dishes (100 × 15 mm) with the cut surface in contact with the medium. Mature fruits were harvested 6 months after anthesis. Each fruit was washed, the skin was peeled off and the fruits were surface-sterilized by immersion for 5 min in ethanol (70% v/v) and 30 min in 2% (w/v) sodium hypochlorite. Without rinsing, the fruits were cut open under sterile conditions, and the undeveloped ovules were dissected and transferred into medium-sized Petri dishes (100 × 15 mm). Ovule integuments were removed with the aid of a stereo microscope and plated. Explants were cultured on Murashige and Skoog (MS) medium [31] supplemented with 146 mM sucrose, 500 mg L<sup>-1</sup> malt extract and 13.3 μM 6-benzylaminopurine. The pH of the media was adjusted to 5.7 ± 0.1 with 0.5 M of KOH before autoclaving. Explants and calluses were subcultured into fresh medium at 4–6-week intervals and maintained in a growth chamber at 25 ± 1 °C under a 16 h day length photoperiod. Germinated embryos were isolated and transferred into test tubes (1 embryo per 55 × 23 mm glass

tube sealed with Parafilm M) containing 20 mL of the above-mentioned medium. Embryos were considered germinated when there was root extension and hypocotyl elongation. For acclimatization, plantlets (about 3 cm in length) were transplanted into autoclaved Jiffy peat pellets and maintained on a heating bench at 25 °C and at high relative humidity (95%). The conditions for the acclimatization of regenerated plants by grafting have been previously described in De Pasquale et al. [32].

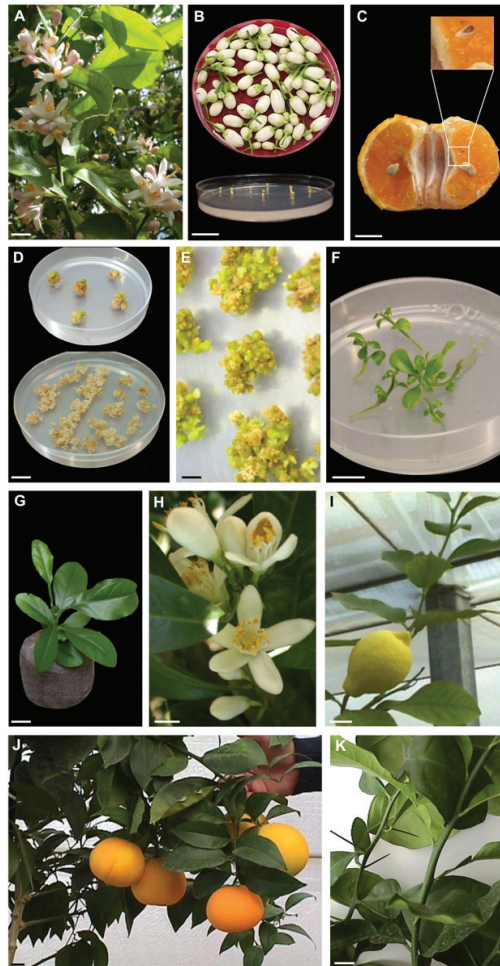


**Figure 1.** Somatic embryogenesis and plant regeneration in *Citrus*. (A) Representative blooming *Citrus* (lemon) (bar = 2 cm); (B) Stigma/style explants dissected from orange flowers collected before opening (bar = 2 cm); (C) Undeveloped ovule in open pollinated fruit of mandarin harvested 6 months after anthesis (bar = 1 cm); (D) Creamy-white callus from the stigma/style and undeveloped ovule explants (bar = 2 cm); (E) Somatic embryos generated after 3–5 months of culture initiation at the surface of stigma/style explant-derived callus (bar = 3 mm); (F) Germinated somatic embryos growing on MS medium (bar = 1 cm); (G) Somatic embryo-derived plant of sweet orange transferred to Jiffy peat pellet (bar = 1 cm); (H) Sweet orange stigma/style regenerants flowering under greenhouse condition (bar = 1 cm); (I,J) Fruits of ‘Femminello comune’ lemon and ‘Brasiliano NL 92’ sweet orange produced by three years old stigma/style regenerated plants growing in greenhouse (bar = 2 cm); (K) Thorny and thornless sour orange shoots from three years old stigma/style regenerants (bar = 2 cm).

### 2.2. Assessment of Ploidy by Flow Cytometric Analysis

Flow cytometry (FCM) was used to analyse the relative nuclear DNA content of the leaf cells collected either from regenerants and from the relative mother plants used as internal diploid standard (STD 2C). The analysis was carried out with the Partec PAS flow cytometer (Sysmex Partec, Görlitz, Germany, <https://www.sysmex-partec.com/>; accessed on 18 January 2021), equipped with a mercury lamp. Fully expanded leaves were chopped, using a sharp razor blade, in 400 µL nuclei extraction buffer (solution A of the ‘High Resolution Kit’ for PlantDNA, Sysmex Partec, Germany) for 30–60 s. After filtration through a 30 µm Cell-Trics disposable filter Cell-Trics Sysmex Partec, Germany, 1.6 mL staining solution containing the dye 4,6-diamidino-2-phenylindole (DAPI; solution B of the kit) was added. Routinely, 4000–5000 nuclei were measured per sample and histograms of DNA content were generated using the Partec FlowMax software package.

### 2.3. Assessment of Genetic Stability in Regenerants by ISSR and RAPD Markers

Leaves collected from regenerants and mother plants for each cultivar were harvested, washed, frozen in liquid nitrogen and stored at  $-80^{\circ}\text{C}$  until analyses. Genomic DNA was isolated from the samples as described by [33] and was quantified by measuring OD260 as described by [34]. The isolated genomic DNA was used for ISSR and RAPD analyses in order to assess genetic fidelity as described by Carra et al. [35].

A total of 6 ISSR primers [36] were used to amplify the DNA (Table S1). The primers were purchased from Life Technologies, Gaithersburg, Md. Each 25 µL amplification reaction consisted of 20 mM Tris-HCl (pH 8.4), 50 mM KCl, 2 mM MgCl<sub>2</sub>, 800 µM dNTP, 0.5 µM of each primer, 1 U of Platinum *Taq* polymerase and 30 ng of template DNA. The amplification was performed under the following cycle program: initial denaturation step for 4 min at 94 °C, followed by 36 cycles at 94 °C for 30 s (denaturation), 48.5–52.0 °C (see Table S1) for 45 s (annealing) and 72 °C for 120 s (extension), followed by a final extension step at 72 °C for 7 min. A total of 25 µL of each PCR-reaction products were electrophoresed on a 1.5% (*w/v*) agarose gel containing 1 × TBE (45 mM Tris-borate, 1 mM EDTA) and 0.5 µg/mL aqueous solution of ethidium bromide. The gel was run for 4 h at 100 V and visualized under UV light lamp. Only those bands showing consistent amplification were considered; smeared and weak bands were excluded from the analysis. Polymorphic ISSR markers were scored for the presence or absence of bands.

RAPD analysis of the grapevine genotypes was performed using six decamer primers [37] (Table S2). DNA amplification reactions were carried out in a volume of 25 µL with 20 mM Tris-HCl (pH 8.4), 50 mM KCl, 3 mM MgCl<sub>2</sub>, 800 µM dNTP, 0.4 µM of each primer, 1.5 U of Platinum *Taq* polymerase and 25 ng of template DNA. The amplification was performed in a MJ Research thermocycler (Genenco) equipped with a Hot Bonnet under the following cycle program: initial denaturation step for 90 s at 94 °C, followed by 36 cycles at 94 °C for 1 min (denaturation), 36 °C for 60 s (annealing) and 72 °C for 2 min (extension), followed by a final extension step at 72 °C for 10 min. Reaction products were visualized and analyzed as cited for ISSR analysis.

### 2.4. Grafting Conditions

In May, scions generated from different embryogenic events were grafted (T-budding) on three-year-old sour orange rootstocks in greenhouse and field trials, 30 cm above the soil line as described in De Pasquale et al. [32]. As control, to represent the ‘true adult’ state, mature scions collected from mother plants were grafted onto sour orange rootstocks. After the successful graft implant, the upper part of the rootstock was removed.

### 2.5. Growth and Flowering Assessment of Plants Maintained in Greenhouse

Grafted plants were maintained in the greenhouse (six plants regenerated *in vitro* for each explant/genotype combination and two mother plants for each genotype) in order to check growth, flowering and thorns production. As *Citrus* plants tend to bloom in the up-

permost part of the canopy, the lateral branches of the grafted plants were removed, starting from the second year of growth, to induce the scion growth in height as a single leader.

### 2.6. Morphological Analyses on Plants Transplanted in the Field

Grafted plants were maintained in the field (20 plants for each explant/genotype combination and eight mother plants for each genotype) for evaluation of leaf area of the plant and morphological characters (thorn length, thorns/nodes ratio). The experiment used a randomized block design (4 blocks) with 5 replications containing regenerated and mother plants. Leaf area of the plant and morphological analyses were performed on plants growing in the field at the end of the vegetative season (November) for one and three years, respectively.

### 2.7. Estimation of Leaf Area Using Linear Leaf Measurements

Non-destructive methods for measuring the leaf area (LA) through linear measurements have been reported for *Citrus* by many authors [38]. The following criteria for the selection of a regression equation were used: coefficients of determination ( $r^2$ ), standard errors of estimates, F test of analysis of variance and significance of the regression coefficients (SPSS-X, Inc., Chicago, IL, USA). We found that the leaf area estimation equations had the relative advantage of simplicity of calculation and the lowest standard error of estimates (Table 1).

**Table 1.** Leaf area estimation equations.

Species	Leaf Area Estimation Equation	$r^2$
Lemon	LA = 1.477 + 0.652 (L × W)	0.982
Mandarin	LA = 0.784 + 0.618 (L × W)	0.974
Sour Orange	LA = −0.442 + 0.690 (L × W)	0.968
Sweet Orange	LA = 1.506 + 0.632 (L × W)	0.990

L = leaf maximum length, LA = leaf area and W = leaf maximum width.

## 3. Results

### 3.1. Somatic Embryogenesis

Most of the explants produced a creamy-white callus after 1–2 weeks of incubation (Figure 1D). The different genotypes showed a different embryogenic potential from stigma/style and undeveloped ovule explants. About 3–5 months after culture initiation, all of the cultivars regenerated somatic embryos from stigma/style explants (Figure 1E). On the contrary, ‘AA-CNR-31’ sour orange, ‘Valencia late’ sweet orange, ‘Femminello comune’ and ‘Lunario’ lemon generated few somatic embryos from undeveloped ovule explants. Only ‘Tardivo di Ciaculli’ mandarin and ‘Brasiliano NL 92’ sweet orange regenerated a sufficient number of somatic embryos from undeveloped ovules from field and greenhouse trials. About 12 weeks after germination, somatic embryos developed into plantlets (Figure 1F) at a high frequency (40–66%). When plantlets were transferred *ex vitro* in Jiffy peat pellets, the percentage of acclimatized plants was about 70% (Figure 1G).

### 3.2. Genetic Fidelity Analysis of the Regenerated Plants

Flow cytometric analysis was used to determine the ploidy level of regenerants. All plants regenerated through somatic embryogenesis of the four different species showed the same ploidy of the mother plants confirming the stability of the ploidy level of plants regenerated from stigma/style and undeveloped ovule explants. Histograms of the DNA content of isolated nuclear suspension of regenerated plants are shown in Figure S1.

Six ISSR and six RAPD primers were screened out and used to amplify 16 DNA samples of regenerants from each cultivar and comparing them to the respective mother plant. A total of 135, 144, 146 and 134 well-resolved band classes were obtained for lemon, mandarin, sour orange and sweet orange, respectively.

The six ISSR primers gave 65, 76, 72 and 66 well-resolved band classes in lemon, mandarin (Figure S2A), sour orange and sweet orange. The sizes of amplified fragments were among 250 bp to 3.1 Kb. The mean number of ISSR bands obtained for each primer varied from 7 [primer (TCC)<sub>5</sub>RY] to 15 [primer (AG)<sub>8</sub>YT].

The six RAPD primers produced 70, 68, 74 and 68 well-resolved band classes in lemon, mandarin, sour orange and sweet orange, respectively, ranging from 300 bp to 3.5 Kb in size. The mean number of bands for each primer varied from 8 in ‘Valencia’ with primer OPM 04 (Figure S2B) to 17 in sour orange with primer OPAT 14. A total of 14,076 bands (number of plantlets analyzed × number of band classes obtained with all the primers) were generated by the RAPD and ISSR techniques. All regenerated plantlets appeared to be completely identical to the respective mother plants.

### 3.3. Growth and Flowering Assessment of Plants Maintained in Greenhouse

Mother plants and regenerated plants, growing under greenhouse conditions, were inspected for the presence or absence of flowers. The presence of flowers in plants maintained in the greenhouse for three years after grafting is reported in Table 2. During the first year of vegetation, mature and regenerated plants did not flower. During the second year, most mother plants were flowering and only few plants of lemon and sour orange produced flowers and some fruits, while juvenile characters started to be lost on some shoots.

**Table 2.** Observations on flowering plants in greenhouse.

Genotype	Origin	Presence of Flowers			Flowering Plants Year 3 (%)	Fruiting Plants Year 3
		Year 1	Year 2	Year 3		
Lemon ‘Femminello comune’	Mother plant	No	Yes	Yes	100	Yes
	Vitro stigma/style	No	No	Yes	50	Yes
Lemon ‘Lunario’	Mother plant	No	Yes	Yes	100	Yes
	Vitro stigma/style	No	No	Yes	50	No
Mandarin ‘Tardivo di Ciaculli’	Mother plant	No	Yes	Yes	100	Yes
	Vitro stigma/style	No	No	Yes	33	Yes
	Vitro ovule	No	No	No	0	No
Sour orange ‘AA-CNR-31’	Mother plant	No	Yes	Yes	100	Yes
	Vitro stigma/style	No	No	Yes	66	Yes
Sweet orange ‘Brasiliano NL 92’	Mother plant	No	Yes	Yes	100	Yes
	Vitro stigma/style	No	No	Yes	50	Yes
	Vitro ovule	No	No	No	0	No
Sweet orange ‘Valencia late’	Mother plant	No	Yes	Yes	100	Yes
	Vitro stigma/style	No	No	Yes	33	Yes

The third year, all the mother plants produced flowers and some of the plants regenerated from stigma/style of lemon, mandarin, sour and sweet orange were flowering under greenhouse condition (Figure 1H). Sour orange (‘AA-CNR-31’) showed the higher percentage of flowering plants (66%), whereas a lower percentage (50%) was observed in lemons (‘Femminello comune’ and ‘Lunario’) and ‘Brasiliano NL 92’ sweet orange. The lowest percentage was detected in ‘Tardivo di Ciaculli’ mandarin and ‘Valencia late’ sweet orange (33%). The third year some of the plants of ‘Femminello comune’ lemon, ‘Brasiliano NL 92’ sweet orange, ‘Tardivo di Ciaculli’ mandarin and ‘AA-CNR-31’ sour orange regenerated by stigma/style produced fruits in greenhouse (Figure 1I,J). Fruits produced by the plants regenerated in vitro from stigma/style did not show differences to those produced

by mother plants. Juvenile characters of all genotypes regenerated through stigma/style culture started to be lost in several shoots (Figure 1K).

In contrast, none of the plants regenerated from undeveloped ovules ('Tardivo di Ciaculli' mandarin and 'Brasiliano NL 92' sweet orange) produced flowers in the first three years of greenhouse cultivation and most of the shoots retained their juvenile characters (Table 2).

### 3.4. Observations of Juvenility Mature and Regenerated Plants Maintained in the Field

Plant leaf area and number of thorns per plant, was measured only the first year. Regenerants (stigma/style and undeveloped ovule) showed a higher vegetative growth as compared to the mother plants (Figure 2). In fact, all regenerants had a higher plant leaf area than the mother plants. The lowest plant leaf area was observed in mandarin mother plants (22.3 dm<sup>2</sup>), higher values were observed in stigma/style and undeveloped ovule regenerants: 32.2 and 38.7 dm<sup>2</sup>, respectively. Generally, the plant leaf area of undeveloped ovules regenerants is superior to stigma/style regenerants (Figure 2).

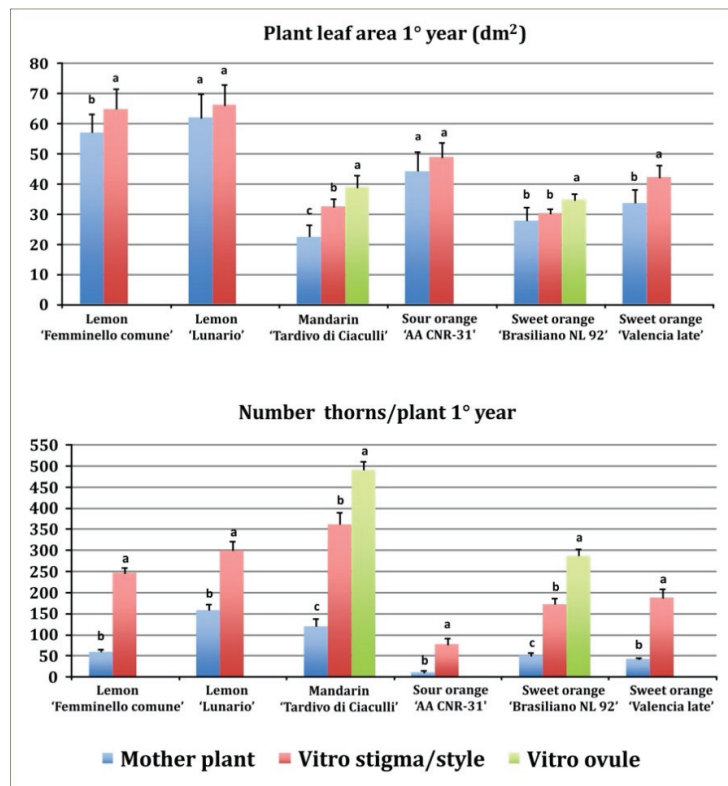


**Figure 2.** Plant leaf area and number of thorns per plant in the first year of growth in the field. Different letters on bars indicate significantly different values at a particular genotype according to the *t*-test for 'Femminello comune', 'Lunario' lemon, 'AA CNR 31' sour orange and 'Valencia late' sweet orange and according to Tukey's multiple comparison test for 'Tardivo di Ciaculli' mandarin and 'Brasiliano NL92' sweet orange. Tests were performed at  $p < 0.05$  significance level. Bars indicate standard error.

All regenerants exhibited a greater number of thorns as compared to mother plants (Figure 2). Mandarin regenerants from stigma/style and undeveloped ovule explants showed the higher number of thorns (361 and 490, respectively) in the first year, never-

theless also the mother plants showed a high number of thorns (119). In the first year, the lowest number of thorns was observed in sour orange mother plants (9). The different genotypes showed different levels of thorniness: both in regenerated plants, ranging from 75 in sour orange (stigma/style regenerants) to 490 in mandarin (undeveloped ovule regenerants) and in mother plants, ranging from 9 in sour orange to 157 in ‘Lunario’ lemon (Figure 2).

The four species showed great differences in thorn length between mother and regenerated plants (Figure 3).

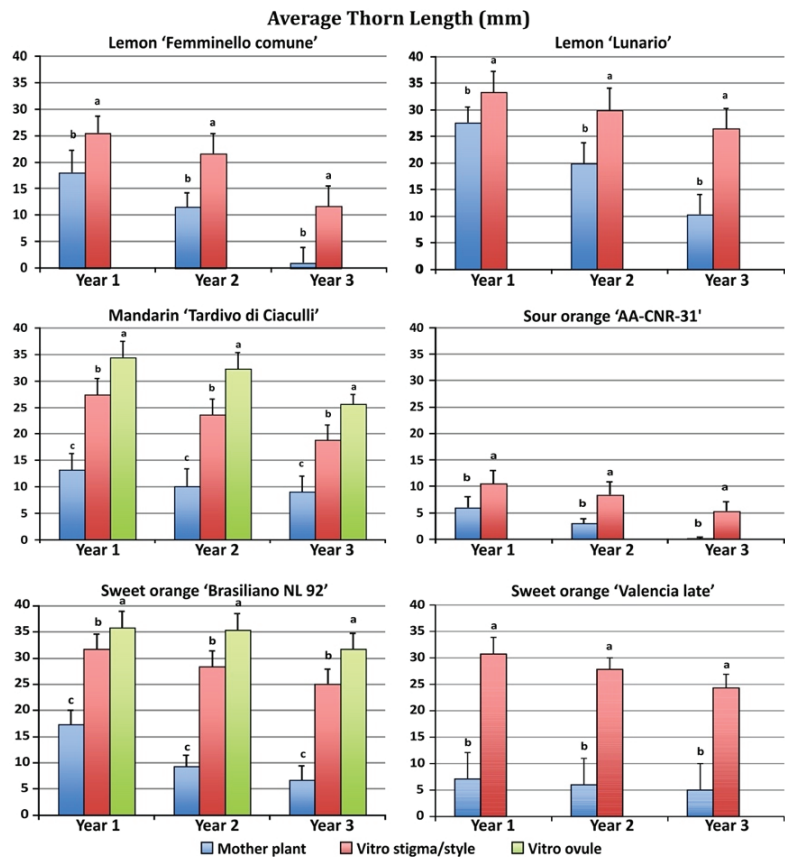


**Figure 3.** Average thorn length in plants regenerated from different explants growing in the field during the first three years after grafting. Different letters on bars indicate significantly different values at a particular genotype according to the *t*-test for ‘Femminello comune’, ‘Lunario’ lemon, ‘AA CNR 31’ sour orange and ‘Valencia late’ sweet orange and according to Tukey’s multiple comparison test for ‘Tardivo di Ciaculli’ mandarin and ‘Brasiliano NL92’ sweet orange. Tests were performed at  $p < 0.05$  significance level within each year. Bars indicate standard error.

Regenerated plants after one year of growth in the field showed much longer thorns than mother plants. Moreover, the undeveloped ovule regenerants showed a longer thorn length when compared to the stigma/style regenerants. ‘Brasiliano NL 92’ sweet orange stigma/style and undeveloped ovule regenerants showed the highest thorn length (31.7 and 35.8 mm, respectively) in the first year, yet also the mother plants showed long thorns (17.3 mm).

A similar behavior was observed in mandarin, with stigma/style and undeveloped ovule regenerants showing the highest thorn length (27.4 and 34.5 mm, respectively) as

compared to the mother plants (13.2 mm). The lowest thorn length was observed in sour orange, in which stigma/style regenerants had an average thorn length of 10.5 mm and the mother plants thorns were 6.0 mm long. During the second and third year of growth, the thorn length of the regenerated plants was reduced as compared to the first year, but thorns were still longer in regenerated compared with mother plants. The second and third years, plants regenerated from undeveloped ovules produced longer spines than plants regenerated from stigma/style.

Consistent differences were observed in thorn/node ratio between mature and regenerated plants during the three years of growth in the field (Figure 4).

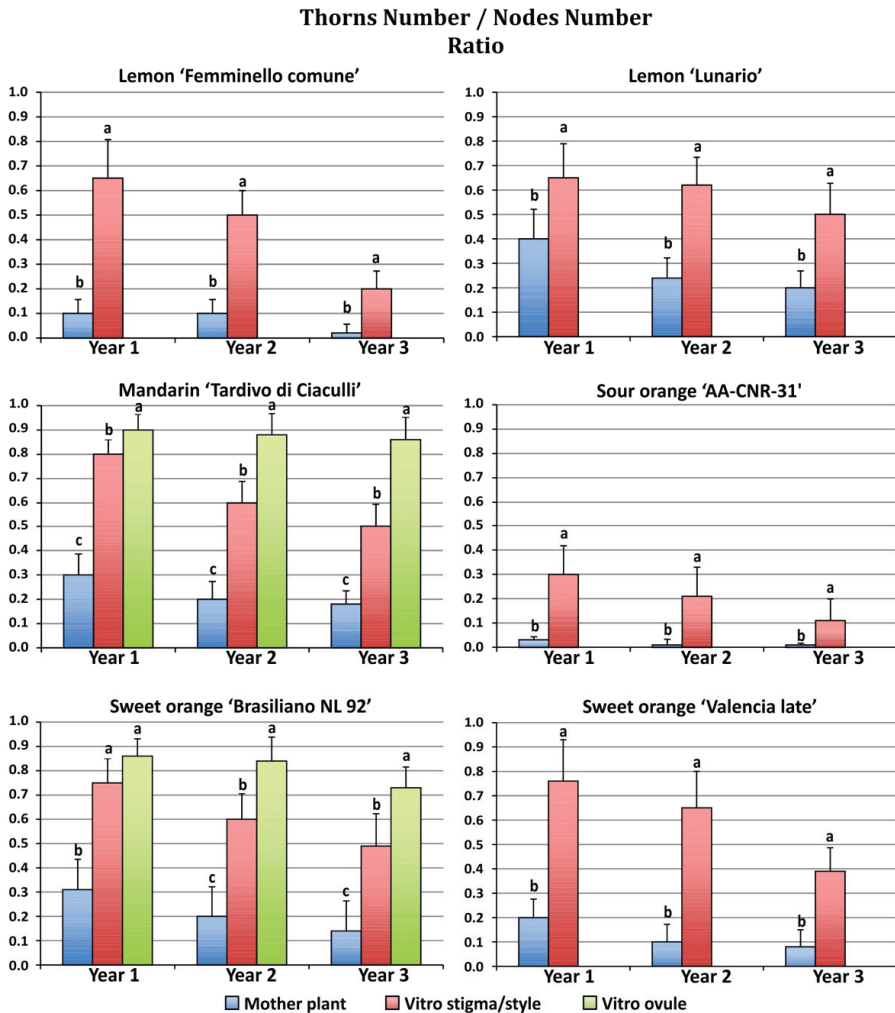


**Figure 4.** Average thorn/node ratio in plants regenerated from different explants growing in the field during the first three years after grafting. Different letters on bars indicate significantly different values at a particular genotype according to the *t*-test for 'Femminello comune', 'Lunario' lemon, 'AA CNR 31' sour orange and 'Valencia late' sweet orange and according to Tukey's multiple comparison test for 'Tardivo di Ciaculli' mandarin and 'Brasiliano NL92' sweet orange. Tests were performed at  $p < 0.05$  significance level within each year. Bars indicate standard error.

All regenerants exhibited a higher thorn/node ratio as compared to mother plants. Among the plants originating from somatic embryogenesis the undeveloped ovule regenerants showed a higher thorn/node ratio when compared to the stigma/style regenerants. Mandarin regenerants from stigma/style and undeveloped ovule explants showed the highest thorn/node ratio (0.80 and 0.90, respectively) in the first year, while the mother plants showed a lower thorn/node ratio (0.30). In the first year, the lowest thorn/node ratio was observed in sour orange mother plants (0.03). The highest thorn/node ratio of the mother plants was observed in 'Lunario' lemon (0.4). During the second and third year of growth, the thorn/node ratio of the regenerated plants was reduced as compared to the first year, with the exception of the mandarin undeveloped ovule regenerants, which maintained similar values in the three years of observation (0.90 and 0.87 for the second and third year, respectively).

At any evaluation time, our observations showed that the thorniness of regenerated plants was higher than those of mother plants; however, some regenerants developed thornless apical shoots. If the thornless shoots were collected and grafted on sour orange, they kept the acquired mature characters (data not reported). Most juvenile characters (thorniness, internode length, absence of flowers, etc.) were no longer present after mature shoots from plants regenerated *in vitro* were grafted again and the new vegetation displayed mature morphology nearly identical to mature plants. The only exception was observed in sweet orange and mandarin, which in some cases reverted to the juvenile form. However, in all species, it was possible to obtain plants regenerated from stigma/style explants that displayed mature morphology within three years after grafting. In contrast, undeveloped ovule regenerants retained their juvenile characteristics during the three years of observation after grafting.

#### 4. Discussion

Since plants cannot escape adversity, they developed a high regeneration ability for survival to biotic or abiotic stresses. Compared to animals, plants generally have a high level of plasticity and exhibit a remarkable regenerative capacity, both *in vivo* and *in vitro*, that varies widely between species and tissue types. Growing evidence suggests that some forms of plant regeneration involve the reprogramming of differentiated somatic cells, while others are induced through the activation of relatively undifferentiated cells in somatic tissues [39]. An extreme example of this adaptation is the generation of adult plants via somatic embryogenesis without the need for fertilization [40]. The regenerative potential can be increased *in vitro* by exogenously supplied plant growth regulators, wherein the interaction between auxin and cytokinin influences the developmental fate of cells inducing shoot or root regeneration. A balanced concentration of auxin and cytokinin induces an unorganized growth of a cell mass known as 'callus' due to its resemblance to the wound-healing plant tissue [41].

Somatic embryogenesis is a powerful biotechnological tool for the propagation and genetic improvement of plants. In *Citrus*, the production of embryogenic callus lines was first reported by Rangan et al. [42] from excised nucelli culture, the regeneration of somatic embryos from stigma and style cultures was first reported by Carimi et al. [43] and, since then, somatic embryogenesis has been induced directly or indirectly via callus formation in several *Citrus* species to produce plants for mass propagation, breeding program [6] and virus-free plants [44–49]. Even if somatic embryogenesis is widely used, little information is available on the behavior of *Citrus* plants regenerated *in vitro* from stigma/style and nucellar culture when grafted on rootstock and transferred under greenhouse conditions.

Here, we tested the genetic fidelity and agronomical aspects of plants regenerated from stigma/style explants or nucellar tissue and grown in the field or greenhouse. Shifts in morphological characters in regenerated plants can be expressed in terms of loss of apical dominance, number and size of leaves and, most importantly, in the time of flowering.

In order to investigate the presence of somaclonal variations on the regenerated plants, we used two different PCR-based techniques, ISSR and RAPD, and flow cytometry to

analyse the regenerants. No somaclonal variation compared to the mother plants was obtained, revealing the homogeneity of the produced plantlets. We also observed that fruits produced by the plants regenerated in vitro (from stigma and style cultures) were identical to those produced by mother plants, confirming that regenerated plants are genetically true-to-type. Moreover, this technology is also effective in the elimination of several viral infections [47]. This strategy can be considered as a possible in vitro process for the healthy plant regeneration of *Citrus* with a very low risk of generating somaclonal variants.

Somatic embryo regeneration from mature explants induced a partial reversion to a juvenile state, as widely demonstrated both for woody and herbaceous plants [50,51]. In fact, with the exception of sour orange, most of the regenerated plants showed strong juvenile characters in the first stages of growth, characterized by a high presence of thorns on stems and branches. During the first year of growth (post-grafting), mature and regenerated plants exhibited juvenile growth, characterized by the absence of flowers and high thorniness. As time passed, both mature and regenerated plants reduced these juvenile characters. Most of the lemons and sour oranges had completely thornless single shoots, whereas, in other shoots, thorns were still abundantly present. The loss of juvenility in the early stages of growth confirms previous observations that lemons and sour oranges produced fruits earlier than other *Citrus* species, with fruits present on thornless branches 3 years after the embryogenic event [46]. Similar results were reported for plantlets of Calamondin *Citrus* derived from somatic embryos grafted onto Japanese citron rootstock which, after one year in the field, produced flowers and fruits normally [52]. Propagated plants obtained by regrafting thornless budwood of stigma/style regenerants onto sour orange rootstock did not show any juvenile characters and they were flowering and fruiting regularly. This suggests that the protocol for plantlets regeneration by somatic embryogenesis from stigma/style explants maintains the genomic integrity of the chosen cultivar, reaching the mature stage in a relatively short time.

The loss of juvenile characters proceeded more quickly in mother plants than in regenerated plants. The most obvious explanation is that since the mother plants scions were derived from adult plants, the rejuvenation process was limited to the first year after grafting. Conversely, regenerants by somatic embryogenesis retained the full juvenile potential for a longer period. However, when comparing scions originated by in vitro somatic embryogenesis to scions taken directly from mother plants in the fields, we always need to keep in mind that the somatic embryogenesis process removes most of the viral and endophytic communities of the parent tissue [53]. Therefore, it is possible that the differences in growth and juvenile characters were (also) a result of the interaction of the microbial community in mother plants, versus the “clean” scions derived from somatic embryos.

Most interestingly, we observed a different behavior in plants regenerated from stigma/style versus ovule explants. Regenerants from ovules showed a greater number and density of thorns and they never flowered within the three years of observation. Conversely, regenerants from stigma/style reduced juvenile characters 12–18 months after grafting in the terminal portion of some shoots, and many showed flowers and fruits in the third year. Since both types of regenerants were derived from somatic embryogenesis in vitro, they were originally both free of the viral and endophytic communities. Therefore, the observed differences probably depended on the source of genetic material. Regenerants derived from nucellus, which is a non-vascularized tissue of maternal origin, can be regarded as a pocket of juvenile tissue in an otherwise adult plant [54]. Our results support the hypothesis that the totipotent cells originated from different cell types are not equivalent, possibly by maintaining memory of their previously differentiated state, possibly by epigenetic modifications. Our future research will address the molecular mechanisms underlying the process of juvenility in regenerants.

**Supplementary Materials:** The following are available online at: <https://www.mdpi.com/article/10.3390/plants11141811/s1>, Figure S1: Flow cytometry and ploidy evaluation of regenerants: *Citrus limon* ‘Lunario’ (A), *Citrus deliciosa* ‘Tardivo di Ciaculli’ (B), *Citrus sinensis* ‘Valencia late’ (C), *Citrus aurantium* ‘AA CNR 31’ (D). Leaf nuclei suspensions were stained with DAPI. Each sample was analysed using the leaf nuclei of the relative mother plant as internal diploid standard (STD 2C). Nuclei DNA fluorescence intensity values and nuclei counts are shown on X and Y axes, respectively, Figure S2: Representative images of molecular markers: (A) Patterns of mother plant (M) and 16 regenerated plantlets (R1-16) of *Citrus deliciosa* ‘Tardivo di Ciaculli’ obtained with the ISSR primer UBC-835. L, 100 bp ladder; (B) Patterns of mother plant (M) and 16 regenerated plantlets (R1-16) of *Citrus sinensis* ‘Valencia late’ obtained with the RAPD primer OPM04. L, 100 bp ladder, Table S1: Primer sequences and annealing temperatures used for ISSR analysis, Table S2: Primer sequences used for RAPD analysis.

**Author Contributions:** Conceptualization, L.A., F.C. and A.C.; methodology, C.C., A.M., F.C. and A.C.; formal analysis, C.C., L.A., F.C. and A.C.; investigation, C.C., L.A., A.M., A.M.D., F.C. and A.C.; resources, A.M.; data curation, R.D.M. and A.C.; writing—original draft preparation, C.C., L.A., S.F.D.B., F.C., R.D.M., F.M., A.M.D. and A.C.; writing—review and editing, C.C., L.A., S.F.D.B., A.M., F.C., R.D.M., F.M., A.M.D. and A.C. All authors have read and agreed to the published version of the manuscript.

**Funding:** This research received no external funding.

**Institutional Review Board Statement:** Not applicable.

**Informed Consent Statement:** Not applicable.

**Data Availability Statement:** The data presented in this study are openly available in Supplementary Materials here.

**Conflicts of Interest:** The authors declare no conflict of interest.

## References

1. Bednarek, P.T.; Orłowska, R. Plant tissue culture environment as a switch-key of (epi) genetic changes. *Plant Cell Tissue Organ Cult.* **2020**, *140*, 245–257. [[CrossRef](#)]
2. Larkin, P.J.; Scowcroft, W.R. Somaclonal variation—A novel source of variability from cell cultures for plant improvement. *Appl. Genet.* **1981**, *60*, 197–214. [[CrossRef](#)] [[PubMed](#)]
3. Kumar, K.; Gill, M.I.S.; Gosal, S.S. Somatic embryogenesis, in vitro selection and plantlet regeneration for citrus improvement. In *Biotechnologies of Crop Improvement*; Springer: Cham, Switzerland, 2018; Volume 1, pp. 373–406.
4. Catalano, C.; Abbate, L.; Motisi, A.; Crucitti, D.; Cangelosi, V.; Pisciotto, A.; Di Lorenzo, R.; Carimi, F.; Carra, A. Autotetraploid Emergence via Somatic Embryogenesis in *Vitis vinifera* Induces Marked Morphological Changes in Shoots, Mature Leaves, and Stomata. *Cells* **2021**, *10*, 1336. [[CrossRef](#)]
5. Bairu, M.W.; Aremu, A.O.; Van Staden, J. Somaclonal variation in plants: Causes and detection methods. *Plant Growth Regul.* **2011**, *63*, 147–173. [[CrossRef](#)]
6. Omar, A.A.; Dutt, M.; Gmitter, F.G.; Grosser, J.W. Somatic embryogenesis: Still a relevant technique in citrus improvement. In *In Vitro Embryogenesis in Higher Plants*; Humana Press: New York, NY, USA, 2016; pp. 289–327.
7. Zhang, S.; Liang, M.; Wang, N.; Xu, Q.; Deng, X.; Chai, L. Reproduction in woody perennial Citrus: An update on nucellar embryony and self-incompatibility. *Plant Reprod.* **2018**, *31*, 43–57. [[CrossRef](#)]
8. Furr, J.R.; Cooper, W.C.; Reece, P.C. An investigation on flower formation in adult and juvenile citrus trees. *Am. J. Bot.* **1947**, *34*, 1–8. [[CrossRef](#)]
9. Hackett, W.P. Juvenility, maturation, and rejuvenation in woody plants. *Hortic. Rev.* **1985**, *7*, 109–155.
10. Huijser, P.; Schmid, M. The control of developmental phase transitions in plants. *Development* **2011**, *138*, 4117–4129. [[CrossRef](#)]
11. Wang, J.W.; Park, M.Y.; Wang, L.J.; Koo, Y.; Chen, X.Y.; Weigel, D.; Poethig, R.S. MiRNA control of vegetative phase change in trees. *PLoS Genet.* **2011**, *7*, e1002012. [[CrossRef](#)]
12. Snowball, A.M.; Warrington, I.J.; Halligan, E.A.; Mullins, M.G. Phase change in citrus: The effects of main stem node number, branch habit and paclobutrazol application on flowering in citrus seedlings. *J. Hortic. Sci.* **1994**, *69*, 149–160. [[CrossRef](#)]
13. Snowball, A.M.; Halligan, E.A.; Warrington, I.J.; Mullins, M.G. Phase change in citrus: Growth and flowering of citrus seedlings from thirteen genetically diverse seedling families. *J. Hortic. Sci.* **1994**, *69*, 141–148. [[CrossRef](#)]
14. Krajewski, A.J.; Rabe, E. Citrus flowering: A critical evaluation. *J. Hortic. Sci.* **1995**, *70*, 357–374. [[CrossRef](#)]
15. Mitani, N.; Matsumoto, R.; Yoshioka, T.; Kuniga, T. Citrus hybrid seedlings reduce initial time to flower when grafted onto shiikuwasha rootstock. *Sci. Hortic.* **2008**, *116*, 452–455. [[CrossRef](#)]
16. Nishikawa, F. Regulation of floral induction in citrus. *J. Jpn. Soc. Hortic. Sci.* **2013**, *82*, 283–292. [[CrossRef](#)]

17. Caruso, M.; Smith, M.W.; Froelicher, Y.; Russo, G.; Gmitter, F.G., Jr. Traditional breeding. In *The Genus Citrus*; Woodhead Publishing: Sawston, UK, 2020; pp. 129–148.
18. Cervera, M.; Juárez, J.; Navarro, L.; Peña, L. Genetic transformation of mature Citrus plants. In *Transgenic Plants: Methods and Protocols. Methods in Molecular Biology*; Peña, L., Ed.; Humana Press: Totowa, NJ, USA, 2005; Volume 286.
19. Endo, T.; Shimada, T.; Fujii, H.; Kobayashi, Y.; Araki, T.; Omura, M. Ectopic expression of an FT homolog from *Citrus* confers an early flowering phenotype on trifoliolate orange (*Poncirus trifoliata* L. Raf.). *Transgenic Res.* **2005**, *14*, 703–712. [[CrossRef](#)]
20. Pena, L.; Cervera, M.; Fagoaga, C.; Romero, J.; Juarez, J.; Pina, J.A.; Navarro, L. Citrus. In *Biotechnology in Agriculture and Forestry, Transgenic Crops*; Pua, E.C., Davey, M.R., Eds.; Springer: Berlin/Heidelberg, Germany; New York, NY, USA, 2007; Volume 60, pp. 35–50.
21. Velázquez, K.; Agüero, J.; Vives, M.C.; Aleza, P.; Pina, J.A.; Moreno, P.; Navarro, L.; Guerri, J. Precocious flowering of juvenile citrus induced by a viral vector based on Citrus leaf blotch virus: A new tool for genetics and breeding. *Plant Biotechnol. J.* **2016**, *14*, 1976–1985. [[CrossRef](#)]
22. Salonia, F.; Ciacciulli, A.; Poles, L.; Pappalardo, H.D.; La Malfa, S.; Licciardello, C. New Plant Breeding Techniques in Citrus for the Improvement of Important Agronomic Traits. A Review. *Front. Plant Sci.* **2020**, *11*, 1234. [[CrossRef](#)]
23. Sim, G.E.; Goh, C.J.; Loh, C.S. Micropropagation of Citrus mitis Blanco- multiple bud formation from shoot and root explants in the presence of 6-benzylaminopurine. *Plant Sci.* **1989**, *59*, 203–210. [[CrossRef](#)]
24. Cervera, M.; Juárez, J.; Navarro, A.; Pina, J.A.; Duran-Vila, N.; Navarro, L.; Peña, L. Genetic transformation and regeneration of mature tissues of woody fruit plants bypassing the juvenile stage. *Transgenic Res.* **1998**, *7*, 51–59. [[CrossRef](#)]
25. Bassan, M.M.; Mourão Filho, F.A.A.; Miyata, L.Y.; Mendes, B.M.J. In vitro organogenesis from internodal segments of adult sweet orange plants. *Pesqui. Agropecuária Bras.* **2011**, *46*, 672–674. [[CrossRef](#)]
26. Cardoso, J.C.; Curtolo, M.; Latado, R.R.; Martinelli, A.P. Somatic embryogenesis of a seedless sweet orange (*Citrus sinensis* (L.) Osbeck). *Vitr. Cell. Dev. Biol. Plant* **2017**, *53*, 619–623. [[CrossRef](#)]
27. Carimi, F.; Tortorici, M.C.; De Pasquale, F.; Crescimanno, F.G. Somatic embryogenesis and plant regeneration from undeveloped ovules and stigma/style explants of sweet orange navel group [*Citrus sinensis* (L.) Osb.]. *Plant Cell Tissue Organ Cult.* **1998**, *54*, 183–189. [[CrossRef](#)]
28. Hidaka, T.; Yamada, Y.; Shichijo, T. Plantlet formation from anthers of *C. aurantium* L. *Proc. Intl. Soc. Citric.* **1981**, *1*, 153–155.
29. Nito, N.; Iwamasa, M. In vitro plantlet formation from juice vesicle callus of satsuma (*Citrus unshiu* Marc.). *Plant Cell Tissue Organ Cult.* **1990**, *20*, 137–140. [[CrossRef](#)]
30. Carimi, F.; De Pasquale, F.; Crescimanno, F.G. Somatic embryogenesis in Citrus from styles culture. *Plant Sci.* **1995**, *105*, 81–86. [[CrossRef](#)]
31. Murashige, T.; Skoog, F. A revised medium for rapid growth and bioassays with tobacco tissue cultures. *Physiol Plant* **1962**, *15*, 473–497. [[CrossRef](#)]
32. De Pasquale, F.; Giuffrida, S.; Carimi, F. Minigrafting of shoots, roots, inverted roots, and somatic embryos for rescue of in vitro Citrus regenerants. *J. Am. Soc. Hort. Sci.* **1999**, *124*, 152–157. [[CrossRef](#)]
33. Doyle, J.J.; Doyle, J.L. A rapid DNA isolation procedure from small quantities of fresh leaf tissue. *Phytochem. Bull.* **1987**, *19*, 11–15.
34. Sambrook, J.; Fritsch, E.F.; Maniatis, T. *Molecular Cloning. A Laboratory Manual*, 2nd ed.; Cold Spring Harbor Laboratory Press: Cold Spring Harbor, NY, USA, 1989.
35. Carra, A.; Sajeva, M.; Abbate, L.; Siragusa, M.; Pathirana, R.; Carimi, F. Factors affecting somatic embryogenesis in eight Italian grapevine cultivars and the genetic stability of embryo-derived regenerants as assessed by molecular markers. *Sci. Hortic.* **2016**, *204*, 123–127. [[CrossRef](#)]
36. Fang, D.Q.; Roose, M.L. Identification of closely related citrus cultivars with inter-simple sequence repeat markers. *Theor. Appl. Genet.* **1997**, *95*, 408–417. [[CrossRef](#)]
37. Coletta Filho, H.D.; Machado, M.A.; Targon, M.L.P.N.; Moreira, M.C.P.Q.D.G.; Pompeu, J., Jr. Analysis of the genetic diversity among mandarins (*Citrus* spp.) using RAPD markers. *Euphytica* **1998**, *102*, 133–139. [[CrossRef](#)]
38. Ascenso, J.C.; Soost, R.K. Relationships between leaf surface area and linear dimension in seedling Citrus populations. *J. Am. Soc. Hort. Sci.* **1976**, *101*, 696–698.
39. Ikeuchi, M.; Ogawa, Y.; Iwase, A.; Sugimoto, K. Plant regeneration: Cellular origins and molecular mechanisms. *Development* **2016**, *143*, 1442–1451. [[CrossRef](#)] [[PubMed](#)]
40. Su, Y.H.; Tang, L.P.; Zhao, X.Y.; Zhang, X.S. Plant cell totipotency: Insights into cellular reprogramming. *J. Integr. Plant Biol.* **2021**, *63*, 228–243. [[CrossRef](#)]
41. Fehér, A. Callus, dedifferentiation, totipotency, somatic embryogenesis: What these terms mean in the era of molecular plant biology? *Front. Plant Sci.* **2019**, *10*, 536. [[CrossRef](#)]
42. Rangan, S.; Murashige, T.; Bitters, W.P. In vitro initiation of nucellar embryos in monoembryonic citrus. *HortScience* **1968**, *3*, 226–227.
43. Carimi, F.; De Pasquale, F.; Crescimanno, F.G. Somatic embryogenesis from styles of lemon (*Citrus limon*). *Plant Cell Tissue Organ Cult.* **1994**, *37*, 209–211. [[CrossRef](#)]
44. D’Onghia, A.M.; De Pasquale, F.; Carimi, F.; Savino, V.; Crescimanno, F.G. Somatic embryogenesis from style culture as possible means for virus elimination in Citrus. *J. Phytopath.* **1997**, *145*, 77–79. [[CrossRef](#)]

45. D’Onghia, A.M.; Carimi, F.; De Pasquale, F.; Djelouah, K.; Martelli, G.P. Somatic embryogenesis from style culture: A new technique for the sanitization, conservation and safe exchange of citrus germplasm. In Proceedings of the Int. Soc. Citric., ‘IXth International Citrus Congress’, Orlando, FL, USA, 3–7 December 2000; Volume 1, pp. 147–149.
46. D’Onghia, A.M.; Carimi, F.; De Pasquale, F.; Djelouah, K.; Martelli, G.P. Elimination of Citrus psorosis virus by somatic embryogenesis from stigma and style cultures. *Plant Pathol.* **2001**, *50*, 266–269. [[CrossRef](#)]
47. Meziane, M.; Frasheri, D.; Carra, A.; Boudjeniba, M.; D’Onghia, A.M.; Mercati, F.; Djelouah, K.; Carimi, F. Attempts to eradicate graft-transmissible infections through somatic embryogenesis in *Citrus* ssp. and analysis of genetic stability of regenerated plants. *Eur. J. Plant Pathol.* **2017**, *148*, 85–95. [[CrossRef](#)]
48. El-Sawy, A.; Gomaa, A.; Abd-El-Zaher, M.H.; Reda, A.; Dania, N. Production of somatic embryogenesis via in vitro culture of stigma and style for elimination of Citrus psorosis virus (CPsV) from some citrus genotypes. *J. Hort. Sci. Ornament. Plants* **2013**, *5*, 110–117.
49. Mahmoud, K.B.; Najjar, A.; Jedidi, E.; Hamdi, I.; Jemmali, A. Detection of two viroids in the Tunisian sweet orange (*Citrus sinensis* L.) cv. Maltese and sanitation via somatic embryogenesis. *J. Chem. Pharm. Res.* **2017**, *9*, 154–159.
50. Ballester, A.; Vieitez, A.M. Partial rejuvenation of mature hardwood trees through somatic embryogenesis: The example of pedunculate oak. In Proceedings of the IUFRO Working Party 2.09.02 Conference on “Integrating Vegetative Propagation, Biotechnologies and Genetic Improvement for Tree Production and Sustainable Forest Management”, Brno, Czech Republic, 25–28 June 2012.
51. Heide, O.M. Juvenility, maturation and rejuvenation in plants: Adventitious bud formation as a novel rejuvenation process. *J. Hortic. Sci. Biotechnol.* **2019**, *94*, 2–11. [[CrossRef](#)]
52. Devy, N.F.; Yenni, Y.; Hardiyanto, H. The growth performance of citrus derived from somatic embryogenesis plantlet and scion stock. *Indones. J. Agric. Sci.* **2014**, *15*, 71–78. [[CrossRef](#)]
53. Carimi, F. Somatic embryogenesis and organogenesis in citrus for sanitation and in vitro conservation. In *Improvement of the Citrus Sector by the Setting up of the Common Conservation Strategies for the Free Exchange of Healthy Citrus Genetic Resources*; D’Onghia, A.M., Menini, U., Martelli, G.P., Eds.; Options Méditerranéennes: Série B; CIHEAM publications: Rome, Italy, 2001; Volume 33, pp. 115–128.
54. Button, J.; Kochba, J. Tissue culture in the citrus industry. In *Applied and Fundamental Aspects of Plant Cell, Tissue, and Organ Culture*; Reinert, J., Bajaj, Y.P.S., Eds.; Springer: Berlin/Heidelberg, Germany, 1977; pp. 70–92.

## Article

# Nutrient Constituents, Bioactive Phytochemicals, and Antioxidant Properties of Service Tree (*Sorbus domestica* L.) Fruits

Manol Ognyanov <sup>1,\*</sup>, Petko Denev <sup>1</sup>, Nadezhda Petkova <sup>2</sup>, Zhana Petkova <sup>3</sup>, Magdalena Stoyanova <sup>4</sup>, Peter Zhelev <sup>5</sup>, Georgi Matev <sup>6</sup>, Desislava Teneva <sup>1</sup> and Yordan Georgiev <sup>1</sup>

<sup>1</sup> Laboratory of Biologically Active Substances, Institute of Organic Chemistry with Centre of Phytochemistry, Bulgarian Academy of Sciences, 139 Ruski Blvd., 4000 Plovdiv, Bulgaria; petko.denev@orgchm.bas.bg (P.D.); desislava.teneva@orgchm.bas.bg (D.T.); yordan.georgiev@orgchm.bas.bg (Y.G.)

<sup>2</sup> Department of Organic Chemistry and Inorganic Chemistry, Technological Faculty, University of Food Technologies, 26 Maritza Blvd., 4002 Plovdiv, Bulgaria; petkovanadejda@abv.bg

<sup>3</sup> Department of Chemical Technology, University of Plovdiv 'Paisii Hilendarski', 24 Tzar Asen Str., 4000 Plovdiv, Bulgaria; zhanapetkova@uni-plovdiv.net

<sup>4</sup> Department of Analytical Chemistry and Physicochemistry, Technological Faculty, University of Food Technologies, 26 Maritza Blvd., 4002 Plovdiv, Bulgaria; magdalena.stoianova@abv.bg

<sup>5</sup> Dendrology Department, University of Forestry, 10 Kliment Ohridski Blvd., 1756 Sofia, Bulgaria; petar.zhelev@ltu.bg

<sup>6</sup> Environmental Executive Agency (ExEA), Regional Laboratory Plovdiv, 1 Perushtitsa Str., 4004 Plovdiv, Bulgaria; georgi\_matev@hotmail.com

\* Correspondence: manol.ognyanov@orgchm.bas.bg; Tel.: +359-32-642759

**Citation:** Ognyanov, M.; Denev, P.; Petkova, N.; Petkova, Z.; Stoyanova, M.; Zhelev, P.; Matev, G.; Teneva, D.; Georgiev, Y. Nutrient Constituents, Bioactive Phytochemicals, and Antioxidant Properties of Service Tree (*Sorbus domestica* L.) Fruits. *Plants* **2022**, *11*, 1832. <https://doi.org/10.3390/plants11141832>

Academic Editors: Antonella Smeriglio and Marcello Salvatore Lenucci

Received: 24 May 2022

Accepted: 11 July 2022

Published: 13 July 2022

**Publisher's Note:** MDPI stays neutral with regard to jurisdictional claims in published maps and institutional affiliations.



**Copyright:** © 2022 by the authors. Licensee MDPI, Basel, Switzerland. This article is an open access article distributed under the terms and conditions of the Creative Commons Attribution (CC BY) license (<https://creativecommons.org/licenses/by/4.0/>).

**Abstract:** The current study aimed to determine the major and minor nutritional constituents of *Sorbus domestica* L. fruits. It was revealed that palmitic acid was the most commonly occurring saturated fatty acid, while linoleic acid represented the major polyunsaturated fatty acid. The sterol fraction consisted mainly of  $\beta$ -sitosterol. Small amounts of lipophilic pigments were quantified. Potassium, iron, and boron were the most abundant macro-, micro-, and ultra-trace elements. The amino acid composition analysis suggested that the non-essential amino acids predominated over the essential ones. Soluble sugars (fructose and glucose) represented a large part of the total carbohydrate content, but pectin formed the major part of polysaccharides. Malic acid was the most abundant organic acid whereas quercetin-3- $\beta$ -glucoside, neochlorogenic, and 3,4-dihydroxybenzoic acids were the major phenolic constituents. Fruits exhibited free-radical scavenging and protecting ability against peroxy and hydroxyl radicals. Service tree fruits provided valuable bioactive constituents having a high nutritional value and potential health benefits.

**Keywords:** carbohydrates; protein; lipids; fatty acids; minerals; polyphenols; antioxidant activity

## 1. Introduction

Service tree (*Sorbus domestica* L.) is a deciduous and long-lived tree with small pear-shaped fruits (average size of 3 cm) that belongs to the Rosaceae family [1,2]. It has a relatively wide distribution across temperate central and southern Europe (the Balkans, Italy, and southern France), but it is also rarely distributed in the northern parts of Africa and western Asia [1–3]. Nevertheless, the service tree is considered an endangered species in some countries due its small proportion of domestication [2,4]. In Bulgaria, the service tree is known as ‘skorusha’ or ‘oskrusha’, and its (over)ripe fruits are often freshly consumed or processed into compôte, jams, jelly, or marmalade [5]. In traditional folk medicine, many people try to cure themselves of gastrointestinal (diarrhea, diabetes, vomiting) and urogenital (kidney stones) illnesses using the striped bark, young twigs, and fruits [1,5]. In general, the service tree is known for its beneficial properties, but nonetheless, it is usually only used by local people who live close to its habitats.

A thorough review of current scientific knowledge of the service tree revealed that scientists have conducted investigations, mainly into different ecological, morphological, and genetic aspects [1–5]. Unfortunately, however, few studies are focused upon the chemical composition and nutritional value of the service tree fruits [4,6–12]. A very minor part of the reports draws attention to the presence and accumulation of some minerals [6,13]. The other reports note evidence that fruits and their extracts are a rich source of phenolic compounds, and they possess a wide range of benefits including anti-inflammatory, antidiabetic, antimicrobial, and antioxidant [7,8,10,14]. Furthermore, in a series of articles, a team of scientists has reached a deep understanding of the phenolic composition of fruits at different maturity stages [9,11,12]. Very few scientists turn their attention to other plant parts such as leaves and their chemical constituents [15,16].

The main conclusion to be drawn from the abovementioned studies is that the main active constituents of the fruits and leaves of the service tree are different polyphenols (flavonoids, proanthocyanidins, etc.) mostly having antioxidant activity. However, the fact remains that details of the other phytochemical constituents of fruits are still scarce or completely missing in the available literature. Service tree fruits have not been exhaustively studied for their lipid constituents (fatty acids, phytosterols, and phospholipids). Moreover, there have not yet been any quantitative data about the presence of polysaccharides (cellulose, starch, and pectin), although they are very important active components responsible for the biological and functional properties of service tree fruits. In addition, there are very little data available about mineral composition, and what is more, the content of elements such as P, Se, B, Al, Co, As, Cd, Hg, Pb, etc., have not yet been evaluated. We could not find any detailed report about the presence and composition of organic and amino acids.

Therefore, the current study is chiefly concerned with conducting an investigation into the presence and composition of different major and minor phytochemical constituents, including lipids, proteins, carbohydrates, organic acids, amino acids, minerals, and polyphenols of service tree fruits collected in Bulgaria.

## 2. Results and Discussion

### 2.1. Protein Content and Amino Acid Composition

The protein content and results of the quantitative estimation of various amino acids are presented in Table 1. It can be seen that a small amount of protein was present in fruits (3.5% dw, 1.1% fw, 35 mg/g dw). It is not surprising, therefore, that 100 g of fresh service tree fruits provides a very small proportion ( $\leq 3.0\%$ ) of the intake of the protein requirement of 0.65 g/kg/day (for 60 kg bw). Furthermore, amino acid composition analysis revealed that the non-essential amino acids (55% of total) predominated slightly higher in comparison to the essential ones (45% of total). The non-essential glutamic and aspartic acids contributed to a large part of the total amino acid content (23%) like in most fruits. This suggested that some protein constituents were acidic in character. These negatively charged amino acids play a major role in proteins. The metal-binding sites of many proteins contain one or several aspartate and glutamate-side chains [17]. However, it should be noted that asparagine and glutamine, if present, may be deaminated to aspartic acid and glutamic acid during acid hydrolysis, and thus the determination of these constituents seemed to be in doubt. The acid hydrolysis used to liberate the acids also provided an adequate explanation for the lack of tryptophan and cysteine which may be recovered in a non-quantifiable yield or destroyed by oxidation under these conditions. Phenylalanine was found in smaller amounts among other amino acids. Together with threonine, they occupied not more than 13% of all essential amino acids. Glycine was also a minor constituent that represented nearly 10% of the total non-essential amino acid content. One further analysis of the data showed that amino acids with non-polar (hydrophobic) and uncharged side chains such as glycine, proline, alanine, valine, leucine, isoleucine, phenylalanine, and methionine were very important major contributors to the total amino acid content (45%) of the service tree fruits. Amino acids with uncharged, polar side chains (serine, threonine, tyrosine, asparagine, and glutamine), on the other hand, seemed to be minor contributors to the

total content (9.2%). Amino acids carrying positively charged side chains (histidine, lysine, and arginine) comprised about 17% of the amino acid pool, and together with negatively charged Asp and Glu, made up about 40% of the total ones.

**Table 1.** Crude protein content and amino acid composition of service tree fruits.

Crude Protein (N × 6.25), w/w%		3.5 ± 0.2	
A. Essential amino acids	mg/g sample	mg/g N	g/100 g protein
Valine (Val)	2.0 ± 0.3	357	5.8
Leucine (Leu)	1.9 ± 0.1	339	5.5
Isoleucine (Ile)	1.4 ± 0.2	250	3.9
Phenylalanine (Phe)	0.7 ± 0.08	125	2.1
Tryptophan (Trp)	-	-	-
Methionine (Met)	1.4 ± 0.1	250	4.1
Threonine (Thr)	1.1 ± 0.0	196	3.2
Histidine* (His)	1.6 ± 0.1	285	4.7
Lysine (Lys)	1.6 ± 0.1	285	4.6
Arginine** (Arg)	2.1 ± 0.1	375	6.1
Total	13.8	2462	40
B. Nonessential amino acids			
Glycine (Gly)	1.6 ± 0.2	285	4.6
Alanine (Ala)	2.4 ± 0.2	428	6.8
Proline (Pro)	2.4 ± 0.1	428	7.0
Serine (Ser)	1.7 ± 0.1	303	4.7
Cysteine (Cys)	-	-	-
Tyrosine (Tyr)	1.7 ± 0.2	303	4.9
Asparagine (Asn)	-	-	-
Glutamine (Gln)	-	-	-
Aspartic acid (Asp)	4.0 ± 0.2	714	11.2
Glutamic acid (Glu)	3.0 ± 0.1	535	8.7
Total	16.8	2996	47.9

\* essential for infants; \*\* “semi-essential” amino acid.

It is a well-known fact that a comparison between the amino acid content of investigated food and amino acid requirements is used for assessing the quality of protein in foods (in vitro). Accordingly, we were interested in calculating the amino acid score of fruits that reflected their overall nutritive value. Not surprisingly, by our calculations (Table S1), it became clear that the protein of the service tree fruits bore no comparison with that of bovine milk, although it seemed that it could contribute to the positive balance of His (167%) and Met (141%) [17]. Nevertheless, in comparison with the amino acid composition of ‘ideal’ protein, the service tree fruits had superior amounts of essential amino acids (His, Met, Val, Phe). Leucine and lysine were considered to be limited acids, not to mention the question of fruit protein digestibility (Table S1).

It is interesting to note that a lower ‘true’ value of the protein content (2.6% or 74.1% recovery of crude protein) of the service tree fruits was calculated when we summed the individual anhydrous amino acid values, assuming that there were not any free amino acids and that all of them were present in polymer form. However, it is important to remember that some amino acids (Trp, Cys, Asn, Gln) were recovered in low non-quantifiable yields, and thus the ‘true’ value would seem to be higher. Another interesting finding of the study was that 78.4% of total nitrogen was recovered in the form of amino acids—in other words, not all nitrogen could be ascribed to the protein. Therefore, about 22% of total nitrogen may be non-protein nitrogen (nucleotides, chlorophylls, polyamines, and amino alcohols of phospholipids, etc.).

There has not yet been any report, to our knowledge, that examined in detail the amino acid composition of service tree fruits, hence to compare with that reported in the current study. Incidentally, several points of similarity between the service tree and apple may

provide a basis for comparison. Methionine, tyrosine, arginine, and proline, for example, predominated in the service tree fruits (Table 1), whereas apple offered superior amounts of aspartic and glutamic acids (1300 and 700 mg/g N) [18].

## 2.2. Lipid Composition

The results of the lipid composition analysis are summarized in Table 2. The crude lipid fraction represented 0.82% (*w/w*) of the dried fruits. It was evident that 16 fatty acids were identified and quantified, including 9 saturated and 7 unsaturated ones. Palmitic acid (16:0; 19.5%) was the most widely occurring saturated fatty acid followed by stearic acid (18:0; 3.3%), which was much less common. Both represented 93% of the total amount of saturated acids. Other saturated acids of chain length smaller than 16 carbon atoms (C<sub>8:0</sub>–C<sub>14:0</sub>) were present at very low levels (0.1–0.4%), in addition to a very small percentage of odd-chain fatty acids (15:0, 17:0), and arachidic acid. Therefore, those components were of lesser nutritional importance. Furthermore, it could be observed that unsaturated fatty acids predominated significantly higher in glyceride oil (75.5%) than in saturated fatty acids (24.5%). Linoleic acid (18:2) represented the major polyunsaturated fatty acid constituent (47.0%). Together with the monounsaturated oleic acid (18:1)—27.3%, they occupied nearly 98% of all unsaturated fatty acids detected in the lipid fraction. Linoleic and linolenic acids are essential fatty acids, and they must be additionally supplied by other sources.

**Table 2.** Lipid composition of service tree fruits.

Total Lipids, <i>w/w</i> %		0.82 ± 0.07 <sup>a</sup>
A. Saturated fatty acids, %		24.5
C8:0	Caprylic acid	0.4 ± 0.05 <sup>b</sup>
C10:0	Capric acid	0.2 ± 0.01
C12:0	Lauric acid	0.1 ± 0.03
C14:0	Myristic acid	0.4 ± 0.03
C15:0	Pentadecylic acid	0.2 ± 0.03
C16:0	Palmitic acid	19.5 ± 0.6
C17:0	Margaric acid	0.3 ± 0.07
C18:0	Stearic acid	3.3 ± 0.3
C20:0	Arachidic acid	0.1 ± 0.02
B. Unsaturated fatty acids, %		75.5
C14:1	Myristoleic acid	0.1 ± 0.02
C16:1	Palmitoleic acid	0.1 ± 0.04
C18:1	Oleic acid	27.3 ± 0.3
C18:2	Linoleic acid	47.0 ± 0.2
C18:3	Linolenic acid	0.5 ± 0.2
C20:3	Eicosatrienoic acid (Dihomo- $\gamma$ -linolenic acid)	0.2 ± 0.02
C20:4	Eicosatetraenoic acid (Arachidonic acid)	0.3 ± 0.04
C. Sterols, %		1.1 ± 0.1
	Cholesterol	1.4 ± 0.02 <sup>c</sup>
	Brassicasterol	1.1 ± 0.04
	Stigmasterol	3.6 ± 0.1
	$\beta$ -Sitosterol	90.2 ± 0.3
	$\Delta^5$ -Avenasterol	0.6 ± 0.02
	$\Delta^7$ -Stigmasterol	2.3 ± 0.1
	$\Delta^7$ -Avenasterol	0.8 ± 0.1
D. Phospholipids, %		3.6 ± 0.1
E. Tocopherols, mg/kg		27.0 ± 2.0
F. Carotenoids, mg/kg		7.6 ± 0.5 <sup>d</sup>
G. Total chlorophylls, mg/kg		37.8 ± 0.8 <sup>d</sup>
	Chlorophyll <i>a</i>	13.7 ± 0.5
	Chlorophyll <i>b</i>	24.2 ± 0.3

<sup>a</sup> Total lipids as *w/w*% of dried fruits, while lipid fractions are expressed as a percent of the total lipids; <sup>b</sup> % of total fatty acids; <sup>c</sup> % of total sterols; <sup>d</sup> mg/kg of dried fruits.

Further useful information could be received from the fatty acid composition data such as PUFA/SFA ratio, AI, TI, and CI (Table S2). These values provide us with a view of the nutritional value and potential health benefits of the lipid fraction. What is more, these values also allow us to compare the results of our study with those of other studies. Keeping in mind a high PUFA content (48%), the value of the PUFA/SFA ratio was computed at 2.0, suggesting that the high intake of fruits would help reduce the risk of cardiovascular disease and oxidative stress. Ideally, it is recommended that the ratio should range in value from 1.0 to 1.5. From the lower values of AI (0.3) and TI (0.6) and the higher CI (3.8) value, it was also evident that the anti-atherogenic, anti-thrombogenic, and hypocholesterolemic fatty acids made up a large proportion of the total fatty acids. This suggested a high nutritional quality of the lipid fraction that might contribute to the minimization of a deficiency in essential fatty acids and consequently to the reduction of atherogenic and thrombogenic factors. It is worth mentioning that the fatty acid composition and corresponding AI and TI were nearly identical to those of soybean, corn, and sunflower oils. However, it stood in clear contrast to those of palm and coconut fats and olive oil [19].

Furthermore, we focused our attention on the quantification of sterol and tocopherol constituents (Table 2), which has not been carried out before. As can be seen, the sterol fraction consisted mainly of  $\beta$ -sitosterol (90%) which is also a major constituent of soybean and sunflower oils [17]. The latter sterol was accompanied by lower levels of stigmasterol (3.6%) and  $\Delta^7$ -stigmasterol (2.3%). Other minor sterol components were cholesterol (1.4%) and brassicasterol (1.1%). Sterols, together with phospholipids (3.6%), play a leading role in the lowering of blood cholesterol levels and as constituents of all biological membranes. Regarding tocopherols, there was only a small amount of them (27 mg/kg). Impressively,  $\alpha$ -tocopherol was a key contributor (100%) to the total tocopherol content. This is not a surprise taking into consideration that the fruits not only have a low concentration of tocopherols but also have barely detectable levels of tocopherols other than  $\alpha$ -tocopherol in contrast to leafy green vegetables. Nevertheless, daily intake of service tree fruits could serve as a beneficial supplement of  $\alpha$ -tocopherol, which is an essential vitamin and antioxidant [17].

Lipophilic pigments (chlorophylls and carotenoids) were found in small quantities. Interestingly, among the chlorophylls, chlorophyll *b*, which is mainly responsible for the yellow-coloring of the fruits, was more predominantly present (24.2 mg/kg) than the blue-green chlorophyll *a* (*a/b* ratio = 0.56). This could be associated with the decomposition of chlorophyll *a* during fruit ripening and/or with specific environmental conditions, especially with low exposure to sunlight. The total chlorophyll content was comparable to those of commercial, red-skinned apple cultivars, and the carotenoid content was in agreement with previously reported values for apples, peas, and lemons (0.9–7.0 ppm) [17]. The vital role of carotenoids in achieving and maintaining health due to their provitamin and antioxidant activity should be emphasized. Chlorophylls, on the other hand, are often used as a marker of food quality.

### 2.3. Carbohydrate and Organic Acid Composition

Table 3 summarizes the carbohydrate compositional data of service tree fruits. The results indicated that carbohydrates made up the major fraction (about 45%) of service tree fruits' dry matter (or nearly 14% fw). Interestingly enough, soluble sugars represented a large part of the total content (nearly 74%). Fructose (5.7% fw) was the main sugar found in the fruits, accounting for almost 56% of the total soluble sugars, followed by glucose (4.0% fw) and nonreducing sucrose (<0.5% fw). Fructose and glucose content was in complete agreement with an earlier study carried out by Brindza et al. who found reduced sugar content not more than 14–16% fw in fruit pulp of *S. domestica* [4]. Sorbitol, a member of sugar alcohols mainly having an osmotic regulation function, was quantified in a small amount.

**Table 3.** Carbohydrates, organic acids, and total titratable acidity of service tree fruits.

<b>A. Total Carbohydrate, w/w%</b>	<b>44.4 ± 1.7</b>
Cellulose	2.3 ± 0.2
Starch	1.1 ± 0.1
Uronic acids (anhydrous)	3.1 ± 0.3
Glucose (Glc)	13.0 ± 1.3
Fructose (Fru)	18.2 ± 1.1
Sucrose (Suc)	1.5 ± 0.1
Sorbitol	1.6 ± 0.1
<b>B. Organic acids, mg/100 g</b>	
Malic acid	1160 ± 130
Quinic acid	363 ± 39
Ascorbic acid	<50 <sup>a</sup>
Shikimic acid	<25 <sup>a</sup>
Citric acid	<50 <sup>a</sup>
α-Ketoglutaric acid	<50 <sup>a</sup>
Tartaric acid	44 ± 5
<b>C. Total titratable acidity (g malic acid/100 g)</b>	<b>1.5</b>

<sup>a</sup> under the limit of detection for this method.

The organoleptic characteristics of fruits could be obtained by calculating sucrose-glucose and glucose-fructose ratios, respectively (Table S3). It was evident that the major contributor to the sweetness index (56.89) was fructose (Glc/Fru = 0.72). The sour index was calculated to be 1.47, which was near that of beverages prepared from apple fruits. The maturity index, an important indicator of commercial and sensory ripeness of fruits, was estimated to be 21.80, which was comparable to reported values for peach and apple cultivars [20]. A higher value of the maturity index was fairly typical of sour-sweet to sweet fruits (17–24) and it suggested a good nutritional and organoleptic quality.

Furthermore, service tree fruits were investigated for their polysaccharide constituents. As shown (Table 3), the uronic acids, which adequately reflected the amount of an acidic polysaccharide such as pectin, were predominantly present in the fruit (3.1% dw, ~1.0% fw). This suggested that pectin formed the major component of polysaccharides (nearly 48%) in service tree fruits. Pectin, a water-soluble dietary fiber, is used in the food industry due to its gelling properties. What is more, increased consumption of pectin is linked to many positive health benefits, especially immunomodulation in the digestive tract [21]. Cellulose (0.7% fw) was observed to be the second most abundant polysaccharide constituent (35%), whereas starch, whose content significantly decreases in the ripened fruits, constituted the minor part of the total carbohydrate content. Thus, service tree fruits could be evaluated as a good source of available carbohydrates and dietary fibers. The intake of 100 g of fresh fruits will provide about 11% of the daily requirements of total carbohydrates (130 g/d). It can also cover about 8% (2 g/100 g fw) of the recommended amounts of dietary fiber (25 g/d). Since carbohydrates represented a major part of dry matter constituents, it is worth estimating their caloric value, just bearing in mind the energy conversion factor for soluble sugars (3.75–4.0 kcal/g) and commonly eaten foods that contain a mixture of fermentable and nonfermentable fibers (0–1.9 kcal/g). It was calculated that carbohydrates in a serving of fruit (100 g fw) will provide the consumer with nearly 45 kcal as a greater share of energy came from sugars (90%), while dietary fiber covered only a minor part (10%). As regards the last point, it should be mentioned that carbohydrates covered not more than 2.5% of the average daily energy requirement of 2000 kcal.

Furthermore, we focused our attention on the investigation of organic acid constituents (see Table 3) because organic acids have a closely related metabolism to carbohydrates. As can be seen, malic acid, one of the Krebs cycle acids, was the most abundant (360 mg/100 g fw), representing 74% of total organic acids. Malic acid content appeared to be quite comparable to the values reported for peach, pear, and strawberry, but it was four times lower than in apples (14.7 mg/g fw). It is widely considered that malic acid makes an important contribution toward providing the substrate used for gluconeogenesis, energy

utilization, and pH regulation in fruits for a short period [22]. In addition, service tree fruits contain quinic acid in an appreciable amount (112.7 mg/100 g fw). By comparison, apples were characterized by a lower amount of quinic acid (0.2–0.7 mg/g fw), whereas medlar, peach, and blackcurrant showed similar levels (1–2 mg/g fw) [22]. In most fruits, quinic acid plays a key role as a reserve compound in phenolic biosynthesis, especially chlorogenic acid. It was easy to identify tartaric acid as a minor constituent in fruits, whereas ascorbic, shikimic, citric, and  $\alpha$ -ketoglutaric acids were qualitatively detected, but these acids appeared to be present in non-quantifiable levels (Table 3). Nonetheless, one thing was for sure—their quantities did not exceed those in banana, pear, blueberry, and raspberry, for example [22].

#### 2.4. Mineral Composition

Table 4 provides data for the total ash content and mineral composition of service tree fruits. As can be seen, potassium (4986 mg/kg; 155 mg/100 g fw) and phosphorus (400 mg/kg; 12.4 mg/100 g fw) were the most abundant macrominerals. The level of potassium, however, bore no comparison with that in well-known sources such as apricots, rose hips, and blackcurrant, but it was comparable to that found in apple, strawberry, or sour cherries [17]. A previous study by Majić et al. showed that service tree fruits collected in Croatia were also rich in potassium [6]. Together, potassium and phosphorus accounted for 55% of the total ash content (nearly 1% *w/w*) or more than 98% of the total amounts of macroelements detected. There is a complex interaction between macrominerals which are to a large extent actively involved in the regulation of acid–alkali balance. Potassium, for instance, is mainly localized within the cells and affects the osmotic pressure in the tissues. Moreover, potassium and sodium have a significant role to play in maintaining electrochemical gradients and secondary active transport in living cells. As a consequence, it exerts a diuretic effect, which can effectively be evaluated by the magnitude of the potassium-to-sodium ratio. The service tree fruits were characterized by a very high K/Na ratio (498:1) comparable to those of other medicinal plants (chamomile, linden, chicory) [23]. Therefore, this fact would seem to indicate that fruits are more likely to affect the sodium-induced hypertensive effect. Despite this, it was calculated that a rather low level of the recommended daily intake of potassium (25%/100 g dw or 7.7%/100 g fw) can come from these fruits, and thus the latter statement is open to doubt. This value was calculated by using 2.0 g as a recommended daily intake of K and assuming that 100% of the ingested element is absorbed [24]. Nevertheless, the consumption of service tree fruits could contribute to a positive K balance. Regarding other macroelements, magnesium, calcium, and sodium were found in smaller amounts (Table 4). Together they represented only 1.5% of the total macroelements; therefore, it seemed unreasonable to expect the service tree fruits to supply a considerable proportion of the intake of these macroelements (<1%/100 g fw). They are closely involved in the activation of many enzymes associated with energy conversion, in addition to the abovementioned functions.

Furthermore, a total of nine essential microelements were quantified. Iron was the most abundant (40.6 mg/kg), followed by copper and zinc (2.2 and 1.3 mg/kg, respectively). Iron, which is an essential constituent of a large number of enzymes, hemoglobin, and myoglobin pigments, accounted for almost 90% of the total, while the remaining part included the other microminerals (Table 4). The iron content (1.3 mg/100 g fw) in the service tree fruits was distinctly superior in comparison to that of fruits such as apples, oranges, apricots, and plums [17]. A daily intake of 100 g of fresh fruits can cover nearly 16% of the requirement (8 mg/day) of iron if its absorption is not disturbed. However, the value sounded very far-fetched, keeping in mind the low extent of iron absorption typical of vegetables and fruits [24]. Service tree fruits provided a relatively small proportion of the daily intake (900  $\mu$ g) of copper (nearly 8%/100 g fw). It is an essential element responsible not only for iron uptake by the organism but also for the activity of enzymes such as polyphenol and ascorbate oxidase which cause fruits to brown. It is worth paying attention to chromium—an essential trace element that functions as an insulin and glucose

level regulator. Inasmuch as 100 g of fresh fruits was estimated to contain 3.7 µg of chromium, a person who had consumed this amount of fruit per day covers nearly 11% of the recommended intake (35 µg).

**Table 4.** Total ash content and mineral composition of service tree fruits.

Total Ash, w/w%	0.98 ± 0.01
Macroelements	Content, mg/kg
Potassium (K)	4986.5 ± 85.5
Phosphorus (P)	400.0 ± 15.5
Magnesium (Mg)	40.9 ± 2.1
Calcium (Ca)	31.6 ± 1.8
Sodium (Na)	10.0 ± 1.0
Micro (Trace) Elements	
Iron (Fe)	40.6 ± 2.5
Copper (Cu)	2.2 ± 0.2
Zinc (Zn)	1.3 ± 0.2
Manganese (Mn)	0.9 ± 0.1
Chromium (Cr)	0.12 ± 0.02
Selenium (Se)	<0.1
Cobalt (Co)	0.07 ± 0.01
Molybdenum (Mo)	0.01 ± 0.00
Nickel (Ni)	0.06 ± 0.001 <sup>a</sup>
Ultra-Trace and Toxic Elements	
Aluminium (Al)	13.0 ± 2.0
Boron (B)	5.4 ± 0.4
Barium (Ba)	4.0 ± 0.6
Strontium (Sr)	3.2 ± 0.4
Arsenic (As)	<0.05
Cadmium (Cd)	0.05 ± 0.005
Mercury (Hg)	<0.03
Lead (Pb)	0.02 ± 0.001
Bismuth (Bi)	-

<sup>a</sup> The value of Ni expressed as µg/kg.

Table 4 contains an important piece of information relating to the levels of ultra-trace elements and toxic metals found in service tree fruits. It is extremely debatable whether aluminum, arsenic, and boron have any benefit to human health, but the very negative effect of the remaining elements (Cd, Hg, and Pb) is a well-known fact. Aluminium and boron accounted for 50% and 21% of the total amount of the elements in this group. One of the most interesting things was that the consumption of 100 g of fresh service tree fruits may meet about 17% of the requirement of boron (1 mg/day). In other words, one serving of fruits provided the highest intake of boron among all other minerals. Boron is a constituent of rhamnogalacturonan-II fragment that composes pectin in particular, and it seems that it plays an important part in the metabolism (Ca, Mg, vit. D) and health of the bones. The boron content (167 µg/100 g fw) was comparable to that in other fruits (apples, oranges, peaches, grapes): 107–187 µg/100 g fw. Further and most importantly, the concentration of toxic elements was well below the permitted levels. Service tree fruits (100 g fw) contained only very small quantities of Cd (1.5 µg), Pb (0.6 µg), and Hg (0.9 µg). For this reason, the risk of exceeding the provisional tolerable daily intake limit of these elements (Cd—60 µg; Pb—214 µg; Hg—43 µg), suggested for 60 kg bw by the Joint FAO/WHO Expert Committee, was considerably reduced even consuming more than one serving per day [25]. The value of Cd was higher than in a previous study, while that of Pb was significantly lower [13].

### 2.5. Phenolic Compounds and Antioxidant Activities

The content of total polyphenols, flavonoids, and tannins was investigated, and the results obtained together with quantitative compositional data are presented in Table 5. Total phenolic content (~36 mg/g dw; 1109 mg/100 g fw) was quite comparable to that reported

for mesocarp and exocarp of service tree fruits collected in Croatia [6]. By comparison, it was significantly higher than in most widely consumed fruits [26]. Regarding total flavonoids, however, some discrepancies in the values existed. Results also showed that quercetin-3- $\beta$ -glucoside was found in the highest amount, while the other flavonoids appeared to be minor constituents in service tree fruits. This result confirmed the findings of previous studies that 3-*O*-glycosylated quercetin was more prevalent among other flavonoids [7,12]. Furthermore, it can be seen that neochlorogenic and 3,4-dihydroxybenzoic acids were major constituents (97%) among phenolic acids detected, whereas ellagic and ferulic acids were found in small amounts. The presence of different phenolic constituents such as hydroxybenzoic acid derivatives in service tree fruits has already been reported [12]. However, in contrast to the study conducted by Piagnani et al., gallic acid was not detected in the current study [8]. The most likely explanation for the discrepancy in phenolic composition could be fruit material origin, its maturity, environmental factors that affect fruit growing, and, last but not least, experimental conditions.

**Table 5.** Phenolic compounds and antioxidant activities of service tree fruits.

<b>A. Total Phenolic Content, mg GAE/100 g</b>	<b>3574 <math>\pm</math> 20</b>
B. Total flavonoids content, mg QE/100 g	76.1 $\pm$ 1.0
Quercetin, mg/100 g	6.1 $\pm$ 0
Quercetin-3- $\beta$ -glucoside	146 $\pm$ 12
Epicatechin	74 $\pm$ 2
Rutin	65 $\pm$ 2
Naringin	53 $\pm$ 7
Myricetin	40 $\pm$ 1
C. Total tannins, mg/100 g	122 $\pm$ 10
D. Phenolic acids, mg/100 g	
Neochlorogenic acid	908 $\pm$ 35
3,4-Dihydroxybenzoic acid	886 $\pm$ 15
Ellagic acid	26 $\pm$ 1
Ferulic acid	22 $\pm$ 1
E. Antioxidant activity	
DPPH assay, mM TE/g	11.3 $\pm$ 1.9
FRAP assay, mM TE/g	9.4 $\pm$ 0.3
ORAC assay, $\mu$ mol TE/g	642.3 $\pm$ 31.9
HORAC assay, $\mu$ mol GAE/g	67.8 $\pm$ 5.3

In general, phenolic constituents contribute not only to the nutritional properties (taste, flavor, color) of foods but also serve a useful function as antioxidants, inhibitors of lipid peroxidation, and enzymatic browning of fruits and vegetables. Thus, we were actively interested in determining the antioxidant activity of service tree fruits (Table 5). The results indicated that fruits had a better ability to scavenge DPPH-radical than the ability to reduce ferric ions. In previous studies, it has been demonstrated that different extracts of *S. domestica* exhibited antioxidant activity evaluated by DPPH, FRAP, and ABTS [6,7,9]. However, we could not draw comparisons with the results, because these authors not only used different extracts/parts for testing the antioxidant activity but also different units of measurement. In addition, the current study also employed ORAC and HORAC methods for a more exhaustive assessment of antioxidant activity. The ORAC method evaluates the peroxy radical chain-breaking ability of antioxidants by the hydrogen atom transfer pathway, while the HORAC measures metal-chelating radical prevention activity of the sample. The results suggested that service tree fruits' constituents had much higher free-radical scavenging ability against the peroxy radical rather than the protection ability against the formation of the hydroxyl radical (the ORAC–HORAC ratio stood at 10:1). Moreover, it was particularly interesting to compare our results with a previously published study on Bulgarian fruits [26]. It came as a genuine surprise to find that service tree fruits had a powerful ORAC antioxidant activity (about 200  $\mu$ M TE/g fw) comparable only to those of rosehip and elderberry. On the other hand, it far exceeded those of apple,

apricot, peach, and even that of chokeberry (161  $\mu\text{M TE/g fw}$ ), well known for its high antioxidant activity [26,27].

### 3. Materials and Methods

#### 3.1. Plant Material

The plant material was picked in the surroundings of Kosti village (Tsarevo Municipality, Burgas Province, 42°03' N, 27°46' E) and immediately transported to the laboratory. We employed 30 fruits, a quantity high enough for morphometric characterization. They were randomly selected from a higher number of fruits which was collected from three trees located relatively close to each other. Fruits were separated from leaves and small twigs, then gently washed clean without damaging the skins and cut into half or quarters. Furthermore, they were freeze-dried, milled into flour, and stored in an exicator, in a Ziploc bag at room temperature. The average ( $n = 30$ ) mass and length of the fresh fruits were  $12.5 \pm 2.9$  g and  $2.6 \pm 0.3$  cm, respectively. The dry matter content of fruits was  $30.0 \pm 0.2\%$ ; 100 g of dry fruits corresponded to 322 g fresh ones—an amount equivalent to 9–10 fresh fruits. The fruit material was identified by the references of the Herbarium of the Institute of Biodiversity and Ecosystem Research where a voucher specimen (SOM 177 441) was deposited.

#### 3.2. Proximate Composition Analysis

For the determination of moisture content, the milled sample (~1.5 g) was dried in an automated moisture analyzer (KERN DLB, Germany) at 105 °C until constant weight. Ash content was determined as the pulverized sample (0.5 g) was placed in a crucible and ignited in a muffle furnace at 550 °C until there was no change in the mass of the sample. For the estimation of crude lipid content, the ground sample (10.0 g) was packed in a cellulose thimble and subjected to an exhaustive extraction with *n*-hexane (500 mL) for 8 h in a Soxhlet extractor. The obtained crude extract was dried under vacuum, and its weight was used for the calculation of the lipid content. The crude protein content was evaluated by the micro-Kjeldahl method ( $N \times 6.25$ ). The determination of nitrogen expressed as ammonia content of the digested sample was performed by the acetylacetone–formaldehyde colorimetric method using ammonium sulfate as a standard [28]. The total carbohydrate content of the fruits was analyzed by the phenol–sulfuric acid method using a mixture of glucose and galacturonic acid (1.5:1) for the calibration curve construction [29]. The dried sample was solubilized in 72% (*w/w*)  $\text{H}_2\text{SO}_4$  (1 h, 30 °C), and after dilution with water to 1 M  $\text{H}_2\text{SO}_4$ , hydrolysis was completed in 3 h at 100 °C. The obtained hydrolyzate was used as a sample for analysis. The absorbance was measured at 490 nm.

#### 3.3. Amino Acid Composition

For the estimation of amino acid composition, the sample (300 mg) was hydrolyzed (5 mL, 6N HCl) in a sealed glass ampule at 105 °C for 24 h. The sample was vacuum-dried, reconstituted in 10 mL 20 mM HCl, and filtered. A total of 20 microliters of the collected filtrate was derivatized using an AccQ•Fluor kit (WATO52880, Waters Corp., Milford, NH, USA) according to the instruction manual of the manufacturer. The resulting derivatives were separated on an ELITE LaChrom HPLC system (VWR™ Hitachi, Tokyo, Japan), equipped with a diode array detector and a reversed-phase column C18 AccQ•Tag (3.9 mm  $\times$  150 mm) operating at 37 °C. The volume of the injected sample was 20  $\mu\text{L}$ . The elution was performed with a flow rate of 1.0 mL/min with two mobile phases: (A) WATO52890 buffer (Waters Corp., Milford, NH, USA) and (B) 60% acetonitrile. The gradient mode was set as follow: 0–0.5 min 100–98% A, 0.5–15 min 98–93% A, 15–19 min 93–90% A, 19–32 min 90–67% A, 34–37 min 0% A, and 38–64 min 100% A. The different amino acid derivatives were detected at 254 nm.

### 3.4. Fatty Acid and Sterol Composition

The fatty acid composition was determined by gas chromatography (GC) after trans-methylation of the sample (2% H<sub>2</sub>SO<sub>4</sub> in CH<sub>3</sub>OH at 50 °C). Fatty acid methyl esters (FAMES) were purified by thin-layer chromatography (TLC) on 20 × 20 cm plates covered with a 0.2 mm silica gel 60 G (Merck) layer with mobile phase hexane:diethyl ether (97:3, *v/v*). GC was performed on a HP 5890 series II (Hewlett Packard GesmbH, Vienna, Austria) apparatus equipped with a 75 m × 0.18 mm (I.D.) × 25 μm (film thickness) capillary column Supelco and a flame ionization detector. The column temperature was programmed from 140 °C (5 min), at 4 °C/min to 240 °C (3 min); injector and detector temperatures were kept at 250 °C. Hydrogen was used as a carrier gas at a flow rate of 0.8 mL/min, and a split ratio of 1:50. The identification of fatty acids was performed by comparison of retention times with those of a standard mixture of FAME (Supelco, Bellefonte, PA, USA 37 comp. FAME mix) [30].

The quantification of sterols was carried out spectrophotometrically after their isolation from unsaponifiable material by TLC on a Silica gel 60 G plate. A mixture of diethyl ether and hexane (1:1 *v/v*) and methanol were employed as a developing solvent and spraying reagent, respectively. Unsaponifiables were obtained after saponification of the oil by boiling under reflux with an ethanolic 2 M KOH solution and extraction by *n*-hexane. The different sterols were identified on the same apparatus used for fatty acid composition analysis with a 25 m × 0.25 mm DB-5 capillary column and flame ionization detector. The temperature gradient was from 90 °C (hold 2 min) up to 290 °C at a rate of change of 15 °C/min and then up to 310 °C at a rate of 4 °C/min (hold 10 min); detector temperature—320 °C; injector temperature—300 °C and carrier gas—hydrogen. Identification was confirmed by the comparison of retention times with those of a standard mixture of sterols [30].

### 3.5. Phospholipid and Tocopherol Content

The quantification of phospholipids was carried out colorimetrically by measuring the phosphorous content at 720 nm by the sulfate–molybdate reagent after mineralization of the oil with a mixture of perchloric acid and sulphuric acid (1:1, *v/v*).

Tocopherols were determined directly in the oil by high-performance liquid chromatography using a Merck-Hitachi apparatus equipped with a 250 mm × 4 mm Nucleosil Si 50-5 column and a fluorescent detector Merck-Hitachi F 1000. The operating conditions are as follows: a mobile phase containing *n*-hexane:dioxan, 96:4 (*v/v*), a flow rate of 1.0 mL/min, excitation 295 nm, emission 330 nm. Twenty microliters of the sample (1% solution of crude oil) was injected. The tocopherols were identified and quantified by comparing the retention time and peak areas of the sample with those of the standard solutions [30].

### 3.6. Total Carotenoid and Chlorophyll Content

The total content of chlorophylls and carotenoids was determined using acetone as a solvent. Absorbance was measured at three different wavelengths 662, 644, and 470 nm according to Lichtenthaler and Wellburn [31].

### 3.7. Uronic Acid, Cellulose, and Starch Content

For the estimation of the uronic acid content of fruits, an automated 3-phenylphenol analysis was performed by a continuous flow analyzer Skalar San<sup>++</sup> system (Skalar Analytical BV, Breda, The Netherlands) according to the instructions of the manufacturer. Absorption was measured at 530 nm, and galacturonic acid (12.5–100.0 μg/mL) was used for a calibration curve construction. Initially, the sample was given a preliminary threefold extraction with 70% (*v/v*) aqueous ethanol at 50 °C for 1 h to remove small molecules. The solids were separated by centrifugation (18.187× *g*) before each repetition. Furthermore, the residue was washed twice with acetone at room temperature and vacuum-dried. Finally,

the sample was hydrolyzed as described above (Section 3.2), and an aliquot of hydrolysate was used as a sample for analysis.

The quantitative estimation of cellulose was performed gravimetrically. Briefly, a sample (0.5 g) was gently boiled (30 min) with 25 mL of acetic acid-HNO<sub>3</sub> reagent (acetic acid:H<sub>2</sub>O:HNO<sub>3</sub> 8:2:1 *v/v/v*) in a round-bottom flask fitted with a reflux condenser. After cooling, the insoluble residue was filtrated through a sintered glass filter (G3) under vacuum, washed with deionized water to neutral pH, then with ethanol (96% *v/v*), and finally with an excess of petroleum ether. The obtained residue was dried in a laboratory oven at 50 °C to a constant weight. The resulting cellulose was corrected for its ash content.

A combination of the  $\alpha$ -amylase/amyloglucosidase method for conversion of starch into glucose and the colorimetric glucose oxidase/oxidase/4-aminoantipyrine (GOPOD) method of measuring glucose content was employed to determine the total starch content. The analysis was conducted according to the analytical protocol described by Hall [32].

### 3.8. High-Performance Liquid Chromatography Analysis of Available Carbohydrates

In a plastic centrifuge tube, about five grams of chopped fresh fruits were weighed out. To this, distilled water (25 mL) was then added. The tube was placed in an ultrasonic bath (Siel UST 5.7-150, Gabrovo, Bulgaria), and an ultrasound-assisted extraction was performed with a frequency of 35 kHz (300 W) at 50 °C. After heating for 20 min, the tube was cooled in running water, then filtrated successively through a paper and PTFE filter (0.45  $\mu$ m). The quantitative chromatographic separation of free sugars was carried out on a Shodex® Sugar SP0810 (300 mm  $\times$  8.0 mm i.d.) column having Pb<sup>2+</sup> as a counter ion and a Shodex SP-G guard column (5  $\mu$ m, 6 mm  $\times$  50 mm) (Shodex Co., Tokyo, Japan) with ultra-purified water (Adrona B30, Riga, Latvia) as a mobile phase. A Shimadzu HPLC system, equipped with an LC-20 AD pump and a Shimadzu RID-10A detector was used. The volume of the sample was 20  $\mu$ L, and it was eluted at 85 °C and a flow rate of 0.5 mL/min.

### 3.9. High-Performance Liquid Chromatography Analysis of Organic Acids

A total of 1 g of the ground sample was extracted with 30 mL of water for 1 h at 30 °C shaking on a thermostatic water bath (NÜVE, Turkey). The residue and extract were then separated through a Büchner funnel (filter paper, KA-4, Czechia) and additionally filtrated through a PTFE filter (0.45  $\mu$ m). The sample was further passed through a Sep-Pak® plus C18 RP cartridge (Waters Corp., Milford, NH, USA), and the eluate was taken for chromatographic analysis. The quantitation of organic acids was conducted on a Nexera-i LC2040C Plus UHPLC system (Shimadzu Corporation, Kyoto, Japan) with a UV detector. The system was controlled by LabSolutions (ver. 5.98) software (Shimadzu Corp.). The separation was performed on a Mediterranean Sea18 (5  $\mu$ m, 4.6 mm  $\times$  150 mm; Teknokroma®, Spain) column at 25 °C and a flow rate of 1.0 mL/min. Then, 20 microliters of the sample was auto-injected and eluted isocratically using a 25 mM solution of K<sub>2</sub>HPO<sub>4</sub> in water as a mobile phase, whose pH was finely adjusted to 2.4 with H<sub>3</sub>PO<sub>4</sub>. The UV detector was set at 210 nm. The concentration of each organic acid in the sample was calculated using a calibration curve obtained by using five different concentrations for each acid. The peak corresponding to different acids was confirmed by comparison of the retention time with that of the standards.

### 3.10. Mineral Composition

The mineralization of the freeze-dried fruits (0.5 g) was performed in a heat-controlled microwave system with 9 mL of HNO<sub>3</sub> (Supra Pure Metal, 65%) in a closed vessel system. The digestion was carried out on Milestone ETHOS PLUS lab station with MPR-300/12S medium pressure rotor and heating in 2 stages (5 and 10 min at 180 °C up to 1000 W power, respectively). The micro and trace elements (Ni, Cu, Zn, As, Cd, Pb, Cr, Mn, Co, Hg, Al, Se, Ba, Sr) of the investigated sample were analyzed using ICP-MS Agilent 7500 (G3272B) (Agilent Technologies, Inc., Tokyo, Japan) spectrometer. The major elements (K, Ca, Na, Mg, Fe) were analyzed by AAS (PerkinElmer 3030 B, Waltham, MA, USA), while Mo, Ba, B, and

P elements were quantified by ICP-OES (Prodigy 7, Teledyne Technologies Incorporated, Hudson, NY, USA). The results were expressed in mg/kg using calibration standards. The reference material was dried peach leaves of the Coronet variety (Standard Reference Material® 1547, National Institute of Standards and Technology, Gaithersburg, MD, USA).

### 3.11. Total Phenolic, Flavonoid, and Condensed Tannin Content

The freeze-dried and ground fruits (0.5 g) were extracted with 40 mL of solvent containing 80% acetone in 0.5% formic acid at room temperature on a magnetic stirrer for 1 h. Then, the sample was centrifuged ( $6000 \times g$ , 20 min), and the supernatant was collected. The total phenolic content was determined according to the method of Singleton and Rossi with Folin–Ciocalteu’s reagent [33]. Gallic acid (10–200  $\mu\text{g}/\text{mL}$ ) was employed as a calibration standard.

About 1.0 g of the freeze-dried and ground sample was extracted with 40 mL of solvent containing 80% ethanol in 0.5% formic acid on a magnetic stirrer at room temperature for 1 h. The sample was centrifuged ( $6000 \times g$ ) for 20 min, and the clear supernatant was used for total flavonoid content analysis. It was determined according to the method of Chang et al. with  $\text{AlCl}_3$  reagent [34]. The calibration curve was constructed with quercetin dihydrate (10–200 mg/L). Part of the extract was taken for the determination of tannins by methylcellulose precipitation assay using epicatechin aqueous solutions as a standard [35].

### 3.12. High-Performance Liquid Chromatography of Phenolic Components

The qualitative and quantitative detection of phenolic components was performed on an HPLC system Agilent 1220 (Agilent Technology, Santa Clara, CA, USA) fully equipped with a binary pump and a UV–Vis detector (Agilent Technology, USA). The separation was performed on an Agilent TC-C18 column (5  $\mu\text{m}$ , 4.6 mm  $\times$  250 mm) at 25 °C and a wavelength of 280 nm with two mobile phases: (A) 0.5% acetic acid and (B) 100% acetonitrile with a flow rate of 0.8 mL/min. The gradient elution started with 14% (B), between 6 and 30 min, linearly increased to 25% (B), and then to 50% (B) at 40 min. The identification of compounds was confirmed by comparison of retention times utilizing standard solutions and standard calibration curves of different phenolics. As a sample for the phenolic profiling, an acidified acetone extract prepared as described in 3.11 was used. The corresponding calibration curves of the authentic standards used are presented as supplementary files (Figures S1 and S2).

### 3.13. In Vitro Antioxidant Activity Assays

Oxygen radical absorbance capacity (ORAC) and hydroxyl radical averting capacity (HORAC) were measured according to the methodology used by Denev et al. [27]. Both analyses were carried out on a FLUOstar OPTIMA plate reader (BMG Labtech, Ortenberg, Germany); 1, 1-Diphenyl-2-picrylhydrazyl (DPPH) radical-scavenging ability and ferric reducing antioxidant power (FRAP) assay and the preparation of extracts were carried out as described by Ivanov et al. [36]. As a sample for ORAC and HORAC analyses, an acidified acetone extract prepared as described in Section 3.11 was used, while for the estimation of DPPH and FRAP activities, a 70% ethanol extract was employed [36].

### 3.14. Lipid and Carbohydrate Indexes Calculation

A polyunsaturated-to-saturated fatty acids (PUFA/SFA) ratio, atherogenic (AI), thrombogenic (TI), and cholesterolemic indexes (CI) were calculated from data from the fatty acid composition following the formulas described in Petkova, Antova, and Angelova-Romova [30]. The maturity index and other carbohydrate indexes were calculated as described in Mihaylova et al. [20].

### 3.15. Statistics

The experimental data were subjected to an analysis of variance, at the confidence level of  $p = 0.05$ , using Statistica v. 8.0 software (Statsoft, Inc., Tulsa, OK, USA). A Fisher test was used for the determination of statistically significant differences if applicable.

## 4. Conclusions

For the first time, we reported an in-depth study that provided valuable insight into the phytochemical composition of service tree fruits. To our knowledge, the current study reveals for the first time the lipid (saturated and unsaturated fatty acids, phytosterols, and phospholipids) composition, the minerals (P, Se, B, Al, Co, As, Cd, Hg, Pb), the polysaccharides (cellulose, starch, and pectin), the amino acids, and the organic acid constituents of service tree fruits. Thus, we believe we not only fill the gaps in scientists' knowledge, but also form a solid basis for a better assessment of the potential for practical applications. The results suggest that a regular intake of fresh fruits may contribute to making up a deficiency of important nutrients. It may contribute, to a higher extent, to maintaining a positive nutritional balance, especially of essential unsaturated fatty acids, potassium, iron, boron, histidine, methionine, and dietary fibers. Therefore, this unique combination of bioactive constituents may help reduce the risk of cardiovascular disease and oxidative stress. In addition, it seems reasonable to suggest that flour made from whole-dried service tree fruits would be a suitable form of practical application used in cooking for making dietary fiber-enriched bread and cakes. Moreover, it can be incorporated as an active natural ingredient in functional beverages and foods.

**Supplementary Materials:** The following supporting information can be downloaded at: <https://www.mdpi.com/article/10.3390/plants11141832/s1>, Table S1: Amino acid score of service tree protein compared with the amino acids of standard and bovine milk protein, %; Table S2: Ratio of polyunsaturated (PUFA) and saturated (SFA) fatty acids, atherogenic, thrombogenic, and cholesterolic indexes of the glyceride oil; Table S3: Sugar ratios, sweetness, total sweetness, sour and maturity indexes of service tree fruits. Figure S1: Calibration curves used for the quantification of flavonoid constituents of service tree fruits; Figure S2: Calibration curves used for the quantification of phenolic acids of service tree fruits.

**Author Contributions:** Conceptualization, M.O.; methodology, M.O. and N.P.; validation, M.O.; formal analysis, M.O., N.P. and Z.P.; investigation, M.O., N.P., Z.P., M.S., G.M. and D.T.; resources, P.D., N.P., P.Z. and G.M.; data curation, M.O., N.P. and Z.P.; writing—original draft preparation, M.O.; writing—review and editing, M.O., P.D., N.P., Z.P., M.S., D.T. and Y.G.; supervision, M.O. and P.D.; project administration, P.D.; funding acquisition, P.D. All authors have read and agreed to the published version of the manuscript.

**Funding:** This research was funded by the Bulgarian Ministry of Education and Science under the National Research Programme “Healthy Foods for a Strong Bio-Economy and Quality of Life” approved by DCM № 577/17.08.2018.

**Institutional Review Board Statement:** Not applicable.

**Informed Consent Statement:** Not applicable.

**Data Availability Statement:** Not applicable.

**Acknowledgments:** The first author acknowledges with gratitude the technical assistance of chemist Irina Z. Yanakieva. He is also thankful to Kalin Nikolov and Iliya Engyozov for service tree fruit picking.

**Conflicts of Interest:** The authors declare no conflict of interest. The funder had no role in the design of the study; in the collection, analyses, or interpretation of data; in the writing of the manuscript, or in the decision to publish the results.

## References

- Enescu, C.M.; de Rigo, D.; Durrant, T.H.; Caudillo, G. *Sorbus domestica* in Europe: Distribution, habitat, usage and threats. In *European Atlas of Forest Tree Species*; San-Miguel-Ayanz, J., de Rigo, D., Caudillo, G., Houston Durrant, T., Mauri, A., Eds.; European Commission: Luxembourg, 2016; p. e019db5+.
- Rotach, P. *EUFORGEN Technical Guidelines for Genetic Conservation and Use for Service Tree (Sorbus domestica)*; International Plant Genetic Resources Institute: Rome, Italy, 2003; 6p.
- George, J.P.; Konrad, H.; Collin, E.; Thevenet, J.; Ballian, D.; Idzjotic, M.; Kamm, U.; Zhelev, P.; Geburek, T. High molecular diversity in true service tree (*Sorbus domestica*) despite rareness: Data from Europe with special reference to the Austrian occurrence. *Ann. Bot.* **2015**, *115*, 1105–1115. [[CrossRef](#)] [[PubMed](#)]
- Brindza, J.; Červeňáková, J.; Tóth, D.; Biro, D.; Sajbidor, J. Unutilized potential of true service tree (*Sorbus domestica* L.). *ISHS Acta Hort.* **2009**, *806*, 717–726. [[CrossRef](#)]
- Mondeshka, P.K. *Skorusha*, 1st ed.; Zemizdat State Publishing House: Sofia, Bulgaria, 1990; pp. 5–67.
- Majić, B.; Šola, I.; Likić, S.; Cindrić, I.J.; Rusak, G. Characterisation of *Sorbus domestica* L. bark, fruits and seeds: Nutrient composition and antioxidant activity. *Food Technol. Biotechnol.* **2015**, *53*, 463–471. [[CrossRef](#)] [[PubMed](#)]
- Mrkonjić, Z.; Nađpal, J.; Beara, I.; Šibul, F.; Knežević, P.; Lesjak, M.; Mimica-Dukić, N. Fresh fruits and jam of *Sorbus domestica* L. and *Sorbus intermedia* (Ehrh.) Pers.: Phenolic profiles, antioxidant action and antimicrobial activity. *Bot. Serbica* **2019**, *43*, 187–196. [[CrossRef](#)]
- Piagnani, M.C.; Debellini, C.; LoScalzo, R. Phyllometry and carpometry, chemical and functional characterization of fruits of *Sorbus domestica* L. (service tree) selections. *J. Berry Res.* **2012**, *2*, 7–22. [[CrossRef](#)]
- Termentzi, A.; Kefalas, P.; Kokkalou, E. Antioxidant activities of various extracts and fractions of *Sorbus domestica* fruits at different maturity stages. *Food Chem.* **2006**, *98*, 599–608. [[CrossRef](#)]
- Termentzi, A.; Alexiou, P.; Demopoulos, V.J.; Kokkalou, E. The aldose reductase inhibitory capacity of *Sorbus domestica* fruit extracts depends on their phenolic content and may be useful for the control of diabetic complications. *Pharmazie* **2008**, *63*, 693–696. [[CrossRef](#)]
- Termentzi, A.; Kefalas, P.; Kokkalou, E. LC–DAD–MS (ESI+) analysis of the phenolic content of *Sorbus domestica* fruits in relation to their maturity stage. *Food Chem.* **2008**, *106*, 1234–1245. [[CrossRef](#)]
- Termentzi, A.; Zervou, M.; Kokkalou, E. Isolation and structure elucidation of novel phenolic constituents from *Sorbus domestica* fruits. *Food Chem.* **2009**, *116*, 371–381. [[CrossRef](#)]
- Zeiner, M.; Cindrić, I.J.; Majić, B.; Stingeder, G. Study of the accumulation of toxic and essential ultra-trace elements in fruits of *Sorbus domestica* L. *Int. J. Environ. Res. Public Health* **2017**, *14*, 341. [[CrossRef](#)]
- Akkol, E.K.; Dereli, F.T.G.; Taştan, H.; Sobarzo-Sánchez, E.; Khan, H. Effect of *Sorbus domestica* and its active constituents in an experimental model of colitis rats induced by acetic acid. *J. Ethnopharmacol.* **2020**, *251*, 112521. [[CrossRef](#)] [[PubMed](#)]
- Matczak, M.; Marchelak, A.; Michel, P.; Owczarek, A.; Piszczan, A.; Kolodziejczyk-Czepas, J.; Nowak, P.; Olszewska, M.A. *Sorbus domestica* L. leaf extracts as functional products: Phytochemical profiling, cellular safety, pro-inflammatory enzymes inhibition and protective effects against oxidative stress in vitro. *J. Funct. Foods* **2018**, *40*, 207–218. [[CrossRef](#)]
- Rutkowska, M.; Balcerczak, E.; Świechowski, R.; Dubicka, M.; Olszewska, M.A. Seasonal variation in phenylpropanoid biosynthesis and in vitro antioxidant activity of *Sorbus domestica* leaves: Harvesting time optimisation for medicinal application. *Ind. Crops Prod.* **2020**, *156*, 112858. [[CrossRef](#)]
- Belitz, H.-D.; Grosch, W.; Schieberle, P. *Food Chemistry*, 4th ed.; Springer: Berlin/Heidelberg, Germany, 2009; pp. 8–428. [[CrossRef](#)]
- FAO Food and Nutrition Series—Collection. Amino-Acid Content of Foods and Biological Data on Proteins. 1981. Available online: <http://www.fao.org/3/AC854T/AC854T00.htm#TOC> (accessed on 24 May 2022).
- Alves, A.Q.; da Silva, V.A., Jr.; Góes, A.J.S.; Silva, M.S.; de Oliveira, G.G.; Bastos, I.V.G.A.; de Castro Neto, A.G.; Alves, A.J. The fatty acid composition of vegetable oils and their potential use in wound care. *Adv. Wound Care* **2019**, *32*, 1–8. [[CrossRef](#)] [[PubMed](#)]
- Mihaylova, D.; Popova, A.; Desseva, I.; Manolov, I.; Petkova, N.; Vrancheva, R.; Peltekov, A.; Slavov, A.; Zhivondov, A. Comprehensive evaluation of late season peach varieties (*Prunus persica* L.): Fruit nutritional quality and phytochemicals. *Molecules* **2021**, *26*, 2818. [[CrossRef](#)] [[PubMed](#)]
- Georgiev, Y.N.; Ognyanov, M.H.; Denev, P.N.; Kratchanova, M.G. Perspective therapeutic effects of immunomodulating acidic herbal heteropolysaccharides and their complexes in functional and dietary nutrition. In *Therapeutic Foods, Handbook of Food Bioengineering*; Holban, A.M., Grumezescu, A.M., Eds.; Academic Press: London, UK, 2018; Volume 8, pp. 285–327. [[CrossRef](#)]
- Walker, R.P.; Famiani, F. Organic acids in fruits: Metabolism, functions and contents. In *Horticultural Reviews*; Warrington, I.J., Ed.; John Wiley & Sons, Inc.: Hoboken, NJ, USA, 2018; Volume 45, pp. 371–430.
- Szentmihályi, K.; Kéry, Á.; Then, M.; Lakatos, L.; Sándor, Z.; Vinkler, P. Potassium–sodium ratio for the characterization of medicinal plant extracts with diuretic activity. *Phytother. Res.* **1998**, *12*, 163–166. [[CrossRef](#)]
- Harris, E.D. *Minerals in Food: Nutrition, Metabolism, Bioactivity*; DEStech Publications, Inc.: Lancaster, PA, USA, 2014; pp. 15–239.
- FAO; WHO. *Evaluation of Certain Food Additives and Contaminants: Seventy-Third Report of the Joint FAO/WHO Expert Committee on Food Additives*; WHO Technical Report Series, № 960; FAO: Rome, Italy; WHO: Geneva, Switzerland, 2011.
- Denev, P.; Lojek, P.; Ciz, M.; Kratchanova, M. Antioxidant activity and polyphenol content of Bulgarian fruits. *Bulg. J. Agric. Sci.* **2013**, *19*, 22–27.

27. Denev, P.; Ciz, M.; Ambrozova, G.; Lojek, A.; Yanakieva, I.; Kratchanova, M. Solid-phase extraction of berries' anthocyanins and evaluation of their antioxidative properties. *Food Chem.* **2010**, *123*, 1055–1061. [[CrossRef](#)]
28. GB 5009.5-2016; Determination of Protein in Foods. National Food Safety Standard (NFSS) of the People's Republic of China. China National Center for Food Safety Risk Assessment: Beijing, China, 2016.
29. DuBois, M.; Gilles, K.A.; Hamilton, J.K.; Rebers, P.A.; Smith, F. Colorimetric method for determination of sugars and related substances. *Anal. Chem.* **1956**, *28*, 350–356. [[CrossRef](#)]
30. Petkova, Z.Y.; Antova, G.A.; Angelova-Romova, M.Y. Biologically active components and health benefits of nettle seed oil. *Grasas Aceites* **2020**, *71*, e347. [[CrossRef](#)]
31. Lichtenthaler, H.K.; Wellburn, A.R. Determinations of total carotenoids and chlorophylls a and b of leaf extracts in different solvents. *Biochem. Soc. Trans.* **1983**, *11*, 591–592. [[CrossRef](#)]
32. Hall, M.B. Determination of starch, including maltooligosaccharides, in animal feeds: Comparison of methods and a method recommended for AOAC collaborative study. *J. AOAC Int.* **2009**, *92*, 42–49. [[CrossRef](#)] [[PubMed](#)]
33. Singleton, V.; Rossi, J. Colorimetry of total phenolic with phosphomolibdophosphotungstic acid reagents. *Am. J. Enol. Vitic.* **1965**, *16*, 144–158.
34. Chang, C.-C.; Yang, M.-H.; Wen, H.-M.; Chern, J.-C. Estimation of total flavonoid content in propolis by two complementary colometric methods. *J. Food Drug Anal.* **2002**, *10*, 178–182. [[CrossRef](#)]
35. Sarneckis, C.J.; Dambergs, R.G.; Jones, P.; Mercurio, M.; Herderich, M.J.; Smith, P.A. Quantification of condensed tannins by precipitation with methyl cellulose: Development and validation of an optimised tool for grape and wine analysis. *Aust. J. Grape Wine Res.* **2006**, *12*, 39–49. [[CrossRef](#)]
36. Ivanov, I.G.; Vrancheva, R.Z.; Marchev, A.S.; Petkova, N.T.; Aneva, I.Y.; Denev, P.P.; Georgiev, V.G.; Pavlov, A.I. Antioxidant activities and phenolic compounds in Bulgarian *Fumaria* species. *Int. J. Curr. Microbiol. Appl. Sci.* **2014**, *3*, 296–306.

## Article

# Gene Losses and Plastome Degradation in the Hemiparasitic Species *Plicosepalus acaciae* and *Plicosepalus curviflorus*: Comparative Analyses and Phylogenetic Relationships among Santalales Members

Widad AL-Juhani <sup>1,\*</sup>, Noha T. Al Thagafi <sup>2</sup> and Rahmah N. Al-Qthanin <sup>3,4</sup><sup>1</sup> Department of Biology, Faculty of Applied Science, Umm Al-Qura University, Makkah 24381, Saudi Arabia<sup>2</sup> Department of Biology, Faculty of Science, Taif University, Taif 21974, Saudi Arabia; noha.t@tu.edu.sa<sup>3</sup> Department of Biology, College of Sciences, King Khalid University, Abha 61421, Saudi Arabia; rngerse@kku.edu.sa<sup>4</sup> Prince Sultan Bin-Abdul-Aziz Center for Environment and Tourism Studies and Researches, King Khalid University, Abha 61421, Saudi Arabia

\* Correspondence: wsjuhani@uqu.edu.sa

**Abstract:** The *Plicosepalus* genus includes hemiparasitic mistletoe and belongs to the Loranthaceae family, and it has several medicinal uses. In the present study, we sequenced the complete plastomes of two species, *Plicosepalus acaciae* and *Plicosepalus curviflorus*, and compared them with the plastomes of photosynthetic species (hemiparasites) and nonphotosynthetic species (holoparasites) in the order Santalales. The complete chloroplast genomes of *P. acaciae* and *P. curviflorus* are circular molecules with lengths of 120,181 bp and 121,086 bp, respectively, containing 106 and 108 genes and 63 protein-coding genes, including 25 tRNA and 4 rRNA genes for each species. We observed a reduction in the genome size of *P. acaciae* and *P. curviflorus* and the loss of certain genes, although this reduction was less than that in the hemiparasite and holoparasitic cp genomes of the Santalales order. Phylogenetic analysis supported the taxonomic state of *P. acaciae* and *P. curviflorus* as members of the family Loranthaceae and tribe Lorantheae; however, the taxonomic status of certain tribes of Loranthaceae must be reconsidered and the species that belong to it must be verified. Furthermore, available chloroplast genome data of parasitic plants could help to strengthen efforts in weed management and encourage biotechnology research to improve host resistance.

**Keywords:** plastome; *Plicosepalus acaciae*; *Plicosepalus curviflorus*; loranthaceae; mistletoe; phylogenetic relationship; plastome structure; comparative analysis

**Citation:** AL-Juhani, W.; Al Thagafi, N.T.; Al-Qthanin, R.N. Gene Losses and Plastome Degradation in the Hemiparasitic Species *Plicosepalus acaciae* and *Plicosepalus curviflorus*: Comparative Analyses and Phylogenetic Relationships among Santalales Members. *Plants* **2022**, *11*, 1869. <https://doi.org/10.3390/plants11141869>

Academic Editors: Cássio Van den Berg and Baohong Zhang

Received: 23 April 2022

Accepted: 7 July 2022

Published: 18 July 2022

**Publisher's Note:** MDPI stays neutral with regard to jurisdictional claims in published maps and institutional affiliations.



**Copyright:** © 2022 by the authors. Licensee MDPI, Basel, Switzerland. This article is an open access article distributed under the terms and conditions of the Creative Commons Attribution (CC BY) license (<https://creativecommons.org/licenses/by/4.0/>).

## 1. Introduction

Parasitic plants completely or partially lose the ability to photosynthesize, and they absorb water and nutrients from the host via the haustorium. Depending on the degree of loss of photosynthetic ability, parasitic plants are divided into photosynthetic parasites (hemiparasites) and nonphotosynthetic parasites (holoparasites) [1]. All hemiparasitic species are capable of photosynthesis (at different levels), whereas holoparasites entirely lose their photosynthetic ability and obtain all nutrients from their hosts [2]. The most parasitic plant species are included in the family Orobanchaceae and the order Santalales.

The family Loranthaceae is the largest in the sandalwood order Santalales, and it includes 76 genera and over 1000 species [3,4]. Loranthaceae are mainly distributed in tropical and subtropical regions of the Americas, Africa, Asia and Australia, with a few species extending to the temperate zones in Europe and East Asia [3,5]. The origin of the Loranthaceae family has been traced back to the Australasian continent in the Late Cretaceous, and it was likely dispersed by birds from Australasia to Asia. African and European species migrated from Asia after the middle Oligocene, and birds also played an

important role in dispersing Loranthaceae from Africa to Madagascar [3]. Loranthaceae mainly include aerial parasitic plants, although they also contain three monotypic genera that are root parasites and considered relicts [5]. Mistletoe is an aerial parasitic plant that depends on pollination and seed dispersal by birds and other pollinators, and it provides a habitat for these organisms; moreover, mistletoe determines the natural structure of the surrounding plant communities [6].

In terms of taxonomic state, initial studies on Loranthaceae included most mistletoes in the genus *Loranthus* or in a section of *Loranthus* [7,8] presented genera with new names, some of which are still used at present. However, the interspecific relationships within genera remain unclear [4].

The Loranthaceae family was divided into tribes and subtribes [5,9] according to morphological data, chromosome numbers, and molecular sequences of the “nuclear gene rDNA and chloroplast genes *rbcl*, *matk*, and *trnL-F*”. The tribe Loranthae has been characterized by a chromosome number  $x = 9$ , the tribe Psittacanthae has been characterized by  $x = 8$ , while the other two tribes (Elytrantheae and Nuytsieae) have been characterized by  $x = 12$  [5].

*P. acaciae* (Zucc.) Wiens and Polhill, and *P. curviflorus* (Benth. ex Oliv.) Tiegh, are hemiparasite species (mistletoe) belonging to Loranthaceae. These plants are woody parasites with brownish slender branchlets, evergreen, rigidly coriaceous, oblong to elliptic-oblong, glabrous leaves, solitary or clustered umbels of scarlet flowers, and berry fruits, and they are widespread parasites of *Acacia* [10]. *P. acaciae* is distributed in Syria to northeast tropical Africa and the southern Arabian Peninsula. *P. curviflorus* is distributed in southeast Egypt to east central and east tropical Africa. *Plicosepalus* is traditionally used as a treatment for diabetes and cancer and as an antioxidant, antimicrobial, anti-inflammatory agent, and it is also used to increase lactation in cattle [11,12].

According to the parsimony, likelihood and Bayesian inference trees presented by [5], *Plicosepalus sagittiflorus* belongs to subtribe Loranthinae (Clade J) and Asian and African taxa ( $x = 9$ ). Furthermore, this study reported 12 species belonging to the genus *Plicosepalus*, which is the same number currently mentioned in Plants of the World Online [13].

Liu et al. conducted taxonomic analyses of Loranthaceae based on floral, inflorescence morphology, phylogenetic and biogeographical analyses using both nuclear and chloroplast DNA regions, and they included 62 of the 76 genera [3]. This study classified the species belonging to family Loranthaceae within five tribes (Psittacanthae, Nuytsieae, Elytrantheae, Gaiadendreae and Loranthae), and species belonging to the tribe Loranthae were distributed within seven subtribes (Tapinanthinae, Scurrellinae, Emelianthinae, Dendrophthoinae, Amyeminae, Loranthinae and Ileostylinae). The species *Plicosepalus sagittiflorus* and *P. curviflorus* are representative of the genus *Plicosepalus*, which appears in the phylogenetic tree within the subtribe Tapinanthinae and belongs to the Africa–Madagascar section (including regions of the coastal area of the Arabian Peninsula and Sub-Saharan Africa and Madagascar). However, the African subtribe Tapinanthinae was not monophyletic but rather was nested within the Emelianthinae subtribe. Therefore, further studies are recommended to resolve the phylogenetic relationship between Tapinanthinae and Emelianthinae and test the monophyly of the African genera.

The chloroplast is an organelle in plant cells that contains its own genome, the plastome, and it has essential roles in photosynthesis [14]. During the evolutionary history of plant families, plastomes have been subjected to strong selective pressures [15]. Thus, chloroplast genomes include useful phylogenetic information that has been used to study evolutionary relationships at different taxonomic levels and resolve difficult problems in plant phylogenetics [3,16]. Investigating the genomes of hemiparasitic plants is important for understanding the changes in the chloroplast genome of a plant when it shifts from an autotrophic to a parasitic state. Moreover, most parasitic plants are medicinally important, and their reliable identification is important for avoiding damage caused by the misidentification of herbal medicinal plants. This study aimed to assemble and compare the complete plastomes of *P. acaciae* and *P. curviflorus*; assess the systematic relationships within the

family and tribes of Loranthaceae; and compare the new plastomes with representatives of hemiparasites and holoparasites to investigate the evolution of plastomes associated with parasitism.

## 2. Results

### 2.1. Characteristics of the Chloroplast Genome

The complete chloroplast genomes of *P. acaciae* and *P. curviflorus* are shown in Figure 1, and they are circular molecules with lengths of 120,181 bp and 121,086 bp, respectively. The chloroplast genome presents a typical four-region structure that consists of a large single copy (LSC), a small single copy (SSC) and two inverted repeats (IRA and IRb). The LSC and SSC regions in *P. acaciae* and *P. curviflorus* are 69,497 bp and 69,947 bp long and 6038 bp and 6187 bp long, respectively, while IRA and IRb are 22,323 bp and 22,476 bp each in *P. acaciae* and *P. curviflorus* (Table 1). The lengths of the coding regions are 58,089 and 64,539 bp, and they represent 48.33% and 53.30% of the entire genome in *P. acaciae* and *P. curviflorus*, respectively, while the noncoding region lengths are 62,092 and 56,547 bp (51.67% and 46.70%), respectively. The percentage of AT in *P. acaciae* and *P. curviflorus* in the entire genome is 63.43% and 63.23%, respectively, whereas the percentage of GC is 36.6% and 36.8%, respectively. The genomic structure of *P. acaciae* and *P. curviflorus* consists of A = (31.50% and 31.34%), T(U) = (31.93% and 31.89%), C = (18.59% and 18.65%) and G = (17.97% and 18.12%), respectively, as shown in Table 1.

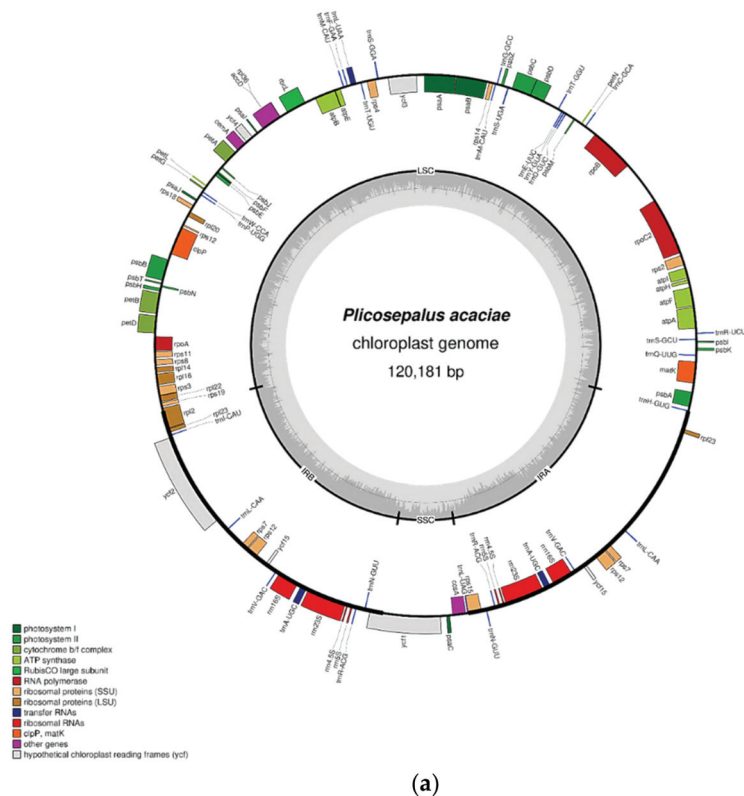
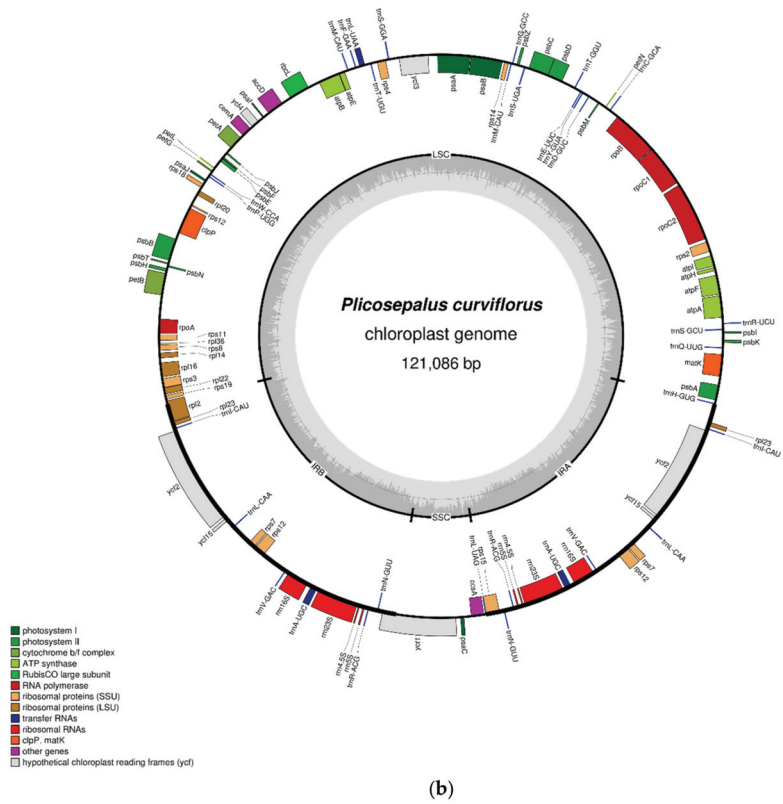


Figure 1. Cont.



**Figure 1.** (a) Gene map of the *Plicosepalus acaciae* plastid genome. (b) Gene map of the *Plicosepalus curviflorus* plastid genome. Small single copy (SSC), large single copy (LSC) and inverted repeats (IRA and IRb) are indicated. Thick lines on the outer complete circle identify the inverted repeat regions (IRA and IRb). The genes outside the circle are transcribed counterclockwise, whereas those inside the circle are transcribed clockwise. Genes belonging to different functional groups are highlighted in different colours. The dark grey area in the inner circle indicates the CG content of the plastome, using OGDRAW tool Version 1.3.1.

**Table 1.** Chloroplast genome features of *Plicosepalus acaciae* & *Plicosepalus curviflorus*.

Feature	<i>P. acaciae</i>	<i>P. curviflorus</i>
Genome size (bp)	120,181	121,086
IRA (bp)	22,323	22,476
IRB (bp)	22,323	22,476
LSC (bp)	69,497	69,947
SSC (bp)	6038	6187
Total No of Genes	106	108
Total No of Unique Genes	92	92
rRNA	4	4
tRNA	25	25
Protein-Coding genes	63	63
A%	31.50	31.34
T (U) %	31.93	31.89
G%	17.97	18.12
C %	18.59	18.65
%GC	36.6	36.8

Figure 1 and Tables S1 and S2 show the results obtained from gene annotation of the chloroplast genomes of *P. acaciae* and *P. curviflorus*: 106 and 108 genes were obtained, respectively, which included 92 of unique genes and 12 and 14 genes that were duplicated in the IR region. The cp contains 63 protein-coding genes, including 25 tRNA and 4 rRNA genes for each species. Most of the protein-coding genes start with a methionine codon (AUG).

Introns play a significant role in gene expression regulation [17,18]. Tables 2 and 3 illustrate that 10 of the 106 and 108 genes in *P. acaciae* and *P. curviflorus* contain introns, and they include 8 protein-coding genes and 2 tRNA genes. The *ycf3* and *clpP* genes have two introns, while the remaining genes have only one intron. The seven introns are included in the LSC, and the rest are specifically located within the IRa and IRb regions.

**Table 2.** Genes with introns in the chloroplast genome of *Plicosepalus acaciae*.

Gene	Strand	Location	Exon I (bp)	Intron I (bp)	Exon II (bp)	Intron II (bp)	Exon III (bp)
atpF	-	LSC	145	801	401		
ycf3	-	LSC	124	762	230	768	153
clpP	-	LSC	71	767	294	675	229
petB	+	LSC	6	814	642		
rps12	-	IRB	56	515	229		
	+	IRA	229	515	56		
rpl2	-	IRB	391	654	431		
rpl16	-	LSC	303	486	9		
petD	+	LSC	8	743	484		
trnL-UAA	+	LSC	35	299	55		
trnA-UGC	-	IRA	55	342	39		
	+	IRB	39	342	55		

**Table 3.** Genes with introns in the chloroplast genome of *Plicosepalus curviflorus*.

Gene	Strand	Location	Exon I (bp)	Intron I (bp)	Exon II (bp)	Intron II (bp)	Exon III (bp)
atpF	-	LSC	145	792	410		
rpoC1	-	LSC	432	830	1617		
ycf3	-	LSC	124	743	230	772	153
clpP	-	LSC	71	752	294	524	229
rpl2	-	IRB	391	654	440		
rps12	-	IRB	56	507	229		
	+	IRA	229	507	56		
rpl16	-	LSC	9	893	81		
petB	+	LSC	6	864	642		
trnL-UAA	+	LSC	35	290	55		
trnA-UGC	-	IRA	55	350	37		
	+	IRB	37	350	55		

## 2.2. Relative Synonymous Codon Usage (RSCU)

Codon usage bias plays an important role in chloroplast genome evolution and occurs as a result of natural selection and mutations [19,20]. The nucleotides of protein-coding and tRNA genes (58,089 bp and 64,539 bp, respectively) in *P. acaciae* and *P. curviflorus* were used to determine the codon usage bias of the plastome. As shown in Tables S3 and S4, these genes are encoded by 19,363 and 21,513 codons in *P. acaciae* and *P. curviflorus*, respectively. As shown in Figure 2, the amino acid leucine was the most frequent amino acid (10.097% and 10.052%, respectively) in *P. acaciae* and *P. curviflorus*, cysteine was the least frequent amino acid (1.097%) in *P. acaciae*, and tryptophan (1.181) was the least frequent amino acid in *P. curviflorus*.

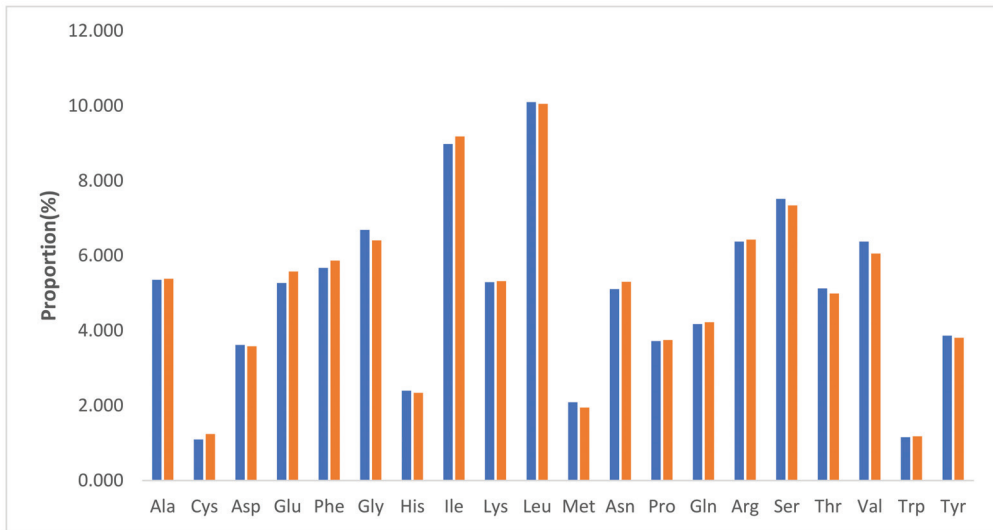


**Figure 2.** Amino acid frequencies of the protein-coding sequences of *Plicosepalus acaciae* (blue) and *Plicosepalus curviflorus* (orange) chloroplast genomes using MEGA software Version 11.0; the most and least frequent amino acids are shown.

The RSCU values in *P. acaciae* in Table S3 show that 27 codons are >1, while 32 codons are <1. The data show that tryptophan, glycine, valine, and methionine with no codon usage bias have an RSCU value of 1. The RSCU values in *P. curviflorus* in Table S4 show that 26 codons are >1 and 32 codons are <1. The data show that tryptophan, glycine, and methionine with no codon usage bias have an RSCU value of 1.

### 2.3. RNA Editing Sites

RNA editing sites include the processes of inserting, deleting or modifying nucleotides, which lead to changes in the DNA coding sequence during RNA transcription processes [21], which in turn allows for the creation of different protein transcripts [22]. The PREP suite was used to predict the RNA editing sites in the *P. acaciae* and *P. curviflorus* plastomes, and the first codon position of the first nucleotide was used in the analysis. The RNA editing sites are presented in Tables S5 and S6. Overall, there are 33 and 40 editing sites in the genomes of *P. acaciae* and *P. curviflorus* distributed among 15 and 16 protein-coding genes. The results show that the highest number of editing sites in *P. curviflorus* are the *rpoB* and *rpoC2* genes (7 and 6 sites, respectively), while the highest number of editing sites in *P. acaciae* are the *rpoB* and *matK* genes (6 and 5 sites). Most of the codon position exchanges involve the amino acids serine (S) and leucine (L) (S to L). The results of RNA editing show that certain genes do not possess a predictable site in the first nucleotide of the first codon, namely, *rpl23*, *accD*, *atpB*, *clpP*, *petG*, *petL*, *psaB*, *psaI*, *psbE*, *psbF*, and *rps14* in *P. acaciae* and *accD*, *atpB*, *clpP*, *ndhA*, *ndhB*, *ndhD*, *ndhF*, *ndhG*, *petD*, *petG*, *petL*, *psaB*, *psaI*, *psbE*, *psbF*, *psbL*, *rpl2*, *rpl23*, and *rps16* in *P. curviflorus*.

### 2.4. Repeat Analysis

#### 2.4.1. Long Repeats

Figure 3 shows that there are four types of repeats in the *P. acaciae* and *P. curviflorus* cp genomes: palindromic (16 and 11), forward (12 and 13), reverse (16 and 19), and complementary (4 and 5). We compared the frequency of repeats (palindromic, forward, reverse, and complementary) in the cp genomes of *P. acaciae*, *P. curviflorus* and six species of Loranthaceae (*Scurrula chingii* (W.C.Cheng) H.S.Kiu, *Taxillus chinensis* (DC.) Danser, *Loranthus*

*europaeus* Jacq., *Dendrophthoe pentandra* (L.) Miq., *Nuytsia floribunda* (Labill.) R.Br. ex G.Don. *Elytranthe albida* (Blume) Blume.) (Figure 3). *T. chinensis* had the highest frequency of palindromic repeats (24), *N. floribunda* had the highest frequency of forward repeats (16), and *P. curviflorus* had the highest frequency of reverse repeats (19). Complement repeats were the least common type of repeat in the genome, with *P. curviflorus* and *E. albida* having five repeats and *N. floribunda* presenting no complementary repeats (Figure 3).

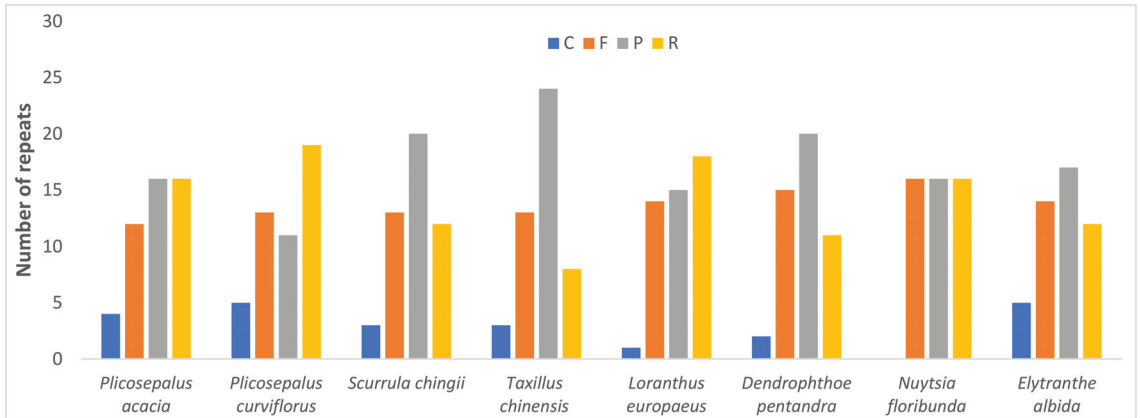


**Figure 3.** Number of each repeat type—F, forward; P, palindromic; R, reverse; and C, complement repeats—in the plastid genome of *Plicosepalus acaciae* and *Plicosepalus curviflorus* and six species from Loranthaceae, using REPUTER 2 software. *Taxillus chinensis* had the highest frequency of palindromic repeats, *Nuytsia floribunda* had the highest frequency of forward repeats, and *Plicosepalus curviflorus* had the highest frequency of reverse repeats. Complement repeats were the least common type of repeat.

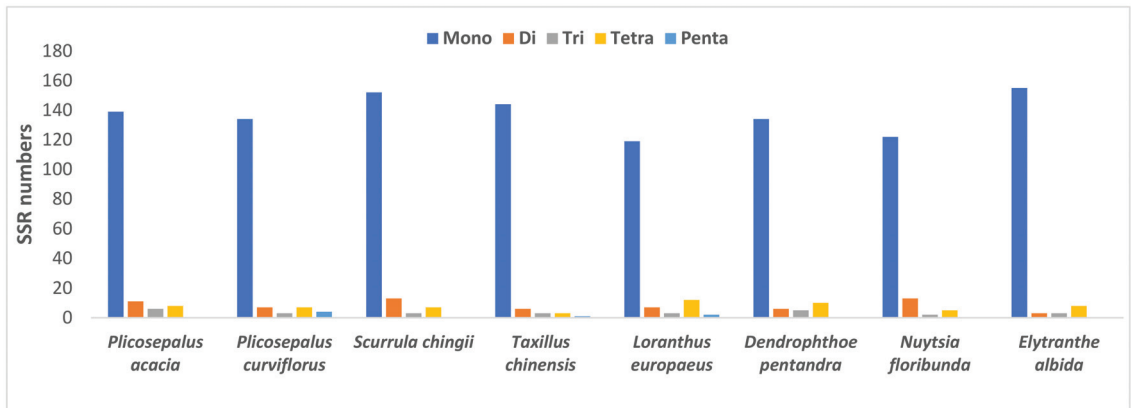
#### 2.4.2. Simple Sequence Repeats

A total of 164 and 155 SSRs are present in the plastid genome of *P. acacia* and *P. curviflorus*, as shown in Table 4, poly T (42.07 and 52.24%) and A (40.85 and 46.27%), and poly C (1.22 and 1.49%) and G (0.61 and 0.00%) repeats. The results obtained from the analysis of microsatellite frequency in the genome of six species from the Loranthaceae family are presented in Table 4. The di-repeat AT/AT is found in the genome of all species, while the dinucleotide AG/CT is found in five species but is absent in three species: *S. chingii*, *T. chinensis* and *E. albida*. Furthermore, there were 3 trinucleotide repeats (AAG/CTT, AAT/ATT and ATC/ATG), 11 tetra repeats (AAAG/CTTT, AAAT/ATTT, ACAG/CTGT, AGGG/CCCT, AAGT/ACTT, AATT/AATT, AATC/ATTG, AAAC/GTTT, AACC/GGTT, AGAT/ATCT, and AATG/ATTC) and 2 penta repeats (AAAAT/ATTTT and AATAT/ATATT) (Table 3).

The frequency of SSRs among the cp genomes of the eight species was also compared (Figure 4), and the results showed that mononucleotides occurred more frequently across all genomes. *N. floribunda* had the highest number of dinucleotides with 13 repeats, *P. acacia* has the highest number of trinucleotides with 6 repeats, and *L. europaeus* had the highest number of tetranucleotides with 12 repeats and pentanucleotides with 4 repeats. The majority of SSRs in the cp genome of *P. acacia* and *P. curviflorus* were monorepeats (84.76 and 86.45%) (Figure 5).

**Table 4.** cpSSRs detected in eight Lornthaceae chloroplast genomes.

SSR Type	Repeat Unit	<i>Plicosepalus acacia</i>	<i>Plicosepalus curviflorus</i>	<i>Scurrula chingii</i>	<i>Taxillus chinensis</i>	<i>Loranthus europaeus</i>	<i>Dendrophthoe pentandra</i>	<i>Nuytsia floribunda</i>	<i>Elytranthe albida</i>
Mono	A	67	62	59	49	44	50	47	60
	C	2	2	4	7	6	6	3	6
	G	1	0	2	2	2	0	3	2
	T	69	70	87	86	67	78	69	87
Di	AG/CT	1	1	0	0	0	1	1	0
	AT/AT	10	6	13	6	7	5	12	3
Tri	AAG/CTT	2	2	2	2	2	2	0	0
	AAT/ATT	4	1	1	1	1	3	2	1
	ATC/ATG	0	0	0	0	0	0	0	2
Tetra	AAAG/CTTT	3	3	1	1	2	2	0	3
	AAAT/ATTT	4	2	1	0	4	5	3	1
	ACAG/CTGT	1	0	1	1	1	1	0	1
	AGGG/CCCT	0	2	2	0	2	2	0	0
	AAGT/ACTT	0	0	1	0	0	0	0	0
	AAAT/AAAT	0	0	1	0	0	0	0	1
	AATC/ATTG	0	0	0	1	0	0	0	0
	AAAC/GTTT	0	0	0	0	1	0	0	0
	AACC/GGTT	0	0	0	0	1	0	0	0
	AGAT/ATCT	0	0	0	0	1	0	1	1
	AATG/ATTC	0	0	0	0	0	0	1	1
Penta	AAAAT/ATTTT	0	1	0	0	0	0	0	0
	AATAT/ATATT	0	3	0	1	2	0	0	0
Total		164	155	175	157	143	155	142	169

**Figure 4.** Number of different simple sequence repeat (SSR) types in the plastid genomes of *Plicosepalus acacia* and *Plicosepalus curviflorus* and six species from Lornthaceae using MISA software v2.1. The majority of SSRs in the cp genome were monorepeats.

### 2.5. Sequence Divergence

To investigate the degree of sequence divergence, the program mVISTA was used to align the complete chloroplast genomic sequences of *P. acacia* and *P. curviflorus* with the six Lornthaceae chloroplast genomes available in GenBank: *S. chingii*, *T. chinensis*, *L. europaeus*, *D. pentandra*, *N. floribunda* and *E. albida*. The annotation of *P. acacia* was used as a reference. The protein-coding genes were more conserved than the noncoding regions (Figure 6). The noncoding regions presented high divergence in the following genes: *trnH-GUG-matK*, *matK-trnQ-UUG*, *atpA-atpH*, *rpoC2-rpoB*, *rpoB-trnC-GCA*, *trnT-GGU-psbD*, *psbC-trnS-UGA*, *pspA-ycf3*, *ycf3-trnS-UGU*, *atpB-rbcL*, *rbcL-rpl36*, *rpl36-pspI*, *pspI-ycf4*, *ycf2-trnL-CAA*, *trnL-CAA-rps7*, *ycf15-trnV-GAC*, *rps12-ycf15*, *ycf15-trnV-GAC*, *trnV-GAC-rrn23S*, *trnR-ACG-trnN-GUU*, *trnN-GUU-trnR-AGG*, *petA-psbJ*, *pspE-petL*, *rpl20-rps12*, *rps12-clpP*,

*clpP-psbB*, *psbN-petB*, *petB-petD*, *rpl14-rps3*, *trnA-UGC-rrn16S*, *trnV-GAC-ycf15*, *ycf15-rps12*, *rps12-rps7*, *rps7-trnL-CAA*, *trnL-CAA-rpl23* and *rpl23-trnH-GUG*. However, the protein-coding genes showed divergence in fewer regions: *matK*, *rpoC2*, *accD-rpl36*, *ycf2* and *ycf1*.

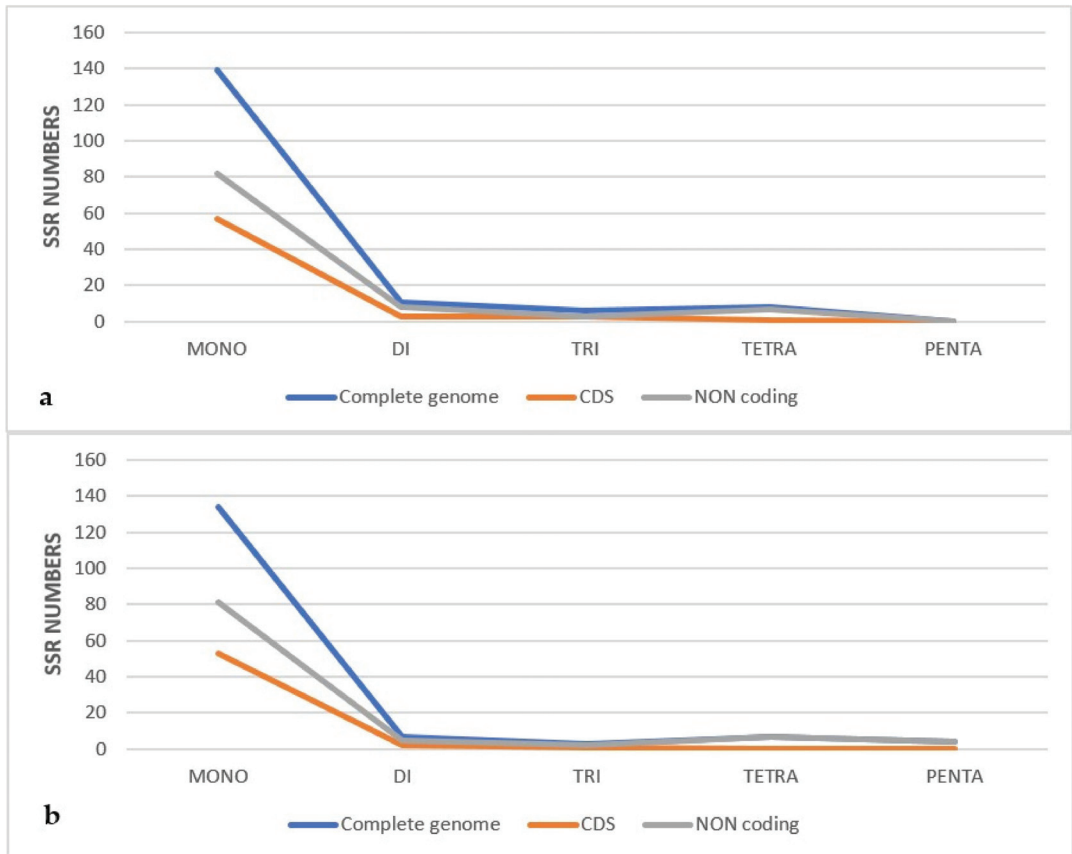


**Figure 5.** Number of SSR types in the complete chloroplast genome, protein-coding regions and non-coding regions of (a) *Plicosepalus acacia*, (b) *Plicosepalus curviflorus*.

### 2.6. Boundary between LSC/SSC and IRs

The difference in the lengths of the LSC, SSC, and IR regions between the species was compared (Figure 7), and a significant reduction in the size of the SSC region was observed, with the shortest SSC (5250 bp) in *E. albida* and the longest SSC in *P. curviflorus* (6187 bp). *E. albida* had the largest LSC region at 72,966 bp, while *D. pentandra* had the shortest LSC at 69,368 bp. Great variation in the length of the IR regions was observed among the species, with the root hemiparasite *N. floribunda* presenting the largest IR region at 26,801 bp and *D. pentandra* presenting the shortest IR region at 20,118 bp.

The four genes *rp12*, *trnL*, *ycf1*, and *trnH*, which were located at the junction of inverted repeats and single copy regions, showed variations in the location and number of base pairs, with the IRA-SSC and IRb border presenting the greatest variations. The two genes *ycf1* and *trnL* were found in the IR/SSC border. The *ycf1* gene crossed the SSC/IRa border in *D. pentandra* (873 bp), *E. albida* (2310 bp), *L. europaeus* (963 bp), *N. floribunda* (2982 bp) and *S. chingii* (945 bp). The SSC/IRa border was distinct in *P. acaciae* and *P. parviflorus* along the *rps15* gene. The *ycf1* gene was in the IRb region of *D. pentandra* (872 bp), *E. albida* (2309 bp)

and *S. chingii* (945 bp), while the extended *ycf1* gene was observed in the SSC region of *P. acaciae* and *P. curviflorus* (4070 bp and 4112 bp, respectively).

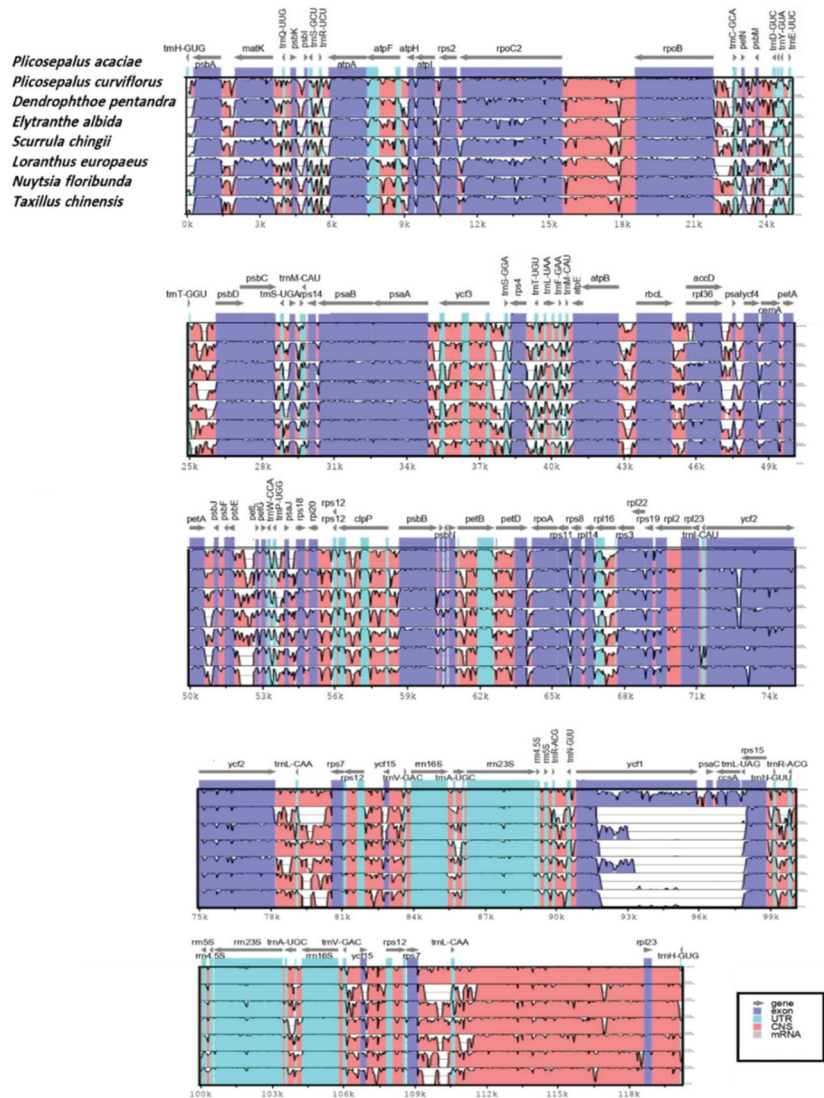


**Figure 6.** Whole chloroplast genome alignments for Loranthaceae species via the mVISTA program, using the annotation of *Plicosepalus acaciae* as reference. The *x*-axis represents the coordinates in the cp genome, while the *y*-axis indicates percentage identity from 50% to 100%. The top grey arrows indicate the position and direction of each gene. Pink indicates non-coding sequences (NCS), blue indicates protein-coding genes, and light green indicates tRNAs and rRNAs.

The *trnL* gene was located in the SSC region in *D. pentandra*, *E. albida* and *S. chingii*, and it was located across the SSC/IRb in *T. chinensis* (15 bp) and *L. europaeus* (45 bp). The root parasite *N. floribunda* differed from the other species, with the *rp132* gene located across the SSC/IRb (26 bp). The *rp12* gene extended across the LSC/IRb in all species: *P. acaciae* (218 bp), *P. curviflorus* (228 bp), *D. pentandra* (231 bp), *E. albida* (300 bp), *L. europaeus* (215 bp),



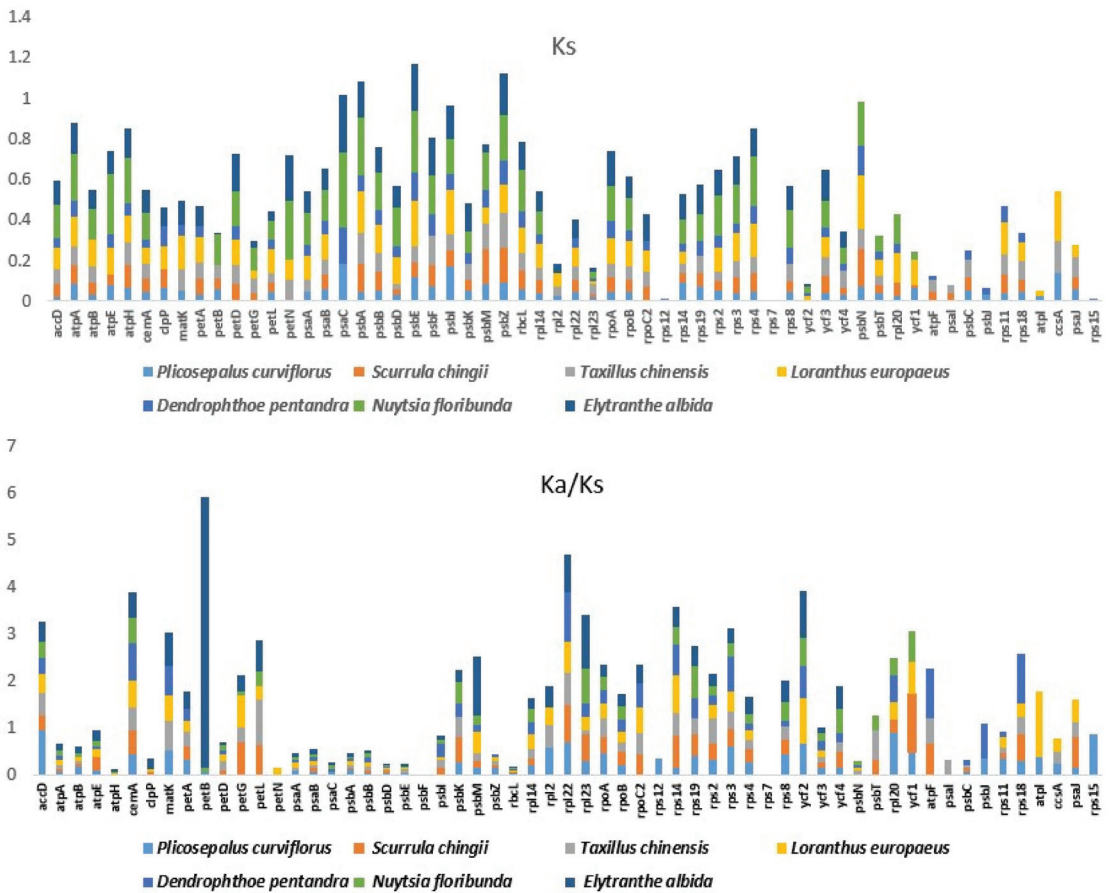


**Figure 8.** Synonymous ( $K_s$ ) and  $K_a/K_s$  ratio values of 59 protein-coding genes of the *Plicosepalus acacia* vs. Lorantheaceae plastomes (*Plicosepalus curviflorus*, *Scurrula chingii*, *Taxillus chinensis*, *Loranthus europaeus*, *Dendrophthoe pentandra*, *Nuytsia floribunda* and *Elytranthe*), using the KaKs Calculator 2.0 to detect substitution, selection, and beneficial mutation genes under selective pressure ( $>1$ ).

### 2.8. Heatmap

The heatmap was created to investigate the evolution of the plastome associated with parasitism in the aerial hemiparasites investigated in this study, i.e., *P. acacia* and *P. curviflorus*, and they were compared to representatives of the Lorantheaceae family: aerial hemiparasitic *S. chingii*, *T. chinensis*, *L. europaeus*, *D. pentandra* and *E. albida*. *N. floribunda* represents a root hemiparasite in Lorantheaceae. In addition to the species *Viscum album* as an aerial hemiparasitic (Viscaceae), *Schoepfia jasminodora* is a root hemiparasite (Santalaceae). *Erythrolalum scandens* (Santalales; Erythrolalaceae) is an example of an autotrophic plant. In contrast, *Epifagus virginiana* was used in the heatmap as a representative of an obligate parasite or holoparasite (Orobanchaceae), (GenBank accession numbers, names are available in Table 5).

**Table 5.** Accession numbers of chloroplast genome analyzed in the study.

Order	Family	Accession Number	Organism
Santalales	Loranthaceae	NC_053563	<i>Scurrula chingii</i> (W.C.Cheng) H.S.Kiu
		MN080717	<i>Taxillus chinensis</i> (DC.) Danser
		MN080718.1	<i>Helixanthera parasitica</i> Lour.
		MT987630	<i>Loranthus europaeus</i> Jacq.
		MT987635.1	<i>Loranthus pseudo-odoratus</i> Lingelsh.
		NC_039376	<i>Macrosolen cochinchinensis</i> (Lour.) Tiegh.
		NC_045107	<i>Dendrophthoe pentandra</i> (L.) Miq.
		NC_045108	<i>Elytranthe albida</i> (Blume) Blume
		NC_058837	<i>Taxillus pseudochinensis</i> (Yamam.) Danser
		NC_058840	<i>Taxillus tsaii</i> S.T.Chiu
	NC_058859	<i>Cecarria obtusifolia</i> (Merr.) Barlow	
	NC_058862.1	<i>Loranthus guizhouensis</i> H.S.Kiu	
	NC_058868	<i>Moquiniella rubra</i> (A.Spreng.) Balle	
	NC_058869	<i>Nuytsia floribunda</i> (Labill.) R.Br. ex G.Don	
	NC_058858.1	<i>Loranthus delavayi</i> Tiegh.	
	Santalaceae	NC_027960	<i>Osyris alba</i> L.
Schoepfiaceae	NC_034228	<i>Schoepfia jasminodora</i> Siebold & Zucc.	
Viscaceae	KT003925.1	<i>Viscum album</i> L.	
	NC_027829	<i>Viscum minimum</i> Harv.	
Erythralaceae	NC_036759.1	<i>Erythralum scandens</i> Blume	
Lamiales	Orobanchaceae	NC_001568.1	<i>Epifagus virginiana</i> (L.) Barton
Solanales	Solanaceae	NC_001879	<i>Nicotiana tabacum</i> L.

As shown in Figure 9, common losses were observed in some protein-coding and tRNA genes as follows: the gene group *ndh* (A, B, C, D, F, H, I, J and K) was absent from most species or present as pseudogenes in some cases, such as the *ndhB* gene pseudogene in *E. virginiana*, *L. europaeus*, and *N. floribunda* and *ndhA* gene in *S. jasminodora*. The *infA* gene was absent in most species and pseudogenes in *L. europaeus*, whereas it was present in *E. virginiana*, *N. floribunda* and *S. jasminodora*.

The *rpl16* gene was present in *E. virginiana*, *P. acacia*, *P. curviflorus*, *D. pentandra*, *E. albida* and *N. floribunda* and *Schoepfia jasminodora*, and the pseudogene in *S. chingii*, *T. chinensis*, and *L. europaeus* was absent from only *V. album*. The *rpl32* gene was missing from all comparison species except *N. floribunda* and *S. jasminodora*. The *rps16* gene was missing from all comparison species except *S. jasminodora*. The *rps15* gene was present in only *P. acacia*, *P. curviflorus* and *S. jasminodora*.

Regarding the tRNA genes, *TrnV-UAC* was lost in all comparison species. The *trnG-UCC* gene was absent in all comparison species except *S. jasminodora*. The *trnI-GAU* gene was absent in all comparison species except *N. floribunda*. The *trnK-UUU* gene was absent in all comparison species except *T. chinensis*, *L. europaeus* and *N. floribunda*. The *trnA-UGC* gene was present in *P. acaciae*, *P. curviflorus*, *T. chinensis* and *N. floribunda* and absent in *E. virginiana*, *S. chingii*, *D. pentandra*, *E. albida*, *V. album* and *S. jasminodora*, while the pseudogene was present in *L. europaeus*. The *trnH-GUG* gene was present in *P. acaciae*, *P. curviflorus*, *S. chingii*, *S. jasminodora* and *N. floribunda*. In contrast, it was absent in *E. virginiana*, *T. chinensis*, *D. pentandra*, *E. albida* and *V. album*, while the pseudogene was present in *L. europaeus*. The gene *trnL-UAG* was present in *P. acaciae*, *Plicosepalus curviflorus*, *S. chingii*, *T. chinensis*, *L. europaeus*, *N. floribunda* and *S. jasminodora*. However, it was absent in *E. virginiana*, *D. pentandra*, *E. albida* and *V. album*.

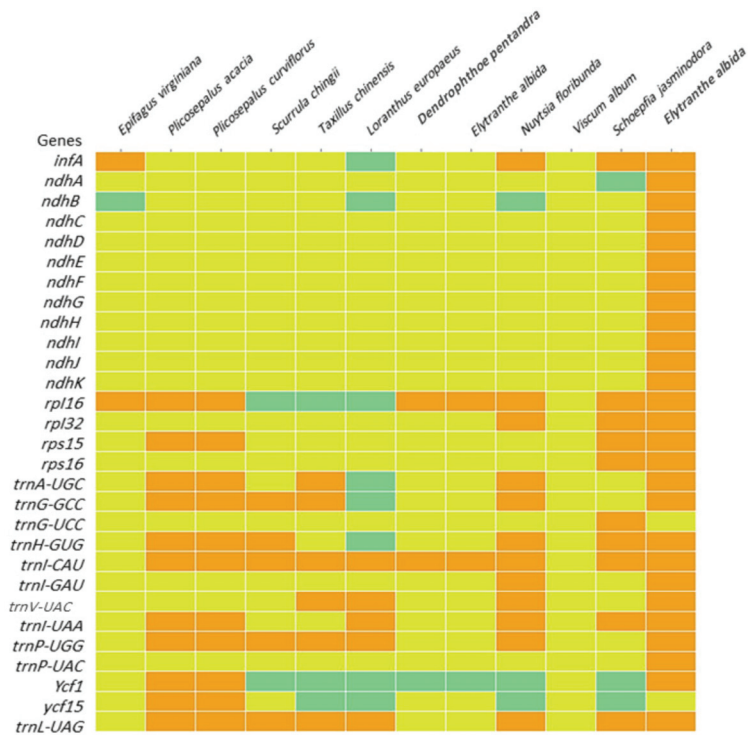


**Figure 9.** Heatmap displaying a comparison of the plastid genome gene content of 11 parasitic plants and 1 autotrophic plant (*Erythralum scandens*) using Plotly software. The common existing genes in the plastid genome of the 12 species are not listed. Orange colour indicates each gene present and seafoam indicates a pseudogene. The yellow indicates an absent gene.

The *trnG-GCC* gene was present in *P. acacia*, *P. curviflorus*, *S. chingii*, *T. chinensis* and *N. floribunda*, while the pseudogene was present in *L. europaeus* but absent in *E. virginiana*, *D. pentandra*, *E. albida*, *V. album* and *S. jasminodora*. The *trnI-CAU* gene was absent only in *V. album* and *E. virginiana*. The *trnI-UAA* gene was present in *P. acacia*, *P. curviflorus*, *L. europaeus*, *N. floribunda* and *S. jasminodora* but absent in *D. pentandra*, *E. albida*, *V. album*, *S. chingii*, *T. chinensis* and *E. virginiana*. The *trnP-UGG* gene was present in *P. acacia*, *P. curviflorus*, *S. chingii*, *T. chinensis*, *N. floribunda* and *L. europaeus*, while it was absent in *E. virginiana*, *D. pentandra*, *E. albida*, *V. album* and *S. jasminodora*.

### 2.9. Phylogenetic Analysis

In the current study, the phylogenetic relationships were assessed among plastomes of *P. acaciae* and *P. curviflorus*, and examples of cp genomes of the Santalales order from GenBank included 15 species belonging to the Loranthaceae family, and they represented different tribes (GenBank accession numbers, names are available in Table 5). The cp genomes from three families (Viscaceae, Santalaceae, and Schoepfiaceae) were also included. The *Nicotiana tabacum* chloroplast genome represents an outgroup.

The phylogenetic trees with all nodes having 100% bootstrap support BS (Figure 10). The monophyly of the Loranthaceae family was strongly supported (BS = 100) by the results.



Typically, chloroplast genome sizes range between 120 and 170 kilobase pairs (kb) [23]. The length of the cp genome is 120,181 bp and 121,086 bp in *P. acaciae* and *P. curviflorus*, respectively. The decrease in the size of the genome is a common feature in parasitic plants as a result of the shift from autotrophic to parasitic life, which is accompanied by several changes, such as pseudogenization, gene loss, structural rearrangement and size reduction [24,25]. Hemiparasites and holoparasite species of the Loranthaceae family have a genome size ranging from 116–139 kb (mean = 122.3 kbp), and a reduction in the plastid of some holoparasites may be more than that, such as in root parasites species of Cynomoriaceae the total Plastid genome length is 45,519 bp [26].

The organization, size, and structure of the chloroplast genome in *Plicosepalus* spp. are analogous to those of other angiosperms, with a typical four-region structure in the chloroplast genome. The size of the LSC regions is 69,497 bp and 69,947 bp, that of the SSC is 6038 bp and 6187 bp, and that of the two IR regions is 22,323 bp and 22,476. The LSC region in angiosperms ranges from 80–90 kb, the SSC regions are approximately 16–27 kb, and the two IRs range from 20–28 kb [27]. Hence, the reduction in the LSC and SSC regions was greater than that in the IR region in the *P. acaciae* and *P. curviflorus* plastomes.

*P. acaciae* and *P. curviflorus* had 106 and 108 genes, including 63 protein-coding genes and 25 tRNA and 4 rRNA genes for each species. A typical angiosperm chloroplast genome consists of 113 genes, including 79 protein-coding genes, 30 tRNA genes and four rRNA genes [21]. The cp genome in autotrophic *E. scandens* (Santalales) consists of almost the same gene number as that observed in angiosperms at 112 genes, including 79 protein-coding genes, 29 tRNA genes and 4 rRNA genes [26]. Other Santalales hemiparasites genomes have gene totals ranging from 80 to 101 [1,2,26–28]. Compared to other parasites in Santalales, fewer genes were lost in the *P. acaciae* and *P. curviflora* plastid genomes. The level of degradation in the chloroplast genome of parasitic plants varies with the level of photosynthesis [1]. Gene losses in the chloroplast genome of hemiparasitic Santalales are not as large as those in holoparasitic plastid genomes, which lose most or all of their genes [1]. *P. acaciae* and *P. curviflora curviflorus* have well-configured green leaves.

We also found that the AT content was higher than the GC content in the *P. acaciae* and *P. curviflorus* cp genomes, which is also observed in the chloroplast genome of holoparasitic species of the Balanophoraceae family [28,29]; nonetheless, some Angiosperms also have high AT contents [30].

The two genes *clpP* and *ycf3* had two introns in each of the *P. acaciae* and *P. curviflorus* plastomes, while the remaining genes presented only one intron, which is consistent with previous reports in the chloroplast genome *Macrosolen* (Santalales) [31] and other cp genomes of angiosperms [32,33].

Codons encoding the amino acid leucine were the most frequent while those encoding cysteine and tryptophan were the least frequent in *P. acaciae* and *P. curviflorus*, respectively. Similar results were reported in the chloroplast genomes of the order Santalales [31], as well in some species of angiosperms [32,33]. The results obtained from the present study show that in the plastid genome of *P. acaciae* and *P. curviflorus*, the amino acid exchange of serine-to-leucine represents the greatest codon transformation. The authors of [31] indicated that the amino acid conversion from serine (S) to leucine (L) occurred most frequently in three parasitic species of the *Macrosolen* genus (Santalales). This agreement between results could be attributed to the high preservation of RNA editing [34,35].

A total of 164 and 155 SSRs are present in the plastid genome of *P. acaciae* and *P. curviflorus*, and most of the microsatellites in repeats are present in the noncoding IGS region. Several reports [36–40] have shown the importance of chloroplast SSRs (cpSSRs) as reliable molecular markers to discriminate between specimens at lower taxonomic levels and for studying the population structure. A previous study using RAPD markers revealed the difference in genetic makeup depending on the host on which the mistletoe grows. The difference in genetic makeup might influence the chemical composition and, in turn, might affect the therapeutic properties of the mistletoe [41]. Thus, we recommend developing the SSRs (cpSSRs) from the cp genome of *Plicosepalus* spp. or available hemiparasitic plastomes

to investigate changes in the genetic structure of the parasitic species when they grow on different hosts and to account for variations within the population of mistletoe.

A heatmap of genes present in the plastomes of *P. acaciae* and *P. curviflorus* and the comparison species showed that all *ndh* genes (A, B, C, D, E, F, G, H, I, D and K) were lost or pseudogenes. The gene *ndh* represents a complex group consisting of approximately 30 subunits, with 11 out of 30 used for encoding subunits of the NADH dehydrogenase complex in plant plastids and involved in photosynthesis [42]. The partial or complete loss (physically or functionally) of genes associated with photosynthesis (*ndh*) is a common phenomenon in hemiparasitic and holoparasites of Santalales and Orobanchaceae [1,2,20,43–45].

In the present study, the *infA* gene was lost in *P. acaciae* and *P. curviflorus* and in most of the compared parasitic species, or it was present as a pseudogene. The *infA* gene is thought to function as a translation initiation factor that assists in the assembly of the translation initiation complex [21]. The *infA* gene is also a common gene lost in parasitic species of Santalales; however, the *infA* gene was also lost in the cp genome in some autotrophic species of angiosperms [46]. The *infA* gene is believed to be the most mobile chloroplast gene and is transferred to the nucleus in angiosperms [44], and it is believed that a similar scenario could also occur in parasitic plants. Several hypotheses have been proposed to explain the reasons for cp gene transfer to the nucleus by [45–49] and was summarised by [49] as three factors: (1) the relatively high frequency of organellar DNA escape to the nucleus provides numerous opportunities for successful functional gene transfers and is essentially a one-way process; (2) the progressive accumulation of detrimental mutations in asexual organelle genomes by Muller's ratchet favours transfer; and (3) smaller, streamlined organelle genomes are favoured selectively. Although all of these hypotheses could be applicable to eukaryote organelles, the first hypothesis is likely more significant in flowering plants [44]. In the history of chloroplast evolution, the *infA* gene has rapidly moved from the chloroplast genome to the nuclear genome. No other chloroplast genes have been reported to undergo multiple evolutionary transfers to the nucleus. Several hypotheses have been proposed to explain why genes are transferred more than once from organelles to plastids, but many have not been applied to *infA* gene [44]. Alternatively, it could be that the small size of *infA* plays a role in repeated transfer of a gene to the nucleus, because it affects both the possibility of transferring genes to the nucleus and the prospect of the transferred gene being damaged by mutation [44].

Additionally, two rRNA (*rpI32*, *rps16*) genes and four tRNA genes (*trnG-UCC*, *trnI-GAU*, *trnK-UUU*, *trnV-UAC*) were lost in the two cp genomes of *P. acaciae* and *P. curviflorus*, and these genes are missing from most of the parasitic plastomes included for comparison. Previous studies indicated that these genes were lost in some species of the family Loranthaceae [4]. However, this loss was not limited to parasitic plants only because similar cases of gene loss were reported in angiosperms [1].

In contrast, previous studies [4,20] indicated the loss or pseudogenesis of some proto-code genes, including *rp16*, *rps15*, *ycf1*, *ycf15* and tRNA (*trnA-UGC*, *trnG-GCC*, *trnH-GUG*, *trnI-CAU*, *trnI-UAA*, *trnP-UGG* and *trnL-UAG*). However, we noticed the presence of these genes in the *P. acaciae* and *P. curviflorus* cp genomes. Our results are consistent with that of [4], who found some of these missing genes after a cp genome reannotation (*ycf1*, *trnH-GUG*, *trnL-UAG* and *trnI-UAA*).

Overall, comparisons between the plastomes of *Plicosepalus* spp. and hemiparasite species showed different degrees of gene loss. A similar pattern of gene loss from the plastome was reported in parasitic species of the family Orobanchaceae as well [20]. Hemiparasites still present varying degrees of photosynthetic ability and use their host to meet some of their nutrient needs, whereas holoparasites lose their photosynthetic ability and depend entirely on the host plant to meet their nutrient needs. Consequently, hemiparasitic plants have different degrees of photosynthesis ability; thus, the chloroplast genomes of parasitic plants are exposed to different levels of selective pressures [24,46]. We suggest that further studies should be conducted on the Plastome structure of different types of

hemiparasitic plants to determine the exact structural changes that occur in the genome and the variation in genes lost during the shift to the parasitic state.

Although close species tend to have similar IR/SC boundaries, several studies have reported variations in the size and boundaries among IR/LSC and IR/SSC regions and variations in the gene location [47,48]. We observed variations in the size of the IR region in the hemiparasitic species. In addition to a reduction in the size of the LSC region and a large reduction in the size of the SSC, a greater amount (more than half) of the SSC region size was lost compared to that in angiosperms [27], which could be the result of contraction and expansion of the IR region.

The *rpl2* gene occupied the LSC/IRb borders in all samples, which is consistent with previous observations [31] in parasitic species of Santalales. In addition, *ycf1* was found at the IR/SC borders in most of the compared species, which is consistent with the results for Loranthaceae species mentioned in previous studies [14,31,50,51]. The IRa/SSC boundaries of the two species *P. acaciae* and *P. curviflorus* were distinguished by the presence of the protein-code gene *rps15*, which is usually lost from many other hemiparasites species, as mentioned by [4,20].

Zong et al. indicated that the *trnL* gene is present in the SSC in the *Macrosolen* genus of the Loranthaceae family [30]. We noticed the same phenomenon in certain species, and the *trnL* gene was extended along the SSC/IRb border in certain species, which could be attributed to the extension in the IR region. The *ycf1* gene present at the SSC/IRb borders of angiosperm plastomes is often pseudogenized, and the expansion length of *ycf1* could influence the IR length and the gene distribution at the SC/IR borders [52–54].

The *trnH* gene is usually located at the IRb/LSC border in angiosperms. We observed variations in the genomes of *Plicosepalus* spp. and the comparison species, where the *trnH* gene was present in the inverted repeat region, which could be a result of expansion in the IR region. A similar finding was reported by [55] in the Acanthoideae family.

The values of synonymous (Ks) and nonsynonymous (Ka) substitutions and the Ka/Ks ratio showed that protein-coding genes (*petB*, *psbM*, *accD*, *ycf1*, *rpl23* and *atp1*) were under positive selection in the *P. acaciae* and *P. curviflorus* chloroplast genomes, and these genes could have a faster evolution rate [56]. Our result corresponds with that of [31], who reported that the *ycf1* gene was a mutational hotspot in hemiparasitic *Macrosolen* species (Santalales). We suggest subjecting these genes to further investigation to identify their ability as indicators of phylogenetic relationships within Loranthaceae.

The plastome consists of many highly efficient genes capable of resolving phylogenetic issues at different levels of angiosperm taxonomy [33,57–59]. In this study, we found that *P. acaciae* and *P. curviflorus* were strongly related to the family Loranthaceae and tribe Lorantheae and all species in the family Loranthaceae represented the monophyletic group. These findings provide additional evidence to confirm the monophyly state of Loranthaceae, as reported by previous studies [3]. In addition, they confirm the taxonomic state of root hemiparasitic *N. floribunda* (tribe Nuytsieae) and *E. albida* (tribe Elytrantheae) as sisters to the Lorantheae tribe (belonging to the family Loranthaceae), as mentioned by [3,5,60].

The current results supported those of previous studies [3]. In the taxonomic state of genera and species belonging to subtribes of Lorantheae, the results corresponded to that of [3], who reported that the subtribe Dendrophile did not represent a monophyletic group. In contrast, we noticed a difference in the taxonomic case of *M. cochinchinensis*, which was previously reported to belong to the tribe Elytrantheae [3]; however, it is a part of the Lorantheae tribe in the current ML and MP trees in a highly supported clade (BP = 100), suggesting the need to rearrange some genera and change the circumscription of some tribes and subtribes of Lorantheae.

## 4. Materials and Methods

### 4.1. Sample Collection

Fresh leaves of *P. curviflorus* were collected from the Al-Taif region, Saudi Arabia (21.218874°, 40.557426°), while those of *P. acacia* were collected from the Al-Wajh district, Saudi Arabia (26.5737260°, 36.3731150°). The plants were identified by Dr. Rahma Alqthanin, the curator of the Sultan bin Abdulaziz for Research and Environmental Studies Centre, based on herbarium specimens and morphologies in the relevant literature. A sample specimen was prepared and deposited in the herbarium of Umm Al-Qura University, Makkah, under accession numbers *P. curviflorus* (UQU012021) and *P. acacia* (UQU062021). Samples of fresh leaves were dried in silica gel for DNA extraction. DNA was extracted from the silica gel-dried leaves of *P. curviflorus* and *P. acacia* using the CTAB Plant DNA extraction protocol [61].

### 4.2. Library Construction

To build the genomic library, 1.0 µg g of DNA was used as input material for sample preparation. The DNA library was constructed using the Illumina TruSeq Nano DNA 350 Kit (Illumina, San Diego, CA, USA) following the manufacturer's recommendations. The library was initially prepared via the random fragmentation of DNA samples to a size of 350 bp, followed by ligation to 5' and 3' adapters. The adapter-ligated fragments were then amplified via PCR and subjected to gel purification. To verify the size of the PCR-enriched fragments, the template size distribution was checked with an Agilent Technologies 2100 Bioanalyzer using a DNA 1000 chip (Agilent Technologies, Santa Clara, CA, USA). The prepared libraries were quantified using qPCR in accordance with the Illumina qPCR Quantification Protocol Guide (Illumina, San Diego, CA, USA).

### 4.3. De Novo Genome Sequencing

Library construction and sequencing was performed using Illumina sequencing (Illumina, San Diego, CA, USA) and a read length of 151 bp paired ends, and the procedures were carried out by Macrogen (<https://dna.macrogen.com/>, Seoul, Korea). The final yield of filtered data was 3.7 Gb and 3.25 Gb for *P. curviflorus* and *Plicosepalus acacia*, respectively.

### 4.4. Genome Assembly and Annotation

The FastQC tool was used to assess the raw read quality using a Phred score above 30. All adapters were removed, vector contamination was removed from the assembly, and the N50 value was high for a single genome. Clean reads were processed for genome assembly using NOVOPlasty 4.3.0 Version [62] with kmer (K-mer = 33) to assemble the complete chloroplast genome from the whole genomic sequence of *Plicosepalus* spp. *Arabidopsis thaliana* (NC\_000932.1) was used as a reference in the assembly. Single contigs containing the complete chloroplast genome were generated. Gene prediction and annotation of the *Plicosepalus* spp. chloroplast (cp) genome were performed using the GeSeq tool [63] with default parameters, and the percent identity cut-off for protein-coding genes and RNAs was set at  $\geq 60$  and  $\leq 85$ , respectively. tRNA genes were identified with tRNA-Scan-SE Version 2.0 [64]. The annotated (gb) format sequence files were used to draw the circular chloroplast genome maps with the OGDRAW tool (Organellar Genome DRAW), Version 1.3.1 [65]. The sequences of the chloroplast genome of *Plicosepalus* spp. were deposited in the GenBank database under accession numbers *P. acacia* (OM640467) and *P. curviflorus* (OM675776).

### 4.5. Sequence Analysis

The relative synonymous codon usage (RSCU) values, base composition, and codon usage were analyzed using MEGA software [66], Version 11.0. Potential RNA editing sites present in the protein-coding genes were predicted by the PREP suite [21], with a cut-off value of 0.8.

#### 4.6. Repeat Analysis in the Chloroplast Genome

The online software MicroSATellite (MISA) v2.1 [67] was used to identify simple sequence repeats (SSRs) in the chloroplast genome of *Plicosepalus* spp. and six other species from the Loranthaceae family, namely, *S. chingii*, *T. chinensis*, *L. europaeus*, *D. pentandra*, *N. floribunda*, and *E. albida*. Parameterwise, eight, five, four and three repeat units were assessed for mononucleotides, dinucleotides, trinucleotides and tetra- and pentanucleotide SSR motifs, respectively.

In addition, REPuter [68] software was used with default settings to detect the size and location of long palindromic, forward, reverse, and complementary repeats in the *Plicosepalus* spp. cp genomes and the genomes of six species from Loranthaceae.

#### 4.7. Sequence Divergence and Boundary

Comparisons between the genome of *Plicosepalus* spp. and six chloroplast genomic sequences of Loranthaceae (*S. chingii*, *T. chinensis*, *L. europaeus*, *D. pentandra*, *N. floribunda*, *E. albida*) were analysed using the mVISTA program [69], and the annotation of *Plicosepalus* spp. was used as a reference in the Shuffle-LAGAN mode. Furthermore, comparisons between the borders of the IR, SSC, and LSC regions were performed using IRSCOPE [70].

#### 4.8. Characterization of the Substitution Rate

Methods for estimating nonsynonymous and synonymous substitution rates (Ka and Ks), selection and beneficial mutations among protein-coding sequences were applied [71]. Nonsynonymous (Ka), synonymous (Ks), and Ka/Ks ratios were calculated to detect plastome genes under selection pressure in *Plicosepalus* spp. and they were compared with those in the six aforementioned Loranthaceae species. We employed KaKs Calculator Version 2.0 [71] with default parameters and the Nei and Gojoberi substitutions.

#### 4.9. Heatmap

A heatmap was created to investigate the evolution of the plastome associated with parasitism in the two plastomes of the aerial hemiparasites evaluated in this study, i.e., *P. acacia* and *P. curviflorus*, and the results were compared to that of the species of the Loranthaceae family, *S. chingii*, *T. chinensis*, *L. europaeus*, *D. pentandra*, and *E. albida*. *N. floribunda* represents a root hemiparasite in Loranthaceae. In addition to the aerial hemiparasitic species *V. album* (Viscaceae), *S. jasminodora* is a root hemiparasite (Santalaceae). *E. virginiana* was used in the heatmap as a representative of an obligate parasite or holoparasite parasite (Orobanchaceae). *E. scandens* (Santalales; Erythralaceae) was included as an example of an autotrophic plant. Heatmaps were generated using Python Version 3.7 [72], and multiple libraries were used to plot the heatmap graph. Pandas was used to import data, and Seaborn and plotly were used to plot the actual heatmap data.

#### 4.10. Phylogenetic Analysis

Phylogenetic analyses were conducted built based on coding genes of genome sequences of Santalales order, including species and families (Loranthaceae, Santalaceae, Schoepfiaceae and Viscaceae). Species of the Solanaceae family (*N. tabacum*) were used as an outgroup. To identify gene families, the OrthoFinder (v 2.5.4) pipeline [73] was sequentially applied to the genomes with all-to-all BLASTP (E-value  $\leq 1 \times 10^{-5}$ ), reciprocity best hit, pairs connected by orthology and in-paralogy, normalize the E-value and cluster pairs by OrthoFinder. Finally, genes were classified into orthologues, paralogues and single copy orthologues (only one gene in each species). To construct the phylogenetic tree, single-copy orthologous genes were used; each gene family nucleotide sequence was aligned using Mafft [74], and the phylogenetic tree was built with both the maximum likelihood (GTR model) and the maximum parsimony using Megatool [66], supports for nodes were assessed with 1000 bootstrapping replicates. The cladograms of the two methods were compared, and we considered that the evolutionary tree constructed by the ML method was more fit. The phylogenetic tree was visualized and modified by ITOL [75].

## 5. Conclusions

The aim of the present research was to provide the complete chloroplast genome of the medicinal species and hemiparasitic species *P. acaciae* and *P. curviflorus* to assess the systematic relationships within the Loranthaceae family. Furthermore, to investigate the evolution of plastome structure associated with parasitism, we compared these the cp genomes of these species with examples of available hemiparasitic and holoparasitic species and autotroph plants. We observed a reduction in the genome size of hemiparasitic *P. acaciae* and *P. curviflorus* and a loss of some genes. However, these losses were much less than those observed in the hemiparasite and holoparasite cp genomes. For a better understanding, we recommend that future studies investigate the chloroplast genome of different species in families of Santalales. This study confirmed the taxonomic status of the species *Plicosepalus acaciae* and *P. curviflorus* as members of the Loranthaceae family and Loranthaceae tribe; however, some species of the Loranthaceae family still require further investigation of their taxonomic status. Moreover, available genome data could facilitate more advanced applications in parasitic plant research, contribute to good parasitic weed management and contribute to modifying the host species to become more resistant.

**Supplementary Materials:** The following supporting information can be downloaded at: <https://www.mdpi.com/article/10.3390/plants11141869/s1>, Table S1: Genes present in the plastome of *P. acaciae*. Table S2: Genes present in the plastome of *P. curviflorus*. Table S3: Codon–anticodon recognition patterns and codon usage in the *P. acacia* chloroplast genome. Table S4: Codon–anticodon recognition patterns and codon usage in the *P. curviflorus* chloroplast genome. Table S5: The predicted RNA editing sites in *P. acacia* chloroplast genome. Table S6: The predicted RNA editing sites in *P. curviflorus* chloroplast genome. Figure S1: Synonymous (Ks) and Ka/Ks ratio values of 59 protein-coding genes of the *Plicosepalus curviflorus* vs. *Loranthaceae* plastomes. Figure S2: Phylogenetic tree construction inferred from the complete chloroplast genomes of 21 taxa, using Maximum Parsimony (MP) methods. The tree shows the relationships between Brassicales (Cleomaceae, Capparaceae and Brassicaceae). The numbers in the branch nodes represent bootstrap support (BP).

**Author Contributions:** Conceptualization, W.A.-J.; methodology, W.A.-J. and N.T.A.T.; software, W.A.-J. and R.N.A.-Q.; validation, W.A.-J., N.T.A.T. and R.N.A.-Q.; formal analysis, W.A.-J. and R.N.A.-Q.; investigation, W.A.-J. and N.T.A.T.; validation, W.A.-J., N.T.A.T. and R.N.A.-Q.; writing—original draft preparation, W.A.-J. and R.N.A.-Q.; supervision, W.A.-J. All authors have read and agreed to the published version of the manuscript.

**Funding:** This research received no external funding.

**Institutional Review Board Statement:** Not applicable.

**Informed Consent Statement:** Not applicable.

**Data Availability Statement:** The data presented in this study are available in this article and Supplementary Materials. The complete chloroplast genome sequence of *P. acacia* and *P. curviflorus* were deposited in GenBank at <https://www.ncbi.nlm.nih.gov>, (accessed on 2 February 2022) (accession numbers: *P. acacia* (OM640467) and *P. curviflorus* (OM675776)).

**Acknowledgments:** We thank the Abdulrahman Al-Johani for his cooperation in collected plants samples from the Al-Wajh district.

**Conflicts of Interest:** The authors declare no conflict of interest.

## Abbreviations

Photosystem 1: PS I is the collection of pigments of chlorophyll, absorbing mostly the wavelength of light at 700 nm; Photosystem 2: PS II is the collection of pigments of chlorophyll, absorbing mostly the wavelength of light at 680 nm; cytochrome b/f complex; clpP: an enzyme complex; matK: a plant plastidial gene; Rubis CO subunit: a binding protein in Chloroplasts; ATP synthase: a protein that catalyzes the formation of the energy storage molecule adenosine triphosphate (ATP) using adenosine diphosphate (ADP) and inorganic phosphate (Pi); RNA polymerase: an enzyme that synthesizes RNA from a DNA

template; Ribosomal protein ssu: the smaller of the two major RNA components of the ribosome; Ycf: hypothetical chloroplast frames; Ribosomal protein lsu: the largest of the two major RNA components of the ribosome; Transfer RNAs: an adaptor molecule that serves as the physical link between the mRNA and the amino acid sequence of proteins; Ribosomal RNAs: a ribozyme which carries out protein synthesis in ribosomes.

## References

1. Shin, H.W.; Lee, N.S. Understanding plastome evolution in hemiparasitic Santalales: Complete chloroplast genomes of three species, *dendrotrophe varians*, *helixanthera parasitica*, and *macrosolen cochinchinensis*. *PLoS ONE* **2018**, *13*, e0200293. [CrossRef] [PubMed]
2. Petersen, G.; Cuenca, A.; Seberg, O. Plastome evolution in hemiparasitic mistletoes. *Genome Biol. Evol.* **2015**, *7*, 2520–2532. [CrossRef] [PubMed]
3. Liu, B.; Le, C.T.; Barrett, R.L.; Nickrent, D.L.; Chen, Z.; Lu, L.; Vidal-Russell, R. Historical biogeography of Loranthaceae (Santalales): Diversification agrees with emergence of tropical forests and radiation of songbirds. *Mol. Phylogenet. Evol.* **2018**, *124*, 199–212. [CrossRef] [PubMed]
4. Su, H.-J.; Liang, S.-I.; Nickrent, D.L. Plastome variation and phylogeny of *Taxillus* (Loranthaceae). *PLoS ONE* **2021**, *16*, 0256345.
5. Vidal-Russell, R.; Nickrent, D.L. Evolutionary relationship in the showy mistletoe family (Loranthaceae). *Am. J. Bot.* **2008**, *95*, 1015–1029. [CrossRef]
6. Watson, D.M. Mistletoe—A keystone resource in forests and woodlands worldwide. *Annu. Rev. Ecol. Syst.* **2001**, *32*, 219–249. [CrossRef]
7. Engler, A. Loranthaceae. In *Die Natürlichen Pflanzenfamilien*, 3rd ed.; Engler, A., Prantl, K., Eds.; Wilhelm Engelmann: Leipzig, Germany, 1894; pp. 156–198.
8. Tieghem, P. Sur le groupement des especes en genres dans les Loranthacees a calice gamosepale et antheres basifixes ou Dendrophthoes. *Bull. Soc. Bot. Fr.* **1895**, *42*, 241–272. [CrossRef]
9. Nickrent, D.L.; Malécot, V.; Vidal-Russell, R.; Der, J.P. A revised classification of Santalales. *Taxon* **2010**, *59*, 538–558. [CrossRef]
10. Migahid, A.M. *Flora of Saudi Arabia*, 4th ed.; King Saud University Press: Riyadh, Saudi Arabia, 1996; Volume 2, pp. 68–69.
11. Orfali, R. Pharmacological evaluation of secondary metabolites and their simultaneous determination in the arabian medicinal plant *picosepalus curviflorus* using hptlc validated. *J. Anal. Methods Chem.* **2019**, *2019*, 7435909. [CrossRef]
12. Nickrent, D.L.; Su, H.-J.; Lin, R.-Z.; Devkota, M.P.; Hu, J.-M.; Glatzel, G. Examining the needle in the haystack: Evolutionary relationships in the mistletoe genus *Loranthus* (Loranthaceae). *Syst. Bot.* **2021**, *46*, 403–415. [CrossRef]
13. Plant of the World, Royal Botanical Gardens (Kew). 2022. Available online: <https://powo.science.kew.org/> (accessed on 5 February 2022).
14. Palmer, J.D. Comparative organization of chloroplast genomes. *Annu. Rev. Genet.* **1985**, *19*, 325–354. [CrossRef] [PubMed]
15. Wicke, S. The evolution of the plastid chromosome in land plants: Gene content, gene order, gene function. *Plant Mol. Biol.* **2011**, *76*, 273–297. [CrossRef] [PubMed]
16. Straub, S.C.K.; Parks, M.; Weitemier, K.; Fishbein, M.; Cronn, R.C.; Liston, A. Navigating the tip of the genomic iceberg: Next-generation sequencing for plant systematics. *Am. J. Bot.* **2012**, *99*, 349–364. [CrossRef]
17. Mattick, J.S.; Gagen, M.J. The evolution of controlled multitasked gene networks: The role of introns and other noncoding RNAs in the development of complex organisms. *Mol. Biol. Evol.* **2001**, *18*, 1611–1630. [CrossRef] [PubMed]
18. Taberlet, P. Power and limitations of the chloroplast trnL (UAA) intron for plant DNA barcoding. *Nucleic Acids Res.* **2007**, *35*, e14. [CrossRef] [PubMed]
19. Staden, R.; McLachlan, A.D. Codon preference and its use in identifying protein coding regions in long DNA sequences. *Nucleic Acids Res.* **1982**, *10*, 141–156. [CrossRef] [PubMed]
20. Li, B. Complete chloroplast genome sequence of *Decaisnea insignis*: Genome organization, genomic resources and comparative analysis. *Sci. Rep.* **2017**, *7*, 10073. [CrossRef]
21. Mower, J.P. The PREP suite: Predictive RNA editors for plant mitochondrial genes, chloroplast genes and user-defined alignments. *Nucleic Acids Res.* **2009**, *37*, 253–259. [CrossRef]
22. Bundschuh, R.; Altmüller, J.; Becker, C.; Nurnberg, P.; Gott, J.M. Complete characterization of the edited transcriptome of the mitochondrion of *Physarum polycephalum* using deep sequencing of RNA. *Nucleic Acids Res.* **2011**, *39*, 6044–6055. [CrossRef]
23. Shaw, J.; Lickey, E.B.; Schilling, E.E.; Small, R.L. Comparison of whole chloroplast genome sequences to choose noncoding regions for phylogenetic studies in angiosperms: The tortoise and the hare III. *Am. J. Bot.* **2007**, *94*, 275–288. [CrossRef]
24. Wicke, S.; Müller, K.F.; Claude, W.D.; Quandt, D.; Bellot, S.; Schneeweiss, G.M. Mechanistic model of evolutionary rate variation en route to a nonphotosynthetic lifestyle in plants. *Proc. Natl. Acad. Sci. USA* **2016**, *113*, 9045–9050. [CrossRef] [PubMed]
25. Wicke, S.; Naumann, J. Molecular evolution of plastid genomes in parasitic flowering plants. *Adv. Bot. Res.* **2018**, *85*, 315–347.
26. Bellot, S.; Cusimano, N.; Luo, S.; Sun, G.; Zarre, S.; Groger, A.; Tensch, E.; Renner, S.S. Assembled plastid and mitochondrial genomes, as well as nuclear genes, place the parasite family cynomoriaceae in the saxifragales. *Genome Biol. Evol.* **2016**, *8*, 2214–2230. [CrossRef] [PubMed]

27. Wang, X.; Dorjee, T.; Chen, Y.; Gao, F.; Zhou, Y. The complete chloroplast genome sequencing analysis revealed an unusual IRs reduction in three species of subfamily Zygothelloideae. *PLoS ONE* **2022**, *17*, e0263253. [[CrossRef](#)] [[PubMed](#)]
28. Schelkunov, M.I.; Nuraliev, M.S.; Logacheva, M.D. *Rhopalocnemis phalloides* has one of the most reduced and mutated plastid genomes known. *PeerJ* **2019**, *7*, e7500. [[CrossRef](#)]
29. Su, H.-J.; Barkman, T.J.; Hao, W.; Jones, S.S.; Naumann, J.; Skippington, E.; Wafula, E.K.; Hu, J.-M.; Palmer, J.D.; dePamphilis, C.W. Novel genetic code and record-setting AT-richness in the highly reduced plastid genome of the holoparasitic plant *Balanophora*. *Proc. Natl. Acad. Sci. USA* **2018**, *116*, 934–943.
30. Zong, D.; Zhang, Y.; Zou, X.; Li, D.; Duan, A.; He, C. Characterization of the complete chloroplast genomes of five *Populus* species from the western Sichuan plateau, southwest China: Comparative and phylogenetic analyses. *PeerJ* **2019**, *7*, e6386. [[CrossRef](#)]
31. Nie, L.; Cui, Y.; Wu, L.; Zhou, J.; Xu, Z.; Li, Y.; Li, X.; Wang, Y.; Yao, H. Gene losses and variations in chloroplast genome of parasitic plant macrosolen and phylogenetic relationships within santalales. *Int. J. Mol. Sci.* **2019**, *20*, 5812. [[CrossRef](#)]
32. Raman, G.; Park, S. The complete chloroplast genome sequence of *Ampelopsis*: Gene organization, comparative analysis, and phylogenetic relationships to other angiosperms. *Front. Plant Sci.* **2016**, *7*, 341. [[CrossRef](#)]
33. Alzahrani, D.A.; Yaradua, S.S.; Albokhari, E.J.; Abba, A. Complete chloroplast genome sequences of *Dipterygium glaucum* and *Cleome chrysantha* and other *Cleomaceae* species, comparative analysis and phylogenetic relationships. *Saudi J. Biol. Sci.* **2021**, *28*, 2476–2490. [[CrossRef](#)]
34. Wang, W.; Yu, H.; Wang, J.; Lei, W.; Gao, J.; Qiu, X.; Wang, J. The complete chloroplast genome sequences of the medicinal plant *Forsythia suspensa* (Oleaceae). *Int. J. Mol. Sci.* **2017**, *18*, 2288. [[CrossRef](#)] [[PubMed](#)]
35. Park, M.; Park, H.; Lee, H.; Lee, B.; Lee, J. The complete plastome sequence of an Antarctic bryophyte *Sanionia uncinata* (Hedw.) Loeske. *Int. J. Mol. Sci.* **2018**, *19*, 709. [[CrossRef](#)] [[PubMed](#)]
36. Provan, J.; Powell, W.; Hollingsworth, P.M. Chloroplast microsatellites: New tools for studies in plant ecology and evolution. *Trends Ecol. Evol.* **2001**, *16*, 142–147. [[CrossRef](#)]
37. Yang, A.-H.; Zhang, J.-J.; Yao, X.-H.; Huang, H.-W. Chloroplast microsatellite markers in *Liriodendron tulipifera* (Magnoliaceae) and cross-species amplification in *L. chinense*. *Am. J. Bot.* **2011**, *98*, e123–e126. [[CrossRef](#)] [[PubMed](#)]
38. Xue, J.; Wang, S.; Zhou, S.-L. Polymorphic chloroplast microsatellite loci in *Nelumbo* (Nelumbonaceae). *Am. J. Bot.* **2012**, *99*, e240–e244. [[CrossRef](#)] [[PubMed](#)]
39. Hu, Y.; Woeste, K.E.; Zhao, P. Completion of the chloroplast genomes of five Chinese *Juglans* and their contribution to chloroplast phylogeny. *Front. Plant Sci.* **2017**, *7*, 1955. [[CrossRef](#)]
40. Ruhsam, M.; Clark, A.; Finger, A.; Wulff, A.S.; Mill, R.R.; Thomas, P.I.; Gardner, M.F.; Gaudeul, M.; Ennos, R.A.; Hollingsworth, P.M. Hidden in plain view: Cryptic diversity in the emblematic *Araucaria* of New Caledonia. *Am. J. Bot.* **2016**, *103*, 888–898. [[CrossRef](#)]
41. Sunil-Kumar, K.N.; Maruthi, K.R.; Alfarhan, A.H.; Rajakrishnan, R.; Thomas, J. Molecular fingerprinting of *Helicanthus elastica* (Desr.) Danser growing on five different hosts by RAPD. *Saudi J. Biol. Sci.* **2016**, *23*, 335–340. [[CrossRef](#)]
42. Friedrich, T.; Klaus, S.; Weiss, H. The proton-pumping respiratory complex I of bacteria and mitochondria and its homologue in chloroplasts. *FEBS Lett.* **1995**, *367*, 107–111. [[CrossRef](#)]
43. Zhu, Z.X.; Wang, J.H.; Cai, Y.C.; Zhao, K.K.; Moore, M.J.; Wang, H.F. Complete plastome sequence of *Erythralum scandens* (Erythralaceae), an edible and medicinally important liana in China. *Mitochondrial DNA Part B* **2018**, *3*, 139–140. [[CrossRef](#)]
44. Su, H.J.; Hu, J.M. The complete chloroplast genome of hemiparasitic flowering plant *Schoepfia jasminodora*. *Mitochondrial DNA Part B* **2016**, *1*, 767–769. [[CrossRef](#)]
45. Frailey, D.C.; Chaluvadi, S.R.; Vaughn, J.N.; Goatney, C.G.; Bennetzen, J.L. Gene loss and genome rearrangement in the plastids of five Hemiparasites in the family Orobanchaceae. *BMC Plant Biol.* **2018**, *18*, 30. [[CrossRef](#)]
46. Wicke, S.; Müller, K.F.; Claude, W.D.; Quandt, D.; Bellot, S.; Schneeweiss, G.M. Mechanisms of functional and physical genome reduction in photosynthetic and nonphotosynthetic parasitic plants of the broomrape family. *Plant Cell* **2013**, *25*, 3711–3725. [[CrossRef](#)]
47. Raubeson, L.A.; Peery, R.; Chumley, T.W.; Dziubek, C.; Fourcade, H.M.; Boore, J.L. Comparative chloroplast genomics: Analyses including new sequences from the angiosperms *Nuphar advena* and *Ranunculus macranthus*. *BMC Genom.* **2007**, *8*, 174. [[CrossRef](#)]
48. Wang, R.J.; Cheng, C.L.; Chang, C.C.; Wu, C.-L.; Su, T.-M.; Chaw, S.-M. Dynamics and evolution of the inverted repeat-large single copy junctions in the chloroplast genomes of monocots. *BMC Evol. Biol.* **2008**, *8*, 3650. [[CrossRef](#)]
49. Millen, R.S.; Olmstead, R.G.; Adams, K.L.; Palmer, J.D.; Lao, N.T.; Heggie, L.; Kavanagh, T.A.; Hibberd, J.M.; Gray, J.C.; Morden, C.W.; et al. Many Parallel Losses of *infA* from Chloroplast DNA during Angiosperm Evolution with Multiple Independent Transfers to the Nucleus. *Plant Cell* **2001**, *13*, 645–658. [[CrossRef](#)]
50. Goulding, S.E.; Wolfe, K.; Olmstead, R.; Morden, C. Ebb and flow of the chloroplast inverted repeat. *Mol. Genet. Genom.* **1996**, *252*, 195–206. [[CrossRef](#)]
51. Sugiura, M. The chloroplast genome. In *10 Years Plant Molecular Biology*; Springer: Dordrecht, The Netherlands, 1992; pp. 149–168.
52. Daniell, H.; Lee, S.-B.; Grevich, J.; Saski, C.; Quesada-Vargas, T.; Guda, C.; Tomkins, J.; Jansen, R.K. Complete chloroplast genome sequences of *Solanum bulbocastanum*, *Solanum lycopersicum* and comparative analyses with other *Solanaceae* genomes. *Theor. Appl. Genet.* **2006**, *112*, 1503. [[CrossRef](#)]

53. Yao, X.; Tan, Y.-H.; Liu, Y.-Y.; Song, Y.; Yang, J.-B.; Corlett, R.T. Chloroplast genome structure in *Ilex* (Aquifoliaceae). *Sci. Rep.* **2016**, *6*, 28559. [\[CrossRef\]](#)
54. Wang, X.; Gussarova, G.; Ruhsam, M.; De Vere, N.; Metherell, C.; Hollingsworth, P.M.; Twyford, A.D. DNA barcoding a taxonomically complex hemiparasitic genus reveals deep divergence between ploidy levels but lack of species-level resolution. *Ann. Bot.* **2018**, *10*, ply026. [\[CrossRef\]](#)
55. Alzahrani, D.A.; Yaradua, S.S.; Albokhari, E.J.; Abba, A. Complete chloroplast genome sequence of *Barleria prionitis*, comparative chloroplast genomics and phylogenetic relationships among Acanthoideae. *BMC Genom.* **2020**, *21*, 393. [\[CrossRef\]](#)
56. Zhou, T.; Ruhsam, M.; Wang, J.; Zhu, H.; Li, W.; Zhang, X.; Xu, Y.; Xu, F.; Wang, X. The complete chloroplast genome of *euphrasia regelii*, pseudogenization of *ndh* genes and the phylogenetic relationships within orobanchaceae. *Front. Genet.* **2019**, *10*, 444. [\[CrossRef\]](#)
57. Yaradua, S.S. Complete chloroplast genome sequence of *justicia flava*: Genome comparative analysis and phylogenetic relationships among acanthaceae. *BioMed Res. Int.* **2019**, *17*, 4370258. [\[CrossRef\]](#)
58. Yang, Y.; Zhou, T.; Duan, D.; Yang, J.; Feng, L.; Zhao, G. Comparative analysis of the complete chloroplast genomes of five quercus species. *Front. Plant Sci.* **2016**, *7*, 959. [\[CrossRef\]](#)
59. Dong, W.; Xu, C.; Li, W.; Xie, X.; Lu, Y.; Liu, Y.; Jin, X.; Suo, Z. Phylogenetic resolution in Juglans based on complete chloroplast genomes and nuclear DNA sequences. *Front. Plant Sci.* **2017**, *8*, 1148. [\[CrossRef\]](#)
60. Cabrera, J.F. Molecular Phylogeny and Historical Biogeography of Loranthaceae (Santalales) Inferred from *Matk* Sequence Data. Master's Thesis, Southern Illinois University, Carbondale, IL, USA, 2002.
61. Doyle, J.; Doyle, J. A rapid DNA isolation procedure for small quantities of fresh leaf tissue. *Phytochem. Bull.* **1987**, *19*, 11–15.
62. Dierckxsens, N.; Mardulyn, P.; Smits, G. NOVOPlasty: De novo assembly of organelle genomes from whole genome data. *Nucleic Acids Res.* **2017**, *45*, e18.
63. Tillich, M.; Lehwark, P.; Pellizzer, T.; Ulbricht-Jones, E.S.; Fischer, A.; Bock, R.; Greiner, S. GeSeq—Versatile and accurate annotation of organelle genomes. *Nucleic Acids Res.* **2017**, *45*, W6–W11. [\[CrossRef\]](#)
64. Chan, P.P.; Lin, B.Y.; Mak, A.J.; Lowe, T.M.; Notes, A. tRNAscan-SE 2.0: Improved detection and functional classification of transfer RNA genes. *Nucleic Acids Res.* **2021**, *49*, 9077–9096. [\[CrossRef\]](#)
65. Greiner, S.; Lehwark, P.; Bock, R. Organellar genome DRAW (OGDRAW) version 1.3.1: Expanded toolkit for the graphical visualization of organellar genomes. *Nucleic Acids Res.* **2019**, *47*, W59–W64. [\[CrossRef\]](#)
66. Kumar, S.; Stecher, G.; Tamura, K. MEGA7: Molecular evolutionary genetics analysis version 7.0 for bigger datasets. *Mol. Biol. Evol.* **2016**, *33*, 1870–1874. [\[CrossRef\]](#)
67. Thiel, T.; Michalek, W.; Varshney, R. Exploiting EST databases for the development and characterization of gene-derived SSR-markers in barley (*Hordeum vulgare* L.). *Theor. Appl. Genet.* **2003**, *106*, 411–422. [\[CrossRef\]](#)
68. Kurtz, S.; Choudhuri, J.V.; Ohlebusch, E.; Schleiermacher, C.; Stoye, J.; Giegerich, R. REPuter: The manifold applications of repeat analysis on a genomic scale. *Nucleic Acids Res.* **2001**, *29*, 4633–4642. [\[CrossRef\]](#)
69. Mayor, C.; Brudno, M.; Schwartz, J.R.; Poliakov, A.; Rubin, E.M.; Frazer, K.A.; Pachter, L.S.; Dubchak, I. VISTA: Visualizing global DNA sequence alignments of arbitrary length. *Bioinformatics* **2000**, *16*, 1046–1047. [\[CrossRef\]](#)
70. Amiryousefi, A.; Hyvönen, J.; Poczai, P. IRscope: An online program to visualize the junction sites of chloroplast genomes. *Bioinformatics* **2018**, *34*, 3030–3031. [\[CrossRef\]](#)
71. Wang, D. KaKs\_Calculator 2.0: A toolkit incorporating gamma-series methods and sliding window strategies. *Genom. Proteom. Bioinform.* **2010**, *8*, 77–80. [\[CrossRef\]](#)
72. Van Rossum, G.; Drake, F.L., Jr. *Python Reference Manual*; Centrum voor Wiskunde en Informatica: Amsterdam, The Netherlands, 1995.
73. Emms, D.M.; Kelly, S. OrthoFinder: Phylogenetic orthology inference for comparative genomics. *Genome Biol.* **2019**, *20*, 238. [\[CrossRef\]](#)
74. Madeira, F.; Pearce, M.; Tivey, A.R.N.; Basutkar, P.; Lee, J.; Edbali, O.; Madhusoodanan, N.; Kolesnikov, A.; Lopez, R. Search and sequence analysis tools services from EMBL-EBI in 2022. *Nucleic Acids Res.* **2022**, *50*, W276–W279. [\[CrossRef\]](#)
75. Letunic, I.; Bork, P. Interactive Tree of Life (iTOL) v5: An online tool for phylogenetic tree display and annotation. *Nucleic Acids Res.* **2021**, *49*, W293–W296. [\[CrossRef\]](#)

## Article

# Characterization of the Water Shortage Effects on Potato Tuber Tissues during Growth Using MRI Relaxometry and Biochemical Parameters

Ghina Hajjar <sup>1</sup>, Stéphane Quellec <sup>1</sup>, Sylvain Challos <sup>1</sup>, Lydia Bousset-Vaslin <sup>2</sup>, Gisèle Joly <sup>3</sup>, Christophe Langrume <sup>2</sup>, Carole Deleu <sup>2</sup>, Laurent Leport <sup>2,\*</sup> and Maja Musse <sup>1,\*</sup>

<sup>1</sup> UR OPAALE, INRAE, 17 Avenue de Cucillé, CS 64427, 35044 Rennes, France; ghina.hajjar@inrae.fr (G.H.); stephane.quellec@inrae.fr (S.Q.); sylvain.challos@inrae.fr (S.C.)

<sup>2</sup> UMR IGEPP, INRAE, Institut Agro-Agrocampus Ouest, Université de Rennes 1, Domaine de la Motte, 35653 Le Rheu, France; lydia.bousset@inrae.fr (L.B.-V.); christophe.langrume@inrae.fr (C.L.); carole.deleu@univ-rennes1.fr (C.D.)

<sup>3</sup> Germicopa, 1 allée Loeiz Herriou, 29334 Quimper, France; gisele.joly@germicopa.fr

\* Correspondence: laurent.leport@univ-rennes1.fr (L.L.); maja.musse@inrae.fr (M.M.)

**Abstract:** The potato is one of the most cultivated crops worldwide, providing an important source of food. The quality of potato tubers relates to their size and dry matter composition and to the absence of physiological defects. It depends on the spatial and temporal coordination of growth and metabolic processes in the major tuber tissues: the cortex, flesh and pith. In the present study, variations in the biochemical traits of each of these tissues were investigated during tuber growth under optimal and water-deficit conditions. MRI relaxometry was used as a non-invasive and quantitative method to access information on cellular water status. The presence of slight but significant variations in organic compound contents quantified in the cortex and flesh revealed a tissue-dependent metabolic pattern. The  $T_2$  and relative  $I_0$  of the bi-exponential relaxation signal allowed a distinction to be made between the pith and the cortex, whereas the flesh could be differentiated from these tissues only through its relative  $I_0$ .  $T_2$  values did not vary significantly during tuber development, in accordance with the typical growth pattern of tubers, but were shown to be sensitive to water stress. The interpretation of the multi-exponential transverse relaxation times is discussed and could be further developed via microscopic analysis.

**Keywords:** magnetic resonance imaging; *Solanum tuberosum*; multi-exponential transverse relaxation; water stress

**Citation:** Hajjar, G.; Quellec, S.; Challos, S.; Bousset-Vaslin, L.; Joly, G.; Langrume, C.; Deleu, C.; Leport, L.; Musse, M. Characterization of the Water Shortage Effects on Potato Tuber Tissues during Growth Using MRI Relaxometry and Biochemical Parameters. *Plants* **2022**, *11*, 1918. <https://doi.org/10.3390/plants11151918>

Academic Editors: Petronia Carillo, Milan S. Stankovic and Paula Baptista

Received: 13 June 2022

Accepted: 21 July 2022

Published: 25 July 2022

**Publisher's Note:** MDPI stays neutral with regard to jurisdictional claims in published maps and institutional affiliations.



**Copyright:** © 2022 by the authors. Licensee MDPI, Basel, Switzerland. This article is an open access article distributed under the terms and conditions of the Creative Commons Attribution (CC BY) license (<https://creativecommons.org/licenses/by/4.0/>).

## 1. Introduction

The potato is one of the most important crops in a number of countries across the world, supplying many important nutrients to the human diet. Potato tubers contain around 80% water and around 10–25% of FW of starch depending on cultivar [1]. Tuber quality relates to size, dry matter composition and the absence of external and internal physiological defects. It is determined by the spatial and temporal coordination of growth and metabolic processes, in particular tuber tissues. Potato tubers are complex organs comprising three major tissues: the flesh (perimedullary zone), the cortex and the pith. Cell division and enlargement in these three tissues during tuber growth occur according to specific tissue-related kinetics [2]. The differentiation of the cortex and pith occurs when the cells in the apex divide, whereas that of the flesh tissue results from the division of the procambial cells [3]. It has been reported that the onset of tuber formation occurs when cells divide longitudinally to the stolon axis [2]. Tuber growth is then associated with the randomly oriented division and enlargement of cells in the flesh until the final size is reached [2]. Since cell size does not increase in the course of tuber growth, the tuber final size is not related to the size of the flesh cells but depends on the number of

cells [4]. Round cells have been observed in the flesh and cortex, those located in the flesh tissue being 1.5 to 2.5 times the size of those in the cortex [5]. The pith tissue is made up of tube-shaped cells orientated along the stolon-top axis with cell transverse-section sizes between those found in the cortex and flesh. In addition to these morphological developments, the formation of tubers also involves the supply of photosynthates from the leaves followed by the biochemical processes that lead to the formation and storage of starch. It has been reported that, during tuber growth, sucrose is provided through phloem symplastic unloading rather than the apoplastic unloading observed before tuberization [6]. During tuber growth, starch accumulates in the flesh and cortex tissues, whereas relatively few starch grains are observed in the pith [7].

Due to its shallow and sparse root system [8], the potato plant is sensitive to water deficit. It responds to drought by initiating complex physiological and metabolic processes. Tuber development is impacted by drought, mainly during the tuber bulking and tuber ripening stages [9]. The relationship between yield components (i.e., the number and size of tubers) depends in a complex way on the timing, duration and severity of the water deficit. In some cases, the number and size of tubers may compensate each other [10]. In addition to tuber size, the water regime may affect the tuber weight and starch content [9] that reflect tuber quality. A differential effect of water regime on tuber tissues was to be expected as a result of their specific composition and growth rate. However, to the best of our knowledge, no such data are available. It is therefore necessary to characterize the individual tissues to gain a better understanding of the effects of drought on tuber quality.

Because it can provide quantitative information on water dynamics and structural features at multiple length scales (from nm to few centimeters) and in a non-destructive way, quantitative magnetic resonance imaging (MRI) offers a valuable approach to the characterization of plant organs. In the case of organs with high water content (fruits, tubers, leaves), the MRI signal is mainly defined by longitudinal ( $T_1$ ) and transverse ( $T_2$ ) relaxation parameters and the self-diffusion coefficient of water molecules. In a number of studies, MRI was used to visualize and quantify morphological features and internal defects in plant organs [11,12]. Additionally, MRI relaxometry has been used to access information on water status, subcellular compartmentalization of water, and membrane permeability/integrity in plant organs [13]. Indeed, in the main cell compartments of plant tissues, water is characterized by different  $T_2$  and  $T_1$  relaxation times that are governed by water mobility and the chemical exchange of water protons with macromolecules (polysaccharides and proteins) and solid surfaces. Since the diffusion exchange of water molecules between compartments separated by a membrane is relatively slow, the relaxation signal is generally multi-exponential, although the process of exchange tends to produce a partially-averaged signal from the water in these compartments. The relaxation signal thus reflects water compartmentalization and is impacted by membrane status and the size of the compartments [14]. The diffusion of water in the random magnetic field gradients that is generated by susceptibility-induced inhomogeneities derived from gas-filled intercellular spaces also affects relaxation times. Several NMR and MRI studies [14–16] have sought to interpret the relaxation data of specific plant tissues in terms of their structure and composition. Among these studies, only two concern tubers [17,18]. Further investigation is therefore required to establish interpretations of relaxation parameters that take into account the specificities of tuber tissues, in particular their high starch content.

In the present study, we investigated the variation in the biochemical traits of tissues during tuber growth under optimal and water-deficit conditions and explored their relationship to changes in transverse relaxation times. Analysis covered the major tuber tissues, i.e., the cortex, the flesh and the pith. The first aim was to characterize the effects of water deficit on the spatial and temporal progress of the biochemical processes occurring in tuber tissues during growth. The second aim was to improve interpretation of the changes in relaxation parameters in tuber tissues so that MRI parameters could be proposed as biomarkers for the assessment of tuber development.

## 2. Results

### 2.1. Changes in Physiological Parameters

Under the water deficit treatment, a loss of 230 g of tuber fresh weight per plant was recorded compared with plants under control conditions. This corresponded to a 63% decrease in final tuber yield measured at 87 days after shoot emergence (DASE). For the three largest tubers (the only tubers selected for further analysis of the effects of the treatment), water stress had an impact on tuber size during the period from 30 to 60 DASE (Figure 1). After 60 DASE, tuber weight did not change significantly, reaching a continuous plateau through to 87 DASE (data not shown).

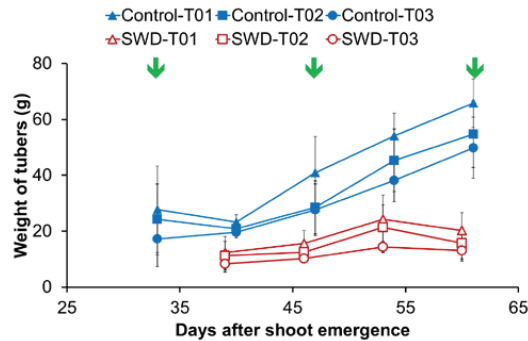


**Figure 1.** Evolution of tuber weight during the growth period expressed in days after shoot emergence (DASE). For each of the eight plants (4 Control & 4 subjected to severe water deficit SWD), the three heaviest tubers were labeled T01 to T03 in decreasing order of mass at harvest. Weight values correspond to the average of four observations ( $n = 4$ ) and standard deviation are indicated by the segment bars. Arrows indicate the measurement dates for physiological parameters. In the case of SWD plants, dates correspond, respectively, to 1 to 5 weeks after irrigation was withheld.

The evolution of the biochemical parameters in the flesh and cortex is shown in Figures 2 and 3 and Tables 1–3. Note that the pith was not subjected to biochemical analysis (Section 4). For the control tubers, the average pH value of the cortex was 6.4 at 32 DASE and differed significantly (Table 1) from that of the flesh, which had an average of 6.2 (Figure 2A). The pH was stable between 32 and 46 DASE and significantly decreased to  $5.9 \pm 0.1$  at 60 DASE in both tissues (Table 2). Overall, severe water deficit (SWD) induced a slight but significant decrease in pH except in the flesh at 32 DASE (Table 3). However, water stress did not modify the pattern of pH evolution during tuber filling (i.e., stable until 45 DASE and then decreasing).

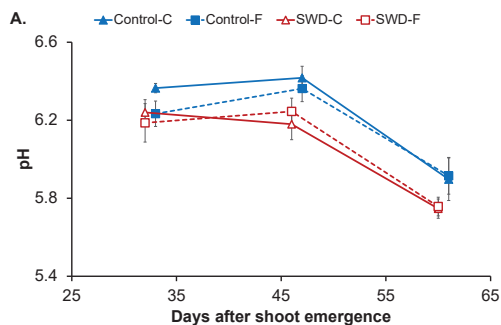


**Figure 2.** Cont.

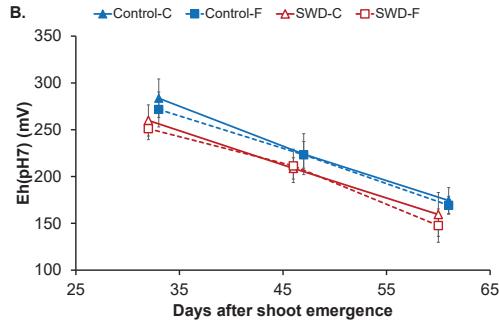


**Figure 2.** Evolution of (A) pH and (B) redox potential corrected for pH = 7 (Eh (pH7)) in potato tuber tissues (C: Cortex; F: Flesh) during tuber filling expressed in days after shoot emergence for both control and severe water-deficit (SWD) conditions. Values correspond to the average of four observations ( $n = 4$ ) and standard deviation are indicated by the segment bars. The statistical significance of differences in value for tissues, growth periods and water regimes is reported in Tables 1–3, respectively.

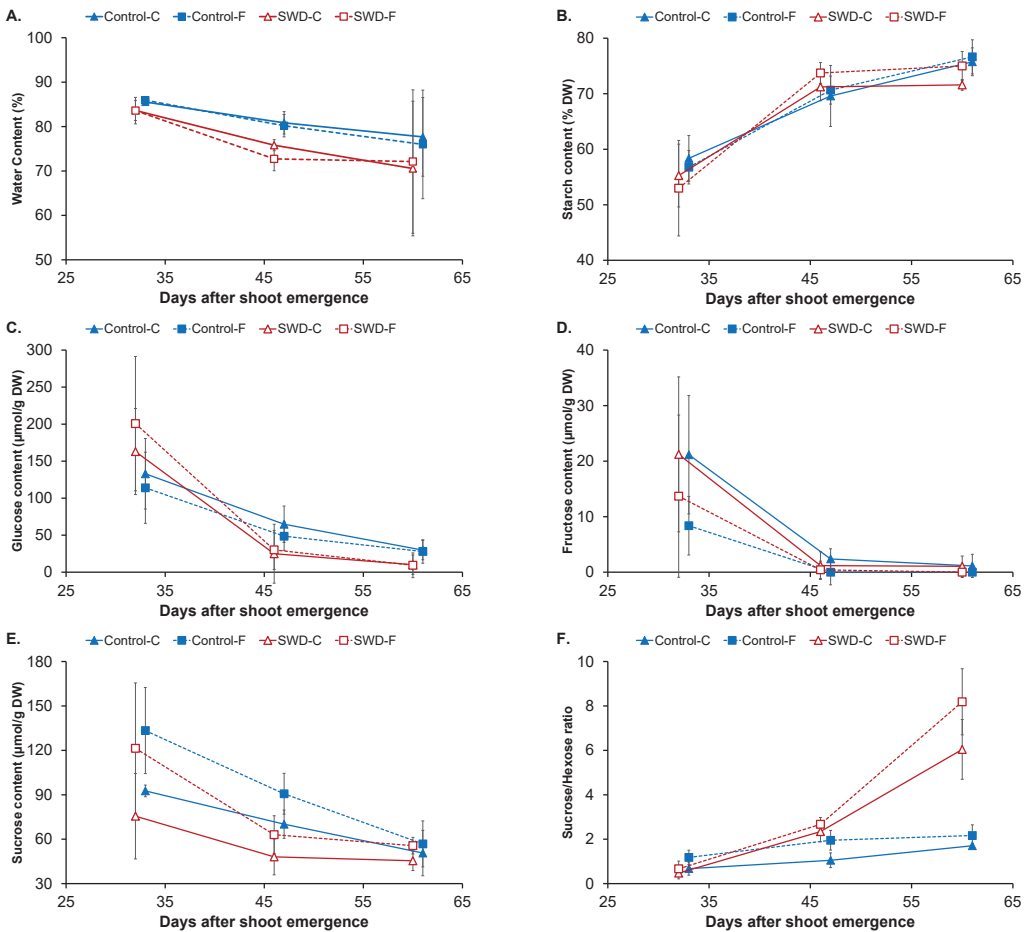


**Figure 3.** *Cont.*

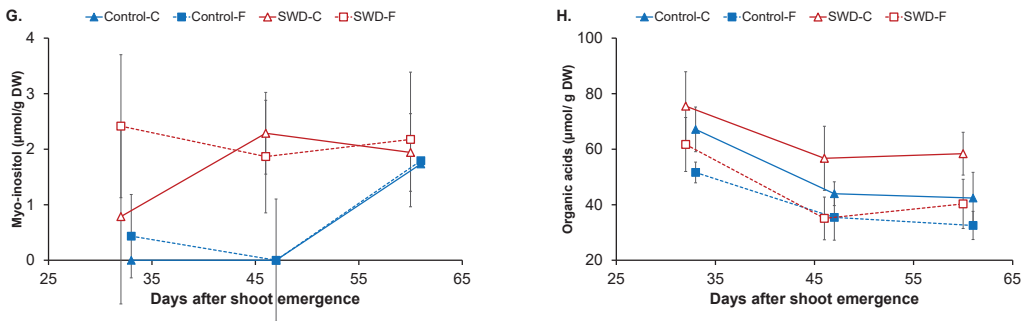


**Figure 3.** Evolution of (A) water content, (B) starch content, (C) glucose content, (D) fructose content, (E) sucrose content, (F) sucrose-to-hexose ratio, (G) myo-inositol content and (H) organic acid content in potato tuber tissues (C: Cortex; F: Flesh) during tuber filling expressed in days after shoot emergence for both control and severe water-deficit (SWD) conditions. Values correspond to the average of four observations ( $n = 4$ ) and standard deviation are indicated by the segment bars. The statistical significance of values between tissues, growth periods and water regimes is reported in Tables 1–3, respectively.

**Table 1.** Statistical evaluation of the effect of tissue type on biochemical parameters (Student t-test or Mann–Whitney test; Statgraphics, alpha = 5%). Different letters between Cortex and Flesh for the same DASE indicate a statistically significant difference.

DASE	32		46		60	
	Control					
Variables	Cortex	Flesh	Cortex	Flesh	Cortex	Flesh
pH	a	b	a	a	a	a
Eh (pH7)	a	a	a	a	a	a
WC	a	a	a	a	a	a
Starch	a	a	a	a	a	a
Glucose	a	a	a	a	a	a
Fructose	a	a	a	a	a	a
Sucrose	a	b	a	a	a	a
S/(G + F)	a	a	a	b	a	a
Myo-inositol	-	-	-	-	a	a
Organic acids	a	b	a	a	a	b
	SWD					
Variables	Cortex	Flesh	Cortex	Flesh	Cortex	Flesh
pH	a	a	a	a	a	a
Eh (pH7)	a	a	a	a	a	a
WC	a	a	a	a	a	a
Starch	a	a	a	a	a	b
Glucose	a	a	a	a	a	a
Fructose	a	a	a	a	a	a
Sucrose	a	a	a	b	a	a
S/(G + F)	a	a	a	a	a	a
Myo-inositol	a	a	a	a	a	a
Organic acids	a	b	a	b	a	b

**Table 2.** Statistical evaluation of the effect of water regime on biochemical parameters (Student t-test or Mann–Whitney test; Statgraphics, alpha = 5%). Different letters between Control and SWD conditions for the same DASE indicate a statistically significant difference.

DASE	32		46		60	
	Cortex					
Variables	Control	SWD	Control	SWD	Control	SWD
pH	a	b	a	b	a	a
Eh (pH7)	a	a	a	a	a	a
WC	a	a	a	b	a	a
Starch	a	a	a	a	a	a
Glucose	a	a	a	b	a	b
Fructose	a	a	a	a	a	a
Sucrose	a	a	a	a	a	a
S/(G + F)	a	a	a	b	a	b
Myo-inositol	-	-	-	-	a	a
Organic acids	a	b	a	b	a	b
	Flesh					
Variables	Control	SWD	Control	SWD	Control	SWD
pH	a	a	a	b	a	b
Eh (pH7)	a	a	a	a	a	a
WC	a	a	a	b	a	a
Starch	a	a	a	a	a	a
Glucose	a	a	a	a	a	b
Fructose	a	a	-	-	-	-
Sucrose	a	a	a	a	a	a
S/(G + F)	a	a	a	a	a	b
Myo-inositol	a	b	-	-	a	a
Organic acids	a	a	a	a	a	a

**Table 3.** Statistical evaluation of the effect of growth phase on biochemical parameters (ANOVA test followed by the Tukey HSD test, or the Kruskal–Wallis test followed by the Bonferroni test; Statgraphics, alpha = 5%). Different letters between 32, 46 and 60 DASE for the same growth condition indicate a statistically significant difference.

DASE	Control			SWD		
	Cortex					
Variables	32	46	60	32	46	60
pH	a	a	b	a	a	b
Eh (pH7)	a	ab	b	a	b	c
WC	a	a	a	a	a	a
Starch	a	ab	b	a	b	b
Glucose	a	b	b	a	ab	b
Fructose	a	ab	b	a	a	a
Sucrose	a	a	a	a	a	a
S/(G + F)	a	a	b	a	a	b
Myo-inositol	-	-	-	a	a	a
Organic acids	a	b	b	a	b	b
	Flesh					
Variables	32	46	60	32	46	60
pH	a	a	b	a	a	b
Eh (pH7)	a	b	c	a	a	b
WC	a	a	a	a	a	a
Starch	a	b	b	a	b	b
Glucose	a	b	b	a	ab	b
Fructose	-	-	-	-	-	-
Sucrose	a	b	b	a	ab	b
S/(G + F)	a	b	b	a	a	b
Myo-inositol	a	-	b	a	a	a
Organic acids	a	b	b	a	b	b

As shown in Figure 2B, the redox potential Eh (adjusted for pH = 7) in the cortex of control tubers was  $284 \pm 21$  mV at 32 DASE with no significant difference compared with values measured in the flesh ( $272 \pm 19$  mV) (Table 1). In both tissues, Eh values significantly decreased to  $224 \pm 22$  mV in the cortex and  $223 \pm 14$  mV in the flesh at 46 DASE and then

to  $174 \pm 14$  and  $169 \pm 10$  mV, respectively, at 60 DASE. Water stress did not have an impact on Eh values in tuber tissues (Table 3) and the same pattern of Eh evolution during filling was observed in the tissues of SWD tubers.

Water content (WC) was approximately 86% of tuber fresh weight (FW) when measurements began (32 DASE), falling to below 80% at 60 DASE in both the cortex and flesh of control tubers (Figure 3A). However, no significant difference was observed between the measurement dates, probably due to the heterogeneity of the samples at 60 DASE (Table 2). In both tissues, water stress induced a significant decrease in WC only at 46 DASE (Table 3).

As expected, starch was the main carbohydrate found in the potato tuber tissues. Its evolution during growth in the cortex and flesh of both control and SWD tubers is shown in Figure 3B. At 32 DASE, the starch content of the control tuber cortex ( $58 \pm 4\%$  of dry weight, DW) was not significantly different from that of the flesh. In both tissues, starch content significantly increased to approximately 70% of DW at 46 DASE and reached  $76 \pm 3$  and  $77 \pm 3\%$  of DW, respectively, at 60 DASE. Other carbohydrates were identified in the potato tuber tissues (sucrose, a disaccharide, fructose and glucose, two monosaccharides) as well as polyols (myo-inositol). In the cortex of control tubers, glucose and fructose contents were  $133 \pm 48$  and  $21 \pm 11$   $\mu\text{mol/g}$  of DW, respectively, at 32 DASE and there was no significant difference in content levels in the flesh of these tubers (Figure 3C,D). Glucose and fructose contents both decreased during filling. At 60 DASE, the greatest decrease was observed in fructose, at 95%, whereas a decrease of 75% was observed for glucose. However, differences were observed between content levels in the flesh and the cortex. As shown in Figure 3E, sucrose content was  $93 \pm 4\%$   $\mu\text{mol/g}$  of DW in the cortex of control tubers at 32 DASE, significantly lower than its content in the flesh ( $133 \pm 29$   $\mu\text{mol/g}$  of DW). Sucrose content also decreased during tuber filling but its decrease was more pronounced in the flesh (57%) than in the cortex (45%). Water deficit had no significant impact on the carbohydrates profile (starch, glucose, fructose and sucrose), with the same pattern of evolution during tuber filling being observed in both tissue types for the SWD tubers (Figure 3B–E).

The sucrose-to-hexose ratio, which is generally considered an indicator for water stress, is shown in Figure 3F. At 32 DASE, this ratio was equal to one in the cortex of the control tubers with no significant difference from the ratio measured in the flesh. This means that in both tissues of the control tubers sucrose and hexose (mainly glucose) contents were equivalent. A slight increase was observed in both the cortex and the flesh of the control tubers, with the sucrose-to-hexose ratio not exceeding two. For both tissue types, water deficit had no impact on the sucrose-to-hexose ratio at the beginning of the filling phase (32 DASE). However, for SWD tubers, an important increase was observed between 46 and 60 DASE, with ratio values above 6 at the end of the filling phase.

Small amounts of myo-inositol in the potato tuber cortex and flesh were quantified (Figure 3G). For both tissue types in the control tubers, myo-inositol content was negligible. Its content levels increased at the late filling stages reaching values of approximately 2  $\mu\text{mol/g}$  DW. By contrast, equivalent amounts of myo-inositol were already quantified in SWD tubers for both tissue types at 32 DASE and remained stable during the filling period.

In addition to carbohydrates and polyols, certain organic acids were also measured in the potato tuber tissues, namely citrate, malate, and quinate (Figure 3H). At 32 DASE, the total content of organic acids in the control cortex was  $67 \pm 8$   $\mu\text{mol/g}$  of DW, differing significantly from levels observed in the flesh ( $52 \pm 4$   $\mu\text{mol/g}$  of DW). Levels decreased significantly in both tissues at 46 DASE, down to  $44 \pm 9$  and  $35 \pm 5$   $\mu\text{mol/g}$  of DW, respectively, in the cortex and flesh, and remained stable until 60 DASE. The same pattern was observed in both the cortex and flesh of the SWD tubers. However, organic acid content levels were significantly higher in the cortex of SWD tubers compared with those of the control tubers on the three measurement dates.

## 2.2. Evolution of MRI Parameters

An example of  $T_2$ -weighted MRI image (TE = 130 ms) acquired with Multi-Spin Echo sequence used for tissue segmentation is shown in Figure 4A. The signal from the pith was

higher, indicating longer  $T_2$  time in this tissue. In the flesh and cortex, the signal had a similar intensity, indicating close  $T_2$  values. However, these two tissues could apparently be distinguished, because of a narrow and bright ring-shaped structure that probably corresponded to vascular bundles at the interface between the cortex and the flesh. Note that the cortex and the pith appeared as homogeneous regions, in contrast to the flesh, characterized by a more heterogeneous signal. This was observed for all tubers as shown in Supplementary Figure S1. The  $T_2$  decay curves for the three different tissue types (cortex, flesh and pith) of both the control and SWD tubers were optimally fitted using a bi-exponential model that reflected two water pools in each tissue: (1) a component with  $T_2$  values below 100 ms and (2) a component with  $T_2$  values above 200 ms (Figure 5 and Supplementary Figure S2).

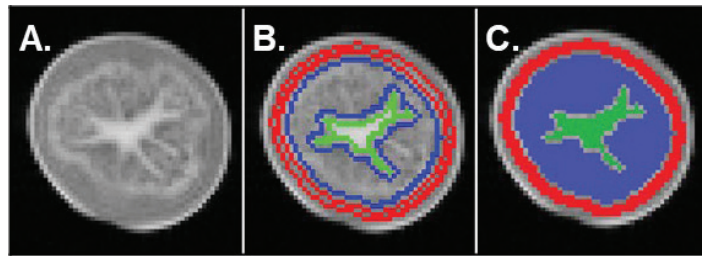


**Figure 4.** (A) MRI image acquired with a Multi-Spin Echo sequence (echo time = 130 ms, repetition time = 10 s,  $0.8 \times 0.8 \times 5 \text{ mm}^3$  voxel) of a potato tuber at 60 days after shoot emergence (DASE). (B) Masks of the three different tissues (cortex, flesh, pith) obtained by means of an automatic segmentation algorithm developed for transverse relaxation time ( $T_2$ ) computation. (C) The three different regions obtained following segmentation according to  $T_2$ : cortex (red), flesh (blue) and pith (green). See Supplementary Figure S1 for images of the other tubers analyzed at 60 DASE.

**Table 4.** Statistical evaluation of the effect of tissue type on MRI parameters (ANOVA test followed by the Tukey HSD test or the Kruskal–Wallis test followed by the Bonferroni test; Statgraphics, alpha = 5%). Different letters between Pith, Cortex and Flesh for the same DASE indicate a statistically significant difference.

DASE	32			39			46			53			60		
	Control														
Variables	Pith (P)	Cortex (C)	Flesh (F)	P	C	F	P	C	F	P	C	F	P	C	F
$I_0$ (comp 2)	a	b	c	a	b	c	a	b	c	a	b	b	a	b	b
$T_2$ (comp 1)	a	a	a	a	a	a	a	a	a	a	a	a	a	a	a
$T_2$ (comp 2)	a	b	b	a	b	b	a	b	b	a	b	b	a	a	a
	SWD														
Variables	Pith (P)	Cortex (C)	Flesh (F)	P	C	F	P	C	F	P	C	F	P	C	F
$I_0$ (comp 2)	a	a	a	a	ab	b	a	b	c	a	b	b	a	ab	b
$T_2$ (comp 1)	a	a	a	a	a	a	a	a	a	a	a	a	a	a	a
$T_2$ (comp 2)	a	b	b	a	b	b	a	b	b	a	b	b	a	a	a

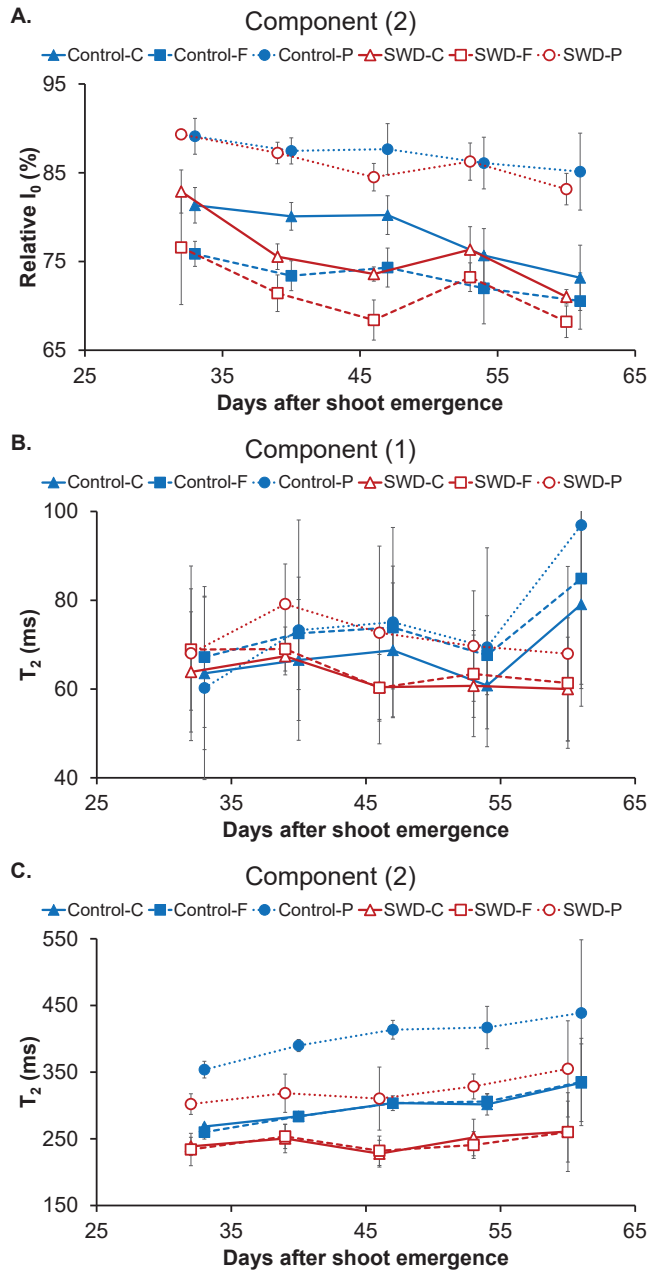


**Figure 5.** Evolution of (A) component (2) relative signal distribution, (B) component (1) transverse relaxation time ( $T_2$ ) and (C) component (2)  $T_2$  in potato tuber tissues (C: Cortex; F: Flesh; P: Pith) during tuber filling expressed in days after shoot emergence for both control and severe water deficit (SWD) conditions. Values correspond to the average of four observations ( $n = 4$ ) and standard deviation are indicated by the segment bars. The statistical significance of values between tissues, growth periods and water regimes is reported in Tables 4–6, respectively.

**Table 5.** Statistical evaluation of the effect of water regime on MRI parameters (Student t-test or Mann–Whitney test; Statgraphics, alpha = 5%). Different letters between Control and SWD conditions for the same DASE indicate a statistically significant difference.

DASE	32		39		46		53		60	
	Pith									
Variables	Control	SWD								
I <sub>0</sub> (comp 2)	a	a	a	a	a	a	a	a	a	a
T <sub>2</sub> (comp 1)	a	a	a	a	a	a	a	a	a	a
T <sub>2</sub> (comp 2)	<b>a</b>	<b>b</b>	<b>a</b>	<b>b</b>	<b>a</b>	<b>b</b>	<b>a</b>	<b>b</b>	<b>a</b>	<b>a</b>
	Cortex									
Variables	Control	SWD								
I <sub>0</sub> (comp 2)	a	a	a	a	a	a	a	a	a	a
T <sub>2</sub> (comp 1)	a	a	<b>a</b>	<b>b</b>	<b>a</b>	<b>b</b>	a	a	a	a
T <sub>2</sub> (comp 2)	a	a	<b>a</b>	<b>b</b>	<b>a</b>	<b>b</b>	<b>a</b>	<b>b</b>	a	a
	Flesh									
Variables	Control	SWD								
I <sub>0</sub> (comp 2)	a	a	a	a	a	a	a	a	a	a
T <sub>2</sub> (comp 1)	a	a	a	a	a	a	a	a	a	a
T <sub>2</sub> (comp 2)	a	a	<b>a</b>	<b>b</b>	<b>a</b>	<b>b</b>	<b>a</b>	<b>b</b>	a	a

**Table 6.** Statistical evaluation of the effect of growth phase on MRI parameters (ANOVA test followed by the Tukey HSD test or the Kruskal–Wallis test followed by the Bonferroni test; Statgraphics, alpha = 5%). Different letters between 32, 39, 46, 53 and 60 DASE for the same growth condition indicate a statistically significant difference.

DASE	Control					SWD				
	Pith									
Variables	32	39	46	53	60	32	39	46	53	60
I <sub>0</sub> (comp 2)	a	a	a	a	a	<b>a</b>	<b>ab</b>	<b>bc</b>	<b>abc</b>	<b>c</b>
T <sub>2</sub> (comp 1)	a	a	a	a	a	a	a	a	a	a
T <sub>2</sub> (comp 2)	a	a	a	a	a	a	a	a	a	a
	Cortex									
Variables	32	39	46	53	60	32	39	46	53	60
I <sub>0</sub> (comp 2)	<b>a</b>	<b>ab</b>	<b>ab</b>	<b>bc</b>	<b>c</b>	<b>a</b>	<b>ab</b>	<b>ab</b>	<b>ab</b>	<b>b</b>
T <sub>2</sub> (comp 1)	a	a	a	a	a	a	a	a	a	a
T <sub>2</sub> (comp 2)	a	a	a	a	a	a	a	a	a	a
	Flesh									
Variables	32	39	46	53	60	32	39	46	53	60
I <sub>0</sub> (comp 2)	a	a	a	a	a	a	a	a	a	a
T <sub>2</sub> (comp 1)	a	a	a	a	a	a	a	a	a	a
T <sub>2</sub> (comp 2)	<b>a</b>	<b>ab</b>	<b>ab</b>	<b>ab</b>	<b>b</b>	a	a	a	a	a

The relative signal intensity of component (2) is shown in Figure 5A since this corresponds to the major water pool in the tissues. At 32 DASE, I<sub>0</sub> of component (2) was 81 ± 2% in the cortex of the control tubers. This value (Tables 4–6) was significantly higher than that found in the flesh (76 ± 2%) and significantly lower than that in the pith (88 ± 2%). At the end of tuber filling (60 DASE), I<sub>0</sub> of component (2) significantly decreased to 73 ± 4% in the cortex of the control tubers, whereas the decreasing trend in the flesh of control tubers (Figure 5A) was not significant. Accordingly, in the control tubers, from 46 DASE, the relative signal distributions between components (1) and (2) in the cortex and the flesh were similar but these differed from that measured in the pith. Water deficit did not change the evolution pattern of I<sub>0</sub> (Tables 4–6).

At 32 DASE, component (1) T<sub>2</sub> was 64 ± 17 ms for the cortex of the control tubers. This value was not significantly different from those measured for the flesh (61 ± 11 ms) or the

pith ( $52 \pm 15$  ms) (Figure 5B and Table 4). Component (1)  $T_2$  remained stable during tuber filling (Table 5) and was not affected by water deficit (Table 6). By contrast, component (2)  $T_2$  was  $268 \pm 4$  ms for the cortex of the control tubers at 32 DASE (Figure 5C). There was no significant difference in the control tubers between component (2)  $T_2$  values for the cortex and the flesh (Table 4). However, the component (2)  $T_2$  value for the pith was  $353 \pm 15$  ms which was significantly higher (~25%) than that measured for both the cortex and the flesh. An increase in component (2)  $T_2$  values over the filling period was observed only for the flesh. However, the component (2)  $T_2$  values measured for the same tissue were significantly lower in the SWD tubers than in the control tubers. Indeed, water deficit induced a decrease of around 20% in all tissues throughout the filling period.

### 2.3. Global Analysis of Physiological and MRI Parameters

By combining all parameters measured in the cortex and the flesh of tubers on the three different dates (32, 46 and 60 DASE), it was possible to carry out a principal component analysis (PCA) and to propose an exploratory global interpretation of the effects of tissue type, water condition and growth phase. Here, two principal components were significant, explaining 65% of observed variance (Figure 6). The first principal component (PC1) accounted for 46% of the variance and made it possible to distinguish between observations by growth phase (Figure 6A). The most significant variables in this component were the content levels of myo-inositol, starch and other carbohydrates as well as redox potential (Figure 6C). Starch content correlated negatively with glucose, fructose and sucrose along the PC1 axis. Starch content also correlated negatively with component (2)  $I_0$ , pH, redox potential and WC. Further, the second principal component (PC2) accounted for 19% of observed variance and made it possible to distinguish between observations by water regime (Figure 6B). The most significant variables in this component were the  $T_2$  values obtained from MRI measurements (Figure 6C). PCA analysis also showed that the difference between control and SWD conditions increased during tuber filling (Figure 6A,B). However, PCA did not make it possible to distinguish between the cortex and flesh of the potato tubers (Supplementary Figure S3). The content levels for organic acids were almost the only discriminating factor between these two tissues (Figure 3H and Tables 1–3).

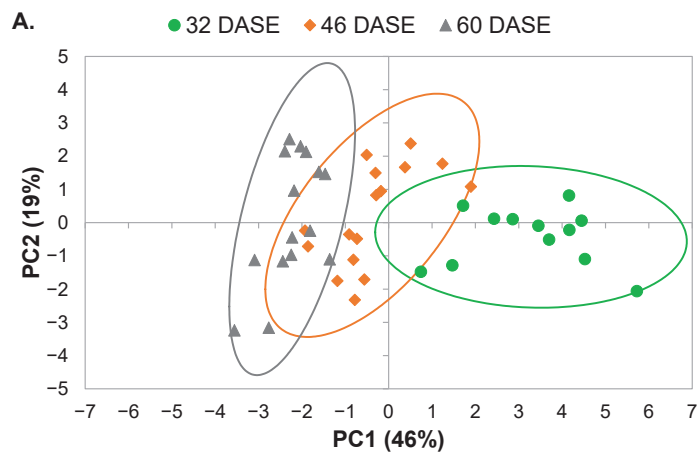
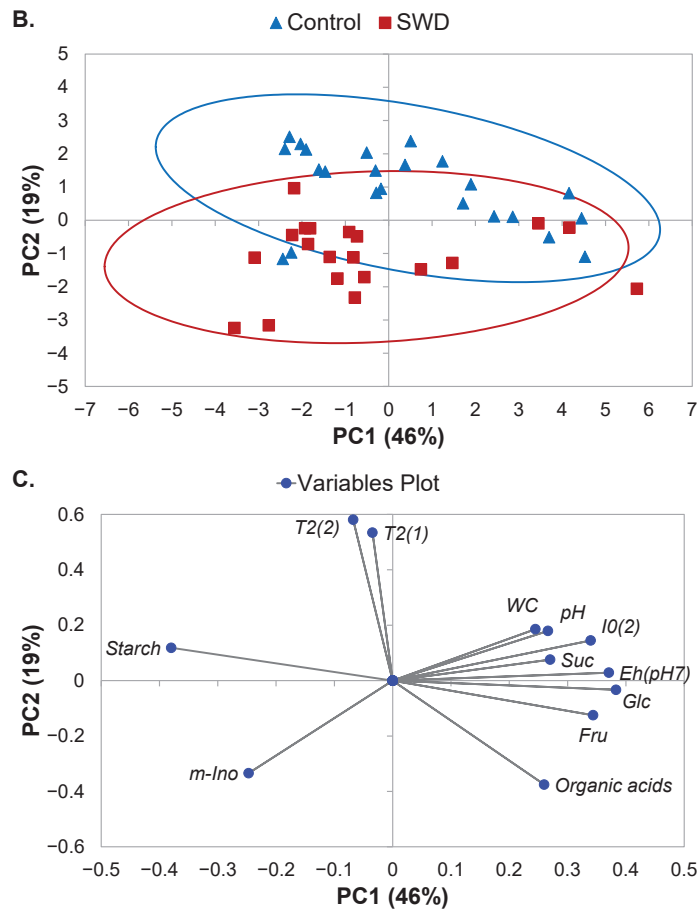


Figure 6. Cont.



**Figure 6.** Principal component analysis (PCA) score plots (A,B) and loading plot for variables (C) derived from data obtained from MRI relaxometry and physiological measurements of potato tuber tissues using principal components 1 (PC1) and 2 (PC2). Observations shown on the score plots are differentiated by colour and symbol to indicate sample classification according to (A) growth period and (B) water regime. Continuous lines on score plots (A,B) represent the ellipsis of confidence at 95% confidence for each group.

### 3. Discussion

#### 3.1. Spatial Changes in Composition during Tuber Filling under Well-Irrigated and Stress Conditions

Tuber growth is sustained by the transport, unloading and utilization of photoassimilates as a substrate for cell respiration, division and enlargement and starch deposition [19]. Under optimal irrigation conditions, adequate leaf-water relations allow unrestricted CO<sub>2</sub> fixation, resulting in the production of large tubers [20]. The results of the present paper confirm those previously obtained [20], showing the continuous growth of individual tubers from two weeks after stolon swelling and tuber initiation through top-kill. During this phase of linear tuber growth, tubers can differ considerably in growth rate, depending on their competing strength [21]. In the present study, the three tubers selected from each plant for analysis were the heaviest and of similar strength; consequently, no such variations were observed.

During tuber growth, the slight decrease in water content observed in the cortex and the flesh (Figure 3A) was mainly due to the increase in dry content associated with starch

synthesis. Indeed, in potatoes, cell division and expansion is rapidly followed by massive starch deposition [22]. Thus, at the beginning of tuber growth, starch already comprised more than half of the total dry-matter component (the latter being around 8% of tuber fresh weight, Figure 3B), in accordance with the literature [22]. The fact that the starch content reached its maximum at this early stage of tuber development may be associated with the particular processes involved in tuber growth, where cell division and enlargement progress from the inner flesh towards the periphery are followed immediately by starch deposition [2,6]. This is consistent with the PCA analysis showing that starch content was one of the main parameters affecting the first PCA component (Figure 6C), explained by the developmental stage (Figure 6A). The present study is original in demonstrating that starch accumulation followed similar patterns in the cortex and flesh tissues. Although the starch content of the pith was not quantified due to experimental constraints, micrographs (Supplementary Figure S4) indicated the starch content of the pith to be lower than that of the other potato tissues in line with Oey et al. [7].

Quantification of organic chemicals in the flesh tissue confirmed earlier results obtained for the whole tuber [6]. For instance, the low fructose content (Figure 3D) observed in the flesh throughout the period of tuber growth is associated with reported high sucrose synthase (SuSy) activity during tuberization [6]. The similar levels of the glucose and sucrose can be linked to the high sucrose hydrolytic activity that has been associated with tuber sink strength [4,6]. It can be noted that the decrease in the quantity of all soluble sugars (i.e., sucrose, glucose and fructose) from 45 DASE is probably explained by a dry-matter dilution effect linked to starch accumulation during this period. Differences between the cortex and flesh tissues in terms of their fructose and sucrose contents can be explained by differences in the carbon metabolism of these tissues. Contrary to expectation, the higher content of organic acids observed in the cortex when compared with the flesh (Figure 3H), produces a slightly higher pH (Figure 2A) rather than greater acidity.

The impact of water stress on tuber size (Figure 1) may be explained by the major change in source-sink relations brought about by, on one hand, a marked decrease in source activity with the stomatal closure and lower CO<sub>2</sub> fixation induced by leaf dehydration and, on the other hand, changes in sink growth depending on sink strength [23]. This sort of change has been recently described in the potato variety under study (Rosanna), despite the fact that this variety has been chosen for its relative drought resistance [20]. Note that, as previously observed [20], the number of tubers was not affected by water stress (data not shown), since stress was induced after onset of tuber swelling. The similar starch and water contents in the control and SWD tubers were consistent with the specific processes of potato tuber growth involving continuous cell proliferation and enlargement.

It is well known that drought has a strong effect on the sucrose-to-hexose ratio in sink organs such as tuber [23]. For the present study, this ratio can be considered a biochemical biomarker of water deficit since stress is known to reduce the degradation of sucrose [24]. Thus, in the growing tuber, there is a cycle of sucrose degradation and resynthesis [25] where the conversion of sucrose to starch represents a possible regulation of the internal osmotic potential.

The myo-inositol content could be considered to be a biochemical biomarker of both water deficit (Figure 3F,G) and plant stress tolerance, as previously reported [26,27]. The study of MIPS sweet potato mutants with low myo-inositol biosynthesis has shown a putative role for this molecule in drought tolerance. Myo-inositol may play a role in osmotic adjustment [28]. Although only trace quantities of myo-inositol were detected in the tissues of the potato tubers, significant differences were observed during growth depending on the water status of the plant (Figure 3G). However, the increase observed in water-stressed tubers may not provide the explanation for this osmotic effect since the content was no more than 1 µM.

So far, it has not been possible to provide an explanation for the concomitant evolution of sucrose content and the acidification of the flesh tissues during tuber filling and under drought conditions. However, it has been reported in a study of orange fruits [29] that

such a decrease in the pH of sink tissues may affect carbohydrate partitioning, with acidity affecting both sucrose hydrolysis and vacuolar sequestration.

### 3.2. Relationship between Transverse Relaxation Times and Tissue Features

Results from the present study indicate that the MRI transverse relaxation signal in the three main potato tuber tissue types can distinguish two water pools with relaxation times of around 60–90 ms and above 200 ms. These relaxation signal components can be linked to particular subcellular compartments only in a limited way. Indeed, as mentioned in the Introduction, the diffusive exchange of water between the compartments partly averages the individual relaxation signals and the contributions from different compartments may overlap. Further, the tissues are potentially composed of cell populations with distinct volume distributions that may result in a bi-exponential signal from the vacuole compartment [15,30]. Nevertheless, the results of the current study that provide transverse relaxation parameters measured by MRI and several tuber biochemical descriptors go some way to improve on previously-proposed transverse relaxation signal assignment. An interpretation was proposed by Hills et al. [31] of the relaxation signal obtained using TD-NMR at 100 MHz (Car-Purcell-Meiboom-Gill sequence (CPMG), TE = 0.4 ms) on potato tubers, following investigation of low-temperature tuber samples and analysis of isolated tissue fractions. At 5 °C (corresponding to the temperature of the present study), the transverse relaxation signals consisting of four peaks centered at (i) approximately a few ms, (ii) 10 ms, (iii) 100 ms and (iv) 200–300 ms, and were attributed to the water in the starch granules, cell walls, cytoplasm and vacuoles, respectively. The differences between the TD-NMR protocols used in [31] and the MRI protocols used in the present study offer a partial explanation for the differences in the results. First, the MRI approach did not allow for measurement of the two fast-relaxing T<sub>2</sub> components recorded by Hills et al. (about a few ms and 10 ms). Second, the differences between the T<sub>2</sub> values measured in [31] and in the present study were to be expected as several studies have demonstrated that relaxation times are affected by experimental conditions (TE, magnetic field strength, temperature) [32,33]. Nevertheless, on the basis of the T<sub>2</sub> and relative amplitude values (Figure 5), it can be hypothesized that the two water pools detected by the MRI relaxation signal correspond to either (i) the cytoplasm and vacuole compartments or (ii) the vacuoles of two cell populations with distinct volume distributions. Note that despite the short TE used in the TD-NMR study of fresh tubers reported in [34] (23 MHz (CPMG), TE = 0.3 ms, 25 °C), the fast-relaxing components remained undetected. Indeed, here, only two water pools with a T<sub>2</sub> of (i) around 60 ms and (ii) around 450–500 ms were distinguishable.

As previously demonstrated for fruit [15,35], the present study shows that MRI relaxometry is effective in revealing differences between tuber tissues, especially those between the pith and the other tissues. Indeed, the T<sub>2</sub> for component (2) was highest in pith and its relative signal distribution differed from that measured in the cortex and flesh throughout the growth period (Figure 5 and Table 4). Multiple relaxation mechanisms are potentially involved in generating these different multi-exponential transverse relaxation times between the tuber regions, and these probably relate to both the specific composition and the structure of this tissue type. Indeed, the greater cell volume in pith (resulting from the cells' particular tubular form [5]) compared with that of the cortex and flesh is a likely contributor to the tissue's higher component (2) T<sub>2</sub>. It has also been reported that pith has a slightly lower starch content than the other potato tissues [7], confirmed in the present study by observation of light micrographs (Supplementary Figure S4). The impact of starch content on the relaxation times of vacuolar and cytoplasmic water pools was observed in banana fruit during ripening [36] and was explained by the occurrence of chemical exchanges between water and starch molecules in amyloplasts and diffusive water exchanges between the amyloplastic, cytoplasmic and vacuolar compartments. Similarly, the lower starch content observed in the defective perimedullary region of a potato tuber compared with neighboring healthy tissues was related to the higher T<sub>2</sub> of component (2) [11]. In the present study, T<sub>2</sub> did not reveal differences between the cortex and flesh, although slight

but significant differences in their pH and sucrose contents were observed at 32 DASE. It was not possible to provide an interpretation of the higher relative signal intensity of component (2) in pith compared with the other two tissues.

The relationship between cell size and relaxation time has been demonstrated for stem [14] and fruit tissues [15]. Indeed, in peaches, apples [15] and pear fruit [37], the increase in  $T_2$  for the component assigned to the vacuolar water pool was related to the increase in cell size in growing fruit. Unexpectedly, in the present study, the developmental stage (expressed in DASE) and, consequently, the increased tuber size only slightly affected component (2)  $T_2$  for the flesh tissue (Figure 5 and Table 5), whereas the effect of developmental stage was insignificant for component (2)  $T_2$  in other tissues and for component (1)  $T_2$ . These differences can be explained by the different processes involved in fruit and tuber growth. In fruits, rapid cell expansion is the dominant mechanism of fruit growth. By contrast, potato enlargement is mainly based on cell division occurring in the cambium-like layer of the perimedullary zone [19]. Consequently, cell sizes remained largely unchanged and the perimedullary cells remained smaller than the pith cells. This explains the absence of any major impact of tuber growth on relaxation parameters. It is also consistent with the fact that  $T_2$  for the control and stressed tubers did not vary significantly at 60 DASE in any of the tissues studied, despite the fact that, at this stage, there was a significant difference in tuber size (Figure 1). The differences between control and SWD conditions observed in component (2)  $T_2$  measured in the tuber tissues at the intermediate stages (DASE 39 to 53), when the tuber growth rate was greatest, may be due to a delay in the growth kinetics of stressed plants. It also may come from differences in water hydration of tuber tissues (Table 2). Note that water stress may also induce changes in cell membrane permeability that can affect the multi-exponential relaxation signal [13].

The relaxation times for the two water pools detected by MRI were the parameters that clearly reflected the impact of water stress on tuber development (Figure 5B,C) and were the principal parameters explaining the second PCA axis (Figure 6C). The possible impact of cell size and water content on relaxation time under stress conditions requires clarification through further microscopic studies.

## 4. Materials and Methods

### 4.1. Experimental Design and Sampling

The potato tubers analyzed in this study were harvested from potato plants of the Rosanna cultivar of *Solanum tuberosum* potato grown under glass (IGEPP, Le Rheu, France). The variety Rosanna was chosen for its high economical potential due to its relatively low sensitivity to drought. Note that it is still sensitive to drought, according to the fact that all potato plants have a more or less sparse and shallow root system. Pre-germinated tubers of similar weight (average  $23 \pm 2$  g fresh weight) and with 1 to 2 sprouts were selected for planting. Single tubers were placed at 25 cm depth in 25 L plastic pots (Airtop<sup>®</sup>, 27 cm diameter, 50 cm high) filled with a mixture (Falienor<sup>®</sup> ref. 992016F1) of sandy loam (40% v/v) and peat moss (60% v/v) with added clay (40 kg m<sup>-3</sup>) and NPK (0.7 kg m<sup>-3</sup> PG-MIX 14-16-18) (soil solution: pH  $5.8 \pm 0.2$  and Ec (1/1.5) 0.7 ms cm<sup>-1</sup>). During the tuber set, which occurred 14 to 24 days after shoot emergence (DASE), soil humidity levels were maintained at 70% of field capacity for all plants. According to a previous study [20], two water regimes were then applied during the tuber-filling period: (i) a 'well-watered' regime, corresponding to soil humidity levels equivalent to 70% of field capacity (control) and (ii) a 'severe water deficit' (SWD) regime, corresponding to humidity levels equivalent to 20% of field capacity. The pot weight equivalent to 70% and 20% was calculated using the method described by Earl [38] to define the soil water holding capacity. In the present study, control and SWD conditions corresponded to a relative soil water of about 20% and below 5%, respectively. In SWD conditions, this value was reached 15 days (39 DASE) after water withholding and it was then maintained by daily water input with the water amount to be supplied determined by daily weighing. Under both regimes, watering ceased for top-kill at 63 DASE and final harvesting was carried out 24 days later.

Four plants grown under each water regime (control and SWD) were harvested during the tuberization growth period at 32, 39, 46, 53 and 60 DASE. In the case of SWD plants, these dates corresponded, respectively, to 1 to 5 weeks after irrigation and were withheld. For each plant, only the three heaviest tubers (labelled T01, T02 and T03 in decreasing weight order) were harvested and stored for a few days before further analysis (Figure 1). In total, 24 tubers (2 water regimes; 4 plants per water regime; 3 tubers per plant) were collected at each the previously mentioned DASE. Different tubers from the same plant were analyzed individually. MRI analysis was carried out on whole potato tubers (T02) on all the above harvesting dates (Supplementary Figure S5A). pH and redox potential were measured at 32, 46 and 60 DASE on a 1 cm thick cross section taken from the center of each potato tuber (T01; Supplementary Figure S5B). Biochemical composition (sugar, organic acid and starch contents) was also determined at 32, 46 and 60 DASE. A 5 mm thick cross section was excised from the center of each potato tuber (T03) and the potato tuber tissues were then separated using a scalpel as shown in Supplementary Figure S5C. Potato tuber tissues were frozen in liquid nitrogen and stored at  $-80^{\circ}\text{C}$ , lyophilized, and then ground to obtain a powder. This allowed the water content (WC) to be determined, expressed as a percentage of the tuber fresh weight for each tissue using the following equation:

$$\text{WC (\%)} = (\text{FW} - \text{DW})/\text{FW} \times 100$$

where FW and DW represent, respectively, the fresh and dry weights (after lyophilization) of the potato tuber tissues. For some tuber sizes and pith structures, the samples obtained from the pith were not sufficient to determine its biochemical composition. For this reason, physiological and biochemical analysis of the pith was not performed.

#### 4.2. MRI Acquisition Protocols and Image Processing

Images of potato tubers were recorded on a 1.5 T MRI scanner (Magnetom Avanto, Siemens, Erlangen, Germany) equipped with a circular polarized head array coil. For the MRI analysis, eight potato tubers were aligned in the center of two rectangular trays (four tubers on each tray; Supplementary Figure S5A). The trays were then inserted in a box placed in the temperature-regulating device installed inside a RF coil designed to conduct MRI acquisitions at  $5 \pm 1^{\circ}\text{C}$ . A 2D Multi-Spin Echo (MSE) sequence [39] was used for the determination of transverse relaxation time ( $T_2$ ) in the tissues of the potato tubers. Images were acquired with the following parameters: imaging matrix  $160 \times 160$ , field of view  $152 \text{ mm} \times 152 \text{ mm}$ , slice thickness 5 mm, repetition time 10 s, echo time 6.5 ms, number of echoes 256, bandwidth 290 Hz/pixel and 2 averages.

Multi-exponential  $T_2$  parameters were estimated for three different tissue types found in potato tubers, i.e., the cortex, the flesh and the pith. Regions of interest (ROIs) corresponding to each tissue were segmented automatically (Figure 4B,C and Supplementary Figure S1) using an algorithm developed using Scilab software. At first, tubers were segmented from the background applying the Otsu automatic thresholding method [40]. According to its position in the images and after a first erosion with a  $5 \times 5$  square kernel in order to remove peripheral pixels (skin), a mask is created for each tuber. The cortex was then delimited by a second erosion with a  $5 \times 5$  square kernel (considering the strip of thickness equal to 3 pixels eroded from the contour of the mask). The pith was delineated by considering the central region of the tuber with a threshold applied by a method based on entropy of the histogram [41]. Any segmented objects on the periphery were manually eliminated. The flesh was the region between the cortex and the pith presenting heterogeneous gray levels. The mean signal from each ROI was computed for all MSE sequence images to generate  $T_2$  decay curves. Values corresponding to a signal-to-noise ratio lower than 7 were removed from the  $T_2$  curves before fitting, making it possible to assume zero-mean noise distribution in magnitude-reconstructed images at all echo times. Then,  $T_2$  relaxation signals were fitted according to the Levenberg-Marquardt algorithm using TableCurve software. The optimal number of components to describe the multi-exponential model was selected, taking account of the coefficient of determination ( $R^2$ ) of the fit, the global fitting

standard error and the errors in all individual parameters. The intensity of individual signal components was expressed as a percentage of the total signal, thereby reflecting the distribution of water between water pools.

#### 4.3. Biochemical Composition

Polar components were extracted from potato tuber powders by using methanol, chloroform, and water in succession. The powder (10–15 mg) was mixed for 15 min with 400  $\mu\text{L}$  of methanol containing internal standard (400  $\mu\text{M}$  adonitol). Then, 200  $\mu\text{L}$  of chloroform was added and the mixture was homogenized for 10 min. Water (400  $\mu\text{L}$ ) was added and the mixture was stirred vigorously for 20 s. The mixture was then centrifuged for 5 min at  $12,000\times g$  at  $15^\circ\text{C}$  (model 3–18KC, Sigma). The chloroform phase was discarded and a volume of 50  $\mu\text{L}$  of the methanol-water phase was dried using a SpeedVac system. Dried extracts were stored at  $-20^\circ\text{C}$  until analysis. For GC-FID analysis, vacuum-dried aliquots were re-suspended in 50  $\mu\text{L}$  of methoxyaminehydrochloride solution in pyridine (20 mg/mL) and the mixture was stirred for 60 min at  $40^\circ\text{C}$ . Then, 50  $\mu\text{L}$  of N-methyl-N-(trimethylsilyl) trifluoroacetamide was added. Derivatization at  $40^\circ\text{C}$  for 30 min and injection were automatically performed using a MultiPurpose Sampler (MPS, Gerstel). Carbohydrates and organic acids were quantified by GC-FID (6890N, Agilent) with a column Tg-5 ms 30 m  $\times$  0.32 mm  $\times$  0.25  $\mu\text{m}$  (Thermo Scientific 26098-1430) as described by [42]. Metabolite contents were estimated through reference to the adonitol signal and expressed in  $\mu\text{mol/g}$  of potato tissue dry weight.

Starch content was determined using an enzymatic method described by [41]. In brief, potato tuber powder (5–10 mg) was mixed in a 2 mL Eppendorf with 1 mL of a methanol-water solution (1:1, *v/v*) followed by 300  $\mu\text{L}$  chloroform. Two liquid phases were separated from the plant powder after 5 min of centrifugation (13,200 rpm,  $4^\circ\text{C}$ , model 5415R, Eppendorf, Le Pecq, France). The lower phase was recovered and 750  $\mu\text{L}$  of methanol was added and continuously mixed for 20 min at  $4^\circ\text{C}$ . The mixture was then centrifuged at 14,000 rpm at  $4^\circ\text{C}$  for 20 min. The supernatant was decanted off and the starch was dispersed by autoclaving (2 bars,  $120^\circ\text{C}$ , 2 h) and then hydrolyzed with amyloglucosidase (6 IU/tube) in a water bath ( $56^\circ\text{C}$ , 1 h 30 min). The glucose content in the supernatant was determined using the microplate method [43]. The starch content was expressed in % of dry weight.

#### 4.4. Redox Potential and pH Measurements

Redox potential (Eh) was measured as described by [44] using a Ag/AgCl Reference electrode Radiometer analytical E21M002 and a Radiometer Analytical platinum plate electrode (5  $\times$  5 mm M241 Pt), with a Voltcraft VC850 multimeter (10  $\times$  106 Ohm input resistance). Electrodes were applied 5 mm apart in the cortex and then in the flesh of potato tubers (Supplementary Figure S5B). The value retained corresponded to that displayed on the multimeter when it was stable for one minute. After being measured using the Ag/AgCl reference electrode, all redox potentials were transformed to give Eh according to the “normal hydrogen electrode”. Redox electrodes were calibrated at the start of the measurements and every 10–12 measurements, with Mettler Toledo Redox buffer solution 220 mV (pH = 7) composed of Potassium hexacyanoferrate (III), Potassium hexacyanoferrate (II), Potassium dihydrogen phosphate and Disodium hydrogen phosphate. All measurements were conducted outdoors in an environment identified as being free from electromagnetic interference.

Once the Eh was measured in the different tissues of the potato tubers, portions of the cortex were excised and quickly ground with a pestle and mortar. The mixture was filtered through cotton wool inserted in a 2 mL syringe. The juice was squeezed onto a Horiba LAQUAtwin-pH-22 m for pH measurement. The same protocol was applied to the flesh.

#### 4.5. Statistical Analysis

Data obtained from biochemical analysis and from the application of MRI relaxometry to potato tuber tissues were used as input variables in statistical analysis performed with Statgraphics Centurion XVII data mining software (statpoint Technologies, Inc., Warrenton, VA, USA). The Student t-test or one-way analysis of variance (ANOVA) were used to determine whether there were any statistically significant differences between the means of independent groups at a 95% confidence level. The Mann–Whitney test or Kruskal–Wallis test were used as non-parametric alternatives to the Student t-test and ANOVA, respectively, whenever the normal distribution of residuals was not observed. Principal component analysis (PCA) was also used as a non-targeted exploratory analysis to predict the effects of water regime, tissue type and growth stage.

#### 5. Conclusions

In the present study, tuber growth was investigated using MRI relaxometry and biochemical parameters, with particular attention paid to the main tissues of the tuber, i.e., the cortex, the flesh and the pith. The study also characterized the differential effect of water regime on the particular composition and growth kinetics of each tissue type. The results indicate that, during the period of tuber enlargement, no major changes specific to tissue type occurred in the biochemical composition of the flesh or cortex. The small number of variations observed were mainly due to the dilution effect of starch accumulation. Nevertheless, variations in the organic compounds made it possible to reveal different patterns in the metabolism of the two tissues that probably relate to the continuous active growing of the flesh. Water deficit affected only the size of the tubers, having no impact on overall tissue functioning, the only exception being the myo-inositol metabolism. On the T2-weighted MRI images, the cortex and the pith appeared clearly as homogeneous regions, whereas the flesh was characterized by a relatively heterogeneous signal. Both T2 values and relative signal intensity allowed distinctions to be made between the pith and the cortex, whereas the flesh could be differentiated from the other two tissue types only through the relative signal intensity. The present study observed no significant changes in T2 at any stage of tuber development. This difference from recorded observations of T2 in fruit is consistent with the specific growth pattern of tubers, consisting in cell proliferation rather than in the increase of final cell size in fruit. In future studies, it could be useful to apply a post-processing scheme that clusters similar voxels according to the multi-exponential relaxation parameters, in order to better discriminate between the tissues [45]. Although MRI relaxation parameters have been shown to act as biomarkers for tuber tissue types and stress response, their interpretation in terms of tissue structure and composition could be further improved via microscopic analysis.

**Supplementary Materials:** The following supporting information can be downloaded at: <https://www.mdpi.com/article/10.3390/plants11151918/s1>. Supplementary Figure S1. A. Multi-spin-echo MRI images (echo time = 130 ms, repetition time = 10 s,  $0.8 \times 0.8 \times 5$  mm<sup>3</sup> voxel) of potato tubers at 60 days after shoot emergence (DASE). B. Masks of the three different tissues (cortex, pith, flesh) obtained by means of an automatic segmentation algorithm developed for transverse relaxation time (T2) computation. C. The three different regions obtained following segmentation according to T2: cortex (red), flesh (blue) and pith (green).; Supplementary Figure S2. T2 decay curves generated from the computation of the mean signal in selected tuber tissue regions of interest (A. Cortex, B. Flesh, C. Pith) from all Mutli-Spin Echo sequence images. Values corresponding to a signal-to-noise ratio lower than 7 were removed from the T2 curves before fitting according to the Levenberg-Marquardt algorithm using TableCurve software. Optimal fitting was reached using a bi-exponential model.; Supplementary Figure S3. Principal component analysis (PCA) score plot derived from data obtained from MRI relaxometry and physiological measurements of potato tuber tissues using principal components 1 (PC1) and 2 (PC2). Sample scores are differentiated by colour and symbol to indicate sample classification according to tissue type. Continuous lines shown on the score plot represent the ellipsis of confidence at 95% for each group.; Supplementary Figure S4: Optical micrographs obtained using a Nikon Eclipse 80i of a 1 mm-thick slice of potato tissue of the cortex (a and b), the

perimedullary region (c and d) and the pith (e and f) of the potato tuber. The tissue was washed with water to remove all excess starch.; Supplementary Figure S5. A. Arrangement of potato tubers on a rectangular tray designed for insertion in a box placed in the temperature-regulating device installed inside an RF coil for transverse relaxation time measurements by MRI. B. Redox-potential measurement of tissue from the cross section of a potato tuber. C. Separation of tissues in a potato slice for metabolite analysis.

**Author Contributions:** Conceptualization, L.B.-V., G.J., C.D., L.L. and M.M.; methodology, G.H., S.Q., S.C., L.B.-V. and C.L.; software, G.H., S.Q., S.C. and C.L.; validation, G.H., L.B.-V., C.D., L.L. and M.M.; formal analysis, G.H., S.Q., S.C., L.B.-V., C.D., L.L. and M.M.; investigation, G.H., S.Q., S.C., L.B.-V., G.J., C.L., C.D., L.L. and M.M.; resources, G.H., S.Q., S.C., L.B.-V., G.J., C.L., C.D., L.L. and M.M.; data curation, G.H., S.Q., S.C. and L.B.-V.; writing—original draft preparation, G.H., L.B.-V., G.J., C.D., L.L. and M.M.; writing—review and editing, G.H., L.L. and M.M.; visualization, G.H., L.L. and M.M.; supervision, L.L. and M.M.; project administration, G.J., L.L. and M.M.; funding acquisition, G.J., L.L. and M.M. All authors have read and agreed to the published version of the manuscript.

**Funding:** This work is part of the Tuberbioscan research project financed by the Brittany region and FEDER as part of the Innovation collaborative au croisement des filières program.

**Institutional Review Board Statement:** Not applicable.

**Informed Consent Statement:** Not applicable.

**Data Availability Statement:** Not applicable.

**Acknowledgments:** Part of this work has been performed using the PRISM core facility (Biogenouest, Univ Rennes, Univ Angers, INRAE, CNRS, FRANCE). We would like to thank Jérémy Pépin from OPAALE for his participation in MRI experiments and Patrick Leconte from IGEPP for providing the pot-grown potato tubers analyzed in this study. We also thank the IGEPP greenhouse team for the set-up of greenhouse facilities. Thanks also go to Solenne Berardocco from the P2M2 platform (IGEPP) for the metabolite analysis and to Doriane Bancel from the PSH research unit (INRAE) for the starch analysis.

**Conflicts of Interest:** The authors declare no conflict of interest.

## References

- Li, L.; Paulo, M.-J.; Strahwald, J.; Lübeck, J.; Hofferbert, H.-R.; Take, E.; Junghans, H.; Wunder, J.; Draffehn, A.; van Eeuwijk, F.; et al. Natural DNA variation at candidate loci is associated with potato chip color, tuber starch content, yield and starch yield. *Theor. Appl. Genet.* **2008**, *116*, 1167–1181. [[CrossRef](#)] [[PubMed](#)]
- Xu, X.; Vreugdenhil, D.; van Lammeren, A.A. Cell division and cell enlargement during potato tuber formation. *J. Exp. Bot.* **1998**, *49*, 573–582. [[CrossRef](#)]
- Reeve, R.M.; Timm, H.; Weaver, M.L. Parenchyma cell growth in potato tubers II. Cell divisions vs. cell enlargement. *Am. Potato J.* **1973**, *50*, 71–78. [[CrossRef](#)]
- Tauberger, E.; Hoffmann-Benning, S.; Fleischer-Notter, H.; Willmitzer, L.; Fisahn, J. Impact of invertase overexpression on cell size, starch granule formation and cell wall properties during tuber development in potatoes with modified carbon allocation patterns. *J. Exp. Bot.* **1999**, *50*, 477–486. [[CrossRef](#)]
- Gancarz, M.; Konstankiewicz, K.; Zgórska, K. Cell orientation in potato tuber parenchyma tissue. *Int. Agrophys.* **2014**, *28*, 15–22. [[CrossRef](#)]
- Viola, R.; Roberts, A.G.; Haupt, S.; Gazzani, S.; Hancock, R.D.; Marmioli, N.; Machray, G.C.; Oparka, K.J. Tuberization in Potato Involves a Switch from Apoplastic to Symplastic Phloem Unloading. *Plant Cell* **2001**, *13*, 385–398. [[CrossRef](#)]
- Oey, I.; Faridnia, F.; Leong, S.Y.; Burritt, D.J.; Liu, T. Determination of Pulsed Electric Fields Effects on the Structure of Potato Tubers. In *Handbook of Electroporation*; Miklavčič, D., Ed.; Springer International Publishing: Cham, Switzerland, 2016; pp. 1489–1507.
- Joshi, M.; Fogelman, E.; Belausov, E.; Ginzberg, I. Potato root system development and factors that determine its architecture. *J. Plant Physiol.* **2016**, *205*, 113–123. [[CrossRef](#)]
- Djaman, K.; Irmak, S.; Koudahe, K.; Allen, S. Irrigation Management in Potato (*Solanum tuberosum* L.) Production: A Review. *Sustainability* **2021**, *13*, 1504. [[CrossRef](#)]
- Kashyap, P.; Panda, R. Effect of irrigation scheduling on potato crop parameters under water stressed conditions. *Agric. Water Manag.* **2003**, *59*, 49–66. [[CrossRef](#)]
- Hajjar, G.; Quellec, S.; Pépin, J.; Challos, S.; Joly, G.; Deleu, C.; Lepout, L.; Musse, M. MRI investigation of internal defects in potato tubers with particular attention to rust spots induced by water stress. *Postharvest Biol. Technol.* **2021**, *180*, 111600. [[CrossRef](#)]
- Herremans, E.; Verboven, P.; Bongaers, E.; Estrade, P.; Verlinden, B.E.; Wevers, M.; Hertog, M.L.A.T.M.; Nicolai, B.M. Characterisation of ‘Braeburn’ browning disorder by means of X-ray micro-CT. *Postharvest Biol. Technol.* **2013**, *75*, 114–124. [[CrossRef](#)]

13. Van As, H. Intact plant MRI for the study of cell water relations, membrane permeability, cell-to-cell and long distance water transport. *J. Exp. Bot.* **2006**, *58*, 743–756. [[CrossRef](#)] [[PubMed](#)]
14. Van der Weerd, L.; Claessens, M.M.; Ruttink, T.; Vergeldt, F.J.; Schaafsma, T.J.; Van As, H. Quantitative NMR microscopy of osmotic stress responses in maize and pearl millet. *J. Exp. Bot.* **2001**, *52*, 2333–2343. [[CrossRef](#)] [[PubMed](#)]
15. Musse, M.; Bidault, K.; Quelled, S.; Brunel, B.; Collewet, G.; Cambert, M.; Bertin, N. Spatial and temporal evolution of quantitative magnetic resonance imaging parameters of peach and apple fruit—relationship with biophysical and metabolic traits. *Plant J.* **2020**, *105*, 62–78. [[CrossRef](#)]
16. Hills, B.P.; Nott, K.P. NMR studies of water compartmentation in carrot parenchyma tissue during drying and freezing. *Appl. Magn. Reson.* **1999**, *17*, 521–535. [[CrossRef](#)]
17. Thybo, A.; Andersen, H.; Karlsson, A.; Dønstrup, S.; Stødkilde-Jørgensen, H. Low-field NMR relaxation and NMR-imaging as tools in differentiation between potato sample and determination of dry matter content in potatoes. *LWT—Food Sci. Technol.* **2003**, *36*, 315–322. [[CrossRef](#)]
18. Hills, B.; Costa, A.; Marigheto, N.; Wright, K. T 1–T 2 NMR correlation studies of high-pressure-processed starch and potato tissue. *Appl. Magn. Reson.* **2005**, *28*, 13–27. [[CrossRef](#)]
19. Borzenkova, R.A.; Borovkova, M.P. Developmental Patterns of Phytohormone Content in the Cortex and Pith of Potato Tubers as Related to Their Growth and Starch Content. *Russ. J. Plant Physiol.* **2003**, *50*, 119–124. [[CrossRef](#)]
20. Musse, M.; Hajjar, G.; Ali, N.; Billiot, B.; Joly, G.; Pépin, J.; Quelled, S.; Challos, S.; Mariette, F.; Cambert, M.; et al. A global non-invasive methodology for the phenotyping of potato under water deficit conditions using imaging, physiological and molecular tools. *Plant Methods* **2021**, *17*, 81. [[CrossRef](#)]
21. Engels, C.H.; Marschner, H. Allocation of Photosynthate to Individual Tubers of *Solanum tuberosum* L.: I. relationship between tuber growth rate and enzyme activities of the starch metabolism. *J. Exp. Bot.* **1986**, *37*, 1795–1803.
22. Visser, R.G.F.; Vreugdenhil, D.; Hendriks, T.; Jacobsen, E. Gene expression and carbohydrate content during stolon to tuber transition in potatoes (*Solanum tuberosum*). *Physiol. Plant.* **1994**, *90*, 285–292. [[CrossRef](#)]
23. Roitsch, T. Source-sink regulation by sugar and stress. *Curr. Opin. Plant Biol.* **1999**, *2*, 198–206. [[CrossRef](#)]
24. Geigenberger, P.; Reimholz, R.; Geiger, M.; Merlo, L.; Canale, V.; Stitt, M. Regulation of sucrose and starch metabolism in potato tubers in response to short-term water deficit. *Planta* **1997**, *201*, 502–518. [[CrossRef](#)]
25. Geigenberger, P.; Stitt, M. Sucrose synthase catalyses a readily reversible reaction in vivo in developing potato tubers and other plant tissues. *Planta* **1993**, *189*, 329–339. [[CrossRef](#)] [[PubMed](#)]
26. Yildizli, A.; Çevik, S.; Ünyayar, S. Effects of exogenous myo-inositol on leaf water status and oxidative stress of Capsicum annum under drought stress. *Acta Physiol. Plant.* **2018**, *40*, 122. [[CrossRef](#)]
27. Valluru, R.; Van Den Ende, W. Myo-inositol and beyond—Emerging networks under stress. *Plant Sci.* **2011**, *181*, 387–400. [[CrossRef](#)] [[PubMed](#)]
28. Loewus, F.A.; Murthy, P.P.N. myo-Inositol metabolism in plants. *Plant Sci.* **2000**, *150*, 1–19. [[CrossRef](#)]
29. Hockema, B.R.; Etxeberria, E. Metabolic Contributors to Drought-enhanced Accumulation of Sugars and Acids in Oranges. *J. Am. Soc. Hortic. Sci.* **2001**, *126*, 599–605. [[CrossRef](#)]
30. Sorin, C.; Musse, M.; Mariette, F.; Bouchereau, A.; Lepout, L. Assessment of nutrient remobilization through structural changes of palisade and spongy parenchyma in oilseed rape leaves during senescence. *Planta* **2014**, *241*, 333–346. [[CrossRef](#)]
31. Hills, B.; Le Floc'H, G. NMR studies of non-freezing water in cellular plant tissue. *Food Chem.* **1994**, *51*, 331–336. [[CrossRef](#)]
32. Leforestier, R.; Mariette, F.; Musse, M. Impact of chemical exchange on transverse relaxation at low and moderate magnetic field strengths for sugar solutions representative of fruit tissues analyzed by simulation and MRI experiments. *J. Magn. Reson.* **2020**, *322*, 106872. [[CrossRef](#)] [[PubMed](#)]
33. Donker, H.; Van As, H.; Edzes, H.; Jans, A. NMR imaging of white button mushroom (*Agaricus bisporis*) at various magnetic fields. *Magn. Reson. Imaging* **1996**, *14*, 1205–1215. [[CrossRef](#)]
34. Mortensen, M.; Thybo, A.K.; Bertram, H.C.; Andersen, H.; Engelsen, S.B. Cooking Effects on Water Distribution in Potatoes Using Nuclear Magnetic Resonance Relaxation. *J. Agric. Food Chem.* **2005**, *53*, 5976–5981. [[CrossRef](#)] [[PubMed](#)]
35. Winisdorffer, G.; Musse, M.; Quelled, S.; Devaux, M.-F.; Lahaye, M.; Mariette, F. MRI investigation of subcellular water compartmentalization and gas distribution in apples. *Magn. Reson. Imaging* **2015**, *33*, 671–680. [[CrossRef](#)]
36. Raffo, A.; Gianferri, R.; Barbieri, R.; Brosio, E. Ripening of banana fruit monitored by water relaxation and diffusion 1H-NMR measurements. *Food Chem.* **2004**, *89*, 149–158. [[CrossRef](#)]
37. Geya, Y.; Kimura, T.; Fujisaki, H.; Terada, Y.; Kose, K.; Haishi, T.; Gemma, H.; Sekozawa, Y. Longitudinal NMR parameter measurements of Japanese pear fruit during the growing process using a mobile magnetic resonance imaging system. *J. Magn. Reson.* **2013**, *226*, 45–51. [[CrossRef](#)]
38. Earl, H.J. A precise gravimetric method for simulating drought stress in pot experiments. *Crop. Sci.* **2003**, *43*, 1868–1873. [[CrossRef](#)]
39. Adriaensen, H.; Musse, M.; Quelled, S.; Vignaud, A.; Cambert, M.; Mariette, F. MSE-MRI sequence optimisation for measurement of bi- and tri-exponential T2 relaxation in a phantom and fruit. *Magn. Reson. Imaging* **2013**, *31*, 1677–1689. [[CrossRef](#)]
40. Otsu, N. A threshold selection method from gray-level histograms. *IEEE Trans. Syst. Man Cybern.* **1979**, *9*, 62–66. [[CrossRef](#)]
41. Kapur, J.N.; Sahoo, P.K.; Wong, A.K.C. A new method for gray-level picture thresholding using the entropy of the histogram. *Comput. Vis. Graph. Image Process.* **1985**, *29*, 273–285. [[CrossRef](#)]

42. Thouvenot, L.; Deleu, C.; Berardocco, S.; Haury, J.; Thiébaud, G. Characterization of the salt stress vulnerability of three invasive freshwater plant species using a metabolic profiling approach. *J. Plant Physiol.* **2015**, *175*, 113–121. [[CrossRef](#)] [[PubMed](#)]
43. Gomez, L.; Bancel, D.; Rubio, E.; Vercambre, G. The microplate reader: An efficient tool for the separate enzymatic analysis of sugars in plant tissues-validation of a micro-method. *J. Sci. Food Agric.* **2007**, *87*, 1893–1905. [[CrossRef](#)]
44. Husson, O.; Husson, B.; Brunet, A.; Babre, D.; Alary, K.; Sarthou, J.-P.; Charpentier, H.; Durand, M.; Benada, J.; Henry, M. Practical improvements in soil redox potential (Eh) measurement for characterisation of soil properties. Application for comparison of conventional and conservation agriculture cropping systems. *Anal. Chim. Acta* **2016**, *906*, 98–109. [[CrossRef](#)] [[PubMed](#)]
45. Collewet, G.; Musse, M.; El Hajj, C.; Moussaoui, S. Multi-exponential MRI T2 maps: A tool to classify and characterize fruit tissues. *Magn. Reson. Imaging* **2021**, *87*, 119–132. [[CrossRef](#)]



## Article

# Effect of Melatonin in Broccoli Postharvest and Possible Melatonin Ingestion Level

Antonio Cano, Manuela Giraldo-Acosta, Sara García-Sánchez, Josefa Hernández-Ruiz and Marino B. Arnao \*

Phytohormones and Plant Development Lab, Department of Plant Biology (Plant Physiology), University of Murcia, 30100 Murcia, Spain; aclario@um.es (A.C.); manuela.giraldo@um.es (M.G.-A.); sara.garcias@um.es (S.G.-S.); jhruiz@um.es (J.H.-R.)

\* Correspondence: marino@um.es

**Abstract:** The post-harvest stage of broccoli production requires cold storage to obtain enough days of shelf life. It has been proved that melatonin is useful as a post-harvest agent in fruits and vegetables, including broccoli. In this study, the broccoli heads treated with melatonin have a longer shelf life than the control samples, which was reflected in parameters such as fresh weight, hue angle (expresses color quality), and chlorophyll and carotenoid contents. Treatments with 100  $\mu$ M melatonin for 15 or 30 min seem to be the most appropriate, extending the broccoli's shelf life to almost 42 days, when it is normally around 4 weeks. In addition, a study on the possible impact that melatonin treatments in broccoli could have on melatonin intake in humans is presented. The levels of superficial melatonin, called washing or residual melatonin, are measured, showing the possible incidence in estimated blood melatonin levels. Our results suggest that post-harvest treatments with melatonin do not have to be a handicap from a nutritional point of view, but more research is needed.

**Keywords:** broccoli; human nutrition; improved health; melatonin; postharvest; vegetables

**Citation:** Cano, A.; Giraldo-Acosta, M.; García-Sánchez, S.; Hernández-Ruiz, J.; B. Arnao, M. Effect of Melatonin in Broccoli Postharvest and Possible Melatonin Ingestion Level. *Plants* **2022**, *11*, 2000. <https://doi.org/10.3390/plants11152000>

Academic Editors: Milan S. Stankovic, Paula Baptista and Petronia Carillo

Received: 17 July 2022  
Accepted: 29 July 2022  
Published: 31 July 2022

**Publisher's Note:** MDPI stays neutral with regard to jurisdictional claims in published maps and institutional affiliations.



**Copyright:** © 2022 by the authors. Licensee MDPI, Basel, Switzerland. This article is an open access article distributed under the terms and conditions of the Creative Commons Attribution (CC BY) license (<https://creativecommons.org/licenses/by/4.0/>).

## 1. Introduction

Increasing the consumption of fruit and vegetables is a key component in a healthy diet to reduce diseases [1,2]. The cruciferous vegetables have shown an important inverse correlation between their intake and oncogenic and cardiovascular diseases [3,4]. Broccoli is a common component of the human diet that has recently seen a growth in demand and increased consumption due to its high nutritional values. Broccoli is easily perishable during the post-harvest period, and its visual and sensory quality is significantly reduced, the loss of sepal greenness accompanied by yellowing being the most visible sign of deterioration. This phenomenon is a major limitation to the post-harvest storage and transportation of broccoli [5]. The green/blue color is the main important commercial quality index in broccoli, due to chlorophyll degradation which is the first visible symptom of senescence [6].

Melatonin (*N*-acetyl-5-methoxytryptamine) is an indolic compound derived from tryptophan discovered in cows [7,8], which plays a role as a hormone in vertebrates. Numerous roles have been proposed for melatonin in mammals, such as the regulator of sleep cycles [9], sexual behavior [10], endocrine rhythms [11–13], amongst others. More recently, its implications have been shown in glucose metabolism and insulin [14–16], as a sensitizer in anti-oncogenic therapies [17], its positive effects in Parkinson's and Alzheimer's diseases [18], and its therapeutic efficiency in COVID-19 treatment [19–21].

In plants, melatonin (phytomelatonin) was identified in 1995 [22–24]. Since then, a variety of studies have been carried out to understand the role that melatonin plays in plant physiology [25–27]. Practically all of the responses in plants have been shown to be modulated by melatonin, which improves processes such as germination, growth,

flowering, etc. [28–31], but the most important action of melatonin is as a mediator in stress situations [32–36].

There is evidence that suggests an important role for melatonin in the regulation of both the biochemical and physiological aspects of postharvest [28,30,37,38]. Concerning broccoli postharvest, melatonin treatment could be an effective technique to improve the quality of fresh-cut broccoli during cold storage [5,39–43]. A recent review on the role of melatonin in broccoli and other Brassicaceae can be consulted [44].

This paper presents a study on the ability of melatonin to improve the conservation of broccoli, both at room temperature and under cold commercial conditions. The changes in weight loss, color and chlorophyll, and carotenoid contents were studied, and, as a novelty, the contents of melatonin (endogenous and exogenous) produced in treated broccoli and its possible impact on human health.

## 2. Material and Methods

### 2.1. Chemicals

The solvents (ethanol, acetone, acetonitrile, and ethyl acetate) and reagents used were from Sigma-Aldrich Co. (Madrid, Spain). Milli-Q system (Milli-Q Corp, Merck KGaA, Darmstadt, Germany) ultra-pure water was used.

### 2.2. Plant Material

The broccoli (*Brassica oleracea* L. var. *italica*, cv. *Parthenon*) was harvested at commercial maturity by a horticultural company in Lorca (37°40′16.28″ N; 1°42′6.12″ W) from the region of Murcia (Murcia, Spain). The harvested samples were placed in polystyrene boxes with ice to avoid bruising and hold moisture. The broccoli heads were transported to our laboratory where pieces of uniform size and color and without apparent disease or injuries were randomly selected for the experiments or treatments.

### 2.3. Broccoli Head Treatments

The broccoli heads were immersed in 0 (distilled water as the control for 30 min), 50 and 100 µM melatonin water-solutions for 15 min and 30 min. The heads were then removed and air-dried for 30 min. All of the procedures were performed at room temperature. Afterward, each head was wrapped in transparent plastic film and stored at 5 °C and 75% relative humidity for 42 days in the dark. In addition, a preliminary study at 20 °C for 7 days with broccoli heads and florets was completed. Each treatment was made three times. The sampling was performed every 7 days to determine weight loss, color, chlorophyll, carotenoid, and phytomelatonin content. The broccoli florets were obtained from heads, and they were immediately frozen in liquid nitrogen and stored at −80 °C for later analysis of chlorophyll, carotenoid, and melatonin contents.

### 2.4. Weight Loss

The weight loss of the broccoli heads was calculated as the percentage change relative to the initial weight using the following formula: weight loss (%) =  $(IW - FW)/IW \times 100$ ; where IW is the initial weight and FW is the weight on a certain day after storage.

### 2.5. Color

The color parameters of the broccoli heads were measured at four points over the surface of each piece with an automatic colorimeter PCE-XXM 20, (PCE Instruments, Tobarra, Spain), calibrated following the instructions. The values determined were L\* (changes in L\* indicate lightness of plant tissues), and the hue angle (main color quality marker), which was calculated as  $H = 180^\circ + \tan^{-1}(b^*/a^*)$  when  $a^* < 0$  and  $b^* > 0$  [45].

### 2.6. Determination of Chlorophyll and Carotenoid Contents

The changes in the chlorophyll and carotenoid levels were determined according to Lichtenthaler (1987). Briefly, 0.3 g of the frozen powdered broccoli florets (the most

superficial tissue of the broccoli heads) were placed in a glass tube with absolute ethanol and then incubated at 100 °C for 30 min (until the tissues were colorless). During the extraction, hot ethanol was refilled when needed. The final volume of extraction was adjusted to 10 mL. The absorbance of the supernatant was measured at 470, 649, and 665 nm to determine chlorophyll a, b, and total, and total carotenoid contents. All of the procedures were performed under diffused light.

### 2.7. Determination of Residual and Endogenous Melatonin

In order to know how the exogenously applied melatonin is distributed in the broccoli heads during the different treatments, the content of the residual melatonin on the surface and the content of the melatonin absorbed by the tissue (endogenous melatonin) were determined. Three broccoli heads were treated with 0 (control) and 100 µM melatonin at two immersion times (15 and 30 min). After drying in the air, the entire surface of the broccoli head was washed homogeneously with 200 mL of ethanol:water (50:50) and drained for 10 min. The final volume collected (ethanol:water washes) was determined and kept in the dark at 5 °C until the analysis of the melatonin content. In addition, after the ethanol:water washes, all of the florets of each broccoli head were crushed to determine the content of endogenous melatonin. The determination of the residual and endogenous melatonin content was carried out by LC with fluorescence detection.

The melatonin was measured by liquid chromatography with fluorescence detection (LC-FLUO) [46]. Briefly, the crushed florets (0.2 g) were mixed with ethyl acetate (4 mL) and shaken overnight (15 h) in the dark. The samples were filtered, and the solvent was evaporated to dryness under vacuum using a SpeedVac (ThermoSavant SPD11V, Thermo-Fisher Sci, Waltham, MA, USA) coupled to a refrigerated RCT400 vapor trap. The dry residue was redissolved in acetonitrile (1 mL), filtered (0.2 µm), and analyzed. A Jasco liquid chromatograph Serie-2000 (Tokyo, Japan) equipped with an online degasser, quaternary pump, autosampler, thermostatted column, and a Jasco FP-2020-Plus fluorescence detector were used to analyze the melatonin content. A Waters XBridge C18-S5 column (2.1 mm × 100 mm) thermostatted at 36 °C was used. The mobile phase consisted of water:acetonitrile (80:20) at an isocratic flow rate of 0.5 mL/min. The fluorescence detector was programmed with an excitation value of 280 nm and 350 nm of emission. The data were analyzed using the JascoChromNAV v.1.09.03 Data System Software (Tokyo, Japan). The melatonin identification was carried out by comparing the excitation and emission spectra of standard melatonin with the corresponding peak of melatonin in the samples. The melatonin quantification was determined using a standard curve and the data were expressed as ng residual melatonin/broccoli head or as ng melatonin/g FW.

### 2.8. Graphic and Statistical Analysis

The graphical analysis of the data was made using SigmaPlot program version 14 (SYSTAT Software Inc., San José, CA, USA). Analysis of variance was performed using IBM SPSS Statistics 22.0 (IBM, New York, NY, USA). The statistical significance was considered for *p*-values less than 0.05 in ANOVA and a post-hoc with the Tukey HSD test.

## 3. Results and Discussion

### 3.1. Effect on Color Parameters of Broccoli Intact (Heads) and Florets Treated with Melatonin and Stored at 20 °C

A preliminary study was carried out on the broccoli heads (intact) and florets (about 7 cm high and 28 g weight) at a storage temperature of 20 °C, since at this temperature the physiological changes occur more quickly. The following melatonin concentrations were applied: 0 (control), 50, 100, 200, and 500 µM in the broccoli florets, and in the broccoli heads at 0, 50, and 100 µM melatonin, and at a fixed immersion time of 30 min. In all of the cases, they were left to air dry and wrapped in a plastic film. They were left in a culture chamber, at a controlled temperature in the dark; the color was measured before treatment and after 7 days of storage.

The results obtained in the color measurements on the broccoli florets stored at 20 °C are shown in Figure 1. The initial value of  $L^*$  on day 0 gave a mean value of 47.8. After 7 days, a slight increase is observed for all of the concentrations of the melatonin-tested broccoli, but the highest increase is observed in the control ( $L^* = 54.0$ ); this turns out to be 6.95% higher (1.07 times) compared to the mean of the  $L^*$  values of all of the broccoli florets treated with melatonin ( $L^* = 50.48$ ) (Figure 1A). The  $L^*$  parameter indicates the brightness or luminosity of the broccoli surface. Generally, it is desirable that it remains constant.

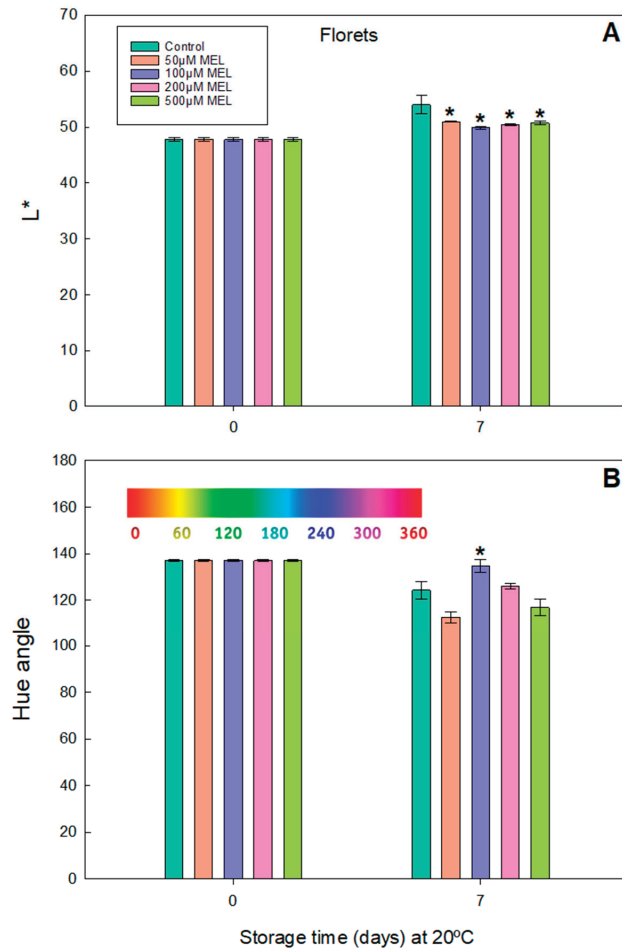


**Figure 1.** Color parameters in broccoli florets stored at 20 °C. (A) Luminosity ( $L^*$ ) and (B) Hue angle of broccoli florets treated with 50, 100, 200 and 500 µM of melatonin and stored in the dark at 20 °C for 0 and 7 days. Each bar represents the mean value  $\pm$  standard error ( $n = 3$ ) obtained for each concentration used. Asterisks indicate significant differences with the control of that day based on a Tukey HSD test with a significance level of  $p < 0.05$ . In (B), the Hue angle scale has been incorporated as a color guide.

The initial reading of the mean value of the hue angle (H) was 137.02 for all of the florets analyzed, observing a general decrease after 7 days (Figure 1B). The hue angle indicates the color changes, according to the equation presented in Section 2, using as a reference the color bar that appears in Figure 1. These results indicated that the green/blue color of the florets was lost at 20 °C after 7 days of storage. However, when analyzed by treatment on 7th day, it is observed that 100 µM MEL preserved a better green/blue color

( $H = 134.67$ ) and followed by 200  $\mu\text{M}$  MEL ( $H = 125.94$ ) relative to the control ( $H = 124.24$ ) after 7 days. The largest drops in the hue value were observed for the MEL 50 and 500  $\mu\text{M}$  treatments ( $H$  value was 112.50 and 116.75, respectively).

In the intact broccoli heads, the changes in the color parameters in the control and melatonin treatments are shown in Figure 2. The initial value of  $L^*$  on day 0 was 49.62. After 7 days, a significant increase for 50  $\mu\text{M}$  MEL ( $L^* = 59.21$ ) concerning the control ( $L = 51.62$ ) was measured, and a practically maintained value in 100  $\mu\text{M}$  of MEL ( $L = 49.77$ ) (Figure 2A).

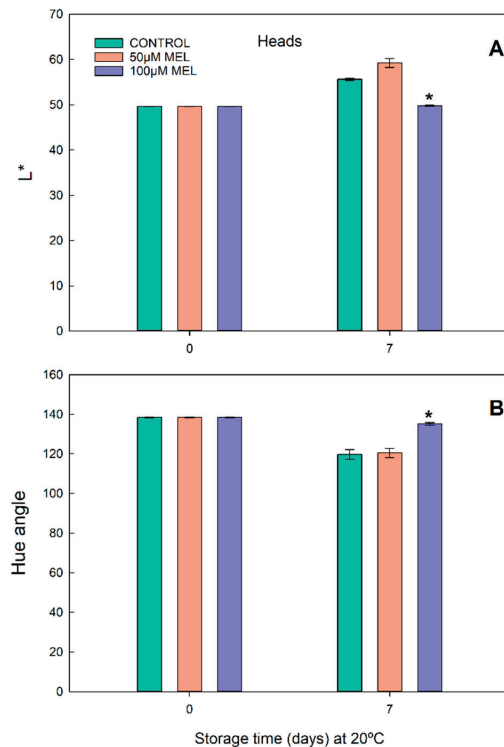


**Figure 2.** Color parameters in broccoli heads stored at 20 °C. (A) Luminosity ( $L^*$ ) and (B) Hue angle of broccoli heads treated with 50 and 100  $\mu\text{M}$  of melatonin and stored in the dark at 20 °C for 0 and 7 days. Each bar represents the mean value  $\pm$  standard error ( $n = 3$ ) obtained for each concentration used. Asterisks indicate significant differences with the control of that day based on a Tukey HSD test with a significance level of  $p < 0.05$ .

Regarding hue angle ( $H$ ) in the broccoli heads (Figure 2B), a general decrease was observed after 7 days (control,  $H = 119.70$  and 50  $\mu\text{M}$  MEL,  $H = 120.46$ ) vs. day 0 ( $H = 138.49$ ), with a very slight increase for 100  $\mu\text{M}$  MEL ( $H = 135.15$ ) in respect to the control of day 7. The  $H$  data pointed to better maintenance of the color after 7 days at 20 °C for 100  $\mu\text{M}$  MEL.

### 3.2. Effect on Weight Loss, Color, and Photosynthetic Pigment Contents of Broccoli Heads Treated with Melatonin over Storage Time at 5 °C

Based on the preliminary results obtained at 20 °C and 30 min of immersion with melatonin, it was decided to carry out a study of the effects of cold storage (5 °C) in melatonin-treated broccoli. For this purpose, 100  $\mu\text{M}$  MEL was selected since, at 20 °C, it produced a significant delay in the loss of color compared to the control and the other melatonin concentrations applied (Figures 1 and 2). On the other hand, it was proposed

to study the relevance of the immersion time, and to observe if a time less than 30 min could improve the melatonin effect, because timing can be an important parameter in the vegetable packaging industry.

The weight loss of the broccoli heads during storage at 5 °C were determined, because water loss is one of the main issues during broccoli storage, causing stalk hardening and bud-cluster turgidity loss [47,48]. As can be seen in Figure 3, the weight loss was always greater in the control samples than in the melatonin-treated samples, throughout all of the measured days. Regarding the different melatonin treatments, it was observed that melatonin, in all of the cases tested, acted by delaying water loss, which is related to its participation in the closing/opening of the stomata [49]. Of all of the treatments, the 100 µM MEL applied for 15 min was the most effective, since it reduced water loss by 6% compared to the control, while the rest of the treatments did not show significant differences between them (Figure 3).

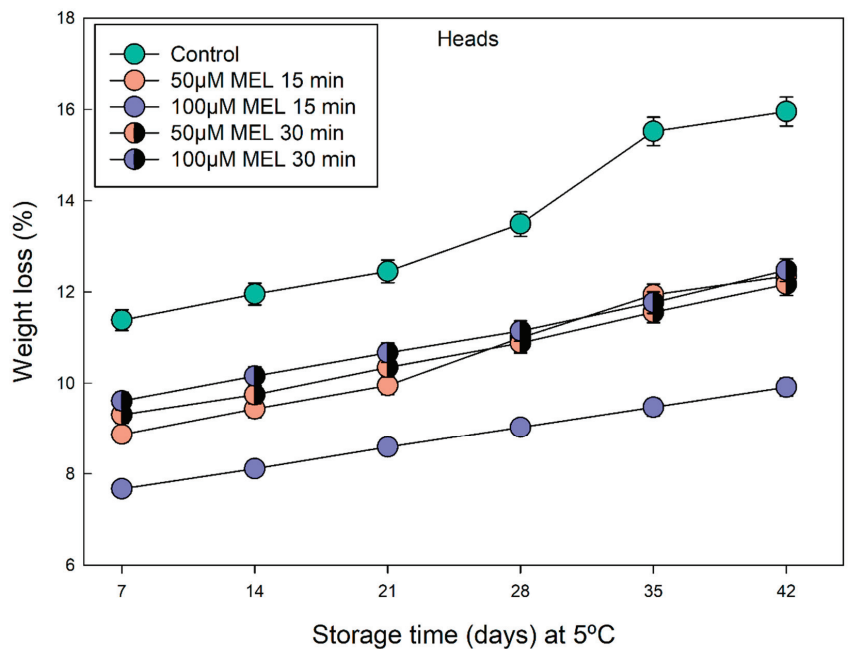


**Figure 3.** Weight loss of broccoli heads treated with 50 and 100 µM of melatonin during 15 and 30 min and stored in the dark at 5 °C for 0, 7, 14, 21, 28, 35 and 42 days. Each point represents the mean value and  $\pm$  standard error ( $n = 3$ ) obtained for each concentration used.

Variations in the visual quality during the broccoli yellowing were measured through the parameters  $L^*$  and hue angle (H) (Figure 4). The  $L^*$  values in both the control and the melatonin-treated broccoli heads increased gradually during storage at 5 °C. The melatonin-treated heads showed a slightly lower rate of increase in the  $L^*$  value than the control heads, at 28, 35, and 42 days, being statistically similar for all of the melatonin concentrations and immersion times tested (Figure 4A).

The initial H value was 132.13 (day 0), remaining more or less constant during the 5 °C storage until days 35 and 42, where the control presented a significant drop, reaching an H value of 124.59. However, the treatments with melatonin for both of the immersion times (15 and 30 min) delayed this drop, with a H value of 132.78 (Figure 4B), in 35 days. After 42 days, only the melatonin treatments of 15 min could maintain the color, showing a mean H value of 133.27. These results indicate that the color of the heads, stored at 5 °C, was gradually lost and that the melatonin delays it; this indicated that a treatment with

melatonin would increase the shelf life of the broccoli beyond 21 days, and may even reach 42 days of storage with acceptable color.

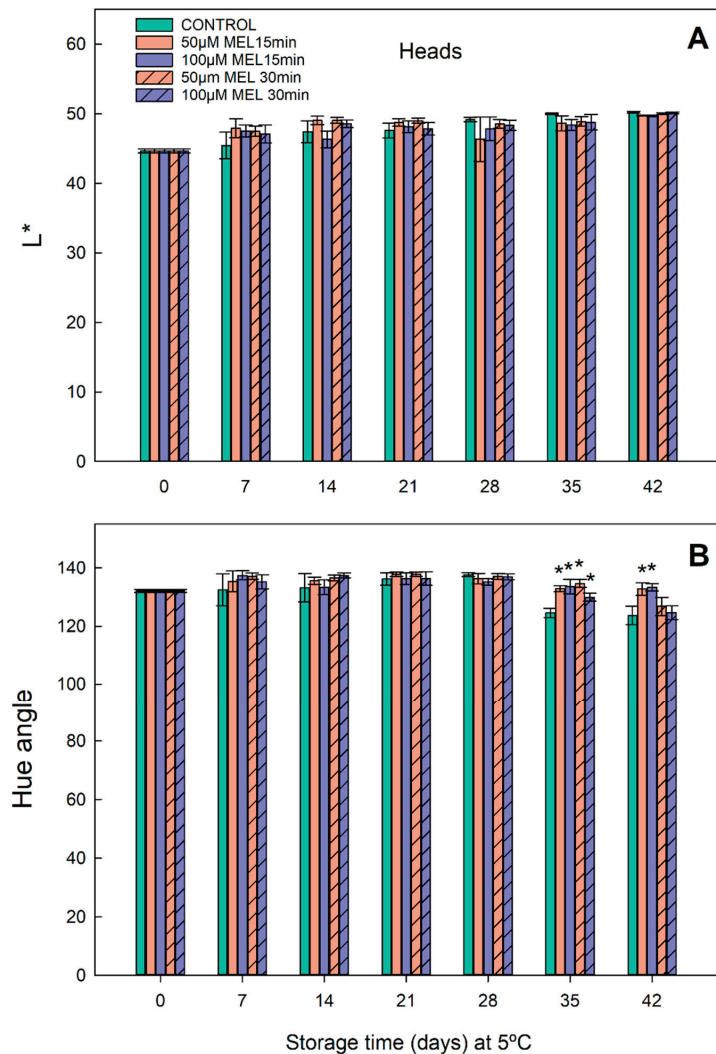


**Figure 4.** Color parameters in broccoli heads stored at 5 °C. (A) Luminosity ( $L^*$ ) and (B) Hue angle of broccoli heads treated with 50 and 100  $\mu\text{M}$  of melatonin during 15 and 30 min and stored in the dark, at 5 °C, for 0, 7, 14, 21, 28, 35 and 42 days. Each bar represents the mean value  $\pm$  standard error ( $n = 3$ ) obtained for each concentration used. Asterisks indicate significant differences with the control of that day based on a Tukey HSD test with a significance level of  $p < 0.05$ .

In order to search for a correlation between the color parameters and chlorophyll and carotenoid contents, these were determined in the melatonin-treated broccoli throughout the cold storage time. A net symptom of senescence in the broccoli heads is the loss of green/blue color or yellowing mainly due to the catabolism of chlorophylls. Based on the results obtained from the evaluation of the color (Figure 4), the pigment contents in the 100  $\mu\text{M}$  melatonin-treated samples for 15 and 30 min were determined.

The total chlorophyll content showed a decrease in both the treated and the control samples, indicating postharvest senescence (Figure 5A). However, in the case of the

melatonin-treated heads, the loss of chlorophyll appears clearly attenuated compared to the control. Moreover, especially from day 28 to the last day of storage, the total chlorophyll values were higher than those of the control. In addition, on day 42 of storage, the 15 min immersion treatment of 100  $\mu$ M MEL resulted in a total chlorophyll value of 0.42 mg/g FW, being 0.23 mg/g FW for the control, that is, approximately twice the chlorophyll content.

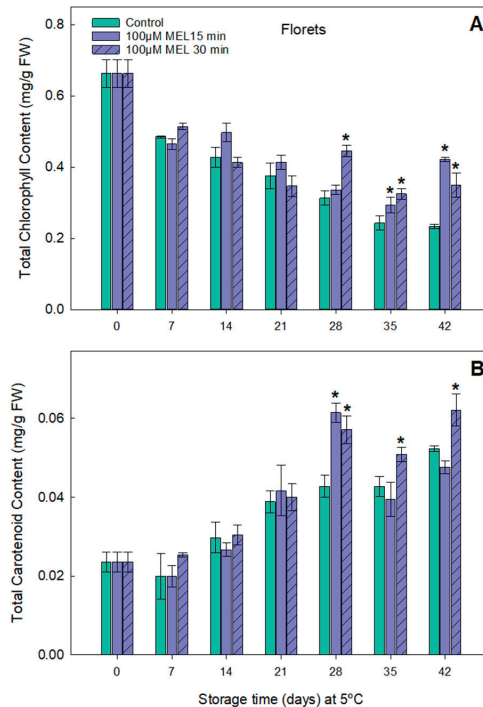


**Figure 5.** Effect on total content of chlorophylls (A) and carotenoids (B) in broccoli treated with 100  $\mu$ M of melatonin during 15 and 30 min and stored in the dark, at 5  $^{\circ}$ C, for 0, 7, 14, 21, 28, 35 and 42 days. Each bar represents the mean value  $\pm$  standard error ( $n = 3$ ) obtained for each concentration used. Asterisks indicate significant differences with the control of that day based on a Tukey HSD test with a significance level of  $p < 0.05$ .

Similarly, the total carotenoid contents remain constant for up to 14 days (Figure 5B). After 21 days of storage, an increase in the carotenoid levels was observed, with a different behavior in the control and the melatonin-treated broccoli heads. In general, and after a significant carotenoid content increase after 21 days, the values in the control remained constant until the last day of the study. In contrast, the melatonin-treated broccoli showed an increase in the carotenoid levels, reaching up to 40% more than the control. Regarding the treatment times tested, higher carotenoid values were obtained on day 42 for the 30-min treatment.

There are several actions to be applied to achieve a longer shelf life of broccoli, preserving its excellent nutritional qualities due to its high contents of several vitamins, highlighting pro-vitamin A, B3, and C, and other substances such as lutein, quercetin, folic acid, glucosinolates, and fiber [50]. The coating of the broccoli in plastic film, the packaging in a tray, or its distribution in bulk are processes that all must go through an adequate cold chain. In some cases, the ethylene absorbers and modified atmospheres have been used with acceptable results [47]. The use of alcohol vapors has also been proposed as an alternative [51]. The artificial preservatives have been used, with poor results. Lately, the use of natural compounds is an ideal strategy, given the EU regulatory constraints. The

use of phyto regulators, such as cytokinins, jasmonates, polyamines, and others, has had very variable results [52,53]. In some cases, the natural preservatives, such as essential oils, have been used, which due to their antimicrobial activity can have some beneficial effects if thermal control is not rigorous [54]. However, the essential oils have the downside of providing undesirable odors and flavors to the fresh product. In addition, generally the cost–benefit balance must be considered, since in most of the cases the treatments are expensive.

Today, the product is usually transported refrigerated in polystyrene boxes containing the heads of broccoli with ice; all of this to ensure a temperature as close to 4 °C, where the broccoli usually maintains its organoleptic qualities [55]. The refrigerated transport is usually carried out in days, achieving good results since the product can have an optimal commercial life of around 25 days. Other studies have suggested that transport conditions of total darkness do not favor its conservation, suggesting that small light treatments can extend the half-life of the product and improve its visual and organoleptic qualities [48]. In other cases, the vibrations due to transport have been shown to cause significant deterioration and a decrease in quality and useful life.

As usual, the temperature is a decisive factor in ensuring the stability in color, appearance, and nutrient contents of broccoli. Thus, a clear difference can be found in conditions of 20 °C and 5 °C for each of the estimated parameters. Generally, the shelf life of the broccoli preserved at 20 °C is about 3–4 days, and can be extended up to almost 5–8 days with melatonin treatments [5,39]. However, in our assays after 7 days at 20 °C, both the luminosity ( $L^*$ ) and the color index (H) were quite well maintained (without increasing  $L^*$  too much and without decreasing H) in the case of the broccoli treated with melatonin (Figures 1 and 2). For other authors, in these conditions, the melatonin treatments significantly prevented the increase in the  $L^*$  value and delayed the decrease in the H index [5,39,40].

When cold storage and melatonin treatments were combined, a significant improvement in the broccoli quality can be determined, even at extended shelf life. At 5 °C, the melatonin-treated broccoli heads with 100  $\mu$ M melatonin preserved considerably the weight loss in the period 7–42 days (Figure 3), indicating that melatonin can regulate open/closed stomata in the broccoli heads as it occurs in the leaves, saving water losses [28,49,56]. Concerning the values of  $L^*$  and H, the melatonin treatments slightly decrease the luminosity of the broccoli heads especially at long times (days 28, 35 and 42) (Figure 4A). The opposite occurs with the color (H index), a significant maintenance of the bluish-green color compared to the respective controls occurs in melatonin treatments on days 35 and 42, (Figure 4B), presenting a significantly less yellowing level.

The chlorophyll and carotenoids are the main items responsible for the broccoli color. Their chlorophyll content losses occur as a habitual senescence process similar to leaves [6]. In the control broccoli heads, the total chlorophyll contents decreased exponentially, reaching a chlorophyll loss of 62% after 42 days of storage at 5 °C (Figure 5A). The melatonin preserved the chlorophyll content in the treated broccoli all of the time, being very significant on days 28, 35, and 42, reaching a chlorophyll content in 42 days similar to the control broccoli after 14 days of conservation, a differential of 4 weeks. This regulatory action of the melatonin on senescence was first described by our group in barley leaves [57]. Subsequently, melatonin was found to have improved the rate of photosynthesis, PSII efficiency, Rubisco activity, the chlorophyll and carotenoid levels, stomatal conductance, and leaf-intercellular CO<sub>2</sub> contents. The Rubisco small subunit (RbcS) and many chlorophyll *a/b* binding-protein transcripts were upregulated by melatonin. Instead, the senescence transcription factor SAG12 and some chlorophyll degradation factors, such as pheophorbide *a* oxygenase (PaO), were downregulated [58,59].

As far as the carotenoid contents are concerned, there was an increase in their levels that appeared from day 21, due to the senescence process. However, in the case of the broccoli treated with melatonin, a greater increase in the carotenoid biosynthesis can be observed (Figure 5B). This carotenoid promoting effect can be explained because

melatonin upregulates the carotenoid biosynthesis genes, thereby increasing the levels of several carotenenes, including  $\alpha$ -,  $\beta$ -carotene, lutein, zeaxanthin, and lycopene, and up-regulating several carotenogenesis genes, such as DXS, DXR, GGPPS, PSY, PDS, ZDS, CRTISO, and CYCB. This action is mediated by ethylene since melatonin also upregulates ethylene biosynthesis enzyme transcripts (ACO and ACS), several ethylene-signal elements (*EIL1*, *EIL3*, and *ERF2*), and ripening factors (*RIN*, *CNR*, and *NOR*), and downregulating *AP2a*, [28,60,61]. As a result, melatonin can prolong the shelf life in numerous fruits, including tomato, strawberry, peach, banana, litchi, plum, grape, pear, and mango [30]. This carotenoid-promoting biosynthesis by melatonin has been also described in microalgae [62].

### 3.3. Residual and Endogenous Melatonin Contents: Implications for Human Consumption

As already mentioned, melatonin is a molecule with numerous beneficial functions for humans. Therefore, it is of interest to know the amount of melatonin that we could ingest in our diet, due to vegetable/fruit post-harvest treatments with melatonin. In the present study, the residual melatonin levels appearing in the melatonin-treated broccoli heads were quantified. Thus, after the melatonin treatments, the broccoli heads were washed with ethanol:water (50:50) and these washing solutions were subjected to the quantification of residual melatonin by LC-FLUO. Other ethanol:water ratios, such as 80:20 and 60:40, showed results very similar to those of 50:50. This is logical since melatonin is an amphoteric molecule with ease of solubilization in aqueous and also organic media. Figure 6A shows the residual melatonin quantifications present in the washing solutions by each broccoli head. As can be seen, a similar amount of residual melatonin can be found in all of the treatments carried out (100  $\mu$ M melatonin-treated samples during 15 and 30 min).

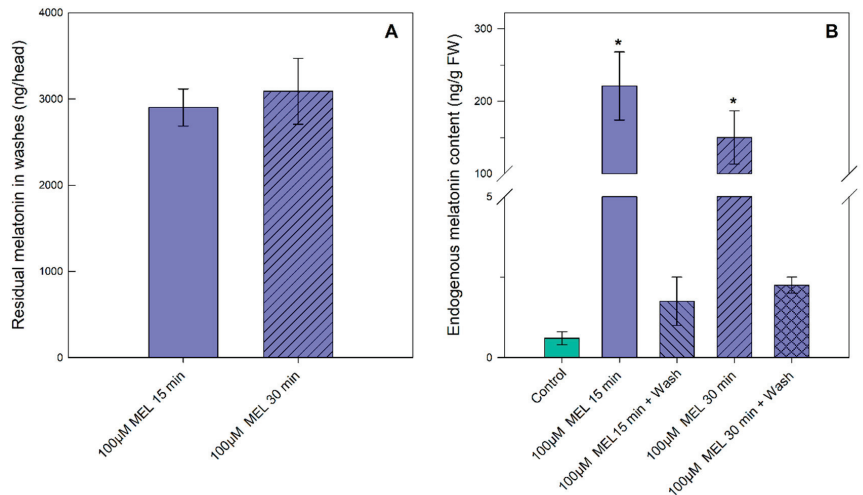


**Figure 6.** Melatonin quantification by LC-FLUO: (A) in the wash solutions of melatonin-treated broccoli heads; (B) endogenous melatonin content of diverse broccoli treated samples. Each bar represents the mean value  $\pm$  standard error ( $n = 3$ ) obtained for each concentration used. Asterisks indicate significant differences between washed and unwashed broccoli heads based on a Tukey HSD test with a significance level of  $p < 0.05$ .

It is also important to know the amount of endogenous melatonin absorbed due to the exogenous treatments. As can be seen in Figure 6B, the values of the endogenous melatonin in the control and the melatonin-treated broccoli after washing were similar, being very low (0.5–2.2 ng/g FW) in all of the cases. In the cases of the broccoli heads treated with melatonin that were not subsequently washed, levels between 150 and 225 ng/g FW were measured (Figure 6B).

Therefore, we can establish that melatonin with the possibility of being ingested is the one that can be removed by washing vegetables, and that we can assess its intake. Figure 7 shows a diagram that helps us to make a quantitative estimation of the possible intake of melatonin present in the treated broccoli. A first possibility is to wash the broccoli before intake. As we have seen in Figure 6B, if the broccoli is washed, all of the superficial melatonin, called washing or residual melatonin, is practically removed. The second possibility would be to eat the melatonin-treated broccoli without washing it. In this case, if we consider a serving size of 76 g (according to FoodData Central of USDA), we could ingest about 570 ng/cup. We consider that approximately 75% of the melatonin that is ingested orally is not absorbed or catabolized in the liver, occurring in feces, mainly through bile. Overall, the pharmacokinetic data of the melatonin pointed to a non-absorption in the gastro-intestinal mucosa and a catabolism of melatonin in the liver around 70–90% of intake, with a half-life of melatonin in blood of 10–30 min [63–68]. Thus, only 25% would reach the bloodstream, or about 142 ng in blood. Considering that the total volume of blood per person ranges between 4.5 and 6 L, an ingested melatonin level of 24–32 pg/mL can be expected; an amount in the usual range for a middle-aged person (see graph in Figure 7) [69–71]. Therefore, in our trials with the broccoli treated with melatonin; its theoretical intake would not alter the usual levels of melatonin in the blood.

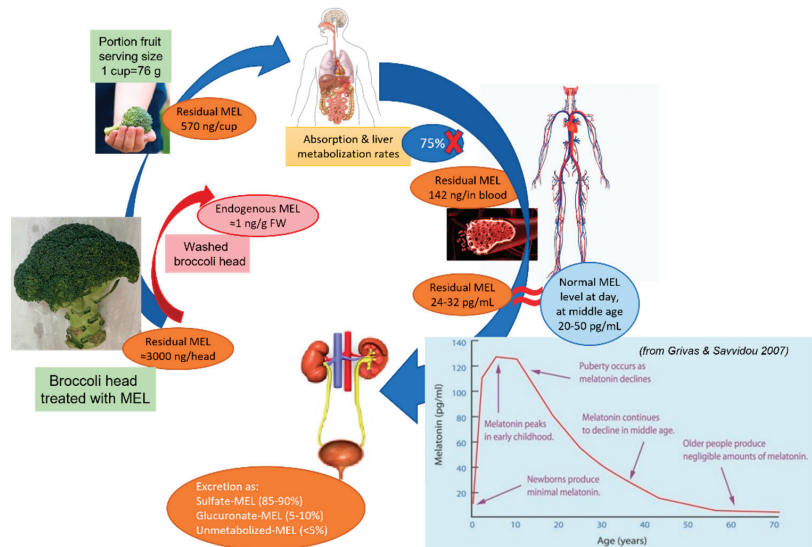


**Figure 7.** Schematic representation of the exogenous melatonin intake of broccoli treated with melatonin and its theoretical evolution in the human body.

In conclusion, the intake and absorption of melatonin after post-harvest treatments should be carefully studied to determine the possible impact on melatonin levels in the diets and subsequently in the blood. Studies so far are controversial, with some pointing to a possible effect of melatonin ingested in fruits on blood levels, while in other cases no such increases are observed [72–79]. In general, there has been criticism on the lack of quantitative correlation between the ingested phytemelatonin and its plasma levels [80]. Therefore, more studies and models are needed on aspects such as the bioavailability of phytemelatonin, its time course of assimilation and degradation, and the possible effects on melatonin release rhythms from the pineal gland [71,81,82].

According to our data, the recommendations for the use of melatonin as a natural agent for post-harvest control of fruits and vegetables point to null or low inference in the usual levels of melatonin in humans, indicating that it does not have to be a handicap from a nutritional point of view, but more research is needed.

**Author Contributions:** A.C., J.H.-R. and M.B.A. contributed to the planning of the main ideas and visualization. S.G.-S., M.G.-A., A.C., J.H.-R. and M.B.A. contributed to experimental works. J.H.-R., A.C. and M.B.A. contributed to the writing of the first draft of the manuscript and final version. All authors have read and agreed to the published version of the manuscript.

**Funding:** This work has been funded through the project of the Ministry of Science and Innovation “R+D+I Projects”, State Program for the Generation of Knowledge and Scientific and Technological Strengthening of the R+D+I System and R+D+I Oriented to the Challenges of Society of the State Plan for Scientific and Technical Research and Innovation 2017–2020, Grant PID2020-113029RB-I00 funded by MCIN/AEI/10.13039/501100011033. More information in: <https://www.um.es/en/web/phytohormones/> (accessed on 17 July 2022) (Phytohormones and Plant Development Lab).

**Institutional Review Board Statement:** Not applicable.

**Informed Consent Statement:** Not applicable.

**Acknowledgments:** The authors would like to thank SACOJE Co. (La Hoya, Lorca, Murcia), for their willingness to provide broccoli samples for our studies. Our sincere thanks to Cristóbal Ruiz Méndez as well for his essential collaboration.

**Conflicts of Interest:** The authors declare that there is no conflict of interest.

## Abbreviations

ACC	1-aminocyclopropane-1-carboxylic acid
ACO	ACC oxidase
ACS	ACC synthase
AP2a	ripening-inhibitor factor
CRTISO	carotene isomerase
CYCB	chromoplast-specific lycopene $\beta$ -cyclase
EIL1, EIL3, and ERF2	ethylene-signal elements and
DXR	1-deoxy-D-xylulose 5-phosphate reductoisomerase
DXS	1-deoxy-D-xylulose 5-phosphate synthase
FW	fresh weight
GGPPS	geranylgeranyl pyrophosphate synthase
H	angle hue (color index)
L*	brightness or luminosity
LC-FLUO	liquid chromatography with fluorescence detection
MEL	melatonin
PaO	chlorophyll degradation factors, such as pheophorbide <i>a</i> oxygenase
PDS	phytoene desaturase
PSY	phytoene synthase
RIN, CNR, and NOR	regulatory ripening factors
SAG12	senescence transcription factor
ZDS	$\zeta$ -carotene desaturase

## References

1. Kushi, L.H.; Doyle, C.; McCullough, M.; Rock, C.L.; Demark-Wahnefried, W.; Bandera, E.V.; Gapstur, S.; Patel, A.V.; Andrews, K.; Gansler, T.; et al. American Cancer Society guidelines on nutrition and physical activity for cancer prevention. *CA Cancer J. Clin.* **2012**, *62*, 30–67. [[CrossRef](#)]
2. Lichtenstein, A.H.; Appel, L.J.; Brands, M.; Carnethon, M.; Daniels, S.; Franch, H.A.; Franklin, B.; Kris-Etherton, P.; Harris, W.S.; Howard, B.; et al. Diet and Lifestyle Recommendations Revision 2006. *Circulation* **2006**, *114*, 82–96. [[CrossRef](#)] [[PubMed](#)]
3. Kirsh, V.A.; Peters, U.; Mayne, S.T.; Subar, A.F.; Chatterjee, N.; Johnson, C.C.; Hayes, R.B. Prospective Study of Fruit and Vegetable Intake and Risk of Prostate Cancer. *JNCI J. Nat. Cancer Inst.* **2007**, *99*, 1200–1209. [[CrossRef](#)]
4. Zhang, X.; Shu, X.-O.; Xiang, Y.-B.; Yang, G.; Li, H.; Gao, J.; Cai, H.; Gao, Y.-T.; Zheng, W. Cruciferous vegetable consumption is associated with a reduced risk of total and cardiovascular disease mortality. *Am. J. Clin. Nutr.* **2011**, *94*, 240–246. [[CrossRef](#)] [[PubMed](#)]
5. Wu, C.; Cao, S.; Xie, K.; Chi, Z.; Wang, J.; Wang, H.; Wei, Y.; Shao, X.; Zhang, C.; Xu, F.; et al. Melatonin delays yellowing of broccoli during storage by regulating chlorophyll catabolism and maintaining chloroplast ultrastructure. *Postharvest Biol. Technol.* **2021**, *172*, 111378. [[CrossRef](#)]

6. Tian, M.S.; Downs, C.G.; Lill, R.E.; King, G.A. A Role for Ethylene in the Yellowing of Broccoli after Harvest. *J. Am. Soc. Hortic. Sci.* **1994**, *119*, 276–281. [[CrossRef](#)]
7. Lerner, A.B.; Case, J.D.; Takahashi, Y.; Lee, T.H.; Mori, W. Isolation of Melatonin, the Pineal Gland Factor That Lightens Melanocytes<sup>1</sup>. *J. Am. Chem. Soc.* **1958**, *80*, 2587. [[CrossRef](#)]
8. Lerner, A.B.; Case, J.D.; Heinzelman, R.V. Structure of Melatonin. *J. Am. Chem. Soc.* **1959**, *81*, 6084–6085. [[CrossRef](#)]
9. Xie, Z.; Chen, F.; Li, W.A.; Geng, X.; Li, C.; Meng, X.; Feng, Y.; Liu, W.; Yu, F. A review of sleep disorders and melatonin. *Neurol. Res.* **2017**, *39*, 559–565. [[CrossRef](#)]
10. Vadnie, C.A.; McClung, C.A. Circadian Rhythm Disturbances in Mood Disorders: Insights into the Role of the Suprachiasmatic Nucleus. *Neural Plast.* **2017**, *2017*, e1504507. [[CrossRef](#)]
11. Blume, C.; Angerer, M.; Raml, M.; del Giudice, R.; Santhi, N.; Pichler, G.; Kunz, A.B.; Scarpatetti, M.; Trinkla, E.; Schabus, M. Healthier rhythm, healthier brain? Integrity of circadian melatonin and temperature rhythms relates to the clinical state of brain-injured patients. *Eur. J. Neurol.* **2019**, *26*, 1051–1059. [[CrossRef](#)]
12. Majidinia, M.; Reiter, R.J.; Shakouri, S.K.; Yousefi, B. The role of melatonin, a multitasking molecule, in retarding the processes of ageing. *Ageing Res. Rev.* **2018**, *47*, 198–213. [[CrossRef](#)]
13. Socaciu, A.I.; Ionut, R.; Socaciu, M.A.; Ungur, A.P.; Bârsan, M.; Chiorean, A.; Socaciu, C.; Răjnovceanu, A.G. Melatonin, an ubiquitous metabolic regulator: Functions, mechanisms and effects on circadian disruption and degenerative diseases. *Rev. Endocr. Metab. Disord.* **2020**, *21*, 465–478. [[CrossRef](#)]
14. Fernández, V.G.; Reiter, R.J.; Agil, A. Melatonin increases brown adipose tissue mass and function in Zucker diabetic fatty rats: Implications for obesity control. *J. Pineal Res.* **2018**, *64*, e12472. [[CrossRef](#)]
15. Lauritzen, E.S.; Kampmann, U.; Pedersen, M.G.B.; Christensen, L.-L.; Jessen, N.; Møller, N.; Støy, J. Three months of melatonin treatment reduces insulin sensitivity in patients with type 2 diabetes—A randomized placebo-controlled crossover trial. *J. Pineal Res.* **2022**, *73*, e12809. [[CrossRef](#)]
16. Santos-Ledo, A.; de Luxán-Delgado, B.; Caballero, B.; Potes, Y.; Rodríguez-González, S.; Boga, J.A.; Coto-Montes, A.; García-Macia, M. Melatonin Ameliorates Autophagy Impairment in a Metabolic Syndrome Model. *Antioxidants* **2021**, *10*, 796. [[CrossRef](#)]
17. Di Bella, G.; Mascia, F.; Gualano, L.; Di Bella, L. Melatonin Anticancer Effects: Review. *Int. J. Mol. Sci.* **2013**, *14*, 2410–2430. [[CrossRef](#)]
18. Alghamdi, B.S. The neuroprotective role of melatonin in neurological disorders. *J. Neurosci. Res.* **2018**, *96*, 1136–1149. [[CrossRef](#)] [[PubMed](#)]
19. Bologna, C.; Madonna, P.; Pone, E. Efficacy of Prolonged-Release Melatonin 2 mg (PRM 2 mg) Prescribed for Insomnia in Hospitalized Patients for COVID-19: A Retrospective Observational Study. *J. Clin. Med.* **2021**, *10*, 5857. [[CrossRef](#)]
20. Okeke, E.S.; Ougofor, M.O.; Nkwoemeka, N.E.; Nweze, E.J.; Okoye, C.O. Phytomelatonin: A potential phytotherapeutic intervention on COVID-19-exposed individuals. *Microbes Infect.* **2022**, *24*, 104886. [[CrossRef](#)]
21. Tan, D.-X.; Reiter, R.J. Melatonin reduces the mortality of severely-infected COVID-19 patients. *Melatonin Res.* **2021**, *4*, 613–616. [[CrossRef](#)]
22. Dubbels, R.; Reiter, R.J.; Klenke, E.; Goebel, A.; Schnakenberg, E.; Ehlers, C.; Schiwara, H.W.; Schloot, W. Melatonin in edible plants identified by radioimmunoassay and by high performance liquid chromatography-mass spectrometry. *J. Pineal Res.* **1995**, *18*, 28–31. [[CrossRef](#)] [[PubMed](#)]
23. Hattori, A.; Migitaka, H.; Iigo, M.; Yamamoto, K.; Ohtani-Kaneko, R.; Hara, M.; Suzuki, T.; Reiter, R.J. Identification of melatonin in plants and its effects on plasma melatonin levels and binding to melatonin receptors in vertebrates. *Biochem. Mol. Biol. Int.* **1995**, *35*, 627–634. [[PubMed](#)]
24. Kolar, J.; Machackova, I.; Illnerova, H.; Prinsen, E.; van Dongen, W.; van Onckelen, H. Melatonin in higher plant determined by radioimmunoassay and liquid chromatography-mass spectrometry. *Biol. Rhythm Res.* **1995**, *26*, 406–409.
25. Arnao, M.B. Phytomelatonin: Discovery, content, and role in plants. *Adv. Bot.* **2014**, *2014*, e815769. [[CrossRef](#)]
26. Arnao, M.B.; Hernández-Ruiz, J. Functions of melatonin in plants: A review. *J. Pineal Res.* **2015**, *59*, 133–150. [[CrossRef](#)]
27. Arnao, M.B.; Hernández-Ruiz, J. Melatonin in its relationship to plant hormones. *Ann. Bot.* **2018**, *121*, 195–207. [[CrossRef](#)]
28. Arnao, M.B.; Cano, A.; Hernández-Ruiz, J. Phytomelatonin: An unexpected molecule with amazing performances in plants. *J. Exp. Bot.* **2022**, erac009. [[CrossRef](#)]
29. Arnao, M.B.; Hernández-Ruiz, J. Melatonin: Plant growth regulator and/or biostimulator during stress? *Trends Plant Sci.* **2014**, *19*, 789–797. [[CrossRef](#)]
30. Arnao, M.B.; Hernández-Ruiz, J. Melatonin in flowering, fruit set and fruit ripening. *Plant Reprod.* **2020**, *33*, 77–87. [[CrossRef](#)]
31. Arnao, M.B.; Hernández-Ruiz, J. Melatonin as a regulatory hub of plant hormone levels and action in stress situations. *Plant Biol.* **2021**, *23*, 7–19. [[CrossRef](#)] [[PubMed](#)]
32. Altaf, M.A.; Shahid, R.; Ren, M.X.; Mora-Poblete, F.; Arnao, M.B.; Naz, S.; Anwar, M.; Altaf, M.M.; Shahid, S.; Shakoore, A.; et al. Phytomelatonin: An overview of the importance and mediating functions of melatonin against environmental stresses. *Physiol. Plant.* **2021**, *172*, 820–846. [[CrossRef](#)] [[PubMed](#)]
33. Arnao, M.B.; Hernández-Ruiz, J. Melatonin: A new plant hormone and/or a plant master regulator? *Trends Plant Sci.* **2019**, *24*, 38–48. [[CrossRef](#)]
34. Moustafa-Farag, M.; Almoneafy, A.; Mahmoud, A.; Elkesh, A.; Arnao, M.B.; Li, L.; Ai, S. Melatonin and its protective role against biotic stress impacts on plants. *Biomolecules* **2020**, *10*, 54. [[CrossRef](#)] [[PubMed](#)]

35. Moustafa-Farag, M.; Elkelish, A.; Dafea, M.; Khan, M.; Arnao, M.B.; Abdelhamid, M.T.; El-Ezz, A.A.; Almoneafy, A.; Mahmoud, A.; Awad, M.; et al. Role of Melatonin in Plant Tolerance to Soil Stressors: Salinity, pH and Heavy Metals. *Molecules* **2020**, *25*, 5359. [[CrossRef](#)] [[PubMed](#)]
36. Moustafa-Farag, M.; Mahmoud, A.; Arnao, M.B.; Sheteiwy, M.; Dafea, M.; Soltan, M.; Elkelish, A.; Hasanuzzaman, M.; Ai, S. Melatonin-induced water stress tolerance in plants: Recent advances. *Antioxidants* **2020**, *9*, 809. [[CrossRef](#)]
37. Aghdam, M.S.; Mukherjee, S.; Flores, F.B.; Arnao, M.B.; Luo, Z.; Corpas, F.J. Functions of Melatonin During Postharvest of Horticultural Crops. *Plant Cell Physiol.* **2021**, pcab175. [[CrossRef](#)] [[PubMed](#)]
38. Arnao, M.B.; Hernández-Ruiz, J. Melatonin as a plant biostimulant in crops and during post-harvest: A new approach is needed. *J. Sci. Food Agric.* **2021**, *101*, 5297–5304. [[CrossRef](#)] [[PubMed](#)]
39. Luo, F.; Cai, J.H.; Zhang, X.; Tao, D.B.; Zhou, X.; Zhou, Q.; Zhao, Y.B.; Wei, B.D.; Cheng, S.C.; Ji, S.J. Effects of methyl jasmonate and melatonin treatments on the sensory quality and bioactive compounds of harvested broccoli. *RSC Adv.* **2018**, *8*, 41422–41431. [[CrossRef](#)]
40. Miao, H.; Zeng, W.; Zhao, M.; Wang, J.; Wang, Q. Effect of melatonin treatment on visual quality and health-promoting properties of broccoli florets under room temperature. *Food Chem.* **2020**, *319*, 126498. [[CrossRef](#)] [[PubMed](#)]
41. Wei, L.; Liu, C.; Wang, J.; Younas, S.; Zheng, H.; Zheng, L. Melatonin immersion affects the quality of fresh-cut broccoli (*Brassica oleracea* L.) during cold storage: Focus on the antioxidant system. *J. Food Process. Preserv.* **2020**, *44*, e14691. [[CrossRef](#)]
42. Wei, L.; Liu, C.; Zheng, H.; Zheng, L. Melatonin treatment affects the glucoraphanin-sulforaphane system in postharvest fresh-cut broccoli (*Brassica oleracea* L.). *Food Chem.* **2020**, *307*, 125562. [[CrossRef](#)]
43. Zhu, L.; Hu, H.; Luo, S.; Wu, Z.; Li, P. Melatonin delaying senescence of postharvest broccoli by regulating respiratory metabolism and antioxidant activity. *Trans. Chin. Soc. Agric. Eng.* **2018**, *34*, 300–308.
44. Hernández-Ruiz, J.; Ruiz-Cano, D.; Giraldo-Acosta, M.; Cano, A.; Arnao, M.B. Melatonin in Brassicaceae: Role in Postharvest and Interesting Phytochemicals. *Molecules* **2022**, *27*, 1523. [[CrossRef](#)]
45. McLellan, M.R.; Lind, L.R.; Kime, R.W. HUE angle determinations and statistical analysis for multiquadrant hunter L,a,b data. *J. Food Qual.* **1995**, *18*, 235–240. [[CrossRef](#)]
46. Arnao, M.B.; Hernández-Ruiz, J. Assessment of different sample processing procedures applied to the determination of melatonin in plants. *Phytochem. Anal.* **2009**, *20*, 14–18. [[CrossRef](#)] [[PubMed](#)]
47. Serrano, M.; Martínez-Romero, D.; Guillén, F.; Castillo, S.; Valero, D. Maintenance of broccoli quality and functional properties during cold storage as affected by modified atmosphere packaging. *Postharvest Biol. Technol.* **2006**, *39*, 61–68. [[CrossRef](#)]
48. Pintos, F.M.; Hasperué, J.H.; Ixtaina, P.; Vicente, A.R.; Lemoine, M.L.; Rodoni, L.M. Short light exposure preserves broccoli head quality and nutrients during refrigerated storage. *J. Food Process. Preserv.* **2021**, *45*, e15801. [[CrossRef](#)]
49. Wei, J.; Li, D.; Zhang, J.; Shan, C.; Rengel, Z.; Song, Z.; Chen, Q. Phytomelatonin receptor PMTR1-mediated signaling regulates stomatal closure in *Arabidopsis thaliana*. *J. Pineal Res.* **2018**, *65*, e12500. [[CrossRef](#)]
50. Herr, I.; Büchler, M.W. Dietary constituents of broccoli and other cruciferous vegetables: Implications for prevention and therapy of cancer. *Cancer Treat. Rev.* **2010**, *36*, 377–383. [[CrossRef](#)]
51. Han, J.; Tao, W.; Hao, H.; Zhang, B.; Jiang, W.; Niu, T.; Li, Q.; Cai, T. Physiology and Quality Responses of Fresh-cut Broccoli Florets Pretreated with Ethanol Vapor. *J. Food Sci.* **2006**, *71*, S385–S389. [[CrossRef](#)]
52. Ku, K.M.; Choi, J.H.; Kim, H.S.; Kushad, M.M.; Jeffery, E.H.; Juvik, J.A. Methyl Jasmonate and 1-Methylcyclopropene Treatment Effects on Quinone Reductase Inducing Activity and Post-Harvest Quality of Broccoli. *PLoS ONE* **2013**, *8*, e77127. [[CrossRef](#)]
53. Xu, D.; Zuo, J.; Li, P.; Yan, Z.; Gao, L.; Wang, Q.; Jiang, A. Effect of methyl jasmonate on the quality of harvested broccoli after simulated transport. *Food Chem.* **2020**, *319*. [[CrossRef](#)] [[PubMed](#)]
54. Navarro-Martínez, A.; López-Gómez, A.; Martínez-Hernández, G.B. Potential of Essential Oils from Active Packaging to Highly Reduce Ethylene Biosynthesis in Broccoli and Apples. *ACS Food Sci. Technol.* **2021**, *1*, 1050–1058. [[CrossRef](#)]
55. Suzuki, Y.; Kato, K.; Okabayashi, H. Transportation method kept quality of broccoli by ice and absorbing sheet. *Bull. Kochi Agric. Res. Center* **1998**, *7*, 155–160.
56. Li, D.; Wei, J.; Peng, Z.; Ma, W.; Yang, Q.; Song, Z.; Sun, W.; Yang, W.; Yuan, L.; Xu, X.; et al. Daily rhythms of phytomelatonin signaling modulate diurnal stomatal closure via regulating reactive oxygen species dynamics in *Arabidopsis*. *J. Pineal Res.* **2020**, *68*, e12640. [[CrossRef](#)]
57. Arnao, M.B.; Hernández-Ruiz, J. Protective effect of melatonin against chlorophyll degradation during the senescence of barley leaves. *J. Pineal Res.* **2009**, *46*, 58–63. [[CrossRef](#)]
58. Shi, X.; Xu, S.; Mu, D.; Sadeghnezhad, E.; Li, Q.; Ma, Z.; Zhao, L.; Zhang, Q.; Wang, L. Exogenous Melatonin Delays Dark-Induced Grape Leaf Senescence by Regulation of Antioxidant System and Senescence Associated Genes (SAGs). *Plants* **2019**, *8*, 366. [[CrossRef](#)]
59. Wang, P.; Yin, L.; Liang, D.; Li, C.; Ma, F.; Yue, Z. Delayed senescence of apple leaves by exogenous melatonin treatment: Toward regulating the ascorbate-glutathione cycle. *J. Pineal Res.* **2012**, *53*, 11–20. [[CrossRef](#)]
60. Sun, Q.Q.; Zhang, N.; Wang, J.; Zhang, H.J.; Li, D.B.; Shi, J.; Li, R.; Weeda, S.; Zhao, B.; Ren, S.; et al. Melatonin promotes ripening and improves quality of tomato fruit during postharvest life. *J. Exp. Bot.* **2015**, *66*, 657–668. [[CrossRef](#)]
61. Sun, Q.; Liu, L.; Zhang, L.; Lv, H.; He, Q.; Guo, L.; Zhang, X.; He, H.; Ren, S.; Zhang, N.; et al. Melatonin promotes carotenoid biosynthesis in an ethylene-dependent manner in tomato fruits. *Plant Sci.* **2020**, *298*, 110580. [[CrossRef](#)] [[PubMed](#)]

62. Ding, W.; Zhao, P.; Peng, J.; Zhao, Y.; Xu, J.W.; Li, T.; Reiter, J.; Ma, H.; Yu, X. Melatonin enhances astaxanthin accumulation in the green microalga *Haematococcus pluvialis* by mechanisms possibly related to abiotic stress tolerance. *Algal Res.* **2018**, *33*, 256–265. [[CrossRef](#)]
63. Bubenik, G. Gastrointestinal melatonin: Localization, function, and clinical relevance. *Digest Dis. Sci.* **2002**, *47*, 2336–2348. [[CrossRef](#)] [[PubMed](#)]
64. Gomes Domingos, A.L.; Hermsdorff, H.H.M.; Bressan, J. Melatonin intake and potential chronobiological effects on human health. *Crit. Rev. Food Sci. Nutr.* **2017**, *59*, 133–140. [[CrossRef](#)]
65. Grivas, T.B.; Savvidou, O.D. Melatonin the “light of night” in human biology and adolescent idiopathic scoliosis. *Scoliosis* **2007**, *2*, 6. [[CrossRef](#)]
66. Jones, R.L.; Mcgeer, P.L.; Greiner, A.C. Metabolism of exogenous melatonin in schizophrenic and non-schizophrenic volunteers. *Clin. Chim. Acta* **1969**, *26*, 281–285. [[CrossRef](#)]
67. Abeysuriya, R.G.; Lockley, S.W.; Robinson, P.A.; Postnova, S. A unified model of melatonin, 6-sulfatoxymelatonin, and sleep dynamics. *J. Pineal Res.* **2018**, *64*, e12474. [[CrossRef](#)]
68. Kopin, I.J.; Pare, C.M.; Axelrod, J.; Weissbach, H. The fate of melatonin in animals. *J. Biol. Chem.* **1961**, *236*, 3072–3075. [[CrossRef](#)]
69. Haimov, I.; Laudon, M.; Zisapel, N.; Souroujon, M.; Nof, D.; Shlitner, A.; Herer, P.; Tzischinsky, O.; Lavie, P. Sleep disorders and melatonin rhythms in elderly people. *BMJ* **1994**, *309*, 167. [[CrossRef](#)]
70. Brzezinski, A. Melatonin in Humans. *N. Engl. J. Med.* **1997**, *336*, 186–195. [[CrossRef](#)] [[PubMed](#)]
71. Arnao, M.B.; Hernández-Ruiz, J. Melatonin: Synthesis from tryptophan and its role in higher plants. In *Amino Acids in Higher Plants*; D’ Mello, J., Ed.; CAB Intern: Boston, MA, USA, 2015; pp. 390–435.
72. Garrido, M.; Espino, J.; González-Gómez, D.; Lozano, M.; Cubero, J.; Toribio-Delgado, A.F.; Maynar-Mariño, J.I.; Terrón, M.P.; Muñoz, J.L.; Pariente, J.A.; et al. A nutraceutical product based on Jerte Valley cherries improves sleep and augments the antioxidant status in humans. *Eur. e-J. Clin. Nutr. Metab.* **2009**, *4*, e321–e323. [[CrossRef](#)]
73. Garrido, M.; Paredes, S.D.; Cubero, J.; Lozano, M.; Toribio-Delgado, A.F.; Muñoz, J.L.; Reiter, R.J.; Barriga, C.; Rodríguez, A.B. Jerte valley cherry-enriched diets improve nocturnal rest and increase 6-sulfatoxymelatonin and total antioxidant capacity in the urine of middle-aged and elderly humans. *J. Gerontol. A Biol. Sci. Med. Sci.* **2010**, *65*, 909–914. [[CrossRef](#)] [[PubMed](#)]
74. Gonzalez-Flores, D.; Velardo, B.; Garrido, M.; González-Gómez, D.; Lozano, M.; Ayuso, M.; Barriga, C.; Paredes, S.D.; Rodriguez, A.B. Ingestion of Japanese plums (*Prunus salicina* Lindl. cv. Crimson Globe) increases the urinary 6-sulfatoxymelatonin and total antioxidant capacity levels in young, middle-aged and elderly humans: Nutritional and functional characterization of their content. *J. Food Nutr. Res.* **2011**, *50*, 229–236.
75. Gonzalez-Flores, D.; Gamero, E.; Garrido, M.; Ramirez, R.; Moreno, D.; Delgado, J.; Valdes, E.; Barriga, C.; Rodriguez, A.B.; Paredes, S.D. Urinary 6-sulfatoxymelatonin and total antioxidant capacity increase after the intake of a grape juice cv. Tempranillo stabilized with HHP. *Food Funct.* **2012**, *3*, 34–39. [[CrossRef](#)]
76. Johns, N.P.; Johns, J.; Porasupthana, S.; Plaimée, P.; Sae-Teaw, M. Dietary intake of melatonin from tropical fruit altered urinary excretion of 6-sulfatoxymelatonin in healthy volunteers. *J. Agric. Food Chem.* **2013**, *61*, 913–919. [[CrossRef](#)]
77. Maldonado, M.D.; Moreno, H.; Calvo, J.R. Melatonin present in beer contributes to increase the levels of melatonin and antioxidant capacity of the human serum. *Clin. Nutr.* **2009**, *28*, 188–191. [[CrossRef](#)]
78. Molfino, A.; Laviano, A.; Fanelli, F.R. Sleep-inducing effect of beer: A melatonin- or alcohol-mediated effect? *Clin. Nutr.* **2010**, *29*, 272. [[CrossRef](#)]
79. Sae-Teaw, M.; Johns, J.; Johns, N.P.; Subongkot, S. Serum melatonin levels and antioxidant capacities after consumption of pineapple, orange, or banana by healthy male volunteers. *J. Pineal Res.* **2013**, *55*, 58–64.
80. Kennaway, D.J. Are the proposed benefits of melatonin-rich foods too hard to swallow? *Crit. Rev. Food Sci. Nutr.* **2017**, *57*, 958–962. [[CrossRef](#)]
81. Arnao, M.B.; Hernández-Ruiz, J. The potential of phyto-melatonin as a nutraceutical. *Molecules* **2018**, *23*, 238. [[CrossRef](#)]
82. Arnao, M.B.; Hernández-Ruiz, J. Phyto-melatonin, natural melatonin from plants as a novel dietary supplement: Sources, activities and world market. *J. Funct. Foods* **2018**, *48*, 37–42. [[CrossRef](#)]



## Article

# Self-Incompatibility in Apricot: Identifying Pollination Requirements to Optimize Fruit Production

Sara Herrera <sup>1,2</sup>, Jorge Lora <sup>3</sup>, José I. Hormaza <sup>3</sup> and Javier Rodrigo <sup>1,2,\*</sup>

<sup>1</sup> Departamento de Ciencia Vegetal, Centro de Investigación y Tecnología Agroalimentaria de Aragón (CITA), Avda. Montañana 930, 50059 Zaragoza, Spain; sherreral@aragon.es

<sup>2</sup> Instituto Agroalimentario de Aragón-IA2, CITA-Universidad de Zaragoza, 50013 Zaragoza, Spain

<sup>3</sup> Subtropical Fruit Crops Department, Instituto de Hortofruticultura Subtropical y Mediterránea La Mayora (IHSM La Mayora-CSIC-UMA), 29750 Algarrobo-Costa, Spain; jlora@eelm.csic.es (J.L.); ihormaza@eelm.csic.es (J.I.H.)

\* Correspondence: jrodrigo@aragon.es; Tel.: +34-976-716-314

**Abstract:** In recent years, an important renewal of apricot cultivars is taking place worldwide, with the introduction of many new releases. Self-incompatible genotypes tolerant to the sharka disease caused by the plum pox virus (PPV), which can severely reduce fruit production and quality, are being used as parents in most breeding programs. As a result, the self-incompatibility trait present in most of those accessions can be transmitted to the offspring, leading to the release of new self-incompatible cultivars. This situation can considerably affect apricot management, since pollination requirements were traditionally not considered in this crop and information is lacking for many cultivars. Thus, the objective of this work was to determine the pollination requirements of a group of new apricot cultivars by molecular identification of the *S*-alleles through PCR amplification of *RNase* and *SFB* regions with different primer combinations. The *S*-genotype of 66 apricot cultivars is reported, 41 for the first time. Forty-nine cultivars were considered self-compatible and 12 self-incompatible, which were allocated in their corresponding incompatibility groups. Additionally, the available information was reviewed and added to the new results obtained, resulting in a compilation of the pollination requirements of 235 apricot cultivars. This information will allow an efficient selection of parents in apricot breeding programs, the proper design of new orchards, and the identification and solution of production problems associated with a lack of fruit set in established orchards. The diversity at the *S*-locus observed in the cultivars developed in breeding programs indicates a possible genetic bottleneck due to the use of a reduced number of parents.

**Keywords:** apricot; pollen tube; pollination; *Prunus armeniaca*; *S*-alleles; self-incompatibility

**Citation:** Herrera, S.; Lora, J.; Hormaza, J.I.; Rodrigo, J. Self-Incompatibility in Apricot: Identifying Pollination Requirements to Optimize Fruit Production. *Plants* **2022**, *11*, 2019. <https://doi.org/10.3390/plants11152019>

Academic Editors: Milan S. Stankovic, Paula Baptista and Petronia Carillo

Received: 28 June 2022  
Accepted: 1 August 2022  
Published: 3 August 2022

**Publisher's Note:** MDPI stays neutral with regard to jurisdictional claims in published maps and institutional affiliations.



**Copyright:** © 2022 by the authors. Licensee MDPI, Basel, Switzerland. This article is an open access article distributed under the terms and conditions of the Creative Commons Attribution (CC BY) license (<https://creativecommons.org/licenses/by/4.0/>).

## 1. Introduction

Apricot (*Prunus armeniaca* L.) belongs to the genus *Prunus* in the Rosaceae family. This crop was domesticated in different domestication events ca. 2000–3000 years ago in Central Asia, which is considered the center of origin of the crop [1,2]. Later, apricot was introduced into the Mediterranean Basin from the Caucasus, a secondary center of diversification [3]. Nowadays, apricot world production has reached 3.7 million tons [4] and it is considered one of the most economically important fruit crops in temperate regions [5].

Apricot cultivars have been traditionally classified into six eco-geographical groups according to their geographical origin: Central Asian, East Chinese, North Chinese, Dzhungar-Zailij, Irano-Caucasian, and European [6]. Apricot cultivars from the Central Asian, which is the oldest and most diverse, the Dzhungar-Zailij, and the Iranian-Caucasian groups, are mostly self-incompatible. Commercial cultivars of Europe, North America, South Africa, and Australia are mainly self-compatible and belong to the European group [7], which has two main gene pools: Continental Europe and Mediterranean Europe [8].

Gametophytic Self-Incompatibility (GSI) is a mechanism to prevent self-fertilization and promote outcrossing present in the Rosaceae [9]. It is controlled by a multiallelic locus named *S* that contains several genes involved in the pollen-pistil recognition. The *S-RNase* gene encodes pistil-expressed glycoproteins with ribonuclease activity that act as highly selective cytotoxins that cause rejection of pollen when its *S*-allele is the same as either of the two *S*-alleles expressed in the pistil [10,11]. Consequently, pollen tube growth is arrested in the style preventing fertilization [12]. The *SFB* gene, which codifies an F-box protein, is specifically expressed in the pollen, and determines the pollen allele specificity [13]. Nowadays, there are self-incompatible and self-compatible apricot cultivars, as in other *Prunus* species such as almond (*Prunus dulcis*), sweet cherry (*Prunus avium*), Japanese plum (*Prunus salicina*), European plum (*Prunus domestica*) and sour cherry (*Prunus cerasus*) [7]. In recent years, the system seems to be more complicated, with the report of different modifier genes involved in the incompatibility response [14,15].

The pollination requirements of cultivars can be established by evaluation of fruit set after self- and cross-pollination under field conditions [16,17], by pollen tube growth observations in self- and cross-pollinated flowers under fluorescence microscopy with the advantage of avoiding failures caused by adverse weather conditions [18–22], and by molecular techniques based on PCR and sequencing approaches of the *S*-locus [23]. In apricot, 33 *S*-alleles ( $S_1$  to  $S_{20}$ ,  $S_{22}$  to  $S_{30}$ ,  $S_{52}$ ,  $S_{53}$ ,  $S_v$ , and  $S_x$ ) have been identified so far, including one allele linked to self-compatibility ( $S_c$ ) [16,24–27].

In recent years, an important renewal of apricot cultivars is taking place worldwide, with the introduction of many new releases in response to productive and industrial changes in the crop [28]. The main objectives of breeding programs for the development of new commercial cultivars include sharka-tolerance/resistance, climate adaptability and improved organoleptic properties fruit such as firmness, skin and fresh color, and aroma [29]. The sharka disease was reported for the first time in plum around 1915 and, since then, it has become the most economically important virus disease of *Prunus* species [30]. PPV is usually transmitted by aphids, and probably spread by the propagation of infected plant material [31]. Sharka disease causes discoloration on leaves, petals and fruits, severely reducing fruit production and quality [31].

Self-(in)compatibility and inter-(in)compatibility relationships in apricot have been characterized in traditional and local cultivars from different regions such as China [26], Hungary [32], Morocco [33], North America and Spain [16,21,34], Tunisia [17,35], and Turkey [32,36,37]. Although self-(in)compatibility of new apricot releases are evaluated in some public breeding programs (‘Centro de Edafología y Biología Aplicada del Segura’ (CEBAS-CSIC) in Murcia [38,39], and the ‘Instituto Valenciano de Investigaciones Agrarias’ (IVIA) in Valencia [40], both in Spain; ‘Institut National de la Recherche Agronomique’ (INRA) in France [41–43]; University of Bologna and University of Milan in Italy [44]; ‘Agricultural Research Service’ in Parlier, CA, and Rutgers University in New Brunswick, NJ, in the USA [45]), the pollination requirements of many cultivars are still unknown.

In this work, we evaluate the hypothesis that a significant proportion of new apricot cultivars are self-incompatible and that knowing the incompatibility relationships between cultivars is needed to select appropriate pollinating cultivars in the design of orchards. For this purpose, the *S*-genotype of 66 apricot cultivars was analyzed; of them, 49 were self-compatible and the other 12 were self-incompatible. The results allowed allocating the self-incompatible cultivars in their corresponding incompatibility groups according to their *S*-alleles. In addition, a compilation of the available *S*-genotype data was carried out to evaluate the distribution of the *S*-alleles in the main apricot cultivars grown worldwide and to assess their current genetic diversity.

## 2. Results

### 2.1. *S*-Alleles and Incompatibility Groups

PCR analysis based on the amplification of *RNase* and *SFB* genes allowed identifying the *S*-genotype in 66 apricot cultivars, 41 of them reported for the first time (Tables 1 and 2). Firstly,

the combination of the primers SRC-F/SRC-R amplified the first intron of the *RNase*, and the different alleles were classified according to the sizes of the fragments previously established by Vilanova et al. [25] (Figure 1A; Supplementary Table S1). To our knowledge, the sequence of the first intron has only been reported in the  $S_1$ ,  $S_2$ ,  $S_4$ ,  $S_6$ ,  $S_7$  and  $S_c$ -alleles [22]. The PruC2/PruC4R primer combination amplified the second intron and was used to differentiate the  $S_6$  and  $S_9$  alleles in 15 genotypes, whose sequences were also previously reported [21,46]. The SHLM1 and SHLM2 primer combination amplified a fragment of 650 bp in 17 cultivars, indicating the presence of the  $S_1$ -allele. A 413 bp fragment, that corresponds to the  $S_7$ -allele, was only detected in ‘Charisma’ and ‘Ninfa’ using the primer pair SHLM3/SHLM4 [22].

**Table 1.** Incompatibility group (I.G.) and S-genotype of 103 apricot cultivars.

I.G. (S-Genotype)	Cultivars Analyzed in This Study	Cultivars Analyzed in Previous Studies
I ( $S_1S_2$ )		AC1 [21], Castleton [16], Farmingdale [47], Giovanniello [47], Goldrich [48], Hargrand [48], Lambertin-1 [48]
II ( $S_8S_9$ )		Ceglédi óriás [24], Cologlu [32], Ligeti óriás [24], Perlecot [21], Pinkcot [21], Szegegi M. [16]
III ( $S_2S_4$ )	Muñoz <sup>b</sup> , Pandora <sup>b</sup>	ASF0401 [21], Avirine (Bergarouge) [21], Moniqui [49]
IV ( $S_2S_7$ )		Ouardi [35], Priana [34]
V ( $S_2S_8$ )	Sweet Cot <sup>d</sup> [21]	Alyanak [32], Holly Cot [21]
VIII ( $S_6S_9$ )	Apribang (ASF0405) <sup>a</sup>	ASF0402 [21], Cataloglu [32], Cheyenne [22], Feria Cot [21], Flashcot [50], JNP [21], Ninja [50], Orangered [16,21], Soganci [32], Stark Early Orange [16,21], Sunny Cot [21], Wonder Cot [21]
X ( $S_7S_{12}$ )		Bedri Ahmar [35], Oud Rhayem [35]
XI ( $S_9S_{13}$ )		Haci Haliloglu [32], Kabaasi [32]
XII ( $S_{11}S_{13}$ )		Voski [24]
XIII ( $S_6S_{19}$ )		Levent [32]
XV ( $S_7S_8$ )		Ouelid El Oud [35]
XVI ( $S_7S_{11}$ )		Bouk Ahmed [35], Hamidi [35]
XVII ( $S_8S_{12}$ )		Adedi Ahmar [35]
XVIII ( $S_1S_3$ )	IPS23214 <sup>a</sup> , Monred <sup>a</sup>	Cooper Cot [21], Perfection [48]
XIX ( $S_2S_3$ )		Mayacot [21], Sun Glo [49]
XX ( $S_2S_9$ )		Goldstrike 02 [21], Hasانبey [32], Magic Cot [21]
XXI ( $S_3S_8$ )	Samourai <sup>a,c</sup>	Lilly Cot [21], Spring Blush [21]
XXII ( $S_3S_9$ )		Almadulce [21], Flodea [21], Henderson [16,21], Kosmos [22], Tsunami [50]
XXIII ( $S_7S_9$ )		Goldbar [21], Kurukabuk [32]
XXVI ( $S_1S_6$ )		Primaya [22]
XXV ( $S_1S_9$ )	Farely <sup>b</sup> , Megatea <sup>b</sup> , Monster Cot <sup>b</sup> , Priabel <sup>b</sup>	Almater [50], Aurora [50], Medaga [50]
XXVI ( $S_6S_8$ )		Robada [50]
Group 0	Harcot <sup>b</sup> ( $S_1S_4$ ) [49]	Bouthani Ben Friha ( $S_{12}S_{13}$ ) [35], Cow-1 ( $S_1S_{31}$ ) [16], Cow-2 ( $S_{20}S_{31}$ ) [16], Estrella ( $S_1S_7$ ) [51], Harlayne ( $S_3S_{20}$ ) [16], Harmat ( $S_{10}S_{11}$ ) [24], Korai zamatos ( $S_{12}S_{13}$ ) [24], Mariem ( $S_7S_{20}$ ) [16], Martinet ( $S_2S_2$ ) [16], Oud Hmida ( $S_2S_{12}$ ) [35], Perla ( $S_2S_{20}$ ) [16], Portici ( $S_2S_{20}$ ) [16], Shalakh (Erevani) ( $S_5S_{11}$ ) [16], Velázquez ( $S_5S_{20}$ ) [16]
Unclassified		
$S_1$	Dama taronja <sup>a</sup> , Tornado <sup>a</sup> , Vitillo <sup>a</sup>	IBCOT 18-2 [50]
$S_2$	Fuego <sup>a</sup>	Cyrano [22], IBCOT 29-5 [50], Veecot [21]
$S_3$	Mogador <sup>a</sup>	Colorado [21], Mikado [22]
$S_6$		Stella [21]
$S_8$		Vanilla Cot [21]
$S_9$		Goldstrike 01 [21]

<sup>a</sup> *S-RNase* genotypes first reported in this study; <sup>b</sup> S-genotype completed in cultivars in which previously only one allele could be identified [21]; <sup>c</sup>  $S_c/S_8$  allele identified using fluorescence microscopy; <sup>d</sup>  $S_c/S_8$  allele confirmed using the primers AprFBC8-F/AprFBC8-R.

PCR amplification of the  $S_c$ - and  $S_8$ -alleles using the primers designed based on the first and second introns of the *RNase* sequence produced identical size fragments [52]. Thus, the AprFBC8-F/AprFBC8-R primers for the *SFB* region were used for distinguishing both S-alleles [32]. This primer combination amplified a fragment of 150 bp, allowing to identify the  $S_8$ -haplotype in 3 cultivars, whereas a 500 bp fragment from V2 region was amplified to characterize the  $S_c$ -allele in 47 cultivars (Figure 1B; Supplementary Table S1). However, the primers AprFBC8-F/AprFBC8-R did not produce amplification fragments in two cultivars (‘Samourai’ and ‘Water’). Thus, controlled pollinations were carried out to differentiate the  $S_c$ - and  $S_8$ -alleles in these two cultivars. All self-pollinated pistils showed germinated pollen grains on the stigma in both cultivars (Figure 2A). ‘Water’ behaved as self-compatible since all the self-pollinated pistils ( $n = 17$ ) showed pollen tubes arriving to the base of the style (Figure 2B). In ‘Samourai’, pollen tubes reached the upper third of the style in all the self-pollinated pistils analyzed (Figure 2C), but pollen tube growth ceased in the middle part of the style, forming a callose tip (Figure 2D), with a mean percentage of style traveled by the pollen tubes of 62.5% ( $n = 10$ ). Thus, ‘Samourai’ was considered as

self-incompatible. In addition, all the examined pistils cross-pollinated with ‘Katy’ showed pollen tubes at the base of the style in ‘Water’ ( $n = 20$ ) and ‘Samourai’ ( $n = 5$ ).

**Table 2.** S-genotype of 153 self-compatible apricot cultivars.

S-Genotype	Cultivars Analyzed in This Study	Cultivars Analyzed in Previous Studies
$S_1S_c$	Big Red <sup>a</sup> , Dama Rosa <sup>a</sup> , Flavorcot <sup>a</sup> , Rojo Pasión <sup>a</sup> , Rubissia <sup>a</sup> , Water <sup>a,c</sup>	Mauricio [34]
$S_2S_c$	Bergecot <sup>d</sup> [21], Canino <sup>d</sup> [21,34], Harval <sup>a</sup> , Justo Cot <sup>a</sup> , Paviot <sup>d</sup> [21], Primidi <sup>d</sup> [21], Tilton [47]	Berdejo [21,50], Bergeron [52], Budapest [52], Dulcinea [16], Galta Vermella Valenciana [16], Kalao [22], Konservnyi Pozdnyi [52], Mamaia [52], Mandulakajsz [52], Mediva [21,50], Peñaflo 02 [21,50], Pepito del Rubio [49,50], Rakovszky [52], Regibus [22], Roxana [52], Rózsakajsz [16], Sandy cot [21,50], Trevatt [16]
$S_3S_c$	Rubista <sup>d</sup> [21]	Pricia [21], Rambo [22]
$S_5S_c$	Búlida [16]	
$S_6S_c$	Fartoly <sup>b,d</sup> [21], Ladycot <sup>b,d</sup> [21], Medflo <sup>d</sup> [21], Mediabel <sup>d</sup> [21]	Aprix20 [21,50], Aprix9 [21,50], Bebecou [47], Falaria [21,50], Farlis [21,50], Lito [16]
$S_7S_c$	Charisma <sup>d</sup> [21], Ninfa [16]	Beliana [34], Sayeb [35]
$S_8S_c$	Gönci Magyarakajsz [52], Luizet <sup>b,d</sup> [21]	Andornaktályai magyarakajsz [52], Cacansko zlato [52], Callatis [52], Crvena ungarska [52], Darunec malahoyeva [52], Effect [52], Kásna ungarska [52], Krimskiy Amur [52], Nagygyümölcsü magyarakajsz [52], Nikitskiy [52], Paksi magyarakajsz [52], Pisana [52], Venus [52]
$S_9S_c$	Alba <sup>a</sup> , Aprisweet (ASF0409) <sup>a</sup> , Micaelo <sup>a</sup> , Tadeo <sup>b</sup> [21]	AC2 [21,50], Ceglédi arany [52], Ceglédi bíborkajsz [52], Flopria [21], Lido [22], Tom Cot [21]
$S_{13}S_c$		Modesto [24]
$S_{19}S_c$		Mari de Cenad [16]
$S_{20}S_c$		Cristali [16], Gavatxet [16]
$S_{24}S_c$		Ezzine [16]
$S_cS_c$		Ananasnyi ciurpinski [52], Asli [35], Borsi-féle kései róza [52], Ceglédi kedves [52], Currot [34], GaltaRoja [16], Gandia [16], Ginesta [25], Grandir [47], Manri [16], NJA-8 [52], Nyujtó Ferenc emléke [52], Palabras [16], Palau [25], Pannónia [52], Pasinok [52], Patterson [47], Raki [35], Rojo Carlet [16], Sirena [52], Sulmona [52], Tiryntos [16], Xirivello [16], Zaposdolye [52]
$S_c$	Aprix 116 <sup>a</sup> , Cebas Red [53], Cocot <sup>a</sup> , Corbato <sup>d</sup> [21], Delice cot <sup>d</sup> [21], Fantasma <sup>a</sup> , Farhial <sup>d</sup> [21], IPS21512 <sup>a</sup> , IPS2712 <sup>a</sup> , Laguna <sup>a</sup> , Merino <sup>a</sup> , Mirlo anaranjado <sup>d</sup> [21,54], Mirlo blanco <sup>d</sup> [21,54], Mirlo Rojo [54], Mitger <sup>d</sup> [21], Orange rubis <sup>a</sup> , Precoz de Tiryntos <sup>a</sup> , Primorosa [53], Soledane <sup>d</sup> [21], Tardorange <sup>a</sup> , Valorange <sup>a</sup> , Katy [55]	Aprix 33 [21,50], ASF0404 (Apriqueen) [21,50], Dorada [22], Facló [21,50], Farbaly [21,50], Farbela [21,50], Fardao [21,50], Farfia [21,50], Farius [21,50], IBCOT 13-12 [50], IPS16121 [50], Kioto [50], Memphis [22], Milord [22], Murciana [22], Oscar [22], Playa cot [21,50], Rouge cot [21], Rubely [50], Sherpa [22] Swired [21,50]
$S_1S_2$		Lorna [21], Palsteyn [21]
$S_2S_9$		Victor 1 [21]
$S_1$		IPS20390 [50], Rubilis [50]
$S_3$		Golden Sweet [21]

<sup>a</sup> S-RNase genotype first reported in this study; <sup>b</sup> S-genotype completed in cultivars in which previously only one allele could be identified [21]; <sup>c</sup>  $S_c/S_8$  allele identified using fluorescence microscopy; <sup>d</sup>  $S_c/S_8$  allele confirmed using the primers AprFBC8-F/AprFBC8-R.

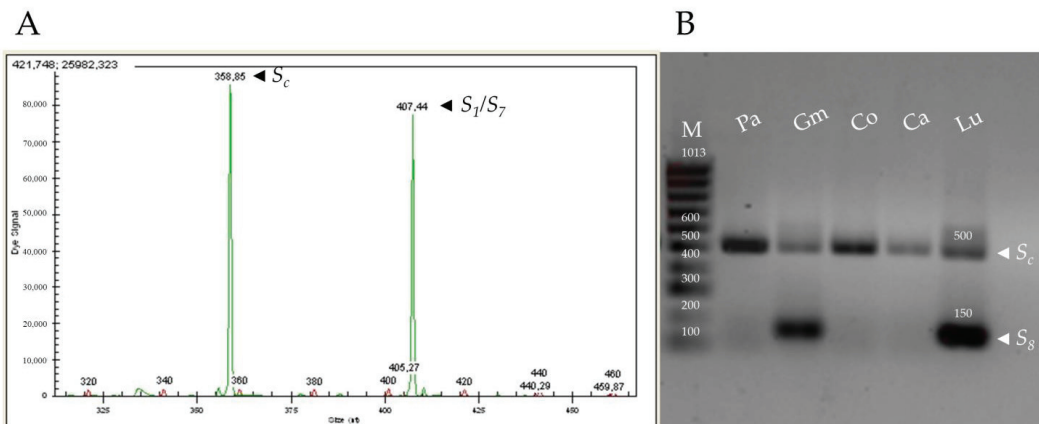


**Figure 1.** Size of the PCR amplification fragments using different primer pair combinations for the identification of S-alleles. (A) Gene analyzer output for the SRc-(F/R) primers showing the size of the two amplified fragments of the RNase first intron region corresponding to the S-alleles  $S_c$  (358 bp, left) and  $S_1/S_7$  (408 bp, right) in apricot cv. ‘Rojo Pasión’. (B) PCR amplification with the AprFBC8-(F/R) primers for identifying  $S_c$ - and  $S_8$ -alleles in five apricot cultivars (Pa: ‘Paviot’, Gm: ‘Gönci Magyarakajsz’, Co: ‘Corbato’, Ca: ‘Canino’, and Lu: ‘Luizet’). M: 100 bp DNA Ladder.

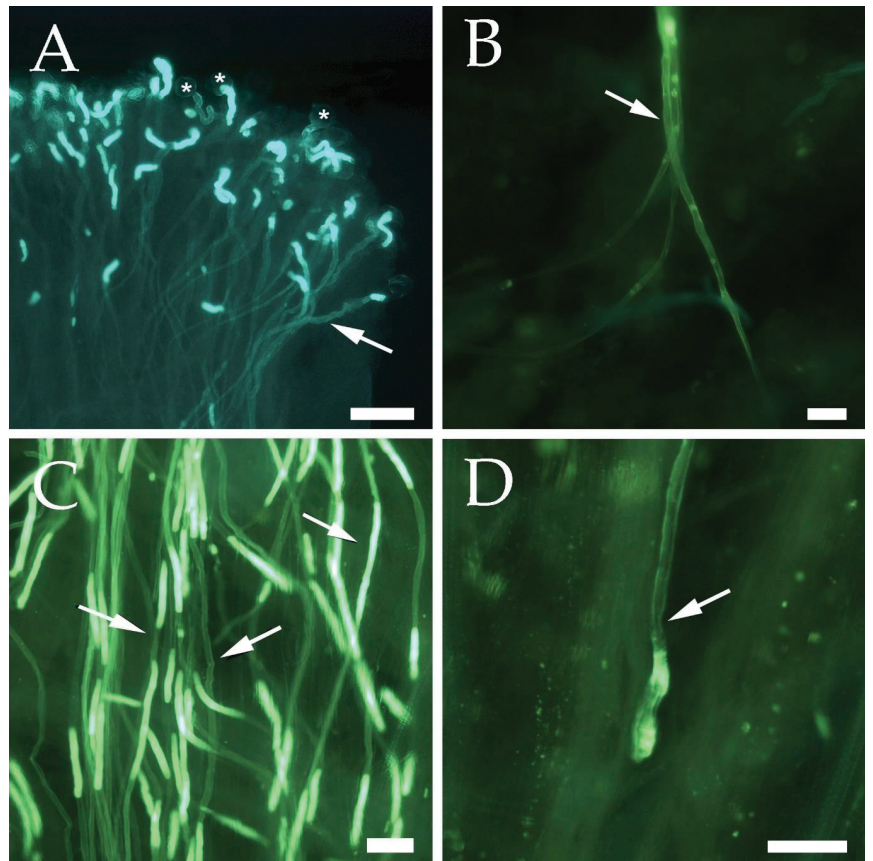


**Figure 2.** Pollen germination and pollen tube growth in self-pollinated apricot flowers observed under the microscope. In Gametophytic Self-Incompatibility (GSI), both compatible and incompatible pollen grains germinate on the stigma. The pollen grain carries one of the two *S*-alleles of the original genotype. In self-incompatible cultivars, if the *S*-allele of the pollen grain matches one of the two *S*-alleles of the pistil, pollen tube growth is inhibited in the middle part of the style. (A) Pollen grains (\*) germinating at the stigma surface with pollen tubes emerging towards the style the style (arrow) in the self-compatible cultivar ‘Water’. (B) Pollen tubes (arrow) reaching the base of the style (down) in the self-compatible cultivar ‘Water’. (C) Pollen tubes (arrows) growing along the style in the self-compatible cultivar ‘Water’. (D) Pollen tube (arrow) arrested in the middle part of the style in the self-incompatible cultivar ‘Samourai’. Aniline blue staining for callose of squash preparations. Scale bars = 100  $\mu$ m.

The *S*-genotype of eleven cultivars, in which a unique allele could be previously characterized [21], has been completed using several primer combinations. The specific primers SHLM1 and SHLM2 allowed to identify the *S*<sub>1</sub>-allele in five cultivars (‘Farely’ (*S*<sub>1</sub>*S*<sub>9</sub>), ‘Harcot’ (*S*<sub>1</sub>*S*<sub>4</sub>), ‘Megatea’ (*S*<sub>1</sub>*S*<sub>9</sub>), ‘Monster Cot’ (*S*<sub>1</sub>*S*<sub>9</sub>), and ‘Priabel’ (*S*<sub>1</sub>*S*<sub>9</sub>)). Primers PruC2 and PruC4R enabled the identification of a second *S*-allele, *S*<sub>6</sub> in ‘Pandora’ (*S*<sub>2</sub>*S*<sub>6</sub>), ‘Muñoz’ (*S*<sub>2</sub>*S*<sub>6</sub>), ‘Fartoly’ (*S*<sub>c</sub>*S*<sub>6</sub>), ‘Lady Cot’ (*S*<sub>c</sub>*S*<sub>6</sub>), and *S*<sub>9</sub> in ‘Tadeo’ (*S*<sub>c</sub>*S*<sub>9</sub>). The genotype of ‘Luizet’ (*S*<sub>c</sub>*S*<sub>8</sub>) was identified using the AprFBC8-F/AprFBC8-R primer combination. Additionally, the presence of the *S*<sub>c</sub>- and *S*<sub>8</sub>-alleles was confirmed in 19 cultivars using the AprFBC8-F and AprFBC8-R primers. In these 19 cultivars, observations of pollen tube growth in pollination experiments were previously used to establish self(in)compatibility; the *S*<sub>c</sub>-allele was assigned to self-compatible cultivars, and the *S*<sub>8</sub>-allele to self-incompatible accessions [21]. Moreover, the

results allowed to confirm the  $S$ -genotype of eight cultivars; ‘Búlida’ ( $S_5S_c$ ) [16], ‘Canino’ ( $S_2S_c$ ) [34], ‘Cebas Red’ ( $S_c$ ) [53], ‘Gönci magyarkajszi’ ( $S_8S_c$ ) [52], ‘Harcot’ ( $S_1S_4$ ) [49], ‘Katy’ ( $S_1S_2$ ) [55], ‘Ninfa’ ( $S_7S_c$ ) [16] and ‘Tilton’ ( $S_2S_c$ ) [47]; a single  $S_c$ -allele amplification was obtained in ‘Mirlo rojo’ and ‘Primorosa’, which were reported previously as self-compatible ( $S_cS_c$ ) [53,54].

In order to establish the compatibility relationships among cultivars, the 12 self-incompatible cultivars were allocated in their corresponding incompatibility groups according to their  $S$ -genotypes. In five cultivars (‘Dama Toronja’, ‘Tornado’, ‘Vitillo’, ‘Fuego’, ‘Mogador’), self-(in)compatibility could not be established by their  $S$ -genotype because only one allele other than  $S_c$  could be identified and, consequently, they were considered unclassified (Table 1).

## 2.2. Diversity in the $S$ -Locus Region

The  $S$ -genotypes of 235 apricot accessions, including the 60 cultivars analyzed herein in which two  $S$ -alleles could be identified together with 175 accessions previously reported (Tables 1 and 2; Supplementary Table S2) were used to assess the diversity and differentiation at the gametophytic self-incompatibility  $S$ -locus.

Fourteen  $S$ -alleles in 32  $S$ -locus combinations were identified within 70 traditional apricot accessions, whereas 36  $S$ -genotype combinations with 17  $S$ -alleles were found in the group of 157 releases from breeding programs (Tables 3 and 4). Both groups of accessions showed the same value of the average number of alleles per country ( $N_a = 4$ ). Thirteen  $S$ -alleles were present in both groups (Figure 3). However, the alleles  $S_4$ ,  $S_{10}$ ,  $S_{24}$ , and  $S_{31}$  were only identified in the commercial cultivars ‘Ezzine’ ( $S_{24}$ ), ‘Harmat’ ( $S_{10}$ ), ‘Harcot’ ( $S_4$ ), ‘Cow-1’ ( $S_{31}$ ), and ‘Cow-2’ ( $S_{31}$ ), and the  $S_5$ -allele was only found in the traditional cultivars ‘Búlida’ and ‘Velázquez’, from Spain, and ‘Shalakh’, from Armenia.

**Table 3.** Genetic parameters of apricot traditional cultivars including landraces and local selections. Number of cultivars, number of alleles ( $N_a$ ), allelic richness ( $A_r$ ), and number of private alleles ( $P_a$ ) for each country of origin. SD: standard deviation; SE: standard error.

Country	Number of Cultivars	Number of Alleles ( $N_a$ )	Allelic Richness ( $A_r$ )	Number of Private Alleles ( $P_a$ )
Armenia	1	2	1.67	-
Australia	1	2	1.67	-
France	2	2	1.57	-
Greece	5	3	1.67	-
Hungary	7	4	1.75	-
Italy	4	4	1.70	-
Romania	1	2	1.67	1 ( $S_{19}$ )
Spain	26	7	1.61	-
Tunisia	9	7	1.80	1 ( $S_{12}$ )
Turkey	8	6	1.77	-
Ukraine	1	2	1.67	-
The USA	5	6	1.84	1 ( $S_3$ )
<b>Total</b>	<b>70</b>	<b>47</b>		<b>3</b>
<b>Mean <math>\pm</math> SD</b>		<b>4 <math>\pm</math> 2</b>	<b>1.70 <math>\pm</math> 0.08</b>	
<b>SE</b>		<b>0.63</b>	<b>0.02</b>	

In both traditional cultivars and cultivars released from breeding programs,  $S_c$  was the most frequent  $S$ -allele as it was found in 38 and 101 cultivars, respectively. The  $S_c$ -allele was not detected in Armenian and Turkish germplasm but was present in more than 50% of the genotypes from Australia, France, Greece, Romania, Spain, and Ukraine (Figure 3A; Supplementary Table S3). A similar trend was observed in cultivars from breeding programs, except for cultivars from North America (Canada and the USA), in which the  $S_c$ -allele appeared in less than 20% of the cultivars (Figure 3B; Supplementary Table S4).

**Table 4.** Genetic parameters of apricot cultivars released from breeding programs. Number of cultivars, number of alleles ( $N_a$ ), allelic richness ( $A_r$ ), and number of private alleles ( $P_a$ ) for each country of origin. SD: standard deviation; SE: standard error.

Country	Number of Cultivars	Number of Alleles ( $N_a$ )	Allelic Richness ( $A_r$ )	Number of Private Alleles ( $P_a$ )
Bulgaria	1	2	1.67	-
Canada	4	6	1.87	1 ( $S_4$ )
France	58	10	1.83	1 ( $S_{31}$ )
Hungary	13	8	1.72	3 ( $S_{10}, S_{11}, S_{12}$ )
Italy	2	3	1.71	-
Macedonia	1	2	1.67	-
Romania	5	3	1.48	-
Serbia	1	2	1.67	-
South Africa	1	2	1.67	-
Spain	33	7	1.76	-
Switzerland	2	2	1.71	-
Tunisia	6	5	1.70	1 ( $S_{24}$ )
Turkey	1	2	1.67	1 ( $S_{19}$ )
Ukraine	4	2	1.50	-
Unknown	1	2	1.67	-
The USA	24	9	1.84	-
<b>Total</b>	157	67		7
<b>Mean <math>\pm</math> SD</b>		4 $\pm$ 3.05	1.70 $\pm$ 0.10	
<b>SE</b>		0.76	0.03	

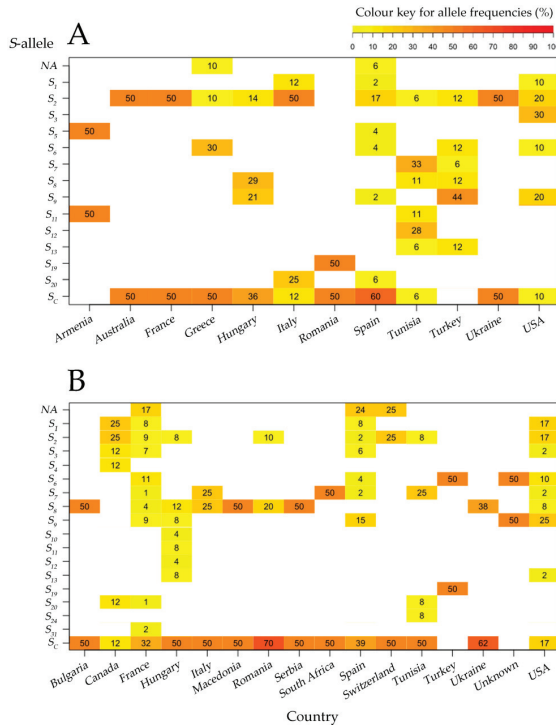


**Figure 3.** Heatmaps of allele frequencies in traditional cultivars (A) and cultivars from breeding programs (B) for each country of origin using “PopGenReport” v. 3.0.4 R package. Cell color indicates the proportion of the total number of alleles, and the numbers within a cell show the percentage of the number of alleles in each country. The frequency of each S-allele was calculated in each country within each group of accessions, showing statistically significant relationships ( $p < 0.05$ ) between S-alleles and countries in the groups of both traditional cultivars and releases from breeding programs.

In traditional cultivars,  $S_2$  was the second most frequent  $S$ -allele ( $n = 24$ ), followed by  $S_9$  ( $n = 13$ ),  $S_6$  and  $S_8$  ( $n = 8$ ),  $S_7$  ( $n = 7$ ),  $S_{12}$  and  $S_{20}$  ( $n = 5$ ),  $S_1$ ,  $S_3$ ,  $S_5$ ,  $S_{11}$ , and  $S_{13}$  ( $n = 3$ ), and  $S_{19}$  ( $n = 1$ ). In cultivars from breeding programs,  $S_9$  was the second most frequent  $S$ -allele ( $n = 35$ ) followed by  $S_2$  ( $n = 26$ ),  $S_1$  ( $n = 24$ ),  $S_6$  ( $n = 23$ ),  $S_8$  ( $n = 21$ ),  $S_3$  ( $n = 14$ ),  $S_7$  ( $n = 8$ ),  $S_{13}$  and  $S_{20}$  ( $n = 3$ ),  $S_{11}$  and  $S_{31}$  ( $n = 2$ ) and  $S_4$ ,  $S_{10}$ ,  $S_{12}$ ,  $S_{19}$ ,  $S_{24}$  ( $n = 1$ ) (Supplementary Tables S2–S4).

A higher percentage of single alleles was observed in cultivars from breeding programs compared to traditional cultivars: 17% in France, 24% in Spain, and 25% in Switzerland for the cultivars from breeding programs compared to 10% in Greece and 6% in Spain for the traditional cultivars (Figure 3).

Regarding the allele frequencies, the chi-squared tests showed a statistically significant relationship ( $p < 0.05$ ) between  $S$ -alleles and countries in the groups of both traditional cultivars and releases from breeding programs (Supplementary Tables S3 and S4).

The existence of private alleles,  $S$ -alleles that are found only in a single population, was used as an indicator of genetic differentiation between both groups. Three alleles ( $P_a$ ) were found in the group of traditional cultivars.  $S_3$  was only found in ‘Perfection’ and ‘Sun Glo’ from the USA,  $S_{12}$  in ‘Bedri Ahmar’, ‘Bouthani Ben Friha’, ‘Oud Rhayem’, and ‘Oud Hmida’, from Tunisia, and  $S_{19}$  in ‘Mari de Cenad’ from Romania. In the group of releases from breeding programs, seven private alleles were identified, three of them,  $S_{10}$ ,  $S_{11}$  and  $S_{12}$ , present in Hungarian accessions (‘Harmat’, ‘Korai zamatos’, and ‘Voski’).

Although the number of genotypes in the group of cultivars from breeding programs was nearly twice than those in the group of traditional cultivars, the same value of average allelic richness ( $A_r = 1.70$ ) was found in both groups. Comparisons of traditional cultivars with cultivars from breeding programs revealed a slight loss of diversity for the  $S$ -locus in Hungarian, Tunisian, and Turkish modern cultivars. On the contrary, higher allelic richness in cultivars from breeding programs than in traditional cultivars were observed in France, Italy, and Spain.

### 3. Discussion

#### 3.1. Self- and Cross-Incompatibility in Apricot

The  $S$ -genotype of 66 apricot cultivars was reported herein, 41 for the first time. A total of 49 cultivars were characterized as self-compatible since their genotype contained the  $S_c$ -allele, which is associated with self-compatibility [56]. However, the self-compatibility of two cultivars was determined through controlled pollinations due to mismatching of PCR primers resulting in no amplification. When self(in)compatibility cannot be determined by identifying the  $S$ -genotype, laboratory pollination experiments have proven to be an accurate method because they avoid weather-related failures under field conditions [23,57,58].

Here, the  $S$ -genotype has been characterized in 11 cultivars [‘Pandora’ and ‘Muñoz’ ( $S_2S_6$ ), ‘Farely’, ‘Megatea’, ‘Monster Cot’, and ‘Priabel’ ( $S_1S_9$ ), ‘Harcot’ ( $S_1S_4$ ), ‘Fartoly’ and ‘Ladycot’ ( $S_6S_c$ ), ‘Luizet’ ( $S_8S_c$ ), and ‘Tadeo’ ( $S_9S_c$ )], in which only one  $S$ -allele could be previously identified [21], probably by the mismatching of PCR primers or preferential amplification of the detected allele. The use of specific primers for the  $S_1$ -allele [22] allowed the identification of this allele in 15 cultivars for the first time. The  $S_c$ -allele was confirmed in 19 cultivars in which self-compatibility was previously assessed by cross-pollinations [21]. AprFBC8-(F/R) primers allowed to distinguish between the  $S_c$ - and  $S_8$ -alleles, since an insertion of 358 bp in the  $SFB$  gene causes a loss of the incompatibility that has been observed in the  $SFB_c$  gene but not in the sequence of  $SFB_8$  [52,56]. Therefore, the cultivars carrying the  $S_8$ -allele but not the  $S_c$ -allele, such as ‘Sweet Cot’, might be considered as self-incompatible. A single  $S_c$ -allele was identified in 21 genotypes. As this allele is associated with self-compatibility [56], these cultivars could present homozygosity, as it has been considered in previous reports for some cultivars that have been characterized as  $S_cS_c$  [16,25,34,35,47,52]. Our results agree with previous reports of the  $S$ -genotype for ‘Búlida’ [16], ‘Cebas Red’ [53], ‘Canino’ [34], ‘Gönci magyarkajszai’ [52], ‘Harcot’ [49], ‘Katy’ [55], ‘Ninfa’ [16] and ‘Tilton’ [47]. According to Egea et al. [59], ‘Rojo Pasión’ resulted

from a cross between ‘Orange Red’ ( $S_6S_9$  [16,21]) and ‘Currot’ ( $S_cS_c$  [34]). However, our results for the  $S$ -genotype ( $S_1S_c$ ) differ from this pedigree. Additionally, our results for three cultivars, ‘Alba’, ‘Corbato’, and ‘Tadeo’, differ from the  $S$ -genotype previously reported [16].

According to their  $S$ -allele composition, 12 self-incompatible cultivars were allocated in their corresponding cross-incompatibility groups together with the 77 self-incompatible cultivars previously analyzed [16,21,22,24,32,34,35,47–50]. To date, a total of thirty-five incompatibility groups (I to XXXV) have been described in apricot [17,21,22,32,35,48]. Self-incompatible cultivars within the same incompatibility group have the same  $S$ -genotype and are genetically incompatible with each other. On the other hand, cultivars from different incompatibility groups are inter-compatible, since at least one of the  $S$ -alleles of their genotype is different [60]. Although lower yields have been related to semi-compatible pollinizers (when one  $S$ -allele is identical and the other differs) in Japanese plum and sweet cherry [61–63], there is no information on the effects of semi-compatibility in apricot. In addition, 16 cultivars are included in group 0 since no other cultivars with the same  $S$ -genotype have been reported until now. Thus, the cultivars from group 0 as well as the self-compatible cultivars could act as universal pollinizers. This could be highly valuable information since the knowledge of incompatibility relationships aims to help breeders to choose parental genotypes for breeding programs and fruit growers to select compatible pollinizers coincident at flowering time.

### 3.2. Current Genetic Diversity at the $S$ -Locus

To provide an overview of the genetic diversity at the  $S$ -locus of currently grown apricot cultivars, results herein have been combined with previous results [16,21,22,24,25,32,34,35,39,47–50,52,54,55] to analyze the frequency and distribution of the  $S$ -alleles. A total of 33  $S$ -alleles ( $S_1$  to  $S_{20}$ ,  $S_{22}$  to  $S_{30}$ ,  $S_{52}$ ,  $S_{53}$ ,  $S_c$ ,  $S_v$ , and  $S_x$ ) have been described in apricot cultivars [16,24–27]. Fourteen  $S$ -alleles were detected within the group of 70 traditional cultivars from Armenia, Australia, France, Greece, Hungary, Italy, Romania, Spain, Tunisia, Turkey, Ukraine, and the USA, whereas 17  $S$ -alleles were identified in the group of cultivars from breeding programs, reflecting lower  $S$ -allele diversity in the group of traditional cultivars. Twenty  $S$ -alleles (20) were reported in a group of 67 cultivars from Europe and North America [16], but fewer  $S$ -alleles were found when local accessions or landraces were studied separately in Tunisia [17,35], Turkey [32,36,37], and Morocco [33].

Four  $S$ -alleles ( $S_{10}$ ,  $S_{24}$ ,  $S_{31}$  and  $S_4$ ) were exclusively found in the group of cultivars from breeding programs, which could be related to the use of landraces instead of commercial cultivars in some breeding programs. Two of these  $S$ -alleles showed a clear relationship with a specific breeding program:  $S_{24}$  was found in ‘Ezzine’ from INRAT (Tunisia) [64], and  $S_{31}$  was found in ‘Cow-1’ and ‘Cow-2’ from INRA (France) [65];  $S_4$  was present in the North American cultivar ‘Harcot’ [49]. Although this cultivar has been used as a parental genotype in several breeding programs to introduce Sharka-resistance to new releases [29], the  $S_4$ -allele has not been found in any recent releases. On the other hand, the  $S_5$ -allele has been previously reported only in some traditional cultivars from Spain and Armenia. Our results differed in the  $S$ -genotype of the Spanish landrace ‘Corbato’ in which this allele has been previously reported, ( $S_c$  vs.  $S_2S_5$  [16]). The presence of the  $S_5$ -allele in this cultivar, as well as in other traditional cultivars from Spain and Armenia, has been reported by Muñoz-Sanz et al. [16]. They suggested that the presence of the  $S_5$ -allele in those populations could be the result of a connection between Southern-Spanish accessions with the Armenian and Eastern-Turkish accessions; in addition, they suggested that Moroccan accessions are a part of the Southwest-Mediterranean apricot diffusion route.

Traditionally, the main marker for self-compatibility in apricot has been  $S_c$  [49]. For this reason, one of the main objectives of breeding programs has been to introduce this  $S$ -allele into new releases [11]. Our results showed that  $S_c$  was the most frequent  $S$ -allele in both the groups of traditional and cultivars from breeding programs. Although we did not detect the  $S_c$ -allele in traditional cultivars from Armenia and Turkey, previous reports found some self-compatible Turkish cultivars carrying this  $S$ -allele [32,37]. The  $S_c$ -allele might

have evolved in Southeastern Turkey as a result of a pollen-part mutation within  $SFB_8$ , causing the pollen with the mutated  $S_8$  haplotype to be self-compatible [52]. Subsequently, it is hypothesized that the allele  $S_c$  was disseminated to the Mediterranean Basin since the cultivars from Central Asia, the center of origin of apricot, are self-incompatible [52,66]. The  $S_c$ -allele was present in cultivars from breeding programs in most countries except for Turkey, probably due to the low number of new releases from this country studied in this work. However, the low presence of the  $S_c$ -allele in North American cultivars (the USA and Canada) is probably due to the fact that most of these cultivars are self-incompatible [28,67].

The presence of just one allele has been observed in a high number of cultivars, mostly cultivars released from breeding programs, mainly as genotype  $S_c$ - (Supplementary Table S2) that would presumably correspond to  $S_cS_c$ . Homozygote cultivars can arise as a result of self- and cross-pollinations with self-compatible parents in breeding programs. Although this genotype has been frequently found in apricot cultivars from most European countries [16,25,34,52], results herein as well as those from previous studies could not confirm homozygosity since sequencing would be needed [22].

The distribution of  $S$ -alleles varied considerably between countries, with a significant association ( $p < 0.05$ ) between  $S$ -alleles and geographical origin, both in the group of traditional accessions and in the group of breeding program releases. Within traditional cultivars, the  $S_3$ -allele was found exclusively in North American cultivars [16]. The  $S_{12}$ -allele was only found in four cultivars from Tunisia [35], being one of the most frequent  $S$ -alleles in this country [17]. The  $S_{19}$ -allele was only found in one cultivar from Romania, 'Mari de Cenad', despite having been associated with Hungarian and Turkish local apricots [32]. Muñoz-Sanz et al. [16] reported that the  $S_{19}$ -allele found in this cultivar could be  $S_{20}$ ; however, further sequencing would be required to confirm this.

Alleles  $S_{10}$  to  $S_{14}$  have Armenian origin [24] but they have also been described in cultivars from Eastern Europe [32], Morocco [33], Tunisia [17,35] and Turkey [32,37]. Our results showed three of these alleles ( $S_{10}$ ,  $S_{11}$ , and  $S_{12}$ ) in three Hungarian traditional cultivars, 'Harmat', 'Korai zamatos', and 'Voski'.

Thus, in addition to providing useful information to know the self-compatibility of cultivars,  $S$ -genotyping can be a valuable tool in elucidating the evolution and dissemination of the crop.

### 3.3. Self-Compatibility and Diversity

Self-compatibility has been described as a cause of loss of genetic diversity since it promotes inbreeding [68]. Self-incompatibility not only reduces inbreeding by preventing self-fertilization but also reduces mating between close relatives, ensuring the exchange of genetic material [69]. It has been suggested that the loss of genetic diversity affecting the  $S$ -locus is due to crop dissemination [16]. In fact, a bottleneck has been observed in apricot diversity as a consequence of the domestication and diffusion of the apricot throughout the history of the crop [8]. Additionally, a decrease in genetic diversity from the eastern (Iran-Caucasian area) to the south-western (North Mediterranean Basin and South Mediterranean Basin areas) distribution of the crop has been detected, analyzing local cultivars from Algeria, France, Italy, Morocco, Spain, Tunisia, and Turkey [70]. A lower number of  $S$ -alleles were found in accessions from Moroccan oases as compared to the whole allele pool in this country, probably due to the pressure to increase production and self-compatibility in the genotypes, allowing a higher level of endogamy [33]. A similar situation was described in landraces from Central Europe [52].

Apricots belonging to the European group have been traditionally considered to be self-compatible [71]. However, the number of self-incompatible commercial cultivars in the European group increased rapidly over the last two decades due to the use of self-incompatible North American cultivars as parentals in breeding programs [21,28]. Recent studies show that about half of the new releases are self-compatible: 51.1% (47 of 92) [21] and 49.6% (61 of 123) [20].

Recently, additional sources of self-compatibility have been described in apricot in addition to the  $S_c$ -allele. Thus, some works have reported the existence of an additional mutation in the  $M$ -locus not linked to the  $S$ -locus, which causes a loss of pollen  $S$ -activity [16,55,56,72]. Pollen-part mutations (PPMs) in the  $M$ -locus were mapped at the distal end of chromosome three in ‘Canino’ (called  $m$  [72]) and in ‘Katy’ (called  $m'$  [55]). Muñoz-Sanz et al. [73] proposed the *ParMDO* gene as a relevant gene involved in pollen part SI function. In order to optimize the screening of self-compatible genotypes, a new useful method based on both loci has been recently developed [74].

Although a clear trend towards releasing self-compatible cultivars is shown, our results exhibited similar allelic richness values in both groups, traditional cultivars, and cultivars from breeding programs. A clear differentiation between apricot landraces and cultivars from breeding programs was recently revealed using SSR markers, showing an unexpected higher diversity in cultivars from breeding programs, which was related to the use of North American genotypes as parents [75]. Our results showed a slight loss of diversity for the  $S$ -locus in Hungarian, Tunisian, and Turkish cultivars comparing landraces with releases from breeding programs. However, this situation was not observed in the countries included in the North Mediterranean Basin group such as France, Italy, and Spain. This could be due to the higher number of new releases from breeding programs of these countries.

Although there is no evidence of a reduction in the diversity at the  $S$ -locus in cultivars developed in breeding programs, results herein suggests that the use of a reduced number of parents in breeding programs can lead to a genetic bottleneck.

#### 4. Materials and Methods

##### 4.1. Plant Material

Young leaves from 66 apricot cultivars, including traditional cultivars (landraces and local selections) and releases from breeding programs of several origins (Tables 1 and 2), were collected in spring from germplasm collections and orchards in Spain. Moreover, flowers were collected from two cultivars (‘Samourai’ and ‘Water’) for pollination experiments to establish the self-(in)compatibility by microscopic observations. The apricot accessions analyzed originated from 12 countries: Armenia, Australia, France, Greece, Hungary, Italy, Romania, Spain, Tunisia, Turkey, Ukraine, and the USA.

##### 4.2. DNA Extraction and $S$ -Allele Identification

Genomic DNA of each sample was extracted using DNeasy Plant Mini Kit (Qiagen, Hilden, Germany) according to Hormaza [76] and quantified by NanoDrop™ ND-1000 spectrophotometer (Bio-Science, Budapest, Hungary).

The  $S$ -genotype of each cultivar was identified through PCR amplification of *RNase* and *SFB* regions with different primer combinations (Table 5) [23]. The first intron of the *S-RNase* gene was amplified with the fluorescently labeled primer combination SRC-(F/R) [25,77]. PCR amplifications were carried out in 15  $\mu$ L reaction volumes, containing 10 $\times$  NH<sub>4</sub> Reaction Buffer, 25 mM MgCl<sub>2</sub>, 2.5 mM of each dNTP, 10  $\mu$ M of each primer, 100 ng of genomic DNA and 0.5 U of BioTaq™ DNA polymerase (Bioline, London, UK). The temperature profile used had an initial step of 3 min at 94 °C, 35 cycles of 1 min at 94 °C, 1 min at 55 °C and 3 min at 72 °C, and a final step of 5 min at 72 °C. The amplified fragments were analyzed in a CEQ™ 8000 capillary electrophoresis DNA analysis system (Beckman Coulter, Fullerton, CA, the USA) and classified according to Vilanova et al. [25] and Herrera et al. [21].

**Table 5.** SSR primers used in this study for the identification of *S*-alleles in apricot (*Prunus armeniaca*).

Amplified Region	Name	Specificity	Primer Sequence (5' → 3')	Reference
<i>S</i> -RNase 1st intron	SRc-(F/R)		F: CTCGCTTTCCTGTCTCTG R: GGCCATTGTTGCACCCCTTG	[77]
<i>S</i> -RNase 2nd intron	Pru-C2/C4R		F: CTTGGCCAAGTAATTATTCAAACC R: GGATGTGGTACGATTGAAGCG	[78]
	SHLM1/SHLM2	<i>S</i> <sub>1</sub> -allele	F: GGTGGAGGTGATAAGGTAGCC R: GGCTGCATAAGGAAGCTGTAGG	[22]
	SHLM3/SHLM4	<i>S</i> <sub>7</sub> -allele	F: TATATCTTACTCTTTGGC R: CACTATGATAATGTGTATG	[22]
<i>SFB</i>	AprFBC8-(F/R)		F: CATGGAAAAGCTGACTTATGG R: GCCTCTAATGTCATCTACTCTTAG	[32]

Because two pairs of alleles, *S*<sub>6</sub>/*S*<sub>9</sub> and *S*<sub>1</sub>/*S*<sub>7</sub>, showed similar fragment sizes, specific primers based on the second intron of the *RNase* were used to distinguish between them. For the identification of the *S*<sub>6</sub>- and *S*<sub>9</sub>-alleles, the PruC2/PruC4R primer combination designed from *P. avium S-RNase*-cDNA sequences [78] was used to differentiate both alleles in 15 genotypes. Specific primers SHLM1/SHLM2 and SHLM3/SHLM4 were required to distinguish between *S*<sub>1</sub> and *S*<sub>7</sub>, respectively [22]. PCR reactions were carried out according to Vilanova et al. [25], but with the addition of 10 cycles and using 55 °C of annealing temperature [79]. The amplified fragments were separated on 1% (*w/v*) agarose gels and the DNA bands were visualized using the nucleic acid stain SYBR Green (Thermo Fisher Scientific, St Leon-Rot, Germany). For the identification of the *S*<sub>1</sub>-allele, the specific primers SHLM1 and SHLM2 were used following the protocol described by Herrera et al. [22] for *Taq* DNA polymerase (Qiagen, Hilden, Germany). Primers SHLM3 and SHLM4 were used for *S*<sub>7</sub>-allele identification. PCR reactions were performed with Phusion® High-Fidelity DNA Polymerase (Thermo Fisher Scientific, St Leon-Rot, Germany) according to Herrera et al. [22].

Since PCR amplification of the *S*<sub>6</sub>- and *S*<sub>8</sub>-alleles using the primers SRc-(F/R) provides a fragment of similar size [24,56], the specific primers AprFBC8-F and AprFBC8-R, designed based on the V2 and HVb variable region of *SFB* gene, were used to distinguish between both alleles [32]. The PCR amplifications were carried out using the program previously described by Halász et al. [32].

#### 4.3. Pollination Experiments

In cultivars ‘Samourai’ and ‘Water’, no amplification was produced with the primers AprFBC8-F/AprFBC8-R. Thus, controlled pollinations were carried out in these two cultivars to differentiate the *S*<sub>6</sub>- and *S*<sub>8</sub>-alleles. Self-(in)compatibility was established by laboratory-controlled pollinations and the observation of pollen tube growth under fluorescence microscopy [23]. Self-pollinations were carried out in the two cultivars. Pollen of the cultivar ‘Katy’, known as universal pollinizer for apricot [55], was used to pollinize another set of flowers of each cultivar as control.

Flowers from each cultivar were collected at the balloon stage one day before anthesis and emasculated to avoid self-pollination. Pistils were placed on wet florist foam and maintained at laboratory temperature. After 24 h, a group of 20–25 flowers were hand-pollinated with the help of a paintbrush for each self- and cross-pollination [80]. Pollen was obtained from flowers at the same balloon stage by removing and drying the anthers at laboratory temperature during 24 h. Pollen grains were then sieved by using a fine mesh (0.26 mm) and used immediately or frozen at −20 °C until further use. Seventy-two hours after pollination, pistils were fixed in ethanol (95%)/acetic acid (3:1, *v/v*) during 24 h, and conserved at 4 °C in 75% ethanol. After hand pollinations, pollen viability was evaluated. Pollen from each pollen donor was scattered on a solidified pollen germination medium [81] and pollen germination was observed under the microscope after 24 h. Pollen

grains were considered viable when the length of the growing pollen tube was higher than the pollen grain diameter.

For histochemical preparations, the fixed pistils were washed three times for 1 h with distilled water and left in 5% sodium sulphite in distilled water at 4 °C for 24 h. Then, they were autoclaved at 1 kg/cm<sup>2</sup> during 10 min in sodium sulphite to soften the tissues [82]. Pistils were squashed and stained with 0.1% (*v/v*) aniline blue in 0.1N K<sub>3</sub>PO<sub>4</sub> [83] to observe callose. Examination of pollen tube growth was carried out by fluorescence microscopy using by a Leica DM2500 microscope (Cambridge, UK) with UV epifluorescence using 340–380 bandpass and 425 longpass filters.

Pollen tube behavior was observed in at least 10 pistils in each self-pollination. Cultivars were considered as self-incompatible when pollen tube growth was arrested along the style in most self-pollinated pistils. On the other hand, when the pollen tube reached the base of the style in most self-pollinations, the cultivars were considered as self-compatible.

#### 4.4. S-Allele Diversity Analysis

In order to analyze the *S*-allele genetic diversity, the *S*-*RNase* genotypes of the 60 cultivars identified herein were compiled with those of the 175 cultivars previously reported (Tables 1 and 2; Supplementary Table S2). Cultivars were first classified into two groups according to the pedigree origin of the accessions, traditional, and releases from breeding programs. Statistical analyses were performed using the R programming environment (R Core Team, 2022, version 4.1.0, Vienna, Austria). The *S*-genetic profiles were stored in a csv file which was converted into a matrix of allelic frequencies stored in a genind class with the “loci2genind” function using the R package “pegas” version 1.0–1 [84]. Missing data (<0.1%) were replaced with the mean frequency of the corresponding allele, which avoids adding artefactual between-group differentiation [85].

The number of alleles ( $N_a$ ), allelic richness ( $A_r$ ), and private alleles ( $P_a$ ) were calculated for all countries on the traditional and cultivars from breeding programs using the adegenet 2.1.3 [85], and PopGenReport 3.0.4 [86] packages. Additionally, the frequency of each *S*-allele was calculated in each country within each group and the results were plotted as a heatmap with the R package PopGenReport version 3.0.4 [86]. To analyze the relationship between the *S*-alleles and their distribution by country, a contingency table of absolute frequencies of alleles by country was created and a chi-square test was performed with the “chisq.test” function using the R package “stats” v. 4.1.2. Due to the low number of observations in some countries, a Monte Carlo simulation with 2000 replicates was indicated.

## 5. Conclusions

Results reveal that a significant proportion of new apricot releases are self-incompatible and, therefore, require cross-pollination to produce fruit. Knowing the incompatibility relationships between cultivars will help breeders to select suitable parental genotypes in crosses. This information, combined with the flowering dates in each geographical area, will allow the selection of appropriate inter-compatible pollinizers for self-incompatible cultivars in the design of new orchards. The identification of the *S*-alleles, in addition to the determination of the pollination requirements of the cultivars, can elucidate missing gaps in the evolution, domestication, and dissemination of the crop. The diversity at the *S*-locus observed in the cultivars developed in breeding programs indicates a possible genetic bottleneck due to the use of a reduced number of parents in breeding programs.

**Supplementary Materials:** The following supporting information can be downloaded at: <https://www.mdpi.com/article/10.3390/plants11152019/s1>, Table S1: Sizes of PCR fragment amplification using five primer pair combinations for the identification of *S*-alleles and *S*-genotype of the analyzed apricot accessions; Table S2: Origin and *S*-genotype of the 235 analyzed apricot accessions; Table S3: Contingency table of absolute allele frequencies by country in apricot traditional cultivars including landraces and local selections and Pearson’s chi-squared test with simulated *p*-value (based on 2000 replicates); Table S4: Contingency table of absolute allele frequencies by country in apricot

cultivars released from breeding programs and Pearson's chi-squared test with simulated *p*-value (based on 2000 replicates).

**Author Contributions:** Conceptualization, J.I.H., J.L. and J.R.; methodology S.H.; data curation, S.H.; writing—original draft preparation, S.H., J.I.H., J.L. and J.R.; writing—review and editing, S.H., J.I.H., J.L. and J.R. All authors have read and agreed to the published version of the manuscript.

**Funding:** This research was funded by the projects PCI2020-111966, PID2019-109566RB-I00 and PID2020-115473RR-I00 funded by MCIN/AEI/10.13039/501100011033, the grant PRE2018-084962 funded by MCIN/AEI/10.13039/501100011033, and FSE “El FSE invierte en tu futuro” and Gobierno de Aragón—European Social Fund, European Union (Grupo Consolidado A12\_17R).

**Data Availability Statement:** Not applicable.

**Acknowledgments:** We thank Yolanda Verdún for technical assistance.

**Conflicts of Interest:** The authors declare no conflict of interest. The funders had no role in the design of the study; in the collection, analyses, or interpretation of data; in the writing of the manuscript, or in the decision to publish the results.

## References

- Janick, J. The Origin of Fruits, Fruit Frowing and Fruit Breeding. *Plant Breed. Rev.* **2005**, *25*, 255–320. [CrossRef]
- Groppi, A.; Liu, S.; Cornille, A.; Decroocq, S.; Bui, Q.T.; Tricon, D.; Cruaud, C.; Arribat, S.; Belser, C.; Marande, W.; et al. Population genomics of apricots unravels domestication history and adaptive events. *Nat. Commun.* **2021**, *12*, 3956. [CrossRef]
- Faust, M.; Surányi, D.; Nyujtó, F. Origin and Dissemination of Apricot. *Hortic. Rev.* **1998**, *22*, 225–266. [CrossRef]
- FAOSTAT. Available online: <http://www.fao.org/faostat/es/> (accessed on 24 June 2022).
- Dirlwanger, E.; Graziano, E.; Joobeur, T.; Garriga-Caldere, F.; Cosson, P.; Howad, W.; Arus, P. Comparative mapping and marker-assisted selection in Rosaceae fruit crops. *Proc. Natl. Acad. Sci. USA* **2004**, *101*, 9891–9896. [CrossRef] [PubMed]
- Layne, R.E.C.; Bailey, C.; Hough, L.F. Apricots. In *Fruit Breeding, Volume I: Tree and Tropical Fruits*; Janick, J., Moore, J.N., Eds.; JohnWiley & Sons, Inc.: New York, NY, USA, 1996; pp. 79–111.
- Herrera, S.; Lora, J.; Hormaza, J.I.; Rodrigo, J. Pollination Management in Stone Fruit Crops. In *Production Technology of Stone Fruits*; Mir, M.M., Iqbal, M., Mir, S.A., Eds.; Springer: Singapore, 2021; pp. 75–102.
- Bourguiba, H.; Scotti, I.; Sauvage, C.; Zhebentyayeva, T.; Ledbetter, C.; Krška, B.; Remay, A.; D'Onofrio, C.; Iketani, H.; Christen, D.; et al. Genetic Structure of a Worldwide Germplasm Collection of *Prunus armeniaca* L. Reveals Three Major Diffusion Routes for Varieties Coming From the Species' Center of Origin. *Front. Plant Sci.* **2020**, *11*, 638. [CrossRef]
- Hegedűs, A.; Lénárt, J.; Halász, J. Sexual incompatibility in Rosaceae fruit tree species: Molecular interactions and evolutionary dynamics. *Biol. Plant.* **2012**, *56*, 201–209. [CrossRef]
- Tao, R.; Yamane, H.; Sassa, H.; Mori, H.; Gradziel, T.M.; Dandekar, A.M.; Sugiura, A. Identification of stylar RNases associated with gametophytic self-incompatibility in almond (*Prunus dulcis*). *Plant Cell Physiol.* **1997**, *38*, 304–311. [CrossRef]
- Muñoz-Sanz, J.V.; Zuriaga, E.; Cruz-García, F.; McClure, B.; Romero, C. Self-(In)compatibility Systems: Target Traits for Crop-Production, Plant Breeding, and Biotechnology. *Front. Plant Sci.* **2020**, *11*, 195. [CrossRef]
- de Nettancourt, N. *Incompatibility and Incongruity in Wild and Cultivated Plants*; Springer: Berlin/Heidelberg, Germany, 2001.
- Ushijima, K.; Sassa, H.; Dandekar, A.M.; Gradziel, T.M.; Tao, R.; Hirano, H. Structural and transcriptional analysis of the self-incompatibility locus of almond: Identification of a pollen-expressed *F-box* gene with haplotype-specific polymorphism. *Plant Cell* **2003**, *15*, 771–781. [CrossRef]
- Cachi, A.M.; Hedhly, A.; Hormaza, J.I.; Wunsch, A. Pollen tube growth in the self-compatible sweet cherry genotype, ‘Cristobalina’, is slowed down after self-pollination. *Ann. Appl. Biol.* **2014**, *164*, 73–84. [CrossRef]
- Socias i Company, R.; Kodad, O.; Fernández, A.; Alonso, J.M. Mutations conferring self-compatibility in *Prunus* species: From deletions and insertions to epigenetic alterations. *Sci. Hortic.* **2015**, *192*, 125–131. [CrossRef]
- Muñoz-Sanz, J.V.; Zuriaga, E.; López, I.; Badenes, M.L.; Romero, C. Self-(in)compatibility in apricot germplasm is controlled by two major loci, *S* and *M*. *BMC Plant Biol.* **2017**, *17*, 82. [CrossRef]
- Boubakri, A.; Krichen, L.; Batnini, M.A.; Trifi-Farah, N.; Roch, G.; Audergon, J.M.; Bourguiba, H. Self-(in)compatibility analysis of apricot germplasm in Tunisia: *S-RNase* allele identification, *S*-genotype determination and crop history evolution. *Sci. Hortic.* **2021**, *276*, 109758. [CrossRef]
- Milatović, D.; Nikolic, D.; Fotiric-Aksic, M.; Radovic, A. Testing of self-(in)compatibility in apricot cultivars using fluorescence microscopy. *Acta Sci. Pol. Hortorum Cultus* **2013**, *12*, 103–113. [CrossRef]
- Milatović, D.; Nikolić, D.; Krška, B. Testing of self-(in)compatibility in apricot cultivars from European breeding programmes. *Hortic. Sci.* **2013**, *40*, 65–71. [CrossRef]
- Milatović, D.; Nikolić, D.; Radović, A.; Krška, B. Fluorescence microscopy as a tool for determining self-incompatibility in apricot cultivars. *Acta Hortic.* **2018**, *1214*, 7–14. [CrossRef]

21. Herrera, S.; Lora, J.; Hormaza, J.I.; Herrero, M.; Rodrigo, J. Optimizing production in the new generation of apricot cultivars: Self-incompatibility, *S-RNase* allele identification, and incompatibility group assignment. *Front. Plant Sci.* **2018**, *9*, 527. [[CrossRef](#)]
22. Herrera, S.; Rodrigo, J.; Hormaza, J.I.; Lora, J. Identification of self-incompatibility alleles by specific PCR analysis and *S-RNase* sequencing in apricot. *Int. J. Mol. Sci.* **2018**, *19*, 3612. [[CrossRef](#)] [[PubMed](#)]
23. Herrera, S.; Lora, J.; Hormaza, J.I.; Rodrigo, J. Determination of Self- and Inter-(in)compatibility Relationships in Apricot Combining Hand-Pollination, Microscopy and Genetic Analyses. *JoVE J. Vis. Exp.* **2020**, *160*, e60241. [[CrossRef](#)]
24. Halász, J.; Hegedus, A.; Hermán, R.; Stefanovits-Bányai, É.; Pedryc, A. New self-incompatibility alleles in apricot (*Prunus armeniaca* L.) revealed by stylar ribonuclease assay and S-PCR analysis. *Euphytica* **2005**, *145*, 57–66. [[CrossRef](#)]
25. Vilanova, S.; Romero, C.; Llacer, G.; Badenes, M.L.; Burgos, L. Identification of Self-(in)compatibility Alleles in Apricot by PCR and Sequence Analysis. *J. Am. Soc. Hortic. Sci.* **2005**, *130*, 893–898. [[CrossRef](#)]
26. Zhang, L.; Chen, X.; Chen, X.; Zhang, C.; Liu, X.; Ci, Z.; Zhang, H.; Wu, C.; Liu, C. Identification of self-incompatibility (S-) genotypes of Chinese apricot cultivars. *Euphytica* **2008**, *160*, 241–248. [[CrossRef](#)]
27. Murathan, Z.T.; Kafkas, S.; Asma, B.M.; Topçu, H. S<sub>1</sub> allele identification and genetic diversity analysis of apricot cultivars. *J. Hortic. Sci. Biotechnol.* **2017**, *92*, 251–260. [[CrossRef](#)]
28. Zhebentyayeva, T.; Ledbetter, C.; Burgos, L.; Llácer, G. Apricot. In *Fruit Breeding*; Badenes, M.L., Byrne, D.H., Eds.; Springer: Boston, MA, USA, 2012; ISBN 978-1-4419-0762-2.
29. Krška, B. Genetic Apricot Resources and their Utilisation in Breeding. In *Breeding and Health Benefits of Fruit and Nut Crops*; Soneji, J.R., Nageswara-Rao, M., Eds.; IntechOpen: London, UK, 2018.
30. Roy, A.S.; Smith, I.M. Plum pox situation in Europe. *EPPO Bull.* **1994**, *24*, 515–523. [[CrossRef](#)]
31. García, J.A.; Cambra, M. Plum pox virus and sharka disease. *Plant Viruses* **2007**, *1*, 69–79.
32. Halász, J.; Pedryc, A.; Ercisli, S.; Yilmaz, K.U.; Hegedüs, A. S-genotyping supports the genetic relationships between Turkish and Hungarian apricot germplasm. *J. Am. Soc. Hortic. Sci.* **2010**, *135*, 410–417. [[CrossRef](#)]
33. Kodad, O.; Hegedüs, A.; Socias i Company, R.; Halász, J. Self-(in)compatibility genotypes of Moroccan apricots indicate differences and similarities in the crop history of European and North African apricot germplasm. *BMC Plant Biol.* **2013**, *13*, 196. [[CrossRef](#)]
34. Alburquerque, N.; Egea, J.; Pérez-Tornero, O.; Burgos, L. Genotyping apricot cultivars for self-(in)compatibility by means of *RNases* associated with S alleles. *Plant Breed.* **2002**, *121*, 343–347. [[CrossRef](#)]
35. Lachkar, A.; Fattouch, S.; Ghazouani, T.; Halasz, J.; Pedryc, A.; Hegedüs, A. Identification of self-(in)compatibility S-alleles and new cross-incompatibility groups in Tunisian apricot (*Prunus armeniaca* L.) cultivars. *J. Hortic. Sci. Biotechnol.* **2013**, *88*, 497–501. [[CrossRef](#)]
36. Halasz, J.; Hegedus, A.; Szikriszt, B.; Ercisli, S.; Orhan, E.; Unlu, H.M. The S-genotyping of wild-grown apricots reveals only self-incompatible accessions in the Erzincan region of Turkey. *Turk. J. Biol.* **2013**, *37*, 733–740. [[CrossRef](#)]
37. Yilmaz, K.U.; Basbug, B.; Gurcan, K.; Halasz, J.; Ercisli, S.; Uzun, A.; Cocen, E. S-Genotype Profiles of Turkish Apricot Germplasm. *Not. Bot. Horti Agrobi.* **2016**, *44*, 67–71. [[CrossRef](#)]
38. Egea, J.; Dicenta, F.; Burgos, L.; Martínez-Gómez, P.; Rubio, M.; Campoy, J.; Ortega, E.; Patiño, J.; Nortes, L.; Molina, A.; et al. New Apricot Cultivars From Cebas-Csic (Murcia, Spain) Breeding Programme. *Acta Hortic.* **2010**, *862*, 113–118. [[CrossRef](#)]
39. Ruiz, D.; Molina, A.; Nortes, M.D.; Molina Jr., A.; Ortega, E.; Martínez-Gómez, P.; Dicenta, F.; Rubio, M.; Egea, J. New apricot selections from the CEBAS-CSIC breeding program (Murcia, Spain) that broaden fruit ripening time. *Acta Hortic.* **2018**, *1214*, 217–220. [[CrossRef](#)]
40. Badenes, M.L.; Martínez-Calvo, J.; Gómez, H.; Zuriaga, E. ‘Dama taronja’ and ‘dama rosa’ apricot cultivars that are resistant to sharka (Plum pox virus). *HortScience* **2018**, *53*, 1228–1229. [[CrossRef](#)]
41. Audergon, J.M.; Duffillol, J.M.; Gilles, F.; Clauzel, G.; Chaffour, D.; Giard, A.; Blanc, A.; Broquaire, J.M.; Moulon, B. “Solédane”, “Florilège” and “Bergarouge ®” Avirine: Three new apricot cultivars for French country. *Acta Hortic.* **2006**, *701*, 395–398. [[CrossRef](#)]
42. Audergon, J.M.; Blanc, A.; Gilles, F.; Clauzel, G.; Broquaire, J.M.; Gouble, B.; Grotte, M.; Reich, M.; Bureau, S.; Frémondrière, G.; et al. An integrated apricot breeding program in France joining CEP innovation—CENTREX and INRA. *Acta Hortic.* **2012**, *966*, 17–22. [[CrossRef](#)]
43. Frémondrière, G.; Blanc, A.; Gilles, F.; Clauzel, G.; Broquaire, J.M.; Roch, G.; Gouble, B. Selections issued from CEP Innovation, Centrex and INRA: The apricot breeding program in France. *Acta Hortic.* **2018**, *1214*, 207–210. [[CrossRef](#)]
44. Bassi, D.; Rizzo, M.; Foschi, S. Breeding apricot in northern Italy. *Acta Hortic.* **2010**, *862*, 151–158. [[CrossRef](#)]
45. Ledbetter, C.A. Apricot Breeding in North America: Current Status and Future Prospects. *Acta Hortic.* **2010**, *862*, 85–92. [[CrossRef](#)]
46. Feng, J.; Chen, X.; Wu, Y.; Liu, W.; Liang, Q.; Zhang, L. Detection and transcript expression of *S-RNase* gene associated with self-incompatibility in apricot (*Prunus armeniaca* L.). *Mol. Biol. Rep.* **2006**, *33*, 215–221. [[CrossRef](#)]
47. Donoso, J.M.; Aros, D.; Meneses, C.; Infante, R. Identification of S-alleles associated with self-incompatibility in apricots (*Prunus armeniaca* L.) using molecular markers. *J. Food Agric. Environ.* **2009**, *7*, 270–273.
48. Egea, J.; Burgos, L. Detecting Cross-incompatibility of Three North American Apricot Cultivars and Establishing the First Incompatibility Group in Apricot. *J. Am. Soc. Hortic. Sci.* **1996**, *121*, 1002–1005. [[CrossRef](#)]
49. Burgos, L.; Pérez-Tornero, O.; Ballester, J.; Olmos, E. Detection and inheritance of stylar ribonucleases associated with incompatibility alleles in apricot. *Sex. Plant Reprod.* **1998**, *11*, 153–158. [[CrossRef](#)]

50. Herrera, S.; Lora, J.; Hormaza, I.; Rodrigo, J. Pollination requirements of new apricot (*Prunus armeniaca* L.) cultivars. *Acta Hortic.* 2022; *in press*.
51. Campoy, J.A.; Dicenta, F.; Burgos, L.; Patin, J.L. ‘Estrella’ and ‘Sublime’ Apricot Cultivars. *HortScience* 2009, 44, 469–470.
52. Halász, J.; Pedryc, A.; Hegedus, A. Origin and dissemination of the pollen-part mutated SC haplotype which confers self-compatibility in apricot (*Prunus armeniaca*). *New Phytol.* 2007, 176, 792–803. [[CrossRef](#)] [[PubMed](#)]
53. Ruiz, D.; Rubio, M.; Martínez-Gómez, P.; López-Alcolea, J.; Dicenta, F.; Ortega, E.; Nortes, M.D.; Molina, A.; Egea, J. ‘Cebasred’ and ‘Primorosa’ Apricots: Two New Self-compatible, Plum pox virus (Sharka)-resistant, and Very Early Ripening Cultivars for the Fresh Market. *HortScience* 2018, 53, 1919–1921. [[CrossRef](#)]
54. Egea, J.; Rubio, M.; Campoy, J.A.; Dicenta, F.; Ortega, E.; Nortes, M.D.; Martínez-Gómez, P.; Molina, A.; Molina, A.; Ruiz, D. ‘Mirlo Blanco’, ‘Mirlo anaranjado’, and ‘Mirlo Rojo’: Three new very early-season apricots for the fresh market. *HortScience* 2010, 45, 1893–1894. [[CrossRef](#)]
55. Zuriaga, E.; Muñoz-Sanz, J.V.; Molina, L.; Gisbert, A.D.; Badenes, M.L.; Romero, C. An S-Locus Independent Pollen Factor Confers Self-Compatibility in “Katy” Apricot. *PLoS ONE* 2013, 8, e53947. [[CrossRef](#)]
56. Vilanova, S.; Soriano, J.M.; Lalli, D.A.; Romero, C.; Abbott, A.G.; Llácer, G.; Badenes, M.L. Development of SSR markers located in the G1 linkage group of apricot (*Prunus armeniaca* L.) using a bacterial artificial chromosome library. *Mol. Ecol. Notes* 2006, 6, 789–791. [[CrossRef](#)]
57. Guerra, M.E.; Rodrigo, J. Japanese plum pollination: A review. *Sci. Hortic.* 2015, 197, 674–686. [[CrossRef](#)]
58. Guerra, M.E.; Guerrero, B.I.; Casadomet, C.; Rodrigo, J. Self-(in)compatibility, *S-RNase* allele identification, and selection of pollinizers in new Japanese plum-type cultivars. *Sci. Hortic.* 2020, 261, 109022. [[CrossRef](#)]
59. Egea, J.; Dicenta, F.; Burgos, L. ‘Rojo Pasión’ Apricot. *HortScience* 2004, 39, 1490–1491. [[CrossRef](#)]
60. Kao, T.; Tsukamoto, T. The Molecular and Genetic Bases of *S-RNase*-Based Self-Incompatibility. *Plant Cell* 2004, 16 (Suppl. S1), S72–S84. [[CrossRef](#)]
61. Ganopoulos, I.V.; Argiriou, A.; Tsaftaris, A.S. Determination of self-incompatible genotypes in 21 cultivated sweet cherry cultivars in Greece and implications for orchard cultivation. *J. Hortic. Sci. Biotechnol.* 2015, 85, 444–448. [[CrossRef](#)]
62. Sapir, G.; Stern, R.A.; Shafir, S.; Goldway, M. Full compatibility is superior to semi-compatibility for fruit set in Japanese plum (*Prunus salicina* Lindl.) cultivars. *Sci. Hortic.* 2008, 116, 394–398. [[CrossRef](#)]
63. Sapir, G.; Stern, R.A.; Shafir, S.; Goldway, M. *S-RNase* based S-genotyping of Japanese plum (*Prunus salicina* Lindl.) and its implication on the assortment of cultivar-couples in the orchard. *Sci. Hortic.* 2008, 118, 8–13. [[CrossRef](#)]
64. Lachkar, A.; Mlika, M. New apricot varieties selected from the Tunisian Breeding Programme. *Acta Hortic.* 2006, 717, 189–192. [[CrossRef](#)]
65. Muñoz-Sanz, J.V. Crossability barriers in *Prunus*: The Role of Modifiers in the Regulation of the Gametophytic Self-Incompatibility System. Ph.D. Thesis, Universitat Politècnica de València, Valencia, Spain, 2016.
66. Zaurov, D.E.; Molnar, T.J.; Eisenman, S.W.; Ford, T.M.; Mavlyanova, R.F.; Capik, J.M.; Funk, C.R.; Goffreda, J.C. Genetic resources of apricots (*Prunus armeniaca* L.) in Central Asia. *HortScience* 2013, 48, 681–691. [[CrossRef](#)]
67. Hormaza, J.I.; Yamane, H.; Rodrigo, J. Apricot. In *Fruits and Nuts. Genome Mapping and Molecular Breeding in Plants*; Kole, C., Ed.; Springer: Berlin/Heidelberg, Germany, 2007; Volume 4, pp. 171–187.
68. Igic, B.; Lande, R.; Kohn, J.R. Loss of self-incompatibility and its evolutionary consequences. *Int. J. Plant Sci.* 2008, 169, 93–104. [[CrossRef](#)]
69. Bedinger, P.A.; Broz, A.K.; Tovar-mendez, A.; McClure, B. Pollen-Pistil Interactions and Their Role in Mate Selection. *Plant Physiol.* 2017, 173, 79–90. [[CrossRef](#)]
70. Bourguiba, H.; Audergon, J.M.; Krichen, L.; Trifi-Farah, N.; Mamouni, A.; Trabelsi, S.; D’Onofrio, C.; Asma, B.M.; Santoni, S.; Khadari, B. Loss of genetic diversity as a signature of apricot domestication and diffusion into the Mediterranean Basin. *BMC Plant Biol.* 2012, 12, 49. [[CrossRef](#)]
71. Burgos, L.; Egea, J.; Guerriero, R.; Viti, R.; Monteleone, P.; Audergon, J.M. The self-compatibility trait of the main apricot cultivars and new selections from breeding programmes and new selections from breeding programmes. *J. Hortic. Sci.* 1997, 72, 147–154. [[CrossRef](#)]
72. Zuriaga, E.; Molina, L.; Badenes, M.L.; Romero, C. Physical mapping of a pollen modifier locus controlling self-incompatibility in apricot and synteny analysis within the Rosaceae. *Plant Mol. Biol.* 2012, 79, 229–242. [[CrossRef](#)] [[PubMed](#)]
73. Muñoz-Sanz, J.V.; Zuriaga, E.; Badenes, M.L.; Romero, C. A disulfide bond A-like oxidoreductase is a strong candidate gene for self-incompatibility in apricot (*Prunus armeniaca*) pollen. *J. Exp. Bot.* 2017, 68, 5069–5078. [[CrossRef](#)]
74. Orlando Marchesano, B.M.; Chiozzotto, R.; Baccichet, I.; Bassi, D.; Cirilli, M. Development of an HRMA-Based Marker Assisted Selection (MAS) Approach for Cost-Effective Genotyping of S and M Loci Controlling Self-Compatibility in Apricot (*Prunus armeniaca* L.). *Genes* 2022, 13, 548. [[CrossRef](#)]
75. Herrera, S.; Hormaza, J.I.; Lora, J.; Ylla, G.; Rodrigo, J. Molecular characterization of genetic diversity in apricot cultivars: Current situation and future perspectives. *Agronomy* 2021, 11, 1714. [[CrossRef](#)]
76. Hormaza, J.I. Molecular characterization and similarity relationships among apricot (*Prunus armeniaca* L.) genotypes using simple sequence repeats. *Theor. Appl. Genet.* 2002, 104, 321–328. [[CrossRef](#)]

77. Romero, C.; Vilanova, S.; Burgos, L.; Martínez-Calvo, J.; Vicente, M.; Llácer, G.; Badenes, M.L. Analysis of the S-locus structure in *Prunus armeniaca* L. Identification of S-haplotype specific S-RNase and F-box genes. *Plant Mol. Biol.* **2004**, *56*, 145–157. [[CrossRef](#)] [[PubMed](#)]
78. Tao, R.; Yamane, H.; Sugiura, A.; Murayama, H.; Sassa, H.; Mori, H. Molecular typing of S-alleles through Identification, characterization and cDNA cloning for S-RNases in Sweet Cherry. *J. Am. Soc. Hortic. Sci.* **1999**, *124*, 224–233. [[CrossRef](#)]
79. Sonneveld, T.; Tobutt, K.R.; Robbins, T.P. Allele-specific PCR detection of sweet cherry self-incompatibility (S) alleles S<sub>1</sub> to S<sub>16</sub> using consensus and allele-specific primers. *Theor. Appl. Genet.* **2003**, *107*, 1059–1070. [[CrossRef](#)] [[PubMed](#)]
80. Rodrigo, J.; Herrero, M. The onset of fruiting in apricot (*Prunus armeniaca* L.). *J. Appl. Bot.* **2002**, *76*, 13–19.
81. Hormaza, J.I.; Pinney, K.; Polito, V.S. Correlation in the tolerance to ozone between sporophytes and male gametophytes of several fruit and nut tree species (Rosaceae). *Sex. Plant Reprod.* **1996**, *9*, 44–48. [[CrossRef](#)]
82. Jefferies, C.J.; Belcher, A.R. A fluorescent brightener used for pollen tube identification in vivo. *Stain Technol.* **1974**, *49*, 199–202. [[CrossRef](#)] [[PubMed](#)]
83. Linskens, H.F.; Esser, K. Über eine spezifische Anfarbung der Pollenschlauche im Griffel und die Zahl der Kallosepfropfen nach Selbstung und Fremdung. *Die Nat.* **1957**, *44*, 16. [[CrossRef](#)]
84. Paradis, E. Pegas: An R package for population genetics with an integrated–modular approach. *Bioinformatics* **2010**, *26*, 419–420. [[CrossRef](#)]
85. Jombart, T. Adegenet: A R package for the multivariate analysis of genetic markers. *Bioinformatics* **2008**, *24*, 1403–1405. [[CrossRef](#)] [[PubMed](#)]
86. Adamack, A.T.; Gruber, B. POPGENREPORT: Simplifying basic population genetic analyses in R. *Methods Ecol. Evol.* **2014**, *5*, 384–387. [[CrossRef](#)]



## Article

# Genome-Wide Survey and Expression Analyses of Hexokinase Family in Poplar (*Populus trichocarpa*)

Mei Han <sup>1,†</sup>, Xianglei Xu <sup>1,2,†</sup>, Yuan Xiong <sup>1,2,†</sup>, Haikun Wei <sup>1</sup>, Kejun Yao <sup>1</sup>, Tingting Huang <sup>1</sup>, Yingle Long <sup>1</sup> and Tao Su <sup>1,2,\*</sup>

- <sup>1</sup> Co-Innovation Center for Sustainable Forestry in Southern China, College of Biology and the Environment, Nanjing Forestry University, Nanjing 210037, China; sthanmei@njfu.edu.cn (M.H.); 1736164453@njfu.edu.cn (X.X.); xiongyuan@njfu.edu.cn (Y.X.); weihaikun@njfu.edu.cn (H.W.); yaokejun@njfu.edu.cn (K.Y.); huangtingting2002@163.com (T.H.); 13613033020@163.com (Y.L.)
- <sup>2</sup> Key Laboratory of State Forestry Administration on Subtropical Forest Biodiversity Conservation, Nanjing Forestry University, Nanjing 210037, China
- \* Correspondence: sutao@njfu.edu.cn; Tel.: +86-1589-598-3381
- † These authors contributed equally to this paper.

**Abstract:** Hexokinase (HXK) family proteins exert critical roles in catalyzing hexose phosphorylation, sugar sensing, and modulation of plant growth and stress adaptation. Nevertheless, a large amount remains unknown about the molecular profile of HXK enzymes in *Populus trichocarpa*, a woody model tree species. A genome-wide survey of HXK-encoding genes, including phylogenies, genomic structures, exon/intron organization, chromosomal distribution, and conserved features, was conducted, identifying six putative HXK isogenes (*PtHXK1-6*) in the *Populus* genome. The evolutionary tree demonstrated that 135 homologous HXKs between 17 plant species were categorized into four major subfamilies (type A, B, C, and D), clustering one plastidic (*PtHXK3*) and five mitochondrial *PtHXKs* grouped into type A and B, respectively. The in silico deduction prompted the presence of the conserved sugar-binding core (motif 4), phosphorylation sites (motif 2 and 3), and adenosine-binding domains (motif 7). The transcriptomic sequencing (RNA-seq) and the quantitative real-time PCR (qRT-PCR) assays revealed that three isogenes (*PtHXK2*, 3, and 6) were abundantly expressed in leaves, stems, and roots, while others appeared to be dominantly expressed in the reproductive tissues. Under the stress exposure, *PtHXK2* and 6 displayed a significant induction upon the pathogenic fungi (*Fusarium solani*) infection and marked promotions by glucose feeding in roots. In contrast, the *PtHXK3* and 6 are ABA-responsive genes, following a dose-dependent manner. The comprehensive analyses of the genomic patterns and expression profiling provide theoretical clues and lay a foundation for unraveling the physiological and signaling roles underlying the fine-tuned *PtHXKs* responding to diverse stressors.

**Keywords:** *Populus*; hexokinase; sucrose metabolism; sugar signaling; stress and defense

**Citation:** Han, M.; Xu, X.; Xiong, Y.; Wei, H.; Yao, K.; Huang, T.; Long, Y.; Su, T. Genome-Wide Survey and Expression Analyses of Hexokinase Family in Poplar (*Populus trichocarpa*). *Plants* **2022**, *11*, 2025. <https://doi.org/10.3390/plants11152025>

Academic Editors: Petronia Carillo, Milan S. Stankovic and Paula Baptista

Received: 20 July 2022  
Accepted: 2 August 2022  
Published: 3 August 2022

**Publisher's Note:** MDPI stays neutral with regard to jurisdictional claims in published maps and institutional affiliations.



**Copyright:** © 2022 by the authors. Licensee MDPI, Basel, Switzerland. This article is an open access article distributed under the terms and conditions of the Creative Commons Attribution (CC BY) license (<https://creativecommons.org/licenses/by/4.0/>).

## 1. Introduction

Sucrose is the primary form of photosynthetic carbohydrates produced in source leaves. Depending on symplastic and apoplasmic pathways, sucrose is translocated and unloaded to sink tissues (e.g., roots and stems), where it is further metabolized into glucose and fructose (hexoses), maintaining cellular metabolism in different compartmentations [1]. In plants, hexoses are the central carbon energy source and signaling molecules influencing the whole life cycle [2]. During the sucrose metabolism, the catalysis of hexose phosphorylation is intermediated by hexokinase (HXK, EC 2.7.1.1) or fructokinase (FRK, EC 2.7.1.4), involving multiple biological processes [3]. HXKs may evolve from the actin fold protein family, sharing a conserved ATP binding site, surrounded by more variable sequences that determine the substrate affinities and other biochemical properties [4]. The phosphorylated hexoses play fundamental functions in various metabolic processes, including intracellular

hexose homeostasis and storage of the phosphate group that is transformed into the energy molecules, adenosine diphosphate (ADP) [4,5]. In contrast to FRKs that catalyze fructose phosphorylation into fructose-6-phosphate (F-6P), HXKs can phosphorylate several hexose substrates, including fructose, mannose, and glucose. Remarkably, the latter is converted to glucose-6-phosphate (G-6P), which triggers the release of the stored energy for plant growth and development [6].

HXKs are moonlighting enzymes virtually in all living organisms, from prokaryotes to eukaryotes, modulating sugar metabolism, signaling transduction, and crosstalk with phytohormone pathways [7]. Molecular and biochemical studies have demonstrated that a small multi-gene family encodes HXKs in model plant species [8,9]. In *Arabidopsis*, six HXKs have been characterized, comprising three isoenzymes (AtHXK1-3) that phosphorylate glucose, and the other three (AtHKL1-3) designated as hexokinase-like (HKL) proteins are deficient in catalytic activity [10]. Only three members (*AtHXK1*, 3, and *AtHKL1*) are verified as glucose sensors, but display different subcellular targets [11]. In rice (*Oryza sativa*), ten HXK isogenes (*OsHXK1-10*) have been isolated, whereas the physiological functions appeared to be diversified owing to playing actions as the positive or negative growth regulator [12–14]. Moreover, extensive surveys of several HXK families have been reported in *Zea Mays*, *Manihot esculenta*, *Gossypium hirsutum*, *Phyllostachys dullish*, *Physcomitrella patens*, and *Jatropha curcas*, suggesting the HXK conserved patterns in diverse plant species [15–20].

The typical HXKs contain glucose-binding sites and adenosine phosphate-binding domains [1]. In plants, HXKs are commonly classified into two major groups (type A and type B) based on the subcellular targets determined by the N-terminal signal sequences. The type A HXKs (e.g., *AtHXK3*) contain transit peptides, showing a plastidic target, while HXKs in type B are mitochondrial-associated proteins, possessing a conserved hydrophobic membrane anchor domain [8]. While a few HXK isogenes in monocots that identified the localization to the cytoplasm and nucleus are grouped in type C [7,21]. In addition, the HXKs in bryophytes, lycophytes, and gymnosperms likely lack the conserved peptides, thus belonging to type D [19]. The various intracellular localizations in classified HXKs could envision the physiological roles regarding specific metabolic regulation and stress adaptation in plants [1,8].

Emerging reports implicated that HXKs are involved in glycolysis, sugar sensing, and signaling, affecting plant growth and development. Previous research revealed that the *Arabidopsis* transgenic mutants exhibited sugar insensitive and hypersensitive phenotypes in seedlings via up- and downregulation of *AtHXK1* transcript, suggesting that the dual-functional *AtHXK1* acts as a glucose sensor [22]. The HXK's roles in sugar sensing were evidenced by the ectopic induction of *AtHXK1* in tomatoes (*Solanum lycopersicum*), leading to the retarded growth, reduced photosynthesis efficiency, and accelerated leaf senescence [23]. Exogenous glucose input in *AtHXK1*-overexpressing *Arabidopsis* repressed the leaf expansion, suggesting an AtHXK1-dependent manner, whereas decreases in *AtHXK1* expression prompted a delayed leaf expansion and senescence process [24]. These results indicated that *AtHXK1* played a dual role in glycolysis and sugar sensing for vital metabolic and physiological processes [25]. In contrast, the *AtHKL1*-overexpressing lines displayed phenotypes very similar to those of the *AtHXK1* mutant (*gin2-1*), suggesting that HKL1 was a negative regulator-mediated crosstalk between glucose and phytohormone pathways [26–28]. According to a previous report, the *OsHXK5* and 6 are evolutionarily related to *AtHXK1*, playing roles as glucose sensors in rice [14]. Recently, a rice cytosolic hexokinase *OsHXK7* was identified as involved in sugar signaling and metabolism that impacted seed germination in a glycolysis-dependent manner; however, its signaling role was depressed under O<sub>2</sub>-deficient conditions [12]. Nevertheless, in plants and yeast (*Saccharomyces cerevisiae*), the HXK-mediated glucose-sensing functions constantly throughout the life cycle that appears to be independent of catalytic activities in phosphorylating glucose to G-6P [29,30]. Therefore, it is speculated that HXKs are very diversified that some isoforms may be capable of functioning essentially as metabolic regulators, and others may act as glucose sensors [9].

Sugar signaling in regulating plant growth is coordinated with phytohormone signaling pathways [29,31,32]. Recent work in *Arabidopsis* demonstrated that *AtHXX1* was involved in the regulation of the salicylic acid (SA)-dependent programmed cell death (PCD), which is mediated by the alternation of the myo-inositol biosynthesis [33]. In grape (*Vitis vinifera*), the exogenous abscisic acid (ABA) cannot block the glucose-induced repression of sucrose metabolic genes in *CsHXX1*- or *CsHXX2*-silencing mutants that were insensitive to glucose treatment [34]. Ectopic expression of *AtHXX1* in citrus (*Citrus sinensis* × *Poncirus trifoliata*) guard cells reduced the stomatal conductance and transpiration, leading to improved water-use efficiency (WUE) [35]. *AtHXX1* could reduce hydraulic conductance in response to increased glucose levels via controlling aquaporin gene expression, preserving water levels in leaves [36]. Similarly, the constant induction of *OsHXX1* in rice led to rapid leaf senescence and a reduced chlorophyll level, suggesting that *OsHXX1* may modulate glucose homeostasis and reactive oxygen species (ROS) accumulation [37]. This finding supported the fact that HXKs might maintain a steady state of ADP recycling, which affect  $H_2O_2$  formation in the mitochondrion [38]. Suppression of *OsHXX10* expression in rice led to the aberrant anther and impaired pollen development [13]. Surprisingly, silencing tomato *SlHXX1* resulted in stunted plant growth and stimulated leaf senescence, associated with an altered starch turnover [39].

HXKs are also involved in stress adaptation and defense regulation in response to various environmental cues and pathogen infection [40,41]. Constantly expressing *AtHXX1* in tobacco (*Nicotiana tabacum*), tomato, and potato (*S. tuberosum*) guard cells increased WUE, conferring tolerance to various abiotic stress (e.g., drought, salt, and heat) [42–44]. In a recent report, the different subcellular allocation of serine may be the reason for the retarded growth of the *gin2-1* under high irradiant conditions [45]. It was shown that *AtHXX1* acts as a positive regulator of plant immunity in leaves challenged by *Pseudomonas syringae* pv. *tomato* DC3000 through the glucose effect mediated by *AtHXX1*-related pathways [46]. Overexpression of native *OsHXX1* in rice led to improved ROS accumulation and leaf resistance to virus infection [47]. Moreover, a recent report demonstrated that constant induction of *MdHXX1* expression in apple (*Malus domestica*) enhanced resistance to ring rot fungi pathogen and ROS production related to glucose signaling [48]. In *Populus*, a GATA transcription factor (TF), *PdGNC* was characterized to modulate stomatal aperture and influence WUE and drought tolerance, resulting from activation of hexokinase that promoted NO and  $H_2O_2$  accumulation in guard cells [49].

The essential catalytic and signaling roles of HXKs in plant growth and development have been well attempted in *Arabidopsis* and other herbaceous crops. Nevertheless, the molecular conception in genomic patterns and expression profiles, particularly in response to various stress factors, remains largely unknown in forest trees. In this work, we performed a genome-wide survey and expression analyses of the HXKs family in *Populus trichocarpa*, a model woody plant species. The primary objective was to gain novel insights into the molecular aspects of the HXKs family in *Populus*. Our data provide a theoretical clue for further unveiling the physiological significance of *PtHXXs* in sucrose metabolism and signaling transduction during plant growth and stress acclimation.

## 2. Results

### 2.1. Genome-Wide Identification and Evolutionary Relationship of HXKs

A systematic pBLAST search using homologs from *Arabidopsis* as queries was conducted in Phytozome v13.1. A total of six putative isogenes were retrieved, proposing to be *PtHXX* after the manual removal of redundant sequences. These gene isoforms were annotated from *PtHXX1* to *PtHXX6* based on the chromosome (Chr) ascending ID number. The gene name, DNA and transcript size, open reading frame (ORF) and protein length, molecular weight (MW), isoelectric point (pI), transit peptide (TP), and subcellular targets are in silico deduced (Table S1). The sequence length of six *Populus* HXK proteins varied from 494 to 508 amino acid (AA) residues, ranging the MW from 53.09 kDa (*PtHXX3*) to 54.97 kDa (*PtHXX2*). All *PtHXXs* displayed the theoretical acid pI from 5.63 to 6.54. The

prediction of intracellular localization indicated that most PtHXXs were localized to the mitochondria, except for PtHXX3, targeting chloroplasts.

The homologous HXXs were identified in 16 other plants, including five monocots: *Brachypodium distachyon*, *O. sativa*, *P. edulis*, *Sorghum bicolor*, and *Z. mays*; eight eudicots: *A. thaliana*, *Eucalyptus grandis*, *Glycine max*, *G. raimondii*, *M. esculenta*, *Medicago truncatula*, *N. tabacum*, and *S. lycopersicum*, alongside one gymnosperm: *Ginkgo biloba*, one bryophyte: *P. patens*, and one lycophyte: *Selaginella moellendorffii*. One hundred and thirty-five homologous HXXs were characterized, varying the numbers from 4 to 14 in all selected plant species (Table 1 and Table S2). The phylogenetic tree revealed that HXXs were clustered into four major subfamilies: Type A, B, C, and D. Type A was typically composed of HXXs from monocots and eudicots with plastidic targets. Type B contained mitochondrial HXXs that were further clustered into three subgroups: Type B-I, type B-II, and type B-III (Figure 1). Few of HXXs, particularly in eudicots, belong to type B-I. While other mitochondrial HXXs shared the common feature between monocots and eudicots, comprising the type B-II. In contrast, type B-III included mitochondrial HXXs, particularly in type B-III. The cytosolic HXXs in monocots were categorized into the type C subfamily. The remaining HXXs in bryophytes, lycophytes, and gymnosperms were grouped in type D, appearing to have variable subcellular patterns. In *Populus*, three members (PtHXX1, 4, and 6) were classified into the type B-I subfamily, two PtHXXs (PtHXX2 and 5) in type B-II, and one (PtHXX3) in type C.

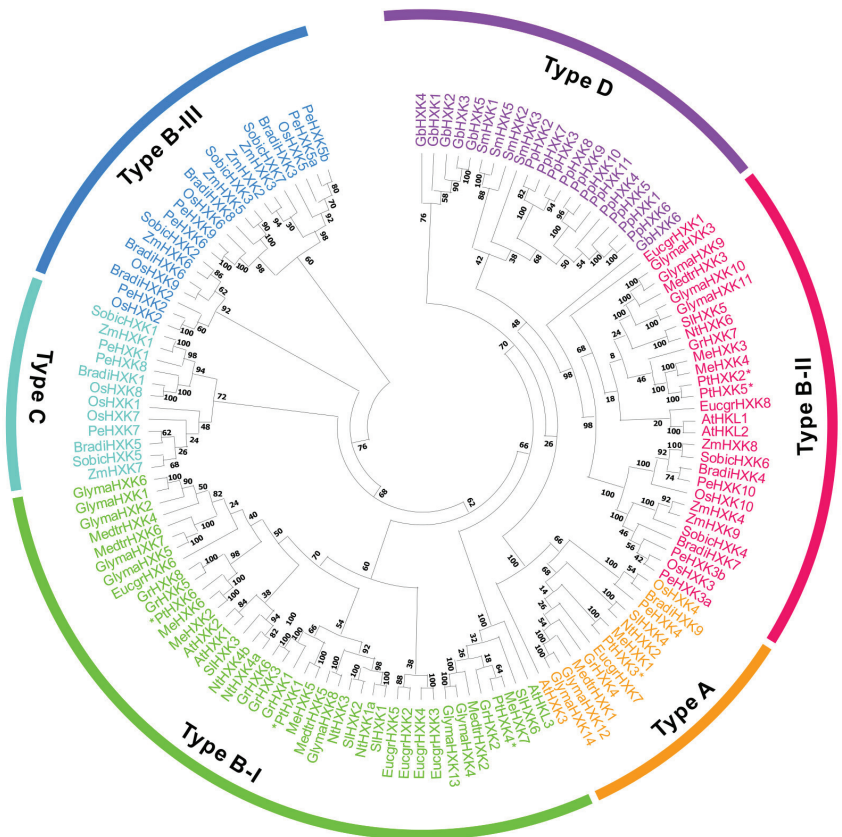


**Figure 1.** Phylogenetic relationships of clustered homologous HXXs between 17 plant species. The evolution tree was generated using the Maximum Likelihood method in MEGA X with 1000 bootstrap replicates. The four classified HXXs subgroups were represented as type A, B, C, and D.

**Table 1.** List of the classification and numbers of HXKs in various plant species.

Groups	Species	Type A	Type B			Type C	Type D	Total
			I	II	III			
Bryophytes	<i>Physcomitrella patens</i>						11	11
Lycophytes	<i>Selaginella moellendorffii</i>						4	4
Gymnosperms	<i>Ginkgo biloba</i>						6	6
Monocots	<i>Brachypodium distachyon</i>	1		2	4	2		9
	<i>Oryza sativa</i>	1		2	4	3		10
	<i>Phyllostachys edulis</i>	1		3	5	3		12
	<i>Sorghum bicolor</i>			2	3	2		7
	<i>Zea mays</i>			3	4	2		9
Eudicots	<i>Arabidopsis thaliana</i>	1	3	2				6
	<i>Eucalyptus grandis</i>	1	5	2				8
	<i>Glycine max</i>	2	8	4				14
	<i>Gossypium raimondii</i>	1	6	1				8
	<i>Manihot esculenta</i>	1	4	2				7
	<i>Medicago truncatula</i>	1	4	1				6
	<i>Nicotiana tabacum</i>	1	4	1				6
	<i>Populus trichocarpa</i>	1	3	2				6
	<i>Solanum lycopersicum</i>	1	4	1				6

## 2.2. Chromosomal Location, Cis-Regulatory Elements, and Genomic Structure of HXKs

Analyses of the chromosomal location revealed that the six *PtHXKs* were mapped on five of the 19 Chrs in *Populus*. Two members (*PtHXK1* and 2) of *PtHXKs* were located on Chr 1, whereas others showed individual distribution on Chr 5, 7, 9, and 18, respectively (Figure 2a). The evolutionary relationship of *PtHXK2* and 5 may propose the occurrence of segmental duplication events during the genome evolution. Comparative analyses of gene promoters between *Arabidopsis* and *Populus* showed that three potential *cis*-regulatory elements in *PtHXKs* represented the most widely spread elements, including the anaerobic induction (ARE), methyl jasmonate (MeJA) (CGTCA/TGACG), and low temperature (LTR). Within phytohormone-regulated elements, ABA-responsive elements (ABRE) and auxin response elements (TGA/AuxRR-core) were identified in three *PtHXKs*. The gibberellin (GA)-responsive elements (GARE/P-box/TATC-box) showed the presence in two *PtHXKs*. The SA-responsive elements (TCA), MYB TF binding site involved in drought response (MBS), and defense and stress response elements (TC-rich) were distributed in a few members of *PtHXKs*. Thereafter, analyses of genomic patterns revealed a more conserved organization of exon/intron in *Populus*, showing eight introns in all *PtHXKs*, whereas the number of introns varied from 6 to 8 in *Arabidopsis* (Figure 2c). *PtHXK2* and 5 were clustered with the maximal length of the DNA sequence owing to the extended sizes of its introns. The high protein sequence identity to HXK homologs in *Arabidopsis* suggested that *PtHXK2*, 4, and 5 were postulated to be HKL proteins deficient in catalytic activity (Table S1 and Figure 2b).

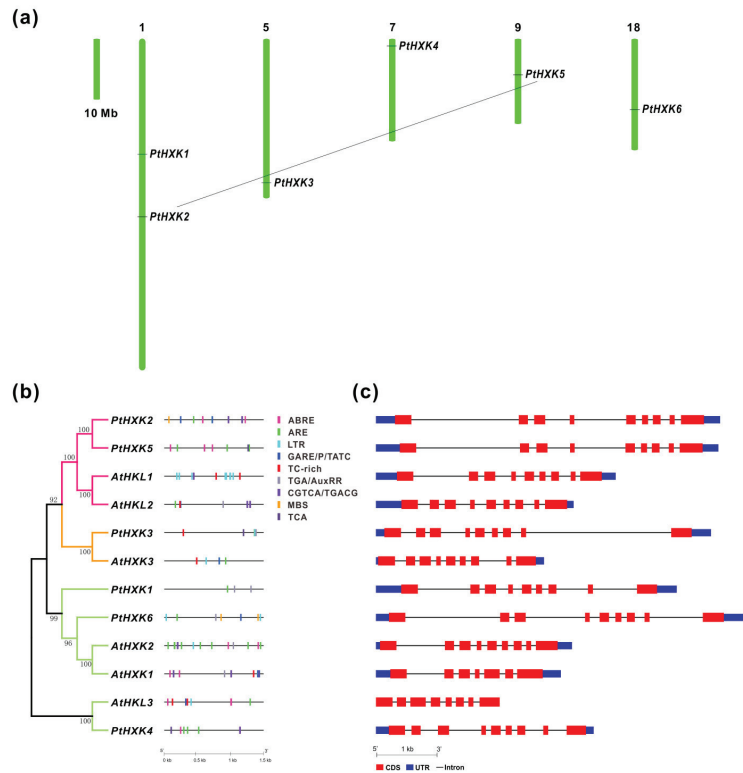


**Figure 2.** The genomic features of the HXKs between *P. trichocarpa* and *Arabidopsis*. (a) The chromosomal distribution of isogenes shows the duplicated gene pair with a straight line. (b) The in silico prediction of the *cis*-regulatory elements in 1.5 kb gene promoters labeled in colors. (c) Genomic structures show the patterns of the exon/intron organization. The exon lengths are displayed proportionally to the scale on the bottom.

### 2.3. Conserved Motifs and Domains in Protein Sequences of PtHXKs

Using the MEME web server, two essential HXK domains (HXK1 and HXK2) were typically present in HXKs between *Arabidopsis* and *Populus* (Figure 3a). A total of ten individual motifs were programmed to vary the length of AA residues from 30 to 50 (Figure 3b). The commonly shared motifs showed a more conserved pattern in the HXK family, except for AtHLK2 and PtHXK4, lacking motif 4 due to the missing specific AA residues. A longer sequence distance between motif 6 and 7 was observed mainly for HXKs (e.g., AtHLK1, 2, PtHXK2, and 5). The multiple sequence alignments were conducted using the functional HXKs in various plants (Figure 4). It was revealed the presence of several conserved fragments, including the N-terminal transmembrane anchor domain (5–24 AA), two phosphate domains (97–118 AA and 248–267 AA), sugar-binding core for substrate recognition (167–186 AA), adenosine phosphate-binding domain (425–461 AA), and C-terminal low complexity domain (477–491 AA). The divergent indel (6–10 AA) within the N-terminal adenosine-binding domain was verified as the critical sequences to distinguish the HXK and HLK subfamilies. These conserved features have been characterized widely in *Arabidopsis*, rice, tobacco, wheat, and *Sorghum* [1]. Two active amino acid residues (Asp104 and Ser177) labeled with stars were identified to possess HXK catalytic activity, demonstrated in rice and *Arabidopsis* [37,50].

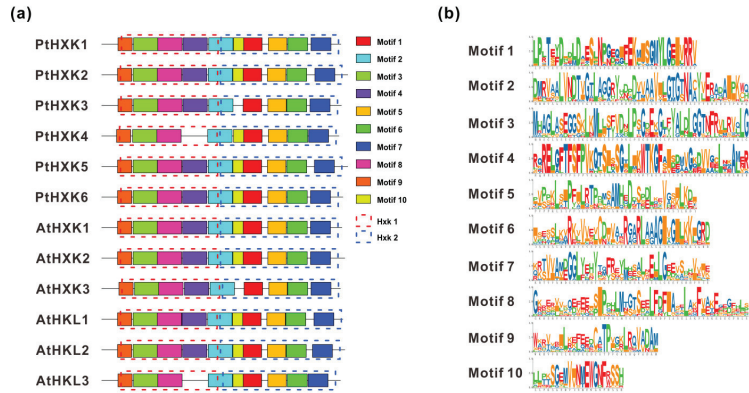


**Figure 3.** The conserved motif distribution in HXKs. (a) Motifs were analyzed using the MEME web server, and ten conserved motifs were boxed in colors. (b) The amino acid logos of respective motifs were detailed on the right side.

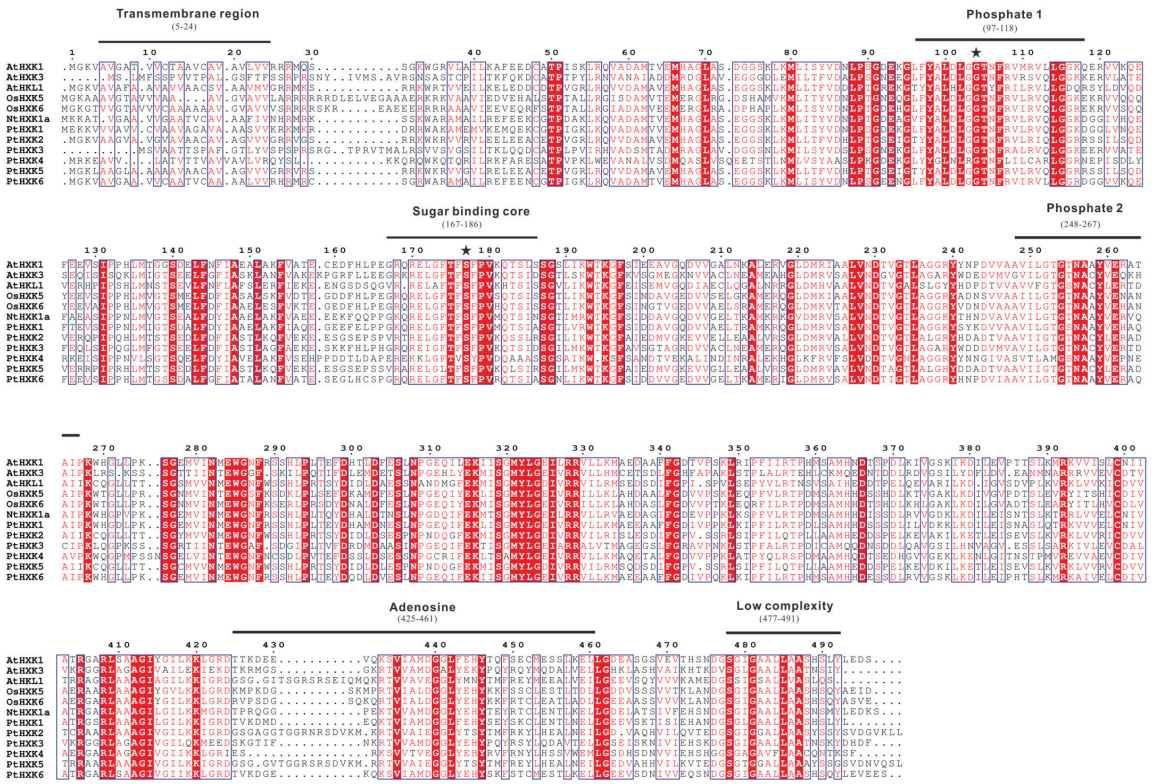


**Figure 4.** The conserved fragments and amino acid residues between PthXKs and other functional homologs. Six conserved sites with different numbers of amino acids were lined in black annotated based on homologous regions to the HXK II in yeast, and two active binding sites were marked with asterisks.

**2.4. Transcriptomics of PthXKs in Vegetative Tissues and upon Pathogenic Fungi Infection**

The spatiotemporal expression patterns of PthXKs were initially analyzed using transcriptomic sequencing (RNA-seq) retrieved from the Phytosome (v13.1). It was demon-

strated that a varied transcript abundance was detected in seven selected vegetative tissues, including the root tips (RTP), roots (RT), stem internodes (STI), stem nodes (STN), leaf expanded fully (LFF), leaf immature (LFI), and leaf young (LFY). As depicted in the heat map, *PtHXX2* and 6 were more abundantly expressed in all vegetative tissues, mainly showing the highest levels in the roots and stems (Figure 5a). While *PtHXX3* displayed explicit transcript abundance in the stems, followed by the root tips. The *PtHXX1* and 5 appeared to be not significantly expressed. However, along with *PtHXX4*, their transcripts were predominantly detected in the inflorescence (Figure S1). The expression patterns of six *PtHXXs* in young leaves (YL), mature leaves (ML), stems (ST), and roots (RT) were further evaluated using the in vitro cultured plants by quantitative real-time PCR (qRT-PCR) that was compatible with the RNA-seq data except for *PtHXX5*, showing exceptional levels of low expression (Figure 5b). In addition, the responding *PtHXXs* were investigated in the roots under the time-coursed infection of the pathogenic fungi, *Fusarium solani* (Fs). Taken together, analyses of the tissue-specific expression confirmed that three *PtHXXs* (*PtHXX2*, 3, and 6) showed a higher expression level in the roots than other isogenes. These three genes also showed a strong induction upon the Fs infection, particularly after 24 h (h) post-inoculation (hpi) (Figure 5c). The *PtHXX1* transcript appeared to be merely affected before 24 hpi. The time coursed expression evaluated via qRT-PCR assay confirmed that *PtHXX3* and 6 were the Fs responsive genes.

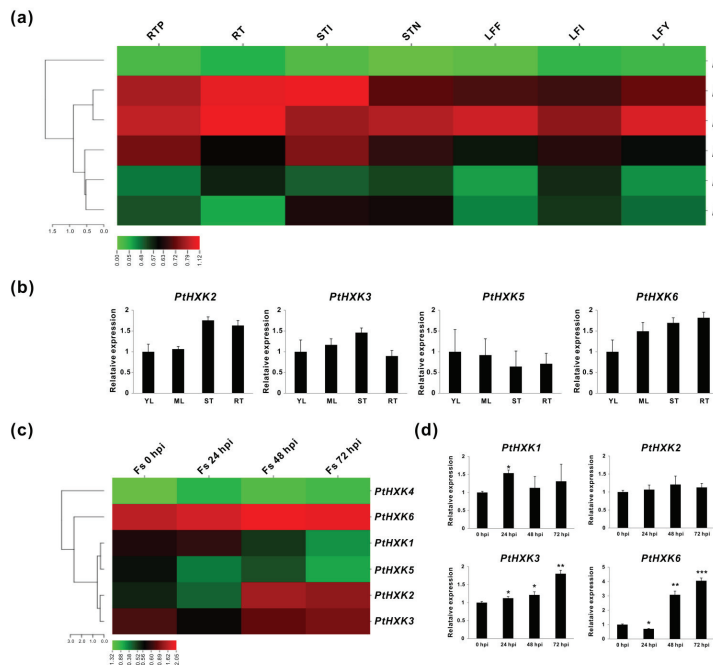


**Figure 5.** Transcriptomic and expression profiles of *PtHXXs* in vegetative tissues and roots challenged by *F. solani* (Fs). (a) The heatmap shows the transcript in vegetative tissues of *P. trichocarpa*. (b) The qRT-PCR evaluation shows the tissue-specific expression of *PtHXXs*. (c) The heatmap shows the transcriptomic profile of *PtHXX* isogenes in Fs infected roots (0, 24, 48, and 72 h of post-inoculation, hpi). (d) Validation of responsive *PtHXXs* compared to the control (0 hpi) by qRT-PCR. The RNA-seq data were given in the Log10 of the fragments per kilobase per million reads (FPKM) expression values. At least three independent biological replicates were conducted for qRT-PCR analyses. *PtβActin*, *PtUBIC*, and *PtEF-α1* were used as the internal control. Data represent mean values standard error ( $\pm$ SE) of at least three independent biological replicates. Asterisks indicate significant differences relative to the control using the Student's *t*-test: \*\*\*  $p < 0.001$ , \*\*  $p < 0.01$ , and \*  $p < 0.05$ .

### 2.5. Effects of *PtHXXs* Expression Responding to Sugars and ABA treatments

The deduced *cis*-regulatory elements on promoters reflect spatiotemporal expressions of specific genes that may be affected by various environmental cues and phytohormone exposures. The gene promoters' analyses revealed a few ABA-related response elements (Figure 2b). Under the input of different sugars (e.g., glucose, fructose, and sucrose) with gradient levels, the compared expression profile of *PtHXXs* was explored between 0 and 24 h by qRT-PCR assay (Figure 6). The significant inductions of *PtHXX2* and 6 were identified in the roots by adding glucose when the amount increased higher than 3%. In contrast to the control (0 h), the *PtHXX3* appeared to be significantly promoted by 6% sucrose and fructose owing to the observed high expression levels after 24 h of inoculation. In addition, the marked upregulation of *PtHXX6* expression was detected in response to sucrose feeding, following a dose-dependent manner. The HXK-mediated sugar signaling profoundly affects promoting or arresting plant morphogenesis in association with altered ABA levels [8]. In line with this, the effect on *PtHXX* transcripts was inspected in roots upon different dose feeding of ABA. Notably, the constant promotions of *PtHXX3* and 6 were observed to be correlated with the increase in the ABA concentration. Nevertheless, detecting other *PtHXXs* expressions was unsuccessful due to the low transcript abundance in the selected tissues.

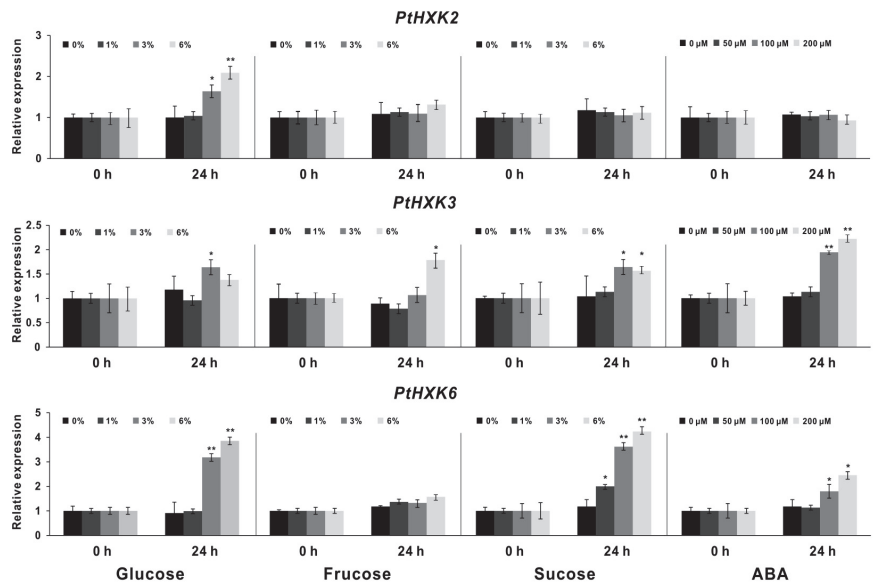


**Figure 6.** Expression effects of three *PtHXXs* in the roots feeding with various sugars and ABA. The qRT-PCR analyses show the transcript responsiveness upon the altered concentration of sugars (glucose, fructose, and sucrose) and ABA. The relative expression of the control was set as 1. Data represent mean values  $\pm$  SE of at least three independent biological replicates. *Pt $\beta$ Actin*, *PtUBIC*, and *PtEF- $\alpha$ 1* were used as reference genes. Asterisks indicate significant differences in comparison with the control using the Student's *t*-test: \*\*  $p < 0.001$ , \*  $p < 0.01$ .

## 3. Discussion

### 3.1. The HXKs Family and Conserved Profiles in Plant Species

Recent advances in high-throughput technologies and multi-omics-based strategy have boosted the framework in functional genomics and metabolic research in plants [51]. As a model perennial woody plant species, the entire genome of *Populus* has been released for over 15 years, whereas a thorough survey of the *PtHXXs* family remains unknown. The putative HXK-encoding genes were identified within 17 selected plant species, including

6–14 members (Table 1). Along with other plant species, the phylogenies of 135 HXK homologs revealed a classification of four subfamilies (type A, B, C, and D), showing one plastidic *PtHXK3* in type A and five members of mitochondrial *PtHXKs* in type B [1,8]. However, there were no cytosolic HXKs identified in the *Populus* genome. Based on phylogenetic relationships and the protein sequence identity to *Arabidopsis*, three members (*PtHXK2*, 4, and 5) most likely belong to HKL-like proteins, while other gene isoforms are HXK candidates in *P. trichocarpa*. The genome duplication facilitates woody perennials to variable environments adaption during million years of evolution [52]. One gene pair (*PtHXK2* and 6) was speculated to undergo a segmental duplication combined with the sequence analyses, suggesting notable physiological roles associated with evolved mechanisms to adapt to stress stimuli (Figure 2a). The *cis*-regulatory elements predicted in promoter regions indicated the dynamic regulation and evolution of specific gene expression upon various environmental cues [53]. Therefore, the deduction of principal diverse *cis*-regulatory elements related to phytohormone response (ABA, GA, MeJA, and Auxin) and stress factors (e.g., MBS, TC-rich, and LRT), along with TF binding sites, provided a hint that the molecular regulation of *PtHXKs* depends significantly on the crosstalk between phytohormone and glucose signaling pathways [31]. In addition, the analyses of the genomic structure of *PtHXKs* compared with homologs in *Arabidopsis* suggested a similar exon and intron organization (e.g., eight introns included) within the same subgroup (Figure 2c).

Furthermore, approximately ten conserved motifs (30–50 AA) of HXKs have predicted distribution between *Arabidopsis* and *Populus*, which was in line with the previous reports [1,15,16,34]. The multiple alignments of *PtHXK* protein sequences with other functional homologs led to the identification of six hallmarks, including 19–50 AA transit peptide sequences (membrane anchor domain) at the N-terminus for the plastidic or mitochondrial targets (Table S1). The prediction of theoretical core sites for glucose and phosphate binding demonstrated that all homologous HXKs possessed the conserved AA residues (e.g., Asp-101, Gly-104, and Ser-177) except for *AtHKL1* and *PtHXK4*, suggesting that *PtHXK4* may be a catalytically inactive glucose sensor (Figure 4). These results were supported by several recent works performed on Cassava, bamboo, and cotton [16–18]. These conserved features of HXKs may be more variable in gymnosperms, bryophytes, and lycophytes, suggesting that the plant-derived HXKs probably evolved from prokaryotic ancestors, common primordial actin fold protein [54,55]. Nevertheless, despite the advanced molecular information concerning functional HXKs in various plants, hitherto, no strategy was potentially used to predict the sensor role of a specific HXK, and not all HXKs played identical functions in *Arabidopsis* [8].

Investigating gene expression patterns is one of the strategies to imply whether candidates may be involved in specific metabolic processes or signaling roles. The significant challenge for the tree functional study of a particular gene family is to overpass the relationships between the transcript abundance and corresponding variation of the enzyme kinetics [56]. In our work, the depicted gene expression profiling revealed that a few genes (e.g., *PtHXK2* and 6) displayed specific expression patterns in vascular tissues, including the roots and stems, reflecting the potential role during plant growth and development. However, the expression of gene pairs (*PtHXK2* and 5) with segmental duplication was observed to show a divergent pattern (Figure 5). The gene alternative splicing (AS) was prevalent in generating variation in protein structure, functional diversity, and stress adaptation among different plant tissues, cell types, and treatments [57]. Therefore, it was hypothesized that the expression variation of gene duplication might be due to the overlapped levels of transcript variants derived from AS. It is worthwhile to note that when focusing on the effects of *PtHXKs* in the roots responding to the *F. solani* infection, the *PtHXK3* and 6 showed significant increases in expression, particularly at Fs 48 hpi. In contrast to the control, the *PtHXK2* and 6 identified showed a marked promotion in roots upon the gradient glucose (3% and 6%) feeding at 24 h, suggesting the role of the sugar sensor. Only the *PtHXK2* was expressed significantly by adding the highest amount (6%) of fructose.

Moreover, the *PtHXX3* and 6 were highly responsive to the sucrose and ABA treatments, suggesting the crosstalk regulation between the sugar and phytohormone under the biotic stress conditions. In contrast, a much lower number of HXX transcripts were significantly influenced in mature leaves than in roots under the above conditions, indicating that this chemical concentration was a significant dosage for roots, but not for aerial leaf tissues within 24 h (data not shown). Overall, transcriptional and post-transcriptional interferences of HXX isogenes in specific tissue types indicate the subsequent exploration of physiological and signaling functions under different stress regimes. Analysis of *cis*-elements and gene expression revealed that *PtHXXs* contained various defense/stress-related response sequences that might be modulated by phytohormone (e.g., ABA), indicating the crosstalk between HXXs and sugar/phytohormone signals during the root development and stress tolerance.

### 3.2. The Regulatory Role of HXXs in Defense and Stress Acclimation

According to the previous research, *Arabidopsis AtHXX1* was identified as a glucose sensor to interrelate nutrient, light, and phytohormone signaling networks for regulating growth and development by responding to various environmental cues [50]. Increasing evidence implicated that HXXs are primary enzymes and exert numerous regulatory actions other than merely catalyzing the phosphorylation of hexoses, the central energy nutrients, and signaling molecules in the effect of sugars on morphogenesis and stress adaptation [7,58]. The glucose acts as a signal molecule through interactions with IAA, GA, and ABA, while the HXX-catalyzed G-6P was regarded as the core intermediate in glucose signal transduction [59]. HXXs with catalytic activity significantly impact multi-cellular processes and sugar signaling, accounting for the metabolite biosynthesis on the glycolytic pathways, providing energy for cell growth [8]. During the plant-pathogen interaction, the host defense and immune responses are mounted with a profound modulation of the primary plant metabolism, including biosynthesis of carbohydrates, amino acids, and the derived secondary metabolites [60].

Feeding experiments elucidated the link between carbohydrate metabolism and defense mechanisms and revealed the induction of pathogenesis-related (PR) genes by sugars, suggesting that carbohydrate metabolism positively regulates the expression of defense-related genes [61]. As an evolutionarily conserved glucose sensor, the *AtHXX1* played dual functions in sugar metabolism, sensing, and defense response [62]. In transgenic tobacco, overexpressing invertase led to sugar accumulation, and the induction of *PR-1* and *PR-5* by glucose in correlation with *AtHXX1* mediated the signaling and catalytic activities, suggesting the positive regulation of defense-related genes through carbohydrate metabolism [24]. Constant induction of *AtHXX1* and 2 transcripts in *Arabidopsis* resulted in elevated resistance to the infections of necrotrophic fungi (*Alternaria brassicicola*) and bacterial *P. syringae*, indicating the defense and immunity roles of HXX against various pathogens [40,46]. The underlying mechanisms of HXX involved in regulating immunity and defense appeared to be related to altered ROS accumulation, further supported by several recent works performed on rice and apples [47,48].

Nevertheless, the *AtHXX1* might play a negative role as the suppression/deletion of *AtHXX1* led to the increased H<sub>2</sub>O<sub>2</sub> production associated with defense-related genes and accelerated SA-dependent PCD, prompting that *AtHXX1* might exert dual regulatory roles mediating up- and downregulation of sugar responsive genes [33]. The HXX-derived metabolic processes regulate plant defense and immunity to the pathogen, reaching far beyond phytohormone cues and crosstalk between signaling pathways and sucrose metabolism. Recently, two grape HXX isoforms and sucrose metabolic enzyme genes increased concomitantly with elevated levels of endogenous glucose and ABA during grape berry development, postulating the regulatory role of glucose and ABA on HXX-dependent sugar metabolism [34]. Emerging reports revealed that ABA signaling pathways regulate water status and mediate drought tolerance by controlling stomatal aperture, water conductance, and gene expression, which were conserved in tree species [63,64]. In line with the previous work, the transcriptional activation of *PdHXX1* via the GATA transcription factor

(PdGNC) resulted in the ABA-induced NO and H<sub>2</sub>O<sub>2</sub> accumulation, mediating the stomatal closure and drought tolerance in woody *Populus* [35,49,65]. In summary, the HXK-derived crosstalk of phytohormone signaling and sugar metabolism deploys defense-related genes and yields profound compounds associated with metabolic conversion, ROS control, and stressor scavenging while remaining a blank in *Populus*.

#### 4. Materials and Methods

##### 4.1. Plant Materials, Growth Conditions, and Treatments

The *P. trichocarpa* (genotype *Nisqually-1*) grows under long-day conditions (25 °C, 16/8 h day/night photoperiod, 50 μE), culturing in vitro on a traditional woody plant medium (WPM) with 30 g L<sup>-1</sup> sucrose, 0.1 mg L<sup>-1</sup> IBA, and solidified with 8 g L<sup>-1</sup> plant agar. The Fs culture, the fungal spore calculation (1.0 × 10<sup>6</sup> spores/mL), and the root infection were conducted according to the report [66]. For feeding experiments, the 4-week in vitro cultured plants were transferred to conical flasks containing 40 mL gradient concentrations (0%, 1%, 3%, and 6%) of solution and incubated in an artificial chamber for 24 h. For RNA-seq data, different vegetative tissues and roots with time-course (0, 24, 48, and 72 hpi) of Fs infection were sampled based on the previous research [67]. The roots of eight randomly selected plants with Fs infection and 24-h-feeding by sugars (glucose, fructose, and sucrose) and ABA (0, 50, 100, and 200 μM) were pooled for one biological replication to evaluate gene expressions using the 0 h treatment as the control.

##### 4.2. Sequence Mining, Identification, and Genomic Analyses of HXKs

The *Arabidopsis* HXK homologs were collected in TAIR. Available online: <https://www.arabidopsis.org> (accessed on 24 October 2000) as queries to search for candidate iso-genes in *P. trichocarpa* genome assembly (v3.1) from the JGI gene catalog. Available online: [https://phytozome-next.jgi.doe.gov/info/Ptrichocarpa\\_v3\\_1](https://phytozome-next.jgi.doe.gov/info/Ptrichocarpa_v3_1) (accessed on 30 November 2018) with the E-value cutoff set as 1e-5. Incomplete protein sequences with short lengths (<300 AA) were eliminated. The upstream 1.5 kb sequences of gene promoters were predicted by the program PlantCARE. Available online: <http://bioinformatics.psb.ugent.be/webtools/plantcare/html> (accessed on 11 September 2000) to obtain overviews of *cis*-regulatory elements associated with the responsiveness of biotic and abiotic stresses, according to the previous reports [60]. The gene structure was deduced by comparing CDS and the corresponding DNA sequence in GSDS. Available online: <http://gsds.gao-lab.org> (accessed on 1 January 2015). The chromosomal distribution of *PtHXKs* was obtained from the PopGenIE. Available online: <http://popgenie.org/chromosome-diagram> (accessed on 1 January 2021), and physical locations were drawn by the program MapInspect. Available online: <http://www.softsea.com/review/MapInspect.html> (accessed on 9 November 2010) [68]. Subcellular localization of *PtHXKs* was predicted by the program DeepLoc 2.0. Available online: <https://services.healthtech.dtu.dk/service.php?DeepLoc-2.0> (accessed on 22 March 2021). Protein sequences of HXKs in *B. distachyon*, *S. bicolor*, *E. grandis*, *G. max*, and *M. truncatula* are available from the Phytozome v13. Available online: <https://phytozome-next.jgi.doe.gov> (accessed on 28 July 2021) and homologs of *G. biloba* are retrieved from the database. Available online: <https://ginkgo.zju.edu.cn/genome> (accessed on 1 January 2022). Other protein sequences in *O. sativa*, *P. edulis*, *Z. mays*, *A. thaliana*, *G. raimondii*, *M. esculenta*, *N. tobacum*, *S. lycopersicum*, *P. patens*, and *S. moellendorffii* were obtained from the literatures [1,10,15–18].

##### 4.3. Phylogenetic Tree Construction and Analyses of Conserved Motifs

The alignments of multiple protein sequences were conducted by Clustal Omega. Available online: <https://www.ebi.ac.uk/Tools/msa/clustalo> (accessed on 23 May 2018). The reciprocal pBLAST was conducted to establish the genetic relationship between gene pairs. The phylogenetic tree was constructed by MEGA X. Available online: <https://www.megasoftware.net/v10.2.2> (accessed on 1 October 2020), using the Maximum Likelihood method with 1000 bootstrap replicates [69]. The evolutionary distances were computed

using the Poisson correction method and the number of AA substitutions per site. The conserved motifs were analyzed by MEME. Available online: <http://meme-suite.org/index.html> (accessed on 1 August 2022), setting the maximum numbers and widths of motifs to 10 and 50, respectively [70]. Transmembrane region and low complexity were predicted in the SMATE database. Available online: <https://smart.embl-heidelberg.de> (accessed on 26 October 2020) based on AtHXK1. The motif was annotated by CDD in NCBI. Available online: <https://www.ncbi.nlm.nih.gov/cdd> (accessed on 5 November 2021) and ScanProsite. Available online: <http://prosite.expasy.org/scanprosite> (accessed on 25 May 2022) [71].

#### 4.4. Transcriptome and Expression Validation by qRT-PCR

Transcriptome and data processing were performed on the Phytozome (v13.1) and based on a previous report [67]. Gene transcript levels in various tissues were valued by fragments per kilobase of exon model per million mapped reads (FPKM). For Fs infection, the significance of differentially expressed genes (DEGs) (FPKM > 5) was judged by the  $p < 0.05$ . Both Fisher's exact test ( $p < 0.05$ ) and multi-test adjustment (false discovery rate (FDR) < 0.05) were applied in DEGs identification based on the report [67]. For the qRT-PCR assay, the RNA extraction and cDNA synthesis were performed, according to the previous report [72]. The primer amplification efficiency was evaluated with dilutions of cDNA, producing an  $R^2 \geq 0.99$ . The cDNA samples were loaded to a TB green Premix ExTap™ Tli RNaseH Plus (Takara, China). The mixture was subjected to StepOnePlus™ Real-Time PCR System (AB, USA). The relative gene expression was normalized by the geometric mean of three housekeeping genes (*Ptβ-Actin*, *PtUBIC*, and *PtEF-1α*). The primers used for targeting specific genes are listed in Table S3. Heatmaps were constructed by the program CIMminer. Available online: <http://discover.nci.nih.gov/cimminer/home.do> (accessed on 19 July 2018).

## 5. Conclusions

HXKs are multifaceted enzymes, playing essential roles in various metabolic processes and signaling that significantly impact the whole plant cycle, including regulating vegetative growth and reproduction, male fertility, and senescent signals. Despite the substantial evidence of the regulatory role of HXK in plant defense and stress adaptation, still more studies are needed to integrate molecular information on the biochemical properties, cellular localization, and sensor capacities with other sugar-sensing pathways to improve performance in woody plants. Among the six putative *PtHXKs* identified in *Populus*, three isogenes (*PtHXK2*, 3, and 6) showed predominant expressions in the vascular tissues (e.g., roots and stems). *PtHXK3* and 6 were significantly induced upon the sugar and ABA treatment, suggesting potential in vivo activities for catalyzing the hexose phosphorylation and signaling effects on *Populus* growth and development. Moreover, the genomic characterization of HXK families is primary for the fine-tuning of HXK-dependent pathways by engineering the activities or expressions of critical HXKs, which might be sufficient to achieve pathogen resistance and abiotic stress tolerance without compromising plant biomass. Therefore, the inspected *PtHXKs* with dominant responsive features to selected stimuli will be the modifying target for functional analyses under stress exposure in *Populus*.

**Supplementary Materials:** The following supporting information can be downloaded at: <https://www.mdpi.com/article/10.3390/plants11152025/s1>. Figure S1: The heatmap shows the transcript in reproductive tissues of *P. trichocarpa*. Table S1: List of HXK candidate genes identified in *P. trichocarpa*; Table S2: Phylogenetic relationship related species and gene IDs; Table S3: List of primers used for qRT-PCR analyses.

**Author Contributions:** Conceptualization, T.S. and M.H.; methodology, X.X., Y.X. and T.S.; software, X.X., Y.X. and H.W.; validation, M.H., X.X., H.W. and K.Y.; formal analysis, X.X., Y.X., H.W., K.Y., T.H. and Y.L.; investigation, X.X., Y.X., H.W., M.H., K.Y. and T.H.; resources, H.W., M.H., K.Y., T.H. and Y.L.; data curation, X.X. and Y.X.; writing—original draft preparation, M.H., X.X. and Y.X.; writing—review

and editing, M.H. and T.S.; visualization, K.Y., T.H. and Y.L.; supervision, M.H. and T.S.; project, M.H.; funding acquisition, T.S. and M.H. All authors have read and agreed to the published version of the manuscript.

**Funding:** This research was funded by the National Natural Science Foundation of China (NSFC), grant number (31870589; 31700525); the Natural Science Foundation of Jiangsu Province (NSFJ) (BK20170921); and the Undergraduate Innovation and Entrepreneurship Training Programs in NJFU (202010298064Z).

**Data Availability Statement:** The raw sequence reads of RNA-seq were deposited in the NCBI database with the accession BioProject of PRJNA680933 and the accession BioSample, SAMN16927537, including twelve accession numbers of SRR13347970-981 for triplicate data of each *F. solani* treatment (Fs0, Fs24, Fs48, and Fs72).

**Acknowledgments:** The authors would like to thank the NSFC and NSFJ for funding this work and the Co-Innovation Center for Sustainable Forestry in Southern China and PAPD for the instrument use.

**Conflicts of Interest:** The authors declare no conflict of interest.

## References

1. Karve, R.; Lauria, M.; Virnig, A.; Xia, X.; Rauh, B.L.; Moore, B.D. Evolutionary Lineages and Functional Diversification of Plant Hexokinases. *Mol. Plant* **2010**, *3*, 334–346. [[CrossRef](#)] [[PubMed](#)]
2. Rolland, F.; Baena-Gonzalez, E.; Sheen, J. Sugar Sensing and Signaling in Plants: Conserved and Novel Mechanisms. *Annu. Rev. Plant Biol.* **2006**, *57*, 675–709. [[CrossRef](#)] [[PubMed](#)]
3. Wan, H.; Wu, L.; Yang, Y.; Zhou, G.; Ruan, Y.-L. Evolution of Sucrose Metabolism: The Dichotomy of Invertases and Beyond. *Trends Plant Sci.* **2018**, *23*, 163–177. [[CrossRef](#)] [[PubMed](#)]
4. Granot, D.; David-Schwartz, R.; Kelly, G. Hexose Kinases and Their Role in Sugar-Sensing and Plant Development. *Front. Plant Sci.* **2013**, *4*, 1–17. [[CrossRef](#)] [[PubMed](#)]
5. Claeysen, É.; Dorion, S.; Clendenning, A.; He, J.Z.; Wally, O.; Chen, J.; Auslender, E.L.; Moisan, M.-C.; Jolicoeur, M.; Rivoal, J. The Futile Cycling of Hexose Phosphates Could Account for the Fact That Hexokinase Exerts a High Control on Glucose Phosphorylation but Not on Glycolytic Rate in Transgenic Potato (*Solanum tuberosum*) Roots. *PLoS ONE* **2013**, *8*, e53898. [[CrossRef](#)] [[PubMed](#)]
6. Pego, J.V.; Smeekens, S.C.M. Plant fructokinases: A sweet family get-together. *Trends Plant Sci.* **2000**, *5*, 531–536. [[CrossRef](#)]
7. Granot, D.; Kelly, G.; Stein, O.; David-Schwartz, R. Substantial roles of hexokinase and fructokinase in the effects of sugars on plant physiology and development. *J. Exp. Bot.* **2014**, *65*, 809–819. [[CrossRef](#)]
8. Aguilera-Alvarado, G.P.; Sánchez-Nieto, S. Plant Hexokinases are Multifaceted Proteins. *Plant Cell Physiol.* **2017**, *58*, 1151–1160. [[CrossRef](#)]
9. Sheen, J. Master regulators in plant glucose signaling networks. *J. Plant Biol.* **2014**, *57*, 67–79. [[CrossRef](#)]
10. Karve, A.; Rauh, B.L.; Xia, X.; Kandasamy, M.; Meagher, R.B.; Sheen, J.; Moore, B.D. Expression and evolutionary features of the hexokinase gene family in Arabidopsis. *Planta* **2008**, *228*, 411–425. [[CrossRef](#)]
11. Cho, Y.-H.; Yoo, S.-D.; Sheen, J. Regulatory Functions of Nuclear Hexokinase1 Complex in Glucose Signaling. *Cell* **2006**, *127*, 579–589. [[CrossRef](#)]
12. Kim, H.-B.; Cho, J.-I.; Ryoo, N.; Shin, D.-H.; Park, Y.-I.; Hwang, Y.-S.; Lee, S.-K.; An, G.; Jeon, J.-S. Role of rice cytosolic hexokinase OsHXK7 in sugar signaling and metabolism. *J. Integr. Plant Biol.* **2016**, *58*, 127–135. [[CrossRef](#)]
13. Xu, F.-Q.; Li, X.-R.; Ruan, Y.-L. RNAi-mediated suppression of hexokinase gene OsHXK10 in rice leads to non-dehiscent anther and reduction of pollen germination. *Plant Sci.* **2008**, *175*, 674–684. [[CrossRef](#)]
14. Cho, J.-I.; Ryoo, N.; Eom, J.-S.; Lee, D.-W.; Kim, H.-B.; Jeong, S.-W.; Lee, Y.-H.; Kwon, Y.-K.; Cho, M.-H.; Bhoo, S.H.; et al. Role of the Rice Hexokinases OsHXK5 and OsHXK6 as Glucose Sensors. *Plant Physiol.* **2009**, *149*, 745–759. [[CrossRef](#)]
15. Zhang, Z.; Zhang, J.; Chen, Y.; Li, R.; Wang, H.; Ding, L.; Wei, J. Isolation, structural analysis, and expression characteristics of the maize (*Zea mays* L.) hexokinase gene family. *Mol. Biol. Rep.* **2014**, *41*, 6157–6166. [[CrossRef](#)]
16. Geng, M.-T.; Yao, Y.; Wang, Y.-L.; Wu, X.-H.; Sun, C.; Li, R.-M.; Fu, S.-P.; Duan, R.-J.; Liu, J.; Hu, X.-W.; et al. Structure, Expression, and Functional Analysis of the Hexokinase Gene Family in Cassava. *Int. J. Mol. Sci.* **2017**, *18*, 1041. [[CrossRef](#)]
17. Dou, L.; Li, Z.; Wang, H.; Li, H.; Xiao, G.; Zhang, X. The hexokinase Gene Family in Cotton: Genome-Wide Characterization and Bioinformatics Analysis. *Front. Plant Sci.* **2022**, *13*, 1–17. [[CrossRef](#)]
18. Zheng, W.; Zhang, Y.; Zhang, Q.; Wu, R.; Wang, X.; Feng, S.; Chen, S.; Lu, C.; Du, L. Genome-Wide Identification and Characterization of Hexokinase Genes in Moso Bamboo (*Phyllostachys edulis*). *Front. Plant Sci.* **2020**, *11*, 600. [[CrossRef](#)]
19. Nilsson, A.; Olsson, T.; Ulfstedt, M.; Thelander, M.; Ronne, H. Two novel types of hexokinases in the moss *Physcomitrella patens*. *BMC Plant Biol.* **2011**, *11*, 32. [[CrossRef](#)]
20. Wang, H.; Xin, H.; Guo, J.; Gao, Y.; Liu, C.; Dai, D.; Tang, L. Genome-wide screening of hexokinase gene family and functional elucidation of HXK2 response to cold stress in *Jatropha curcas*. *Mol. Biol. Rep.* **2019**, *46*, 1649–1660. [[CrossRef](#)]

21. Cheng, W.; Zhang, H.; Zhou, X.; Liu, H.; Liu, Y.; Li, J.; Han, S.; Wang, Y. Subcellular localization of rice hexokinase (OsHXK) family members in the mesophyll protoplasts of tobacco. *Biol. Plant.* **2011**, *55*, 173–177. [[CrossRef](#)]
22. Jang, J.C.; León, P.; Zhou, L.; Sheen, J. Hexokinase as a sugar sensor in higher plants. *Plant Cell* **1997**, *9*, 5–19.
23. Dai, N.; Schaffer, A.; Petreikov, M.; Shahak, Y.; Giller, Y.; Ratner, K.; Levine, A.; Granot, D. Overexpression of Arabidopsis Hexokinase in Tomato Plants Inhibits Growth, Reduces Photosynthesis, and Induces Rapid Senescence. *Plant Cell* **1999**, *11*, 1253–1266. [[CrossRef](#)]
24. Xiao, W.; Sheen, J.; Jang, J.C. The role of hexokinase in plant sugar signal transduction and growth and development. *Plant Mol. Biol.* **2000**, *44*, 451–461. [[CrossRef](#)]
25. Feng, J.; Zhao, S.; Chen, X.; Wang, W.; Dong, W.; Chen, J.; Shen, J.-R.; Liu, L.; Kuang, T. Biochemical and structural study of Arabidopsis hexokinase 1. *Acta Crystallogr. Sect. D Biol. Crystallogr.* **2015**, *71*, 367–375. [[CrossRef](#)]
26. Karve, A.; Moore, B.D. Function of Arabidopsis hexokinase-like1 as a negative regulator of plant growth. *J. Exp. Bot.* **2009**, *60*, 4137–4149. [[CrossRef](#)]
27. Kushwah, S.; Jones, A.M.; Laxmi, A. Cytokinin Interplay with Ethylene, Auxin, and Glucose Signaling Controls Arabidopsis Seedling Root Directional Growth. *Plant Physiol.* **2011**, *156*, 1851–1866. [[CrossRef](#)]
28. Gupta, A.; Singh, M.; Laxmi, A. Interaction between Glucose and Brassinosteroid during the Regulation of Lateral Root Development in Arabidopsis. *Plant Physiol.* **2015**, *168*, 307–320. [[CrossRef](#)]
29. Smeeckens, S.; Hellmann, H.A. Sugar sensing and signaling in plants. *Front. Plant Sci.* **2014**, *5*, 113. [[CrossRef](#)]
30. Mayordomo, I.; Sanz, P. Hexokinase PII: Structural analysis and glucose signalling in the yeast *Saccharomyces cerevisiae*. *Yeast* **2001**, *18*, 923–930. [[CrossRef](#)]
31. Sami, F.; Siddiqui, H.; Hayat, S. Interaction of glucose and phytohormone signaling in plants. *Plant Physiol. Biochem.* **2019**, *135*, 119–126. [[CrossRef](#)] [[PubMed](#)]
32. Barbier, F.F.; Cao, D.; Fichtner, F.; Weiste, C.; Perez-Garcia, M.; Caradeuc, M.; Le Gourrierec, J.; Sakr, S.; Beveridge, C.A. HEXOKINASE1 signalling promotes shoot branching and interacts with cytokinin and strigolactone pathways. *New Phytol.* **2021**, *231*, 1088–1104. [[CrossRef](#)] [[PubMed](#)]
33. Bruggeman, Q.; Prunier, F.; Mazubert, C.; de Bont, L.; Garmier, M.; Lugan, R.; Benhamed, M.; Bergounioux, C.; Raynaud, C.; Delarue, M. Involvement of Arabidopsis Hexokinase1 in Cell Death Mediated by Myo-Inositol Accumulation. *Plant Cell* **2015**, *27*, 1801–1814. [[CrossRef](#)] [[PubMed](#)]
34. Wang, X.-Q.; Zheng, L.-L.; Lin, H.; Yu, F.; Sun, L.-H.; Li, L.-M. Grape hexokinases are involved in the expression regulation of sucrose synthase- and cell wall invertase-encoding genes by glucose and ABA. *Plant Mol. Biol.* **2017**, *94*, 61–78. [[CrossRef](#)] [[PubMed](#)]
35. Lugassi, N.; Kelly, G.; Fidel, L.; Yaniv, Y.; Attia, Z.; Levi, A.; Alchanatis, V.; Moshelion, M.; Raveh, E.; Carmi, N.; et al. Expression of Arabidopsis Hexokinase in Citrus Guard Cells Controls Stomatal Aperture and Reduces Transpiration. *Front. Plant Sci.* **2015**, *6*, 1114. [[CrossRef](#)]
36. Kelly, G.; Sade, N.; Doron-Faigenboim, A.; Lerner, S.; Shatil-Cohen, A.; Yeselson, Y.; Egbaria, A.; Kottapalli, J.; Schaffer, A.A.; Moshelion, M.; et al. Sugar and hexokinase suppress expression of PIP aquaporins and reduce leaf hydraulics that preserves leaf water potential. *Plant J.* **2017**, *91*, 325–339. [[CrossRef](#)]
37. Zheng, S.; Lu, J.; Yu, D.; Li, J.; Zhou, H.; Jiang, D.; Liu, Z.; Zhuang, C. Hexokinase gene OsHXK1 positively regulates leaf senescence in rice. *BMC Plant Biol.* **2021**, *21*, 580. [[CrossRef](#)]
38. Valluru, R.; Van den Ende, W. Myo-inositol and beyond—Emerging networks under stress. *Plant Sci.* **2011**, *181*, 387–400. [[CrossRef](#)]
39. Li, J.; Chen, G.; Zhang, J.; Shen, H.; Kang, J.; Feng, P.; Xie, Q.; Hu, Z. Suppression of a hexokinase gene, SlHXK1, leads to accelerated leaf senescence and stunted plant growth in tomato. *Plant Sci.* **2020**, *298*, 110544. [[CrossRef](#)]
40. Sarowar, S.; Lee, J.Y.; Ahn, E.R.; Pai, H.S. A role of hexokinases in plant resistance to oxidative stress and pathogen infection. *J. Plant Biol.* **2008**, *51*, 341–346. [[CrossRef](#)]
41. Atanasov, V.; Fürtauer, L.; Nägele, T. Indications for a Central Role of Hexokinase Activity in Natural Variation of Heat Acclimation in Arabidopsis thaliana. *Plants* **2020**, *9*, 819. [[CrossRef](#)]
42. Lugassi, N.; Yadav, B.S.; Egbaria, A.; Wolf, D.; Kelly, G.; Neuhaus, E.; Raveh, E.; Carmi, N.; Granot, D. Expression of Arabidopsis Hexokinase in Tobacco Guard Cells Increases Water-Use Efficiency and Confers Tolerance to Drought and Salt Stress. *Plants* **2019**, *8*, 613. [[CrossRef](#)]
43. Kelly, G.; Egbaria, A.; Khamaisi, B.; Lugassi, N.; Attia, Z.; Moshelion, M.; Granot, D. Guard-Cell Hexokinase Increases Water-Use Efficiency Under Normal and Drought Conditions. *Front. Plant Sci.* **2019**, *10*, 1499. [[CrossRef](#)]
44. Lehretz, G.G.; Sonnewald, S.; Lugassi, N.; Granot, D.; Sonnewald, U. Future-Proofing Potato for Drought and Heat Tolerance by Overexpression of Hexokinase and SP6A. *Front. Plant Sci.* **2021**, *11*, 614534. [[CrossRef](#)]
45. Küstner, L.; Fürtauer, L.; Weckwerth, W.; Nägele, T.; Heyer, A.G. Subcellular dynamics of proteins and metabolites under abiotic stress reveal deferred response of the Arabidopsis thaliana hexokinase-1 mutant gin2-1 to high light. *Plant J.* **2019**, *100*, 456–472. [[CrossRef](#)]
46. Jing, W.; Uddin, S.; Chakraborty, R.; Van Anh, D.T.; Macoy, D.M.; Park, S.O.; Ryu, G.R.; Kim, Y.H.; Cha, J.; Kim, W.-Y.; et al. Molecular characterization of HEXOKINASE1 in plant innate immunity. *Appl. Biol. Chem.* **2020**, *63*, 76. [[CrossRef](#)]

47. Wang, Z.; Chen, D.; Sun, F.; Guo, W.; Wang, W.; Li, X.; Lan, Y.; Du, L.; Li, S.; Fan, Y.; et al. ARGONAUTE 2 increases rice susceptibility to rice black-streaked dwarf virus infection by epigenetically regulating HEXOKINASE 1 expression. *Mol. Plant Pathol.* **2021**, *22*, 1029–1040. [[CrossRef](#)]
48. Yu, J.; Li, X.; Wang, W.; Gu, K.; Sun, C.; You, C.; Hu, D. Glucose sensor MdHXK1 activates an immune response to the fungal pathogen *Botryosphaeria dothidea* in apple. *Physiol. Plant.* **2022**, *174*, e13596. [[CrossRef](#)]
49. Shen, C.; Zhang, Y.; Li, Q.; Liu, S.; He, F.; An, Y.; Zhou, Y.; Liu, C.; Yin, W.; Xia, X. PdGNC confers drought tolerance by mediating stomatal closure resulting from NO and H<sub>2</sub>O<sub>2</sub> production via the direct regulation of PdHXK1 expression in *Populus*. *New Phytol.* **2021**, *230*, 1868–1882. [[CrossRef](#)]
50. Moore, B.; Zhou, L.; Rolland, F.; Hall, Q.; Cheng, W.-H.; Liu, Y.-X.; Hwang, I.; Jones, T.; Sheen, J. Role of the Arabidopsis Glucose Sensor HXK1 in Nutrient, Light, and Hormonal Signaling. *Science* **2003**, *300*, 332–336. [[CrossRef](#)]
51. Hasin, Y.; Seldin, M.; Lusic, A. Multi-omics approaches to disease. *Genome Biol.* **2017**, *18*, 83. [[CrossRef](#)]
52. Polle, A.; Douglas, C. The molecular physiology of poplars: Paving the way for knowledge-based biomass production. *Plant Biol.* **2010**, *12*, 239–241. [[CrossRef](#)] [[PubMed](#)]
53. Schmitz, R.J.; Grotewold, E.; Stam, M. Cis-regulatory sequences in plants: Their importance, discovery, and future challenges. *Plant Cell* **2022**, *34*, 718–741. [[CrossRef](#)]
54. Zhang, L.; Li, B.; Zhang, Y.; Jia, X.; Zhou, M. Hexokinase plays a critical role in deoxynivalenol (DON) production and fungal development in *Fusarium graminearum*. *Mol. Plant Pathol.* **2016**, *17*, 16–28. [[CrossRef](#)] [[PubMed](#)]
55. Bork, P.; Sander, C.; Valencia, A. An ATPase domain common to prokaryotic cell cycle proteins, sugar kinases, actin, and hsp70 heat shock proteins. *Proc. Natl. Acad. Sci. USA* **1992**, *89*, 7290–7294. [[CrossRef](#)]
56. Rocca, J.D.; Hall, E.K.; Lennon, J.T.; Evans, S.E.; Waldrop, M.P.; Cotner, J.B.; Nemergut, D.R.; Graham, E.B.; Wallenstein, M.D. Relationships between protein-encoding gene abundance and corresponding process are commonly assumed yet rarely observed. *ISME J.* **2015**, *9*, 1693–1699. [[CrossRef](#)]
57. Chaudhary, S.; Khokhar, W.; Jabre, I.; Reddy, A.S.N.; Byrne, L.J.; Wilson, C.M.; Syed, N.H. Alternative splicing and protein diversity: Plants versus animals. *Front. Plant Sci.* **2019**, *10*, 708. [[CrossRef](#)]
58. Li, L.; Sheen, J. Dynamic and diverse sugar signaling. *Curr. Opin. Plant Biol.* **2016**, *33*, 116–125. [[CrossRef](#)]
59. Sakr, S.; Wang, M.; Dédaldéchamp, F.; Perez-García, M.D.; Ogé, L.; Hamama, L.; Atanassova, R. The sugar-signaling hub: Overview of regulators and interaction with the hormonal and metabolic network. *Int. J. Mol. Sci.* **2018**, *19*, 2506. [[CrossRef](#)]
60. Han, M.; Xu, X.; Li, X.; Xu, M.; Hu, M.; Xiong, Y.; Feng, J.; Wu, H.; Zhu, H.; Su, T. New Insight into Aspartate Metabolic Pathways in *Populus*: Linking the Root Responsive Isoenzymes with Amino Acid Biosynthesis during Incompatible Interactions of *Fusarium solani*. *Int. J. Mol. Sci.* **2022**, *23*, 6368. [[CrossRef](#)]
61. Rojas, C.M.; Senthil-Kumar, M.; Tzin, V.; Mysore, K.S. Regulation of primary plant metabolism during plant-pathogen interactions and its contribution to plant defense. *Front. Plant Sci.* **2014**, *5*, 17. [[CrossRef](#)] [[PubMed](#)]
62. Granot, D.; Kelly, G. Evolution of Guard-Cell Theories: The Story of Sugars. *Trends Plant Sci.* **2019**, *24*, 507–518. [[CrossRef](#)] [[PubMed](#)]
63. Papacek, M.; Christmann, A.; Grill, E. Interaction network of ABA receptors in grey poplar. *Plant J.* **2017**, *92*, 199–210. [[CrossRef](#)] [[PubMed](#)]
64. Estravis-Barcala, M.; Mattera, M.G.; Soliani, C.; Bellora, N.; Opgenoorth, L.; Heer, K.; Arana, M.V. Molecular bases of responses to abiotic stress in trees. *J. Exp. Bot.* **2020**, *71*, 3765–3779. [[CrossRef](#)]
65. Kelly, G.; Moshelion, M.; David-Schwartz, R.; Halperin, O.; Wallach, R.; Attia, Z.; Belausov, E.; Granot, D. Hexokinase mediates stomatal closure. *Plant J.* **2013**, *75*, 977–988. [[CrossRef](#)]
66. Su, T.; Han, M.; Min, J.; Zhou, H.; Zhang, Q.; Zhao, J.; Fang, Y. Functional Characterization of Invertase Inhibitors PtC/VIF1 and 2 Revealed Their Involvements in the Defense Response to Fungal Pathogen in *Populus trichocarpa*. *Front. Plant Sci.* **2020**, *10*, 1654. [[CrossRef](#)]
67. Su, T.; Zhou, B.; Cao, D.; Pan, Y.; Hu, M.; Zhang, M.; Wei, H.; Han, M. Transcriptomic Profiling of *Populus* Roots Challenged with *Fusarium* Reveals Differential Responsive Patterns of Invertase and Invertase Inhibitor-Like Families within Carbohydrate Metabolism. *J. Fungi* **2021**, *7*, 89. [[CrossRef](#)]
68. Hu, B.; Jin, J.; Guo, A.-Y.; Zhang, H.; Luo, J.; Gao, G. GSDS 2.0: An upgraded gene feature visualization server. *Bioinformatics* **2015**, *31*, 1296–1297. [[CrossRef](#)]
69. Kumar, S.; Stecher, G.; Li, M.; Niyaz, C.; Tamura, K. MEGA X: Molecular Evolutionary Genetics Analysis across Computing Platforms. *Mol. Biol. Evol.* **2018**, *35*, 1547–1549. [[CrossRef](#)]
70. Bailey, T.L.; Williams, N.; Misleh, C.; Li, W.W. MEME: Discovering and analyzing DNA and protein sequence motifs. *Nucleic Acids Res.* **2006**, *34*, W369–W373. [[CrossRef](#)]
71. De Castro, E.; Sigrist, C.J.A.; Gattiker, A.; Bulliard, V.; Langendijk-Genevaux, P.S.; Gasteiger, E.; Bairoch, A.; Hulo, N. ScanProsite: Detection of PROSITE signature matches and ProRule-associated functional and structural residues in proteins. *Nucleic Acids Res.* **2006**, *34*, W362–W365. [[CrossRef](#)]
72. Han, M.; Heppel, S.C.; Su, T.; Bogs, J.; Zu, Y.; An, Z.; Rausch, T. Enzyme Inhibitor Studies Reveal Complex Control of Methyl-D-Erythritol 4-Phosphate (MEP) Pathway Enzyme Expression in *Catharanthus roseus*. *PLoS ONE* **2013**, *8*, e62467. [[CrossRef](#)]

Review

# Management and Utilization of Plant Genetic Resources for a Sustainable Agriculture

Ranjith Pathirana <sup>1,2,\*</sup> and Francesco Carimi <sup>3</sup>

<sup>1</sup> Plant & Food Research Australia Pty Ltd., Waite Campus Research Precinct—Plant Breeding WT46, University of Adelaide, Waite Rd, Urrbrae, SA 5064, Australia

<sup>2</sup> School of Agriculture, Food and Wine, Waite Campus Research Precinct—Plant Breeding WT46, University of Adelaide, Waite Rd, Urrbrae, SA 5064, Australia

<sup>3</sup> Istituto di Bioscienze e BioRisorse (IBBR), C.N.R., Corso Calatafimi 414, 90129 Palermo, Italy

\* Correspondence: ranjith.pathirana@adelaide.edu.au

**Abstract:** Despite the dramatic increase in food production thanks to the Green Revolution, hunger is increasing among human populations around the world, affecting one in nine people. The negative environmental and social consequences of industrial monocrop agriculture is becoming evident, particularly in the contexts of greenhouse gas emissions and the increased frequency and impact of zoonotic disease emergence, including the ongoing COVID-19 pandemic. Human activity has altered 70–75% of the ice-free Earth’s surface, squeezing nature and wildlife into a corner. To prevent, halt, and reverse the degradation of ecosystems worldwide, the UN has launched a Decade of Ecosystem Restoration. In this context, this review describes the origin and diversity of cultivated species, the impact of modern agriculture and other human activities on plant genetic resources, and approaches to conserve and use them to increase food diversity and production with specific examples of the use of crop wild relatives for breeding climate-resilient cultivars that require less chemical and mechanical input. The need to better coordinate in situ conservation efforts with increased funding has been highlighted. We emphasise the need to strengthen the genebank infrastructure, enabling the use of modern biotechnological tools to help in genotyping and characterising accessions plus advanced ex situ conservation methods, identifying gaps in collections, developing core collections, and linking data with international databases. Crop and variety diversification and minimising tillage and other field practices through the development and introduction of herbaceous perennial crops is proposed as an alternative regenerative food system for higher carbon sequestration, sustaining economic benefits for growers, whilst also providing social and environmental benefits.

**Keywords:** centres of origin; crop wild relatives; crop domestication; cryopreservation; genebank; conservation; in vitro storage; germplasm; ecosystem restoration; plant breeding; climate change

**Citation:** Pathirana, R.; Carimi, F. Management and Utilization of Plant Genetic Resources for a Sustainable Agriculture. *Plants* **2022**, *11*, 2038. <https://doi.org/10.3390/plants11152038>

Academic Editors: Milan S. Stankovic, Paula Baptista and Petronia Carillo

Received: 29 June 2022

Accepted: 1 August 2022

Published: 4 August 2022

**Publisher’s Note:** MDPI stays neutral with regard to jurisdictional claims in published maps and institutional affiliations.



**Copyright:** © 2022 by the authors. Licensee MDPI, Basel, Switzerland. This article is an open access article distributed under the terms and conditions of the Creative Commons Attribution (CC BY) license (<https://creativecommons.org/licenses/by/4.0/>).

## 1. Introduction

With the global population expected to reach 9 billion by the middle of this century and the land area available for food production stagnating, or even reducing, the challenge of global food security is ever increasing. Almost one out of every nine people in the world suffers from hunger, and the number of hungry people is growing, albeit slowly [1]. The 2030 Agenda for Sustainable Development puts forward a transformational vision recognizing that our world is changing, bringing with it new challenges that must be overcome if we are to live in a world without hunger, food insecurity, and malnutrition in any of its forms. More than 820 million people in the world go hungry today, up from 784 million in 2015, emphasising the immense challenge of achieving the United Nations Zero Hunger target by 2030 [2]. Hunger is rising in almost all subregions of Africa and, to a lesser extent, in Latin America and Western Asia. It is heartening to see progress in Southern Asia in the last 5 years, but the prevalence of undernourishment in this subregion is still the highest in Asia. Another disturbing scenario is the fact that about 2 billion people

in the world experience moderate to severe food insecurity, thus experiencing greater risk of malnutrition and poor health. With the drop in economic growth, food access disruptions, increasing unemployment, rising food costs, and exacerbated poverty, food insecurity will affect a further 83–132 million people [3].

Concurrently with some regions of the global population increasingly experiencing hunger, around one million animal and plant species are threatened with extinction purely because of human activity—many within decades [4]. Even though natural ecosystem services are critical for our survival—providing oxygen, regulating weather patterns, pollinating our crops, and providing us with food, fibre, and feed for livestock—human activity has altered 70–75% of the global ice-free Earth’s surface [5], squeezing natural ecosystems into an ever-decreasing corner of the planet. The health of ecosystems on which we and all other species depend is deteriorating more rapidly than ever, affecting the very foundations of our economies, livelihoods, food security, health, and quality of life worldwide.

Using a data harmonisation procedure to reduce uncertainties in satellite-based land cover maps, Song [6] estimated the annual value of the world’s total terrestrial ecosystem services at USD 49.4 trillion. Land and its biodiversity also represent essential, intangible benefits to humans, such as cognitive and spiritual enrichment, a sense of belonging, and aesthetic and recreational values. Valuing ecosystem services with economic methods often overlooks these intangible services that shape societies, cultures, and quality of life, as well as the intrinsic value of biodiversity. The Earth’s land area is finite. Using land resources sustainably is fundamental to human well-being. Despite commitments made in 2010, biodiversity has further declined in the past decade [7]. To prevent, halt, and reverse the degradation of ecosystems worldwide, the UN has launched a Decade of Ecosystem Restoration (2021–2030). This action plan is globally coordinated through the governing body of the Convention on Biological Diversity and is in response to a call from scientists, as articulated in the Special Report on Climate Change and Land of the Intergovernmental Panel on Climate Change, the Rio Conventions on Climate Change and Biodiversity, and the UN Convention to Combat Desertification. This new draft for the post-2020 Global Biodiversity Framework comprises 21 targets and 10 milestones [8].

The Green Revolution aimed to resolve the global food crisis through breeding cultivars for mechanized monocultures with high inputs of pesticides and fertilizers. Although the increased yield helped to save the cultivation of an estimated 17.9–26.7 million hectares of new land under crops [9], the resulting increase in food production during the past five decades was accompanied by environmental degradation and deficiency in micronutrients in populations [10]. Furthermore, there is strong evidence that modern farming practices and intensified systems may be linked to disease emergence and amplification. There are many examples of zoonotic disease emerging at the wildlife–livestock–human interface which are associated with agricultural intensification and environmental change, such as habitat fragmentation and ecotones, reduced biodiversity, agricultural changes, and increasing human density in ecosystems [11,12], including Ebola virus [13,14] and recently, COVID-19 [15]. It is now clear that, as predicted by Borlaug in his acceptance speech for the Nobel Peace Prize (1970), further actions are needed to resolve the worsening environmental and social crises limiting food production and planetary health.

We have seen unprecedented levels of global warming since the beginning of the industrial era. Modelling has shown that each degree in temperature rise would cause a drop in crop production of 7.4% for corn, 6% for wheat, 3.2% for rice, and 3.1% for soybean [16]. This is significant because these four crops provide two-thirds of the human caloric intake. It is not only production, but also the quality of food that is at stake. Increased temperature and, to a lesser extent, increased atmospheric CO<sub>2</sub>, will affect soil biogeochemical processes by altering microbial community dynamics and activity, and geochemical reactions. This will result in alterations of ionic composition of the rhizosphere, hence affecting their uptake by crop plants. For example, it has been shown that future conditions will likely lead to a greater proportion of the more toxic form of arsenic, pore-

water arsenite, in the rhizosphere of Asian and Californian rice soils. Simulating these conditions under controlled environmental conditions, Muehe et al. [17] showed that elevated temperatures not only reduced rice yield by 39%, but also increased the amount of inorganic arsenic twofold in rice grain. Arsenic accumulation in rice is already becoming a problem in many South and Southeast Asian countries [18,19]. Therefore, agriculture requires more resilient varieties that can address likely problems induced by climate change; germplasm collections hold the key to developing such cultivars.

In broad terms, germplasm is the diversity of a cultivated species and its wild relatives that can hybridise and produce fertile progeny. Germplasm is of great importance for plant breeding because it carries genes that have potential value for improving crop yield, quality, and adaptation to the environment, including biotic and abiotic stresses. Thus, recognising the increasing frequency of natural disasters affecting the agricultural sector and their impact on food security, the introduction of longer-term measures to increase farmers' and households' resilience to natural disasters and climate change, such as the promotion of drought-tolerant crops and varieties, and livelihood diversification, is important. It is in this context that this paper on genetic diversity of cultivated species is presented, discussing the current situation and possible response options to contribute positively to sustainable development.

## 2. Origin of Cultivated Species and Geographic Distribution of Crop Diversity

Although the first land plants, the embryophytes, appeared some 515–470 million years ago in the Middle Cambrian–Early Ordovician period [20], humans who domesticated plants appeared much later, just 195,000–160,000 years ago and migrated from Africa about 130,000–120,000 years ago [21]. They were roaming the wild as hunter–gatherers, relying on wild plants and hunting wild animals for their food for another ~110,000 years before they settled to cultivate plants and rear animals in the Neolithic period—the start of the domestication of species (Table 1). Thanks to plant domestication and the resulting availability of food, humans became the predominant, most successful species on Earth, with a subsequent population explosion (Table 1) that demanded for more and more food.

**Table 1.** Evolutionary timescale of life on land illustrating that crop domestication is a very recent event compared with evolution of land plants. mya—million years ago, ya—years ago. Data from multiple sources referred in text.

Time in History	Event
515–470 mya	First land plants
350 mya	Emergence of angiosperms
160 mya	Monocots separated from dicots
6.5 mya	Hominids appear
2 mya	<i>Homo habilis</i>
1.75 mya	<i>Homo erectus</i>
195,000–160,000 ya	<i>Homo sapiens</i>
130,000–120,000 ya	Human migration out of Africa
13,000 ya	Settled agriculture and beginning of crop domestication

### 2.1. Vavilov's Centres of Origin of Cultivated Plants and the Theory of Homologous Series of Variation

The domestication of crops took place independently in eight geographic regions, described by Nikolai Vavilov [22] as primary centres of origin of cultivated plants in 1926 (Figure 1, Table 2). The criteria for these centres were high varietal diversity of the crop, presence of wild ancestors along with the domesticated ones, and a long history of the crop in the region. Vavilov was the first to observe that diversity of cultivated

plants was not distributed equally around the world, but was associated with ancient civilisations. It was in the 1920s that he recognised the existence of these centres and started collecting germplasm through numerous expeditions [23,24]. He established the world's first genebank in Petrograd (Saint Petersburg), with branches across the Soviet Union where almost any crop could be grown because of the vastness and diverse climatic zones in the country. The current status of this genebank and its activities are described by Dzyubenko [25].

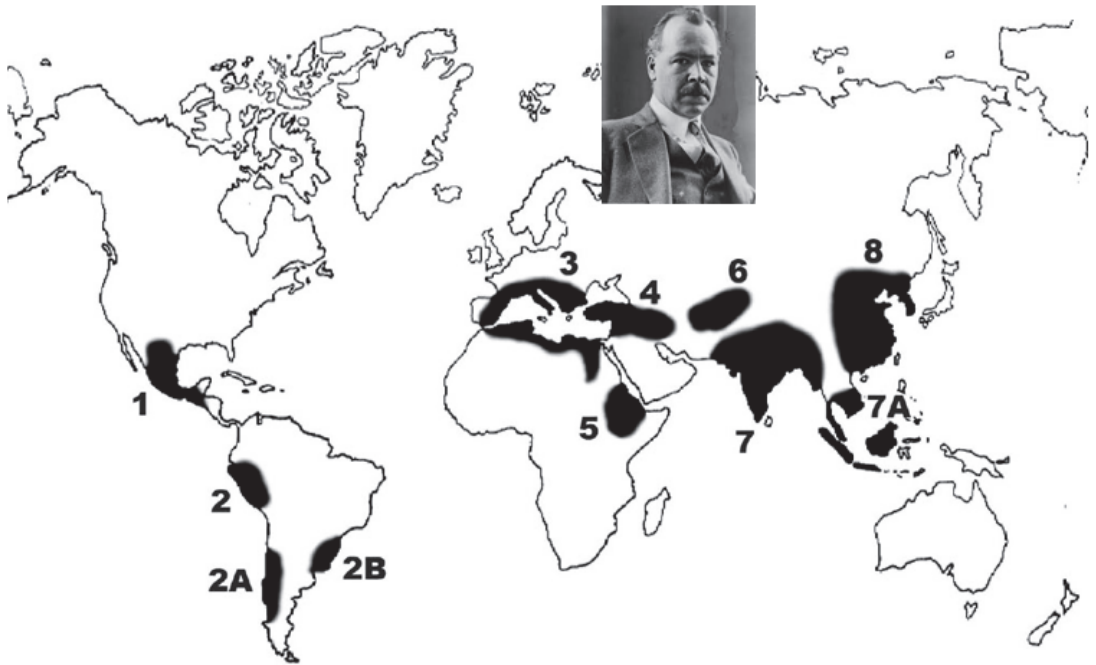


**Figure 1.** Eight main centres of the origin of cultivated plants according to Nikolai Vavilov (inset). 1. Mexico–Guatemala, 2. Peru–Ecuador–Bolivia, 2A. Southern Chile, 2B. Southern Brazil, 3. Mediterranean, 4. Middle East, 5. Ethiopia, 6. Central Asia, 7. Indo-Burma, 7A. Siam–Malaya–Java, and 8. China and Korea.

During his study of cultivated plants and wild species, Vavilov noted regularities of genotypical and phenotypical variation within the polymorphism between related species of the same genus, between species in related plant genera of the same family, or even between close families [26]. The first law of homologous series of variation states that “closely allied Linnean species are characterized by similar and parallel series of variation; and, as a rule, the nearer these Linneons are genetically, the more precise is the similarity of morphological and physiological variability. Genetically nearly related Linneons have consequently similar series of hereditary variation”. As a sequence to the first law, the second law states that “not only genetically closely related Linnean species, but also closely allied genera, display similarity in their series of phenotypical, as well as genotypical, variability”. Thanks to this discovery, the variation within a less studied species can be predicted if the variability of a related species is known. Voigt [27] has illustrated practical examples of the use of such predictions by Vavilov in plant breeding.

Such parallelism has been observed in recent molecular analyses of related crop species, for example, in resequenced *Brassica rapa* and *B. oleracea* [28]. Understanding of the existence of such parallelism is important in plant breeding because if a variant is predicted to be present, the required genotype can be found through hybridisation and

selection in segregating populations or using mutagenic techniques [29,30]. Use of induced mutations to produce semi-dwarf rice mutants in *Japonica* and *Javonica* backgrounds in California [31,32] and phytophthora (*Phytophthora nicotianae* var. *parasitica*)-resistant sesame (*Sesamum indicum*) mutants in Sri Lanka [33,34] are some examples of such practical use.

**Table 2.** Some of the crop species domesticated in different centres of diversity according to Zhukovsky [35].

Region	Crop
South Mexico–Central America	Avocado, Maize, Sweet Potato, Tomato, <i>Capsicum</i> spp., Tobacco, <i>Cucurbita pepo</i> , <i>C. moschata</i> , <i>Phaseolus</i> spp., <i>Amaranthus cruentus</i> , <i>A. hypochondriacus</i> , and <i>Gossypium hirsutum</i>
South American Andes (Peru, Bolivia, and Ecuador)	Potato, Quinoa, Lima Bean, Common Bean, Tomato, <i>Capsicum</i> spp., <i>Cucurbita maxima</i> , <i>C. moschata</i> , Grain amaranth ( <i>Amaranthus caudatus</i> ), Oca ( <i>Oxalis tuberosa</i> ), Ulluco ( <i>Ullucus tuberosus</i> ), Añu ( <i>Tropaeolum tuberosum</i> ), Achira ( <i>Canna edulis</i> ), Coca, <i>Gossypium barbadense</i>
Tropical lowland South America (Chile, Paraguay, and Southern Brazil)	Cassava, Arrowroot, Cocoyam, Peanut, Pineapple, and <i>Capsicum chinense</i>
Mediterranean	Grapevine, Carrot, Cabbage, Olive, Sugar Beet, European Pear, <i>Vicia faba</i> , <i>V. sativa</i> , <i>Lathyrus ochrus</i> , <i>Cicer arietinum</i> , and Almond
Asia Minor (Middle East)	<i>Cicer arietinum</i> (secondary centre), <i>Lens culinaris</i> , <i>L. orientalis</i> , <i>Vicia ervilia</i> , <i>Pisum sativum</i> , <i>Medicago sativa</i> , <i>Trifolium resupinatum</i> , <i>Trigonella foenum-graecum</i> , <i>Onobrychis</i> spp., <i>Lathyrus cicera</i> , <i>Vicia</i> spp., Date Palm, and Lettuce
Abyssinia (Ethiopian Centre)	Millet, Sorghum, Castor, Coffee ( <i>Coffea arabica</i> L.), Peanut, Teff ( <i>Eragrostis abyssiniaca</i> Link.), Finger Millet, Sesame, and Niger ( <i>Guizotia abyssiniaca</i> Cass.)
Inner Asia	Wheat, Barley, Apple, and Onion
India	Mung Bean, Rice, Black Gram, Pigeon Pea, Horsegram, Mango, Little Millet ( <i>Panicum sumatrense</i> ), and Flax
Indo-Malaya	Rambuttan, Banana, Sugarcane, and Yam
China	Rice, Soybean, Peach, Foxtail Millet ( <i>Setaria italica</i> ), Proso Millet ( <i>Panicum miliaceum</i> ), Hemp, Tea, Chinese Cabbage, Mulberry, and <i>Citrus</i> spp.

Study of crop domestication is complex, and was especially so during Vavilov’s time because of difficulty in accessing the many areas of crop domestication spanning different continents. Later studies have shown that high varietal diversity does not exist for some crops in the centre of origin [36]. Archaeological findings in recent times have added further complexity to the theme of crop domestication. This has revealed smaller independent areas of domestication within large centres. For example, Vavilov considered India as one major centre. Archaeological evidence suggests that there are five independent centres within India [37]. Other broad regions, such as Near Oceania, Amazonia, Eastern North America, and the river deltas of Western Africa, have also been identified as a result of new archaeological and molecular biological findings. Thus, for example, the Niger River basin in West Africa is now considered a major cradle of crop domestication in Africa, with sequencing and microsatellite marker studies confirming the origin of African rice (*Oryza glaberrima*) [38], African yam (*Dioscorea rotundata*) [39], and pearl millet (*Pennisetum glaucum*) [40] in this area. Li [41] discussed the complexity of Vavilov’s Chinese Centre and identified four belts of origin of cultivated plants in this region: I. Northern China, II. Southern China, III. Southern Asia, and IV. Southern Islands, according to their latitude. Archaeological evidence also suggests that in the early period, the focus on domestication was on a few crop species, mainly cereals. Plant domestication resulted in a lifestyle change for humans, from foraging to a more sedentary lifestyle. Increased agricultural productivity supported larger populations, and the first civilisations arose as a result. Purugganan and Fuller [42] describe 24 regions of domestication, most of them in and around Vavilov’s main centres.

## 2.2. Landrace and Modern Cultivars; Their Genetic Structure in Relation to Diversity Management

In later periods, large-scale breeding programmes or natural adaptation of crops outside the main centres after introduction by humans resulted in the diversity of particular species that Vavilov called secondary centres of diversity. The main difference in these secondary centres is the poor representation of wild relatives. In primary centres where the crop was domesticated, one sees wild relatives including the progenitors. Genetic diversity studies of domesticated crops and their wild ancestors can provide insight into the history and timing of domestication, shedding light on the food habits of our ancestors. Additionally, we can understand the genes that underlie the main phenotypic and genetic shifts in populations leading to domestication events, giving clues for the better use of underutilised crops for breeding. Most importantly, from crop genetic diversity studies, we can identify genetic groups within populations that need to be retained as germplasm for conservation and utilisation. The value of wild populations is in the large genomic variation and novel genes and alleles they carry that can be introgressed into cultivated species where there is typically lower genetic diversity due to domestication and selective breeding [43–45]. Therefore, once candidate genes associated with adaptation to emerging biotic and abiotic stresses in wild populations are identified, they can be introgressed into new cultivars. This approach can contribute to increased resilience of the cultivated species in new crop varieties destined to keep feeding the increasing population under climate change.

Soybean (*Glycine max*) is a well-studied domesticated crop, arising in an area covering parts of present-day China (Manchuria), Korea, and Southern Russia, where its progenitor *G. soja* exists [46]. The genetic diversity measured using different genetic markers, such as simple sequence repeat (SSR) [47], single-nucleotide polymorphism (SNP), 5S ribosomal RNA polymorphism [48] markers, and a de novo assembly of sequence data [44] all point to the larger variation and presence of novel alleles in *G. soja* compared with the domesticated *G. max*, including rare alleles [43]. Furthermore, the genetic diversity of the cultivated species in the centre of origin is far greater than in secondary centres. For example, North America is a secondary centre of diversity of soybean, with more than 30 million ha and 2242 cultivars registered in the USA alone within the period 1970–2008 [49]. However, only a limited number of ancestral introductions have contributed to the germplasm developed there, with only five introductions being the cytoplasm source for 121 of the 136 cultivars studied by Specht and Williams [50]. The ancestry of nuclear material also was narrow, with only 12 introductions contributing to 88% of the germplasm [50]. This indicates the value and need for conservation of genetic resources at the source of origin, with special attention to wild progenitors and other wild relatives because of the presence of a wider diversity of alleles.

Despite the narrow genetic variability, secondary centres of diversity offer valuable agronomic traits in their germplasm; hence, some countries can directly adopt some of these cultivars until national breeding efforts commence. A good example was the adoption of U.S. soybean cultivars such as ‘Hardy’, ‘Lee’, ‘Improved Pelican’, ‘Davis’, and ‘Bragg’ in north-central India in the 1960s [51,52] and in Sri Lanka in 1974 [53] until local breeding programmes were initiated resulting in superior cultivars suitable for release [52,54].

Few cultivated species have been domesticated outside their region of origin. For example, sunflower from South America was developed into oilseed sunflower in Russia [55–57]; grapefruit, a hybrid of *Citrus sinensis* from Southeast Asia and *Citrus maxima* from Indonesia, was domesticated in Barbados in the 1820s [58]; and Chinese gooseberry (*Actinidia* spp.) from East Asia was domesticated and commercialised in New Zealand as kiwifruit [59,60]. Again, the diversity of wild species is richer in the source region, with many wild species of sunflower in South America, and 57 species of *Actinidia* in China [61] against 19 in New Zealand introduced before China embargoed further export of kiwifruit genetic resources [62].

### 3. Crop Domestication and Domestication Traits

#### 3.1. Primary Domestication Traits

Humans who had traditionally foraged (Table 1) started cultivating limited plant species as food sources in the early Neolithic period (13,000 to 11,000 years ago). The morphological, physiological, and biochemical changes in species during evolution can take different directions under domestication depending on the part of the plant used. For example, in cereals and pulses, there is evidence for an increase in grain size and non-shattering at maturity [22,42]. As a result of acquiring the non-shattering grain character, cereal crops lost their ability for dispersal and became dependant on humans for reproduction by sowing. Many tuber and root crops, on the other hand, lost the ability to sexually reproduce as a result of selection for larger tuber or root, associated with selection for polyploid types resulting in sterility. In *Dioscorea alata*, a dioecious tuber crop, all 73 male genotypes studied by Abraham and Gopinathan Nair [63] were tetraploid, whereas most of the 30 female germplasm accessions were of higher ploidy (hexa and octaploids) and completely sterile.

Meyer and Purugganan [64] describe domestication traits as those selected during the initial transformation and establishment of a new domesticated species from its wild ancestor. Changes in resource allocation to the part of the plant commonly used for food are typical in many crop categories, whereas loss of dormancy, determinate growth habit, increase in seed size with thinner seed coat, and changes in inflorescence architecture are hallmark domestication traits in seed crops. These traits arose either through conscious human selection or ability of the particular genotype to survive under deforested or disturbed habitats. Traits to facilitate harvest (e.g., non-shattering in cereals) represent the former, and larger seed size the latter because of the ability of larger seeds to emerge after burial during planting (competitive advantage) [37,42,65].

Archaeological evidence from wheat, barley, and rice suggests that the seed size increase was one of the first traits selected under cultivation followed by the non-shattering of grains, the latter taking a much longer time for fixation. Seed size increases in barley and rye were achieved within 500–1000 years, whereas in rice it happened at a much slower pace, over the period 9000–5500 years ago [42,66,67]. On the other hand, pearl millet seed size enlargement occurred only 2000 years after domestication [42] and occurred at several locations [66]. Similarly, a 1500–2000-year period for seed size enlargement in mung bean is evident from recent archaeological findings from Indian sites [65,66].

For the first time, Li et al. [68] cloned and characterised a gene, *sh4*, for the loss of shattering in a grain crop (in rice), a hallmark trait of domestication, which, interestingly, is expressed at a slower rate during grain maturation in cultivated *O. sativa* than in the seed shattering progenitor *O. nivara*. This was probably the result of selection in the regulatory region of the gene for finer adjustment of the shattering/threshing balance in cultivated rice.

Another trait of domestication is tillering and branching. Generally, in most seed crops, apical dominance has increased, with the suppression of lateral branching or tillering during domestication. Doebley et al. [69] cloned *teosinte branched 1* (*tb1*), the key gene contributing to the increased apical dominance in maize (*Zea mays* ssp. *mays*) compared with its ancestor teosinte (*Z. mays* ssp. *parviglumis*) (Figure 2). Their research led to the discovery that *tb1* acts both to repress the growth of axillary organs and to enable the development of female inflorescences. The gene is not expressed in the primary axillary meristems of teosinte, enabling them to develop into long branches with a tassel at the tip (Figure 2). During domestication, the selection of forms that have high expression of *tb1* in primary axillary meristems led to the development of ear shoots rather than elongated tassel-tipped branches. Thus, during maize domestication for less branching, an alteration of the gene regulation of *tb1* has occurred rather than loss/gain or change in function. The most critical step in maize domestication was the liberation of the kernel from the hardened, protective casing that envelops the kernel in teosinte. This evolutionary step exposed the kernel on the surface of the ear, such that it could readily be used by humans as a food source (Figure 2). Wang et al. [70] mapped the factor controlling the phenotypic difference between maize

and teosinte for this trait to a 1 kilobase region, within which maize and teosinte show only seven fixed differences in their DNA sequences. They demonstrated that this key event in maize domestication is thus controlled by a single gene (*teosinte glume architecture 1* or *tga1*), belonging to the SBP-domain family 2 of transcriptional regulators [70].

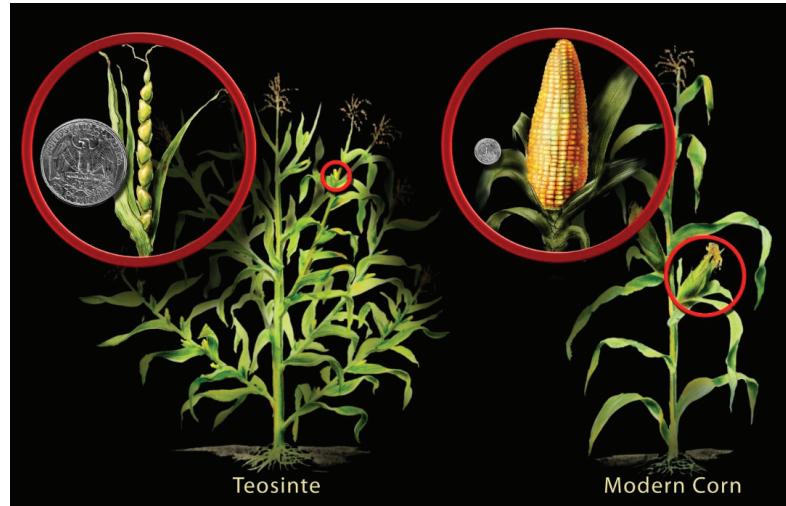


**Figure 2.** Domestication promotes rapid phenotypic evolution through artificial selection. Pictured here is wild grass teosinte (*Zea mays* ssp. *parviglumis*) that was domesticated into modern maize (*Z. mays* ssp. *mays*). The main traits selected during domestication included the ear and seed size (compared in relation to a USD coin in the inset) and the suppression of axillary branching. Figure courtesy National Science Foundation, USA.

Plant size can be reduced either as in the case of wheat and rice during the Green Revolution or from indeterminate growth habits to determinate growth, such as in beans and soybean. Plant architecture has been selected to suit harvesting practices, e.g., single-ear corn or single-head sunflower. Plants are also selected for ease of handling, thus losing their natural protective features such as thorns and spines in the case of some *Citrus* spp. and *Solanum* spp., respectively.

### 3.2. Diversification Events

After initial domestication, crops underwent diversification as a secondary event. For example, sticky and aromatic rice and popcorn were selected from the commonly grown rice and maize types, and a whole range of *Brassica oleraceae* vegetables (kohlrabi, cabbage, Brussels sprout, kale, broccoli, and cauliflower) were selected from mustard (Figure 3) as a result of diversification events. Most of the diversification traits evolve under targeted selection. Another interesting vegetable that has experienced through much diversification is lettuce (*Lactuca sativa* L.). Grown and used in ancient Egypt and depicted in Egyptian ancient art circa 2500 BC, it was a plant with narrow, erect leaves with prickles [71]. It has been used as an oil-yielding crop, and de Vries [72] considers that it was domesticated even earlier in the Kurdistan–Mesopotamia area. The fact remains that conscious selection has produced the many forms of lettuce in production today: cos, stalk, butterhead, crispbread (iceberg), and Latin. The oil type of lettuce is still used in Greece as a soporific [71].

Purugganan and Fuller [42] reviewed the genes directly involved in crop domestication that have been isolated and characterised to date. Of the nine domestication loci identified, eight encode transcriptional activators, including rice shattering genes *sh4* and *qSH1*, maize architecture gene *tb1* (suppresses axillary branch formation), and wheat inflorescence structure-determining *AP2*-like wheat gene *Q*. In contrast, more than half of

the 26 genes involved in diversification where molecular function has been characterised encode enzymes. Thus, domestication events are associated with transcription regulatory networks, whereas crop diversification involves a larger proportion of enzyme-coding loci.

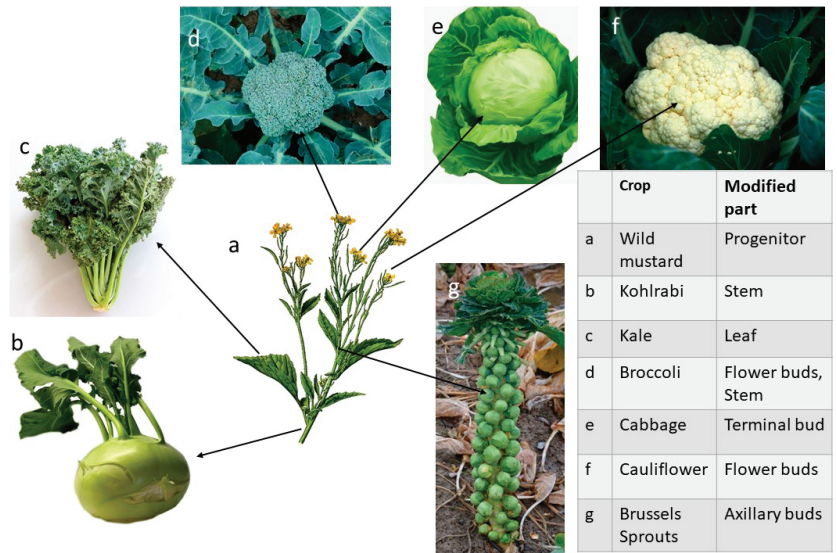


**Figure 3.** A whole range of Brassica vegetables have been selected during the diversification of *Brassica oleracea* (mustard), first domesticated as an oil-yielding crop in the Kurdistan/Mesopotamia area. Brussels sprouts are the youngest in the family of these vegetables, selected in Belgium in the mid-18th century.

### 3.3. Physiological and Biochemical Changes

During domestication, changes in morphological features as well as physiological and biochemical features, such as photoperiodism, vernalisation requirements, and seed and tuber dormancy, were very common. Changes in life cycle to suit different seasons in different climates have occurred. Some crops have been turned into annuals from their original perennial habit, such as cotton, castor, pigeon pea and cassava; others have lost their natural protective toxins, e.g., many crops of the Solanaceae family, as humans selected against those features. Another example of major physiological change following selection is the evolution from wild *Ananas bracteatus* to domesticated pineapple *A. comosus* (Figure 4).



**Figure 4.** The difference in wild *Ananas bracteatus* (left) and domesticated pineapples *A. comosus* (right).

### 3.4. Genetic and Cytogenetic Changes

Polyploidy, the increase in genome copy number, is a central feature of plant diversification. This could be autopolyploidy, where the same genome is represented multiple times (whole genome duplication) as a result of sexual polyploidisation via unreduced gametes, or somatic polyploidisation followed by sexual reproduction [30]. A classic example is cultivated potato (*Solanum tuberosum*) ( $2n = 4 \times = 48$ ), which has tetrasomic inheritance.

The other common form of polyploidy in domesticated species is allopolyploidy (amphidiploidy), where genomes of two or more species are represented in the new species. Durum wheat (*T. durum*) ( $2n = 4 \times = 28$ ; tetraploid) and bread wheat (*T. aestivum*) ( $2n = 6 \times = 42$  hexaploid) are well-known examples. Canola (*B. napus*) provides an example of how heterozygosity at polyploid level can increase selection advantage. It carries genomes of *B. oleraceae* ( $2n = 18$ , CC genome) and *B. rapa* ( $2n = 20$ , AA genome). Using quantitative trait loci analysis for yield, it was shown that canola yields were lower when it had allelic arrangements similar to the parental types, but when the arrangement differed from those of the parents, the yield was higher [73].

The majority of cultivated bananas are derived from inter- and intra-specific crosses between two diploids ( $2n = 2 \times = 22$ ): *Musa acuminata* (AA genome) and *M. balbisiana* (BB genome). The parent species have seeded fruit with little starch and are of no value as a crop (Figure 5). Most of the cultivated bananas are parthenocarpic seedless triploids ( $2n = 3 \times = 33$ ) with AAA (dessert bananas), AAB, or ABB (mostly cooking bananas) genomes. These variations have been collected from multiple independent sources in the wild; thus, the hybridisation events and mutations giving rise to the seedless and parthenocarpic characters have occurred many hundreds of times [74], meaning that bananas were domesticated in several areas of the Malayan centre of diversity.



**Figure 5.** Wild banana is diploid and produces seeds (left), whereas cultivated banana is sterile and seedless because it is a triploid (right).

## 4. Current Status of Plant Genetic Resources in the Centres of Diversity

As already described, along the path of domestication, humans have selected for only a few traits in our crops over time, resulting in the narrowing of the gene pool available for breeding. Landrace cultivars, although not as productive under high-input conditions of modern agriculture, carry alleles that are useful in many other ways, including pest and disease resistance, and tolerance to adverse soils, drought, salinity, and other abiotic stresses, while also carrying valuable quality traits such as a better nutritional value than many modern cultivars. For example, using whole-genome shotgun data from seeds of ancient and modern common bean, Trucchi et al. [75] showed that selection strategies during the past few centuries, as compared with historically, more intensively reduced genetic variation within cultivars and produced further improvements by focusing on a few plants carrying the traits of interest, at the cost of marked genetic erosion within Andean landraces. Using data from collecting missions and survey data since 1927, Hammer and Laghetti [76] found higher historical rates of genetic erosion of wheat in Italy (13.2%) compared with the period after 1950 (0.48–4%). Similar trends in genetic erosion have been found to occur in rice in India and China, *T. durum* and *T. dicoccum* in Ethiopia, and in traditional wheat varieties in Greece [77]. Crop wild relatives (CWRs) evolving in their natural habitat can also have many useful traits. Contemporary plant breeders are aware of the need to broaden the genetic structure of the crops they breed, although it is not easy to incorporate this aspect into breeding schemes because hybridisation with landrace

cultivars, more so with wild species, requires time-consuming back-crossing to achieve the high yields and other traits expected under modern cultural practices. As a result, the gene pool of our crops often continues to narrow in breeders' hands; at the same time, because of urbanisation, deforestation, monocropping, etc., the genetic diversity of crops is reducing at the centres of diversity.

Some of the centres of origin of cultivated species have recently become areas for large-scale irrigation and hydroelectric projects. By 2000, there were over 45,000 large dams in more than 150 countries, and each year 160 to 320 new schemes are being built worldwide [78], at the expense of habitat loss for terrestrial ecosystems. For example, the world's largest dam, the Three Gorges Dam in central China, was inserted in the middle of a biodiversity hotspot. Located in the upper reaches of the Yangtze River, little affected by the quaternary glaciations, the Three Gorges Reservation Area is one of the richest areas in biodiversity in China and was considered to have had the highest diversity of genera and families globally. It is the home of 6388 species of higher plants, belonging to 238 families and 1508 genera, and accounting for 20% of all seed plant species in China, with 57 of them being endangered [79].

In addition to industrial development, in some centres of crop diversity, protracted wars have induced the displacement of farming communities, in some cases with the complete abandonment of farmland along with the crop genetic resources they contained. Good examples are in the Middle East—Syria, Iraq, Yemen, and Palestine. The depletion of crop genetic resources is thus happening both at the centres of diversity, in what is left of the natural environment, and on farmers' lands. This is part of the larger problem of environmental degradation, and the COVID-19 pandemic could be viewed as a symptom of a bigger problem of deforestation and biodiversity loss that needs addressing urgently.

Without continued genetic enhancement using diverse germplasm from both CWRs and landrace cultivars, gains in crop yields obtained over the past seven decades are not sustainable, and yields might eventually grow more slowly or even decline, as already discussed [16]. Hence, comprehensive integrated programmes are needed for the conservation of plant genetic resources.

## 5. Role of Perennial Species in Sustainable Agriculture

Plants show a wide variability in the distribution of the limited resources available, allocating them to growth, defence, and reproduction, with two contrasting strategies: annual species, which complete their life cycle and die within a year; and perennial species, which usually delay their flowering to a later year, sometimes interrupted by periods of quiescence. Ensuring the need for agricultural products by a growing and more demanding world population through the intensification of conventional agriculture without causing significant damage to the environment is unrealistic. In recent decades, the environmental costs of intensifying conventional agriculture have begun to cause serious concern. Ecological intensification has been proposed as a nature-based alternative that complements or partially replaces external inputs [80]. Perennial plants are key components that offer previously unattainable levels of ecological intensification in agriculture, reducing the impact on the environment [81].

Although annual crops are the main source of our diet, several perennial crops could also be important players in the coming decades. Approximately one-eighth of the total area of global food production is composed of perennials, which are therefore a fundamental source of nutrition worldwide [82]. Perennial crops have several advantages from the point of view of environmental impact. One benefit is that they do not have to be reseeded or replanted every year, so they do not require annual ploughing to establish. Moreover, to successfully grow annuals, farmers must chemically or mechanically control weeds to avoid competition with crops for light, nutrients, and water, especially in the early stages of seedling development. The resulting soil disturbance has caused significant amounts of carbon loss in the soil (which ends up in the atmosphere as CO<sub>2</sub>), soil erosion, nutrient loss, and an impact on soil organisms [83]. From a study on the dynamics of soil organic

carbon, it was estimated that over a 20-year period, encompassing a change from annual to perennial crops led to an average 20% increase in organic carbon at 0–30 cm soil profile [84]. Compared with organic and conventional cultivation systems of annual wheat, recently commercialised perennial intermediate wheatgrass (IWG) cultivation increased the soil organic carbon in 30–60 cm soil depth, including the amount of carbon in the particulate organic matter, implying reduced carbon losses and high carbon use efficiency [83]. Another study found that carbon flux, as well as carbon and nitrogen storage in soil were greatest in IWG systems compared with both restored native vegetation and the annual monocropping rotation of wheat, sorghum, and soybean [85].

In general, compared with annual crops, perennial crops are more robust, protect the soil from erosion and improve its structure, increase the retention of nutrients, organic carbon, water [83–85], and therefore can contribute to the adaptation and mitigation of climate change. Overall, they help ensure long-term food and water security. Another advantage of perennial crops is that they can free farmers from economic instability by significantly reducing tillage and planting costs and their time in the field. In recent years, research has contributed to improving agricultural techniques and practices to support environmentally friendly agricultural systems based on perennial crops. All these ecological benefits were recently proven in 14 woody perennial polyculture farmlands when compared with annual monocultures in the U.S. Midwest, one of the most industrialised food-producing regions in the world [86]. A similar beneficial effect was found in semi-arid West Africa when the correct woody perennials and shrubs were chosen for growing along with annual cereals or legumes, particularly in farmer-managed natural regeneration systems as an agroforestry strategy [87]. However, perennial species are particularly recalcitrant to conventional breeding programs, because there are many obstacles to their improvement when compared with annual crops [82]. Many perennial species have long juvenile phases and thus require up to several years before the yield and quality can be evaluated. Not only are the time, space, and infrastructure required for breeding perennials often far greater than for breeding annuals, but the evaluation of commercially relevant traits is also often more complex, time-consuming, and expensive [82].

#### *Herbaceous Perennial Crops*

Agroecosystems are in constant evolution, in order to adapt to the needs of a growing population in a sustainable manner. Debates on the ecological impacts of agricultural intensification, including soil degradation and erosion, have concentrated attention on crops that provide both agricultural products and ecological services. Annual crops sown every year deplete the soil and expose it to erosion, requiring weed control with herbicides. Moreover, during the first phases of growth, shallow root systems are not efficient in absorbing water and nutrients, resulting in ground and surface water pollution by nitrate leaching [88]. Perennial herbaceous crops, which can be harvested mechanically, are perceived as a sustainable alternative to annual crops used as a source of human and animal food. They can grow for several years, produce a large root system that helps to reduce soil erosion and increases the soil organic matter, and can support several below-ground microbial communities that make plants more competitive, with better performance and, at the same time, with a lower impact on the environment. However, these species, which provide an opportunity to explore potential alternatives to annual crops, have been almost absent from agriculture, and were rarely domesticated for seed or fruit production [81,84].

Different possible biological mechanisms have been proposed to explain the rareness of herbaceous perennial crops. Among these, compromises between vegetative and reproductive tissues stand out, and it is now possible to develop these through phenotypic and genotypic selection [89]. The presence of genome sequences in wheat relatives such as *Thinopyrum intermedium* that may be orthologous to domestication genes identified in annual grain crops gives optimism [88]. Plants must devote limited resources towards a variety of processes, including growth, defence, and reproduction. In wild species, allocation strategies must reflect trade-offs between these processes and are therefore central

to a species' ecology. During the domestication process, artificial selection on allocation was carried out, which generated high-yielding crops that often invest reduced resources in defence or longevity, thus limiting the number of herbaceous perennial crops [89,90].

Need in developing new perennial crops and better understanding domesticated perennials has led to an increase in interest in the physiology, genetics, and evolution of these species. Our ability to understand or predict evolutionary transitions between strategies and their adaptive significance is limited by the lack of integration between the different fields. The evolutionary transition between perenniality and annuality in plants is exceptionally common among angiosperms. Reconstructions of the ancestral status using phylogenetic approaches have generally found that annuals derive from perennial ancestors; however, the evolution of perenniality was also observed. Empirical data support the hypothesis that evolutionary changes to annual life histories are associated with arid, disturbed/unstable environments in which adult survival is low or unpredictable [91].

The interest in developing new perennial crops through wide hybridization led to the crossing of annual crops with perennial relatives and the de novo domestication of wild, perennial, herbaceous species [92]. However, the idea of developing new perennial crops to replace annual grains is controversial [89,93]. The opportunity costs associated with the low grain yield compared with the high yield index of annual crops are one of the most persistent criticisms of perennial crops [94]. In his review, Smaje [94] raises three arguments against developing perennial grain agriculture: (a) ecological theory suggests that perennial grains may yield less than annual grains; (b) strong criticisms of annual agriculture are unfounded, both socially and ecologically; and (c) focus on perennial grains detracts from more important strategies for achieving agricultural sustainability. Crews and DeHaan [95] counter these three arguments, concluding that perennial herbaceous crops constitute a valid solution for enhancing sustainability in agriculture.

Many researchers have suggested that a more sustainable agricultural system will need to consist of mostly perennial species, and will need to be more diverse than is the case with present agroecosystems [96,97]. In the early 1980s, Wes Jackson [98] proposed the idea of growing perennial grain crops, including cereals, pulses, and oilseeds, and by planting them in complementary arrangements in prairie. This idea, which was considered utopian by many researchers in the past, seems to be achievable today thanks to new plant biotechnologies. In fact, the rapid deployment of technologies, such as CRISPR-Cas systems and other genome editing processes, provides new opportunities for crop breeding. The de novo domestication strategy can be adopted to improve the elite foundation materials from wild or semi-wild plant species in nature to achieve the main goals of genetic improvement, followed by the introduction of desired traits through the application of new genetic engineering technologies while retaining their desired features, resulting in plants harbouring new traits of interest [99]. If the new technologies that have been developed in recent years are applied to perennial proto-crops, it would enable the development of new genotypes of interest, probably in decades as opposed to the centuries that were required to create our current annual food crops [96].

The idea of rapid neodomestication was propagated as a promising strategy for future sustainable agriculture [100]. Despite accelerating the process, neodomestication through crosses would still suffer from the accumulation of deleterious mutations linked with domestication traits alleles, the so-called domestication cost [101]. Although the scientific community is not completely unanimous on the potential impact of crop neodomestication, there are several successful studies rendering this concept of potential interest to agriculture [102]. Neodomestication was first utilized for a rapid sunflower breeding program that introduced domestication traits into wild relatives through crosses [103]. In this regard, the high phenotypic gains, approaching 320% in breeding sunflower as a perennial oil crop [104], are encouraging. Subsequently, species of the genus *Vigna* were nominated as candidates for neodomestication due to their stress resilience and common use as edible wild plants [105].

Identifying the right herbaceous perennial species and germplasm for domestication can be challenging. The construction of an online resource of wild, perennial, herbaceous species—the Perennial Agriculture Project Global Inventory (PAPGI), comprising details of perennial members of the three of the largest known plant families, Asteraceae, Fabaceae, and Poaceae, containing details of taxonomy, growth descriptors, ecology, reproductive biology, genetics, economic uses, and toxicity [106] in this regard is invaluable. As the first component of the PAPGI project, focus has been on wild, perennial, herbaceous Fabaceae species, with records of 6644 species and over 60 agriculturally important traits. Food and forage uses of 314 legume species and toxicological data for 278 species have been incorporated into searchable online resources [81].

## 6. Approaches to Germplasm Conservation

There are two main approaches to conserving crop germplasm: in situ and ex situ. Article 2 of the Convention on Biological Diversity defines ex situ conservation as the conservation of components of biological diversity outside their natural habitat. In situ conservation relates to the conservation of ecosystems and natural habitats, and the maintenance and recovery of viable populations of species and, in the case of domesticated or cultivated species, in the surroundings where they have developed their distinctive properties. Thus, in situ conservation has two major facets: (a) the conservation of ecosystems and natural habitats, mainly facilitating the conservation of CWR in the natural ecosystems; and (b) the conservation of domesticated species in the habitats where they were developed [107]. The latter is called on-farm conservation and is part of wider in situ conservation.

### 6.1. In Situ Conservation

In situ conservation is important for conserving CWRs and landrace varieties of the cultivated species. In 1989, the Commission on Genetic Resources for Food and Agriculture (CGRFA) called for the establishment of networks of in situ conservation areas for plant genetic resources for agriculture, for both crops and CWR.

#### 6.1.1. Identity of Crop Wild Relatives

CWRs are commonly defined as wild species that are relatively closely related to agricultural and horticultural crops. Therefore, any taxon belonging to the same genus as a crop would fall into the CWR category. However, this definition covers large numbers of taxa and can result in the inclusion of species that are too remotely related to the crop or a large proportion of the species, e.g., in the Mediterranean Region and Europe almost 80% of flowering species are CWRs [108]. Considering the limited resources available for ex situ conservation efforts, a more rational approach would be to use the gene pool concept [109], where the close relatives are categorised as the primary gene pool, the more remote relatives as the secondary gene pool, and the most distant relatives as the tertiary gene pool. For many tropical species, where the relatedness in terms of crossing ability and genetic diversity is not well understood, the taxonomic hierarchy may be used to identify the relatedness of CWR to the cultivated species [110]. Even if relatedness is not yet established, new-found taxa can become high priority for conservation, such as the case with *Oryza rhizomatis* Vaughan, discovered in the late 1980s, mainly occurring in the driest areas of Sri Lanka (Figure 6). It is rhizomatous [111] and has drought-avoidance traits. It is in the near-threatened category in the IUCN Red List [112] and is a high priority rice taxon in terms of in situ conservation with another three species (*O. longiglumis*, *O. minuta*, and *O. schlechteri*).



**Figure 6.** Distribution of *Oryza rhizomatis* discovered in the late 1980s in the periphery of Yala and Wilpattu National Parks in the driest areas of Sri Lanka [113]. Reproduced with permission from the Food and Agriculture Organization of the United Nations.

#### 6.1.2. Why In Situ Conservation?

The evolution of crop species is continuing in the centres of diversity of crop plants, with new landraces emerging and genetic frequencies changing, as shown, for example, in the evolution of cultivated rice [114]. Thus, the main difference in maintaining the diversity in situ as against ex situ conservation in field genebanks or seed banks is that we have a continually evolving population responding to the changing environment. Allele frequencies vary over time in response to the changes in environment, thus making available genotypes of particular interest for contemporary plant breeding problems. Older ex situ collections, if not updated, remain frozen snapshots of a particular epoch of evolution and will subsequently have genotypes that are not adapted to the changed environment of the original collection site.

In addition to the conservation of genetic resources in the wild, on-farm conservation also helps to protect the conditions that allow the emergence of new germplasm. This idea of dynamic conservation extends to the whole farming system. This type of conservation enables the maintenance of genetic resources at all levels—ecosystem, species, and intraspecific—supporting and contributing to the overall agroecosystem health in locally tested farming systems. This includes minimising the use of pesticides, restricting emissions, conserving soil, and preventing pest and disease outbreaks as multiple crops and heterogeneous varieties within a farming community provide less than ideal conditions for such outbreaks.

CWRs and landrace varieties provide new sources of variation for crop improvement programmes. There are many examples of novel cultivars produced using these genetic resources from the past and present. For example, when late blight (*Phytophthora infestans*) decimated the potato industry in Europe as a result of the import of infested seed potatoes

from the United States in 1845, the introgression of phytophthora disease resistance from wild relatives, such as *Solanum demissum* from South America [115], helped to revive the industry; most modern potato cultivars carry resistance genes from this wild species. Potato blight caused one million deaths and the displacement of another one million people from Ireland, a country that was totally dependent on potato at the time [115]; a historical lesson of the importance of diversification of food sources.

In recent times, rice improvement has greatly benefitted from wild relatives. Brown plant hopper (BPH—*Nilaparvata lugens* Stål.) is one of the most destructive pests of rice throughout Asia, causing severe yield reduction by directly sucking the plant sap and acting as a vector of virus diseases such as rice grassy stunt and ragged stunt. *O. glaberrima* and *O. minuta* have durable resistance to this pest. Using embryo rescue techniques, this trait was transferred to cultivated rice [116]. The resulting lines are being used worldwide in rice breeding programmes. For example, screening of the introgression lines from the crosses IR 64 × *O. glaberrima* and IR 31917-45-3-2 × *O. minuta* showed that the two wild rice parents and the introgression lines had greater resistance to BPH than any of the local tolerant genotypes or IR 64, which has a *Bph1* gene which imparts some tolerance to BPH [117]. Examples of different wild rice species used in the improvement of targeted traits in cultivated rice are given in Table 3. Considering the value of such germplasm, both the Convention on Biological Diversity and the International Treaty on Plant Genetic Resources for Food and Agriculture (ITPGRFA—termed Plant Treaty) highly recommend the implementation of in situ conservation strategies.

**Table 3.** Some examples of traits of wild rice used in improving *Oryza sativa*—the cultivated species of rice.

<i>Oryza</i> Species	Genome	Trait of Interest	Line Number	Reference
<i>O. glaberrima</i>	AA	Brown planthopper ( <i>Nilaparvata lugens</i> Stål.) resistance	IR 75870-5-8-5-B-1-B), IR 75870-5-8-5-B-2-B)	[117]
<i>O. nivara</i>	AA	Brown planthopper tolerance	IR28, IR29, IR30, IR34, IR36, IR38, IR40, IR48, IR50, IR56, IR58,	[118]
<i>O. minuta</i>	BBCC	Brown plant hopper resistance	IR 71033-62-15, IR 71033-121-15	[117]
<i>O. nivara</i>	AA	Sheath blight ( <i>Rhizoctonia solani</i> ) tolerance	RPBio4918-10-3	[119]
<i>O. nivara</i>	AA	Salinity tolerance	14S, 75S, 166S, IL 3-1K	[120]
<i>O. rufipogon</i>	AA	Salinity tolerance	Chinsurah Nona 2	[118]
<i>O. nivara</i>	AA	Heat tolerance	166-2, 175-2, 3-1K	[121]
<i>O. rufipogon</i>	AA	Heat tolerance	377-13, 50	[121]
<i>O. nivara</i>	AA	Heat tolerance	24S, 70S, 14-3S	[122]
<i>O. nivara</i>	AA	High yield	220S, 10-2S	[123]
<i>O. nivara</i>	AA	100 grain weight, early flowering	NSL-15, NSL-22	[124]
<i>O. sativa</i> f. <i>spontanea</i>	AA	Cytoplasmic male sterility		Mondal and Henry [118]
<i>O. rufipogon</i>	AA	Rice tungro bacilliform virus resistance	Matatag 9	[118]
<i>O. longistaminata</i>	AA	Bacterial blight ( <i>Xanthomonas oryzae</i> pv. <i>oryzae</i> )	Shanyou63-Xa21	[125]

Table 3. Cont.

<i>Oryza</i> Species	Genome	Trait of Interest	Line Number	Reference
<i>O. rufipogon</i>	AA	Acid sulphate tolerance	AS 996	[118]
<i>O. minuta</i>	BBCC	Bacterial blight	41 Lines	[126]
<i>O. minuta</i>	BBCC	Brown planthopper	11 Lines	[126]
<i>O. minuta</i>	BBCC	Whitebacked planthopper ( <i>Sogatella furcifera</i> )	7 Lines	[126]
<i>O. grandiglumis</i>	CCDD	Grain weight and other yield traits	HG 101	[127]
<i>O. meridionalis</i>	AA	Iron tolerance	CM 23, CM 24	[128]
<i>Oryza rufipogon</i> 'DXWR'	AA	Drought tolerance	Restorer line BIL627	[129]

### 6.1.3. Implementation of In Situ Conservation

In general, implementing in situ conservation has been more challenging than ex situ conservation for several reasons. The in situ conservation of traditional cultivars is not well funded, unlike traditional genebank activities. Management and coordination activities of in situ collections have logistical problems because on-farm programmes have a poor connection with mainstream genebanking activities at both national and international level. In many environments, in situ conservation is still in an experimental stage and not supported through mainstream funding which is available for genebanking.

About forty years ago, it was widely assumed that traditional varieties would be rapidly and completely replaced by modern varieties [130]; this did not happen in several agricultural regions around the world [131]. For example, maize landraces in the U.S. corn belt were completely replaced between 1925 and 1950, whereas those in Mesoamerica continue to be cultivated [132]. A substantial amount of information has been documented in the last few years on the continuing maintenance and use of traditional varieties by small-scale farmers around the world [131–133]. Farmers seem to find that diversity, in the form of traditional varieties, remains important for their production systems. In fact, traditional varieties seem to adapt better than modern varieties to climate change and require lower chemical inputs. There are different ways of supporting farmers and farming communities in the maintenance of traditional varieties and crop genetic diversity within their production systems: (i) on-farm diversity assessment; (ii) access to diversity and information; (iii) the extent of use of available materials and information; and (iv) benefits derived by the farmer or farming community from their use of local crop diversity [131,133].

Different studies carried out around the world have demonstrated the value of the use of traditional varieties by small-scale farmers for conservation [131,134,135]. However, most studies on this topic suggest that there is insufficient knowledge about the social, cultural, and methodological dimensions on the topic, particularly how seed exchange networks cope under climate change, and under changes in socioeconomic factors, and family structures that have supported seed exchange systems to date [136,137]. Four core criteria have recently been proposed that characterize diverse Seed Commons arrangements at local and regional scales: (1) collective responsibility; (2) protection from private enclosure; (3) collective, polycentric management; and (4) the sharing of formal and practical knowledge [138].

A successful in situ on-farm conservation programme would usually have awareness raising as its first step. This will encourage not only the growing of local crops, but also their use by consumers. Local policy makers, journalists, and rural leaders, including farmers themselves, need to be educated through different activities, such as school programmes, poetry, essay and drama, village fairs, news, social media, etc. Through their daily interactions with the on-farm crop diversity and with neighbouring farmers, a local farming community is likely to know more about the local crop genetic resources than

anyone else. This is a good reason for the incorporation of farmers into the national plant genetic resources (PGRs) system, making them partners. The interaction of genebank operators with the local community helps make farmers aware of their activities. This interaction will benefit both parties because it facilitates farmer access to genebank material, and the genebank will receive farmer cooperation to maintain crop genetic diversity in situ. Genebanks can also facilitate the communication between farmer groups scattered throughout a country, sharing resources and learning from one another. In this model, on-farm conservation recognises local farmers as the curators of the crop genetic diversity and links it with indigenous knowledge.

On-farm conservation should be targeted at uplifting the livelihoods of resource-poor farmers. This can be achieved if development efforts are targeted at local resources to empower farmers, leading to the sustainable development of their livelihoods. This can be approached through infrastructure development, securing new marketing opportunities for underutilised crops and varieties with identified nutritional value or other traits with consumer preference. With demand growing for organic foods, organic certification programmes can be introduced at village level. In many developing countries, where industrialisation/mechanisation has yet to occur in some areas and farming traditions go back many centuries, farmers have developed a sense of community and collaborative relationships where they exchange seeds, planting material, and labour. In contrast to this, in industrialised countries, farmers compete with each other and decisions are made based on economic reasons, with tradition having much less influence on how farming is practiced—this makes it more difficult to introduce on-farm conservation. Increased mechanisation has also seen farm sizes increase and mono-cropping replacing traditional farming systems. As a result of the introduction of modern agricultural practices in Germany, for example, 90% of the original diversity of landraces has been lost [139]. Nevertheless, with a strong genebanking tradition, Germany has managed to introduce on-farm conservation practices better than many other industrialised countries, with about 50 initiatives launched for in situ conservation [139].

Some wild species are threatened by overexploitation by communities living in the periphery of conservation areas. The domestication of such species and propagation through seed gardens with the participation of users has been proposed as an approach for the conservation of genetic diversity of such species [140]. Studies on the changes in the diversity of landraces on farms have been critically analysed and recommendations for further studies and conservation measures needed have been proposed in a recent review by Khoury et al. [132].

## 6.2. *Ex Situ Conservation*

### 6.2.1. Origin of Genebanks and Their Spread

Nicolai Vavilov was one of the first to realise that the traditional crop varieties and land races were being lost from farmers' fields where they originated. This led him to establish the genebank in Petrograd in the 1920s, with 50,000 seed samples collected from more than 50 countries as a result of his expeditions. Since then, several genebanks have been established, and seed exchanges with Western Europe, the USA, Australia, and New Zealand have commenced. Those that are large or with a particularly wide scope include the All Union Institute for Plant Industry (VIR), Leningrad (Saint Petersburg), established in 1920; the Empire Potato Collection, Cambridge, UK (1938), now operating from James Hutton Institute, Invergowrie, Scotland; the Rockefeller Foundation Collections of maize under the Mexican Agricultural Programme (1943) [141]; and the National Seed Storage Laboratory, Fort Collins, CO, USA (1958). Similar collection efforts were commenced in many other South American countries in collaboration with American Land Grant Universities. By 1952, the USA had established four plant introduction stations in Ames (Iowa), Pullman (Washington), Geneva (New York), and Griffin (Georgia). In Europe, other than the VIR in the Soviet Union, significant work was conducted at the Institut für Kulturpflanzenforschung in Vienna, where Hans Stubbe carried out collection missions:

this institute was moved to Gatersleben in 1946 and now operates as the Leibniz-Institut für Pflanzengenetik und Kulturpflanzenforschung (IPK).

### 6.2.2. International and National Genebanks

The FAO, despite commencing the Plant Introduction Newsletter as far back as 1957, did not have any on-ground programmes for collection and conservation until 1964. This started to be addressed following an FAO Technical Meeting on Plant Exploration and Introduction, where the recommendation for setting up national and regional plant introduction centres was proposed and adopted. The FAO Expert Panel on Plant Exploration and Introduction was established in 1965 and held six meetings up to 1974, when the International Board for Plant Genetic Resources (IBPGR) was established. By the 1970s, many initiatives on international collaboration were in place, which gained further momentum with the establishment of the IBPGR [142] which, in 1991, became the International Plant Genetic Resources Institute—IPGRI. Within two decades, its network supported collections of over 200,000 accessions in 136 countries and coordinated the creation of an internationally linked system of genebanks called the Registry of Base Collections (Figure 7). Its aim is to conserve and make a subset of those materials available for national programmes [143]. The international genebanks were established in the centres of diversity of particular crops, but circumstances required moving some. For example, the war in Syria resulted in the relocation of the International Centre for Agricultural Research in the Dry Areas (ICARDA) from Aleppo, Syria, to Beirut, Lebanon, with most of the research activities moved to Morocco [144]. In addition to the traditional eight centres (Figure 7), Bioversity International holds a banana collection and supports aroid and yam genebanks in the Pacific. The Centre for International Forestry Research (CIFOR) and the World Agroforestry Institute have tree and fruit crop collections, and the International Livestock Research Institute (ILRI) has a fodder crops collection.



**Figure 7.** The location of the major international crop genebanks under the Consortium of International Agricultural Research Centres (CGIAR) network. CIMMYT—International Wheat and Maize Improvement Centre, CIAT—International Centre for Tropical Agriculture, ICARDA—International Centre for Agricultural Research, IRRI—International Rice Research Institute, ICRISAT—International Crops Research Institute for the Semi-Arid Tropics, ILRI—International Livestock Research Institute, IITA—International Institute for Tropical Agriculture, CIP—International Potato Centre. Inset—location of the Svalbard Global Seed Vault in the Arctic Circle.

In 2006, IPGRI centres signed an agreement with the Governing Body of the ITPGRFA, as a result of which the work of the centres is now influenced by Plant-Treaty-related activities. In the 1970s and 1980s, many national genebanks were set up both in industrialised and developing countries. Generally poorer in crop genetic diversity, industrialised countries gave technical support for setting up national genebanks in developing tropical countries with a rich diversity of plant genetic resources. For example, Sri Lanka's Plant Genetic Resources Centre was set up with the Japanese Technical Cooperation in 1988. The FAO estimates that 1750 genebanks exist worldwide with a total holding of about 7.4 million accessions. Of these, about 6.6 million are held in the national genebanks of individual countries [145]. For example, India's National Genebank holds around 0.39 million accessions, with similar numbers spread across 41 National Active Germplasm Sites [146].

To further safeguard the collections, the Svalbard Global Seed Vault (SGSV) was opened in 2008 under a partnership between the Ministry of Agriculture and Food of the Government of Norway, the Nordic Genetic Resource Centre (NordGen), and the Crop Trust. It is a backup facility for all the genebanks around the world and holds 1.15 million accessions in some 5000 species. It has a capacity for 4.5 million accessions and seeds are held under black box conditions, i.e., the seed boxes and containers stored in SGSV will not be opened. The seeds are indisputably owned by the depositing genebank, and only that genebank can request the return of seeds stored in SGSV [147]. For example, when the access to ICARDA genebank in Syria was finally closed in September 2015 due to war, seed boxes safely deposited in SGSV were systematically retrieved, regenerated, and multiplied in Lebanon and Morocco for the continuation of ICARDA operations [144]. Thus, located halfway between Norway and the North Pole, carved into ice in the permafrost 110 m above sea level, SGSV provides back-up for individual collections in the event that the original samples in conventional genebanks are lost due to natural disasters, human conflict, changing policies, mismanagement, or any other circumstances [147]. Engels and Ebert [148] recently critically reviewed the current global system of ex situ collections in the context of political and legal frameworks.

### 6.3. Management of Ex Situ Collections

#### 6.3.1. Management in Time

Under ex situ conservation, once the plant or seed samples are removed from the centre where they have evolved, natural processes of selection and adaptation to the environment cease. Thus, the collected sample is a "frozen snapshot" of the genetic structure at the time of collection [149]. In the case of seeds, particularly in cross-pollinated species, the representativeness of the sample is further reduced every time it is regenerated, because of genetic drift and natural selective pressures under different environmental conditions.

In the centres of diversity, on the other hand, crop evolution is an ongoing phenomenon: the "loss" and origin of "new" alleles frequently occur; indeed, land race cultivar dynamics are quite high [149,150]. Even in extensive collections from the Mediterranean region, researchers have found low geographic coverage and poor representation of on-farm genetic diversity in ex situ collections established in Europe [151]. This is perhaps because as for wild species diversity, a stratified sampling strategy is required for full coverage [152]. Notwithstanding, no matter how well sampled, ex situ collections do not represent the natural population in the diversity hotspot, after a few decades. Therefore, a regular and systematic monitoring programme of the landrace cultivar population dynamics in well-defined in situ hotspots is needed to better understand the drivers of change [150] and to supplement existing collections. Systematic monitoring programmes would enable proper sampling at regular intervals to capture the changing allelic frequencies, which is particularly important for meeting breeding challenges in a changing climate.

#### 6.3.2. Identification of Duplicates

With large numbers of accessions in genebanks, another issue confronted by curators is the duplication of samples resulting from poor passport data and collection strategies,

inconsistent documentation, and a lack of characterisation, amongst other factors. Labelling errors, hybridisation between stocks, and confusion about origins have also been identified as problems in *ex situ* collections. With over 7 million existing accessions in genebanks around the world [145] and increasing storage demands and costs, methods for efficient characterization and curation are required to avoid duplication. Genebanks have used molecular markers, such as simple sequence repeat (SSR), single-nucleotide polymorphism (SNP), amplified fragment length polymorphic (AFLP), and chloroplast DNA markers to characterise collections for their diversity and to identify duplicates with the aim of rationalising future collection and conservation efforts.

Lately, genome sequencing is being used to identify new patterns of variation [153,154], alleles of interest for breeding programmes [155], as well as duplicates [156] in collections. Methods are being developed to sequence large populations at low cost, including complex polyploid genomes [157–159]. Additionally, genome sequencing enables the unravelling of patterns of evolution of ancient crops, such as apple [160], grape [161], rice [114], and wheat [162], giving insights to their progenitors and conservation needs. Furthermore, they enable quantitative trait mapping and novel allele mining from large genetic collections [163]. When applied across different genebanks, these methods will enable the cost-effective and efficient management of germplasm and better stewardship of valuable genetic resources.

### 6.3.3. What to Conserve and Use—The Concept of Core Collections

It is practically impossible to cover the entire range of landraces or the diversity within CWR in a genebank. To manage the increasing number of accessions in collections and the resultant difficulties in monitoring, regeneration, evaluation, etc., the concept of core collections arose [164]. Identifying ‘representative’ samples within large collections helps to better utilise genetic resources when there are tens of thousands of accessions to choose from with just basic passport data. Such subsets in a collection represent the maximum diversity without redundancy. This allows the supply of a set of accessions for evaluation or breeding purposes without compromising the diversity within the collection.

With the introduction of the core set concept, genebanks now has a tool to manage their collections more efficiently. Core collections have since become focal points for conservation prioritisation, phenotypic evaluation, genotyping, and exchange. In the early years, the objective was to develop a single entry point for users, providing them with the widest diversity within a manageable number of accessions. Collections were defined hierarchically using taxonomic characterisation, genomic distance, and geographic data, dividing the collection into clusters and selecting ‘core’ genotypes within those clusters using methods such as proportional allocation, log frequency allocation, and constant allocation groups. Once a core collection is developed, it can be validated using several methods, such as mean comparisons with the entire collection, the homogeneity of variances and frequency distributions among traits between the entire collection and the core, and optimising correlations [165].

Alternatively, diversity can be assessed using molecular markers, and core sets developed using a maximization of the number of alleles observed in each marker locus without relying on a stratification strategy. This M (maximization) strategy examines all the accessions for the alleles in the collection and identifies those that maximize the number of observed alleles at the marker loci. These can then be chosen as final candidates for the core. The superiority of this marker-based method is derived from the correlation between observed allelic richness at the marker loci and allelic richness at other loci. The software uses iterative procedures to select samples with the highest diversity as measured by the number of alleles and the trait classes that account for the greatest proportion of the collection variability based on the M strategy. The method can also be applied for both quantitative and qualitative data [166]. For example, this method enabled the production of a mini core subset of 217 accessions representing a core of 1794 accessions from the United States Department of Agriculture Agricultural Research Service (USDA-ARS) collection of

rice, comprising more than 18,000 accessions [167], and to produce a core of 20 accessions within 450 apple accessions of the New Zealand apple germplasm repository, which was targeted for the first round of cryopreservation using winter dormant buds [168,169].

Core collections can also be developed using a multivariate distance approach [170] to develop the clusters followed by selection within those. Applying these methods, the International Crops Research Institute for the Semi-Arid Tropics (ICRISAT) has developed core sets from global collections of eleven crop species in ICRISAT genebank accessions [171]. Subsequently, mini core collections have been developed within the core collection using the same principles.

Core subsets for global collections, such as those maintained by the CGIAR, often serve as reference panels so that researchers around the world can evaluate the same genetic resources in different environments. Individuals in those reference sets may be selected as “controls” for phenotyping efforts (particularly relevant for disease and pathogen resistance/susceptibility and adaptation to different agro-ecological zones) so that results can be compared among research and breeding programmes. Some plant collections, particularly those that are clonally propagated, are difficult to distribute across international borders. Hence, multinational plantings of international core subsets for clonally propagated collections would help ensure that international communities have access to the same plant materials for comparative research.

#### 6.4. Types of Collections in Genebanks, Their Management and Utilization

Ex situ collections are conserved in different forms depending on the reproductive behaviour, genetic composition of the population, use of the crop (seed, fruit, fibre, vegetative materials, etc.) and other considerations. These aspects are briefly discussed below, with references to recent studies for details.

##### 6.4.1. DNA Banks

Plant DNA banks were initially developed to create genetic libraries for evolutionary studies, to understand biological diversity, and to collect genomic information [172]. However, with habitat loss, species extinction is happening at a rapid rate, particularly in areas with high genetic diversity. Therefore, DNA banks are increasingly used to store genomic and diversity information of species in these vulnerable hot spots. Additionally, our ability to extract DNA from fossilised plant remains is providing new research opportunities in paleoecology, phylogeography, and evolution, including crop domestication. Therefore, the number of DNA specimens from extinct species is increasing in DNA banks.

Genomic research has seen unprecedented advances in recent years. However, the physical DNA from the published sequences is generally not accessible to researchers. Access to the original samples is important for conducting new studies, to extend or complement existing results, and to support good scientific practice, enabling the verification of published results. To address these needs, the Global Genome Biodiversity Network (GGBN) was formed in 2011, with the aim of developing high-quality, well-documented, and vouchered collections that store DNA or tissue samples, as well as to encourage and enable scientists to complete documentation chains between vouchers, tissues, physical DNA, sequences, and publications [173,174]. The GGBN currently has 99 member organisations from 35 countries, with over 4.1 million samples from 5152 families, covering 38,074 genera and 140,182 species. Their updates can be viewed in annual newsletters [175] and the data can be accessed through their data portal [176].

DNA banking is considered the most economical way of conserving genetic information of plant genetic resources, and is also the easiest way of exchanging genetic information across borders because DNA samples occupy less space, are more stable, and phytosanitary certification is not needed.

#### 6.4.2. Orthodox Seeds

There are three types of seeds from a conservation perspective. Orthodox seeds can be dried to low moisture contents (about 3% for oily seeds and about 7% for starchy seeds) without damage and be stored dry at low temperatures without losing their viability over long periods. Recalcitrant seeds cannot withstand desiccation to moisture contents below 20%. Intermediate seeds can be dried to a moisture content of 10% to 12%, but further desiccation reduces viability and/or dry seeds are injured by low temperatures. Seeds of most of the main crop species belong to the orthodox category, meaning that they can be safely cooled to standard long-term storage conditions of  $-18\text{ }^{\circ}\text{C}$  without losing viability once dried to appropriate moisture contents. Seed storage is well researched and is the most efficient and cost-effective method of the conservation of plant germplasm, with about 96% of accessions held in genebanks worldwide as seeds [177]. In most of the genebanks, the seed vaults are maintained at  $-18\text{ }^{\circ}\text{C}$  for long-term storage, whereas active collections are maintained at  $5\text{ }^{\circ}\text{C}$  to  $10\text{ }^{\circ}\text{C}$ . Seeds may be stored in dedicated cold rooms (Figure 8) or in domestic deep chest freezers or refrigerators, for which genebank standards and technical guidelines have been published by the FAO [178].



**Figure 8.** Seed vaults for long-term storage at the United States Department of Agriculture—Agricultural Research Service genebank in Fort Collins, Colorado.

There are many advantages of conserving germplasm as seeds, including better security than in the natural environment, less space required, methods being simple, easily accessed and exchanged, and long storage periods. Additionally, seed collections capture more allelic diversity of the population than clonal collections. Therefore, in the case of fruit crop wild relatives, seed conservation is an option. However, as mentioned above, the evolutionary processes are frozen in time: as in any *ex situ* conservation method, regeneration is required from time to time. There can be gaps in the collection and initial set-up, and ongoing maintenance can be costly, including providing a constant power supply.

Under the ITPGRFA multilateral system, there are over 730,000 accessions available from the collections of the CGIAR system. The majority of these accessions are held in the form of seeds, with only 23,862 conserved as clones *in vitro* and 29,122 in field collections [143]. The number of accessions according to the species and the 11 participating genebanks are listed [143]. Additionally, the IBPGR has also coordinated the creation of an internationally linked system of genebanks known as the Registry of Base Collections (RBC) to conserve and make a subset of those materials available. Under this system, 144,000 accessions are available in 52 selected genebanks spread across all continents, covering 80 genera and 250 species [179]. Engels and Ebert [177] recently critically reviewed the current status of global seed banking with recommendations for improvement, emphasising the role of functional genomics and phenomics as well as strengths and weaknesses within regulatory frameworks and the strategies for linking national programmes with the global network.

### 6.4.3. Genebanking of Clonal Crops and Recalcitrant Species Field Collections

The traditional approach for maintaining germplasm of clonal species, species that are sterile or semi-sterile, and those producing recalcitrant seeds, is in field genebanks. They provide an excellent opportunity for curators to assess the diversity by phenotyping and for plant breeders to directly use accessions in their breeding programmes. Woody perennial crops (WPCs) represent about one-half of crop plant diversity and one-third of the 167 major crops. WPCs are usually clonally propagated because they are obligately outcrossing. Therefore, the conservation of germplasm through seed banks is not applicable to maintain the genetic characteristics of different heterozygous individuals. Moreover, the seeds of many species are recalcitrant, and therefore cannot be stored in traditional seed banks. Additionally, WPC species have a juvenile stage that can last for several years. In fact, plants generated from seeds usually exhibit strong, undesirable juvenile characters, such as a thorny habit and delayed flowering and fruit production [180]. In order to avoid these problems, the long-term conservation of WPC germplasm can be effectuated as field collections with clonal material in order to maintain the elite genotypes that form the foundation of woody perennial agriculture. However, WPCs represents only 5.8% of ex situ germplasm collections. Despite their importance, field collections are expensive to establish, and maintenance requires high costs for specialized technical personnel and land. Usually, woody perennials have a large plant size and therefore need large areas for maintenance in the field. Moreover, field collections have high risks of loss because they are exposed to natural disasters and are subject to biotic and abiotic stresses. In particular, the risk of pathogen infections transmitted through vegetative propagation is high and difficult to avoid. There are many examples of such cases, e.g., the loss of accessions in the apple germplasm collection in USDA due to fireblight (*Erwinia amylovora*) [181] and the loss of kiwifruit germplasm in New Zealand due to the incursion of *Pseudomonas syringae* pv. *actinidiae* [182]. Therefore, many genebanks back up their field collections in separate locations and also, more reliably, using lab-based conservation methodologies such as in vitro storage or cryostorage.

Establishing field genebanks may seem straightforward, but there are established best practices for sampling, the duplication of collections, and cataloguing the accessions. These can be found, for example, in the IPGRI training manual on “Establishment and management of field genebanks” [183], which has separate chapters on principles, legal issues, plant health, choice of materials, genetic considerations, planting layout, management characterisation and evaluation, utilisation, and economics. Another useful document is the IPGRI handbook No 7 on “Technical guidelines for the management of field and in vitro genebanks” [184]. Field genebanks of horticultural crops are a long-term commitment. Therefore, in many countries, field collections and genebank operations are undertaken by government departments.

#### In Vitro Collections

In general, lab-based germplasm conservation strategies fall under two major categories: slow growth procedures and cryopreservation. Both strategies require efficient regeneration system with high regeneration efficiency via organogenesis and/or somatic embryogenesis. In vitro storage has the advantage of maintaining collections under disease-free conditions and the cultures have fewer biosecurity requirements when material is exchanged across borders. On the other hand, because collections have high genetic diversity, the response to tissue culture media will be variable, which therefore requires prior research to optimise media for different species and even genotypes within species. There have been many studies on the tissue culture of cultivated species; therefore, this is not as daunting as it used to be a few decades ago. In vitro genebanks enable the rapid multiplication of material when required and provide a safe environment for managing germplasm collections in a confined space away from the field. To avoid somaclonal variation (genetic variation induced under tissue culture conditions), pathways using dedifferentiation and

adventitious regeneration should be avoided. Therefore, intact shoot tips and axillary buds are typically used with minimal use of plant growth regulators.

After initiation and the multiplication of accessions in tissue culture, they are stored under slow-growth conditions to increase the period between subcultures, thus significantly reducing the cost of labour and materials. Generally, this is achieved by a combination of several factors: (a) decreased light (generally about 5–10% of the standard culture conditions); (b) low temperature between 4 and 21 °C with tropical species requiring higher temperatures; (c) lower concentration of mineral nutrients and sucrose in media, often without growth regulators; (d) smaller size of culture vessel/vial; (e) inclusion of growth retardants in media; and (f) osmotic stress using chemicals [62,185,186]. Unless available in the literature, these conditions need to be determined for each species by experimentation. Many genebanks around the world have *in vitro* storage for some species. Genebanks holding large numbers of accessions *in vitro* are given in Table 4.

Synthetic seed technology (SST) is an innovative and sustainable approach to preserve the biodiversity of clonally propagated woody perennials. A synthetic seed is defined as an artificially encapsulated somatic embryo, vegetative bud, or any other micropropagule that plays the role of a seed and has the ability to give rise to a complete true-to-type plant. SST offers opportunities to conserve clonal genetic resources safely at low cost.

General guidelines for the storage [187] and status of *in vitro* storage under the CGIAR network, particularly CIP, IITA, CIAT, and Bioversity International [188], have been published. Additionally, *in vitro* techniques have proven useful in collecting germplasm when seeds are not available (off-season), or in situations where seeds are not likely to remain viable because of their recalcitrant nature. Pence et al. [189] recently reviewed basic approaches and principles of *in vitro* collection, and one of the crop species for which *in vitro* collection is routinely used is coconut.

**Table 4.** Genebanks with large *in vitro* collections.

Genebank	Country	Crop	Number of Accessions	Reference			
International Potato Centre	Peru	Potato, Andean Root and Tubers	>11,000	CIP-Genebank [190]			
		Cassava	>2500				
International Institute for Tropical Agriculture	Nigeria	Yam	>2500	IITA-GRC [191]			
		Banana	>500				
		24 genera, 63 species	1250		Cunha Alves, et al. [192]		
EMBRAPA Genebank	Brazil	24 genera, 63 species	1250	Cunha Alves, et al. [192]			
Agricultural Research Council	South Africa	Potato	1100	Myeza and Visser [193]			
		Fruit crops	743				
		Tuber crops	611				
		Spices	380				
National Bureau of Plant Genetic Resources	India	Bulbous crops	171	Tyagi and Agrawal [194]			
		Medicinal and Aromatic	170				
		Total 24 Genera, 63 spp.	1250				
		Bioversity International Transit Centre	Belgium		<i>Musa</i> spp.	>1500	ITC [195]
		International Centre for Tropical Agriculture (CIAT)	Columbia		Cassava	6632	Rondon [186]
The New Zealand Institute for Plant and Food Research Limited	New Zealand	Kiwifruit ( <i>Actinidia</i> spp.)	1012	Debenham and Pathirana [62]			
United States Department of Agriculture Agricultural Research Service	USA	Potato	~1000	Bamberg et al. [196]			

### Cryopreserved Collections—Stopping the Biological Clock

Cryopreservation is the storage of biological samples in liquid nitrogen (LN) at −196 °C or in its vapour phase (LNV) at −165 °C to −196 °C. The demonstration that win-

ter shoots of woody species can be conserved in liquid nitrogen in 1960 by Sakai [197] gave the impetus to undertake research on cryopreservation of fruit tree germplasm [198]. In the meantime, Latta [199] demonstrated the survival of carrot and sweet potato cell cultures in LN when pre-treated with high concentrations of sucrose followed by freezing to  $-40\text{ }^{\circ}\text{C}$  and subsequent transfer to LN. This method came to be called classical two-step freezing or slow freezing. However, it was the advent of vitrification methods in the 1990s that allowed genebanks to take up cryopreservation on a mass scale as it became applicable across different families and genera. The method relies on the dehydration of cellular content to the extent that sudden freezing does not allow water molecules to form lethal ice crystals, but enters a state of metastable glass—hence the term vitrification. Vitrification can be applied to naked meristematic explants, such as shoot tips and embryogenic cells, or to propagules protected by encapsulation in alginate beads [200,201]. The most widely used vitrification solution is Plant Vitrification Solution 2 [202] and the method is droplet vitrification, where propagules are held on an aluminium strip covered in a droplet of vitrification solution and directly immersed in LN. However, the recently developed V cryo-plate technique, where droplet vitrification and encapsulation techniques are combined, has shown an improvement in recovery over droplet vitrification in some crops [203–205]. The two methods as applied to grapevine have been described by Bettoni et al. [206]. Another advantage of cryopreservation using vitrification is its ability to eliminate viruses, phytoplasma, and bacteria [169,207–213] for the delivery of high-health propagation material.

Through cryopreservation, viable explants can be brought to a state where cellular division and metabolic processes are minimized to the extent that they cease, preserving the structure and function of the biological system—virtually stopping the biological clock. There are no biochemical processes or gene expression; therefore, the genetic material is safe from any changes, and is hence ideal for conservation. Most of the protocols depend on a tissue culture phase (except the dormant bud technique used mainly for apple cryopreservation); thus, it is important to ensure the precautions mentioned in the previous section are taken to avoid somaclonal variation. It is also cost-effective to maintain collections for extended periods of time in LN compared with field or in vitro collections [214], and the cost effectiveness increases as more accessions are added to the collection [215]. LN is used to freeze material, so the method is not dependent on an electric power supply; hence, it is an attractive method for countries with an insecure power supply, although it is dependent on a reliable LN supply.

The use of cryobanking in genebanks using vitrification methods has recently been summarised by Wang et al. [200], and for the USDA, currently the world's largest cryo collection, by Jenderek and Reed [216]. Panis [217] recently summarised the major cryopreserved collections worldwide. It is estimated that about 10,000 accessions are in long-term cryostorage using explants from in vitro culture material (mainly vitrification methods). Of these, over 80% belong to five species: potato (38%), cassava (22%), bananas and plantains (11%), mulberry (12%), and garlic (5%). Other large collections are in apple, using winter dormant buds. Cryopreservation is also used for intermediate and recalcitrant seed crop conservation, such as coconut [218] and coffee [215], as well as for pollen. Pollen is naturally dehydration-tolerant and can be used to conserve the nuclear genetic diversity of CWR, recalcitrant species, endangered and rare species, and fruit and ornamental crops. The cryopreservation of pollen allows access to pollen when needed by breeders, particularly useful when breeding lines have differing flowering times, the use of CWR in breeding programmes, and for hybrid seed production programmes. Cryopreserving the pollen of male sterile lines for use on female lines can save large amounts of land in hybrid seed production fields and labour to collect pollen during busy periods of hybridisation. Pollen of many tropical plant species has successfully been cryopreserved: for example, the Indian Institute of Horticultural Research in Bangalore holds 650 samples of pollen from 45 species belonging to 15 plant families [219].

Synthetic seeds can be stored for long periods using vitrification-based cryopreservation [220,221]; both somatic embryos and other somatic tissues with meristematic regions

have been used in cryopreservation and methods have been optimized to achieve post-thaw regeneration rates that meet genebank standards for the implementation of cryopreservation [201,206,222,223]. However, high genetic variability in the somatic embryogenesis response [224,225] is a barrier to use this propagule in cryopreservation.

Cryopreservation is only applied to a limited number of crops in some tropical genebanks outside the CGIAR system. Interestingly, the banana genebank, including the cryo-collection, is in Europe [226]. Since the introduction of vitrification methods, cryopreservation has become operationally simple and easily adaptable to any laboratory with tissue culture facilities. Collections of many tropical species, such as cassava, banana, sweet potato, and taro, are already being cryopreserved for their long-term security. The challenge is with CWR plus rare and endangered species of the tropics because their seeds are often recalcitrant and therefore cannot be preserved in traditional seed banks. Botanic gardens may only have one or a few specimens of each species in their field genebanks; however, the cryopreservation of seeds/embryonic axes and pollen enables the conservation of a much broader genetic diversity of CWRs or endangered species. Genebanks therefore need to invest in infrastructure and human resources for cryo-conservation. The integrated conservation strategies described above were recently used to save iconic New Zealand Myrtaceae species after the incursion of myrtle rust (*Austropuccinia psidii*) into New Zealand in 2017 [227]. The techniques used included the cryopreservation of pollen of *Metrosideros excelsa* and zygotic embryos of recalcitrant *Syzygium maire*, along with the successful hand pollination of flowers of *Metrosideros bartlettii*, a critically endangered species with only a few plants in the wild. Ex situ conservation strategies in field genebanks, in vitro slow growth, and the advantages and disadvantages of cryopreservation have recently been reviewed by Panis et al. [226].

## 7. Challenges to Plant Breeding in Search of Right Germplasm

Germplasm resources including CWRs carry alleles that are integral to creating new crop cultivars that can meet increasing consumer and environment demands. As changes in environmental conditions accelerate, so does the need for germplasm resources to breed more environmentally resilient crops. Properly characterised germplasm with information available to the plant breeding community will enable the deployment of improved cultivars on an ongoing basis. New cultivars with better water use efficiency, tolerance to soil toxicities, fertiliser response, and pest and disease tolerance will enable the replacement of at least some part of the costs for fertiliser, irrigation, and pesticides. Selection of the right genotype is the most effective means to achieve yield and quality improvements in crops, keeping other inputs to a minimum. Although plant breeders are often well aware of the necessity of maintaining genetic diversity in their breeding populations, they may lack the information to determine which of the thousands of accessions of a given crop would prove most beneficial for their breeding objectives. They may also be reluctant to introduce unadapted germplasm, with potentially negative impacts on quality, into their elite breeding materials. In some cases, they may lack the technical expertise or facilities to make interspecific crosses, for example, between CWR and cultivars of different ploidy levels that often require embryo rescue, in vitro pollination, and other interventions. Therefore, plant breeders should have access to facilities and expertise in plant biotechnology for the better utilisation of PGR.

Many international genebanks have a mandate to supply germplasm if the requests are justified. With more and more accessions being characterised and accessible databases made available, plant breeders should be trained in accessing the germplasm that matches their needs. The USDA-ARS holds over 576,000 accessions from 15,116 species and in 2015 alone, distributed over 239,000 accessions on request to national and international researchers [228]. The accessions available for supply can be searched in the Germplasm Resources Information Network-Global (GRIN-Global) database and ordered [229]. The CGIAR system of 11 genebanks holds over 736,000 accessions, with wheat and rice accounting for >196,000 and >144,000, respectively. Other major collections are in sorghum

(>39,200), beans (~38,000), barley (>31,500), maize (>29,700), pearl millet (>23,000), and forages and fodder (>44,000). The CGIAR system distributed over 3.9 million samples over a 10-year period from 2007 to 2016 [143]. The CGIAR system of networks has developed a Global Information System (GLIS), with an emphasis of assigning a unique digital object identifier (DOI) to each accession; these are linked to the GRIN-Global searchable database and to Genesys—an online database for global plant collections managed by the Crop Trust [230]. The VIR collection holds 346,666 accessions of PGR and CWRs, representing 64 botanical families, 376 genera, and 2169 species. Annually, 12,000–14,000 accessions are distributed by the genebank, of which 2000–3000 accessions are supplied outside Russia [25].

## 8. Conclusions

Significant improvements have been made for the better management of PGRs within international and national genebanks in the last few decades. More attention is being paid to managing ‘difficult’ species with recalcitrant seeds, clonal crops, and CWRs. Effective research and development mechanisms and policies have been established for the protection and conservation of biodiversity worldwide. Many countries have signed international treaties on biodiversity, as well as PGR conservation and exchange. Coordination among genebank curators, breeders, farming communities, government organisations, and different stakeholders should be strengthened to meet global obligations for sustainable management and the use of PGR for food and nutritional security. Genebank accessions are of no use unless they are accessible online or can be observed in the field. Therefore, conserved PGRs need to be characterised using advanced technologies and results with passport data made available for online access by users. The emphasis should be on duplicating collections for better security, creating and securing core collections, identifying gaps in collections and remediating them, and using advanced and integrated strategies for the conservation and dissemination of information. CWR and landrace varieties need to be secured for the future, using multiple strategies including in situ, on-farm, and ex situ conservation. Further exploration and collection of PGR from diversity-rich centres should also assume priority, recognising the high rate of loss of genetic diversity.

**Author Contributions:** Conceptualization, R.P. and F.C.; writing-original draft preparation, R.P. and F.C.; Writing-review and editing, R.P. and F.C. All authors have read and agreed to the published version of the manuscript.

**Funding:** This research received no external funding.

**Institutional Review Board Statement:** Not applicable.

**Informed Consent Statement:** Not applicable.

**Data Availability Statement:** Not applicable.

**Conflicts of Interest:** The authors declare no conflict of interest.

## References

1. FAO. The Food and Agriculture Organisation. *The State of Food Security and Nutrition in the World 2019. Safeguarding against Economic Slowdowns and Downturns*. Available online: <http://www.fao.org/3/ca5162en/ca5162en.pdf> (accessed on 2 February 2022).
2. UN. United Nations 2030 Agenda for Sustainable Development—Sustainable Development Goals. *Goal 2: Zero Hunger*. Available online: <https://www.un.org/sustainabledevelopment/hunger/> (accessed on 7 June 2022).
3. FAO. The State of Food Security and Nutrition in the World 2021: Transforming Food Systems for Food Security, Improved Nutrition and Affordable Healthy Diets for All. Available online: <https://www.fao.org/3/cb4474en/online/cb4474en.html> (accessed on 25 May 2022).
4. IPBES. *Global Assessment Report of the Intergovernmental Science-Policy Platform on Biodiversity and Ecosystem Services*; The Intergovernmental Science-Policy Platform on Biodiversity and Ecosystem Services (IPBES)—IPBES Secretariat: Bonn, Germany, 2019; p. 1144.
5. IPCC. An IPCC Special Report on Climate Change, Desertification, Land Degradation, Sustainable Land Management, Food Security, and Greenhouse Gas Fluxes in Terrestrial Ecosystems. Available online: [https://www.ipcc.ch/site/assets/uploads/2019/11/Headline-statements\\_Final.pdf](https://www.ipcc.ch/site/assets/uploads/2019/11/Headline-statements_Final.pdf) (accessed on 5 May 2022).

6. Song, X.-P. Global estimates of ecosystem service value and change: Taking into account uncertainties in satellite-based land cover data. *Ecol. Econ.* **2018**, *143*, 227–235. [CrossRef]
7. Xu, H.; Cao, Y.; Yu, D.; Cao, M.; He, Y.; Gill, M.; Pereira, H.M. Ensuring effective implementation of the post-2020 global biodiversity targets. *Nat. Ecol. Evol.* **2021**, *5*, 411–418. [CrossRef] [PubMed]
8. CBD. A New Global Framework for Managing Nature Through 2030: First Detailed Draft Agreement Debuts. Available online: <https://www.cbd.int/article/draft-1-global-biodiversity-framework> (accessed on 7 June 2022).
9. Stevenson, J.R.; Villoria, N.; Byerlee, D.; Kelley, T.; Maredia, M. Green Revolution research saved an estimated 18 to 27 million hectares from being brought into agricultural production. *Proc. Natl. Acad. Sci. USA* **2013**, *110*, 8363–8368. [CrossRef] [PubMed]
10. Pingali, P.L. Green Revolution: Impacts, limits, and the path ahead. *Proc. Natl. Acad. Sci. USA* **2012**, *109*, 12302–12308. [CrossRef]
11. Karesh, W.B.; Dobson, A.; Lloyd-Smith, J.O.; Lubroth, J.; Dixon, M.A.; Bennett, M.; Aldrich, S.; Harrington, T.; Formenty, P.; Loh, E.H.; et al. Ecology of zoonoses: Natural and unnatural histories. *Lancet* **2012**, *380*, 1936–1945. [CrossRef]
12. Jones, B.A.; Grace, D.; Kock, R.; Alonso, S.; Rushton, J.; Said, M.Y.; McKeever, D.; Mutua, F.; Young, J.; McDermott, J.; et al. Zoonosis emergence linked to agricultural intensification and environmental change. *Proc. Natl. Acad. Sci. USA* **2013**, *110*, 8399–8404. [CrossRef]
13. Olivero, J.; Fa, J.E.; Real, R.; Márquez, A.L.; Farfán, M.A.; Vargas, J.M.; Gaveau, D.; Salim, M.A.; Park, D.; Suter, J.; et al. Recent loss of closed forests is associated with Ebola virus disease outbreaks. *Sci. Rep.* **2017**, *7*, 14291. [CrossRef]
14. Rulli, M.C.; Santini, M.; Hayman, D.T.S.; D’Odorico, P. The nexus between forest fragmentation in Africa and Ebola virus disease outbreaks. *Sci. Rep.* **2017**, *7*, 41613. [CrossRef]
15. Everard, M.; Johnston, P.; Santillo, D.; Staddon, C. The role of ecosystems in mitigation and management of COVID-19 and other zoonoses. *Environ. Sci. Policy* **2020**, *111*, 7–17. [CrossRef]
16. Zhao, C.; Liu, B.; Piao, S.; Wang, X.; Lobell, D.B.; Huang, Y.; Huang, M.; Yao, Y.; Bassu, S.; Ciais, P.; et al. Temperature increase reduces global yields of major crops in four independent estimates. *Proc. Natl. Acad. Sci. USA* **2017**, *114*, 9326–9331. [CrossRef]
17. Muehe, E.M.; Wang, T.; Kerl, C.F.; Planer-Friedrich, B.; Fendorf, S. Rice production threatened by coupled stresses of climate and soil arsenic. *Nat. Commun.* **2019**, *10*, 4985. [CrossRef] [PubMed]
18. Meharg, A.A. Arsenic in rice—understanding a new disaster for South-East Asia. *Trends Plant Sci.* **2004**, *9*, 415–417. [CrossRef] [PubMed]
19. Hassan, F.I.; Niaz, K.; Khan, F.; Maqbool, F.; Abdollahi, M. The relation between rice consumption, arsenic contamination, and prevalence of diabetes in South Asia. *EXCLI J.* **2017**, *16*, 1132–1143. [CrossRef] [PubMed]
20. Morris, J.L.; Puttick, M.N.; Clark, J.W.; Edwards, D.; Kenrick, P.; Pressel, S.; Wellman, C.H.; Yang, Z.; Schneider, H.; Donoghue, P.C.J. The timescale of early land plant evolution. *Proc. Natl. Acad. Sci. USA* **2018**, *115*, E2274–E2283. [CrossRef]
21. Petraglia, M.D.; Haslam, M.; Fuller, D.Q.; Boivin, N.; Clarkson, C. Out of Africa: New hypotheses and evidence for the dispersal of *Homo sapiens* along the Indian Ocean rim. *Ann. Hum. Biol.* **2010**, *37*, 288–311. [CrossRef]
22. Vavilov, N.I. *Origin and Geography of Cultivated Plants*; Nauka: Leningrad, Russia, 1987. (In Russian)
23. Cohen, B.M. Nikolai Ivanovich Vavilov: The explorer and plant collector. *Econ. Bot.* **1991**, *45*, 38–46. [CrossRef]
24. Zakharov, I.A. Nikolai I Vavilov (1887–1943). *J. Biosci.* **2005**, *30*, 299–301. [CrossRef]
25. Dzyubenko, N.I. Vavilov’s collection of worldwide crop genetic resources in the 21st Century. *Biopreservation Biobanking* **2018**, *16*, 377–383. [CrossRef]
26. Vavilov, N.I. The law of homologous series in variation. *J. Genet.* **1922**, *12*, 47–89. [CrossRef]
27. Voigt, W. Einige Gedanken zu Vavilovs Gesetz der homologen Reihen und zu den Ursachen homologer genetischer Variationen aus wissenschaftstheoretischer Sicht. *Die Kulturpflanze* **1988**, *36*, 163–168. [CrossRef]
28. Cheng, F.; Sun, R.; Hou, X.; Zheng, H.; Zhang, F.; Zhang, Y.; Liu, B.; Liang, J.; Zhuang, M.; Liu, Y.; et al. Subgenome parallel selection is associated with morphotype diversification and convergent crop domestication in *Brassica rapa* and *Brassica oleracea*. *Nat. Genet.* **2016**, *48*, 1218–1224. [CrossRef]
29. Maluszynski, M.; Ahloowalia, B.S.; Sigurbjörnsson, B. Application of in vivo and in vitro mutation techniques for crop improvement. *Euphytica* **1995**, *81*, 303–315. [CrossRef]
30. Pathirana, R. Plant mutation breeding in agriculture. *CAB Rev. Perspect. Agric. Vet. Sci. Nutr. Nat. Resour.* **2011**, *6*, 1–20. [CrossRef]
31. Foster, K.W.; Rutger, J.N. Inheritance of semidwarfism in rice *Oryza sativa* L. *Genetics* **1978**, *88*, 559–574. [CrossRef] [PubMed]
32. Rutger, J.N. *Plant Mutation Breeding for Crop Improvement, Volume 1, Proceedings of the FAO/IAEA Symposium on Plant Mutation Breeding for Crop Improvement, Vienna, Austria, 18–22 June 1990*; International Atomic Energy Agency: Vienna, Austria, 1991; pp. 155–165.
33. Pathirana, R. Gamma-ray-induced field tolerance to Phytophthora blight in Sesame. *Plant Breed.* **1992**, *108*, 314–319. [CrossRef]
34. Pathirana, R.; Weerasena, L.A.; Priyanthi, B. Development and release of gamma ray induced sesame mutant ANK-S2 in Sri Lanka. *Trop. Agric. Res. Ext.* **2000**, *3*, 19–24.
35. Zhukovsky, P.M. *Cultivated Plants and Their Progenitors*; Kolos: Leningrad, Russia, 1971; p. 750. (In Russian)
36. Harlan, J.R. *Crops and Man*; Crop Science Society of America: Madison, WI, USA, 1992.
37. Meyer, R.S.; DuVal, A.E.; Jensen, H.R. Patterns and processes in crop domestication: An historical review and quantitative analysis of 203 global food crops. *New Phytol.* **2012**, *196*, 29–48. [CrossRef]

38. Wang, M.; Yu, Y.; Haberer, G.; Marri, P.R.; Fan, C.; Goicoechea, J.L.; Zuccolo, A.; Song, X.; Kudrna, D.; Ammiraju, J.S.S.; et al. The genome sequence of African rice (*Oryza glaberrima*) and evidence for independent domestication. *Nat. Genet.* **2014**, *46*, 982–988. [[CrossRef](#)]
39. Scarcelli, N.; Cubry, P.; Akakpo, R.; Thuillet, A.C.; Obidiegwu, J.; Baco, M.N.; Otoo, E.; Sonke, B.; Dansi, A.; Djedatin, G.; et al. Yam genomics supports West Africa as a major cradle of crop domestication. *Sci. Adv.* **2019**, *5*, eaaw1947. [[CrossRef](#)]
40. Oumar, I.; Mariac, C.; Pham, J.-L.; Vigouroux, Y. Phylogeny and origin of pearl millet (*Pennisetum glaucum* [L.] R. Br) as revealed by microsatellite loci. *Theor. Appl. Genet.* **2008**, *117*, 489–497. [[CrossRef](#)]
41. Li, H.-L. The origin of cultivated plants in Southeast Asia. *Econ. Bot.* **1970**, *24*, 3–19.
42. Purugganan, M.D.; Fuller, D.Q. The nature of selection during plant domestication. *Nature* **2009**, *457*, 843–848. [[CrossRef](#)]
43. Hyten, D.L.; Song, Q.; Zhu, Y.; Choi, I.-Y.; Nelson, R.L.; Costa, J.M.; Specht, J.E.; Shoemaker, R.C.; Cregan, P.B. Impacts of genetic bottlenecks on soybean genome diversity. *Proc. Natl. Acad. Sci. USA* **2006**, *103*, 16666–16671. [[CrossRef](#)] [[PubMed](#)]
44. Li, Y.-H.; Zhou, G.; Ma, J.; Jiang, W.; Jin, L.-G.; Zhang, Z.; Guo, Y.; Zhang, J.; Sui, Y.; Zheng, L.; et al. De novo assembly of soybean wild relatives for pan-genome analysis of diversity and agronomic traits. *Nat. Biotechnol.* **2014**, *32*, 1045–1052. [[CrossRef](#)]
45. Khush, G.S. Green revolution: The way forward. *Nat. Rev. Genet.* **2001**, *2*, 815–822. [[CrossRef](#)]
46. Zakharova, E.S.; Epishin, S.M.; Vinetski, Y.P. An attempt to elucidate the origin of cultivated soybean via comparison of nucleotide sequences encoding glycinin B4 polypeptide of cultivated soybean, *Glycine max*, and its presumed wild progenitor, *Glycine soja*. *Theor. Appl. Genet.* **1989**, *78*, 852–856. [[CrossRef](#)] [[PubMed](#)]
47. Wang, K.-J.; Takahata, Y. A preliminary comparative evaluation of genetic diversity between Chinese and Japanese wild soybean (*Glycine soja*) germplasm pools using SSR markers. *Genet. Resour. Crop Evol.* **2007**, *54*, 157–165. [[CrossRef](#)]
48. Doyle, J.J. 5S ribosomal gene variation in the soybean and its progenitor. *Theor. Appl. Genet.* **1988**, *75*, 621–624. [[CrossRef](#)]
49. Mikel, M.A.; Diers, B.W.; Nelson, R.L.; Smith, H.H. Genetic diversity and agronomic improvement of North American soybean germplasm. *Crop Sci.* **2010**, *50*, 1219–1229. [[CrossRef](#)]
50. Specht, J.E.; Williams, J.H. Contribution of Genetic Technology to Soybean Productivity—Retrospect and Prospect. In *Genetic Contributions to Yield Gains of Five Major Crop Plants*; Fehr, W.R., Ed.; Crop Science Society of America: Madison, WI, USA, 1984; pp. 49–74.
51. Bisaliah, S. *Soybean Development in India*; UN/ESCAP CGPRT Centre: Bogor, Indonesia, 1986; p. 11.
52. Agarwal, D.K.; Billore, S.D.; Sharma, A.N.; Dupare, B.U.; Srivastava, S.K. Soybean: Introduction, improvement, and utilization in India—Problems and prospects. *Agric. Res.* **2013**, *2*, 293–300. [[CrossRef](#)]
53. Herath, E. Cultivation and uses of soybeans in Sri Lanka. In *INTSOY Series—International Soybean Program (USA)*; College of Agricultural, University of Illinois at Urbana-Champaign: Champaign, IL, USA, 1976; Volume 10, pp. 250–252.
54. Chithrapala, N.H.M.S.; Aberathne, M.S.; Samarakoon Manike, S.M.; Pushpakumara, U. MISB 01—A new soybean [*Glycine max* (L.) Merrill] variety for the dry and intermediate zones of Sri Lanka. *Ann. Sri Lanka Dep. Agric.* **2015**, *17*, 180–186.
55. Škorić, D. Achievements and future directions of sunflower breeding. *Field Crops Res.* **1992**, *30*, 231–270. [[CrossRef](#)]
56. Goryunova, S.V.; Goryunov, D.V.; Chernova, A.I.; Martynova, E.U.; Dmitriev, A.E.; Boldyrev, S.V.; Ayupova, A.F.; Mazin, P.V.; Gurchenko, E.A.; Pavlova, A.S.; et al. Genetic and phenotypic diversity of the sunflower collection of the Pustovoit All-Russia Research Institute of Oil Crops (VNIIMK). *Helia* **2019**, *42*, 45–60. [[CrossRef](#)]
57. Gavrilova, V.A.; Anisimova, I.N. Genealogy of the sunflower lines created on the basis of Russian varieties. *Helia* **2017**, *40*, 133–146. [[CrossRef](#)]
58. Kumamoto, J.; Scora, R.W.; Lawton, H.W.; Clerx, W.A. Mystery of the forbidden fruit: Historical epilogue on the origin of the grapefruit, *Citrus paradisi* (Rutaceae). *Econ. Bot.* **1987**, *41*, 97–107. [[CrossRef](#)]
59. Ferguson, A.R. Kiwifruit: The wild and the cultivated plants. *Adv. Food Nutr. Res.* **2013**, *68*, 15–32. [[CrossRef](#)]
60. Ferguson, A.R.; Huang, H. Genetic resources of kiwifruit: Domestication and breeding. *Hortic. Rev.* **2007**, *33*, 1–121.
61. Huang, H.; Wang, Y.; Zhang, Z.; Jiang, Z.; Wang, S. *Actinidia* germplasm resources and kiwifruit industry in China. *Hortscience* **2004**, *39*, 1165–1172. [[CrossRef](#)]
62. Debenham, M.; Pathirana, R. Establishment and management of an in vitro repository of kiwifruit (*Actinidia* spp.) germplasm. In *Meta-Topolin: A Growth Regulator for Plant Biotechnology and Agriculture*; Ahmad, N., Strnad, M., Eds.; Springer Nature: Cham, Switzerland, 2020; pp. 279–291.
63. Abraham, K.; Gopinathan Nair, P. Polyploidy and sterility in relation to sex in *Dioscorea alata* L. (Dioscoreaceae). *Genetica* **1991**, *83*, 93–97. [[CrossRef](#)]
64. Meyer, R.S.; Purugganan, M.D. Evolution of crop species: Genetics of domestication and diversification. *Nat. Rev. Genet.* **2013**, *14*, 840–852. [[CrossRef](#)]
65. Fuller, D.Q.; Harvey, E.L. The archaeobotany of Indian pulses: Identification, processing and evidence for cultivation. *Environ. Archaeol.* **2006**, *11*, 219–246. [[CrossRef](#)]
66. Fuller, D.Q. Contrasting patterns in crop domestication and domestication rates: Recent archaeobotanical insights from the Old World. *Ann. Bot.* **2007**, *100*, 903–924. [[CrossRef](#)] [[PubMed](#)]
67. Fuller, D.Q.; Denham, T.; Arroyo-Kalin, M.; Lucas, L.; Stevens, C.J.; Qin, L.; Allaby, R.G.; Purugganan, M.D. Convergent evolution and parallelism in plant domestication revealed by an expanding archaeological record. *Proc. Natl. Acad. Sci. USA* **2014**, *111*, 6147–6152. [[CrossRef](#)] [[PubMed](#)]
68. Li, C.; Zhou, A.; Sang, T. Rice domestication by reducing shattering. *Science* **2006**, *311*, 1936–1939. [[CrossRef](#)]

69. Doebley, J.; Stec, A.; Hubbard, L. The evolution of apical dominance in maize. *Nature* **1997**, *386*, 485–488. [[CrossRef](#)]
70. Wang, H.; Nussbaum-Wagler, T.; Li, B.; Zhao, Q.; Vigouroux, Y.; Faller, M.; Bomblies, K.; Lukens, L.; Doebley, J.F. The origin of the naked grains of maize. *Nature* **2005**, *436*, 714–719. [[CrossRef](#)]
71. Harlan, J.R. Lettuce and the Sycomore: Sex and romance in ancient Egypt. *Econ. Bot.* **1986**, *40*, 4–15. [[CrossRef](#)]
72. de Vries, I.M. Origin and domestication of *Lactuca sativa* L. *Genet. Resour. Crop Evol.* **1997**, *44*, 165–174. [[CrossRef](#)]
73. Vaughan, D.A.; Balázs, E.; Heslop-Harrison, J.S. From crop domestication to super-domestication. *Ann. Bot.* **2007**, *100*, 893–901. [[CrossRef](#)] [[PubMed](#)]
74. Heslop-Harrison, J.S.; Schwarzacher, T. Domestication, genomics and the future for banana. *Ann. Bot.* **2007**, *100*, 1073–1084. [[CrossRef](#)] [[PubMed](#)]
75. Trucchi, E.; Benazzo, A.; Lari, M.; Iob, A.; Vai, S.; Nanni, L.; Bellucci, E.; Bitocchi, E.; Raffini, F.; Xu, C.; et al. Ancient genomes reveal early Andean farmers selected common beans while preserving diversity. *Nat. Plants* **2021**, *7*, 123–128. [[CrossRef](#)] [[PubMed](#)]
76. Hammer, K.; Laghetti, G. Genetic erosion—Examples from Italy. *Genet. Resour. Crop Evol.* **2005**, *52*, 629–634. [[CrossRef](#)]
77. Hammer, K.; Teklu, Y. Plant genetic resources: Selected issues from genetic erosion to genetic engineering. *J. Agric. Rural. Dev. Trop. Subtrop. (JARTS)* **2008**, *109*, 15–50.
78. WCD. Dams and Development: A New Framework for Decision-Making. In *The Report of the World Commission on Dams*; Earthscan Publications Ltd.: London, UK, 2000; p. 356.
79. Wu, J.; Huang, J.; Han, X.; Xie, Z.; Gao, X. Three-Gorges Dam—Experiment in Habitat Fragmentation? *Science* **2003**, *300*, 1239–1240. [[CrossRef](#)] [[PubMed](#)]
80. Kleijn, D.; Bommarco, R.; Fijen, T.P.M.; Garibaldi, L.A.; Potts, S.G.; van der Putten, W.H. Ecological intensification: Bridging the gap between science and practice. *Trends Ecol. Evol.* **2019**, *34*, 154–166. [[CrossRef](#)]
81. Ciotir, C.; Applequist, W.; Crews, T.E.; Cristea, N.; DeHaan, L.R.; Frawley, E.; Herron, S.; Magill, R.; Miller, J.; Roskov, Y.; et al. Building a botanical foundation for perennial agriculture: Global inventory of wild, perennial herbaceous Fabaceae species. *Plants People Planet* **2019**, *1*, 375–386. [[CrossRef](#)]
82. McClure, K.A.; Sawler, J.; Gardner, K.M.; Money, D.; Myles, S. Genomics: A potential panacea for the perennial problem. *Am. J. Bot.* **2014**, *101*, 1780–1790. [[CrossRef](#)]
83. Audu, V.; Rasche, F.; Martensson, L.M.D.; Emmerling, C. Perennial cereal grain cultivation: Implication on soil organic matter and related soil microbial parameters. *Appl. Soil Ecol.* **2022**, *174*, 104414. [[CrossRef](#)]
84. Ledo, A.; Smith, P.; Zerihun, A.; Whitaker, J.; Vicente-Vicente, J.L.; Qin, Z.; McNamara, N.P.; Zinn, Y.L.; Llorente, M.; Liebig, M.; et al. Changes in soil organic carbon under perennial crops. *Glob. Chang. Biol.* **2020**, *26*, 4158–4168. [[CrossRef](#)]
85. Means, M.; Crews, T.; Souza, L. Annual and perennial crop composition impacts on soil carbon and nitrogen dynamics at two different depths. *Renew. Agric. Food Syst.* **2022**, *1*–8. [[CrossRef](#)]
86. Kreitzman, M.; Eyster, H.; Mitchell, M.; Czajewska, A.; Keeley, K.; Smukler, S.; Sullivan, N.; Verster, A.; Chan, K.M.A. Woody perennial polycultures in the U.S. Midwest enhance biodiversity and ecosystem functions. *Ecosphere* **2022**, *13*, e03890. [[CrossRef](#)]
87. Félix, G.F.; Scholberg, J.M.S.; Clermont-Dauphin, C.; Courmac, L.; Tittone, P. Enhancing agroecosystem productivity with woody perennials in semi-arid West Africa. A meta-analysis. *Agron. Sustain. Dev.* **2018**, *38*, 57. [[CrossRef](#)] [[PubMed](#)]
88. DeHaan, L.; Larson, S.; López-Marqués, R.L.; Wenkel, S.; Gao, C.; Palmgren, M. Roadmap for accelerated domestication of an emerging perennial grain crop. *Trends Plant Sci.* **2020**, *25*, 525–537. [[CrossRef](#)] [[PubMed](#)]
89. Van Tassel, D.L.; DeHaan, L.R.; Cox, T.S. Missing domesticated plant forms: Can artificial selection fill the gap? *Evol. Appl.* **2010**, *3*, 434–452. [[CrossRef](#)] [[PubMed](#)]
90. Lundgren, M.R.; Des Marais, D.L. Life history variation as a model for understanding trade-offs in plant–environment interactions. *Curr. Biol.* **2020**, *30*, R180–R189. [[CrossRef](#)]
91. Friedman, J. The evolution of annual and perennial plant life histories: Ecological correlates and genetic mechanisms. *Annu. Rev. Ecol. Syst.* **2020**, *51*, 461–481. [[CrossRef](#)]
92. DeHaan, L.R.; Van Tassel, D.L. Useful insights from evolutionary biology for developing perennial grain crops. *Am. J. Bot.* **2014**, *101*, 1801–1819. [[CrossRef](#)]
93. Vico, G.; Manzoni, S.; Nkurunziza, L.; Murphy, K.; Weih, M. Trade-offs between seed output and life span—A quantitative comparison of traits between annual and perennial congeneric species. *New Phytol.* **2016**, *209*, 104–114. [[CrossRef](#)]
94. Smaje, C. The Strong perennial vision: A critical review. *Agroecol. Sustain. Food Syst.* **2015**, *39*, 471–499. [[CrossRef](#)]
95. Crews, T.E.; DeHaan, L.R. The strong perennial vision: A response. *Agroecol. Sustain. Food Syst.* **2015**, *39*, 500–515. [[CrossRef](#)]
96. Crews, T.E.; Carton, W.; Olsson, L. Is the future of agriculture perennial? Imperatives and opportunities to reinvent agriculture by shifting from annual monocultures to perennial polycultures. *Glob. Sustain.* **2018**, *1*, e11. [[CrossRef](#)]
97. Crews, T.E.; Blesh, J.; Culman, S.W.; Hayes, R.C.; Jensen, E.S.; Mack, M.C.; Peoples, M.B.; Schipanski, M.E. Going where no grains have gone before: From early to mid-succession. *Agric. Ecosyst. Environ.* **2016**, *223*, 223–238. [[CrossRef](#)]
98. Jackson, W. *New Roots for Agriculture*; Friends of the Earth: San Francisco, CA, USA, 1980.
99. Yu, H.; Li, J. Breeding future crops to feed the world through de novo domestication. *Nat. Commun.* **2022**, *13*, 1171. [[CrossRef](#)]
100. Duhamel, M.; Vandenkoornhuyse, P. Sustainable agriculture: Possible trajectories from mutualistic symbiosis and plant neodomestication. *Trends Plant Sci.* **2013**, *18*, 597–600. [[CrossRef](#)] [[PubMed](#)]
101. Gaut, B.S.; Seymour, D.K.; Liu, Q.; Zhou, Y. Demography and its effects on genomic variation in crop domestication. *Nat. Plants* **2018**, *4*, 512–520. [[CrossRef](#)] [[PubMed](#)]

102. Zhao, Y.; Zhong, L.; Zhou, K.; Song, Z.; Chen, J.; Rong, J. Seed characteristic variations and genetic structure of wild *Zizania latifolia* along a latitudinal gradient in China: Implications for neo-domestication as a grain crop. *AoB Plants* **2018**, *10*, ply072. [CrossRef]
103. Nooryazdan, H.; Serieys, H.; David, J.; Bacilieri, R.; Bervillé, A.J. Construction of a crop—Wild hybrid population for broadening genetic diversity in cultivated sunflower and first evaluation of its combining ability: The concept of neodomestication. *Euphytica* **2010**, *178*, 159–175. [CrossRef]
104. Kantar, M.B.; Hüber, S.; Herman, A.; Bock, D.G.; Baute, G.; Betts, K.; Ott, M.; Brandvain, Y.; Wyse, D.; Stupar, R.M.; et al. Neo-domestication of an interspecific tetraploid *Helianthus annuus* × *Helianthus tuberosus* population that segregates for perennial habit. *Genes* **2018**, *9*, 422. [CrossRef]
105. Tomooka, N.; Naito, K.; Kaga, A.; Sakai, H.; Isemura, T.; Ogiso-Tanaka, E.; Iseki, K.; Takahashi, Y. Evolution, domestication and neo-domestication of the genus *Vigna*. *Plant Genet. Resour.* **2014**, *12*, S168–S171. [CrossRef]
106. Ciotir, C.; Townesmith, A.; Applequist, W.; Herron, S.; Van Tassel, D.; DeHaan, L.; Crews, T.; Schlautman, B.; Jackson, W.; Miller, A. *Global Inventory and Systematic Evaluation of Perennial Grain, Legume, and Oilseed Species for Pre-Breeding and Domestication*; Missouri Botanical Garden: St. Louis, MO, USA, 2016; Available online: <http://www.tropicos.org/Project/PAPGI> (accessed on 3 July 2022).
107. Maxted, N.; Guarino, L.; Myer, L.; Chiwona, E.A. Towards a methodology for on-farm conservation of plant genetic resources. *Genet. Resour. Crop Evol.* **2002**, *49*, 31–46. [CrossRef]
108. Kell, S.P.; Knüpfper, H.; Jury, S.L.; Ford-Lloyd, B.V.; Maxted, N. Crops and wild relatives of the EuroMediterranean region: Making and using a conservation catalogue. In *Crop Wild Relative Conservation and Use*; Maxted, N., Ford-Lloyd, B.V., Kell, S.P., Iriondo, J., Dulloo, E., Turok, J., Eds.; CAB International: Wallingford, UK, 2008; pp. 69–109.
109. Harlan, J.R.; de Wet, J.M.J. Toward a rational classification of cultivated plants. *Taxon* **1971**, *20*, 509–517. [CrossRef]
110. Maxted, N.; Ford-Lloyd, B.V.; Jury, S.; Kell, S.; Scholten, M. Towards a definition of a crop wild relative. *Biodivers. Conserv.* **2006**, *15*, 2673–2685. [CrossRef]
111. Vaughan, D.A. A new rhizomatous *Oryza* species (Poaceae) from Sri Lanka. *Bot. J. Linn. Soc.* **1990**, *103*, 159–163. [CrossRef]
112. Phillips, J.; Yang, L. *Oryza Rhizomatis*. The IUCN Red List of Threatened Species. Available online: <https://www.iucnredlist.org/species/112680830/113899786> (accessed on 12 July 2020).
113. GBIF. *Oryza Rhizomatis* D.A.Vaughan. Available online: <https://www.gbif.org/species/4135750> (accessed on 17 August 2020).
114. Huang, X.; Kurata, N.; Wei, X.; Wang, Z.-X.; Wang, A.; Zhao, Q.; Zhao, Y.; Liu, K.; Lu, H.; Li, W.; et al. A map of rice genome variation reveals the origin of cultivated rice. *Nature* **2012**, *490*, 497–501. [CrossRef]
115. Nowicki, M.; Foolad, M.R.; Nowakowska, M.; Kozik, E.U. Potato and tomato late blight caused by *Phytophthora infestans*: An overview of pathology and resistance breeding. *Plant Dis.* **2012**, *96*, 4–17. [CrossRef]
116. Brar, D.S.; Khush, G.S. Alien introgression in rice. In *Oryza: From Molecule to Plant*; Sasaki, T., Moore, G., Eds.; Springer: Dordrecht, The Netherlands, 1997; pp. 35–47.
117. Ram, T.; Deen, R.; Gautam, S.K.; Ramesh, K.; Rao, Y.K.; Brar, D.S. Identification of new genes for Brown Planthopper resistance in rice introgressed from *O. glaberrima* and *O. minuta*. *Rice Genet. Newsl.* **2010**, *25*, 67–68.
118. Mondal, T.; Henry, R. *The Wild Oryza Genomes*; Springer: Cham, Switzerland, 2018.
119. Dey, S.; Badri, J.; Prakasam, V.; Bhadana, V.P.; Eswari, K.B.; Laha, G.S.; Priyanka, C.; Rajkumar, A.; Ram, T. Identification and agro-morphological characterization of rice genotypes resistant to sheath blight. *Australas. Plant Pathol.* **2016**, *45*, 145–153. [CrossRef]
120. Ganeshan, P.; Jain, A.; Parmar, B.; Rao, A.R.; Sreenu, K.; Mishra, P.; Mesapogu, S.; Subrahmanyam, D.; Ram, T.; Sarla, N.; et al. Identification of salt tolerant rice lines among interspecific BILs developed by crossing *Oryza sativa* × *O. rufipogon* and *O. sativa* × *O. nivara*. *Aust. J. Crop Sci.* **2016**, *10*, 220–228.
121. Prasanth, V.V.; Chakravarthi, D.V.; Kiran, T.V.; Rao, Y.V.; Panigrahy, M.; Mangrauthia, S.K.; Viraktamath, B.C.; Subrahmanyam, D.; Voleti, S.R.; Sarla, N. Evaluation of rice germplasm and introgression lines for heat tolerance. *Ann. Biol. Res.* **2012**, *3*, 5060–5068.
122. Prasanth, V.V.; Basava, K.R.; Babu, M.S.; V.G.N., V.T.; Devi, S.J.S.R.; Mangrauthia, S.K.; Voleti, S.R.; Sarla, N. Field level evaluation of rice introgression lines for heat tolerance and validation of markers linked to spikelet fertility. *Physiol. Mol. Biol. Plants* **2016**, *22*, 179–192. [CrossRef] [PubMed]
123. Surapaneni, M.; Balakrishnan, D.; Mesapogu, S.; Addanki, K.R.; Yadavalli, V.R.; Tripura Venkata, V.G.N.; Neelamraju, S. Identification of major effect QTLs for agronomic traits and CSSLs in rice from Swarna/*Oryza nivara* derived backcross inbred lines. *Front. Plant Sci.* **2017**, *8*, 1027. [CrossRef] [PubMed]
124. Furuta, T.; Uehara, K.; Angeles-Shim, R.B.; Shim, J.; Nagai, K.; Ashikari, M.; Takashi, T. Development of chromosome segment substitution lines harboring *Oryza nivara* genomic segments in Koshihikari and evaluation of yield-related traits. *Breed. Sci.* **2016**, *66*, 845–850. [CrossRef] [PubMed]
125. Zhai, W.; Wang, W.; Zhou, Y.; Li, X.; Zheng, X.; Zhang, Q.; Wang, G.; Zhu, L. Breeding bacterial blight-resistant hybrid rice with the cloned bacterial blight resistance gene *Xa21*. *Mol. Breed.* **2002**, *8*, 285–293. [CrossRef]
126. Guo, S.-B.; Wei, Y.; Li, X.-Q.; Liu, K.-Q.; Huang, F.-K.; Chen, C.-H.; Gao, G.-Q. Development and identification of introgression lines from cross of *Oryza sativa* and *Oryza minuta*. *Rice Sci.* **2013**, *20*, 95–102. [CrossRef]

127. Yoon, D.B.; Kang, K.H.; Kim, K.J.; Ju, H.G.; Kwon, S.J.; Suh, J.P. Mapping quantitative trait loci for yield components and morphological traits in an advanced back cross population between *Oryza grandiglumis* and the *O. sativa japonica* cultivar Hwaseongbyeo. *Theor. Appl. Genet.* **2006**, *112*, 1052–1062. [CrossRef]
128. Wairich, A.; de Oliveira, B.N.; Wu, L.B.; Murugaiyan, V.; Margis-Pinheiro, M.; Fett, J.P.; Ricachenevsky, F.K.; Frei, M. Chromosomal introgressions from *Oryza meridionalis* into domesticated rice *Oryza sativa* result in iron tolerance. *J. Exp. Bot.* **2021**, *72*, 2242–2259. [CrossRef]
129. Luo, Y.; Lao, L.Y.; Ai, B.; Zhang, M.; Xie, J.K.; Zhang, F.T. Development of a drought stress-resistant rice restorer line through *Oryza sativa-rufipogon* hybridization. *J. Genet.* **2019**, *98*, 55. [CrossRef]
130. Frankel, O.H.; Frankel, O.; Soulé, M.E. *Conservation and Evolution*; Cambridge University Press: Cambridge, UK, 1981.
131. Jarvis, D.I.; Hodgkin, T.; Sthapit, B.R.; Fadda, C.; Lopez-Noriega, I. An heuristic framework for identifying multiple ways of supporting the conservation and use of traditional crop varieties within the agricultural production system. *Crit. Rev. Plant Sci.* **2011**, *30*, 125–176. [CrossRef]
132. Khoury, C.K.; Brush, S.; Costich, D.E.; Curry, H.A.; Haan, S.; Engels, J.M.M.; Guarino, L.; Hoban, S.; Mercer, K.L.; Miller, A.J.; et al. Crop genetic erosion: Understanding and responding to loss of crop diversity. *New Phytol.* **2022**, *233*, 84–118. [CrossRef]
133. Jarvis, D.J.; Hodgkin, T.; Brown, A.H.D.; Tuxill, J.; Noriega, I.L.; Smale, M.; Sthapit, B. *Crop Genetic Diversity in the Field and on the Farm: Principles and Applications in Research Practices*; Yale University Press: New Haven, CT, USA; London, UK, 2016.
134. Porcuna-Ferrer, A.; Fiala, V.; Freyer, B.; van Etten, J.; Vernooy, R.; Probst, L. Do community seed banks contribute to the social-ecological resilience of communities? A case-study from western Guatemala. *Int. J. Agric. Sustain.* **2020**, *18*, 232–249. [CrossRef]
135. Diez, M.J.; De la Rosa, L.; Martin, I.; Guasch, L.; Cartea, M.E.; Mallor, C.; Casals, J.; Simo, J.; Rivera, A.; Anastasio, G.; et al. Plant Genebanks: Present Situation and Proposals for Their Improvement. the Case of the Spanish Network. *Front. Plant Sci.* **2018**, *9*, 1794. [CrossRef] [PubMed]
136. Pautasso, M.; Aistara, G.; Barnaud, A.; Caillon, S.; Clouvel, P.; Coomes, O.T.; Delètre, M.; Demeulenaere, E.; De Santis, P.; Döring, T.; et al. Seed exchange networks for agrobiodiversity conservation. A review. *Agron. Sustain. Dev.* **2012**, *33*, 151–175. [CrossRef]
137. Sievers-Glotzbach, S.; Euler, J.; Frison, C.; Gmeiner, N.; Kliem, L.; Mazé, A.; Tschersich, J. Beyond the material: Knowledge aspects in seed commoning. *Agric. Hum. Values* **2021**, *38*, 509–524. [CrossRef]
138. Sievers-Glotzbach, S.; Tschersich, J.; Gmeiner, N.; Kliem, L.; Ficiyan, A. Diverse seeds—Shared practices: Conceptualizing seed commons. *Int. J. Commons* **2020**, *14*, 418–438. [CrossRef]
139. Hammer, K.; Gladis, T.; Diederichsen, A. In situ and on-farm management of plant genetic resources. *Eur. J. Agron.* **2003**, *19*, 509–517. [CrossRef]
140. Bush, D.; Thomson, L.; Bolatolu, W.; Dutt, S.; Hamani, S.; Likiafu, H.; Mateboto, J.; Tauraga, J.; Young, E. Domestication provides the key to conservation of *Santalum yasi*—A threatened Pacific sandalwood. *Aust. For.* **2020**, *83*, 186–194. [CrossRef]
141. Curry, H.A. From working collections to the World Germplasm Project: Agricultural modernization and genetic conservation at the Rockefeller Foundation. *Hist. Philos. Life Sci.* **2017**, *39*, 5. [CrossRef]
142. FAO. Commission on Plant Genetic Resources: FAO Activities and Future Programme on Plant Genetic Resources. Available online: <http://www.fao.org/3/a-aj427e.pdf> (accessed on 22 March 2022).
143. Noriega, I.L.; Halewood, M.; Abberton, M.; Amri, A.; Angarawai, I.I.; Anglin, N.; Blümmel, M.; Bouman, B.; Campos, H.; Costich, D.; et al. CGIAR Operations under the Plant Treaty Framework. *Crop Sci.* **2019**, *59*, 819–832. [CrossRef]
144. Westengen, O.T.; Lusty, C.; Yazbek, M.; Amri, A.; Asdal, Å. Safeguarding a global seed heritage from Syria to Svalbard. *Nature Plants* **2020**, *6*, 1311–1317. [CrossRef]
145. FAO. The Second Report on the State of the World’s Plant Genetic Resources for Food and Agriculture. Available online: <http://www.fao.org/3/i1500e/i1500e.pdf> (accessed on 22 March 2022).
146. Singh, A.K.; Varaprasad, K.S.; Venkateswaran, K. Conservation costs of plant genetic resources for food and agriculture: Seed genebanks. *Agric. Res.* **2012**, *1*, 223–239. [CrossRef]
147. SGSV. Svalbard Global Seed Vault. Available online: <https://www.croptrust.org/work/svalbard-global-seed-vault/> (accessed on 18 July 2022).
148. Engels, J.M.M.; Ebert, A.W. A critical review of the current global ex situ conservation system for plant agrobiodiversity. I. History of the development of the global system in the context of the political/legal framework and its major conservation components. *Plants* **2021**, *10*, 1557. [CrossRef] [PubMed]
149. Bellon, M.R.; Dulloo, E.; Sardos, J.; Thormann, I.; Burdon, J.J. In situ conservation-harnessing natural and human-derived evolutionary forces to ensure future crop adaptation. *Evol. Appl.* **2017**, *10*, 965–977. [CrossRef] [PubMed]
150. de Haan, S.; Núñez, J.; Bonierbale, M.; Ghislain, M.; van der Maesen, J. A Simple Sequence Repeat (SSR) marker comparison of a large in- and ex-situ potato landrace cultivar collection from Peru reaffirms the complementary nature of both conservation strategies. *Diversity* **2013**, *5*, 505–521. [CrossRef]
151. Casals, J.; Casanas, F.; Simo, J. Is it still necessary to continue to collect crop genetic resources in the Mediterranean Area? A case study in Catalonia. *Econ. Bot.* **2017**, *71*, 330–341. [CrossRef]
152. Smykal, P.; Hradilova, I.; Trneny, O.; Brus, J.; Rathore, A.; Bariotakis, M.; Das, R.R.; Bhattacharyya, D.; Richards, C.; Coyne, C.J.; et al. Genomic diversity and macroecology of the crop wild relatives of domesticated pea. *Sci. Rep.* **2017**, *7*, 17384. [CrossRef]

153. Abe, A.; Kosugi, S.; Yoshida, K.; Natsume, S.; Takagi, H.; Kanzaki, H. Genome sequencing reveals agronomically important loci in rice using MutMap. *Nat. Biotechnol.* **2012**, *30*, 174–178. [[CrossRef](#)]
154. Kumar, S.; Kirk, C.; Deng, C.; Wiedow, C.; Knaebel, M.; Brewer, L. Genotyping-by-sequencing of pear (*Pyrus* spp.) accessions unravels novel patterns of genetic diversity and selection footprints. *Hortic. Res.* **2017**, *4*, 17015. [[CrossRef](#)]
155. Norelli, J.L.; Wisniewski, M.; Fazio, G.; Burchard, E.; Gutierrez, B.; Levin, E.; Droby, S. Genotyping-by-sequencing markers facilitate the identification of quantitative trait loci controlling resistance to *Penicillium expansum* in *Malus sieversii*. *PLoS ONE* **2017**, *12*, e0172949. [[CrossRef](#)]
156. Singh, N.; Wu, S.Y.; Raupp, W.J.; Sehgal, S.; Arora, S.; Tiwari, V.; Vikram, P.; Singh, S.; Chhuneja, P.; Gill, B.S.; et al. Efficient curation of genebanks using next generation sequencing reveals substantial duplication of germplasm accessions. *Sci. Rep.* **2019**, *9*, 650. [[CrossRef](#)]
157. Melo, A.T.O.; Bartaula, R.; Hale, I. GBS-SNP-CROP: A reference-optional pipeline for SNP discovery and plant germplasm characterization using variable length, paired-end genotyping-by-sequencing data. *BMC Bioinform.* **2016**, *17*, 1–15. [[CrossRef](#)]
158. Schlotterer, C.; Tobler, R.; Kofler, R.; Nolte, V. Sequencing pools of individuals—mining genome-wide polymorphism data without big funding. *Nat. Rev. Genet.* **2014**, *15*, 749–763. [[CrossRef](#)] [[PubMed](#)]
159. Wells, R.; Trick, M.; Fraser, F.; Soumpourou, E.; Clissold, L.; Morgan, C.; Pauquet, J.; Bancroft, I. Sequencing-based variant detection in the polyploid crop oilseed rape. *BMC Plant Biol.* **2013**, *13*, 111. [[CrossRef](#)] [[PubMed](#)]
160. Duan, N.B.; Bai, Y.; Sun, H.H.; Wang, N.; Ma, Y.M.; Li, M.J.; Wang, X.; Jiao, C.; Legall, N.; Mao, L.Y.; et al. Genome re-sequencing reveals the history of apple and supports a two-stage model for fruit enlargement. *Nat. Commun.* **2017**, *8*, 249. [[CrossRef](#)]
161. Bouquet, A. Sequencing of the grapevine genome: A brilliant demonstration of a 55-year-old hypothesis. *Prog. Agric. Vitic.* **2007**, *124*, 337–341.
162. Brenchley, R.; Spannagl, M.; Pfeifer, M.; Barker, G.L.A.; D’Amore, R.; Allen, A.M.; McKenzie, N.; Kramer, M.; Kerhornou, A.; Bolser, D.; et al. Analysis of the bread wheat genome using whole-genome shotgun sequencing. *Nature* **2012**, *491*, 705. [[CrossRef](#)] [[PubMed](#)]
163. Graner, A.; Kilian, B. NGS technologies for analyzing germplasm diversity in genebanks. *Brief. Funct. Genom.* **2012**, *11*, 38–50. [[CrossRef](#)]
164. Frankel, O.H.; Brown, A.H.D. Current plant genetic resources: A critical appraisal. In *Genetics: New Frontiers*; Oxford & IBH Publishing Company: New Delhi, India, 1984; pp. 3–13.
165. Franco, J.; Crossa, J.; Díaz, J.; Taba, S.; Villaseñor, J.; Eberhart, S.A. A sequential clustering strategy for classifying gene bank accessions. *Crop Sci.* **1997**, *37*, 1656–1662. [[CrossRef](#)]
166. Gouesnard, B.; Bataillon, T.M.; Decoux, G.; Rozale, C.; Schoen, D.J.; David, J.L. MSTRAT: An algorithm for building germplasm core collections by maximizing allelic or phenotypic richness. *J. Hered.* **2001**, *92*, 93–94. [[CrossRef](#)]
167. Agrama, H.A.; Yan, W.; Lee, F.; Fjellstrom, R.; Chen, M.-H.; Jia, M.; McClung, A. Genetic assessment of a mini-core subset developed from the USDA Rice Genebank. *Crop Sci.* **2009**, *49*, 1336–1346. [[CrossRef](#)]
168. Pathirana, R.; Molloy, C.; Erridge, Z.; McLachlan, A.; Seelye, J.; Kumar, S. Towards a cryopreserved germplasm collection of apple—Results of dormant bud cryopreservation in the mild maritime winter climate of Hawkes Bay, New Zealand. *Acta Hortic.* **2018**, *1205*, 769–778. [[CrossRef](#)]
169. Pathirana, R.; Mathew, J.; Jibrán, R.; Hunter, D.A.; Morgan, E.R. Cryopreservation and cryotherapy research on horticultural crops in New Zealand. *Acta Hortic.* **2019**, *1234*, 29–36. [[CrossRef](#)]
170. Rana, J.C.; Sharma, T.R.; Tyagi, R.K.; Chahota, R.K.; Gautam, N.K.; Singh, M.; Sharma, P.N.; Ojha, S.N. Characterisation of 4274 accessions of common bean (*Phaseolus vulgaris* L.) germplasm conserved in the Indian gene bank for phenological, morphological and agricultural traits. *Euphytica* **2015**, *205*, 441–457. [[CrossRef](#)]
171. ICRISAT. ICRISAT Sorghum Core. Available online: <http://genebank.icrisat.org/IND/Core?Crop=Sorghum> (accessed on 20 May 2022).
172. Mattick, J.S.; Ablett, E.M.; Edmonson, D.L. The gene library-preservation and analysis of genetic diversity in Australasia. In *Conservation of Plant Genes*; Academic Press: Cambridge, MA, USA, 1992; pp. 15–35.
173. Droege, G.; Barker, K.; Astrin, J.J.; Bartels, P.; Butler, C.; Cantrill, D.; Coddington, J.; Forest, F.; Gemeinholzer, B.; Hobern, D.; et al. The Global Genome Biodiversity Network (GGBN) Data Portal. *Nucleic Acids Res.* **2014**, *42*, D607–D612. [[CrossRef](#)]
174. Gemeinholzer, B.; Dröge, G.; Zetzsche, H.; Haszprunar, G.; Klenk, H.; Güntsch, A.; Berendsohn, W.G.; Wägele, J. The DNA Bank Network: The start from a German initiative. *Biopreservation Biobanking* **2011**, *9*, 51–55. [[CrossRef](#)]
175. GGBN. Newsletter. Available online: <https://wiki.ggbn.org/ggbn/Newsletters> (accessed on 20 June 2022).
176. GGBN. The GGBN Data Portal. Available online: [http://www.ggbn.org/ggbn\\_portal/](http://www.ggbn.org/ggbn_portal/) (accessed on 27 June 2022).
177. Engels, J.M.M.; Ebert, A.W. A critical review of the current global ex situ conservation system for plant agrobiodiversity. II. Strengths and weaknesses of the current system and recommendations for its improvement. *Plants* **2021**, *10*, 1904. [[CrossRef](#)] [[PubMed](#)]
178. FAO. Genebank Standards for Plant Genetic Resources for Food and Agriculture, Revised Edition. Available online: <http://www.fao.org/3/a-i3704e.pdf> (accessed on 20 May 2022).
179. Thormann, I.; Engels, J.M.M.; Halewood, M. Are the old International Board for Plant Genetic Resources (IBPGR) base collections available through the Plant Treaty’s multilateral system of access and benefit sharing? A review. *Genet. Resour. Crop Evol.* **2019**, *66*, 291–310. [[CrossRef](#)]

180. Migicovsky, Z.; Warschefsky, E.; Klein, L.L.; Miller, A.J. Using living germplasm collections to characterize, improve, and conserve woody perennials. *Crop Sci.* **2019**, *59*, 2365–2380. [CrossRef]
181. Forsline, P.L.; Aldwinckle, H.S. Natural occurrence of fire blight in USDA apple germplasm collection after 10 years of observation. *Acta Hort.* **2002**, *590*, 351–357. [CrossRef]
182. Datson, P.; Nardoza, S.; Manako, K.; Herrick, J.; Martinez-Sanchez, M.; Curtis, C.; Montefiori, M. Monitoring the *Actinidia* germplasm for resistance to *Pseudomonas syringae* pv. *actinidiae*. *Acta Hort.* **2015**, *1095*, 181–184. [CrossRef]
183. IPGRI-APO. Establishment and Management of Field Genebank, a Training Manual. Available online: [https://www.bioversityinternational.org/fileadmin/\\_migrated/uploads/tx\\_news/Establishment\\_and\\_management\\_of\\_field\\_genebank\\_786.pdf](https://www.bioversityinternational.org/fileadmin/_migrated/uploads/tx_news/Establishment_and_management_of_field_genebank_786.pdf) (accessed on 19 April 2022).
184. IPGRI. Technical Guidelines for the Management of Field and In Vitro Genebanks: IPGRI Handbooks for Genebanks No. 7. Available online: [https://cropgenebank.sgrp.cgiar.org/images/file/learning\\_space/genebankmanual7.pdf](https://cropgenebank.sgrp.cgiar.org/images/file/learning_space/genebankmanual7.pdf) (accessed on 19 March 2022).
185. Carimi, F.; Pathirana, R.; Carra, A. Biotechnologies for germplasm management and improvement. In *Grapevines—Varieties, Cultivation and Management*; Szabo, P.V., Shojania, J., Eds.; Nova Science Publishers: New York, NY, USA, 2012; pp. 199–249.
186. Aranzales, E.R. Use of Tissue Culture Techniques in the Conservation and Exchange of Cassava Germplasm Material: CIAT Case. International Course on Modern Technologies for Production, Processing and Utilization of the Cassava Crop. “Support to sustainable development of the cassava sector in the Caribbean Region.” CIAT, Palmira, Colombia, 28 July 2014. Available online: <https://cgspace.cgiar.org/handle/10568/82943> (accessed on 15 February 2022).
187. CGIAR-SGRP. Refinement and Standardization of Storage Procedures for Clonal Crops—Global Public Goods Phase 2: Part III. *Multi-Crop Guidelines for Developing In Vitro Conservation Best Practices for Clonal Crops*. Available online: [https://cropgenebank.sgrp.cgiar.org/images/file/learning\\_space/gpg2%20part%20iii\\_final%20for%20web.pdf](https://cropgenebank.sgrp.cgiar.org/images/file/learning_space/gpg2%20part%20iii_final%20for%20web.pdf) (accessed on 5 April 2022).
188. CGIAR-SGRP. Refinement and Standardization of Storage Procedures for Clonal Crops—Global Public Goods Phase 2: Part II. *Status of In Vitro Conservation Technologies for: Andean Root and Tuber Crops, Cassava, Musa, Potato, Sweetpotato and Yam*. Available online: [https://cropgenebank.sgrp.cgiar.org/images/file/learning\\_space/gpg2%20part%20ii%20\\_07022012.pdf](https://cropgenebank.sgrp.cgiar.org/images/file/learning_space/gpg2%20part%20ii%20_07022012.pdf) (accessed on 5 April 2022).
189. Pence, V.C.; Engelmann, F.; Guarino, L.; RamanathaRao, V.; Goldberg, E. Collecting in vitro for genetic resources conservation. In *Collecting Plant Genetic Diversity: Technical Guidelines*; Bioversity International: Rome, Italy, 2011; Volume 47, pp. 5–16.
190. CIP-Genebank. In Vitro Conservation. Available online: <https://cipotato.org/genebankcip/process/in-vitro/> (accessed on 23 June 2022).
191. IITA-GRC. Genetic Resources Center. Available online: <https://www.genebanks.org/genebanks/iita/>; <https://www.genebanks.org/wp-content/uploads/2021/04/IITA-Closure-Report-IN-VITRO-CONS-2018-Round-2.xlsx> (accessed on 22 May 2022).
192. Cunha Alves, C.; Azevedo, A.A.; Rennó, V.C. EMBRAPA Network for Brazilian Plant Genetic Resources Conservation. *Biopreservation Biobanking* **2018**, *16*, 350–360. [CrossRef]
193. Myeza, P.N.; Visser, A. Agricultural Research Council’s potato in vitro genebank. *Acta Hort.* **2013**, *1007*, 727–731. [CrossRef]
194. Tyagi, R.K.; Agrawal, A. Genetic Resources Conservation: Ex Situ Conservation Strategies. Available online: [http://www.nbpgg.ernet.in/genomic\\_resources/03\\_rktyagi\\_ex-situ.pdf](http://www.nbpgg.ernet.in/genomic_resources/03_rktyagi_ex-situ.pdf) (accessed on 20 February 2022).
195. ITC. International Musa Germplasm Transit Center (ITC). Available online: <https://www.bioversityinternational.org/banana-genebank/> (accessed on 22 August 2020).
196. Bamberg, J.B.; Martin, M.W.; Abad, J.; Jenderek, M.M.; Tanner, J.; Donnelly, D.J.; Nassar, A.M.K.; Veilleux, R.E.; Novy, R.G. In vitro technology at the US Potato Genebank. *Vitr. Cell. Dev. Biol.—Plant* **2016**, *52*, 213–225. [CrossRef]
197. Sakai, A. Survival of the twig of woody plants at  $-196^{\circ}\text{C}$ . *Nature* **1960**, *185*, 392–394. [CrossRef]
198. Sakai, A.; Nishiyama, Y. Cryopreservation of winter vegetative buds of hardy fruit-trees in liquid-nitrogen. *Hortscience* **1978**, *13*, 225–227.
199. Latta, R. Preservation of suspensions cultures of plant cells by freezing. *Can. J. Bot.* **1971**, *49*, 1253–1254. [CrossRef]
200. Wang, M.-R.; Lambardi, M.; Engelmann, F.; Pathirana, R.; Panis, B.; Volk, G.M.; Wang, Q.-C. Advances in cryopreservation of in vitro-derived propagules: Technologies and explant sources. *Plant Cell Tiss. Organ Cult.* **2020**, *144*, 7–20. [CrossRef]
201. Carra, A.; Carimi, F.; Bettoni, J.C.; Pathirana, R. Progress and challenges in the application of synthetic seed technology for ex situ germplasm conservation in grapevine (*Vitis* spp.). In *Synthetic Seeds: Germplasm Regeneration, Preservation and Prospects*; Faisal, M., Alatar, A.A., Eds.; Springer International Publishing: Cham, Switzerland, 2019; pp. 439–467.
202. Sakai, A.; Kobayashi, S.; Oiyama, I. Cryopreservation of nucellar cells of navel orange (*Citrus sinensis* Osb. var. *brasiliensis* Tanaka) by vitrification. *Plant Cell Rep.* **1990**, *9*, 30–33. [CrossRef]
203. Niino, T.; Wunna; Watanabe, K.; Nohara, N.; Rafique, T.; Yamamoto, S.; Fukui, K.; Arizaga, M.V.; Martinez, C.R.C.; Matsumoto, T.; et al. Cryopreservation of mat rush lateral buds by air dehydration using aluminum cryo-plate. *Plant Biotechnol.* **2014**, *31*, 281–287. [CrossRef]
204. Yamamoto, S.; Rafique, T.; Fukui, K.; Sekizawa, K.; Niino, T. V-cryo-plate procedure as an effective protocol for cryobanks: Case study of mint cryopreservation. *Cryoletters* **2012**, *33*, 12–23.
205. Yamamoto, S.; Rafique, T.; Priyantha, W.S.; Fukui, K.; Matsumoto, T.; Niino, T. Development of a cryopreservation procedure using aluminium cryo-plates. *Cryoletters* **2011**, *32*, 256–265.

206. Bettoni, J.C.; Pathirana, R.; Bonnart, R.; Shepherd, A.; Volk, G. Cryopreservation of grapevine shoot tips from in vitro plants using droplet vitrification and V cryo-plate techniques. In *Synthetic Seeds: Germplasm Regeneration, Preservation and Prospects*; Faisal, M., Alatar, A.A., Eds.; Springer International Publishing: Cham, Switzerland, 2019; pp. 469–482.
207. Bettoni, J.C.; Mathew, L.; Pathirana, R.; Wiedow, C.; Hunter, D.A.; McLachlan, A.; Khan, S.; Tang, J.; Nadarajan, J. Eradication of *Potato Virus S*, *Potato Virus A*, and *Potato Virus M* from infected in vitro-grown potato shoots using in vitro therapies. *Front. Plant Sci.* **2022**, *13*, 878733. [\[CrossRef\]](#)
208. Bettoni, J.C.; Souza, J.A.; Volk, G.M.; Dalla Costa, M.; da Silva, F.N.; Kretschmar, A.A. Eradication of latent viruses from apple cultivar ‘Monalisa’ shoot tips using droplet-vitrification cryotherapy. *Sci. Hortic.* **2019**, *250*, 12–18. [\[CrossRef\]](#)
209. Farhadi-Toolii, S.; Ghanbari, A.; Kermani, M.J.; Zeinalabedini, M.; Bettoni, J.C.; Naji, A.M.; Kazemi, N. Droplet-vitrification cryotherapy and thermotherapy as efficient tools for the eradication of apple chlorotic leaf spot virus and apple stem grooving virus from virus-infected quince in vitro cultures. *Eur. J. Plant Pathol.* **2022**, *162*, 31–43. [\[CrossRef\]](#)
210. Mathew, L.; Tiffin, H.; Erridge, Z.; McLachlan, A.; Hunter, D.; Pathirana, R. Efficiency of eradication of Raspberry bushy dwarf virus from infected raspberry (*Rubus idaeus*) by in vitro chemotherapy, thermotherapy and cryotherapy and their combinations. *Plant Cell Tiss. Organ Cult.* **2021**, *144*, 133–141. [\[CrossRef\]](#)
211. Pathirana, R.; McLachlan, A.; Hedderley, D.; Carra, A.; Carimi, F.; Panis, B. Removal of leafroll viruses from infected grapevine plants by droplet vitrification. *Acta Hortic.* **2015**, *1083*, 491–498. [\[CrossRef\]](#)
212. Wang, Q.; Valkonen, J.P.T. Elimination of viruses and phytoplasma by cryotherapy of in vitro-grown shoot tips: Analysis of all cases. *Adv. Hortic. Sci.* **2007**, *21*, 265–269.
213. Wang, Q.C.; Valkonen, J.P.T. Efficient elimination of sweetpotato little leaf phytoplasma from sweetpotato by cryotherapy of shoot tips. *Plant Pathol.* **2008**, *57*, 338–347. [\[CrossRef\]](#)
214. Keller, E.R.J.; Zanke, C.D.; Senula, A.; Breuing, A.; Hardeweg, B.; Winkelmann, T. Comparing costs for different conservation strategies of garlic (*Allium sativum* L.) germplasm in genebanks. *Genet. Resour. Crop Evol.* **2013**, *60*, 913–926. [\[CrossRef\]](#)
215. Dulloo, M.E.; Ebert, A.W.; Dussert, S.; Gotor, E.; Astorga, C.; Vasquez, N.; Rakotomalala, J.J.; Rabemiafara, A.; Eira, M.; Bellachew, B.; et al. Cost efficiency of cryopreservation as a long-term conservation method for coffee genetic resources. *Crop Sci.* **2009**, *49*, 2123–2138. [\[CrossRef\]](#)
216. Jenderek, M.M.; Reed, B.M. Cryopreserved storage of clonal germplasm in the USDA National Plant Germplasm System. *Vitr. Cell. Dev. Biol.-Plant* **2017**, *53*, 299–308. [\[CrossRef\]](#)
217. Panis, B. Sixty years of plant cryopreservation: From freezing hardy mulberry twigs to establishing reference crop collections for future generations. *Acta Hortic.* **2019**, *1234*, 1–8. [\[CrossRef\]](#)
218. Wilms, H.; Rhee, J.H.; Rivera, R.L.; Longin, K.; Panis, B. Developing coconut cryopreservation protocols and establishing cryo-genebank at RDA; a collaborative project between RDA and Bioversity International. *Acta Hortic.* **2019**, *1234*, 343–348. [\[CrossRef\]](#)
219. Rajasekharan, P.E.; Ravish, B.S.; Kumar, T.V.; Ganeshan, S. Pollen Cryobanking for Tropical Plant Species. In *Conservation of Tropical Plant Species*; Normah, M.N., Chin, H.F., Reed, B.M., Eds.; Springer: New York, NY, USA, 2013; pp. 65–75.
220. Carimi, F.; Carra, A.; Panis, B.; Pathirana, R. Strategies for conservation of endangered wild grapevine (*Vitis vinifera* L. subsp. *silvestris* (C.C. Gmel.) Hegi). *Acta Hortic.* **2016**, *1115*, 81–86. [\[CrossRef\]](#)
221. O’Brien, C.; Hiti-Bandaralage, J.; Folgado, R.; Hayward, A.; Lahmeyer, S.; Folsom, J.; Mitter, N. Cryopreservation of woody crops: The avocado case. *Plants* **2021**, *10*, 934. [\[CrossRef\]](#)
222. Pathirana, R.; Mathew, L.; McLachlan, A. A simplified method for high recovery of kiwifruit (*Actinidia* spp.) shoot tips after droplet vitrification cryopreservation suitable for long-term conservation. *Plant Cell Tiss. Organ Cult.* **2021**, *144*, 97–102. [\[CrossRef\]](#)
223. Mathew, L.; Burritt, D.J.; McLachlan, A.; Pathirana, R. Combined pre-treatments enhance antioxidant metabolism and improve survival of cryopreserved kiwifruit shoot tips. *Plant Cell Tiss. Organ Cult.* **2019**, *138*, 193–205. [\[CrossRef\]](#)
224. Carra, A.; Sajeva, M.; Abbate, L.; Siragusa, M.; Pathirana, R.; Carimi, F. Factors affecting somatic embryogenesis in eight Italian grapevine cultivars and the genetic stability of embryo-derived regenerants as assessed by molecular markers. *Sci. Hortic.* **2016**, *204*, 123–127. [\[CrossRef\]](#)
225. Niskanen, A.-M.; Lu, J.; Seitz, S.; Keinonen, K.; Von Weissenberg, K.; Pappinen, A. Effect of parent genotype on somatic embryogenesis in Scots pine (*Pinus sylvestris*). *Tree Physiol.* **2004**, *24*, 1259–1265. [\[CrossRef\]](#)
226. Panis, B.; Nagel, M.; Van den houwe, I. Challenges and prospects for the conservation of crop genetic resources in field genebanks, in in vitro collections and/or in liquid nitrogen. *Plants* **2020**, *9*, 1634. [\[CrossRef\]](#)
227. Nadarajan, J.; van der Walt, K.; Lehnebach, C.A.; Saeiahagh, H.; Pathirana, R. Integrated ex situ conservation strategies for endangered New Zealand Myrtaceae species. *N. Z. J. Bot.* **2020**, *59*, 72–89. [\[CrossRef\]](#)
228. Byrne, P.F.; Volk, G.M.; Gardner, C.; Gore, M.A.; Simon, P.W.; Smith, S. Sustaining the future of plant breeding: The critical role of the USDA-ARS National Plant Germplasm System. *Crop Sci.* **2018**, *58*, 451–468. [\[CrossRef\]](#)
229. GRIN-Global. U.S. National Plant Germplasm System. Available online: <https://npgsweb.ars-grin.gov/gringlobal/search.aspx> (accessed on 25 March 2022).
230. CGIAR-Genebank-Platform. CGIAR Centers’ Use of Digital Object Identifiers (DOIs): A Submission to the Advisory Committee on the Global Information System 10 p. Available online: <https://cgispace.cgiar.org/handle/10568/102457> (accessed on 22 May 2022).

## Article

# Seasonal Xylem Sap Acidification Is Governed by Tree Phenology, Temperature and Elevation of Growing Site

Manuel Pramsöhler<sup>1,\*</sup>, Edith Lichtenberger<sup>2</sup> and Gilbert Neuner<sup>2,\*</sup><sup>1</sup> Laimburg Research Centre, Laimburg 6, Pfatten/Vadena, 39040 Auer/Ora, Italy<sup>2</sup> Unit of Functional Plant Biology, Department of Botany, University of Innsbruck, Sternwartestraße 15, 6020 Innsbruck, Austria

\* Correspondence: manuel.pramsöhler@laimburg.it (M.P.); gilbert.neuner@uibk.ac.at (G.N.); Tel.: +39-0471-969-649 (M.P.); +43-512-51026 (G.N.)

**Abstract:** pH of xylem sap (pHx) was determined in three trees (*Malus domestica* (apple tree), *Picea abies* and *Pinus cembra*) in response to seasonal changes. Conifer trees from lowland (600 m) were compared to trees growing at the alpine timberline (1950 m a.s.l.). Xylem sap was extracted with a Scholander pressure bomb and pHx was measured with a pH microsensor. In all species, pHx changed markedly with season. In spring, pHx was acidic; during winter, the pHx was more alkaline. In apple trees, the pHx did not show a significant correlation with temperature but was rather affected by developmental stage. During flushing in spring, xylem sap acidification took place concomitant to the developmental stage “tight cluster”, when foliar development enables a significant transpiration and a consequent movement of water in the xylem. The xylem sap of the two studied conifers showed a significantly larger seasonal alkalisation (+2.1) than found in apple trees (+1.2) and was significantly more pronounced at the timberline. Xylem sap acidification took place before bud break. pHx had a significant negative correlation with soil temperatures and corresponded to already reported pHx of angiosperms. Overall, pHx appears to be a sensitive stress marker and indicator of activity status in tree xylem.

**Keywords:** acidification; alkalisation; bud burst; freezing; *Malus domestica*; pH; *Picea abies*; *Pinus cembra*

**Citation:** Pramsöhler, M.; Lichtenberger, E.; Neuner, G. Seasonal Xylem Sap Acidification Is Governed by Tree Phenology, Temperature and Elevation of Growing Site. *Plants* **2022**, *11*, 2058. <https://doi.org/10.3390/plants11152058>

Academic Editors: Milan S. Stankovic, Paula Baptista and Petronia Carillo

Received: 30 June 2022  
Accepted: 1 August 2022  
Published: 6 August 2022

**Publisher’s Note:** MDPI stays neutral with regard to jurisdictional claims in published maps and institutional affiliations.



**Copyright:** © 2022 by the authors. Licensee MDPI, Basel, Switzerland. This article is an open access article distributed under the terms and conditions of the Creative Commons Attribution (CC BY) license (<https://creativecommons.org/licenses/by/4.0/>).

## 1. Introduction

The pH of the xylem sap (pHx) of plants ranges from acidic values of 4.5 to about 7.4 [1], which is in contrast to the milieu of the symplast, which has an alkaline pH ranging from 7.2 to 7.5 [2]. Only a few studies report on seasonal changes of pHx. In deciduous temperate trees, xylem sap usually becomes more alkaline in winter and then acidifies during spring [3–9]. In contrast, it can also be the other way round, as in *Juglans regia* pHx acidifies during winter and becomes more alkaline in spring [10].

Various mechanisms are reported to be responsible for the regulation of the pHx. All factors that affect proton pump activity [8,11,12] and xylem sap composition, especially the concentration of cations/anions and organic compounds, might be involved [13–15]. In addition, the pHx influences the concentration of dissolved CO<sub>2</sub> in the xylem sap and therefore regulates the amount of CO<sub>2</sub> that can be transported through the xylem in trees [1,9,16]. Seasonal pHx changes in deciduous species may be linked to the onset of the ascent of xylem sap, which is coupled to transpiration in the foliated stage. Unfortunately, studies reporting on seasonal changes of pHx in deciduous trees lack information on phenology and short-term variations during flushing in spring. For evergreen trees and gymnosperms, where the end of winter dormancy and the ascent of xylem sap are not linked to the formation of new leaves, only very few reports about seasonal changes of pHx are currently available. In conifers growing at the alpine timberline a marked pHx alkalisation during winter is reported [17].

Seasonal pHx changes are likely the consequence of steadied water and nutrient transport in the xylem that, in turn, is under environmental control and affected by winter stress. Under laboratory and field conditions, several abiotic and biotic stresses have been shown to cause an alkalisation of the xylem or apoplastic sap, including drought [18–20], salt stress [21,22], flooding [23,24], chilling temperatures [25] and fungal infection [25,26]. Additionally, it has been shown that environmental factors that influence transpiration rates, such as increased solar irradiation, vapour pressure deficit (VPD) and increased temperatures can influence the pHx [16,27,28]. Particularly in response to drought, alkalination of the xylem sap induces accumulation of the phytohormone abscisic acid (ABA) in the leaf apoplast triggering stomatal closure [18,20,29]. During winter, soil frosts can induce drought stress, which becomes even more severe at high elevations, where winter desiccation is a widespread phenomenon observed in woody plants [30]. Little is known about the effects of subalpine winter environmental conditions on the alkalisation of the pHx.

The aims of the present study were (1) to determine seasonal changes of pHx in a deciduous angiosperm (apple tree, *Malus domestica*) and in two evergreen gymnosperm tree species (*Picea abies*, *Pinus cembra*) and to correlate pHx values with seasonal temperature changes, (2) to compare seasonal changes of pHx in the same species under contrasting environmental conditions and growing sites (greenhouse versus field conditions in apple trees in order to advance tree phenology, low versus high elevation in evergreen gymnosperms) and (3) to assess the short-term dynamic of pHx in relation to developmental phenology during flushing of apple trees in spring.

## 2. Results

The pHx of apple trees was found to change significantly with season, with a mean value of pH  $5.0 \pm 0.03$  in spring and pH  $5.6 \pm 0.05$  in winter (Figure 1). The range between the minimum (pH 4.7) and maximum pH value (pH 5.9) recorded during the two measurement years was 1.2 pH units. In winter, the xylem sap was more alkaline. Acidification of the xylem sap occurred during regrowth in spring and was strongly linked to the developmental stage of buds during flushing. While in the early developmental stages, “green tip” and “half inch green”, the pH remained unchanged; in later stages, beginning with a “tight cluster”, the pH of the xylem sap decreased significantly ( $p < 0.05$ ). In all later developmental stages, pHx values were more acidic and significantly different from the early developmental stages.

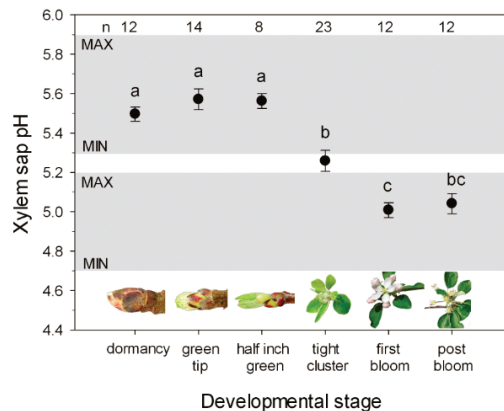


**Figure 1.** Seasonal change of pHx of twigs of *M. domestica* as related to the developmental stage of buds during flushing in spring. The grey boxes indicate the minimum and maximum for the respective season. Data (mean values  $\pm$  SE, replicate numbers are given in the figure) are from December

to May from two measurement years and were obtained on potted trees and orchard trees at field sites. Different letters indicate significant differences (tested by ANOVA and the Tamhane test at  $p < 0.05$ ). The pictures illustrate the phenology or stage of bud development.

The onset of or release from soil frost had no effect on pHx in apple trees. The seasonally occurring temperature fluctuations (mean values of soil and air temperatures 7 days before sampling) did not have any immediate effect on pHx of apple trees (see Table 1).

**Table 1.** Effect of air and soil temperatures (mean values from 7 days before sampling) on pHx (mean values,  $n = 5$ ). The Pearson correlation coefficient ( $r$ ) is given for calculations obtained with data from eight different sampling dates.

Species	Air Temperature		Soil Temperature	
	R	$p$	R	$p$
<i>Malus domestica</i> <sup>1</sup>	−0.345	0.402	−0.375	0.407
<i>Picea abies</i> <sup>2</sup>	−0.887	0.003	−0.901	0.002
<i>Pinus cembra</i> <sup>2</sup>	−0.669	0.069	−0.756	0.03
<i>Picea abies</i> <sup>3</sup>	−0.768	0.075	−0.924	0.008
<i>Pinus cembra</i> <sup>3</sup>	−0.660	0.153	−0.826	0.043

<sup>1</sup> measured on twig samples in an apple orchard from October 2010 till May 2011; <sup>2</sup> measured on twigs sampled at 600 m a.s.l. from October 2008 till April 2009; <sup>3</sup> measured on twigs sampled at 1950 m a.s.l. from October 2008 till April 2009.

Similar seasonal pHx changes were obtained for potted apple trees exposed to two contrasting temperature conditions (Figure 2). The range between mean values measured in spring (pH  $4.4 \pm 0.02$ ) and mean values measured in winter (pH  $5.7 \pm 0.1$ ) was 1.3 pH units. In potted trees, pHx values in spring were slightly more acidic than in trees from the field site. In the trees exposed to greenhouse conditions xylem sap acidification and flushing occurred earlier. In the greenhouse, apple trees were already at the developmental stage of “first bloom” in the middle of March. In the field, potted trees started to bloom nearly one month later.

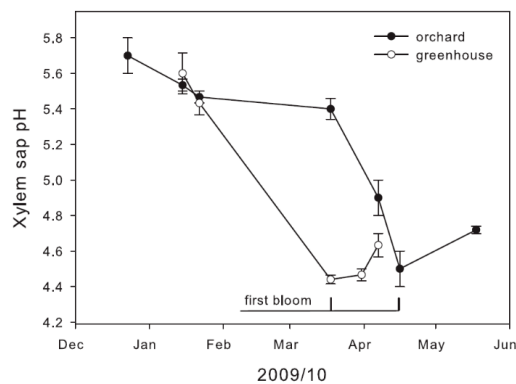


**Figure 2.** Seasonal change of pHx of twigs of potted *M. domestica* trees grown in an orchard (closed circles) or under greenhouse conditions (10/25 °C; open circles). Data are mean values  $\pm$  SE ( $n = 4$ ). Trees were transferred into the greenhouse on 15 January 2010.

In the investigated evergreen gymnosperms, a significant seasonal change of pHx was also found. In *P. abies* at 600 m a.s.l. alkalinisation in winter was more pronounced than in

apple with mean values of pH  $5.4 \pm 0.08$  in spring and pH  $6.9 \pm 0.13$  in winter (Figure 3). The range between the minimum (pH 5.2) and maximum pH value (pH 7.3) measured was 2.1 pH units. In *P. cembra* at 600 m a.s.l., mean values of pH  $6.1 \pm 0.3$  in spring and pH  $6.8 \pm 0.07$  in winter were found (data not shown).

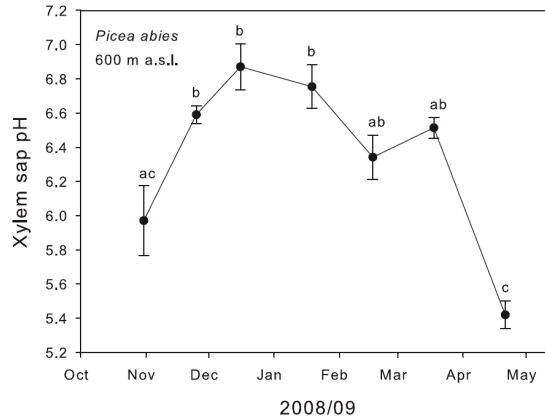


**Figure 3.** Seasonal change of pHx of twigs of *P. abies* sampled in the Botanical Garden in Innsbruck at 600 m a.s.l. Different letters indicate significant differences between mean values ( $\pm$ SE;  $n = 5$ ) tested by ANOVA and the Bonferroni test at  $p < 0.05$ .

Soil and air temperatures at the two contrasting field sites clearly differed (Figure 4). Particularly at the high elevation site (1950 m a.s.l.), there was a prolonged soil frost period during winter. Winter xylem sap alkalisation of *P. abies* and *P. cembra* from lowland (600 m a.s.l.) and from the timberline ecotone sites (1950 m a.s.l.) are compared in Figure 5. In winter, xylem sap was more alkaline at the growing site at 1950 m independent of species ( $p < 0.001$ ). In both evergreen gymnosperms, a significant alkalisation was observed during winter at both elevations, with a stronger alkalisation at the high elevation growing site ( $p < 0.001$ ). pHx values in the gymnosperms showed a negative correlation with the seasonally occurring air and soil temperatures (*P. abies* at 600 m and soil temperature  $r = -0.901$ ,  $p < 0.05$  see Table 1). In contrast to apple trees, the xylem sap of the evergreen gymnosperms acidified before bud break in spring.

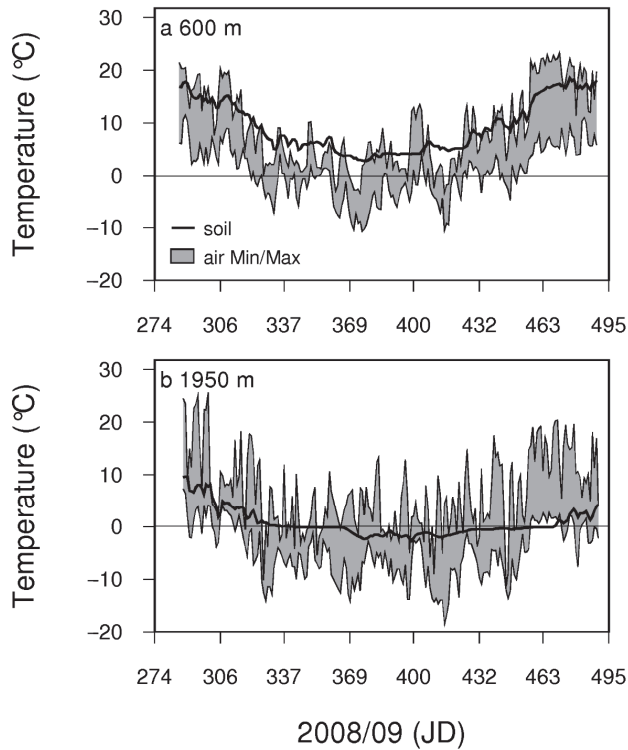


**Figure 4.** Temperature conditions in the Botanical Garden at 600 m a.s.l. (a) and at the field site at the timberline at 1950 m a.s.l. on Mt. Patscherkofel (b). The solid line shows the daily mean soil temperature at 5 cm depth, the grey area marks the daily minimum and maximum air temperatures measured at a height of 2 m.

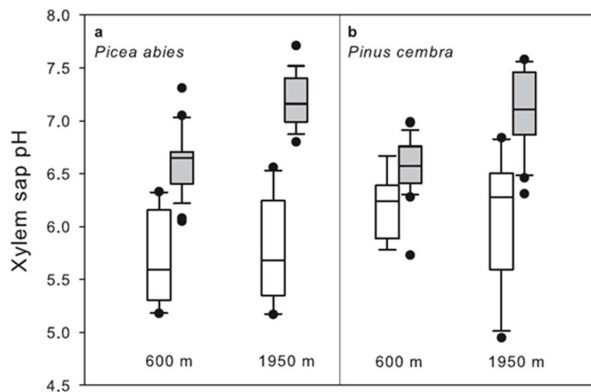


**Figure 5.** Seasonal change of pHx of (a) *P. abies* and (b) *P. cembra* twigs sampled at 600 m a.s.l. in comparison to samples from the alpine timberline at 1950 m. White boxes show values obtained during the growing period ( $n = 9$ ), grey boxes show winter values ( $n = 25$ ). The boxplots present the median and the 10th, 25th, 75th and 90th percentiles; outliers are shown as dots. For both species at both growing sites winter values were significantly different (Bonferroni at  $p < 0.05$ ) from values obtained during the growing period. Winter alkalisation was significantly higher ( $t$ -test at  $p < 0.001$ ) at 1950 m for both species.

### 3. Discussion

In the three investigated species, the pHx showed a pronounced seasonal variation. While in spring and autumn, pHx was acidic, a significant alkalisation took place during winter. The measured pHx values were in the range of other published values for pHx [1,19]. The alkalisation measured over winter corroborates earlier observations for a number of temperate deciduous angiosperm trees (*Acer pseudoplatanus* pH 5.4–6.9 [3]; *Actinidia chinensis* pH 5.3–6.2 [4]; *Betula pendula* pH 5.7–7.5 [5]; *Populus × canadensis* “robusta” pH 5.4–7.5 [6]; *Fagus sylvatica* pH 4.8–6.7 [31]; *Robinia pseudoacacia* pH 5.2–6.0 [8]).

In spring and autumn pHx of the gymnosperms *P. cembra* and *P. abies* was acidic. Acidification was also reported for other gymnosperms (pH 5.3 in *Abies koreana* [32]; pH 5.6 in *Pinus taeda* [33]). The seasonal dynamic of pHx in gymnosperms has recently been studied [17]; as for deciduous angiosperms, we found a significant winter alkalisation in evergreen gymnosperms. The seasonal pHx amplitude in the two studied evergreen gymnosperms was higher than in apple trees, but still in the range of the reported maximum seasonal amplitude of 2.3 pH units as reported for *Fagus sylvatica* [7,31]. Our results allow us to compare between the studied species but not between the functional groups of trees. Further studies with a higher number of conifer and deciduous tree species are needed to compare between functional groups of trees at different environments.

In apple trees, xylem sap acidification in spring was linked to the bud developmental stage “tight cluster” and there was no significant correlation between xylem sap acidification and the seasonally occurring soil or air temperatures. A close relationship between developmental stages during flushing and pHx values was found in trees grown under field conditions and individuals exposed to greenhouse conditions. At the onset of bud break, when the release from winter dormancy first becomes visible, no significant changes of pHx values were found. In the developmental stage of “tight cluster” when foliation had proceeded to such an extent that a significant transpiration and consequent ascent of water and nutrients in the xylem were possible, pHx began to decrease. Concomitant measurements of transpiration and xylem conductivity reveal that in the developmental stage of “tight cluster” the developing leaves are already transpiring; however, xylem hydraulic conductance is not yet fully restored [34,35].

For apple trees, significant seasonal variations in the quantitative mineral and amino acid composition of the xylem sap are reported [36,37]. Moreover, for *P. abies*, the mineral composition of the xylem sap and its seasonal variation are reported [38,39]. In the investigated evergreen gymnosperms xylem sap acidification in spring occurred before bud break and therefore before the new needles of the current season emerged. We assume that in evergreen species the absence of water movement in the xylem in winter is directly related to winter stress and low environmental temperatures; therefore, a correlation between pHx values and temperatures can be found. In deciduous tree species, transpiration and water movement in the xylem can start only after foliation in spring and therefore pHx values might not be directly related to the environmental temperatures in spring. Tree phenology is linked to occurring environmental temperatures and therefore climate change can lead to phenological shifts [40]. These shifts in tree phenology will directly influence the timing of the seasonal variations in pHx for apple trees. In the two studied conifers at the alpine timberline, a correlation between pHx and the seasonal occurring soil temperatures was found. Increasing temperatures due to climate change will therefore also affect the seasonal changes of pHx in timberline conifers.

The underlying mechanisms for the seasonal variation of pHx are not fully understood. All factors affecting proton pumping activity might be involved [11]. Fromard et al. [8] showed that in *Robinia pseudoacacia* the plasma membrane H<sup>+</sup>-ATPase of the vessel-associated cells is responsible for the control of pHx, and its activity changes with season. In winter the activity of the H<sup>+</sup>-ATPase was low and therefore xylem sap was more alkaline. Seasonal changes in the amount of the H<sup>+</sup>-ATPase in cambial and expanding xylem cells are reported for twigs of two *Populus* species [12]. Furthermore, the xylem sap composition has been shown to influence the pHx due to the buffering capacity of distinct compo-

nents [14,15,41,42]. In the xylem sap of beech roots, a significant correlation between low pH values and high concentrations of  $\text{Ca}^{2+}$ ,  $\text{Mg}^{2+}$  and malate was found [13]. The author concluded that the increase in malic acid, which forms complexes with cations, is responsible for the springtime acidification of the xylem sap in beech roots.

In the case of the winter acidification of the xylem sap of *Juglans regia* [10], the pHx values were not directly related to the activity of the  $\text{H}^+$ -ATPase of vessel-associated cells, but depended on the seasonal variation of the sugar content in the xylem sap. Proton-coupled active sugar transport mechanisms were shown to be responsible for this [10,43,44]. There is a strong relationship between pHx and the concentration of dissolved  $\text{CO}_2$  in the xylem sap. Therefore, pHx regulates the amount of  $\text{CO}_2$  transported through the xylem and, furthermore, the exchange of  $\text{CO}_2$  between the different stem tissues [1,45,46]. Knowledge about the species-specific xylem sap pH might be useful for the calculation of  $\text{CO}_2$  budgets of individual trees.

The comparison of pHx values of the same species from contrasting elevations clearly revealed that at 1950 m a.s.l. winter alkalisation was more pronounced than at 600 m in both investigated gymnosperms. The amount of mean winter alkalisation in *P. abies* was 1.5 pH units at 600 m compared to 2.0 pH units at 1950 m. Similarly, in *P. cembra* we measured a mean winter alkalisation of 0.6 pH units at 600 m compared to 1.5 pH units at 1950 m. In spring, pHx values were unaffected by elevation in the two gymnosperms. In both species at both growing sites, a significant correlation between pHx values and soil temperatures was found. At the timberline during winter the soil was frozen for a prolonged period causing winter drought stress that increased in severity with duration [30]. Timberline conifers are growing at the upper distribution boundaries of the respective tree species. Information on pHx and xylem sap composition may help to understand the survival mechanisms of the respective tree species at the timberline [17]. Under laboratory and field conditions, drought has been repeatedly identified as a factor in xylem sap alkalisation, due to a reduced proton pumping activity, leading to the accumulation of abscisic acid (ABA) in the leaf apoplast and inducing stomatal closure [11,18,27,28,47]. The alkalisation of the xylem sap in response to drought stress is not a universal mechanism in higher plant species [32]. However, the response to the apoplastic alkalisation—elevated ABA concentration in the apoplast and induction of stomatal closure—is thought to be a universal mechanism in plants [32]. The winter alkalisation of the xylem sap in evergreen gymnosperms might be part of a physiological stress response in evergreen trees, which keeps the stomata securely closed during winter. Nevertheless, irrespective of its physiological function, pHx can be nicely used to assess the current activation state of the xylem tissue in trees.

#### 4. Materials and Methods

##### 4.1. Study Site and Plant Material

Seasonal changes of the pHx were studied in a deciduous (apple tree, *Malus domestica* Borkh. cv. “Golden Delicious” growing on “M9” rootstock) and two evergreen tree species (*Picea abies* L. Karst. and *Pinus cembra* L.). Samples from apple trees were either taken from trees growing in an apple orchard in Tarsch, Italy (46°36' N, 10°53' E, 860 m a.s.l., 20 trees were used for sampling) or from 20 potted trees cultivated in the Botanical Garden, University of Innsbruck, Austria (47°16' N, 11°23' E, 600 m a.s.l.). To break dormancy ahead of field sites and to advance tree phenology, four potted apple trees were transferred into a greenhouse (10/25 °C night/day) on 15 January 2010. pHx values of these trees growing in the greenhouse were then compared to potted trees kept under field conditions. Apple trees were from 5 to 6 years old, and 2-year-old and 3-year-old shoots were used for xylem sap extraction. Samples from the evergreen gymnosperms were taken from two different field sites with contrasting elevations: at 600 m a.s.l. from trees growing in the Botanical Garden of the University of Innsbruck, and from trees growing close to the timberline ecotone on Mt. Patscherkofel (1950 m a.s.l.; 47°12' N, 11°27' E). Xylem sap samples from *P. abies* and *P. cembra* (twigs with a diameter of 0.7–0.9 cm, detached from adult trees) were

taken from the end of October 2008 to the end of May 2009. Apple trees were sampled over two years from December 2009 to May 2011. Twig samples were always taken between 10.00 and 12.00 a.m.

#### 4.2. Temperature Conditions

At the field sites, soil and air temperatures were recorded with sets of type T thermocouples. Soil temperatures were measured at a depth of 5, 10 and 20 cm, air temperatures were measured at a height of 2 m. Thermocouples were connected to a multiplexer (AM16/32B, Campbell Scientific, Logan, UT, USA) and temperatures were recorded at 7 min intervals with a CR10 data logger (Campbell Scientific, Logan, UT, USA). Temperatures of the potted apple trees in the greenhouse experiment and in the field were measured every 30 min with TidBit temperature data loggers (Onset, Pocasset, MA, USA).

#### 4.3. Xylem Sap Collection

For xylem sap extraction, twigs with a diameter of 0.7–0.9 cm were used. Twig samples were detached from the trees and transported in plastic bags from the field sites to the laboratory. Samples were either prepared for immediate measurement or stored overnight in a cold room at +4 °C until measurements started. When twigs from the alpine timberline site were frozen at the time of sampling, they were stored overnight at −8 °C in commercial freezers until the beginning of measurements. Xylem sap was collected using a Scholander pressure bomb (Model 3115, Soil moisture Equipment Corp., Santa Barbara, CA, USA). Twigs were cut into pieces of a mean length of about 15 cm. The bark, including the phloem and the cambium layer, was peeled off to ensure that the expressed liquid came only from the xylem. The pieces of wood were then sealed into the lid of the pressure chamber. After closure of the pressure chamber, the pressure was gradually increased to a maximum pressure of between 0.2 and 2.5 MPa. Xylem sap leaking out at the cut surface of the wood was then collected with glass capillaries until the volume was sufficient for pH measurements. pH<sub>x</sub> was measured immediately after xylem sap collection. This sampling methodology may affect xylem sap composition [48]. To minimise this aspect, we applied only the minimum pressure necessary for xylem sap collection and worked with pH microsensors that allowed measurements with small quantities of xylem sap (see following paragraph).

#### 4.4. pH Measurements

In apple twigs the pH<sub>x</sub> of the expressed xylem sap was measured with two different pH sensor types. With a needle-type pH microsensor (pH-1 micro, PreSens, Regensburg, Germany) measurements could be conducted inside glass capillaries (inner capillary diameter: 1.15 mm), which were used to suck up xylem sap. The pH-1 micro was connected to a PC for digital registration of the pH values. Because of the small dimension of the sensor (sensor tip < 150 µm), measurements were possible even within sap volumes < 0.02 mL. The second sensor type employed to measure apple xylem sap pH was a PHR-146 micro electrode (Lazar Research Laboratories, Los Angeles, CA, USA). For measurements with this sensor type the extracted xylem sap was also collected within glass capillaries, but then transferred to microtiter plates and measured in the microtiter plate. One droplet of xylem sap (0.05 mL) was sufficient for pH measurement. The pH sensor was connected to a digital pH meter (Jenco Model 60, Jenco Instruments, San Diego, CA, USA) and pH values could be read from the display. Calibration of the pH sensors was performed with certified buffer solutions (Merck, Darmstadt, Germany) according to the user instructions of the respective pH sensor. Additionally, all recordings were cross checked with non bleeding pH-indicator strips (Merck, Darmstadt, Germany). Measurements of the xylem sap of gymnosperms were taken using a micro combination pH electrode (Amani-1000, Innovative Instruments, Tampa, FL, USA). This sensor has a tip diameter of 1 mm and was also injected into the glass capillaries (inner diameter 1.6 mm) containing the collected xylem sap. The sensor was connected to a data logger (CR10X, Campbell Scientific, Logan,

UT, USA) for digital registration of the values. Between 4 and 5 twig samples were used for the pHx measurements.

#### 4.5. Tree Phenology

Classification of floral bud phenology in apple trees was conducted according to the descriptions given in the BBCH scale [49]. In the text the following terminology is used: “dormancy” (BBCH 00), “green tip” (BBCH 53), “half inch green” (BBCH 54), “tight cluster” where leaves are unfolding (BBCH 56), “first bloom” (BBCH 60) and “post bloom” (BBCH 69). In the two studied conifer species the timing of bud break in spring was observed.

#### 4.6. Statistical Data Analysis

pHx values are given as mean  $\pm$  standard error of the mean (SE). After values passed the Kolmogorov–Smirnov and the Levene tests, significant differences between mean values were tested using one-way ANOVA and the Bonferroni post hoc test ( $p < 0.05$ ). If homogeneity of variances was not established, significant differences between mean values were tested with one-way ANOVA and the Tamhane test. pHx values of gymnosperms from the two contrasting elevations were compared using Student’s *t*-test. Correlations between mean pHx values and the seasonally occurring air and soil temperatures were calculated using Pearson’s correlation analysis. All analyses are carried out using PASW Statistics 18 (formerly SPSS, IBM Corporation, New York, NY, USA). Replicate numbers are given in the figures or in the figure legends.

**Author Contributions:** Conceptualization, G.N. and M.P.; methodology, M.P. and E.L.; formal analysis, M.P. and E.L.; investigation, M.P. and E.L.; resources, G.N.; writing—original draft preparation, M.P.; writing—review and editing, G.N. and M.P.; funding acquisition, M.P. and G.N. All authors have read and agreed to the published version of the manuscript.

**Funding:** This work was financially supported by ‘Forschungsförderungsmittel der Südtiroler Landesregierung’ [PJ 81817] and a grant from ‘Verein zur Förderung der wissenschaftlichen Ausbildung und Tätigkeit von Südtirolern an der Landesuniversität Innsbruck’. The authors thank the Department of Innovation, Research, University and Museums of the Autonomous Province of Bozen/Bolzano for covering the Open Access publication costs.

**Acknowledgments:** We thank M. Abler from ‘Südtiroler Beratungsring für Obst- und Weinbau’ and O. Buchner for assistance at the field sites. Further, we thank the Patscherkofel Bergbahnen for free transportation to Mt. Patscherkofel.

**Conflicts of Interest:** The authors declare no conflict of interest.

## References

1. Teskey, R.O.; Saveyn, A.; Steppe, K.; McGuire, M.A. Origin, fate and significance of CO<sup>2</sup> in tree stems. *New Phytol.* **2008**, *177*, 17–32. [[CrossRef](#)] [[PubMed](#)]
2. Felle, H.H. pH: Signal and messenger in plant cells. *Plant Biol.* **2001**, *3*, 577–591. [[CrossRef](#)]
3. Essiamah, S.K. Spring sap of trees. *Ber. Deut. Bot. Ges.* **1980**, *93*, 257–267.
4. Ferguson, A.R.; Eiseman, J.A.; Leonard, J.A. Xylem sap from *Actinidia chinensis*—Seasonal changes in composition. *Ann. Bot.* **1983**, *51*, 823–833. [[CrossRef](#)]
5. Sauter, J.J.; Ambrosius, T. Changes in the partitioning of carbohydrates in the wood during bud break in *Betula pendula* Roth. *J. Plant Physiol.* **1986**, *124*, 31–43. [[CrossRef](#)]
6. Sauter, J.J. Seasonal changes in the efflux of sugars from parenchyma cells into the apoplast in poplar stems (*Populus x canadensis* “robusta”). *Trees Struct. Funct.* **1988**, *2*, 242–249. [[CrossRef](#)]
7. Glavac, V.; Koenies, H.; Ebben, U. Seasonal variation of calcium, magnesium, potassium, and manganese contents in xylem sap of beech (*Fagus sylvatica* L.) in a 35-year-old limestone beech forest stand. *Trees Struct. Funct.* **1990**, *4*, 75–80. [[CrossRef](#)]
8. Fromard, L.; Babin, V.; Fleuratlessard, P.; Fromont, J.C.; Serrano, R.; Bonnemain, J.L. Control of vascular sap pH by vessel-associated cells in woody species—Physiological and immunological studies. *Plant Physiol.* **1995**, *108*, 913–918. [[CrossRef](#)]
9. Erda, F.G.; Bloemen, J.; Steppe, K. Quantifying the impact of daily and seasonal variation in sap pH on xylem dissolved inorganic carbon estimates in plum trees. *Plant Biol.* **2014**, *16*, 43–48. [[CrossRef](#)]

10. Alves, G.; Ameglio, T.; Guillot, A.; Fleurat-Lessard, G.; Lacoine, A.; Sakr, S.; Petel, G.; Julien, J.L. Winter variation in xylem sap pH of walnut trees: Involvement of plasma membrane H<sup>+</sup>-ATPase of vessel-associated cells. *Tree Physiol.* **2004**, *24*, 99–105. [[CrossRef](#)]
11. Wilkinson, S. PH as a stress signal. *Plant Growth Regul.* **1999**, *29*, 87–99. [[CrossRef](#)]
12. Arend, M.; Weisenseel, M.H.; Brummer, M.; Osswald, W.; Fromm, J.H. Seasonal changes of plasma membrane H<sup>+</sup>-ATPase and endogenous ion current during cambial growth in poplar plants. *Plant Physiol.* **2002**, *129*, 1651–1663. [[CrossRef](#)] [[PubMed](#)]
13. Schell, J. Interdependence of pH, malate concentration, and calcium and magnesium concentrations in the xylem sap of beech roots. *Tree Physiol.* **1997**, *17*, 479–483. [[CrossRef](#)] [[PubMed](#)]
14. Gerendas, J.; Schurr, U. Physicochemical aspects of ion relations and pH regulation in plants—A quantitative approach. *J. Exp. Bot.* **1999**, *50*, 1101–1114. [[CrossRef](#)]
15. Wang, Y.S.; Liu, F.L.; Jensen, C.R. Comparative effects of deficit irrigation and alternate partial root-zone irrigation on xylem pH, ABA and ionic concentrations in tomatoes. *J. Exp. Bot.* **2012**, *63*, 1907–1917. [[CrossRef](#)] [[PubMed](#)]
16. Aubrey, D.P.; Boyles, J.G.; Krysinaky, L.S.; Teskey, R.O. Spatial and temporal patterns of xylem sap pH derived from stems and twigs of *Populus deltoides* L. *Environ. Exp. Bot.* **2011**, *71*, 376–381. [[CrossRef](#)]
17. Losso, A.; Nardini, A.; Damon, B.; Mayr, S. Xylem sap chemistry: Seasonal changes in timberline conifers *Pinus cembra*, *Picea abies*, and *Larix decidua*. *Biol. Plant.* **2018**, *62*, 157–165. [[CrossRef](#)]
18. Wilkinson, S.; Davies, W.J. Xylem sap pH increase: A drought signal received at the apoplastic face of the guard cell that involves the suppression of saturable abscisic acid uptake by the epidermal symplast. *Plant Physiol.* **1997**, *113*, 559–573. [[CrossRef](#)]
19. Wilkinson, S.; Corlett, J.E.; Oger, L.; Davies, W.J. Effects of xylem pH on transpiration from wild-type and flacca tomato leaves—A vital role for abscisic acid in preventing excessive water loss even from well-watered plants. *Plant Physiol.* **1998**, *117*, 703–709. [[CrossRef](#)]
20. Gloser, V.; Korovetska, H.; Martin-Vertedor, A.I.; Hajickova, M.; Prokop, Z.; Wilkinson, S.; Davies, W. The dynamics of xylem sap pH under drought: A universal response in herbs? *Plant Soil* **2016**, *409*, 259–272. [[CrossRef](#)]
21. Pitann, B.; Kranz, T.; Zorb, C.; Walter, A.; Schurr, U.; Muhling, K.H. Apoplastic pH and growth in expanding leaves of *Vicia faba* under salinity. *Environ. Exp. Bot.* **2011**, *74*, 31–36. [[CrossRef](#)]
22. Geilfus, C.M.; Muhling, K.H. Transient alkalization in the leaf apoplast of *Vicia faba* L. depends on NaCl stress intensity: An in situ ratio imaging study. *Plant Cell Environ.* **2012**, *35*, 578–587. [[CrossRef](#)] [[PubMed](#)]
23. Jackson, M.B.; Saker, L.R.; Crisp, C.M.; Else, M.A.; Janowiak, F. Ionic and pH signalling from roots to shoots of flooded tomato plants in relation to stomatal closure. *Plant Soil* **2003**, *253*, 103–113. [[CrossRef](#)]
24. Else, M.A.; Taylor, J.M.; Atkinson, C.J. Anti-transpirant activity in xylem sap from flooded tomato (*Lycopersicon esculentum* Mill.) plants is not due to pH-mediated redistributions of root- or shoot-sourced ABA. *J. Exp. Bot.* **2006**, *57*, 3349–3357. [[CrossRef](#)]
25. Felle, H.H.; Herrmann, A.; Huckelhoven, R.; Kogel, K.H. Root-to-shoot signalling: Apoplastic alkalization, a general stress response and defence factor in barley (*Hordeum vulgare*). *Protoplasma* **2005**, *227*, 17–24. [[CrossRef](#)]
26. Felle, H.H.; Herrmann, A.; Schaefer, P.; Hueckelhoven, R.; Kogel, K.H. Interactive signal transfer between host and pathogen during successful infection of barley leaves by *Blumeria graminis* and *Bipolaris sorokiniana*. *J. Plant Physiol.* **2008**, *165*, 52–59. [[CrossRef](#)]
27. Davies, W.J.; Wilkinson, S.; Loveys, B. Stomatal control by chemical signalling and the exploitation of this mechanism to increase water use efficiency in agriculture. *New Phytol.* **2002**, *153*, 449–460. [[CrossRef](#)]
28. Wilkinson, S.; Davies, W.J. Manipulation of the apoplastic pH of intact plants mimics stomatal and growth responses to water availability and microclimatic variation. *J. Exp. Bot.* **2008**, *59*, 619–631. [[CrossRef](#)]
29. Wilkinson, S.; Davies, W.J. ABA-based chemical signalling: The co-ordination of responses to stress in plants. *Plant Cell Environ.* **2002**, *25*, 195–210. [[CrossRef](#)]
30. Sakai, A.; Larcher, W. *Frost Survival of Plants. Responses and Adaptation to Freezing Stress*; Springer: Berlin/Heidelberg, Germany, 1987; Volume 62, p. 321.
31. Glavac, V.; Koenigs, H.; Ebben, U. Seasonal-variations in mineral concentrations in the trunk xylem sap of beech (*Fagus sylvatica* L.) in a 42-year-old beech forest stand. *New Phytol.* **1990**, *116*, 47–54. [[CrossRef](#)]
32. Sharp, R.G.; Davies, W.J. Variability among species in the apoplastic pH signalling response to drying soils. *J. Exp. Bot.* **2009**, *60*, 4361–4370. [[CrossRef](#)] [[PubMed](#)]
33. Carter, M.L.H. Soil nutrients and loblolly pine xylem sap composition. *For. Sci.* **1965**, *11*, 216–220.
34. Beikircher, B.; Mittmann, C.; Mayr, S. Prolonged soil frost affects hydraulics and phenology of apple trees. *Front. Plant Sci.* **2016**, *7*, 867. [[CrossRef](#)] [[PubMed](#)]
35. Beikircher, B.; Mayr, S. Annual patterns of xylem embolism in high-yield apple cultivars. *Funct. Plant Biol.* **2017**, *44*, 587–596. [[CrossRef](#)]
36. Tromp, J. Seasonal-variations in the composition of xylem sap of apple with respect to K, Ca, Mg, and N. *Z. Pflanzenphysiol.* **1979**, *94*, 189–194. [[CrossRef](#)]
37. Tromp, J.; Ovaa, J.C. Spring composition of xylem sap of apple with respect to amino-nitrogen and mineral elements at two root temperatures. *Z. Pflanzenphysiol.* **1981**, *102*, 249–255. [[CrossRef](#)]
38. Osonubi, O.; Oren, R.; Werk, K.S.; Schulze, E.D.; Heilmeyer, H. Performance of two *Picea abies* (L.) Karst. stands at different stages of decline. 4. Xylem sap concentrations of magnesium, calcium, potassium and nitrogen. *Oecologia* **1988**, *77*, 1–6. [[CrossRef](#)]

39. Berger, A.; Oren, R.; Schulze, E.D. Element concentrations in the xylem sap of *Picea abies* (L.) Karst. seedlings extracted by various methods under different environmental conditions. *Tree Physiol.* **1994**, *14*, 111–128. [[CrossRef](#)]
40. Vitasse, Y.; Baumgarten, F.; Zohner, C.M.; Rutishauser, T.; Pietragalla, B.; Gehrig, R.; Dai, J.; Wang, H.; Aono, Y.; Sparks, T.H. The great acceleration of plant phenological shifts. *Nat. Clim. Chang.* **2022**, *12*, 300–302. [[CrossRef](#)]
41. Gollan, T.; Schurr, U.; Schulze, E.D. Stomatal response to drying soil in relation to changes in the xylem sap composition of *Helianthus annuus*. 1. The concentration of cations, anions, amino acids in, and pH of, the xylem sap. *Plant Cell Environ.* **1992**, *15*, 551–559. [[CrossRef](#)]
42. Schurr, U.; Schulze, E.D. Effects of drought on nutrient and ABA transport in *Ricinus communis*. *Plant Cell Environ.* **1996**, *19*, 665–674. [[CrossRef](#)]
43. Alves, G.; Decourteix, M.; Fleurat-Lessard, P.; Sakr, S.; Bonhomme, M.; Ameglio, T.; Lacoïnte, A.; Julien, J.L.; Petel, G.; Guilliot, A. Spatial activity and expression of plasma membrane H<sup>+</sup>-atpase in stem xylem of walnut during dormancy and growth resumption. *Tree Physiol.* **2007**, *27*, 1471–1480. [[CrossRef](#)] [[PubMed](#)]
44. Bonhomme, M.; Peuch, M.; Ameglio, T.; Rageau, R.; Guilliot, A.; Decourteix, M.; Alves, G.; Sakr, S.; Lacoïnte, A. Carbohydrate uptake from xylem vessels and its distribution among stem tissues and buds in walnut (*Juglans regia* L.). *Tree Physiol.* **2010**, *30*, 89–102. [[CrossRef](#)] [[PubMed](#)]
45. Teskey, R.O.; McGuire, M.A. Measurement of stem respiration of sycamore (*Platanus occidentalis* L.) trees involves internal and external fluxes of CO<sub>2</sub> and possible transport of CO<sub>2</sub> from roots. *Plant Cell Environ.* **2007**, *30*, 570–579. [[CrossRef](#)] [[PubMed](#)]
46. Etzold, S.; Zweifel, R.; Ruehr, N.K.; Eugster, W.; Buchmann, N. Long-term stem CO<sub>2</sub> concentration measurements in norway spruce in relation to biotic and abiotic factors. *New Phytol.* **2013**, *197*, 1173–1184. [[CrossRef](#)] [[PubMed](#)]
47. Secchi, F.; Zwieniecki, M.A. Accumulation of sugars in the xylem apoplast observed under water stress conditions is controlled by xylem pH. *Plant Cell Environ.* **2016**, *39*, 2350–2360. [[CrossRef](#)]
48. Schurr, U. Xylem sap sampling—New approaches to an old topic. *Trends Plant Sci.* **1998**, *3*, 293–298. [[CrossRef](#)]
49. Lancashire, P.D.; Bleiholder, H.; Vandenboom, T.; Langeluddeke, P.; Stauss, R.; Weber, E.; Witzemberger, A. A uniform decimal code for growth-stages of crops and weeds. *Ann. Appl. Biol.* **1991**, *119*, 561–601. [[CrossRef](#)]



## Article

# Genome-Wide Identification and Spatial Expression Analysis of Histone Modification Gene Families in the Rubber Dandelion *Taraxacum kok-saghyz*

Francesco Panara<sup>1</sup>, Carlo Fasano<sup>1</sup>, Loredana Lopez<sup>1</sup>, Andrea Porceddu<sup>2</sup>, Paolo Facella<sup>1</sup>, Elio Fantini<sup>1</sup>, Loretta Daddiego<sup>1</sup> and Giorgio Perrella<sup>3,\*</sup>

<sup>1</sup> Trisaia Research Center, Italian National Agency for New Technologies Energy and Sustainable Economic Development (ENEA), 75026 Rotondella, MT, Italy

<sup>2</sup> Department of Agriculture, University of Sassari, Viale Italia, 39a, 07100 Sassari, SS, Italy

<sup>3</sup> Department of Biosciences, University of Milan, Via Giovanni Celoria 26, 20133 Milan, MI, Italy

\* Correspondence: giorgio.perrella@unimi.it

**Abstract:** *Taraxacum kok-saghyz* (*Tks*), also known as the Russian dandelion, is a recognized alternative source of natural rubber quite comparable, for quality and use, to the one obtained from the so-called rubber tree, *Hevea brasiliensis*. In addition to that, *Tks* roots produce several other compounds, including inulin, whose use in pharmaceutical and dietary products is quite extensive. Histone-modifying genes (HMGs) catalyze a series of post-translational modifications that affect chromatin organization and conformation, which, in turn, regulate many downstream processes, including gene expression. In this study, we present the first analysis of HMGs in *Tks*. Altogether, we identified 154 putative *Tks* homologs: 60 HMTs, 34 HDMs, 42 HATs, and 18 HDACs. Interestingly, whilst most of the classes showed similar numbers in other plant species, including *M. truncatula* and *A. thaliana*, HATs and HMT-PRMTs were indeed more abundant in *Tks*. Composition and structure analysis of *Tks* HMG proteins showed, for some classes, the presence of novel domains, suggesting a divergence from the canonical HMG model. The analysis of publicly available transcriptome datasets, combined with spatial expression of different developmental tissues, allowed us to identify several HMGs with a putative role in metabolite biosynthesis. Overall, our work describes HMG genomic organization and sets the premises for the functional characterization of epigenetic modifications in rubber-producing plants.

**Keywords:** histone modification; gene expression; *Taraxacum kok-saghyz*; natural rubber

**Citation:** Panara, F.; Fasano, C.; Lopez, L.; Porceddu, A.; Facella, P.; Fantini, E.; Daddiego, L.; Perrella, G. Genome-Wide Identification and Spatial Expression Analysis of Histone Modification Gene Families in the Rubber Dandelion *Taraxacum kok-saghyz*. *Plants* **2022**, *11*, 2077. <https://doi.org/10.3390/plants11162077>

Academic Editor: Pavel Kerchev

Received: 1 July 2022

Accepted: 4 August 2022

Published: 9 August 2022

**Publisher's Note:** MDPI stays neutral with regard to jurisdictional claims in published maps and institutional affiliations.



**Copyright:** © 2022 by the authors. Licensee MDPI, Basel, Switzerland. This article is an open access article distributed under the terms and conditions of the Creative Commons Attribution (CC BY) license (<https://creativecommons.org/licenses/by/4.0/>).

## 1. Introduction

The genus *Taraxacum* Wigg. (dandelion) is included in the large family of Asteraceae (Compositae), which counts more than 2800 species [1]. Most of these species of dandelions live in the temperate zones of the northern hemisphere, although they are native to Eurasia [2]. Among all the dandelions species, the Russian dandelion (*Taraxacum kok-saghyz*, *Tks*) can produce from its roots natural rubber (NR) of excellent quality, quite comparable to that obtained from *Hevea brasiliensis*, the so-called rubber tree [3]. In *Tks*, the length of the rubber polymer is greater than that of *Hevea*, with a molecular weight of approximately 2180 kDa, but its productivity per hectare is lower [4]. Nevertheless, *Tks* mature roots can contain up to 5% of rubber and 20% of inulin in dry weight in wild plants and, therefore, this dandelion is considered as a valid alternative natural rubber source. *Tks* can extensively grow both in cold and temperate areas, presents a short life cycle, and can be easily harvested [5]. Moreover, *Tks* is a species suitable for genetic manipulation and it could be used as a model plant to investigate the molecular pathways that regulate NR biosynthesis [6,7].

NR is a polymer composed of cis-1,4-polyisoprene and it represents a very important raw material, used to produce more than 50,000 both industrial and medical products [8].

The *Tks* genome has been recently published, showing that this dandelion (a diploid species  $2n = 16$ ) has a genome size of 1.29 Gb, comprising 46,731 predicted protein-coding genes [9].

*Tks* presents tissues specialized in the production of NR, called laticifers [3]. Laticifers contain latex in specific structures, the rubber particles, that are spherical organelles surrounded by a lipid monolayer membrane [8]. Several proteins are bound to the membrane of the rubber particles and some of them play an important role in rubber biosynthesis. In the roots of *Taraxacum* spp., there are also present in significant quantities the carbohydrate inulin and other metabolites that are relevant in various applications [2,10–13].

In plants, chromatin is comprised in nucleosomes that are constituted by two copies of each histone protein (H2A, H2B, H3, and H4) wrapped around ~146 base pairs of DNA [14]. Together with canonical histone proteins, nucleosomes can also contain histone variants that are usually integrated in specific chromatin regions and in response to external stimuli [15]. Histones are composed of N-terminal tails that are enriched in basic amino acids that are subjected to different post-translational modifications (PTMs) [16]. The simultaneous presence of different modifications defines the so-called histone code that is superimposed over the genetic code to regulate most cellular mechanisms [17]. Histone H3 and H4 tails can indeed be methylated, acetylated, and phosphorylated at different levels (mono-di-and tri). Interestingly, different lysine and arginine residues can be subjected to different modifications that ultimately work as positive or negative regulators of gene expression [18]. Histone methylation is catalyzed by histone methyltransferases (HMTs) and can occur primarily at H3 Lys4 (K4), Lys9 (K9), Lys27 (K27), and Lys36 (K36) [19]. HMTs comprise mostly of the SET domain group (SDG) enzymes that are divided in seven different classes: (1) E(Z) (enhancer of zeste) homologs, (2) ASH1 (absent, small, or homeotic discs 1) groups (ASH1 homologs (ASHH) and ASH1-related proteins (ASHR)), (3) TRX (Trithorax) groups (TRX homologs and TRX-related proteins), (4) SET and PhD domain, (5) SU(VAR)3–9 groups (together with SU(VAR)3–9 homologs (SUVH) and SU(VAR)3–9-related proteins (SUVR)), (6) truncated SET domain class and (7) Rubisco large (RBLSM) and small (RBSSM) subunit methyltransferases SET-related class [20–22]. In addition to that, plants also do present a second HMT family that includes the protein arginine methyl-transferases that contain the PRMA domain (PRMTs) [23].

While histone methylation is catalyzed by HMTs', histone demethylases (HDMs) are responsible for its removal [24]. In plants, there are two main classes of HDM enzymes that are distinguished through their mechanism of action. Indeed, the KDM1/LSD1-like (HDMAs) operate through amine oxidation to remove methylation marks, while JmjC domain-containing (JMJs) demethylases use hydroxylation [25–27]. At the same time, cofactors and the substrates change based on the type of HDMs. HDMAs only demethylate residues that have been mono- or dimethylated by a flavin adenine dinucleotide (FAD)-dependent reaction. Instead, JMJs demethylate lysines independently on the type of methylation and use Fe(II) and  $\alpha$ -ketoglutarate ( $\alpha$ KG) as cofactors [28].

Histone acetyltransferases (HATs) and deacetylases (HDACs) catalyze the addition and the removal of the acetyl-CoA groups over the histone tails, respectively [29]. This modification is usually correlated with changes in gene expression as well as chromosome condensation. In Arabidopsis, HATs are divided in four groups: GNAT and MYST families (HAGs and HAMs, respectively), CBP (HACs), and the TAFII250 (HAFs) [30]. HAGs are then classified in three main classes: GCN5 or GCN5-like, ELP3, and HAT1. MYSTs, instead, contain mostly HAM members [31]. HDACs in plants are grouped in three main groups: RPD3/HDA1 superfamily, similar to the yeast large RPD3 complex (HDAs), the sirtuins (SIR2/SRTs), and the HD2/HDT enzymes, whose class appears to be specific in plants [32,33]. Both HATs and HDACs have been largely characterized in plants. Indeed, their function is involved in different developmental processes and transitions, including germination, cell differentiation, and leaf and floral organogenesis [34–37]. Furthermore, their role has been linked with changes in gene expression upon different abiotic and biotic stress conditions, such as salinity, light, temperature, and immuno-responses [38–42].

Here, we report for the first time an extensive in silico analysis and identification of the histone-modifying genes (HMGs) in *Tks*. Using publicly available genome and transcriptome data, we analyzed the gene and protein structure of the identified HMGs and monitored their expression in various *Tks* tissues, including latex. In addition, we measured transcript levels in *Tks* young and adult leaves and roots and identified those per each class of enzymes that appeared to be abundant in relevant tissues.

## 2. Results

### 2.1. HMG Genes Identification

In the *Tks* genome [9], we identified a total of 154 HMGs: 60 HMTs, 34 HDMs, 42 HATs, and 18 HDACs. We compared the total number with a close relative of *Tks*, *Lactuca sativa* (*Ls*) and with the reference plants *Arabidopsis thaliana* (*At*) [43] and *Medicago truncatula* (*Mt*) [44]. While some classes were similar in numbers, others showed divergent expansion among different species. PRMTs were indeed more abundant in *Tks*, indicating an expansion of this class of proteins similarly to *Litchi chinensis* [45]. Altogether, HAGs were more abundant in both *Tks* and *Ls* compared to *At*, confirming the possibility for this group to expand divergently in different taxa (Table 1). The complete list of *Tks* HMGs is reported in Table S1.

**Table 1.** Number of genes identified in the different classes of HMGs in *Taraxacum kok-saghyz* and in three reference species: *Lactuca sativa*, *Arabidopsis thaliana*, and *Medicago truncatula*.

Family	Group	PFAM	Taraxacum Kok-Saghyz	Lactuca Sativa	Arabidopsis Thaliana	Medicago Truncatula v.4.01
HMT	SDG	PF00856	46	46	41	78
	PRMT	PF05185	14	4	7	3
HDM	JMJ	PF02373	27	47	21	34
	HDMA	PF04433	7	8	4	12
	HAG	PF00583	38	34	3	51
HAT	HAM	PF01853	1	2	2	1
	HAC	PF08214	3	14	5	11
	HAF	PF09247	0	1	2	1
	HDA	PF00850	9	19	12	10
HDAC	SRT	PF02146	4	3	2	2
	HDT		5	3	4	3
			<b>154</b>	<b>181</b>	<b>103</b>	<b>206</b>

Gene duplication events contributed to the high number of HMGs in the *Tks* genome. Synteny analysis on the *Tks* genome assembly was not effective for the identification of segmentally duplicated HMGs, while five couples of tandemly duplicated genes were identified: *TksHDA5/TksHDA6*, *TksHAG30/TksHAG31*, *TksHAG36/TksHAG37*, *TksJMJ11/TksJMJ12*, and *TksSDG44/GWHPAAAA005121*. In the last pair, GWHPAAAA005121 was not classified as an HMG due to the absence of a representative domain. We identified 32 additional couples of putative duplicated HMGs based on phylogenetic analysis. The Ka/Ks ratio was calculated for all the gene pairs in order to estimate the occurring evolutionary dynamics (Table S3). Most of the couples showed Ka/Ks <1, suggesting purifying or stabilizing selection. Only the *TksHAG13/14* pair with a Ka/Ks ratio of 1.54 and *TksPRMT7/8* with 1.05 showed values compatible with positive and neutral selection.

#### 2.1.1. HMTs

Among HMTs, 46 were identified belonging to SDG and 14 to the PRMT group. SDGs are similar in number to *At* and the same amount in *Tks* and *Ls* (Table 1). SDGs are divided in seven classes [22,46]. Four *Tks*SDGs cluster with Class I, E(Z)-like SDGs (Figure 1A) and show the expected SANT-CXC-SET domains except for *TksSDG8* lacking the SANT domain (Figure 2).

Five clusters with Class II, ASH1-like. *TksSDG29*, *TksSDG16*, and *TksSDG19* have the same domain composition of corresponding *At* proteins. *TksSDG15* encodes for a short (52aa) and a probably aberrant protein where only the SET domain was identified. *TksSDG37* lacks the PostSET domain compared to *AtSDG26*. Five proteins cluster with Class III, TRX-like. *TksSDG41* differs from *AtSDG14* as the first PHD module is substituted by a SAND domain that is often associated to PHDs and could contribute to their function. *TksSDG45* showed an additional TUDOR domain at the N-terminal. The TUDOR domain was previously identified in *D. melanogaster* TUDOR proteins and its function is unknown. Several human MJJ/KDM4 proteins harbour a TUDOR domain at the C-terminal [44]. *TksSDG4* clusters with *AtSDG25* but differs in domain composition and sequence length: GYF-SET and 1057aa the former, and SET-PostSET 1424aa the latter. This was previously observed in *S. lycopersicum* (*Sl*), where *AtSDG25* and *SlSDG20* showed similar differences [45]. Two Class IV SDGs exist in both *Tks* and *At*. Six *Tks* proteins cluster with class V subclass I and six with class V subclass II with a similar domain composition to *At* proteins. Eighteen SDGs can be classified as belonging to class VI/VII and show an interrupted SET domain. *TksSDG40* is a short protein of 158aa, probably aberrant, and the presence of the SET domain was not confirmed by SMART analysis.

*TksSDG5* and *TksSDG25* encode for putative long proteins with an additional/unexpected domain composition, probably resulting from exon gain or, more likely, a defect in genome assembly/annotation.

As shown in Figure S1, three PRMTs form a separate cluster: *TksPRMT2*, *TksPRMT7*, and *TksPRMT8* and contains two PRMT domains (Figure 2). The PRMT5 domain was not confirmed for *TksPRMT9* and *TksPRMT11* by SMART analysis. *TksPRMT6* shows four C2H2 modules at the N-terminal similarly to HMGs belonging to other groups such as *AtSDG6*/*TksSDG24* (Figure 2).

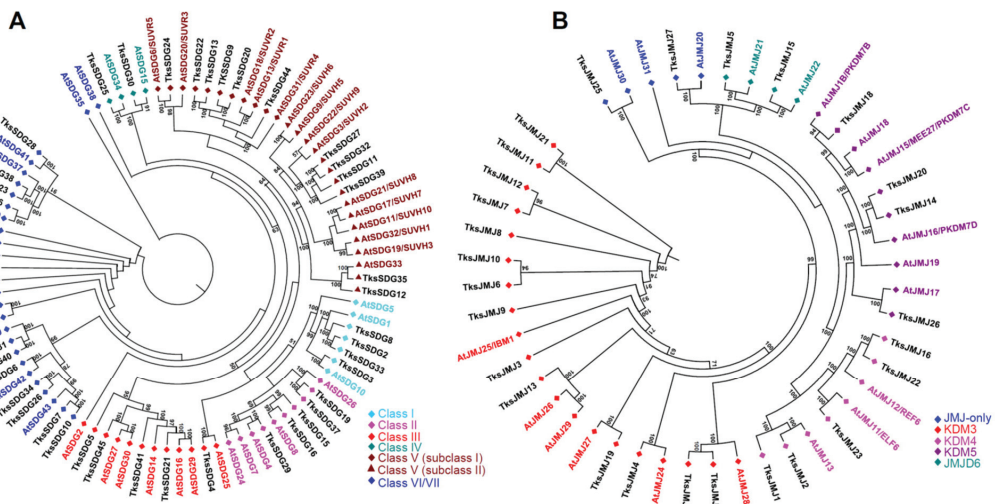
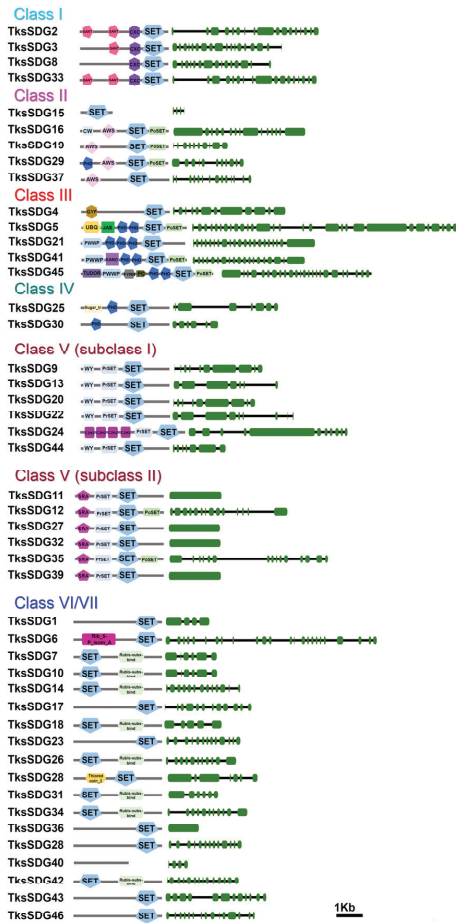
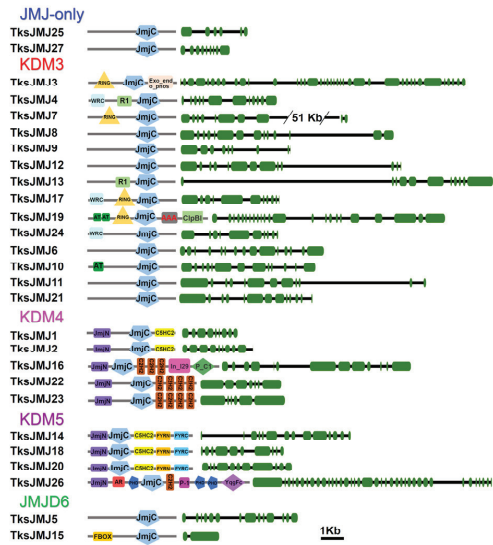


**Figure 1.** Phylogenetic tree of SDG (A) and MJJ (B) proteins of *Taraxacum kok-saghyz* and *Arabidopsis thaliana* (in colour according to their respective classes). The numbers near the tree branches represent bootstrap values.

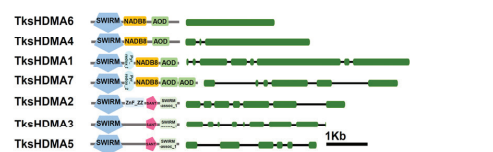
### TksSDGs



### TksJMJs



### TksHDMAs



#### SDGs Legend:



#### PRMTs Legend:



#### JMJs Legend:



#### HDMAs Legend:



Exon Intron

Figure 2. Domain composition and intron-exon structure of *Taraxacum kok-saghyz* HMTs and HDMs.

### 2.1.2. HDMs

In *Tks*, we identified 27 proteins containing the JmjC domain (PF02373) (Table 1). Despite that nine harbour the JmjC domain alone and could be classified as JMJ-only, only *Tks*JMJ25 and *Tks*JMJ27 clustered with *At* JMJ-only proteins (Figures 1B and 2). The other

seven are closer to other JMJ groups but underwent the loss of representative domains. In addition, only four out of fourteen proteins show the presence of the RING domain typical of the KDM3 group (Figure 2). KDM4 JMJs present N-terminal JmjN (PF02375) and JmjC, and C-terminal C5HC2 (PF02928) (subgroup I) or C2H2 (PF00096) (subgroup II). In *Tks*, two proteins belong to subgroup I and three to subgroup II. Four proteins cluster with KDM5 JMJs and show the expected domain composition (Figures 1B and 2).

In addition, among *Tks*JMJs, several proteins revealed additional C-terminal domains (*Tks*JMJ19, *Tks*JMJ3, *Tks*JMJ16, and *Tks*JMJ26) or exceptionally long introns (*Tks*JMJ7) that likely derive from errors in genome annotation (Figure 2). In the JMJD6 group, *Tks*JMJ15 has the expected F-Box domain while *Tks*JMJ5, although clustering with *At*JMJ21, retains only the JmjC domain (Figures 1B and 2).

Seven HDMA5s were identified by our analysis (Table 1). *Tks*HDMA1, *Tks*HDMA7, and *Tks*HDMA4 are grouped with *At*HDMA4, 2, and 1, respectively (Figure S2). The above-mentioned proteins and *Tks*HDMA6 show the presence of SWIRM-NADB8-AOD domains (Figure 2). *Tks*HDMA2, *Tks*HDMA3, and *Tks*HDMA5 form a subgroup harbouring a SANT domain (Figures S2 and 2).

### 2.1.3. HATs

We identified 42 HATs in *Tks*. Most of them, 38, belong to the HAG group (Table 1). An expansion of HAGs compared to *At* was already observed in other species analysed so far such as *Medicago truncatula* [44], *Malus domestica* [26], *Solanum lycopersicum* [47], *Citrus sinensis* [48], and *Vitis vinifera* [49].

GCN5-type HAGs, *Tks*HAG36, and *Tks*HAG37 have a C-terminal Bromodomain similar to *At*HAG1. Three additional proteins clustering with *At*HAG1 are shorter and probably underwent loss of the Bromodomain: *Tks*HAG8 193 aa, *Tks*HAG33 250 aa, and *Tks*HAG34 192 aa (Figures 3A and 4 and Table S1).

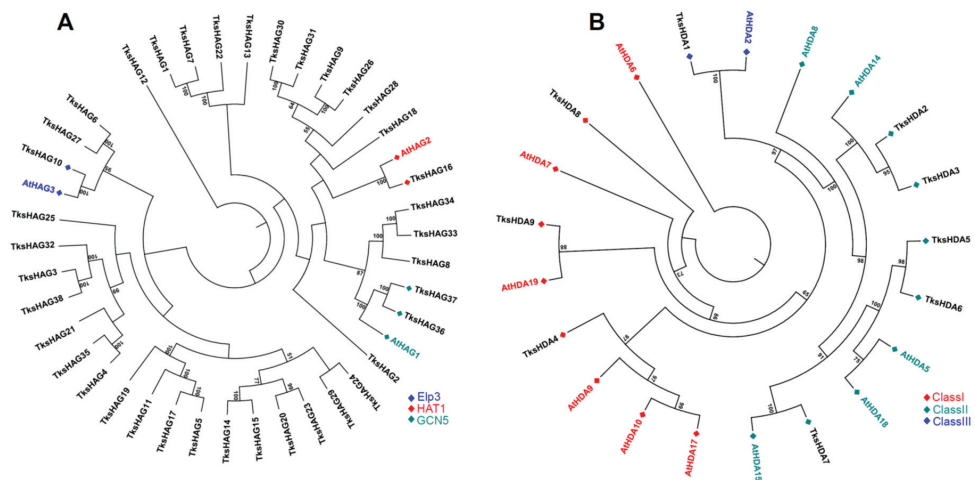


**Figure 3.** Phylogenetic tree of HAG (A) and HDA (B) proteins of *Taraxacum kok-saghyz* and *Arabidopsis thaliana* (in colour according to their respective classes). The numbers near the tree branches represent bootstrap values.

## TksHAGs

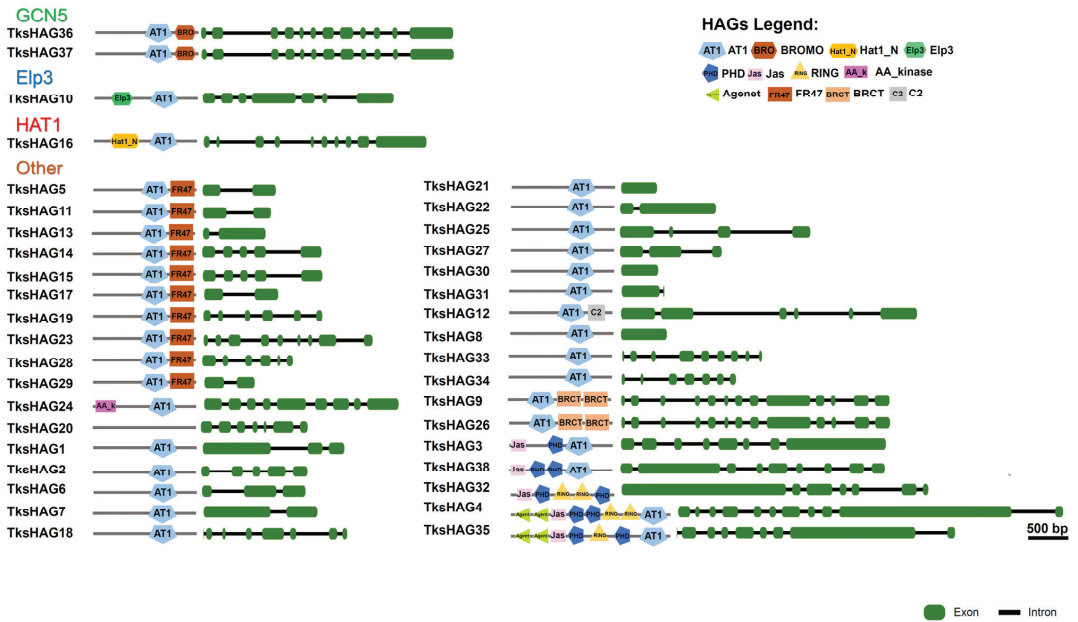


**Figure 4.** Domain composition and intron–exon structure of *Taraxacum kok-saghyz* HAGs.

*TksHAG16* clusters with *AtHAG2* and harbours the Hat1 domain. *TksHAG10* clusters with *AtHAG3* and harbours the ELP3 domain. Two additional proteins clustering with *AtHAG3*, *TksHAG27*, and *TksHAG6* show the AT1 domain alone (Figures 3A and 4). Furthermore, other AT1 domain-containing proteins can be observed.

A first group of seven proteins forms a definite cluster that is characterized by the presence of Jas and PHD domains except for two shorter proteins, probably derived from the others, that lost specific domains: *TksHAG21* and *TksHAG25*. In *TksHAG32*, the AT1 domain was not identified as below the threshold for SMART analysis (Figures 3A and 4).

Ten proteins are characterized by the presence of an additional FR47 domain at the C-terminal. Four of them, *TksHAG5*, *TksHAG11*, *TksHAG17*, and *TksHAG19* form a definite cluster. Instead, a second cluster includes *TksHAG14*, *TksHAG15*, *TksHAG23*, *TksHAG29*, and two additional proteins: *TksHAG20* where no domain was identified by SMART, and *TksHAG24*, where the FR47 domain is missing and there is an N-terminal AAK domain. Interestingly, *TksHAG13*, containing both AT1–FR47, do not cluster with the other FR47 domain-containing proteins (Figures 3A and 4).

Two proteins, *TksHAG9* and *TksHAG26* show two C-terminal BRCT domains and form a cluster with *TksHAG30* and *TksHAG31* that are shorter and without a BRCT domain. *TksHAG12* harbours AT1 and C2 domains. All other *TksHAG* proteins show the AT1 domain alone (Figures 3A and 4).

One MYST acetyltransferase was identified: *TksHAM1* with Chromo-C2H2-MYST-Syja\_N domain composition (Figure S3).

Two HACs identified in *Tks* have a TAZ-PHD-KAT11-ZZ-ZZ-TAZ domain composition, a third HAC, *TksHAC2*, lost the N-terminal TAZ domain and clusters with *AtHAC2* (Figures S3 and S4). No proteins showing the HAF domain were identified by our analysis.

#### 2.1.4. HDACs

We identified 18 histone deacetylases (Table 1). Nine are HDAs, three belong to class I, RPD3-like, five to class II, HDAC1-like, and one to class III, HDAC11-like. In class I, *TksHDA9*, clustering with *AtHDA19*, is a long protein (1634 aa) showing six additional N-terminal TPR domains probably resulting from exon gain or a defect in genome assembly/annotation. In the class II, *TksHDA7* similarly to *MtHDA8* [44] harbours an N-terminal Znf\_RBZ domain (Figures 3B and S5).

Four proteins are SRTs containing the SIR2 (PF02146) domain. Interestingly, with the exception of *TksSRT4*, all other SRTs have a double SIR2 domain (Figures S5 and S6).

Five *TksHDTs* were identified by BLASTp analysis (Table 1). The most conserved are *TksHDT1* and *TksHDT2* if compared with *AtHDTs*. *TksHDT1* showed a C2H2 domain. In *TksHDT5*, C2H2 modules are six (Figures S5 and S7). In plants, HD2-Types are related to cis–trans isomerases found in insects and yeast [30]. Similarly, their function as HDACs remains debatable.

### 2.2. In Silico Expression Analysis of HMG Genes in Different Organs and Developmental Stages

To shed light on the spatial expression of the HMGs in *Tks*, we analyzed publicly available datasets [9], based on the following tissues/organs: leaves, stems, the main root, and the lateral root in both young and mature stages (eight samples); latex and three additional samples from reproductive organs: flower, peduncle, and seeds. Expression patterns of HMGs were evaluated for each gene as log<sub>2</sub> fold change (Fc) compared to the average among samples. Hierarchical clustering was used to assess groups with similar expression patterns.

#### 2.2.1. HMTs

Among SDGs, a first group presents a peak of expression in young/mature leaves compared to other organs. Within this group, *TksSDG28* shows an additional peak in the latex. A second large group includes genes with higher expression in reproductive organs, mainly flowers and seeds. In group 3 we identified genes with higher expression in young organs and flowers. Group 4 shows higher expression in stem and roots with lower expression in the latex. The last group harbours the most expressed genes, showing an expression pattern primarily in mature roots (Figure 5).

*TksPRMTs* exhibit less modulated expression patterns. Three groups can be identified: the first with higher expression in latex and reproductive organs; the second with a peak in flowers; and the third group with higher expression in stem and roots. In the first group, *TksPRMT7* is the one showing the most abundant peak of expression in latex (Figure 5).

#### 2.2.2. HDMs

Among *TksJMs*, a first group includes genes with higher expressions in reproductive organs. In addition to that, *TksJM22* presents a relevant peak also in the latex, indicating a strong modulation compared to whole roots. A second group includes genes with a higher expression in stem-root and flower, and little expression in latex and leaf. The third group shows a higher expression in stem-root but, differently from most *JMs*, not in flower. This group includes *JMs* with high levels of expression. The fourth group shows a relevant expression in stem and flower (Figure 5).

All *HDMAs* exhibit higher expression in stem, flower, and seeds, with two groups that can be distinguished by high and low expression in mature root and latex (Figure 5).

#### 2.2.3. HATs

Four groups were identified among *TksHAGs*: a first one with peaks in the roots (mainly in mature roots); a second group predominantly in reproductive organs; a third with the same pattern with addition of leaves; and interestingly, the fourth group is made of highly expressed genes showing a peak in the latex similarly to the single *HAM* gene detected by our analysis. *HACs* are less expressed in leaves and latex (Figure 6).

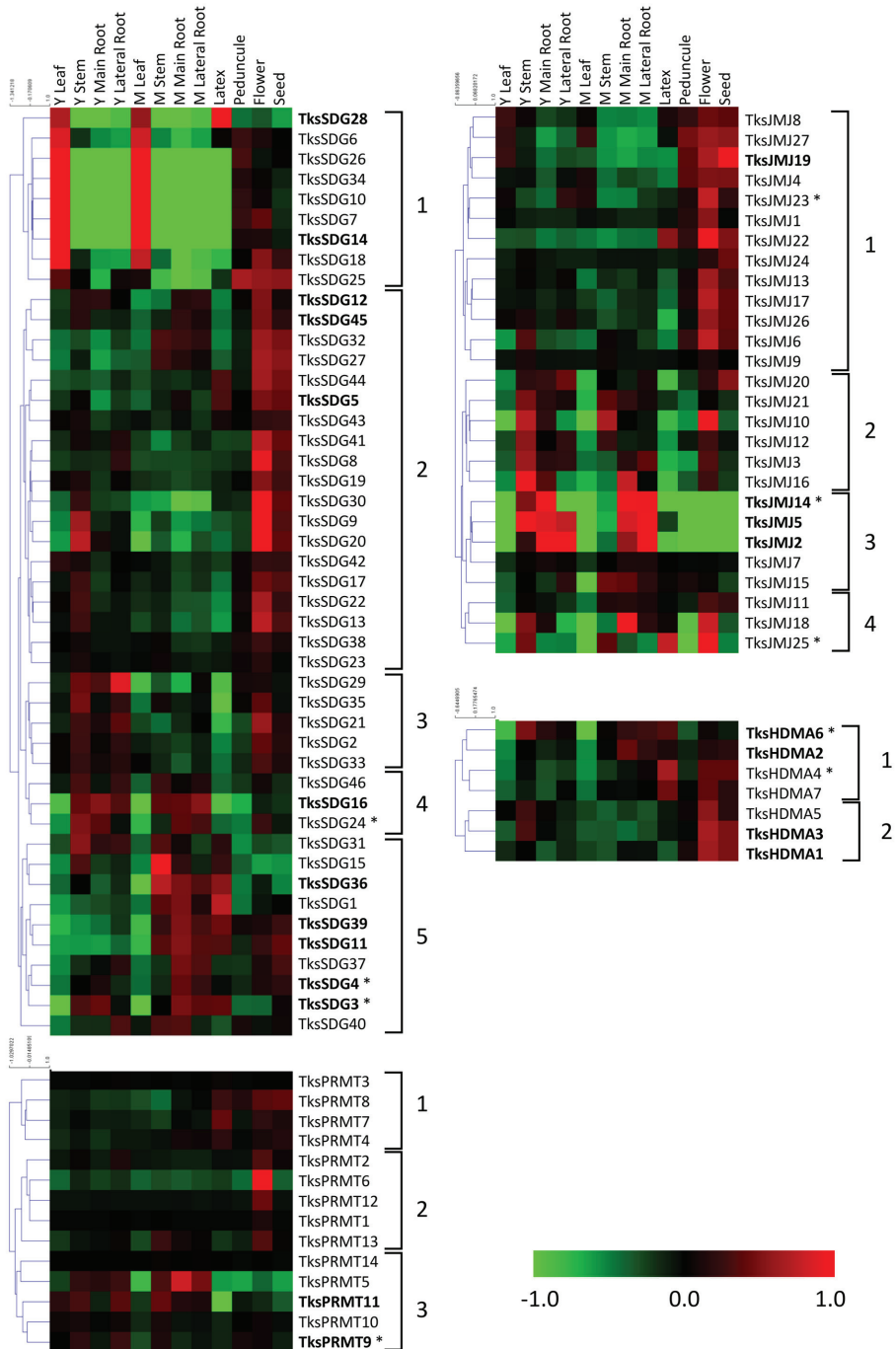


**Figure 5.** Heat map of *TksHMTs* and *TksHDMs* in different organs and developmental stages. The main clusters are indicated by square brackets. Genes with higher expression are indicated in bold. Asterisks indicate the genes analyzed by qPCR.

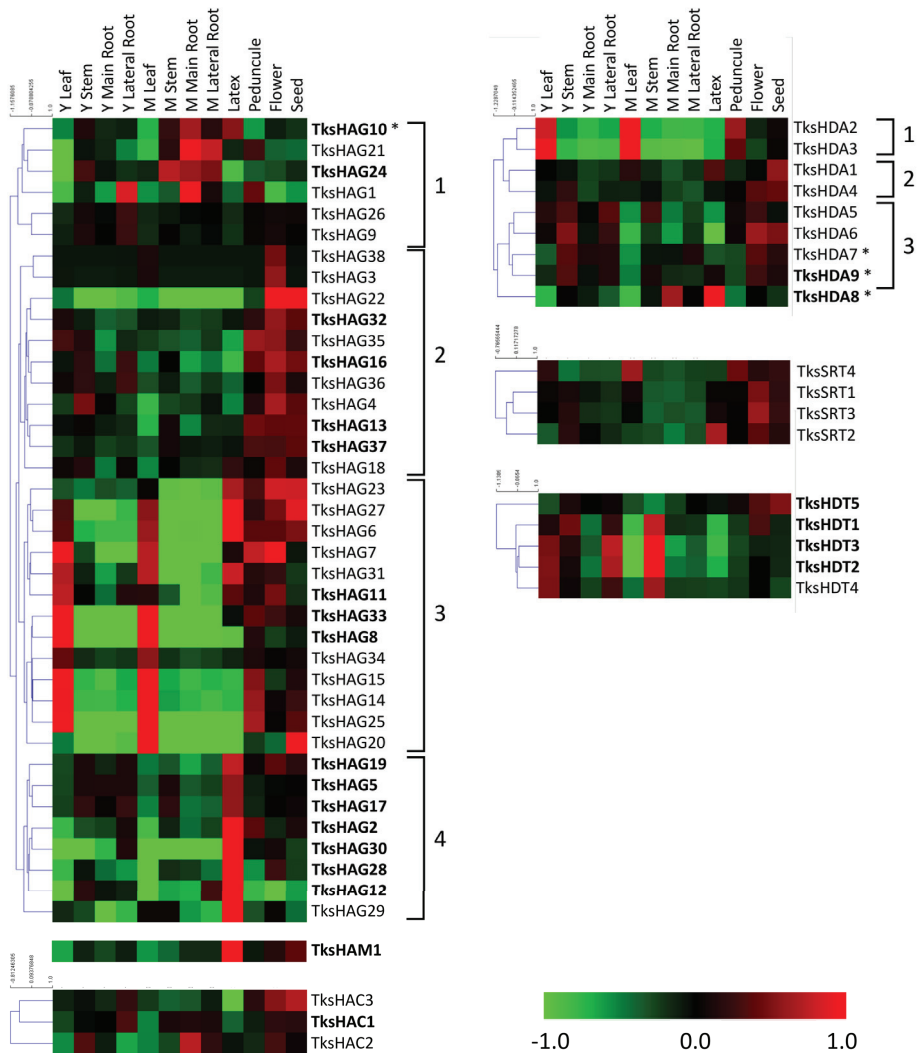


**Figure 6.** Heat map of *TksHATs* and *TksHDACs* in different organs and developmental stages. The main clusters are indicated by square brackets. Genes with a higher expression are indicated in bold. Asterisks indicate the genes analysed by qPCR.

### 2.2.4. HDACs

*TksHDAs* can be divided into three groups: a first one with peaks of expression in leaves and peduncle; a second group with lower levels in the roots; and a third group more relevant in young and reproductive organs. *TksHDA8* shows a peculiar pattern with peaks in the main root and latex. *TksSRTs* were present in reproductive organs with *TksSRT4* and *TksSRT2* having an additional peak in mature leaf and in the latex, respectively. *HDTs*, instead, show peaks of expression in young leaf, stem, lateral root, and in the mature stem with the exception of *TksHDT5*, which shows peaks in reproductive organs.

### 2.3. HMGs Expression

Using the absolute quantification method, we measured the expression of 13 different *Tks*HMGs belonging to four families in four different tissues: developing leaves (DL), fully developed leaves (FL), root tips (RT), and mature roots (R). Figure 7 shows the spatial gene expression pattern of four HMTs (*TksSDG3*, *TksSDG4*, *TksSDG24*, and *TksPRMT9*), five HDMs (*TksJM14*, *TksJM23*, *TksJM25*, *TksHDMA4*, and *TksHDMA6*), one HAT (*TksHAG10*), and three HDACs (*TksHDA7*, *TksHDA8*, and *TksHDA9*). Five genes (*TksHDMA4*, *TksHDA9*, *TksHDMA6*, *TksJM23*, and *TksHAG10*) have at least one tissue expression level higher than 1 femtogram (fg)/ $\mu$ L (Figure 7a). The most expressed gene is *TksHDMA4*, with an average tissue quantification of 6 fg/ $\mu$ L but no significative modulation between the different tissues. Among the remaining eight genes, *TksSDG3* and *TksJM25* expressions never exceed 0.1 fg/ $\mu$ L (Figure 7b). With an average tissue quantification of 0.05 and 0.01 fg/ $\mu$ L, respectively, they are the lowest expressed HMG genes. Overall, there is no difference of global HMG gene expression between the four different tissues analyzed, with an average expression of 1.38 and 1.29 fg/ $\mu$ L in fully developed leaves (FL) and the root (R), respectively. *TksJM25* and *TksHDA8* expression increased significantly, 319 and 174%, respectively, in FL in comparison to DL. *TksHAG10*, *TksSDG24*, and *TksPMRT9* are up-regulated in a less strong way. The remaining eight genes confirm an FL up-regulation with respect to DL; however, below a 50% change. *TksSDG4*, *TksHDA8*, and *TksSDG3* expression increased clearly with a 276, 249, and 104%, respectively, in R compared to RT. *TksHDA7* and *TksHAG10* are up-regulated by 85 and 56%. As for leaves, all eight remaining genes are up-regulated in R tissue in comparison to RT with a percentage below 50%.

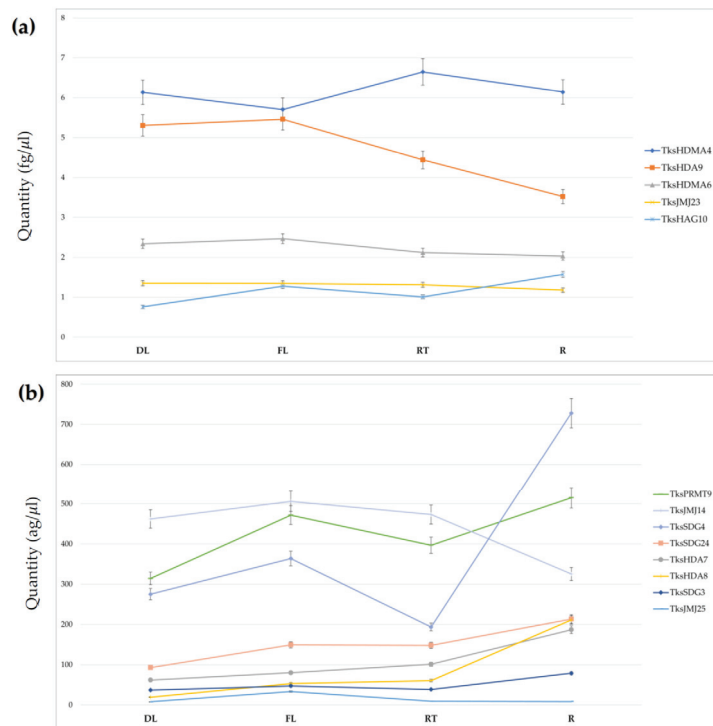


**Figure 7.** qPCR expression analysis of 13 HM genes in *Taraxacum kok-saghyz* developing leaves (DL), fully developed leaves (FL), root tips (RT), and mature roots (R). (a) Absolute quantification (mean  $\pm$  SD fg/ $\mu$ L) of HM genes with an average expression above 1 fg/ $\mu$ L; (b) Absolute quantification (mean  $\pm$  SD ag/ $\mu$ L) of HMG genes with an average expression below 1 fg/ $\mu$ L.

### 3. Discussion

#### 3.1. HMG Members in *Taraxacum Kok-Saghyz*

Natural rubber represents a biopolymer of major importance due to its wide properties that cannot be found in synthetic material, including resilience, elasticity, and abrasion [50]. The demands to develop new sources of natural rubbers have quickly increased over the years due to the constant reductions of petroleum-based materials and the efforts towards renewables [3]. Currently, the main resource for commercial natural rubber, *Hevea brasiliensis*, has generated major concerns because of its high sensitivity towards pathogen infections [51]. Furthermore, latex can induce several allergic reactions due to their protein content [52]. As an alternative to *H. Brasiliensis*, two plant species are so far known to produce rubber in similar amounts and a high molecular weight: *Parthenium argentatum* Gray, also known as guayule, and *Taraxacum kok-saghyz*, the Russian dandelion [53]. *Tks* latex, for instance, is broadly investigated for non-medical applications such as tire production [54].

In *Tks*, rubber biosynthesis occurs through different pathways that are responsible for NR chain elongation, small rubber particles (SRPPs), and rubber elongation factors, respectively [7]. Therefore, to improve rubber quality and quantity, it becomes paramount to functionally characterize the genes involved in those pathways.

Histone modifications are well established to control gene expression [15]. Thus, they represent a promising strategy to manipulate different signalling pathways, unlike the gene-by-gene approach [55].

In this study, we presented for the first time a comprehensive analysis of the HMGs in *Tks*, identified by the presence of representative domains recognized through their hidden Markov profiles. HMGs sequences and/or composition were compared with the model species *A. thaliana* and *M. truncatula*, as well as the close relative *L. sativa*.

Overall, the identification recorded an increase in the number of HMG genes in *Tks* (154) compared to *A. thaliana* (102), which is similar to what is observed in *L. sativa* and *M. truncatula*. Due to limitations in the assembly, it was not possible to assess gene duplication.

A closer investigation revealed that such an increase did not occur on all the HMG classes, but it was indeed specific. Thus, while HDMs were similar in numbers (34 in *Tks* vs. 24 in Arabidopsis), HATs were predominantly higher in the former (42) than in the latter (12). This is not necessarily surprising, as an expansion of HAGs was already revealed in other crops when compared to Arabidopsis (Table 1) [44].

Among the HMTs family, analyses on *Tks* indicated the presence of 46 genes encoding for SDGs, a similar number to those of lettuce and Arabidopsis. Instead, the PRMTs were doubled up in *Tks* compared to the other species. Overall, the *Tks* SDGs showed a similar structure to those already annotated with SANT-CXC-SET domains except for *Tks*SGD8 that showed a shorter structure (Figure 2). SANT domains are essential to ensure histone substrates for the SGD enzymatic activity [56], while the CXC allows binding to RNA molecules as the SET represents the signature domain to cluster the SDGs [57,58]. *Tks*SDG5 appears to be much longer than the other SDGs, perhaps due to fusion between two different proteins (Figure 2). The presence of a bag6-A domain could implicate a divergent function among the other SDGs, including a possible interaction with heat shock proteins [59]. A functional study is therefore required to address this question.

Deeper investigation on the PRMTs indicated that *Tks*PRMT2, 7, and 8 contained two PRMT domains whilst the majority had only one. Structural analyses combined with domain deletion could retrieve more information on that regard.

*Tks* HDMs were classified in JMJs and HDMAs. Interestingly, many JMJ-only clustered with the KDM3 groups although they lacked the additional RING domain (Figure 5). However, they all presented a very extensive introns and exons structure that is typical of the KDM3s [60].

Over 90% of *Tks* HATs belonged to the HAG group. Similar to previous reports [48], the majority of the members contained only the AT1 protein domain (Figure 4). Whilst *Tks*HAG36 and 37 were identified as GCN5 likes due to the presence of the bromodomain, others included Jas and PhD domains or the FR47, or the BRCT domain in combination with

AT1. This appears to be quite divergent from the canonical HAGs structure, suggesting a novel class of HMG HATs in *Tks*. Indeed, Jas domains are present in JASMONATE ZIM-domain (JAZ) proteins that are repressors of jasmonate (JA) signalling [61]. FR47 domain resembles the C-terminal region of the *Drosophila melanogaster* hypothetical protein FR47. Interestingly, a member of the HATs in *Plasmodium falciparum* also contains that domain, suggesting a class of acetyltransferases targeting nonhistone proteins [62].

Our approach identified 18 HDACs in *Tks*. The three classes showed numbers comparable to Arabidopsis (Figure S5). Interestingly, *TksHDA9*, which shows similarities with *AtHDA19*, appears to have additional domains. *AtHDA19* is a major regulator of development and growth [41,63]. Whether *TksHDA9* has developed similar functions remains to be assessed.

### 3.2. In Silico and Spatial Analysis of HMGs in *Tks* Tissues Identified Putative Regulators of NR Biosynthesis

Histone modifications are well known to regulate important functions in plants [15], but very little is known about their expression patterns and behaviour in *Tks*. To unveil new roles for the HMGs, we took advantage of publicly available datasets in *Tks* and measured their mRNA levels as fold-change normalized to the average amounts. Among the different tissues analyzed, latex represented the most interesting as it is directly connected to natural rubber production. Indeed, the biosynthesis of NR occurs in the latex of laticifers, organized in rubber particles [64]. Within the SDG class VI, *TksSDG28* presented a distinct expression in latex (Figure 5). Instead, *TksSDG3* and 4 showed an abundant level of transcripts in young leaves and roots. Interestingly, *TksSDG4* was more abundant in roots, whilst *TksSDG3* showed similar levels in both tissues. The Arabidopsis *TksSDG3* homolog, SWINGER, is part of a large protein complex that includes VRN2 (VERNALIZATION 2) and VIN3 (VERNALIZATION INSENSITIVE 3), together with FERTILIZATION INDEPENDENT ENDOSPERM (FIE) and CURLY LEAF (CLF). They are responsible for establishing FLC (FLOWERING LOCUS C) repression during vernalization [65]. Notably, the *TksSDG4* homolog in Arabidopsis is ATXR7 that instead promotes H3K4me3 on the FLC locus, hence its transcriptional activation [66]. A similar function is associated with *AtSDG8*, a homolog of *TksSDG24* [67]. Whether their function is indeed conserved in *Tks* and is based on tissue specificity remains to be assessed.

Heatmaps for *Tks* PRMTs did not show major modulations among tissues, with the exception for *TksPRMT9* and *TksPRMT11* that portrayed an elevated expression in young leaves (Figure 5). Real time qPCR analyses of some of the indicated genes revealed a tendency towards root samples. Interestingly, *TksSDG4* was expressed primarily in mature roots and *TksPMRT9* showed major peaks in fully developed leaves as well as roots, making them interesting targets for a functional approach (Figure 7b).

In silico expression of the histone demethylases revealed a predominance on the reproductive tissues (Figure 5). However, *TksJM14* showed a preferential expression in roots. Our qRT-PCR data showed instead that levels were different between root tips and adult roots, suggesting a modulation associated with plant development. Furthermore, it is important to highlight that, while mature roots contain laticifers already producing rubber, in the root tips the laticifers are still developing. Therefore, our qPCR analysis presents dual significance: first, it identifies putative HMGs involved in regulating the expression of genes related to rubber or laticifers production; second, the comparison between the expression in leaves and roots is pivotal to distinguish between overall growth and rubber-specific mechanisms. The analysis of other two JMJs *TksJM23*, a homolog of Arabidopsis ELF6 [67] and *TksJM25*, confirmed in silico results as none of them were modulated but instead they showed similar expression levels among the analyzed tissues (Figure 7a,b). A similar pattern was observed for the HDMAs, where only *TksHDMA4* turned out to be the most abundant among the analyzed genes. Interestingly, the heatmaps showed a major expression in the latex tissue.

Heatmaps for histone acetyltransferases indicated only a few HATs were expressed in root tissues, whilst the group 3 was majorly present in young and mature leaves (Figure 6). We focused our attention on *TksHAG10* that indeed showed to be mostly abundant in roots (Figure 7a). Interestingly, our qPCR data also showed a peak in fully developed leaves that was not observed in the datasets analysis. However, the plant material used in the datasets experiment might not fully correspond to the one obtained for expression analysis.

Among the histone deacetylases, *TksHDA9* was the most expressed within the family (Figure 7a). Interestingly, *TksHDA9* revealed a drop in expression between leaves and roots, while *TksHDA8* was instead more abundant in mature roots. It will be interesting to assess whether *TksHDA9* action is counteracted by histone acetyltransferases GCN5-likes.

## 4. Materials and Methods

### 4.1. Plant Material

A *Tks* plant belonging to the W6-35166 population obtained from USDA-ARS (Regional Plant Introduction Station, 295 CLARK HALL, WSU Pullman, WA 99164, Washington State University, USA) was grown and clonally propagated from root cuttings. Fully developed clones have been cultivated in trays filled with topsoil under controlled conditions (12/12 light cycle, 20 °C) for three weeks, then transplanted in 85 × 39 × 34 cm rectangular pots, 8 plants each. Potted plants were cultivated from January to November 2021 under near natural conditions for photoperiod, temperature, humidity, and exposure to atmospheric events, in ENEA Trisaia Research Center (40°09′47.4″ N 16°38′00.1″ E, Italy). Plants were supplemented with fertilisers, treated against pests and fungal pathogens, and shaded during summer. Four different tissues have been harvested and snap-frozen in liquid nitrogen: developing leaves, fully developed leaves, root tips, and mature roots.

### 4.2. In Silico Identification and Analysis of HMG Loci

To identify HMGs loci, the hidden Markov profiles of each gene family were used as a query input for the HMM software against the protein subject datasets of *Taraxacum kok-saghyz* and *Lactuca sativa* [9]. Since for the HDT family no PFAM domain is available, we used *Arabidopsis* HDTs as query input for BLASTp searches against the protein datasets. The identified loci were analysed with the SMART software to characterise the domain composition [68,69]. The cases pointing to two different domains for the same protein region were resolved based on the domain that was associated to the smaller E-value. The intron/exon structures were graphically represented with GSDS 2.0 [70].

### 4.3. Phylogenetic Analysis

The HM protein families identified in this work from *Taraxacum kok-saghyz* genome annotation database [9] along with HM proteins from *Arabidopsis* were aligned using ClustalW program in CLC Genomics Workbench version 9.5.2 (Qiagen, Hilden, Germany). A phylogenetic tree was then constructed using a neighbor-joining algorithm and Kimura protein substitution model. Reliability of the internal branching was obtained by a bootstrap test of 1000 replicates.

Collinearity analysis was performed using MCSCANX [71]. In brief, *Taraxacum* proteins were searched for sequence homology using BLASTp [72] according to McScanX default settings. Collinear blocks were identified by McSCANX with default settings and sequence duplication were classified with the duplicate gene classifier tool integrated in the McSCANX suite. Protein of duplicated HMG were aligned with ClustalO [73] and codon-based alignments were obtained with PRANK software [74]. The synonymous and non-synonymous substitution patterns were calculated with PAML [75] using YN00 procedure [76].

### 4.4. Transcriptome Analysis

RNA reads included in project PRJCA000437 were downloaded from the National Genomics Data Center (NGDC), part of the China National Center for Bioinformatics

(CNGB) and quality checked using Trimmomatic [77] according to Corchete et al. (2020) [78]. The reads were then aligned to the *Tks* indexed genome using STAR [79] with default settings. HTSeq-count script [80] was used to determine raw counts for each feature and experiment. The raw count matrix was normalised using edgeR and TMM method [78,81].

#### 4.5. RNA Extraction, cDNA Synthesis, and Gene Expression Analysis

Total RNA from the above-mentioned plant material was extracted using innuPREP Plant RNA Kit (Analytik, Jena, Germany) according to the manufacturer's protocol. RNA quality and concentration were estimated by Nanodrop™ 1000 Spectrophotometer (Thermo Fisher Scientific Waltham, MA, USA). A total of 1 µg of total RNA was used for cDNA synthesis using SuperScript IV kit (ThermoFisher Waltham, MA, USA) with oligo(dT)<sub>20</sub> as primers in a 20 µL final volume. Primer pairs for SYBR-Green based qPCR have been designed for each candidate gene using Geneious Prime 2022.1.1 (<https://www.geneious.com>). Each primer has been subjected to off-target analysis using local BLAST-2.11.0+ [72,82,83] against the *Taraxacum kok-saghyz* genome annotation [9] downloaded from <https://ngdc.cncb.ac.cn/gwh/>. Pairs with both forward and reverse primers matching an off-target transcript were rejected. Primer sequences are reported in Supplementary Table S2. qPCR was performed using an ABI Prism 7900HT instrument (Applied Biosystems, Waltham, MA, USA) and Platinum SYBR Green qPCR SuperMix-UDG with ROX (ThermoFisher, Waltham, MA, USA) following manufacturer's instructions. Reactions were performed in two technical replicates on three biological replicates. The following cycling conditions were used for quantitative PCR: 5 min at 95 °C followed by 45 cycles at 95 °C for 15 s and at 58 °C for 60 s. Melting curve analysis from 60 to 90 °C was performed to monitor the specificity of the amplification. mRNA levels of each genes analysed were calculated using absolute quantification based on the standard curve method [84] as reported by D'Amelia et al., (2014) [85] expect for standard curves obtained by purified and quantified conventional PCR normalised to a concentration of 33 pg/µL and 10-fold serial dilutions (ranging from 10<sup>2</sup> to 10<sup>8</sup>). Expression data were analysed using Tukey's pairwise test.

**Supplementary Materials:** The following supporting information can be downloaded at: <https://www.mdpi.com/article/10.3390/plants11162077/s1>, Figure S1: Phylogenetic tree of PRMT proteins of *Taraxacum kok-saghyz* and *Arabidopsis* (in bold). The numbers near the tree branches. Figure S2: Phylogenetic tree of HDMA proteins of *Taraxacum kok-saghyz* and *Arabidopsis* (in bold). The numbers near the tree branches represent bootstrap values. Figure S3: Domain composition and intron–exon structure of *Taraxacum kok-saghyz* HAMs and HACs. Figure S4: Phylogenetic tree of HAC proteins of *Taraxacum kok-saghyz* and *Arabidopsis* (in bold). The numbers near the tree branches represent bootstrap values. Figure S5: Domain composition and intron–exon structure of *Taraxacum kok-saghyz* HDAs, SRTs, and HDTs. Figure S6: Phylogenetic tree of SRT proteins of *Taraxacum kok-saghyz* and *Arabidopsis* (in bold). The numbers near the tree branches represent bootstrap values. Figure S7: Phylogenetic tree of PRMT proteins of *Taraxacum kok-saghyz* and *Arabidopsis* (in bold). The numbers near the tree branches represent bootstrap values. Table S1: List of *T. kok-saghyz* HMGs. Table S2: Primer list. Table S3: Pairs of putative duplicated HM genes in the *Tks* genome. Table S4: Tukey's pairwise test

**Author Contributions:** Conceptualization, F.P., L.L. and G.P.; methodology, F.P., L.L., A.P., E.F. and L.D.; validation, C.F. and P.F.; writing—review and editing, F.P., C.F., L.L., A.P., P.F., E.F., L.D. and G.P. All authors have read and agreed to the published version of the manuscript.

**Funding:** This research was partly funded by University of Sassari (FAR 2020 to AP).

**Institutional Review Board Statement:** Not applicable.

**Informed Consent Statement:** Not applicable.

**Data Availability Statement:** RNAseq reads archived as part of the PRJCA000437 bioproject were downloaded from <https://ngdc.cncb.ac.cn/search/?dbId=gwh&q=%20PRJCA000437> (accessed at 15 May 2022) which is included in the CNGB/NGDC genome warehouse.

**Acknowledgments:** We would like to thank USDA-ARS (Regional Plant Introduction Station, Washington State University, USA for donating the *Tks* population used in this study and National Genomics Data Center (NGDC), part of the China National Center for Bioinformation (CNCB) for making publicly available the RNA reads from *Taraxacum* RNAseq. Graphical abstract was created with [Biorender.com](https://biorender.com).

**Conflicts of Interest:** The authors declare no conflict of interest.

## References

- Sharifi-Rad, M.; Roberts, T.H.; Matthews, K.R.; Bezerra, C.F.; Morais-Braga, M.F.B.; Coutinho, H.D.M.; Sharopov, F.; Salehi, B.; Yousaf, Z.; Sharifi-Rad, M.; et al. Ethnobotany of the Genus *Taraxacum*—Phytochemicals and Antimicrobial Activity. *Phytother. Res.* **2018**, *32*, 2131–2145. [[CrossRef](#)]
- Schütz, K.; Carle, R.; Schieber, A. *Taraxacum*-A Review on Its Phytochemical and Pharmacological Profile. *J. Ethnopharmacol.* **2006**, *107*, 313–323. [[CrossRef](#)]
- Van Beilen, J.B.; Poirier, Y. Establishment of New Crops for the Production of Natural Rubber. *Trends Biotechnol.* **2007**, *25*, 522–529. [[CrossRef](#)]
- Kirschner, J.; Štěpánek, J.; Černý, T.; De Heer, P.; van Dijk, P.J. Available Ex Situ Germplasm of the Potential Rubber Crop *Taraxacum Koksaghyz* Belongs to a Poor Rubber Producer, *T. Brevicorniculatum* (Compositae-Crepidinae). *Genet. Resour. Crop Evol.* **2013**, *60*, 455–471. [[CrossRef](#)]
- Mooibroek, H.; Cornish, K. Alternative Sources of Natural Rubber. *Appl. Microbiol. Biotechnol.* **2000**, *53*, 355–365. [[CrossRef](#)]
- Zhang, Y.; Iaffaldano, B.J.; Xie, W.; Blakeslee, J.J.; Cornish, K. Rapid and Hormone-Free Agrobacterium Rhizogenes-Mediated Transformation in Rubber Producing Dandelions *Taraxacum Kok-Saghyz* and *T. Brevicorniculatum*. *Ind. Crops Prod.* **2015**, *66*, 110–118. [[CrossRef](#)]
- Panara, F.; Lopez, L.; Daddiego, L.; Fantini, E.; Facella, P.; Perrotta, G. Comparative Transcriptomics between High and Low Rubber Producing *Taraxacum Kok-Saghyz* R. Plants. *BMC Genom.* **2018**, *19*, 875. [[CrossRef](#)]
- Yamashita, S.; Takahashi, S. Molecular Mechanisms of Natural Rubber Biosynthesis. *Annu. Rev. Biochem.* **2020**, *89*, 821–851. [[CrossRef](#)]
- Lin, T.; Xu, X.; Ruan, J.; Liu, S.; Wu, S.; Shao, X.; Wang, X.; Gan, L.; Qin, B.; Yang, Y.; et al. Genome Analysis of *Taraxacum Kok-Saghyz* Rodin Provides New Insights into Rubber Biosynthesis. *Natl. Sci. Rev.* **2018**, *5*, 78–87. [[CrossRef](#)]
- Junkong, P.; Ikeda, Y. 7—Properties of Natural Rubbers from Guayule and Rubber Dandelion. In *Chemistry, Manufacture, and Application of Natural Rubber*, 2nd ed.; Kohjiya, S., Ikeda, Y., Eds.; Woodhead Publishing in Materials; Woodhead Publishing: Sawston, UK, 2021; pp. 177–201, ISBN 978-0-12-818843-9.
- Chadwick, M.; Trewin, H.; Gawthrop, F.; Wagstaff, C. Sesquiterpenoids Lactones: Benefits to Plants and People. *Int. J. Mol. Sci.* **2013**, *14*, 12780–12805. [[CrossRef](#)]
- Arias, M.; Herrero, J.; Ricobaraza, M.; Hernández, M.; Ritter, E. Evaluation of Root Biomass, Rubber and Inulincontents in Nine *Taraxacum Koksaghyz* Rodin Populations. *Ind. Crops Prod.* **2016**, *83*, 316–321. [[CrossRef](#)]
- Esatbeyoglu, T.; Obermair, B.; Dorn, T.; Siems, K.; Rimbach, G.; Birringer, M. Sesquiterpene Lactone Composition and Cellular Nrf2 Induction of *Taraxacum Officinale* Leaves and Roots and Taraxinic Acid  $\beta$ -d-Glucopyranosyl Ester. *J. Med. Food* **2017**, *20*, 71–78. [[CrossRef](#)]
- Perrella, G.; Kaiserli, E. Light behind the Curtain: Photoregulation of Nuclear Architecture and Chromatin Dynamics in Plants. *New Phytol.* **2016**, *212*, 908–919. [[CrossRef](#)]
- Perrella, G.; Bäurle, I.; van Zanten, M. Epigenetic Regulation of Thermomorphogenesis and Heat Stress Tolerance. *New Phytol.* **2022**, *234*, 1144–1160. [[CrossRef](#)]
- Bannister, A.J.; Kouzarides, T. Regulation of Chromatin by Histone Modifications. *Cell Res.* **2011**, *21*, 381–395. [[CrossRef](#)]
- Kouzarides, T. Chromatin Modifications and Their Function. *Cell* **2007**, *128*, 693–705. [[CrossRef](#)]
- Barneche, F.; Malapeira, J.; Mas, P. The Impact of Chromatin Dynamics on Plant Light Responses and Circadian Clock Function. *J. Exp. Bot.* **2014**, *65*, 2895–2913. [[CrossRef](#)]
- Liu, S.; de Jonge, J.; Trejo-Arellano, M.S.; Santos-González, J.; Köhler, C.; Hennig, L. Role of H1 and DNA Methylation in Selective Regulation of Transposable Elements during Heat Stress. *New Phytol.* **2021**, *229*, 2238–2250. [[CrossRef](#)]
- Baumbusch, L.O.; Thorstensen, T.; Krauss, V.; Fischer, A.; Naumann, K.; Assalkhou, R.; Schulz, I.; Reuter, G.; Aalen, R.B. The Arabidopsis Thaliana Genome Contains at Least 29 Active Genes Encoding SET Domain Proteins That Can Be Assigned to Four Evolutionarily Conserved Classes. *Nucleic Acids Res.* **2001**, *29*, 4319–4333. [[CrossRef](#)]
- Zhao, Z.; Shen, W.H. *Plants Contain a High Number of Proteins Showing Sequence Similarity to the Animal SUV39H Family of Histone Methyltransferases*; New York Academy of Sciences: New York, NY, USA, 2004; Volume 1030, pp. 661–669.
- Ng, D.W.-K.; Wang, T.; Chandrasekharan, M.B.; Aramayo, R.; Kertbundit, S.; Hall, T.C. Plant SET Domain-Containing Proteins: Structure, Function and Regulation. *Biochim. Biophys. Acta* **2007**, *1769*, 316. [[CrossRef](#)]
- Ahmad, A.; Dong, Y.; Cao, X. Characterization of the PRMT Gene Family in Rice Reveals Conservation of Arginine Methylation. *PLoS ONE* **2011**, *6*, e22664. [[CrossRef](#)] [[PubMed](#)]

24. Luo, M.; Hung, F.-Y.; Yang, S.; Liu, X.; Wu, K. Histone Lysine Demethylases and Their Functions in Plants. *Plant Mol. Biol. Rep.* **2014**, *32*, 558–565. [\[CrossRef\]](#)
25. Schneider, J.; Shilatfard, A. Histone Demethylation by Hydroxylation: Chemistry in Action. *ACS Chem. Biol.* **2006**, *1*, 75–81. [\[CrossRef\]](#) [\[PubMed\]](#)
26. Fan, S.; Wang, J.; Lei, C.; Gao, C.; Yang, Y.; Li, Y.; An, N.; Zhang, D.; Han, M. Identification and Characterization of Histone Modification Gene Family Reveal Their Critical Responses to Flower Induction in Apple. *BMC Plant Biol.* **2018**, *18*, 173. [\[CrossRef\]](#) [\[PubMed\]](#)
27. Yamaguchi, N. Removal of H3K27me3 by JMJ Proteins Controls Plant Development and Environmental Responses in Arabidopsis. *Front. Plant Sci.* **2021**, *12*, 1212. [\[CrossRef\]](#) [\[PubMed\]](#)
28. Klose, R.J.; Zhang, Y. Regulation of Histone Methylation by Demethylination and Demethylation. *Nat. Rev. Mol. Cell Biol.* **2007**, *8*, 307–318. [\[CrossRef\]](#)
29. Asensi-Fabado, M.-A.; Amtmann, A.; Perrella, G. Plant Responses to Abiotic Stress: The Chromatin Context of Transcriptional Regulation. *Biochim. Biophys. Acta—Gene Regul. Mech.* **2017**, *1860*, 106–122. [\[CrossRef\]](#)
30. Pandey, R.; Müller, A.; Napoli, C.A.; Selinger, D.A.; Pikaard, C.S.; Richards, E.J.; Bender, J.; Mount, D.W.; Jorgensen, R.A. Analysis of Histone Acetyltransferase and Histone Deacetylase Families of Arabidopsis Thaliana Suggests Functional Diversification of Chromatin Modification among Multicellular Eukaryotes. *Nucleic Acids Res.* **2002**, *30*, 5036–5055. [\[CrossRef\]](#)
31. Servet, C.; Conde e Silva, N.; Zhou, D.-X. Histone Acetyltransferase AtGCN5/HAG1 Is a Versatile Regulator of Developmental and Inducible Gene Expression in Arabidopsis. *Mol. Plant* **2010**, *3*, 670–677. [\[CrossRef\]](#)
32. Tahir, M.S.; Tian, L. HD2-Type Histone Deacetylases: Unique Regulators of Plant Development and Stress Responses. *Plant Cell Rep.* **2021**, *40*, 1603–1615. [\[CrossRef\]](#)
33. Yruela, I.; Moreno-Yruela, C.; Olsen, C.A. Zn<sup>2+</sup>-Dependent Histone Deacetylases in Plants: Structure and Evolution. *Trends Plant Sci.* **2021**, *26*, 741–757. [\[CrossRef\]](#) [\[PubMed\]](#)
34. Luo, M.; Liu, X.; Singh, P.; Cui, Y.; Zimmerli, L.; Wu, K. Chromatin Modifications and Remodeling in Plant Abiotic Stress Responses. *Biochim. Biophys. Acta—Gene Regul. Mech.* **2012**, *1819*, 129–136. [\[CrossRef\]](#)
35. Kim, D.; Perrea, G.; Trapnell, C.; Pimentel, H.; Kelley, R.; Salzberg, S.L. TopHat2: Accurate Alignment of Transcriptomes in the Presence of Insertions, Deletions and Gene Fusions. *Genome Biol.* **2013**, *14*, R36. [\[CrossRef\]](#)
36. Tanaka, M.; Kikuchi, A.; Kamada, H. The Arabidopsis Histone Deacetylases HDA6 and HDA19 Contribute to the Repression of Embryonic Properties after Germination. *Plant Physiol.* **2008**, *146*, 149–161. [\[CrossRef\]](#) [\[PubMed\]](#)
37. Krogan, N.T.; Hogan, K.; Long, J.A. APETALA2 Negatively Regulates Multiple Floral Organ Identity Genes in Arabidopsis by Recruiting the Co-Repressor TOPLESS and the Histone Deacetylase HDA19. *Dev. Camb.* **2012**, *139*, 4180–4190. [\[CrossRef\]](#)
38. De Rooij, P.G.H.; Perrella, G.; Kaiserli, E.; van Zanten, M. The Diverse and Unanticipated Roles of Histone Deacetylase 9 in Coordinating Plant Development and Environmental Acclimation. *J. Exp. Bot.* **2020**, *71*, 6211–6225. [\[CrossRef\]](#) [\[PubMed\]](#)
39. Van Der Woude, L.C.; Perrella, G.; Snoek, B.L.; Van Hoogdalem, M.; Novák, O.; Van Verk, M.C.; Van Kooten, H.N.; Zorn, L.E.; Tonckens, R.; Dongus, J.A.; et al. HISTONE DEACETYLASE 9 Stimulates Auxin-Dependent Thermomorphogenesis in Arabidopsis Thaliana by Mediating H2A.Z Depletion. *Proc. Natl. Acad. Sci. USA* **2019**, *116*, 25343–25354. [\[CrossRef\]](#)
40. Shen, R.; Tao, L.; Yang, B. Techno-Economic Analysis of Jet-Fuel Production from Biorefinery Waste Lignin. *Biofuels Bioprod. Biorefining* **2019**, *13*, 486–501. [\[CrossRef\]](#)
41. Jing, Y.; Guo, Q.; Lin, R. The SNL-HDA19 Histone Deacetylase Complex Antagonizes HY5 Activity to Repress Photomorphogenesis in Arabidopsis. *New Phytol.* **2021**, *229*, 3221–3236. [\[CrossRef\]](#)
42. Chen, L.T.; Wu, K. Role of Histone Deacetylases HDA6 and HDA19 in ABA and Abiotic Stress Response. *Plant Signal. Behav.* **2010**, *5*, 1318–1320. [\[CrossRef\]](#)
43. The Arabidopsis Genome Initiative. Analysis of the Genome Sequence of the Flowering Plant Arabidopsis Thaliana. *Nature* **2000**, *408*, 796–815. [\[CrossRef\]](#) [\[PubMed\]](#)
44. Lopez, L.; Perrella, G.; Calderini, O.; Porceddu, A.; Panara, F. Genome-Wide Identification of Histone Modification Gene Families in the Model Legume Medicago Truncatula and Their Expression Analysis in Nodules. *Plants* **2022**, *11*, 322. [\[CrossRef\]](#) [\[PubMed\]](#)
45. Peng, M.; Ying, P.; Liu, X.; Li, C.; Xia, R.; Li, J.; Zhao, M. Genome-Wide Identification of Histone Modifiers and Their Expression Patterns during Fruit Abscission in Litchi. *Front. Plant Sci.* **2017**, *8*, 639. [\[CrossRef\]](#)
46. Springer, N.M.; Napoli, C.A.; Selinger, D.A.; Pandey, R.; Cone, K.C.; Chandler, V.L.; Kaeppler, H.F.; Kaeppler, S.M. Comparative Analysis of SET Domain Proteins in Maize and Arabidopsis Reveals Multiple Duplications Preceding the Divergence of Monocots and Dicots. *Plant Physiol.* **2003**, *132*, 907–925. [\[CrossRef\]](#) [\[PubMed\]](#)
47. Aiese Cigliano, R.; Sanseverino, W.; Cremona, G.; Ercolano, M.R.; Conicella, C.; Consiglio, F.M. Genome-Wide Analysis of Histone Modifiers in Tomato: Gaining an Insight into Their Developmental Roles. *BMC Genom.* **2013**, *14*, 57. [\[CrossRef\]](#)
48. Xu, J.; Xu, H.; Liu, Y.; Wang, X.; Xu, Q.; Deng, X. Genome-Wide Identification of Sweet Orange (Citrus Sinensis) Histone Modification Gene Families and Their Expression Analysis during the Fruit Development and Fruit-Blue Mold Infection Process. *Front. Plant Sci.* **2015**, *6*, 607. [\[CrossRef\]](#)
49. Wang, L.; Ahmad, B.; Liang, C.; Shi, X.; Sun, R.; Zhang, S.; Du, G. Bioinformatics and Expression Analysis of Histone Modification Genes in Grapevine Predict Their Involvement in Seed Development, Powdery Mildew Resistance, and Hormonal Signaling. *BMC Plant Biol.* **2020**, *20*, 412. [\[CrossRef\]](#)

50. Zhou, M.; Wan, G.; Mou, P.; Teng, S.; Lin, S.; Wang, G. CNT@NiO/Natural Rubber with Excellent Impedance Matching and Low Interfacial Thermal Resistance toward Flexible and Heat-Conducting Microwave Absorption Applications. *J. Mater. Chem. C* **2021**, *9*, 869–880. [[CrossRef](#)]
51. Tran, D.M.; Clément-Demange, A.; Déon, M.; Garcia, D.; Le Guen, V.; Clément-Vidal, A.; Soumahoro, M.; Masson, A.; Label, P.; Le, M.T.; et al. Genetic Determinism of Sensitivity to *Corynespora Cassiicola* Exudates in Rubber Tree (*Hevea Brasiliensis*). *PLoS ONE* **2016**, *11*, e0162807. [[CrossRef](#)]
52. Parisi, C.A.S.; Kelly, K.J.; Ansotegui, I.J.; Gonzalez-Díaz, S.N.; Bilò, M.B.; Cardona, V.; Park, H.S.; Braschi, M.C.; Macias-Weinmann, A.; Piga, M.A.; et al. Update on Latex Allergy: New Insights into an Old Problem. *World Allergy Organ. J.* **2021**, *14*, 100569. [[CrossRef](#)]
53. Hodgson-Kratky, K.J.M.; Stoffyn, O.M.; Wolyn, D.J. Recurrent Selection for Rubber Yield in Russian Dandelion. *J. Am. Soc. Hortic. Sci.* **2017**, *142*, 470–475. [[CrossRef](#)]
54. Salehi, M.; Bahmankar, M.; Naghavi, M.R.; Cornish, K. Rubber and Latex Extraction Processes for *Taraxacum Kok-Saghyz*. *Ind. Crops Prod.* **2022**, *178*, 114562. [[CrossRef](#)]
55. Mladenov, V.; Fotopoulos, V.; Kaiserli, E.; Karalija, E.; Maury, S.; Baranek, M.; Segal, N.; Testillano, P.S.; Vassileva, V.; Pinto, G.; et al. Deciphering the Epigenetic Alphabet Involved in Transgenerational Stress Memory in Crops. *Int. J. Mol. Sci.* **2021**, *22*, 7118. [[CrossRef](#)]
56. Boyer, L.A.; Latek, R.R.; Peterson, C.L. The SANT Domain: A Unique Histone-Tail-Binding Module? *Nat. Rev. Mol. Cell Biol.* **2004**, *5*, 158–163. [[CrossRef](#)]
57. Heo, J.B.; Sung, S. Vernalization-Mediated Epigenetic Silencing by a Long Intronic Noncoding RNA. *Science* **2011**, *331*, 76–79. [[CrossRef](#)] [[PubMed](#)]
58. Zhou, H.; Liu, Y.; Liang, Y.; Zhou, D.; Li, S.; Lin, S.; Dong, H.; Huang, L. The Function of Histone Lysine Methylation Related SET Domain Group Proteins in Plants. *Protein Sci.* **2020**, *29*, 1120–1137. [[CrossRef](#)] [[PubMed](#)]
59. Lee, J.-G.; Ye, Y. Bag6/Bat3/Scythe: A Novel Chaperone Activity with Diverse Regulatory Functions in Protein Biogenesis and Degradation. *BioEssays* **2013**, *35*, 377–385. [[CrossRef](#)]
60. Dong, Y.; Lu, J.; Liu, J.; Jalal, A.; Wang, C. Genome-Wide Identification and Functional Analysis of JmjC Domain-Containing Genes in Flower Development of *Rosa Chinensis*. *Plant Mol. Biol.* **2020**, *102*, 417–430. [[CrossRef](#)]
61. Hoo, S.C.; Howe, G.A. A Critical Role for the TIFY Motif in Repression of Jasmonate Signaling by a Stabilized Splice Variant of the JASMONATE ZIM-Domain Protein JAZ10 in Arabidopsis. *Plant Cell* **2009**, *21*, 131–145. [[CrossRef](#)]
62. Kanyal, A.; Rawat, M.; Gurung, P.; Choubey, D.; Anamika, K.; Karmodiya, K. Genome-Wide Survey and Phylogenetic Analysis of Histone Acetyltransferases and Histone Deacetylases of *Plasmodium Falciparum*. *FEBS J.* **2018**, *285*, 1767–1782. [[CrossRef](#)]
63. Chen, C.Y.; Wu, K.; Schmidt, W. The Histone Deacetylase HDA19 Controls Root Cell Elongation and Modulates a Subset of Phosphate Starvation Responses in Arabidopsis. *Sci. Rep.* **2015**, *5*, 1–11. [[CrossRef](#)] [[PubMed](#)]
64. Schmidt, T.; Lenders, M.; Hillebrand, A.; van Deenen, N.; Munt, O.; Reichelt, R.; Eisenreich, W.; Fischer, R.; Prüfer, D.; Schulze Gronover, C. Characterization of Rubber Particles and Rubber Chain Elongation in *Taraxacum Koksaghyz*. *BMC Biochem.* **2010**, *11*, 1–11. [[CrossRef](#)] [[PubMed](#)]
65. De Lucia, F.; Crevillen, P.; Jones, A.M.E.; Greb, T.; Dean, C. A PHD-Polycomb Repressive Complex 2 Triggers the Epigenetic Silencing of FLC during Vernalization. *Proc. Natl. Acad. Sci. USA* **2008**, *105*, 16831–16836. [[CrossRef](#)]
66. Berr, A.; McCallum, E.J.; Ménard, R.; Meyer, D.; Fuchs, J.; Dong, A.; Shen, W.H. Arabidopsis SET DOMAIN GROUP2 Is Required for H3K4 Trimethylation and Is Crucial for Both Sporophyte and Gametophyte Development. *Plant Cell* **2010**, *22*, 3232–3248. [[CrossRef](#)] [[PubMed](#)]
67. Crevillen, P.; Yang, H.; Cui, X.; Greeff, C.; Trick, M.; Qiu, Q.; Cao, X.; Dean, C. Epigenetic Reprogramming That Prevents Transgenerational Inheritance of the Vernalized State. *Nature* **2014**, *515*, 587–590. [[CrossRef](#)] [[PubMed](#)]
68. Letunic, I.; Bork, P. 20 Years of the SMART Protein Domain Annotation Resource. *Nucleic Acids Res.* **2018**, *46*, D493–D496. [[CrossRef](#)]
69. Letunic, I.; Khedkar, S.; Bork, P. SMART: Recent Updates, New Developments and Status in 2020. *Nucleic Acids Res.* **2021**, *49*, D458–D460. [[CrossRef](#)]
70. Hu, B.; Jin, J.; Guo, A.Y.; Zhang, H.; Luo, J.; Gao, G. GSDS 2.0: An Upgraded Gene Feature Visualization Server. *Bioinformatics* **2015**, *31*, 1296–1297. [[CrossRef](#)]
71. Wang, Y.; Tang, H.; DeBarry, J.D.; Tan, X.; Li, J.; Wang, X.; Lee, T.; Jin, H.; Marler, B.; Guo, H.; et al. MCScanX: A Toolkit for Detection and Evolutionary Analysis of Gene Synteny and Collinearity. *Nucleic Acids Res.* **2012**, *40*, e49. [[CrossRef](#)]
72. Altschul, S.F.; Gish, W.; Miller, W.; Myers, E.W.; Lipman, D.J. Basic Local Alignment Search Tool. *J. Mol. Biol.* **1990**, *215*, 403–410. [[CrossRef](#)]
73. Sievers, F.; Wilm, A.; Dineen, D.; Gibson, T.J.; Karplus, K.; Li, W.; Lopez, R.; McWilliam, H.; Remmert, M.; Söding, J.; et al. Fast, Scalable Generation of High-Quality Protein Multiple Sequence Alignments Using Clustal Omega. *Mol. Syst. Biol.* **2011**, *7*, 539. [[CrossRef](#)] [[PubMed](#)]
74. Löytynoja, A.; Goldman, N. An Algorithm for Progressive Multiple Alignment of Sequences with Insertions. *Proc. Natl. Acad. Sci. USA* **2005**, *102*, 10557–10562. [[CrossRef](#)] [[PubMed](#)]
75. Yang, Z. PAML: A Program Package for Phylogenetic Analysis by Maximum Likelihood. *Bioinformatics* **1997**, *13*, 555–556. [[CrossRef](#)] [[PubMed](#)]

76. Yang, Z.; Nielsen, R. Estimating Synonymous and Nonsynonymous Substitution Rates Under Realistic Evolutionary Models. *Mol. Biol. Evol.* **2000**, *17*, 32–43. [[CrossRef](#)] [[PubMed](#)]
77. Bolger, A.M.; Lohse, M.; Usadel, B. Trimmomatic: A Flexible Trimmer for Illumina Sequence Data. *Bioinformatics* **2014**, *30*, 2114–2120. [[CrossRef](#)] [[PubMed](#)]
78. Corchete, L.A.; Rojas, E.A.; Alonso-López, D.; De Las Rivas, J.; Gutiérrez, N.C.; Burguillo, F.J. Systematic Comparison and Assessment of RNA-Seq Procedures for Gene Expression Quantitative Analysis. *Sci. Rep.* **2020**, *10*, 1–15. [[CrossRef](#)]
79. Dobin, A.; Davis, C.A.; Schlesinger, F.; Drenkow, J.; Zaleski, C.; Jha, S.; Batut, P.; Chaisson, M.; Gingeras, T.R. STAR: Ultrafast Universal RNA-Seq Aligner. *Bioinformatics* **2013**, *29*, 15. [[CrossRef](#)]
80. Putri, G.H.; Anders, S.; Pyl, P.T.; Pimanda, J.E.; Zanini, F. Analysing High-Throughput Sequencing Data in Python with HTSeq 2.0. *Bioinformatics* **2022**, *38*, 2943–2945. [[CrossRef](#)]
81. Robinson, M.D.; McCarthy, D.J.; Smyth, G.K. EdgeR: A Bioconductor Package for Differential Expression Analysis of Digital Gene Expression Data. *Bioinform. Oxf. Engl.* **2010**, *26*, 139–140. [[CrossRef](#)]
82. Altschul, S.F.; Madden, T.L.; Schäffer, A.A.; Zhang, J.; Zhang, Z.; Miller, W.; Lipman, D.J. Gapped BLAST and PSI-BLAST: A New Generation of Protein Database Search Programs. *Nucleic Acids Res.* **1997**, *25*, 3389–3402. [[CrossRef](#)]
83. Camacho, C.; Coulouris, G.; Avagyan, V.; Ma, N.; Papadopoulos, J.; Bealer, K.; Madden, T.L. BLAST+: Architecture and Applications. *BMC Bioinform.* **2009**, *10*, 421. [[CrossRef](#)] [[PubMed](#)]
84. Whelan, J.A.; Russell, N.B.; Whelan, M.A. A Method for the Absolute Quantification of cDNA Using Real-Time PCR. *J. Immunol. Methods* **2003**, *278*, 261–269. [[CrossRef](#)]
85. D’Amelia, V.; Aversano, R.; Batelli, G.; Caruso, I.; Moreno, M.C.; Castro-Sanz, A.B.; Chiaiese, P.; Fasano, C.; Palomba, F.; Carputo, D. High AN1 Variability and Interaction with Basic Helix-Loop-Helix Co-Factors Related to Anthocyanin Biosynthesis in Potato Leaves. *Plant J.* **2014**, *80*, 527–540. [[CrossRef](#)] [[PubMed](#)]



Article

# $\beta$ -Cyclocitral Does Not Contribute to Singlet Oxygen-Signalling in Algae, but May Down-Regulate Chlorophyll Synthesis

Thomas Roach \*, Theresa Baur and Ilse Kranner

Department of Botany, University of Innsbruck, Sternwartestraße 15, 6020 Innsbruck, Austria

\* Correspondence: thomas.roach@uibk.ac.at; Tel.: +43-512-507-51030

**Abstract:** Light stress signalling in algae and plants is partially orchestrated by singlet oxygen ( $^1\text{O}_2$ ), a reactive oxygen species (ROS) that causes significant damage within the chloroplast, such as lipid peroxidation. In the vicinity of the photosystem II reaction centre, a major source of  $^1\text{O}_2$ , are two  $\beta$ -carotene molecules that quench  $^1\text{O}_2$  to ground-state oxygen.  $^1\text{O}_2$  can oxidise  $\beta$ -carotene to release  $\beta$ -cyclocitral, which has emerged as a  $^1\text{O}_2$ -mediated stress signal in the plant *Arabidopsis thaliana*. We investigated if  $\beta$ -cyclocitral can have similar retrograde signalling properties in the unicellular alga *Chlamydomonas reinhardtii*. Using RNA-Seq, we show that genes up-regulated in response to exogenous  $\beta$ -cyclocitral included *CAROTENOID CLEAVAGE DIOXYGENASE 8 (CCD8)*, while down-regulated genes included those associated with porphyrin and chlorophyll anabolism, such as tetrapyrrole-binding protein (*GUN4*), magnesium chelatases (*CHL11*, *CHL12*, *CHLD*, *CHLH1*), light-dependent protochlorophyllide reductase (*POR1*), copper target 1 protein (*CTH1*), and coproporphyrinogen III oxidase (*CPX1*). Down-regulation of this pathway has also been shown in  $\beta$ -cyclocitral-treated *A. thaliana*, indicating conservation of this signalling mechanism in plants. However, in contrast to *A. thaliana*, a very limited overlap in differential gene expression was found in  $\beta$ -cyclocitral-treated and  $^1\text{O}_2$ -treated *C. reinhardtii*. Furthermore, exogenous treatment with  $\beta$ -cyclocitral did not induce tolerance to  $^1\text{O}_2$ . We conclude that while  $\beta$ -cyclocitral may down-regulate chlorophyll synthesis, it does not seem to contribute to  $^1\text{O}_2$ -mediated high light stress signalling in algae.

**Keywords:** high light stress; singlet oxygen; signalling; GPX5; beta cyclocitral; acrolein; glutathione peroxidase; carbonyl; transcription

**Citation:** Roach, T.; Baur, T.; Kranner, I.  $\beta$ -Cyclocitral Does Not Contribute to Singlet Oxygen-Signalling in Algae, but May Down-Regulate Chlorophyll Synthesis. *Plants* **2022**, *11*, 2155. <https://doi.org/10.3390/plants11162155>

Academic Editors: Milan S. Stankovic, Paula Baptista and Petronia Carillo

Received: 2 June 2022

Accepted: 15 August 2022

Published: 19 August 2022

**Publisher's Note:** MDPI stays neutral with regard to jurisdictional claims in published maps and institutional affiliations.



**Copyright:** © 2022 by the authors. Licensee MDPI, Basel, Switzerland. This article is an open access article distributed under the terms and conditions of the Creative Commons Attribution (CC BY) license (<https://creativecommons.org/licenses/by/4.0/>).

## 1. Introduction

Photosynthetic organisms often encounter suboptimal conditions, leading to the absorption of excess light energy and 'high light' (HL) stress. Therefore, light harvesting must be regulated, requiring acclimation to the current environment [1]. As part of acclimation, signals from the chloroplast can alter transcription in the nucleus in so-called retrograde signalling [2,3]. For example, levels of tetrapyrrole intermediates (chlorophyll precursors) in the chloroplast provide feedback cues to the nucleus during chlorophyll synthesis [4,5]. Stress signalling is also partially orchestrated by reactive oxygen species (ROS), including singlet oxygen ( $^1\text{O}_2$ ), which is produced by energy transfer from excited chlorophyll to molecular oxygen in photosystem II (PSII) [6–8]. Singlet oxygen oxidises almost anything in its path and the  $^1\text{O}_2$  signal leaves the chloroplast in the form of down-stream reaction products.  $\beta$ -cyclocitral, a  $^1\text{O}_2$ -derived breakdown product of  $\beta$ -carotene, has emerged as an aldehyde electrophile involved in  $^1\text{O}_2$  retrograde signalling of *Arabidopsis thaliana* [9]. However, the contribution of  $\beta$ -cyclocitral to  $^1\text{O}_2$  signalling in algae is unknown.

Other  $^1\text{O}_2$ -derived molecules with potent signalling activity include  $\alpha,\beta$ -unsaturated carbonyl derivatives, known as reactive carbonyl/electrophile species (RES). These are produced as a consequence of lipid peroxidation [10,11]. Thylakoid membranes are particularly

enriched in 1-linolenoyl/2-linolenoyl (di-C18:3) found in monogalactosyldiacylglycerol, a polar lipid that improves fluidity for membrane functionality, but is highly prone to peroxidation by  $^1\text{O}_2$ . One of the most abundant RES produced by lipid peroxidation in chloroplasts due to HL stress is acrolein [10,11], which can activate a significant proportion of transcriptional changes that occur in response to  $^1\text{O}_2$  [12,13]. In *Chlamydomonas reinhardtii*, an electrophile response element (ERE)-containing bZIP transcription factor called SOR1 participates in  $^1\text{O}_2$  signalling [12,13]. SOR1 up-regulates transcription of a large suite of genes, including glutathione transferases (e.g., *GST51*) and an isoflavone reductase-like protein (*IRL1*), which contribute to RES-associated antioxidant defences [12,14,15].

Although they are potent signalling molecules, RES are also toxic to cells by forming Michael addition adducts with nucleophilic thiolate anions [16], such as redox-active cysteine residues of proteins. As a thiol, the antioxidant glutathione (GSH), can detoxify RES. *Chlamydomonas reinhardtii* rapidly responds to low concentrations of the RES acrolein ( $\leq 600$  ppm) by increasing GSH contents, but is critically GSH-depleted at higher acrolein concentrations [13]. Another component of RES detoxification putatively includes glutathione peroxidases (GPX), whereby *GPX5* (also known as GPXh) transcription is strongly up-regulated by sub-lethal levels of  $^1\text{O}_2$  [17,18] and acrolein [13]. Moreover, overexpression of *GPX5* in *C. reinhardtii* can increase tolerance to  $^1\text{O}_2$  [18].

In summary, low levels of ROS/RES can activate signalling pathways implicated in acclimation, whereas an excess ROS/RES load leads to intolerable stress. Thus, stress responses can be distinguished into eustress and distress: Eustress leads to increased stress tolerance via acclimation in which  $^1\text{O}_2$  signalling can be involved, and distress leads to loss of viability due to excess stress (e.g., high RES load) beyond a level that can be compensated for by acclimation [18–20].

Here, we explored the potential role for  $\beta$ -cyclocitral in  $^1\text{O}_2$ -mediated signalling and inducing  $^1\text{O}_2$  tolerance in the unicellular model green alga, *C. reinhardtii*. First, we confirmed that  $\beta$ -cyclocitral could enter cells by measuring increased concentrations of the molecule in treated cells, and observing the concentration-dependent effect on chlorophyll fluorescence. Then, using RNA-Seq analysis, we analysed the transcriptional response of cells to  $\beta$ -cyclocitral and compared this to previously published data of differential gene expression induced by the photosensitizer rose bengal (RB), to reveal if elements of  $^1\text{O}_2$  signalling were activated by  $\beta$ -cyclocitral. Further experiments investigated if  $\beta$ -cyclocitral can induce  $^1\text{O}_2$  tolerance, and comparisons are drawn with responses to acrolein, a  $^1\text{O}_2$ -derived signal resulting from lipid peroxidation of the thylakoid membrane.

## 2. Results

As an aldehyde,  $\beta$ -cyclocitral could be cytotoxic as well as a signalling molecule. Therefore, to assess toxicity, the impact of various concentrations of  $\beta$ -cyclocitral on photosynthesis was probed via chlorophyll fluorescence. The maximum quantum yield of PSII ( $F_v/F_m$ ), which is an often-used health marker of photosynthetic organisms, decreased in both wild types (WT), cell-wall containing WT-4A and cell-wall-less *cw15*, in response to  $\beta$ -cyclocitral treatment with  $\geq 10$   $\mu\text{L}$ /Petri dish (Figure 1A), corresponding to  $\geq 50,000$  ppm atmospheric concentration (see methods for calculation). In contrast, NPQ that is also measured via chlorophyll fluorescence was affected at much lower  $\beta$ -cyclocitral concentrations (Figure 1B), including at 0.12  $\mu\text{L}$ /Petri dish (Figure S1), which corresponds to the 600 ppm treatment used for the RNA-Seq analysis. Cellular concentrations of  $\beta$ -cyclocitral before treatment were 0.2  $\text{nmol g}^{-1}$  fresh weight, and increased 400 fold 2 h after exogenous treatment at 600 ppm (Figure S2). There was no difference in the influence of  $\beta$ -cyclocitral on NPQ or  $F_v/F_m$  between WT-4A and *cw15* strains (Figure 1). Furthermore, the reduction of NPQ was also found in the *npq4*, *stt7*, and *npq4stt7* mutants (Figure S1), and thus was independent of LHCSR3- and STT7-mediated NPQ, which are the major NPQ mechanisms in *C. reinhardtii* [1,21]. Therefore, our results are indicative of a direct physical effect of  $\beta$ -cyclocitral on NPQ that occurs at the level of the thylakoid membrane, similar to an uncoupler. To test this, the activity of the pH-dependent violaxanthin cycle was measured

in response to HL. Less zeaxanthin accumulated in  $\beta$ -cyclocitral-treated cells (Figure S1), indicating that the proton gradient was dissipated by  $\beta$ -cyclocitral.

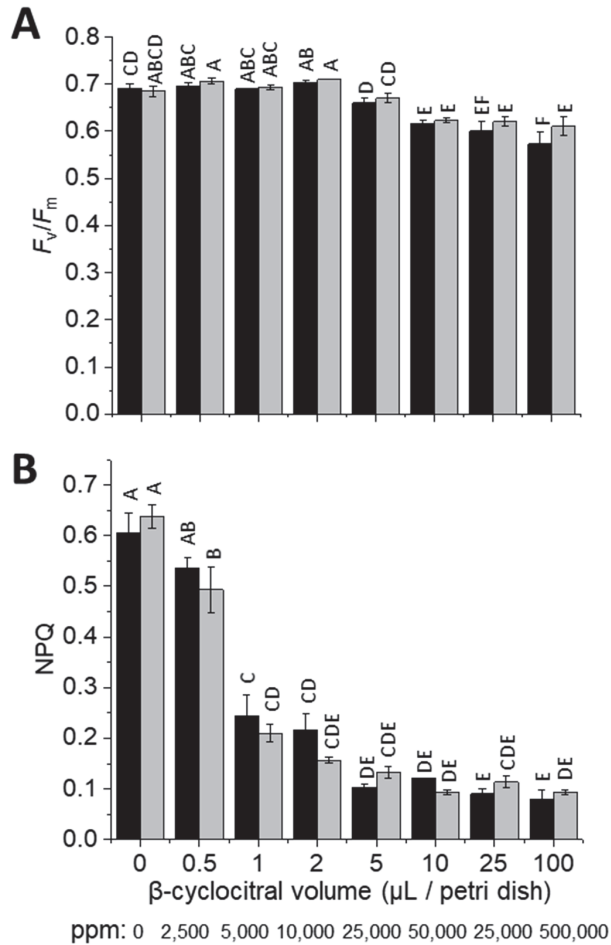


**Figure 1.** Effect of exogenous  $\beta$ -cyclocitral on  $F_v/F_m$  and NPQ in *Chlamydomonas reinhardtii*. (A) Measurements of  $F_v/F_m$  and (B) NPQ in 4 h HL-acclimated cultures were made after 4 h of treatment under very LL (see methods), of cell-wall-containing wild type (WT-4A; black bars) and cell-wall-less (cw15; grey bars) cultures,  $n = 3 \pm$  SD, with distinct letters indicating significant differences ( $p < 0.05$ ).

Aldehydes can be detoxified by GSH and associated enzymes, such as GSTS1. Thus, the response of  $\beta$ -cyclocitral on GSH concentrations was also measured up to 1500 ppm (0.3  $\mu$ L/Petri dish), and after 4 h, no effect was observed (Figure S3).

Overall, the lack of decrease in  $F_v/F_m$  and lack of change in GSH concentrations indicated that  $\beta$ -cyclocitral was not a cytotoxic aldehyde at treatment with up to 1500 ppm, a concentration at which the RES acrolein is lethal [13]. Moreover, the significant impact of  $\beta$ -cyclocitral on NPQ in WT-4A and cw15 showed that this aldehyde could enter the chloroplast of *C. reinhardtii* and that the cell wall was not a hindrance to influx. Therefore, we felt confident to be able to assess the signalling properties of  $\beta$ -cyclocitral in exogenously-treated cells.

One of the most  $^1\text{O}_2$ -responsive genes in *C. reinhardtii* is *GPX5*, and GPXs likely have a role in mitigating HL stress by detoxifying aldehydes/RES that are produced as a consequence of  $^1\text{O}_2$  production [18]. We screened three mutants over-expressing *GPX5* in the WT-4A background [18] and found clearly elevated protein levels of *GPX5* in *GPXHGX-11* and *GPX5OX-14*, relative to WT-4A, in low light (LL)-treated cells (Figure 2A). This led to the selection of *GPXHGX-11* for further experiments to see how  $\beta$ -cyclocitral, acrolein, and HL influence *GPX5* levels, and how elevated levels of *GPX5* affect the response to these treatments and subsequent tolerance to  $^1\text{O}_2$ . Levels of *GPX5* increased in WT-4A cells after 4 h of HL, indicating that this treatment induced  $^1\text{O}_2$  production. However, 4 h treatments with 600 ppm of  $\beta$ -cyclocitral or 600 ppm of acrolein did not increase *GPX5* levels (Figure 2B). After 4 h of HL, WT cells increased the GSH contents, indicating that cells were under mild oxidative stress, whereas in *GPXHGX-11*, no change in the GSH contents occurred, indicating that cells were under less stress. In support of this, after 4 h of HL, *GPXHGX-11* accumulated less aldehydes (propanal and hexanal) and RES (acrolein and 4-hydroxynonenal) than WT-4A, whereas the fold change of  $\beta$ -cyclocitral was equally low in both genotypes (Figure 3). After a 4 h treatment with 600 ppm of acrolein, both WT and *GPXHGX-11* accumulated GSH (Figure S3).

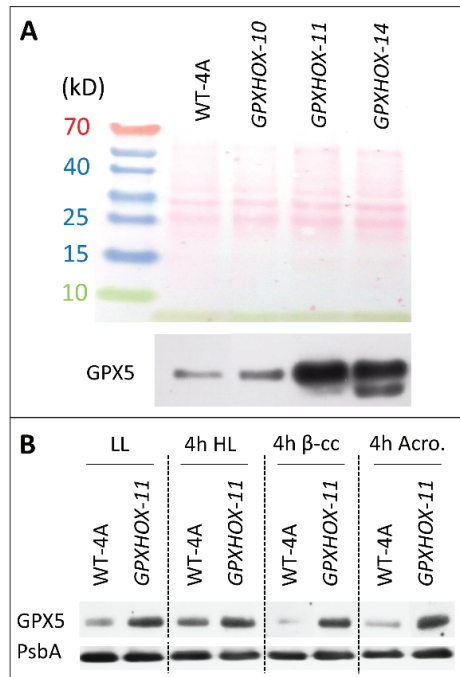


**Figure 2.** Protein levels of *GPX5* in WT-4A and *GPX5*-overexpressor (*GPXHGX*) mutants under LL and in response to HL,  $\beta$ -cyclocitral and acrolein. (A) Three *GPXHGX* lines and WT-4A were analysed for *GPX5* protein levels under LL. Shown above is the Ponceau-stained membrane for loading control. (B) The effect of LL, 4 h with HL, and 4 h with 600 ppm of  $\beta$ -cyclocitral ( $\beta$ -cc) or with 600 ppm of acrolein (4 h Acro.) under LL, on *GPX5* levels. The D1 reaction centre of photosystem II (*PsbA*) was used for loading control.

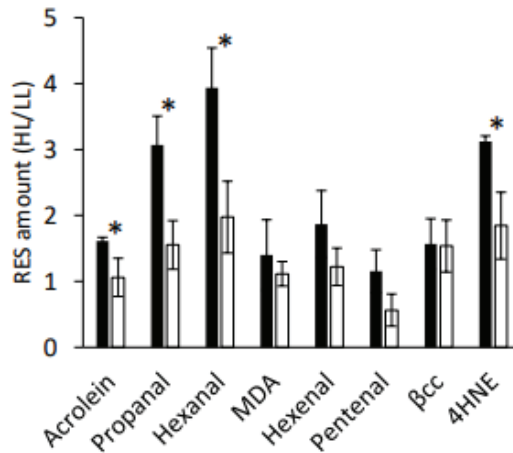


**Figure 3.** Influence of GPX5 overexpression on aldehyde/RES accumulation. Change in RES concentrations in response to HL ( $600 \mu\text{mol photons m}^{-2} \text{s}^{-1}$ ) for 4 h, relative to levels before treatment at LL ( $50 \mu\text{mol photons m}^{-2} \text{s}^{-1}$ ), in wild-type (black) and *GPXHOX-11* (white). MDA: malondialdehyde,  $\beta\text{cc}$ :  $\beta$ -cyclocitral, 4HNE: 4-hydroxynonenal.  $n = 4 \pm \text{SD}$  with \* denoting significant differences between genotypes ( $p < 0.05$ ).

A function of  $^1\text{O}_2$ -related signalling is partly towards increasing tolerance of this ROS [18]. Therefore, the influence of exogenous  $\beta$ -cyclocitral and acrolein treatments under LL (as potential components of  $^1\text{O}_2$ -mediated signalling) on the tolerance to  $^1\text{O}_2$  was measured. The influence of HL stress, which increases endogenous  $^1\text{O}_2$  levels, was also included as pre-treatment before testing  $^1\text{O}_2$  tolerance, and all comparisons were made to LL-treated 'control' cells. Tolerance to  $^1\text{O}_2$  was tested by incubating cells with the photosensitizer RB. Since the amount of  $^1\text{O}_2$  that RB produces is dependent on the degree of photoexcitation (i.e., intensity and duration of light treatment) and RB concentration, various treatments were conducted to test cell tolerance. These constituted  $4 \mu\text{M}$ ,  $7 \mu\text{M}$ , and  $10 \mu\text{M}$  of RB, either for 10 min at  $250 \mu\text{mol photons m}^{-2} \text{s}^{-1}$  to provide a short  $^1\text{O}_2$  shock, or 24 h at  $50 \mu\text{mol photons m}^{-2} \text{s}^{-1}$  to test longer term endurance. The 24 h endurance test was more severe and led to less cell survival of control cells, under which *GPXHOX-11* was significantly less affected than WT-4A (Figure 4), with  $p < 0.05$  when comparing genotype as a factor with MANOVA across all RB concentrations. Pre-treatment with HL increased the tolerance of WT-4A to the  $^1\text{O}_2$  shock treatment with  $7 \mu\text{M}$  and  $10 \mu\text{M}$  of RB (Figure 4A), and the 24 h treatment with  $4 \mu\text{M}$  (Figure 4B), while affecting *GPXHOX-11* less. This resulted in HL-treated WT-4A and *GPXHOX-11* having a similar  $^1\text{O}_2$  tolerance (Figure 4). Relative to control cells, pre-treatment with 600 ppm of  $\beta$ -cyclocitral had no impact on  $^1\text{O}_2$  tolerance in either genotype under all treatments (average  $p = 0.895$ ), whereas pre-treatment with 600 ppm of acrolein increased the tolerance of both genotypes (average  $p = 0.034$ ). In summary, acrolein and HL induced tolerance to severe  $^1\text{O}_2$  stress, whereas  $\beta$ -cyclocitral did not significantly affect tolerance.

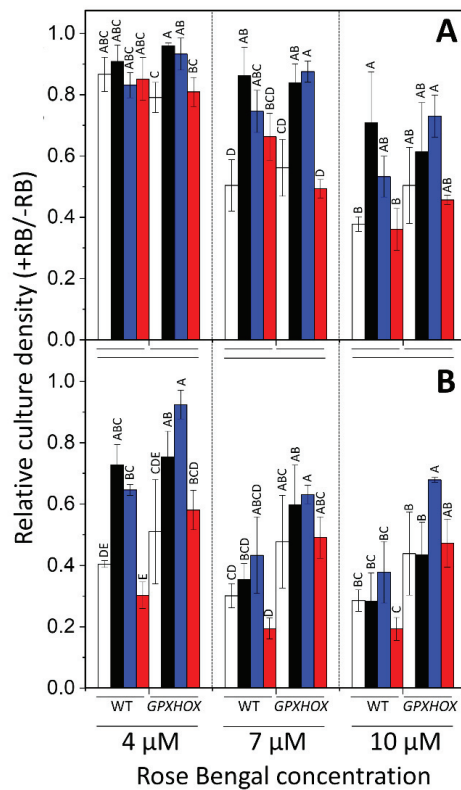


**Figure 4.** Influence of *GPX5*-overexpression and effect of HL,  $\beta$ -cyclocitral, and acrolein pre-treatments on tolerance to  $^1\text{O}_2$ . Tolerance to  $^1\text{O}_2$  was tested by exposing WT 4A or *GPXOX-11* cultures to (A) 250  $\mu\text{mol photons m}^{-2} \text{s}^{-1}$  for 10 min or (B) 50  $\mu\text{mol photons m}^{-2} \text{s}^{-1}$  for 24 h, in a medium that initially contained 4  $\mu\text{M}$ , 7  $\mu\text{M}$ , or 10  $\mu\text{M}$  of rose bengal (RB). Before treatment with RB, cells were from LL (control; white) or pre-treated with 4 h of HL (black), 600 ppm of acrolein (blue) or 600 ppm of  $\beta$ -cyclocitral (red) under LL. To reveal tolerance to  $^1\text{O}_2$ , cell density was monitored for 24 h after RB treatment by turbidity of culture at 650 nm and is shown relative to turbidity of the respective pre-treated cultures not treated with RB. Bars labelled with different letters within the same RB treatment denote significant differences from each other (Tukey's post hoc after arcsine transformation,  $p < 0.05$ ,  $n = 3 \pm \text{SD}$ ).

To investigate if  $\beta$ -cyclocitral could contribute to  $^1\text{O}_2$ -mediated signalling in *C. reinhardtii*, an RNA-Seq analysis of cells treated for 2 h with 600 ppm of  $\beta$ -cyclocitral under LL (Table S1) was conducted and compared to the transcriptional response of cells treated with the  $^1\text{O}_2$ -producing photosensitizer RB at 1  $\mu\text{M}$  under LL (data from [13]). In response to the  $\beta$ -cyclocitral treatment, only six genes were significantly up-regulated, and 57 genes were down-regulated, when considering a fold change of  $>2$  and modified *t*-test *p* values of  $<0.01$  (Table S1). Of the genes down-regulated by  $\beta$ -cyclocitral, 18 and 6 were significantly down-regulated and up-regulated, respectively, by RB (Table S1; Figure S4). Differentially expressed genes associated with carotenoid metabolism include carotenoid cleavage dioxygenase 8 (*Cre08.g365851*), up-regulated five-fold, and  $\beta$ -carotene ketolase (*BKT1*), up-regulated two-fold, but not significantly (Table S1). Of all significantly down-regulated genes, the only ontological group with  $>1$  hit was 'porphyrin and chlorophyll metabolism' with 10 hits: *Cre01.g015350* (*POR1*), *Cre01.g050950*, *Cre02.g085450* (*CPX1*), *Cre05.g242000* (*CHLD*), *Cre05.g246800* (*GUN4*), *Cre06.g306300* (*CHL11*), *Cre07.g325500* (*CHL11*), *Cre09.g396300* (*PPX1*), *Cre12.g510050* (*CTH1*), *Cre12.g510800* (*CHL12*), and *Cre16.g663900*. Collectively,

these genes covered several steps of chlorophyll anabolism (Figure S5), but the overall overlap of differential gene expression with RB-treated cells was low, as shown by a  $R^2$  linear correlation of  $<0.01$  when including all genes, which increases to 0.15, considering only the 63 genes with significantly altered expression (Figure 5). In comparison, this contrasts with the much tighter relationship between differential gene expression shared between acrolein-treated and RB-treated cells [13], which has an  $R^2$  linear correlation of 0.34 and 0.70 when considering expression of total genes and only significantly affected genes, respectively (Figure 5).

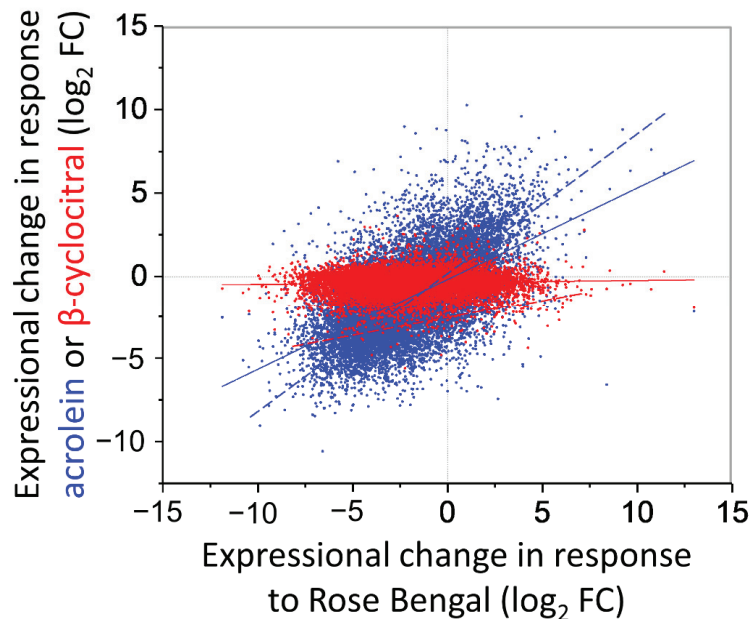


**Figure 5.** Correlation of differential gene expression induced by treatment with  $^1\text{O}_2$  and acrolein (blue) or  $^1\text{O}_2$  and  $\beta$ -cyclocitral (red). Levels of mRNA are expressed as  $\log_2$  fold changes ( $\log_2\text{FC}$ ), relative to mock-treated cells, calculated from RNA-Seq analyses;  $n = 3$  for treatments and controls. Treatments with acrolein and  $\beta$ -cyclocitral were at 600 ppm and  $^1\text{O}_2$  was induced by rose bengal (RB;  $1 \mu\text{M}$  under growth light at  $50 \mu\text{mol quanta m}^{-2} \text{s}^{-1}$ ). Continuous and dashed lines of best fit consider all and only significantly affected genes, respectively. See Table S1 for expression levels of each gene. RNA-Seq data for acrolein and RB treatments adapted with permission from [13] 2018, Copyright Elsevier.

### 3. Discussion

Ten years ago, the discovery that  $\beta$ -cyclocitral in *A. thaliana* effects transcription of several genes known to be affected by  $^1\text{O}_2$  [9] made a coherent link between HL-induced  $^1\text{O}_2$  production and ROS-associated retrograde signalling. Subsequently, it was found that  $\beta$ -cyclocitral functions up-stream of MBS1 [22], a zinc finger protein that regulates  $^1\text{O}_2$ -dependent gene expression, not only in *A. thaliana* but also in *C. reinhardtii* [23]. However, the fact of whether  $\beta$ -cyclocitral actually has a role in  $^1\text{O}_2$  signalling in alga remained unknown. Since then, other RES (i.e., acrolein), related to lipid peroxidation rather than carotenoid cleavage, emerged as retrograde signals acting in  $^1\text{O}_2$ -mediated stress acclimation [13]. Here, we investigated how  $\beta$ -cyclocitral modulates the physiology and transcription in *C. reinhardtii* and made comparisons with transcriptional responses of cells to the photosensitizer RB and the RES acrolein.

The very minor effect of  $\beta$ -cyclocitral on  $F_v/F_m$  showed how tolerant cells were of this molecule. For example, decreases in  $F_v/F_m$  occurred at  $>1000$  fold concentrations

compared to the effects of acrolein (Figure 1A; [13]). The concentration of  $\beta$ -cyclocitral even in very light-stressed *C. reinhardtii* has never been measured at  $>1 \text{ nmol g}^{-1}$  fresh weight [13,24], which is below the cellular concentrations after exogenous treatment with 600 ppm (Figure S2). Therefore, our data supports that, unlike acrolein,  $\beta$ -cyclocitral does not build up to toxic concentrations in light-stressed cells. Despite the insensitivity of  $F_v/F_m$  to  $\beta$ -cyclocitral, NPQ was affected at much lower concentrations (Figures 1B and S1), confirming that  $\beta$ -cyclocitral was able to enter cells, which otherwise may have contributed to tolerance. Inhibition of NPQ in various NPQ mutants indicates that  $\beta$ -cyclocitral directly affected an over-riding NPQ mechanism, such as the requirement of low luminal pH. This was indeed shown by the lower accumulation of zeaxanthin under HL, which is a process requiring a low luminal pH for violaxanthin de-epoxidase activity, in  $\beta$ -cyclocitral-treated cells (Figure S1). Therefore, we suggest that  $\beta$ -cyclocitral may act as an uncoupler of the thylakoid membrane potential, comparable to the inhibitory activity of structurally similar monoterpene ketones, such as pulegone, on respiration [25]. The relevance of this observation is that NPQ protects from  $^1\text{O}_2$  production under HL [1,24], and thus exogenous  $\beta$ -cyclocitral may increase  $^1\text{O}_2$  production and may confound observations of  $\beta$ -cyclocitral involvement in  $^1\text{O}_2$  signalling under HL. Here, exogenous treatments for the RNA-Seq were conducted under very LL ( $2 \mu\text{mol photons m}^{-2} \text{ s}^{-1}$ ), thus unaffected by lowered NPQ.

Defence against  $^1\text{O}_2$  requires many enzymes that mitigate lipid peroxidation, including GPX5 [18]. In mammalian cells, GSH is the typical GPX substrate to break down  $\text{H}_2\text{O}_2$ , whereas in *C. reinhardtii*, a thioredoxin is the reductant of GPX5 that has a close association with  $^1\text{O}_2$  stress [26]. In WT cells, HL induced accumulation of GPX5 (Figure 2B), alongside higher levels of RES, which were attenuated in *GPXHGX-11* (Figure 3), a *GPX5* over-expressing mutant with elevated GPX5 levels (Figure 2). This supports that GPX5 has a role in metabolising HL-induced RES production, and explains why HL stress is associated with elevated GPX5 levels [26,27]. *GPXHGX-11* also possessed significantly elevated tolerance to long-term  $^1\text{O}_2$  treatment with the photosensitizer RB (Figure 4B), in agreement with results from Ledford et al. [18]. Comparing the influence of pre-treatments on  $^1\text{O}_2$  tolerance, acrolein was able to induce tolerance of WT and *GPXHGX-11*, whereas  $\beta$ -cyclocitral could not (Figure 4).  $\beta$ -cyclocitral did not induce GSH synthesis, whereas acrolein and HL did (Figure S3), as also previously shown [13]. Thus, enhanced  $^1\text{O}_2$  tolerance can be partially attributed to elevated GSH and GPX5 levels.

A molecule involved in stress signalling would be expected to increase in concentration in response to the relevant stress. The amounts of  $\beta$ -cyclocitral in *C. reinhardtii* were  $\leq 1 \text{ nmol g}^{-1}$  fresh weight (Figure S2), and not affected by HL stress (Figures S2 and 3), also in agreement with previous data [13,24]. In comparison, levels of RES increased in HL-stressed cells, similar to after treatment with RB [13], supporting that  $^1\text{O}_2$  production under HL is involved in RES production, but hardly with  $\beta$ -cyclocitral production. Acrolein has received attention in the field of redox biology for its high electrophilic nature and high endogenous levels of  $>5 \text{ nmol g}^{-1}$  fresh weight in stressed plants and algae alike [13,28,29]. Previously, we showed that exogenous acrolein treatments induce a ‘eustress’ (i.e., acclimation) response by up-regulating thiol-disulfide-dependent defence mechanisms required for tolerating  $^1\text{O}_2$  [13]. Of note, around half of global gene expression (up and down) occurring in response to 600 ppm of acrolein, the dose that induced a eustress response with highest tolerance to  $^1\text{O}_2$ , was shared with the gene regulation in response to RB [13]. While we did not find a similar transcriptional response to  $\beta$ -cyclocitral (Figure 5), in line with a lack of inducing  $^1\text{O}_2$  tolerance (Figure 4), there was evidence that  $\beta$ -cyclocitral may have some signalling properties in *C. reinhardtii*. Collectively down-regulated genes (Table S1) covered many steps of chlorophyll anabolism (Figure S5), such as porphobilinogen deaminase/HemC (*Cre16.g663900.t1.2*), coproporphyrinogen III oxidase (*CPX1*), and protoporphyrinogen oxidase (*PPX1*), which are involved in early steps of porphyrin synthesis, as well as genes coding for proteins that insert  $\text{Mg}^{2+}$  into protoporphyrin, including tetrapyrrole-binding protein (*GUN4*) and magnesium chelatase (*CHL11*, *CHL12*, *CHLD*, *CHLH1*) to form Mg-protoporphyrin IX (MgP), the first dedicated intermediate of the

chlorophyll branch. In *C. reinhardtii*, *CHL2* seems to be redundant to *CHL1* [30]. Gene expression associated with later steps of chlorophyll synthesis, such as copper target 1 protein (*CTH1*) and light-dependent protochlorophyllide reductase (*POR1*) were also down-regulated by  $\beta$ -cyclocitral. In *A. thaliana*,  $\beta$ -cyclocitral also down-regulated expression of *CHL2* and a few other genes involved in porphyrin/chlorophyll biosynthesis, such as *PORB*, *CHLM* and *HEME1* alongside an up-regulation of *CLH1* and *CLH2* involved in chlorophyll catabolism (Ramel et al., 2102), indicating a conserved signalling role for  $\beta$ -cyclocitral in decreasing chlorophyll contents, which existed before the evolution of vascular plants. Chlorophyll synthesis needs to be tightly regulated because MgP and protochlorophyllide are, similar to free chlorophyll, highly efficient photosensitizers [6]. MgP provides feedback on chlorophyll synthesis by repressing nuclear transcription in a signalling pathway that requires GUN4 [4]. There are contrasting reports on whether the GUN4-MgP complex produces more or less  $^1\text{O}_2$  than MgP alone, and if  $^1\text{O}_2$  is a component of the retrograde signal [31,32].

In summary, in *C. reinhardtii*,  $\beta$ -cyclocitral does not seem to have a role in  $^1\text{O}_2$  signalling or inducing  $^1\text{O}_2$  tolerance. Nonetheless, the influence of carotenoid cleavage products on chlorophyll synthesis and how  $^1\text{O}_2$  integrates into the retrograde signalling of this pathway warrants further investigation.

## 4. Materials and Methods

### 4.1. Strains and Growth Conditions

*Chlamydomonas reinhardtii* WT-4A<sup>+</sup> (CC-4051) and *GPXHOX*<sup>+</sup> strains *GPXHOX-10* (CC-4606), *GPXHOX-11* (CC-4607), and *GPXHOX-14* (CC-4608) in the WT-4A<sup>+</sup> background, from Ledford et al., [18], were initiated in Tris-Acetate-Phosphate (TAP) liquid media, pH 7.0. For agar-grown cultures, 1 mL of liquid culture was evenly spread across 11 cm Petri dishes half-filled with 1.5% (*w:v*) TAP agar media. The liquid medium was evaporated for 0.5 h in a sterile air-flow bench before the lid was replaced, but not sealed. Liquid and agar-grown cultures were grown under constant LL (50  $\mu\text{mol photons m}^{-2} \text{s}^{-1}$ ) at 20 °C in a growth chamber (Percival PGC-6HO, CLF Plant Climatics GmbH, Wertingen, Germany). HL was provided by increasing the light intensity of the growth chamber to 600  $\mu\text{mol photons m}^{-2} \text{s}^{-1}$  for 4 h.

### 4.2. Chlorophyll Fluorescence Measurements

Pulse-amplitude modulation (PAM) measurements of chlorophyll fluorescence (*F*) parameters were performed with an Imaging PAM (WALZ). After dark treatment, minimum (*F*<sub>0</sub>) and maximum fluorescence (*F*<sub>m</sub>) was measured immediately before and during a 200 ms saturating pulse (6000  $\mu\text{mol photons m}^{-2} \text{s}^{-1}$ ), respectively. The maximum quantum yield of photosystem II (*F*<sub>v</sub>/*F*<sub>m</sub>) was calculated via (*F*<sub>m</sub>−*F*<sub>0</sub>)/*F*<sub>m</sub> after 1.5 h recovery in dark. NPQ was calculated via (*F*<sub>m</sub>−*F*<sub>m</sub><sup>'</sup>)/*F*<sub>m</sub>, with *F*<sub>m</sub><sup>'</sup> measured after 2 min at 750  $\mu\text{mol photons m}^{-2} \text{s}^{-1}$ .

### 4.3. Exogenous $\beta$ -Cyclocitral Treatments

For treatments, advantage was taken of the volatility of  $\beta$ -cyclocitral (Sigma-Aldrich), which was placed on a paper wick within the middle of a sealed Petri dish to treat agar-grown cells, in an identical approach used for acrolein treatments [13].  $\beta$ -cyclocitral was diluted in 100% p.a. methanol and 1  $\mu\text{L}$  containing 0–0.3  $\mu\text{L}$  of diluted  $\beta$ -cyclocitral (mock = 1  $\mu\text{L}$  pure methanol) was placed on a paper wick in an Eppendorf lid in the centre of a 11 cm Petri dish, which was immediately sealed with Parafilm and left under very LL (2  $\mu\text{mol photons m}^{-2} \text{s}^{-1}$ ). After 2–4 h, as indicated, cells within 2 cm of the middle of the plate were gently scraped from the agar with a spatula and immediately frozen in liquid nitrogen prior to biochemical analyses.  $\beta$ -cyclocitral concentrations in parts per million (ppm) were calculated on a volume basis, considering a 30 cm<sup>3</sup> air space in a 11 cm Petri dish, a  $\beta$ -cyclocitral density of 0.943 g mL<sup>−1</sup>, 95% purity, and the particle-related gas

concentration of  $0.0241 \text{ m}^3/\text{mol}$ , so that  $0.12 \text{ }\mu\text{L}$  of  $\beta$ -cyclocitral corresponded to 600 ppm inside the Petri dish.

#### 4.4. HPLC Analysis of Glutathione and Pigments, Western Blotting of Glutathione Peroxidase 5, and LC-MS/MS Measurement of RES

All methods were conducted according to Roach et al., [13], after 4 h treatment. For HPLC analyses (glutathione and pigments), cells were first freeze-dried for 3 days and each replicate was composed of 8–10 mg dry weight. For Western blotting of GPX5 levels and LC-MS/MS analyses of RES, cells were not freeze-dried. Loading of protein extracts and normalisation of pigments was made to total chlorophyll of the extract, according to [13]. For western blotting, the GPXh antibody (AS15 2882, Agrisera, Vännäs, Sweden) at a ratio of 1:10.000 and PsbA antibody (AS05 084, Agrisera, Vännäs, Sweden) at a ratio of 1:25.000 were used.

#### 4.5. Singlet Oxygen Resistance Test

Resistance to singlet oxygen was performed by suspending liquid cultures in fresh TAP media with RB at 0, 4, 7, and  $10 \text{ }\mu\text{M}$  of RB in a 96-well multiwall plate with a total volume of  $200 \text{ }\mu\text{L}$  per well. One light treatment consisted of a  $^1\text{O}_2$  shock by exposure to  $250 \text{ }\mu\text{mol photons m}^{-2} \text{ s}^{-1}$  for 10 min before recovery at  $20 \text{ }\mu\text{mol photons m}^{-2} \text{ s}^{-1}$ , and another was constant exposure to  $50 \text{ }\mu\text{mol photons m}^{-2} \text{ s}^{-1}$ . After 24 h, cell density at 650 nm was measured as an indicator of cell number for calculating differences between each RB treatment and cells without RB for each genotype and pre-treatment individually.

#### 4.6. RNA-Seq Analysis

Total RNA was extracted with the Rneasy Plant Mini Kit (Qiagen, Hilden, Germany) and additional on-column Dnase treatment (Rnase-free Dnase set, Qiagen) from ca. 15 mg (fresh weight) per replicate (=1 Petri dish). Cells were harvested after a 2 h treatment with 600 ppm of  $\beta$ -cyclocitral diluted in methanol, or for control with methanol only. Poly A-enriched library preps were sequenced with an Illumina HiSeq2500 using single-end 50 bp read lengths, by the NGS Core Facility of the Vienna Biocentre, Austria, resulting in an average of 24,063,263 reads per replicate,  $n = 3$ . Reads were aligned against the *C. reinhardtii* reference genome (JGI v5.5 release) with STAR version 2.5.1b, created by Dobin et al. [33] (Cold Springs Harbour, New York, NY, USA), using 2-pass alignment mode.

#### 4.7. Data Analysis and Statistics

For all measurements, one Petri dish of cell culture counted as an individual biological replicate. The RNA-Seq analysis data was analysed by the Bioinformatics and Scientific Computing Core of the Vienna Biocenter Core Facilities with the R package limma for selecting genes that were differently expressed more than two-fold between control and treatment (i.e., mock cells v  $\beta$ -cyclocitral-treated cells). The  $p$ -values used for filtering differentially expressed genes were cut off at  $p < 0.01$ . KEGG pathways and gene ontology annotations (*Chlamydomonas*-based) were conducted using the Algal Functional Annotation Tool [34].

Significant differences for biochemical measurements and chlorophyll fluorescence at  $p < 0.05$  were calculated in IBM SPSS Statistics, version 24, IBM, (New York, NY, USA) using one-way ANOVA with Tukey's post hoc test, or for pairwise comparisons using t-test with independent samples. A multivariate general linear model (MANOVA) was additionally calculated to evaluate the influence of genotype on RES tolerance.

## 5. Conclusions

Overall, we first conclude that  $\beta$ -cyclocitral is not a particularly reactive aldehyde since it does not lead to loss of  $F_v/F_m$  or modulate GSH concentrations like RES do. Second, unlike most RES,  $\beta$ -cyclocitral concentrations are not associated with HL stress in *C. reinhardtii*. Third, GPX5 helps mitigate HL stress by breaking down RES produced by  $^1\text{O}_2$ .

Fourth,  $\beta$ -cyclocitral is unable to induce tolerance to  $^1\text{O}_2$ , and does not seem to contribute to  $^1\text{O}_2$  signalling in *C. reinhardtii*, but instead may have a specific role in down-regulating chlorophyll synthesis.

**Supplementary Materials:** The following supporting information can be downloaded at: <https://www.mdpi.com/article/10.3390/plants11162155/s1>, Figure S1: Effect of  $\beta$ -cyclocitral treatments on NPQ, the xanthophyll cycle, and  $F_v/F_m$  in high light-treated cells. Figure S2: Effect of exogenous treatment with acrolein or  $\beta$ -cyclocitral on RES levels. Figure S3: Effect of  $\beta$ -cyclocitral, HL, and acrolein treatments on total glutathione (GHS + GSSG) contents. Figure S4: Overlap in differential gene expressional changes between  $^1\text{O}_2$  stress, acrolein, and  $\beta$ -cyclocitral treatments. Figure S5: Genes with transcription down-regulated by 600 ppm of  $\beta$ -cyclocitral that are involved in porphyrin and chlorophyll metabolism. Table S1: Transcriptional levels from an RNA-Seq analysis of *Chlamydomonas reinhardtii* treated with 600 ppm of  $\beta$ -cyclocitral in comparison to control (mock-treated) identically grown cells.

**Author Contributions:** Conceptualization, T.R.; methodology, T.R. and T.B.; investigation, T.R. and T.B.; resources, T.R. and I.K.; writing—original draft preparation, T.R.; writing—review and editing, T.R. and I.K.; funding acquisition, T.R. All authors have read and agreed to the published version of the manuscript.

**Funding:** This research was funded by The Austrian Research Promotion Agency (FFG) BRIDGE programme (project ALAS, grant number 41863779).

**Institutional Review Board Statement:** Not applicable.

**Informed Consent Statement:** Not applicable.

**Data Availability Statement:** Raw data is available from the corresponding author upon request.

**Acknowledgments:** We thank Wolfgang Stöggel and Bettina Lehr (University of Innsbruck) for LC-MS measurements and general lab assistance, respectively.

**Conflicts of Interest:** The authors declare no conflict of interest.

## References

- Roach, T.; Krieger-Liszkay, A. Photosynthetic regulatory mechanisms for efficiency and prevention of photo-oxidative stress. In *Annual Plant Reviews Online*; John Wiley & Sons, Inc.: Hoboken, NJ, USA, 2019; pp. 273–306.
- Crawford, T.; Lehotai, N.; Strand, Å. The role of retrograde signals during plant stress responses. *J. Exp. Bot.* **2018**, *69*, 2783–2795. [[CrossRef](#)] [[PubMed](#)]
- Chan, K.X.; Phua, S.Y.; Crisp, P.; McQuinn, R.; Pogson, B.J. Learning the languages of the chloroplast: Retrograde signaling and beyond. *Annu. Rev. Plant Biol.* **2016**, *67*, 25–53. [[CrossRef](#)] [[PubMed](#)]
- Larkin, R.M.; Alonso, J.M.; Ecker, J.R.; Chory, J. GUN4, a regulator of chlorophyll synthesis and intracellular signaling. *Science* **2003**, *299*, 902–906. [[CrossRef](#)] [[PubMed](#)]
- Shimizu, T.; Masuda, T. The role of tetrapyrrole- and GUN1-dependent signaling on chloroplast biogenesis. *Plants* **2021**, *10*, 196. [[CrossRef](#)] [[PubMed](#)]
- Fischer, B.B.; Hideg, É.; Krieger-Liszkay, A. Production, detection, and signaling of singlet oxygen in photosynthetic organisms. *Antioxid. Redox Signal.* **2013**, *18*, 2145–2162. [[CrossRef](#)] [[PubMed](#)]
- Kim, C.; Apel, K. Singlet oxygen-mediated signaling in plants: Moving from flt to wild type reveals an increasing complexity. *Photosynth. Res.* **2013**, *116*, 455–464. [[CrossRef](#)]
- Erickson, E.; Wakao, S.; Niyogi, K.K. Light stress and photoprotection in *Chlamydomonas reinhardtii*. *Plant J.* **2015**, *82*, 449–465. [[CrossRef](#)]
- Ramel, F.; Birtic, S.; Ginies, C.; Soubigou-Taconnat, L.; Triantaphylidès, C.; Havaux, M. Carotenoid oxidation products are stress signals that mediate gene responses to singlet oxygen in plants. *Proc. Natl. Acad. Sci. USA* **2012**, *109*, 5535–5540. [[CrossRef](#)]
- Mano, J.; Biswas, M.S.; Sugimoto, K. Reactive carbonyl species: A missing link in ROS signaling. *Plants* **2019**, *8*, 391. [[CrossRef](#)]
- Farmer, E.E.; Mueller, M.J. Ros-mediated lipid peroxidation and RES-activated signaling. *Annu. Rev. Plant Biol.* **2013**, *64*, 429–450. [[CrossRef](#)]
- Fischer, B.B.; Ledford, H.K.; Wakao, S.; Huang, S.G.; Casero, D.; Pellegrini, M.; Merchant, S.S.; Koller, A.; Eggen, R.I.L.; Niyogi, K.K. Singlet oxygen resistant 1 links reactive electrophile signaling to singlet oxygen acclimation in *Chlamydomonas reinhardtii*. *Proc. Natl. Acad. Sci. USA* **2012**, *109*, E1302–E1311. [[CrossRef](#)] [[PubMed](#)]
- Roach, T.; Stöggel, W.; Baur, T.; Kranner, I. Distress and eustress of reactive electrophiles and relevance to light stress acclimation via stimulation of thiol/disulfide-based redox defences. *Free Radic. Biol. Med.* **2018**, *122*, 65–73. [[CrossRef](#)] [[PubMed](#)]

14. Venkanna, D.; Südfeld, C.; Baier, T.; Homburg, S.V.; Patel, A.V.; Wobbe, L.; Kruse, O. Knock-down of the IFR1 protein perturbs the homeostasis of reactive electrophile species and boosts photosynthetic hydrogen production in *Chlamydomonas reinhardtii*. *Front. Plant Sci.* **2017**, *8*, 1347. [CrossRef] [PubMed]
15. Mano, J.; Ishibashi, A.; Muneuchi, H.; Morita, C.; Sakai, H.; Biswas, M.S.; Koeduka, T.; Kitajima, S. Acrolein-detoxifying isozymes of glutathione transferase in plants. *Planta* **2017**, *245*, 255–264. [CrossRef] [PubMed]
16. LoPachin, R.M.; Gavin, T. Reactions of electrophiles with nucleophilic thiolate sites: Relevance to pathophysiological mechanisms and remediation. *Free Radic. Res.* **2016**, *50*, 195–205. [CrossRef]
17. Fischer, B.B.; Eggen, R.I.L.; Trebst, A.; Krieger-Liszakay, A. The glutathione peroxidase homologous gene *gpxh* in *Chlamydomonas reinhardtii* is upregulated by singlet oxygen produced in photosystem II. *Planta* **2006**, *223*, 583–590. [CrossRef]
18. Ledford, H.K.; Chin, B.L.; Niyogi, K.K. Acclimation to singlet oxygen stress in *Chlamydomonas reinhardtii*. *Eukaryot. Cell* **2007**, *6*, 919–930. [CrossRef]
19. Selye, H. A syndrome produced by diverse noxious agents. *Nature* **1936**, *138*, 32. [CrossRef]
20. Kranner, I.; Minibayeva, F.V.; Beckett, R.P.; Seal, C.E. What is stress? Concepts, definitions and applications in seed science. *New Phytol.* **2010**, *188*, 655–673. [CrossRef]
21. Allorent, G.; Tokutsu, R.; Roach, T.; Peers, G.; Cardol, P.; Girard-Bascou, J.; Seigneurin-Berny, D.; Petroustos, D.; Kuntz, M.; Breyton, C.; et al. A dual strategy to cope with high light in *Chlamydomonas reinhardtii*. *Plant Cell* **2013**, *25*, 545–557. [CrossRef]
22. Shumbe, L.; D’Alessandro, S.; Shao, N.; Chevalier, A.; Ksas, B.; Bock, R.; Havaux, M. Methylene blue sensitivity 1 (MBS1) is required for acclimation of *Arabidopsis* to singlet oxygen and acts downstream of  $\beta$ -cyclocitral. *Plant Cell Environ.* **2017**, *40*, 216–226. [CrossRef] [PubMed]
23. Shao, N.; Duan, G.Y.; Bock, R. A mediator of singlet oxygen responses in *Chlamydomonas reinhardtii* and *Arabidopsis* identified by a luciferase-based genetic screen in algal cells. *Plant Cell* **2013**, *25*, 4209–4226. [CrossRef] [PubMed]
24. Mucciarelli, M.; Camusso, W.; Berteza, C.M.; Bossi, S.; Maffei, M. Effect of (+)-pulegone and other oil components of *mentha* × *piperita* on cucumber respiration. *Phytochemistry* **2001**, *57*, 91–98. [CrossRef]
25. Roach, T.; Na, C.S.; Stöggel, W.; Krieger-Liszakay, A. The non-photochemical quenching protein LHCSR3 prevents oxygen-dependent photoinhibition in *Chlamydomonas reinhardtii*. *J. Exp. Bot.* **2020**, *71*, 2650–2660. [CrossRef] [PubMed]
26. Fischer, B.B.; Dayer, R.; Schwarzenbach, Y.; Lemaire, S.D.; Behra, R.; Liedtke, A.; Eggen, R.I.L. Function and regulation of the glutathione peroxidase homologous gene *gpxh/gpx5* in *Chlamydomonas reinhardtii*. *Plant Mol. Biol.* **2009**, *71*, 569–583. [CrossRef]
27. Roach, T.; Baur, T.; Stöggel, W.; Krieger-Liszakay, A. *Chlamydomonas reinhardtii* responding to high light: A role for 2-propenal (acrolein). *Physiol. Plant.* **2017**, *161*, 75–87. [CrossRef]
28. Mano, J. Reactive carbonyl species: Their production from lipid peroxides, action in environmental stress, and the detoxification mechanism. *Plant Physiol. Biochem.* **2012**, *59*, 90–97. [CrossRef]
29. Biswas, M.S.; Mano, J. Lipid peroxide-derived short-chain carbonyls mediate hydrogen peroxide-induced and salt-induced programmed cell death in plants. *Plant Physiol.* **2015**, *168*, 885–898. [CrossRef]
30. Brzezowski, P.; Sharifi, M.N.; Dent, R.M.; Morhard, M.K.; Niyogi, K.K.; Grimm, B. Mg chelatase in chlorophyll synthesis and retrograde signaling in *Chlamydomonas reinhardtii*: CHLI2 cannot substitute for CHLI1. *J. Exp. Bot.* **2016**, *67*, 3925–3938. [CrossRef]
31. Tabrizi, S.T.; Sawicki, A.; Zhou, S.; Luo, M.; Willows, R.D. GUN4-protoporphyrin IX is a singlet oxygen generator with consequences for plastid retrograde signaling. *J. Biol. Chem.* **2016**, *291*, 8978–8984. [CrossRef]
32. Brzezowski, P.; Schlicke, H.; Richter, A.; Dent, R.M.; Niyogi, K.K.; Grimm, B. The GUN4 protein plays a regulatory role in tetrapyrrole biosynthesis and chloroplast-to-nucleus signalling in *Chlamydomonas reinhardtii*. *Plant J.* **2014**, *79*, 285–298. [CrossRef] [PubMed]
33. Dobin, A.; Davis, C.A.; Schlesinger, F.; Drenkow, J.; Zaleski, C.; Jha, S.; Batut, P.; Chaisson, M.; Gingeras, T.R. STAR: Ultrafast universal RNA-seq aligner. *Bioinformatics* **2013**, *29*, 15–21. [CrossRef] [PubMed]
34. The Algal Functional Annotation Tool. Available online: <http://pathways.mcdb.ucla.edu/algal/index.html> (accessed on 7 June 2018).

## Article

# The C-Terminal Region of SLIM1 Transcription Factor Is Required for Sulfur Deficiency Response

Justyna Piotrowska <sup>1,†</sup>, Yuki Jodoi <sup>2,†</sup>, Nguyen Ha Trang <sup>2</sup>, Anna Wawrzynska <sup>1</sup>, Hideki Takahashi <sup>3,4</sup>, Agnieszka Sirko <sup>1</sup> and Akiko Maruyama-Nakashita <sup>2,3,\*</sup>

<sup>1</sup> Institute of Biochemistry and Biophysics Polish Academy of Sciences, ul. Pawinskiego 5A, 02-106 Warsaw, Poland

<sup>2</sup> Department of Bioscience and Biotechnology, Graduate School of Bioresource and Bioenvironmental Sciences, Faculty of Agriculture, Kyushu University, 744 Motooka, Nishi-ku, Fukuoka 819-0395, Fukuoka, Japan

<sup>3</sup> RIKEN Plant Science Center, 1-7-22 Suehiro-cho, Tsurumi-ku, Yokohama 230-0045, Kanagawa, Japan

<sup>4</sup> Department of Biochemistry and Molecular Biology, Michigan State University, East Lansing, MI 48824, USA

\* Correspondence: amaru@agr.kyushu-u.ac.jp; Tel.: +81-92-802-4712

† These authors contributed equally to this work.

**Abstract:** Sulfur LIMitation1 (SLIM1) transcription factor coordinates gene expression in plants in response to sulfur deficiency (−S). SLIM1 belongs to the family of plant-specific EIL transcription factors with EIN3 and EIL1, which regulate the ethylene-responsive gene expression. The EIL domains consist of DNA binding and dimerization domains highly conserved among EIL family members, while the N- and C-terminal regions are structurally variable and postulated to have regulatory roles in this protein family, such that the EIN3 C-terminal region is essential for its ethylene-responsive activation. In this study, we focused on the roles of the SLIM1 C-terminal region. We examined the transactivation activity of the full-length and the truncated SLIM1 in yeast and *Arabidopsis*. The full-length SLIM1 and the truncated form of SLIM1 with a deletion of C-terminal 106 amino acids ( $\Delta$ C105) transactivated the reporter gene expression in yeast when they were fused to the GAL4 DNA binding domain, whereas the deletion of additional 15 amino acids to remove the C-terminal 120 amino acids ( $\Delta$ C120) eliminated such an activity, identifying the necessity of that 15-amino-acid segment for transactivation. In the *Arabidopsis slim1-2* mutant, the transcript levels of *SULTR1;2* sulfate transporter and the GFP expression derived from the *SULTR1;2* promoter-GFP (*P<sub>SULTR1;2</sub>-GFP*) transgene construct were restored under −S by introducing the full-length SLIM1, but not with the C-terminal truncated forms  $\Delta$ C105 and  $\Delta$ C57. Furthermore, the transcript levels of −S-responsive genes were restored concomitantly with an increase in glutathione accumulation in the complementing lines with the full-length SLIM1 but not with  $\Delta$ C57. The C-terminal 57 amino acids of SLIM1 were also shown to be necessary for transactivation of a −S-inducible gene, *SHM7/MSA1*, in a transient expression system using the *SHM7/MSA1* promoter-GUS as a reporter. These findings suggest that the C-terminal region is essential for the SLIM1 activity.

**Keywords:** SLIM1 transcription factor; sulfur deficiency; *Arabidopsis thaliana*; sulfate transporter; sulfate assimilation

**Citation:** Piotrowska, J.; Jodoi, Y.; Trang, N.H.; Wawrzynska, A.; Takahashi, H.; Sirko, A.; Maruyama-Nakashita, A. The C-Terminal Region of SLIM1 Transcription Factor Is Required for Sulfur Deficiency Response. *Plants* **2022**, *11*, 2595. <https://doi.org/10.3390/plants11192595>

Academic Editors: Milan S. Stankovic, Paula Baptista and Petronia Carillo

Received: 27 August 2022

Accepted: 27 September 2022

Published: 2 October 2022

**Publisher's Note:** MDPI stays neutral with regard to jurisdictional claims in published maps and institutional affiliations.



**Copyright:** © 2022 by the authors. Licensee MDPI, Basel, Switzerland. This article is an open access article distributed under the terms and conditions of the Creative Commons Attribution (CC BY) license (<https://creativecommons.org/licenses/by/4.0/>).

## 1. Introduction

Sulfur (S) is an essential nutrient for all organisms. Plants use sulfate as an S source to assimilate it into cysteine and synthesize various organic S compounds [1,2]. The importance of plants in the global S cycle in nature is evident because animals cannot assimilate sulfate and they rather consume S-containing amino acids and proteins as dietary S sources [1,2].

SLIM1/EIL3 is a transcription factor (TF) that controls the S deficiency (−S) responsive gene expression, while it belongs to the plant-specific EIL family of TFs (EIL-TFs) [3,4]. The EIL domain is conserved among the EIL-TFs, but the N- and C-terminal regions are variable (Figure 1) [5]. The best-characterized member of the EIL-TFs family is EIN3

(Ethylene-INsensitive3) which initiates downstream transcriptional cascades for ethylene responses [6–8]. Studies of ethylene-responsive elements demonstrated that EIN3 binds to the upstream sequence in an ethylene-responsive gene, *ERF1*, through the DNA binding domains, BD I to IV (1 to 359 amino acids of EIN3) [7]. The DNA binding domain was further narrowed down to a specific region from 174 to 306 amino acids (aa) containing BD III and IV [9]. Despite that the N-terminal half region of EIN3 controls the DNA binding and its dimerization, the protein stability of EIN3 is controlled via its C-terminal region, which interacts with EBF1 (EIN3-Binding F-box Protein 1) and EBF2, responding to ethylene and the plant carbon status [7,10–12].

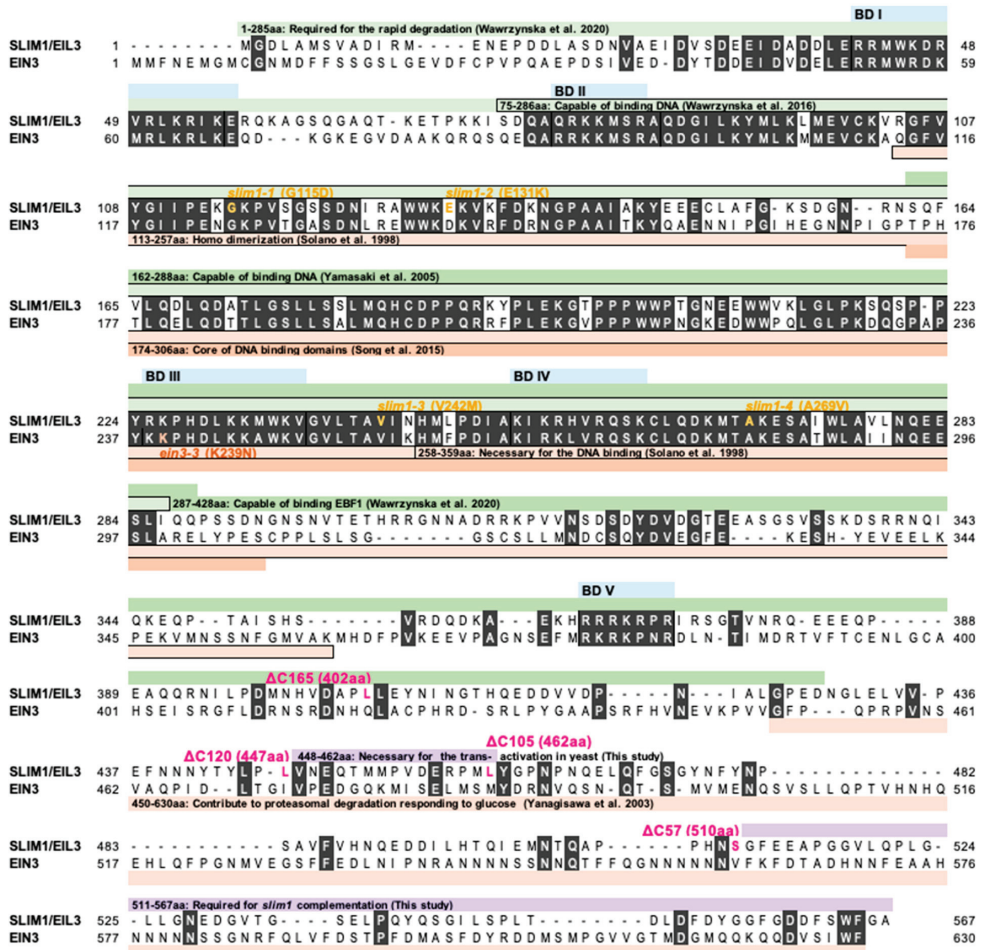


**Figure 1.** Alignment of SLIM1 and EIN3 proteins in *Arabidopsis thaliana*. Alignment of full protein sequences was performed by the ClustalW program at the DNA Data Bank of Japan (DDBJ) (<http://www.ddbj.nig.ac.jp/search/clustalw-j.html>, accessed on 8 May 2017). Amino acid residues conserved between SLIM1 and EIN3 are shown with white characters and dark gray background. Predicted DNA binding domains (BD I to BD V) are shown with pale blue bars. Yellow and brown characters indicate the positions of *slim1* mutations (*slim1-1*, *slim1-2*, *slim1-3*, and *slim1-4*) and *ein3-3* mutation, respectively. Magenta characters show the last amino acid in each C-terminal truncated form of SLIM1. Green and orange bars describe existing knowledge about domain structures of SLIM1 and EIN3, respectively. Violet bars highlight the findings in this study.

The domain structure for SLIM1 has been studied concurrently (Figure 1). Like EIN3, the N-terminal region of SLIM1 (75 to 286 aa), including BD II, III, and IV, can bind to the UPE-box (AGATACATTGAACCTGGACA), which has been shown as the conserved sequence among several  $-S$  responsive genes [13,14]. The 162-to-288 aa region of SLIM1, including BD III and IV, can interact with the conserved EIL binding sequence, AYGWAYCT [7,15], although with less affinity compared to EIN3 [16]. The *slim1* mutations in the protein coding region are only found in the conserved region spanning BD II, III, and IV [3]. Despite the genetic evidence and information that supports specific DNA binding capabilities of SLIM1, molecular mechanisms involved in  $-S$  responses via the regulation of the SLIM1 protein activity has not been elucidated yet.

The activity of SLIM1 seems to be controlled post-transcriptionally based on the observation that SLIM1 transcript levels did not increase under  $-S$ , and the complementation of *slim1* mutants only occurred under  $-S$  even though the expression of SLIM1 was driven by a cauliflower mosaic virus (CaMV) 35S promoter which allows constitutive expression [3]. Recently, it has been demonstrated that SLIM1 undergoes proteasomal degradation facilitated by the N-terminal 285 aa region [17]. In contrast to EIN3, SLIM1 interacts only with EBF1 but not EBF2, and the protein region to interact with EBF1 has been shown to be localized at the C-terminal portion (residues 287-428 of SLIM1) [17]. Further characterization of proteasomal degradation through dissection of the C-terminal region may clarify mechanisms that control the SLIM1 protein activity.

In this study, we focused on investigating the role of the SLIM1 C-terminal region by dissecting the region required for transactivation of target gene expression under  $-S$ . Our results indicated that the C-terminal region of SLIM1 is indispensable to its activity under  $-S$ .

## 2. Results and Discussion

### 2.1. The C-Terminal Region of SLIM1 Is Required for Transactivation in Yeast

To explore the function of the C-terminal region of SLIM1, the full-length and the C-terminal truncated forms of SLIM1 were expressed as fusion proteins with the DNA binding domain of GAL4 (BD-GAL4) in a histidine (His) auxotrophic yeast strain AH109, which allowed us to characterize the ability of these BD-GAL4 fusion proteins to bind to the upstream activation sequence and transactivate the *HIS3* reporter gene by monitoring the growth on the selective medium lacking His (Figure 2). For preparation of the C-terminal truncation of SLIM1, 57, 105, 120, 137, 150, and 165 aa were deleted from the C-terminal end of SLIM1 and named  $\Delta C57$ ,  $\Delta C105$ ,  $\Delta C120$ ,  $\Delta C137$ ,  $\Delta C150$ , and  $\Delta C165$ , respectively. Each plasmid construct with the BD-GAL4 fusion for the full-length or the C-terminal truncated SLIM1 was integrated into the yeast strain AH109 and grew on agar plates lacking tryptophan ( $-Trp$ ) or Trp and His ( $-Trp/-His$ ) supplemented with or without 3-AT (Figure 2). The yeast cells expressing the BD-GAL4 full-length SLIM1 fusion protein grew well on both the control ( $-Trp$ ) and selective ( $-Trp/-His$ ,  $-Trp/-His$  10 mM 3-AT) media, while the empty plasmid with the BD-GAL4 alone could grow only on the control medium ( $-Trp$ ). Among the yeast cells expressing the BD-GAL4 fusion proteins with the C-terminal truncated forms of SLIM1, only the  $\Delta C57$  and  $\Delta C105$  variants grew well on both the control and selective media, but others with longer deletions did not grow on the selective medium. These results indicated that the 15 aa (VNEQTMMPVDERPML) located at the positions 448 to 462 aa of SLIM1 (105 to 119 from the C-terminal end of SLIM1) are necessary for transactivation of the *HIS3* gene expression in yeast.

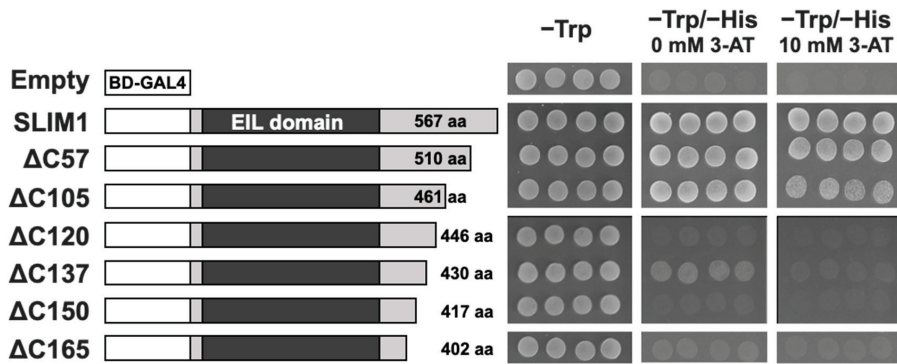


**Figure 2.** Trans-activation of *HIS3* gene expression in yeast. The left panel shows the schematic representations of SLIM1 proteins fused to the GAL4 DNA-binding domain (BD-GAL4). Empty: no insertion, SLIM1: full-length SLIM1, ΔC57, ΔC105, ΔC120, ΔC137, ΔC150, and ΔC165: C-terminal truncated forms of SLIM1 lacking the C-terminal 57, 105, 120, 137, 150, and 165 amino acids, respectively. BD-GAL4: DNA binding domain of yeast GAL4 protein. Four independent colonies obtained from each plasmid transformation of yeast strain AH109 were spotted on the minimal SD agar medium lacking Trp (–Trp) or Trp and His (–Trp/–His) with or without 10 mM 3-amino-1,2,4-triazole (3-AT). The right panel shows the yeast growth at 30 °C for 3 days after spotting.

### 2.2. C-Terminal 57 Amino Acids in SLIM1 Are Necessary for *slim1* Complementation

To further investigate the roles of the SLIM1 C-terminal region in plants, the full-length and the C-terminal truncated forms of SLIM1 were expressed in *Arabidopsis slim1-2* mutant, which allows monitoring of plant –S responses displayed as fluorescence of GFP expressed under the control of the promoter region of *SULTR1;2* sulfate transporter [3,18].

In plants exposed to –S, both the GFP fluorescence and the *SULTR1;2* transcript expression recovered by expression of the full-length SLIM1 in the *slim1-2* mutant, but not with the C-terminal 57 and 105 aa truncated forms, ΔC57 and ΔC105 (Figure 3; S0 condition). However, consistent with our previous observation [3], the recovery of these phenotypes was only seen under –S, although the CaMV 35S promoter was used for SLIM1 overexpression. We also found that both the overexpression of ΔC57 and ΔC105 weakened the *P<sub>SULTR1;2</sub>-GFP* derived expression of GFP fluorescence relative to *slim1-2* (Figure 3a), as well as the *SULTR1;2* transcript expression, particularly under –S conditions (Figure 3b). We obtained the similar results with the C-terminal 165 aa truncated form, ΔC165 (data not shown).

The transcript levels of other –S-responsive genes, *BGLU28*, *SDI1*, *SULTR2;1*, and *APR3*, were similarly influenced in the complemented lines; i.e., their –S responses were restored by introducing the full-length SLIM1 but not by ΔC57 (Figure 4). Interestingly, the induction of *SULTR2;1* and *APR3* gene expression under –S were also influenced by the C-terminal 57 aa, although their –S induction was reported as SLIM1-independent [3]. These results indicate that the C-terminal 57 aa region of SLIM1 is required for complementation of the *slim1-2* mutant.

To gain further insights into the –S-responsive phenotypes affected by the C-terminal 57 aa deletion (ΔC57), we analyzed the tissue sulfate, cysteine, and GSH levels. Sulfate levels were not different among the plant lines under both S1500 (S-sufficient) and S0 (–S) conditions (Figure 5). Cysteine levels were similar between the parental line and *slim1-2* but slightly increased in ΔC57/*slim1-2* compared to SLIM1/*slim1-2* under both S1500 and S0 conditions. GSH levels were lower in *slim1-2* than in the parental line under S1500 and lower in ΔC57/*slim1-2* than in SLIM1/*slim1-2* under S0 conditions (Figure 5). These results suggest that sulfate assimilation is restored by overexpression of the full-length SLIM1 to complement *slim1-2* under –S, but not with the C-terminal truncated form ΔC57.

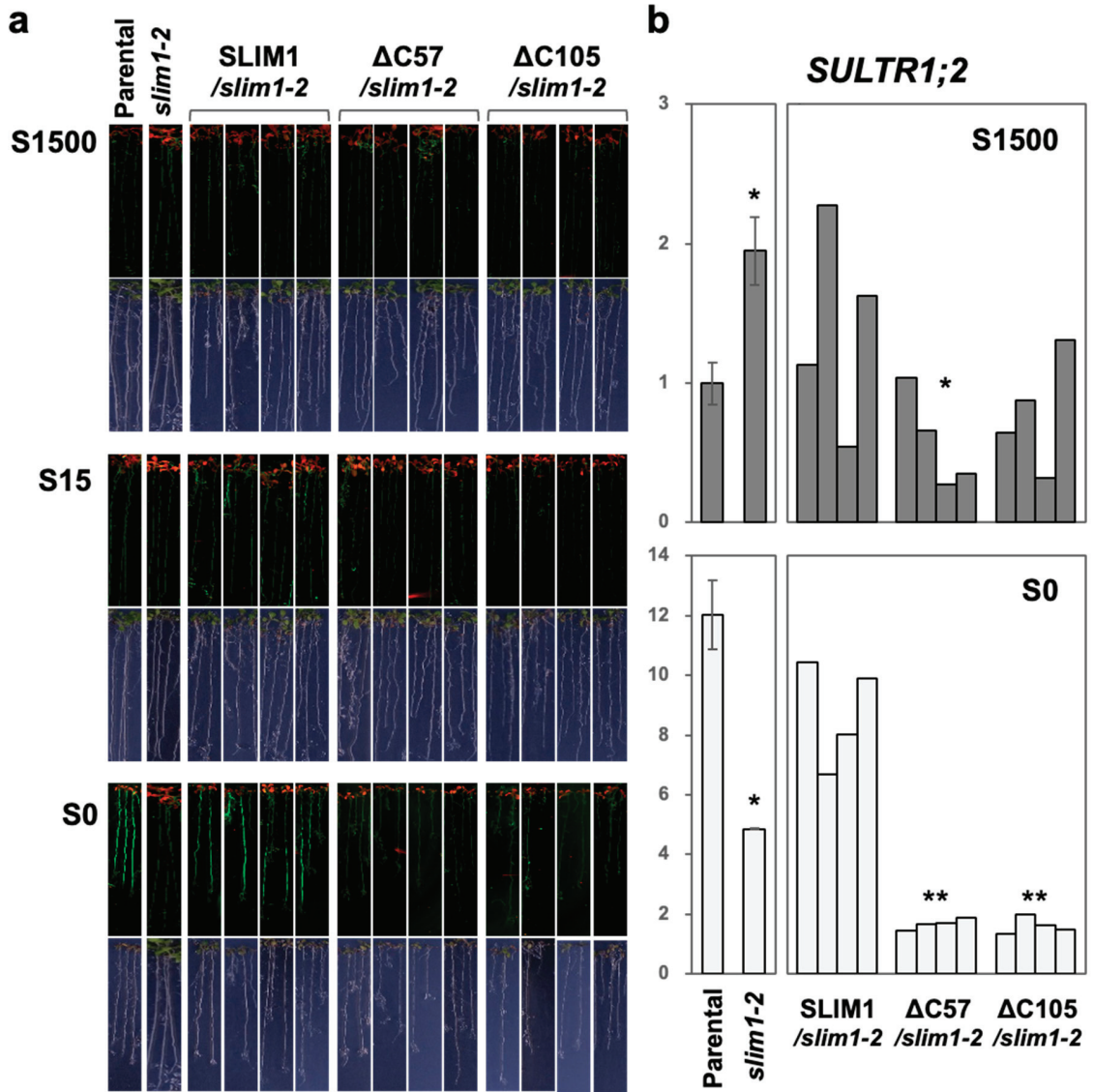


**Figure 3.** Complementation of *Arabidopsis slim1-2* by expressing the full-length and C-terminal truncated forms of *SLIM1*. The full-length *SLIM1* or the C-terminal truncated variants were expressed in *slim1-2* under CaMV 35S promoter (*SLIM1/slim1-2*,  $\Delta C57/slim1-2$ , and  $\Delta C105/slim1-2$ ). Parental (*P<sub>SULTR1;2</sub>-GFP*), *slim1-2*, and four independent lines of *SLIM1/slim1-2*,  $\Delta C57/slim1-2$ , and  $\Delta C105/slim1-2$  were grown on S1500, S15, and S0 media for 10 days. (a) GFP fluorescence in plants is visualized using an image analyzer. Fluorescent images (upper panels) and bright-field images (lower panels) are shown. (b) Transcript levels of *SULTR1;2* in roots. The average values are indicated with error bars denoting SEM ( $n = 3$ ) for Parental and *slim1-2* (left), and the single values are indicated for four independent transgenic lines generated for complementation with the full-length *SLIM1* or the C-terminal truncated variants. Asterisks indicate significant differences between Parental and *slim1-2* determined by Student's *t*-test (left), and between *SLIM1/slim1-2* and  $\Delta C57/slim1-2$  or  $\Delta C105/slim1-2$  by Dunnet's test (right) under S1500 and S0 conditions (\*\*  $p < 0.01$ , \*  $0.01 \leq p < 0.05$ ).

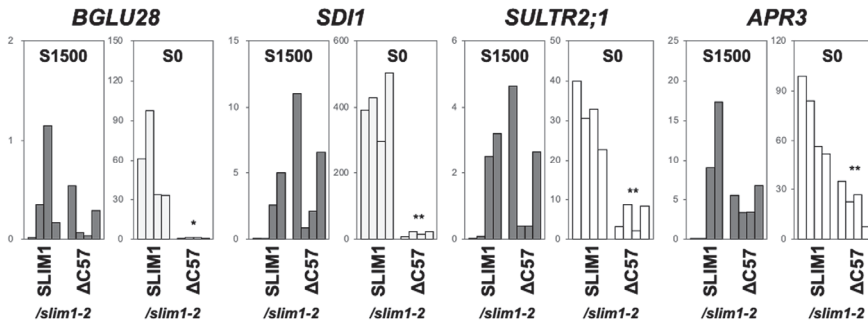


**Figure 4.** Transcript levels of *–S*-responsive genes in the complemented lines. Transcript levels of *BGLU28*, *SDI1*, *SULTR2;1*, and *APR3* in the roots of four independent lines of *SLIM1/slim1-2* and  $\Delta C57/slim1-2$  were determined by qRT-PCR with the same root-derived RNA used for the *SULTR1;2* transcript expression analysis in Figure 3b. Asterisks indicate significant differences between *SLIM1/slim1-2* and  $\Delta C57/slim1-2$  in S1500 and S0 conditions (Student’s *t*-test; \*\*  $p < 0.01$ , \*  $0.01 \leq p < 0.05$ ).

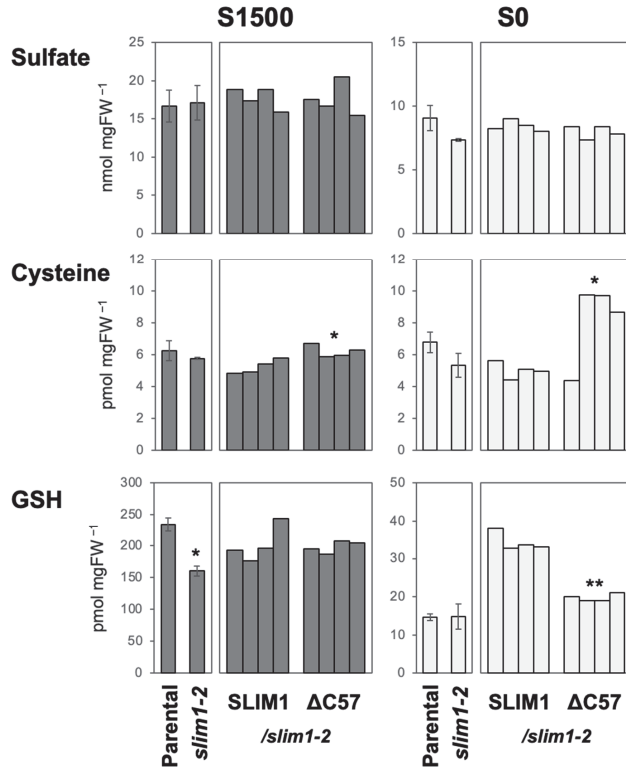


**Figure 5.** Sulfate, cysteine, and glutathione (GSH) levels in the complementation lines. Shoots of Parental (*P<sub>SULTR1;2-GFP</sub>*), *slim1-2*, and four independent lines of *SLIM1/slim1-2* and  $\Delta C57/slim1-2$  grown on S1500 and S0 media for 10 days were used for the metabolite analysis. The average values are indicated with error bars denoting SEM ( $n = 3$ ) for Parental and *slim1-2*, and the single values are indicated for four independent transgenic lines generated for complementation with the full-length *SLIM1* or  $\Delta C57$ . Asterisks indicate significant differences between Parental and *slim1-2* (left), and between *SLIM1/slim1-2* and  $\Delta C57/slim1-2$  (right) under S1500 and S0 conditions (Student’s *t*-test; \*\*  $p < 0.01$ , \*  $0.01 \leq p < 0.05$ ).

### 2.3. Transactivation of a $-S$ -Inducible Gene, *SHM7/MSA1*, Requires C-Terminal 57 Amino Acids of SLIM1

Next we tested how SLIM1 activity is affected by the C-terminal deletion using the transient *in planta* transactivation test (Figure 6). For this purpose, we selected one of the  $-S$ -inducible and SLIM1-dependent genes, *SHM7/MSA1* [3,19]. We constructed the reporter plasmid containing an *SHM7/MSA1* promoter-GUS expression cassette to monitor the transactivation of the *SHM7/MSA1* promoter by assessing the GUS activity. The reporter plasmid was transfected with the effector plasmids expressing either the full-length SLIM1 (SLIM1), or the C-terminal 57-aa truncated SLIM1 ( $\Delta$ C57) under the control of CaMV 35S promoter in *Nicotiana benthamiana* leaves. The GUS activity was analyzed after 3 days of transfection (Figure 6).

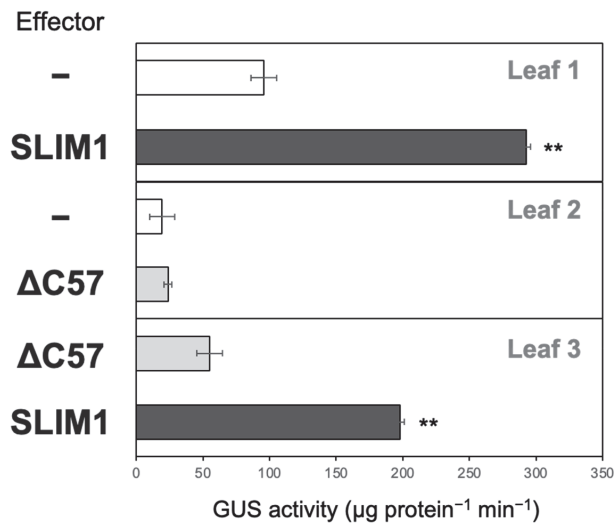


**Figure 6.** Transactivation of *SHM7/MSA1* promoter by full-length and C-terminal 57 aa truncated SLIM1. GUS activity was measured in transiently transformed *Nicotiana benthamiana* leaves incubated for 72 h after the infiltration with the reporter (*SHM7/MSA1* promoter-GUS) or the combination of the reporter and effectors (SLIM1 or  $\Delta$ C57). The *uidA* gene in the reporter constructs was driven by the *SHM7/MSA1* promoter (569 bp upstream of ATG), and the effector expressions were driven by the CaMV 35S promoter. The mean values are indicated with error bars denoting SD ( $n = 3$ ). Asterisks indicate significant differences between the two combinations of reporter and effector transfected in each leaf (Student's *t*-test; \*\*  $p < 0.01$ ).

The full-length SLIM1 increased the GUS activity compared to the leaf part, where only the reporter plasmid was introduced alone (Leaf 1 in Figure 6). In contrast,  $\Delta$ C57 did not show such an increase after the infiltration (Leaf 2 in Figure 6). When compared between the full-length SLIM1 and  $\Delta$ C57, the GUS activity was highly increased with the full-length SLIM1 infiltration (Leaf 3 in Figure 6). These results indicate that the C-terminal 57 aa region of SLIM1 is essential for activating SLIM1-controlled genes in plants.

### 2.4. Roles of SLIM1 C-Terminal Region

In this study, we found that the C-terminal region of SLIM1 is important for its protein functionality. We demonstrated the importance of the C-terminal 57 aa in activating expression of SLIM1-responsive genes in plants by using transgenic plants expressing *P<sub>SULTR1,2</sub>-GFP*. Besides the importance of this C-terminal 57 aa region *in planta*, our experiments revealed the function of an additional 15 aa region located between the positions 105 to 119 aa from the C-terminal end of SLIM1 to function as a transcriptional activator

in yeast. The contribution of this putative 15 aa activation domain remains an unsolved question *in planta*, because its presence in  $\Delta C57$  deletion was not sufficient to complement the *slim1* mutant.

Domain search tools in InterPro (<http://www.ebi.ac.uk/interpro/>, accessed on 9 July 2022) and Conserved Domains (<https://www.ncbi.nlm.nih.gov/Structure/cdd/cdd.shtml>, accessed on 9 July 2022) did not detect presence of significant domains in the C-terminal 120 aa of SLIM1, indicating that our findings may lead the novel molecular machinery controlling the SLIM1 functions. The SLIM1 protein stability is controlled by the N-terminal half (1–285 aa) [17]. In contrast, the C-terminal region could play roles in other aspects implicated for SLIM1 function, such as possible interaction with other proteins or protein modification required for transactivation. It would be necessary to examine the function of C-terminal 57 aa by further dissecting this region for *slim1* mutant complementation to clarify the molecular machinery of transcriptional activation associated with SLIM1 and connect these findings with the question of how plants respond to  $-S$ .

### 3. Materials and Methods

#### 3.1. Yeast Assay

Full-length or truncated *SLIM1* coding sequences were amplified with PCR using the forward primer SLIM1-F (5'-CACCATGGGCGATCTTGCTATGTCCGTAGC-3') in combination with the reverse primer, SLIM1-R (5'-CTAAGCTCAAACCATGAGAAATCATCACCA-3' for full length), SLIM1-510R (5'-ACTGTTGTGAGGTGGTGTGTTGTTATCATTCT-3' for truncation of C-terminal 57 aa,  $\Delta C57$ ), SLIM1-461R (5'-AAGCATTGGCCTTTCGTCTACAGGCATCATAGT-3' for  $\Delta C105$ ), SLIM1-446R (5'-GTGGAAGATAAGTATAGTTGTTATTGAATCAGGA-3' for  $\Delta C120$ ), SLIM1-430R (5'-CAGACCATTATCCTCTGGTCCTAAGGCA-3' for  $\Delta C137$ ), SLIM1-417R (5'-GACAACATCGTCCTCTTGATGAGTACCGT-3' for  $\Delta C150$ ), or SLIM1-402R (5'-CAGAGGGGCATCAACATGATTATCATCAGGT-3' for  $\Delta C165$ ), and KOD-Plus (TOYOBO, Osaka, Japan). The resultant fragments were purified from the agarose gel and cloned into pENTR/D-TOPO vector (Invitrogen, Waltham, MA, USA). After validating the sequence, each coding sequence was integrated into pBD-GAL4-GWRFC [20] using LR clonase (Invitrogen). The resultant plasmids were then transferred to *S. cerevisiae* strain AH109 (Clontech, Mountain View, CA, USA) according to the manufacturer's instructions (Matchmaker GAL4 Two-Hybrid System 3, Clontech). The yeast transformants were incubated at 30 °C on minimal SD medium (Clontech) lacking tryptophan (Trp) for three days. To verify the transcriptional activation through the function of GAL4-BD fusion proteins with the full-length and the C-terminal truncated forms of SLIM1 in yeast cells, four independent colonies per each plasmid were resuspended in sterilized double-distilled water and dropped on minimal SD medium lacking Trp or Trp and His with or without 10 mM 3-AT (TCI, Tokyo, Japan). pBD-GAL4 Cam plasmid (Stratagene, San Diego, CA, USA) was used as the negative control.

#### 3.2. Plant Materials and Growth Conditions

*P<sub>SULTRI;2</sub>-GFP* plants (Parental, *Arabidopsis thaliana* Columbia-0 (Col-0) accession) [18], *slim1-2* [3], and *slim1-2* complemented with the full-length or truncated *SLIM1* coding sequences were used as the plant samples.

To introduce the full-length *SLIM1* (SLIM1) and truncated *SLIM1* variants named  $\Delta C57$  and  $\Delta C105$ , their coding sequences cloned into pENTR/D-TOPO vector were integrated into pH35GS binary vector [21] using LR clonase (Invitrogen). The resultant binary plasmids were transferred to *Agrobacterium tumefaciens* GV3101 (pMP90) [22] and used for the transformation of *slim1-2* plants [23]. The transgenic plants were selected on GM media containing 30 mg L<sup>-1</sup> hygromycin sulfate.

The T<sub>2</sub> progenies of SLIM1/*slim1-2*,  $\Delta C57$ /*slim1-2*, and  $\Delta C105$ /*slim1-2* transgenic lines, and the parental line and *slim1-2* plants were vertically grown for 10 days on the agar medium [24] supplied with 1500  $\mu$ M (S1500), 15  $\mu$ M (S15), or 0  $\mu$ M (S0) sulfate at 22 °C and 16 h/8 h light (40  $\mu$ mol m<sup>-2</sup> s<sup>-1</sup>) and dark cycles.

### 3.3. Imaging of GFP Fluorescence

The expression of GFP in the whole intact seedlings was visualized by using the image analyzer, Amersham Typhoon scanner 5, equipped with a 525BP20 filter and a 488-nm laser (GE Healthcare, Chicago, IL, USA) as described previously [25].

### 3.4. Quantitative RT-PCR

Total RNA was extracted from root tissues using Sepasol-RNA I (Nacalai Tesque, Kyoto, Tapan) and reverse transcription was conducted using the PrimeScript RT Reagent Kit with gDNA Eraser (Takara, Japan). Subsequently, quantitative PCR was conducted using SYBR Premix Ex Taq II (Takara, Japan) and a Thermal Cycler Dice Real Time System (Takara, Japan). Relative mRNA abundance was calculated using ubiquitin (UBQ2, accession no. J05508) as a constitutive internal control. Gene-specific primers for quantitative PCR were previously described [3,26,27].

### 3.5. Measurements of Sulfate and Thiols (Cysteine and GSH)

Plant tissues were flash frozen in liquid nitrogen and extracted with 5 volumes of 10 mM HCl by homogenizing with Tissue Lyser MM300 (Retsch, Haan, Germany). The resultant mixtures were centrifuged at 4 °C, 13,000 rpm for 15 min, and the supernatant was used for sulfate and thiols analyses.

Sulfate contents were determined by ion chromatography (IC-2001, TOSOH, Tokyo, Japan) as described previously [28]. Cysteine and GSH contents were determined by HPLC-fluorescent detection system after labeling of thiol bases by monobromobimane as described previously [27]. The labeled products were separated by HPLC using the TSKgel ODS-120T column (150 × 4.6 mm, TOSOH) and detected using a scanning fluorescence detector FP-920 (JASCO, Oklahoma City, OK, USA), monitoring for fluorescence of thiol-bimane adducts at 478 nm under excitation at 390 nm. Cysteine and GSH (Nacalai Tesque, Kyoto, Japan) were used as standards.

### 3.6. Transient Trans-Activation Assay

pH35GS-SLIM1 and pH35GS-ΔC57 were used as the effector plasmids. For the reporter plasmid, we inserted *SHM7/MSA1* promoter sequence (569 bp upstream of ATG) amplified by PCR using the *A. thaliana* genomic DNA and primers, F: 5'-CACCTACCATAGTCCAACTCCATCC-3' and R: 5'-ACGTTGAAGATGATGAAGATTGG-3', into *NotI* and *XbaI* sites of the modified pGreenII0029 binary vector [29] and validated the sequence. The *trans*-activation assay was performed as previously described [13]. In brief, the reporter plasmid (*SHM7/MSA1* promoter-GUS), and the effector plasmids (pH35GS-SLIM1 and pH35GS-Δ57) were introduced into the *A. tumefaciens* strains LBA4404 and GV3101, respectively. After over-night growth of *A. tumefaciens* cultures at 28 °C, the cells were collected by centrifugation and resuspended in water to an OD600 = 0.1 (reporter plasmid) or 0.4 (effector plasmids). The same aliquots of resuspended cells were mixed and infiltrated to three well-expanded leaves of 5-week-old *N. benthamiana* plants using 2 mL needleless syringes. Samples were collected for protein extractions 72 h after leaf inoculation and used for the quantitative GUS assay. The three leaf discs (8 mm diameter) collected from three different leaves were extracted with buffer (100 mM sodium phosphate pH 8.0, 10 mM EDTA, 14 mM β-mercaptoethanol, 0.1% Triton X-100) and centrifuged at 11,000 × *g* for 5 min at 4 °C. Soluble protein level was quantified using the Bradford method [30]. GUS activity was measured as the absorbance at 415 nm after mixing 10 μL of extract and 140 μL of the extraction buffer containing 1 mM PNPG (*p*-nitrophenyl-β-D-glucuronide) and incubating the mixture at 37 °C for 30 min. The data were normalized with the absorbance of the sample without PNPG. The activity was calculated as μmol processed substrate mg<sup>-1</sup> total soluble protein min<sup>-1</sup>.

### 3.7. Statistical Analysis

The student's *t*-test (two-tailed) was used for pairwise comparisons between the parental plants and *slim1-2* mutants, between the SLIM1/*slim1-2* and  $\Delta$ C57/*slim1-2* lines, or between the two conditions in a leaf described in Figures 3–6. The Dunnett's *t*-test (two-tailed) was used for multiple comparisons between the SLIM1/*slim1-2* and  $\Delta$ C57/*slim1-2* or  $\Delta$ C105/*slim1-2* in Figure 3. Significant differences under the same treatment were shown with asterisks (\*\*  $p < 0.01$ , \*  $0.01 \leq p < 0.05$ ).

**Author Contributions:** Conceptualization, A.M.-N.; methodology, A.W. and A.M.-N.; formal analysis, J.P., Y.J., N.H.T., A.W. and A.M.-N.; writing—original draft preparation, A.W. and A.M.-N.; writing—review and editing, A.W., H.T., A.S. and A.M.-N.; supervision, A.W., H.T., A.S. and A.M.-N.; funding acquisition, A.W., A.S. and A.M.-N. All authors have read and agreed to the published version of the manuscript.

**Funding:** This work was supported by Japan Society for the Promotion of Science KAKENHI grant Number JP24380040, JP17H03785, JP22H02229, JP22H05573, and Initiative for Realizing Diversity in the Research Environment (for A.M.-N.), by National Science Centre in Poland, grants Number 2018/31/F/NZ1/02234 (for A.S.), and 2014/15/B/NZ1/01887 (for A.W.).

**Data Availability Statement:** All data were provided within the article.

**Acknowledgments:** We thank Masatoshi Yamaguchi (Saitama University) and Taku Demura (Nara Institute of Science and Technology) for providing us with the yeast plasmids. We thank Yukiko Okuo and Tomoko Yoshida-Ono for technical support. Plant growth and seed harvesting were performed at the Biotron Application Center, Kyushu University, Japan.

**Conflicts of Interest:** The authors have no conflict of interest to declare. The funders had no role in the design of the study; in the collection, analyses, or interpretation of data; in the writing of the manuscript, or in the decision to publish the results.

## References

1. Takahashi, H.; Kopriva, S.; Giordano, M.; Saito, K.; Hell, R. Sulfur assimilation in photosynthetic organisms: Molecular functions and regulations of transporters and assimilatory enzymes. *Annu. Rev. Plant Biol.* **2011**, *62*, 157–184. [[CrossRef](#)] [[PubMed](#)]
2. Long, S.R.; Kahn, M.; Seefeldt, L.; Tsay, Y.F.; Kopriva, S. Nitrogen and Sulfur. In *Biochemistry & Molecular Biology of Plants*, 2nd ed.; Buchana, B.B., Gruissem, W., Jones, R.L., Eds.; Wiley Blackwell: Oxford, UK, 2015; pp. 746–768.
3. Maruyama-Nakashita, A.; Nakamura, Y.; Tohge, T.; Saito, K.; Takahashi, H. *Arabidopsis* SLIM1 is a central transcriptional regulator of plant sulfur response and metabolism. *Plant Cell* **2006**, *18*, 3235–3251. [[CrossRef](#)] [[PubMed](#)]
4. Maruyama-Nakashita, A. Metabolic changes sustain the plant life in low-sulfur environments. *Curr. Opin. Plant Biol.* **2017**, *39*, 144–151. [[CrossRef](#)] [[PubMed](#)]
5. Li, Q.; Shen, Y.; Guo, L.; Wang, H.; Zhang, Y.; Fan, C.; Zheng, Y. The EIL transcription factor family in soybean: Genomewide identification, expression profiling and genetic diversity analysis. *FEBS Open Bio* **2019**, *9*, 629–642. [[CrossRef](#)]
6. Chao, Q.; Rothenberg, M.; Solano, R.; Roman, G.; Terzaghi, W.; Ecker, J.R. Activation of the ethylene gas response pathway in *Arabidopsis* by the nuclear protein ETHYLENE-INSENSITIVE3 and related proteins. *Cell* **1997**, *89*, 1133–1144. [[CrossRef](#)]
7. Solano, R.; Stepanova, A.; Chao, Q.; Ecker, J.R. Nuclear events in ethylene signaling: A transcriptional cascade mediated by ETHYLENE-INSENSITIVE3 and ETHYLENE-RESPONSE-FACTOR1. *Genes Dev.* **1998**, *12*, 3703–3714. [[CrossRef](#)]
8. Guo, H.; Ecker, J.R. The ethylene signaling pathway: New insights. *Curr. Opin. Plant Biol.* **2004**, *7*, 40–49. [[CrossRef](#)]
9. Song, J.; Zhu, C.; Zhang, X.; Wen, X.; Liu, L.; Peng, J.; Guo, H.; Yi, C. Biochemical and structural insights into the mechanism of DNA recognition by *Arabidopsis* ETHYLENE INSENSITIVE3. *PLoS ONE* **2015**, *10*, e0137439. [[CrossRef](#)]
10. Guo, H.; Ecker, J.R. Plant responses to ethylene gas are mediated by SCF<sup>EBF1/EBF2</sup>-dependent proteolysis of EIN3 transcription factor. *Cell* **2003**, *115*, 667–677. [[CrossRef](#)]
11. Potuschak, T.; Lechner, E.; Parmentier, Y.; Yanagisawa, S.; Grava, S.; Koncz, C.; Pascal, G. EIN3-dependent regulation of plant ethylene hormone signaling by two *Arabidopsis* F box proteins: EBF1 and EBF2. *Cell* **2003**, *115*, 679–689. [[CrossRef](#)]
12. Yanagisawa, S.; Yoo, S.-D.; Sheen, J. Differential regulation of EIN3 stability by glucose and ethylene signalling in plants. *Nature* **2003**, *425*, 521–525. [[CrossRef](#)] [[PubMed](#)]
13. Wawrzynska, A.; Lewandowska, M.; Sirko, A. *Nicotiana tabacum* EIL2 directly regulates expression of at least one tobacco gene induced by sulphur starvation. *J. Exp. Bot.* **2010**, *61*, 889–900. [[CrossRef](#)]
14. Wawrzynska, A.; Sirko, A. EIN3 interferes with the sulfur deficiency signaling in *Arabidopsis thaliana* through direct interaction with the SLIM1 transcription factor. *Plant Sci.* **2016**, *253*, 50–57. [[CrossRef](#)]
15. Kosugi, S.; Ohashi, Y. Cloning and DNA binding properties of a tobacco Ethylene-Insensitive3 (EIN3) homolog. *Nucl. Acids Res.* **2000**, *28*, 960–967. [[CrossRef](#)]

16. Yamasaki, K.; Kigawa, T.; Inoue, M.; Yamasaki, T.; Yabuki, T.; Aoki, M.; Seki, E.; Matsuda, T.; Tomo, Y.; Terada, T.; et al. Solution structure of the major DNA-binding domain of *Arabidopsis thaliana* Ethylene-insensitive3-like3. *J. Mol. Biol.* **2005**, *348*, 253–264. [[CrossRef](#)] [[PubMed](#)]
17. Wawrzynska, A.; Sirko, A. Proteasomal degradation of proteins is important for the proper transcriptional response to sulfur deficiency conditions in plants. *Plant Cell Physiol.* **2020**, *61*, 1548–1564. [[CrossRef](#)] [[PubMed](#)]
18. Maruyama-Nakashita, A.; Nakamura, Y.; Yamaya, T.; Takahashi, H. A novel regulatory pathway of sulfate uptake in *Arabidopsis* roots: Implication of CRE1/WOL/AHK4-mediated cytokinin-dependent regulation. *Plant J.* **2004**, *38*, 779–789. [[CrossRef](#)] [[PubMed](#)]
19. Huang, X.Y.; Chao, D.Y.; Koprivova, A.; Danku, J.; Wirtz, M.; Müller, S.; Sandoval, F.J.; Bauwe, H.; Roje, S.; Dilkes, B. Nuclear Localised MORE SULPHUR ACCUMULATION1 Epigenetically Regulates Sulphur Homeostasis in *Arabidopsis thaliana*. *PLoS Genet.* **2016**, *12*, e1006298. [[CrossRef](#)]
20. Yamaguchi, M.; Kubo, M.; Fukuda, H.; Demura, T. VASCULAR-RELATED NAC-DOMAIN7 is involved in the differentiation of all types of xylem vessels in *Arabidopsis* roots and shoots. *Plant J.* **2008**, *55*, 652–664. [[CrossRef](#)]
21. Kubo, M.; Udagawa, M.; Nishikubo, N.; Horiguchi, G.; Yamaguchi, M.; Ito, J.; Mimura, T.; Fukuda, H.; Demura, T. Transcription switches for protoxylem and metaxylem vessel formation. *Genes Dev.* **2005**, *19*, 1855–1860. [[CrossRef](#)]
22. Koncz, C.; Schell, J. The promoter of T-DNA gene 5 controls the tissue-specific expression of chimaeric genes carried by a novel types of *Agrobacterium* binary vector. *Mol. Gen. Genet.* **1986**, *204*, 383–396. [[CrossRef](#)]
23. Clough, S.J.; Bent, A.F. Floral dip: A simplified method for *Agrobacterium*-mediated transformation of *Arabidopsis thaliana*. *Plant J.* **1998**, *16*, 735–743. [[CrossRef](#)] [[PubMed](#)]
24. Fujiwara, T.; Hirai, M.Y.; Chino, M.; Komeda, Y.; Naito, S. Effects of sulfur nutrition on expression of the soybean seed storage protein genes in transgenic petunia. *Plant Physiol.* **1992**, *99*, 263–268. [[CrossRef](#)] [[PubMed](#)]
25. Yamaguchi, C.; Khamsalath, S.; Takimoto, Y.; Suyama, A.; Mori, Y.; Ohkama-Ohtsu, N.; Maruyama-Nakashita, A. SLIM1 transcription factor promotes sulfate uptake and distribution to shoot, along with phytochelatin accumulation, under cadmium stress in *Arabidopsis thaliana*. *Plants* **2020**, *9*, 163. [[CrossRef](#)] [[PubMed](#)]
26. Maruyama-Nakashita, A.; Watanabe-Takahashi, A.; Inoue, E.; Yamaya, T.; Saito, K.; Takahashi, H. Sulfur-responsive elements in the 3'-nontranscribed intergenic region are essential for the induction of *Sulfate Transporter 2;1* gene expression in *Arabidopsis* roots under sulfur deficiency. *Plant Cell* **2015**, *27*, 1279–1296. [[CrossRef](#)]
27. Zhang, L.; Ryota, K.; Tomomi, M.I.; Allahham, A.; Kim, S.J.; Maruyama-Nakashita, A. Sulfur Deficiency-induced glucosinolate catabolism attributed to two  $\beta$ -Glucosidases, *BGLU28* and *BGLU30*, is required for plant growth maintenance under sulfur deficiency. *Plant Cell Physiol.* **2020**, *61*, 803–813. [[CrossRef](#)]
28. Kimura, Y.; Ushiwatari, T.; Suyama, A.; Tominaga-Wada, R.; Wada, T.; Maruyama-Nakashita, A. Contribution of root hair development to sulfate uptake in *Arabidopsis*. *Plants* **2019**, *8*, 106. [[CrossRef](#)]
29. Hellens, R.P.; Edwards, E.A.; Leyland, N.R.; Bean, S.; Mullineaux, P.M. pGreen: A versatile and flexible binary Ti vector for *Agrobacterium*-mediated plant transformation. *Plant Mol. Biol.* **2000**, *42*, 819–832. [[CrossRef](#)]
30. Bradford, M. A rapid and sensitive method for the quantification of microgram quantities of protein utilizing the principle of dye-binding. *Anal. Biochem.* **1976**, *72*, 248–254. [[CrossRef](#)]



Review

# Receptor-like Kinases (LRR-RLKs) in Response of Plants to Biotic and Abiotic Stresses

Aigerim Soltabayeva <sup>1,\*</sup>, Nurbanu Dauletova <sup>1</sup>, Symbat Serik <sup>1</sup>, Margulan Sandybek <sup>1</sup>, John Okoth Omondi <sup>2</sup>, Assylay Kurmanbayeva <sup>3</sup> and Sudhakar Srivastava <sup>4</sup>

<sup>1</sup> Biology Department, School of Science and Humanities, Nazarbayev University, Astana 010000, Kazakhstan

<sup>2</sup> International Institute of Tropical Agriculture, Lilongwe P.O. Box 30258, Malawi

<sup>3</sup> Department of Biotechnology and Microbiology, L.N. Gumilyov Eurasian National University, Astana 010000, Kazakhstan

<sup>4</sup> NCS-TCP, National Institute of Plant Genome Research, New Delhi 110067, India

\* Correspondence: aigerim.soltabayeva@nu.edu.kz

**Abstract:** Plants live under different biotic and abiotic stress conditions, and, to cope with the adversity and severity, plants have well-developed resistance mechanisms. The mechanism starts with perception of the stimuli followed by molecular, biochemical, and physiological adaptive measures. The family of LRR-RLKs (leucine-rich repeat receptor-like kinases) is one such group that perceives biotic and abiotic stimuli and also plays important roles in different biological processes of development. This has been mostly studied in the model plant, *Arabidopsis thaliana*, and to some extent in other plants, such as *Solanum lycopersicum*, *Nicotiana benthamiana*, *Brassica napus*, *Oryza sativa*, *Triticum aestivum*, *Hordeum vulgare*, *Brachypodium distachyon*, *Medicago truncatula*, *Gossypium barbadense*, *Phaseolus vulgaris*, *Solanum tuberosum*, and *Malus robusta*. Most LRR-RLKs tend to form different combinations of LRR-RLKs-complexes (dimer, trimer, and tetramers), and some of them were observed as important receptors in immune responses, cell death, and plant development processes. However, less is known about the function(s) of LRR-RLKs in response to abiotic and biotic stresses. Here, we give recent updates about LRR-RLK receptors, specifically focusing on their involvement in biotic and abiotic stresses in the model plant, *A. thaliana*. Furthermore, the recent studies on LRR-RLKs that are homologous in other plants is also reviewed in relation to their role in triggering stress response processes against biotic and abiotic stimuli and/or in exploring their additional function(s). Furthermore, we present the interactions and combinations among LRR-RLK receptors that have been confirmed through experiments. Moreover, based on GENEINVESTIGATOR microarray database analysis, we predict some potential LRR-RLK genes involved in certain biotic and abiotic stresses whose function and mechanism may be explored.

**Keywords:** abiotic stress; biotic stress; stress tolerance; LRR-RLK receptors; *Arabidopsis*

**Citation:** Soltabayeva, A.; Dauletova, N.; Serik, S.; Sandybek, M.; Omondi, J.O.; Kurmanbayeva, A.; Srivastava, S. Receptor-like Kinases (LRR-RLKs) in Response of Plants to Biotic and Abiotic Stresses. *Plants* **2022**, *11*, 2660. <https://doi.org/10.3390/plants11192660>

Academic Editors: Milan S. Stankovic, Paula Baptista and Petronia Carillo

Received: 8 August 2022

Accepted: 1 October 2022

Published: 10 October 2022

**Publisher's Note:** MDPI stays neutral with regard to jurisdictional claims in published maps and institutional affiliations.



**Copyright:** © 2022 by the authors. Licensee MDPI, Basel, Switzerland. This article is an open access article distributed under the terms and conditions of the Creative Commons Attribution (CC BY) license (<https://creativecommons.org/licenses/by/4.0/>).

## 1. Introduction

Biotic and abiotic stresses have detrimental effects on growth and development in plants that are at risk of biotic and abiotic stresses. To counteract these adversities, plants have developed diverse stimuli and activation strategies. The receptors in plants are one of the primary components of plant–environment interaction that transduces the information and makes the plant aware of its surroundings. In plants, a large number of different types of receptor-like kinases (RLKs) have evolved, and they are classified based on their kinase domain and extracellular domain sequences [1–3]. Among the RLKs, the biggest group are the Leucine-rich-repeats–RLKs (LRR-RLKs), which have an extracellular domain LRR motif that facilitates the binding of ligands (proteins, signaling peptides, hormones, etc.). In addition to their regulatory role in plant development, shoot and root apical meristem, xylem differentiation, and BL (Brassinolide) pathways, they also play a role in the immune system and activation of cell death [4–9]. A small number of LRR-RLKs have been shown

to be involved in the abiotic stress response of plants [2,10–12]. It is mainly achieved through the investigation of *LRR-RLK* mutant lines by inserting tDNA fragments into their exon [8,13,14], intron, UTR (untranslated region), or into the promoter region [8,15,16] and then testing them under different stresses (Tables S1 and S2). There are plenty of genetic tools that are used for the investigation of *LRR-RLK* gene function, but these studies were mostly conducted in model plant *Arabidopsis thaliana*, and thereafter in tomato (*Solanum lycopersicum*) and tobacco (*Nicotiana benthamiana*). The ubiquitous presence of *LRR-RLK* with varying sequences across the plant genera underscores the need for its investigation in other plants in order to expand the knowledge and thereby to understand their role more specifically. *RLKs* were classified into different groups based on their functions, such as growth and development processes and biotic and abiotic stress responses (reviewed Yuriko Osakabe, and Beg Hab Kim review articles [2,17]). Some of the well-studied *LRR-RLKs*, such as *BRASSINOSTEROID INSENSITIVE 1 (BR1)* or *SOMATIC EMBRYOGENESIS RECEPTOR KINASE 3 (SERK3)*; *SOMATIC EMBRYOGENESIS RECEPTOR KINASE 1, 2, and 4 (SERK1/2/4)*; *BR1-ASSOCIATED RECEPTOR KINASE 1 (BAK1)*; *BAK1-INTERACTING RECEPTOR-LIKE KINASE1 (BIR1)*; and *SUPPRESSOR OF BIR1-1 (SOBIR1)*, *ELONGATION FACTOR-Tu (EF-Tu) RECEPTOR (EFR)* were discussed as being essential for immune responses [2,17,18]. Credible evidence has been provided to demonstrate that some of the *RLKs*, such as *RECEPTOR-LIKE PROTEIN KINASE1 (RPK1)* and *RECEPTOR-LIKE KINASE 7 (RLK7* or other name *LRR XI-23*), are involved in water stress [2,16], and *PHLOEM INTERCALATED WITH XYLEM-LIKE 1 (PXL1)* in cold stress [19]. Notably, some of the above-mentioned *LRR-RLKs*, such as *BAK1/SERK3*; *SERK1*, -2, and -4; and *BR1*, share the same signaling pathways in Mitogen-Activated Protein Kinase (MAPK) activation,  $Ca^{2+}$  influx, and the production of reactive oxygen species (ROS) in order to initiate plant responses to biotic or abiotic stresses and/or developmental cues (see review [20]). Among the *SERK*-mediated signaling pathways, crosstalk occurs at multiple levels, and it is possible to have crosstalk with other *LRR-RLKs*. Recent *LRR-RLK* studies showed additional crosstalk of *LRR-RLKs*, and also new achievements for additional functions of known *LRR-RLKs*. Despite the exploration of so many *LRR-RLKs* from *A. thaliana* over a period of time, the functional role of several of these has not yet been explored.

The *in silico* studies have shown that *LRR-RLK* harbors a transmembrane domain (TM), intracellular kinase domain (KD), and *LRR*-containing extracellular domain (ECD) [21]. This extracellular domain of *LRR-RLKs* was classified according to the structure of *LRR*, where the *LRR* II, III, VI, IX, X, XI, XII, and XIII sub-families contained the cysteine residues in the amino-terminal of the *LRR* motifs [21]. This extracellular domain could have an impact on oligomerization [21]. Moreover, it was shown that *LRR-RLKs* with short extracellular domains are mainly co-receptors [22], which help to hold the ligand and stabilize and enhance transduction of the intracellular signal together with the ligand-binding receptor [23–25]. Some of the *LRR-RLKs* interact with each other, which allows for the formation of different heterodimers or trimers, thereby allowing them to become multifunctional [26,27]. *In vitro* and *in vivo* studies confirmed the heterodimer complexes of *LRR-RLK* and few trimeric complexes [15,16,28–32]. These formations are important for triggering immune responses, metabolic pathways, stem development, etc. Therefore, the use of double, triple, or quadruple mutants proved to be a useful tool for achieving their function and/or interactions [16,29–33]. The interaction of *LRR-RLKs* and its mechanism was mainly studied in *A. thaliana*.

Here, we update the functioning of *LRR-RLKs* in response to biotic and abiotic stresses in *A. thaliana*, and in other plants as well, such as *N. benthamiana*, *S. lycopersicum*, *Oryza sativa*, *Triticum aestivum*, *Hordeum vulgare*, *Brachypodium distachyon*, *Brassica napus*, *Medicago truncatula*, *Gossypium barbadense*, *Phaseolus vulgaris*, *Solanum tuberosum*, and *Malus robusta*. Additionally, we compiled the information on genetic tools used in the investigation of *LRR-RLK*'s role in biotic and abiotic stress response. The Microarray data analysis (GENEINVESTIGATOR, <https://geneinvestigator.com/>, accessed on 3 August 2022) of the *LRR-RLK* genes, which responded to biotic and abiotic stimuli, suggested

the possibility of additional functions and their cross-link in triggering different signaling processes. Furthermore, we have presented the information on stress-related LRR-RLKs as dimer, trimer, and tetramer complexes, which were experimentally achieved in *A. thaliana*. Furthermore, an ATTED databases (<https://atted.jp/hclust/>, accessed on 2 February 2022) analysis for protein interactions pointed towards additional possible interactions among the LRR-RLKs, however, these need to be validated experimentally [33].

## 2. Abundance of LRR-RLKs Genes in the Plant Genome

The abundant availability of genome and RNA sequences allowed us to identify the potential LRR-RLK in different plants, such as annual and perennial plants, crops, trees, herbs, etc. (Table 1). In primitive plants such as *Sedum alfredii*, *Selaginella moellendorffii*, *Amborella trichopoda*, and *Physcomitrella patens*, there are about 60–134 genes. In higher plants, the identified LRR-RLK gene numbers vary from 200 to 600 (LRR-RLK genes) (See Table 1). It was shown that algae do not contain any LRR-RLK genes similar to plants and it was suggested that the structural combination of LRRs and kinase domains (KD) to form new genes may have occurred after the divergence of land plants from green algae [34]. An in silico analysis revealed that the expansion in LRR-RLKs is a result of tandem and segmental duplication events (Table 1). Additionally, the exon/intron compositions and motif arrangements were considerably conserved among members in the same groups or subgroups in plants (Table 1).

**Table 1.** Number of LRR-RLKs present in different plants. Whole genome sequence data of the enlisted plant species was analyzed for the identification of LRR-RLKs. The identified LRR-RLK genes (numbers) with their expansion characteristic (presence of tandem duplication, motif conservation, and duplication) were based on different studies. Genome size for each species was given. Mb indicates mega base pairs. “-” indicates no data available.

Numbers of LRR-RLK	Plant Species	Genome Size	Presence of Tandem Duplication	LRR-RLK Organizations	References
0	<i>Chlamydomonas reinhardtii</i>	120 Mb	-	-	[34]
60	<i>Sedum alfredii</i>	39.1 Mb	-	motif conservation	[35]
67–81	<i>Selaginella moellendorffii</i>	100 Mb	present	motif conservation	[34]
94	<i>Amborella trichopoda</i>	870 Mb	present	motif conservation	[36]
134	<i>Physcomitrella patens</i>	500 Mb	-	-	[34,37]
176	<i>Phoenix dactylifera</i>	658 Mb	present	-	[37,38]
180	<i>Cucumis sativus</i>	367 Mb	present	segmental duplication	[37,39]
201	<i>Fragaria vesca</i>	240 Mb	present	-	[40]
211	<i>Medicago truncatula</i>	465 Mb	present	exon/intron organization, motif conservation	[37,41]
215	<i>Vitis vinifera</i>	500 Mb	present	segmental duplication	[37,42]
226	<i>Arabidopsis thaliana</i>	133 Mb	present	-	[37,43]
227	<i>Jatropha curcas</i>	320 Mb	present	-	[37,44]
230–236	<i>Vernicia fordii</i> <i>Vernicia montana</i>	1310 Mb	Present ( <i>V. fordii</i> )	motif conservation (both), segmental duplications ( <i>V. fordii</i> )	[45,46]
239	<i>Solanum lycopersicum</i>	900 Mb	present	-	[37,47]
247	<i>Theobroma cacao</i>	430 Mb	present	motif conservation	[37,48]
250	<i>Zea mays</i>	2400 Mb	present	random chromosomal distribution	[37,49]
267	<i>Prunus mume</i>	280 Mb	present	-	[40]
268	<i>Solanum tuberosum</i>	840 Mb	present	lineage-specific expansion	[37,50]
268	<i>Prunus persica</i>	265 Mb	present	-	[37,40]
292	<i>Raphanus sativus</i>	574 Mb	present	motif conservation	[51]
298	<i>Gossypium arboreum</i>	1750 Mb	present	conserved exon/intron organization	[52]

Table 1. Cont.

Numbers of LRR-RLK	Plant Species	Genome Size	Presence of Tandem Duplication	LRR-RLK Organizations	References
297–300	<i>Citrus clementina</i> <i>Citrus sinensis</i>	370 Mb 380 Mb	present	-	[53]
300	<i>Brassica rapa</i>	455 Mb	present	intron/exon pattern organization, motif conservation	[37,54]
310	<i>Setaria italica</i>	515 Mb	present	motif conservation, segmental duplication	[37,55]
312	<i>Brassica nigra</i>	522 Mb	present	intra-chromosomal duplication, conserved loci duplication	[56]
332	<i>Oryza sativa</i>	430 Mb	present	exon duplication, mutation, and exon shuffling	[37,57]
367	<i>Glycine latifolia</i>	939 Mb	present	-	[58]
384	<i>Gossypium raimondii</i>	761 Mb	present	motif conservation	[37,59]
427	<i>Pyrus bretschneideri</i>	512 Mb	present	exon/intron organization, motif conservation	[60]
441	<i>Populus trichocarpa</i>	500 Mb	present	segmental duplication, exon/intron organization and motif conservation	[37,61]
484	<i>Brassica juncea</i>	920 Mb	present	segmental duplications, intra-/inter-genomic duplications	[62]
485	<i>Malus domestica</i>	750 Mb	present	-	[37,40]
494	<i>Glycine max</i>	1100–1150 Mb	present	exon/intron organizations, motif arrangements	[37,63]
531	<i>Triticum aestivum</i>	17,000 Mb	present	segmental duplications, intra-genomic duplications	[64]
548	<i>Arachis hypogaea</i>	2700 Mb	present	segmental duplication, exon/intron organization and motif conservation	[65]
589	<i>Thinopyrum elongatum</i>	4780 Mb	present	segmental duplications	[66]

The research on *LRR-RLKs* were mainly conducted in *A. thaliana* due to the availability of a large dataset. The increase in DNA and RNA sequencing in different crops and *A. thaliana* allowed for the identification of the numbers of stress-related *LRR-RLKs* (Table S1) and their sequence in other plants such as *O. sativa*, *G. max*, *M. truncatula*, *Populus*, *V. vinifera*, *S. lycopersicum*, *B. napus*, and *Z. mays* (Table S2). Note that some of the stress-related *LRR-RLKs* in *A. thaliana* have bigger numbers of orthologs in some plants, such as *G. max*, *M. truncatula*, *O. sativa*, and *Z. mays*, as compared to *A. thaliana* (Table S2). Only a few orthologs of stress-related *LRR-RLK* genes were investigated under biotic and abiotic stresses and their functions were elucidated in different plants by using different mutants of *LRR-RLKs* (Table S3).

### 3. Stress-Related *LRR-RLKs* in Plants

From a pool of 223 *LRR-RLKs* identified in *A. thaliana* (Table 1), some were clustered as regulators of various growth and development processes (stem cell maintenance, anther development, determination of the fate of a cell and organ development, cell expansion, stem stomata development) [67–71], while others were shown or suggested to be important in biotic and abiotic stress responses (Figure 1). One of the extensively studied genes among *LRR-RLKs* is *BAK1/SERK3*, which regulates multiple processes such as Brassinosteroid (BR) signaling, growth and development, and stomatal patterning, and also activates the expression of antimicrobial proteins [20,72]. Recently, the role of BAK1 in guard cell ABA signaling was demonstrated and *bak1* mutants showed more loss of water as compared to wild-type. The ABA increased the formation of a complex between BAK1 and OPEN STOMATA1 (OST1) near the plasma membrane [73]. In addition, *bak1–5* mutants revealed

that the post-invasive resistance of *A. thaliana* to *Alternaria brassicicola* is independent of pathogen-triggered indole-3-carboxylic acid and its derivatives (ICAs) and camalexin biosynthesis [74]. Notably, the function of BAK1/SERK3 in the immune response was shown in tobacco and tomato plants against the late blight pathogen (*Phytophthora infestans*) and bacterial and nematode infection [75,76]. Other SERKs, such as SERK1 and SERK2, were also important genes for conferring resistance against bacterial leaf blight and fungal infection, respectively [20,77,78]. In rice, OsSERK2 was shown as a positive regulator of immunity, interacting with the rice immune receptor kinases (XA21 and XA3) [78]. It was suggested that SERK2 could be a target for sRNAs of *Sclerotinia sclerotiorum* and the resulting action may contribute to the silencing of immune components in plants [79]. Recently, using the *serk2* mutant lines, it was observed that SERK2 is a component of BR signaling and it regulates BR signaling and salt resistance in rice [80]. Previously, SERK4 together with SERK3 were shown to trigger a series of defense responses [20], but in recent studies using knock-out and overexpressing lines of SERK4, it was observed that SERK4 negatively regulates the leaves senescence process [81].

Another well-studied LRR-RLK gene is *BRI1*, which interacts with SERK3 by mediating BR signaling through the BRI1/BAK1 complex [72], and it regulates stem elongation, vascular differentiation, seed size, fertility, flowering time, and senescence [8,17,82]. Moreover, the mutant of *BRI1* shows pleiotropic effects on disease resistance along with plant development regulation [83], and it displays ABA-hypersensitive primary root growth [84,85]. In *B. napus*, *S. lycopersicum*, and *B. distachyon*, the role of *BRI1* in BR signaling was confirmed [86–88]. Furthermore, *BRI1* was involved in BR signaling through MAPK and Ca<sup>2+</sup>-dependent protein kinases in rice [89]. Additionally, it was suggested that *SIBRI1* is related with systemin-mediated systemic defense response [90], however it was not established conclusively [87]. In tobacco, *NbBRI1* was involved in BR-mediated systemic defense signaling by regulating H<sub>2</sub>O<sub>2</sub> and NO production [91]. Recently, *BRI1* manipulation in different cereals resulted in drought tolerance [86], and disease resistance [83]. Additionally, the overexpression of wheat *TaBRI1* in *A. thaliana* revealed early flowering and enhancement of seed production [92], while overexpression of *SIBRI1* promoted fruit ripening and ethylene production, and increased the levels of carotenoids, ascorbic acid, soluble solids, and soluble sugars during fruit ripening [93]. In potato (*S. tuberosum*), *BRI1* was involved in the regulation of tuberization, thus suggesting other possible roles of *BRI1* [94]. *BIR1* is another LRR-RLK that forms a complex with SERK3/BAK1 or with other SERKs, and these complexes were shown to repress the effector-triggered immunity (ETI) in the absence of pathogen effectors [72]. The LRR-RLK *SOBIR1* also interacts with SERKs, serving as a stabilizer of the protein complex and aids receptor complexes in triggering defense responses [18]. Notably, the homolog of *SOBIR1* activated the immune response in tomato against fungal infection [18], but not in antiviral infection [95]. In tobacco plants, *NbSOBIR1* was involved in the immunity of *N. benthamiana* through monitoring the production of ROS [96]. Furthermore, the manipulation of *GbSOBIR1* in cotton (*G. barbadense*) plants resulted in resistance to *Verticillium* [97]. While EFR regulated the immune response of plants after perceiving bacterial flagellin and EF-Tu by forming complexes with SERKs [72], it was observed that *A. thaliana efr* mutants lacking EF-Tu perception are more susceptible to transformation by *Agrobacterium tumefaciens* [98]. This revealed the importance of the EF-Tu perception system for plant defense. The homologs of *EFR* in tobacco and in tomato were also involved in pathogen-associated molecular patterns (PAMP)-triggered immunity, and suggesting transgenic expression of *EFR* could be used as an engineering tool against broad-spectrum bacterial infections [99]. In rice, it was shown that receptors EFR and XA21 recruit similar immune signaling [100]. The overexpression of *AtEFR* in different crops shows resistance to bacterial infection and/or symptoms. In wheat and apple, the overexpression of *AtEFR* enhanced resistance against bacterial disease, fire, and blight [101], respectively. Similarly, in *M. truncatula*, it reduced the bacterium infection [102] and in potato it enhanced bacterial wilt resistance [103].

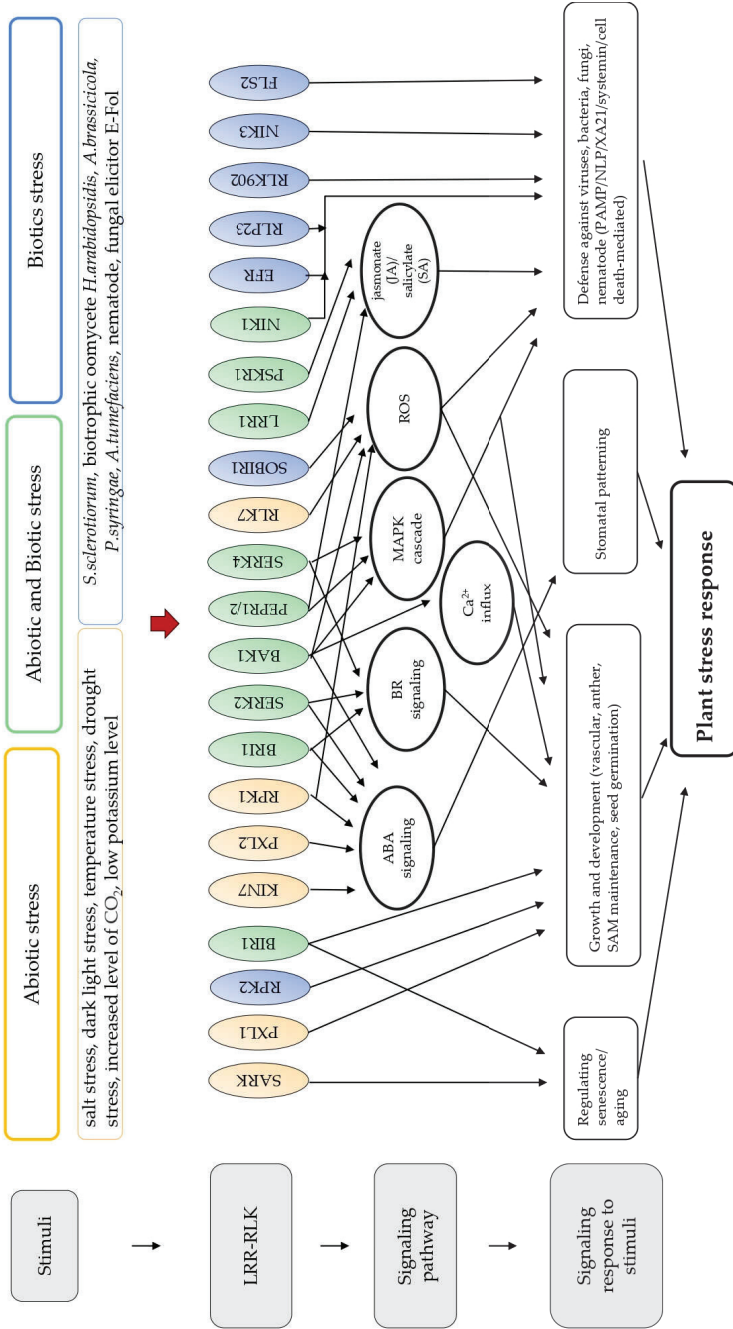


**Figure 1. Scheme of signaling pathways triggered by biotic- and abiotic-tested LRR-RLKs and cross-talk among them.** The LRR-RLKs regulate various plant processes, including growth, development, and responses to biotic and abiotic stresses. After perceiving abiotic and/or biotic stimuli by the LRR-RLKs, activation of diverse signaling, such as MAPK activation (BAK1, PEPR1/2, SERK4), Ca<sup>2+</sup> influx (BAK1), reactive oxygen species (ROS) production (RPK1, BAK1, RLK7, SOBIR1), BR signaling (BR1, SERK2, SERK4), ABA signaling (KIN7, PXL2, RPK1, BR1, SERK2, BAK1), jasmonate (JA), and salicylate (SA) (PEPR1/2, LRR1, PSKR1) occurs. Some LRR-RLKs may activate several signaling pathways depending on the type of stimuli: RPK1-ABA and ROS pathways; BR1 and SERK2—ABA and BR pathway; PEPR1/2—MAPK and JA/SA pathway; SERK4—BR and MAPK pathway; BAK1-BR signaling, Ca<sup>2+</sup> and MAPK pathways. Senescence may be associated with SARK and BIR1. Defense mechanisms against biotic stress stimuli are mediated by JA, SA, ROS, and MAPK pathways, and also additionally followed by LRR-RLKs: NIK1, EFR, RLP23, RLK902, NIK3, and FLS2. Yellow color indicates tested abiotic stimuli, blue color is for tested biotic stimuli, and green for both stimuli.

SERKs also form complexes with PHYTOSULFOKINE (PSK) RECEPTOR 1 (PSKR1), which is known to regulate root growth and hypocotyl elongation [20]. Moreover, *PSKR1* was also identified as an important component of plant defense [104]. *PSKR1* suppresses salicylate-dependent defense responses, where the *pskr1* mutants exhibit early senescence, a salicylate (SA)-associated response, and are impaired in wound healing, a jasmonate (JA)-associated response [104]. Moreover, *OsPSKR1* was involved in the immune response against bacterial leaf streak in rice through salicylic acid (SA) pathway signaling [105]. *PEP1 RECEPTOR 1 (PEPR1)* and *PEPR2* were involved in immune responses through interaction with SERK3 through AtPep1-triggered ROS production and ethylene signaling [20]. Furthermore, PEPR1 recognizes AtPep3 and increases tolerance to salt stress as well as immune response [106]. Furthermore, it was suggested that AtPeps-PEPR signaling pathway is involved in stomatal closure through an OST1-independent mechanism under biotic stress [107]. *PEPR1/2 ORTHOLOG RECEPTOR-LIKE KINASE1* from *S. lycopersicum* was shown to regulate responses to systemin, necrotrophic fungi, and insect herbivory [108]. Previously, RECEPTOR-LIKE PROTEIN KINASE1 (RPK1) was linked to the water stress response [2], wherein it regulates ABA/stress signaling by controlling ROS homeostasis. Additionally, RPK1 and BAK1 form complexes with OST1 to regulate ABA-induced stomatal closure [73,109].

The LEUCINE-RICH REPEAT PROTEIN 1 (LRR1) forms a complex with pathogenesis-related protein10 (PR10), and it leads to cell-death-mediated defense signaling [110]. Additionally, it was shown in vivo and in vitro that during plant responses to drought stress, LRR1 and KINASE 7 (KIN7) are degraded by PLANT U-BOX PROTEIN 11 (PUB11), an E3 ubiquitin ligase [111]. This KIN7 phosphorylates and activates tonoplast-located channels during ABA- and CO<sub>2</sub>-mediated stomatal closure [112]. Recently, Leucine-rich receptor-like kinase homologs in cereals such as barley and wheat showed important components of defense responses against *Fusarium* by disbalancing salicylic acid signaling [113]. The silencing of *LRR1* in rice in the *XA21* genetic background (*XA21-LRR1Ri*, *XA21* is 21 amino acid tyrosine-sulfated epitope derived from the bacterial protein) compromises resistance to bacterial leaf blight, indicating involvement in *XA21*-mediated immune response [114]. Other *LRR-RLK*, RECEPTOR-LIKE KINASE 902 (RLK902) previously showed importance in resistance to *Hyaloperonospora arabidopsidis* (downy mildew) in *A. thaliana* [115]. RLK902 associates with ENHANCED DISEASE RESISTANCE 4 (EDR4) and with BRASSINOSTEROID-SIGNALING KINASE1 (BSK1), a key component of plant immunity [116]. Not much is known about LRR-RLK-like NSP-interacting kinases (NIKs), such as NIK1, NIK2, and NIK3, and their interaction with geminivirus nuclear shuttle protein (NSP). The binding of NSP to NIK inhibits its kinase activity in vitro, and a phenotypic analysis of NIKs mutant lines suggests that NIKs are involved in the antiviral defense response [117]. It was shown that *At-FEI2* (cell wall receptor-like kinase) plays a positive role in *Arabidopsis* and in tomato defense against *Botrytis cinerea* based on the study using knockout mutants of the Bc-siR37 [118].

The *LRR-RLK* genes have been shown to play important roles in response to abiotic stresses. In previous studies, *ERECTA-LIKE1 (ERL1)*, a member of the gene family closely related to LRR-RLKs, was shown to synergistically regulate plant development and morphogenesis and functions in response to abiotic stresses, especially for heat response and drought [2,119]. Recently, it was observed that the *ERECTA* family was involved in sensing salt and osmotic stresses [120]. Furthermore, other *LRR-RLK* genes like *PXY-Like 2 (PXL2)* have been proven to be essential in vascular development through recognizing small signaling peptides, and they play a role in ABA signaling [121]. While the *PHLOEM INTERCALATED WITH XYLEM-LIKE 1 (PXL1)* is essential in cold and heat stress (through the ROS), the PXL1 regulates HISTIDINE-RICH DEHYDRIN1 (AtHIRD1) and LIGHT-HARVESTING PROTEIN COMPLEX I (AtLHCA1) by phosphorylation [122]. Another *LRR-RLK* gene, such as *SCHENGEN 3 (SGN3)*, is related with developmental processes, particularly with microdomain organization and enhanced suberization in the endodermis. Additionally, it was shown that the *sgn3* mutant was extremely sensitive to environmental

conditions, such as different temperatures and nutrient deficiency [123]. Moreover, the role of BRI1-LIKE3 (BRL3) was reported in sensing glucose and flg22, where BRL3 together with REGULATOR OF G-PROTEIN SIGNALING 1 (AtRGS1) prevents excess ROS burst and control growth inhibition [124]. Additionally, the overexpression of BRL3 resulted in drought stress tolerance in *A. thaliana* through the accumulation of osmoprotectant metabolites, such as proline and sugars [125]. In rice, the *OsBRL1* and *OsBRL3* were shown to be partly involved in BR perception in the roots [126]. Another LRR-RLK, *RLK7/LRR XI-23*, was involved in the regulation of seed germination and oxidative stress [127]. Furthermore, the LRR-RLKs, RECEPTOR-LIKE PROTEIN KINASE 2 (RPK2) also known as TOAD2) together with CLAVATA3 (CLV3), regulate the development of anthers, embryo, and stem cell homeostasis in the shoot apical meristem [2]. Single mutants of *RPK2* and *CLAVATA1 (CLV1)* and *CLAVATA2 (CLV2)* showed importance in nematode parasitism [128]. Furthermore, RPK2 interacts with other LRR-RLK, such as SENESCENCE-ASSOCIATED RECEPTOR-LIKE KINASE (SARK)—also known as CLAVATA3 INSENSITIVE RECEPTOR KINASE 3 (CIK3)—to maintain stem cell homeostasis [129] and anther development [33]. SARK was shown to be a positive regulator of senescence through hormone imbalances [130]. Interestingly, *PpSARK* in moss was shown as a positive regulator of senescence in salt stress responses and was also suggested to be a negative regulator of senescence [131]. In common bean's SARK, it did not coordinate senescence in nodules [132].

Thus, the mentioned *LRR-RLK* gene(s), which were tested in different biotic or abiotic stress/senescence processes, shared similar signaling pathways, such as reactive oxygen species (ROS) production,  $\text{Ca}^{2+}$  influx, activation of MAPK, regulation of defense genes, regulation of stomatal patterning, hormonal regulation, and regulation of senescence-related gene(s), to trigger the response of plants (See the scheme in Figure 1). Remarkably, some *LRR-RLK* genes show crosstalk in triggering different programs (Figure 1) and their numbers increased compared to the most recent review articles, which mentioned *LRR-RLK* genes in biotic and abiotic stresses [17,20]. Therefore, we have additionally collected all of the known single mutants of *LRR-RLK* genes and enlisted their phenotypic changes under experimentally tested biotic and/or abiotic stresses in Table S1, where their crosstalk can be easily observed. The information was gathered from the available microarray and RNA sequencing data (online available GENEINVESTIGATOR), which is also useful in predicting the potential role of genes for a particular stress stimulus [133]. Several *LRR-RLK* genes were identified in biotic or abiotic stresses (Table S1). The microarray data analysis of these *LRR-RLK* genes showed the alterations in expression under both types of stress stimuli i.e., biotic and abiotic (Figure S1). For example, *FEI2*, *NIK3*, *RLK902*, *RPK2*, *EFR*, *SOBIR1*, and *NIK1*, which were tested only in biotic stresses, showed a change in the expression under abiotic stress as well (Figure S2). Similarly, the reverse was observed for genes involved in abiotic stresses, such as *RPK1*, *BRL3*, *ERL1*, *PXL1*, *PXL2*, *SARK*, *RLK7/LRR XI-23*, *SGN3*, *KIN7*, and *PEPR1*, as it showed a change in expression for biotic stress too (Figure S3). The detailed characterization of these *LRR-RLK* genes under both stresses is likely to provide additional information on their mechanistic role and may give insight into the crosstalk among the LRR-RLKs.

#### 4. Interactions among the Stress-Related LRR-LRKs

Several mutant lines, such as single, double, triple, and/or quadruple mutants, were generated (Table S1) to investigate the function of these genes [8,15,33,134,135]. In these studies, it was shown that the formation of complexes (dimer, trimer, or tetramer) is important in relaying the signals to the downstream components [13,14,28–31]. The genetic evidence for interactions was confirmed by pull-down, gel filtration, bimolecular fluorescence complementation (BiFC), co-immunoprecipitation (CoIP), and protein kinase assay, as presented in Table 2, Figures S4–S7. Most of the known functional interactions among the LRR-RLK were shown as heterodimers and, in a few cases, as homodimers, e.g., SERK 1 and SERK2 (Table 2). The trimers were also shown and they perform different functions, e.g., SOBIR-BAK1-RLP23, BON1-BAK1-BIR1, ER-BAK1-TMM, BIK1-BAK1-ERL1/2, FLS2-

BAK-BIK1, and FLS2-BIK1-RBOHD play a role in the immune system [14,28,29,31,136,137]; and CLV1-CLV2-CRN in stem cell regulation [32,138]. The formation of some of the LRR-RLK complexes were dependent on ligand stimulation, for example, ligands such as flg22 [fragment of bacterial flagellin that binds the FLAGELLIN SENSITIVE 2 (FLS2) receptor] and elf18 (the N-terminal of EF-Tu) stimulate the formation of BAK-FLS2 or BAK-EFR dimers, respectively [16]. Similarly, SCFE1 (SCLEROTINIA CULTURE FILTRATE ELICITOR1) or nlp20 (peptide motif) ligands stimulate the formation of the BAK1-SOBIR1-RLP23 complex [14], while the binding of AtPep1 (endogenous peptide elicitor) induces PEPR1-BAK1 heterodimerization [139]. The INFLORESCENCE DEFICIENT IN ABSCIS- SION (IDA) stimulate the formation of heterodimers of SERK1 and SERK2 with HAESA (HAE) and HAESA-LIKE2 (HSL2), and Cf-4 of the SERK1-SOBIR1 complex [14,30] (see Figures S4–S7). Steroids may induce the generation of a LRR-RLKs complex, such as SERKs and TETRATRICOPEPTIDE-REPEAT THIOREDOXIN-LIKE 3 (TTL3), which activate the BR signaling pathway [16,140,141], and an application of brassinolide (BL) stimulates the formation of BAK1-BRI1 [16]. However, it was shown that the formation of heterotrimers, BAK1-ER-TMM, BAK1-ERL1-TMM, and BAK1-ERL2-TMM, are not dependent on stimulation ligands (EPF1 and EPF2) [29].

The formation of heterodimers with other LRR-RLKs, so-called co-receptors that usually have short extracellular domains, is important for holding the ligand and stabilizing it for the enhancement of the transduction of the intracellular signal [22]. The role of heterodimers was mainly as a defense response, development process, BR signaling, or cell death (Figures S4–S7). For example, BRI1 generated complexes with SERKs (BAK1/SERK3, SERK1, and SERK4) and TTL3—only for BR pathway activation [16,140,141], BRI1 can interact with BAK1, SERK1, SERK2, and SERK4 to inhibit plant cell death [14,30], and EFR with SERK1, BAK1, and SERK4/BKK1 can activate the immune response [16,98] and EFR with GLYCINE-RICH PROTEIN7 (GRP7) activates the PAMP-triggered immune (PTI) response against *Pseudomonas syringae* [142]. SOBIR1 forms a complex with BAK1 for immune responses against *P.infestans* and *S. sclerotiorum* [14,30], and the heterotrimer with AtRLP23 is formed in the absence of BRI1 to activate cell death [14]. Additionally, PSKR1 may interact with SERK1/2 and BAK1 [143]. Furthermore, CLV1 forms heterodimers with BAM1 (BARELY ANY MERISTEM1), SARK, and CRN (CORYNE), RPK2 [32,138,144,145], which are important for apical and young floral meristem development. Conversely, other LRR-RLKs that form variant complexes were shown to perform different roles. For example, BAK1 interacts with FLS2, SOBIR1, NIK1, BKK1, BIR2, PEPR1, PSKR1, EFR, BIK1, RLP23, ERL2, ERL1, ER, and TMM to activate immune responses [14,16,28–31]; with BRI1 to inhibit plant cell death; with RPK1, BIR1, BON1 (BONZAI1), SOBIR1, and HSL2 to activate cell death [30,109,146]; with BRI1 to activate BR pathway [8,16]; and with ER or ERL1 to regulate stomatal patterning [147] (Figure S4). Other multifunctional LRR-RLK genes are SERK1 and SERK2, which interact with EXCESS MICROSPOROCYTES 1 (EMS1) for anther development [135]; with PXY to regulate procambial cell proliferation [23,148]; with ER or ERL1 to regulate stomatal patterning; and with FLS2 and EFR, BRI1 and BAK1 for other functions (Figure S5).

Some multifunctional LRR-RLKs, such as BAK1, SERK 1, SERK2, SERK4, SARK, NIK1, and NIK3, were classified as co-receptors based on the length of the extracellular domain (ECD) [22], which are able interact with other LRR-RLKs, and they are grouped as the LRR (II) family. Some of the examples of members belonging to a particular family are as follows: LRR (II)—SERK 4, NIK1, NIK3, SARK, and SERK5; LRR(III)—RPK1, RLK902, PRK1, PRK2A, PRK4, PRK5, PRK6, MRLK; LRR(VII)—HYDROGEN PEROXIDASE-RESISTANT 1 (GHR1); LRR(IX)—BIR1; and LRR(V)—SRF1, SRF2, SRF3, SRF5, SRF6, SRF7, and SRF8 (STRUBBELIG-RECEPTOR FAMILY 1–3, 5–8). Other LRR-RLKs such as SOBIR1, FEI1, EFR, FLS2, BRI1, CLV1, ERL1, ERL2, ER, HSL2, PXY, BAM1, BAM2, PEPR1, GSO1 (GASSHO1), PSKR1, EMS1, RPK2, BRL1, BRL2, BRL3, PSY1R (PHYTOSULFOKINE RECEPTOR), and IOS1 (IMPAIRED OOMYCETE SUSCEPTIBILITY1) (Table 2 and Table S4), which are classified as ligand-perceiving receptors with long ECD and are grouped as LRR (I), LRR

(X), LRR (XI), and (LRR XII) [22]. Mainly, these co-receptors potentially bind with ligand-perceiving receptor groups for the activation and stabilization of complexes that sense signals [8,13,16,22,28]. They also enhance signaling through sequential reciprocal receptor transphosphorylation [149]. Different combinations of interactions among co-receptors with different ligand-binding LRR-RLKs allows for the substitution of each other. This creates difficulties in using a single mutant line for LRR-RLK gene studies. For example, SERK1, SERK2, and BAK1 share the same players, like EFR and FLS2, although BAK1 is preferred by FLS2 among other SERKs, whereas EFR does not show preference to BAK1 [16]. Yet, SERK1 and SERK2 could easily substitute each other for activation of a similar plant response [16]. This regulation of stability of complexes is less studied, with only a few reported cases. For example, BAK1 interacts with BIR1 or BIR2 to prevent heterodimerization of the BAK1-FLS2 complex, and thereby inhibits an immune system response [14,30]. Furthermore, BRI1 and SERK3 do not ubiquitously interact, they only show interaction in the endosomes and in restricted areas on the plasma membrane. In these sites, BAK1 is shown as a redistributor of BRI1 receptors [15]. Thus, most LRR-RLKs form complexes, and some of the LRR-RLK in the complexes play key roles in the complex, such as BAK1 [16,28], and some components in the complexes are able to substitute for each other.

Additionally, the ATTED database showed different interactions among the proteins based on various experiments and data (Table 2). The analysis of these interactions confirmed the known interactions of BAK1, SERK 1, SERK 2, SERK 4, NIK1, NIK3, and SARK (Figures S4–S7), but also the additional potential heterodimerizations for these co-receptors (Table 2). The less investigated co-receptors, like NIK1 and SARK, according to this database, have a potential for binding with BAK1. Importantly, the CIKs, such as NIK1, NIK3, and SARK, were shown in the stress response and in natural senescence [4,22], but their co-receptors' (heterodimers or homodimer) involvement in senescence or the stress response was not shown (Table 2). It will be exciting in the future to reveal the additional functions of these CIKs and to show the new interactions of the collected LRR-RLKs mentioned in Table S4. The interactions among the LRR-RLKs in other plants are less studied, and only a few were confirmed in tomato and tobacco [75,150], rice [77], *M. truncatula* [151], and wheat [92] (Table S4), and that was mainly done by using the yeast two-hybrid assays, co-immunoprecipitation, and BiFC methods. Altogether, the study of new interactions of LRR-RLKs in *A. thaliana* and other plants and the generation of new double or triple mutants could help in functional and interactional analyses of LRR-RLKs.

**Table 2.** Experimentally proven and potential interactions of stress-related LRR-RLKs with LRR-RLK co-receptors from LRR II. Data taken from different well-studied research manuscripts and from ATTED database. The formation of heterodimers between the LRR-RLKs were labeled as “heterodimer” inside of box cross between two LRR-RLKs one from column and second from row. Below the heterodimer formation were shown the method/s of identifications heterodimer formation such as CoIP—coimmunoprecipitation; BiFC—bimolecular fluorescence complementation, gel filtration, pull-down, in vivo, genetically (by mutants analysis), kinase assay, co-sedimentation in solution, solid-phase assay. NA indicates not available data reported the formation of heterodimer/s. Grey colored box indicates that information taken from ATTED database about interaction was confirmed experimentally (published data), and white zone was not confirmed experimentally.

LRR-RLK	SERK2	SERK1	SERK4/BKK1	SERK3/BAK1	SARK/Cik3	NIKI	NIK3/Cik1	References
	<b>co-receptors (LRR-RLKs from LRR II family according classification of [22])</b>							
<b>BIR1</b>	heterodimer (BiFC)	heterodimer (BiFC)	heterodimer (BiFC)	heterodimer (genetically, in vivo, pull-down)	heterodimer (solid-phase assay)	heterodimer (solid-phase assay)	NA	[14,152]
<b>FLS2</b>	NA	heterodimer (in vivo)	heterodimer (in vivo)	heterodimer (in vivo, CoIP, gel filtration)	NA	heterodimer (in vitro, pull down)	NA	[16,153,154]
<b>ERL1</b>	heterodimer (CoIP)	heterodimer (CoIP)	heterodimer (CoIP)	heterodimer (in vivo, CoIP)	heterodimer (solid-phase assay)	heterodimer (solid-phase assay)	NA	[147,152,153]
<b>BRI1</b>	NA	heterodimer (genetically, in vivo)	heterodimer (in vivo)	heterodimer (genetically, in vivo, in vitro)	NA	NA	NA	[146,149,155]
<b>EFR</b>	NA	heterodimer (in vivo)	heterodimer	heterodimer (genetically, CoIP, in vivo)	heterodimer (solid-phase assay)	heterodimer (solid-phase assay)	NA	[16,152,156]
<b>ER</b>	heterodimer (genetically, CoIP)	heterodimer (genetically, CoIP)	heterodimer (solid-phase assay)	heterodimer (genetically, pull-down, in vivo)	heterodimer (solid phase assay)	heterodimer (solid-phase assay)	NA	[29,147,152,153]
<b>PXY</b>	heterodimer (genetically, in vivo, in vitro)	heterodimer (genetically, in vivo, in vitro)	NA	heterodimer (genetically, in vivo, in vitro)	heterodimer (solid-phase assay)	heterodimer (solid-phase assay)	heterodimer (solid-phase assay)	[23,153]
	<b>co-receptors (LRR-RLKs from LRR II family according classification of [22])</b>							
<b>HSL2</b>	heterodimer (CoIP)	heterodimer (CoIP)	NA	heterodimer (CoIP)	heterodimer (solid-phase assay)	heterodimer (solid-phase assay)	NA	[152,157]
<b>BAK1</b>	heterodimer (genetically, CoIP)	heterodimer (BiFC, CoIP)	heterodimer (genetically)	NA	heterodimer (solid-phase assay)	heterodimer (genetically, in vivo, in vitro)	heterodimer (solid-phase assay)	[127,130–132]
<b>SERK1</b>	heterodimer (genetically, in vivo)	homodimer (genetically, in vivo)	heterodimer (solid-phase assay)	heterodimer (BiFC, CoIP)	heterodimer (solid-phase assay)	heterodimer (solid-phase assay)	NA	[152,153,155,158]
<b>SERK2</b>	homodimer (genetically, in vivo)	heterodimer (genetically, in vivo)	NA	NA	NA	NA	heterodimer (solid-phase assay)	[152,158]
<b>EMS1</b>	heterodimer (genetically, kinase assay, BiFC)	heterodimer (genetically, kinase assay, BiFC)	NA	NA	NA	NA	NA	[135]

Table 2. Cont.

LRR-RLK	SERK2	SERK1	SERK4/BKK1	SERK3/BAK1	SARK/CiK3	NIKI	NIK3/CiK1	References
SERK4	heterodimer (genetically, ColP)	heterodimer (solid-phase assay)	NA	heterodimer (genetically)	Heterodimer (solid-phase assay)	Heterodimer (solid-phase assay)	NA	[16,152]
NIKI	NA	heterodimer (solid-phase assay)	heterodimer (solid-phase assay)	Heterodimer (genetically, in vivo, in vitro)	Heterodimer (solid-phase assay)	NA	NA	[152–154]
PSK1	heterodimer (solid-phase assay, co-sedimentation in solution)	heterodimer (molecular sieving)	NA	heterodimer (genetically, ColP, gel filtration)	heterodimer (solid-phase assay)	NA	NA	[143,153]
<b>co-receptors (LRR-RLKs from LRR II family according to classification of [22])</b>								
SOBIR1	heterodimer (solid-phase assay)	NA	NA	heterodimer (genetically, ColP)	NA	NA	NA	[30,153]
RPK1	NA	NA	NA	heterodimer (genetically, pull-down, kinase assay)	heterodimer (solid-phase assay)	heterodimer (solid-phase assay)	NA	[109,152]
PEPR 1	NA	NA	NA	heterodimer (pull-down, gel filtration)	NA	NA	heterodimer (solid-phase assay)	[153,159]
ERL2	NA	heterodimer (solid-phase assay)	heterodimer (solid-phase assay)	heterodimer (genetically)	heterodimer (solid-phase assay)	heterodimer (solid-phase assay)	NA	[29,152]
RPK2	NA	NA	NA	NA	heterodimer (in vivo, pull-down)	heterodimer (solid-phase assay)	heterodimer (genetically)	[129,153]
CLV1	NA	NA	NA	NA	heterodimer (in vivo, pull-down)	NA	heterodimer (genetically)	[129]
BAM1	heterodimer (solid-phase assay)	NA	NA	NA	heterodimer (pull-down)	heterodimer (solid-phase assay)	heterodimer (genetically, BiFC, ColP)	[33,153]
BAM2	NA	NA	NA	NA	heterodimer (pull-down)	heterodimer (solid-phase assay)	heterodimer (genetically, BiFC, ColP)	[33,153]

## 5. Conclusions

Plants must evolve to adapt and tolerate harsh environments. The perception of biotic and abiotic stimuli is crucial for the survival of plants. Among the large numbers of receptors, the LRR-RLK are not only involved in different development biological processes but also in stress response processes. The rapid development of genome and RNA sequence analyses have allowed for the identification of the many LRR-RLKs genes in different monocot and dicot plants. As compared to *A. thaliana*, not much is known about the functions of LRR-RLKs in other plants such as tomato, tobacco, wheat, rice, *H. vulgare*, *B. distachyon*, etc. Additionally, stress-related LRR-RLKs in *A. thaliana* are mainly shown to play a role in biotic stresses, and to some extent in abiotic stresses. For the functional study of LRR-RLKs, a single mutant is of little use to capture all their functions, and, as LRR-RLKs can be substituted by other members, they do not have non-specific ligand binding and they have the ability to make different protein complexes (di-, tri-, or tetramer). The double, triple, and quadruple mutant generation for LRR-RLKs in *A. thaliana* and/or crop plants is a powerful tool for identifying the function role of LRR-RLKs.

**Supplementary Materials:** The following are available online at <https://www.mdpi.com/article/10.3390/plants11192660/s1>, Figure S1: Microarray analysis of the biotic and abiotic stress related LRR-RLK genes transcripts in response to biotic and abiotic stresses in WT (Col ecotype). Figure S2: Microarray analysis of the biotic stress related LRR-RLK genes transcripts in response to biotic and abiotic stresses in WT (Col ecotype). Figure S3: Microarray analysis of the abiotic stress related LRR-RLK genes transcripts in response to biotic and abiotic stresses in WT (Col ecotype). Figure S4: Protein interactions of BAK1/SERK3 with other LRR-RLK with experimental proved functional role. Figure S5: Protein interactions of SERK1 and SERK4 with other LRR-RLK with experimental proved functional role. Figure S6: Protein interactions of SERK2 with other LRR-RLK with experimental proved functional role. Figure S7: Protein interactions of CIK's (NIK1, NIK3 and SARK) with other LRR-RLK with experimental proved functional role. Table S1: Phenotypes of single mutants of LRR-RLK genes in *A. thaliana* tested under different biotic and abiotic stresses. Table S2: Orthologous of stress related LRR-RLKs genes in *A. thaliana*, *O. sativa*, *G. max*, *M. truncatula*, *Populus*, *V. vinifera*, *S. lycopersicum*, *B. napus*, *Z. mays*. Table S3: Genetic tools in different crop plants in investigation of stress-related LRR-RLKs. Table S4: Potential interactions of stress-related LRR-RLKs (from LRR II family) with other LRR-RLKs. References [160–181] are cited in the supplementary materials.

**Author Contributions:** Conceptualization, Aigerim Soltabayeva, N.D. and S.S. (Symbat Serik); data curation, M.S. and N.D. analysis of data from Geneinvestigator, Aigerim Soltabayeva, N.D. and S.S. (Symbat Serik) writing—original draft preparation, A.K. and S.S. (Sudhakar Srivastava) review and editing, J.O.O. visualization, A.S. supervision, project administration, A.S.; funding acquisition, A.S. All authors have read and agreed to the published version of the manuscript.

**Funding:** This research was funded by Faculty Development Competitive Research Grant Program (FDCRG 2020) at Nazarbayev University, Kazakhstan. Grant ID number 240919FD3939.

**Institutional Review Board Statement:** Not applicable.

**Informed Consent Statement:** Not applicable.

**Data Availability Statement:** Data is contained within the article or supplementary material.

**Acknowledgments:** The authors would like to thank Damira Kanayeva for moral support. Temirlan Nurtazin for supporting the project.

**Conflicts of Interest:** The authors declare no conflict of interest. The funders had no role in the design of the study; in the collection, analyses, or interpretation of data; in the writing of the manuscript, or in the decision to publish the results.

## References

- Gish, L.A.; Clark, S.E. The RLK/Pelle Family of Kinases. *Plant J.* **2011**, *66*, 117–127. [[CrossRef](#)] [[PubMed](#)]
- Osakabe, Y.; Yamaguchi-Shinozaki, K.; Shinozaki, K.; Tran, L.S.P. Sensing the Environment: Key Roles of Membrane-Localized Kinases in Plant Perception and Response to Abiotic Stress. *J. Exp. Bot.* **2013**, *64*, 445–457. [[CrossRef](#)] [[PubMed](#)]

3. Dievart, A.; Gottin, C.; Peacuterin, C.; Ranwez, V.; Chantret, N. Origin and Diversity of Plant Receptor-like Kinases. *Annu. Rev. Plant Biol.* **2020**, *71*, 131–156. [[CrossRef](#)] [[PubMed](#)]
4. Dievart, A.; Clark, S.E. LRR-Containing Receptors Regulating Plant Development and Defense. *Development* **2004**, *131*, 251–261. [[CrossRef](#)]
5. Wang, J.; Kucukoglu, M.; Zhang, L.; Chen, P.; Decker, D.; Nilsson, O.; Jones, B.; Sandberg, G.; Zheng, B. The Arabidopsis LRR-RLK, PXC1, Is a Regulator of Secondary Wall Formation Correlated with the TDIF-PXY/TDR-WOX4 Signaling Pathway. *BMC Plant Biol.* **2013**, *13*, 94. [[CrossRef](#)]
6. Wang, R.; Ji, Y.; Wang, J.; Yang, S.; Song, Y. Vascular Expression of Populus LRR-RLK Genes and the Effects of Their Overexpression on Wood Formation. *Mol. Breed.* **2015**, *35*, 220. [[CrossRef](#)]
7. Li, X.; Salman, A.; Guo, C.; Yu, J.; Cao, S.; Gao, X.; Li, W.; Li, H.; Guo, Y. Identification and Characterization of LRR-RLK Family Genes in Potato Reveal Their Involvement in Peptide Signaling of Cell Fate Decisions and Biotic/Abiotic Stress Responses. *Cells* **2018**, *7*, 120. [[CrossRef](#)]
8. Li, J.; Wen, J.; Lease, K.A.; Doke, J.T.; Tax, F.E.; Walker, J.C. BAK1, an Arabidopsis LRR Receptor-like Protein Kinase, Interacts with BRI1 and Modulates Brassinosteroid Signaling. *Cell* **2002**, *110*, 213–222. [[CrossRef](#)]
9. Zhou, J.; Wang, P.; Claus, L.A.N.; Savatin, D.V.; Xu, G.; Wu, S.; Meng, X.; Russinova, E.; He, P.; Shan, L. Proteolytic Processing of Serk3/Bak1 Regulates Plant Immunity, Development, and Cell Death. *Plant Physiol.* **2019**, *180*, 543–558. [[CrossRef](#)]
10. Park, S.J.; Moon, J.C.; Park, Y.C.; Kim, J.H.; Kim, D.S.; Jang, C.S. Molecular Dissection of the Response of a Rice Leucine-Rich Repeat Receptor-like Kinase (LRR-RLK) Gene to Abiotic Stresses. *J. Plant Physiol.* **2014**, *171*, 1465–1653. [[CrossRef](#)]
11. Liu, X.S.; Liang, C.C.; Hou, S.G.; Wang, X.; Chen, D.H.; Shen, J.L.; Zhang, W.; Wang, M. The LRR-RLK Protein HSL3 Regulates Stomatal Closure and the Drought Stress Response by Modulating Hydrogen Peroxide Homeostasis. *Front. Plant Sci.* **2020**, *11*, 548034. [[CrossRef](#)]
12. Lin, F.; Li, S.; Wang, K.; Tian, H.; Gao, J.; Zhao, Q.; Du, C. A Leucine-Rich Repeat Receptor-like Kinase, OsSTLK, Modulates Salt Tolerance in Rice. *Plant Sci.* **2020**, *296*, 110465. [[CrossRef](#)]
13. Albert, I.; Böhm, H.; Albert, M.; Feiler, C.E.; Imkamp, J.; Wallmeroth, N.; Brancato, C.; Raaymakers, T.M.; Oome, S.; Zhang, H.; et al. An RLP23-SOBIR1-BAK1 Complex Mediates NLP-Triggered Immunity. *Nat. Plants* **2015**, *1*, 15140. [[CrossRef](#)]
14. Gao, M.; Wang, X.; Wang, D.; Xu, F.; Ding, X.; Zhang, Z.; Bi, D.; Cheng, Y.T.; Chen, S.; Li, X.; et al. Regulation of Cell Death and Innate Immunity by Two Receptor-like Kinases in Arabidopsis. *Cell Host Microbe* **2009**, *6*, 34–44. [[CrossRef](#)]
15. Russinova, E.; Borst, J.W.; Kwaaitaal, M.; Caño-Delgado, A.; Yin, Y.; Chory, J.; De Vries, S.C. Heterodimerization and Endocytosis of Arabidopsis Brassinosteroid Receptors BRI1 and AtSERK3 (BAK1). *Plant Cell* **2004**, *16*, 3216–3229. [[CrossRef](#)]
16. Roux, M.; Schwessinger, B.; Albrecht, C.; Chinchilla, D.; Jones, A.; Holton, N.; Malinovsky, F.G.; Tör, M.; de Vries, S.; Zipfel, C. The Arabidopsis Leucine-Rich Repeat Receptor-like Kinases BAK1/SERK3 and BKK1/SERK4 Are Required for Innate Immunity to Hemibiotrophic and Biotrophic Pathogens. *Plant Cell* **2011**, *23*, 2440–2455. [[CrossRef](#)]
17. Nam, K.H.; Li, J. BRI1/BAK1, a Receptor Kinase Pair Mediating Brassinosteroid Signaling. *Cell* **2002**, *110*, 203–212. [[CrossRef](#)]
18. Liebrand, T.W.H.; Van Den Berg, G.C.M.; Zhang, Z.; Smit, P.; Cordewener, J.H.G.; America, A.H.P.; Sklenar, J.; Jones, A.M.E.; Tameling, W.I.L.; Rotbatsch, S.; et al. Receptor-like Kinase SOBIR1/EVR Interacts with Receptor-like Proteins in Plant Immunity against Fungal Infection. *Proc. Natl. Acad. Sci. USA* **2013**, *110*, 10010–10015. [[CrossRef](#)]
19. Ye, Y.; Ding, Y.; Jiang, Q.; Wang, F.; Sun, J.; Zhu, C. The Role of Receptor-like Protein Kinases (RLKs) in Abiotic Stress Response in Plants. *Plant Cell Rep.* **2017**, *36*, 235–242. [[CrossRef](#)]
20. Ma, X.; Xu, G.; He, P.; Shan, L. SERKING Coreceptors for Receptors. *Trends Plant Sci.* **2016**, *21*, 1017–1033. [[CrossRef](#)]
21. Diévar, A.; Clark, S.E. Using Mutant Alleles to Determine the Structure and Function of Leucine-Rich Repeat Receptor-like Kinases. *Curr. Opin. Plant Biol.* **2003**, *6*, 507–516. [[CrossRef](#)]
22. Xi, L.; Wu, X.N.; Gilbert, M.; Schulze, W.X. Classification and Interactions of LRR Receptors and Co-Receptors within the Arabidopsis Plasma Membrane—An Overview. *Front. Plant Sci.* **2019**, *10*, 472. [[CrossRef](#)] [[PubMed](#)]
23. Zhang, H.; Lin, X.; Han, Z.; Wang, J.; Qu, L.J.; Chai, J. SERK Family Receptor-like Kinases Function as Co-Receptors with PXY for Plant Vascular Development. *Mol. Plant* **2016**, *9*, 1406–1414. [[CrossRef](#)] [[PubMed](#)]
24. Hohmann, U.; Nicolet, J.; Moretti, A.; Hothorn, L.A.; Hothorn, M. The SERK3 Elongated Allele Defines a Role for BIR Ectodomains in Brassinosteroid Signalling. *Nat. Plants* **2018**, *4*, 345–351. [[CrossRef](#)]
25. Hohmann, U.; Santiago, J.; Nicolet, J.; Olsson, V.; Spiga, F.M.; Hothorn, L.A.; Butenko, M.A.; Hothorn, M. Mechanistic Basis for the Activation of Plant Membrane Receptor Kinases by SERK-Family Coreceptors. *Proc. Natl. Acad. Sci. USA* **2018**, *115*, 3488–3493. [[CrossRef](#)]
26. Chinchilla, D.; Shan, L.; He, P.; de Vries, S.; Kemmerling, B. One for All: The Receptor-Associated Kinase BAK1. *Trends Plant Sci.* **2009**, *14*, 535–541. [[CrossRef](#)]
27. Postel, S.; Küfner, I.; Beuter, C.; Mazzotta, S.; Schwedt, A.; Borlotti, A.; Halter, T.; Kemmerling, B.; Nümberger, T. The Multifunctional Leucine-Rich Repeat Receptor Kinase BAK1 Is Implicated in Arabidopsis Development and Immunity. *Eur. J. Cell Biol.* **2010**, *89*, 169–174. [[CrossRef](#)]
28. Lin, W.; Li, B.; Lu, D.; Chen, S.; Zhu, N.; He, P.; Shan, L. Tyrosine Phosphorylation of Protein Kinase Complex BAK1/BIK1 Mediates Arabidopsis Innate Immunity. *Proc. Natl. Acad. Sci. USA* **2014**, *111*, 3632–3637. [[CrossRef](#)]
29. Jordá, L.; Sopena-Torres, S.; Escudero, V.; Nuñez-Corcuera, B.; Delgado-Cerezo, M.; Torii, K.U.; Molina, A. ERECTA and BAK1 Receptor like Kinases Interact to Regulate Immune Responses in Arabidopsis. *Front. Plant Sci.* **2016**, *7*, 897. [[CrossRef](#)]

30. Liu, Y.; Huang, X.; Li, M.; He, P.; Zhang, Y. Loss-of-Function of Arabidopsis Receptor-like Kinase BIR1 Activates Cell Death and Defense Responses Mediated by BAK1 and SOBIR1. *New Phytol.* **2016**, *212*, 637–645. [[CrossRef](#)]
31. Wang, Z.; Meng, P.; Zhang, X.; Ren, D.; Yang, S. BON1 Interacts with the Protein Kinases BIR1 and BAK1 in Modulation of Temperature-Dependent Plant Growth and Cell Death in Arabidopsis. *Plant J.* **2011**, *67*, 1081–1093. [[CrossRef](#)]
32. Bleckmann, A.; Weidtkamp-Peters, S.; Seidel, C.A.M.; Simon, R. Stem Cell Signaling in Arabidopsis Requires CRN to Localize CLV2 to the Plasma Membrane. *Plant Physiol.* **2010**, *152*, 166–176. [[CrossRef](#)]
33. Cui, Y.; Hu, C.; Zhu, Y.; Cheng, K.; Li, X.; Wei, Z.; Xue, L.; Lin, F.; Shi, H.; Yi, J.; et al. Clk Receptor Kinases Determine Cell Fate Specificity during Early Anther Development in Arabidopsis. *Plant Cell* **2018**, *30*, 2383–2401. [[CrossRef](#)]
34. Liu, P.L.; Du, L.; Huang, Y.; Gao, S.M.; Yu, M. Origin and Diversification of Leucine-Rich Repeat Receptor-like Protein Kinase (LRR-RLK) Genes in Plants. *BMC Evol. Biol.* **2017**, *17*, 47. [[CrossRef](#)]
35. He, X.; Feng, T.; Zhang, D.; Zhuo, R.; Liu, M. Identification and Comprehensive Analysis of the Characteristics and Roles of Leucine-Rich Repeat Receptor-like Protein Kinase (LRR-RLK) Genes in *Sedum alfredii* Hance Responding to Cadmium Stress. *Ecotoxicol. Environ. Saf.* **2019**, *167*, 95–106. [[CrossRef](#)]
36. Liu, P.L.; Xie, L.L.; Li, P.W.; Mao, J.F.; Liu, H.; Gao, S.M.; Shi, P.H.; Gong, J.Q. Duplication and Divergence of Leucine-Rich Repeat Receptor-like Protein Kinase (LRR-RLK) Genes in Basal Angiosperm *Amborella trichopoda*. *Front. Plant Sci.* **2016**, *7*, 1952. [[CrossRef](#)]
37. Dufayard, J.F.; Bettembourg, M.; Fischer, I.; Droc, G.; Guiderdoni, E.; Périn, C.; Chantret, N.; Diévert, A. New Insights on Leucine-Rich Repeats Receptor-like Kinase Orthologous Relationships in Angiosperms. *Front. Plant Sci.* **2017**, *8*, 381. [[CrossRef](#)]
38. Xiao, Y.; Xia, W.; Yang, Y.; Mason, A.S.; Lei, X.; Ma, Z. Characterization and Evolution of Conserved MicroRNA through Duplication Events in Date Palm (*Phoenix dactylifera*). *PLoS ONE* **2013**, *8*, e71435. [[CrossRef](#)]
39. Huang, S.; Li, R.; Zhang, Z.; Li, L.; Gu, X.; Fan, W.; Lucas, W.J.; Wang, X.; Xie, B.; Ni, P.; et al. The Genome of the Cucumber, *Cucumis sativus*, L. *Nat. Genet.* **2009**, *41*, 1275–1281. [[CrossRef](#)]
40. Sun, J.; Li, L.; Wang, P.; Zhang, S.; Wu, J. Genome-Wide Characterization, Evolution, and Expression Analysis of the Leucine-Rich Repeat Receptor-like Protein Kinase (LRR-RLK) Gene Family in Rosaceae Genomes. *BMC Genom.* **2017**, *18*, 763. [[CrossRef](#)]
41. Meng, J.; Yang, J.; Peng, M.; Liu, X.; He, H. Genome-Wide Characterization, Evolution, and Expression Analysis of the Leucine-Rich Repeat Receptor-like Protein Kinase (Lrr-Rlk) Gene Family in *Medicago truncatula*. *Life* **2020**, *10*, 176. [[CrossRef](#)] [[PubMed](#)]
42. Zhuang, J.; Peng, R.H.; Cheng, Z.M.; Zhang, J.; Cai, B.; Zhang, Z.; Gao, F.; Zhu, B.; Fu, X.Y.; Jin, X.F.; et al. Genome-Wide Analysis of the Putative AP2/ERF Family Genes in *Vitis vinifera*. *Sci. Hort.* **2009**, *123*, 73–81. [[CrossRef](#)]
43. Wu, Y.; Xun, Q.; Guo, Y.; Zhang, J.; Cheng, K.; Shi, T.; He, K.; Hou, S.; Gou, X.; Li, J. Genome-Wide Expression Pattern Analyses of the Arabidopsis Leucine-Rich Repeat Receptor-like Kinases. *Mol. Plant* **2016**, *9*, 289–300. [[CrossRef](#)] [[PubMed](#)]
44. Hirakawa, H.; Tsuchimoto, S.; Sakai, H.; Nakayama, S.; Fujishiro, T.; Kishida, Y.; Kohara, M.; Watanabe, A.; Yamada, M.; Aizu, T.; et al. Upgraded Genomic Information of *Jatropha curcas* L. *Plant Biotechnol.* **2012**, *29*, 123–130. [[CrossRef](#)]
45. Zhu, H.; Wang, Y.; Yin, H.; Gao, M.; Zhang, Q.; Chen, Y. Genome-Wide Identification and Characterization of the LRR-RLK Gene Family in Two *Vernicia* Species. *Int. J. Genom.* **2015**, *2015*, 823427. [[CrossRef](#)]
46. Cao, Y.; Mo, W.; Li, Y.; Li, W.; Dong, X.; Liu, M.; Jiang, L.; Zhang, L. Deciphering the Roles of Leucine-Rich Repeat Receptor-like Protein Kinases (LRR-RLKs) in Response to *Fusarium* Wilt in the *Vernicia fordii* (Tung Tree). *Phytochemistry* **2021**, *185*, 112686. [[CrossRef](#)]
47. Sakamoto, T.; Deguchi, M.; Brustolini, O.J.B.; Santos, A.A.; Silva, F.F.; Fontes, E.P.B. The Tomato RLK Superfamily: Phylogeny and Functional Predictions about the Role of the LRR-RLK Subfamily in Antiviral Defense. *BMC Plant Biol.* **2012**, *12*, 229. [[CrossRef](#)]
48. Shen, S.; Zhang, Q.; Shi, Y.; Sun, Z.; Zhang, Q.; Hou, S.; Wu, R.; Jiang, L.; Zhao, X.; Guo, Y. Genome-Wide Analysis of the NAC Domain Transcription Factor Gene Family in *Theobroma cacao*. *Genes* **2020**, *11*, 35. [[CrossRef](#)]
49. Song, W.; Wang, B.; Li, X.; Wei, J.; Chen, L.; Zhang, D.; Zhang, W.; Li, R. Identification of Immune Related LRR-Containing Genes in Maize (*Zea mays* L.) by Genome-Wide Sequence Analysis. *Int. J. Genom.* **2015**, *2015*, 231358. [[CrossRef](#)]
50. Dezhsetan, S. Genome Scanning for Identification and Mapping of Receptor-like Kinase (RLK) Gene Superfamily in *Solanum tuberosum*. *Physiol. Mol. Biol. Plants* **2017**, *23*, 755–765. [[CrossRef](#)]
51. Wang, J.; Hu, T.; Wang, W.; Hu, H.; Wei, Q.; Bao, C. Investigation of Evolutionary and Expressional Relationships in the Function of the Leucine-Rich Repeat Receptor-like Protein Kinase Gene Family (LRR-RLK) in the Radish (*Raphanus sativus* L.). *Sci. Rep.* **2019**, *9*, 6937. [[CrossRef](#)]
52. Sun, R.; Wang, S.; Ma, D.; Liu, C. Genome-Wide Analysis of LRR-RLK Gene Family in Four *Gossypium* Species and Expression Analysis during Cotton Development and Stress Responses. *Genes* **2018**, *9*, 592. [[CrossRef](#)]
53. Magalhães, D.M.; Scholte, L.L.S.; Silva, N.V.; Oliveira, G.C.; Zipfel, C.; Takita, M.A.; De Souza, A.A. LRR-RLK Family from Two *Citrus* Species: Genome-Wide Identification and Evolutionary Aspects. *BMC Genom.* **2016**, *17*, 623. [[CrossRef](#)]
54. Rameneni, J.J.; Lee, Y.; Dhandapani, V.; Yu, X.; Choi, S.R.; Oh, M.H.; Lim, Y.P. Genomic and Post-Translational Modification Analysis of Leucine-Rich-Repeat Receptor-like Kinases in *Brassica rapa*. *PLoS ONE* **2015**, *10*, e0142255. [[CrossRef](#)]
55. Li, W.; Chen, M.; Wang, E.; Hu, L.; Hawkesford, M.J.; Zhong, L.; Chen, Z.; Xu, Z.; Li, L.; Zhou, Y.; et al. Genome-Wide Analysis of Autophagy-Associated Genes in Foxtail Millet (*Setaria italica* L.) and Characterization of the Function of SiATG8a in Conferring Tolerance to Nitrogen Starvation in Rice. *BMC Genom.* **2016**, *17*, 797. [[CrossRef](#)]
56. Truco, M.J.; Quiros, C.F. Structure and Organization of the B Genome Based on a Linkage Map in *Brassica nigra*. *Theor. Appl. Genet.* **1994**, *89*, 590–598. [[CrossRef](#)]

57. Sun, X.; Wang, G.L. Genome-Wide Identification, Characterization and Phylogenetic Analysis of the Rice LRR-Kinases. *PLoS ONE* **2011**, *6*, e16079. [[CrossRef](#)]
58. Liu, Q.; Chang, S.; Hartman, G.L.; Domier, L.L. Assembly and Annotation of a Draft Genome Sequence for *Glycine latifolia*, a Perennial Wild Relative of Soybean. *Plant J.* **2018**, *95*, 71–85. [[CrossRef](#)]
59. Yang, W.; Yu, M.; Zou, C.; Lu, C.; Yu, D.; Cheng, H.; Jiang, P.; Feng, X.; Zhang, Y.; Wang, Q.; et al. Genome-Wide Comparative Analysis of RNA-Binding Glycine-Rich Protein Family Genes between *Gossypium arboreum* and *Gossypium raimondii*. *PLoS ONE* **2018**, *14*, e0218938. [[CrossRef](#)]
60. Cao, Y.; Han, Y.; Meng, D.; Li, D.; Jin, Q.; Lin, Y.; Cai, Y. Structural, Evolutionary, and Functional Analysis of the Class III Peroxidase Gene Family in Chinese Pear (*Pyrus bretschneideri*). *Front. Plant Sci.* **2016**, *7*, 1874. [[CrossRef](#)]
61. Zan, Y.; Ji, Y.; Zhang, Y.; Yang, S.; Song, Y.; Wang, J. Genome-Wide Identification, Characterization and Expression Analysis of *Populus* Leucine-Rich Repeat Receptor-like Protein Kinase Genes. *BMC Genom.* **2013**, *14*, 318. [[CrossRef](#)] [[PubMed](#)]
62. Yang, H.; Bayer, P.E.; Tirnaz, S.; Edwards, D.; Batley, J. Genome-Wide Identification and Evolution of Receptor-like Kinases (RLKs) and Receptor like Proteins (RLPs) in *Brassica juncea*. *Biology* **2021**, *10*, 17. [[CrossRef](#)] [[PubMed](#)]
63. Zhou, F.; Guo, Y.; Qiu, L.J. Genome-Wide Identification and Evolutionary Analysis of Leucine-Rich Repeat Receptor-like Protein Kinase Genes in Soybean. *BMC Plant Biol.* **2016**, *16*, 58. [[CrossRef](#)] [[PubMed](#)]
64. Shumayla; Sharma, S.; Kumar, R.; Mendu, V.; Singh, K.; Upadhyay, S.K. Genomic Dissection and Expression Profiling Revealed Functional Divergence in *Triticum aestivum* Leucine Rich Repeat Receptor like Kinases (TaLRRKs). *Front. Plant Sci.* **2016**, *7*, 1374. [[CrossRef](#)]
65. Wang, X.; Wu, M.H.; Xiao, D.; Huang, R.L.; Zhan, J.; Wang, A.Q.; He, L.F. Genome-Wide Identification and Evolutionary Analysis of RLKs Involved in the Response to Aluminium Stress in Peanut. *BMC Plant Biol.* **2021**, *21*, 281. [[CrossRef](#)]
66. Mishra, D.; Suri, G.S.; Kaur, G.; Tiwari, M. Comprehensive Analysis of Structural, Functional, and Evolutionary Dynamics of Leucine Rich Repeats-RLKs in *Thinopyrum elongatum*. *Int. J. Biol. Macromol.* **2021**, *183*, 513–527. [[CrossRef](#)]
67. Zoulias, N.; Harrison, E.L.; Casson, S.A.; Gray, J.E. Molecular Control of Stomatal Development. *Biochem. J.* **2018**, *475*, 441–454. [[CrossRef](#)]
68. Zhu, Y.; Hu, C.; Cui, Y.; Zeng, L.; Li, S.; Zhu, M.; Meng, F.; Huang, S.; Long, L.; Yi, J.; et al. Conserved and Differentiated Functions of CIK Receptor Kinases in Modulating Stem Cell Signaling in *Arabidopsis*. *Mol. Plant* **2021**, *14*, 1119–1134. [[CrossRef](#)]
69. Ou, Y.; Kui, H.; Li, J. Receptor-like Kinases in Root Development: Current Progress and Future Directions. *Mol. Plant* **2021**, *14*, 166–185. [[CrossRef](#)]
70. Nadeau, J.A. Stomatal Development: New Signals and Fate Determinants. *Curr. Opin. Plant Biol.* **2009**, *12*, 29–35. [[CrossRef](#)]
71. Cammarata, J.; Scanlon, M.J. A Functionally Informed Evolutionary Framework for the Study of LRR-RLKs during Stem Cell Maintenance. *J. Plant Res.* **2020**, *133*, 331–342. [[CrossRef](#)]
72. Kim, B.H.; Kim, S.Y.; Nam, K.H. Assessing the Diverse Functions of BAK1 and Its Homologs in *Arabidopsis*, beyond BR Signaling and PTI Responses. *Mol. Cells* **2013**, *35*, 7–16. [[CrossRef](#)]
73. Shang, Y.; Dai, C.; Lee, M.M.; Kwak, J.M.; Nam, K.H. BRI1-Associated Receptor Kinase 1 Regulates Guard Cell ABA Signaling Mediated by Open Stomata 1 in *Arabidopsis*. *Mol. Plant* **2016**, *9*, 447–460. [[CrossRef](#)]
74. Kosaka, A.; Pastorczyk, M.; Piślewska-Bednarek, M.; Nishiuchi, T.; Ono, E.; Suemoto, H.; Ishikawa, A.; Frerigmann, H.; Kaido, M.; Mise, K.; et al. Tryptophan-Derived Metabolites and BAK1 Separately Contribute to *Arabidopsis* Postinvasive Immunity against *Alternaria brassicicola*. *Sci. Rep.* **2021**, *11*, 1488. [[CrossRef](#)]
75. Peng, H.C.; Kaloshian, I. The Tomato Leucine-Rich Repeat Receptor-like Kinases SISERK3A and SISERK3B Have Overlapping Functions in Bacterial and Nematode Innate Immunity. *PLoS ONE* **2014**, *9*, e93302. [[CrossRef](#)]
76. Chaparro-Garcia, A.; Wilkinson, R.C.; Gimenez-Ibanez, S.; Findlay, K.; Coffey, M.D.; Zipfel, C.; Rathjen, J.P.; Kamoun, S.; Schornack, S. The Receptor-like Kinase Serk3/Bak1 Is Required for Basal Resistance against the Late Blight Pathogen *Phytophthora Infestans* in *Nicotiana benthamiana*. *PLoS ONE* **2011**, *6*, e16608. [[CrossRef](#)]
77. Chen, X.; Zuo, S.; Schwessinger, B.; Chern, M.; Canlas, P.E.; Ruan, D.; Zhou, X.; Wang, J.; Daudi, A.; Petzold, C.J.; et al. An XA21-Associated Kinase (OsSERK2) Regulates Immunity Mediated by the XA21 and XA3 Immune Receptors. *Mol. Plant* **2014**, *7*, 874–892. [[CrossRef](#)]
78. Hu, H.; Xiong, L.; Yang, Y. Rice SERK1 Gene Positively Regulates Somatic Embryogenesis of Cultured Cell and Host Defense Response against Fungal Infection. *Planta* **2005**, *222*, 107–117. [[CrossRef](#)]
79. Derbyshire, M.; Mbengue, M.; Barascud, M.; Navaud, O.; Raffaele, S. Small RNAs from the Plant Pathogenic Fungus *Sclerotinia sclerotiorum* Highlight Host Candidate Genes Associated with Quantitative Disease Resistance. *Mol. Plant Pathol.* **2019**, *20*, 1279–1297. [[CrossRef](#)]
80. Dong, N.; Yin, W.; Liu, D.; Zhang, X.; Yu, Z.; Huang, W.; Liu, J.; Yang, Y.; Meng, W.; Niu, M.; et al. Regulation of Brassinosteroid Signaling and Salt Resistance by SERK2 and Potential Utilization for Crop Improvement in Rice. *Front. Plant Sci.* **2020**, *11*, 621859. [[CrossRef](#)]
81. Li, X.; Ahmad, S.; Ali, A.; Guo, C.; Li, H.; Yu, J.; Zhang, Y.; Gao, X.; Guo, Y. Characterization of Somatic Embryogenesis Receptor-like Kinase 4 as a Negative Regulator of Leaf Senescence in *Arabidopsis*. *Cells* **2019**, *8*, 50. [[CrossRef](#)]
82. Wang, X.; Li, X.; Meisenhelder, J.; Hunter, T.; Yoshida, S.; Asami, T.; Chory, J. Autoregulation and Homodimerization Are Involved in the Activation of the Plant Steroid Receptor BRI1. *Dev. Cell* **2005**, *8*, 855–865. [[CrossRef](#)]

83. Goddard, R.; Peraldi, A.; Ridout, C.; Nicholson, P. Enhanced Disease Resistance Caused by BRI1 Mutation Is Conserved between *Brachypodium distachyon* and Barley (*Hordeum vulgare*). *Mol. Plant-Microbe Interact.* **2014**, *27*, 1095–1106. [[CrossRef](#)]
84. Clouse, S.D.; Langford, M.; McMorris, T.C. A Brassinosteroid-Insensitive Mutant in *Arabidopsis thaliana* Exhibits Multiple Defects in Growth and Development. *Plant Physiol.* **1996**, *111*, 671–678. [[CrossRef](#)]
85. Li, J.; Lease, K.A.; Tax, F.E.; Walker, J.C. BRS1, a Serine Carboxypeptidase, Regulates BRI1 Signaling in *Arabidopsis thaliana*. *Proc. Natl. Acad. Sci. USA* **2001**, *98*, 5916–5921. [[CrossRef](#)]
86. Feng, Y.; Yin, Y.; Fei, S. Down-Regulation of BdBRI1, a Putative Brassinosteroid Receptor Gene Produces a Dwarf Phenotype with Enhanced Drought Tolerance in *Brachypodium distachyon*. *Plant Sci.* **2015**, *234*, 163–173. [[CrossRef](#)] [[PubMed](#)]
87. Holton, N.; Harrison, K.; Yokota, T.; Bishop, G.J. Tomato BRI1 and Systemin Wound Signalling. *Plant Signal. Behav.* **2008**, *3*, 54–55. [[CrossRef](#)]
88. Huang, S.; Wang, H.; Gan, S.; Hussein, M.A.M.; Wang, Q.; Wang, X.; Zhang, Y.; Wang, X. Molecular Identification and Functional Analysis of Brbri1 as Brassinosteroid Receptor Gene in *Brassica rapa*. *Pak. J. Bot.* **2018**, *50*, 85–95.
89. Sharma, A.; Matsuoka, M.; Tanaka, H.; Komatsu, S. Antisense Inhibition of a BRI1 Receptor Reveals Additional Protein Kinase Signaling Components Downstream to the Perception of Brassinosteroids in Rice. *FEBS Lett.* **2001**, *507*, 346–350. [[CrossRef](#)]
90. Scheer, J.M.; Pearce, G.; Ryan, C.A. Generation of Systemin Signaling in Tobacco by Transformation with the Tomato Systemin Receptor Kinase Gene. *Proc. Natl. Acad. Sci. USA* **2003**, *100*, 10114–10117. [[CrossRef](#)]
91. Deng, X.G.; Zhu, T.; Zou, L.J.; Han, X.Y.; Zhou, X.; Xi, D.H.; Zhang, D.W.; Lin, H.H. Orchestration of Hydrogen Peroxide and Nitric Oxide in Brassinosteroid-Mediated Systemic Virus Resistance in *Nicotiana benthamiana*. *Plant J.* **2016**, *85*, 478–493. [[CrossRef](#)] [[PubMed](#)]
92. Singh, A.; Breja, P.; Khurana, J.P.; Khurana, P. Wheat Brassinosteroid-Insensitive1 (TaBRI1) Interacts with Members of TaSERK Gene Family and Cause Early Flowering and Seed Yield Enhancement in *Arabidopsis*. *PLoS ONE* **2016**, *11*, e0153273. [[CrossRef](#)] [[PubMed](#)]
93. Nie, S.; Huang, S.; Wang, S.; Cheng, D.; Liu, J.; Lv, S.; Li, Q.; Wang, X. Enhancing Brassinosteroid Signaling via Overexpression of Tomato (*Solanum lycopersicum*) SIBRI1 Improves Major Agronomic Traits. *Front. Plant Sci.* **2017**, *8*, 1386. [[CrossRef](#)] [[PubMed](#)]
94. Huang, S.; Zheng, C.; Zhao, Y.; Li, Q.; Liu, J.; Deng, R.; Lei, T.; Wang, S.; Wang, X. RNA Interference Knockdown of the Brassinosteroid Receptor BRI1 in Potato (*Solanum tuberosum* L.) Reveals Novel Functions for Brassinosteroid Signaling in Controlling Tuberization. *Sci. Hortic.* **2021**, *290*, 110516. [[CrossRef](#)]
95. Costa, A.T.; Bravo, J.P.; Krause-Sakate, R.; Maia, I.G. The Receptor-like Kinase SISOBIR1 Is Differentially Modulated by Virus Infection but Its Overexpression in Tobacco Has No Significant Impact on Virus Accumulation. *Plant Cell Rep.* **2016**, *35*, 35–75. [[CrossRef](#)]
96. Huang, S.; R.H.H.; Schol, C.; Villanueva, S.L.; Heidstra, R.; Joosten, M.H.A.J. Knocking out SOBIR1 in *Nicotiana benthamiana* Abolishes Functionality of Transgenic Receptor-like Protein Cf-4. *Plant Physiol.* **2021**, *185*, 290–294. [[CrossRef](#)]
97. Zhou, Y.; Sun, L.; Wassan, G.M.; He, X.; Shaban, M.; Zhang, L.; Zhu, L.; Zhang, X. GbSOBIR1 Confers Verticillium Wilt Resistance by Phosphorylating the Transcriptional Factor GbbHLH171 in *Gossypium barbadense*. *Plant Biotechnol. J.* **2019**, *17*, 152–163. [[CrossRef](#)]
98. Zipfel, C.; Kunze, G.; Chinchilla, D.; Caniard, A.; Jones, J.D.G.; Boller, T.; Felix, G. Perception of the Bacterial PAMP EF-Tu by the Receptor EFR Restricts Agrobacterium-Mediated Transformation. *Cell* **2006**, *125*, 749–760. [[CrossRef](#)]
99. Lacombe, S.; Rougon-Cardoso, A.; Sherwood, E.; Peeters, N.; Dahlbeck, D.; Van Esse, H.P.; Smoker, M.; Rallapalli, G.; Thomma, B.P.H.J.; Staskawicz, B.; et al. Interfamily Transfer of a Plant Pattern-Recognition Receptor Confers Broad-Spectrum Bacterial Resistance. *Nat. Biotechnol.* **2010**, *28*, 365–369. [[CrossRef](#)]
100. Holton, N.; Nekrasov, V.; Ronald, P.C.; Zipfel, C. The Phylogenetically-Related Pattern Recognition Receptors EFR and XA21 Recruit Similar Immune Signaling Components in Monocots and Dicots. *PLoS Pathog.* **2015**, *11*, e1004602. [[CrossRef](#)]
101. Piazza, S.; Campa, M.; Pompili, V.; Costa, L.D.; Salvagnin, U.; Nekrasov, V.; Zipfel, C.; Malnoy, M. The Arabidopsis Pattern Recognition Receptor EFR Enhances Fire Blight Resistance in Apple. *Hortic. Res.* **2021**, *8*, 204. [[CrossRef](#)]
102. Pfeilmeier, S.; George, J.; Morel, A.; Roy, S.; Smoker, M.; Stransfeld, L.; Downie, J.A.; Peeters, N.; Malone, J.G.; Zipfel, C. Expression of the *Arabidopsis thaliana* Immune Receptor EFR in *Medicago truncatula* Reduces Infection by a Root Pathogenic Bacterium, but Not Nitrogen-Fixing Rhizobial Symbiosis. *Plant Biotechnol. J.* **2019**, *17*, 569–579. [[CrossRef](#)]
103. Boschi, F.; Schwartzman, C.; Murchio, S.; Ferreira, V.; Siri, M.I.; Galván, G.A.; Smoker, M.; Stransfeld, L.; Zipfel, C.; Vilaró, F.L.; et al. Enhanced Bacterial Wilt Resistance in Potato through Expression of Arabidopsis Efr and Introgression of Quantitative Resistance from *Solanum commersonii*. *Front. Plant Sci.* **2017**, *8*, 1642. [[CrossRef](#)]
104. Mosher, S.; Seybold, H.; Rodriguez, P.; Stahl, M.; Davies, K.A.; Dayaratne, S.; Morillo, S.A.; Wierzbza, M.; Favery, B.; Keller, H.; et al. The Tyrosine-Sulfated Peptide Receptors PSKR1 and PSY1R Modify the Immunity of Arabidopsis to Biotrophic and Necrotrophic Pathogens in an Antagonistic Manner. *Plant J.* **2013**, *73*, 469–482. [[CrossRef](#)]
105. Yang, W.; Zhang, B.; Qi, G.; Shang, L.; Liu, H.; Ding, X.; Chu, Z. Identification of the Phytosulfokine Receptor 1 (OsPSKR1) Confers Resistance to Bacterial Leaf Streak in Rice. *Planta* **2019**, *250*, 1603–1612. [[CrossRef](#)]
106. Nakaminami, K.; Okamoto, M.; Higuchi-Takeuchi, M.; Yoshizumi, T.; Yamaguchi, Y.; Fukao, Y.; Shimizu, M.; Ohashi, C.; Tanaka, M.; Matsui, M.; et al. AtPep3 Is a Hormone-like Peptide That Plays a Role in the Salinity Stress Tolerance of Plants. *Proc. Natl. Acad. Sci. USA* **2018**, *115*, 5810–5815. [[CrossRef](#)]

107. Zheng, X.; Kang, S.; Jing, Y.; Ren, Z.; Li, L.; Zhou, J.M.; Berkowitz, G.; Shi, J.; Fu, A.; Lan, W.; et al. Danger-Associated Peptides Close Stomata by OST1-Independent Activation of Anion Channels in Guard Cells. *Plant Cell* **2018**, *30*, 1132–1146. [[CrossRef](#)]
108. Xu, S.; Liao, C.J.; Jaiswal, N.; Lee, S.; Yun, D.J.; Lee, S.Y.; Garvey, M.; Kaplan, I.; Mengiste, T. Tomato PEPR1 ORTHOLOG RECEPTOR-LIKE KINASE1 Regulates Responses to Systemin, Necrotrophic Fungi, and Insect Herbivory. *Plant Cell* **2018**, *30*, 2214–2229. [[CrossRef](#)]
109. Shang, Y.; Yang, D.; Ha, Y.; Nam, K.H. BAK1-Induced RPK1 Phosphorylation Is Essential for RPK1-Mediated Cell Death in *Arabidopsis*. *Biochem. Biophys. Res. Commun.* **2021**, *573*, 125–131. [[CrossRef](#)]
110. Choi, D.S.; Hwang, I.S.; Hwang, B.K. Requirement of the Cytosolic Interaction between PATHOGENESIS-RELATED PROTEIN10 and LEUCINE-RICH REPEAT PROTEIN1 for Cell Death and Defense Signaling in Pepper. *Plant Cell* **2012**, *24*, 1675–1690. [[CrossRef](#)]
111. Chen, X.; Wang, T.; Rehman, A.U.; Wang, Y.; Qi, J.; Li, Z.; Song, C.; Wang, B.; Yang, S.; Gong, Z. *Arabidopsis* U-Box E3 Ubiquitin Ligase PUB11 Negatively Regulates Drought Tolerance by Degrading the Receptor-like Protein Kinases LRR1 and KIN7. *J. Integr. Plant Biol.* **2021**, *63*, 494–509. [[CrossRef](#)]
112. Isner, J.C.; Begum, A.; Nuehse, T.; Hetherington, A.M.; Maathuis, F.J.M. KIN7 Kinase Regulates the Vacuolar TPK1 K<sup>+</sup> Channel during Stomatal Closure. *Curr. Biol.* **2018**, *28*, 466–472.e4. [[CrossRef](#)]
113. Thapa, G.; Gunupuru, L.R.; Hehir, J.G.; Kahla, A.; Mullins, E.; Doohan, F.M. A Pathogen-Responsive Leucine Rich Receptor like Kinase Contributes to Fusarium Resistance in Cereals. *Front. Plant Sci.* **2018**, *9*, 867. [[CrossRef](#)]
114. Caddell, D.F.; Park, C.J.; Thomas, N.C.; Canlas, P.E.; Ronald, P.C. Silencing of the Rice Gene LRR1 Compromises Rice Xa21 Transcript Accumulation and XA21-Mediated Immunity. *Rice* **2017**, *10*, 23. [[CrossRef](#)]
115. ten Hove, C.A.; de Jong, M.; Lapin, D.; Andel, A.; Sanchez-Perez, G.F.; Tarutani, Y.; Suzuki, Y.; Heidstra, R.; van den Ackerveken, G. Trans-Repression of Gene Activity Upstream of T-DNA Tagged Rik902 Links *Arabidopsis* Root Growth Inhibition and Downy Mildew Resistance. *PLoS ONE* **2011**, *6*, e19028. [[CrossRef](#)]
116. Zhao, Y.; Wu, G.; Shi, H.; Tang, D. RECEPTOR-LIKE KINASE 902 Associates with and Phosphorylates BRASSINOSTEROID-SIGNALING KINASE1 to Regulate Plant Immunity. *Mol. Plant* **2019**, *12*, 59–70. [[CrossRef](#)]
117. Fontes, E.P.B.; Santos, A.A.; Luz, D.F.; Waclawovsky, A.J.; Chory, J. The Geminivirus Nuclear Shuttle Protein Is a Virulence Factor That Suppresses Transmembrane Receptor Kinase Activity. *Genes Dev.* **2004**, *18*, 2545–2556. [[CrossRef](#)]
118. Wang, M.; Weiberg, A.; Dellota, E.; Yamane, D.; Jin, H. Botrytis Small RNA Bc-SiR37 Suppresses Plant Defense Genes by Cross-Kingdom RNAi. *RNA Biol.* **2017**, *14*, 421–428. [[CrossRef](#)] [[PubMed](#)]
119. Liu, T.; Jiang, G.Q.; Yao, X.F.; Liu, C.M. The Leucine-Rich Repeat Receptor-like Kinase OsERL Plays a Critical Role in Anther Lobe Formation in Rice. *Biochem. Biophys. Res. Commun.* **2021**, *563*, 85–91. [[CrossRef](#)] [[PubMed](#)]
120. Nanda, A.K.; El Habti, A.; Hocart, C.H.; Masle, J. ERECTA Receptor-Kinases Play a Key Role in the Appropriate Timing of Seed Germination under Changing Salinity. *J. Exp. Bot.* **2019**, *70*, 6417–6435. [[CrossRef](#)] [[PubMed](#)]
121. Yu, Z.; Zhang, D.; Xu, Y.; Jin, S.; Zhang, L.; Zhang, S.; Yang, G.; Huang, J.; Yan, K.; Wu, C.; et al. CEPR2 Phosphorylates and Accelerates the Degradation of PYR/PYLs in *Arabidopsis*. *J. Exp. Bot.* **2019**, *70*, 5457–5469. [[CrossRef](#)]
122. Jung, C.G.; Hwang, S.G.; Park, Y.C.; Park, H.M.; Kim, D.S.; Park, D.H.; Jang, C.S. Molecular Characterization of the Cold- and Heat-Induced *Arabidopsis* PXL1 Gene and Its Potential Role in Transduction Pathways under Temperature Fluctuations. *J. Plant Physiol.* **2015**, *176*, 138–146. [[CrossRef](#)]
123. Pfister, A.; Barberon, M.; Alassimone, J.; Kalmbach, L.; Lee, Y.; Vermeer, J.E.M.; Yamazaki, M.; Li, G.; Maurel, C.; Takano, J.; et al. A Receptor-like Kinase Mutant with Absent Endodermal Diffusion Barrier Displays Selective Nutrient Homeostasis Defects. *elife* **2014**, *3*, e03115. [[CrossRef](#)]
124. Tunc-Ozdemir, M.; Jones, A.M. BRL3 and AtRGS1 Cooperate to Fine Tune Growth Inhibition and ROS Activation. *PLoS ONE* **2017**, *12*, e0177400. [[CrossRef](#)]
125. Fàbregas, N.; Lozano-Elena, F.; Blasco-Escámez, D.; Tohge, T.; Martínez-Andújar, C.; Albacete, A.; Osorio, S.; Bustamante, M.; Riechmann, J.L.; Nomura, T.; et al. Overexpression of the Vascular Brassinosteroid Receptor BRL3 Confers Drought Resistance without Penalizing Plant Growth. *Nat. Commun.* **2018**, *9*, 4680. [[CrossRef](#)]
126. Nakamura, A.; Fujioka, S.; Sunohara, H.; Kamiya, N.; Hong, Z.; Inukai, Y.; Miura, K.; Takatsuto, S.; Yoshida, S.; Ueguchi-Tanaka, M.; et al. The Role of OsBRI1 and Its Homologous Genes, OsBRL1 and OsBRL3, in Rice. *Plant Physiol.* **2006**, *140*, 580–590. [[CrossRef](#)]
127. Pitorre, D.; Llauro, C.; Jobet, E.; Guillemot, J.; Brizard, J.P.; Delseny, M.; Lasserre, E. RLK7, a Leucine-Rich Repeat Receptor-like Kinase, Is Required for Proper Germination Speed and Tolerance to Oxidative Stress in *Arabidopsis thaliana*. *Planta* **2010**, *232*, 1339–1353. [[CrossRef](#)]
128. Replogle, A.; Wang, J.; Paolillo, V.; Smeda, J.; Kinoshita, A.; Durbak, A.; Tax, F.E.; Wang, X.; Sawa, S.; Mitchum, M.G. Synergistic Interaction of Clavata1, Clavata2, and Receptor-like Protein Kinase 2 in Cyst Nematode Parasitism of *Arabidopsis*. *Mol. Plant-Microbe Interact.* **2013**, *26*, 87–96. [[CrossRef](#)]
129. Hu, C.; Zhu, Y.; Cui, Y.; Cheng, K.; Liang, W.; Wei, Z.; Zhu, M.; Yin, H.; Zeng, L.; Xiao, Y.; et al. A Group of Receptor Kinases Are Essential for CLAVATA Signalling to Maintain Stem Cell Homeostasis. *Nat. Plants* **2018**, *4*, 205–211. [[CrossRef](#)]
130. Xu, F.; Meng, T.; Li, P.; Yu, Y.; Cui, Y.; Wang, Y.; Gong, Q.; Wang, N.N. A Soybean Dual-Specificity Kinase, GmSARK, and Its *Arabidopsis* Homolog, ATsARK, Regulate Leaf Senescence through Synergistic Actions of Auxin and Ethylene. *Plant Physiol.* **2011**, *157*, 2131–2153. [[CrossRef](#)]

131. Li, P.; Yang, H.; Liu, G.; Ma, W.; Li, C.; Huo, H.; He, J.; Liu, L. PpSARK Regulates Moss Senescence and Salt Tolerance through ABA Related Pathway. *Int. J. Mol. Sci.* **2018**, *19*, 2609. [\[CrossRef\]](#)
132. da Silva, H.A.P.; Caetano, V.S.; Pessoa, D.D.V.; Pacheco, R.S.; Simoes-Araujo, J.L. Molecular and Biochemical Changes of Aging-Induced Nodules Senescence in Common Bean. *Symbiosis* **2019**, *79*, 33–48. [\[CrossRef\]](#)
133. Soltabayeva, A.; Ongaltay, A.; Omondi, J.O.; Srivastava, S. Morphological, Physiological and Molecular Markers for Salt-Stressed Plants. *Plants* **2021**, *10*, 243. [\[CrossRef\]](#)
134. Meng, X.; Zhou, J.; Tang, J.; Li, B.; de Oliveira, M.V.V.; Chai, J.; He, P.; Shan, L. Ligand-Induced Receptor-like Kinase Complex Regulates Floral Organ Abscission in Arabidopsis. *Cell Rep.* **2016**, *14*, 1330–1338. [\[CrossRef\]](#)
135. Li, Z.; Wang, Y.; Huang, J.; Ahsan, N.; Biener, G.; Paprocki, J.; Thelen, J.J.; Raicu, V.; Zhao, D. Two SERK Receptor-like Kinases Interact with EMS1 to Control Anther Cell Fate Determination. *Plant Physiol.* **2017**, *173*, 326–337. [\[CrossRef\]](#)
136. Lu, D.; Wu, S.; Gao, X.; Zhang, Y.; Shan, L.; He, P. A Receptor-like Cytoplasmic Kinase, BIK1, Associates with a Flagellin Receptor Complex to Initiate Plant Innate Immunity. *Proc. Natl. Acad. Sci. USA* **2010**, *107*, 496–501. [\[CrossRef\]](#)
137. Li, L.; Li, M.; Yu, L.; Zhou, Z.; Liang, X.; Liu, Z.; Cai, G.; Gao, L.; Zhang, X.; Wang, Y.; et al. The FLS2-Associated Kinase BIK1 Directly Phosphorylates the NADPH Oxidase RbohD to Control Plant Immunity. *Cell Host Microbe* **2014**, *15*, 329–338. [\[CrossRef\]](#) [\[PubMed\]](#)
138. Zhu, Y.; Wang, Y.; Li, R.; Song, X.; Wang, Q.; Huang, S.; Jin, J.B.; Liu, C.M.; Lin, J. Analysis of Interactions among the CLAVATA3 Receptors Reveals a Direct Interaction between CLAVATA2 and CORYNE in Arabidopsis. *Plant J.* **2010**, *61*, 223–233. [\[CrossRef\]](#) [\[PubMed\]](#)
139. Schulze, B.; Mentzel, T.; Jehle, A.K.; Mueller, K.; Beeler, S.; Boller, T.; Felix, G.; Chinchilla, D. Rapid Heteromerization and Phosphorylation of Ligand-Activated Plant Transmembrane Receptors and Their Associated Kinase BAK1. *J. Biol. Chem.* **2010**, *285*, 9444–9451. [\[CrossRef\]](#) [\[PubMed\]](#)
140. Amorim-Silva, V.; García-Moreno, A.; Castillo, A.G.; Lakhssassi, N.; Del Valle, A.E.; Pérez-Sancho, J.; Li, Y.; Posé, D.; Pérez-Rodríguez, J.; Lin, J.; et al. TTL Proteins Scaffold Brassinosteroid Signaling Components at the Plasma Membrane to Optimize Signal Transduction in Arabidopsis. *Plant Cell* **2019**, *31*, 1807–1828. [\[CrossRef\]](#) [\[PubMed\]](#)
141. Santiago, J.; Henzler, C.; Hothorn, M. Molecular Mechanism for Plant Steroid Receptor Activation by Somatic Embryogenesis Co-Receptor Kinases. *Science* **2013**, *341*, 889–892. [\[CrossRef\]](#)
142. Nicaise, V.; Joe, A.; Jeong, B.R.; Korneli, C.; Boutrot, F.; Westedt, I.; Staiger, D.; Alfano, J.R.; Zipfel, C. Pseudomonas HopU1 Modulates Plant Immune Receptor Levels by Blocking the Interaction of Their MRNAs with GRP7. *EMBO J.* **2013**, *32*, 701–712. [\[CrossRef\]](#)
143. Wang, J.; Li, H.; Han, Z.; Zhang, H.; Wang, T.; Lin, G.; Chang, J.; Yang, W.; Chai, J. Allosteric Receptor Activation by the Plant Peptide Hormone Phytosulfokine. *Nature* **2015**, *525*, 265–268. [\[CrossRef\]](#)
144. Kinoshita, A.; Betsuyaku, S.; Osakabe, Y.; Mizuno, S.; Nagawa, S.; Stahl, Y.; Simon, R.; Yamaguchi-Shinozaki, K.; Fukuda, H.; Sawa, S. RPK2 Is an Essential Receptor-like Kinase That Transmits the CLV3 Signal in Arabidopsis. *Development* **2010**, *137*, 3911–3920. [\[CrossRef\]](#)
145. Guo, Y.; Han, L.; Hymes, M.; Denver, R.; Clark, S.E. CLAVATA2 Forms a Distinct CLE-Binding Receptor Complex Regulating Arabidopsis Stem Cell Specification. *Plant J.* **2010**, *573*, 125–131. [\[CrossRef\]](#)
146. He, K.; Gou, X.; Yuan, T.; Lin, H.; Asami, T.; Yoshida, S.; Russell, S.D.; Li, J. BAK1 and BKK1 Regulate Brassinosteroid-Dependent Growth and Brassinosteroid-Independent Cell-Death Pathways. *Curr. Biol.* **2007**, *17*, 1109–1115. [\[CrossRef\]](#)
147. Meng, X.; Chen, X.; Mang, H.; Liu, C.; Yu, X.; Gao, X.; Torii, K.U.; He, P.; Shan, L. Differential Function of Arabidopsis SERK Family Receptor-like Kinases in Stomatal Patterning. *Curr. Biol.* **2015**, *25*, 2361–2372. [\[CrossRef\]](#)
148. Mou, S.; Zhang, X.; Han, Z.; Wang, J.; Gong, X.; Chai, J. CLE42 Binding Induces PXL2 Interaction with SERK2. *Protein Cell* **2017**, *8*, 612–617. [\[CrossRef\]](#)
149. Wang, X.; Kota, U.; He, K.; Blackburn, K.; Li, J.; Goshe, M.B.; Huber, S.C.; Clouse, S.D. Sequential Transphosphorylation of the BRI1/BAK1 Receptor Kinase Complex Impacts Early Events in Brassinosteroid Signaling. *Dev. Cell* **2008**, *15*, 220–235. [\[CrossRef\]](#)
150. Franco-Orozco, B.; Berepiki, A.; Ruiz, O.; Gamble, L.; Griffe, L.L.; Wang, S.; Birch, P.R.J.; Kanyuka, K.; Avrova, A. A New Proteinaceous Pathogen-Associated Molecular Pattern (PAMP) Identified in Ascomycete Fungi Induces Cell Death in Solanaceae. *New Phytol.* **2017**, *214*, 1657–1672. [\[CrossRef\]](#)
151. Crook, A.D.; Schnabel, E.L.; Frugoli, J.A. The Systemic Nodule Number Regulation Kinase SUNN in *Medicago truncatula* Interacts with MtCLV2 and MtCRN. *Plant J.* **2016**, *88*, 108–119. [\[CrossRef\]](#)
152. Smakowska-Luzan, E.; Mott, G.A.; Parys, K.; Stegmann, M.; Howton, T.C.; Layeghifard, M.; Neuhold, J.; Lehner, A.; Kong, J.; Grünwald, K.; et al. An Extracellular Network of Arabidopsis Leucine-Rich Repeat Receptor Kinases. *Nature* **2018**, *553*, 342–346. [\[CrossRef\]](#)
153. Mott, G.A.; Smakowska-Luzan, E.; Pasha, A.; Parys, K.; Howton, T.C.; Neuhold, J.; Lehner, A.; Grünwald, K.; Stolt-Bergner, P.; Provart, N.J.; et al. Data Descriptor: Map of Physical Interactions between Extracellular Domains of Arabidopsis Leucine-Rich Repeat Receptor Kinases. *Sci. Data* **2019**, *6*, 190025. [\[CrossRef\]](#)
154. Li, B.; Ferreira, M.A.; Huang, M.; Camargos, L.F.; Yu, X.; Teixeira, R.M.; Carpinetti, P.A.; Mendes, G.C.; Gouveia-Mageste, B.C.; Liu, C.; et al. The Receptor-like Kinase NIK1 Targets FLS2/BAK1 Immune Complex and Inversely Modulates Antiviral and Antibacterial Immunity. *Nat. Commun.* **2019**, *10*, 4996. [\[CrossRef\]](#)

155. Karlova, R.; Boeren, S.; Russinova, E.; Aker, J.; Vervoort, J.; De Vries, S. The Arabidopsis SOMATIC EMBRYOGENESIS RECEPTOR-LIKE KINASE1 Protein Complex Includes BRASSINOSTEROID-INSENSITIVE1. *Plant Cell* **2006**, *18*, 626–638. [[CrossRef](#)]
156. Sun, Y.; Li, L.; Macho, A.P.; Han, Z.; Hu, Z.; Zipfel, C.; Zhou, J.-M.; Chai, J. Structural Basis for Flg22-Induced Activation of the Arabidopsis FLS2-BAK1 Immune Complex. *Science* **2013**, *342*, 624–628. [[CrossRef](#)]
157. He, Y.; Zhou, J.; Shan, L.; Meng, X. Plant Cell Surface Receptor-Mediated Signaling-A Common Theme amid Diversity. *J. Cell Sci.* **2018**, *131*, jcs209353. [[CrossRef](#)]
158. Albrecht, C.; Russinova, E.; Hecht, V.; Baaijens, E.; de Vries, S. The Arabidopsis thaliana SOMATIC EMBRYOGENESIS RECEPTOR-LIKE KINASES1 and 2 Control Male Sporogenesis. *Plant Cell* **2005**, *17*, 3337–3349. [[CrossRef](#)] [[PubMed](#)]
159. Tang, J.; Han, Z.; Sun, Y.; Zhang, H.; Gong, X.; Chai, J. Structural Basis for Recognition of an Endogenous Peptide by the Plant Receptor Kinase PEPR1. *Cell Res.* **2015**, *25*, 110–120. [[CrossRef](#)]
160. Xiang, T.; Zong, N.; Zou, Y.; Wu, Y.; Zhang, J.; Xing, W.; Li, Y.; Tang, X.; Zhu, L.; Chai, J.; et al. Pseudomonas Syringae Effector AvrPto Blocks Innate Immunity by Targeting Receptor Kinases. *Curr. Biol.* **2008**, *18*, 74–80. [[CrossRef](#)]
161. Ranf, S.; Eschen-Lippold, L.; Pecher, P.; Lee, J.; Scheel, D. Interplay between Calcium Signalling and Early Signalling Elements during Defence Responses to Microbe- or Damage-Associated Molecular Patterns. *Plant J.* **2011**, *68*, 100–113. [[CrossRef](#)] [[PubMed](#)]
162. Kim, S.Y.; Warpeha, K.M.; Huber, S.C. The Brassinosteroid Receptor Kinase, BRI1, Plays a Role in Seed Germination and the Release of Dormancy by Cold Stratification. *J. Plant Physiol.* **2019**, *241*, 153031. [[CrossRef](#)] [[PubMed](#)]
163. Kemmerling, B.; Halter, T.; Mazzotta, S.; Mosher, S.; Nürnberger, T. A Genome-Wide Survey for Arabidopsis Leucine-Rich Repeat Receptor Kinases Implicated in Plant Immunity. *Front. Plant Sci.* **2011**, *2*, 88. [[CrossRef](#)] [[PubMed](#)]
164. Wang, X.; Jiang, N.; Liu, J.; Liu, W.; Wang, G.L. The Role of Effectors and Host Immunity in Plant–Necrotrophic Fungal Interactions. *Virulence* **2014**, *5*, 722–732. [[CrossRef](#)] [[PubMed](#)]
165. Loivamäki, M.; Stührwohldt, N.; Deeken, R.; Steffens, B.; Roitsch, T.; Hedrich, R.; Sauter, M. A Role for PSK Signaling in Wounding and Microbial Interactions in Arabidopsis. *Physiol. Plant.* **2010**, *139*, 348–357. [[CrossRef](#)]
166. Furukawa, K.; Hoshi, Y.; Maeda, T.; Nakajima, T.; Abe, K. Aspergillus Nidulans HOG Pathway Is Activated Only by Two-Component Signalling Pathway in Response to Osmotic Stress. *Mol. Microbiol.* **2005**, *56*, 1246–1261. [[CrossRef](#)]
167. Carvalho, C.M.; Santos, A.A.; Pires, S.R.; Rocha, C.S.; Saraiva, D.I.; Machado, J.P.B.; Mattos, E.C.; Fietto, L.G.; Fontes, E.P.B. Regulated Nuclear Trafficking of RpL10A Mediated by NIK1 Represents a Defense Strategy of Plant Cells against Virus. *PLoS Pathog.* **2008**, *4*, e1000247. [[CrossRef](#)]
168. Shang, Y.; Yang, D.; Ha, Y.; Shin, H.Y.; Nam, K.H. Receptor-like Protein Kinases RPK1 and BAK1 Sequentially Form Complexes with the Cytoplasmic Kinase OST1 to Regulate ABA-Induced Stomatal Closure. *J. Exp. Bot.* **2020**, *71*, 1491–1502. [[CrossRef](#)]
169. Osakabe, Y.; Mizuno, S.; Tanaka, H.; Maruyama, K.; Osakabe, K.; Todaka, D.; Fujita, Y.; Kobayashi, M.; Shinozaki, K.; Yamaguchi-Shinozaki, K. Overproduction of the Membrane-Bound Receptor-like Protein Kinase 1, RPK1, Enhances Abiotic Stress Tolerance in Arabidopsis. *J. Biol. Chem.* **2010**, *285*, 9190–9201. [[CrossRef](#)]
170. Schoonbeek, H.J.; Wang, H.H.; Stefanato, F.L.; Craze, M.; Bowden, S.; Wallington, E.; Zipfel, C.; Ridout, C.J. Arabidopsis EF-Tu Receptor Enhances Bacterial Disease Resistance in Transgenic Wheat. *New Phytol.* **2015**, *206*, 606–613. [[CrossRef](#)]
171. Shen, H.; Zhong, X.; Zhao, F.; Wang, Y.; Yan, B.; Li, Q.; Chen, G.; Mao, B.; Wang, J.; Li, Y.; et al. Overexpression of Receptor-like Kinase ERECTA Improves Thermotolerance in Rice and Tomato. *Nat. Biotechnol.* **2015**, *33*, 996–1003. [[CrossRef](#)] [[PubMed](#)]
172. Sakai, K.; Citerne, S.; Antelme, S.; Le Bris, P.; Daniel, S.; Boudier, A.; D’Orlando, A.; Cartwright, A.; Tellier, F.; Pateyron, S.; et al. BdERECTA Controls Vasculature Patterning and Phloem-Xylem Organization in Brachypodium Distachyon. *BMC Plant Biol.* **2021**, *21*, 196. [[CrossRef](#)] [[PubMed](#)]
173. Zhang, Y.; Li, S.; Xue, S.; Yang, S.; Huang, J.; Wang, L. Phylogenetic and CRISPR/Cas9 Studies in Deciphering the Evolutionary Trajectory and Phenotypic Impacts of Rice ERECTA Genes. *Front. Plant Sci.* **2018**, *9*, 473. [[CrossRef](#)] [[PubMed](#)]
174. De Gruijl, F.R.; Rebel, H. Early Events in UV Carcinogenesis-DNA Damage, Target Cells and Mutant P53 Foci. *Photochem. Photobiol.* **2008**, *84*, 382–387. [[CrossRef](#)] [[PubMed](#)]
175. Jaiswal, N.; Liao, C.J.; Mengesha, B.; Han, H.; Lee, S.; Sharon, A.; Zhou, Y.; Mengiste, T. Regulation of Plant Immunity and Growth by Tomato Receptor-like Cytoplasmic Kinase TRK1. *New Phytol.* **2022**, *233*, 458–478. [[CrossRef](#)]
176. Araya, T.; Miyamoto, M.; Wibowo, J.; Suzuki, A.; Kojima, S.; Tsuchiya, Y.N.; Sawa, S.; Fukuda, H.; Von Wirén, N.; Takahashi, H. CLE-CLAVATA1 Peptide-Receptor Signaling Module Regulates the Expansion of Plant Root Systems in a Nitrogen-Dependent Manner. *Proc. Natl. Acad. Sci. USA* **2014**, *111*, 2029–2034. [[CrossRef](#)]
177. Wang, L.; Xu, Y.Y.; Li, J.; Powell, R.A.; Xu, Z.H.; Chong, K. Transgenic Rice Plants Ectopically Expressing AtBAK1 Are Semi-Dwarfed and Hypersensitive to 24-Epibrassinolide. *J. Plant Physiol.* **2007**, *164*, 655–664. [[CrossRef](#)]
178. Hu, L.; Ye, M.; Kuai, P.; Ye, M.; Erb, M.; Lou, Y. OsLRR-RLK1, an Early Responsive Leucine-Rich Repeat Receptor-like Kinase, Initiates Rice Defense Responses against a Chewing Herbivore. *New Phytol.* **2018**, *219*, 1097–1111. [[CrossRef](#)]
179. Brotman, Y.; Landau, U.; Pnini, S.; Lisek, J.; Balazadeh, S.; Mueller-Roeber, B.; Zilberstein, A.; Willmitzer, L.; Chet, I.; Viterbo, A. The LysM Receptor-like Kinase LysM RLK1 Is Required to Activate Defense and Abiotic-Stress Responses Induced by Overexpression of Fungal Chitinases in Arabidopsis Plants. *Mol. Plant* **2012**, *5*, 1113–1124. [[CrossRef](#)]
180. Qu, X.; Cao, B.; Kang, J.; Wang, X.; Han, X.; Jiang, W.; Shi, X.; Zhang, L.; Cui, L.; Hu, Z.; et al. Fine-Tuning Stomatal Movement through Small Signaling Peptides. *Front. Plant Sci.* **2019**, *10*, 69. [[CrossRef](#)]
181. Ali, S.S.; Gunupuru, L.R.; Kumar, G.B.S.; Khan, M.; Scofield, S.; Nicholson, P.; Doohan, F.M. Plant Disease Resistance Is Augmented in Uzu Barley Lines Modified in the Brassinosteroid Receptor BRI1. *BMC Plant Biol.* **2014**, *14*, 227. [[CrossRef](#)] [[PubMed](#)]

## Article

# *Cuscuta australis* Parasitism-Induced Changes in the Proteome and Photosynthetic Parameters of *Arabidopsis thaliana*

Lyuben Zagorchev <sup>1,2</sup>, Zhaokui Du <sup>1</sup>, Yongbin Shi <sup>1</sup>, Denitsa Teofanova <sup>2</sup> and Junmin Li <sup>1,\*</sup>

<sup>1</sup> Zhejiang Provincial Key Laboratory of Plant Evolutionary Ecology and Conservation, Taizhou University, Taizhou 318000, China

<sup>2</sup> Department of Biochemistry, Faculty of Biology, Sofia University “St. Kliment Ohridski”, 8 Dragan Tsankov blvd., 1164 Sofia, Bulgaria

\* Correspondence: lijm@tzc.edu.cn; Tel.: +86-576-88660396

**Abstract:** *Cuscuta australis* is a widely distributed stem parasitic plant, infecting a variety of host plants. Its parasitism has a negative effect on the hosts, mainly due to the exhaustion of nutrients, thus negatively affecting the growth and development. However, recent studies indicated that the effect of parasitism may extend beyond the simple extraction of organic compounds, water, and minerals. In the present study, the model plant *Arabidopsis thaliana* was used as a host for *Cuscuta australis*, to study the effect of the parasite on the photosynthetic parameters and the proteome after short-term infection. To test this, a highly sensitive portable photosynthesis system and gel-based MS/MS proteomics were employed. It was found that the parasite has a dramatic negative effect on the photosynthetic ability of the host, as well as causing the up-regulation of stress-related proteins. Simultaneously, proteins involved in both decreased permeability and loosening of the cell wall of the host were found to be up-regulated.

**Keywords:** dodders; parasitic plants; proteomics; photosynthesis

**Citation:** Zagorchev, L.; Du, Z.; Shi, Y.; Teofanova, D.; Li, J.

*Cuscuta australis* Parasitism-Induced Changes in the Proteome and Photosynthetic Parameters of *Arabidopsis thaliana*. *Plants* **2022**, *11*, 2904. <https://doi.org/10.3390/plants11212904>

Academic Editors: Milan S. Stankovic, Paula Baptista and Petronia Carrillo

Received: 15 August 2022

Accepted: 26 October 2022

Published: 28 October 2022

**Publisher’s Note:** MDPI stays neutral with regard to jurisdictional claims in published maps and institutional affiliations.



**Copyright:** © 2022 by the authors. Licensee MDPI, Basel, Switzerland. This article is an open access article distributed under the terms and conditions of the Creative Commons Attribution (CC BY) license (<https://creativecommons.org/licenses/by/4.0/>).

## 1. Introduction

Dodders (*Cuscuta* spp. L., Convolvulaceae, Solanales) are prominent parasitic angiosperms infecting a wide range of predominantly eudicotyledonous host plants [1]. Dodders are stem parasites, e.g., infecting the aerial organs, either stems or leaves, of the hosts. They lack or have limited photosynthesis [2] and lose soil contact after the first successful infection. Instead of autotrophic carbon fixation, they acquire organic as well as mineral nutrients and water from their hosts by establishing a physiological xylem/phloem link, known as haustoria [3]. By doing this, they largely exhaust their host plants and exhibit a negative impact on their growth and development [4].

Most of the current research on dodders is focused on prevention and management strategies due to their potential to be agricultural pests. Several species, indeed, are considered a serious threat to contemporary agriculture and cause significant yield reduction in over 50 economically important crop plants [5]. Although generally regarded as harmful, more and more reports suggest the important role of dodders as biodiversity regulators and an important part of healthy plant societies. They are known to selectively forage on certain species under changing environmental conditions, thus benefiting the growth of other species [6]. Recently it was shown that native *Cuscuta* spp. might be key players in reducing the spreading of invasive species [7]. In China, both *C. australis* R. Br. and *C. chinensis* Lam. were proven as efficient regulators of invasions of several introduced weeds, most notably *Mikania micrantha* Kunth. [8,9].

Although dodders were extensively studied for their agricultural and ecological impact, knowledge of the host–parasite interactions is still fragmented. A typical dodder lifecycle includes germination, host localization, coiling (also twining), and haustoria formation through penetration to vascular elements of the host, formation of secondary

stem and infectious sites, ending with flowering, seed formation, and dispersal [1]. Host localization is believed to involve both light [10] and chemical [11] signal perception. Formation of haustoria was recently reviewed by Shimizu and Aoki [12] and divided into three distinct phases. First, a tight adhesion is achieved through the secretion of adhesive substances and elongation of *Cuscuta* stem cells toward the host tissue. There are reports, that both pectic substances [13] and arabinogalactan proteins (AGPs) are responsible for the adhesion [14]. The intrusive phase involves differentiation of various cell types, forming searching hyphae and penetrating the host tissue by pushing the host's cells aside [13]. Various cell wall hydrolyzing and modifying enzymes are also involved in this process in order to loosen host cells' walls and facilitate the process [15,16]. Finally, during the conductive phase, the searching hyphae differentiate into xylem and establish a xylem (and probably phloem) bridge with the host [12].

Further growth of the parasite results in continuous host exhaustion of both assimilated carbon and nitrogen, and thus, significant host growth restriction [4]. While Jeschke and Hilpert [17] reported increased photosynthetic activity in the host as a compensatory mechanism, more recent literature reported a decrease in photosynthetic parameters [18,19]. We also recently demonstrated that at least the light phase of photosynthesis may be inhibited even in *Cuscuta* association with poor hosts, where the growth of the parasite is not abundant [20]. This is an important question as it seems that, even at a slow growth rate, the parasite could inhibit the overall performance of the affected hosts.

Accumulation of new knowledge about the molecular mechanisms of dodder–host plants interaction is crucial from a fundamental point of view, but also important for the development of new strategies for control and eradication in agriculture. Such efforts are impeded by both the long seed longevity and continuous germination over the years [10], but most importantly by the difficulties during post-attachment control. By establishing a physiological link with the host plant, dodders are difficult to remove without harm to their hosts and there is a need for highly selective herbicides, affecting only the parasite and no other plants [21]. Elucidation of the host's response to dodder infection could also help the selection of resistant cultivars [22,23].

Recent reports demonstrated the dodder-specific response of at least some host species, accomplished by specific receptors and response proteins [24], as well as Jasmonic acid and Salicylic acid response pathways [25]. Research on these aspects of dodder–host interactions is still scarce, inconclusive, and further obstructed by the apparent interspecific and intraspecific variations. It was not until recently that dodder research was focused on the use of *Arabidopsis thaliana* (L.) Heynh. as a model host plant [26]. In the present study, we performed combined measurement of photosynthetic parameters with gel-based proteomics study on the effect of *C. australis* parasitism on *A. thaliana*. The aim was to assess both the photosynthetic performance, which was proposed to be significantly affected by parasitism, and differentially abundant proteins in the host, separately, in the affected stem and the relatively distant leaves.

## 2. Results

### 2.1. Effect of Parasitism on Photosynthetic Parameters

Attachment and haustoria formation were macroscopically visible at the 24th hour in most cases (Figure 1a) and were further confirmed microscopically (Figure 1b). Despite the fact that there were slight differences in terms of time to attachment, further analyses were performed on infected *Arabidopsis* plants with the most uniform pattern of infection. *Cuscuta australis* parasitism decreased most of the photosynthetic parameters in the host, *A. thaliana*, within 72 h of infection (Table 1). A notable drop in relative chlorophyll content—almost two-fold from 17.5 to 8.8—as well as a significant decrease in photosynthetic rate ( $P_n$ ), stomatal conductance ( $g_s$ ), and transpiration rate ( $T_s$ ) was observed. The change in intercellular  $CO_2$  ( $C_i$ ) was not significant but followed the pattern of decrease.

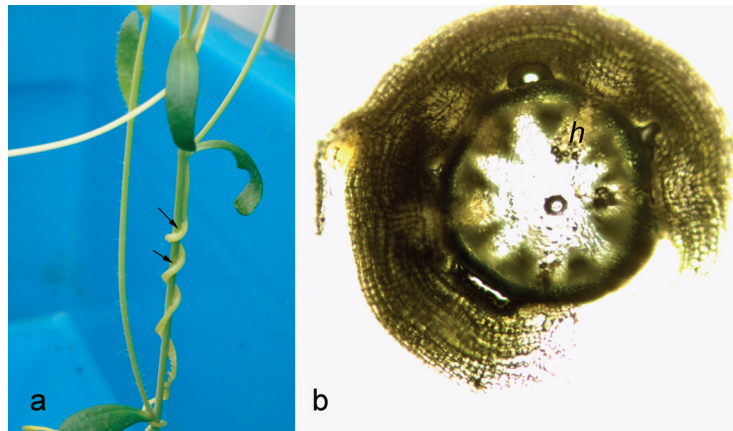


**Figure 1.** Point of infection of *Arabidopsis thaliana* by *Cuscuta australis* (a) with arrows, showing the site of haustoria formation after 24 h and microscopic cross-section of haustoria (h) after 72 h (b).

**Table 1.** Effect of parasitism on the chlorophyll content and photosynthetic characteristics of the host. Data were shown as mean  $\pm$  standard errors ( $n = 6$ ). Different small letters indicate significant (Student's *t*-test) differences between parasitized and non-parasitized treatments.

Traits	Non-Parasitized	Parasitized
Photosynthetic rate ( $P_n$ )/( $\mu\text{mol CO}_2 \text{ m}^{-2} \text{ s}^{-1}$ )	3.61 $\pm$ 0.73 <sup>a</sup>	2.71 $\pm$ 0.33 <sup>b</sup>
Stomatal conductance ( $g_s$ )/( $\mu\text{mol H}_2\text{O m}^{-2} \text{ s}^{-1}$ )	0.19 $\pm$ 0.05 <sup>a</sup>	0.12 $\pm$ 0.01 <sup>b</sup>
Concentration of intercellular CO <sub>2</sub> ( $C_i$ )/( $\mu\text{mol CO}_2 \text{ m}^{-2} \text{ s}^{-1}$ )	305.66 $\pm$ 1.34 <sup>a</sup>	301.58 $\pm$ 6.23 <sup>a</sup>
Transpiration rate ( $T_r$ )/( $\mu\text{mol CO}_2 \text{ m}^{-2} \text{ s}^{-1}$ )	3.30 $\pm$ 0.74 <sup>a</sup>	2.31 $\pm$ 0.097 <sup>b</sup>
Relative chlorophyll content	17.51 $\pm$ 2.06 <sup>a</sup>	8.79 $\pm$ 1.96 <sup>b</sup>

## 2.2. Quantitative Analysis of Protein Spots on 2D Gels

Differential protein abundance was assessed by two-dimensional polyacrylamide gel electrophoresis, separately in stem and leaves of the host plants. Images were analyzed using PDQuest 8.0 (Bio-Rad, Hercules, CA, USA) Software by deriving a master gel image (Figure 2a,b). Original images are provided as (Supplementary Figures S1–S4). Only protein spots with 2.5-fold difference between non-parasitized and parasitized samples, statistically significant at  $p < 0.05$ , Student's *t*-test (Figure 2c,d) were considered for further analysis. A total of 21 protein spots in leaves and 24 protein spots in the stem met the above criteria (Figure 3). Of them, the proportion of up-regulated to down-regulated protein spots were almost equal in leaves (Figure 3a), while in the stem (Figure 3b) the number of up-regulated protein spots was substantially higher than down-regulated (only four). The fold difference in leaves was also higher, reaching 40-fold down-regulation for SSP 0007 and above 20-fold for SSP 1213 and 1103 (Figures 2c and 3a). The fold difference in stem was much lower for all of the protein spots (Figure 3b). All protein spots are indicated by their SSP number, automatically assigned by PDQuest 8.0 Software.

## 2.3. Protein MS/MS Identification

A total of five protein spots in the leaves and two protein spots in the stem failed to be identified (Figure 3)—protein score, lower than the identity or extensive homology score at  $p < 0.05$ . The additional broad database search (Viridiplantae) aimed to find any possible proteins of *Cuscuta* origin, as such are known to be transferred into hosts [27]. However, no such were found. Out of the identified protein spots (Tables 2 and 3), one protein was found in a total of four down-regulated spots in leaves glyceraldehyde-3-phosphate dehydrogenase (SSP 1210, 1212, 1213, and 1303). One protein was found in two

up-regulated spots in stem Atmp 24.1 glutathione S transferase (SSP 2201 and 3001), but also two isoforms of aspartate aminotransferase were found in two up-regulated spots (SSP 0315 and 1403). Chloroplastic transketolase 1 was found in up-regulated spots in both leaves and stem (SSP 2601 and 1715, respectively) and chloroplastic phosphoribulokinase was found in down-regulated spots in both leaves and stem (SSP 0508 and 8008, respectively). Finally, a member of the glycine cleavage T-protein family was found in a down-regulated spot in leaves (SSP 0105) and up-regulated spot in the stem (SSP 0407).

According to the annotation to gene ontology (GO) biological process, proteins, associated with a variety of stress, including biotic (response to bacterial pathogens) and abiotic (salinity, cold, heavy metals) were equally distributed between both up-regulated and down-regulated protein spots (Tables 2 and 3). Except for down-regulated protein spots in the stem, the stress-related proteins were not the predominant fraction in either of the identified proteins. A substantial amount, however, is associated with either photosynthesis or carbohydrate metabolism.

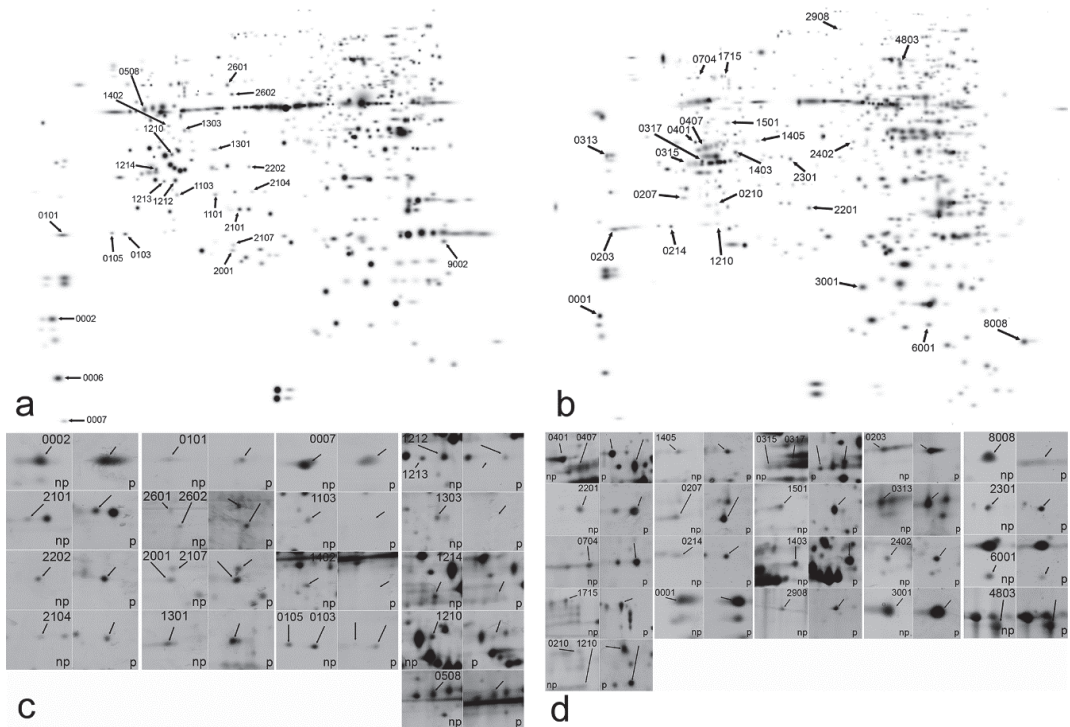


**Figure 2.** PDQuest master gel images of 2D-electrophoregrams of Arabidopsis leaves (a) and stem (b) and the respective differentially regulated protein spots (c,d). Arabidopsis was either parasitized (p) or non-parasitized (np) by *Cuscuta australis*. Protein spot numbers correspond to the assigned by PDQuest.

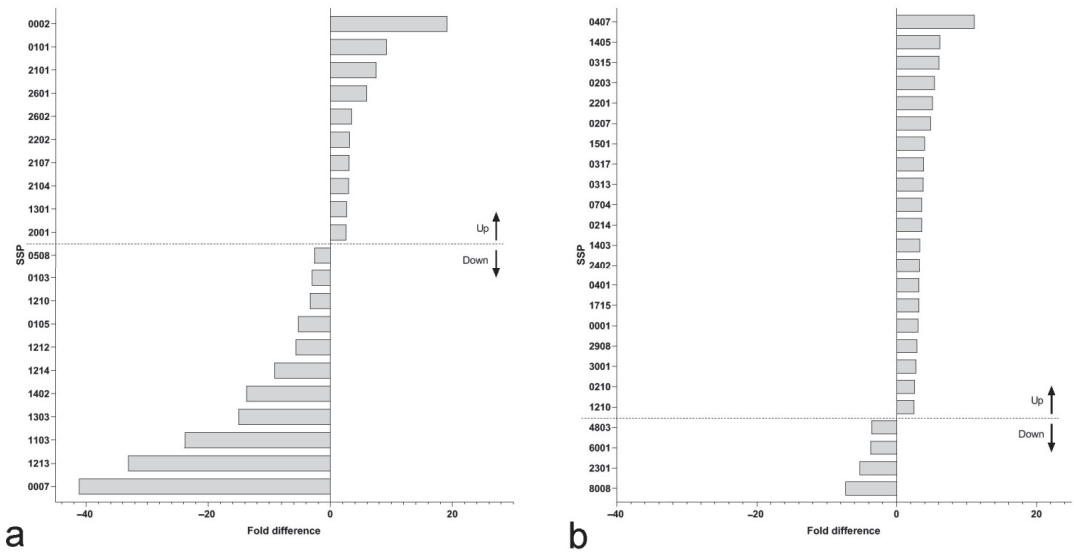


**Figure 3.** Differentially regulated protein spots, shown as SSP numbers, assigned by PDQuest with 2.5-fold difference in leaves (a) and stem (b) of *Cuscuta australis*—parasitized *Arabidopsis thaliana*.

**Table 2.** MS/MS identified protein spots, up-regulated in leaves and stem of *Cuscuta australis*—parasitized *Arabidopsis thaliana*. SSP is the standard spot number.

SSP	Mascot Score	UniProt Accession	Protein Identity	GO Localization	GO Biological Process
<b>Leaves</b>					
0002	98	Q41932	Oxygen-evolving enhancer protein 3-2, chloroplastic	chloroplast thylakoid membrane	photosynthetic electron transport chain
0101	69	Q9LUT2	S-adenosylmethionine synthase 4	cytoplasm	lignin biosynthetic process response to cold stress
2101	54	Q9SAJ4	Phosphoglycerate kinase 3, cytosolic	Cytoplasm	gluconeogenesis
2601	175	Q8RWW0	Transketolase-1, chloroplastic	Chloroplast	Pentose-phosphate shunt Response to cadmium ions/salt stress
2602	53	P10795	Ribulose bisphosphate carboxylase small chain 1A, chloroplastic	Chloroplast	chloroplast ribulose bisphosphate carboxylase complex assembly response to cold
2107	130	O49344	Putative oxygen-evolving enhancer protein 2-2	Chloroplast	photosynthesis
1301	212	Q42560	Aconitate hydratase 1	Mitochondrion Cytoplasm	citrate metabolic process response to salt stress
<b>Stem</b>					
0407	269	O65396	Glycine cleavage T-protein family	Mitochondrion	glycine decarboxylation via glycine cleavage system response to cadmium ion
1405	229	B9DHX4	Malate dehydrogenase		carbohydrate metabolic process
0315	194	Q56YR4	aspartate aminotransferase	Multiple	Biosynthetic process

Table 2. Cont.

SSP	Mascot Score	UniProt Accession	Protein Identity	GO Localization	GO Biological Process
0203	229	A0A178UUR9	VDAC2	Mitochondrial outer membrane	voltage-gated anion channel
2201	169	Q8LC43	Atpm24.1 glutathione S transferase	Cytosol/ER	response to bacteria response to abiotic stress
1501	49	A0A178VU56	Succinate-CoA ligase [ADP-forming] subunit beta	Mitochondrion	tricarboxylic acid cycle
0317	352	Q9FWA3	6-phosphogluconate dehydrogenase family protein	Cytosol/Peroxisome	D-gluconate metabolic process response to salt stress
0313	49	A0A178VDL9	Pectin methyl esterase 3	Cell Wall	Cell wall modification
0704	550	O50008	methionine synthase	Cytoplasm	response to cadmium ion response to salt stress
1403	551	P46645	aspartate aminotransferase 2	Cytoplasm	2-oxoglutarate metabolic process
2402	191	Q944G9	Fructose-bisphosphate aldolase 2	Chloroplast stroma	gluconeogenesis response to abscisic acid/ response to cadmium ion
0401	170	Q96533	glutathione-dependent formaldehyde dehydrogenase	Cytoplasm	ethanol oxidation
1715	197	Q8RWW0	Transketolase-1	chloroplast stroma	pentose-phosphate shunt response to cadmium ion/ response to salt stress
0001	111	A0A178VBH5	PSBO2	Chloroplast thylakoid	photosystem II assembly
2908	334	Q93ZF2	putative 2,3-bisphosphoglycerate-independent phosphoglycerate mutase	Cytoplasm	glucose catabolic process
3001	168	Q8LC43	Atpm24.1 glutathione S transferase	Cytosol/ER	response to bacteria response to abiotic stress
0210	76	O24616	Proteasome subunit alpha type-7-B	Nucleus/Cytoplasm	proteasomal protein catabolic process
1210	127	Q42029	photosystem II subunit P-1	chloroplast thylakoid	Photosynthesis defense response to bacterium

Table 3. MS/MS identified protein spots, down-regulated in leaves and stem of *Cuscuta australis*—parasitized *Arabidopsis thaliana*. SSP is the standard spot number.

SSP	Mascot Score	UniProt Accession	Protein Identity	GO Localization	GO Biological Process
<b>Leaves</b>					
1213	259	A0A178VKK2	Glyceraldehyde-3-phosphate dehydrogenase		glucose metabolic process
1103	138	A0A0K1CVP8	Ribulose biphosphate carboxylase large chain	Chloroplast	Photorespiration
1303	232	A0A178VKK2	Glyceraldehyde 3-phosphate dehydrogenase A subunit		glucose metabolic process
1402	138	P22954	dnaK-type molecular chaperone hsc70.1—like, partial	Nucleus Cytoplasm	cellular response to heat response to multiple stresses
1212	213	A0A178VKK2	Glyceraldehyde-3-phosphate dehydrogenase		glucose metabolic process

Table 3. Cont.

SSP	Mascot Score	UniProt Accession	Protein Identity	GO Localization	GO Biological Process
0105	200	O65396	Glycine cleavage T-protein family	Mitochondrion	glycine decarboxylation via glycine cleavage system response to cadmium ion
1210	137	P25856	Glyceraldehyde 3-phosphate dehydrogenase A subunit	Chloroplast	glucose metabolic process response to cold
0103	82	F4KDZ4	Peroxisomal NAD-malate dehydrogenase 2	Peroxisome	carbohydrate metabolic process
0508	99	P25697	Phosphoribulokinase, chloroplastic	Chloroplast	defense response to bacterium response to cold
<b>Stem</b>					
8008	40	P25697	Phosphoribulokinase, chloroplastic	Chloroplast	Defense response to bacteria Response to cold
2301	115	P06525	Alcohol dehydrogenase class-P	Cytoplasm	Response to multiple abiotic stresses
6001	47	P31265	translationally controlled tumor protein-like protein	Cytosol	Auxin homeostasis Response to multiple stresses
4803	481	O23654	vacuolar ATP synthase subunit A	Vacuole	ATP hydrolysis coupled proton transport Response to salt stress

### 3. Discussion

The pronounced effect of *C. australis* parasitism on the host's photosynthetic parameters is consistent with previously reported results for the *C. campestris*—*M. micrantha* association [18], who reported a significant decrease in  $P_n$  after 18 days of infection and *C. australis*—*Bidens pilosa* [28,29]. Chen [30] suggested the involvement of abscisic acid (ABA) in the suppression of stomatal conductance and transpiration rate, hence the net photosynthetic rate. Despite differences in the host response in terms of time needed for the adverse effect of *Cuscuta* infection on photosynthesis to occur, which might be host-specific and dependent on the parasite size, an overall decrease in photosynthetic parameters seems like a common response. Considering the light reactions, we also recently demonstrated a certain negative effect of *C. campestris* parasitism on the semi-compatible host *Ipomoea tricolor* [20], suggesting a dramatic effect on the host plant even when the parasite is not developing successfully. Overall, it seems that suppression of photosynthesis in the early stages of *Cuscuta* parasitism is a global stress response, similar or sharing common signal mechanisms to other abiotic, mainly drought [31] and biotic [32] stresses.

The decrease in CO<sub>2</sub> assimilation could be further explained by the down-regulation of at least the large RuBisCO subunit (Table 3), but also the down-regulation of the chloroplastic Glyceraldehyde-3-phosphate dehydrogenase and Phosphoribulokinase (Table 3), both of which are involved in the regeneration of ribulose-1,5-bisphosphate. Accordingly, down-regulation leads to a reduction in CO<sub>2</sub> assimilation, otherwise designated as “Calvin-Benson Cycle slow down” [33,34]. In all cases, such down-regulation of CO<sub>2</sub> assimilation would largely contribute to the growth inhibition of parasitized hosts, reported previously [18,35] in addition to the reduction in organic nutrients [4]. Furthermore, many of the differentially regulated proteins in the present study are related to the modulation of the carbohydrate or amino acid metabolism and according to GO biological processes are related to the response to different kind of stresses. In contrast, we also found up-regulation of the small RuBisCO subunit, several thylakoid complex proteins—Oxygen-evolving enhancer proteins (PSBO2), and photosystem II subunit P-1 (Table 2). The small RuBisCO subunit is encoded in nuclear DNA and synthesized in the cytoplasm, then it is transferred into the chloroplast [36]. The up-regulation of the small RuBisCO subunit indicated that the compensatory reaction of the nuclear gene to decreased accumulation of photosynthates would be quicker than genes encoded in chloroplast DNA, such as the large RuBisCO subunit gene. PsbO proteins in

Arabidopsis are encoded by two genes, *psbO1* and *psbO2* [37]. A low level of PSBO2 would limit the photosynthetic activity [37] and the function of PSBO2 showed under high light stress. In this study, Arabidopsis plants were grown under natural sunlight conditions in the greenhouse for successful infection of *Cuscuta*. The up-regulation of PSBO2 might be due to the high light stress response.

Overall, the host's response to *Cuscuta* infection is believed to trigger Jasmonic acid and Salicylic acid defense pathways [25] and up-regulation of numerous pathogen-response related genes and proteins was previously reported. Borsics and Lados [38] reported up-regulation of *PPRG2* in dodder-infected alfalfa, encoding a homologous to pathogenesis-related (PR-10) protein family product. In *Mikania micrantha*, infected by *C. campestris*, up-regulation of a homologous to chitinase gene, *Mmchi1*, was reported [39]. In our study glutathione S-Transferase Atpm24.1, commonly involved in response to pathogenic fungi, bacteria, and viruses, mainly governing the antioxidant response [40] was found to be up-regulated in the stem of infected plants. More interestingly, it was found that S-adenosylmethionine synthase 4 was up-regulated in leaves and Pectin methyl esterase 3 in the stem. The former is involved in the synthesis of S-adenosylmethionine, an important methyl donor for methylation of lignin precursors for lignin synthesis [41]. As such, it is expected to be involved in the lignification and reinforcement of the cell wall, a common defense mechanism and systemic response against different pathogens [42]. Lignin-based resistance to *C. campestris* in the tomato plant was established in a particular cultivar, governed by up-regulation of numerous related genes [22]. The up-regulation of Pectin methyl esterase, especially in the stem of the host plants, where infection with the dodder mainly occur is probably involved in the de-esterification of pectic polysaccharides, which in turn facilitates pectin hydrolyses and penetration of the parasite [43]. It is yet to be concluded whether this is a mechanism by which the parasite manipulates the metabolism of the host to increase susceptibility, but it was reported that pectinolytic enzymes are essential in host tissue penetration during haustoria formation [43].

The possibility that some of the up-regulated proteins in the parasitized group are of *Cuscuta* origin was taken into consideration because of several studies reporting extensive protein exchange between the parasite and the host [27,44], including translation of transferred mRNAs in the host [45]. Liu et al. [27] reported more than 1000 dodder proteins, translocated to the infected *Arabidopsis* stems. Interestingly, most of the up-regulated and none of the down-regulated proteins in our study were also found to be dodder-to-*Arabidopsis* mobile proteins [27].

## 4. Materials and Methods

### 4.1. Plant Material and Growing Conditions

Seeds of *Arabidopsis thaliana* ecotype Columbia-0 (Col-0) were kindly provided by Dr Zhongnan Yang (Shanghai Normal University, Shanghai, China). Arabidopsis seeds were surface sterilized using 70% (*v/v*) ethanol for 10 min, then washed three times with sterile water and stratified for 48 h at 4 °C in the dark. The treated seeds were sown evenly in vermiculite: peat substrate: perlite (16:3:1) mixture and germinated in a growth chamber under 16 h light/8 h dark photoperiod, 150  $\mu\text{mol m}^{-2} \text{s}^{-1}$  white light intensity, 22 °C, 70% relative humidity. Two-week-old healthy seedlings were transferred to a plastic tray (one seedling per tray), containing a controlled-release fertilizer (Osmocote<sup>®</sup>, Scotts International B.V., Harderwijk, The Netherlands), and grown under the same conditions. Twenty plants were chosen when the height reached approximately 5 cm in a growth chamber, then separated into the control group and parasitized group (each group had 10 plants) and grown for further 5 days.

Fifteen cm long stems of *C. australis* were collected from a field population at Taizhou University, Linhai City, Zhejiang Province, China. The parasite's stem was coiled around the inflorescence stem (the upper one-third, approximately 5 cm from the rosette leaves) of *A. thaliana* (one parasite per host) in a counter-clockwise direction and plants were grown under natural sunlight conditions in the greenhouse for infection—usually, haustoria are

formed after 24 h. After 72 h, a total of six plants from the parasitized group with the most uniform *Cuscuta* infection and six plants from the control group, respectively, were chosen for photosynthetic measurements and protein analyses.

#### 4.2. Photosynthesis Measurements

Relative chlorophyll content was measured using CCM-200 chlorophyll content meter (OPTI-SCIENCES, Hudson, NH, USA) on fully expanded 5th rosette leaves of *Arabidopsis*, one leaf per plant. Photosynthetic rate ( $P_n$ ), stomatal conductance ( $g_s$ ), the concentration of intercellular  $\text{CO}_2$  ( $C_i$ ), and transpiration rate ( $T_s$ ) were measured using a portable photosynthesis system Li-6400 (LI-COR, Lincoln, NE, USA) according to the manufacturer's instructions on fully expanded rosette leaves. Gas exchange measurements were determined under 25 °C, 1200  $\mu\text{mol m}^{-2} \text{s}^{-1}$  photons, 400  $\mu\text{mol mol}^{-1}$   $\text{CO}_2$  concentration and 70% relative humidity.

#### 4.3. Protein Extraction and Quantification

For proteomics analyses, *Arabidopsis* inflorescence stem (2 cm up and down the site of dodder parasitism) and leaves (5th rosette, two leaves per plant) were studied separately after 72 h of infection. Total protein was extracted from the control and parasitized tissues of *Arabidopsis* as previously described [46]. Two grams of fresh plant material were powder-grounded in liquid nitrogen, dissolved in 20 mL cold acetone, containing 10% (*w/v*) trichloroacetic acid (TCA), and proteins were precipitated for 1 h at −20 °C. The samples were centrifuged at 15,000 *g* for 15 min at 4 °C. The procedure was repeated with TCA-free cold acetone, then the pellets were dried by vacuum freeze dryer and dissolved in protein lysis buffer, containing 9 M Urea, 4% (*w/v*) CHAPS, 1% (*w/v*) DTT, 1% (*v/v*) IPG buffer (pH 4–7, GE Healthcare, Danderyd, Sweden) and vortexed at 30 °C for 1 h. The protein concentrations were determined by Bradford's method [47]. If not immediately used for isoelectric focusing separation, proteins were stored at −80 °C.

#### 4.4. Two-Dimensional Gel Electrophoresis

Equal amounts of protein (100  $\mu\text{g}$ ) were separated on Immobiline Dry Strip Gels (pH = 4–7, 24 cm, GE Healthcare, Danderyd, Sweden). Isoelectric focusing (IEF) was performed according to the producer's recommendations at 20 °C as follows: 250 V for 1 h, 1000 V for 2 h, on a linear gradient from 1000 V to 10,000 V for 1 h, 10,000 V for 1 h. The strips were then incubated under constant gentle shaking in equilibration buffer I (6M urea, 30% *v/v* glycerol, 2% *w/v* SDS, 50 mM Tris-HCl pH 8.8, 1% *w/v* DTT) and buffer II, in which DTT was replaced with 2.5% *w/v* Iodoacetamide, for 15 min each. Twelve percent T SDS polyacrylamide gels were used for the second-dimension electrophoresis and the gels were stained with Coomassie Brilliant Blue (CBB) G-250 according to the procedure described by Neuhoff [48].

#### 4.5. Image Analysis and Mass Spectrometric Identification

The stained gels (in triplicates, each representing an individual plant) were scanned on Image Scanner (GE Healthcare, Waukesha, WI, USA) at a resolution of 300 dots per inch and the images were analyzed using PDQuest 2-D analysis software 8.0 (Bio-Rad, Hercules, CA, USA), following the steps of spot detection, volumetric quantification and matching. Protein spots, identified to show 2.5-fold higher or lower difference ( $n = 3$ ,  $p < 0.05$ , Student's *t*-test) in intensity between control and parasitized *Arabidopsis* plants were selected as the differentially abundant proteins, designated up-regulated and down-regulated, respectively, and extracted for MS analysis. Selected protein spots were excised from 2-DE gels, de-stained, dehydrated, and digested with trypsin according to the procedure of Shevchenko [49]. Peptide MS and MS/MS were performed on an ABI 5800 MALDI-TOF-TOF plus mass spectrometer (Applied Biosystems, Foster City, CA, USA).

Both the MS and MS/MS data were integrated and processed using the GPS Explorer V3.6 software (Applied Biosystems, Foster City, CA, USA) with default parameters.

Based on combined MS and MS/MS spectra, the protein identification was performed using the MASCOT V2.1 search engine (Matrix Science, London, UK), with the following search parameters: NCBIprot (also performed against SwissProt database) thale cress (*Arabidopsis thaliana*) database (repeated against green plants, Viridiplantae), trypsin as the digestion enzyme, one missed cleavage site; variable modifications: Oxidation (M), Acetyl (Protein N-term), Deamidated (N and Q) and Dioxidation (W); fixed modifications: Carbamidomethyl (C), and a mass deviation of less than 100 ppm. Statistically significant search scores (>95% confidence, equivalent to MASCOT expect value  $p < 0.05$ ) were chosen [50]. All confirmed proteins—MASCOT  $p < 0.05$  were searched in UniProt database and GO annotated for localization and biological process.

## 5. Conclusions

In conclusion, it was shown that *Cuscuta australis* parasitism negatively affected most of the photosynthetic parameters of the host plants. The differential abundance of proteins, however, could not entirely explain such effect. Nevertheless, multiple proteins related to the carbohydrate metabolism were differentially regulated, as well as proteins with known function in abiotic and biotic stress response and defense mechanisms. Notably, S-adenosylmethionine synthase 4 and Pectin methyl esterase 3, involved in cell wall modifications and the parasite–host interaction, are up-regulated in stem and leaves, respectively. Accumulation of data on proteins involved in plant-to-plant interaction could further elucidate the mechanisms of haustoria formation in *Cuscuta* spp. and allow us to identify individual players in the hosts' defense with a putative role in at least partial resistance to infection.

**Supplementary Materials:** The following supporting information can be downloaded at: <https://www.mdpi.com/article/10.3390/plants11212904/s1>, Figure S1: Representative 2D gel of proteins from leaves of control *Arabidopsis thaliana* plant; Figure S2: Representative 2D gel of proteins from leaves of *Cuscuta australis*-parasitized *Arabidopsis thaliana* plant; Figure S3: Representative 2D gel of proteins from stem of control *Arabidopsis thaliana* plant; Figure S4: Representative 2D gel of proteins from stem of *Cuscuta australis*-parasitized *Arabidopsis thaliana* plant.

**Author Contributions:** J.L. designed the experiment. J.L., Z.D. and Y.S. performed the experiments. L.Z. and D.T. analyzed the data. L.Z. and J.L. wrote the manuscript. All authors have read and agreed to the published version of the manuscript.

**Funding:** This work was financially supported by the Talented Young Scientist Program of the Ministry of Science and Technology of People's Republic of China (given to Lyuben Zagorchev), the Ten Thousand Talent Program of Zhejiang Province (given to Junmin Li), and the National Natural Science Foundation of China (No. 30800133) (given to Junmin Li) and grant KP-06-H31/10 of the National Science Fund of Ministry of Education and Science, Bulgaria.

**Institutional Review Board Statement:** Not applicable.

**Informed Consent Statement:** Not applicable.

**Data Availability Statement:** The data presented in this study are available on request from the corresponding author.

**Acknowledgments:** We thank Zhongnan Yang from Shanghai Normal University, China, for his kind grant of seeds of *Arabidopsis thaliana* ecotype Columbia-0 (Col-0).

**Conflicts of Interest:** The authors declare no conflict of interest.

## References

1. Kaiser, B.; Vogg, G.; Fürst, U.B.; Albert, M. Parasitic plants of the genus *Cuscuta* and their interaction with susceptible and resistant host plants. *Front. Plant Sci.* **2015**, *6*, 45. [[CrossRef](#)] [[PubMed](#)]
2. Reville, M.J.; Stanley, S.; Hibberd, J.M. Plastid genome structure and loss of photosynthetic ability in the parasitic genus *Cuscuta*. *J. Exp. Bot.* **2005**, *56*, 2477–2486. [[CrossRef](#)] [[PubMed](#)]
3. Birschwilks, M.; Haupt, S.; Hofius, D.; Neumann, S. Transfer of phloem-mobile substances from the host plants to the holoparasite *Cuscuta* sp. *J. Exp. Bot.* **2006**, *57*, 911–921. [[CrossRef](#)] [[PubMed](#)]
4. Hibberd, J.M.; Dieter Jeschke, W. Solute flux into parasitic plants. *J. Exp. Bot.* **2001**, *52*, 2043–2049. [[CrossRef](#)]

5. Parker, C. Parasitic weeds: A world challenge. *Weed Sci.* **2012**, *60*, 269–276. [[CrossRef](#)]
6. Koch, A.M.; Binder, C.; Sanders, I.R. Does the generalist parasitic plant *Cuscuta campestris* selectively forage in heterogeneous plant communities? *New Phytol.* **2004**, *162*, 147–155. [[CrossRef](#)]
7. Yu, H.; Liu, J.; He, W.-M.; Miao, S.-L.; Dong, M. *Cuscuta australis* restrains three exotic invasive plants and benefits native species. *Biol. Invasions* **2011**, *13*, 747–756.
8. Yu, H.; He, W.-M.; Liu, J.; Miao, S.-L.; Dong, M. Native *Cuscuta campestris* restrains exotic *Mikania micrantha* and enhances soil resources beneficial to natives in the invaded communities. *Biol. Invasions* **2009**, *11*, 835. [[CrossRef](#)]
9. Yu, H.; Liu, J.; He, W.-M.; Miao, S.-L.; Dong, M. Restraints on *Mikania micrantha* by *Cuscuta campestris* facilitates restoration of the disturbed ecosystems. *Biodiversity* **2009**, *10*, 72–78. [[CrossRef](#)]
10. Benvenuti, S.; Dinelli, G.; Bonetti, A.; Catizone, P. Germination ecology, emergence and host detection in *Cuscuta campestris*. *Weed Res.* **2005**, *45*, 270–278. [[CrossRef](#)]
11. Runyon, J.B.; Mescher, M.C.; De Moraes, C.M. Volatile chemical cues guide host location and host selection by parasitic plants. *Science* **2006**, *313*, 1964–1967. [[CrossRef](#)] [[PubMed](#)]
12. Shimizu, K.; Aoki, K. Development of parasitic organs of a stem holoparasitic plant in genus *Cuscuta*. *Front. Plant Sci.* **2019**, *10*, 1435. [[PubMed](#)]
13. Vaughn, K. Attachment of the parasitic weed dodder to the host. *Protoplasma* **2002**, *219*, 227–237. [[CrossRef](#)] [[PubMed](#)]
14. Striberny, B.; Krause, K. Cell wall glycoproteins at interaction sites between parasitic giant dodder (*Cuscuta reflexa*) and its host *Pelargonium zonale*. *Plant Signal. Behav.* **2015**, *10*, e1086858. [[CrossRef](#)] [[PubMed](#)]
15. Bleischwitz, M.; Albert, M.; Fuchsbaumer, H.-L.; Kaldenhoff, R. Significance of Cuscutain, a cysteine protease from *Cuscuta reflexa*, in host-parasite interactions. *BMC Plant Biol.* **2010**, *10*, 227. [[CrossRef](#)]
16. Olsen, S.; Striberny, B.; Hollmann, J.; Schwacke, R.; Popper, Z.; Krause, K. Getting ready for host invasion: Elevated expression and action of xyloglucan endotransglucosylases/hydrolases in developing haustoria of the holoparasitic angiosperm *Cuscuta*. *J. Exp. Bot.* **2016**, *67*, 695–708. [[CrossRef](#)]
17. Jeschke, W.; Hilpert, A. Sink-stimulated photosynthesis and sink-dependent increase in nitrate uptake: Nitrogen and carbon relations of the parasitic association *Cuscuta reflexa*–*Ricinus communis*. *Plant Cell Environ.* **1997**, *20*, 47–56. [[CrossRef](#)]
18. Shen, H.; Hong, L.; Ye, W.; Cao, H.; Wang, Z. The influence of the holoparasitic plant *Cuscuta campestris* on the growth and photosynthesis of its host *Mikania micrantha*. *J. Exp. Bot.* **2007**, *58*, 2929–2937. [[CrossRef](#)]
19. Le, Q.V.; Tennakoon, K.U.; Metali, F.; Lim, L.B.; Bolin, J.F. Impact of *Cuscuta australis* infection on the photosynthesis of the invasive host, *Mikania micrantha*, under drought condition. *Weed Biol. Manag.* **2015**, *15*, 138–146.
20. Zagorchev, L.; Traianova, A.; Teofanova, D.; Li, J.; Kouzmanova, M.; Goltsev, V. Influence of *Cuscuta campestris* Yunck. on the photosynthetic activity of *Ipomoea tricolor* Cav.—In Vivo chlorophyll a fluorescence assessment. *Photosynthetica* **2020**, *58*, 237–247. [[CrossRef](#)]
21. Goldwasser, Y.; Rabinovitz, O.; Hayut, E.; Kuzikaro, H.; Sibony, M.; Rubin, B. Selective and effective control of field dodder (*Cuscuta campestris*) in chickpea with granular pendimethalin. *Weed Technol.* **2019**, *33*, 586–594. [[CrossRef](#)]
22. Jhu, M.-Y.; Farhi, M.; Wang, L.; Philbrook, R.N.; Belcher, M.S.; Nakayama, H.; Zumstein, K.S.; Rowland, S.D.; Ron, M.; Shih, P.M. Heinz-resistant tomato cultivars exhibit a lignin-based resistance to field dodder (*Cuscuta campestris*) parasitism. *Plant Physiol.* **2022**, *189*, 129–151. [[CrossRef](#)] [[PubMed](#)]
23. Córdoba, E.M.; Fernández-Aparicio, M.; González-Verdejo, C.I.; López-Grau, C.; del Valle Muñoz-Muñoz, M.; Nadal, S. Search for Resistant Genotypes to *Cuscuta campestris* Infection in two legume species, *Vicia sativa* and *Vicia ervilia*. *Plants* **2021**, *10*, 738. [[CrossRef](#)] [[PubMed](#)]
24. Hegenauer, V.; Fürst, U.; Kaiser, B.; Smoker, M.; Zipfel, C.; Felix, G.; Stahl, M.; Albert, M. Detection of the plant parasite *Cuscuta reflexa* by a tomato cell surface receptor. *Science* **2016**, *353*, 478–481. [[CrossRef](#)]
25. Runyon, J.B.; Mescher, M.C.; Felton, G.W.; De Moraes, C.M. Parasitism by *Cuscuta pentagona* sequentially induces JA and SA defence pathways in tomato. *Plant Cell Environ.* **2010**, *33*, 290–303. [[CrossRef](#)]
26. Birschwilks, M.; Sauer, N.; Scheel, D.; Neumann, S. *Arabidopsis thaliana* is a susceptible host plant for the holoparasite *Cuscuta spec.* *Planta* **2007**, *226*, 1231–1241. [[CrossRef](#)]
27. Liu, N.; Shen, G.; Xu, Y.; Liu, H.; Zhang, J.; Li, S.; Li, J.; Zhang, C.; Qi, J.; Wang, L. Extensive inter-plant protein transfer between *Cuscuta* parasites and their host plants. *Mol. Plant* **2020**, *13*, 573–585. [[CrossRef](#)]
28. Yang, B.; Li, J.; Zhang, J.; Yan, M. Effects of nutrients on interaction between the invasive *Bidens pilosa* and the parasitic *Cuscuta australis*. *Pak. J. Bot.* **2015**, *47*, 1693–1699.
29. Li, J.; Hettenhausen, C.; Sun, G.; Zhuang, H.; Li, J.-H.; Wu, J. The parasitic plant *Cuscuta australis* is highly insensitive to abscisic acid-induced suppression of hypocotyl elongation and seed germination. *PLoS ONE* **2015**, *10*, e0135197. [[CrossRef](#)]
30. Chen, H.; Shen, H.; Ye, W.; Cao, H.; Wang, Z. Involvement of ABA in reduced photosynthesis and stomatal conductance in *Cuscuta campestris*–*Mikania micrantha* association. *Biol. Plant.* **2011**, *55*, 545–548. [[CrossRef](#)]
31. Flexas, J.; Medrano, H. Drought-inhibition of photosynthesis in C3 plants: Stomatal and non-stomatal limitations revisited. *Ann. Bot.* **2002**, *89*, 183–189. [[CrossRef](#)] [[PubMed](#)]
32. Bonfig, K.B.; Schreiber, U.; Gabler, A.; Roitsch, T.; Berger, S. Infection with virulent and avirulent *P. syringae* strains differentially affects photosynthesis and sink metabolism in *Arabidopsis* leaves. *Planta* **2006**, *225*, 1–12. [[CrossRef](#)] [[PubMed](#)]

33. Price, G.D.; Evans, J.R.; von Caemmerer, S.; Yu, J.-W.; Badger, M.R. Specific reduction of chloroplast glyceraldehyde-3-phosphate dehydrogenase activity by antisense RNA reduces CO<sub>2</sub> assimilation via a reduction in ribulose biphosphate regeneration in transgenic tobacco plants. *Planta* **1995**, *195*, 369–378. [[CrossRef](#)]
34. Elena López-Calcagno, P.; Omar Abuzaid, A.; Lawson, T.; Anne Raines, C. Arabidopsis CP12 mutants have reduced levels of phosphoribulokinase and impaired function of the Calvin–Benson cycle. *J. Exp. Bot.* **2017**, *68*, 2285–2298. [[CrossRef](#)] [[PubMed](#)]
35. Zagorchev, L.; Albanova, I.; Tosheva, A.; Li, J.; Teofanova, D. Salinity effect on *Cuscuta campestris* Yunc. Parasitism on *Arabidopsis thaliana* L. *Plant Physiol. Biochem.* **2018**, *132*, 408–414. [[CrossRef](#)]
36. Portis, A.R.; Parry, M.A. Discoveries in Rubisco (Ribulose 1,5-bisphosphate carboxylase/oxygenase): A historical perspective. *Photosynth. Res.* **2007**, *94*, 121–143. [[CrossRef](#)]
37. Murakami, R.; Ifuku, K.; Takabayashi, A.; Shikanai, T.; Endo, T.; Sato, F. Functional dissection of two *Arabidopsis* PsbO proteins: PsbO<sub>1</sub> and PsbO<sub>2</sub>. *FEBS J.* **2005**, *272*, 2165–2175.
38. Borsics, T.; Lados, M. Dodder infection induces the expression of a pathogenesis-related gene of the family PR-10 in alfalfa. *J. Exp. Bot.* **2002**, *53*, 1831–1832. [[CrossRef](#)]
39. Li, D.-M.; Staehelin, C.; Wang, W.-T.; Peng, S.-L. Molecular cloning and characterization of a chitinase-homologous gene from *Mikania micrantha* infected by *Cuscuta campestris*. *Plant Mol. Biol. Rep.* **2010**, *28*, 90–101. [[CrossRef](#)]
40. Gullner, G.; Komives, T.; Király, L.; Schröder, P. Glutathione S-transferase enzymes in plant-pathogen interactions. *Front. Plant Sci.* **2018**, *9*, 1836. [[CrossRef](#)] [[PubMed](#)]
41. Boerjan, W.; Ralph, J.; Baucher, M. Lignin biosynthesis. *Annu. Rev. Plant Biol.* **2003**, *54*, 519–546. [[PubMed](#)]
42. Bhuiyan, N.H.; Selvaraj, G.; Wei, Y.; King, J. Role of lignification in plant defense. *Plant Signal. Behav.* **2009**, *4*, 158–159. [[CrossRef](#)] [[PubMed](#)]
43. Johnsen, H.R.; Striberny, B.; Olsen, S.; Vidal-Melgosa, S.; Fangel, J.U.; Willats, W.G.; Rose, J.K.; Krause, K. Cell wall composition profiling of parasitic giant dodder (*Cuscuta reflexa*) and its hosts: A priori differences and induced changes. *New Phytol.* **2015**, *207*, 805–816. [[CrossRef](#)] [[PubMed](#)]
44. Kim, G.; Westwood, J.H. Macromolecule exchange in *Cuscuta*–host plant interactions. *Curr. Opin. Plant Biol.* **2015**, *26*, 20–25. [[CrossRef](#)]
45. Park, S.-Y.; Shimizu, K.; Brown, J.; Aoki, K.; Westwood, J.H. Mobile Host mRNAs Are Translated to Protein in the Associated Parasitic Plant *Cuscuta campestris*. *Plants* **2021**, *11*, 93. [[CrossRef](#)]
46. Wu, X.; Xiong, E.; Wang, W.; Scali, M.; Cresti, M. Universal sample preparation method integrating trichloroacetic acid/acetone precipitation with phenol extraction for crop proteomic analysis. *Nat. Protoc.* **2014**, *9*, 362. [[CrossRef](#)]
47. Bradford, M.M. A rapid and sensitive method for the quantitation of microgram quantities of protein utilizing the principle of protein-dye binding. *Anal. Biochem.* **1976**, *72*, 248–254. [[CrossRef](#)]
48. Neuhoff, V.; Arold, N.; Taube, D.; Ehrhardt, W. Improved staining of proteins in polyacrylamide gels including isoelectric focusing gels with clear background at nanogram sensitivity using Coomassie Brilliant Blue G-250 and R-250. *Electrophoresis* **1988**, *9*, 255–262.
49. Shevchenko, A.; Tomas, H.; Havli, J.; Olsen, J.V.; Mann, M. In-gel digestion for mass spectrometric characterization of proteins and proteomes. *Nat. Protoc.* **2006**, *1*, 2856. [[CrossRef](#)]
50. Sharmin, S.A.; Alam, I.; Rahman, M.A.; Kim, K.-H.; Kim, Y.-G.; Lee, B.-H. Mapping the leaf proteome of *Miscanthus sinensis* and its application to the identification of heat-responsive proteins. *Planta* **2013**, *238*, 459–474. [[CrossRef](#)]

## Article

# Cucumber mosaic virus Is Unable to Self-Assemble in Tobacco Plants When Transmitted by Seed

Antonella Vitti <sup>1,2,\*</sup>, Israel Pagán <sup>3</sup>, Brigida Bochicchio <sup>4</sup>, Angelo De Stradis <sup>5</sup>, Pasquale Piazzolla <sup>1</sup>, Antonio Scopa <sup>1</sup> and Maria Nuzzaci <sup>1</sup>

<sup>1</sup> School of Agricultural, Forestry, Food and Environmental Sciences, University of Basilicata, Viale dell'Ateneo Lucano 10, 85100 Potenza, Italy

<sup>2</sup> Department of Pharmacy, University of Salerno, Via Giovanni Paolo II, 132, Fisciano, 84084 Salerno, Italy

<sup>3</sup> Centre for Plant Biotechnology and Genomics UPM-INIA/CSIC, Polytechnic University of Madrid, Campus Montegancedo, M40 Highway km.38, Pozuelo de Alarcón, 28223 Madrid, Spain

<sup>4</sup> Laboratory of Protein Chemistry, Laboratory of Bioinspired Materials (LaBIM), Department of Science, University of Basilicata, Viale dell'Ateneo Lucano, 10, 85100 Potenza, Italy

<sup>5</sup> Institute for Sustainable Plant Protection, CNR, Via Amendola 122/D, 70126 Bari, Italy

\* Correspondence: avitti.uni@gmail.it

**Abstract:** *Cucumber mosaic virus* (CMV), which has great impact on agronomic production worldwide, is both aphid and seed transmitted. Although the mechanisms of aphid transmission have been widely studied, those underlying the ability of CMV to survive and remain infectious during the passage from one generation to the next through the seeds are still to be clarified. Moreover, the viral determinants of seed transmission rate are poorly understood. Three viral genotypes produced from same RNA 1 and 2 components of CMV-Fny but differing in RNA 3 (the wild type CMV-Fny, a pseudorecombinant CMV-Fny/CMV-S and a chimeric CMV previously obtained by our group, named F, FS and CS, respectively) were propagated in *Nicotiana tabacum* cv Xanthi plants in order to assess differences in tobacco seed transmission rate and persistence through plant generations in the absence of aphid transmission. Seed-growth tests revealed CMV infection in the embryos, but not in the integuments. Seedlings from seed-growth tests showed the presence of all considered viruses but at different rates: from 4% (F, FS) to 16% (CS). Electron microscopy revealed absence (CS) of viral particles or virions without the typical central hole (F and FS). In agreement, structural characteristics of purified CMV particles, assessed by circular dichroism spectroscopy, showed anomalous spectra of nucleic acids rather than the expected nucleoproteins. These alterations resulted in no seed transmission beyond the first plant generation. Altogether, the results show for the first time that correct virion assembly is needed for seed infection from the mother plant but not to seedling invasion from the seed. We propose that incorrect virion formation, self-assembly and architecture stability might be explained if during the first stages of germination and seedling development some tobacco seed factors target viral regions responsible for protein-RNA interactions.

**Keywords:** virus vertical transmission; CMV-Fny strain; pseudorecombinant virus; chimeric virus; infection rate; seed-growth tests; electron microscopy; circular dichroism spectroscopy; viral assembly

**Citation:** Vitti, A.; Pagán, I.; Bochicchio, B.; De Stradis, A.; Piazzolla, P.; Scopa, A.; Nuzzaci, M. *Cucumber mosaic virus Is Unable to Self-Assemble in Tobacco Plants When Transmitted by Seed*. *Plants* **2022**, *11*, 3217. <https://doi.org/10.3390/plants11233217>

Academic Editors: Milan S. Stankovic, Paula Baptista and Petronia Carillo

Received: 20 October 2022

Accepted: 21 November 2022

Published: 24 November 2022

**Publisher's Note:** MDPI stays neutral with regard to jurisdictional claims in published maps and institutional affiliations.



**Copyright:** © 2022 by the authors. Licensee MDPI, Basel, Switzerland. This article is an open access article distributed under the terms and conditions of the Creative Commons Attribution (CC BY) license (<https://creativecommons.org/licenses/by/4.0/>).

## 1. Introduction

*Cucumber mosaic virus* (CMV, family *Bromoviridae*, genus *Cucumovirus*) is a plant virus with great impact on agronomic production worldwide due to its extremely wide host range and geographical distribution [1]. CMV is a positive-sense RNA virus whose genome is encapsidated in icosahedral particles of about 30 nm in diameter. The virus genome consists of three single-stranded RNAs (RNA 1, 2 and 3), all necessary for infectivity. RNA 1 encodes for the 1a protein, involved in virus replication together with the 2a protein, which is encoded by RNA 2. RNA 2 also harbors the 2b gene, which encodes for a protein involved in suppressing the host RNA silencing defense response. RNA3

encodes for the movement protein (MP) and the coat protein (CP), the latter being expressed through the subgenomic RNA 4. CMV is mainly transmitted horizontally from plant-to-plant by aphids, but vertical transmission from-parent-to-offspring through seeds was reported few years after the virus was first described in cucumber [2–4]. In the last twenty years, CMV vertical transmission has been described in several plant species, such as some legumes [5–9], spinach (*Spinacia oleracea* L.) [10], pepper (*Capsicum annuum* L. cv Marengo) [11] and *Arabidopsis thaliana* [12–14]. Thus, seed transmission is an essential mode for CMV persistence (the virus can survive within the seed as long as this remains viable) and long-distance dissemination (even at trans-continental scale). Moreover, it also provides an inoculum source for subsequent spread by aphids, having substantial epidemiological effects and therefore a far-reaching impact on crop production [10,15]. Indeed, it has been shown that very low CMV seed transmission rates are enough to start an outbreak [15].

In *A. thaliana*, it has been determined that the efficiency of vertical transmission depends on the host-virus genotypes per genotype interaction [14]. In agreement, another recent study conducted on *Capsicum* species reported that the CMV ability to be transmitted by seeds, and the rate of seed transmission, are cultivar-dependent [16]. The host determinants controlling CMV seed transmission are not well understood yet. In *A. thaliana*, virus multiplication and speed of within-host movement through the inflorescence have been shown to chiefly predict the CMV seed transmission rate [14]. In addition, Genome-Wide Association Studies (GWAS) indicated that the same host functions that modulate CMV virulence (i.e., the effect of pathogen infection on host progeny production) are important for CMV seed transmission rate [17]. However, the host genes controlling virus multiplication and movement have not been identified, and GWAS results need to be experimentally validated. On the virus side, as soon as 1992, a study with pseudorecombinants obtained from strains that were, or were not, seed transmissible in *Phaseolus vulgaris* demonstrated that RNA 1, co-governing viral replication and affecting virus movement, has a great influence on CMV transmissibility by seeds [5]. These results are compatible with those of works focused on the plant side. Therefore, RNA 1 is considered to affect the efficiency of seed transmission. However, Pagán (2019) [15] suggested that RNAs 2 and 3 could also represent viral genetic determinants of CMV seed transmission, although there is no experimental test of this hypothesis, and information on the amino acids potentially involved in this process is not available. Efforts have been made to explore whether the virus is vertically transmitted over several generations [13]. However, in line with the lack of information on the genetic determinants of CMV seed transmission, the mechanisms underlying the ability of CMV to survive and remain infectious in seeds across plant generations have not been defined.

This work aims to better understand the role played by the proteins encoded by the genomic segments RNA 1, 2, and 3 (and particularly the latter segment) in CMV seed transmission, by searching for possible unknown virus determinants, as well as by clarifying if the virus has the capacity to remain viable across host generations and what are the mechanisms underlying this ability. To address these questions, we used *Nicotiana tabacum* as a model host and three different virus genotypes: CMV-Fny (F), a pseudorecombinant CMV-Fny/CMV-S (FS) and a chimeric CMV previously obtained by our group (CS) [18]. All genotypes have RNA 1 and 2 components from CMV-Fny, and different RNA 3: of CMV-Fny (F), of CMV-S (FS) and a version of the CMV-S mutated in the amino acid 131 of CP and carrying an exogenous peptide of 11 aa (CMV<sub>392</sub>, CS). Using these genetic materials, we analyzed the location of CMV within the seed, we explored the relationship between modifications in RNA 3 and seed transmission rate and we determined for how many generations CMV persisted in the plant through strict vertical transmission.

## 2. Results

### 2.1. Symptoms of Virus Infection in Mother Plants

Fourteen days after inoculation, as well as during seed harvesting, plants inoculated with all viral genotypes showed typical infection symptoms (Figure 1a,b,d,e,g,h) compatible with those reported previously [18], thus proving that the viruses replicated, assembled and systemically spread. Virus presence was corroborated by molecular and serological means (see Section 2.3). Seeds obtained from tobacco mother plants infected with the wild type CMV-Fny (F), the pseudorecombinant CMV-Fny/CMV-S (FS) and the chimeric CMV<sub>392</sub> (CS) were collected 120–135 days post inoculation (d.p.i.). All seedlings obtained by the germination of these seeds resulted symptomless (Figure 1c,f,i).

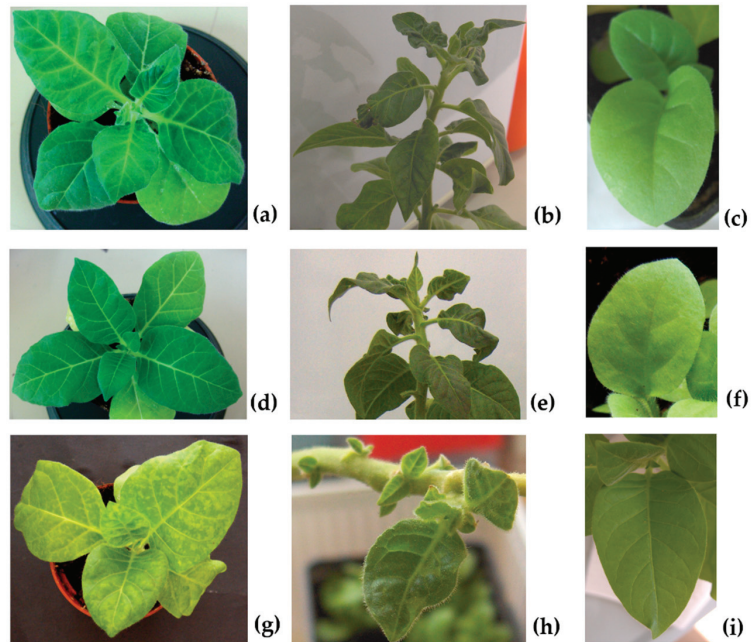


**Figure 1.** Symptoms induced on *N. tabacum* cv Xanthi mother plants 14 days post-inoculation (first column) and during seeds harvest (second column). Seedlings of the first generation showing no symptoms (third column). Images correspond to plants infected with F (CMV-Fny) (a–c); FS (CMV-Fny/CMV-S) (d–f); CS (chimeric CMV<sub>392</sub>) (g–i).

As a control, virions from the purified three CMV genotypes, as well as systemically infected tissues of mother plants were used to mechanically inoculate healthy plants. In all cases, RT-PCR and serological analyses revealed the presence of the replicase gene and CP in all infected plants 14 d.p.i. The typical CMV symptoms were also shown and virions were observed under EM (data not shown).

### 2.2. Location of CMV within Infected Tobacco Seeds

Grow-out tests of first-generation seeds allowed us to separate seed integuments from embryos and then to detect the presence of CMV infection in the two different tissues (Figure 2).

Both RT-PCR and Immuno-dot blot (IB) analyses revealed seed infection only in the embryo but not at the integument level, as shown in Figure 2. Specifically, RT-PCR analysis of the separated seed tissues showed the presence of amplicons of the expected size (513 bp) for all nucleic acids extracted from plants infected by the three viral genotypes F,

FS and CS, so confirming the presence of the RNA-dependent RNA polymerase (*RdRp*) gene only in the embryos and never in the integuments (Figure 2a). Similarly, IB analysis confirmed this finding through detecting the viral CP by CMV polyclonal antiserum (Figure 2b).

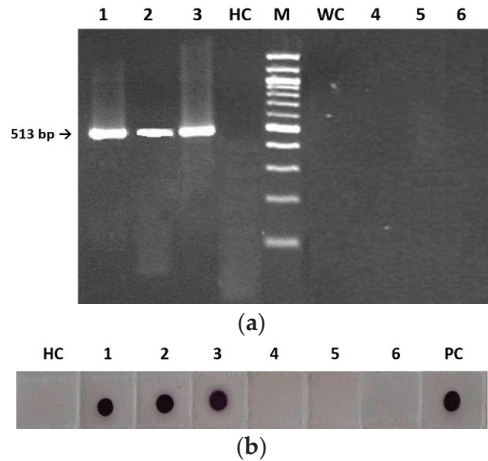


**Figure 2.** Detection of wild type (F), pseudorecombinant (FS) and chimeric (CS) CMVs in tobacco seed embryonal (1–3) and integumental (4–6) tissues by RT-PCR (a) and Immuno-dot blot (b) analyses. (a): lines 1–3, DNA fragment of 513 bp derived from embryonal tissues infected with F (1), FS (2), and CS (3); HC, healthy control; M, 100 bp DNA Ladder (BioLabs); WC, water control; lines 4–6, no fragment derived from integumental tissues infected with F (4), FS (5), and CS (6). (b): membrane probed with CMV polyclonal antiserum (Bioreba AG). HC, healthy control; 1–3, CP revealed from embryonal tissues infected with F (1), FS (2), and CS (3); 4–6, no CP revealed from integumental tissues infected with F (4), FS (5), and CS (6). PC, positive control.

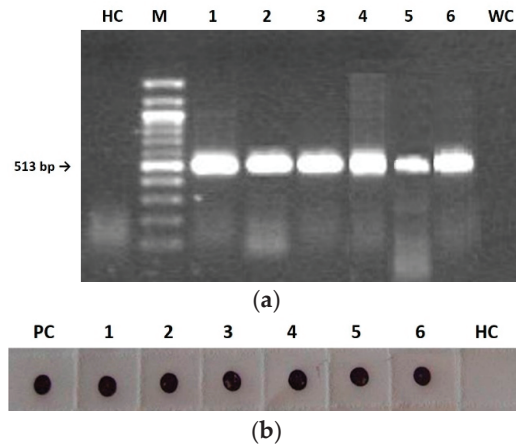
### 2.3. CMV Seed Transmission Rate in Tobacco

First-generation seedlings, obtained from the germination in pot of seeds derived from CMV-infected mother plants, were monitored for virus presence after 6–8 weeks post-germination, and were used to analyze CMV seed transmission rate in tobacco plants. For comparison purposes, virus infection in mother plants was also analyzed.

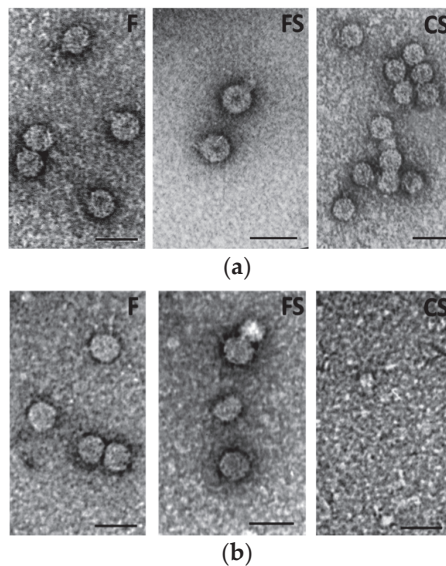
For all three considered viruses, the analyses on mother plants during seed collection and on first-generation seedling leaf tissues showed the presence of both *RdRp* gene by RT-PCR (Figure 3a) and CP by IB (Figure 3b).

For each considered viral genotype, 400 seedlings derived from mature seeds collected from the 30 infected mother plants were randomly chosen and analyzed by IB, in order to establish the CMV vertical transmission rate. The results indicated that the CMV seed-transmission rate ranged from 4% for F and FS to 16% in the case of CS, in spite of symptomless infection in all seedlings (Figure 1c,f,i).

Purified virions from both mother plants and first-generation seedlings were analyzed by electron microscopy (EM), as reported in Figure 4. In mother plants, all CMV viral genotypes displayed the characteristic lesser density central region, named “hole” (Figure 4a). On the contrary, when virions derived from first-generation seedlings were analyzed, they were absent (CS) or the viral particles had not the typical central hole (F and FS) (Figure 4b).



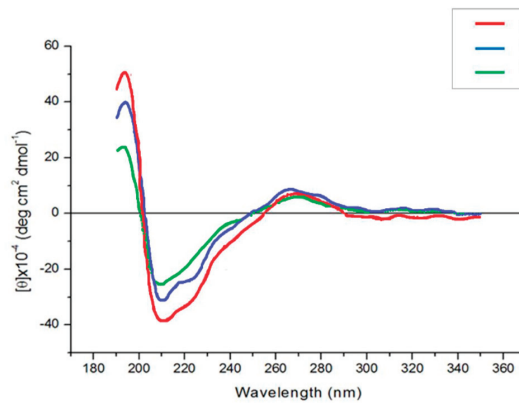
**Figure 3.** Detection of wild type (F), pseudorecombinant (FS) and chimeric (CS) CMVs in tobacco mother plants (1–3) and first-generation seedlings (4–6) by RT-PCR (a) and Immuno-dot blot (b). (a): HC, healthy control; M, 100 bp DNA Ladder (BioLabs); line 1–3, DNA fragment of 513 bp derived from mother plants tissues infected with F (1), FS (2), and CS (3); line 4–6, DNA fragment of 513 bp derived from first-generation seedlings tissues infected with F (4), FS (5), and CS (6); WC, water control. (b): membrane probed with CMV polyclonal antiserum (Bioreba AG). PC, positive control; 1–3, CP revealed from mother plants tissues infected with F (1), FS (2), and CS (3); 4–6, CP revealed from first-generation seedlings tissues infected with F (4), FS (5), and CS (6); HC, healthy control.



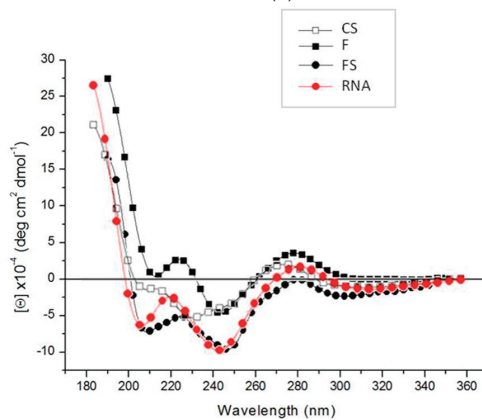
**Figure 4.** Electron micrograph of purified wild type (F), pseudorecombinant (FS) and chimeric (CS) virions isolated from tobacco mother plants (a) or from first-generation seedlings (b). Bar = 100 nm.

Figure 5 shows circular dichroism (CD) spectra of purified virions isolated from mother plants and first-generation tobacco seedlings. The conformational features are those expected for the typical CMV bands when obtained from mother plants (Figure 5a). CD spectra of viruses extracted from mother plants showed a strong positive band at about 200 nm, two negative bands at about 208 nm and 220 nm, and a small positive band at

about 270 nm. Both the positive, at 200 nm, and negative band, at 208 nm, reached the maximum ellipticity value in the case of F, and the minimum for CS, with FS showing intermediate values (Figure 5a). In contrast, the positive band at about 270 nm displayed the same intensity for all three viruses. CD spectra of first-generation seedling viruses are shown in Figure 5b. CMV viral RNA was used to compare the CD spectra of these viruses. All CD spectra were similar to the RNA spectrum, with some exceptions for CS. They were characterized by a positive peak below 200 nm even if with lower ellipticity values than those shown in Figure 5a. A positive band at about 270 nm, with the highest ellipticity for F and values around zero for FS, was found (Figure 5b). Furthermore, two negative bands at about 240 and 200 nm were evident for all samples, except CS. The RNA CD spectrum shows a trend toward positive values at about 220 nm, analogously to F and FS that showed positive values and a red wavelength shift. Summarizing, a typical CD profile of a CMV nucleic acid, rather than the expected nucleoprotein, was revealed for all three virus genotypes in the first-generation seedlings (Figure 5b).



(a)



(b)

**Figure 5.** CD spectra of CMV purified wild type (F), pseudorecombinant (FS) and chimeric (CS) virions isolated from tobacco mother plants (a) or first-generation seedlings (b). CMV viral RNA was used to compare the CD spectra of first-generation seedling viruses. Note the different scale in each panel.

#### 2.4. Second Generation Seeds and Seedlings

Second-generation seedlings, obtained from the germination in pot of seeds deriving from 30 CMV-infected first-generation plants, were monitored after 6–8 weeks post germination. In all 400 s-generation seedlings, none of the CMV genotypes were detected for either by RT-PCR or by IB analyses. Similarly, purified F, FS and CS particles were never observed by ME. These findings indicate that, in tobacco, the vertical transmission of CMV was unable to proceed beyond the first generation.

### 3. Discussion

*Cucumber mosaic virus* can be transmitted both horizontally and vertically, by aphids and seeds, respectively. To develop efficient strategies to control virus outbreaks, understanding the mechanisms and determinants underlying the ability of CMV to survive and remain infectious in seeds and to persist during strict vertical passage from one generation to the next, are of pivotal importance. However, CMV seed-borne infections and their implications for virus epidemiology, as well as the factors and processes that affect vertical transmission, are not fully understood yet [15].

In the present study, we show that in tobacco the CMV seed-borne infection was associated with the virus presence in the embryo for the wild type, the pseudorecombinant and the chimeric CMVs (Figure 2). This is probably due to virion instability, which reduces viability outside living cells and therefore on seed coats [9], although host-specific factors may also be involved. Indeed, in other plant species the embryo infection is not necessary for seedling infection. For instance, using CMV-Fny as in this work, Ali and Kobayashi (2010) [11] reported a high rate of seed coat infection linked to virus vertical transmission. These authors also reported embryo infection at low rates and showed that embryo infection had not guaranteed CMV seed transmission, which was attributed to an inactivation suffered by the virus during the seedling germination phase [11]. Regardless the route of transmission, our findings seem to confirm that seed invasion and virus multiplication into the seed are necessary (but not sufficient) for CMV transmission, which would be therefore affected by RNA 1 and 2, through their participation in viral replication and movement from mother plants to seeds (Figures 2 and 3) [5].

Results regarding the seedling infection rate suggest the existence of potential viral genetic determinants of seed transmission in CMV RNA 3. Specifically, seed-borne infection transferred to seedlings ranged from 4% for F and FS to 16% in the case of CS. These values overlap with those reported by other researchers on CMV in several plant species, such as incarnate clover and pumpkin (5%) [8,19] or the above-mentioned pepper (from 10 to 14%) [11] and spinach (nearly 15%) [10]. Notably, the rate registered in CS quadrupled that of F and FS. As indicated in Section 4.1., all three CMV genotypes were produced starting from the same RNA 1 and RNA 2 components of CMV-Fny; whereas the RNA 3 component was derived from CMV-Fny in F and from CMV-S in FS and CS. This latter chimeric CMV differs from FS by the presence of an exogenous sequence in position 392 of the CP gene, obtained via the site-directed mutagenesis T<sub>391</sub>→G and C<sub>392</sub>→G in the codon for the aa 131 (changed from Ser<sub>131</sub> to Gly<sub>131</sub>), and located in the βE-αEF region, without affecting to any significant degree the stability of chimeric subunits during serial mechanical plant-to-plant horizontal passages [18]. Therefore, we may point to RNA 3 (and particularly the CP) as a possible viral genetic determinant of CMV seed transmission rate. Moreover, we can also speculate, for the first time, on the eventual amino acids implicated, such as 131 and/or those belonging to βE-αEF region of the CP, provided that the other factors potentially to be considered (i.e., host, time of plant infections, absence of mixed infections with other viruses) are the same for all the studied CMVs and therefore not involved [15]. The possible role of the βE-αEF region in seed transmission rate is also supported by the recognized function of the amino acid 129 of the CP, the first of the βE-αEF region. In fact, this amino acid is considered a virulence determinant and key regulator of symptoms induced in plants by CMV [20,21], with effects that are not host specific, but dependent on the CMV strain [22]. In agreement, in our experiments no symptoms on seedlings derived from

infected seeds by all virus genotypes were observed (Figure 1c,f,i), as already demonstrated for other species in which CMV is seed transmitted [11,23]. Nevertheless, the absence of symptoms observed in first-generation seedlings in this work may well be related to an involvement of  $\beta$ E- $\alpha$ EF region of the CP due to incorrect or lack of virion assembly, as observed for all three genotypes F, FS and CS by EM and CD spectra (Figures 4b and 5b). The  $\beta$ E- $\alpha$ EF region of the CP is a flexible loop and this property is conferred by its first amino acid 129 [24,25]. Suzuki et al. (1995) [26] observed that the substitution of the amino acid 129 from Serine to Phenylalanine ( $S_{129} \rightarrow F_{129}$ ) in the CP of the CMV-Y strain is able to disrupt the virion assembly and provoke the aggregation of CP molecules, to elicit necrosis in tobacco plants. In that amino acid substitution, a polar uncharged group (S) was replaced with a non-polar uncharged group (F). In the current study, we used a chimeric CMV where a similar substitution occurred in the same  $\beta$ E- $\alpha$ EF region of the CP, but in the nearby amino acid position 131. In fact, in the genotype CS, the amino acid Serine at position 131 of the CP was replaced with a non-polar uncharged group, that is the aa Glycine ( $S_{131} \rightarrow G_{131}$ ). Besides the mentioned substitution, and starting from the same position, an exogenous peptide of 11 amino acids was also inserted in the CP. These modifications resulted in some variation of the electrostatic potential in the CP, which is known to play an important role in the protein folding and stability, as well as in the protein-protein and protein-nucleic acid interactions [18,27]. Therefore, these modifications, although they did not interfere with virus stability in serial plant-to-plant passages, as reported in a previous research of this group [18], could be the reason for the total inability to assemble by CS (Figure 4b) under strict vertical transmission. Other studies with mutation of the aa 131 (without carrying the exogenous peptide) or in different positions of the CP (i.e., from 129 to 136, that are the first and the last aa of the  $\beta$ E- $\alpha$ EF region) will be useful for validating the role of the CP in CMV vertical transmission.

In *A. thaliana*, an autogamous species like the tobacco used in this work, seed transmission rates for three different CMV strains increased after five serial passages of strict vertical transmission, in association with an analogous reduction of virus accumulation and virulence [13,28]. These observations were explained by the authors as a result of a reciprocal co-evolutionary selection/interaction between host and virus during the seed transmission, aimed to reduce the damage in the plant induced by the virus infection, to favor CMV maintenance in the plant population via seed infection, and also to increase plant fitness [13]. Although symptoms were never observed in seedlings of the first generation, our results disagree with a co-evolution towards lower virulence because the virions are not anymore infectious after the first generation, regardless of the differences on seed transmission rate between F and FS and CS in this first progeny. However, our results are in accordance with a study on pea plants contaminated by *Pea seed-borne mosaic virus* (PSbMV) through seed transmission, where infected plants of the second generation expressed no symptom and, at the same time, the virus was not detectable in their vegetative parts [29]. We might think that an extinction of the virus population could have occurred, maybe due to severe population bottlenecks responsible to hamper the virus ability to pass on through generations and preventing the adaptation of all virus genotypes here studied to seed transmission in tobacco. Such bottlenecks during seed transmission have been previously reported [30]. Supporting this idea, we detected few defective virions passing to the first generation, which were unable to recover the virus population and therefore the virus did not invade the seeds again. However, this might not be the only force at play: while F and FS were at least able to form viral particles, although without the typical central hole, CS showed a complete inability to self-assemble (Figure 4b). Notably, both the replicase gene and the CP were detected in seedlings infected with all three CMVs (Figure 3) and the highest seed transmission rate was observed for CS in the first-generation seedlings. This suggests that the capacity of the virus to invade seedlings from infected seeds does not require virion formation and perhaps nude RNA molecules are enough. In contrast, seed invasion from mother plants and/or virus survival within the seed would need correct

virion assembly. Indeed, virions of the three CMV genotypes purified from mother plants were infectious and assembled correctly (see Results).

EM analysis and CD spectra indicated analogous peculiarities for the three CMVs in mother plants. For example, the positive band revealed by CD spectra for the purified virions at about 270 nm displayed the same intensity for all three viruses, indicating the same stacking of RNA bases and structural organization [27]. At odds with this, EM and CD analyses on first-generation seedlings confirmed that abnormal virus particles (F and FS) or no virions at all (CS) were detected (Figures 4b and 5b). As above mentioned, the purified virions appeared to be dissociated as a mixture of RNA and proteins interacting with each other, although in a different manner for CS than for the other two CMV genotypes (Figure 5b). Altogether, our findings suggest that for all three viruses, something seems to happen certainly not in the mother plants, but during seed germination and first-generation seedlings development. We could also speculate that some tobacco seed substances able to interfere with some viral components responsible for protein-RNA interactions could be involved. Chemical analysis of tobacco seeds has indicated a high tocopherol content in different genotypes of *Nicotiana tabacum* (L.) [31,32]. These compounds, also known as vitamin E, are considered lipophilic antioxidants with a possible role in activating both basal and induced resistance in plants [33], thanks to the ability to remove reactive oxygen species (ROS) or polyunsaturated fatty acid radical species [34]. In our case, it can be argued that CMV particles are able to infect seeds but, during germination, some substance (e.g., tocopherols contained in the seed) could be responsible for targeting CMV components, such as CP N-terminal region, rich in basic amino acids; this could disturb (F and FS) or disrupt (CS) the correct virion formation, self-assembling and architecture stability in the developed seedlings of first generation [27]. As a consequence, a second round of seed infection turns out to be not possible. Currently, no data are available from sequencing of viruses from first-generation seedlings to establish also a possible shift in the RNAs sequence of the infecting CMV viruses. Therefore, a next step in this research would be focused on checking the integrity of individual virus RNAs and verifying possible mutations responsible for hampering the ability of the virus to pass on through generations during vertical transmission.

#### 4. Materials and Methods

##### 4.1. Virus and RNA Sources

The wild type CMV-Fny strain (F), pseudorecombinant CMV-Fny/CMV-S (FS) and chimeric CMV<sub>392</sub> (CS) were used [18]. They were propagated in *Nicotiana tabacum* cv Xanthi plants and virions were purified as described by Lot et al. (1972) [35]. All three CMV genotypes were produced starting from the same RNA 1 and RNA 2 components of CMV-Fny strain; whereas the RNA 3 component was derived from the same Fny strain in F and from CMV-S strain in FS and CS. This latter chimeric CMV differs from FS by the presence of an exogenous sequence in position 392 of the CP gene, obtained via the site-directed mutagenesis T<sub>391</sub>→G and C<sub>392</sub>→G in the codon for the aa 131 (changed from Ser<sub>131</sub> to Gly<sub>131</sub>) [18].

##### 4.2. Virus Inoculation and Production of Infected Seeds

Tobacco seeds were sterilized using 1% Na-hypochlorite solution for 1 min and then rinsed with sterile distilled H<sub>2</sub>O, before imbibition on moist filter paper at 4 °C for 24 h in the dark. Seeds germinated on water-dampened filter paper in a sterile Petri dish at 26 °C. One day after germination, seedlings were transferred to sterilized soil-filled pots. Throughout the experiment, plants were kept in a growth chamber with a 16 h photoperiod, at 26/23 °C (day/night), and watered with tap water, according to the needs of the seedlings, daily checked. Ten µg of virions from each purified CMV genotype were used to mechanically inoculate 30 tobacco plants at the four-leaf stage, which were kept in the growth chamber as infected mother plants until obtaining developed and mature tobacco seeds. The mechanically inoculated tobacco plants were monitored for symptom

development. Ten uninfected control plants were also kept in a separate growth chamber as mother healthy plants. The seeds were collected as they matured, in a scaled manner from each mother plant, pooled and stored all together. In the same way, 30 infected tobacco plants obtained from first-generation seeds were grown and represented the mother plants for second-generation seeds. Again, second-generation seeds were pooled and stored. During all experimentation, plants were carefully checked to ensure absence of aphids.

The following samples were tested for virus presence by RT-PCR and Immuno-dot blot (IB), as described in the subsequent subsections: systemically infected tissues of each mother plant (collected at 14 d.p.i. and during seeds harvesting); embryos and seed coats separated after germination of CMV-infected seeds on water dampened filter paper; 400 seedlings of first generation and 400 of second generation obtained from the germination in pot of CMV-infected seeds, 6–8 weeks post germination. Each seedling of first and second generation was derived from seeds randomly chosen from the total sets collected from mother plants and first-generation mother plants, respectively.

CMVs from both tobacco mother plants and first- and second-generation seedlings were purified according to Lot et al. (1972) [35]. All purified CMV particles were analyzed by electron microscopy (EM), and assessed by circular dichroism (CD) spectroscopy.

#### 4.3. Reverse Transcription (RT)-PCR Analysis

Total plant RNAs of samples infected with F, FS and CS were extracted by the PureLink™ Micro-to-Midi Total RNA Purification System (Invitrogen, Milan, Italy). Five hundred ng were reverse transcribed and amplified in a single tube using the SuperScript™ III One-Step RT-PCR System with Platinum® Taq DNA Polymerase (Invitrogen). The RT-PCR reaction mixture (a final volume of 50 µL) was prepared as described by the manufacturer adding 1 µL of both the reverse and forward 10 µM primers. The following pairs of primers were used: P<sub>RevRep</sub> (5'-CCATCACCTTAGCTTCCATGT-3'), complementary to position 1895–1915 of the CMV RNA-dependent RNA polymerase (*RdRp*) gene, and P<sub>ForRep</sub> (5'-TAACCTCCCAGTTCTCACCGT-3'), homologous to position 1403–1423 of the CMV *RdRp* gene (accession NC\_002035), according to Grieco et al. (2000) [36]. The PCR fragments were fractionated on 1.5% agarose gel and stained with SYBR Safe™ DNA gel stain (Invitrogen).

In the case of seedlings obtained from germination of CMV-infected seeds in pots, pairs of leaves for each plantlet (of the 400 total) were harvested, pooled in groups of ten (a total of 40 pool), and mixed for total nucleic acid extraction. When CMV was detected in a pool, total RNA extraction and RT-PCR from each single plant were performed, accordingly.

#### 4.4. Immuno-Dot Blot (IB) Analysis

Samples infected with F, FS and CS were homogenized in 0.2 M Tris, 1.5 M NaCl (TBS 10×) and centrifuged at 10,000 rpm for 10 min at 4 °C. The supernatant was gently dropped (2 µL) onto nitrocellulose membrane (Invitrogen). The membrane was air-dried, blocked for 45 min in 5% milk Tween–TBS and incubated for 1 h with CMV polyclonal antiserum (Bioreba AG, Switzerland) (diluted 1:2000). The membrane was then treated with anti-rabbit (Pierce Biotechnology, Rockford, IL, USA) alkaline phosphatase-conjugated antibodies (Abs) (diluted 1:2000), and the reactivity was detected using the Sigma Fast™ kit (Sigma Chemical Co., St. Louis, MO, USA). All incubations were performed at room temperature; after each incubation the membrane was washed three times with 20 mM Tris, 150 mM NaCl, 0.05% Tween-20 (Tween–TBS 1×).

#### 4.5. Electron Microscopy (EM)

Purified virions isolated from tobacco plants were examined via negative staining with 2% aqueous uranyl acetate and immediately processed for electron microscopy assays. Observations were performed with a Philips Morgagni 282D electron microscope at 60 kV.

#### 4.6. Circular Dichroism (CD) Spectroscopy

Circular dichroism (CD) spectra of purified virion (0.2 mg/mL) samples in aqueous solution were recorded on a Jasco J600 CD spectropolarimeter at 24 °C using a cell with a 1 mm optical path length. A HAAKE water bath was used to control the temperature. Data are expressed as molar ellipticity  $[\theta]M$  in  $\text{deg cm}^2 \text{dmol}^{-1}$  [37].

### 5. Conclusions

For the first time, this study demonstrated the ability of three different genotypes of CMV to be seed-borne in tobacco plants, and the inability to proceed beyond the first generation of plants. The three different genotypes varied in seed transmission rate and in the genomic sequence at RNA 3. Thus, our data allows a speculation on this genomic segment as a possible viral genetic determinant of seed transmission, and on the amino acids potentially implicated in this process and their position: codon for Ser<sub>131</sub>→Gly<sub>131</sub> (nt 391–393), located in the βE-αEF region of the CP.

In addition, we show that in tobacco plants CMV is unable to persist for more than one generation of strict vertical transmission. An explanation of mechanisms determining the lack of second-generation seedlings infection is that defective or few virions passing to the first generation are unable to recover the virus population after severe population bottlenecks associated with seed transmission, so that the virus does not invade the seeds again. We hypothesize that during the first stages of germination and seedling development some tobacco seed compounds (i.e., tocopherols) may target, for example, the viral CP N-terminal region, rich in basic amino acids and responsible for protein-RNA interactions. In this way, the correct virion formation, self-assembling and architecture stability are interfered with and cannot occur. As a consequence, the vertical transmission is restricted to the first generation of plants, without the ability to achieve a second round of progeny infection, regardless of the transmission rate.

**Author Contributions:** Conceptualization, A.V., M.N. and P.P.; methodology, A.V. and M.N.; investigation, A.V., M.N., B.B. and A.D.S.; resources, M.N., A.S. and A.V.; data curation, A.V. and M.N.; writing—original draft preparation, A.V. and M.N.; writing—review and editing, I.P. and A.V.; visualization, A.V., B.B., A.D.S. and I.P.; supervision, A.S., M.N. and P.P.; funding acquisition, A.S. All authors have read and agreed to the published version of the manuscript.

**Funding:** This research received no external funding.

**Data Availability Statement:** Data presented in this study are available on request from the corresponding author.

**Conflicts of Interest:** The authors declare no conflict of interest.

### References

- Palukaitis, P.; García-Arenal, F. *Cucumber Mosaic Virus*, 1st ed.; The American Phytopathological Society (APS) Publications: St. Paul, MN, USA, 2019. [\[CrossRef\]](#)
- Doolittle, S.P. A new infectious mosaic disease of cucumber. *Phytopathology* **1916**, *6*, 145–147.
- Jagger, I.C. Experiments with the cucumber mosaic disease. *Phytopathology* **1916**, *6*, 148–151.
- Doolittle, S.P. The mosaic disease of cucurbits. *US Dept. Agric. Bull.* **1920**, *879*, 1–69.
- Hampton, R.O.; Francki, R.I.B. RNA-1 dependent seed transmissibility of cucumber mosaic virus in *Phaseolus vulgaris*. *Phytopathology* **1992**, *82*, 127–130. [\[CrossRef\]](#)
- Abdullahi, I.; Ikotun, T.; Winter, S.; Thottappilly, G.; Atiri, G.I. Investigation on seed transmission of cucumber mosaic virus in cowpea. *Afr. Crop Sci. J.* **2001**, *9*, 677–684. [\[CrossRef\]](#)
- Latham, L.J.; Jones, R.A.C. Incidence of virus infection in experimental plots, commercial crops, and seed stocks of cool season crop legumes. *Aust. J. Agric. Res.* **2001**, *52*, 397–413. [\[CrossRef\]](#)
- Latham, L.J.R.; Jones, A.C.; McKirdy, S.J. Cucumber mosaic cucumovirus infection of cool-season crop, annual pasture, and forage legumes: Susceptibility, sensitivity, and seed transmission. *Aust. J. Agric. Res.* **2001**, *52*, 683–697. [\[CrossRef\]](#)
- O’Keefe, D.C.; Berryman, D.I.; Coutts, B.A.; Jones, R.A. Lack of seed coat contamination with Cucumber mosaic virus in lupin permits reliable, large-scale detection of seed transmission in seed samples. *Plant Dis.* **2007**, *91*, 504–508. [\[CrossRef\]](#)
- Yang, Y.; Kim, K.S.; Anderson, E.J. Seed transmission of cucumber mosaic virus in spinach. *Phytopathology* **1997**, *87*, 924–931. [\[CrossRef\]](#)

11. Ali, A.; Kobayashi, M. Seed transmission of Cucumber mosaic virus in pepper. *J. Virol. Meth.* **2010**, *263*, 234–237. [[CrossRef](#)]
12. Pagán, I.; Alonso-Blanco, C.; García-Arenal, F. Host responses in life-history traits and tolerance to virus infection in *Arabidopsis thaliana*. *PLoS Pathog.* **2008**, *4*, e1000124. [[CrossRef](#)]
13. Pagán, I.; Montes, N.; Milgroom, M.G.; García-Arenal, F. Vertical transmission selects for reduced virulence in a plant virus and for increased resistance in the host. *PLoS Pathog.* **2014**, *10*, e1004293. [[CrossRef](#)]
14. Cobos, A.; Montes, N.; López-Herranz, M.; Gil-Valle, M.; Pagán, I. Within-Host Multiplication and Speed of Colonization as Infection Traits Associated with Plant Virus Vertical Transmission. *J. Virol.* **2019**, *93*, e01078–e01119. [[CrossRef](#)]
15. Pagán, I. Movement between plants: Vertical transmission. In *Cucumber Mosaic Virus*; Palukaitis, P., García-Arenal, F., Eds.; APS Press: Washington, DC, USA, 2019; pp. 185–198. [[CrossRef](#)]
16. Arogundade, O.; Balogun, O.S.; Kumar, P.L. Seed transmissibility of Cucumber mosaic virus in Capsicum species. *Int. J. Veg. Sci.* **2018**, *25*, 146–153. [[CrossRef](#)]
17. Montes, N.; Cobos, A.; Gil-Valle, M.; Caro, E.; Pagán, I. *Arabidopsis thaliana* Genes Associated with Cucumber mosaic virus Virulence and Their Link to Virus Seed Transmission. *Microorganisms* **2021**, *9*, 692. [[CrossRef](#)]
18. Vitti, A.; Piazzolla, G.; Condelli, V.; Nuzzaci, M.; Lanorte, M.T.; Boscia, D.; de Stradis, A.; Antonaci, S.; Piazzolla, P.; Tortorella, C. Cucumber mosaic virus as the expression system for a potential vaccine against Alzheimer’s disease. *J. Virol. Methods* **2010**, *69*, 332–340. [[CrossRef](#)]
19. Sevik, M.A.; Balkaya, A. Seed transmissibility of viruses in winter squash landraces collected from the Black Sea region of Turkey. *Plant Prot. Sci.* **2015**, *51*, 195–199. [[CrossRef](#)]
20. Shintaku, M.; Zhang, L.; Palukaitis, P. A single amino acid substitution in the coat protein of Cucumber mosaic virus induces chlorosis in tobacco. *Plant Cell* **1992**, *4*, 751–757. [[CrossRef](#)]
21. Mochizuki, T.; Ohki, S.T. Single amino acid substitutions at residue 129 in the coat protein of cucumber mosaic virus affect symptom expression and thylakoid structure. *Arch. Virol.* **2011**, *156*, 881–886. [[CrossRef](#)]
22. Kobori, T.; Miyagawa, M.; Nishioka, K.; Ohki, S.T.; Osaki, T. Amino acid 129 of Cucumber mosaic virus coat protein determines local symptom expression and systemic movement in *Tetragonia expansa*, *Momordica charantia* and *Physalis floridana*. *J. Gen. Plant Pathol.* **2002**, *68*, 81–88. [[CrossRef](#)]
23. Gallitelli, D. The ecology of Cucumber mosaic virus and sustainable agriculture. *Virus Res.* **2000**, *71*, 9–21. [[CrossRef](#)] [[PubMed](#)]
24. Smith, T.J.; Chase, E.; Schmidt, T.; Perry, K.L. The structure of cucumber mosaic virus and comparison to cowpea chlorotic mottle virus. *J. Virol.* **2000**, *74*, 7578–7586. [[CrossRef](#)] [[PubMed](#)]
25. Gellert, A.; Salanki, K.; Naray-Szabo, G.; Balazs, E. Homology modelling and protein structure based functional analysis of five cucumovirus coat proteins. *J. Mol. Graph. Model.* **2006**, *24*, 319–327. [[CrossRef](#)] [[PubMed](#)]
26. Suzuki, M.; Kuwata, S.; Masuta, C.; Takanami, Y. Point mutations in the coat protein of cucumber mosaic virus affect symptom expression and virion accumulation in tobacco. *J. Gen. Virol.* **1995**, *76*, 1791–1799. [[CrossRef](#)]
27. Nuzzaci, M.; Bochicchio, I.; de Stradis, A.; Vitti, A.; Natilla, A.; Piazzolla, P.; Tamburro, A.M. Structural and biological properties of Cucumber mosaic virus particles carrying hepatitis C virus-derived epitopes. *J. Virol. Methods* **2009**, *155*, 118–121. [[CrossRef](#)]
28. Pagán, I.; Fraile, A.; Fernández-Fueyo, E.; Montes, N.; Alonso-Blanco, C.; García-Arenal, F. *Arabidopsis thaliana* as a model for the study of plant–virus co-evolution. *Philos. Trans. R Soc. Lond. B* **2010**, *365*, 1983–1995. [[CrossRef](#)]
29. Ligat, J.S.; Randles, J.W. An eclipse of pea seed-borne mosaic virus in vegetative tissue of pea following repeated transmission through the seed. *Ann. Appl. Bio.* **1993**, *122*, 39–47. [[CrossRef](#)]
30. Fabre, F.; Moury, B.; Johansen, E.I.; Simon, V.; Jacquemond, M.; Senoussi, R. Narrow bottlenecks affect pea seedborne mosaic virus populations during vertical seed transmission but not during leaf colonization. *PLoS Pathog.* **2014**, *10*, e1003833. [[CrossRef](#)]
31. Zlatanov, M.; Angelova, M.; Antova, G. Lipid composition of tobacco seeds. *Bulg. J. Agric. Sci.* **2007**, *13*, 539–544.
32. Mohammad, M.; Tahir, N.A.R. Evaluation of Chemical Compositions of Tobacco (*Nicotiana tabacum* L) Genotypes Seeds. *Annu. Res. Rev. Biol.* **2014**, *4*, 1480–1489. [[CrossRef](#)]
33. Boubakri, H.; Gargouri, M.; Mliki, A.; Brini, F.; Chong, J.; Jbara, M. Vitamins for enhancing plant resistance. *Planta* **2016**, *244*, 529–543. [[CrossRef](#)] [[PubMed](#)]
34. Caretto, S.; Nisi, R.; Paradiso, A.; de Gara, L. Tocopherol production in plant cell cultures. *Mol. Nutr. Food Res.* **2010**, *54*, 726–730. [[CrossRef](#)] [[PubMed](#)]
35. Lot, H.; Marrou, J.; Quiot, J.B.; Esvan, C. Contribution à l’étude du virus de la mosaïque du cocombre (CMV). I. Méthode de purification rapide du virus. *Annls. Phytopath.* **1972**, *4*, 25–38.
36. Grieco, F.; Alkowni, R.; Saponari, M.; Savino, V.; Martelli, G.P. Molecular detections of olive viruses. *EPPO Bull.* **2000**, *30*, 469–473. [[CrossRef](#)]
37. Piazzolla, P.; Guantieri, V.; Tamburro, A.M. Spectroscopic studies on purified particles and isolated RNA of cucumber mosaic virus. *J. Gen. Virol.* **1986**, *67*, 69–74. [[CrossRef](#)]

## Article

# Ecological Features and Conservation of *Urtica rupestris* Guss. (Urticaceae): A Narrow Endemic Species of Sicily

Saverio Sciandrello <sup>1,\*</sup>, Salvatore Cambria <sup>1</sup>, Gianpietro Giusso del Galdo <sup>1</sup>, Pietro Minissale <sup>1</sup>, Marta Puglisi <sup>1</sup>, Gianmarco Tavilla <sup>1,\*</sup> and Valeria Tomaselli <sup>2</sup>

<sup>1</sup> Department of Biological, Geological and Environmental Sciences, University of Catania, Via A. Longo 19, 95125 Catania, Italy

<sup>2</sup> Department of Biosciences, Biotechnologies and Environment, University of Bari “Aldo Moro”, Via Orabona 4, 70125 Bari, Italy

\* Correspondence: s.sciandrello@unict.it (S.S.); gianmarco.tavilla@phd.unict.it (G.T.)

**Abstract:** The conservation actions of endangered plant species require a clear knowledge of their habitats. *Urtica rupestris* Guss. (Urticaceae) is a rare endemic plant species occurring on shady cliffs in the southern-eastern part of Sicily. In the last century, the extreme anthropogenic alterations of Hyblaean plateau have caused the continuous and unrestrained fragmentation of natural habitats and consequently the reduction and disappearance of some plant species. A total of 52 vegetation plots, of which 34 are unpublished, were analyzed in order to characterize the floristic composition of the *U. rupestris* community. All the relevés were classified using classification and ordination methods. The species is mainly linked to shady and wet rock habitats, and only secondarily colonizes the undergrowth shrubs. According to IUCN criteria, we propose a new risk status for this species and the establishment of a new habitat (92/43CEE) for correct long-term conservation. Finally, a new association, *Urtico rupestris-Adiantetum capilli-veneris*, which falls within the *Polysticho setiferi-Phyllitidion scolopendrii* alliance (*Adiantetea capilli-veneris* class), was described. This study can provide useful information for the management and conservation of *U. rupestris*.

**Keywords:** *Adiantetea capilli-veneris*; conservation; demographic analysis; ecology; IUCN; plant conservation; phytosociology; rupicolous habitat

**Citation:** Sciandrello, S.; Cambria, S.; Giusso del Galdo, G.; Minissale, P.; Puglisi, M.; Tavilla, G.; Tomaselli, V. Ecological Features and Conservation of *Urtica rupestris* Guss. (Urticaceae): A Narrow Endemic Species of Sicily. *Plants* **2023**, *12*, 164. <https://doi.org/10.3390/plants12010164>

Academic Editors: Milan S. Stankovic, Paula Baptista and Petronia Carillo

Received: 24 November 2022

Revised: 23 December 2022

Accepted: 26 December 2022

Published: 29 December 2022



**Copyright:** © 2022 by the authors. Licensee MDPI, Basel, Switzerland. This article is an open access article distributed under the terms and conditions of the Creative Commons Attribution (CC BY) license (<https://creativecommons.org/licenses/by/4.0/>).

## 1. Introduction

Defining effective plant conservation strategies has become a crucial issue in the Mediterranean area due to strong human pressure on the natural landscape, which has led to the loss of habitats and some endemic plant species [1,2]. Sicily is one of the most important centers of plant diversity in the Mediterranean region, with many habitats included in Annex I of the Habitat Directive [3–9]. The importance of the vascular flora of Sicily lies not only in the total number of taxa (2763 species according to Bartolucci et al. [10]), but also in the considerable number of endemic species (400 species according to Peruzzi et al. [11]). In particular, the south-eastern sector of the island (Hyblaean territory), despite relatively low altitudes, hosts an extraordinary floristic richness and several plant communities, as well as many habitat types [12–14]. This high biological variety is due to the great geological, geomorphological, and bioclimatic complexity of the Hyblaean territory. In this area, several rare and narrow endemic species grow, such as *Zelkova sicula* Di Pasq., Garfi & Quézel, *Trachelium caeruleum* L. subsp. *lanceolatum* (Guss.) Ar-cang., *Anthemis pignattiorum* Guarino, Raimondo & Domina, *Limonium syracusanum* Brullo, *L. pachynense* Brullo, *L. pavonianum* Brullo, *Ferulago nodosa* (L.) Boiss. subsp. *geniculata* (Guss.) Troia & Raimondo, *Myosotis tineoi* C.Brullo & Brullo, *Epipactis hyblaica* Brullo & Zimmitti, and *Solenopsis laurentia* (L.) C.Presl. subsp. *hyblaica* Brullo et al. [15–17]. In the list of endemic species of the Hyblean territory, there is also *Urtica rupestris*, which shows some

affinities (*morifolia*-clade) with *U. morifolia* Poir. (Macaronesian Islands) and a strong similarity with *U. fragilis* J.Thiébaud (Syria, SE Turkey, Lebanon) [18]. *Urtica rupestris*, exclusive to the southern-eastern part of Sicily, is an Urticaceae woody nettle species that grows on the shady cliffs of the Hyblaean district. It was listed in the Red Book of Italian flora [19,20] as a vulnerable species (VU). The aim of our research was to study the scattered surviving *U. rupestris* population, in particular, analyzing the floristic composition, identifying the ecological requirements, and re-evaluating the conservation status at a regional level. Moreover, we propose the establishment of a new habitat type according to the European Directive 92/43CEE in order to achieve long-term conservation of the species.

## 2. Results and Discussion

### 2.1. Description of the Species (Based on our Specimens Collected in Monello and Palombara Localities)

Based on our morphological investigations of *Urtica rupestris*, we report below an updated and more detailed description of the species than those available in the literature.

*Urtica rupestris* Guss., Cat. Pl. Hort. Boccadifalco: 83(–84). 1821. Type (lectotype designated by Corsi et al. [21]: 218) “Militello di Val di Noto nel vallone detto il Carcarone. *Ad rupes vulcanicas in umbrosis vallibus, Aprili. Majo*”. (Herb. Guss. NAP).

The species is an erect, perennial, rhizomatous herb 0.3–0.8(–1.0 m) that is woody at the base and forms a perennial root with many unbranched stems. The plants are mostly dioecious and sometimes monoecious. The plant has a very sparse cover of erect stinging hairs that are 0.9–1.2 mm long, with a pluricellular straight base and a ca. 1/3–1/2 of the overall length of the seta. It is subglabrous with scattered, simple trichomes that are 0.1–0.4 mm long. The leaf lamina are 50–100 × 30–50 Mm ovate-acuminate, cuneate, or truncate at the base. The surface is poorly pubescent with short simple trichomes that are 0.1–0.5 mm long and has very few stinging hairs. The margins are coarsely and regularly serrate, with 8–9 teeth on each side. These teeth are 5–7 mm long and are usually undivided. The leaves are opposite and are deciduous with an apex acute to acuminate. The stipules are free (4 per node) and 3–4 mm long. The petioles are 25–45 mm long. The leaves are thin, dark green, and shiny on the upper side and lighter green on the lower leaf page. The racemes are unisexual. The plant has staminate flowers with tepals that are 0.6–0.8 mm long and pistillate flowers with tepals that are 1–1.2 mm long, which are sparsely pubescent. The female inflorescence is 8–18 mm long and is shorter than the subtending petiole, patent, or pendent in fruit. The male inflorescence is 20–40 mm long and is erecto-patent. The female flowers have subglabrous perianth segments. The mature fruit has tepals of 1.2–1.3 mm long and are achenes ovoid, wrinkled, and 1.2–1.3 × 0.8–0.9 mm.

Chromosome number: 2n = 26 according to Corsi et al. [21].

### 2.2. Ecological Data and Habitat Analysis

*Urtica rupestris* is a hemicryptophyte scapose, is rhizomatous, and flowers between April and June. It grows on shady cliffs exclusively in the Hyblaean district (south-eastern Sicily), mainly on carbonate rocks and sporadically on volcanic outcrops (Figure 1), although the specimens used to describe the plant species were collected on the volcanic substrates of Calcarone valley near Militello (Type: *Militello di Val di Noto nel vallone detto il Carcarone. Ad rupes vulcanicas in umbrosis vallibus, Aprili. Majo*) [21]. The species thrives within valleys that mainly comprise evergreen woodlands dominated by *Quercus ilex* L., of fluvial tectonic origin, with steep slopes. They are locally named “Cave”. It is a member of the highly specialized shady rupicolous community that is rich in bryophytes and pteridophytes and grows in the water dripping crevices of calcareous rocks. It only secondarily colonizes the *Rubus ulmifolius* shrubs (*Scutellario-Urticetum rupestris* Brullo, Minissale, Scelsi, and Spampinato 1993), and in the presence of rock outcrops, also the *Quercus ilex* woods (*Ostryo-Quercetum ilicis* Lapraz 1975, *Doronico-Quercetum ilicis* Barbagallo, Brullo, & Fagotto 1979, *Pistacio-Quercetum ilicis* Brullo & Marcenò 1985), as well as the rare *Laurus nobilis* communities of the *Hedero helicis-Lauretum nobilis* Bueno & Pri-

eto 1991 [22]. Considering the high phytogeographic value of *U. rupestris* and the remarkable naturalistic value of its habitat, as well as its vulnerability, we propose the inclusion of this habitat with the name “Shady wet cliffs (*Adiantetea capilli-veneris*)”, as a new habitat type in Annex I of the Habitat Directive. This shady and wet habitat, with high edaphic humidity, includes the dripping cliffs/walls of the Mediterranean areas that are characterized by chomophytic and chasmophytic vegetation (edaphohygrophylous) related to the *Adiantetea capilli-veneris* class. In the Mediterranean area, this class includes one order and three alliances [23]. In particular, the alliance *Adiantion capilli-veneris* groups plant communities dominated by *Adiantum capillus-veneris* L., which are particularly rich in bryophytes that grow on siliceous or calcareous dripping cliffs. The second one, *Pinguiculion longifoliae*, includes a relict herb-rich chomophytic vegetation of shaded and water-splashed habitats that are dominated by *Pinguicula* L. sp. pl., whereas the *Polysticho setiferi-Phyllitidion scolopendri* groups the fern-rich communities of damp walls and narrow and shady ravines. This shady, wet, and rocky habitat type is characterized by the occurrence of many ferns (*Adiantum capillus-veneris*, *Struthiopteris spicant* (L.) Weiss, *Pteris vittata* L., *Pteris cretica* L., *Osmunda regalis* L., *Asplenium scolopendrium* L. subsp. *scolopendrium*, and *Woodwardia radicans* (L.) Sm.), bryophytes (*Eucladium verticillatum* (Brid.) Bruch & Schimp., *Didymodon tophaceus* (Brid.) Lisa, *Pellia endiviifolia* (Dicks.) Dumort., *Conocephalum conicum* (L.) Dumort., and *Palustriella commutata* (Hedw.) Ochyra), and vascular plants (*Urtica rupestris*, *Cymbalaria pubescens* (C.Presl) Cufod., *Hypericum hircinum* L. subsp. *hircinum*, *Hypericum androsaemum* L., and *Samolus valerandi* L., etc.). As such, this vegetation type is typically found under the Mediterranean macrobioclimate, and occasionally under the sub-Mediterranean variant of the temperate macrobioclimate [24,25]. In Italy, it has been observed in the southern part of the peninsula and in the main islands, as well as in the coastal and sub-coastal areas of the central-northern part of the country [26–30]. These fern-rich plant communities, on thicker and water-rich soils, often come into catenal contact with the phytocoenoses that are dominated by bryophytes of the *Cratoneurion commutati* alliance, including in the Habitat 7220\* “Petrifying springs with tufa formation (Cratoneurion)”. The need for a specific habitat type concerning shady dripping cliffs with communities dominated by bryophytes and pteridophytes that belong to the *Adiantetea capilli-veneris* class (shady dripping cliffs with *Woodwardia radicans* and other large ferns) has already been highlighted by Spampinato [31], as well as recently by Guarino et al. [32] and Sciandrello et al. [33]. This proposed Mediterranean dripping cliff habitat includes sciaphilous-hygrophilous communities, in which the density of pteridophytes and bryophytes is high, and rare or endangered ferns of remarkable phytogeographic interest, such as *Woodwardia radicans*, *Osmunda regalis*, *Pteris vittata*, *Pteris cretica*, and *Asplenium scolopendrium* subsp. *scolopendrium*.

### 2.3. Phytosociological Insights

The cluster and ordination analysis of all the relevés (52 rel. × 72 sp.) carried out in the Hyblaean territory showed two main groups (Table S1, Appendix A, Figures 2 and 3). The first group (cluster A) includes the shady rupicolous vegetation of the *Adiantetea capilli-veneris* class (20rel. × 46sp.), whereas the second (cluster B) group (32rel. × 56sp.) includes the thermophilous scrub vegetation of the *Scutellario-Urticetum rupestris* (*Pruno spinosae-Rubion ulmifolii* alliance, *Crataego-Prunetea* class). In this last association, *U. rupestris*, together with *Scutellaria rubicunda* Hornem., was indicated by Brullo et al. [34] as a characteristic species for the Hyblaean territory [35]. It is a nemoral and sciaphilous association characterized by species belonging to the *Rhamno-Prunetea* class, such as *Rubus ulmifolius* Schott, *Smilax aspera* L., *Clematis cirrhosa* L., *C. vitalba* L., and *Crataegus monogyna* Jacq. This phytocoenosis is essentially localized in the thermo-mesophilous woods of the *Doronico-Quercetum ilicis*, *Ostryo-Quercetum ilicis*, and *Pistacio-Quercetum ilicis*. Most species of this phytocoenosis belong to the Mediterranean element (45%), with the dominant life form corresponding to phanerophytes/nanophanerophytes (34%) and hemicryptophytes (31%).

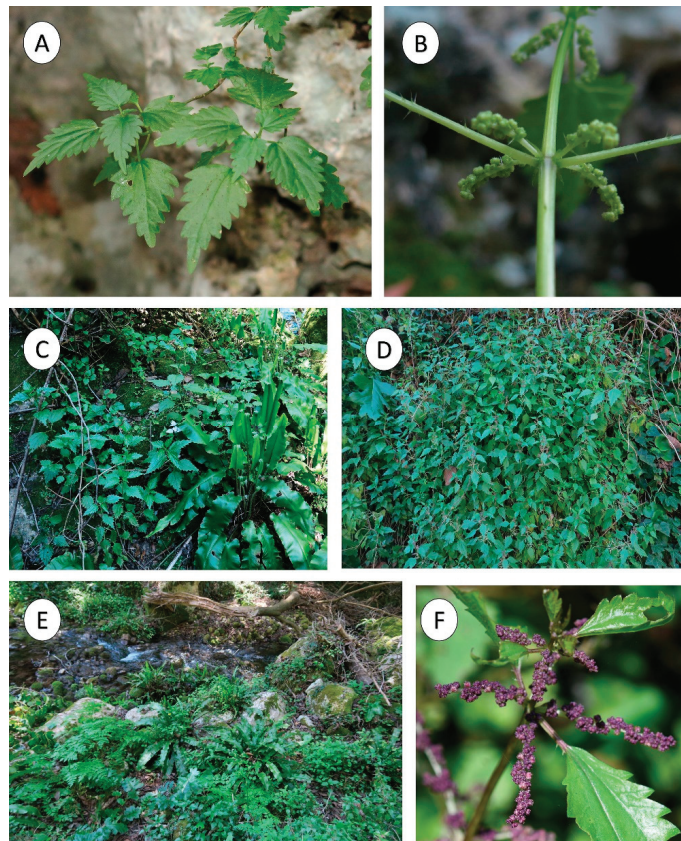


**Figure 1.** Some views of *Urtica rupestris*. (A) On a limestone cliff; (B) Female inflorescence; (C) *Urtica rupestris* with *Asplenium scolopendrium* from Cava Bibbinello (Syracuse); (D) Undergrowth plant from Anapo valley (Syracuse); (E) *Urtica rupestris*-*Adiantum capillus-veneris* from Cava Bibbinello (Syracuse); (F) Male inflorescence.

Cluster A includes perennial vegetation growing mainly on dripping vertical limestone cliffs and shady ravines, which are humid for most of the year, in the shade of wooded formations that are dominated by *Quercus ilex* within the Hyblaeen caves. The structure of the community is determined by *U. rupestris*, together with several hygrophilous species of bryophytes and pteridophytes, such as *Pellia endiviifolia*, *Thamnobryum alopecurum* (Hedw.) Gangulee, *Asplenium scolopendrium* subsp. *scolopendrium*, *Dryopteris filix-mas* (L.) Schott, and *Adiantum capillus-veneris*, *Asplenium sagittatum* (DC.) Bange. Moreover, this vegetation is enriched with several lianose species, such as *Hedera helix* L., *Rubia peregrina* L., *Dioscorea communis* (L.) Caddick & Wilkin, *Clematis vitalba*, and *Aristolochia sempervirens* L. Due to its ecological features, *U. rupestris* has been proposed as a characteristic species of a new association named *Urtica rupestris*-*Adiantum capillus-veneris* ass. nova hoc loco (\* holotypus: Table 1, Rel. 10) within the *Polysticho setiferi*-*Phyllitidion scolopendrii* alliance (*Adiantetea capilli-veneris* class, Appendix B). From a chorological and structural viewpoint, this vegetation highlights the relevance of this species with a Mediterranean distribution (29%), with hemicryptophytes (53%) being the dominant life forms. This new association shows floristic-ecological affinities with *Thamnobryo alopecuri*-*Phyllitidetum scolopendrium* Brullo, Privitera & Puglisi 1993, which have been described for southern Italy and Sicily [27]. Furthermore, it shows edaphic-ecological characteristics similar to *Conocephalo conici-*

*Woodwardietum radicans* Brullo, Lo Giudice, & Privitera 1989, *Adiantum capilli veneris-Pteridetum vittatae* Brullo, Lo Giudice & Privitera 1989, *Adiantum capilli veneris-Osmundetum regalis* Brullo, Lo Giudice & Privitera 1989. These chasmo-comophytic associations are rich in bryophytes and pteridophytes of shady/humid cliffs, which were described for the Peloritani Mountains in the north-eastern sector of Sicily [26]. From a bioclimatic point view, the *Urtico rupestris-Adiantum capilli-veneris* falls within the upper Thermomediterranean and lower Mesomediterranean belts with lower dry and upper ombrotypes [36].

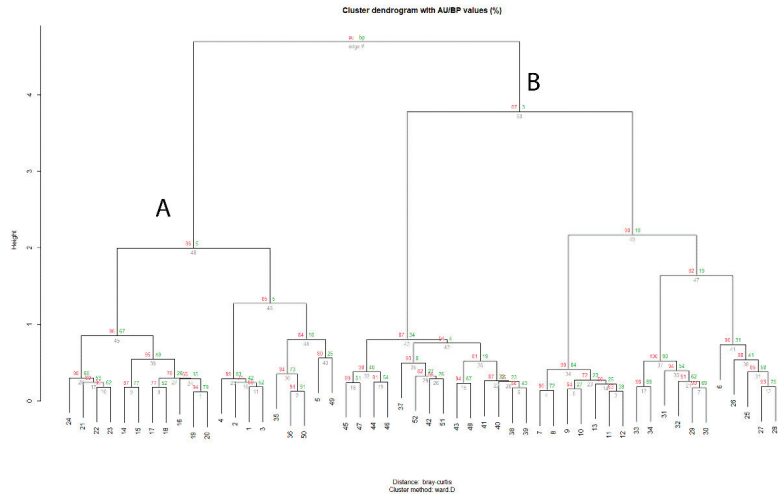


**Figure 2.** Dendrogram resulting from the cluster analysis (Cophenetic correlation = 0.808) of the surveyed plant communities: (A). *Urtico rupestris-Adiantum capilli-veneris*; (B). *Scutellario-Urticetum rupestris*. Approximately unbiased (AU—values printed in red) and bootstrap probability (BP—values printed in green) *p*-values are shown next to the nodes.

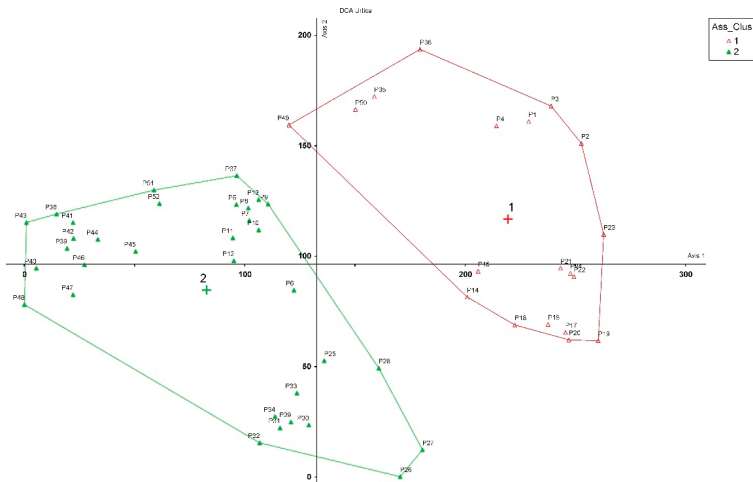


**Figure 3.** Ordination scatter diagram (DCA). Total variance (‘inertia’) in the species data: 2.1536. The *r*<sup>2</sup> value of axis 1 is (Eig = 0.44982) and the *r*<sup>2</sup> value of axis 2 is (Eig = 0.15224). Plant communities: 1. *Urtico rupestris-Adiantum capilli-veneris*; 2. *Scutellario-Urticetum rupestris*.

**Table 1.** *Urtica rupestris-Adiantetum capilli-venensis* ass. nova hoc loco. Phytosociological relevés of the plant community investigated. The symbol \* display the holotypus.

Chorotype	Life form	Floristic richness	Cluster number																		Presence																												
			1	2	3	4	5	6	7	8	9	10	11	12	13	14	15	16	17	18		19	20	21	22	23	24	25	26	27	28	29	30	31	32	33	34	35	36	37	38	39	40	41	42	43	44	45	46
			20	14	18	16	10	20	20	22	16	19	15	16	22	22	16	19	15	16	22	22	16	22	20	21	10	12	10	11	11	320																	
			341	345	351	355	140	461	461	460	465	465	465	465	465	465	465	465	465	465	465	465	465	465	465	465	464	320	320	320	320																		
			45	35	30	35	85	90	80	80	75	90	90	20	70	80	80	70	80	80	70	80	80	70	80	70	80	60	80	100																			
			N	N	N	N	N	N	N	-	NE	NE	-	NE	-	-	-	-	-	-	-	-	-	-	-	-	-	-	-	-	-																		
			85	80	85	95	35	90	85	16	16	16	16	16	16	16	16	16	16	16	16	16	16	16	16	16	16	16	16	16	16																		
			16	16	16	16	16	16	16	16	16	16	16	16	16	16	16	16	16	16	16	16	16	16	16	16	16	16	16	16	16	16																	
			1	2	3	4	5	6	7	8	9	10	11	12	13	14	15	16	17	18	19	20	21	22	23	24	25	26	27	28	29																		
			1	2	3	4	5	6	7	8	9	10	11	12	13	14	15	16	17	18	19	20	21	22	23	24	25	26	27	28	29																		
			1	2	3	4	5	6	7	8	9	10	11	12	13	14	15	16	17	18	19	20	21	22	23	24	25	26	27	28	29																		
			1	2	3	4	5	6	7	8	9	10	11	12	13	14	15	16	17	18	19	20	21	22	23	24	25	26	27	28	29																		
			1	2	3	4	5	6	7	8	9	10	11	12	13	14	15	16	17	18	19	20	21	22	23	24	25	26	27	28	29																		
			1	2	3	4	5	6	7	8	9	10	11	12	13	14	15	16	17	18	19	20	21	22	23	24	25	26	27	28	29																		
			1	2	3	4	5	6	7	8	9	10	11	12	13	14	15	16	17	18	19	20	21	22	23	24	25	26	27	28	29																		
			1	2	3	4	5	6	7	8	9	10	11	12	13	14	15	16	17	18	19	20	21	22	23	24	25	26	27	28	29																		
			1	2	3	4	5	6	7	8	9	10	11	12	13	14	15	16	17	18	19	20	21	22	23	24	25	26	27	28	29																		
			1	2	3	4	5	6	7	8	9	10	11	12	13	14	15	16	17	18	19	20	21	22	23	24	25	26	27	28	29																		
			1	2	3	4	5	6	7	8	9	10	11	12	13	14	15	16	17	18	19	20	21	22	23	24	25	26	27	28	29																		
			1	2	3	4	5	6	7	8	9	10	11	12	13	14	15	16	17	18	19	20	21	22	23	24	25	26	27	28	29																		
			1	2	3	4	5	6	7	8	9	10	11	12	13	14	15	16	17	18	19	20	21	22	23	24	25	26	27	28	29																		
			1	2	3	4	5	6	7	8	9	10	11	12	13	14	15	16	17	18	19	20	21	22	23	24	25	26	27	28	29																		
			1	2	3	4	5	6	7	8	9	10	11	12	13	14	15	16	17	18	19	20	21	22	23	24	25	26	27	28	29																		
			1	2	3	4	5	6	7	8	9	10	11	12	13	14	15	16	17	18	19	20	21	22	23	24	25	26	27	28	29																		
			1	2	3	4	5	6	7	8	9	10	11	12	13	14	15	16	17	18	19	20	21	22	23	24	25	26	27	28	29																		
			1	2	3	4	5	6	7	8	9	10	11	12	13	14	15	16	17	18	19	20	21	22	23	24	25	26	27	28	29																		
			1	2	3	4	5	6	7	8	9	10	11	12	13	14	15	16	17	18	19	20	21	22	23	24	25	26	27	28	29																		
			1	2	3	4	5	6	7	8	9	10	11	12	13	14	15	16	17	18	19	20	21	22	23	24	25	26	27	28	29																		
			1	2	3	4	5	6	7	8	9	10	11	12	13	14	15	16	17	18	19	20	21	22	23	24	25	26	27	28	29																		
			1	2	3	4	5	6	7	8	9	10	11	12	13	14	15	16	17	18	19	20	21	22	23	24	25	26	27	28	29																		
			1	2	3	4	5	6	7	8	9	10	11	12	13	14	15	16	17	18	19	20	21	22	23	24	25	26	27	28	29																		
			1	2	3	4	5	6	7	8	9	10	11	12	13	14	15	16	17	18	19	20	21	22	23	24	25	26	27	28	29																		
			1	2	3	4	5	6	7	8	9	10	11	12	13	14	15	16	17	18	19	20	21	22	23	24	25	26	27	28	29																		
			1	2	3	4	5	6	7	8	9	10	11	12	13	14	15	16	17	18	19	20	21	22	23	24	25	26	27	28	29																		
			1	2	3	4	5	6	7	8	9	10	11	12	13	14	15	16	17	18	19	20	21	22	23	24	25	26	27	28	29																		
			1	2	3	4	5	6	7	8	9	10	11	12	13	14	15	16	17	18	19	20	21	22	23	24	25	26	27	28	29																		
			1	2	3	4	5	6	7	8	9	10	11	12	13	14	15	16	17	18	19	20	21	22	23	24	25	26	27	28	29																		
			1	2	3	4	5	6	7	8	9	10	11	12	13	14	15	16	17	18	19	20	21	22	23	24	25	26	27	28	29																		
			1	2	3	4	5	6	7	8	9	10	11	12	13	14	15	16	17	18	19	20	21	22	23	24	25	26	27	28	29																		
			1	2	3	4	5	6	7	8	9	10	11	12	13	14	15	16	17	18	19	20	21	22	23	24	25	26	27	28	29																		
			1	2	3	4	5	6	7	8	9	10	11	12	13	14	15	16	17	18	19	20	21	22	23	24	25	26	27	28	29																		
			1	2	3	4	5	6	7	8	9	10	11	12	13	14	15	16	17	18	19	20	21	22	23	24	25	26	27	28	29																		
			1	2	3	4	5	6	7	8	9	10	11	12	13	14	15	16	17	18	19	20	21	22	23	24	25	26	27	28	29																		
			1	2	3	4	5	6	7	8	9	10	11	12	13	14	15	16	17	18	19	20	21	22	23	24	25	26	27	28	29																		
			1	2	3	4	5	6	7	8	9	10	11	12	13	14	15	16	17	18	19	20	21	22	23	24	25	26	27	28	29																		
			1	2	3	4	5	6	7	8	9	10	11	12	13	14	15	16	17	18	19	20	21	22	23	24	25	26	27	28	29																		
			1	2	3	4	5	6	7	8	9	10	11	12	13	14	15	16	17	18	19	20	21	22	23	24	25	26	27	28	29																		
			1	2	3	4	5	6	7	8	9	10	11	12	13	14	15	16	17	18	19	20	21	22	23	24	25	26	27	28	29																		
			1	2	3	4	5	6	7	8	9	10	11	12	13	14	15	16	17	18	19	20	21	22	23	24	25	26	27	28	29																		
			1	2	3	4	5	6	7	8	9	10	11	12	13	14	15	16	17	18	19	20	21	22	23	24	25	26	27	28	29																		
			1	2	3	4	5	6	7	8	9	10	11	12	13	14	15	16	17	18	19	20	21	22	23	24	25	26	27	28	29																		
			1	2	3	4	5	6	7	8	9	10	11	12	13	14	15	16	17	18	19	20	21	22	23	24	25	26	27	28	29																		
			1	2	3	4	5	6	7	8	9	10	11	12	13	14	15	16	17	18	19	20	21	22	23	24	25	26	27	28	29																		
			1	2	3	4	5	6	7	8	9	10	11	12	13	14	15	16	17	18	19	20	21	22	23	24	25	26	27	28	29																		
			1	2	3	4	5	6	7	8	9	10	11	12	13	14	15	16	17	18	19	20	21	22	23	24	25	26	27	28	29																		
			1	2	3	4	5	6	7	8	9	10	11	12	13	14	15	16	17	18	19	20	21	22	23	24	25	26	27	28	29																		
			1																																														



#### 2.4. Distribution and Conservation Status

Our investigations confirmed 13 sites with *U. rupestris* (Figure 4): 1. Vallone Carcarone—Militello (1 plot); 2. Torrente Belluzza—Villasmundo (1 plot, SAC-ITA090024); 3. Cava Sorciaro, Cava Mostringiano—Monti Climiti (3 plots, SAC-ITA090020); 4. Grotta Palombara—Siracusa (1 plot, SAC-ITA090012); 5. Grotta Monello—Siracusa (1 plot, SAC-ITA090011; 1 plot out of the SAC); 6. Vallone Caradonna—Canicattini Bagni (1 plot); 7. Cava Grande del Cassibile e Cava di Bauli, Manghisi (2 plots, SAC-ITA090007; 2 plots out of the SAC); 9. Cava del Prainito, Rosolini (1 plot, SAC-ITA080012); 10. Cava Grande, Valle dell’Anapo e Bibinello—Buscemi, Cassaro, Ferla, Palazzolo Acreide, Sortino (5 plots, SAC-ITA090009); 11. Sant’Andrea, Valle Cupa—Buccheri (1 plot, SAC-ITA090015); 12. Cava Rosolini (La Rosa A., Aprile. 2016) (1 plot); 13. Cava Bruccoli (Alicata I., 6.11.2016) (1 plot). The species was no longer found in two of the sites: first in Syracuse “*scendendo dal Belvedere a oriente verso il mare*” (Lojacono 1904) and second in “*Pantani Capo Passero*” (Lopriore 1900). In total, *U. rupestris* falls within 22 cells ( $2 \times 2$  km) and eight special areas of conservation (SAC), and outside of four Natura 2000 sites. The area hosting the largest number of individuals was the N2000 “Valle del Fiume Anapo, Cavagrande del Calcinara, Cugni di Sortino” (ITA090009) site. Currently, almost all *U. rupestris* sites are located in the Syracuse province, with the exception of the *locus classicus*, which falls within the Catania territory, and one in the Ragusa province. Despite the many records of the distribution of the species, *U. rupestris* is threatened by many factors that, over time, have altered and reduced its natural habitat. *Urtica rupestris* was listed in the Red Book of Italian plants [37] as lower risk (LR), which was subsequently reconsidered by Brullo et al. [13] as a vulnerable species (VU), and, more recently, has been classified as a vulnerable species [19,20]. Our accurate field surveys allowed us to have a deeper knowledge of the distribution and conservation status of *U. rupestris*. Considering our current assessments and observations in the field, the species is currently recorded in 22 cells in the Hyblaean territory. According to the reference grid for Italy [38] and the GeoCAT tool, based on the IUCN criterion B, we propose a new status for this species, which should be considered endangered (EN) B2ab (ii, iii). In fact, we assessed this using the GeoCAT web tool, and calculated an EOO area equal to 1880 km<sup>2</sup> and an AOO equal to 104 km<sup>2</sup>. This decline in the original population, because of habitat loss and fragmentation, suggests that this species could be classified as endangered (EN).

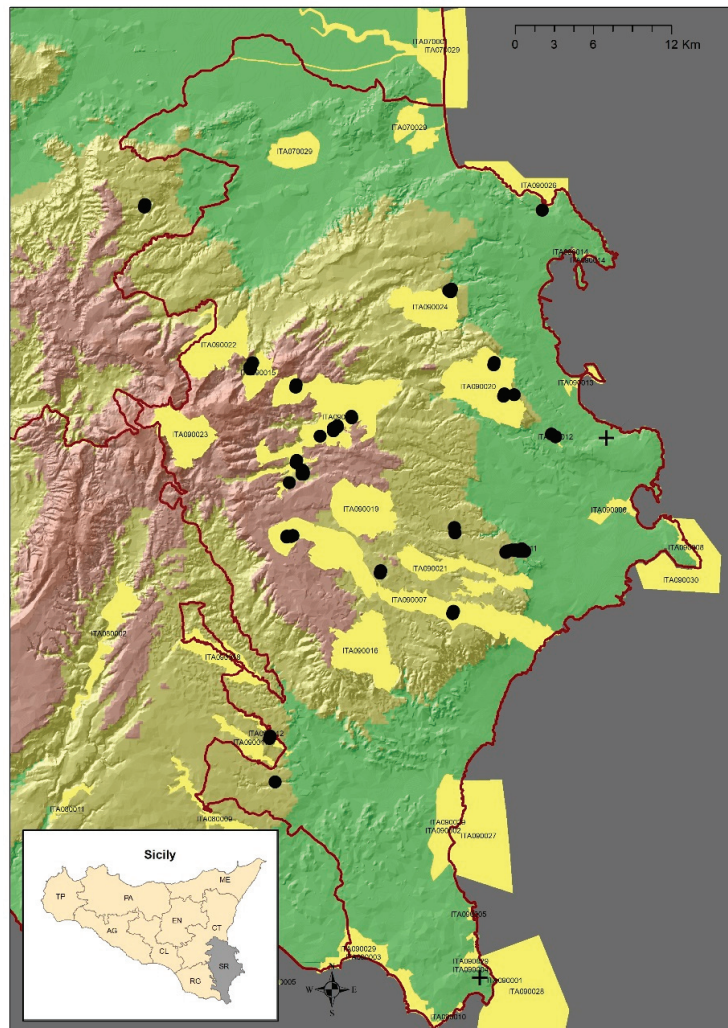


**Figure 4.** Geographical distribution of *Urtica rupestris* in Sicily. Black dot, current distribution; black cross, no longer recorded; yellow polygons, Special Areas Conservation.

### 3. Materials and Methods

Data in the literature regarding the distribution of this species were reviewed [39–43], and specimens of herbaria of Catania (CAT) and Palermo (PA) were also examined. Based on these starting data, all the sites in which *U. rupestris* has been reported were visited. In addition, other sites that were potentially suitable for the species were investigated. In order to analyze the floristic composition of the *U. rupestris* plant community in the Hyblaean territory, several field activities were carried out in the years between 2015 and 2020. A total of 52 relevés were collected, of which 34 were unpublished and 18 from bibliographic data [34,44,45]. The floristic composition and cover of the species in each plot were determined using the standard phytosociological method [46]. All the phytosociological relevés were processed using classification and ordination methods. The numerical analysis was performed using the software package “PCORD” 6.08 and R software. A multivariate analysis (linkage method: Ward’s, distance measure:

Bray–Curtis) was applied. Clustering was performed using the R package “pvclust” [47]. Pvcust computes *p*-values for each cluster’s uncertainty using bootstrap resampling. The bootstrap sample size was set to 1000. Detrended correspondence analyses (DCA) were utilized in order to develop a hypothesis about the vegetation/environmental interactions and to establish geographic patterns in the scatter-gram [48]. The DCA takes into account different quantitative data, such as the vegetation coverage (%), number of species (N. sp.), altitude (m a.s.l.), and slope (°). Quantum GIS software version 3.6 and GPS Garmin Montana were used to geolocalize the surveyed population. For the risk assessment at the regional scale (Sicily), we followed the IUCN protocol and the most recent guidelines for its application [49]. In particular, we applied the IUCN criterion B for estimating the trends in the Area of Occupancy (AOO) using the 2 × 2 km grid for the Italian territory proposed by Gargano [38]. On the other hand, in order to obtain an accurate assessment, we also calculated the Area of Occupancy (AOO, km<sup>2</sup>) and Extent of Occurrence (EOO) using the Geo-CAT web tool (Geospatial Conservation Assessment Tool) programme [50], which performs a rapid geospatial analysis of species in a simple way.

The identification of vascular plants was carried out according to Pignatti et al. [51–54], and the nomenclature follows the Portal to the Flora of Italy (<http://dryades.units.it/floritaly/> accessed on 15 October 2022) [55], whereas the nomenclature of bryophytes is in accordance with Cortini Pedrotti [56,57]. The syntaxonomical nomenclature follows Mucina et al. [58]. The bioclimatic units refer to Bazan et al. [36].

#### Study Area

The study area, located in the southeast of Sicily, is represented by the Hyblaean plateau which belongs to the African plate. It comprises of a crust of continental types different from that of the rest of Sicily [59], whereas, from a geophysicist standpoint, it is characterized by a strong gravimetric and magnetic anomaly (Bouguer anomalies) chiefly due to its composition. Outcropping successions in the Hyblaean plateau consist mostly of carbonate and carbonate-marly sediments ranging from Lower Cretaceous to Pleistocene, where basic volcanics of considerable power [60] are intercalated. One of the most typical landscapes of the Hyblaean area is the “Cave”, which are valleys of fluvial-tectonic origin, with a cross-section very similar to a V with steep slopes. Water courses flowing in the “Cave” usually have temporary arrangements or a permanent regime. Furthermore, the Hyblaean territory is characterized by the presence of very important coastal wetlands [61–64], as well as several rocky pools and temporary ponds that host very specialized vascular flora [65–69]. Blasi et al. [70] identified six important plant areas (IPAs) for the Hyblaean territory, which are essential for the conservation of plant biodiversity. Furthermore, the Hyblaean territory is affected by 43 special areas of conservation (SAC), and 9 regional protected areas. According to the bioclimatic classification proposed by Rivas-Martinez [71,72], the area under study is referred to as the Mediterranean pluviseasonal oceanic bioclimate, with thermotypes ranging from low thermomediterranean to supramediterranean, and ombrotypes from semiarid to lower humid.

#### 4. Conclusions

The ecological and phytosociological analyses carried out on *U. rupestris* in the Sicilian territory pointed out the biogeographical importance of this rupicolous species and of the shady dripping cliff habitat that deserves to be included in Annex I of the 93/42 EEC Directive. The re-assessment of the conservation status of this species (EN) highlights the urgent need to primarily preserve the habitats of the “Hyblaean Cave”, which hosts *U. rupestris* and several other restricted endemic species, such as *Zelkova sicula*, *Trachelium caeruleum* subsp. *lanceolatum*, *Anthemis pignattiorum*, *Limonium pachynense*, *L. pavonianum*, *Epipactis hyblaea*, etc. Therefore, the outcomes of this research can be included in future conservation and management strategies for this rare endemic taxon.

**Supplementary Materials:** The following are available online at <https://www.mdpi.com/article/10.3390/plants12010164/s1>, Table S1: Phytosociological relevés; Scheme S1: Old records and Specimina visa of *U. rupestris*.

**Author Contributions:** Conceptualization, S.S.; methodology, S.S. and G.T.; investigation, S.S., S.C., G.T., V.T., G.G.d.G., P.M. and M.P.; data curation, S.S. and G.T.; writing—original draft preparation, S.S. and G.T.; writing—review and editing, S.S., S.C., G.T., V.T., G.G.d.G., P.M. and M.P. All authors have read and agreed to the published version of the manuscript.

**Funding:** This research was financially supported by the research programme (PIA.CE.RI. 2020–2022 Line 2 cod. 22722132149 and Line 3 Starting Grant Progetto HAB-VEG cod. 22722132172) funded by the University of Catania, and by Convention with PIM within the project MedIsWet funded by the MAVA Foundation.

**Data Availability Statement:** Not applicable.

**Conflicts of Interest:** The authors declare no conflict of interest.

### Appendix A Localities and Dates of Relevés (Table 1)

Rel. 1, Cava Grande del Cassibile, 6.05.2014 (Minissale & Sciandrello); Rel. 2–4, Cava Grande del Cassibile, 09.06.2014 (Minissale & Sciandrello); Rel. 5, 07.04.2015, Villasmundo, Belluzza (Sciandrello); Rel. 6–15, Cava Bibinello, Palazzolo Acreide, 30.03.2021 (Cambria, Minissale, Sciandrello); Rel. 16–17, Pantalica (Minissale et al. 2007); Rel. 18–19, Pantalica (Brullo et al. 1993).

### Appendix B Syntaxonomical Scheme

*Adiantetea capilli-veneris* Br.-Bl. in Br.-Bl., Roussine & Negre 1952

*Adiantetalia capilli-veneris* Br.-Bl. ex Horvatic 1934

*Polysticho setiferi-Phyllitidion scolopendri* Ubaldi ex Ubaldi & Biondi in Biondi, Allegrezza, Casavecchia, Galdenzi, Gasparri, Pesaresi, Vagge & Blasi 2014

*Urtico rupestris-Adiantetum capilli-veneris* ass. nova hoc loco

*Crataego-Prunetea spinosae* R.Tx. 1962

*Pyro spinosae-Rubetalia ulmifolii* Biondi, Blasi & Casavecchia in Biondi et al. 2014

*Pruno spinosae-Rubion ulmifolii* O. Bolòs 1954

*Scutellario rubicundae-Urticetum rupestris* Brullo, Minissale, Scelsi & Spamp. 1993.

### References

- Schröter, D.; Cramer, W.; Leemans, R.; Prentice, I.C.; Araújo, M.B.; Arnell, N.W.; Bondeau, A.; Bugmann, H.; Carter, T.R.; Gracia, C.A.; et al. Ecosystem service supply and vulnerability to global change in Europe. *Science* **2005**, *310*, 1333–1337. [[CrossRef](#)] [[PubMed](#)]
- Tomaselli, V.; Tenerelli, P.; Sciandrello, S. Mapping and quantifying habitat fragmentation in small coastal areas: A case study of three protected wetlands in Apulia (Italy). *Environ. Monitor. Assessm.* **2012**, *184*, 693–713. [[CrossRef](#)] [[PubMed](#)]
- Médail, F.; Quézel, P. Hot-spots analysis for conservation of plant biodiversity in the Mediterranean Basin. *Ann. Mo. Bot. Gard.* **1997**, *84*, 112–127. [[CrossRef](#)]
- Médail, F.; Quézel, P. Biodiversity Hotspots in the Mediterranean Basin: Setting global conservation priorities. *Conserv. Biol.* **1999**, *13*, 1510–1513. [[CrossRef](#)]
- Sciandrello, S.; Guarino, R.; Minissale, P.; Spampinato, G. The endemic vascular flora of Peloritani Mountains (NE Sicily): Plant functional traits and phytogeographical relationships in the most isolated and fragmentary micro-plate of the Alpine orogeny. *Plant Biosyst.* **2015**, *149*, 838–854. [[CrossRef](#)]
- Sciandrello, S.; Cambria, S.; Giusso del Galdo, G.; Guarino, R.; Minissale, P.; Pasta, S.; Tavilla, G.; Cristaudo, A. Floristic and Vegetation Changes on a Small Mediterranean Island over the Last Century. *Plants* **2021**, *10*, 680. [[CrossRef](#)]
- Sciandrello, S.; Minissale, P.; Giusso del Galdo, G. Vascular plant species diversity of Mt. Etna (Sicily): Endemicity, insularity and spatial patterns along the altitudinal gradient of the highest active volcano in Europe. *PeerJ* **2020**, *8*, e9875. [[CrossRef](#)]
- Brullo, S.; Cambria, S.; Crisafulli, A.; Tavilla, G.; Sciandrello, S. Taxonomic remarks on the *Centaurea aeolica* (Asteraceae) species complex. *Phytotaxa* **2021**, *483*, 9–24. [[CrossRef](#)]
- Tavilla, G.; Angiolini, C.; Bagella, S.; Bonini, F.; Cambria, S.; Caria, M.C.; Esposito, A.; Fanfarillo, E.; Ferri, V.; Fiaschi, T.; et al. New national and regional Annex I Habitat records: From #37 to #44. *Plant Sociol.* **2022**, *59*, 49–66. [[CrossRef](#)]

10. Bartolucci, F.; Peruzzi, L.; Galasso, G.; Albano, A.; Alessandrini, A.; Ardenghi, N.M.G.; Astuti, G.; Bacchetta, G.; Ballelli, S.; Banfi, E.; et al. An updated checklist of the vascular flora native to Italy. *Plant Biosyst.* **2018**, *152*, 179–303. [CrossRef]
11. Peruzzi, L.; Conti, F.; Bartolucci, F. An inventory of vascular plants endemic to Italy. *Phytotaxa* **2014**, *168*, 1–75. [CrossRef]
12. Brullo, S.; Grillo, M.; Guglielmo, A. Considerazioni fitogeografiche sulla flora iblea. *Boll. Acc. Sci. Nat.* **1998**, *29*, 45–111.
13. Brullo, C.; Minissale, P.; Sciandrello, S.; Spampinato, G. Phytogeographic survey on the endemic vascular flora of the Hyblaean territory (SE Sicily-Italy). *Acta Bot. Gall.* **2011**, *158*, 617–631. [CrossRef]
14. Pavone, P.; Spampinato, G.; Tomaselli, V.; Sciandrello, S.; Ronsisvalle, F. Map of the habitats of the EEC Directive 92/43 in the biotopes of the Syracuse province (eastern Sicily). *Fitosociologia* **2007**, *44*, 183–193.
15. Garfi, G.; Carimi, F.; Pasta, S.; Rühl, J.; Trigila, S. Additional insights on the ecology of the relic tree *Zelkova sicula* Di Pasquale, Garfi & Quézel (Ulmaceae) after the finding of a new population. *Flora* **2011**, *206*, 407–417.
16. Guarino, R.; Raimondo, F.M.; Domina, G. A new species of *Anthemis* sect. *Hiorthia* (Asteraceae) from SE Sicily. *Plant Biosyst.* **2013**, *147*, 821–825. [CrossRef]
17. Brullo, S.; Brullo, C.; Sciandrello, S.; Tavilla, G.; Cambria, S.; Tomaselli, V.; Ilardi, V.; Giusso Del Galdo, G.; Minissale, P. The Plant Communities of the Class *Isoëto-Nanojuncetea* in Sicily. *Plants* **2022**, *11*, 1214. [CrossRef]
18. Grosse-Veldmann, B.; Nürk, N.M.; Smissen, R.; Breitwieser, I.; Quandt, D.; Weigend, M. Pulling the sting out of nettle systematics—A comprehensive phylogeny of the genus *Urtica* L. (Urticaceae). *Mol. Phylogenet. Evol.* **2016**, *102*, 9–19. [CrossRef]
19. Rossi, G.; Orsenigo, S.; Gargano, D.; Montagnani, C.; Peruzzi, L.; Fenu, G.; Abeli, T.; Alessandrini, A.; Astuti, G.; Bacchetta, G.; et al. *Lista Rossa Della Flora Italiana. 2 Endemiti e Altre Specie Minacciate*; Ministero dell’Ambiente e della Tutela del Territorio e del Mare, 2020; Available online: <https://http://www.iucn.it/pdf/LISTAROSSAvol-2-FLORAITALIANA.pdf> (accessed on 24 October 2022).
20. Orsenigo, S.; Fenu, G.; Gargano, D.; Montagnani, C.; Abeli, T.; Alessandrini, A.; Bacchetta, G.; Bartolucci, F.; Carta, A.; Castello, M.; et al. Red list of threatened vascular plants in Italy. *Plant Biosyst.* **2021**, *155*, 310–335. [CrossRef]
21. Corsi, G.; Garbari, F.; Maffei, F. Il genere *Urtica* L. (Urticaceae) in Italia. Revisione biosistemica. *Webbia* **1999**, *53*, 193–239. [CrossRef]
22. Brullo, S.; Costanzo, E.; Tomaselli, V. Étude phytosociologique sur les formations à *Laurus nobilis* L. dans le Monts Iblei (Sicile sud-orientale). *Phytocoenologia* **2001**, *31*, 249–270. [CrossRef]
23. Foucault, B. Contribution au prodrome des végétations de France: Les *Adiantetea capilli-veneris* Braun-Blanq. ex Braun-Blanq., Roussine & Nègre 1952. *Acta Bot. Gall.* **2015**, *162*, 375–403.
24. Biondi, E.; Blasi, C.; Allegrezza, M.; Anzellotti, I.; Azzella, M.M.; Carli, E.; Casavecchia, S.; Copiz, R.; Del Vico, E.; Facioni, L.; et al. Plant communities of Italy: The Vegetation Prodrome. *Plant Biosyst.* **2014**, *148*, 728–814. [CrossRef]
25. Biondi, E.; Allegrezza, M.; Casavecchia, S.; Galdenzi, D.; Gasparri, R.; Pesaresi, S.; Vagge, I.; Blasi, C. New and validated syntaxa for the checklist of Italian vegetation. *Plant Biosyst.* **2014**, *148*, 318–332. [CrossRef]
26. Brullo, S.; Lo Giudice, R.; Privitera, M. La classe *Adiantetea* in Sicilia. *Arch. Bot. Ital.* **1989**, *65*, 81–99.
27. Brullo, S.; Privitera, P.; Puglisi, M. *Thamnobryo alopecuri-Phyllitidum scolopendrium* nuova associazione centro-mediterranea della classe *Adiantetea*. *Arch. Bot. Ital.* **1993**, *68*, 35–43.
28. Brullo, S.; Scelsi, F.; Spampinato, G. *La Vegetazione dell’Aspromonte*. *Studio Fitosociologico*; Laruffa Editore: Reggio Calabria, Italy, 2001; pp. 525–774.
29. Cortini Pedrotti, C. Associations de la classe *Adiantetea* dans quelques grottes de la gorge de Frasassi. Guide-Itinéraire. Excursion Internationale de Phytosociologie en Italie centrale (2-11 juillet 1982). *Univ. Di Camerino* **1982**, 201–207.
30. Puglisi, M. *Homalio lusitanicae-Adiantetum*, nuova associazione della classe *Adiantetea* Br.-Bl. 1947. *Boll. Acc. Gioenia Sci. Nat.* **1994**, *27*, 93–98.
31. Spampinato, G. Rupi Stillicidiose Mediterranee dell’*Adiantum*: Nuovo habitat proposto per l’inserimento nell’allegato i della Direttiva (92/43CEE). In *Specie e Habitat di Interesse Comunitario in Italia: Distribuzione, Stato di Conservazione e Trend*; Genovesi, P., Angelini, P., Bianchi, E., Dupré, E., Ercole, S., Giacanelli, V., Ronchi, F., Stoch, F., Eds.; Serie Rapporti, 194/201; ISPRA: Rome, Italy, 2014; pp. 276–279.
32. Guarino, R.; Pasta, S.; Bazan, G.; Crisafulli, A.; Caldarella, O.; Giusso del Galdo, G.; Silvestre Gristina, A.; Ilardi, V.; La Mantia, A.; Marcenò, C.; et al. Relevant habitats neglected by the Directive 92/43 EEC: The contribution of Vegetation Science for their reappraisal in Sicily. *Plant Sociol.* **2021**, *58*, 49–63. [CrossRef]
33. Sciandrello, S.; Cambria, S.; Crisafulli, A.; Giusso del Galdo, G.; Minissale, P.; Musarella, C.M.; Puglisi, M.; Tavilla, G.; Tomaselli, V.; Spampinato, G. A new habitat of the shady wet cliffs (*Adiantetea capilli-veneris*) of the Mediterranean region. In Proceedings of the 54th SISV Congress, Twenty years in the third millennium with Vegetation Science, Online, 28–29 September 2021.
34. Brullo, S.; Minissale, P.; Scelsi, F.; Spampinato, G. Note fitosociologiche miscellanee sul territorio ibleo (Sicilia sud-orientale). *Boll. Accad. Gioenia Sci. Nat.* **1993**, *26*, 19–48.
35. Bartolo, G.; Brullo, S.; Fichera, G.; Scelsi, F. Osservazioni fitosociologiche sulla vegetazione a *Urtica rupestris* Guss. del territorio ibleo (Sicilia sudorientale). *Giorn. Bot. Ital.* **1989**, *123*, 90.
36. Bazan, G.; Marino, P.; Guarino, R.; Domina, G.; Schicchi, R. Bioclimatology and vegetation series in Sicily: A geostatistical approach. *Ann. Bot. Fenn.* **2015**, *52*, 1–18. [CrossRef]

37. Conti, F.; Manzi, A.; Pedrotti, F. *Liste rosse Regionali delle Piante d'Italia*; WWF Italia, Società Botanica Italiana: Camerino, Italy, 1997; pp. 1–139.
38. Gargano, D. Proposta metodologica. Verso la realizzazione di nuove Liste Rosse della flora d'Italia: Una griglia standard per la misura dell'Area of Occupancy (AOO). *Inf. Bot. Ital.* **2011**, *43*, 455–456.
39. Giardina, G.; Raimondo, F.M.; Spadaro, V. A catalogue of plants growing in Sicily. *Boccone* **2007**, *20*, 5–582.
40. Gussone, J. *Catalogus Plantarum Quae Observantur in Regio Horto ser. Fr. Borbonii Principis Juventutis in Boccadifalco prope Panormum*; Typis Angeli Trani: Neapoli, Greece, 1821; pp. 1–84.
41. Gussone, J. *Florae Siculae Synopsis 2 (2)*; Ex Typis Tramater: Neapoli, Greece, 1845; pp. 525–774.
42. Lopriore, C. *Studi Comparativi Sulla Flora Lacustre Della Sicilia*; Tip. Sicula di Monaco & Mollica: Catania, Italy, 1900; pp. 1–116.
43. Lojacono Pojero, M. *Flora Sicula o Descrizione Delle Piante Vascolari Spontanee o Indigenate in Sicilia*; Tipo-Litografia Salvatore Bizzarri: Palermo, Italy, 1904; Volume 2, pp. 1–428.
44. Minissale, P.; Sciandrello, S.; Spampinato, G. Analisi della biodiversità vegetale e relativa cartografia della Riserva Naturale Orientata “Pantolica, Valle dell'Anapo e Torrente Cava Grande” (Sicilia sudorientale). *Quad. Bot. Amb. Appl.* **2007**, *18*, 241–303.
45. Zimmiti, A.; Ronsisvalle, F.B.F.; Ronsisvalle, G.A. Aree di interesse naturalistico per la rete ecologica dei M.ti Iblei (Sicilia sud-orientale): Il territorio dei Monti Climiti. *Quad. Bot. Amb. Appl.* **2007**, *8*, 319–342.
46. Braun-Blanquet, J. *Pflanzensoziologie. Grundzüge der Vegetationskunde*, 3rd ed.; Springer: Wien, Austria, 1964; pp. 1–330.
47. Suzuki, R.; Shimodaira, H. Pvclust: An R package for assessing the uncertainty in hierarchical clustering. *Bioinformatics* **2006**, *22*, 1540–1542. [[CrossRef](#)]
48. Hill, M.O.; Gauch, H.G. Detrended correspondence analysis: An improved ordination technique. *Vegetatio* **1980**, *42*, 47–58. [[CrossRef](#)]
49. IUCN Standards and Petitions Committee. Guidelines for Using the IUCN Red List Categories and Criteria. Version 15.1. Prepared by the Standards and Petitions Committee. Available online: <https://www.iucnredlist.org/documents/RedListGuidelines.pdf> (accessed on 24 October 2022).
50. Bachman, S.; Moat, J.; Hill, A.W.; Torre, J.; Scott, B. Supporting Red List threat assessments with GeoCAT: Geospatial conservation assessment tool. *ZooKeys* **2011**, *150*, 117–126. [[CrossRef](#)]
51. Pignatti, S.; Guarino, R.; La Rosa, M. *Volume 1: Flora d'Italia & Flora Digitale*. In *Flora d'Italia: In 4 Volumi*, 2nd ed.; Edagricole-Edizioni Agricole di New Business Media srl: Milano, Italy, 2017.
52. Pignatti, S.; Guarino, R.; La Rosa, M. *Volume 2: Flora d'Italia & Flora Digitale*. In *Flora d'Italia: In 4 Volumi*, 2nd ed.; Edagricole-Edizioni Agricole di New Business Media srl: Milano, Italy, 2017.
53. Pignatti, S.; Guarino, R.; La Rosa, M. *Volume 3: Flora d'Italia & Flora Digitale*. In *Flora d'Italia: In 4 Volumi*, 2nd ed.; Edagricole-Edizioni Agricole di New Business Media srl: Milano, Italy, 2018.
54. Pignatti, S.; Guarino, R.; La Rosa, M. *Volume 4: Flora d'Italia & Flora Digitale*. In *Flora d'Italia: In 4 Volumi*, 2nd ed.; Edagricole-Edizioni Agricole di New Business Media srl: Milano, Italy, 2019.
55. Martellos, S.; Bartolucci, F.; Conti, F.; Galasso, G.; Moro, A.; Pennesi, R.; Peruzzi, L.; Pittao, E.; Nimis, P.L. FlorItaly—The portal to the Flora of Italy. *PhytoKeys* **2020**, *156*, 55–71. [[CrossRef](#)]
56. Cortini Pedrotti, C. *Flora dei Muschi d'Italia. Sphagnopsida, Andreaeopsida, Bryopsida (I Parte)*; Antonio Delfino Editore: Rome, Italy, 2001.
57. Cortini Pedrotti, C. *Flora dei Muschi d'Italia. Bryopsida (II Parte)*; Antonio Delfino Editore: Rome, Italy, 2005.
58. Mucina, L.; Bültmann, H.; Dierßen, K.; Theurillat, J.-P.; Raus, T.; Carni, A.; Šumberová, K.; Willner, W.; Dengler, J.; García, R.G.; et al. Vegetation of Europe: Hierarchical floristic classification system of vascular plant, bryophyte, lichen, and algal communities. *Appl. Veg. Sci.* **2016**, *19*, 3–264. [[CrossRef](#)]
59. Ben Avraham, Z.; Grasso, M. Collisional zone segmentation in Sicily and surrounding areas in the Central Mediterranean. *Ann. Tecton.* **1990**, *4*, 131–139.
60. Bianchi, F.; Carbone, S.; Grasso, M.; Invernizzi, G.; Lentini, F.; Longaretti, G.; Merlini, G.; Mostardini, F. Sicilia orientale: Profilo geologico Nebrodi-Iblei. *Mem. Soc. Geol. Ital.* **1989**, *38*, 429–445.
61. Minissale, P.; Santo, A.; Sciandrello, S. The coastal vegetation of the SCI “Capo Murro di Porco, Penisola della Maddalena e Grotta Pellegrino” (Siracusa). *Fitosociologia* **2011**, *48*, 77–98.
62. Sciandrello, S.; Guglielmo, A.; Spampinato, G. Spatial patterns and floristic composition of plant communities in coastal salt marshes of south-eastern Sicily (Italy). *Acta Bot. Gall.* **2014**, *161*, 99–109. [[CrossRef](#)]
63. Sciandrello, S.; Musarella, C.M.; Puglisi, M.; Spampinato, G.; Tomaselli, V.; Minissale, P. Updated and new insights on the coastal halophilous vegetation of southeastern Sicily (Italy). *Plant Sociol.* **2019**, *56*, 81–98.
64. Sciandrello, S. Coastal saltmarsh vegetation in Sicily (Italy): Phytosociological insights and plant diversity. *Plant Biosyst.* **2020**, *154*, 860–876. [[CrossRef](#)]
65. Minissale, P.; Molina, J.A.; Sciandrello, S. *Pilularia minuta* Durieu (Marsileaceae) discovered in south-eastern-Sicily: New insights on its ecology, distribution and conservation status. *Bot. Lett.* **2017**, *164*, 197–208. [[CrossRef](#)]
66. Minissale, P.; Sciandrello, S. Ecological features affect patterns of plant communities in Mediterranean temporary rock pools. *Plant Biosyst.* **2016**, *150*, 171–179. [[CrossRef](#)]

67. Minissale, P.; Trigilia, A.; Brogna, F.; Sciandrello, S. Plants and vegetation in the archaeological park of Neapolis of Siracusa (Sicily–Italy). A management effort but also an opportunity for a better enjoyment of the site. *Conserv. Manag. Archeol.* **2015**, *17*, 340–369.
68. Sciandrello, S.; Privitera, M.; Puglisi, M.; Minissale, P. Plant communities diversity and spatial patterns in volcanic temporary pond of Sicily (S-Italy). *Biologia* **2016**, *71*, 793–803. [[CrossRef](#)]
69. Brullo, S.; Brullo, C.; Tavilla, G.; Cambria, S.; Minissale, P.; Sciandrello, S.; Giusso del Galdo, G.; Siracusa, G.; Del Guacchio, E. About the occurrence of *Elatine macropoda* and *E. gussonei* (Elatinaceae) in Sicily and lectotypification of their names. *Acta Bot. Croat.* **2022**, *81*, 129–139. [[CrossRef](#)]
70. Blasi, C.; Marignani, M.; Copiz, R.; Fipaldini, M.; Bonacquisti, S.; Del Vico, E.; Rosati, L.; Zavattero, L. Important plant areas in Italy: From data to mapping. *Biol. Conserv.* **2011**, *144*, 220–226. [[CrossRef](#)]
71. Rivas Martínez, S. Bases para una nueva clasificacion bioclimatica de la tierra. *Folia Bot. Matritensis* **1993**, *10*, 1–23.
72. Rivas-Martínez, S. *Bioclimatic Map of Europe: Bioclimates, Scale 1:16 Mill*; Cartographic Service; University of León: León, Spain, 2004.

**Disclaimer/Publisher’s Note:** The statements, opinions and data contained in all publications are solely those of the individual author(s) and contributor(s) and not of MDPI and/or the editor(s). MDPI and/or the editor(s) disclaim responsibility for any injury to people or property resulting from any ideas, methods, instructions or products referred to in the content.

MDPI  
St. Alban-Anlage 66  
4052 Basel  
Switzerland  
[www.mdpi.com](http://www.mdpi.com)

*Plants* Editorial Office  
E-mail: [plants@mdpi.com](mailto:plants@mdpi.com)  
[www.mdpi.com/journal/plants](http://www.mdpi.com/journal/plants)



Disclaimer/Publisher's Note: The statements, opinions and data contained in all publications are solely those of the individual author(s) and contributor(s) and not of MDPI and/or the editor(s). MDPI and/or the editor(s) disclaim responsibility for any injury to people or property resulting from any ideas, methods, instructions or products referred to in the content.





Academic Open  
Access Publishing

[mdpi.com](https://www.mdpi.com)

ISBN 978-3-0365-8423-2